

Proceedings of the

15th North American



Mine Ventilation Symposium

Blacksburg, Virginia

20-25 June 2015

Edited by

Edmund Jong

Emily Sarver

Steven Schafrik

Kray Luxbacher

Proceedings of the 15th North American Mine Ventilation Symposium

June 20-25, 2015

Blacksburg, Virginia

Editors

Edmund Jong

Emily Sarver

Steven Schafrik

Kray Luxbacher

Published by the Virginia Tech Department of Mining and Minerals Engineering

2015

Foreword

The following conference proceedings are a compilation of technical papers representing subjects related to underground mine ventilation. All of the papers included in these proceedings were presented at the 15th North American Mine Ventilation Symposium (NAMVS) from June 20, 2015 to June 25, 2015, held on the Virginia Tech campus in Blacksburg, Virginia. All papers were peer-reviewed prior to publication. The 2015 NAMVS is championed by the Underground Ventilation Committee of the Society for Mining, Metallurgy, and Exploration (a joint committee of the Coal and Energy Division and Mining and Exploration Division).

First held in 1982, the biannual Symposium has become a major international venue attracting subject matter experts in the field of underground mine ventilation from major industrial partners, advanced research laboratories, and prestigious academic institutions. Symposium attendees congregate for the presentation of technical papers representing the state-of-the-art in underground mine ventilation research and technology. The Symposium venue additionally facilitates open collaboration between underground mine ventilation professionals from industry, academia, and government in an environment that fosters innovation. The 15th NAMVS was organized by the Mining and Minerals Engineering Department of Virginia Tech with significant help from Keith Wallace, Brian Prosser, Jürgen Brune, Ian Loomis, Phil Patton, and John Kelleher. Special thanks are extended to the Virginia Tech help team: Gwen Davis, Kathryn Dew, Heather Dougherty, Betsy Duane, Michael Karmis, Kyle Louk, Erin McCullough, Lucas Rojas-Mendoza, Nino Ripepi, Daniel Stinnette, Charles Schlosser, and Carol Trutt.

Over 90 abstracts were received as a result of the “call for papers.” Seventy of these papers were selected and published in these proceedings. The included papers were selected by Symposium organizers because they reflect both present day critical challenges that underground mine ventilation professionals face as well as new innovative ideas that will propel the profession into the future. The content in the proceedings represents topics that include diesel exhaust and other contaminants in the mine atmosphere, dust in the underground mine environment, mine atmospheric monitoring, mine fans, mine fires, mine gases, mine heating and cooling, case studies, ventilation planning, and ventilation system design.

Kray Luxbacher, Chair, and Emily Sarver, Co-Chair
Blacksburg, Virginia, USA
June 2015

The Underground Ventilation Committee of the SME

Phil Patton, 2014 Chair

Anu Martikainen, 2015 Chair

Kray Luxbacher

Gerrit Goodman

Daniel Stinnette

Charles Kocsis

Heather Dougherty

Exhibits Chair

John Kelleher

Sponsors

Chasm Consulting

Howden

Maestro Mine Ventilation

Spendrup Fan Co.

SME CAS

Exhibitors

ABC

ACI – Canefco

Accutron

Advanced Fan Systems

Chasm Consulting

Clarage

Coalfield Services Inc.

Cradle

Howden

Hurley Ventilation Technologies Inc.

G+ Plastics

Maestro Mine Ventilation

Mine Ventilation Services

NIOSH

Pauls Fans

Schauenburg Flexadux Corp.

Shaft Drillers International (SDI)

SMJ Fans

Turbo

Contributing Editors

Angelo Biviano

Eric Watkins

Proceedings of the 15th North American Mine Ventilation Symposium

ISBN 978-0-692-47348-1

Copyright © 2015 by the Virginia Tech Department of Mining and Minerals Engineering. All rights reserved excepted as noted below. This book, or parts thereof, may not be reproduced without permission of the publisher.

The following papers were prepared as part of government work or by authors employed by the U.S. government working for the National Institute of Occupational Safety and Health (NIOSH) and the United States Environmental Protection Agency (U.S. EPA).

Diesel Oxidation Catalytic Converters for Underground Mining Applications. *Bugarski, A.D., Hummer, J. A., Robb, G. M. NIOSH Office of Mine Safety Health and Research (OMSHR)*

A New End-of-Shift Monitoring Approach for Respirable Crystalline Silica in Coal Mine Dust. *Cauda, E., Miller, A., Drake, P. NIOSH/CDC*

Effect of Discrete Fracture Network Representation of Gob on Airflow Distribution Near the Longwall Face. *Karacan, C.Ö., Yuan, L. CDC/NIOSH/OMSHR*

Improvement in Booster Fan Applications for US Coal and Metal/Non-metal Mines through the Application of Technology, International Operating Experience, and NIOSH Research. *Pritchard, C. J., Martikanien, A. L. NIOSH.*

The Use of Atmospheric Monitoring Systems for Fire Detection in Underground Coal Mines. *Smith, A.C., Litton, C. D. NIOSH*

Numerical Study on the Effects of Water Spray Characteristics on Suppression of Conveyor Belt Fires. *Yuan, L., Smith, A. C. CDC/NIOSH*

Computational Fluid Dynamics Modeling of Methane Distribution at a Continuous Miner Face Under Various Methane Release Conditions. *Zhou, L., Pritchard, C., Zheng, Y. CDC/NIOSH*

Ventilation Air Methane Abatement Opportunities for the Coal Industry. *Ruiz, F., Talkington, C., Olson, E. U.S. EPA*

The following paper is Copyright © to Her Majesty the Queen in Right of Canada, as represented by the Ministry of Natural Resources, 2015

The Assessment of Specialized Clothing Worn by Underground Miners and its Heat Stress Management Implications. *Hardcastle, S.G., Poirier, M.P., Friesen, B.J., McGinn, R., Meade, R., and Kenny, G.P.*

Table of Contents

Mine Atmospheric Monitoring

A Review of Good Practice Standards and Re-entry Procedures after Blasting and Gas Detection Generally in Underground Hardrock Mines (15-01). *Brake, D.J.*

The Use of Atmospheric Monitoring Systems for Fire Detection in Underground Coal Mines (15-02). *Smith, A.C. and Litton, C.D.*

An Investigation of Mine Gas Stability in Sampling Containers Over Time Using Gas Chromatography Analysis (15-03). *Dougherty, H., Jeter, T.S., Luxbacher, K., Brashear, K. Jong, E., McNair, H., Shan, L., Zhang, A.*

Gas Chromatography Techniques in Detecting Toxic Exhaust Gases in Underground Mines (15-04). *Alghamdi, Y.H. and Gillies, A.D.S.*

Comparison of Turbulence Models for Estimation of Fugitive Dust Retention in Open-Pit Mines (15-46). *Bhowmick, T. and S. Bandopadhyay*

Mine Fans

Considerations for the Selection of Variable Frequency Drives for Primary Fans (15-06). *De Souza, E.*

Improvement in Booster Fan Applications for US Coal and Metal/non-Metal Mines through the Application of Technology, International Operating Experience, and NIOSH Research (15-07). *Pritchard, C.J., Martikainen, A.L.*

Axial Fan Failures Related to Improper VFD Operation (15-08). *Ray, R.E., Gouge, A.P., Wilchek, S.B.*

Utilization of Booster Fans in Underground Coal Mines (15-09). *Calizaya, F., Nelson, M. G.*

Optimal Combination of Main and Booster Fans Pressure - Application of Genetic Algorithms (15-10). *Shriwas, M., Calizaya, F.*

Mine Heating and Cooling

Liquefied Natural Gas as a Mine Intake Air Heating Fuel (15-11). *Loomis, I.A., Ramirez, M.*

Conveyor Tunnel Airflow Requirement Update Based on Heat Exchange for the New Level Mine Project (15-12). *Montecinos, C., Acuña, E.I., Wallace, K.G.*

Investigating the Importance of Climatic Monitoring and Modeling in Deep and Hot US Underground Mines (15-13). *Carpenter, K. E., Roghanchi, P., Kocsis, K.C.*

The Assessment Of Specialized Clothing Worn By Underground Miners And Its Heat Stress Management Implications (15-14). *Hardcastle, S.G., Poirier, M.B., Friesen, B.J., McGinn, R., Meade, R., Flouris, A.D., Allen, C., Kenny, G.P.*

Understanding the Human Thermal Balance and Heat Stress Indices as they apply to Deep and Hot US Mines (15-15). *Roghanchi, P., Sunkpala, M., Kocsis, K.C.*

Heat Management in a Potash Mine (15-16). *Anderson, R.I., De Souza, E.*

Ventilation Planning and Design

Applications of Modelling Software for Safety and Health Training in US Underground Coal Mines (15-17). *Dougherty, H., Stewart, C.*

Acoustic Directivity of Mine Ventilation Systems (15-18). *Dobson, A.*

Development and Implementation of a Data Management Platform for Atmospheric Data in Underground Coal Mines (15-19). *Agioutantis, Z., Luxbacher, K., Dougherty, H., Karmis, M.*

Reconciliation of Ventilation and Production Expansion in a Potash Mine (15-20). *Penner, K., De Souza, E.*

A Case Study of Optimization of Costs for Trackless Mining Ventilation and Cooling Systems (15-21). *Rostami, P., Rawlins, A.C.*

Mine Ventilation Model Calibration with Numerical Optimization (15-22). *Danko, G.L., Bahrami, D., Lu, C.*

Behavior of Flow Through Mine Elbows and Louvers (15-23). *Haghighat, A., Gillies, S. Luxbacher, K.*

Study of Ventilation in the Mine CERRO LINDA CIA. MINERA MILPO S.A. to Increase Production from 15000 TPD to 18000 TPD (15-24 English). *Corimanya, J.A., Herrera, F.A.*

Estudio de Ventilacion de la Mina Cerro Lindo CIA. Minera Milpo S.A. para Ampliar la Produccion de 15 000 a 18 000 TPD (15-24 Spanish). *Corimanya, J.A., Herrera, F.A.*

Effect of the Air Gap Associated with Cave Evolution on Cave Resistance (15-25). *Erogul, D., Baysal, A., Ajayi, K.M., Tukkaraja, P., Shahbazi, K., Katzenstein, K., Loring, D.*

Assessment of Ventilation Circuit for Block Caving Production Level Drifts (15-26). *Hurtado-Cruz, J.P., Acuña-Duhart, E., San Martín-Lizana, Y.H., Vargas-Norambuena, J.P.*

Ventilation and Mine Atmosphere Case Studies

An Engineer's Guide to Ventilation Surveys and Ventilation Modelling: A Case Study from a Large Underground Metal Mine (15-27). *Slaughter, C. and Tien, J.*

Primary Mine Ventilation Solution for the New Level Mine Project During the Construction Period 2015 – 2020 (15-28). *Acuña, E.I., Wallace, K. G., Soto, H.*

Sinking of Resolution No.10 Shaft in Extreme Heat Conditions (15-29). *von Glehn, F., Bluhm, S., Goodell, T., Lunderstedt, D.*

Ventilation Analyses at the Waste Isolation Pilot Plant Post Radiological Event (15-30). *Wallace, K.G., Farnsworth, J.I., Rodriguez, E.C.*

Arctic Mine Air Heating (15-31). *Wilson, A., De Souza, E.*

A Discussion of the Automated Ventilation Systems at the Henderson Mine (15-32). *Loring, D.M., Brokering, R.D., Rogers, A., Dhyne, B.P.*

Technical Ventilation Services of a Large Coal Mining Company (15-33). *Boskovich, B., Thadisina, R.R., Persinski, B.*

Modeling the ventilation network at NIOSH's Safety Research Coal Mine (15-34). *Iannacchione, A., Jose, A., Horn, T., Iannacchione, G., Iannacchione, S.*

Impact of Air Inversions on Natural Ventilation in Open Pit Mines (15-35). *Raj, K.V., Fochesatto, G.J., Bandopadhyay, S.*

Improving the Expected Cooling Capacity of the Conditioning System at Creighton Mine (15-36). *Acuña, E. I., Allen, C., O'Connor, D.*

Diesel Exhaust and Other Contaminants

Diesel Oxidation Catalytic Converters for Underground Mining Applications (15-37). *Bugarski, A.D., Hummer, J.A., Robb, G.M.*

Simulation of DPM Dispersion for Different Mining Operations Inside a Dead-end Entry (15-38). *Zheng, Y., Thiruvengadama, M., Lan, H., Tien, J.C.*

Overview of DPM Control Strategies during Longwall Moves (15-39). *Gillies, A.D.S., Wu, H.*

Real-time monitoring of DPM, Airborne Dust and Correlating Elemental Carbon Measured by Two Methods in Underground Mines in USA (15-40). *Khan, M.U., Gillies, A.D.S.*

DPM Monitoring in Underground Metal/Nonmetal Mines (15-41). *McCullough, E., Rojas-Mendoza, L., Sarver, E.*

A Preliminary Investigation of DPM Scavenging by Water Sprays (15-42). *Rojas-Mendoza, L., McCullough, E., Sarver, E., Saylor, J.R.*

Computational Fluid Dynamics Study of Radon Gas Migration in a Block Caving Mine (15-43). *Ajayi, K.M., Tukkaraja, P., Shahbazib, K., Katzenstein, K., Loring, D.*

Economics of Diesel Fleet Replacement by Electric Mining Equipment (15-44). *Varaschin, J., De Souza, E.*

Dust in the Underground Mine Environment

A New End-of-Shift Monitoring Approach for Respirable Crystalline Silica in Coal Mine Dust (15-45). *Cauda, E., Miller, A., Drake, P.*

Introducing the Ultrasonic Scrubber: Potential Applications in Dust Control (15-74). *Saylor, J.R., Ran, W.*

Considerations for an Automated SEM-EDX Routine for Characterizing Respirable Coal Mine Dust (15-47). *Johann, V.A., Sarver, E.A.*

Considerations for TGA of Respirable Coal Mine Dust Samples (15-48). *Scaggs, M., Sarver, E., Keles, C.*

CFD Modeling of a Flooded-Bed Scrubber Concept for a Longwall Shearer Operating in a U.S. Coal Seam (15-49). *Wedding, W., Novak, T., Arya, S., Kumar, A.*

Development of a Mine Dust Sampling Instrument for Use in Underground Coal Mines (15-50). *Goertz, B.J., Brune, J., McDaniel, S., Rockley, T., Soares Barreto, F., Demontigny, N.*

Application of Box-Wilson Experimental Design Method for Underground Mine Respirable Coal Dust Studies (15-51). *Chen, Y., Xu, G., Kuruppu, M., Albijan, B.*

Preliminary Laboratory Experiments Design for the Study of Bauxite Residue Dust Control (15-52). *Ding, X., Xu, G., Kuruppu, M., Albijan, B.*

Mine Gases

Computational Fluid Dynamics Modeling of Methane Distribution at a Continuous Miner Face Under Various Methane Release Conditions (15-53). *Zhou, L., Pritchard, C., Zheng, Y.*

A Critical Look at Longwall Bleeder Ventilation (15-54). *Brune, J.F., Grubb, J.W., Bogin, G.E., Zipf, R.K., Marts, J.A., Gilmore, R.C., Lolon, S., Saki, S.A.*

Experimental Investigation of Fusing Thin Spray-On Liners as a Gas Management Tool in Underground Coal Mines (15-55). *Li, Z., Chalmers, D., Saydam, S., Mitra, R., Hussain, F.*

Effect of Decreasing Barometric Pressure on Explosive Gas Zones in Bleeder Ventilated Longwall Gobs (15-56). *Lolon, S. A., Gilmore, R.C., Brune, J.F., Bogin, G.E., Grubb, J.W., Zipf, R.K., Juganda, A., Saki, S.A.*

Ventilation Air Methane Abatement Opportunities to the Coal Industry (15-57). *Ruiz, F., Talkington, C., Olson, E.*

Gob Ventilation Boreholes Design Optimization for Longwall Coal Mining (15-58). *Saki, S.A., Brune, J.F., Bogin, G.E., Gilmore, R.C., Grubb, J.W., Zipf, R.K., Marts, J.A.*

Effect of Discrete Fracture Network Representation of Gob on Airflow Distribution Near the Longwall Face (15-59). *Karacan, C.Ö., Yuan, L.*

Ventilation Methane Emissions of Coal Mines in Zonguldak Coal Basin, Turkey (15-73). *Fişne, A., Özer, S.C., Esen, O.*

Evaluation of Coal Seam Gas Content in Kozlu Mine, Zonguldak, Turkey (15-62). *Özer, S.C., Esen, O., Fişne, A.*

Mine Fires

Analysis of all Reported Mine Fire Incidents: 2000-2013 in All Types of United States Mines (15-63). *Slaughter, C., Tien, J., Cao, Y.*

Principle Roles of Mine Fire Simulation in Mine Management and Emergency Planning (15-64). *Fox, J., Bowling, J., Schafrik, S.*

Spontaneous Combustion Prediction and Remediation Techniques (15-65). *Jha, A., Clizaya, F., Nelson, M.G.*

Fire Behavior Analysis of a Mine Future Plan (15-66). *Haghighat, A., Gillies, S.*

Underground Fire Rollback Simulation in Large Scale Ventilation Models (15-67). *Stewart, C., Aminossadati, S.M., Kizil, M.S.*

Numerical Study on the Effects of Water Spray Characteristics on Suppression of Conveyor Belt Fires (15-68). *Yuan, L., Smith, A.C.*

Modeling and Simulation of Multiple Underground Mine Fire Scenarios at Freeport Indonesia (15-69). *Brake, R., Hatt, A., Sani, R.*

Managing the Risk of Spontaneous Combustion in Underground Coal Mines (15-70). *Grubb, J.W., Brune, J. F., Zipf, R.K., Bogin, G.E., Marts, J.A., Gilmore, R.C., Saki, S.A., Lolon, S.A.*

CFD analysis of Truck Fire in Large-Opening Limestone Mine (15-71). *Lee, C., Kim, H.*

Mine Atmospheric Monitoring

A Review of Good Practice Standards and re-Entry Procedures after Blasting and Gas Detection Generally in Underground Hardrock Mines

Derrick J Brake

Mine Ventilation Australia, Brisbane, Australia

There have been many single and multiple fatalities over generations of underground mining due to workers being gassed by toxic blasting fumes or an irrespirable atmosphere after re-entering the area that was blasted, or some area connected to it. The traditional approach to determining safe re-entry (clearance) times was to use a fixed time interval after blasting based on either experience, limited testing with chemical stain tubes, or simple dilution calculations, as well as training miners to “use their nose” to smell for fumes. With the advent of relatively inexpensive and reliable electronic gas monitors, combined with the now well-established principal of managing risks to the “as low as reasonably achievable” (ALARA) standard, re-entry procedures have been undergoing considerable changes. Gas monitors are now frequently used to test all “potentially” affected locations. However, the risks from migrating blasting fumes have also increased due to the trends to allow or even design ventilation circuits with major short-circuiting through open stopes and other leakage paths, as well as using the main ramp in some mines as a “dirty intake” with one level effectively in series with another. In all of these cases, blasting fumes from one location may be introduced into non-blasted locations. Moreover, the introduction of 12 hour shifts and “long” rosters has created some divergence in the industry with respect to the gas limit standards for “safe” gas levels for re-entry. This paper reviews modern procedures for safe re-entry after both development and production blasting, including how it is being undertaken, the target gases being used for re-entry clearance criteria, and general risk management considerations. It makes recommendations for safe standards.

Keywords: gas, monitors, blasting, re-entry, ALARA.

1. Introduction

Incidents resulting in serious injury and fatalities due to being exposed to toxic blasting gases continue in the mining industry. A key problem is that most hardrock mines blast between two and six times each day, so that it is easy to become “over-familiar” with the issue of blasting fumes and complacent so that when the unexpected or unusual happens, workers can be gassed.

This paper deals solely with the safe re-entry in terms of noxious gases; it does not discuss any of the other important safety aspects of preparing for blasting, or safety requirements at the conclusion of blasting such as disconnecting firing lines, checking for misfires, barring down, setting up water sprays, etc.

Most Australian mines now have a system of written “Authorized Firing Plans” (AFPs) or similar documentation (one AFP for every blast), that sets out the “check and clear” information for the blasting crew and the re-entry information and required checks for the re-entry crew. In effect, an AFP is a standard checklist that is customized for each particular blast and includes extracts from level plans showing where barricades are required, etc. These AFPs are issued by the mine design staff (including the ventilation engineer), completed in writing by the re-entry crew and handed back to the supervisor after each blast. Just as airline pilots, no matter how experienced, complete written checklists before take-off, so these AFPs reduce the potential for human error in blasting checks.

2. Gases produced from blasting

With modern explosives (ANFO and/or emulsion [or various mixtures of the two]), the amount of toxic gases or fumes produced from blasting varies according to the explosive mix, the degree of confinement in the hole, the amount of water in the hole and the sleep time of the explosive, among other factors.

It is always difficult to predict how much blasting fumes will be produced, and also how long it will take for the fumes to “clear”. Empirical methods have been developed but these are at best an indicator of the likely clearance time and hence are more intended to provide an estimate of the impact on mine productivity, and should never be considered to be “prescriptive” or sufficient in terms of safely allowing persons back into the area.

In the following discussion, “safe” re-entry gas concentrations are taken as being the current Australian TWA values: CO (30 ppm), CO₂ (5000 ppm), NO₂ (3 ppm) and NO (25 ppm). Other gases such as NH₃ and SO₂ are unlikely to be critical. As will be seen below, SO₂ and H₂S are not strictly substantial products from explosives, but where present are usually due to the use of explosives in sulphide-containing rocks. NH₃ should also be minimal unless lime is present (e.g. due to cement).

Table 1 summarizes key available data in terms of the toxicity of the concentrations of blasting gases. The values in columns A to C of this table are expressed as m³/s of fresh air required to dilute the volume of blasting fumes produced from 1 kg of explosive to the TWA values as noted above. Column D is discussed separately.

- Column A of Table 1 is from Rowland, Mainiero and Hurd [5] who also found that for fresh emulsion, an average NO/NO₂ ratio is about 30% (see also figure 1 and 2).
- Column B of Table 1 is from Lovitt [3] who also found that emulsion (“Powergel”) has a NO/NO₂ ratio of about 30% (see also table 2).
- Column C of Table 1 relates to non-ideal detonation of ANFO and is from Lovitt [2]. See also figure 4.

- Column D of Table 1 is from Hardcastle [1]. Whilst numerical data is not available, Hardcastle found the critical gas was CO, followed in descending order by NO₂, NO and CO₂.

Effectively Table 1 shows that for emulsion, the most critical blasting gases are CO and NO₂, with NO and CO₂ much less significant. The critical gases with ANFO are much harder to predict as it suffers much greater production of toxic gases (from ideal detonation values) due to presence of water. However, the most toxic gases for ANFO and emulsions will remain CO, NO₂, CO₂ and NO in *some* order.

Table 1. "Criticality of gases from blasting" expressed as m³/s of fresh air to dilute blasting fumes from 1 kg of explosive to the TWA as above, except for column D which is by critical order

	A	B	C	D
Explosive	Emulsion	Emulsion	ANFO (non-ideal det)	Unspecified
CO	500	583	833	1
NO ₂	333	307	2500	2
NO	40	97	700	3
CO ₂	30	21	35	4

Examples of actual gas concentrations from blasting (production and development) are shown in Figures 6 and 7.

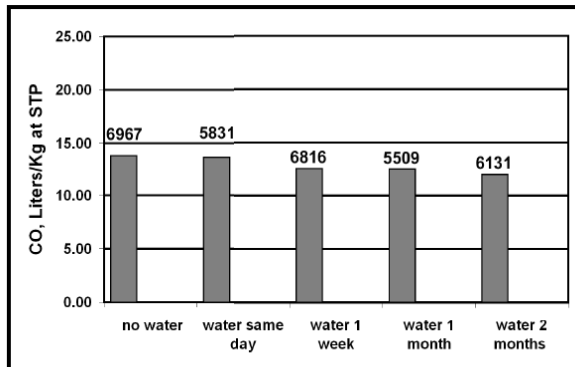


Fig. 1. Carbon monoxide production of emulsion shot in steel pipe following exposure to water for up to two months. Numbers above bars are detonation velocity in m/s (Rowland, Mainiero and Hurd [5])

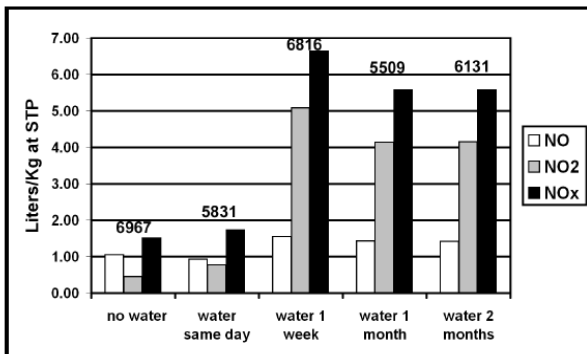


Fig. 2. Nitrogen oxides production for emulsion shot in steel pipe following exposure to water for up to two months.

Numbers above bars are detonation velocity in m/s (Rowland, Mainiero and Hurd [5])

Table 2. Data from Lovitt [2] (original source 1984)

Explosive type	Computed toxic gas value (L/kg)				
	NO _x	NO	NO ₂	CO	CO ₂
AN60	8.53	5.93	2.60	65.95	195.38
Powergel	3.35	2.43	0.92	17.51	105.02
Molanite 115	5.70	4.66	1.04	27.84	70.15

Component	ANFO	ANFO
	litres/Kg	Percent
Methane	minor	minimal
Carbon Monoxide	5 to 44	1% to 4%
Carbon Dioxide	100 to 250	9% to 24%
Hydrogen	minor	minimal
Ammonia	0.3 to 3	0.03 to 0.3 %
Water	580 to 680	53% to 63%
Hydrogen Sulphide	minor	minor
Nitrogen	100 to 250	9% to 24%
Nitric Oxides	10 to 40	1% to 4%
Oxygen	minor	minor
Sulphur Dioxide	minor	minor

Fig. 3. Data from Lovitt [2] who states “In normal use, the following rates of production...can reasonably be expected. Water is the main cause for non-ideal nature.”

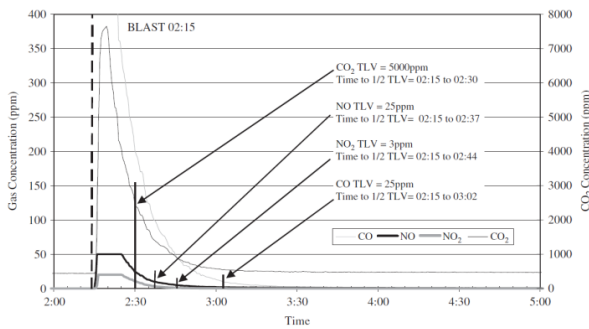


Fig. 4. Data from Hardcastle [1]

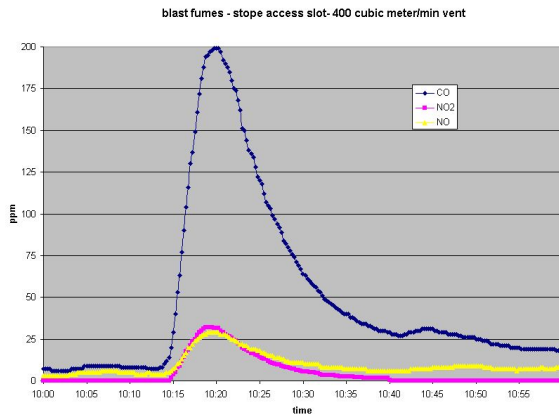


Fig. 5. Data from stope blast

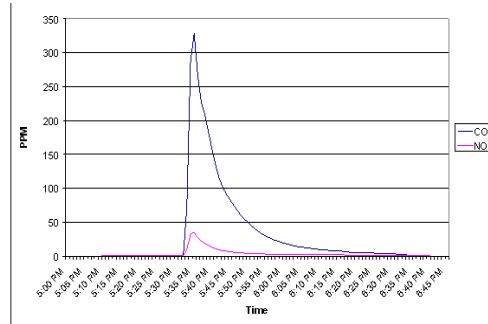


Fig. 6. Data from development blast (same mine and time period as Figure 6)

3 Blast gas measurement procedures

Whilst supervisors have often been used in the past to check the blast-affected areas for fumes, most Australian mines now use dedicated, trained re-entry crews. These crews are usually either development charge-up or production blasting personnel and usually operate as “pairs” (two persons per crew). They operate to strict procedures. They usually have two persons per crew for safety, although often using only one gas monitor providing it is maintained, operated and calibrated strictly in accordance with the manufacturer’s requirements.

Based on the earlier discussion, the minimum gases that need to be measured before re-entry are shown in Table 2. This table also shows other gases commonly installed on these monitors, as the monitors are often used for other purposes than re-entry after blasting.

Table 2 also shows the recommended maximum gas concentration in any part of the area before the area can be considered safe (in terms of atmosphere). Note that some mining operators use different values for these levels. Typical values/criteria across the industry would be to use the:

- STEL (short-term exposure level)
- 8-hour TWA (time-weighted average)
- Roster-adjusted TWA (for 12 hour shifts, this is usually 50% of the 8-hour TWA for most gases).

This author recommends use of the roster-adjusted TWA, as this is the “safe” level even if no further dilution of blasting fumes in that location were to occur. This is conservative but most Australian mines use this approach.

Less conservative criteria could be used if careful risk assessment finds this acceptable; however, often the extra time required for the gas concentration to fall from (say) 30 ppm to 15 ppm in well-ventilated areas is only

1. Some operations do allow single persons in this role providing they are carrying reliable, accurate gas monitors. However, the author would not recommend this practice.

Table 3. Usual minimum gases to be measured in hardrock mine (TWA and STEL values are those applicable in Australia)

Situation	Gas	Criteria (8 hr shifts, 40 hr week)	Criteria (12 hour shifts, 42 hr week)	STEL
Minimum gas checks for blasting in inert material	CO	<30 ppm ^c	<15 ppm	<50 ppm ^c
	NO ₂	<3 ppm	<1.5 ppm	<5 ppm
Extra gas to be checked if sulphides present	SO ₂	<2 ppm	<1 ppm	<5 ppm
Extra gases-desirable	NH ₃	<25 ppm	<12.5 ppm	<25 ppm
	CO ₂	<5000 ppm	<2500 ppm	<30 000 ppm
Confined spaces ^d LEL should also be measured where flammable gases may be present, e.g. strata gases or large lead-acid battery charging stations	H ₂ S	<10 ppm	<5 ppm	<10 ppm
	O ₂	>18 % ^e	>18 % ^e	
	CH ₄ /H ₂	>20 % LEL	>20 % LEL	
	LEL			

Some operations do allow the re-entry crew, who are carrying gas monitor(s) and are specially trained, to enter an area above the TWA but below the STEL, solely for purposes of making the area safe (e.g. turning fans on, or shorting-out firing lines), providing the exposure meets STEL guidelines (maximum of 15 minutes no more than 4 times per shift separated by at least one hour per exposure). Some gas monitors now have the facility to continuously monitor on a time-weighted basis for TWA and STEL values and alarm accordingly.

There is a limit to the number of sensors that can be fitted to a handheld gas monitor, and more sensors also mean higher initial purchase cost and more expensive recalibration, etc. Fitting the maximum number of sensors to a monitor is not always the best option. In some cases it may be better to have two monitors (say an "A" monitor and a "B" monitor—each with different sensors), if the mine does want to measure a number of gases.

Effectively Table 2 shows that the minimum gases to be checked in most hardrock mines (most of which have some sulfides present) would be: CO, NO₂ and SO₂, with NH₃ also desirable. A second monitor could carry: CO₂, H₂S, O₂, CH₄/LEL and NH₃ (if not on the first monitor).

In Australia, current good practice gas re-entry procedures for blasting is as follows:

1. Blast-proof barricades⁶ are placed to prevent entry to any area which could be affected by the blast directly (concussion, flyrock) or by fumes from the blast. An AFP is essential for production blasts other than small blasts (e.g. opening up the cutoff slot, often to a limit of (say) 3000 tonnes ore) and good practice would be to have at least a "generic" AFP for development headings on various levels of the mine or in various sub-circuits of the ventilation system. As noted earlier, some operations require an AFP for all blasts.
2. With parallel ventilation circuits, barricades may not be required on the ramp and on many non-blasted levels. This should be resolved in the risk assessment used to develop the AFP.
3. All potentially affected persons are then removed to safe locations (usually the surface or a cribroom that is also a secure fresh air base). All persons are accounted for.
4. The blasts are initiated.
5. The priority for re-entry checks is usually the ramp so that most if not all persons can get back to work assuming they can get to their workplace without going past a blasting barricade. The re-entry crew will give priority to checking the ramp (if required under the AFP) and then these areas are declared 'all clear' and any barricades on the ramp removed.
6. If fans (including development fans) on fume-affected levels can be restarted immediately and automatically from a safe central location, this is done immediately after the blast. Alternately, and assuming the development fan "electrical starters" are located in a "safe" area with fresh air, the re-entry crew might be required to wait (say) 10 to 15 minutes after the blast and then, with gas monitors, proceed to turn on the fans manually. If gas levels exceed the allowable value before they reach the fan starter, they retreat to the surface or cribroom and wait a further 10 to 15 minutes. If fan starters still cannot be reached safely, then trained persons (e.g. mine rescue crew) using breathing apparatus may be required.
7. If that fan can be turned on, then the re-entry crew may proceed to the next fan allowing time for the fumes in that heading to clear.
8. A minimum of (say) 15 to 30 minutes *after the ventilation is re-established*, the re-entry crew will start from the "safe" area and proceed to each barricade and then into the firing area, checking for fumes as they go. If they encounter fumes above the re-entry criteria, they withdraw and leave the barricade up. If they check the entire potentially affected area (including blind headings) and gases are below (within) the re-entry level criteria, then they remove the barricade.

2. Hour TWA for CO in Australia is 30 ppm; in North America it is 25 ppm

3. There is no STEL for CO although there is a special Guidance Note in Australia. This is a typical value used for short-term re-entry.

4. The "standard" gases to be checked in Australia for confined spaces entry are O₂, CH₄/LEL (flammables) and two toxic gases which are usually H₂S and CO₂. However, confined space gas entry requirements can vary with circumstances and regulatory authority. Check first.

5. At normal barometric pressure.

6. Blast proof in the sense that the personnel barricade (e.g. chain) and sign cannot be blown away due to the blast. In some cases, sentries are posted. Some operations also use flashing blue lights at the barricade.

9. The gas levels at the fan inlet (for a blind heading) should be checked first to ensure no recirculation is occurring.
10. The gas monitor must be exposed to the air that potentially contains the toxic gases, i.e. if travelling by vehicle (normal practice) the re-entry crew passenger's arm is held safely out the window with the gas monitor exposed to the outside atmosphere. It is unsafe to just have the gas monitor on the seat of the vehicle, or held inside the vehicle.
11. In some mines, workers who then enter the area that was fired once it is "cleared" and declared safe *also* carry a gas monitor (in case of residual gas not detected by the re-entry crew).
12. If the mine has many areas to "clear", then more than one re-entry crew can be utilised, according to a carefully constructed and coordinated plan.
13. When considering areas that may be affected by blasting fumes it is essential to understand the following:
 - a. Fumes are initially and instantly produced as a concentrated cloud that then starts to move through the mine towards the exhaust (for that area) as a "plug" (diluting and dispersing as it goes). It is therefore possible that the fume level may be falling, or even safe, in an area close to the blast, *but still be increasing or unsafe in another area between the blast and the exhaust.*
 - b. This issue is particularly the case in mines with series ventilation of multiple levels, where the fumes from a blast on a level will return to the ramp and then move down the ramp so that a gas monitor on the ramp will show levels increasing and decreasing as the fumes from the first blast pass. However, a blast fired on a level further up in the mine may then have its "plug" move down the ramp past the same monitor *which will then show a second peak.*
 - c. The fumes produced as part of the blast are "thrown back" instantly filling a substantial volume. This means they can be pushed into areas other than the region directly between the blast position and the local exhaust.
 - d. Ducting may be blown off development fans or "broken" part-way along the duct meaning the fan may be on but the fresh air may not be reaching the face. Therefore as noted earlier, solely adopting a time-limit for re-entry is not acceptable.
 - e. For a similar reason, it is possible that the ramp and "general" mine areas can be declared "clear" of fumes, but the re-entry crew then enters a fired area and finds a fan is off. If this fan is turned on, the plug of fumes may enter an area into which workers have already proceeded. Therefore once an all-clear has been given, fans that may disperse blasting fumes must not be turned on until workers are cleared from potential return paths for those fumes.
 - f. Fumes can migrate or be pushed or pulled from the level on which the blast occurred to other areas even down blastholes or raisebore holes or through open stopes due to leakage or short-circuiting. Circuit fans that "should" be on after the blast to clear fumes may not be (due to

damage) or ventilation controls may be damaged. To follow on from the example in dot point a, as fumes proceed down the ramp, any fan on the ramp that is "on" will pick up those fumes and push them into levels that may not have been fired. Therefore it is essential to take care to ensure that all potentially affected areas have been checked. As a minimum ALL levels that are open (via *any sort of vertical opening*) to a stope that is blasted (even if the blast is not on that level) should be checked, as well as any area fed by a fan that could have taken in blast fumes to its inlet.

- g. Fumes can be contained within the muck pile and only released into the air once loading operations commence, i.e. after re-entry is allowed. The conversion of NO to NO₂ in the presence of oxygen can be constrained by the low-oxygen potential in the muckpile (see Mainiero et al [4] and Sapko et al [6]).

Ventilation modelling can be useful in understanding blast fume behaviour and clearance times, especially in complex mines or mines with disseminated blasts. Some packages offer substantially better techniques for this purpose than others.

References

- [1] Hardcastle S, Kocsis C & O'Connor D, 2009. Justifying ventilation-on-demand in a Canadian mine and the need for process based simulations. 11th U.S./North American Mine Ventilation Symposium 2006 – Mutmanský & Ramani (eds)
- [2] Lovitt M, 2008. Explosive gases from ANFO and Powerbulk VE (pers comm).
- [3] Lovitt M, 2014. Personal communication.
- [4] Mainiero R, Rowland III J, Harris M and Sapko M, 2006. Behavior of Nitrogen Oxides in the Product Gases from Explosive Detonations, NIOSH.
- [5] Rowland J, Mainiero R and Hurd D, 2001. Factors affecting fumes production of an emulsion and ANFO/Emulsion blends (NIOSH). Proc 27th Ann conf explos blasting Tech. Vol II (28-31 Jan 2001, Cleveland OH: Int Soc of Explos Eng, 2001:133-141)
- [6] Sapko M, Rowland J, Mainiero R, and Zlochower I, 2002. Chemical and Physical Factors That Influence NO_x Production During Blasting - Exploratory Study (NIOSH).

The Use of Atmospheric Monitoring Systems for Fire Detection in Underground Coal Mines

Alex C. Smith and Charles D. Litton

NIOSH, Office of Mine Safety and Health Research, Pittsburgh, Pennsylvania, 15236 USA

The use of atmospheric monitoring systems (AMS) for early warning fire detection has significant potential to enhance the safety and well-being of underground miners. When fires occur in underground mines, significant levels of toxic gases and smoke can enter the mine ventilation airflow and be carried throughout the mine ventilation network, thus increasing the hazard potential for personnel far-removed from the actual fire. Different stages of the fire development generate different gas and smoke toxicity hazards, and although fires that develop to the point of rapid flame spread pose imminent hazards, even fires in their smoldering, pre-flaming stages can contaminate the mine atmosphere with debilitating levels of smoke and toxic gases. In addition, fires are known to increase the resistance of a mine entry, producing a reduced, or “throttled,” ventilation airflow that results in increased contaminant concentrations and affects the rate of contamination of other mine entries downstream of the fire.

Using an AMS, large numbers of sensors can be deployed within the underground workings to provide extensive coverage of critical areas where the potential for fire is of concern. These areas would be continuously monitored and readings/alerts/alarms displayed at a central control station in a secure above-ground location that is staffed around the clock. Identified problems can then be communicated quickly to underground personnel in order to implement appropriate reactions to a developing situation. The basic AMS requirements for underground mines are defined by 30 CFR 75 [1]. AMS sensors and systems are readily available, and these various sensors/systems represent the most efficient means for early and reliable detection of a variety of underground fires typically occurring throughout the mining industry. Once an AMS is installed, the extension to a mine-wide monitoring system for other locations is relatively straightforward. Enhancements to these systems could also be made, such as the use of alternative techniques for sensor/system interface and the interfacing of the AMS with mine ventilation simulators to provide for a more dynamic and interactive system. This paper provides guidance for deploying existing technologies for mine-wide atmospheric monitoring systems capable of detecting fires in the underground coal mine environment.

Disclaimer: The findings and conclusions in this report are those of the authors and do not necessarily represent the views of the National Institute for Occupational Safety and Health.

Keywords: atmospheric monitoring systems, fire detection, methane detection, ventilation.

1. Introduction

Mine fires continue to be a serious hazard to the safety and health of U.S. miners. From 1990 through 2001, there were 1,060 reported fires, resulting in 560 injuries and 6 fatalities, at U.S. mine operations [2]. Although there was a significant drop in the number of fires, to about 13 per year for underground mines from 2000 to 2004, this number is starting to increase slightly since 2004. Fire in an underground mine is especially hazardous because of the confined space, problems with ventilation and mine gases, and limited and long evacuation routes. Fires also have the potential to contaminate mine atmospheres at distances far-removed from the fire location with potentially lethal and debilitating levels of toxic gases and smoke. Although early warning fire detection is intended to prevent miner exposure to these hazards, the actual levels of toxic gases such as CO, HCl, SO₂, H₂S, and NO_x produced, along with the impact of the fire size on the mine's ventilation system, are strategic pieces of information that can be of significant benefit, both before, during, and subsequent to mine fire emergencies. With the advances in instrumentation and computer power, NIOSH is in position to obtain sound scientific data on mine fires to support performance-based regulations for the installation and performance of mine atmospheric monitoring systems, mine fire detection systems, and mine fire suppression systems.

In the late 1980s and early 1990s, the Mine Safety and Health Administration (MSHA) began to receive significant numbers of petitions from underground coal mine operators for variances to locate conveyor belt transport systems in intake entries used to ventilate working sections in order to make more efficient use of mine ventilation systems. Because fires along conveyor belts are a major concern of MSHA, the variances were generally granted if the mine installed sensors (CO, CH₄, O₂, smoke) along the intake conveyor belt entry in order to provide early warning of either fire, excessive methane, or reduced oxygen before the contaminated air could reach the working section. In the mid 1990s, these systems, called atmospheric monitoring systems (AMS), and the requirements for their installation and use were added to Title 30, Code of Federal Regulations (30 CFR). In 2004, more specific language was added to 30 CFR to remove the necessity of petitioning for the use of intake entries for conveyor belt transport. More recently, the recommendations of The Technical Study Panel on the Utilization of Belt Air and The Composition and Fire Retardant Properties of Belt Materials in Underground Coal Mining (2007) reaffirmed the need for continuous use of AMS for early warning fire detection, along with recommendations to require smoke sensors and, under certain conditions, the use of diesel-discriminating fire sensors. In addition, MSHA responded rapidly to the Panel's recommendation to discontinue the requirement for point-type heat sensors for fire detection in all conveyor belt entries, and to require the use of AMS-

based smoke or CO sensors with new regulations that went into effect January 1, 2010.

2. Current AMS Status

Existing regulations relevant to AMS are limited to monitoring for products of combustion (POC) for fire detection and the use of methane sensors in belt entries that use belt air as an intake airway. 30 CFR Part 75 identifies the location and spacing of the monitoring devices and mandates either automatic fire detection and/or automatic fire suppression for protection and for early warning of developing fires. Other underground locations exist that are not specified in 30 CFR Part 75 where there is sufficient combustible material loading to warrant continuous monitoring for fire.

A number of companies sell AMSs at various levels of capability and complexity, along with the typical sensors used for their systems. For fire detection, these systems typically use a diffusion-type electrochemical CO sensor. Such sensors are manufactured and configured to specifications supplied by the particular AMS vendor in order to satisfy constraints of intrinsically safe equipment or mine-permissible equipment, although some AMS vendors have elected to manufacture their own electrochemical cells and resultant sensors. Electrochemical CO sensors used for fire detection are typically sensitive over the range of 0 to 50 parts per million (ppm) or 0 to 100 ppm of CO, and usually with stated accuracies of around ± 0.10 ppm of CO.

Smoke sensors may also be used for fire detection as a part of an AMS. Not all AMS vendors market smoke sensors for use with their systems. However, all vendors market AMS interface units, or similar devices, that allow sensors from other vendors to be integrated into and used by their AMS system. At least one AMS vendor is currently developing its own in-house smoke sensor that will compete with only two other smoke sensors available here in the U.S. from AMS vendors. Other sensor types, such as metal oxide semiconductors (MOS), also have potential for use as fire detectors as a component of an AMS.

3. Potential for expansion of AMS for mine-wide monitoring

The use of AMS for early warning fire detection has significant potential to enhance the safety and well-being of underground miners. When fires occur in underground mines, significant levels of toxic gases and smoke can enter the mine ventilation airflow and can be carried throughout the mine ventilation network, thus increasing the hazard potential for personnel far-removed from the actual fire. Different stages of the fire development generate different gas and smoke toxicity hazards, and although fires that develop to the point of rapid flame spread pose imminent hazards, even fires in their smoldering, pre-flaming stages can contaminate the mine atmosphere with debilitating levels of smoke and toxic gases. In addition, fires are known to increase the resistance of a mine entry producing a reduced, or "throttled," ventilation airflow that results in increased contaminant concentrations and affects the rate of contamination of other mine entries downstream of the fire.

Using an AMS, large numbers of sensors can be deployed within the underground workings to provide

extensive coverage of critical areas where the potential for fire is of concern. These areas would be continuously monitored and readings/alerts/alarms displayed at a central control station in a secure above-ground location that is staffed around the clock. Identified problems can then be communicated quickly to underground personnel in order to implement appropriate reactions to a developing situation. The basic AMS requirements for underground mines are defined by 30 CFR 75.351. AMS sensors and systems are readily available, and these various sensors/systems represent the most efficient means for early and reliable detection of a variety of underground fires typically occurring throughout the mining industry. Given the installation of an AMS, the extension to a mine-wide monitoring system for other locations is relatively straightforward. Enhancements to these systems could be made as well, such as the use of alternative techniques for sensor/system interface and the interfacing of the AMS with mine ventilation simulators to provide for a more dynamic and interactive system.

4. Proposed AMS Fire Detection Locations

It is proposed that automatic fire sensors be installed as a major component of a mine-wide AMS at any and all underground locations or installations where potential significant hazards for fire exist. 30 CFR Part 75 identifies some of these locations and mandates either automatic fire detection and/or automatic fire suppression for protection and for early warning of developing fires. Other underground locations exist that are not specified in 30 CFR Part 75 where the combustible material loading is sufficient to warrant the continuous monitoring for fire.

In addition, because the types of fires that are likely to occur can vary dramatically from one location to the next, along with the characteristic times for fire development and spread, different types of fire sensors may also be required at these various locations and installations in order to provide adequate fire protection and detection capabilities. In some cases, there may also exist alternative sensors that can be expected to perform as well as or better than the sensor types mandated in 30 CFR Part 75. Guidance for installation of both mandated and optional fire sensor locations, including the types of sensors, are discussed below.

4.1 Conveyor belt entries when the ventilation airflow in the entry is used to ventilate a working section

Regulation: 30 CFR Part 75.351 defines requirements for the use of an AMS in conveyor belt entries when the ventilation airflow within such an entry is used to ventilate a working section. The use of CO and smoke sensors as the primary sensors for early warning fire detection is specified within Part 75.351, including alert/alarm levels and spacing of sensors as a function of the ventilation air velocity. Litton (1991) and Litton (2012) contain comprehensive alarm and spacing guidelines as a function of entry cross-sectional area and airflow. Briefly, CO or smoke fire sensors are to be located at distances no greater than 100 feet within the entry immediately downstream of a conveyor belt drive and/or belt take-up, transfer point, or tailpiece and, for CO sensors, at subsequent intervals not to exceed 1000 feet along the remainder of the conveyor belt entry shown in figure 1. Both CO and smoke sensors are to be

located as near the midpoint of the entry as is practical and at a distance from the entry roof not to exceed one-third the entry height. These specifications for the use and deployment of these sensors as part of an AMS are reasonable and adequate with the exception of the maximum allowable spacing of 3000 feet for smoke sensors.

Best practice: NIOSH research has shown that an allowable spacing of 1000 feet for smoke sensors would provide a much greater margin of safety because of the reduced contaminant travel times at low to moderate ventilation air velocities [2, 3].

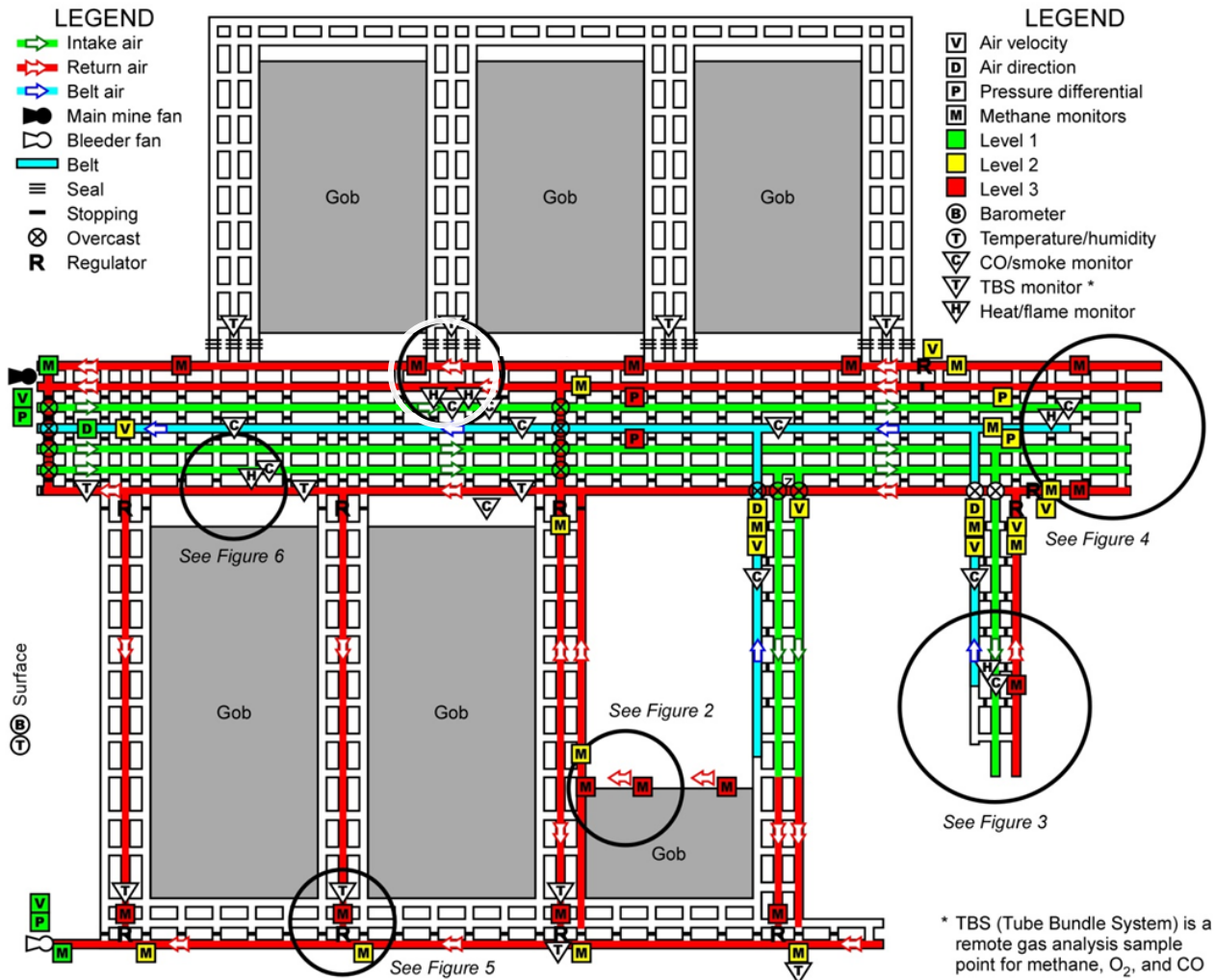


Fig 1. Schematic of typical underground coal mine showing proposed new AMS fire monitoring locations.

4.2 Conveyor belt entries regardless of the use of ventilation airflow

Regulation: 30 CFR Part 75.1103-4 defines requirements for automatic fire detection within any conveyor belt entry using CO sensors or sensors responding to radiation, smoke, gases, or other indications of fire, as long as such sensors provide protection equivalent to carbon monoxide sensors. 30 CFR Part 75.1103-5 specifies CO sensor alarm levels and locations where alarms shall be given, including a manned surface location, and additional requirements for minimum sensor/system operating time in the event of loss of electrical power.

Best practice: Because neither the two Parts discussed above, nor any other parts within 30 CFR 75.1100, contain any requirement for these sensors to be part of an AMS, it is suggested that the system of CO or

smoke sensors for fire protection in conveyor belt entries be connected to an AMS as part of the mine-wide system for fire detection.

4.3. Unattended underground equipment

Regulation: 30 CFR Part 75.1107-4 defines requirements for automatic fire detection using point-type heat sensors for unattended underground equipment, such as compressors, high-voltage power centers, transformer stations, etc. This part also requires the use of these sensors to actuate an automatic fire suppression system.

Best practice: Although these requirements for fire detection specify point-type heat sensors, optical flame sensors would also provide equivalent protection. Further, an additional POC sensor, such as a CO or

smoke sensor, located near the roof in the entry downstream of the equipment at a distance of 150 to 200 feet, would provide improved protection. Both the mandated fire sensor used to activate the fire suppression system and the downstream POC sensor should be

connected to the AMS. This will alert the AMS operator that the system has activated. A load center and sensor locations are shown in figures 2 and 3.

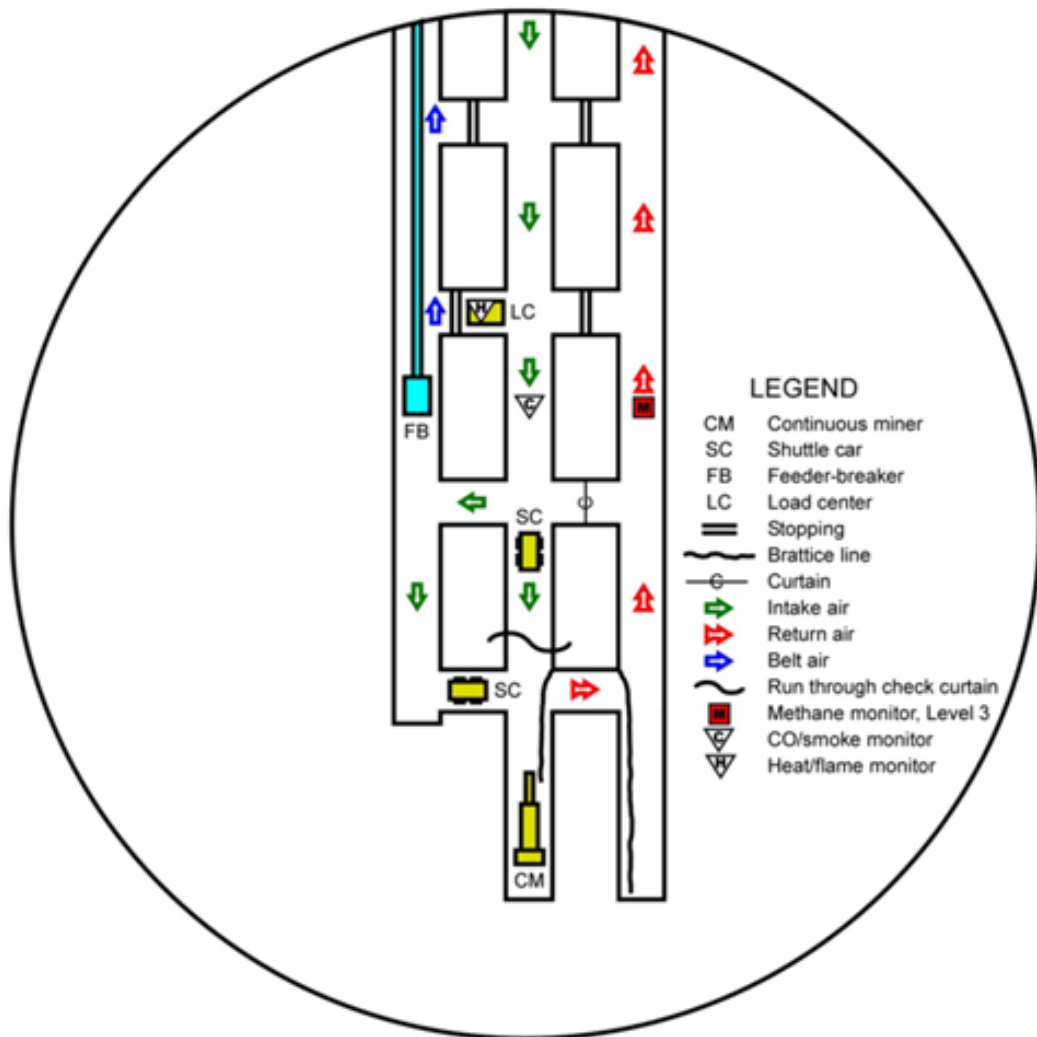


Figure 2. Schematic of gateroad development area showing proposed CO/smoke and heat/flame monitoring locations.

4.4 Permanent underground diesel fuel storage areas:

Regulation: 30 CFR Part 75.1912 sets forth the requirements for automatic fire detection using fire sensors to activate an automatic fire suppression system

for permanent underground fuel storage areas. It is worth noting that these regulations do not specify any particular type of fire sensor, the only requirement being that it must actuate the automatic fire suppression system.

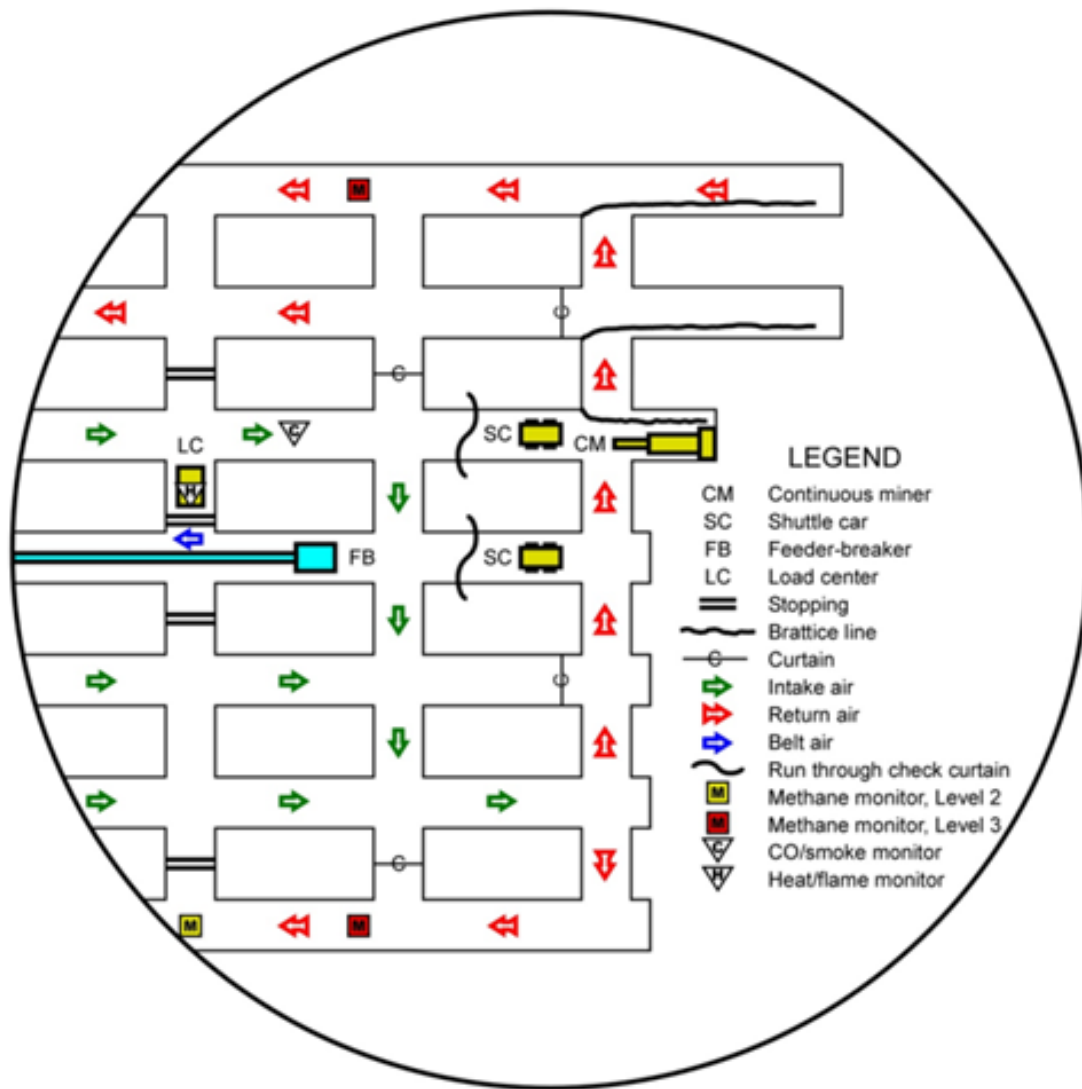


Figure 3. Schematic of room-and-pillar development area showing proposed CO/smoke and heat/flame monitoring locations.

Best practice: Because fires that occur within diesel fuel storage areas can be expected to develop rapidly and produce high levels of heat within seconds to minutes, either heat sensors or optical flame sensors would be the best fire sensors to use. Again, as was the case for unattended underground equipment, it is strongly suggested that a POC sensor (CO or smoke) be located in the entry downstream of the fuel storage area, as shown in figure 4, and that both the primary fire sensor used to activate the automatic fire suppression system and the POC sensor should be connected to the AMS.

4.5 Mobile diesel-powered equipment and fuel transportation units

Regulation: 30 CFR Part 75.1911 defines requirements for automatic fire detection and fire suppression for mobile diesel equipment and fuel transportation units. In this Regulation, automatic fire detection is an option, not a requirement, for use in activating the fire suppression system.

Best practice: Because diesel-powered equipment and fuel transport units are mobile and can move

throughout the mine, connection to a central AMS is not practical, although some form of on-board suppression should be used.

4.6 Battery charging stations

Regulation: No current regulation exists for fire detection for this location.

Best practice: 30 CFR Part 77.1106 requires that the air passing through a battery charging area be diverted into a return, yet no regulations exist for fire detection within these areas. It is proposed that POC sensors (CO or smoke) be installed near the roof at locations both near the exhaust that goes into the return and in the entry just downstream of the battery charging area, shown in figure 5, and that these sensors be connected to an AMS as part of the mine-wide fire detection system.

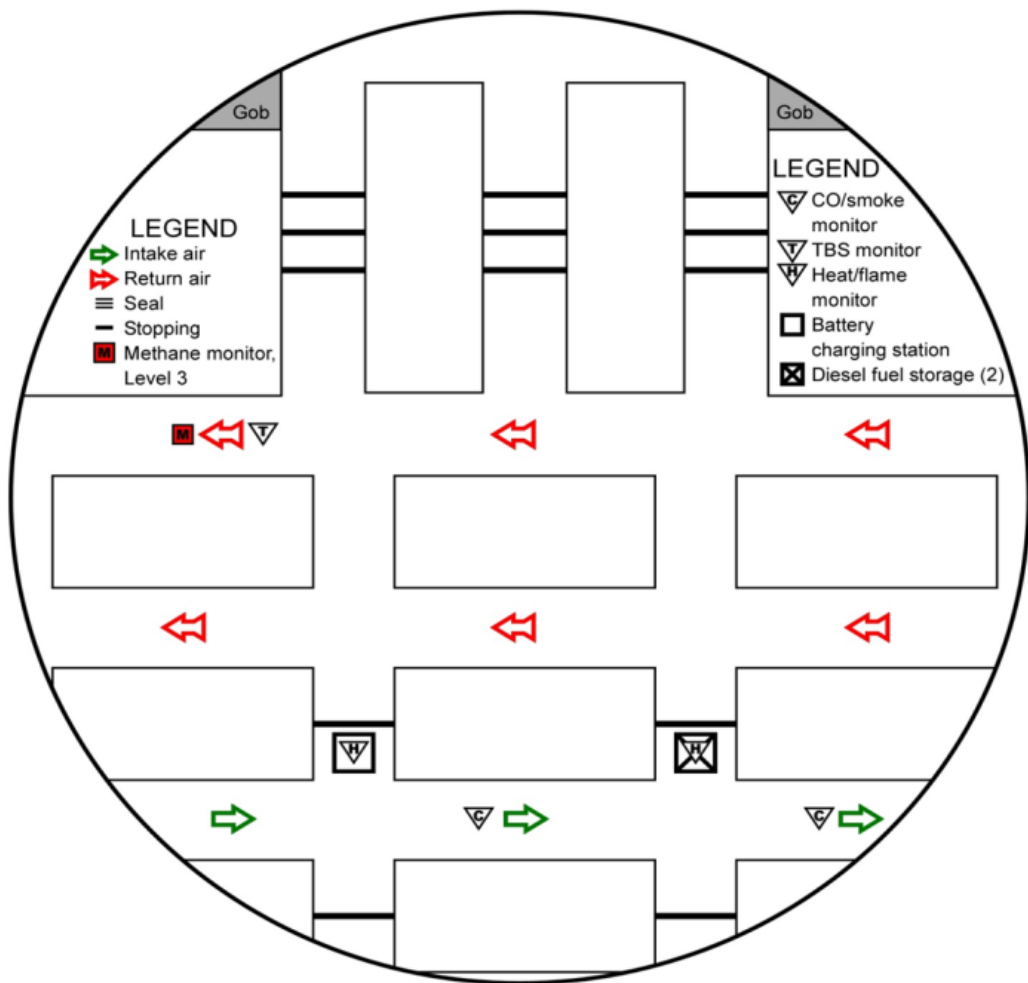


Figure 4. Schematic of intake and returns showing diesel fuel storage area, battery charging station, and permanent seals and associated CO/smoke and heat/flame monitoring locations.

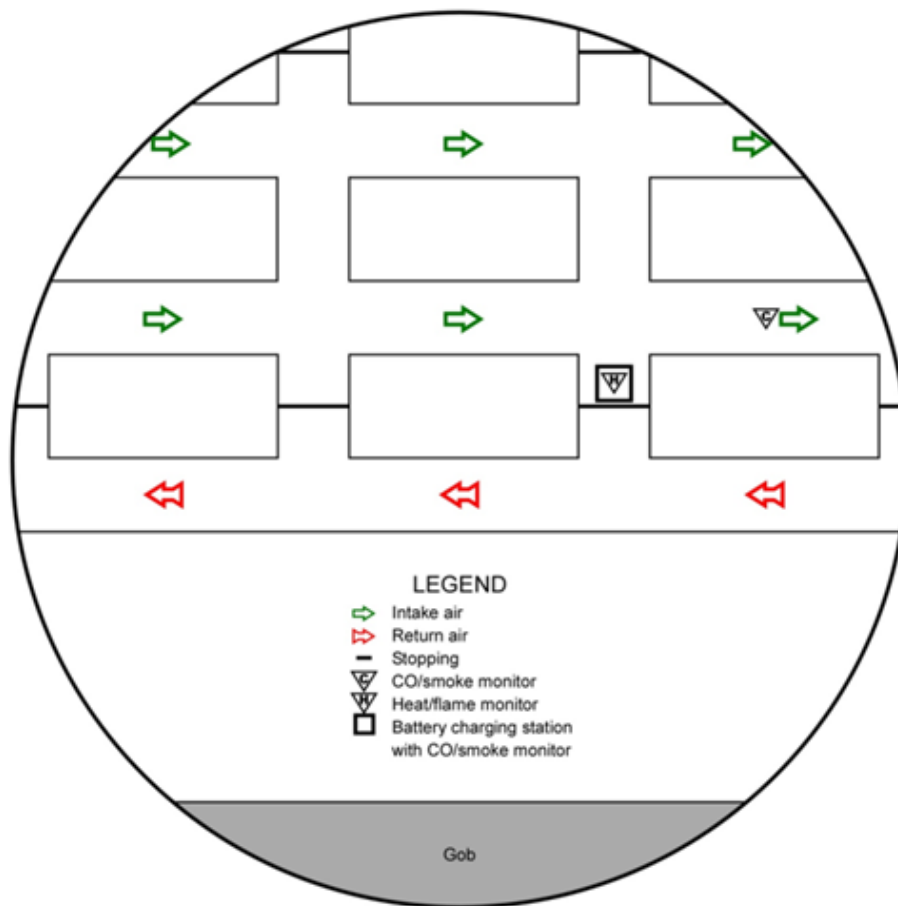


Figure 5. Schematic of location of battery charging station and heat/flame monitor.

4.7 Underground shops or maintenance areas

Regulation: No current regulation exists for fire detection for this location.

Best practice: Because underground shops or maintenance areas may often contain significant quantities of combustibles or involve activities such as flame-cutting or welding, there is a high potential for fires to occur within these areas. It is proposed that either heat or optical flame sensors be installed in these areas to provide for rapid and early detection of any developing fire within these locations and, where warranted, that such sensors also be used to actuate an automatic fire suppression system. It is further proposed that a POC sensor (CO or smoke) also be located in the entry downstream of the shop or maintenance area and that both the primary fire sensor used to activate the automatic fire suppression system and the POC sensor be connected to an AMS as part of the mine-wide fire detection system.

4.8 Trolley and/or track entries

Regulation: No current regulation exists for fire detection for this location.

Best practice: Because there is sufficient energy expended should any electrical short or power surge occur within an entry utilizing electrical track for transportation of either personnel or equipment/supplies, it is suggested that CO or smoke sensors, or sensors that can provide equivalent protection, be installed within

such entries and connected to an AMS as part of a mine-wide fire detection system. CO or smoke sensors would be spaced similarly to those in belt entries at intervals not to exceed 1000 ft.

4.9 Mined-out and caved areas, such as gobs or sealed areas

Regulation: No current regulation exists for fire detection for this location.

Best practice: Because these areas are often prone to either self-heating due to repeated, often cyclic, changes in atmospheric conditions within the gob or sealed area, or to spontaneous heating of the coal that is abundant in such areas, it is proposed that a tube bundle system (TBS) be used to monitor either behind seals (if such areas are bleederless) or within the bleeder airflow returns. TBSs convey air samples from these underground locations via rigid plastic tubing to a central, above-ground location where the air samples can subsequently be analyzed for combustion product gases, such as CO or CO₂, for O₂, and for flammable/explosive gases, such as methane (CH₄), ethane (C₂H₆), or hydrogen (H₂). Furthermore, it is proposed that the TBS be a sub-component of the AMS as part of a mine-wide fire detection system. Gob monitoring locations using a TBS are shown in figures 1 and 6. It should be noted that at the TBS monitoring locations, the tubing should extend behind the seals into the gob or sealed area from which the gas sample is drawn.

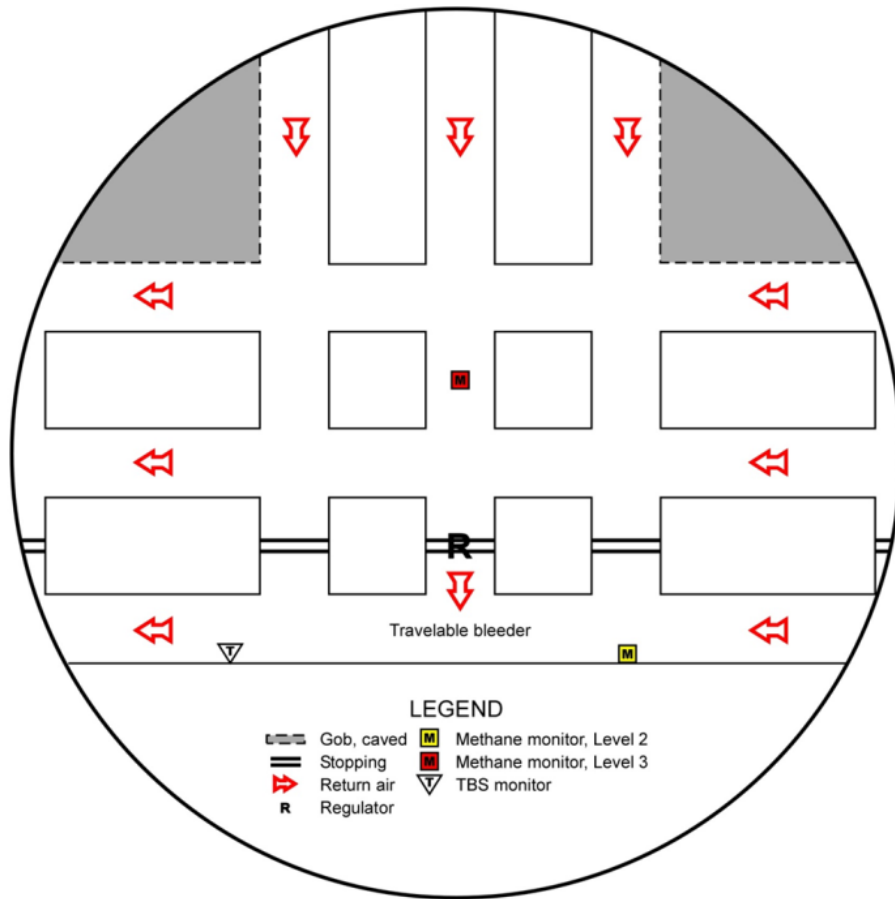


Figure 6. Schematic of bleeder area airstreams showing proposed tube bundle monitor locations.

Table 1 summarizes the locations and the mandated, alternative, or suggested sensors for each location, along

with any relevant location specifics for siting of the sensors.

Table 1. Summary of fire detection locations, regulations, and sensors for AMS.

Location	Applicable Regulation	Mandatory Sensor	Alternative Sensor	Location Specifics
Conveyor belt entries when the ventilation airflow in the entry is used to ventilate a working section	30 CFR Part 75.351	CO	Smoke	Located at distances no greater than 100 feet downstream of a conveyor belt drive and/or belt take-up, transfer point, or tailpiece; at subsequent intervals not to exceed 1000 feet
Conveyor belt entries regardless of the use of ventilation airflow	30 CFR Part 75.1107-4 and 30 CFR Part 5.1103-5	CO	Sensors responding to radiation, smoke, gases, or other indications of fire as long as such sensors provide protection equivalent to CO sensors	Located at distances no greater than 100 feet downstream of a conveyor belt drive and/or belt take-up, transfer point, or tailpiece; at subsequent intervals not to exceed 1000 feet
Unattended underground equipment	30 CFR Part 75.1107-4	Heat	Optical flame sensor and CO or smoke sensor	CO or smoke sensor near the roof in the entry downstream of the equipment at a distance of 150 to 200 feet
Permanent underground diesel fuel storage areas	30 CFR Part 75.1912	None	Heat or optical flame sensor for primary and CO or smoke sensor as backup	CO or smoke sensor near the roof in the entry downstream of the equipment at a distance of 150 to 200 feet
Mobile diesel-powered equipment and fuel transportation units	30 CFR Part 75.1911	None	On-board heat or flame sensor	Some method to keep track of location for AMS
Battery charging stations	None	None	CO or smoke sensor	Near the roof at locations both near the exhaust that goes into the return and in the entry just downstream of the battery charging area
Underground shops or maintenance areas	None	None	Heat or optical flame sensor for primary and CO or smoke sensor as backup	CO or smoke sensor near the roof in the entry downstream of the area at a distance of 150 to 200 feet
Trolley and/or track entries	None	None	CO or smoke sensors	Spaced along such entries at intervals not to exceed 1000 feet
Mined-out, caved areas, such as gobs or sealed areas	None	None	Tube bundle system	Analysis at central, above-ground location for CO, CO ₂ , O ₂ , and CH ₄ .

5. Areas for future research

Because the operational principle of CO sensors requires fine-tuning of the operating voltages of the measurement electrode in an attempt to be specific to CO, such fine-tuning is not often as good as is needed. As a result, these sensors may be subject to cross-interferences from other gases that can either appear as negative or positive influences on the true CO concentration. Attempts to eliminate much of this interference are usually in the form of charcoal filters that can remove some, but not all, of the interfering gases. One such interfering gas is H₂ that is produced at underground battery charging stations, where exposure to 30 ppm of H₂ will produce a CO sensor reading of 12 ppm; or NO produced from the

exhaust of diesel engines, where exposure to 10 ppm of NO may produce a CO sensor reading of 3 ppm. In spite of some of these drawbacks and limitations, these CO sensors are proving to be reliable and robust in underground environments when subjected to the recommended maintenance and calibration intervals.

Within the next 2–5 years, it is expected that the use of CO and smoke sensors will increase as the primary method of fire detection in underground mines. Additional sensors may also become available, such as metal oxide semiconductor (MOS) sensors, which have potential for fire detection. Within this time period, the integration of AMS with ventilation software, such as NIOSH’s MFIRE code, is underway to develop real-

time, dynamic, and interactive systems that can be used to deal with mine emergencies. Improved strategies and/or sensors to deal with interfering gases such as H₂ and NO, as well as diesel particulate matter (DPM), need to be developed and implemented as part of the AMS software.

If fire detection using AMS is to find widespread use and acceptance by the mining industry, these systems must be shown to be accurate and reliable in their depiction of the underground environment and the events that occur. Currently, there are no MSHA standards of performance for approval of these systems and the sensors that they use. The sensors, in particular, are evaluated by MSHA for their intrinsic safety or mine permissibility based solely upon their electrical/electronic characteristics. MSHA relies upon information supplied by the vendors that the sensors/systems will perform adequately and reliably. Some of these sensors/systems may have been evaluated using performance standards for other applications, or they may have been subjected to tests that were devised and conducted by the manufacturer to provide some assurance that they will function as intended. The result is a virtual smorgasbord of tests and test results with little or no uniformity from one vendor to the next. As these systems find increased usage in the Nation's mines, it is imperative that some uniform path of approval be defined for components used by these AMS units based upon a consistent set of performance standards. The various performance standards developed by Underwriters Laboratories (UL) for both residential and industrial smoke sensors, the signaling systems used with these sensors, and the National Fire Protection Association (NFPA) standards, are excellent models to use for such metrics. Alternatively, UL and NFPA models can be adopted as minimum criteria that sensors and systems must satisfy for subsequent MSHA approval.

6. Conclusions

The use of AMS for early warning fire detection has significant potential to enhance the safety and well-being of underground miners. A large number of sensors can be deployed within the underground workings to provide extensive coverage of critical areas where the potential for fire is of concern by expanding on any of the above existing systems for monitoring. In summary, it is proposed that additional fire sensors be deployed and integrated into the AMS at the following locations:

- conveyor belt entries regardless of the use of ventilation airflow
- unattended underground equipment
- permanent underground diesel fuel storage areas
- mobile diesel-powered equipment and fuel transportation units
- battery charging stations
- underground shops or maintenance areas
- trolley and/or track entries
- mined-out, caved areas, such as gobs or sealed areas

References

- [1] U.S. Code of Federal Regulations, 30 CFR 75.
- [2] M. DeRosa, Analysis of mine fires for all U.S. underground and surface coal mining categories, 1990-1999. NIOSH Information Circular 9470, (2004), 36 pp.
- [3] C.D. Litton, C.P. Lazzara, and F.J. Perzak, Fire detection for conveyer belt entries. Report of Investigations, US Bureau of Mines, No. 9380, (1991), 23 pp.
- [4] C.D. Litton and I.E. Perera, Evaluation of criteria for the detection of fires in underground conveyor belt haulageways, Fire Safety Journal, v. 5, pp. (2012), 110-119.

An Investigation of Mine Gas Stability in Sampling Containers Over Time Using Gas Chromatography Analysis

Heather Dougherty^a, Timothy Scott Jeter^a, Kray Luxbacher^a, Ali Haghghat^a, Kyle Brashear^b, Edmund Jong^a, Harold McNair^a

^a Virginia Tech, Blacksburg, VA

^b Martin Marietta, Raleigh, NC

Gas chromatography (GC) is the most widely used analytical technique for the qualitative and quantitative characterization of volatile compounds. This usage is derived from GC's ability to accurately quantify analytes down to sub parts per trillion (PPT) level concentrations. Various sampling methods are available to collect mine air samples for processing using GC. In this study, four different types of sample containers regularly used in the mining industry were investigated. These containers were multi-layered Teflon coated Mylar gas sampling bags, glass vacutainers, plastic vacutainers, and plastic syringes. Each container was filled with a known standard mixture of gases commonly found in subsurface mine atmospheres, such as methane (CH₄), oxygen (O₂), and carbon monoxide (CO). The performance of each container type is presented and accompanied by a detailed explanation of the experimental methodology.

Keywords: Mine Gas, Gas Chromatography, Mine Gas Sampling, Ventilation

1. Introduction

The accurate sampling of underground mine air is essential in determining the levels of gases in standard operating and emergency situations. Detailed sampling and analysis of mine air is typically performed in outby areas, behind underground mine seals, or in emergency situations. GC analysis is used to perform these detailed analyses.

Various sampling containers have been used in the mining atmosphere but none have been created specifically for this application. An analysis of six variations of the four containers commonly used, were tested over a period of two months to determine the reaction of mine gases in the containers over time.

A variety of containers that are commonly used in collecting mine atmosphere for GC analysis, including new and reused gas collection bags, glass and plastic evacuated vacutainers, and plastic syringes. Xu [1] discussed gas sampling bags, hypodermic syringes, and vacutainers for use with tracer gasses in underground applications. His review of gas sampling bags recommended being cognizant of their constituent materials, additional supply requirements, and sample containment stability constraints. He concluded that plastic syringes were easy to use and durable. However, plastic syringes have proven to be subject to significant losses of gasses over a short time frame. Vacutainers,

which are convenient to use and yield consistent results [2] have a longer sample storage life, but Freedman et al. warn that a maximum of two months should not be exceeded for sample storage and recommend analysis of the samples within one week.

There is a dearth of literature on the use of containers for the collection of underground mine atmosphere. Much of the recent literature is focused on tracer gas use for ventilation network characterization [3] rather than sampling and analysis of mine gases. Accuracy and shelf life are not addressed in literature, but they are addressed in some manufacturer literature for gas sampling container guidelines.

2. Experimental Design

For this study, four common types of mine atmosphere collecting containers were chosen: tedlar bags, glass vacutainers, plastic vacutainers and plastic syringes. A calibration gas containing common mine gases in concentrations as seen in Table 2 was chosen to use as the testing gas for all the containers. Seven of each container were filled at the onset of the experiment to have samples for each time segment in Table 1. Each container was randomly filled and sampled to minimize bias for analysis. This was done once for the initial experiment and a second time for the replication.

Of the four container types, it was determined that six specific variations of these containers would be tested over a time frame of two months. The data would be analyzed to determine the effect from leakage and other effects on the gas from the container over time. Table 1 lists the time frame and containers chosen for this initial study. All samples were run in duplicate from a new container for each analysis, for a total of 84 samples.

Table 1: Study time frame and container listing

Time	Container
0 hour	New 1L Foil bag #1
1 day	New 1L Foil bag #2
2 days	Used 1L Foil bag #1
1 week	10ml Glass Vacutainer
2 weeks	6ml Plastic Vacutainer
1 month	60ml Plastic Syringe
2 months	

2.1 Gas chromatography (GC)

Gas chromatography is a common method utilized for the separation and analysis of volatile compounds. In this experiment, a Mine Gas Analyzer equipped with a flame ionization detector (FID) and a thermal conductivity detector (TCD) was used. The Mine Gas Analyzer was specifically designed to analyze hydrogen, oxygen, nitrogen, methane, ethane, ethylene, acetylene, carbon monoxide, and carbon dioxide. The Mine Gas Analyzer is equipped with a 1 mL sample loop that requires at least 3 mL of sample to be introduced for accurate processing. The volume required per sample restricted the number of analyses that could be made from the smaller containers. A triplicate of each sample was run to ensure adequate precision was achieved.

2.2 Sampling Gas

The gas that was chosen for use in this study was a calibration gas mixture. The canister contained approximately 100ppm of each gas, as listed in Table 2. The balance of this mixture was Argon, which is the carrier gas used in this GC. The gases directly measured in this study are bolded in Table 2, and include, acetylene, carbon monoxide, ethane, ethylene, hydrogen, methane, and oxygen.

Table 2: Study gas concentration

Gas	Concentration (ppm)
Acetylene (C₂H₂)	100
Carbon Dioxide (CO ₂)	399
Carbon Monoxide (CO)	100
Ethane (C₂H₆)	101
Ethylene (C₂H₄)	100
Hydrogen (H)	101
Methane (CH₄)	100
Nitrogen (N ₂)	16869
Oxygen (O₂)	2509
Argon (Ar)	Balance

2.3 Gas Sampling Containers

Since the majority of underground mines do not have the ability to analyze gas samples on-site, gas samples must be sent to GC laboratories. Sampling containers are used to collect samples of the underground mine atmosphere and transport them to the laboratory. This sampling and analysis process is generally accomplished in under one week.

Some gas sampling containers recommend a maximum hold time of 48 hours. Although this is probably a conservative estimate, it is important to understand the implications of time and storage on the mine gas sample. In various situations, such as during emergencies, samples may require more time for analysis. It may also be beneficial to understand the life of a mine gas sample in a container. A time frame of two months was chosen due to recommendations by Freedman et al. for a maximum of two months for sample analysis [2].

Four different types of commonly used underground gas collection containers were used in this study. Two different manufactures were utilized for new multi-layer foil 1 liter (L) capacity bags and also obtained some used 1L capacity bags. The foil bags from two different manufacturers had different valves, one made of plastic, the other metal (Figure 1). These bags are manufactured specifically for the collection of gases. Used bags were also analyzed because it is common mining practice to reuse these bags in mine sampling. Both the glass and plastic vacutainers are used primarily for biological purposes like blood collection. Vacutainers are manufactured with an approximate 70% partial vacuum applied, which is unsuitable for mine gas sampling purposes. The vacutainers were further evacuated to approximately 98% to allow for a complete gas sample to be collected [3]. The last tested container used was the 60 mL disposable plastic (polypropylene) syringe that is

multipurpose and is mainly used for laboratory applications.

Foil bags, as seen in Figure 1, are specifically made for gas sampling applications. To fill these bags to the maximum of 80% full as recommended by the manufacturer, a pump must be used. It is also suggested that the bag be filled with atmosphere and purged at least once to collect a representative sample of atmosphere. Both bag manufactures recommend sampling for analysis within 48 hours and a single use for the bags to avoid potential sample adsorption onto the bag film, although it is common practice in mines that bags are re-used.

Foil bags in this test ranged in cost from \$9.00 to \$20.00 each. They can easily be rolled up and carried into the mine to obtain an air sample but can be cumbersome once filled. Filled bags must be handled carefully to prevent contamination caused by damage to the bag. Inspection of each bag for damage prior to use is imperative to ensure contamination-free sampling. These sample bags are convenient because of their size, 1L, which allows for multiple samples to be run from one vessel from one sampling area.

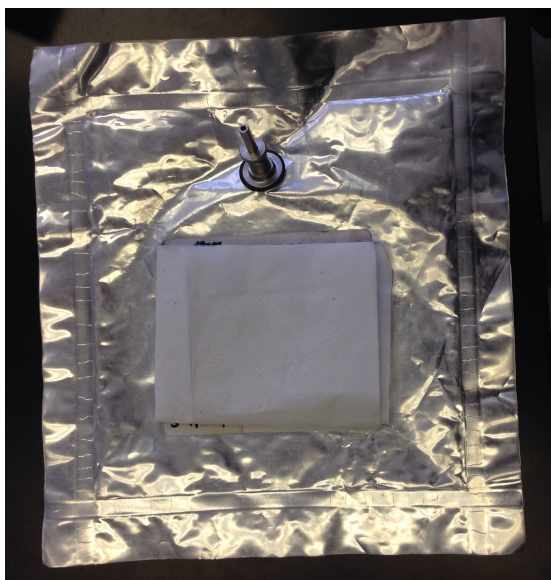


Figure 1: Tedlar gas sampling bag

Vacutainers are repurposed for mine atmosphere sampling and are popular for both mine atmospheres and underground tracer gas sampling [4]. Glass vacutainers are approximately 10ml, and plastic vacutainers are approximately 6ml capacity as shown in Figure 2. Due to the fact that they cannot be entirely evacuated, there is higher dilution when using these containers. Vacutainer use includes an extra step, they must be evacuated to an appropriate level within a reasonable time frame prior to

sampling. The vacutainers may be stored up to a week to be sure that the containers maintain their evacuation pressure, but time frames up to one month have been observed with minimal vacuum loss. Vacutainers are small and rigid and easy to carry in and out of the mine. Due to their size of approximately 10ml, a minimum of three samples must be taken at each air sampling location. Three samples of approximately 3ml is standard procedure for precision when using a GC. A needle is used to puncture the septum of the vacutainer to obtain a sample. This needle should be changed out at regular intervals so that it does not become obstructed which can invalidate a sample. Vacutainer prices are the least of all of the sample containers, ranging from \$0.08 to \$0.41 each for bulk orders.

It is crucial to properly use vacutainers for atmospheric sampling. It is essential to use an evacuated container, and a sharp needle to pierce the septum. If the septum is removed when taking a sample, the integrity of the seal to keep the sample within the container is compromised.

The plastic syringe is also a repurposed laboratory tool used for mine atmosphere sampling and is shown in Figure 2. Plastic syringes used in this study hold a maximum of 60ml when entirely filled and are easily and quickly purged and fill with atmosphere. No needle is used and a rubber septum is ordered separately to seal the end of the syringe and is used to draw a sample through from the syringe for analysis. The plastic material is rigid and easy to carry in and out of the mine when taking samples. The capacity of 60ml is large enough that only one sample needs to be taken at each sampling location. Although reuse of the syringe is not recommended, it is common practice. The cost of both the syringe and septum is approximately \$2.30.

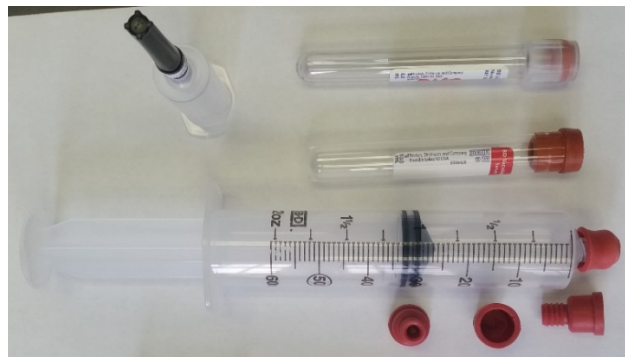


Figure 2: Example of (from top to bottom) a 9.5ml plastic vacutainer, needle in sheath used to pierce septum for sample collection, 13ml glass vacutainer, and plastic syringe. Removed rubber septum are shown below containers.

3. Experimental data and analysis

During the initial data collection period a few problems were encountered that are common when collecting and sampling gas. First, it was determined that both new and used foil bags, even when handled with the utmost care lost sample within a week, to the degree that it was not acceptable to use them as a valid sample. It was speculated that used bags would have a greater likelihood of damage and lost sample due to their prior use. However, similar sample loss was seen in new gas sampling bags. During initial analysis a great difference was not observed in the gas data between the new and used bags, so the use of the used sample bags was discontinued in the replication of the test. The used gas sample bag test data will not be used in this analysis. Additional delays caused by equipment were encountered.

The data were prepared and tabulated by factors including gas, container, and time. The determining variable was the concentration (in ppm) of the gas, or the change in the concentration of the gas over the allotted time frame. The average of the two observed values for each gas, time, and container were graphed as seen in Figure 3, Figure 4, and Figure 5. Oxygen was graphed separately due to its difference in concentration.

It can be observed in Figure 3 that the hydrocarbons, acetylene, ethane, and ethylene all display similar trends in the containers over time. Observation of Figure 3 and **Error! Reference source not found.** indicates:

- The glass vacutainer shows the least amount of change over the time period
- Other than carbon monoxide, all the gases tend to lose concentration over time

- Although both gas sampling bags were initially considered similar, they were not, and one lost gas at a considerably faster rate
- The plastic syringe shows little change over the time period
- If hydrogen is an important species in the analysis, a short time frame for testing is imperative, and the glass vacutainer is the best container to minimize gas variation

Figure 3 and Figure 4 display gases that decrease over time, Figure 5 shows the increase of oxygen over time. Gas sampling bag #1 shows an increase in concentration of all gases but oxygen between the one and two month sampling times. When averaging the two values for the experiment and repeat it was found that one value was similar to the one month value, but the second was significant enough to increase the average of the two. This change of approximately 10ppm was determined to be a variance in sampling and analysis technique. Figure 5 shows that oxygen was the largest contaminant in the experiment. The scale of concentration was much larger than all of the other study gases and would have complicated the interpretation of the data graphically.

Figure 5 identifies that the initial concentration and contamination of oxygen in the container was much less when using a gas sample bag or plastic syringe. This is most likely due to the fact that those containers can be totally empty when filled with sample. Unlike sample bags vacutainers cannot be completely evacuated because of equipment constraints. The increased concentration of oxygen in the vacutainers is due to the containers themselves being not fully evacuated at the time they are filled.

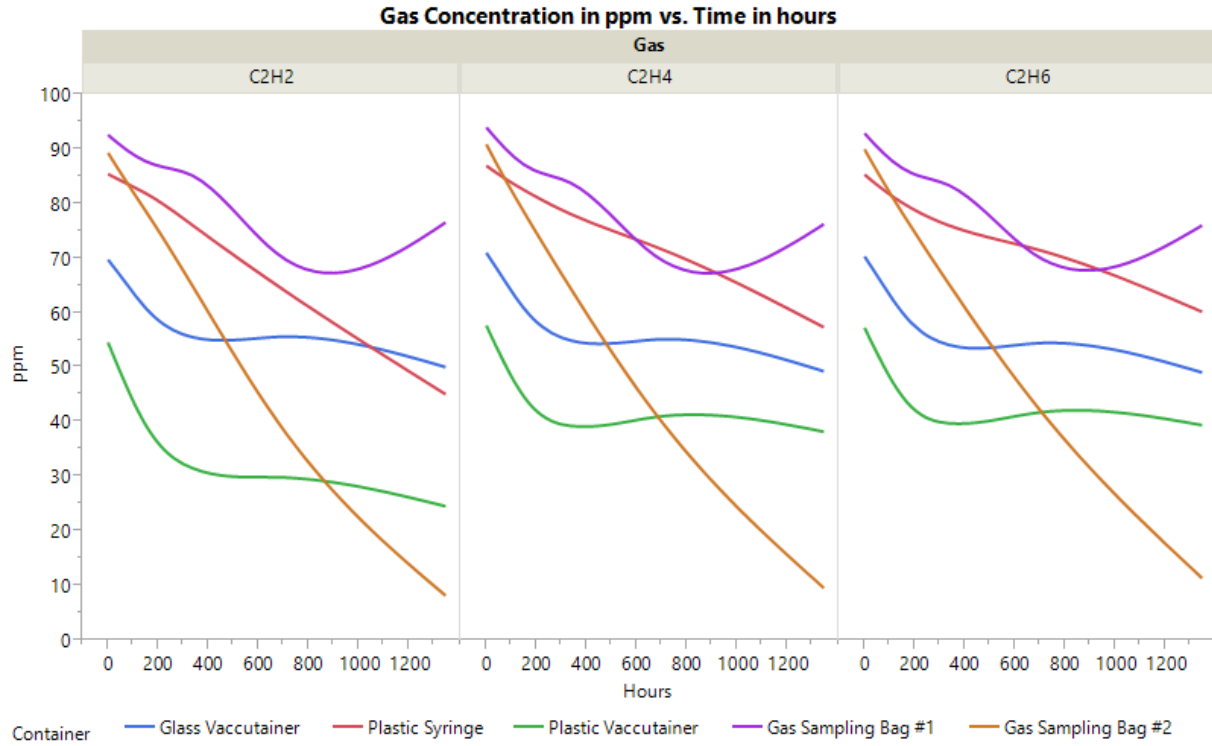


Figure 3: Gas concentration in ppm vs time in hours for acetylene, ethane, and ethylene

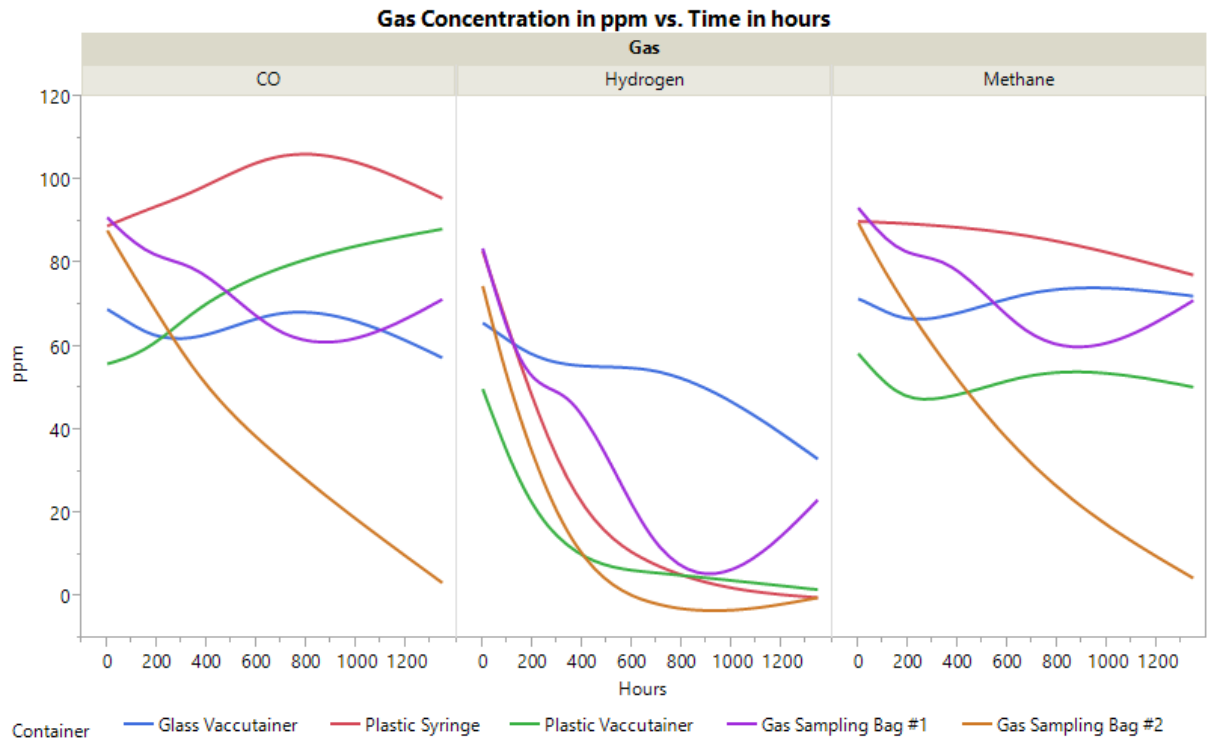


Figure 4: Gas concentration in ppm vs time in hours for CO, Hydrogen, and Methane

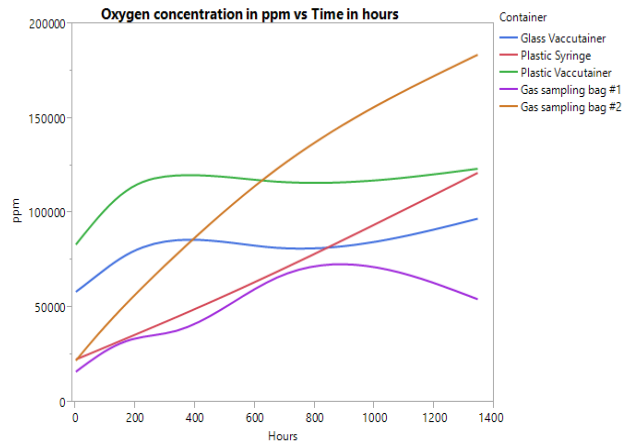


Figure 5: Oxygen concentration in ppm over time for all studied containers

4. Discussion

Each container has its advantages and disadvantages for use in an underground application. Either the plastic or glass vacutainer are small, cheap, easy to carry, rigid and are easily and quickly filled. The disadvantages of the vacutainers are that they require a minimum of triplicate sampling, a needle is needed for sample collection, and they require a re-evacuation with a vacuum pump prior to use. Glass containers can pose a safety hazard if broken during travel and sampling, but the plastic containers are a viable alternative. Another disadvantage of this container is that running three separate samples from three separate containers decreases the repeatability of the GC analysis. All vacutainers have a small percentage of air within them prior to sampling, which was very evident with the low concentration of gas we were using for this experiment. This results in dilution and higher concentrations of oxygen as compared with other containers. However, vacutainers appear to have the lowest leakage over time, which is evident in Figure 5.

The gas collection bags are manufactured specifically for gas sampling purposes. They are easy to carry, purge and fill, have a large enough volume to easily re-sample, and in many cases have been successfully reused. The authors would caution that best analytical practice would not include the reuse of sampling containers, including bags. This initial experiment showed large variability in the two gas sampling bags that were used. One of these bags (sampling bag #1) performed well over the time

frame, but the other (sampling bag #2) performed poorly, with difference of greater than 50 ppm over the life of the experiment. It was unforeseen that issues were observed with the integrity of both new and used bags, there was an apparent loss of sample.

Plastic syringes are simple, easy to use and are common for gas sampling purposes in mines. As repurposed containers, they are not made for gas-tight air sampling purposes. They were found to be easy to fill, purge, and carry around the mine for sampling, in addition their cost is very reasonable. They did not perform as accurately as a glass vacutainer, but the plastic syringe had less dilution when compared with the vacutainers, and held the sample well over the testing time period.

Depending on the use of the sample, importance of the different mine gas data, and the equipment available to the operation various containers are suitable. The glass vacutainers consistently had the least change in gas over the studied time frame for all gases, but with the small size, additional steps needed for further evacuation and sample extraction, this may not always be the best fit for every operation. The plastic vacutainers would also have similar advantages and disadvantages, and are safer, if they are accidentally broken. Because the plastic syringe is not designed for gas tight applications, we hypothesized that it would not perform well, but it demonstrated surprisingly good results over the studied time frame and is recommended for atmospheric sampling. If the gases of hydrogen or carbon monoxide are important, it is important that sampling and analysis are accomplished quickly, preferably within 48 hours to preserve integrity of the sample.

Multiple air samples from the same area are needed when sampling containers of less than 30ml are used, in this study this includes both of the vacutainers. Precision or repeatability of the sample when running triplicates of each sample is much lower when pulling the samples from three separate containers. When three separate containers are used, additional error can be introduced during collection and after the sample is collected. The precision is much better when using a single container, like a bag or 60ml syringe. Using a multiple sample technique when air sampling using a GC method, errors can be more easily identified and outliers removed, particularly when small containers are considered.

5. Conclusion

From this initial analysis the most robust container over the entire time frame of all the gases is the glass vacutainer. This does not necessarily indicate that its use is the best for all applications and sampling procedures. The plastic syringe and plastic vacutainer were also very good and viable alternatives for mine atmosphere sampling. Gas sampling bags demonstrated high variability during this testing, which was not anticipated. Although one of the sampling bags did yield consistent result, one should choose a bag and manufacturer with caution and invest some time in testing the bags.

For best results, sampling of mine atmosphere should be carefully planned and considered. Some best practices are:

- Have a well-trained person taking the samples, and it is preferred if it is consistently the same individual(s)
- Clean out and purge containers (the gas sampling bags and syringe only) prior to filling, specifically with sample air if possible
- Take multiple samples in the same place if possible, particularly if it is an important point. This allows for identification of outliers, quantification of sampling error, and further investigation of data that seem unusual.
- The careful handling of the sample container prior to and after the sample is taken is important to container integrity. Containers should not be exposed to rough handling or extreme temperature changes.

Moving forward it has been determined that both the time and choice of container have an impact on the level of gas or rate of change within the container. The next step in experimentation would be to use a sample that more closely resembles a normal mine atmosphere or hazardous mine atmosphere that would be encountered. Another factor that could be studied is the effect, if any, of shipping of these samples for analysis.

References

1. Xu, G., *Remote Characterization of Underground Ventilation Systems using Tracer Gas and CFD*. 2013, Virginia Polytechnic Institute & State University.
2. Freedman, R.W., W.G. Humphrey, and R.L. Craft, *Use of vacutainers for collection of mine atmosphere samples*. Vol. 7999. 1975: US Bureau of Mines.
3. Louk, A.K., *Monitoring for enhanced gas and liquids recovery from a CO₂ 'Huff-and-puff' injection test in a horizontal chattanooga shale well*, in *Mining and Minerals Engineering*. 2015, Virginia Polytechnic Institute and State University.
4. Jong, E.C., *Development and Evaluation of a Permeation Plug Release Vessel (PPRV) for the Release of Perfluoromethylcyclohexane (PMCH) in Underground Mine Tracer Gas Studies*, in *Mining and Minerals Engineering*. 2014, Virginia Polytechnic and State University. p. 192.

Gas Chromatography Techniques in Detecting Toxic Exhaust Gases in Underground Mines

Yasir Helal Alghamdi^a, Argyle Douglas Stewart Gillies^b.

Missouri University of Science and Technology, Missouri, USA

Many gas emissions in mines can threaten human health. Gases can be emitted from mining sources such as geological strata, chemical treatment and exhaust emissions. Exhaust emissions include carbon monoxide, carbon dioxide, nitrogen and sulfur oxides and are considered as some of the most important and hazardous gases. These gases are dangerous in terms of human's health. They can cause toxic materials to be absorbed by the lungs and throat. They also can cause a situation under which an explosion may possibly occur. The Environmental Protection Agency (EPA) and Mine Safety and Health Administration (MSHA) specify maximum levels for various gases such as 50 ppm for carbon monoxide, 5000 ppm for carbon dioxide, 25 ppm for nitrogen monoxide, 5 ppm for nitrogen dioxide, and 5 ppm for sulfur dioxide. During this study, measurements have been taken by using GC (Gas Chromatograph) analyses to determine the amount and the concentration of each of the gases when high concentrations may indicate an emergency in a mine. The GC has been used in underground coal mines for over 30 years. Early models were too slow for high volume sampling and analyses required during a mine emergency. Improved GC models received wide acceptance in many industries and have become commonly used. The main use of a GC is for determining contaminants in air and water. This GC analyzing method can be useful in monitoring and investigating the underground mine atmosphere. Samples of mixed gases are often taken in bags and subsequently the gas is injected into the GC. Samples proceed through several analysis stages ending with the detector measuring the concentration of gases to provide accurate quantitative measurements of the different components of the gas mixture. Modern GCs provide high accuracy with fast analysis, have become popular analytical instruments and are considered as economical and reliable analyzers.

Keywords: Gas Chromatography, Exhaust Gas, Contaminents

1. Introduction

A gas chromatograph (GC) is used to isolate gas mixtures and analyze compounds that can be vaporized and injected into the instrument. The GC is commonly used in laboratories for gas mixture analysis. The GC consists of various components that help to separate, prepare and analyze the gas where the inert carrier gas is pumped continuously through coils that contain gas adsorbents. Small pulses of the gas mixture sample are injected into the line upstream from the GC columns. Initially, the coil materials absorb the selected gases and the continued flow of the carrier gas will cause desorption of each gas at a time and rate based on its particular adsorption characteristics. The result is that the gases leave the adsorbent columns as discrete and separated pulses. The subsequent concentrations can then be measured by using one or more of the detection techniques as described by McPherson, 1993. [1]

The GC technique can be used in detecting various kinds of naturally occurring mine gases. It is also used to detect engine exhaust gases from combustion processes such as carbon dioxide, carbon monoxide, hydrocarbons, and nitrogen oxides. GC laboratory testing can determine gas concentrations accurately. It can make accurate determination of gases found in the underground environment such as hydrogen, nitrogen, ethylene and ethane as described by Brady, 2008. [2]

Samples are often taken and stored in containers from which air has been totally evacuated. A container often used by NIOSH personnel is the 10-to-20 ml air-evacuated glass sampling tube. These are blood collection tubes that have at least 95% of air evacuated [3]. The other method for sampling gas is by using sampling plastic bags. These have been used successfully to collect air samples that contain organic and inorganic gases. This provides a simple,

uncomplicated, and economical means of collecting and transferring gas samples. Also it offers an option of either short-term sampling or alternatively sampling for a full work shift depending on the size of the bag and the pump flow rate [4].

2. GC types

There are four GC types that are commonly used in determining mine gas concentrations based on the type of the detectors that have been incorporated.

2.1 Flame ionization detector-type gas chromatograph (GC - FID)

This type is used for low gas concentrations and is constructed of a small volume chamber into which the gas chromatograph's capillary column is directly plumbed. Usually the small diameter capillary column is fitted directly into the bottom of the detector's jet. The gaseous eluents from the column are mixed with separately delivered H₂ and air and all are burned on the jet's tip. After H₂ and O₂ are introduced to the Flame Ionization Detector (FID), the flame is lit using an electronic ignitor. The charged particles in that combustion process create a current between the detector's electrodes. The gaseous products leave the detector chamber through the detector's exhaust as shown in Fig 1. The detector housing has been heated so that gases produced by combustion do not condense before leaving its exhaust [5]. This type of GC is very sensitive and can detect a large range of concentrations. The FID is a relatively inexpensive instrument and needs low maintenance. FIDs can measure organic materials concentrations at very low substances. The FID flame is oxidizing all the mixture that is passing through. This analytical method destroys the gas sample [3,5].

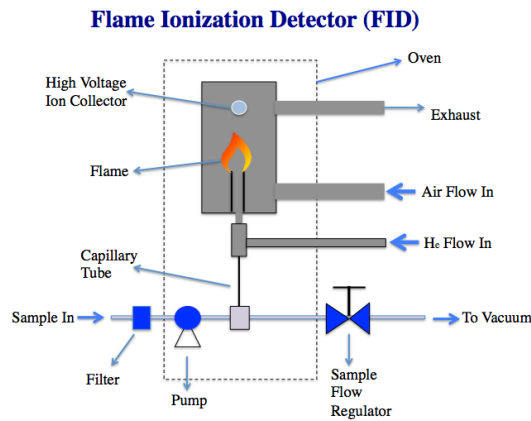


Fig. 1. Illustration of the GC – FID type.

2.2 Thermal conductivity detector-type gas chromatograph (GC – TCD)

The thermal conductivity detector – type gas chromatograph (GC-TCD) is used to analyze inorganic gases and small hydrocarbon molecules. It compares the thermal conductivity of two gas flows – the pure carrier gas and the sample. Changes in the temperature of the electrically heated wires in the detector are affected by the thermal conductivity of the gas which flows around it. The changes in this thermal conductivity are sensed as a change in electrical resistance and then can be measured [6]. The GC – TCD type is used in the presence of high gas concentrations. Unlike the FID, the TCD does not destroy the sample and it is less sensitive.

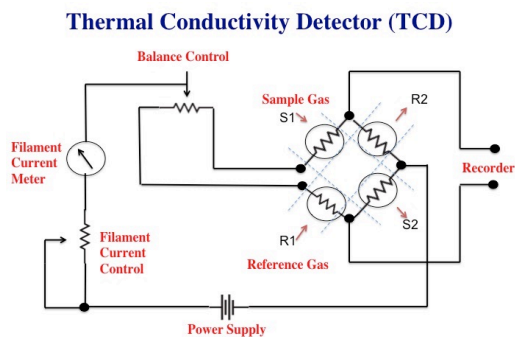


Fig. 2 . Illustration of the GC – TCD type.

2.3 Gas Chromatography – Mass spectrometry (GC – MS)

This type of GC is a combination of gas – liquid chromatography and gas spectrometry that will allow identification of different substances in a test sample. It identifies substances by electrically charging the specimen molecules, accelerating them through a magnetic field, breaking the molecules into charged fragments and detecting the different charges. A spectral plot displays the mass of each fragment. A technician can use a compound's mass spectrum for qualitative identification. The technician uses these fragment masses as puzzle pieces to piece together the mass of the original molecule, the "parent mass [7]. The GC – MS is popular for detecting engine exhaust gases analysis. From a mining perspective it is efficient in detecting gases in case of fire and explosives investigations. In addition it can identify the organic materials. On the

other hand, the GC – MS requires pure samples to be injected in in order to give accurate measurements.

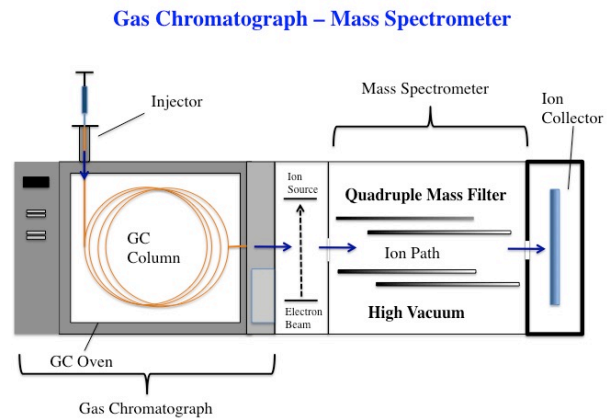


Fig. 3. The GC – MS type components.

2.4 Gas Chromatography Infrared Spectrometry (GC-IR)

The combination of Chromatography and Infrared Spectrometry enables the separation of the mixture and identifies the component. The Infrared spectrophotometer determines the relative strengths and positions of the infrared region and it measures the IR absorption spectrum of the measurement target gas introduced into the gas cell. The measured IR absorption spectrum is used for qualification and quantification. The analysis can be completed rapidly without pretreatment.

3. Previous research

There are many studies that have been done to investigate mine atmospheres by using gas chromatography techniques to analyze the collected gas samples and to identify their type as well as measuring their concentrations.

Within a study done by [9] a gas chromatograph equipped with thermal conductivity detector was used. Two gas chromatographic columns were used where column 1 consisted of a 3 m of Porapak Q, 50-80 mesh, in series with 1.5 m of Porapak R, 100-120 mesh, in 3.2 mm internal diameter teflon tubing. Column 2 consisted of 25 mm of calcium sulphate in series with 3 m of Porapak Q, 50-80 mesh, and 1.5 m of Porapak R, 100-120 meshes, in 3 mm internal diameter Teflon tubing. The detector is maintained at a temperature of 200° C and 200 milliamps detector current. The Porapak is a packing material that delivers separated volatile compounds. It consists of cross linked polystyrene beads. There are different types of Porapak packing materials and for each there are three different kinds based on mesh size and temperature limit. Table 1 illustrates some types of Porapak.

Lamb, Larson and Tollefson have used the Q types as it is very effective with hydrocarbons, organic compounds in water and oxides of nitrogen. R types are useful because they have moderate polarity.

Table 1. Some types of the Porapak packing materials.

Porapak type	Mesh sizea	Temp. Limits
P	50 - 80	250° C
	80 - 100	250° C
	100 - 120	250° C
Q	50 - 80	250° C
	80 - 100	250° C
	100 - 120	250° C
R	50 - 80	250° C
	80 - 100	250° C
	100 - 120	250° C

Column 1 has been immersed in dry ice for about 15 mins after a sample was injected into the column and the column maintained at minus 78° C until the CO was eluted approximately 15 mins after sample injection. The column was then removed and left to adjust to room temperature. Methane and all inorganic components except NH₃, NO₃, and H₂O were obtained from the analysis using this column.

Column 2 was maintained at 160°C for the duration of the analysis of about one hour. The analysis of hydrocarbon components including methane was performed on this column. Ammonia analysis was not possible in this column.

The results showed that column 1 gave an excellent separation of O₂ and CO. The component separations indicate that these separations suggest that column 1 could be used with great facility in the study of NO reduction by H₂ or CO and in the study of the formation of nitrous oxide (N₂O) as an intermediate in the reduction process. Most of components used in column 1 are eluted. In column 2 it is apparent that CO₂ and N₂O have equal retention times.

This study showed that the combination of the column packings Porapak Q and R in a single column could be used for partial gas chromatographic analysis of automobile exhaust gas mixture components including hydrocarbons, oxides of nitrogen (except nitrogen dioxide which is detected in- directly when present in sufficient quantity) and carbon monoxide. [9].

Another study was conducted by Bagley and others, [10]. The researchers undertook this project to ensure a safe atmospheric condition in an underground mine after the use of modern, electronically controlled, low emission diesel engines in a mine. DPM samples were collected in the underground mine and analyzed by using two separate gas chromatography/mass spectrometry (GC-MS) methods. The first method was used to quantify the polycyclic aromatic hydrocarbon. The second GC-MS method was used for the measurement of nitro-polycyclic aromatic hydrocarbon. Researchers have analyzed separate aliquots of DPM-associated soluble organic fractions (SOF) for nitro - polycyclic aromatic hydrocarbon. Aliquots in the range of 5.0 to 6.0 ml of the SOF extracts were spiked with 4-nitro-biphenyl and then concentrated to a final volume of 1.0 ml. 1.0 µl of the concentrated extract was introduced in the GC/MS instrument with the injector and transfer line at 300°C and the GC oven at 65°C. The injector and transfer line are held at constant temperature throughout the sample analysis and the column was ramped to 240° C at a rate of 30°C per minute followed by a ramp to 300°C at a rate of 10°C per minute. After reaching the final temperature the column was held at the final temperature for 20mins as shown by Bagley, and others, 2002. [10]

The usage of GC- MS was vital for this study to obtain the results. However, the researchers concluded that the use of electronically controlled, modern diesel engines with a low sulfur fuel in Cote Balanch Mine (and underground salt mine) resulted in large reductions in DPM and all DPM-related components. The measured potentially health related components showed similar reductions. However, the use of electronically, controlled, modern engines cannot be relied upon to reduce concentrations below 0.15 mg/m³ in all circumstances. A substantial reduction in DPM levels was observed at the downwind sampling location in this study. The traditional metric and the < 0.8 µm respirable fraction were reduced by > 60% and 43%, respectively. The nontraditional metric continuous reading instruments such as diffusion charger, photoelectric aerosol sensor, and condensation particle counter all showed 50% reduction.

Another study was conducted by (Heaton, and Wentworth, 1959) [12] based on the necessity of studying distinct hydrocarbons in vehicle emissions. The organic elements of vehicle exhaust have given rise to the common recognition that these mostly consist of hydrocarbons. A suitable method for defining emission hydrocarbons should qualitatively and quantitatively regulate distinct hydrocarbons. In addition it is important to ensure a sensitivity of above of 10 ppm, without intrusion of non-hydrocarbon constituents. The analysis should not be costly, and should be quick, precise, correct, functional, simple to adjust, and give easily understandable and interpretable results. There is a void in previous approaches regarding the study of emission gas that provides for the necessity of understanding and solving the gas emission problems in mines.

Gas chromatography can give the required separations of gas mixtures but typical current energy sensors are not sensitive enough without the sample being concentrated. The mass spectrometer detectors are relatively expensive and do not have an ease of adjustability or understandings of the resulting data. Furthermore, an improved type of GC, Gas Chromatography Infrared Spectrometry (GC-IR) has been developed that generally meets the aforementioned pre-requisites.

Through the use of the GC – IR the information conveyed for emission hydrocarbons associated with untainted hydrocarbon fuels led to the conclusion that there were considerable quantities of unreacted fuel. The emissions from scented fuels held the most unreacted fuel, while olefin fuels emission held the least. It was found that 45 percent of all hydrocarbons in emissions were unreacted isooctane when utilizing isooctane energy sources. Furthermore, scented fuels travel within the engine with fewer cracked products, which were defined as components no more present in the original fuels than non-scented fuels. These outcomes qualitatively correlate with the given data. With the concentration of olefin in the gasoline there was a transmission of strong variances regarding the olefin concentration in the emission. The investigational indications gave the conclusion that the amount of olefin within the emission grew as the amount of olefin within the fuel was enlarged. Finally, the majority of the analysis and evidence conveys that the emissions hydrocarbon structure is contingent on the fuel structure.

4. Conclusions

The gas chromatograph with its different types and features can be very useful for determining the exhaust gases concentrations that they give accurate readings and measurements that the researchers can rely on. The GCs vary in hardware types and the variety of the detectors that can be built in them, which give a flexibility to choose the appropriate type of GC and detector based on the feature of the sample. However, the GC sometimes requires time to analyze the sample where a real time reading is not given since the samples are taken to the laboratory. Also, some of the gas chromatography might be too expensive and sensitive – a reason why they might not in preference to be used. Nevertheless, the GC is a favored instrument for gas or liquid analysis as it gives accurate concentration readings.

References

- [1] M. J. McPherson, Subsurface Ventilation and Environmental Engineering, Springer Publishing 1993, ch.11, pp 23 – 24.
- [2] D. Brady, “The Role of Gas Monitoring in Prevention and Treatment of Mine Fires”, Coal Operators’ Conference, 2008, University of Wollongong.
- [3] R. J. Timko, and R. L. Derick, “Methods to Determine the Status of Mine Atmosphere – an overview”, 2006 Journal of Mine Ventilation Society of South Africa.
- [4] M. J. Peach, and W.G. Carr, “Air Sampling and Analysis for Gases and Vapors”, Occupational Respiratory Diseases, 1986, CDC
- [5] Y. Posudin, Methods of Measuring Environmental Parameters, Ch 18.3.2, John Wiley & Sons 2014 .
- [6] “Thermal Conductivity Detector- Type Gas Chromatograph” brochure, Air products website, Analytical Laboratory Applications.
- [7] F. Douglas, “GC/MS Analysis”, 1999, Scientific Testimony, an Online Journal, Department of Criminology, Law & Society, University of California, Irvine.
- [8] “Gas Chromatography,MS” LC GC’s CHROMacademy website, by Crawford Scientific.
- [9] A. Lamb, K. A. Larson and E. L. Tollefson, “A Gas Chromatographic Method for Exhaust Gas Analysis”, Journal of the Air Pollution Control Association, March 2012.
- [10] S. T. Bagley, W. F. Watts, J. P. Johnson, D. B. Kittelson, J. H. Johnson, and J. J. Schauer, “Impact of Low-Emission Diesel Engine on Underground Mine Air Quality”, U.S. Office of Research Integrity, National Institute of Health, 2002.
- [11] W. B. Heaton and J. T. Wentworth, “Exhaust Gas Analysis by Chromatograph Combined with Infrared Detection”, Research Laboratories, General Motors Corp., Detroit, Michigan, 1959.
- [12] B. K. Blashich, W. J. Francart, and M. D. Calhoun, “Use of automated micro gas chromatograph to monitor mine atmospheres during mine emergencies”, 12th U.S./North American Mine Ventilation Symposium, 2008 – Wallace
- [13] B. M. Tissue, “FLAME-Ionization Detectors”, 1996, SCIMEDIA.com
- [14] T. Taylor, and J. V. Hinshaw, “GC Troubleshooting Column and Detector Issues”, LC GC’s CHROMacademy website, by Crawford Scientific.

Comparison of Turbulence Models for Estimation of Fugitive Dust Retention in Open-Pit Mines

Taraprasad Bhowmick^a, Sukumar Bandopadhyay^a

^a University of Alaska Fairbanks, Fairbanks, Alaska, USA

The ventilation of an open-pit mine is mostly dependent on natural airflow pattern. The dispersion behavior of the pollutants, generated in a mine, is also dependent on the atmospheric conditions. Therefore, various modeling inputs of CFD simulations are quantified based on the meteorological data collected from weather stations. As the weather conditions vary from season to season, the fugitive dust dispersion simulation for the selected open-pit mine is conducted for various seasonal conditions. In each scenario, fugitive dust particles varying in size (PM_{0.1} to PM₁₀) and concentration are generated at various locations of mine.

In this paper, the behavior of the dust particles and the dispersion or retention phenomena inside the mine is calculated using 'Particle Tracking' function of CFD software SC/Tetra developed by Software Cradle. The simulation results presented the expected variations in dust dispersion for different seasons. However, in simulation of the clear sky conditions, a significant contrast is observed in the simulation results of the various turbulence models. The simulation results of the LES (Large Eddy Simulation) and the standard k-ε RANS (Reynolds-Averaged Navier-Stokes) turbulence model are therefore compared and analyzed to estimate the fugitive dust retention in the selected open-pit mine.

Keywords: CFD, Mine Ventilation, LES, RANS, Fugitive Dust, Particle Tracking.

1. Introduction

The generation and entrainment of pollutants is inherent to many of the unit and auxiliary operations of mining. In surface mining, in general, most of these operations are carried out in open atmosphere and the resulting pollutants are generally released to the atmosphere. Advances in mathematical and computer fields in recent years have enabled better modeling of pollutant dispersion phenomenon around mines using computational fluid dynamics (CFD). Modeling of fugitive dust dispersion in open-pit mines using CFD is a convenient method to approximate the pollutant concentrations within and around the open-pit mines. Flores et al. [1] used OpenFOAM CFD simulation package to simulate and predict the pollutant dispersion in an idealized as well as an actual open-pit mine in Chile with an intense insolation condition. Flores et al. [1] concluded that the buoyant currents modify the purely mechanical-turbulence induced flow pattern and reduce the particle residence time. In a recent paper, Bhowmick et al. [2] presented various constraints in development of 3-Dimensional CFD models to predict the fugitive dust dispersion in open-pit mines. In their research, Bhowmick et al. [3] estimated the fugitive dust retention in two open-pit domains for various weather conditions.

In this paper, the efficacy of the simulation method to predict the fugitive dust dispersion in open-pit mines by Bhowmick et al. [3] is evaluated. Since the flow patterns of fugitive dust particle in an open-pit mine is dependent on the airflow pattern, various turbulence models are investigated to identify the appropriate model that would simulate the dust dispersion phenomena with reasonable accuracy. The simulation of the Atmospheric Boundary Layer (ABL) is an important area for modeling of the dust dispersion in open-pit mines. ABL

is the part of the troposphere that is directly influenced by the presence of the earth's surface and responds to the surface forcing in a time scale of about one hour or less. The turbulent characteristic of the ABL is developed due to the buoyancy generated by sensible heat flux (thermal forcing) and the wind shear generated by surface roughness (mechanical forcing) [4, 5]. The dispersion and the entrainment of the dust particles, generated in an open-pit mine, take place within the ABL and thus, the dispersion or the retention of the dust particles is governed by the state of turbulence of the open-pit ABL [6].

In this paper, the ABL is simulated for the clear sky condition in an open-pit. During the clear sky conditions, overcast cloud cover above the open-pit domain is absent. The amount of radiation, reflected from the cloud cover, is therefore negligible. Clear sky conditions of the ABL are simulated with similar sets of initial and boundary conditions using both the RANS and LES turbulence models. The dispersion models differ in its assumptions, structures and the algorithm of the solving approach; and as a result, the simulation results also vary from model to model. Therefore the fugitive dust dispersion phenomenon in an open-pit mine under various weather conditions is investigated using various dispersion models.

2. Model Domain

Two idealized geometries are used for the simulation purpose. The idealized pits have several advantages over an actual open-pit domain [3]. The Trapezoidal and Conical open-pit domains used for this study are presented in figure 1. The pit cavities approximately contain the same volume similar to an actual open-pit. The ultimate pit slope is 40° for both the geometries. The

numbers of mesh elements are in the order of 1.2 million and 1.3 million for the trapezoidal and the conical domains respectively. A detailed discussion of the complexities of meshing of a large open-pit mine is beyond the scope of this paper and therefore is not presented here, but can be found elsewhere (Bhowmick et al. [2], Raj et al. [7]).

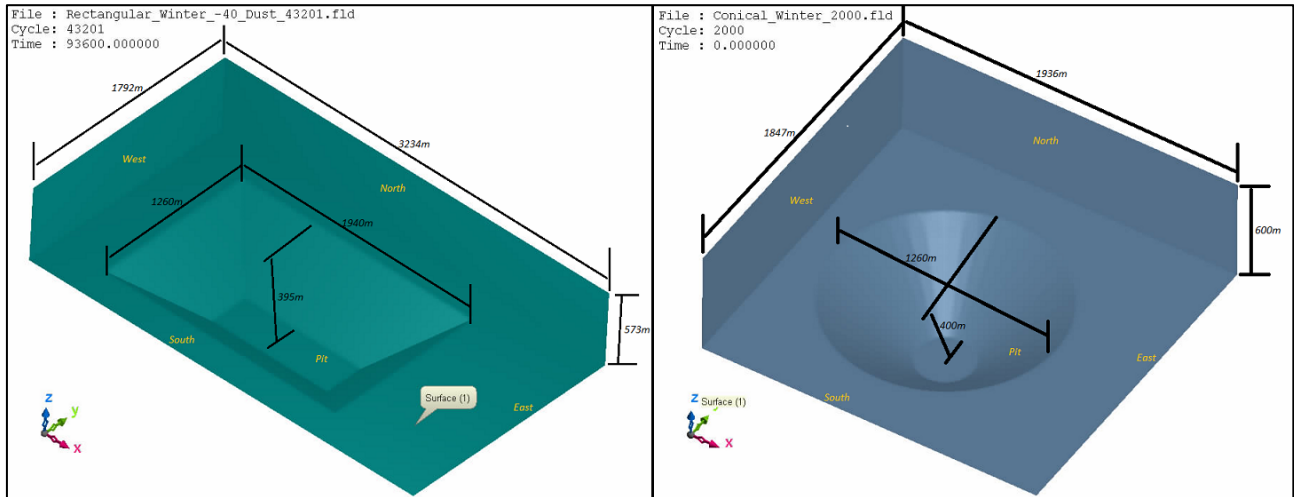


Fig. 1. Idealized trapezoidal (left) and conical (right) open-pit domain.

3. Simulation Setup

Initial conditions, boundary conditions, choices of the turbulence models, the turbulent parameters along with the generation and tracking process of fugitive dust particles are the important criteria for the simulation setup. The simulation setup is defined using the 'Analysis Condition' setup of SC/Tetra Preprocessor [3]. The idealized domains are simulated for the clear sky conditions.

3.1 Boundary Conditions

All the model boundaries are required to be defined to initiate a simulation. An Inlet (East) and an Outlet (West) boundary (Figure 1) along with various Wall boundaries are used for the simulation. Inlet boundary is defined as the velocity boundary with a Power law profile of velocity [3]. The Free Atmosphere (FA) boundary is located at 600m from the surface [3]. Two four-component net radiation sensors, temperature sensor and weather station data are processed for categorizing the boundary conditions based on the various climatic conditions. Table 1 presents the input values for various boundary conditions for simulation of the winter and the summer sessions.

Table 1. Input values for the winter and the summer sessions.

Season	Intensity	Wind Speed	Initial Temp.	Heat Flux (W/m ²)
Winter	Moderate Winter	4.7 mph = 2.1 m/s	-10 C	-20
	Extreme Winter	4.7 mph = 2.1 m/s	-10 C	-40
Summer	Fair Insolation	5.6 mph = 2.5 m/s	10 C	60
	Moderate Insolation	5.6 mph = 2.5 m/s	10 C	100
	Extreme Insolation	5.6 mph = 2.5 m/s	10 C	160

3.1.1 Clear Sky Condition

In simulation of the clear sky conditions, the FA boundary is defined as an adiabatic free surface. The adiabatic property of the FA boundary stops heat transfer through this boundary. The free surface simulates the FA boundary as a virtual surface which has no influence on the airflow pattern nearby the boundary.

3.2 Initial Conditions

A steady state velocity profile is established for both the summer and the winter conditions and is used as an initial velocity condition for the transient simulations. In a transient simulation, the time dependent variables such as the temperature and the heat flux are the input variables [2].

3.3 Turbulence Model

RANS (Reynolds-Averaged Navier-Stokes) using Standard k- ϵ turbulence models and LES (Large Eddy Simulation) using SGS/DSGS/WALE models are used to model the turbulent dispersion of fugitive dust in the selected domains. The turbulent flow in k- ϵ turbulence model is treated through Reynolds averaging. In Reynolds averaging, the transitional and the unsteady physical phenomena are time-averaged and divided into their mean values and fluctuating components. Whereas, Large Eddy Simulation (LES) models the various sizes of turbulence eddies generated by the cascading process of turbulence [8]. The model domains are simulated to capture the ABL and the micrometeorological flow due to the surface roughness induced mechanical turbulence and surface radiation induced thermal buoyancy. The surface roughness results in formation of the velocity boundary layers. The sensible heat flux of the surface radiation results in formation of the thermal boundary layers. In order to model the thermal forces, Boussinesq approximation is used in both the simulations. For resolving the thermal boundary layers, the LES method shows better resolution than other turbulent models [2].

3.4 Fugitive Dust Particles

For the selected two idealized domains, a total of 25 dust source polygons are defined. Due to the extensive requirement of computational space, the number of particles from each source is kept to a maximum of one hundred particles. All the dust particles are defined as mass particles with density and gravitational settling velocity. Four types of particles are generated from each source: (i) PM_{0.1}, (ii) PM_{2.5}, (iii) PM₅ and (iv) PM₁₀ [3].

3.5 Time Step of the Transient Simulation

In an open-pit mine, the fugitive dust dispersion is a time dependent phenomenon which requires a transient analysis approach. In a transient simulation, the simulation clock advances with the specified time step. The SC/Tetra offers two different approaches for defining the time step: (i) time step in temporal units and (ii) time step based on Courant number. In the first approach, the time step can be defined either as a constant time step or as a variable time step which will be a function of simulation time. In the second approach also, the time step can be defined either as a constant courant number or variable courant number. The time step defined by the courant number is an adaptive time step scheme, where the time step is determined by the Courant-Friedrich-Levy (CFL) criterion [8].

In order to converge the solution, the time step must be small. Ideally the choice of the time step should result in a CFL number of one, however, a very small time step is required for that. Therefore a fixed time step is used. Initially various constant time step duration is applied to examine the convergence and stability of the solution. However, for time step greater than two seconds, the solution did not converge and resulted instability in the solution. Therefore, a constant time step of two seconds is applied throughout the model run for both the RANS and LES methods.

4. Comparison of the LES and the standard k- ϵ RANS method

The dust dispersion phenomenon under the clear sky conditions is simulated using both the RANS and the LES method. The amount of dust retention and the time required for the dust particles to clear out of the domain is observed to depend on the choice of the turbulence model. In order to compare the turbulence models, the initial downfall and the pathlines of the dust particles are analyzed.

4.1 Initial Downfall of the Dust Particles

With the RANS simulation, an extensive amount of dust particles settles down at the pit surface within initial four minutes of simulation. Whereas, in the LES simulation, the number of settled dust particle is more realistic. Table 2 presents the initial downfall of dust particles for the two different methods. The extensive initial downfall of dust particles in the RANS simulation results in reduced dust retention and a shorter time for the dust particles to clear out of the pit.

Table 2. The initial downfall of dust particles in RANS and LES simulation.

Season	Intensity	Settled dust (out of 2460 particles)		Live dust (out of 2460 particles)	
		RANS	LES	RANS	LES
Winter	Moderate Winter	705	138	1755	2322
	Extreme Winter	574	132	1886	2328
Summer	Fair Insolation	1498	36	962	2424
	Moderate Insolation	1726	25	734	2435
	Extreme Insolation	1609	83	851	2377

4.2 Irregularity in the Pathlines of Dust Particles

Figure 2 presents the pathlines for LES and RANS simulation. The pathlines of the dust particles for RANS simulation show small scale irregularities on its way out of the domain. Whereas for the LES simulation; the pathlines of the dust particles follow well-developed smooth re-circulatory patterns. The pathlines in LES simulation resembles the re-circulatory patterns of the airflow inside the model domain. However, the irregular pathlines in RANS simulation represents the lack of accuracy in calculation of the net resultant forces on the dust particles.

Following the generation of the dust particles, the pathlines of the dust particles for RANS simulation also display very complicated pattern for the initial stage of dust dispersion. Some of the pathlines are also observed

to collapse abruptly at the pit surface after being dispersed for a short duration. The initial downfall of the dust particles are resulted due to this lack of accuracy in net resultant force calculation.

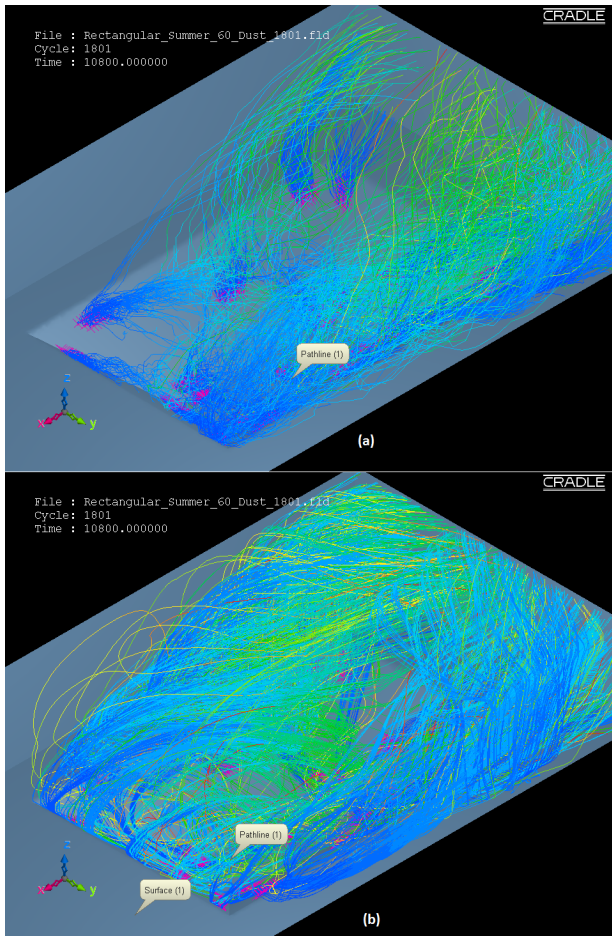


Fig. 2. Pathlines of the Dust Particles for (a) RANS and (b) LES simulation.

5. Simulation Results

Since the flow pattern of fugitive dust particle in an open-pit mine is not known a-priori, various turbulence models needs to be investigated to identify the appropriate model that would simulate the dust dispersion phenomena with reasonable accuracy. The clear sky condition is therefore simulated with similar initial and boundary conditions using both the RANS and LES. The initial downfall of dust particles in the RANS simulation has significant effect in estimation of (i) the particles, settled down at the pit surface, (ii) the particles, transported outside the pit domain and (iii) the duration of dust retention inside the pit. While for the

LES simulation, as the quantity of initial downfall of dust particle is comparatively small, the simulation requires longer duration to clear the dispersed dust particles out of the pit.

The simulation results of clear sky condition using both the RANS and LES methods are shown in Table 3. The results of RANS simulation predict that the gravitational settling is the foremost mechanism for removal of the fugitive dust particles. However, the results of LES simulation present that the re-circulatory airflow inside the domain is the primary mechanism for removal of the fugitive dust. The RANS simulation result for the fair insolation condition in the conical model domain predicted that a maximum of 45% of the particles would be removed. While the LES simulation results for the summer conditions predicted more than 95% of the particles would be removed. The settling time calculated from the terminal gravitational settling velocities of PM_{10} and smaller particles indicates that the downfall of a large percentage of fugitive dust particles within a short duration is not feasible. Therefore the LES method seems to be a better choice than the RANS method in this research.

The simulation results of the winter conditions in both the domains show extensive fugitive dust retention. This is due to the existence of air inversion which results from the negative heat flux at the pit surface. However, the percentage of fugitive dust particles settling down at the pit surface represents a more feasible value in the LES simulation. In LES simulation, the number of dust particles trapped below the inversion layer is larger than the RANS simulation. The absence of strong re-circulatory airflow within the inversion layer results in extensive fugitive dust retention for a long duration. The simulated time to clear out the dust particles during the winter condition is beyond the computational capabilities of this research.

Table 3. The simulation results of clear sky condition using the RANS and the LES simulation.

Domain	Climate Condition	Heat Flux (W/m ²)	% settled down		% reported outside		Time to clear out	
			RANS	LES	RANS	LES	RANS	LES
Trapezoidal	Moderate Winter	-20	~92	~23	4.10 (6 hrs.)	2.68 (6 hrs.)	Unknown	Unknown
	Extreme Winter	-40	~96	~27.8	0.12 (6 hrs.)	1.2 (6 hrs.)	Unknown	Unknown
	Fair Insolation	60	73	1.8	27	98.2	52 min	116 min
	Moderate Insolation	100	81	3	19	97	48 min	144 min
	Extreme Insolation	160	75	4.6	25	95.4	53 min	80 min
	Conical	Moderate Winter	-20	~89	~25.2	6.06 (6 hrs.)	18.66 (6 hrs.)	Unknown
Conical	Extreme Winter	-40	~88	~26.14	0.53 (6 hrs.)	2.1 (6 hrs.)	Unknown	Unknown
	Fair Insolation	60	55	0.07	45	99.93	36 min	80 min
	Moderate Insolation	100	61	1.18	39	98.82	32 min	80 min
	Extreme Insolation	160	72	1.07	28	98.93	48 min	104 min

6. Conclusions

Two idealized open-pit domains are simulated to predict fugitive dust retention for various weather conditions. The input values for the initial and the boundary conditions are obtained from various net radiation sensors, temperature sensors and weather stations installed in an open-pit mine. The modeling domains are simulated to capture the ABL and the micrometeorological flow inside the open-pit. After simulating the airflow pattern in the domain, fugitive dust particles are generated from various dust sources inside the model domain. Two different methods, namely RANS using Standard k- ϵ turbulence models and LES using SGS/DSGS/WALE modeling are used for simulation with similar simulation setup. The simulation results for the LES and the standard k- ϵ RANS turbulence models are not in agreement in prediction of the fugitive dust retention in the model domain.

The analysis of results of the standard k- ϵ RANS turbulence model shows an extensive downfall of the dust particles during the initial stage of simulation. This phenomenon significantly reduces the number of dispersed dust particles in the airflow. In simulation of the summer conditions; excessive downfall of the dust particles also reduces the duration to clear the dust particles out of the domain. While the LES shows very negligible downfall of dust particles during the initial stage. The settling time based on the terminal gravitational settling velocities of PMs also suggests that the LES provides a more feasible estimate than the RANS model. The pathlines of the dust particles for the RANS model also show small scale irregularities which represent the lack of accuracy in calculation of the net resultant force on the dust particle. Whereas the pathlines of the dust particles in the LES follow a well-

developed smooth re-circulatory pattern which resembles the re-circulatory pattern of the airflow. The results of RANS simulation predicts the gravitational settling as the foremost mechanism for removal of the fugitive dust. While the re-circulatory airflow inside the domain, is the primary mechanism for removal of the fugitive dust in the LES simulation. Based on the results of this research, LES seemed to be a better choice than the RANS model.

Acknowledgments

The authors would like to acknowledge the National Institute for Occupational Safety and Health (NIOSH) for its financial support for this research. Technical support from the CRADLE North America Technical Support team is also gratefully acknowledged.

References

- [1] F. Flores, R. Garreaud, and R.C. Muñoz, OpenFOAM applied to the CFD simulation of turbulent buoyant atmospheric flows and pollutant dispersion inside large open pit mines under intense insolation, *Computers & Fluids*, Vol. 90 (2014) © 2013 Elsevier Ltd, pp. 72–87.
- [2] T. Bhowmick, K.V. Raj, and S. Bandopadhyay, Constraints and Consequences in 3-Dimensional CFD Modeling of Open-Pit Mines, Preprint 15-017, SME Annual Meeting (2015), Denver, CO, pp. 1–6.
- [3] T. Bhowmick, K.V. Raj, and S. Bandopadhyay, Three-Dimensional Modeling of Fugitive Dust Dispersion in Idealized Open-Pit Mines, Preprint 15-018, SME Annual Meeting (2015), Denver, CO, pp. 1–6.
- [4] R.B. Stull, *An Introduction to Boundary Layer*

Meteorology, Kluwer Academic Publishers, Netherlands
1988.

- [5] J.R. Garratt, The Atmospheric Boundary Layer, Cambridge University Press, 1994.
- [6] K.V. Raj, Three Dimensional Computational Fluid Dynamics Models of Pollutant Transport in a Deep Open Pit Mine Under Arctic Air Inversion and Mitigation Measures , PhD Thesis, University of Alaska Fairbanks, Fairbanks, Alaska, 2015.
- [7] K.V. Raj, W. Collingwood, and S. Bandopadhyay, Challenges In CFD Modeling Of Air Flow In Open-Pit Mines, Transactions of the SME, Vol. 334 (2013), No. 1, pp. 449-456.
- [8] Software Cradle Co., Ltd., User's Guide Basics of CFD Analysis, SC/Tetra Version 11, 2013.

Mine Fans

Considerations for the Selection of Variable Frequency Drives for Primary Fans

Euler De Souza

Queen's University, Kingston, Ontario, Canada

The operation of primary mine fans must be well configured, yet flexible, to provide the required airflow for underground production activities under changing mine resistance characteristics and surface air conditions and temperatures. Under certain conditions, a Variable Frequency Drive (VFD) may be successfully used to achieve and maintain the fan design operating requirements. A VFD controls the voltage and frequency supplied to a motor to vary the speed, power, and torque in order to meet load conditions. The motivation behind the use of a VFD is to increase energy efficiency and thus reduce energy costs. However, the decision to use VFDs in favor over Reduced Voltage Starters (RVS) is not straight forward. The justification must be made on an engineering and economic basis. The VFD must be carefully specified to match the specific motor otherwise it will destroy the motor. The larger capital costs of VFDs must be offset by savings in operating costs. This paper presents a case study in which main surface fresh air fans were sized for operation in a new ventilation raise under extreme environmental conditions in Northern climates. Ventilation costs for the remote mining operation are high and every opportunity for savings was carefully investigated during design of the fresh air system. Use of VFDs was considered as a potential alternative to increase system energy efficiency. The decision on the selection between RVS and VFD was based on detailed engineering and economic analysis.

Keywords: primary fans, variable frequency drives, reduced voltage starters, energy efficiency, cost savings

1. Introduction

In an operating mine, the system resistance and air density vary regularly and, as such, the fan operation needs to be routinely adjusted in order to achieve or maintain the required operating point of flow and pressure.

During the winter season in Northern climates, when extremely low air temperatures (below -45°C) can persist for extended periods of time and when natural ventilation pressure is at its maximum, substantial savings in energy costs can be realized by reducing the fan operating pressure.

In order to regulate fan flow and pressure, inlet and outlet dampers can be used. However, this practice usually results in inefficient operation and energy loss because of the increased resistance.

Fan operation can also be adjusted by changing the fan blade setting. However the costs associated with production downtime sometimes makes the procedure prohibitive. An attractive alternative is to integrate a means of controlling the fan operating speed. One of the main justifications for selecting a VFD is if the load profile varies frequently.

Alternating current induction motors are constant speed machines. When the motor is started, the electrical system experiences a current surge and the mechanical system experiences a torque surge. With line voltage applied to the motor, the current can reach up to ten times the motor full-load current and the magnitude of the torque the fan could be in excess of 200% of the motor full-load torque [1]. RVS are used in induction motors to reduce the starting current draw of the motor and to reduce the starting torque provided by the motor. Their use results in smooth acceleration with gradually increasing torque and voltage. Reduced voltage starting minimizes the shock on the fan, and potential damage to shaft, bearings, couplings, etc., by reducing the starting

torque of the motor. With RVS alone, one cannot regulate fan flow and pressure.

When the load profile varies frequently, it is desirable to have a fan motor with fully variable speed operation. This can be accomplished by incorporating variable speed operation using a VFD.

A VFD is a device that controls the voltage and frequency being supplied to a fan induction motor thus controlling the speed, power and torque of the motor and of the fan. Since the VFD is capable of adjusting the speed and torque of the fan motor it provides a continuous range fan speed control. By precisely meeting the specific system resistance the fan, efficiency can be maximized.

A number of benefits may be realized using VFDs. Because the brakepower varies with the cube of the speed, adjusting the fan operating speed will result in significant energy savings. Also, when a fan is operated at reduced speeds, significant maintenance savings are achieved due to reduced wear on shafts, bearings, seals, etc. The purpose of a VFD is thus to increase energy efficiency, reduce energy costs and reduce fan operating and maintenance costs.

The decision on use of VFDs in favor of RVSs is however not straight forward. The justification must be made on an engineering and economic basis. A case study in which main surface fresh air fans were sized for operation under variable load profiles is presented. Additionally, a decision on the selection between RVS and VFD is presented to demonstrate the decision-making process.

2. Fan motor controller selection – A case study

An engineering design associated with commissioning of a new fresh air raise to supply 200 m/s and operation under extreme environmental conditions in Northern

climates was completed [2]. Primary fans were sized and a detailed engineering and economic analysis was conducted for the selection of the fan motor controllers (RVSS versus VFDs).

2.1 Operational parameters

The following engineering and operational parameters were considered for sizing of the primary fans.

- The design flow rate is 200 m³/s.
- The raise is a bored raise of diameter 4.5 m.
- The raise length is 610 m.
- The fresh air fans will be operated 24 hours/day, 365 days per year.
- The target availability of the fan system is to be 100% excluding scheduled outages.
- The fans will be exposed to ambient air temperatures ranging between +40°C and -50°C.
- Power cost is 9 cents per kWh.

2.2 Fan sizing

For the required airflow volume it is more economical to install multiple fans. The proposed main surface fresh air fan system consists of two fans operating in parallel configuration.

All fan assemblage components were designed for maximum efficiency (low shock resistance losses) and for lowest fan operating cost. Figure 1 presents a schematic of the fan assemblage design.

For the design flow, the raise resistance pressure was estimated at 0.65 kPa. The fan assemblage resistance pressure was estimated as 0.56 kPa based on system losses associated with the heater house, fan screen, inlet bell, backdraft damper, transition sections, fan cones,

duct junction and elbow. The fan total pressure was estimated at 1.49 kPa.

Based on the design operating point a 2.13 m diameter axial flow fan, with a 0.8 m hub diameter hub was selected. A 225 kW motor, running at 1180 rpm was installed. Figure 2 shows the fan curve, the system curve and fan operating point.

2.3 Fan operation

Under extreme winter temperature conditions in Northern climates, natural ventilation pressures are so significant that, by adjusting the fan operating point, substantial savings in energy costs can be realized.

Based on the monthly temperature profile at the mine site and psychrometric surveys, the monthly variations of natural ventilation pressure were determined. The required fan operating point as a function of surface air temperatures was then determined, as presented in Figure 3. This allowed for the selection of the fan operating point during any time of the year.

If VFDs are used, the fan operation can be instantly adjusted under varying environmental conditions, thus maintaining its operation at the design requirements and guaranteeing the required airflow for underground production. The fan operating point and operating power was determined for each month of the year when using a VFD.

If using RVS, the surface fresh air fans will operate at full demand year round, with an estimated brake power of 200 kW. At extremely low temperatures, the fan blade setting would need to be changed in order to meet the design flow requirements. This would result in additional costs associated with downtime during blade setting changes.

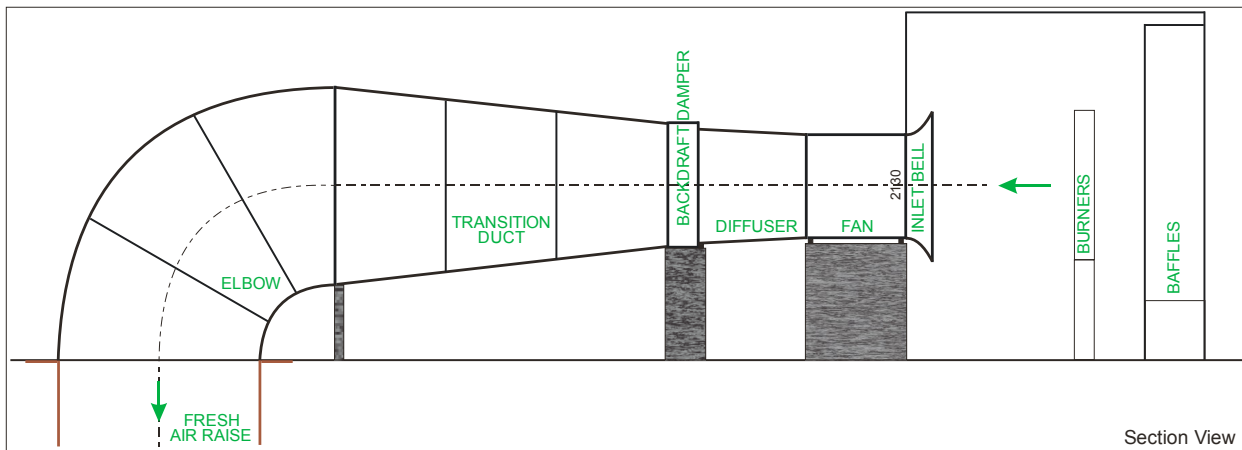


Fig. 1. Fan assemblage design schematic.

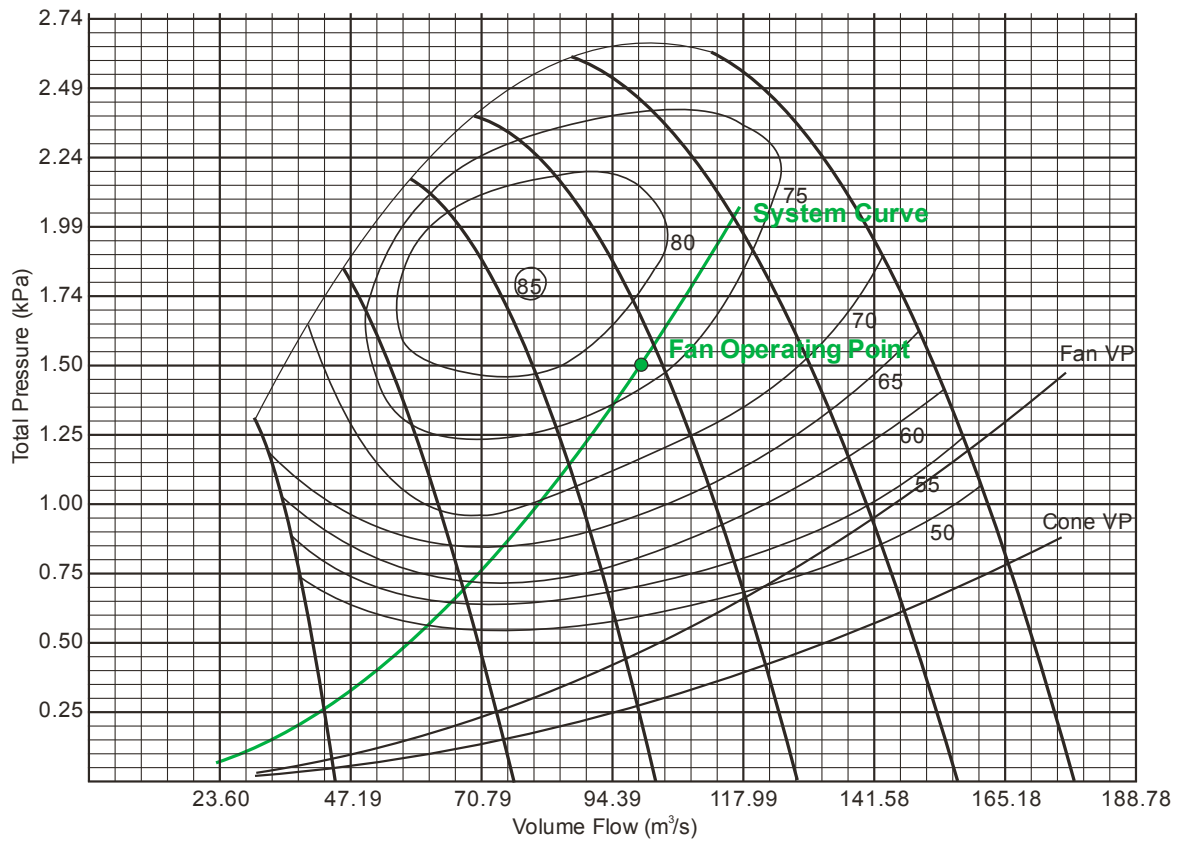


Fig. 2. Fan curve and design operating point.

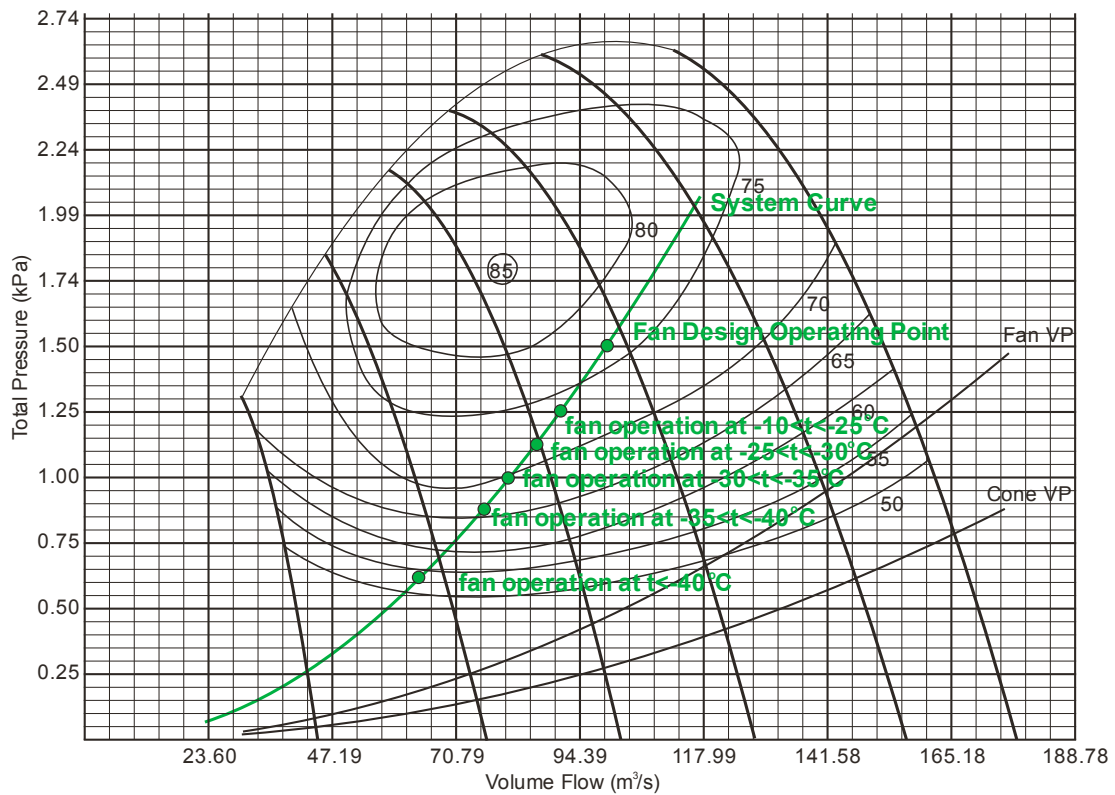


Fig. 3. Fan operating point as a function of surface air temperature.

2.4 Cost analysis

The Net Present Value (NPV) method was used to compare the alternatives.

The capital cost, expressed in total dollars, and operating costs, expressed in dollars per unit time, for purchasing VFDs or RVSs was evaluated. The discount rate and growth rate of electrical costs were also determined.

The capital cost for two VFDs, including switch gear, was \$500,000 and the capital cost for two RVSs was \$122,000. The capital cost difference is thus \$378,000.

The annual operating cost for the fans fitted with VFDs or with RVSs was determined based on the monthly operating cost for each alternative. The month operating cost was a function of the fan operating point, previously described, and cost of power.

The annual operating cost for the fans fitted with VFDs was \$200,720 and the annual operating cost when fitted with RVSs was \$321,771. The savings in operating cost when using VFDs approximate \$121,051.

The economic analysis considered a 5 year period and a power increase rate of 7%. The cost of power in year 1 was \$0.09/kWh.

The discount rate was determined using the weighted average cost of capital and cost of debt (WACC), which is a combination of the cost of equity and the after tax cost of debt.

The number of years was selected as a reasonable payback period.

2.4.1 Net Present Value

NPV allows one to consider the time value of money. It is defined as the present value of the expected future cash flows less the initial cost of the investment.

To evaluate the NPV of the project, the expected net present value of the future cash flows from the project was estimated, including the project's initial investment as a negative amount. A comparison between VFDs and RVSs was made by using the relative difference between the two options for the cost factors and finding the NPV for each year in consideration. The time at which NPV = 0 would represent the payback period for the VFD project. For the determination of the NPV, the initial capital outlay was \$378,000 and a discount rate of 12% was considered. The NPV analysis indicated a payback period of 3 years when the fans are operated with VFDs.

2.4.2 Internal Rate of Return

In evaluating this capital project, Internal Rate of Return (IRR) was used as a measure of the estimated percentage return from the project.

It uses the initial cost of the project and estimates of the future cash flows to figure out the interest rate. The IRR is the return rate that makes the NPV from a particular investment equal to zero. It is the discount rate at which the present value of all future cash flows is equal to the initial investment, that is, the rate at which an investment breaks even. In general, the project is accepted if the IRR exceeds the cost of capital.

Using the NPV method, the Internal Rate of Return was determined through trial and error and interpolation techniques; by trying different interest rates until finding the interest rate which delivered an NPV closest to zero. For the project, the internal rate of return is 23.2%.

2.5 Final recommendation

Based on a 3 year payback period and IRR of 23.2%, and considering the guidelines previously presented, it was recommended that VFDs be installed with the surface fans.

In addition, VFDs offer the following advantages over RVSs: custom control is provided; provides controlled starting, stopping and acceleration; provides advanced overload protection; provides easily adjustable fan speed control; reduces peak energy demand; allows for power cost savings. Table 1 presents a summary of the project economics.

Table 1. Project economics.

	VFD	RVS	Cost difference
Capital cost	\$500,000	\$122,000	\$378,000
Operating cost	\$200,720	\$321,771	\$121,051
NVP year 3	\$3,306		
IRR	23.2%		

3. Conclusions

When deciding of the type the fan motor controller, the process is not straight forward. The justification must be made on an engineering and economic basis. On the engineering front, only under certain conditions, a VFD may be successfully used to achieve and maintain the fan design operating requirements. The VFD must be carefully specified to match the specific motor otherwise it will destroy the motor. On the economic front, the larger capital costs of VFDs must be offset by savings in operating costs. A case study has been presented to detail how these two aspects are applied for the selection of a fan motor controller.

References

- [1] Schneider Electric. Reduced Voltage Starting of Low Voltage, Three-Phase Squirrel Cage Induction Motors. Technical Overview. Bulletin No. 8600PD9201. 16 (1992).
- [2] AirFinders Inc. Surface Fresh Air Fan System Design. Technical report. 54 (2014).

Improvement in Booster Fan Applications for US Coal and Metal/non-Metal Mines through the Application of Technology, International Operating Experience, and NIOSH Research

C. J. Pritchard^a, A.L. Martikainen^b

^a NIOSH, Spokane Mining Research Division, Spokane, WA
^b Outokumpu Ferrochrome, Kemi, Finland

Booster fans have been effectively used in underground gassy and non-gassy, metal, non-metal, and international coal mines for increasing airflow to difficult-to-ventilate areas. Health and safety aspects of booster fans were evaluated based on the previous body of domestic and international research, which showed that except for US-based non-anthracite coal mines, booster fans are perceived as a safe option to achieve increased ventilation capacity that results in health, safety, and environmental benefits.

Inherently, booster fans themselves are not a hazard; it is their installation and operation that are of concern. This analysis showed that when located, sized, and operated correctly, booster fans are a tool to be considered to safely increase mine airflow. Improved technology in ventilation network modeling, atmospheric monitoring, and control of ventilation systems can reduce the risk associated with underground mine booster fan applications. Based on this body of knowledge and recent National Institute for Occupational Safety and Health (NIOSH) research, a compilation of effective booster fan installation and operation recommendations is presented that can be incorporated to improve the use of booster fans in underground coal and metal/non-metal (M/NM) mining applications.

Keywords: Mine Ventilation, Underground Mining, Booster Fans, Recirculation, Coal Mining, Metal Non-metal Mining

1. Introduction

There are two frequently cited examples of booster fan failure in mines. The first is the Sunshine Mine Fire in 1972 where a bulkhead fire caused a short circuit in the ventilation system, recirculating fire contaminants [1,2]. The second is the 1959 Auchengeich Colliery fire in Scotland where the booster fan drive belt caught fire, spreading to roadway timber [3,4]. The former led to passage of the 1977 Federal Mine Safety and Health Act and the second resulted in a major redesign of underground fan installations, both milestones in mine safety regulation.

Regulatory concerns related to booster fan operation are the recirculation of methane (in coal mines) and fire contaminants, monitoring and control issues, increased potential for spontaneous combustion, and leakage around the booster installation. Despite these concerns, booster fans have been successfully operated in US and international M/NM mines, including gassy mines, as well as in selective international coal mines. Also, controlled recirculation has been successfully implemented in international coal mines. Years of operating experience have shown that booster fans have safely provided additional mine airflow to improve miner health and safety in both gassy and non-gassy coal and metal/non-metal mines, with and without the use of recirculation.

1.1 Booster Fan Use and Issues – M/NM mines

Booster fan use has a successful recent history in underground mining, such as at the Homestake Mine [5], Ruttan Mine [6], FMC Trona Mine [7] and Barrick Meikle Rodeo Mine [8], encompassing metal, non-metal, multi-

level, and single-level applications. The Homestake mine recirculated return air through an underground cooling facility to improve the deep mine's working environment, the Canadian Ruttan Mine recirculated at the mine level to save heating costs, the FMC booster allowed safe and effective ventilation of a gassy metal/non-metal longwall retreat mining block at the far extent of the mine's workings, and the Meikle-Rodeo mine assured ventilation of a complex multi-deposit underground operation. Booster fan applications add ventilation pressure, assisting main fans in distributing airflow to areas not effectively ventilated by main fans.

Health and safety issues relevant to operating a M/NM booster fan system are: allowance for changes in the existing ventilation system, such as main fan maintenance [9]; recirculation of dust and gasses [10,11]; and minimized recirculation of mining-generated and fire contaminants [5]. An extreme example of a related health and safety issue is the Sunshine Mine fire [1], which resulted in the death of 91 miners—although this example is not of a booster fan failure, but one of ventilation system component failure exacerbated by booster fan operation.

1.2 Experience and Research with Booster Fans in Coal and Gassy M/NM Mining

Coal mine booster fans have been primarily utilized overseas (South Africa [12]; United Kingdom [13]; Australia [14,15] and have been effectively summarized by Martikainen and Taylor [16]. Use of boosters in US coal mines has been prohibited in §75.302 [17] but has been recommended as a potential option to increase airflow by Ramani [18], McPherson [19], Moraru et al. [20], and

others [16, 21].

Meyer's experience with a South African coal mine booster fan utilized in a district recirculation system for partial air re-use concluded:

To date, the continuous gas monitoring systems have not recorded any increase of the gases found in the underground workings as a result of the recirculation of the air.

It can therefore be concluded that the recirculation project showed the use of recirculated air in a ventilation district, to increase airflow to problem areas, to be a feasible and economical short term solution, as opposed to the use of additional ventilation shafts.

The Mine and Health Safety Administration (MSHA) allows booster fan installations in gassy Class III metal/non-metal mines per 30CFR §57.22207 [17] which also emit methane and utilize similar mining methods and equipment as coal mines. Noted previously, a gassy trona mine has safely and effectively operated a booster fan in a longwall retreat section utilizing room and pillar development while emitting over 3 million cubic feet of methane per day. Most methane from this mine is emitted in the active longwall face and gob area [22]. The booster fan installation was utilized in a difficult-to-ventilate area distant from intake and return shafts. Larger methane inflows and outby leakage required additional airflow to keep methane levels below statutory limits. Once mining retreated closer to shaft areas, the booster fan was placed on standby and ultimately removed from service.

Booster fans have also been effectively used internationally in the United Kingdom, South Africa, China, and Australian coal mines [14, 15, 23]. Motivation to re-examine US booster fan use came about as one of three priority research areas cited by the Technical Study Panel (TSP) meetings [24], which recommended investigation of coal mine booster fan use as a means to improve airflow to mining areas, thus minimizing fire and explosion risks. MSHA's later response to the TSP final report [25] did not address TSP recommendations regarding booster fans [26]. MSHA's approach to potential use of booster fans continues to focus on managing recirculation, leakage, poor mine design, float and coal dust, recirculation of smoke, and utilizing other alternatives [27]. These are reasonable concerns that have been examined in the international mining community, and have been successfully addressed.

Many coal mines have allowed recirculation of return air [23, 28] with success, giving confidence that the booster fan use and recirculation issue may be managed and resolved safely. Because increased airflow to improve safety by more effective dilution of contaminants is the goal, booster fan installations often have the potential to more quickly provide increased airflow and increased velocity to a ventilation-challenged mine than other options such as additional shafts or upgraded surface fan facilities.

2. Atmospheric monitoring and control technology and booster fans

M/NM mines have been safely utilizing booster fans for decades and their use is an accepted industry practice.

A recent development is the concept of Ventilation on Demand (VOD) [29], which involves incorporating control of ventilation systems through monitoring airflow control devices such as fans, sensors, and regulators in conjunction with the variable airflow demands related to variable mining equipment use, blasting, and personnel. The thrust of the VOD system is two-fold: to direct air to where it is actively needed during changing mine operations and to drive operational cost savings from reduced airflow when possible. From a safety standpoint, the additional air is welcomed as the standard ventilation system is often slow to react or does not respond to changes in production requirements. Through the use of contaminant and ventilation control monitoring, additional information is provided to mine management and operations to better control all facets of the ventilation system. When incorporated with the total ventilation system, this marriage of monitoring and control technology through development of VOD systems may improve airflow within the changing mine environment, benefitting not only the day-to-day working conditions, but response to emergency situations, such as excessive contaminant levels or a mine fire.

Advances in monitoring and control ventilation technology has been more prevalent in M/NM mines, but may be further implemented in coal mines to achieve greater knowledge of the state of contaminants and mine airflow for the benefit of management and miners. With this knowledge, management can make better decisions regarding production planning, airflow distribution, and emergency response, and allow miners to better know the present state of their work areas. The use of atmospheric monitoring systems (AMS) technology in coal mines has been locally applied in belt monitoring systems for CO and smoke to allow use of belt air as additional intake capacity [26]. Ultimately, the successful application of belt air at many mines, which mines accomplish through MSHA's Petition for Modification process, has resulted in MSHA amending existing underground mine safety standards to incorporate this successful method [30]. Additionally, since the 1980s mine network modeling programs have improved from simple network programs on mainframe computers to those capable of modeling natural ventilation, contaminants, and mine fires, which can be displayed with exceptional graphics on an engineer's desktop. Recent technology has combined real time in-mine contaminant and airflow quantity monitoring from an AMS system with the Ventsim network model [31], which allows for three-dimensional modeling based on ventilation data.

Booster fans have had a long history of successful operation in various international coal mines. Concerns about recirculation, methane, and fires have been effectively addressed to the satisfaction of the mines and inspectorate. Successful methods were outlined in Gillies and Calizaya [23]. There are serious challenges in all underground booster fan installations but as experience has shown, with effective engineering, management, training, and inspection, they can and have been overcome. In the extreme case of booster fan-induced recirculation, safe operation is noted by Meyer [12], Marks [5], and Robinson [28] with the major concern of methane recirculation being managed. Effective use of contaminant, fan, and pressure differential monitoring in conjunction with variable frequency drives (VFD) allows close control of differential pressures and changing mine conditions to

minimize recirculation. Favorable experience has been documented in applying VOD technology to actively control main, booster, and auxiliary fans in Canadian [29] and US metal mines [8], and can be further applied to coal mine booster fan systems. AMS monitoring has improved and developed dramatically in conjunction with VOD systems in the past few years.

3. NIOSH booster fan research in coal and M/NM mines

NIOSH has been involved with booster fan and recirculation research since the late 1980s, beginning with examining health and safety issues involved with increasing airflow in M/NM gassy trona mines [10, 23-34]. These tests involved utilizing auxiliary and booster fans in continuous miner sections (Figure 1) and mining districts

(Figure 2) to improve airflow to the mining face. This work showed that contaminant levels did not increase, total dust rapidly settled in return airways, and respirable dust levels remained fairly constant in section recirculation scenarios but greatly decreased in mining district applications. This reduction was due to dilution from idle mining sections, leakage, and the addition of relatively uncontaminated air from shops and sumps. Dust reduction methods utilizing water sprays at the face in exhaust tubing and in return airways showed limited success. It was also noted that increased district airflow from recirculation booster fans reduced total mine intake airflow, slightly lowering the dilution effect. Researchers noted that recirculated contaminants could be effectively managed by diligent monitoring and control in conjunction with good planning.

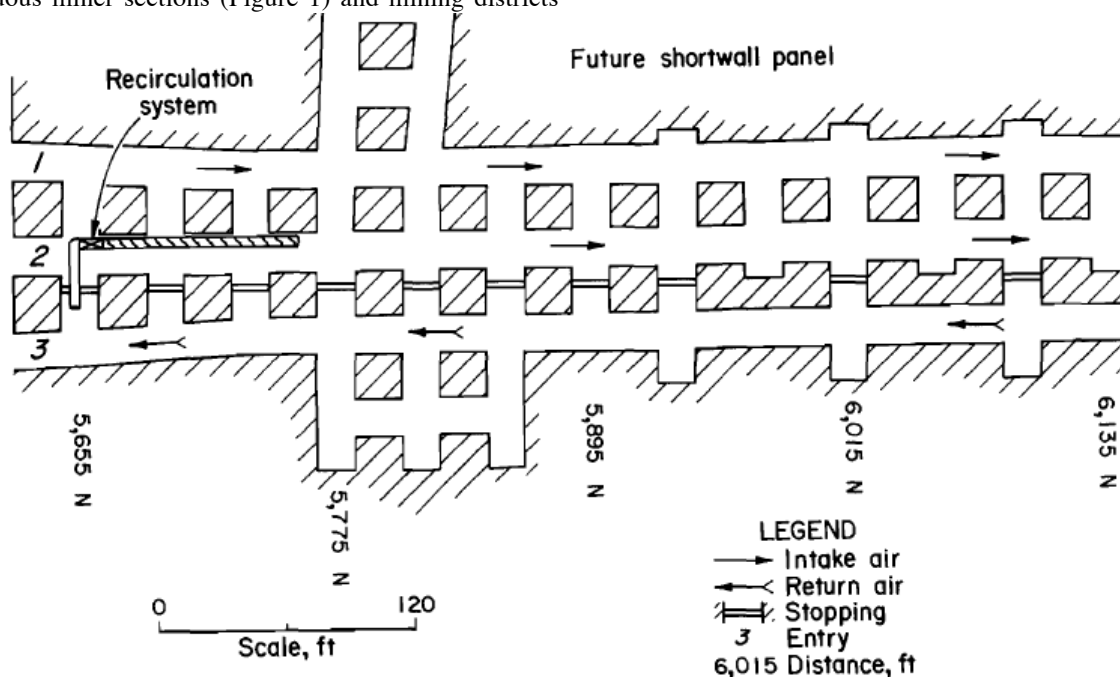


Fig 1. Three-entry auxiliary fan induced section recirculation test layout.

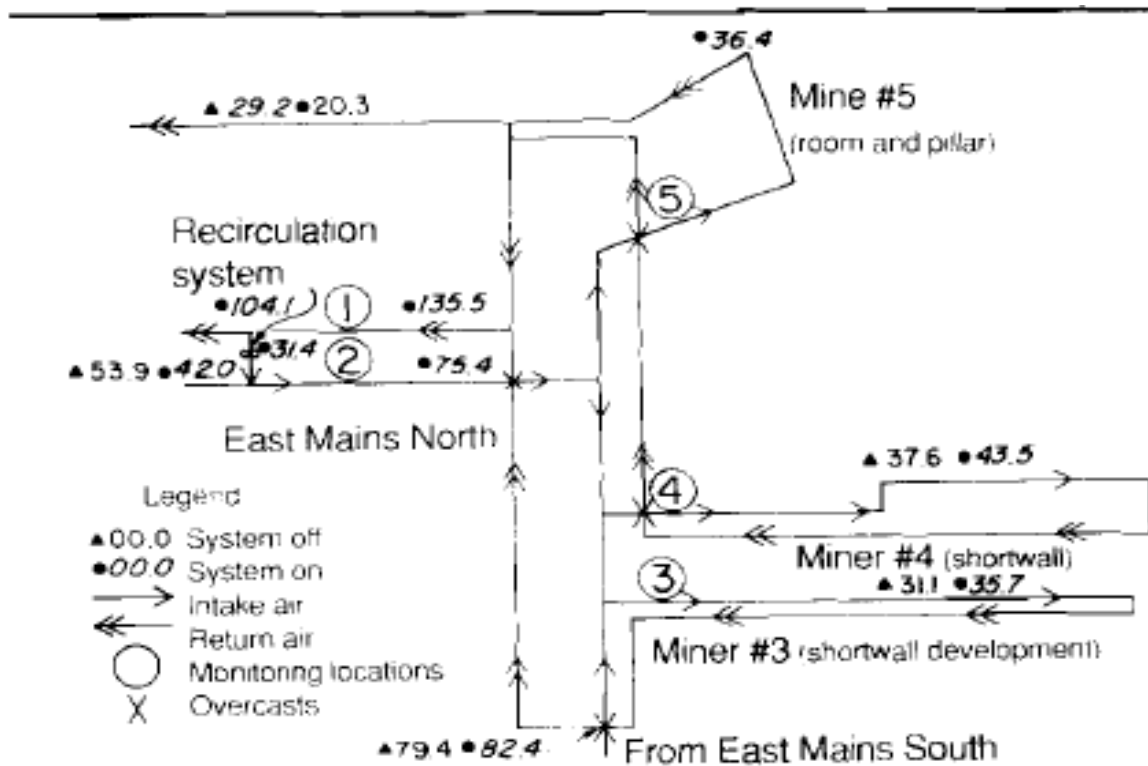


Fig 2. District recirculation system layout, with recirculation/booster fan (arrow) located between monitoring location 1 & 2.

More recently, field research was conducted in the Bruceeton Safety Research Coal Mine and at a large iron mine (Figure 3 and 4) in combination with network modeling [21]. This work was driven by a recommendation from the Belt Air Study Panel [24] and geared towards examining booster fan use in a room-and-pillar environment on a small and large scale, to determine its effect on the overall ventilation system. Research concluded that booster fans can be an effective tool to increase airflow in underground

coal and M/NM mines. The combination of both large and small mine field tests with network modeling showed: booster fans can be used to increase face airflow; outby booster fan locations can minimize recirculation; moderate booster fan pressure-induced localized recirculation would result in undetectable amounts of recirculated methane in intake air; and multiple booster fans can be used to manage leakage and recirculation.

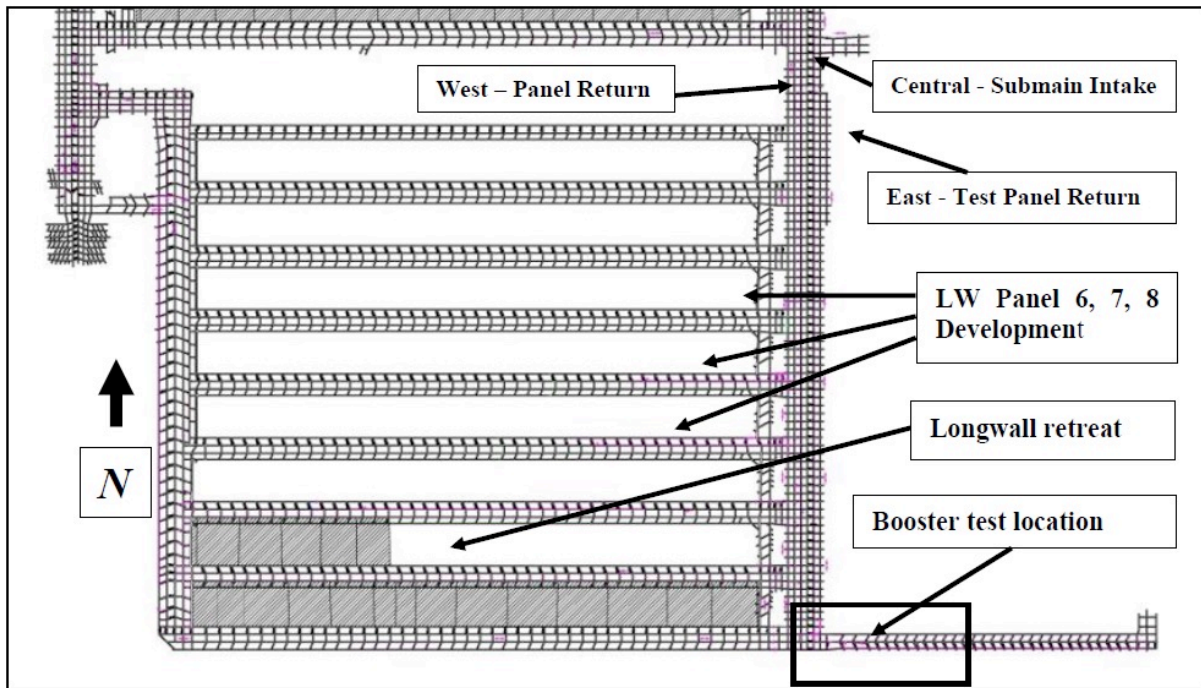


Fig 3. Booster fan test location in relation to mining areas in a large room and pillar mine.

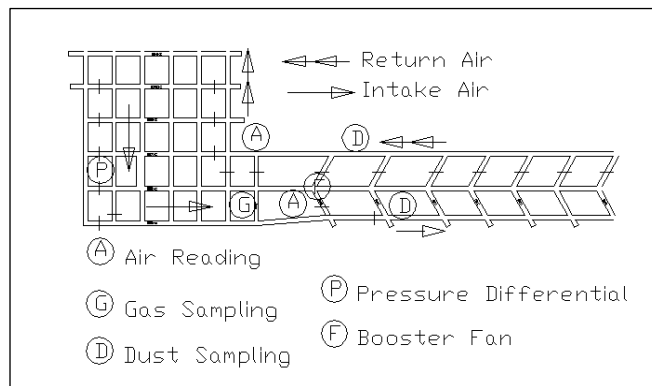


Fig 4. In-line intake booster fan test location detail from Figure 3.

A comparison of field vs. network modeling (Typical Ventgraph network model shown in Figure 5) results showed that leakage of stoppings did not behave identically when pressures across them changed from an intake/return direction to return/intake due to booster fan over-pressure. As such, resistance models needed to be modified; and to ensure that leakage volumes did not significantly change, stoppings near a booster fan needed to be sealed on both sides and be constructed in a substantial manner. In coal mines, safety is enhanced by pressurizing the intake entry, which minimizes the

potential influx of methane from the return. Using moderate booster fan pressures less than 125 Pa/0.5 in wg will minimize recirculation, making detection of methane in intake air unlikely with normal mine gas monitors because of concentrations less than 0.1%. Multiple booster fan installations contribute to safety and efficiency, but ultimately complicate the ventilation system. Any booster fan system requires considerable vigilance in a constantly changing mine ventilation environment, and should be well designed initially with network models kept up to date.

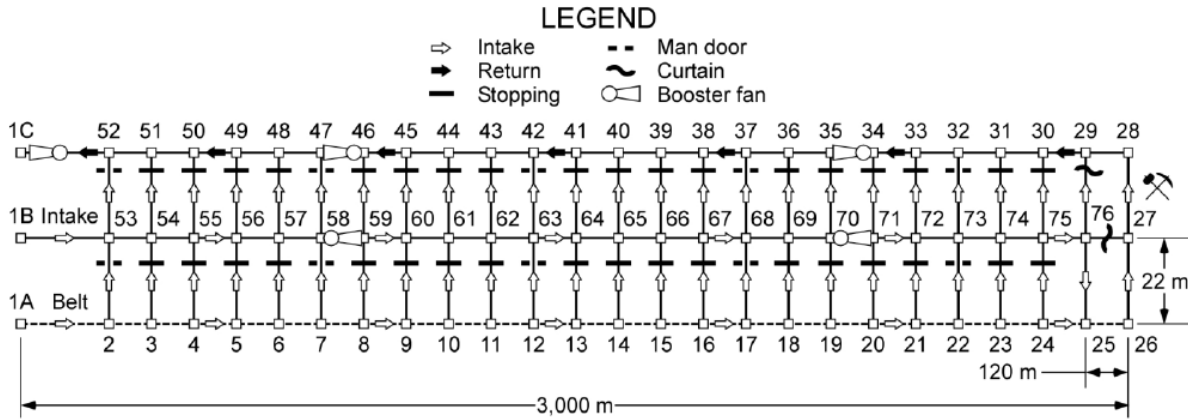


Fig 5. Extended development model with four booster fans utilizing Ventgraph.

Further NIOSH field work focused on booster fan applications in M/NM two mines: a multi-level room-and-pillar mine and the second a multi-level multi-deposit hardrock mine. The first project [35] investigated utilizing a booster fan in a controlled recirculation setting (Figure 6) to improve airflow to a multi-level room-and-pillar operation with limited options to increase airflow. The intent was to evaluate a ventilation system for potential use of recirculated air by determining existing air quality, site selection, modeling, and implementation. Ultimate implementation was not possible due to the mine being classified as gassy by MSHA, but offered a good proving ground for the evaluation concept for other mines interested in utilizing district recirculation. Data showed this mine was a good candidate for booster fan-induced controlled district recirculation by virtue of low return air contaminant concentrations, resulting from considerable idle panel dilution and settling of dust in return airways. Key

findings for booster fan installation were that return air quality was actually better than intake due to dust settling, leakage and dilution, except in the presence of very low methane levels that would be undetectable in intake air at proposed recirculation levels, as noted in previous NIOSH modeling and field research. However, due to long return air system travel times, any mine fire would take many hours to reach the booster fan site, and encounter considerable dilution by other merging return air splits. Findings showed that booster fan-induced controlled district recirculation in conjunction with monitoring and control technology may result in improving air quality and quantity in underground workings. It is important to remember that the use of recirculation to increase local circuit airflow will moderately reduce total mine intake fresh air airflow due to the main fan response to increased inby circuit airflow.

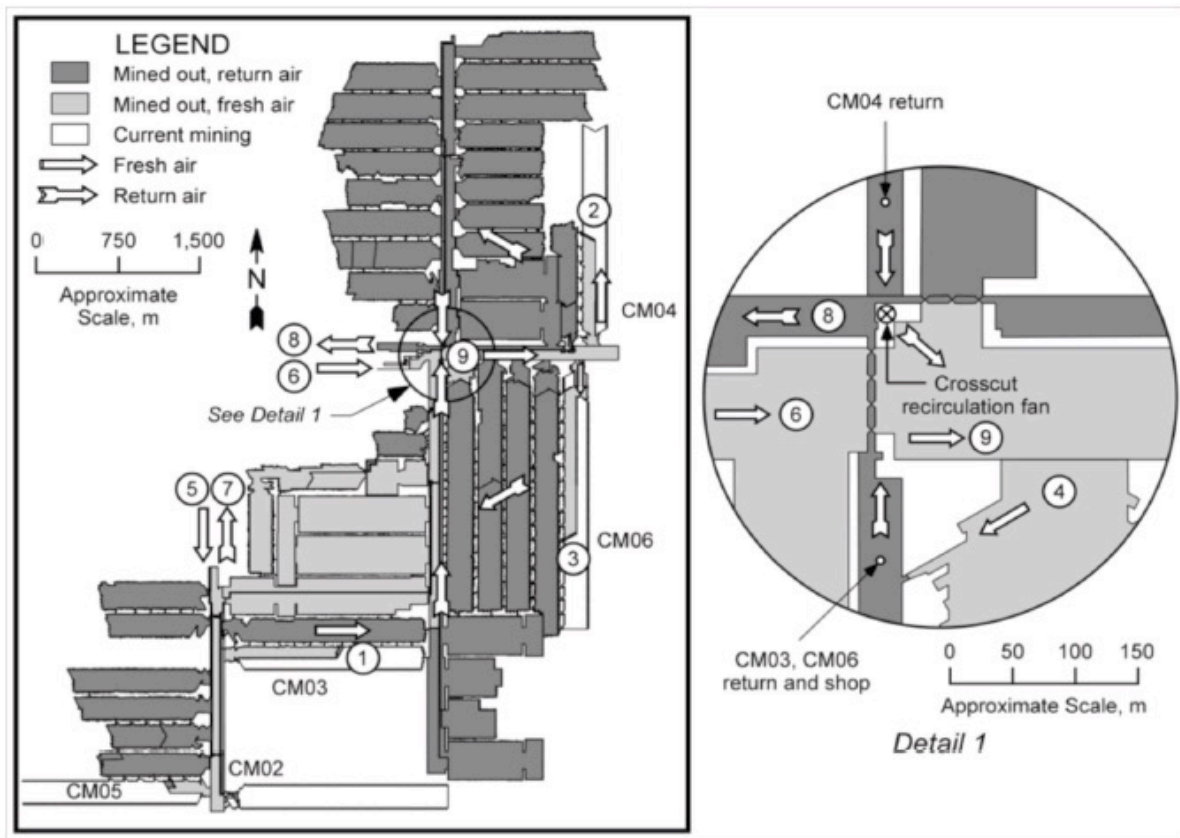


Fig 6. Plan view of upper mine level, with detail 1 showing the recirculation area crosscut recirculation fan connecting intake and return through a stopping bulkhead. Circled areas are mining locations or underground facilities.

Another project [9] involved induced recirculation by underground booster fans during main fan maintenance, in which one of the two underground main mine fans was shut down to allow for shaft maintenance. Booster fan operation was not adjusted during shutdown, inducing recirculation in the studied mining district (Figure 7). The intent was to examine the state of the recirculation zone air quality during this upset condition, and also to examine uncontrolled district recirculation. Although the recirculation percentage approached 20% and the district fresh air supply was slightly reduced, total dust levels increased slightly and respirable dust levels remained low. Diesel particulate matter (DPM) levels increased modestly in line with the recirculation level, but still remained low.

4. Summary of NIOSH Research Findings

National and international experience has shown that utilization of booster fans can effectively improve airflow to increase miner safety and health in normal and district recirculation applications [8][13][16][23]. Safety is enhanced through application of new technologies as confirmed in coal

mine AMS systems for intake belt air and in VOD systems. Leakage around the booster installation has the potential to recirculate return air contaminants, but at a low concentration if booster fan pressures are kept at moderate levels (250 Pa) and local stoppings are effectively sealed, especially if fans are installed in an outby location where mine ventilation pressure differentials are higher. At these outby locations, return air contaminants have been shown to often be much lower, further minimizing recirculation issues and improving air quality.

Modelling and planning are very important, with variations in modeling and pre-booster operation leakage noted due to stopping behavior being different when pressures in the return airway have changed due to booster fan over-pressure. Modeling must be calibrated with operational data and include fire scenarios to plan for booster fan shutdown, mine evacuation, and the effect on the circuit.

Increased inby airflow in both the booster and recirculation circuit can reduce main fan airflow and ultimately total fresh air flow to the area, which must be taken into account as total fresh air is the key component for effective ventilation. Any null points

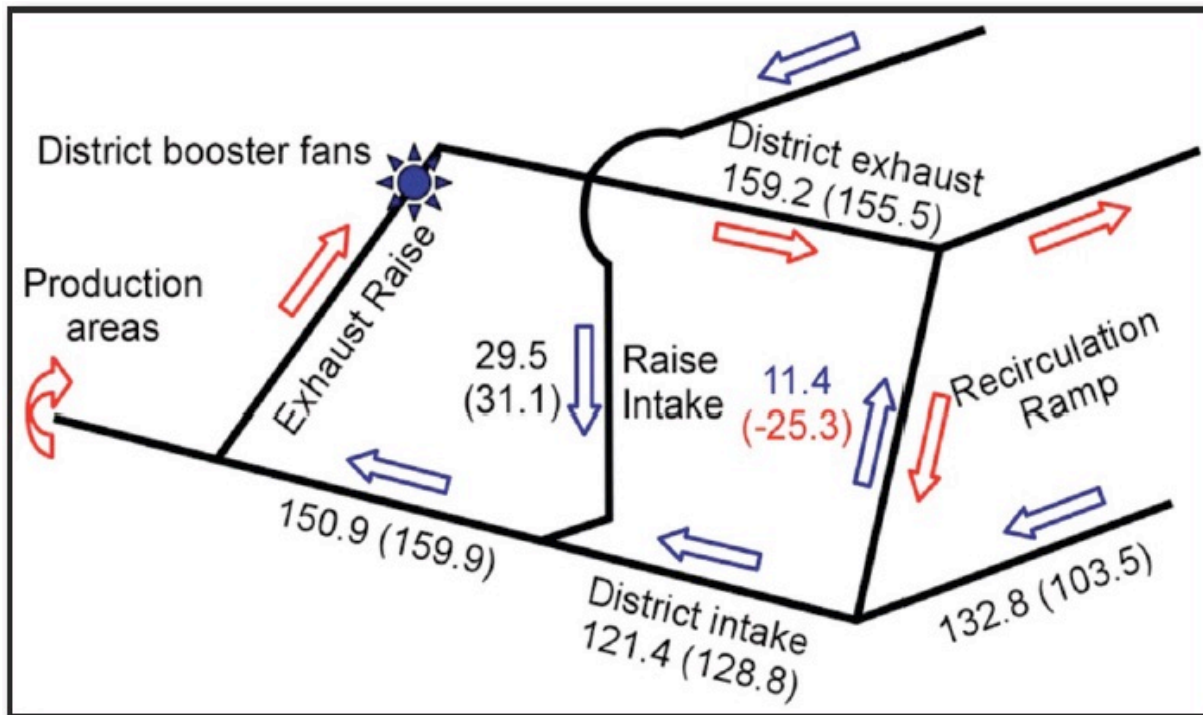


Figure 7. Survey Schematic – Airflow m/s: Normal (recirculation). Intake (blue), return (red).

which involve marginal or reduced flow zones must be managed to increase local flows or to include the option of using air doors, especially if actively travelled. Areas affected by booster fans require diligent monitoring of contaminants, fan performance, and airflow.

5. Operational guidelines and procedures for booster fan use

Booster fans must use proven methods to ensure miner health and safety during normal and abnormal operation, by utilizing successful techniques noted previously and incorporating monitoring and control technology. M/NM mines have begun implementing Airflow Optimization (AO)/VOD monitoring and control systems to optimize airflow and minimize energy consumption [29]. However, due to restrictions in airflow quantity changes when miners are underground [17] in 30 CFR 75. 324, the full capability of AO/VOD cannot be utilized in US coal mines and often in gassy M/NM mines. Refined technologies associated with AO/VOD have greatly improved the ability to monitor and control ventilation systems, increasing awareness of and potentially improving response to contaminants that affect miners' health and safety.

Operational issues noted with coal mine booster fans were reported by Gillies and Calizaya [23] showed that mines recirculated an average of 10% of the air, while Marlborough [36] stated that many air locks needed to be installed for safe personnel access due to increased pressure differentials. Leeming and Webb [13] concluded that booster fans were a

beneficial addition to the ventilation system at large and deep coal and potash mines and that with correct standards, safety of personnel was not compromised. Operational guidelines and procedures noted in the above three references are a comprehensive guideline to good practices in operation of booster fan installations in coal and M/NM mines, in addition to those noted here. Extensive information from years of operating experience on fan system monitoring, controls, management and supervision, communication, training, and system shutdown is described, allowing the booster fan application to be tailored to the individual mine's needs.

M/NM booster fans can induce recirculation during operational upsets and as mining circuit balances change with mine development and seasonal natural ventilation variations. It is often normal practice for mining to take place in series or return circuits, where operations can be complicated by these changes and booster fan use. Many of the above proven guidelines for coal mines from Leeming and Webb, and Gillies and Calizaya can be applied to M/NM mines, especially for monitoring fire contaminants and fan pressures, and for remote fan startup and shutdown.

Vigilance is required in mine work areas during main and booster fan maintenance with reduced system airflow. These conditions are addressed by performing additional personnel exposure and air quality monitoring procedures for contaminants such as carbon monoxide. When these situations are known in advance, ventilation modelling should be conducted to determine airflow changes and

increased contaminant exposures, especially at critical work faces and in recirculation zones. Employees should be notified of system changes and their effects. Again, application of monitoring and control technology is a key component to optimize reduced airflow and ensure a safe and healthy mine environment.

Ventilation system complications from booster fan operation place a higher responsibility on management to educate and train affected employees in emergency procedures specific to the individual mine. As booster fan/AO/VOD systems are implemented, the reactions by persons supervising the AMS system or software programmed to control the system need to be well thought out and failsafe.

Potential hazards and risks such as harmful recirculation and fires can be mitigated by utilizing state of the art monitoring and control, employee training, maintaining ventilation expertise and dedicated management support. Regular assessment of the operational state of the booster fan system must be performed and adjustments made to assure minimal leakage and safe operation.

6. Conclusion

Booster fans have been successful in providing additional airflow to dilute contaminants and safely improve the mine environment in M/NM mines and international coal mines for many years.

The key advantage to booster fans is the timely manner in which they can be installed, improving airflow much more quickly over standard options such as upgrading main fan pressure which increases air leakage considerably, or additional ventilation shafts. Today, mining is intimately affected by the complex world economy, and mines are often started with minimal knowledge of total ore reserves. Reserves and mining areas often expand, challenging the ventilation system in meeting health and safety levels. Booster fans can be an effective tool to combat these issues.

The other key ingredient to effective booster fan implementation is the recent improvement in monitoring and control systems technology, notably AMS and AO/VOD, adding a level of safety not available even a few years ago. Knowledge of the current state of the overall mine ventilation system, mine contaminants and individual fan operation allows miners and management to make informed health, safety and emergency decisions. This provides miners the best conditions during changing operations during the current shift or for short term mine planning challenges.

Utilizing technological improvements and international and NIOSH research results in combination with proven experience from successful international and domestic mining operations will result in booster fan applications that provide airflow improvements resulting in improved miner health and safety.

Acknowledgements

The assistance of Dr. B. K. Belle of Anglo American, Australia, is much appreciated as is the guidance from Mr. John Marks throughout the years for NIOSH's work in booster fans and district recirculation.

Disclosure

The findings and conclusions in this report are those of the authors and do not necessarily represent the views of the National Institute for Occupational Safety and Health. Mention of any company or product does not imply endorsement by NIOSH.

References

- [1] S. Jarrett et al, Health and Safety Report. Final Report of Major Mine Fire Disaster, Sunshine Mine, Sunshine Mining Company, Kellogg, Shoshone County, Idaho, May 2, 1972. US Department of the Interior, (1972) 175 pp
- [2] C. Pritchard, Validation of the Ventgraph Program for use in Metal/Non-Metal Mines, 13th US/North American Mine Ventilation Symposium, Sudbury, ON, Canada. (2010) 455-462.
- [3] Saxton, Coal Mine Ventilation from Agricola to the 1980's, Part VIII. *Min. Eng.* (London). 147: (1986) 395-405.
- [4] R. Robinson, and T. Harrison, Controlled recirculation of air at Wearmouth Colliery, *Min. Eng.* (London). 146 (May) (1987) 661-671.
- [5] J.R. Marks, Rationale and Methodology in Designing Controlled Recirculation Ventilation Systems, American Mining Congress Mining Convention '89', September (1989) 10 pp.
- [6] A.E. Hall et al, Controlled Recirculation Investigation at Ruttan Mine, *In Proceedings of the 3rd Mine Ventilation Symposium, Chapter 3-Recirculation Issues* (1987) 14-23
- [7] A Habibi, Personal communication (2013)
- [8] A.M. Meyer, Implementing a tracking and ventilation control system at Barrick Goldstrike's underground division, 12th US/North American Mine Ventilation Symposium (2008) 13-18.
- [9] C.J. Pritchard et al, Investigation of Induced Recirculation During Planned Ventilation System Maintenance, *Mining Engineering Magazine*, October (2014) 43-48.
- [10] A.B. Cecala et al, Case study of controlled district recirculation, *Mining Engineering*, Vol. 43, No. 11. (1991) 1351-1355.
- [11] B.K. Belle, Personal Communication (2013)
- [12] C.F.Meyer, Controlled Recirculation of Mine Air in a South African Colliery, *Proceedings of the 6th US Mine Ventilation Symposium, Chapter 5* (1993)

- [13] J.R. Leeming and D.J.T. Webb, Underground booster fans – current UK practice for safe installation and management, 14th US/North American Mine Ventilation Symposium, Salt Lake City, UT (2012) 467-473.
- [14] M. Ogle, The Design and Installation of a Booster Fan at Tahmoor Colliery, *Australian Mine Ventilation Conference*, Sydney, NSW (2011)
- [15] D. Benson, Use of Booster Fan Ventilation at West Cliff Colliery, In Coal Operators' Conference, University of Wollongong, the AusIMM Illawarra Branch, NSW, Australia. February 6–8 (2002)
- [16] A.L. Martikainen and C.D. Taylor, Breaking the ice on the booster fan dilemma in US underground coal mines, *Mining Engineering*, October (2003) 47-53.
- [17] MSHA, 30 CFR <http://www.msha.gov/30cfr/0.0.htm> (2013)
- [18] R.V. Ramani, Current issues in US mine ventilation, *Proceedings of the 6th US mine ventilation symposium*, Vol. 45, No. 10 (1993) 1262-1265.
- [19] M.J. McPherson, Booster fans and recirculation of air in coal mines, *American Mining Congress Coal Convention and Longwall USA, International Exhibition and Conference*, (1991) 21-47.
- [20] R. Moraru, G. Babu, I. Mate. The feasibility of district recirculation ventilation system in Romanian mining, *Proceedings of the 6th US Mine Ventilation Symposium*, Chapter (1997) 460-472.
- [21] C.J. Pritchard et al, Booster fan applications for sections in longwall and room and pillar mining, 14th US/North American Mine Ventilation Symposium, Salt Lake City, UT (2012) 449-458.
- [22] A.D.S Gillies, F Calizaya, Use of underground booster fans in foreign prominent coal mining countries compared with the ban in the United States., 13th United States/North American Mine Ventilation Symposium, Sudbury, Ontario, Canada (2012) 475-480.
- [23] J.M. Mutmansky et al, Final Report of the Technical Study Panel on the Utilization of the Belt Air and the Composition and Fire Retardant Properties of Belt Materials in Underground Coal Mining. Report to the Mine Safety and Health Administration, U.S. Department of Labor, Arlington, VA (2007) 131 pp.
- [24] Federal Register, Safety Standards Regarding the Recommendations of the Technical Study Panel on the Utilization of Belt Air and the Composition and Fire Retardant Properties of Belt Materials in Underground Coal Mining, Conveyor Belt Combustion Toxicity and Smoke Density; Proposed Rules, Mine Safety and Health Administration (2008) 34 pp.
- [25] J.C. Tien and F Calizaya, Use of belt air in underground coal mines – with special emphasis on TSP recommendations, 12th US/North American Mine Ventilation Symposium, Reno, NV (2008) 213-217
- [26] D. Beiter, et al, Personal Communication (2013)
- [27] R. Robinson. The use of booster fans and recirculation systems for environmental control in British coal mines, In *Proceedings of the 4th US Mine Ventilation Symposium*. Berkley, CA (1989) 235-242.
- [28] K. Lagowski, Ventilation Air supply on demand, *CIM Magazine*, Vol. 8, No. 2 March/April (2013) 58-60
- [29] Federal Register <https://www.federalregister.gov/articles/2003/01/27/03-1307/underground-coal-mine-ventilation-safety-standards-for-the-use-of-a-belt-entry-as-an-intake-air#h-11>, (2003)
- [30] Maestro Mine Ventilation, *Ventilation Voice*, May Newsletter, Vol 1, Issue 4 (2014)
- [31] A.B. Cecala et al, Controlled Recirculation of Section Air in a Trona Mine, 4th U. S. Mine Ventilation Symposium, Berkeley, CA (1989)
- [32] L. Xu L et al, Respirable Dust Issues Relative to Recirculation of Air in Trona Mines, *SME Annual Meeting*, Feb, Phoenix, AZ (1992) Preprint 92-237.
- [33] C.J. Pritchard, Preparatory Work Required for a Long-Term District Recirculation Test in a Gassy Underground Metal-Non Metal Mine, 7th U. S. Mine Ventilation Symposium, Lexington, KY (1995)
- [34] C. Pritchard et al, Ventilation Systems for Underground Trona Mines, 10th U. S. Mine Ventilation Symposium, Anchorage, AK (2004)
- [35] L. Marlborough, The installation of underground booster fans at North Goonyella coal mine, *ACARP Gas and Outburst Workshop*, http://uow.edu.au/html.ourburst_pres.html (2003)

Axial Fan Failures Related to Improper VFD Operation

Richard E. Ray, Jr.^a, Andrew P. Gouge^b, Stephen B. Wilchek^c

^a*Parsons Brinckerhoff, Inc., New York, NY, USA*
^b*New York University, New York, NY, USA (formerly of Parsons Brinckerhoff, Inc.)*
^c*National Railroad Passenger Corp., New York, NY, USA*

When the power circuit of a motor operating at full speed is opened and then quickly reclosed the result can be sudden high currents that produce high transient torques on the motor shaft. Depending upon the synchronization of the motor rotation and the power circuit phase, reclosure torques may be more than 10 times the rated torque of the motor. This paper provides a case study of the investigation of the catastrophic failure of three tunnel ventilation axial flow fans related to unintentional reclosing of the power supply from a variable frequency drive (VFD) to a VFD bypass direct drive starter. The failure of all fans occurred shortly after the installation of replacement VFDs. The impellers of each of the three reversible fans were directly coupled to the shafts of three phase, 460V, totally enclosed air over (TEAO) induction motors, with the motors foot-mounted inside the fan casings. The investigation included the review of the forensic evaluation of damaged fan impellers, post failure inspection and vibration testing of the motors, and observations of the replacement VFD installations, setup parameters and control logic for operation of the fans. In all three failures, cracks were visible along the keyway of the cast iron hub adapter connecting the fan rotor to the motor shaft. The timing of the three fan failures and the forensic study ruled out possible material defects or fatigue failure of hub or blade components. Field observations confirmed incorrect configuration of the replacement VFD control circuit terminal wiring and programmable parameters that likely resulted in unintentional transfer from the VFD output contactor to the bypass contactor while the motor was operating at full speed. The unintentional reclosing of the motor circuit would have created a transient torque on the motor shaft that would have exceeded the ultimate tensile strength of hub adapter and initiated the failures.

Keywords: fan, failure, VFD, reclosing

1. Introduction

Three of eleven (11) reversible, axial flow ventilation fans comprising the platform ventilation system for a large passenger rail station in New York City experienced catastrophic failures within a two-week period in late 2011. Each of the failed fans was 2.8 m (110 in.) in diameter with a 1-m (39.4-in.)-dia. hub equipped with nine (9) airfoil blades. They were driven by three phase, 460V, 186.5 kW (250 HP) TEAO (totally enclosed air over) motors coupled directly to the fan impellers and foot-mounted inside the fan casings. The rotational speed of the fans when operated at 60 Hz by variable frequency drives (VFDs) was 892 RPM (high speed). When run at high speed, the fans delivered 155.74 m³/s (330,000 cfm) at 0.45 to 0.55 kPa (1.8 to 2.2 in. w.g.) total pressure. Two of the fans were installed in a vertical orientation and one in a horizontal orientation.

Each of the station fans can be operated by a Supervisory Control and Data Acquisition (SCADA) system from remotely located consoles or locally from the individual fan rooms. Control logic for running the fans remotely is provided by Programmable Logic Controllers (PLCs) located in each fan room. For a fire or smoke emergency in the station, fans are run at high speed in the exhaust mode. Selected fans can also be operated at low speed, supply or exhaust for cooling or track maintenance activities conducted in the station. In case of VFD failure, a "Bypass" mode is provided for across-the-line starting.

Site acceptance testing of the original fan and drive systems was performed in 2002. All of the VFDs originally supplied for the platform ventilation system were from a single manufacturer. One of the drives was replaced in 2008 and five more of the original drives were replaced with VFDs produced by a different manufacturer, including the drives for all three failed fans, several weeks prior to the fan failures.

According to information provided by the station owner/operator, one of two vertically-oriented station ventilation fans installed in parallel in the same fan room failed on November 16, 2011. Two additional fan failures occurred on December 1, 2011 -- a vertically-oriented fan in a second fan room and one of two horizontally-mounted fans installed in parallel in a third fan room. In all three instances, the cast iron hub adapters that attached the aluminum fan hub assemblies to the fan motors failed, as did the cast aluminum fan hub assemblies, which split into two or more pieces. Some of the cast aluminum fan blades remained intact, still attached to the rotors, while others were broken into two or more pieces. Since all three failed fans had recently been equipped with new VFDs, the two other fans with the new VFDs that were still operational at that time were subsequently idled due to concerns about potential impeller failures related to possible incompatibilities between the station platform ventilation system equipment and the new VFDs. Upon completion of repairs, all fans were eventually placed back into service for remote emergency operations in late April 2012.

Immediately after the fan failure incidents, Parsons Brinckerhoff Inc. was retained by the station owner/operator to compile the findings of a group of consultants and manufacturers brought in to investigate the failures and prepare a report summarizing the possible root causes of the fan failures. The report was based on site observations and photographs prepared and obtained by Parsons Brinckerhoff and data, analyses, documents and information supplied by the investigation team, which was comprised of the following entities:

- An engineering firm to perform a forensic evaluation of the damaged fan parts
- The fan manufacturer to perform inspections of the failed fan impellers and the remainder of the station fans

- The station ventilation system maintenance contractor and installer of the replacement VFDs to investigate the set-up and performance of the replacement drives
- A motor repair/rebuild shop to inspect and recertify the fan motors
- The engineering firm that performed the original control logic design for the ventilation system to evaluate the control logic for SCADA operation of the fans

2. Review and observations

2.1 General

Confirmation of the rotational direction of each failed fan was not available. However, photographs of the failed horizontal fan indicated that the fan was most likely operating in exhaust at the time of failure (or just prior to failure, if the failure occurred during an unintentional plug reversal) since the leading edge of the blade that penetrated the fan ductwork would had to have been rotating in a counterclockwise direction as viewed from the station platform side of the fan-motor unit (see Figure 1).



Fig. 1. Fan blade penetrating casing for horizontal fan failure.

Fan impeller components included a clamp style sand cast aluminum alloy ASTM B26/B26M A356-T6 hub assembly attached to the motor shaft with a cast iron BS1452 Grade 260 hub adaptor. The hub assembly was comprised of an aluminum hub (rear portion) and clamp plate (front portion). The sand cast aluminum alloy LM31 airfoil-shaped fan blades were inserted in sockets created by the attachment of the clamp plate to the hub. The impellers and motors were installed in cylindrical fan casings at the fan-motor unit manufacturer's plant prior to shipping to the site in 2001. Field testing of the fans was completed by the installation contractor in 2002.

As stated previously in Section 1, all three failed fans had recently been equipped with new VFDs made by a different manufacturer than the original. No testing reports were available for the replacement drives prior to the fan failure occurrences to evaluate parameter settings on the drives or performance pre-incident. In addition, no records were available to determine if the VFDs tripped at the time of fan failure.

2.2 Mechanical

2.2.1 Fan hub failure description

Photographs of the two vertical failed fans are provided in Figures 2 and 3. The hub adapter for the failed vertical fan no. 1 split longitudinally near its horizontal axis, with half of the hub adapter still attached to a broken section of the hub assembly. The fracture face coincided with the corner of the keyway. The hub was separated from the clamp plate and broke into two main pieces. Some fan blades remained intact, while a number were broken along the length of the airfoil section.

The hub and clamp plate for failed vertical fan no. 2 broke into two main sections. The hub adaptor remained mounted on the motor shaft, but was cracked longitudinally through the corner of the keyway and portions of the flange were broken off. Several fan blades remained intact, while a number were broken along the length of the airfoil section.

The hub adapter for the failed horizontal fan remained on the motor shaft but was cracked longitudinally about the horizontal axis, with the crack intersecting the corner of the keyway. A portion of the flange was also broken off. The hub assembly broke into three main pieces, with two full length blades still attached to one piece with one of the blades impaled through the fan casing as shown in Figure 1. At least four of the nine fan blades remained intact.

For all three failed fans, fan impeller parts that broke away from the motor shaft created dents, or in some cases, penetrated through the blade path portions of the fan casings, which were fabricated from 1/4-in.-thick steel plate. Aluminum shrouds mounted over the fan rotors were also damaged. Based on these observations, it appears that all failed fans experienced a similar mode of failure.



Fig. 2. Vertical fan no. 1 fractured fan hub and hub adapter.



Fig. 3. Vertical fan no. 2 fractured fan hub.

2.2.2 Hub material analysis

A detailed forensic investigation of the horizontal fan revealed that three cracks separated by approximately 120 degrees originated at bolt holes connecting the hub adapter to the hub and propagated outwards toward the outer diameter of the impeller. Visual and magnified examinations of the fractured impeller pieces “exhibited clean, bright, faceted fracture morphologies, with no indication of pre-existing cracks, metallurgical defects, or mechanical damage [1].

Metallurgical analyses of micro-specimens from fractures on the fan blades and hub did not indicate any evidence of pre-existing material defects. Microspecimens for the blades showed a “jagged profile” of fracture surfaces typical for “single occurrence, overstress fracture of cast aluminum” [1].

2.2.3 Fracture analysis

Representatives of the fan-motor unit manufacturer visually inspected damaged parts from all three failed fans on site and performed a more detailed inspection of vertical fan no. 1. The report concluded that the fracture faces of the aluminum hub assembly and fan blades showed “a grainy crystalline structure, consistent with a single event, high stress, fast fracture event, with no evidence of any fatigue” [2]. It also stated that the cast iron hub adapter fracture faces for the same fan were “grainy with crystalline features, again consistent with fast fracture failure” and concluded that the fracture faces examined for vertical fan no. 2 and the horizontal fan also showed evidence of “fast fracture failure only, with the exception of impact marks” [2].

The forensic report concluded that the horizontal fan “failed by way of single occurrence, rapid, unstable fracture as a result of an overstress event” [1]. It further stated that no evidence of progressive, or fatigue, fractures were discovered. In follow up conversations, the forensic consultant stated that the fan failures were not typical of blade initiated failures in axial fans resulting from aerodynamic stall or other sources of overstress [3]. They explained that blade failure incidents are usually initiated with the failure of one or more blades near the base of the airfoil, with remaining blades subsequently breaking off due to the resulting imbalance. Only one of the nine fan blades for the

horizontal fan was broken beneath the airfoil section and none of the vertical fan blades. The break surface for this single blade did not exhibit any evidence of fatigue.

The forensic examination of the cast iron hub adapter for the horizontal fan indicated that a longitudinal crack extended the full length of the adapter and through the entire thickness and that “the sharp corner of the keyway acted as a stress concentrator from which the crack originated and propagated” [1]. As with the aluminum hub materials, fracture surfaces of the cast iron hub adapter “exhibited clean, bright, faceted fracture morphologies” characteristic of “single occurrence, rapid, unstable, overstress fracture of cast iron” [1].

2.2.4 Vibration analysis

Vibration testing was performed on the motors of vertical failed fan no. 1 and the failed horizontal fan, as well as three other station ventilation fans, including the remaining two equipped with replacement VFDs. Acceptable vibration levels were measured for the motors of the failed fans, and moderate vibration levels of 10.2 – 12 mm/sec (0.40 – 0.48 in./sec) were measured between 700 and 750 RPM on the remaining two fans with new VFDs. These speeds coincide with the first natural frequency of the fan motor mounting structure. The fan-motor unit manufacturer recommended avoiding operation at these speeds with the VFDs (40-53 Hz).

2.3 Electrical

2.3.1 VFD unit operating mode

A photograph provided by the station owner/operator with a file date/time stamp of the same day as the first fan failure indicated that a few hours prior to the failure, the VFD cabinet and newly installed internal VFD unit were energized and selected in “Auto” mode. Refer to Section 2.4 for the “Auto” mode operating sequence.

2.3.2 Electrical rating of original and replacement VFD units

There did not appear to be any evidence suggesting that either the original or replacement drives were undersized for their application at the rail station. Visual observations of the replacement VFD units by Parsons Brinckerhoff and the station owner/operator did not indicate any signs of damage, e.g., discoloration from overheating. The only noted damage within the electrical cabinet relates to pitting found on new power contactors, which is covered in Section 2.3.5.

2.3.3 Replacement VFD trip records

The last five (5) trip records experienced by each of the five newly installed VFD units were provided by the drive manufacturer. A review of these records did not reveal any consistent trip information that was common to all failed fans.

Based on the manufacturer’s trip record report, each replacement drive was fitted with a timer and not a real time clock. As a result, it is unknown if the replacement VFD units did or did not experience a trip condition corresponding to the time of ventilation fan failures.

Table 1. Condition of contactors for fans with replacement VFDs

Contactors				
Fan No.	VFD Line	VFD Load	Bypass FWD	Bypass REV
Vertical No. 3	Clean	Clean	Significant Pitting	Clean
Vertical No. 1	Clean	Minor Pitting	Significant Pitting	Clean
Vertical No. 2	Significant Pitting	Clean	Significant Pitting	Clean
Horizontal No. 2	<i>Not Accessed</i>	Minor Pitting	Normal Pitting	Clean
Horizontal No. 1	<i>Not Accessed</i>	Clean	Significant Pitting	Normal Pitting

2.3.4 VFD cabinet and circuit breaker trip settings

According to the station owner/operator, the main circuit breakers within the VFD cabinets for the five fans with new VFDs had been replaced in kind with new circuit breakers. The breaker testing documents and breaker trip settings of these new breakers were not available for review. Based on visual observations of the breaker housings performed by Parsons Brinckerhoff and the station owner/operator, there did not appear to be indications of damage to the circuit breakers.

2.3.5 Pitting on recently replaced contactors

From visual observations made by Parsons Brinckerhoff and the station owner/operator, it was clear that the installer of the replacement drives replaced the four contactors within each VFD cabinet in kind with new contactors. The four contactors in each cabinet were assigned as follows:

- VFD Line
- VFD Load
- Bypass Forward
- Bypass Reverse

A review of documents provided by the VFD installer indicated that the contactors were replaced a few days prior to the first ventilation fan failure. Visual inspections of the contactor surfaces performed by station owner/operator personnel found significant pitting on some of the recently installed contactors. The contactor manufacturer stated that the observed damage to the contactors could be attributed to high currents during contactor closing or opening. The significant pitting found on the “Bypass Forward” contactors was an important factor in determining the cause of the fan failures. A summary of the condition of the contactors for the five replacement VFDs is provided in Table 1.

2.4 Electronic controls

2.4.1 “Auto” fan operation via SCADA system

The original operating mode tables for the station platform ventilation system provided both “Emergency” (high speed fan operation for smoke and fires) and “Maintenance” (low speed fan operation for cooling or work in the station) modes. According to the station owner/operator, the default mode of the station ventilation fans when operated remotely from the SCADA system was “Emergency” mode.

“Emergency” mode operation of a station ventilation fan via the SCADA system will commence with the fan attempting to start with the VFD. If the fan room PLC

does not receive a “RUN” confirmation digital input from the VFD within 1 second of starting, the PLC will automatically remove the VFD start command after a 145-second delay and operate the logic to disconnect the VFD load contactor and connect the bypass contactor to start the fan across-the-line in “Bypass.” There is no evidence that the SCADA system programming or any of the fan room PLC programs had been modified or adjusted from the original programming.

2.4.2 Hardwired VFD to bypass interlock timers

The fan drive cabinets were fitted with hardwired VFD to bypass interlock timers that were observed to be set to 0 seconds. According to the SCADA system designer, it is understood that the fan room PLCs are programmed with the relevant time delays to start the fan in sequence, and delay the fan to start in the reverse direction or in bypass. These time delays assist in preventing damage to the fan motors as a result of multiple motor starts in a short time period.

2.4.3 Inconsistencies with VFD control circuit wiring

While performing visual observations of the Control Circuit Terminals for all five replacement VFDs, inconsistencies were discovered with the control circuit terminal wiring. Of the five units observed, five different wiring configurations were found.

The VFD control circuit terminal wiring is the logical interface between the cabinet relay logic and the VFD. A review of the original as-built VFD drawings and control circuit terminal wiring interfaces with the cabinet relays and contactors indicated that there was no direct circuit connection between the replacement VFD control circuit terminals and the Fan Room PLC Input/Output terminals. All PLC input and output signals were connected to a relay or contactor within the cabinet in the original installations.

2.4.4 VFD Fault Wiring

During site visits conducted after the fan failures it was noted that the applicable VFD fault wiring was not connected to the VFD control terminals for all five replacement VFDs. Instead, the fault wiring had been terminated together via a wire nut, and not interfaced with the replacement VFD units.

The original VFD installation drawings indicate that the “VFD fault” terminals were in a supervised circuit with the fault relay. Any interruption to this fault circuit would de-energize the relay, which in turn would de-energize the VFD output power contactor. While the original VFD configuration would disconnect the VFD

output if the fault safety circuit was interrupted, the configuration observed for the replacement VFDs permanently energized the fault circuit. As a result, the VFD power output for the replacement drives remained connected to the fan motor in the event of a VFD fault, negating the original design that was intended to protect the motor by disconnecting it in the event of a VFD fault. The impact of this fault terminal wiring is discussed in further detail in Section 3 of this report.

2.4.5 VFD programmable outputs

The original installation drawings indicated that the VFDs were programmed with two outputs that powered relay coils in the fan drive cabinet. A list of the replacement VFD assignable outputs provided by the station owner/operator for failed vertical fan no. 1, that was apparently downloaded a few days after the fan failure, indicates that the Assignable Output parameters were not programmed in the replacement VFD unit. If these outputs are not programmed, the "RUN" relay will not energize when the VFD starts the ventilation fan. Consequently, in "Emergency" mode the SCADA system would have operated the fan bypass contactor sequence due to a failure of the VFD to provide "RUN" confirmation.

2.4.6 VFD programmable inputs

Drive parameters received from the station owner/operator indicated that the parameter associated with programmable input "M5" was modified after the ventilation fan failures for vertical fan no. 1 by the installation contractor. The programmable input "M5" is viewed as significant in relation to the ventilation fan failures since it operates as the drive "Stop" function as indicated on the original VFD drawings. A comparison of the relay logic diagrams for the original installation to the text files for the replacement VFD indicated the actual function when M5 was "ON" was "Emergency Stop." This observation is significant as it indicates the possibility that the replacement drive may not have stopped when the "RUN" command from the fan room PLC was discontinued.

3. Findings

3.1 Hub failure due to high transient torque applied to fan motor shaft

It is Parsons Brinckerhoff's professional opinion that there are generally seven possible causes of catastrophic failure of axial ventilation fans:

1. Foreign object impacting the rotating fan
2. Excessive vibration
3. Material defect in the fan motor assembly
4. Overspeed of the fan
5. Material fatigue over time
6. Material fatigue caused by aerodynamic stall
7. High transient torque applied to the motor shaft

Of these possible causes of catastrophic fan failure, it is Parsons Brinckerhoff's opinion that a high transient torque applied to the motor shaft was the most probable cause of the station fan failures for the following reasons:

1. Based on site observations there is no evidence of foreign objects impacting the rotating fans.
2. No excessive vibration levels were measured for any of the fan motors.
3. The metallurgical analyses of fan blades and hub materials indicated inclusions and porosity "typical for aluminum castings and not indicative of a pre-existing material defect." The forensic report concluded that the fans "failed by way of single occurrence, rapid, unstable fracture as a result of an overstress event" [1].
4. The failure mode of the fans was not consistent with an overspeed event, which would typically be characterized by blade failures initiated near the base of the airfoil due to excessive tip speeds.
5. As stated in the forensic report, "the analyses did not reveal any evidence of progressive, that is, fatigue fracture" [1].
6. The failure mode of fans was not consistent with an aerodynamic stall event, which would typically be characterized by a fatigue failure near the base of the airfoil on one or more blades and the subsequent breaking of all blades due to the resulting imbalance.

To quantify the transient torque that would result in

It is possible for the fan motor to produce torques

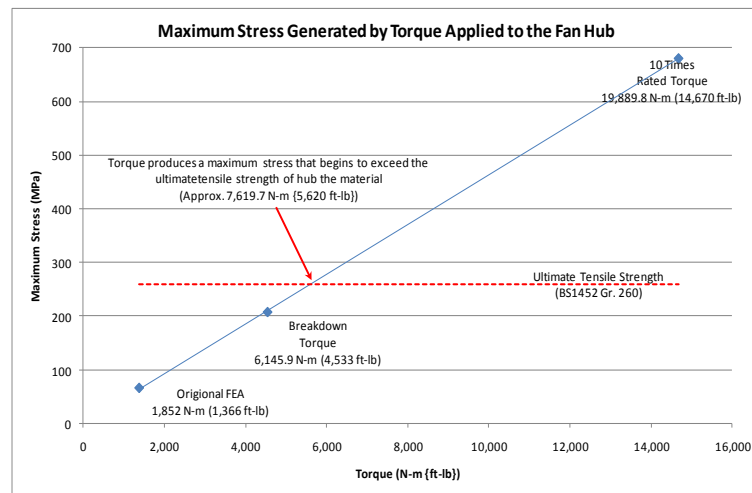


Fig. 4. Maximum stress in cast iron hub keyway vs. torque applied by motor shaft.

catastrophic fan failure the fan manufacturer performed a Finite Element Analysis of the fan hub adapter [4]. A graphical summary of the results is provided in Figure 4. The trend line illustrated in the graph indicates a linear relationship between applied torque and stress, which is as expected since a linear model was used for the FEA analysis, and is “standard for cast material” according to the fan-motor unit manufacturer [4]. The Y axis of the graph is labeled as “Maximum Stress (MPa)” as this is the maximum calculated stress at any point within the model for a given torque” [4]. For all cases modeled the maximum stress was identified in a “corner” of the hub adapter keyway. These results are in line with photographs of all the failed fan hubs that show fractures intersecting a corner of the hub adapter keyway.

The highest transient torque generated by the fan-motor assembly under normal operation is the breakdown torque. The fan-motor unit manufacturer confirmed that “the fan motor can accept a torque value equal to the breakdown torque,” which is 6,149.5 N-m (4,533 ft-lb). Based on the results of the FEA, a torque of at least 7,619.7 N-m (5,620 ft-lb) would be required to produce a maximum stress in the hub that exceeds the hub material tensile strength and result in material failure in the form of a fracture intersecting a corner of the hub adapter keyway.

much higher than the breakdown torque during power switching operations. High transient torques can be generated during the “reclosing” of the motor power source, sometimes referred to as “motor bus transfer.”

3.2 Transient torque due to reclosing of power source

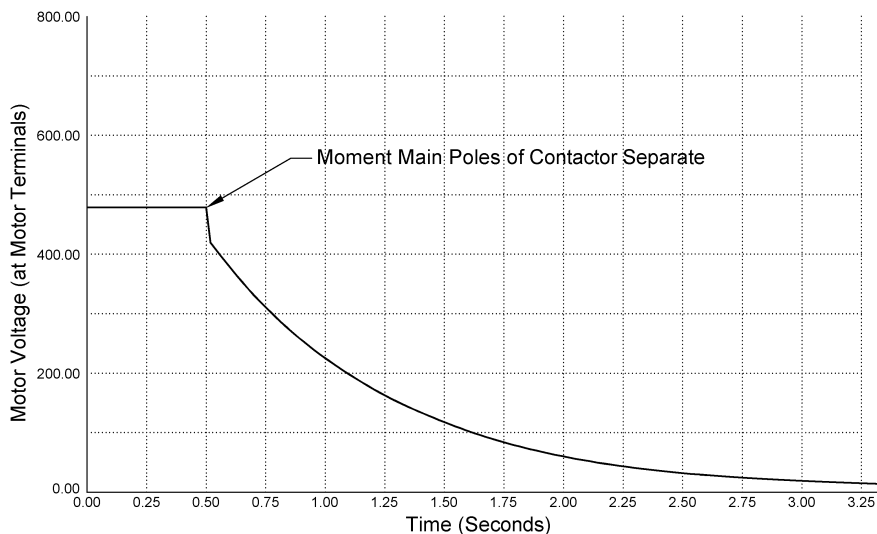
The reclosing of fan motor power supply from one source to another while the fan is operating at speed is capable of generating high transient torques for the following two cases:

1. Two motor power sources having reverse phasing (equivalent to a plug reversal)
2. Two motor power sources that are out of phase

Contactors interlocks within the VFD cabinet prevent the VFD output or bypass contactors from being closed at the same time. Therefore, any reclosing event from one supply to another will involve a time interval when the motor circuit is opened prior to the circuit closing on a different contactor.

During a reclosing event, the time duration between the contactors opening and the second contactor closing will have a significant effect on the magnitude of the transient torque that is generated by the fan motor due to the time constant of the fan motor magnetic flux to decay. For a fan motor experiencing a short circuit, e.g., a three phase fault, the decay time is relatively short. McCulloch explains that for a short circuit “typically the flux will decay to less than 30% of rated flux within 5 to 6 cycles” [5]. However, when the fan motor circuit is opened, as is the case with the opening of the VFD load contactor in a VFD to bypass situation, the decay time of the motor flux is longer. McCulloch describes the flux decay for an open circuit as follows:

“The time constant for this process is that of the open rotor resistance in series with the rotor leakage inductance and the mutual inductance. This time



constant is typically in the order of seconds” [5].

This is consistent with the time constants observed for voltage to decay in the 186.5 kW (250 HP) motor for the horizontal fan when the motor is open circuited, as shown in a voltage vs. time plot in Figure 4 produced from data gathered by a power quality analyzer in May 2012 after the rotor was replaced.

According to data available from the manufacturer, the contactor opening time, measured from the moment the coil supply is switched off to the moment the main poles separate, is in the range of 100 to 170ms (0.10 to 0.17 seconds). The contactor closing time, measured from the moment the coil supply is switched on to the initial contact of the main poles is in the range of 40 to 75ms (0.04 to 0.075 seconds).

For the case where the hardwired bypass contactor interlock timers are set to 0 seconds, as observed, the only time delay between the moment the main poles of the VFD load contactor are opened and the bypass contactor is closed is in the range of 40 to 75ms. Based on the voltage decay curve produced from motor testing that is shown in Figure 5, the residual voltage within the motor after 75ms would be in the range of 400V.

It is the opinion of Parsons Brinckerhoff that for the configuration with a VFD and bypass contactors, the likely reclosing sequence was from VFD to bypass and not the other way around (bypass to VFD) for the following reasons:

1. The VFDs are not capable of producing transient torques consistent with a reclosing event.
2. If the reclosing was from bypass to VFD it is likely that there would have been significant VFD component damage. This was not observed.
3. Damage to bypass contactors was observed, which is consistent with a VFD to bypass reclosing event as described below.

The sequence described above would not have allowed sufficient time for the motor flux to decay below a residual motor voltage of approximately 400V; as such, if the bypass contactors are either in reverse phasing or are out of phase when closed, there would be significant potential across the closing contactors

resulting in high currents and arcing that would produce burning as noted in Section 2.3.5. The lack of damage to any VFD components confirms that the VFD output contactor 2M was open at the time of the bypass contactor closing.

When the power circuit of a motor operating at full speed is opened and then quickly reclosed the result can be sudden high currents that produce high transient torques on the motor shaft. According to Nailen, “some authorities calculate reclosure torque peaks of 10 to 20 times rated (torque). He further states that the damage from switching transients “can be severe -- shafts twisted, rotors loosened on shafts, coils bent out of shape, or a machine ripped clear off its foundation” [6].

While discussing reclosing torques of large induction motors, Shaltout notes (1996) the following:

“When an induction motor is disconnected from the supply, residual fluxes will be trapped in its rotor circuits. Such residual fluxes will produce stator voltages as the motor continues running and, thus, they will interact with the supply voltage at the instant of reclosing” [7].

In describing reclosing of the power supply on an operating motor Patterson states that:

“The problem that is encountered by these disconnected machines maintaining a residual voltage is that when reclosing occurs, the system voltage and machine residual voltage are typically

out-of-phase...The motor(s) may not immediately fail but the resulting high shaft torque and torque on the coils can eventually result in unexplained failure of the machines” [8].

When contacted regarding possible transient torque magnitudes associated with reclosing events for the station fan motors, the motor manufacturer stated that:

“As for the maximum transient torque values, this would depend on many factors, but it would be safe to say that the transient torque can be more than 10 times the design torque value in situations such as this” [9].

Full load torque for the 186.5 kW 250 HP fan motors is 1,988.9 N-m (1,467 ft-lb). The transient torque produced by reclosing on an already operating motor of 10 to 20 times full load torque would be approximately 19,889.8 to 39,779.7 N-m (14,670 to 29,340 ft-lb). The ultimate tensile strength of the BS 1452 Grade 260 cast iron hub adapter is 260 MPa (37,752 psi). As shown in Figure 4, a torque greater than 7,619.7 N-m (5,620 ft-lb) applied to the hub adapter assembly—would likely result in failure of the hub adapter along a corner of the keyway. A transient torque of 10 to 20 times full load torque would produce stress levels in the keyway well in excess of the tensile strength of the cast iron hub adapter.

3.3 Reclosing of power source due to incorrect VFD control circuit terminal wiring and programmable parameters

The original VFD installation was designed with relay logic and VFD I/O to prevent a reclosing event from occurring. As noted in the observations, inconsistencies with the replacement VFD control terminal wiring were discovered between the five replacement VFD units. It is the opinion of Parsons Brinckerhoff that the incorrect installation and configuration of the replacement VFDs allowed the reclosing events to occur when the ventilation fans were operated remotely, specifically in relation to three main installation and configuration items:

1. VFD “Fault” Control Circuit Terminal Wiring
2. Configuration of the VFD “RUN” Assignable Output Relay
3. Configuration of the VFD input terminal “M5” related to Start/Stop function

The observed inconsistencies in the installation of the replacement VFD units would have led to a departure from the correct step-by-step operation of the VFDs. In the opinion of Parsons Brinckerhoff, the incorrect configuration of the replacement VFD control circuit terminal wiring and programmable parameters resulted in uncontrolled ventilation fan operation in which the VFD ran up to full speed, failed to provide run confirmation, failed to latch the VFD output contactor and failed to stop when the Fan Stop Relay opened. As a result, power supply to the motor was allowed to transfer from the VFD output contactor to bypass contactor while the motor was operating at full speed.

As the VFD operated on a generated frequency, it is very likely that the supply from the VFD and the supply from the bypass contactor were out of phase at the time of transfer. Additionally, it is also possible that the direction of the fan operating on bypass was reversed, equivalent to a plug reversal.

4. Recommendations

The unintentional reclosing of the power supply during starting of the three failed fans could have been avoided with the proper wiring of the VFD control circuit and setting of programmable parameters related to the control system. In addition, life safety equipment such as station platform ventilation fans should be locked out to prevent remote operation until testing is completed and all disciplines/groups are confident of the safe operation of the system.

It was recommended that hardwired time delays be added to the control circuits for the station ventilation fans to provide an additional layer of safety to prevent the power contactors in the VFD cabinet from disconnecting the VFD and reconnecting the bypass contactors, or vice versa. The time delays were subsequently installed for each of the station ventilation fans, and set to 15 seconds, since the fans are factory tested to withstand an across the line start in the opposite direction after a time delay of 10 seconds.

References

- [1] Lucius Pitkin, Inc., Evaluation of Rail Station Ventilation Fans, Report No. F11511m, January 11, 2012.
- [2] American Fan Company, Rail Station, 280J1/2TS-100-9 Fan Failure Analysis, Rev A, April 25, 2012.
- [3] J. Crosson, Lucius Pitkin, Inc., Personal communication, April 13, 2012.
- [4] American Fan Company, Rail Station, Hub Adaptor Finite Element Analysis, Rev A, June 14, 2012.
- [5] M.D. McCulloch, The Effect of Voltage Dips on Induction Motors, DIP-Proofing Technologies, Inc., Power Quality Paper No. 3, 1992.
- [6] R.I. Nailen, Avoiding Switching Transients Damage in Motor Circuits, Consulting-Specifying Engineer, March, 1987.
- [7] A. Shaltout, Reclosing Torques of Large Induction Motors with Stator Trapped Flux, IEEE Transactions, Volume 2, Issue 1, March, 1996.
- [8] R.W. Patterson and G.T. Pitts, Reclosing and Tapped Motor Load, 61st Annual Georgia Tech Protective Relaying Conference, May 2-4, 2007.
- [9] Toshiba International, Personal communication, May 22, 2012.

Utilization of Booster Fans in Underground Coal Mines

Felipe Calizaya, Michael G Nelson

University of Utah, Salt Lake City, Utah

This study presents the basic requirements for the installation and operation of booster fans in underground coal mines. It includes a summary of advantages and disadvantages of booster fans, design principles to avoid flow recirculation, standards and regulations adopted by coal mining countries, the requirements for the fail-safe operation of the fan system, the applicable standards for use in the U.S., and the rules of safe practices developed in coal mining where booster fans are used regularly. The study also presents the results of booster fan surveys and inspections conducted in six underground coal mines, three in Australia and three in the United Kingdom. In both countries, the regulations allow mine operators to use booster fans to overcome adverse ventilation conditions provided that certain requirements are met. One of these requirements is that the booster fan installation must be justified. Another is that the fan must be equipped with airlock doors, and an environmental monitoring system. These requirements and practices are discussed in the paper.

Keywords: booster fans, basic requirements, coal mines, fan monitoring

1. Introduction

A booster fan is an underground ventilation device installed in the main airstream to handle the quantity of air circulated by one or more working districts. It is installed to operate in conjunction with the main fan and boost the air pressure of the ventilation air passing through it [1]. To accomplish this objective, the fan is installed in a permanent bulkhead and equipped with airlock doors, electrical interlocking devices between main and booster fans, and a fan monitoring system to continuously assess the operating conditions of the fan.

Booster fans are generally installed in return airways in series with the main surface fan and sized to pressurize the air circulated through a working section of a mine. Although the booster fan is installed in series with a main surface fan, the quantity of air passing through it is usually less than the quantity of air passing through the main fan. In deep coal mines, booster fans can be used to overcome conditions under which surface fans are incapable of providing the airflow demands, or when these requirements can be fulfilled only at extremely high pressures, which cause excessive air leakage and may lead to unsafe conditions [2].

1.1. Basic requirements

The first and foremost basic requirement of any booster fan installation is a thorough evaluation of the existing mine ventilation system. If the ventilation requirement can be fulfilled safely and economically by upgrading the main fan, decreasing the airway resistances, or repairing bulkheads, then these options should be given priority over booster fan installations. The evaluation comprises of ventilation surveys, prediction of future airflow requirements, and simulation studies by means of

numerical simulators such as VnetPC, and Ventsim. Once the decision is made to use a booster fan system, a detailed plan must be developed. This plan must specify the size and type of the fan(s); the number, type, and strength of airlock doors; fan condition and environmental monitors; and an electrical interlocking system.

1.2. Advantages and disadvantages

1.2.1. Advantages

There are several ways of gaining advantage from the use of a booster fan. Even if booster fans are not suitable for every situation, they are capable of providing improvements in various underground environments. Some of the possible advantages of booster fans are:

- The airflow distribution in the mine is enhanced, especially in the difficult-to-ventilate areas.
- The pressure differentials from intake to return are reduced, thus reducing leakage and the need for airlock doors.
- The surface fan pressures are reduced, allowing existing installations to remain in place.
- The fan can be used to boost air flow to single panel(s) rather than the whole mine, to minimize required regulation and mine resistance.
- The overall development costs are much less than those for installation of large surface fans and sinking a new shaft.
- The total electric power cost of a system with booster fans is lower than that of a system with surface fans only.

1.2.2. Disadvantages

The major disadvantages of booster fans are:

- Most coal mines have multiple parallel intake and return airways; therefore, if booster fans are used in the main return airway all the air should be directed to the entries where the fans are located, thus requiring heavy duty stoppings and doors.
- All coal mines are gassy, so the booster fan must be designed with anti-sparking characteristics, which calls for use of a stainless steel rotor, and other fan parts.
- The booster fan must be installed in a flameproof housing, or the motor must be placed in intake air; therefore, an extended drive shaft is required.
- Electric interlocking is required between the main and booster fan systems to prevent uncontrolled recirculation.

The authors believe that, in underground coal mines, the advantages of booster fans outweigh their disadvantages. This is why booster fans are widely used in many coal mining countries, including the U.K., and Australia.

2. Regulations and rules of safe practices

Each country has its own regulations for the use of booster fans in underground coal mines. In this paper, the British and Australian statutory regulations for the use of booster fans are summarized. Although there are similarities between the mining technologies and practices in the United Kingdom, and Australia, there are legal and practical dissimilarities that have led each country to approach coal mine ventilation differently.

In the United Kingdom, the Coal and Other Mines Order of 1956 allows the coal mine operators to use booster fans, provided that certain requirements are met. One of these requirements states that before installing a booster fan, an extensive ventilation survey must be carried out and a detailed report submitted to Mines Inspectorate. Another requirement states that the booster fan must be inspected at 30-minute intervals and the results recorded every two hours. Furthermore, the regulations require the mine operators to equip the booster fan with airlock doors, fan monitors, and other devices to reverse the ventilation to a flow-through system in the event of fan failure [3].

In Australia, booster fans are used in two coal mining states: Queensland and New South Wales. In both states, the installation of booster fans requires a thorough evaluation and risk analysis and a management plan demonstrating adoption of best practice that must be submitted to the state inspectorate for approvals. In Queensland, The Coal Mining Safety and Health

Regulation requires the mine operator to develop standard operating procedures for (i) using a booster fan, and (ii) for actions to be taken if a methane detector monitoring the air passing through the fan activates a visible or audible alarm [4]. In New South Wales, The Coal Mines Regulation states that: "A booster fan must not be installed or used underground at a mine unless the installation and use of the fan is approved by the mines inspectorate." Furthermore, the regulation requires the mine manager the installation and maintenance of a monitoring system to monitor the operation of main surface and underground fans [5]

Table 1 shows a comparative evaluation of current regulations, types of fans used, and basic requirements under which booster fans are designed, installed, and operated in British and Australian coal mines. In both countries, the booster fan installation plan is justified using studies that document the risks associated with booster fan use, the control measures included in the design, and the plan approved by the mine inspectorate. In every case, booster fans are installed in the return airway, and are equipped with heavy duty airlock doors to minimize leakage and recirculation and a monitoring system to evaluate the operating conditions of the fans. Depending on the pressure differential, a booster fan requires at least two airlock doors in series. Furthermore, the fan operating conditions are evaluated by an atmospheric monitoring system.

This table also shows some differences which are attributed to local conditions. One difference is that recirculation is not allowed in Australian mines, while recirculation of less than 10% is accepted in British mines. Another is that electrical interlocking between the main and booster fans is required in Australian mines, but not in British mines. In both countries booster fans are used to assist the main fans in ventilating working areas with higher volumetric requirements and located at great depths.

3. Booster fan surveys and inspections

Personnel of the University of Utah and the Missouri University of Science and Technology conducted booster fan surveys and inspections in six underground coal mines, three in Australia and three in the United Kingdom. In these mines, booster fans are used regularly to overcome adverse conditions created by higher airway resistances and increased airflow requirements. In both countries, booster fans are installed after a period of review by the mines inspectorate, and their uses are justified through studies, and there is no other practical and economic way of ventilating planned production sections [6].

3.1 Surveys in British mines

During the inspection period, three of the five significant coal mines using booster fans were visited. All three mines are located near Rotherham, in South

Yorkshire. In these mines, booster fans are used to assist the main fans in overcoming high airway resistances. Both, axial and centrifugal types are used as booster fans. Figure 1 shows a schematic of a sample booster fan installation in a British coal mine with significant and airflow requirements. In this case, the workings are located at about 1,000 m below the surface, where the rock temperature reaches 42°C. In addition, the mine uses a substantial amount of water to control dust and to cool the mining machinery. The booster fan system consists of a single 1,500-kW axial fan installed in the main return airway, near the neutral point. The motor, also located in the return airway, is protected by a fireproof enclosure. The fan is equipped with a set of heavy duty airlock doors to reduce flow recirculation, and a system that monitors the operating condition of the fan. Because of high pressure differentials across the stoppings, four heavy duty airlock doors are used to isolate the fan from the intake entries. The factors that are monitored include differential pressure, air velocity, and bearing temperatures, to assess the fan operating conditions, methane and carbon monoxide concentrations, to detect the early stages of combustion. The fan system is designed to deliver 160 m³/s at 7.0 kPa pressure with the surface fans delivering 280 m³/s at 5.5 kPa. A site specific safe operating procedure is used to start and stop the fans and the mining machinery in by the fan. Although series ventilation is discouraged because of the high pressure differentials across the stoppings, some recirculation (< 10%) is allowed [7].

3.2 Surveys in Australian mines

In Australia, booster fans are used in the two coal mining states of New South Wales and Queensland. In both states, the installation of booster fans requires a thorough evaluation and risk analysis and a management plan demonstrating adoption of best practice that must be submitted to the state inspectorate for approvals.

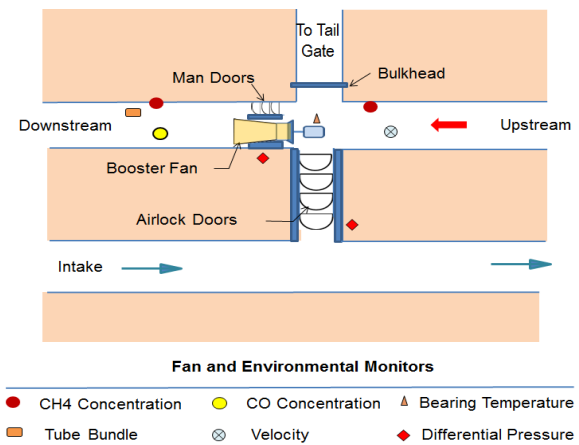


Fig 1. Typical booster fan installation in British coal mines

Before the use of any booster fan is considered, alternate options should be evaluated. Figure 2 shows a schematic of typical booster fan system in an Australian underground coal mine where the working areas are located at about 500 m below surface. The system consists of two double-inlet centrifugal fans, installed in concrete bulkheads in the main return airways. Each fan is equipped with heavy-duty airlock doors, barrier fences, and an environmental monitoring system. Because of regulatory restrictions, the fan motor is located in a specially designed, fire resistant chamber, which is ventilated with fresh air by two separately routed, 30-cm-diameter pipes. Double air-lock doors, designed to withstand high pressure differences, are used to allow machine access to the fan site and to minimize recirculation. The system is equipped with condition and environmental monitors located upstream and downstream of the booster fan and in the motor chamber. The factors that are monitored include methane and carbon monoxide concentrations, differential pressure, and air flow rate. The system is designed to deliver 300 m³/s at 3.0 kPa pressure, with the surface fans delivering 350 m³/s at 3.3 kPa. The fact that the surface fan capacities are larger than those of the booster fans reduces the possibility of flow recirculation.

Table 1. Use of booster fans in U.K. and Australian coal mines

Description	Australia	United Kingdom
Regulations	Coal mine operators are allowed to use booster fans to assist main fans in Australian mines (a)	Booster fans are accepted as safe and effective ventilation control devices in underground coal mines (b)
Reasons for using booster fans	Because of mine depths (± 500 m), remoteness of workings, and economic and environmental reasons	Because of mine depths (> 800 m) and increased resistance, to decrease effective mine resistance, and economic reasons
Basic Requirements	<ul style="list-style-type: none"> - Fan installation plan approved by Mine Inspectorate - Installed in concrete bulkhead - Multiple airlock doors - Set of fan controls and monitors - Safe operating procedure(SOP) for each fan - Maintenance every four months 	<ul style="list-style-type: none"> - Need demonstrated through studies to mine inspector, and results included in the ventilation plan - Installed in concrete bulkhead and equipped with airlock doors - Fan condition and environmental monitoring system - Fan examination every 30 min*
Number and type of booster fans	Single or double inlet centrifugal fans	Centrifugal and axial fans; if multiple axial fans used, each must be equipped with anti-reversal doors at discharge
Fan and motor locations	Booster fan in return airway Motor in a chamber ventilated with fresh air taken from an intake drift	Booster fan and motor both located in return airway. Motor enclosed in fireproof housing
Recirculation	Return air from one production district cannot be used in another production district and recirculation is not an accepted practice. Booster fans are generally located so that the return pressure outby the booster fan remains lower than the adjacent intake roadway.	Recirculation and series ventilation not prohibited; heavy duty airlock doors provided to reduce recirculation.
Fire Prevention	Possibility of fire is major design parameter; booster fans are equipped with CO sensors and alarms activated when TLVs are exceed.	Fan site (20 m upstream and 30 m downstream) maintained free from risk of fire Area equipped with CO and smoke sensors and fire suppression systems
Electrical Interlocking	Electrical interlocking between main and booster fans required	Electrical interlocking between main and booster fans not required
Risk Analysis	Each mine must develop and implement appropriate H&S management system, to ensure that risks are assessed and controls are in place at all times	No fan (not being an auxiliary fan) shall be installed at any place below ground unless the manager is satisfied that it is necessary to install it at that place for proper ventilation of the mine

*: Mine inspector has the power of exemption for all aspects of mining law.

- (a) Queensland: <http://www.legislation.qld.gov.au/LEGISLTN/CURRENT/C/CoalMinSHR01.pdf>
 New South Wales: <http://www.legislation.nsw.gov.au/maintop/view/inforce/subordleg+783+2006+cd+0+N>
- (b) United Kingdom: <http://www.legislation.gov.uk/uksi/1956/1764/made>

4. Design principles to avoid recirculation

Although improved ventilation efficiency and reduced leakage may result from the utilization of booster fans, the possibility of uncontrolled flow recirculation still exists. However, with a proper design and installation, and a reliable monitoring system, this problem can be eliminated or reduced substantially.

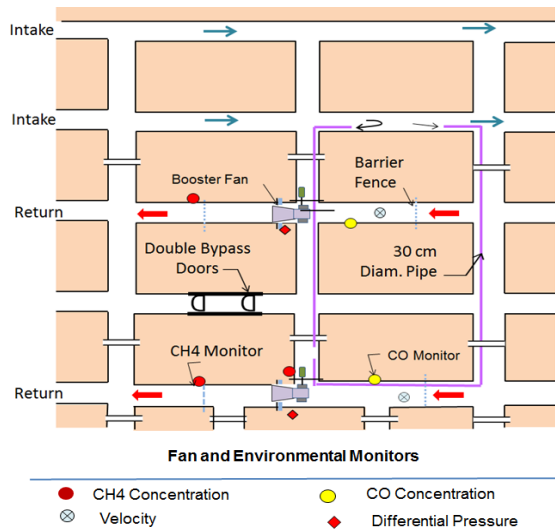


Fig 2. Typical booster fan installation in Australian coal mines

Proper design implies selecting the right fan, and installing it appropriately to ventilate a working district. The booster fan should be sized and sited to assist the main fan to redistribute the fan pressures in the mine efficiently and reduce the leakage quantity. This can be accomplished by selecting the fans adequately, such that booster fan pressure is always lower than the main fan pressure. The best combination of fan pressures can be determined by means of ventilation simulators such as Vnet-PC or by using Genetic Algorithm-based routines such as those developed by Lowndes [8] and Acuña [9]. Proper booster fan installation requires the fan to be installed in a concrete bulkhead, and equipped with airlock doors, and a fan monitoring and control system.

In most coal mining countries where booster fans are used, identification of hazards and risk assessment are part of the ventilation planning process [10]. Oversizing the booster fan, and installing inadequate doors or bulkheads are sample hazards that can be spotted during the planning stage, and fan system failure modes during the operation stage. Once the hazards are identified, they can then be evaluated and the outcomes are compared against the risk acceptance criteria established to this purpose. If requirements are not met, changes to the booster fan system should be made and the evaluation process repeated.

A good practice to avoid recirculation is to size and operate the booster fan at a pressure lower than the surface fan pressure. Another good practice is to equip

the booster fan with an electrical interlocking device to cut off the power to the booster fan in the event of main fan failure. If a booster fan fails for any reason, the equipment nearby must be de-energized and the airlock doors must open automatically.

4.1 Fan selection routines

The placement of booster fans in a mine ventilation network needs to be undertaken with care. The fans must be sized and placed so that the positive pressure added to the circuit does not lead to flow reversal in some cross-cuts and to the return of contaminated air to intake airways. The possibility of recirculation can be reduced by determining the best combination of fan pressures for a set of fan locations.

Currently, this combination is determined by trial and error by means of numerical simulators such as VnetPC, VUMA, and VentSim. For complex networks the process can be tedious and the optimal combination of fans never achieved. The alternative is to use smart programs such the one implemented by Lowndes [8] or the one developed by Shriwas [11]. The latter program, GVENT, combines the features of a set of genetic algorithms (Gas) developed by MIT, and a ventilation solver developed by Mine Ventilation Services, Inc. For any given ventilation network, this program generates randomly the entities of an initial population. In this case, an entity is represented by an array of fan locations and pressures, and a population by a set of entities and their corresponding attributes. Next, the program determines the flow distribution in the network, regulator resistances and the total airpower. These parameters are then evaluated against a fitness function and a set of practical constraints. For any population size, alternative solutions with positive regulator resistances are evaluated and the power function is minimized. This procedure is repeated until the global minimum is obtained. GA techniques can be used to approach the optimum solution of a ventilation network problem quickly and efficiently.

4.2 Fan installation and monitoring

A booster fan should be installed in a concrete bulkhead, in either intake or return airway, and equipped with a set of airlock doors and a monitoring system. To avoid recirculation, the fan should be equipped with at least two bypass ventilation doors, positioned near or next to the booster fan. These doors should be designed to open automatically should the booster fan stop. The monitoring system should include fan condition and environmental monitors, positioned to provide an early warning should abnormal conditions at the fan be detected.

Figure 3 shows a schematic of a booster fan system in a return airway. The fan, with its motor in a flame-proof enclosure, is installed in a concrete bulkhead. The system is equipped with a set of airlock doors to avoid flow recirculation, and a set of condition and environmental monitors to evaluate the health of the fan continuously. The factors to be monitored include (1) methane concentration, upstream and downstream from the fan, (2) carbon monoxide concentration, downstream, (3) air velocity, upstream, (4) differential pressure across the fan and door bulkheads, and (5) bearing temperatures.

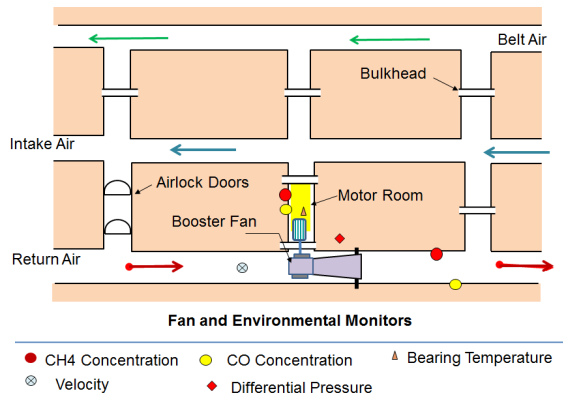


Fig. 3. Sample booster fan installation in a return airway

When the fan is switched on, the pressure on the delivery side is higher than on the intake side. The difference is the effective fan pressure added to the air stream. This pressure is used to increase the airflow rate in a working section. However, this requires airtight doors and bulkheads. Cracks in the bulkheads or poorly maintained airlock doors will allow leakage and recirculation, thus reducing the capacity of the fan. To overcome this problem, bulkheads should be sealed from the high pressure side and the doors affixed with rubber seals. The doors should be designed in such a way that they are always kept closed when the fan is running and open when the fan is down.

4.3 Electrical interlocking system

An interlocking system is a method of preventing the occurrence of any unsafe condition, which in a general sense can include any electrical, electronic, or mechanical problem in the mine ventilation system. The simplest example of fan interlocking is that if the main fan shuts off due to power failure or any other problem, the booster fan and all the mining equipment should automatically switch off to prevent any kind of flow recirculation in the mine. Most mines use electrical interlocking together with the atmospheric monitoring system (AMS), so that if high concentrations of gas are detected, electrical equipment downstream is de-

energized and the booster fans are disabled to allow flow through ventilation and prevent the recirculation of air contaminants.

Main and booster fans are operated as long as the workers are in an underground mine. The monitoring system measures all the relevant parameters including the concentrations of air contaminants. The booster fan is equipped with an interlocking device to cut off the power to the fan in the event of main fan failure. If a booster fan fails for any reason, the equipment nearby must be de-energized and the airlock doors must open automatically. This action is performed to prevent the build-up of air contaminants. If the main fan fails for any reason, the booster fan and all underground equipment must be de-energized. Under this condition, the whole system is down and an alarm must be generated. That alarm may be generated automatically or by a management procedure. Workers must be trained to understand that, in the instance of such an alarm, the mine's emergency evacuation procedure is initiated. A fan start-stop protocol is to be established to restore power after any power outage, including those scheduled for changing the fan duties.

5. Risk analysis

A booster fan, when properly sized and sited, can be used to decrease the main fan pressure, reduce leakage and power consumption. However, an inadequate installation can increase the likelihood of the buildup of air contaminants due to flow recirculation, and may lead to fires. In most coal mining countries, identification of hazards and risks associated with the operation of underground fans are part of the ventilation planning process. In the U.S., the regulations of the Mine Safety and Health Administration (MSHA) require mine operators to apply general hazard awareness and control in all operations, but do not require a comprehensive risk management program. This section summarizes the hazards associated with the usage of booster fans, the risk analysis tools and control measures to mitigate the risks to acceptable levels.

5.1 Hazard identification

When the ventilation plan includes the use of booster fans, the associated hazards should be identified in each of the following stages: mine planning and design, installation and commissioning, and operation. A summary of these is presented below [6, 10].

5.1.1. Planning and design

Potential hazards at this stage include:

Oversizing the booster fan. Oversizing the booster fan may lead to flow recirculation, which in turn can lead to the buildup of air contaminants at the working face.

Determining the best combination of main and booster fan pressures using ventilation simulators may reduce these hazards.

Inadequate monitoring system. Mine monitoring system components are subject to wear and tear and malfunction. They should be maintained regularly, and the sensors calibrated against primary standards. Furthermore, the system must be equipped with redundant units.

Poor design of airlock doors. Poorly installed airlock doors can lead to “struck by” and “caught between” type accidents. These doors should be designed and installed to operate at high pressure.

Installation and commissioning. Inadequate installation and commissioning of the fan may also lead to hazardous situations. Potential hazards include:

Misalignment of shafts. Misalignment can result in excessive vibration, shaft fatigue, and irregular bearing wear. This can act as a source of ignition and trigger a mine fire. Alignment tests must be conducted periodically and after any major repair.

Fan performance tests. During testing, the fan is usually operated under three different conditions: no load, half load, and full load. Parameters such as motor and bearing temperatures and vibration should be measured for each condition and the results compared against pre-set standards.

5.1.2. Operation

The potential hazards during this stage include:

Power Failure to the mine site. Power failure to mine site will result in the buildup of air contaminants and a reduction in the total quantity of air. Controls should be in place to de-energize the mining equipment and to reduce the gas emissions in the mine.

Failure of the main fan. The main fan can fail due to mechanical or electrical problems. If the booster fan is left running, uncontrolled recirculation can create unsafe conditions. To mitigate this hazard, the booster fan and all underground equipment must be de-energized immediately upon main fan failure.

Failure of the booster fan. As soon as booster fan failure is detected, the airlock doors must be opened and the quality of air at the workings re-evaluated. Although a booster fan stoppage reduces the quantity of air directed to a section, the opening of the doors will allow part of the air circulated by the main fan to reach the workings.

Failure of the monitoring system. Workplace assessment using faulty units can result in unsafe and unhealthy conditions. To avoid this problem, transducers should be calibrated frequently. Redundant units and

uninterruptable power supplies should be provided for critical monitors.

Failure of the fan motor or bearings. Motor and bearing temperatures are key indicators of the fan health. When the fan is installed properly, with the right alignment, these temperatures should never exceed the alarm level, which is typically 85°C.

Spontaneous combustion and fire. Although the likelihood of spontaneous combustion near the fan installation is low, it can occur in low rank coal mines, when the coal comes in contact with oxygen through the cracks around the periphery of the fan bulkhead. To control the problem the fan drift should be covered with inert material. An alternative is to install the fan in a drift driven in the overlying strata.

5.2 Risk assessment

Identification of potential hazards and evaluation of risks associated with utilization of booster fans are two major steps of risk assessment for the use of booster fans. If requirements are not met, changes to the system should be made and the process repeated. These are then compared against the risk acceptance criteria. A risk assessment team and a risk matrix are needed to determine the critical hazards.

5.2.1. Risk assessment team

Before any analysis, a team must be formed. The members must be familiar with the hazards to be investigated and capable of identifying the vulnerabilities of the process or facility, analyzing the results, and developing action plans to mitigate the consequences of failures.

5.2.2. Risk matrix

The risk matrix is an evaluation tool used to rank the risk of a potential hazard in terms of the likelihood (L) and consequence © of each of the undesired events. It increases the visibility of the risk and assists the management in making timely, informed decisions [12].

5.2.3. Risk assessment tools

There are number of techniques that can be used to analyze risks associate with the use of booster fans. These include: Workplace Risk Assessment and Control, Failure Mode Effective Analysis, Fault Tree Analysis, Bow Tie Analysis, Job Safety Analysis, and Safe Operating Procedures.

6. Conclusions

A booster fan system is a proven technology used in most coal mining countries including the United Kingdom, Australia, Poland, and South Africa.

However, in these countries, regulations require mine operators to develop a comprehensive ventilation plan showing the need of the booster fan, and that all critical hazards are identified, the risks are evaluated, and the control measures to mitigate these are in place.

A booster fan, when properly sized and sited, can be used to decrease the surface fan pressure, reduce leakage and reduce the total power consumption. However, when the fan is not sized, operated, or maintained properly, it can induce flow recirculation.

For practical reasons, a booster fan is usually installed in the return airway and is equipped with heavy duty airlock doors, condition and environmental monitors, and an electrical interlocking system to avoid flow recirculation in the event of surface fan failure.

As part of this study, six underground coal mines using booster fans were visited: three in Australia and three in the United Kingdom. In these mines, booster fans are used regularly to overcome adverse conditions created by higher airway resistances and increased airflow requirements.

A comparative evaluation of current U.K., and Australian regulations on booster fan usage shows some differences. While recirculation is not allowed in Australian mines, some recirculation of less than 10% is accepted in British mines. Another difference is that electrical interlocking between the main and booster fans is required in Australian mines, but not in British mines. In the U.K., redundant surface fans are used instead.

A monitoring system is a basic requirement for the usage of booster fans in coal mines. The factors to be monitored include (1) methane concentration, upstream and downstream from the fan, (2) carbon monoxide concentration, downstream, (3) air velocity, upstream, (4) differential pressure across the fan and door bulkheads, and (5) bearing temperatures.

Acknowledgements

The authors would like to acknowledge the National Institute for Occupational Safety and Health for providing financial support for this project.

We would like to express our gratitude to Gerrit Goodman and Howard Dale Bish of the NIOSH Office, Keith G. Wallace of Mine Ventilation Services, Inc., and Robert J. Leeming, Health and Safety Executive, Sheffield, S. Yorkshire, UK, for their support and advocacy in developing this project.

References

- [1] M.J. McPherson. Subsurface Ventilation. London: Chapman Hall (1993).
- [2] M. Ogle. The Design and installation of a booster fan at Tahmoor Colliery. Australian Mine Ventilation Conference, Sydney, NSW (2011).
- [3] Legislation, United Kingdom (2014)
<http://www.legislation.gov.uk/ukxi/1956/1764/made>
- [4] Legislation, Queensland (2014).
<http://www.legislation.qld.gov.au/LEGISLTN/CURRENT/C/CoalMinSHR01.pdf>
- [5] Legislation, New South Wales (2014)
<http://www.legislation.nsw.gov.au/maintop/view/inforce/subordleg+783+2006+cd+0+N>
- [6] F. Calizaya, and M.G. Nelson. Booster fans in Australia and British coal mines. *Proceedings of the 10th International Mine Ventilation Congress*. The Mine Ventilation Society of South Africa (2014).
- [7] J.R. Leeming, and D.J.T. Webb. Underground booster fans—Current UK practice for safe installation and management. *Proceedings of the 14th U.S./North American Mine Ventilation Symposium*. Edited by F. Calizaya and M.G. Nelson. Salt Lake City, UT: University of Utah, (2012)
- [8] I. S. Lowndes, and Z.Y. Yang. The application of GA optimization methods to the design of practical ventilation systems for multi-level metal mine operations. *Mining Technology (Trans. Inst. Min. Metal. A)*. March (2004) 43-57.
- [9] E.I. Acuña, R. Maynard, S. Hall, S. Hardcastle, G. Li, I.S. Lowndes, and A. Tonnos. Practical mine ventilation optimization based on genetic algorithms for free splitting networks. In *Proceedings of 13th United States/American Mine Ventilation Symposium*, Sudbury, Ontario, (2010), 379-385.
- [10] D. Benson. Use of booster fan ventilation at West Cliff Colliery. In Coal Operators' Conference, University of Wollongong, the AusIMM Illawarra Branch, NSW, Australia (2002).
- [11] M. Shriwas, *Application of genetic algorithms to determine the best combination of main and booster fans*. Ph.D. thesis. University of Utah, Salt Lake City, UT (2014).
- [12] J. Joy, Safety risk assessment process. Course notes, Mineral Industry Risk Management (MIRM), Modules I through V, University of Utah (2009).

Optimal Combination of Main and Booster Fans Pressure - Application of Genetic Algorithms

Mahesh Shriwas, Felipe Calizaya

University of Utah, Salt Lake City, Utah

One major challenge in the main and booster fan selection for a mine is to determine the optimal combination of fan pressures while minimizing airpower and eliminating the onset of flow recirculation. The solution can be achieved using commercial software packages by trial and error. But the process is very lengthy, and often the optimal solution is not found. Therefore, a new approach to solve the problem is required.

This paper presents a basic overview of genetic algorithm based fan selection program GVENT to solve the problem for two ventilation networks as case studies. This program combines the Genetic Algorithms (GAs) library functions developed by MIT and VnetPC program developed by MVS. The program uses the GAs routines to minimize the total airpower, to reduce leakage, and to prevent the onset of recirculation. To accomplish these objectives, the program requires a ventilation network, possible fan locations, and fixed quantity requirements and generates a solution with fan pressures, total airpower, and regulator resistances. This program was successfully used to optimize the combination of main and booster fan pressures for two ventilation networks to reduce total airpower. The solutions were compared with those generated using a commercial ventilation simulator and were found that these were within 5% of accuracy. Using this program, the solutions were generated faster with less human intervention than those generated by the simulator with trial and error.

Keywords: Genetic algorithms, GVENT, Fan Selection, Optimization

1. Introduction

The modern mining industry demands larger quantities of air to dilute the contaminants generated during the mining process. A main fan alone can serve the purpose of meeting the flow requirements of a mine, but often deep and extensive mines require high fan pressures. High pressure fans can result in “Caught in Between” type safety hazards while operating high pressure airlock doors. Furthermore, high pressure fans may result in excessive leakage through stopping and high power consumption. Alternatives such as sinking new shafts or widening existing airways are not always practical choices because they require heavy capital investment and several months of construction time. An effective alternative is to use booster fans in addition to main surface fans.

A booster fan is an underground ventilation device used to assist the main fan. An adequate utilization of this fan can reduce the main fan pressure, reduce leakage and consequently reduce the total power consumption. But, an inadequate selection or installation of the fan can induce flow recirculation. However the federal law prohibits the use of booster fans in a United States coal mine. But, they are widely used in other countries.

Current practice to determine the combination of main and booster fans is based on trial and error using a ventilation simulator and manual effort. Using this

method, fans of different sizes are tested on a trial-and-error basis until an acceptable solution is found [2, 3]. For complex networks with multiple fans, the process can be tedious and the optimal combination of fans may never be determined. To date, there is no single commercial program that can be used to determine the optimum combination of main and booster fan pressures that fulfills the flow requirements and minimizes the power consumption.

1.1 Fan Selection Problem

One major challenge of mine ventilation is to determine the optimal combination of main and booster fans which reduces the surface fan pressure and eliminating the onset of flow recirculation. The solution can be achieved using commercial software packages by trial and error. But the process is very lengthy, and often the optimal solution is not found. Therefore, a new approach to solve the problem is required.

A Genetic algorithm is a search heuristic that mimics the process of natural selection. The heuristic is routinely used to generate useful solution to optimization and search problems [7]. It is based on survival of fittest in which a better population is evolved in successive generation. Such algorithm based ventilation program, GVENT, has been developed and used to optimize the combination of main and booster fan pressures for two

ventilation networks. The convention search algorithm is based on trial and error method using any commercial ventilation software. The results obtained were compared with those generated using the VnetPC software. The main features of GVENT program along with sample applications to two ventilation network are presented in this paper.

1.2 GVENT Program

GVENT is a modular fan selection program that combines the features of a set of genetic algorithms and library function developed by MIT [8], and a ventilation solver (xyz.c) developed by Mine Ventilation Services, Inc [5]. The GAs library is used to generate a population of individuals represented by fan attributes, and the ventilation solver to determine the flow distribution in a given network [1, 4]. This program can be used to solve a complex ventilation network problem for the optimal combination of fan pressures. It requires a ventilation network, a set of airways with fixed flow requirements (working areas), fan locations, an objective function, and practical constraints. For a given network problem, an input file containing these parameters are first generated. Then the file is updated to include a set of GAs parameters. Upon execution, the program generates an output file showing the fan pressures, flow quantities, regulator resistances, and total airpower. These results are then evaluated against a fitness function and a set of practical constraints. In the process the power function is minimized and the optimal or near optimal solution is achieved. Essentially, the program consists of seven building blocks; a ventilation network, the GA

parameters, the GA routines, a ventilation simulator, a fitness function, the practical constraints, and an evaluation routine [6]. During each trial, a number of individuals are generated. The newly generated individuals are used to update the input file and to solve the network problem for fan duties, regulator resistances (R_R), leakage flow rates (Q_{SL}), and the total air power (AP).

One objective of this paper is to demonstrate the capability and utility of GVENT program by solving two network problems.

2. Network Problem 1

Figure 1 shows the ventilation network used to illustrate the major steps of this program. The network consists of 65 branches, 45 nodes, one surface main fan, one booster fan (when needed), six working areas, one return airway, and two intake airways. Table 1 shows the airflow requirements for six working areas. The problem is to determine the optimum operating pressure for the surface fan, if only one fan is used, and the optimum combination of main and booster fan pressures if two fans are used. In each case, the solution must satisfy the airflow requirements without causing any unwanted recirculation. The ventilation network is solved for the fan pressures and their corresponding airpower and regulator resistances, first using a ventilation simulator (VnetPC) and then using a GAs-based GVENT program. Two scenarios are considered: a single surface fan system, and a two-fan system that includes a booster fan for academic exercise.

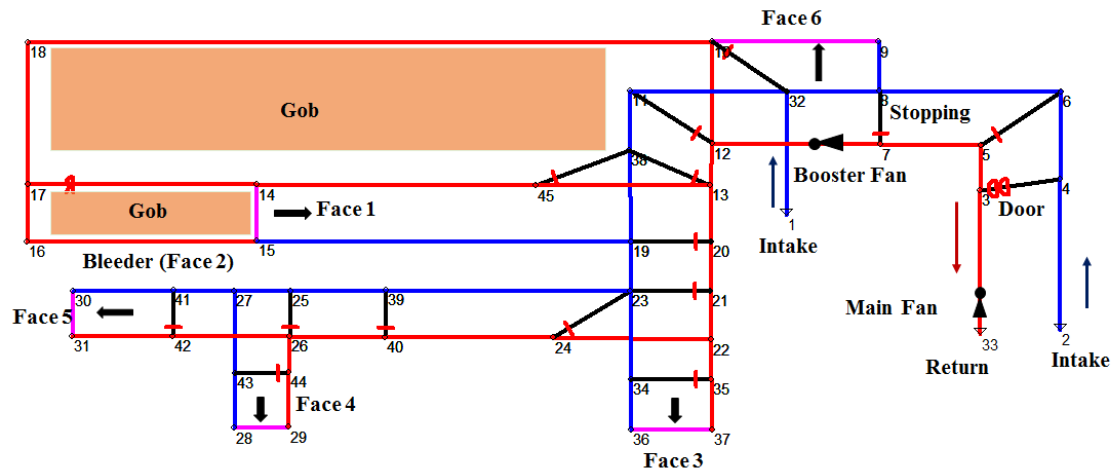


Fig 1. Sample network

Table 1. Flow requirements

Branch	Airflow m ³ /s	Working areas
15-14	47	Face 1
15-16	15	Face 2
36-37	40	Face 3
28-29	33	Face 4
30-31	33	Face 5
9-10	20	Face 6

2.1 VnetPC Approach

A network data file is first created in VnetPC and then solved iteratively for two ventilation scenarios: a) using a surface fan only and b) using two fans, one surface and one booster fan. In each case, the fan pressure is determined to satisfy the airflow requirements and minimize the power consumption.

2.2.1 Single-fan system

For this system, the network was solved in three steps. First, the fan pressure was initialized and the network solved for regulator resistances. Next, the regulator resistances were sorted, and then the critical branch (minimum resistance) was identified. If all the regulator resistances are positive, the trial pressure is decreased by a fixed amount (step size); otherwise, this pressure is increased. This procedure is repeated until the resistance of the critical branch is close to the predefined positive value (0.005 Ns²/m⁸). When this condition is satisfied, the optimal solution is found. Table 2 shows an optimal solution for the single fan system. A quick evaluation of Table 2 shows that a high-pressure fan (5.72 kPa) is needed to meet the total flow requirements (188 m³/s). Furthermore, at this pressure, a significant amount of fresh air (255 m³/s or 58% of total quantity) is short-circuited to surface (leakage flows) before reaching the workings.

Table 2. Optimal solution for single-fan system—VnetPC approach

Description	P, kPa	Q m ³ /s	AP kW	Total AP kW	Q _L m ³ /s
Main Fan	5.72	442.60	2532	2532	255

2.2.2 Two-fan system

In this case, the single-fan system was modified by adding a booster fan in the main return airway (branch 12-7 in Figure 1). The reason for choosing this location was to reduce the possibility of drastic changes in pressure at or near the working places when the booster fan was stopped. The operation of

the booster fan introduced a new dimension to the design problem. Now the major challenge is to determine the optimal combination of two fan pressures (main, and booster). In an attempt to solve the problem, the booster fan pressure was set at 200 Pa, and the main fan pressure was decreased successively from 5720 Pa to 3000 Pa to meet the flow requirements. The total air power for this combination was recorded. This procedure was repeated for other booster fan pressures in the 200–3000 Pa range while minimizing the main fan pressure. For each combination of main and booster fan pressures the total airpower was recorded.

Table 3 shows a summary of results for the two-fan system. In this case, the best combination of fan pressures was given by 2.63 kPa for the main fan and 2.60 kPa for the booster fan. Under these conditions, as compared to the single fan system, the quantity of air circulated through the system decreased from 443 m³/s to 399 m³/s, and the total power requirement decreased from 2532 kW to 2016 kW.

Table 3. Optimal solutions for two-fan system—VnetPC approach

Fan System	P kPa	Q m ³ /s	AP kW	Total AP kW	Q _L m ³ /s
Main Fan	2.630	399	1049	2016	211
Booster Fan	2.600	372	967		

An evaluation of results of these two scenarios (Table 2 and Table 3) shows that the two-fan system requires a lower pressure surface fan and lower total input power than the single-fan system. In addition, because of the lower fan pressure, the leakage quantity is reduced from 255 to 211 m³/s. These results show some of the benefits that can be gained by using booster fans in a ventilation system.

2.2 GVENT Approach

As in the previous section, to solve the sample network problem, two input files were created, one for the single-fan system and another for the two-fan system. In addition, based on trial tests and experience gained from other researchers [9], the following GAs parameters were chosen:

- population size: 100
- cross-over rate: 0.26
- mutation rate: 0.015
- number of generations: 30
- pressure range: 0 to 6 kPa

The reason for selecting a large population size and large number of generations was to enable the program to cover a wide range of alternatives for the proposed ventilation network, irrespective of the size and shape of the mine.

2.2.1 Single-fan system

In this system, first, the input file was updated to include GAs parameters, and then the GVENT program executed. GVENT randomly generated a population of fan pressures. In the process, for each trial fan pressure, a set of regulator resistances were determined. These were then evaluated. Only the trial pressures with positive regulator resistances were preserved and evaluated against the objective function (air power); the others were discarded. The process was repeated for all the individuals of the population. In each generation, to balance the population size, new individuals were generated and the evaluation procedure repeated until the optimal or near optimal solution was found. Table 4 shows a summary of results generated by this program for a single-fan network problem.

Table 4. Optimal solution for single-fan system—GVENT approach

Fan System	P kPa	Q m ³ /s	AP kW	Total AP kW	Q _L m ³ /s
Main Fan	5.722	442.66	2533	2533	255

2.2.2. Two-fan system

In this case, the GVENT randomly generate a population of pairs of fan pressures (one pressure for each fan). As in the previous text, the booster fan was placed in branch 12-7 (Figure 1). Once the input file was updated, the program was executed, and the results evaluated against the fitness function. The procedure of updating and solving the network for flow rates and regulator resistances was repeated for different individuals of a population and for different generations until an optimal or near optimal solution was found. Table 5 shows the optimal solution to the problem using this approach. The solutions were then checked for flow recirculation. However, no recirculation was found for the generated solution.

A quick evaluation of the results of the two scenarios (Table 4 and Table 5) shows that the two fan scenario yields lower surface fan pressure and total power requirement than the single fan scenario. These results are similar to those generated by the VnetPC simulator, but obtained rapidly.

Table 5. Optimal solutions for two-fan system—GVENT approach

Fan System	P kPa	Q m ³ /s	AP kW	Total AP kW	Q _L m ³ /s
Main Fan	2.65595	400.65	1064	2046	213
Booster Fan	2.62778	373.58	982		

2.3 Discussion

A comparison of results of the two approaches (VnetPC and GVENT) used to solve the same network problem for two fan system shows that the GVENT program was able to replicate the results generated by the VnetPC within an accuracy of 0.5% for flow rates rapidly. GVENT produced the optimal combination of fans pressure of 2.65 and 2.62 kPa at 2046 kW as compared to VnetPC result of 2.63 and 2.60 kPa at 2016 kW. Using VnetPC, these results were achieved after several trials and correlation studies, which in this case took about 3 days. Using the GVENT program, it took less than 1 hour to achieve practically the same results with very little manual involvement. The GVENT program is an efficient and effective fan selection tool. The results appears convincing and appealing for small network problems.

3. Network Problem 2

Figure 2 shows the ventilation schematic of the sample XYZ mine. This mine operates three working sections: one longwall and two continuous miner sections. The longwall panel is 305 m wide and 4800 m long. A 15-m slice of coal is removed from the panel each day. In addition to the longwall, this mine also operates two continuous miners in development headings, each with an advance rate of about 61 m per day. On the average, the mine produces about 22,000 tons of coal per day. The potential use of booster fan was demonstrated for academic exercise. In Figure 2, the encircled area shows the possible location for the booster fans in a network.

The mine is ventilated by a U-tube ventilation system made up of five main intake airways, and three exhaust shafts equipped with three surface fans. Fan 1 is used to ventilate the longwall gob, fan 2 to ventilate mined-out areas that are not sealed yet, and fan 3 to ventilate the three working sections. The surface fans, of exhaust type, are located in the following branches: 8-38, 236-237, and 70-239, respectively.

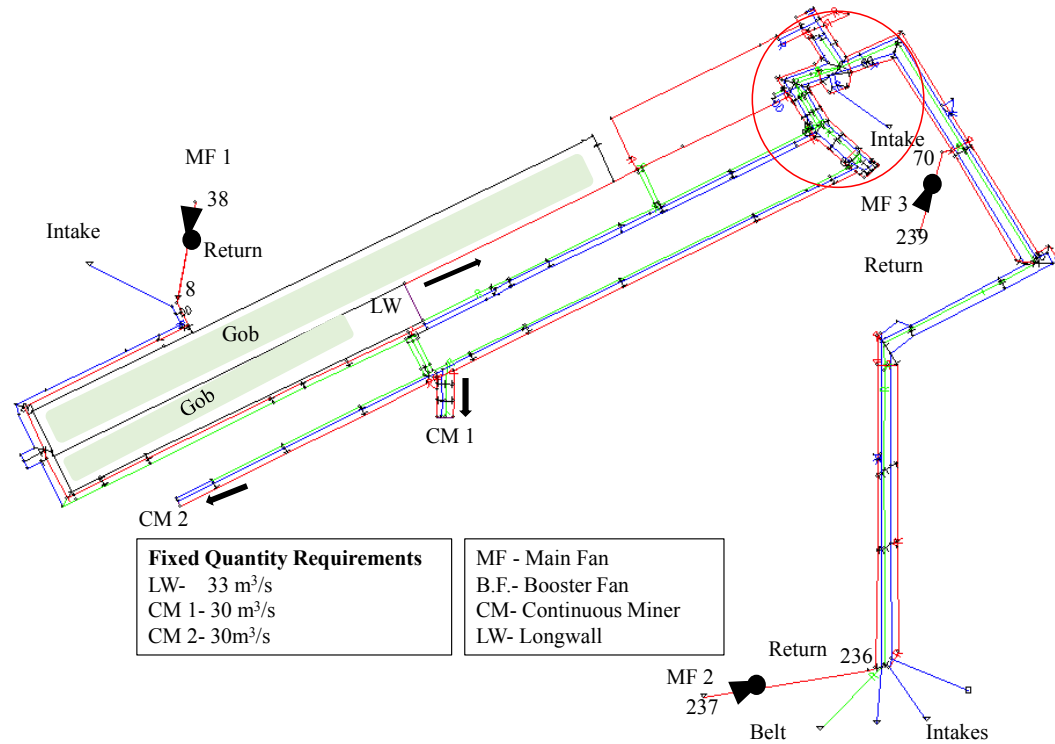


Fig 2 Coal mine ventilation network

Based on the coal strata characteristics and the mining methods used and assuming that the liberation of methane at each section is constant, the following airflow requirements were estimated: 33 m³/s for the longwall section and 30 m³/s for each continuous miner section as per the data provided by the mine. Table 6 shows details of the airflow requirements for each section.

Table 6 Airflow requirements for coal mine network

Working area	Airflow requirements m ³ /s
LW	33
CM1	30
CM2	30

The above quantities were determined based on the methane emission rates, coal production rates, and the threshold limit values stated in the *Code of Federal Regulations* (30CFR §75.321 1977). In the development sections the flow requirements were maintained at the main return, while in longwall panel, they were maintained at the tailgate.

Based on the mine ventilation network of Figure 2, and the flow requirements of Table 6, the problem is to determine the optimum combination of fan pressures that fulfills the flow requirements and

minimizes the total power consumption. The problem is to be investigated using the GVENT program for two fan configurations identified as Alternative A - using three surface fans only, and Alternative B - using three surface fans and two booster fans together. Although booster fans are not used in US coal mines, this alternative has been considered for this mine as an academic exercise to show the benefits that can be achieved by using booster fans.

3.1 GVENT Approach

As in previous section, the GVENT program was used to determine the optimum combination of fan pressures for each alternative. The process was started by creating an input data file, initializing the GAs parameters, and running the program. The solutions were then checked using the VnetPC program and examined for flow recirculation. The formulation details and the calculated fan pressures for each alternative are presented below.

3.1.1. Alternative A - Three surface fan system

In this case, the problem is to determine the optimum combination of three fan pressures that minimizes the total power requirement. The GVENT program was used to accomplish this objective. Prior to running the program, an input file for the network problem was created, and the GAs parameters initialized as explained earlier. These were then used to generate the initial population of fan pressures. These pressures together with the GAs were fed into the GVENT engine to determine the flow distribution in the network, regulator resistances and the power requirement. These results were then evaluated against a fitness function—the total airpower, and a set of constraints—the need to have positive regulator resistances for all fixed quantity branches. The main goal of this exercise was to determine the best combination of fan pressures for the network while satisfying the flow requirements and minimizing the total power consumption. Table 6 shows a summary of results for this problem.

Table 6. GVENT results -Three surface fan system

Fan	Br	P kPa	Q m ³ /s	AP kW	Total AP kW
1	8-38	1.50	26.20	39.33	1395
2	236-237	0.70	65.90	46.26	
3	70-239	3.72	352.11	1309.14	

An evaluation of the results shown in Table 6 shows that the airpower is optimized at 1395 kW when the three surface fans are rated at 1.50, 0.70, and 3.72 kPa, respectively. For these pressures, all the regulator resistances were positive, indicating that no additional booster fan is required; therefore, this is a feasible solution to the problem.

The fan pressures generated by the GVENT program were then checked for the flow recirculation. No unwanted recirculation loops were detected. Therefore, the results shown in Table 6 indeed represent the optimal solution to the problem.

3.1.2. Alternative B - Three surface and two booster fans system

In this case, the location of three surface fans and flow rate requirements remained unchanged. The booster fans were located in branches 5-150 and 171-159 respectively. Figure 3 shows the details of

booster fan locations for the mine ventilation network. Here again, the problem is to determine the optimal combination five fan pressure: three surface and two booster fans. The GVENT program was used to determine the fan pressure, to meet the air flow requirements and minimize the total air power.

Prior to running the GVENT program, an input file was created for the network problem, and the GAs parameters initialized as explained earlier. These were used to generate the initial population of fan pressures including the booster fans. These were used to determine the flow rates, regulator resistances, and the total airpower. These results were then evaluated against the same fitness function and constraints as in the previous cases. The main goal of this approach was to determine the optimum combination of fan pressures while satisfying the flow requirements and minimizing the total power consumption.

Table 7 shows a summary of key results generated by GVENT for this problem. An evaluation of these results shows that the airpower is optimized at 1186 kW, when the fan pressures are rated at 2.62, 1.33, and 2.67 kPa for the three surface fans and at 0.69 and 1.29 kPa for the two booster fans. Under these conditions, all regulator resistances were positive, indicating that no additional booster fans were needed.

Table 7. Summary of GVENT results - Three surface and two booster fan System

Fan	Br	P kPa	Q m ³ /s	A.P. kW	Total kW
MF-1	8-38	2.62	46.00	120.75	1186
MF-2	236-237	1.33	98.88	131.31	
MF-3	70-239	2.67	302.83	810.07	
BF-1	5-150	0.69	76.00	52.28	
BF-2	171-159	1.29	55.72	72.05	

To check the results for flow recirculation, the fan pressures generated by the GVENT program were again fed to the VnetPC simulator, and the network problem solved for flow rates and regulator resistances. The results were then evaluated for flow reversal and recirculation. No unwanted recirculation was found. Therefore, the results shown in Table 7 indeed represent the optimal solution to the problem.

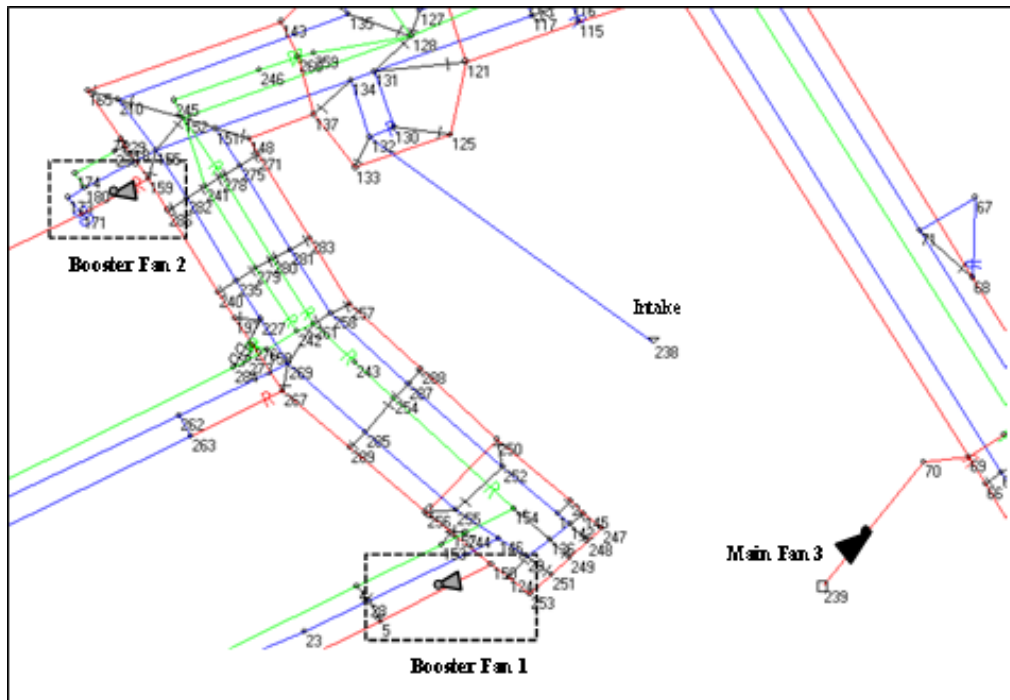


Fig. 3. Locations of booster fans in a coal mine ventilation network

3.2 Discussion

A comparison of the results generated by the GVENT program for the two ventilation scenarios (Table 6 and Table 7) shows that the five-fan scenario (three surface fans and two booster fans) yields a lower air power requirement than the three-surface-fan scenario (1186 kW vs. 1395 kW), resulting in a net savings of 209 kW. Furthermore, when five fans are used, the largest surface fan pressure decreased from 3.72 to 2.67 kPa. These results show two advantages that can be achieved by using booster fans in coal mines: (1) reducing the main fan pressures and (2) reducing the total power requirement. Further evaluation of the results did not detect any flow recirculation for either of the two ventilation scenarios. The complex network may have multiple fans including booster fans. The conventional method of determining the combination of fans pressure becomes tedious and difficult to achieve the optimal solution. Therefore, the GVENT program can be used to determine the optimal combination of fan pressures to complex network problems with multiple fans.

4. Conclusions

GVENT program has been used to determine the optimal combination of main and booster fan pressures

for two ventilation network systems. In the former, network problem 1, the solution converged at 2046 kW of total power, when the main and booster fans were used. The operating pressures of these fans were 2.655 kPa and 2.620kPa respectively. In latter, network problem 2, the solution to the problem converged at 1186 kW of total power, when three main surface fans and two booster fans. In both cases, the regulator resistances were minimized ($\geq 0.005 \text{ Ns}^2/\text{m}^8$). GVENT program is an efficient and effective fan selection tool that can be used to solve multi-fan ventilation network problems for fan duties faster than those based on ventilation simulators. Based on the two network problems, the results appear promising not only for one or two fan ventilation systems, but for real and complex ventilation network problems.

Acknowledgements

The authors would like to acknowledge the National Institute for Occupational Safety and Health for providing financial support for this project. The authors would also like to express our gratitude to Keith G. Wallace of Mine Ventilation Services, Inc., for his support in developing the GVENT program. We would also like to acknowledge the Mathew Wall of Massachusetts Institute of Technology for his open source of GAs Library.

References

- [1]. E.I. Acuña. Multiple period mine ventilation and fan selection optimization. Ph.D. dissertation, Laurentian University, Sudbury, ON (2010).
- [2]. F. Calizaya, M.J. McPherson, and P. Mousset-Jones. An algorithm for selecting the optimum of combination of main and booster fans in underground mines. In *Proceedings of the 3rd Mine Ventilation Symposium* (1987).
- [3]. F. Calizaya, M.J. McPherson, and P. Mousset-Jones. A computer program for selecting the optimum combination of fans and regulators in underground mines. In *Proceedings of the 4th International Mine Ventilation Congress* (1988)
- [4]. I.S. Lowndes, T. Fogarty, T., and Z.Y. Yang. Application of genetic algorithms to optimize the performance of a mine ventilation network: the influence of coding method and population size. *Soft Computing*, 9 (2005), 493–506.
- [5]. M.V.S. *VnetPC: A C++ program XYZ.c*. Clovis, CA: Mine Ventilation Services (2006)
- [6]. M. Shriwas. Application of genetic algorithm to determine the best combination of main and booster fans. Ph.D. dissertation, University of Utah, Salt Lake City, Utah (2014).
- [7]. M. Melanie. *An Introduction to Genetic Algorithms*. Cambridge, MA: MIT Press (1996).
- [8]. M. Wall. *GAlib: A C++ Library of Genetic Algorithm Component*. Library Function. Boston: Massachusetts Institute of Technology (1996).
- [9]. Z. Yang, I. Lowndes, and B. Denby. Application of genetic algorithm to the optimization of large mine ventilation network. *Trans Institute of min. and Metall. Sec A: Mine Industry* (1998b)

Appendix A

Appendix A shows the airway resistance of the network problem 2. This file is used to solve the networks. Table A.1 consists of five columns. Columns show branch ID, From Node, To Node, airway resistance, and remark (Description of Branch).

Table A.1. Airways resistance of network problem 1

From Node	To Node	Resistance Ns^2/m^8	From Node	To Node	Resistance Ns^2/m^8
7	5	0.006	2	4	0.09
6	8	0.006	32	11	0.0015
10	12	0.1	12	7	0.0015
1	32	0.006	11	12	6
3	33	0.006	5	3	0.0015
13	12	0.001	4	6	0.0015
20	13	0.001	18	10	0.0015
21	20	0.001	17	18	0.0015
22	21	0.001	23	39	0.04989
14	17	5	23	24	6
25	27	0.0015	35	22	0.01
24	22	0.0015	34	35	6
26	40	0.03488	34	36	0.05
4	3	6	37	35	0.01
6	5	6	36	37	0.25
8	7	6	23	34	0.0015
19	20	6	38	13	6
8	32	0.0015	11	38	0.001
30	31	0.25	38	19	0.002
16	17	0.0015	14	45	0.04821
15	16	1	39	25	0.03011
15	14	0.25	40	24	0.04512
28	29	0.25	39	40	6
25	26	6	41	30	0.00095
19	23	0.0015	42	26	0.00548
23	21	6	41	42	6
19	15	0.08	43	28	0.00057
8	9	0.08	44	26	0.00066
9	10	0.2	43	44	6
27	41	0.00055	45	13	0.01949
31	42	0.00481	38	45	6
27	43	0.00093	32	10	6
29	44	0.00084			

Appendix B

Appendix B shows the airway resistance of the network problem 2. This file is used to solve the networks. Table B.1 consists of five columns. Columns show branch ID, From Node, To Node, airway resistance, and remark (Description of Branch).

Table B.1. Airways resistance of network problem 2

ID	From	To	R (Ns ² /m ⁸)	Remarks	ID	From	To	R (Ns ² /m ⁸)	Remarks
1	72	87	0.00855	Intake	288	156	93	0.0572	Return
2	92	87	0.00058	Intake	349	142	145	8530.39	Stopping
3	102	95	212.42	Stopping	368	169	294	0.00645	Fixed Q
6	94	95	0.15701	Belt	379	186	176	0.00622	Intake
8	92	95	195.66	Stopping	388	192	191	341.2157	Stopping
18	95	97	0.17816	Belt	394	189	215	0.01496	Fixed Q
29	90	84	41.0190	Stopping	416	211	212	161.77	Seals
63	53	51	37.73	Door	427	220	219	0.16574	Fixed Q
66	53	52	2292.515	Stopping	428	223	224	0.00179	Intake
101	116	117	156.53	Door	430	226	164	0.018	Fixed Q
113	121	126	1.63417	Overcast	489	266	221	0.01312	Belt
158	231	232	0.19225	Belt	493	290	291	0.24425	Fixed Q
164	236	237	0.00011	Fan 1	501	41	43	44.732	Stopping
166	70	239	0.00011	Fan 2	520	288	257	0.02055	Return
273	8	38	0.14775	Fan 3	523	256	289	0.02114	Return
274	93	76	161.77328	Seals	524	285	289	44.732	Stopping

Mine Heating and Cooling

Liquefied Natural Gas as a Mine Intake Air Heating Fuel

Ian M. Loomis¹, Mark Ramirez²

¹Amec Foster Wheeler, Denver, CO, USA

Heating of mine intake air in northern temperate, sub-arctic and arctic environments is often done where there is a requirement to prevent freezing conditions in the mine intake airways and shafts. These mines can be in remote locations with limited access and/or limited options. There is a variety of heating system fuels available for use, each with particular benefits and limitations. A recent review of fuel systems has indicated the potential that exists for liquefied natural gas to be considered as a mine intake air heating fuel of choice. While the infrastructure required to support full scale adoption of liquefied natural gas remains nascent, the fuel does offer benefits where it is available to be trucked to the mine site. Application of a liquefied natural gas fuel system has the potential to make use of the high energy density, low base cost of natural gas and the high efficiency of direct fire combustion; while avoiding the cost of a new delivery pipeline.

Keywords: intake, heating, natural gas, liquefied, ventilation.

1. Introduction

The use of intake air heating at mines in northern temperate, sub-arctic and arctic environments is an established practice generally applied to prevent the freezing of water in mine utility lines and within ventilation intake shafts, adits and ramps. Additionally, this provides safe work conditions for personnel travelling and working in the direct intakes. While the target intake temperatures may vary, an intake temperature just above the freezing point of water is often selected. Depending on a number of factors including the mine location and access to and cost of fuels the approach to heating mine air is very site specific. Terkovic and Kwant [1] recently provided a review of the primary methods of mine intake air heating and fuels applications.

1.1 Mine Intake Air Heating Systems

Mine intake air heating systems fall into two basic categories, direct and indirect heating. In a direct heating system heat is added directly to the intake air from the fuel. The example of this is natural gas or propane burners placed directly within the intake airflow. This is allowable due to the clean burning nature of the fuels. (CO monitoring systems are generally required to ensure that the systems are not creating a potentially hazardous intake.) Since the heat is added directly from the fuel to the air, these systems have a very high thermal efficiency.

Alternatively, an indirect system using some form of heat-exchanger/radiator is used when it is not practical to directly heat the air. These systems are generally either an air-to-air or a liquid-to-air type of heat exchange. Indirect systems suffer from efficiency losses due the nature of the systems and “re-handling” of the heat. However, indirect systems do allow for the use of alternate heat sources that may be readily available such as geothermal heat or power plant waste heat.

1.2 Mine Intake Air Heating Fuels

Fuels used for mine air heating vary widely depending on the location of the use and the access to available fuel sources. Typical fuel/energy sources include:

Geothermal –Where available, the use of geothermal heat can be applied through an indirect radiator system.

Power plant waste heat –At remote sites using generators, the reject heat can be a significant source of energy that can be allocated to providing overall site heat. In the event that sufficient energy is available this waste heat can be applied in part or in full to intake air heating.

Electricity – Electricity provides a heating option that may be available at many mine sites if low-cost electrical power is available and the mine’s electrical distribution system is sized to handle the high load demand of air heating. This may be the option of choice for mines with poor overland/road access but that are serviced by major electrical transmission lines.

Diesel fuel – Most mine sites will rely on diesel fuel for powering their equipment fleets so this is a readily available fuel source for an indirect air heating system. Since the cost per unit of heat is relatively high for diesel fuel it may not prove cost effective where alternatives are available.

Propane – In relatively remote locations propane provides a fuel that is reasonably easy to transport and store as a liquid and can be used in direct-fire heating system. The fuel is subject to delivery schedules and on-site storage. However, the fuel and the aspects of its storage and usage is well understood.

Natural Gas –Where the mine is relatively close to the natural gas distribution infrastructure, natural gas is used as a fuel for mine air heating. When used, natural gas is generally taken directly from the pipeline without storage at the site.

Table 1 shows an example of relative direct costs for the various fuels and does not include the relative delivery charges. While the relation between the costs will vary with respect to variations in the overall economic climate, the relative ranking is likely to be consistent. Given the very low relative cost of natural gas, this would appear to be the obvious fuel of choice, however, if a pipeline sized to meet the peak heating demand must also be provided that may add substantially to the effective delivered cost whether the mine chooses to own the pipeline or pay a service fee to the utility to provide the line. Furthermore, a mine may find that it is placed on an “interruptible” service

program in which their gas supply may be curtailed by the utility to meet other needs at high-demand/extreme cold conditions.

Table 1 – Typical heat cost comparison

Fuel	\$/unit	\$/MMBtu
Natural Gas (NG) [2]	\$5.00/MMBtu	5.00
Liquefied NG [3]	\$10.45/MMBtu	10.45
Electricity (major utility) [4]	\$0.045/kW□hr	13.18
Propane (LPG) [5]	\$2.00/gal	22.00
Diesel Fuel [6]	\$3.20/gal	24.38

Table is direct cost of fuel only (not including efficiency losses.)

Alternatively, if a source of liquefied natural gas (LNG) is reasonably available then it could be given consideration as the fuel of choice. The ability to make use of LNG relies on a number of factors, including: source of liquefied gas, transportation, storage, safety.

Where suitable conditions can be met, it appears that LNG can offer a viable mine heating fuel.

2. Options for Liquefied Natural Gas

Like other liquid fuels, such as diesel fuel and propane, LNG can be transported on-the-road using tanker trucks and it can be stored in above ground tanks similar to propane. See Figure 1. For use in direct-fired heating, LNG would need to be converted back to a gas phase and, then, would be used identically to pipeline supplied natural gas. Thus, the overall model for distribution and consumption of LNG is functionally identical to fuels that are already familiar.

Currently, a limiting factor for use of LNG as a mine heating fuel is its availability. However, the use of LNG as a fuel source is being pushed such that its application in railroads and shipping may prove to be a catalyst that makes the fuel more readily available.

Where it is available, LNG can be transported on the road using production transport trailers as a “virtual pipeline” between source location and the mine storage site. Compared to compressed natural gas (CNG), LNG systems transport/store approximately 2.5 times the fuel on a volumetric basis. Hence, a delivery schedule requiring 12 CNG tankers per day would be accomplished with about 5 LNG tankers per day.

3. Liquefied Natural Gas Marketing

Sourcing of LNG is a critical component of the potential to make use of this fuel. Within the United States there are a limited number of natural gas liquefaction plants that would be capable of providing commercial LNG. Hence, the distance that the fuel must be transported from a source point to a mine site will have a key role in the viability of this approach.

Use for mine air heating may prove to be a relatively small portion of a larger conversion to LNG as a fuel type. Two major uses appear to be on the horizon within the United States and Canada. Reductions in the allowable emissions from locomotives is leading to the consideration of LNG as a rail transportation fuel [7, 8].

Additionally, there are considerations for LNG to become a fuel for freighters on major North American waterways [9]. In order to be viable, both of these approaches appear to require the common availability of LNG.

Given the expectation that a mine will require the average delivery of several tanker loads per day, it is unlikely that the efficient transportation distance would exceed ~150 miles, or the distance of single round-trip per “shift” for each tanker. This means that in order to be an effective fuel source, either a source of LNG must be found or created within that radius.

Even a small to medium sized liquefaction plant, on the order of 100,000 gallons per day, is substantially larger than a mine would require. It is unlikely that a facility could be built to support just the needs of a single mine. A similar situation was seen in Colorado, where Noble Energy planned a liquefaction plant to support the needs of their drilling and other heavy equipment. To support their case, the excess capacity of the plant would be made available to other local users [10]. For the case of a mine user, there may be similar justification to support the construction of a plant rather than supporting the construction of a new, dedicated pipeline to the mine site.

In estimating the cost of LNG, one must consider the following elements: commercial price of the gas with pipeline service charges, liquefaction costs and additional transportation costs. By applying the fuel prices in table 1, an LNG delivered cost of \$11.95 per MMBtu (\$10.45/MMBtu + \$1.50/MMBtu-delivery [11]) would be approximately \$1.01 per gallon. Diesel fuel has a volumetric energy density about 62% higher than LNG, so this would be roughly equivalent on an energy basis to diesel fuel delivered at \$1.62 per gallon.

4. Liquefied Natural Gas Storage and Safety

On-site storage of LNG is a well-established practice that cryogenically maintains the liquid at a low temperature under relatively low pressure. In on-site storage tanks, LNG is typically maintained as a liquid at about -162 °C at approximately 414 kPa. Considering LNG for use as fuel for water-borne shipping, a major fuel company considers “LNG as a fuel with no more of a risk than any of the conventional fuels” [4].

Large, multi-tank storage systems are available for liquid fuel systems (LNG, LPG and diesel fuel) that allow for the storage of as much supply as is required. For a typical mine site, the storage would be based on the real and perceived risks associated with the fuel supply at the source and the ability to transport the fuel to the site. For a very remote site with limited access, the mine operations may require a full season’s worth of fuel storage whereas a less remote mine site with year-round road access may only require several days’ worth of fuel on hand to cover the peak demand periods and the potential for the access road to be closed due to weather. For a typical situation where year-round road access is expected the overall delivery, storage and usage profile for fuel may be represented as illustrated in Figure 2.

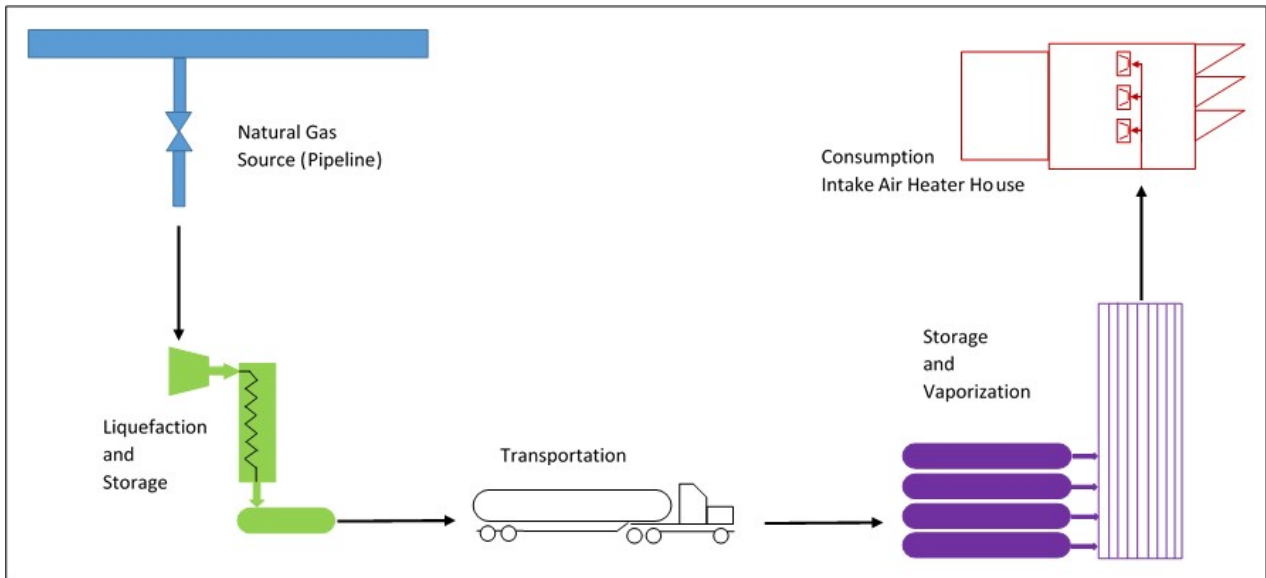


Figure 1: Representative LNG Cycle

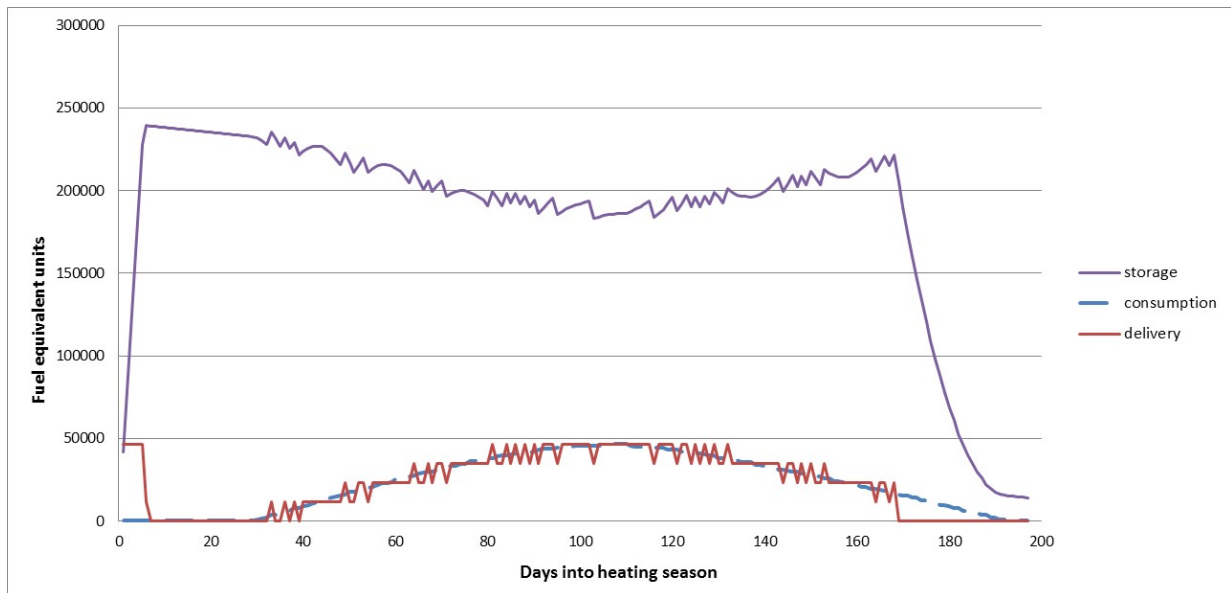


Figure 2: Hypothetical LNG fuel delivery, storage and consumption profile.

Table 2: Fuel type comparisons

	Complexity/ Capital Cost	Fuel Cost	Transportation	Supply/Storage	Source	Additional Risks	Limiting factors
Pipeline Natural Gas	Relatively low on burner systems, capital low if pipeline not included	Lowest direct cost	Pipeline, sized for peak usage (high cost)	Interruptible contract, None – CNG backup possible	Major pipeline or utility pipeline	-	Pipeline and service cost, interruptible nature
Compressed Natural Gas	Relatively low on burner systems, compressed gas storage systems add complexity and cost	low	Compressed gas tanker Limited haul distance	Could have several days backup supply in compressed gas tank farm	Compressor station tied to major pipeline or utility pipeline	-	Required delivery frequency
Liquefied Natural Gas	Relatively low on burner systems, liquid gas storage systems add complexity and cost	Medium (due to liquefaction charges)	LNG Tankers from liquefaction plant Limited haul distance	Could have several days backup supply on hand in LNG tank farm and vaporizers	Liquefaction plant at source or major pipeline	Perception of danger, system complexity	Transportation distance, storage loss

Propane	Relatively low on burner systems, liquid gas storage systems add complexity and cost	High	LPG tankers from various sources Limited haul distances	Could have several days backup supply on hand LPG tank farm and vaporizers	Common fuel from various suppliers	High density vapor from tank leaks, system complexity	Cost
Electricity	Electrical controls and load center capital cost high relative to gas	Medium to high	Primary distribution lines to site, sized for peak usage	None or backup generators (NG/LPG or diesel)	Major utility	System control complexity	Service capacity requirements, interruptible nature, cost
Diesel fuel	Moderate to high capital, complexity depends on system type (air-to-air or glycol-to-air)	High	Fuel transport tankers, supplementing normal diesel fuel deliveries	Could have several days backup supply on hand in diesel fuel tanks	Common fuel from various suppliers	Environmental containment or cleanup of spill, complexity of system	Cost, system inefficiency, emissions

5. Benefits and Limitations of Liquefied Natural Gas

As with any of the heating fuel/energy sources, the viability of LNG as a fuel may be highly dependent on the site location and site conditions. When considering a green fields site that does not have an established natural gas pipeline, an alternative to the capital investment of a physical pipeline may be the development of a “virtual” pipeline to transport LNG from a liquefaction plant to storage tanks at the mine site. By taking this approach, certain costs associated with the pipeline, such as procuring an appropriate right-of-way, capacity limitations and interruptible service contracts may be eliminated while maintaining the overall cost benefits of the natural gas.

However, considering LNG as a fuel does require specialized infrastructure on the mine site, whether owned/operated by the mine or the fuel company, which would not necessarily be associated with pipeline delivery of natural gas or transmission line electrical power. Such storage infrastructure is also required for other fuel alternatives (CNG, LPG and diesel fuel). With LNG storage there are certain associated losses including those of evaporation necessary to maintain the cryogenic state and those that occur during the process of cooling the storage tanks during the initial filling each season if the tanks are allowed to empty.

A comparison of several parameters associated with each of fuels discussed here is given in Table 2 below. This comparison is based on the consideration of the fuels as the sole fuel.

6. Conclusions

The consideration of LNG as a mine intake air heating fuel should take into account the following:

- It is based on using an established clean-burning fuel, NG, that can be applied in a direct fire use.
- If the LNG source is within a reasonable distance, the establishment of a virtual pipeline with on-site storage may be more cost effective than constructing a new natural gas pipeline or upgrading the capacity of an existing one.
- Storage and on-site vaporization, while specialized to a cryogenic system, is consistent with storage of other fuels.

The various fuel sources may or may not share common price pressures, so over the course of a mine life price volatility may alter the apparent benefit of the fuel decision. Thus an awareness of the project’s sensitivity to individual fuel costs is imperative as is an awareness of the individual fuel price cycles and projections for the life of the mine in question.

The cost and handling of the heating fuel/energy is an element in the larger consideration process of specifying a mine intake air heating system and therefore does not constitute the single element of a decision to proceed with one approach over others. However, the current trend in energy sources in North America appears to indicate that for mines currently under consideration for development and operation LNG is worth considering as an intake air heating fuel.

References

- [1] P.J. Terkovics and B.H. Kwant “Heating of mine ventilation air”, *Proceedings, 10th International Mine Ventilation Congress*, 2014, Sun City, South Africa, pp 11-17.
- [2] 2013 data from reference project data sheet. See also EIA city gate price average July 2012 through June 2013 = \$4.94/MMBtu.
- [3] LNG price built-up from city gate price plus service and liquefaction costs based on discussion with NG/LNG supplier regional with reference project.
- [4] 2013 data from reference project data sheet. See also EIA, Electric power monthly, April 2013.
- [5] 2013 data from reference project data sheet. See also EIA, commercial price data from 2011 (latest available) ~\$1.94/gal in respective market.
- [6] 2013 data from reference project data sheet. See also EIA, retail price for No. 2 Diesel fuel ~\$3.03/gal (2011-latest available) in respective market.
- [7] W. Pentland “Railroads Look At Liquefied Natural Gas”, *Forbes*, January 29, 2014, retrieved from <http://www.forbes.com/sites/williampentland/2014/01/29/railroads-look-at-liquefied-natural-gas/> on 3/20/2015.
- [8] B. Tita “First Steam, Then Diesel. Will LNG Be Next to Power the Railroads?”, *The Wall Street Journal*, November 27, 2013, retrieved from <http://blogs.wsj.com/corporate-intelligence/2013/11/27/first-steam-then-diesel-will-Ing-be-next-to-power-the-railway/> on 3/20/2015.
- [9] N. Vanderklippe “Shell aims to fuel Great Lakes freighters

with liquefied natural gas”, *The Globe and Mail*, March 4, 2013, retrieved from <http://www.theglobeandmail.com/report-on-business/industry-news/energy-and-resources/shell-aims-to-fuel-great-lakes-freighters-with-liquefied-natural-gas/article9282660/> on 3/20/2015

- [10] C. Procter “Noble Energy to build Colorado’s first LNG plant”, *Denver Business Journal*, March 21, 2013, retrieved from http://www.bizjournals.com/denver/blog/earth_to_power/2013/03/noble-energy-to-build-colorados-first.html on 3/10/2015.
- [11] Estimated from “maximum practical haulage distance” using dedicated carrier. Compare European study 200 km delivery ~\$1.70 per MMBtu - <http://www.climatetechwiki.org/technology/lng>.

Disclaimer: The opinions expressed in this paper are solely those of the authors and are not the opinions of Amec Foster Wheeler. This material is intended for personal and non-commercial use only. Any other use of this material requires the authors’ prior written consent.

Conveyor Tunnel Airflow Requirement Update Based on Heat Exchange for the New Level Mine Project

Claudio Montecinos^a, Enrique I. Acuña^b, Keith G. Wallace^c

^aSKM, Santiago Chile

^bProyecto Nuevo Nivel Mina, CODELCO, Rancagua, Chile

^cMine Ventilation Services, Inc., Clovis, California USA

The New Mine Level Project (NMLP) is the future underground expansion of the El Teniente mine. This mine is near the city of Rancagua, Chile. The daily production rate is expected to be between 137 kt/d and a maximum of 180 kt/d, with production planned to start at the end of 2020 or early 2021. As part of the NMLP, two main tunnels are being constructed, one for personnel and supply transportation (TAP) and a second one for ore haulage by a belt conveyor system (TC) to bring the ore from the mine to surface. The airflow requirement of the two tunnels were estimated during the prefeasibility engineering phase and only the requirement of the TAP tunnel was updated in this phase of detail engineering according to the available information of diesel vehicle fleet and expected air velocities in the tunnel. This paper presents the findings of a recent study to update the airflow requirement of the TC tunnel based on the velocity range that minimizes dust pick up from the belt becoming airborne and to maintain the air temperature in a reasonable range according to Chilean law. The updated airflow requirement and power demand is compared to the results of the previous engineering phase in terms of magnitude and operational point of the main fans dedicated to the tunnels. A proposed design modification for the ventilation of the tunnel Conveyor N° 2 and 3, which are part of the ore haulage system, is also presented.

Keywords: Mine ventilation design, heat load calculations

1. Introduction

The New Mine Level Project consists of a new block cave mine being developed below the existing El Teniente mine. The mine is operated by the state run company CODELCO. The planned production rate may be as high as 180 kt/d over a ramp up period of about 10 years. The mine will use mechanized methods to move the ore from the draw points to the ore passes. The production level will be at the 1862 masl elevation. Ore passes, approximately 54 m in length, will send the ore to truck loading chutes on the haulage level located at an elevation of 1808 masl. The trucks will dump at one of three identical crushing plants located in the center of the ore body. The primary crushing plants will feed the ore to the 2m wide Conveyor N° 1 that is designed to operate at 6 m/sec and has a capacity of 12,280 t/h. Conveyor N° 1 runs in a nearly 9 km long tunnel which reaches the surface at the Coya river canyon on a specially excavated platform at elevation 1496 masl. At this location, a primary transfer station (Station N°1) is located. The conveyor has a horizontal length of 8,855 m, running down slope at 2%. The elevation difference over the tunnel length is 177.1 m. The conveyor will be driven by two 2.5 MW directly coupled synchronous motors.

At Station N° 1 the ore is transferred from Conveyor N° 1 to Conveyor N° 2 which has a horizontal length of 962.8 m and slopes upward 212.4 m with a maximum slope of 13.5 degrees. Conveyor N° 2 will be driven by four 2.5 MW directly coupled synchronous motors. This conveyor crosses the river and through a tunnel ending on a higher platform at an elevation of 1699.2 m. Transfer Station N° 2 is located at the end of Conveyor N° 2 and transfers the ore to Conveyor N° 3. This conveyor has a horizontal length of 1129.4 m and slopes upward a vertical distance of 213.5 m with a maximum slope of 12.5 degrees. The conveyor will be driven by four 2.5 MW directly coupled synchronous motors.

Conveyor N° 3 has a pant leg chute at his discharge where Transfer Station N° 3 is located. This chute allows for diverting the ore to a future stockpile or to the different processing plants of the concentrator.

Conveyor N° 1 of the project will be supplied with a Low Rolling Resistance (LRR) belt bottom cover and on all idlers of the system in order to reduce belt friction. The power demand estimated for Conveyor N° 1 is only 631 kW at full load since it will operate downhill and gravity will assist in moving the ore. The conveyor motors are primarily sized to be able to start the conveyor. Stopping the conveyor will be by an electro dynamic motor generation. The predicted heat dissipated by the conveyor is 6540 kW giving a per unit length rate of $q = 0.74$ kW/m. For Conveyors N° 2 and 3 the power demand is 8607 kW and 8766 kW giving a per unit length rate 1.44 & 1.35 kW/m, respectively.

The tunnel of Conveyor N° 1 has two ventilation adits one called P-500 and the other P-4600 which divide the tunnel into three separate ventilation sections. These adits were built for the construction of the conveyor tunnel and to divide the airflow in the tunnel in the event of a tunnel fire. P-500 has a length of 2.5km with P-4600 having a length of 2 km. The P-500 will be used as air intake and P-4600 will be an exhaust. The sections from the tunnel of Conveyor N° 1 are described from surface portal to the inner mine as: Portal – P500, P500 – P4600, P4600 – Inner mine end. A scheme of the N°1 conveyor tunnel (TC), the personnel and supply transportation tunnel (TAP), and the two access ramps is shown in Figure 1.

The purpose of the ventilation study described in this paper is to define the minimum air requirements of the three tunnel segments of the Conveyor N° 1 to keep acceptable environmental conditions considering the high energy dissipation of the conveyors. In addition, the natural ventilation effects to ventilate Conveyors N° 2 are described.

2. Results of the previous engineering phase and TAP airflow update

The airflow requirements of the two main tunnels TAP and TC were initially estimated during a prefeasibility engineering phase. Detail engineering studies resulted in the airflow requirement of the TAP tunnel being updated according to new information on

the diesel vehicles fleet and expected air velocities in the tunnel to maintain a flow to assist in dust control. Figure 1 represents the prefeasibility engineering phase and Figure 2 presents the results considering TAP updated requirements.

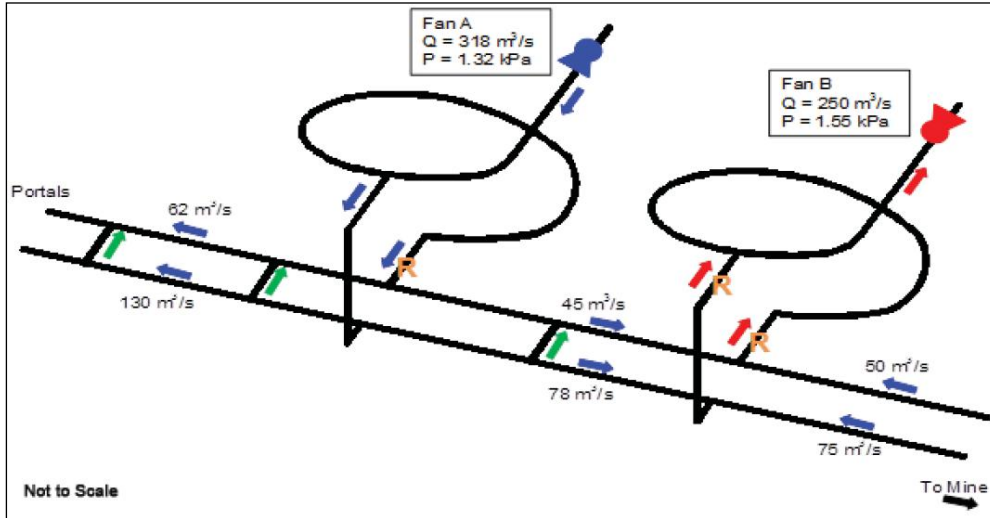


Fig. 1. Schematic of TAP and TC tunnels (original engineering Phase).

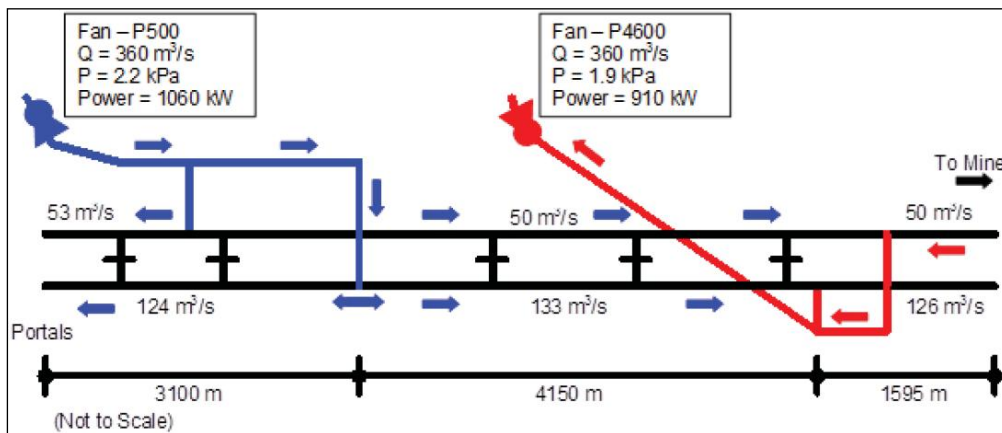


Fig. 2. Schematic of TAP and TC tunnels (TAP updated requirements).

Table 1 presents the expected airflow velocities in each of the three sections of the conveyor tunnel (TC) as a result of the updated requirements of the TAP tunnel study. As can be observed in Table 1, the three sections have almost the same air velocity, slightly over 1 m/s.

A result of the TAP detailed engineering update was the power increase required to move the airflow through both TAP and TC tunnels went from 1,075 kW to 1,970 kW. One of the main concerns of this study for the TC tunnel was to hopefully validate that the current airflow velocities in the tunnel while maintaining acceptable environmental conditions through each tunnel segment.

Table 1. Airflow, area and velocity for each section of TC tunnel

TC sections	Airflow (m³/s)	Area (m²)	Velocity (m/s)
Portal - P500	53	46.3	1.14
P500 - P4600	50	46.3	1.08
P4600 - Mine inner end	50	46.3	1.08

3. Heat exchange model

For this study, a heat exchange model was developed to compute the heat loads in the tunnel and predict the air temperatures within the three tunnel segments. The goal of the study was to predict the tunnel temperatures and determine if they will meet Chilean law requirements.

In the Conveyors N° 2 and 3 tunnels (outside the mine) airflow will occur by natural ventilation generated by the difference in height between the tunnel inlet and outlet. In addition, conveyor and transfer station heat will cause the air to rise in these tunnels also inducing flow.

For the conveyor tunnels the thermal model needs to consider the heat transfer that will occur from the air to/from the rock and from the conveyor to the air. Because the New Level Mine is at elevation (side of a mountain), the natural rock temperatures are not excessive. Furthermore, ore from the mine is also not expected to be a heat source. For this study this phenomenon has a much larger inertia (hours) in comparison to the air heating by the energy dissipated by the conveyors during the short traveling time in the tunnel (minutes). The strata heat sink/source helps to stabilize the air temperature inside the tunnels. For this reason during the time elapsed from the air inlet to the tunnel and the discharge at the other end the heat flow to or from the wall is assumed to be constant. This allows simplifying the model by applying a steady heat flow to the wall reducing it to a one-dimensional problem along the tunnel. With the model the heat flow to the wall is analyzed for different instances of time to see its effect on the air.

The temperature and the absolute humidity of the outside air were assumed to follow a sinusoidal distribution considering that it represents, with minor differences which are not relevant for this study, the day cycle. With the functions of X_m (absolute humidity) and T_m (Temperature) where T_m and X_m are mean values, ΔX & ΔT are the amplitudes, τ the cycle (24 hours) and τ_m the time lag of the maximum relative humidity to the temperature are computed as follows:

$$T_a(t) = T_{am} + \Delta T_a \cdot \sin\left(\frac{2 \cdot \pi \cdot t}{\tau_d}\right)$$

$$X_{ar}(\tau_x) = X_m + \Delta X_a \cdot \sin\left[\frac{2 \cdot \pi \cdot (\tau_x + \tau_{ox})}{\tau_d}\right] \quad (1)$$

The parameters of the temperature and humidity distribution were obtained from measurements made during one year at the Sewell meteorological station located at the 1980 masl elevation. The daily temperature distribution considered corresponds to the average of the hottest summer days. The parameters for Conveyors N° 1 were estimated by correcting the temperature by the altitude temperature gradient of the atmosphere. The relative humidity is considered equal to the values of the station. The absolute humidity was obtained with the atmospheric pressure, relative humidity and air temperature. Figure 3 shows the temperature and humidity curves for a typical summer day.

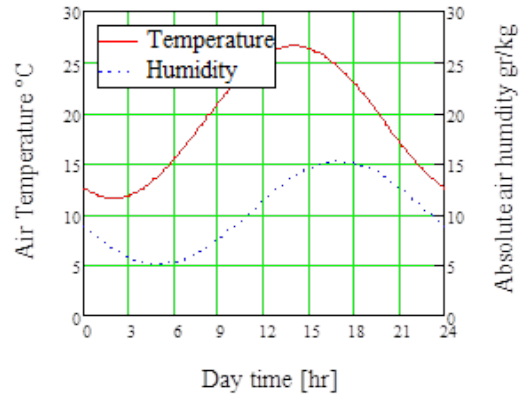


Fig. 3. Air and humidity data.

The absolute humidity was considered for the air temperature calculation in the tunnel since it is constant while travelling along the tunnel. The primary heat source is the sensible heat added by the conveyors. Applying absolute constant humidity assumes the tunnels are dry and no major water infiltrations to the tunnel will occur. For this study, the mean rock temperature was assumed to be equal to the mean air temperature $T_m = 19.15$ °C in ET 1, and $T_m = 17.85$ °C at the tunnel portal as measured in the summer. This data has an air temperature amplitude of $\Delta T = 7.5$ °C, a mean humidity of $X_m = 5.068$ gm/kg, an amplitude of $\Delta X = 5.068$ gm/kg and a time lag of the maximum temperature and humidity of $\tau_m = -3$ hr.

The temperature inside the El Teniente mine is comfortable and very stable all year long. The depth temperature gradient of the rock is lower than in other continental plates (~15 °C/km) due to the mountainous terrain. This makes the above assumptions reasonable for this study. Furthermore, the heating and cooling of the rock during a year cycle is very slow so that the heat flow due for this analysis was neglected. The behavior of the air heating during winter has not been modeled in this analysis since the existing mine shows no problems with excessive air temperature.

To model the heat flow in the rock on the tunnel wall the one dimensional partial differential equation for the heat conduction in a plane solid is used. This assumes the heat penetration is about 1 m deep as compared to the tunnel width of 6 m. This allowed for a plane surface to be assumed, thence we have the following with a thermal diffusivity assumed to be $a = 1.111$ mm²/sec.

$$\frac{\partial}{\partial t} T(x, t) = a_r \cdot \frac{\partial^2}{\partial x^2} T(x, t) \quad (2)$$

To determine the temperature distribution in the rock close to the tunnel wall it was assumed that it follows a sinusoidal fluctuation of the day cycle of the outside air temperature. This allows modeling as a quasi-steady heat flow with an alternating expression for the time dependence with $\omega = 2\pi/\tau$ being the frequency and function $F(x)$ will only depend on the distance x . Equation 3 shows this function.

$$T(x, t) = e^{i\omega \cdot t} \cdot F_x(x) \quad (3)$$

Replacing this expression in the heat conduction equation gives a differential equation for $F(x)$ which depends on x only (whose solution is of the sinusoidal form):

$$\frac{d^2}{dx^2} F_x(x) = \frac{i\omega}{a_r} \cdot F_x(x) \quad (4)$$

The solution of this differential equation is as follows:

$$F_x(x) = A \cdot e^{\sqrt{\frac{i\omega}{a_r}} \cdot x} - \sqrt{\frac{i\omega}{a_r}} \cdot x + B \cdot e^{-\sqrt{\frac{i\omega}{a_r}} \cdot x} \quad (5)$$

The boundary conditions requires that the function $F(x)$ decreases with increasing depth into the rock so that the coefficient $A=0$.

$$\lim_{x \rightarrow \infty} T(x, t) = T_{am} \quad A = 0 \quad (6)$$

On the wall surface, the heat flow by convection of the air inside the tunnel must be equal to the heat conduction in the rock. Here h is the convective heat transfer coefficient, $\lambda = 1.9 \text{ W/m}^\circ\text{K}$ is the heat conduction of the rock, and the air temperature in the tunnel is expressed as a complex function with the same frequency as in the rock:

$$x=0 \quad T_a(t) = T_{am} + \Delta T_a \cdot e^{i\omega \cdot t} \quad h_t [(T_a(t) - T_{am}) - T(0, t)] = -\lambda_r \left(\frac{dT(0, t)}{dx} \right) \quad (7)$$

Replacing $T_a(t)$ from (7) and $T(x, t)$ from (3) at $x=0$ gives the value of the coefficient B of (5).

$$B = \frac{\Delta T_a}{1 + \frac{\lambda_r}{h_t} \cdot \sqrt{\frac{i\omega}{a_r}}} \quad (8)$$

Inserting B into equation (5) and with the function $F(x)$ from equation (3) it is possible to simplify the expression to get the solution of temperature distribution inside the rock. Replacing $w=2\pi/\tau_c$ gives λ_w the wave length. K_p is a parameter that depend on λ the conduction coefficients of the rock and h is the heat convection coefficient inside the tunnel on the wall surface. Considering that the expression has complex numbers to match the phase of the alternating air temperature the imaginary part of the equation is used. With x the distance from the wall into the rock and t the time elapsed during the cycle the temperature distribution inside the rock is computed as follows:

$$\theta(x, t) = T_{am} - T_o + \text{Im} \left[\frac{\Delta T_a}{[1 + K_p \cdot (1 + i)]} \cdot \exp \left[2 \cdot \pi \cdot \left[-\frac{x}{\lambda_o} + i \left(\frac{t}{\tau_d} - \frac{x}{\lambda_o} \right) \right] \right] \right] \quad (9)$$

$$\lambda_o := 2 \cdot \sqrt{\pi \cdot a_r \cdot \tau_d} = 1.098 \text{ m} \quad K_p = \frac{2 \cdot \pi \cdot \lambda_r}{h_t \cdot \lambda_o} \quad (10)$$

The heat flow into the rock wall has the following expression:

$$\varphi(v_x, \tau_x) = \frac{\Delta T_a \cdot \lambda_r}{\lambda_o} \cdot \frac{2 \cdot \pi \cdot (1 + i)}{1 + K_p \cdot (1 + i)} \cdot \exp \left(i \cdot 2 \cdot \pi \cdot \frac{\tau_x}{\tau_d} \right) \quad (11)$$

Balancing the heat in a section of tunnel (dy) was done using: G_a as the air mass flow, the function v_x for air velocity, C_a for air heat capacity, T the air temperature (which is a function of y), \square for the tunnel wall temperature, q_c the heat dissipated by the conveyor per unit length ($= 1.568 \text{ kW/m}$ for Conveyor N° 2), S the perimeter of the tunnel section, and τ_c the time elapsed of the day cycle temperature, the following equation is obtained:

$$G_a \cdot C_a \cdot \left(\frac{d}{dy} T \right) = q_c - h_t \cdot S_a \cdot (T - \theta(0, \tau_x)) \quad (12)$$

Ordering the terms the following first order differential equation is obtained

$$\Lambda \cdot \left(\frac{d}{dy} T \right) + T = \frac{q_c}{h_t \cdot S_a} + \theta(0, \tau_x) \quad \Lambda(v_x) = \frac{G_a(v_x) \cdot C_a}{h_t(v_x) \cdot S_a} \quad (13)$$

Integrating with respect to y considering the boundary condition $T = T_o$ at $y = 0$ the equation reduces to $T(\tau_x, y)$ for the air heating along the tunnel with f the load factor of the conveyor.

$$T_s(\tau_x, y) = T_a(\tau_x) + \left[\frac{f_c \cdot q_c}{h_t(\tau_x) \cdot S_a} - (T_{as}(\tau_x) - \theta(0, \tau_x)) \right] \cdot \left(1 - \exp \left(\frac{-y}{\Lambda(\tau_x)} \right) \right) \quad (14)$$

To calculate the convection heat transfer coefficient h the following relation is used which corresponds to the forced heat transfer along a prismatic conductor since the air movement is created by the air draft due to the heat released by the conveyor or the ventilation fan and not by natural convection from the wall. Here Nu and Re are the Nusselt and Reynolds numbers of the air and are functions mainly of the air velocity v_x , $Pr = 0.712$ is the Prandtl number of the air; $D_h = 6.22 \text{ m}$ the hydraulic diameter of the conductor (i.e. the tunnel of Conveyor N° 2), $\lambda_a = 0.0263 \text{ W/m}^\circ\text{K}$ the heat conduction coefficient of the air, $\nu_a = 0.176 \text{ cm}^2/\text{sec}$ the cinematic viscosity of the air.

$$Nu_a(v_x) = 0.024 Re_c(v_x)^{0.8} \cdot Pr_a^{0.333}$$

$$Re_c(v_x) = \frac{v_x \cdot D_h}{\nu_a}$$

$$h_t(v_x) = \frac{Nu_a(v_x) \cdot \lambda_a}{D_h} \quad (15)$$

The airflow in the tunnels of conveyors 2 and 3 is obtained from the balance of the hot air draft with the pressure drop of the air movement. The air draft corresponds to the buoyancy of the warmer air inside the tunnel with respect to the outside colder air.

The pressure drop of the air flowing in the tunnel is obtained with the Darcy relation in which λ_{ad} is the friction factor of the tunnel wall and $K_{\Sigma} = 3.126$ the sum of the loss factors (entrance loss, curves, contractions, lovers and roof ventilators in the Transfer Stations, etc. in the tunnel of Conveyor N° 2). The friction factor is obtained with the Colebrook relation in this case for the wholly rough zone ($Re \sim 6 \cdot 10^4$) with the absolute roughness $e_c = 360$ mm of the tunnel wall.

$$\lambda_{ad} := \left(2 \cdot \log \left(3.7 \cdot \frac{D_h}{e_c} \right) \right)^{-2} = 0.089 \quad (16)$$

The air draft is calculated with L_a the tunnel length, the height difference H_v between the inlet at the lower end of the conveyor tunnel and exit at the upper end of it, H_c the height difference in the Transfer Station from the tunnel entrance to it and the air outlet in the static roof ventilator, ΔT_c the temperature rise of the air heated in the building and β_a the thermal expansion coefficient of the air at the mean temperature. As the temperature of the air varies while moving along the tunnel, the draft increases and therefore the buoyance force is the integral over the tunnel length.

The air drag of the belt movement generates a pressure raise Δh_c in the same direction as the air draft and is obtained using the resistance to the air movement over a flat rough surface. The resistance factor C_D is obtained with the roughness of the surface and in this case corresponds to the rocks lying on the belt which have a size of $e_m = 350$ mm, L_a is the belt length, B_b the belt width and A_t the tunnel section. The total resistance force F_{ar} which is the action of the movement of the belt on the air is obtained with the expression of relation (16) obtained from reference [2]. So the pressure raise over the whole length of the conveyor can be calculated as follows:

$$C_D := \left(2.635 + 0.618 \ln \left(\frac{L_a}{e_m} \right) \right)^{-2.57} = 5.682 \times 10^{-3} \quad (17)$$

$$F_{ar} := L_a \cdot C_D \cdot B_b \cdot \frac{\rho_g(T_{am}) \cdot v_c^2}{2} = 186.6 \text{ N} \quad \Delta h_c := \frac{F_{ar}}{\rho_g(T_{am}) \cdot A_t} = 6.38 \frac{\text{m}^2}{\text{s}^2}$$

With this the final expression to calculate the air velocity v_x is:

$$\left(K_{eq} + \frac{\lambda_{ad} L_a}{D_h} \right) \cdot \frac{v_x^2}{2} = \Delta h_c + g \cdot \beta_a \left[H_c \cdot \Delta T_c(v_x) + \frac{H_v}{L_a} \int_0^{L_a} H_a (T_s(v_x, \tau_x, u) - T_{as}(\tau_x)) du \right] \quad (18)$$

To get the velocity and outlet temperature of the air in the tunnels of Conveyors N° 2 and 3 an iterative procedure has to be used to solve simultaneously the equations (9), (14), (15) and (18).

As the ventilation of the tunnel of Conveyor N° 1 is with fans, equation (18) has to be replaced by the constant air velocity considered, to get the air temperature at the outlet of the tunnel. Conversely, in this case the air flows through the adits to reach the conveyor tunnel itself, and the ventilation fan power will add heat to the intake air. The heat generated by the fan

power was distributed along the length of the tunnel with $q_c = 0.402$ kW/m and the result was a sinusoidal air temperature with a lower amplitude $\Delta T_a = 4.25$ °C and a mean air temperature $T_{am} = 20.25$ °C (a bit higher than the outside air temperature of relation (1) at the inlet of the conveyor tunnel). This stabilization effect of the air temperature happens due to the heat exchange with the tunnel wall.

4. Results of the model

To assess whether the heat stress in the tunnels are suitable for people working in this environmental condition, the Wet Bulb Globe Temperature (WBGT) according to the Chilean code DS 594 was estimated. As the radiant heat load within these tunnels is negligible the WBGT temperature is calculated considering the dry bulb T_s and the wet bulb temperature T_{wb} of the air. This is a simplification, but it is based on the absolute humidity, and both T_s and T_{wb} are functions of the distance y in the tunnel and τ_x the hour of the day under analysis. The instant and shift mean WBGT temperature are calculated with the following relations with the second equation giving the mean value of the hottest shift.

$$T_G(\tau_x, y) = 0.3 T_s(\tau_x, y) + 0.7 T_{wb}(\tau_x, y)$$

$$T_{GM2} = \frac{1}{8\text{-hr}} \int_{15\text{-hr}}^{23\text{-hr}} T_G(\tau_x, L_a) d\tau_x \quad (19)$$

The permissible limit for heat stress according to the code is $WBGT = 25$ °C for heavy and continuous work within the tunnels. Applying the model to the main tunnel adit of P500 it can be seen that a stabilizing effect on the temperature is noted as shown in Figure 4 with Figure 5 showing the air cooling effect along the adit.

The modeling results for the different variables for Conveyor Tunnel N° 2 are shown on Figures 6 through 9. Figure 6 show the heat exchanged between the air and the rock while Figure 7 illustrates the variation of the different temperatures during the day cycle time.

Figure 8 gives the predicted temperature distributions of the rock wall, dry and wet bulb of the air, and mean day cycle of the air along the tunnel. Figure 9 shows the temperature distribution inside the rock at different times of day. It is noted that the heat penetration is relatively small, around 1 m into the rock.

From the graphs the stabilizing effect the rock has on the temperature inside the tunnel is observed. This is because the rock will absorb heat when the air has a higher temperature and, conversely will release the heat when the air is cooler (at night).

An analysis based on the utilization of the conveyors was done, and the WBGT temperature was predicted based on a daily average utilization factor of 75% and 100%. The last case was considered in order to assess the heat conditions when the conveyors have been operating for several hours at maximum conditions.

Table 2 summarizes the predicted temperatures for the different conditions studied. Relatively small length differences of the main tunnel sections of Conveyor N° 1 shown in Table 2 can be observed if they are compared to the length given in the previous study performed in reference [1].

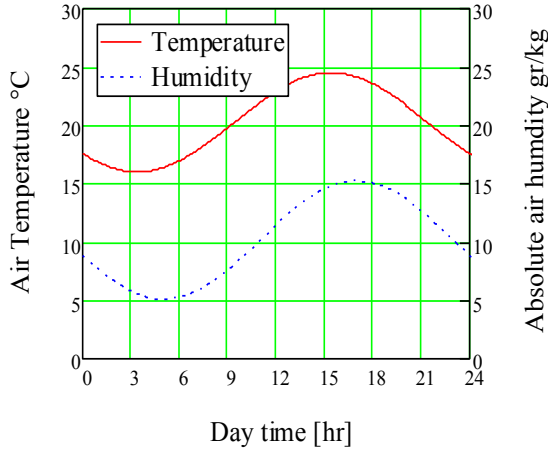


Fig. 4. Air temperature against time of day.

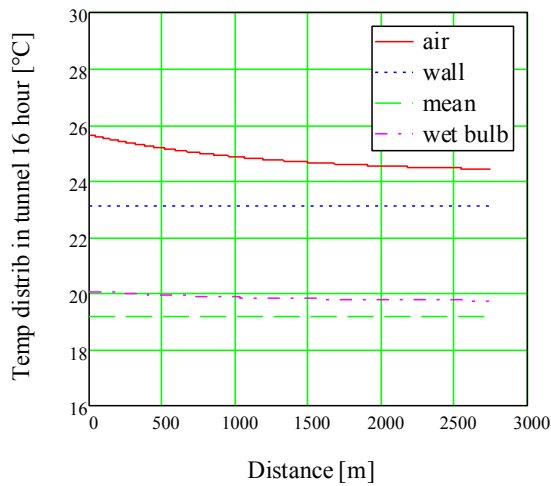


Fig. 5. Temperature against tunnel distance

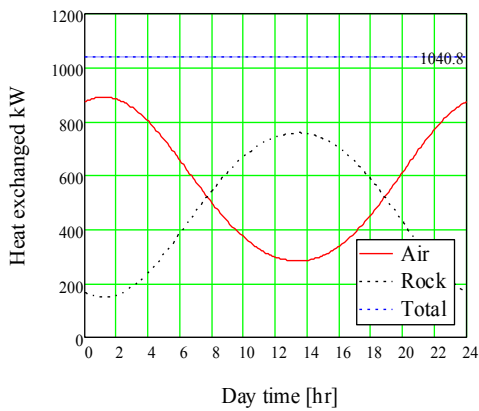


Fig. 6. Heat exchange against time of day

These differences can be attributed to changes during the detail design of the tunnel mainly due to layout requirements and geomechanical constraints observed during the current construction phase. As noted in Table 2, the most demanding section of Conveyor N° 1 tunnel is the one from the injection adit P500 to the extraction adit P4600.

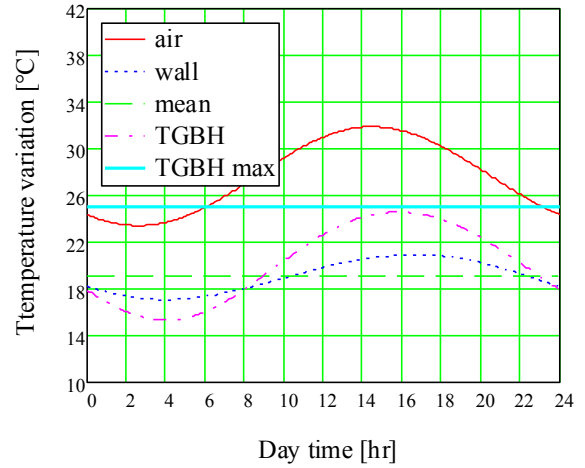


Fig. 7. Temperature variation against time of day

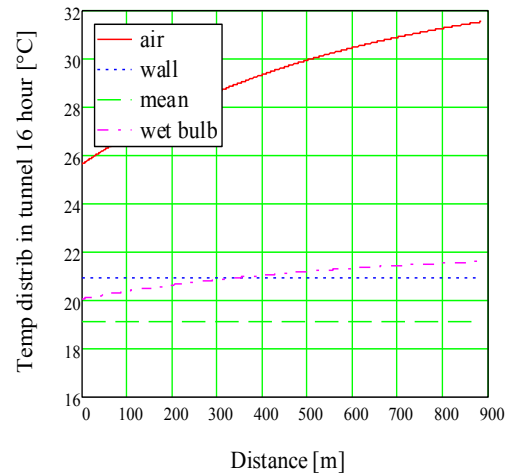


Fig. 8. Temperature distribution vs distance.

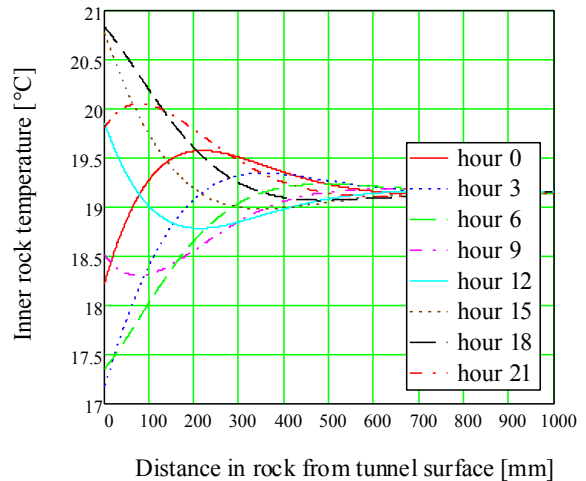


Fig. 9. Rock temperature vs distance in rock

Table 2. Summary of air velocities and temperatures in conveyor tunnels.

16 hrs Air velocity m/s	75 % conveyor heat dissipation			100 % conveyor heat dissipation		
	Air Tdb Tunnel exit °C	Amb heat stress T _g h		Air Tdb Tunnel exit °C	Amb heat stress T _g h	
		instantan. °C	shift mean °C		instantan. °C	shift mean °C
Conveyor 1: Section Portal - P 500 = 3105 m						
0.8	29.90	23.80	23.14	32.94	24.47	24.61
1.0	28.48	23.12	22.43	31.01	24.47	23.66
1.2	27.52	22.65	21.94	29.70	23.70	23.01
1.4	26.22	22.03	21.21	28.75	23.24	22.53
Conveyor 1: Section P500 - P 4600 = 4312 m						
0.8	29.98	23.84	23.19	33.06	25.31	24.67
1.0	28.55	23.15	22.47	31.12	24.16	23.73
1.2	27.57	22.68	21.98	29.79	23.75	23.07
1.4	26.87	22.34	21.62	28.83	23.29	22.59
Conveyor 1: Section P 4600 - Mine inner end = 1431 m						
0.8	29.18	23.40	22.66	31.81	24.66	23.94
1.0	27.91	22.78	22.01	30.08	23.82	23.07
1.2	27.06	22.36	21.57	28.91	23.25	22.48
1.4	26.45	22.06	21.25	28.07	22.84	22.05
Conveyor 2: L = 986 m						
1.90	31.54	24.59	22.76			
2.13				33.63	25.58	23.74
Conveyor 3: L = 1149 m						
1.85	30.18	23.76	22.04			
2.07				32.36	24.80	23.06

However, even in the case of full load (100%) a velocity of ~ 1 m/sec in the tunnels is sufficient to keep the WBGT temperature within the legislated limit of 25 °C.

5. Summary

The results indicate that for all the considered scenarios, including the updated ventilation design of the tunnels, that modification to the current ventilation system design is not required due to heat. The fan operational point will not change and the power consumption determined for the fans will not increase further as it did with the last study.

The previous results also open an additional avenue for study which is the possibility of applying ventilation on demand (VOD) strategy for each tunnel section to minimize the use of energy, while maintaining the permissible limits for temperature and other contaminants. The conveyor tunnel (TC) VOD strategy could be based on temperature, dust control and diesel fleet. On the other hand, the personnel and supply tunnel (TAP) should be based on diesel fleet and mitigating any potential fire risk.

The tunnel ventilation of Conveyor N° 1 is a forced ventilation system with constant flow rate and for the purposes of defining the air velocity the 3 sections, between the Portal and the junction with the P 500 adit, between junctions of adits P 500 and 4600 to end of the tunnel inside the mine were modeled. The air velocity was varied over the range of 0.8 to 1.4 m/sec and the dry bulb temperature and the maximum instantaneous heat stress and average shift WBGT for these air flows were calculated.

According to the results, an air flow of 47.5 m³/s with a speed of 0.9 m/sec is recommended in order to cover the scenarios investigated. Under this condition the heat stress limit WBGT is not met even during maximum conveyor heat dissipation (i.e. 100% of the heat generated by the friction of the idler and belt heating by hysteresis in the indentation of the rollers). This situation should not occur very often since the maximum outside air temperature combined with the belts operating at full load only occur a few times a year. Hence, a WBGT exceeding 25 °C for heavy duty and continuous work would rarely occur.

For the natural draft ventilation of the tunnels of Conveyors N° 2 and 3 the model shows that the concept

works well with the resulting air velocity sufficient in magnitude to assure good ventilation inside the tunnel. Only during the 15 to 17 hour during the summer will the WBGT temperature possibly exceed the 25 °C at the exit of the tunnel.

Tunnel ventilation of Conveyors N° 2 and 3 can be ventilated naturally due to their respective inclined design and from the heat generated by the conveyor system. At the transfer stations air louvers in the lower part of the building need to be considered in addition to Robertson type static roof ventilators to allow air to enter the stations and to release heat from the tunnels and transfer station.

The air intake louvers and roof ventilators were sized to keep the temperature under the values defined by these calculations. The intake louvers must have an area of at least 60 m² and the roof ventilators must be 800 mm wide with an area of 40 m² (50 m long).

During summer the outlet air temperature of the tunnels is not predicted to exceed 34 °C and at the roof ventilator discharge a temperature of 40 °C may be possible. The air flow in the tunnel of Conveyors N° 2 and 3 is in the range of 50 - 70 m³/sec with a speed between 1.8 to 2.1 m/sec which adjusts itself by the heat released by the belts.

This paper presents an approach to predict the heat transfer in a long conveyor tunnel being constructed for the New Level Mine. WBGT was calculated to determine if acceptable environmental conditions could be maintained in the conveyor tunnels. The study was used to verify previous studies on the airflow required for the Conveyor N° 1 tunnel and the proposed natural ventilation of Conveyors N° 2 and 3 tunnels. The results of this study indicate that heat does not appear to be an issue in the conveyor tunnel based on the original design airflows. Furthermore, the predicted maximum WBGT criterion is not expected to be met. This result may give an opportunity to explore the benefit of reduced airflow quantities to save operating power costs. However, such a reduction would also need to consider dust dilution and mitigating any potential fire event.

References

- [1] E. Acuña, R. Alvarez, K. Wallace and B. Prosser. Ventilation Considerations for the New Level Mine Project Access Tunnels, Proc. The Australian Mine Ventilation Conference, (2013), Adelaide.
- [2] Robert D. Blevins Ph.D. - Applied Fluid Dynamics Handbook.

Investigating the Importance of Climatic Monitoring and Modeling in Deep and Hot US Underground Mines

Karena E. Carpenter^a, Pedram Roghanchi^a, Karoly Charles Kocsis^a

^a*University of Nevada Reno, Reno, Nevada, USA*

To understand and model heat and humidity transport, all major heat sources in an underground mine need to be identified and quantified. There can be a considerable difference in the spectrum of the heat and mine power source distributions between different mines due to many factors such as depth, mechanization, power sources, geothermal activity and rock thermal properties. To assess the atmospheric and underground environmental conditions, multi-channel climatic monitoring units will be installed along vertical and horizontal airways from surface to the lowest production level at various underground mines in Northern Nevada. To identify the mining equipment responsible for increasing temperature and humidity in the production workings, equipment activity surveys will also be conducted in parallel with the climatic monitoring program.

This paper aims to begin discussing best practices and provide recommendations in respect to the design and use of atmospheric and environmental monitoring systems involving heat and humidity in deep and hot US mines. The collected climatic and equipment activity data will be used to validate a dynamic climatic model developed by means of a ventilation/climatic software package. Heat flows will be quantified from the mining equipment, strata, auto-compression and other major heat sources. The validated model will be used to predict the underground climatic conditions of yet undeveloped orebodies and future underground mines. Furthermore, this dynamic model can also be used to assess various cooling strategies used world-wide and identify the most effective cooling and refrigeration methods which can be effectively and economically employed in hot US mines.

Keywords: climatic monitoring, heat sources, underground cooling, underground environment, climatic modeling

1. Introduction

Base and precious metal mines in the US are becoming deeper, more productive, and further mechanized. These mining trends will cause the underground environment to become hotter and more humid through an increase in auto-compression as air descends vertical airways, the geothermal gradient, mechanical processes, etc. The thermal and psychrometric working conditions in an underground mine are an important consideration when discussing the performance, productivity, and, most importantly, the health and safety concerns of the workers.

Much has been studied about the effects of hot and humid environments on a human's health and it is known that high levels of heat in the body can cause heat stroke, a very serious illness that carries a high risk of fatality when working in a hot and humid underground environment. Employing a heat stress index to limit the workers exposure to heat has become a standard practice in the mining industry. These indices require certain parameters such as temperature, humidity, and wind velocity to be measured and evaluated.

When a mine exceeds allowable heat levels (whether by MSHA standards or as indicated by a heat stress index), climatic parameters of the intake air can be altered to achieve acceptable underground climatic conditions. If increasing ventilation is not adequate to control the heat load, localized cooling or refrigeration may be necessary.

Climatic data collection will also be essential for validation of mine ventilation and climatic models.

These models can then be used to understand transient heat transport processes, evaluate the heat profile of the mine, and predict the climatic conditions in future developments and working areas.

Inputs needed for indices, the design of mitigation controls for heat, and modeling can be assumed or measured directly at the mines. In this paper, we present important applications and challenges of climatic monitoring. We also discuss how these challenges will be examined in our climate monitoring strategy at our partner underground mines in Nevada.

2. Health and Safety

2.1 The Human Body and Heat Exchange

The human body's mechanisms for heat exchange are convection, radiation, and evaporation. Once the body's skin temperature reaches 93.2°F (34°C) sweating increases to the point that evaporative cooling is most effective, but may be inhibited by a humid environment [1]. When the skin becomes completely wetted the only method of heat transfer is skin temperature increase. If the dry bulb temperature (T_d) of the ventilating air exceeds the skin temperature, convective and radiant heat transfer reverse, adding more heat to the body [1]. At a skin temperature of 96.8°F (36°C) symptoms of heat strain initiate and at 98.6°F (37°C) there is a danger of excessive and fatal core temperatures [1]. According to MSHA [2], a hot work site would include any combination of air temperature, humidity, radiation, and wind speed that exceeds a wet bulb globe temperature of 79°F (26.1°C). It may be more prudent to consider the

workers thermal comfort, or satisfaction with the thermal environment rather than their level of heat strain. Thermal comfort is a very important factor in managing the workers performance, productivity, and health and safety as it relates to the thermal environment.

2.2 Heat Indices

The International Organization for Standardization (ISO) draft on the evaluation of thermal strain [2] lists four principle parameters to consider: body core temperature, heart rate, skin temperature, and weight loss through sweating. Although these measures provide information on the human body's response to thermal stress, they do not result in a simple evaluation of the thermal environment. The measurements of these parameters on a regular basis require accurate, complex, and expensive measuring devices which are not normally available to industry.

Heat stress indices are single values that integrate the effects of the basic parameters in any human environment. Most heat indices are based on the thermal comfort parameters: dry bulb temperature (T_d), wet bulb temperature (T_w), black globe temperature (T_g), wind velocity, clothing and metabolic rate [3]. The first four parameters are considered the environmental parameters and can be directly measured or calculated from measured data. Directly measuring these parameters will confirm if an area has exceeded an acceptable range. It is therefore logical to relate the comfort, and ultimately the health and safety of a worker, with the climatic parameters listed above. In order to ensure the working environment meets the preferred heat index threshold or MSHA requirement, these parameters should be monitored regularly.

Many institutions choose to use a heat stress index to relate a human's physiological response to the environmentally imposed thermal stresses. Some commonly used indices include:

- Wet Bulb Globe Temperature (WBGT)
- Thermal Work Limit (TWL)
- Effective Heat (ET)
- Cooling Power

3. Major Sources of Heat

3.1 Heat Sources

Heat is usually the dominant environmental problem in deep metal mines [1]. Classifying and analyzing the heat sources in a mine allow for calculation of the total heat load. Stationary and moving heat sources are also necessary in understanding and modeling the heat and humidity transport. The potential heat sources in an underground mine are [4]:

- Auto-compression
- Strata heat (geothermal gradient)
- Underground water

- Machinery
- Human metabolism
- Oxidation
- Blasting
- Rock movement
- Pipelines

It was once understood that this was also the order of importance of the heat sources; however, recent studies have shown that each mine is unique in its heat source distribution [4-6].

Table 1 shows the heat load distributions for mines in Canada, Australia, and the US. The relative contributions of the major heat sources are affected by several factors including:

- Depth of the mine
- Level of mechanization
- Mine power sources
- Geothermal activity
- Rock thermal properties, etc.

It is, therefore, advisable to analyze the heat sources for each mine so that an accurate distribution can be determined.

Table 1. Examples of heat load distributions in mines [46].

	Auto-compression	Strata Heat	Equipment	Other
Canada	87%	7%	6%	-
Australia	51%	24%	14%	11%
USA ^a	11%	48%	20%	21%

^aAverage heat balance for hot mines [4]

Measuring climatic parameters including dry bulb temperature (T_d), relative humidity (RH), and barometric pressure (BP) will provide the basis for the heat source distribution. If the area's geothermal gradient is not known, obtaining the rock thermal conductivity and virgin rock temperatures from the mines, as well as an assumption of the heat flow, will enable calculation of the geothermal gradient. Spot measurements of the wall temperatures in old openings and new headings will confirm strata heat transfer. To obtain the mechanical heat load, an equipment survey in selected areas which records equipment presence and their time spent in the area can be used to correlate temperature and humidity spikes to the equipment used. This data will allow for the calculation of heat which was transferred from the mining equipment to the ventilating air.

4. Underground Heat Mitigation

There are several methods of controlling heat in an underground mine including the redesign of primary and auxiliary ventilation systems, localized cooling, or refrigeration. Selecting the most suitable method depends on the level of heat to be removed, the location

of the problem areas, and economic constraints. Design or re-design of primary and/or auxiliary ventilation systems to provide acceptable working conditions should be explored before refrigeration is considered, as the cost savings could be significant. For example, a localized “exhausting” auxiliary ventilation system can be re-designed into a “forcing” system. The higher velocity airstream emerging from a forcing duct can provide cooler air at the face of a dead-end heading, having also taken into account the heat generated by the auxiliary fan. Ventilation is a sufficient mitigating technique when the heat removal capacity of the airflow is greater than the calculated heat loads [1]. The heat removal capacity of the air can be calculated using psychrometric equations and the heat load is determined as discussed in section 3.1. The ability of ventilation systems to effectively cool the air decreases at a depth of about 3,300 ft (1000 m) [5]. Below this depth, use of localized cooling methods and refrigeration might be necessary for heat removal from the active areas of the mine. Climatic monitoring allows for evaluation of the underground environmental conditions and, if necessary, selection and design of a cooling or refrigeration system.

5. Modeling

There are many standard mine ventilation and climatic simulation programs available which model relevant transport processes for heat and humidity and predict the climatic conditions for yet undeveloped orebodies. Successful calibration of numerical models against field measurements allows for validation of the model’s ability to simulate the environment being studied. Therefore, a comprehensive strategy of monitoring for field data collection would be critical to employ an accurate climatic model. Furthermore, studies show that hourly, daily and seasonal temperature changes can produce significant modeling errors [5, 7]. Kocsis et al [5] highlighted that the difference between simulated and measured climatic parameters is the result of the dynamic time delay of temperature and humidity spikes along the advection pathways of the ventilating air due to the “thermal flywheel effect” (TFE). To assess transient heat transport processes and address the impact of TFE on the underground environment, a dynamic “ventilation-thermal-humidity” (V-T-H) model should be developed using measured climatic data.

6. Summary and Discussion

As the increasingly mechanized underground mines in Northern Nevada become deeper, the issue of heat becomes a significant problem. Hot and humid environments can seriously affect the performance, overall productivity and most importantly the ability of the underground workforce to perform work in a safe manner. When the underground working places become excessively hot, the volume of a mine’s intake air, its temperature and humidity can be altered in order to improve the underground climatic conditions. Power

supply modifications may also be exercised. As a last resort, refrigeration of the ventilating air may be required.

Climatic monitoring of the underground mining environment with climatic sensors is a key element in documenting compliance with MSHA regulations, managing worker safety with a heat index, developing a heat source profile, selecting a heat control technique, and successfully calibrating and validating a simulation model. However, the challenges in designing a successful monitoring system are numerous. It can be difficult to identify the critical locations for the placement of monitors so that relevant data is collected. It is not clear if monitoring the exhaust of a district ventilation system will provide sufficient data, whereas placement of monitors in the working areas may. Another issue is that there are many types of climatic monitors available. For example, use of data logging type monitors to collect and then download data may be convenient, but would delay the detection of potentially hazardous conditions underground. Small handheld units may be used for spot checking the parameters, but may run the risk of missing the hazardous changes all together. Newer technology, such as fiber optics, may be able to provide real-time data changes, but may not be able to measure all of the parameters required. The number of monitoring units required and the best schedule for taking measurements are other factors that need to be examined.

In order to study and examine these challenges in the underground environment, and as part of a 5-year NIOSH study, ACR multi-channel data loggers will be installed along vertical and horizontal airways from the surface to the lowest production area, along the main haulage drifts, and throughout the exhaust system at our Nevada partner mines. These small data loggers will continually record temperature (T_d), relative humidity (RH), and barometric pressure (BP) at one minute intervals for two weeks at a time. We will periodically collect the data stored on the loggers and reposition them for further data collection. From the collected data we will calculate the wet bulb temperature (T_w) in the production workings and throughout the mine. During this time we will also perform spot measurements throughout the mine using more accurate handheld climatic and ventilation instruments. These measurements will allow for evaluation of whether the climatic data loggers have the ability to accurately measure, collect, and transfer climatic and ventilation data to be used for a climatic monitoring program at a mine. Using both types of instruments, one with higher accuracy, will allow for checking of measurements for accuracy and make recommendations on units to be used in mines.

At various stages of the climatic monitoring program (e.g. winter, spring, summer) we will also conduct an equipment activity survey. The climatic and equipment activity data will be used to accurately quantify the heat generated by the mining equipment (e.g. diesel,

electrical) and the heat transferred to the ventilating air during various production shifts.

The climatic data (Td, Tw, RH, and BP) collected by the ACR data loggers will be used to calibrate the dynamic V-T-H model being developed and verify the TFE effects on the underground environment.

Acknowledgements

This project is funded by National Institute of Safety and Health (NIOSH). The authors would like to acknowledge the partner mines in the state of Nevada for their collaborations in this project.

References

- [1] M.J. McPherson, *Subsurface Ventilation Engineering*, Mine Ventilation Services, Inc., Fresno, 2009.
- [2] *Heat Stress in Mining*. Mine Safety and Health Administration, National Mine Safety and Health Academy [viewed 17 March 2015]. Available from: <http://www.msha.gov/s&hinfo/heatstress/manual/heatmanual.HTM>.
- [3] K. Parsons, Heat stress standard ISO 7243 and its global application, *Industrial Health*, 44(3) (2006) 368-379.
- [4] Y. Epstein and D.S. Moran, Thermal comfort and the heat stress indices, *Industrial Health*, 44(3) (2006) 388-398.
- [5] H.L. Hartman et al., *Mine Ventilation and Air Conditioning*, John Wiley & Sons, Inc., New York, 1997.
- [6] C. Kocsis and S.G. Hardcastle, Prediction and Analysis of the Underground Climatic Conditions and their Cause in Deep Mechanized Canadian Metal Mines, *Proceedings of the 13th U.S./North American Mine Ventilation Symposium (2010)* 323-332.
- [7] T. Payne and R. Mitra, A review of heat issues in underground metalliferous mines, *Proceedings of the 12th U.S./North American Mine Ventilation Symposium (2008)* 197-201.
- [8] G. Danko, Ventilation and climate control of deep mines, *McGraw-Hill Yearbook of Science and Technology (2012)* 296-299.

The Assessment Of Specialized Clothing Worn By Underground Miners And Its Heat Stress Management Implications

Stephen G. Hardcastle^a, Martin P. Poirier^b, Brian J. Friesen^b, Ryan McGinn^b, Rob Meade^b,
Andreas D. Flouris^c, Cheryl Allen^d, Glen P. Kenny^e

^a*CANMETMining, Natural Resources Canada, Sudbury, Canada*

^b*Human and Environmental Physiology Research Unit, University of Ottawa, Ottawa, Ontario, Canada*

^c*FAME Laboratory, Department of Exercise Science, University of Thessaly, Trikala, Greece, 42100*

^d*Vale, Sudbury, Ontario, Canada*

Clothing plays an important role in heat stress management; if it prevents adequate heat exchange between the human body and the ambient environment when working, the body will store heat causing elevated core temperatures and potential health risks. This paper summarizes a series of tests performed on clothing that could be worn by underground miners in Canada. These evaluations, undertaken using a human calorimeter, were each believed to be the first of their kind addressing human heat storage directly as opposed to using indirect thermometry. These studies initially assessed standard coverall arrangements and popular activewear for prolonged continuous work, continued with tests simulating intermittent work in hot-dry and warm-wet (or humid) environments, and concluded with the recent intermittent work evaluation of arc-flash or flame resistant (AFR) clothing. Throughout the studies, young, healthy, un-medicated, non-acclimated male volunteers were subjected to exercise/recovery test protocols lasting up to 120 minutes. The subjects exercised at 360-400 W rates of metabolic heat production, verging on American Conference of Governmental Industrial Hygienist's (ACGIH) "Heavy" classification, in environments ranging from approximately 23 to 29°C wet-bulb globe temperature (WBGT). The results emphasize the benefits of direct calorimetry in providing a more accurate depiction of heat storage compared to indirect thermometry. The latest AFR tests confirmed the previous findings that coverall arrangements, currently typical of the Canadian industry, may be detrimental to miners' health, as caused by elevated body temperatures. This is as a consequence of reduced heat loss to the environment compared to single-layer, closer-fitting alternatives that promote evaporative cooling. However, in regard to AFR clothing ensembles needing special consideration, or the requiring a clothing adjustment factor when applying the ACGIH heat stress screening criteria, this could not be confirmed. Despite the additional protective properties of the fabrics, the results tend to indicate within each clothing category, i.e. coveralls, or work-pant/long-sleeved t-shirt, that there were no significant differences between comparable AFR and non-AFR options in terms of the progression of increasing core temperature or overall heat storage. Consequently, the closer fitting long-sleeved shirt ensembles tested, as a whole, through allowing greater evaporation, could reduce the rate of increasing body temperatures allowing for longer or more intense activity before core temperatures thresholds are reached.

Keywords: Heat stress, Clothing, WBGT, Arc-flash, Flame resistant, Snellen calorimeter

1. Introduction

Miners wear a variety of clothing ensembles based on durability or specific safety requirements. The fabric material, and any treatment or layering thereof, can adversely affect a worker's core temperature and therefore increase the risk of heat stress. Full coveralls, often worn in conjunction with a full under layer, are the norm in the Canadian mining industry. Furthermore, there is increasing interest in the widespread use of arc-flash or flame resistant (AFR) clothing normally limited to electricians and mine rescue personnel. The Deep Mining Research Consortium (DMRC) identified clothing requirements and heat stress concerns as knowledge gaps that need to be addressed to ensure miner safety. Moisture-wicking garments, similar to those promoted for sporting activities, have been shown to be beneficial in mitigating heat storage and or elevated core body temperatures for both continuous activity in a hot/dry environment and for intermittent activity in both hot-dry and warm-wet (humid) environments. However, their adoption has been limited due to worker preference, other safety concerns, such as protection from cuts and lubricating oils etc. plus the operational considerations of wide scale introduction including cost without a comprehensive benefit analysis. There is also anecdotal belief within industry workers that AFR clothing, such as Nomex® coveralls, results in greater thermal discomfort.

In mining, factors such as rock and ground water temperature as well as artificial heat sources, such as powered machinery, along with ventilation air auto-compression are major determinants in an underground environment's temperature and humidity. In Canada, where mines are reaching 3 km below surface, the effect

Table 1. Screening Criteria for TLV® and Action Limit (AL) for heat stress exposure (to nearest 0.5°C WBGT) [after 1,2]

Demand Category (Median) Allocation Work/Recovery	Light 180 W		Moderate 300 W		Heavy 415 W		Very Heavy 520 W	
	TLV	AL	TLV	AL	TLV	AL	TLV	AL
75%-100% Work	31.0	28.0	28.0	25.0				
50%-75% Work	31.0	28.5	29.0	26.0	27.5	24.0		
25%-50% Work	32.0	29.5	30.0	27.0	29.0	25.5	28.0	24.5
0%-25% Work	32.5	30.0	31.5	29.0	30.5	28.0	30.0	27.0

of auto-compression superimposed over summer climatic conditions can be significant. Also, despite Canadian mines being highly mechanized there are certain regular tasks that have high metabolic demands. Consequently, with increasingly adverse thermal environments, the same level of work activity may not be sustainable. For occupational tasks involving physical activity, the risk of heat stress becomes greater as the level of heat rejection required to maintain thermal homeostasis increases and as metabolic heat loss mechanisms reach their limit. Below mean skin temperatures of ~34-36°C, the body can reject heat through both dry and evaporative heat transfer mechanisms. Above this mean skin temperature, the direction of dry heat transfer is reversed and evaporative heat rejection becomes the primary heat loss mechanism. Hence, efficient and useful evaporation of sweat is critical, and clothing becomes a significant moderator.

The wet-bulb globe temperature (WBGT) is one of the most widely used empirical indices in the management of heat exposure and the heat stress to which workers may be exposed. In Canada, the WBGT threshold limit value (TLV) criteria for heat stress and strain, as published by the American Conference of Governmental Industrial Hygienists (ACGIH) [1,2], are the basis for virtually every province's occupational health and safety regulations or guidelines for thermal stress management. The WBGT combines the ambient dry-bulb air temperature (T_a , °C), the relative humidity (RH) combined with air movement as a natural wet-bulb temperature (T_{wb} , °C), and radiant heating effects, where applicable, through a globe temperature (T_g , °C) into a single environmental measure. The premise behind the threshold limits is to prevent the body's core temperature from exceeding 38.0-38.5°C. The environmental temperature exposure limits, Table 1, are based upon work-rate, the ratio of continued effort to rest periods (work:recovery ratio) and worker acclimation. Other considerations in the application of WBGT based TLVs include temperature adjustments for the clothing worn and body weight corrections to the metabolic work rate categories that are based upon a 70 kg subject.

The insulative effects of clothing ensembles ranging from the standard work coverall, including a modest second layer, through specialized clothing with AFR fabrics, and semi permeable or impermeable suits, as required for particular occupations, have the potential to

limit evaporative cooling to some degree. The number clothing of layers, the fabric, their fit and extent, proximity to the skin, spacing and venting also control effective moisture evaporation. Even tasks performed with a low level of activity or clothing insulation value, or both, can present a significant heat stress risk if they are performed under hot environmental conditions [3]. Conversely, insulative clothing and high activity tasks, such as mine rescue, can present risks at low environmental temperatures. This was evident with core temperatures approaching 39°C in a mine rescue simulation that required an average metabolic work rate of 538 W, "Very Heavy" according to the ACGIH classification, in an environment with an equivalent WBGT of ~16°C (assumes $T_a \approx T_g$ and the psychrometric wet-bulb temperature, $T_{wb} \approx T_{min}$) [4].

To accommodate the effects of clothing, the application of the WBGT criteria incorporates Clothing Adjustment Factors that range from 0°C for cotton coveralls worn over modest undergarments through to an 11°C downward adjustment of the TLV value for encapsulating vapor barrier clothing [1]. With respect to AFR clothing, depending upon the fire retardant rating and the clothing ensemble, downward corrections ranging from 0.5 to 3.2°C have been proposed [2,5]. However, work based on determining the point where there is a clear loss of thermal equilibrium found no significant difference between fire retardant ensembles and cotton work clothes and has proposed a 0°C adjustment [6].

These clothing adjustment factors can have a significant impact. For example, upon applying an adjustment of 2.0-3.0°C to the WBGT screening criteria in Table 1 when wearing specialized clothing, activities previously pertaining to "Light" work with a 75-100% work allocation may now be limited to a 0-25% work allocation. Furthermore, where "Heavy" work was undertaken at a 25-50% allocation, the same order correction would now only accommodate "Light" to "Moderate" work. In deep mines, increasing ventilation rates and/or introducing mechanical cooling could be used to negate the loss of productive time, or the downgrading of maximum work intensity. However, the associated capital and operating costs can be significant, potentially to the point of the operation being uneconomic. Therefore, a better understanding of clothing factors and their appropriateness is imperative.

Table 2. Subject characteristics for the three clothing evaluations performed in the modified Snellen calorimeter.

		Age (yrs)	Height (m)	Weight (kg)	Body Fat (%)	BSA (m ²)	VO ₂ max (mlO ₂ /kg/min)
Test 1	Evaporative Properties	20 ± 1	1.76 ± 0.02	79.5 ± 3.7	16.4 ± 3.5	1.97 ± 0.05	53.6 ± 1.4
Test 2	Work:Rest Hot: Humid	22.9 ± 0.4	1.78 ± 0.03	77.3 ± 2.9	15.7 ± 1.6		58.3 ± 2.1
Test 3	AFR Clothing	23 ± 1	1.73 ± 0.03	79.5 ± 6.8	17.7 ± 2.9	1.93 ± 0.09	46.9 ± 4.4

BSA – Body Surface Area

2. Clothing Tests

The study reported here continues the evaluation of clothing ensembles in a “gold standard” modified Snellen direct air human calorimeter [7]. This testing capacity, at the University of Ottawa, is essentially a precisely controlled and monitored environmental test vessel that can accommodate the testing of human subjects, contained within another precisely controlled and monitored environmental chamber. It provides the rates of whole-body evaporative and dry heat losses (or gains), as well as the change in body heat content (and therefore the level of thermal strain), in humans by performing simultaneous minute-by-minute measurements of the individual heat balance components. As will be described, this sequence of work started with an evaluation of several clothing arrangements against a semi-nude condition for continuous activity. This was used to identify a clothing ensemble with the best evaporative cooling potential under hot conditions. The second study introduced intermittent work to better represent the mining activity observed in field observations [8] plus exploring any differences between hot-dry and warm-wet environments with a common WBGT for standard and modified clothing combinations. The third and latest study explored the added detriments, if any, of those ensembles providing additional AFR protection. Throughout these studies, 6-8 young healthy non-smoking male test subjects were used. Their characteristics (mean ± SE), as given in Table 2, shows the similarity between the test subject groups used. For continuity a semi-nude control condition and certain standard clothing arrangements were also common to all three sets of tests.

2.1 Measurements

Throughout the clothing tests, the prime assessment of clothing effects were indirect measurements to determine the change in body heat content ΔH_b , from the heat balance equation given below, and direct measurements of deep body (core) and mean skin temperatures.

The standard form of the heat balance equation for the human body is:

$$S + M = (R + C + K) + E - W \quad (1)$$

where, S is the rate of body heat storage; M is the rate of metabolic energy expenditure; W is the rate of external work; R , C and K are the rates of radiant convective and conductive heat exchange, respectively, which combined constitute the dry heat exchange; and E is the rate of evaporative heat exchange.

While heat storage is determined indirectly, its derivation should be considered more direct than that of

using a two-compartment model based upon core and skin temperatures. Although the measurement of a temperature is direct, the determination of a mean skin temperature through the application of weighting factors, plus applying multipliers to combine the core and mean skin temperatures renders the two-compartment model approach less direct.

2.1.1 Body Heat Content (ΔH_b)

The differential form of Equation 1, with respect to time, provides the change in body heat content ΔH_b . The individual components of Equation 1 were determined through a combination of direct and indirect calorimetry. The evaporative (E) and combined dry ($R+C+K$) heat exchange of test subjects were established every minute within a modified Snellen direct air calorimeter. This apparatus uses differential air temperature and humidity measurements of the influent and effluent flows to determine the air mass flow rate and then measure total heat loss/gain with an accuracy of $\Delta \pm 2.3W$. External work (W) was regulated to predetermined levels through subjects performing seated pedaling on a constant load eddy current cycle ergometer. The rate of metabolic (M) heat production was calculated from minute-average values of oxygen consumption and respiratory exchange ratio based on inspired and expired air oxygen and carbon dioxide gas contents and a ventilometer derived flow rate measurements.

2.1.2 Core Temperature and Other Measurements

Although not reported throughout, the following measurements are often typical of such calorimeter based studies. Esophageal (T_{es}) and rectal (T_{re}) deep body temperatures were measured every 15 seconds through suitably positioned thermocouple probes. Mean skin temperatures were obtained from the weighted average of four, regional thermocouple temperatures. Heart rate was monitored with a Polar coded transmitter.



Fig. 1. Semi-nude control (CON), activewear undergarments, standard coverall with undergarment (SWU) and work-pant activewear long-sleeved shirt (MWU) clothing ensembles.

Additional measures, as considered relevant to each study or an associated research aim, included blood plasma volume and stress marker changes, urine specific gravity, and subject provided thermal sensation and perceived exertion ratings.

2.2 Prior Calorimeter Clothing Studies Summaries

2.2.1 Evaporative Properties

This initial study [9,10] compared the performance of a standard mining work uniform (SWU) polyester cotton (65:35%) coveralls worn over full cotton or activewear undergarments, against polyester spandex (93:7%) activewear undergarments worn alone, and a semi-nude control (CON). A sub-analysis also evaluated a polyester cotton (65:35%) work pant with activewear top combination termed modified mining work uniform (MWU), see Figure 1. The test protocol involved the subjects performing 60 minutes of upright seated cycling at a constant rate of metabolic heat production ~ 400 W, considered the onset of a “Heavy” work demand according to the ACGIH [2]. This was followed by a 60 minute seated rest period. For both activity regimes the air supply to the calorimeter was regulated to 40°C and 15%RH (equivalent to $\sim 26^{\circ}\text{C}$ WBGT).

The study showed that the effect of the activewear undergarments worn alone were negligible as they were comparable to the semi-nude condition. Their heat storage and loss, core temperature and heart rate changes were similar; the semi-nude and activewear conditions also showed a trend towards temperature stabilization as activity progressed. An example of the different effects of such clothing is demonstrated in Figure 2 which shows the change in rectal temperature starting to plateau at 37.4°C for the semi-nude and activewear undergarments. In comparison, both of the coverall ensembles caused rectal temperature values to continually increase towards 37.7°C until exercise was terminated. The coveralls also resulted in higher heat storage during exercise and lower heat loss during recovery. With a longer exercise period, the coverall arrangements would have resulted in core temperatures

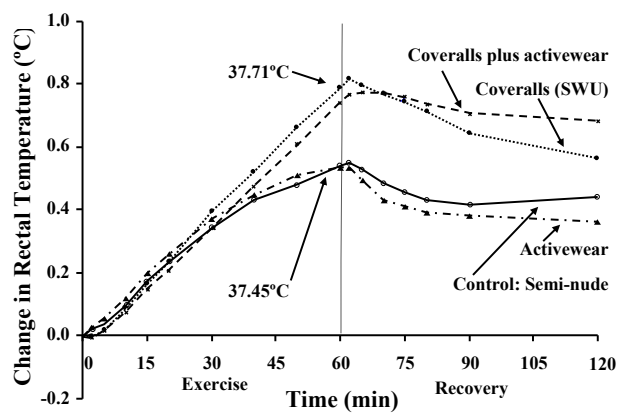


Fig. 2. Average change in rectal temperature example from the evaporative property assessment of mining work-wear

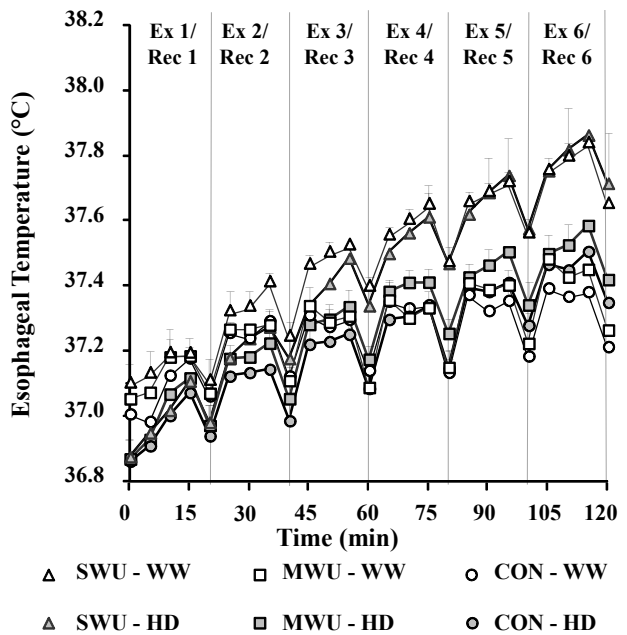


Fig. 3. Average esophageal temperature example from the intermittent work two environment assessment of mining

work-wear (SWU & MWU) versus the semi-nude control condition

in excess of accepted limits. The sub-analysis of an activewear top with work pants showed it to be more favorable than the coveralls with cotton undergarments with respect to producing smaller changes in rectal temperature and heart rate during exercise.

2.2.2 Intermittent Work & Environment

This follow-up study [11,12] explored the effects of three clothing ensembles (CON, SWU and MWU) under a more realistic intermittent work regime while also comparing hot and humid environments with a common WBGT. The 75:25 work test protocol involved the subjects performing six repetitions of 15 minutes of exercise followed by 5 minutes of rest/recovery. The constant cycling exercise metabolic work rate was ~360 W. The hot-dry (HD) and warm-wet (WW), or humid, environmental conditions, were 46°C/10%RH and 33°C/60%RH, respectively, and had a common equivalent WBGT ~29°C.

This second study demonstrated significantly less evaporative heat loss, up to ~50% less, for the humid condition compared to the dry condition through the 6 exercise:recovery cycles, minor dry heat loss for the humid condition and significant dry heat gain for the hot conditions. These losses and gains were all related to the environment's ability to absorb moisture or the temperature difference between the environment and skin temperature. In terms of changes in body heat content, the insulative effect of clothing, increasing through CON, MWU and SWU, produced escalating changes in body heat content under both environmental conditions. Also, it was found that the change in body heat content was consistently greater under the humid condition. The control ensemble (CON) demonstrated a minimal, and possibly diminishing, rate of increased esophageal and rectal temperatures through the 120 minute evaluation. The SWU ensemble caused esophageal and rectal temperatures to continually increase at a faster rate through the 120 minute evaluation. The MWU ensemble demonstrated temperature changes between that of CON and SWU ensembles but more comparable to semi-nude CON. An

example of the different effects of the clothing, as given in Figure 3, highlights the change in esophageal temperature, here the SWU resulted in a ~37.8°C maximum whereas the maxima for the MWU and CON conditions were all <37.6°C. The study also indicated the humid condition could produce greater mean skin temperature increases for each clothing ensemble, and that across conditions the MWU caused the least change in mean skin temperature. These results demonstrate a greater likelihood of workers reaching core temperature limits earlier when wearing the SWU ensemble than if wearing the MWU.

2.3 Arc-Flash and Flame Resistant (AFR) Clothing

To reduce the risk of serious injury there is an increasing interest within Canada for the more widespread use of AFR clothing beyond that used by electricians and mine rescue personnel. The AFR fabrics employed to provide greater protection can come at a cost for human heat balance, as they can be thicker, heavier, less permeable, less moisture absorbent, and looser fitting. As such, there is a belief within the mining industry that these types of clothing may cause greater thermal discomfort and pose a higher heat stress risk in deep mines. As mentioned in the Introduction, there has been research into developing suggested clothing adjustment factors for AFR clothing based upon limiting core temperature change, however it is believed that this is the first study to evaluate such ensembles in terms of body heat storage using a calorimeter.

In this most recent study [13,14] several AFR combinations were compared against the more typical work uniforms (Figure 4) and a semi-nude control as follows:

- The standard polyester cotton work-pant with either a polyester micro-fiber activewear long-sleeve shirt or an AFR long-sleeved shirt (Arc Thermal Performance Value, ATPV 8.1, flame resistant, 70% modacrylic, 15% lenzing, 15% rayon).
- Standard cotton coveralls worn over cotton undershirt.



Fig. 4. Cotton polyester work-pants with activewear and AFR long-sleeved tops; Standard cotton, fire-rated and Nomex® coveralls over AFR top, and full AFR jacket, top and pant clothing ensembles

- AFR coveralls (ATPV 9.5, 65% modacrylic, 33% aramid, 2% carbon nylon antistatic) worn over a cotton undershirt.
- Nomex® coveralls (ATPV 4.5, flame resistant 100% Nomex) worn over a cotton undershirt.
- AFR ensemble of an AFR jacket (ATPV 8.7, flame resistant, 88% cotton, 12% high tenacity nylon) worn over a cotton undershirt along with AFR pants (ATPV 10.1, flame resistant, 45% modacrylic, 35% lyocell, 15% polyamide-imide, 5% aramid).

Here, the evaluations used a 50:50 work/recovery regime across 120 minutes that included four repetitions of 15-minute cycling activity (at ~400 W) followed by a 15-minute recovery. The air supply entering the calorimeter was controlled to 35°C and 15%RH (~23°C WBGT). At this lower ambient temperature, dry heat gain from the environment is negligible

Figures 5 through 7 provide an early indication of the average results obtained from the AFR clothing trials. These figures focus on comparing the change in mean body temperature as derived from the calorimeter determined change in body heat content versus that from core and skin temperatures. Further and more exhaustive analysis is pending peer review for medical publication. This includes additional clothing ensembles for other industry sectors, assessing the progression of evaporative heat loss in relation to the total heat load, hydration, heart rate, physiological strain, thermal sensation and rating of perceived exertion. Consequently, for a more complete understanding of this research, it is highly recommended that the reader review the full results as being published elsewhere [14].

Figure 5 compares the change in mean body temperature of the work-pant long-sleeved shirt combinations, with and without AFR properties, as predicted from rectal (core) and skin thermometry (i.e. a 2-compartment model) or calculated from calorimetry determined body heat storage. Both methods tend to show a staged increasing change through the four exercise/recovery cycles. However, of more significance is that the graph shows the net change in body temperature, as derived from calorimetry, is significantly greater than that predicted from 2-compartment thermometry. Or, conversely thermometry drastically underestimates the amount of heat being stored and thereby the potential risk. Such underestimation had previously been shown for semi-nude male and female subjects to be 15-35% after 90 minutes of exercise [15] but could be in the order of ~95% after only 10 minutes of exercise. As describe above, this clothing study element used 15 minute activity periods.

Figure 6 is a similar presentation of mean body temperature changes for cotton and Nomex® coveralls worn over cotton underwear. This figure shows a similar stepped effect regardless of the fabric, through the four exercise/ recovery cycles. But again, the magnitude of the determined changes is significantly different depending on their derivation.

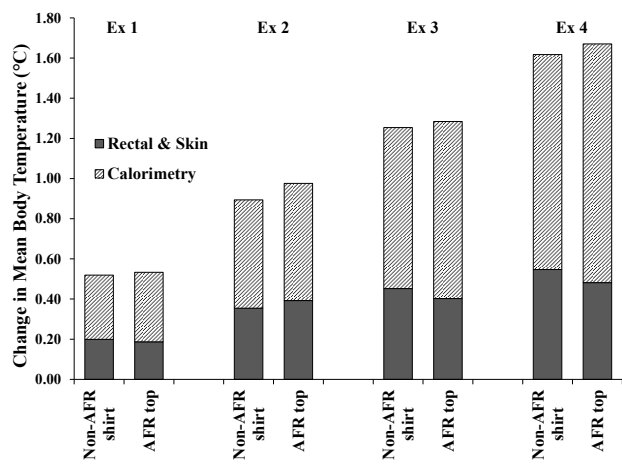


Fig. 5. Mean change in mean body temperature from direct calorimetry and indirect temperature measurement for the standard work-pant with non-AFR and AFR tops

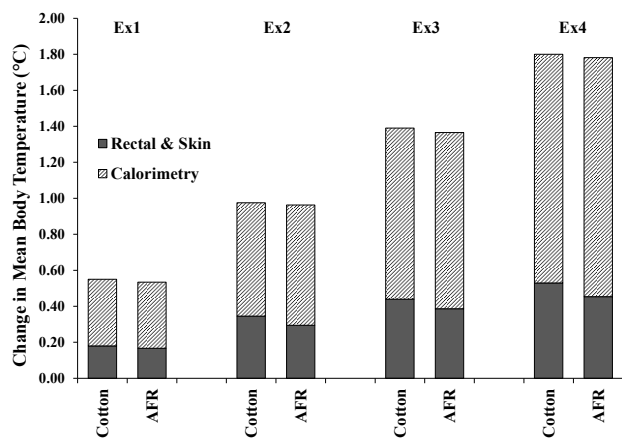


Fig. 6. Mean change in mean body temperature from calorimetry and thermometry for the cotton and AFR coveralls worn over cotton underwear

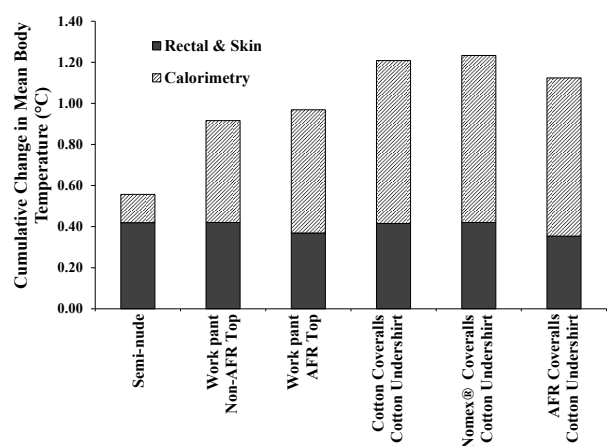


Fig. 7. Mean cumulative change in mean body temperature from calorimetry and thermometry across the control, non-AFR and AFR clothing arrangements

In both Figures 5 and 6, the calorimetry results show more clearly an overall effect of ever increasing mean body temperatures with each exercise and recovery cycle, and no sign of attaining any level of equilibrium.

Considering this trend, although the 38.0°C core temperature TLV criteria was not attained within 120 minutes, it could be a possibility for longer duration activity and would more likely occur earlier for coverall ensembles.

Figure 7 provides an inter-comparison of the cumulative change in mean body temperature through the 120 minute protocol by clothing type. It also generally supports the previous calorimeter based clothing studies that indicated coverall ensembles were more detrimental to heat loss compared to the work pant long-sleeved shirt ensembles. However, it also shows that any discrimination between clothing types and even the semi-nude condition may not have been possible using indirect thermometry.

The potential to reach a temperature limit is demonstrated more quantitatively elsewhere in terms of evaporative heat loss [14]. The results presented there generally showed that through the 120 minute assessment, in relation to the 400 W heat loss required to maintain thermal equilibrium, heat loss peaked at ~350 W for the semi-nude control condition, at ~320 W for the work-pant combinations and was ~300 W for the coverall ensembles.

Throughout, upon comparing the styles of clothing, these calorimeter based mean body temperature change results along with those detailing the evaporative cooling [14], continue to indicate coverall ensembles to be more limiting with respect to heat transfer so causing a greater rate of increasing core temperatures.

3. Discussion

Regardless of these initial results tending to show no decrements from wearing AFR equivalent clothing, with ATPV values reaching ~10 kcal/cm², when compared to their existing work wear, other factors still need to be considered. As shown by Table 2, the test subjects were young, they were also healthy, non-smoking and un-medicated, plus not hydrated prior to commencing each test. They were also heavier with a larger body surface area than the “standard” worker assumed in the WBGT criteria. The same cannot be said for the mining workforce, in the evaluation of miners and their work demands at a Canadian mine [8], the average age was 42 yrs and their average weight at 85 kg; both are even further from the standard than the test subjects. In an underground mine based assessment simulating mine rescue activities, the average age was 47 yrs and average weight 87 kg nude and 109 kg dressed and equipped [4], the latter is nearing a weight 50% greater than the standard. With age, growing health concerns and being increasingly overweight leads to the general acceptance that the body’s capacity to cool itself effectively can be compromised. Calorimetry based studies using semi-nude healthy males in 35°C with 60 & 20%RH environments have showed that the older males (~57 yrs) exhibit greater thermal and cardiovascular strain compared to both middle-aged (~44 yrs) and younger males (~26 yrs) which were comparable [16]. However, when clothed in work-wear, young and old healthy males, under common air velocity conditions, tended to exhibit comparable dehydration, hydration shifts and stress marker changes [17,18].

4. Conclusion

The results presented from the AFR clothing study generally support the need to use a calorimeter to fully understand clothing and its direct impact on human thermoregulation. Calorimeter based studies continue to show significantly more heat storage during activity that needs to be managed to ensure worker safety. Thermometry based decisions may not be sufficient.

Coverall arrangements continue to be shown as more detrimental to human thermoregulation than a work-pant/long-sleeved shirt ensemble. Higher mean body temperatures result from the heavier clothing arrangements that limit heat loss to the environment. However, in regard to the primary focus of this study, it appears within each clothing category that arc-flash or flame resistant clothing may not significantly affect heat storage when compared to its non-treated equivalent. Consequently, close fitting long-sleeved shirt ensembles with enhanced evaporative/wicking performance remain a viable option to maximize evaporative cooling of workers in mines.

Nevertheless, as this paper can only provide a generalized overview of the multi-year DMRC clothing research program, for more specific information the reader is directed to the peer reviewed journal articles referenced with each study, and to Dr. Kenny, the medical lead researcher.

Acknowledgments

In addition to their funding, the authors would like to thank the DMRC for the opportunity to perform this suite of clothing research studies and publish the results. The financial support of the numerous graduate students from other agencies, too many to mention, is greatly appreciated.

Our gratitude is also extended to Vale, Agnico-Eagle and Xstrata Nickel for providing the clothing and mining personal protective equipment throughout the studies, and lastly to the subjects who volunteered for the often demanding calorimeter tests.

References

- [1] American Conference of Industrial Hygienists (ACGIH), Heat Stress and Strain and TLVs® Documentation. (2007) Cincinnati, Ohio, USA.
- [2] ACGIH, TLVs® and BEIs® based on the documentation of the Threshold Limit Values for chemical substances and physical agents & Biological Exposure Indices, (2014), Cincinnati, Ohio, USA.
- [3] O. Jay and G.P. Kenny, Heat exposure in the Canadian workplace, American Journal of Industrial Medicine, (2010), Aug. 53(8):842-53.
- [4] S.G. Hardcastle, F.D. Reardon, G.P. Kenny & C. Allen, Assessing the work intensity of mine rescue activities and its relevance in applying heat stress management protocols, Mine Ventilation – Volume 1, pp 231-241, Proceedings Ninth International Mine Ventilation Congress, India, Ed. D.C. Panigrahi, Oxford & IBH Publishing, New Delhi, (2009).
- [5] T.E. Bernard, Heat Stress and Protective Clothing: an Emerging Approach from the United States, Annals of

- Occupational Hygiene, Vol. 43, No. 5, pp. 321±327 (1999).
- [6] C.D. Ashley & T.E. Bernard, Effects of Hoods and Flame-Retardant Fabrics on WBGT Clothing Adjustment Factors, *Journal of Occupational Environmental Hygiene (JEOH)*, (2008) Jan. 5(1):59-62.
- [7] F.D. Reardon, K.E. Leppik, R. Wegmann, P. Webb., M.B. Ducharme and G.P. Kenny, The Snellen Human Calorimeter Revisited, Re-engineered and Upgraded: Design and Performance Characteristics. *Medical & Biological Engineering & Computing*, (2006) Vol. 44: No. 8, August, pp 721-728.
- [8] G.P. Kenny, M. Vierula, J. Maté, F. Beaulieu, S.G. Hardcastle & F. Reardon, A Field Evaluation of the Physiological Demands of Miners in Canada's Deep Mechanized Mines, *JEOH*, (2012) 9:8, 491-501.
- [9] G.P. Kenny, The influence of different mining clothing ensembles on core temperature regulation, Final Report to the DMRC, (2009).
- [10] J.M. Stapleton, S.G. Hardcastle & G.P. Kenny, The Influence of Activewear Worn Under Standard Work Coveralls on Whole-Body Heat Loss, *JEOH*, (2011), 8:11, 652-661.
- [11] G.P. Kenny, Thermal and hemodynamic consequences of mining clothing systems during intermittent work in the heat, Final Report to the DMRC, (2011).
- [12] J.M. Stapleton, H.E. Wright, S.G. Hardcastle & G.P. Kenny, Body heat storage during intermittent work in hot-dry and warm-wet environments, *Applied Physiology, Nutrition & Metabolism*, (2012) Oct;37(5):840-9.
- [13] G.P. Kenny, Miner's clothing: Effects of whole-body heat dissipation during work in the heat, Final Report to the DMRC, (2013).
- [14] M.P. Poirier, R.D. Meade, R. McGinn, B.J. Friesen, S.G. Hardcastle, A.D. Flouris & G.P. Kenny, The Influence of Arc-Flash and Fire Resistant Clothing on Heat Dissipation During Work in the Heat, (2015), *JOEH* Apr 21:0. [Epub ahead of print]; DOI: 10.1080/15459624.2015.1029615.
- [15] O. Jay, L.M. Gariépy, F.D. Reardon, P. Webb, M.B. Ducharme, T. Ramsay and G.P. Kenny,. A three-compartment thermometry model for the improved estimation of changes in body heat content, *American Journal of Physiology - Regulatory, Integrative and Comparative Physiology*, 292: R167–R175, (2007).
- [16] H.E. Wright, J. Larose, T.M. McLellan, S.G. Hardcastle, P. Boulay & G.P. Kenny, Moderate-Intensity Intermittent Work in the Heat Results in Similar Low-Level Dehydration in Young and Older Males, *BioMed Research International*, (2015), Article ID 619103.
- [17] H.E. Wright-Beatty, J.M. Keillor, S.G. Hardcastle, P. Boulay & G.P. Kenny, Preservation of Cognitive Performance with Age during Exertional Heat Stress under Low and High Air Velocity, *JEOH*, (2014) 11: 144–153.
- [18] H.E. Wright-Beatty, S.G. Hardcastle, P. Boulay, J. Larose & G.P. Kenny, Increased air velocity during exercise in the heat leads to equal reductions in hydration shifts and interleukin-6 with age, *European Journal of Applied Physiology* (2014) 114:2081–2092.

Understanding the Human Thermal Balance and Heat Stress Indices as they apply to Deep and Hot US Mines

Pedram Roghanchi^a, Maurice Sunkpal^a, Karoly Charles Kocsis^a

^aUniversity of Nevada, Reno, Nevada., USA

Thermal heat stress may seriously affect the performance, overall productivity, safety and health of an individual and may decrease tolerance to other environmental hazards. Discomfort, heat illness and heat stroke are three phases of the reaction of the human body when exposed to an unstable heat balance in a hot and humid environment. Heat stroke is the most serious illness, which occurs when the core temperature of the human body exceeds the threshold temperature. Exceeding core temperatures can damage the thermoregulation functions of an underground worker and potentially generate irreversible damage to the brain and other organs. Heat stroke is a very serious illness, which carries a high risk of fatality when the underground climatic conditions are not immediately corrected.

The reaction of the human body to thermal variations involves a complex interrelationship between climatic factors and physiological responses. A heat stress index integrates personal, physiological, and environmental parameters into a single number for a quantitative assessment of thermal environments. Heat stress indices can be divided into three groups: rational, empirical and direct indices. Over decades, more than one hundred heat stress indices have been proposed for various thermal environments. No single heat index has given a holistic assessment of the human thermal environment. However, each heat stress index has special advantages that make it more suitable for use in its particular environment.

This paper aims to review and summarize the existing heat stress indices commonly used for assessing the heat stress conditions in underground mining environments. Heat stress indices will be categorized based on the thermal comfort parameters (dry-bulb temperature, wet-bulb temperature, black-globe temperature, wind velocity, metabolic rate, and clothing). The advantages and shortcomings of using a heat stress index for evaluation of an underground mine environment will be assessed. The physiological response of the human body to thermal stress will be made. Various modes of heat exchange events associated with the human body and its corresponding physiological reactions to hot and humid environments will also be analyzed. Furthermore, a discussion of the possibility of determining an empirical and/or rational index which would offer adequate protection for the underground workforce in the US will be made.

Keywords: Heat, Human Thermal Balance, Thermal Comfort, Energy Balance Equation, Heat Stress Index

1 Introduction

As the base and precious metal mines in the US become deeper, more productive and further mechanized, the underground workforce will be exposed to an increasingly hot and humid environment. Appraisal of the thermal environment is becoming more important due to significant effects of excessive heat on safety and health of the underground miners. These effects on individuals can be from thermal discomfort to heat-related illnesses such as thermal stress, heat cramps, heat rash, and heat stroke.

Assessment of the thermal environment includes an extensive monitoring of temperature and humidity with adequate thermal management protocols established for each underground mine. Controlling methods include reducing heat loads in the development and production workings and throughout the mine by means of ventilation, localized cooling systems, and refrigeration. The evaluation of the climatic conditions of an environment requires extensive measurements and modeling strategies. However, a simple tool is required to have a valid and acceptable evaluation of climatic condition on regular bases. A heat stress index integrates personal, physiological, and thermal environment parameters into a single number for a quantitative assessment of heat stress. Heat stress indices can be grouped into: (1) rational indices, which are based on calculations involving the heat balance equation; (2) empirical indices, based on objective and subjective strain; and (3) direct indices, which involve direct measurements of environmental variables. The use of a

heat stress index makes it possible to evaluate and compare the climatic conditions in an underground mine during development and production processes. Over the decades, more than one hundred heat stress indices have been proposed for various thermal environments. No one single heat index has given a holistic assessment of the human thermal environment. However, each heat stress index has special advantages that make it more suitable for its particular environment.

Our goal is to identify and recommend heat stress indices that are more convenient for underground mining application. We identified twenty eight (28) heat stress indices suitable for an underground climatic assessment. In this paper, we discuss the effect of excessive heat on the human body, the thermal comfort, and energy balance equation. A review of the definition, history, and limitations of heat stress indices is also performed. We present a summary of international standards and regulations. The selection criteria available for underground mining applications are assessed and questioned.

2 Human Response to the Thermal Environment

Humans are comfortable within a very small range of core body temperatures. Biochemical processes in the body will not function if the temperature becomes too low or too high. At high temperatures, enzymes lose their activity and at low temperatures there is inadequate energy to continue metabolic processes. When the core

temperature rises above 40°C (104°F), hyperthermia occurs, and hypothermia occurs below 35°C (95°F). Humans can tolerate extreme core temperatures below 35°C (95°F) or above 41°C (106°F) for only brief periods of time. To maintain the internal temperature within these limits, the human body exhibits very effective and in some instances specialized physiological responses to critical thermal stresses. These responses facilitate the conservation, production or elimination of body heat. This is achieved through finely controlled coordination of several body systems [1].

2.1 Human Heat Regulation

The various human body systems must synchronize their activities to perform physical activity. These systems have the capacity to adapt when exposed to the stresses of specific environments. There are mechanisms by which the body can regulate its core temperature both at rest and during activity, and in both hot and cold or humid environments. [2]. Through its intricate temperature regulation, the human body is able to reach a state of thermal equilibrium with the surrounding environment when the variation of internal energy, at the body core level is equal to zero [3]. The thermal exchange between a subject and the environment is equal to the difference between metabolic heat and thermal losses due to respiration and exchanges of heat through the skin surface.

3. Thermal comfort

Thermal comfort is the condition of mind which expresses satisfaction with the thermal environment [4]. The environmental conditions required for comfort are different for individuals because there are variations, both physiologically and psychologically, from person to person. Hence, the best approach is to provide a thermal environment that satisfies the majority of people in the workplace. Based on ASHARE definition [4], the thermal comfort zone is the condition that “80% of sedentary or slightly active persons find the environment thermally acceptable.” Three parameters need to be satisfied for a person to be in the thermal comfort zone, as follows: (1) sweat rate is within comfort limits; (2) the

body is in heat balance; (3) mean skin temperature is within comfort limits [3].

Assessment of thermal comfort must start with the appreciation that comfort is a state of mind. It is extremely difficult to classify the many factors which affect thermal comfort; the interaction between the physical demand imposed upon the individual, his physiological status and his psychological attitudes must be considered in interaction with social customs, tangible perceptions and among other considerations [5]. Because thermal comfort is subjective, it is difficult to satisfy all individuals with a simple environmental specification.

Regardless of difficulties in defining the thermal comfort zone, attempts to define the parameters affecting the human thermal environment and its sensation to thermal comfort were made. By the end of the nineteenth century, four important components of the environment, temperature, humidity, air speed of movement, and the intensity of radiation, were recognized [6].

Undeniably, thermal comfort depends on the interaction between three groups of elements: environmental factors, clothing factors and physiological factors. Fanger [3] established that the interaction of six fundamental factors can define the human thermal environment. Temperature, radiant temperature, humidity, and air movement are the four basic environmental variables. Behavioral factors are clothing and metabolic rate.

Table 1. Thermal comfort parameters

Environmental	1. Dry bulb temperature (T)
	2. Black-globe temperature (MRT)
	3. Wind velocity (V)
	4. Relative humidity (RH)
Behavioral	5. Clothing (Clo)
	6. Metabolic rate (M)

Table 2. Five thermal effect zones associated with thermal and comfort sensation [2, 7, 8].

Vote	Thermal Sensation	Zone of Thermal Effect	Comfort Sensation	Total Heat Storage (S)
	Very hot	In-compensable heat zone	Very uncomfortable	$S \gg 0$
3	Hot	Sweat evaporation compensable zone	Uncomfortable	$S \approx 0$
2	Warm		Slightly uncomfortable	
1	Slightly warm	Vasomotor compensable zone	Comfortable	$S = 0$
0	Neutral			
-1	Slightly cool			
-2	Cool	Shivering compensable zone	Slightly uncomfortable	$S \approx 0$
-3	Cold			
	Very Cold	In-compensable cold zone	Uncomfortable	$S \ll 0$

4. Heat Balance Equation

Sustaining core temperature involves a balancing act between heat loss and heat production. The body is in a state of thermal equilibrium with its environment when it loses heat at the same rate as it gains heat. The relationship between the body's heat production and its

heat gains and losses can be expressed mathematically using the first law of thermodynamics. This makes it possible to assess the human body's thermal balance with the following well-known equation (see table 3) [9]:

$$S = M - W - (C_{res} + E_{res} \pm C \pm R + E) \quad (1)$$

where:

- M : Metabolic rate
- W : External work rate
- C_{res} : Respiratory convective heat loss,
- E_{res} : Respiratory evaporative heat loss
- E : Evaporation of the sweat
- C : Convection
- R : Radiation
- S : Heat storage in the body

When air is inhaled during respiration its temperature and humidity are at different levels with respect to the core of the body. The body's internal heat is transferred relative to the level of activity, to the external environment by convective (C_{res}) and evaporative (E_{res}) exchanges. Respiratory heat losses depend on the level of activity performed by the subject and the temperature and humidity of the air in the environment. Respired vapor loss, (E_{res}) comprises latent respiration heat loss (E_{res}) and convective or sensible respiration heat loss (E_{res}). Evaporative heat loss from skin surface (E_{sk}), is made of evaporative heat loss by skin diffusion (E_{sk}), and heat loss due to regulatory sweating (E_{sw}) [9].

The human body external surface is characterized by thermo-conditions that are dissimilar from those of the neighboring environment. This prompts thermal exchanges between the subject and environment. These interactions are in the form of “sensible” heat losses: by convection (C), radiation (R), and conduction (K) and “latent” heat losses owing to sweat evaporation, (E) [10]

5. Heat Stress Index

The idea of the thermal index goes back to 18th century [11]. Without considering dry-bulb temperature, perhaps the first published heat stress index was wet-bulb temperature proposed by Hardlane [12]. Since then a large number of heat stress indices have been proposed. Many of the earlier indices only included four environmental factors, such as: Effective Temperature (ET), Equivalent Temperature (E_{eq}), Operative Temperature (OpT), and Wet-bulb Globe Temperature (WBGT). Later, new indices took into account clothing and metabolic rate as behavioral parameters. Furthermore, indices such as WBGT and ET were later modified to take into account the effect of clothing.

As shown in Fig. 1, over the years, more than 162 heat stress indices have been proposed by many authors for use in a specific climatic condition [13]. Fig. 1 shows the trend of heat stress indices proposed from 1905 to 2012. The trend is almost linear after 1950; approximately two heat stress indices were proposed each year. This indicates two important aspects of heat

stress indices. First, the large number of indices demonstrate that none of these indices is valid as a universal heat stress assessment index. Belding [14] and Gagge and Nishi [15] mentioned that having a unique valid system for rating heat stress is not possible since the interaction between the climatic parameters is complicated. An index that integrates these parameters and correlates them with the physiological response of the body has not been developed.

Second, the large number of indices generates confusion. Many of these indices were developed for specific climatic conditions. There may be limitation(s) that make these indices inadequate for other climatic conditions. Therefore, it will be difficult for users to choose an appropriate index, since no one single index includes all environmental and behavioral factors and conditions.

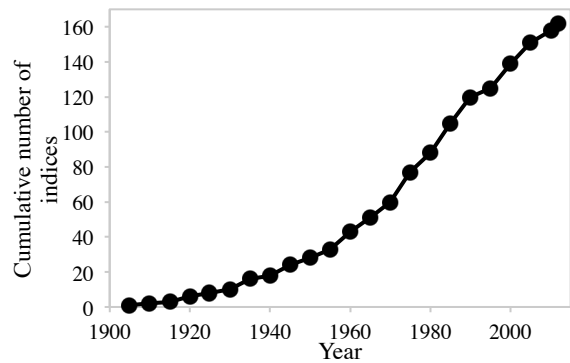


Fig. 1. Cumulative number of indices from 1905 to 2012

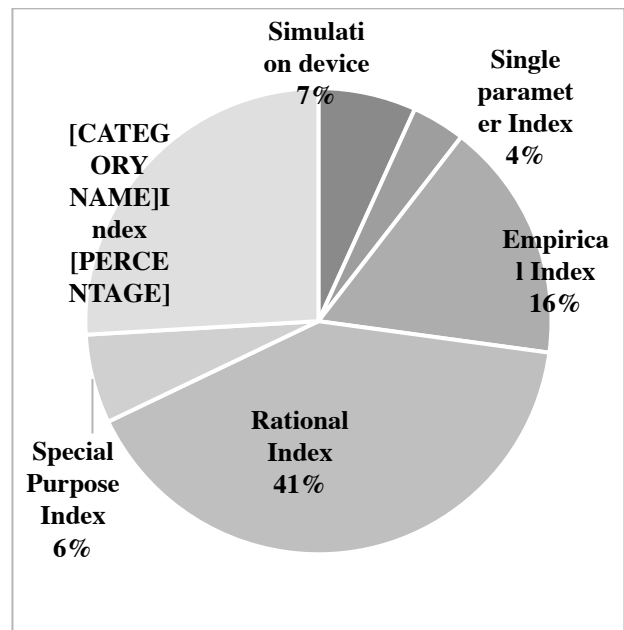


Fig. 2. Heat stress indices classification [13]

Table 3. The terms of the energy balance equation can be logically expressed as a function of the thermal comfort parameters [2]

Terms in the thermal balance equation	Comfort Parameters					
	M	Clo	T	V	MRT	RH
Metabolic power, M	<input type="checkbox"/>					
Mechanical power, W	<input type="checkbox"/>					
Respiratory convective heat loss, C _{res} ,	<input type="checkbox"/>	<input type="checkbox"/>	<input type="checkbox"/>			
Respiratory evaporative heat loss, E _{res}	<input type="checkbox"/>					<input type="checkbox"/>
Convective heat loss, C		<input type="checkbox"/>	<input type="checkbox"/>	<input type="checkbox"/>		
Radiation heat loss, R		<input type="checkbox"/>			<input type="checkbox"/>	

6. Limitations of Heat Stress Indices

Heat stress indices can be divided into three groups:

1. Rational, based on energy balance equation
2. Empirical, based on objective and subjective strain
3. Direct, based on direct measurements of parameters.

Presently, no one single index can be used as universal valid index for all thermal environments. Many of these indices were developed for a specific use. It is thus the user's responsibility to examine each index and choose the one that best suits the defined thermal climate.

There are some general limitations that should be taken into account for many of the heat stress indices, as follows:

1. Many of the indices do not include a wide range of climatic conditions. These indices may be precise for a climatic condition (e.g. warm environment), but inappropriate for others. A good example is the scale of

the 'Equivalent Temperature Index', which does not extend beyond 75 °F. Therefore, an engineer may have to work with more than one heat stress index if the environmental condition changes.

2. Inbuilt errors exist in some of these indices. Several indices (in particular direct indices) are developed based on algebraic or statistical models. There is some degree of error when these mathematical methods are applied. An example is the error of 'Effective Temperature Index' scale in wind speed at high temperature [16].

3. Important factors such as acclimation (the process of becoming adjusted to an environment) cannot be included [6, 17]. In a given level of heat stress, heat strain experienced by an acclimated individual is different from a non-acclimated person. Many of the indices do not distinguish between acclimated and un-acclimated subjects in their application.

4. Brake & Bates [18] states that most heat stress indices were developed for externally paced work. Increasing degree of mechanization of heavy tasks and

new regulations result in informed workers that support self-pacing in thermally stressed climates.

5. Averaging method is not always physiologically valid. Many of the indices are developed based on thermal stress of the workers and averaging of large

experimental data. Though, the reaction of the individuals to heat load can be modified by age, gender, etc. The response of a group of self-paced, acclimated workers to heat will differ from a group of non-acclimated, less experienced workers.

6. The validity and reliability of many indices are questionable. For example, Discomfort Index (DI) was developed as a simplified version of WBGT [16]. In the WBGT index, globe temperature (GT) measures the combined effect of radiant heat, air temperature, and air speed. DI does not take into account air speed by replacing GT with ambient temperature, which may cause significant error in evaluating some climatic conditions.

7. The primary purpose of evaluating climatic conditions is to assess the environment and re-design it so that to be to meet safety, health and comfort of workers [6]. None of the indices can take into account all the comfort determining factors and their interrelation. Therefore, the environment should be assessed on regular bases irrespective of the comprehensives of the applied index.

7. Selection Criteria

Thermal assessment of the underground mine environment, particularly in active areas, should be done routinely by ventilation engineers. The choice of an index for this purpose is of great importance and critical.

An index should be simple to use, accurate for moderate to hot climates and involve minimal manpower and instrumentation in measurements, calculations and interpretation of results.

The following criteria should be satisfied when an index is used for assessing thermal environment in underground mines:

1. Applicability in the chosen industry should be confirmed;
2. All major heat load contributing factors in mining conditions should be included;
3. Measurements, calculations and interpretation should be simple;
4. The included factors should have valid weight in relation to the total strain;
5. The index should be applicable for the purposes of mine climatic guidelines or limits [17, 18].

No existing index meets all these requirements. On the one hand, direct and empirical indices have relatively simple measurement and calculation procedures. They however do not encompass the physiological comfort

parameters for evaluating total strain. This is because many of these indices are developed using statistical and simple mathematical methods and not upon the energy balance equation. On the other hand, rational indices may be more comprehensive and accurate compared with other types of indices. The problem is that the measurement and calculation procedures are complex and difficult to comprehend.

8. Comparison and Selection of Heat Stress Indices

Several research studies looked to assess, compare and select the most appropriate heat stress index for a particular application. These attempts can be grouped into comparison methods including:

(1) *Experiment*: Examination of acclimated and/or un-acclimated individuals in different range of activity and climatic conditions and study of physiological and behavioral responses of human body to hot-humid environments (e.g. [20, 21]).

(2) *Comparison*: Based on thermal comfort parameters (e.g. [8, 20]).

(3) *Climatic data analysis*: Analysis of climatic condition with assumed data or climatic databases as input parameters of (e.g. [21, 22]).

(4) *Rational methods*: Use of different rational methods to examine the accuracy and applicability of heat stress indices (e.g. [23, 24]).

There are other research projects and comparison methods not mentioned in this paper.

9. Summary and Discussion

As the increasingly mechanized underground mines in Northern Nevada become deeper, the issue of heat becomes a significant problem. Hot and humid environments can seriously affect the performance, overall productivity and most importantly the ability of the underground workforce to perform work in a safe manner. Therefore, thermal assessment of the underground mine environment, particularly in the active areas, should be performed regularly by ventilation engineers.

It is not practical to review and compare all the available indices based on the mentioned methods. Generally, we know that in underground mine environments, it is not practical to measure and collect a large number of physiological and human-related factors. A discussion shall be made to debate how accurate a heat stress index should be for the underground mine environments. An investigation of the accuracy of simple indices (e.g. mostly direct indices) may lead to a simple index which is at least precise in its range and accuracy.

The large number of available heat stress indices and shortcomings of current selection criteria would make it difficult to choose an applicable index. Many of the underground mines in the US and around the world choose an index while they are unaware of its limitations. The current criteria do not specify the use of standard instruments and their calibration procedures, which could be a significant source of error. The small size of the black globe (often less than the standard 150

mm) used in the measurement of GT is a typical example.

In the next stage of the NIOSH project, we are working on a new evaluation and selection method for the mining industry to make it easier to choose a heat stress index for thermal climatic assessments. A comprehensive but simple selection criterion seems to be necessary mainly for underground mining application.

Our goal is to define and recommend one or more indices that can effectively protect the underground workers in hot US mines. It will be difficult to suggest one index that can be used in the western US mines, only. Though, it can be a fairly acceptable guideline to show the performance and safeguard of these heat stress indices in various climatic conditions. Based on this principle, we can define heat stress indices for any type of climatic condition including the base and precious metal mines in USA.

So far, for the precious metal mines in western USA we selected 28 heat stress indices (10 direct indices, 8 empirical indices and 10 rational indices) for comparisons. In each particular index we have defined the parameters as well as the weight of each parameter based on model sensitivity. We are presently comparing these heat indices based on:

1. Weights of each parameter
2. Simplicity and applicability
3. Instrumentations and requirements
4. Validity of indices using maximum rate of sweating

By developing our comparison model, we can then compare any other index that contains thermal comfort parameter(s).

Acknowledgement

This project is funded by National Institute of Safety and Health (NIOSH). The authors would like to acknowledge the partner mines in the state of Nevada for their collaborations to this project.

References

- [1] J. Naish et al, Medical sciences, Elsevier Health Sciences, London, 2009.
- [2] J. King, Thermoregulation: Physiological Responses and Adaptations to Exercise in Hot and Cold Environments. Journal of Hyperplasia Research. 4(3) (2004).
- [3] Fanger PO (1970) Thermal Comfort, Danish Technical Press, Copenhagen.
- [4] ASHRAE, 2009. ASHRAE handbook, Fundamentals. 1st Edn. ASHRAE, Atlanta, GA., ISBN: 9781615830015.
- [5] R. Goldman, The handbook on clothing, biomedical effects of military clothing and equipment systems, Report NATO Research Study Group 7, Brussels, 1988.
- [6] R. K. Macpherson, The assessment of the thermal environment. A review, British Journal of Industrial Medicine 19(3) (1962) 151-164.
- [7] Y. Shapiro and Y. Epstein, Environmental physiology and indoor climate—thermoregulation and

- thermal comfort, *Energy and Buildings* 7(1) (1984) 29-34.
- [8] Y. Epstein and D. S. Moran, Thermal comfort and the heat stress indices, *Industrial Health*, 44(3) (2006) 388-398.
- [9] M. Beccali et al, Thermal comfort, *Encyclopedia of Energy*. 6(2004) 55-64.
- [10] JLM. Hensen, On the thermal interaction of building structure and heating and ventilating system. PhD thesis, Technische Universiteit Eindhoven; 1991.
- [11] R. A. Graveling, et al, Working in hot conditions in mining: a literature review, Institute of Occupational Medicine, Edinburgh, 1988.
- [12] J. S. Haldane, The influence of high air temperatures No. I, *Journal of Hygiene* 5(4) (1905) 494-513.
- [13] C. R. de Freitas and E. A. Grigorieva, A comprehensive catalogue and classification of human thermal climate indices, *International Journal of Biometeorology* 59(1) (2015) 109-120.
- [14] H. S. Belding, The search for a universal heat stress index, *Physiological and Behavioral Temperature Regulation*. IL: Springfield, 1970.
- [15] A. P. Gagge and Y. Nishi, Physical indices of the thermal environment, *ASHRAE Journal*, (United States) 18(1) (1976) 47-51.
- [16] F. R. ALFANO et al, Thermal environment assessment reliability using temperature-humidity indices, *Industrial Health*, 49(1) (2011) 95-106.
- [17] G. M. Budd, Wet-bulb globe temperature (WBGT)—its history and its limitations, *Journal of Science and Medicine in Sport*, 11(1) (2008) 20-32.
- [18] D. J. Brake and G. P. Bates, Limiting metabolic rate (thermal work limit) as an index of thermal stress, *Applied Occupational and Environmental Hygiene*, 17(3) (2002) 176-186.
- [18] National Institute for Occupational Safety and Health. Criteria for a recommended standard occupational exposure to hot environments (Publication No. NIOSHHSM-72-10269) Cincinnati: Author, 1972.
- [19] R. A. GRAVELING, Working in hot conditions in mining, a literature review, National Technical Information Service, Report 22161. Springfield, VA., US Department of Commerce, (1988) 53-77.
- [20] P. Mairiaux and J. Malchaire, Comparison and validation of heat stress indices in experimental studies, *Ergonomics*, 38(1) (1995) 58-72.
- [21] C. Pulket et al, A comparison of heat stress indices in a hot-humid environment. *The American Industrial Hygiene Association Journal*, 41(6) (1980) 442-449.
- [22] M. Beshir and J. D. Ramsey, Heat stress indices: a review paper. *International Journal of Industrial Ergonomics*, 3(2) (1988) 89-102.
- [23] K. Blazejczyk et al, Comparison of UTCI to selected thermal indices, *International Journal of Biometeorology*, 56(3) (2012) 515-535.
- [24] A. Zuhairy and A. Sayigh, The development of the bioclimatic concept in building design, *Renewable Energy*, 3(4) (1993) 521-533.

Heat Management in a Potash Mine

Ryan Isaac Anderson^a, Euler De Souza^a

^aMosaic Potash, Esterhazy, Saskatchewan, Canada
^aQueen's University, Kingston, Ontario, Canada

Heat management in mines is crucial to both equipment and personnel. The ability to accurately estimate heat flow and transfer allows the mine ventilation engineer to limit and minimize exposure. This paper looks at both the methods to calculate heat losses from equipment infrastructure and heat transferred into the rock and sumps throughout the area of interest. Verification methods are also presented to further strengthen the techniques used for modeling.

Keywords: heat load, heat flow, heat management, heat monitoring, psychrometry.

1. Introduction

Heat management practices in underground mines, through applied engineering and work practice controls, have a direct impact on the health and safety of workers and the operation of equipment. Heat production control has become a greater focus in underground mining as current mining practices rely more heavily on electrical infrastructure and equipment.

This paper presents a complex study on the management of heat generated from pumping infrastructure in a Saskatchewan Potash Mine. The study area is 5.6 kilometers of underground excavations within series ventilation (cascading) and recirculation circuits. There are over 20,515 kW of electric motors resulting in 305,000 Watts of lost power and atmospheric heating. In addition to these motors there are 49.6 kilometers of electrical power cables and the associated electrical controls and transformers, which also lose energy to heat throughout the area.

This paper describes the methodology and instrumentation used to collect environmental heat load data for interpretation and analysis. Data is collected from environmental monitoring stations located through the circuits in conjunction with equipment monitoring heat penetration into the rock strata. Calculated heat loads are assessed using ventilation modeling software and calibrated using real time data. This data, through application of management control strategies, is used to address current heat conditions underground, eliminate heat stress, and extend the life of equipment. The modeling techniques presented in the paper are valuable tools used in the planning of current and future projects.

2. Heat loads

2.1 Identification of heat sources

The study area within the potash mine is confined to infrastructure excavations required to pump brine to the surface. The brine storage study area encompasses 5.6km of excavation. Within the circuit there are individual areas that have instrumentation installed and monitored. The study area makes up 3.2km of the brine

transport excavations. The remaining 2.4km is inaccessible, with limited monitoring capabilities.

In order to identify the locations and sources of heat, the study area was broken down in 14 zones. Each zone was further broken down into 20 meter sections to be used for future computational modeling. Within each section the heat source components were identified. The 20 meter zones allowed for individual point sources of heat to be applied to the system. This process is used in the ventilation software program Climsim, developed by Mine Ventilation Services Inc. [1]. The Heat Management Study Area and zone locations are identified in Figure 1.

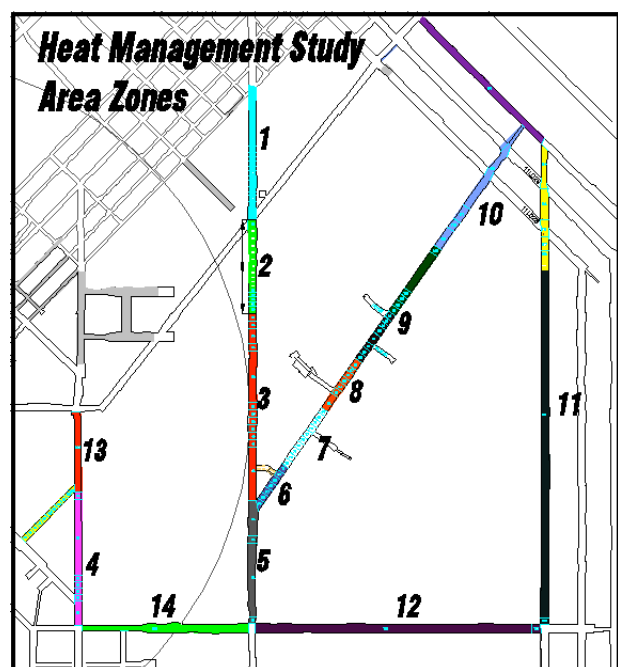


Fig. 1 Heat Management Study Area

To identify the sources of heat, an equipment survey was conducted throughout the 14 zones recognized as potentially containing heat sources. To verify sources of heat and heat sinks an infrared camera was used to visually detect differing surface temperatures. This resulted in some items that were initially identified as sources being negated. Junction boxes, which include

breakers, contactors, feeders, and disconnect switches were excluded from the list and had an equivalent length based on the length of cable within the box added to the total length of the zone. Additionally the sclear piping, used to transport brine from the brine storage areas to the pumps, were removed from the list after a temperature survey was conducted along the external pipe length.

2.2 Electrical cable

The study area consisted of a measured 49.6km of cable. The cable types were surveyed to include the wire gauge, voltage, number of cores, amperage, and core resistance. The resistance characteristics were found using the DC and AC resistance of copper conductors, in nominal ohms per 1000ft, supplied by the manufactures.

The heat losses supplied to the environment were calculated based on the resistances of the cables cores, with 100% of the losses of the electrical energy within the cable being converted to heat, using the equation provided by White et al[2]:

$$\frac{\text{Watt loss}}{ft} = (I + 0.048I)^2 \cdot R \cdot (\text{number of core}) \quad (1)$$

This equation assumes a diversity factor of 60%, where the average load in the cable over time is 60% of full load. The calculation used in Equation (1) assumes an ambient temperature of 26°C. The losses increase by an average of 2.3% when the ambient temperatures increase to 32°C. Different types of insulation may also account for minimal potential variations in losses. The increase in losses due to ambient temperature rise and inconsistency in insulation were excluded from the load calculations.

2.3 Transformers

To provide power to the pumping infrastructure there are banks of transformers set up in areas throughout the circuit. During the survey of the transformers the temperature rise, apparent power load (KVA), and power factor were collected off the name plate. Load factors (LF) were provided by NEMA TP1 Efficiencies [3]. Total Losses were determined using:

$$\text{Total Losses} = \text{no load losses} + \text{load losses} = I^2 R \quad (2)$$

With full load capability in KVA, the full load losses are calculated using:

$$\text{Full load losses} = pf \cdot kVA \cdot \left(\frac{100}{\eta} \right) \cdot \left(\frac{1}{100} \right) \cdot (2 + LF) \cdot \left(\frac{1}{\eta} \right) \quad (3)$$

In the above equations, pf is the power factor, LF is the load fraction for peak efficiency (0.35 or 0.5) and η is the efficiency corresponding to kVA and unit type.

A temperature correction factor must be applied to the full load losses calculation that take into account the dry type transformers used in the pumping infrastructure circuit. The Standard Reference Temperature (C°) T_{REF} was found using limits for temperature rise for dry-type units [2]. The correction factor equation is:

$$\text{Temperature correction factor} = \frac{T_{REF} - T_{AMB}}{T_{REF} - T_{MIN}} \quad (4)$$

$T_K = 234.5^\circ\text{C}$ for copper windings

No load losses were calculated using:

$$\text{No load losses} = pf \cdot kVA \cdot 1000(LF) \cdot \left(\frac{100}{\eta} \right) \cdot LF^2 \cdot \text{load loss} \quad (5)$$

There is a calculated 100% utilization of the transformers throughout the excavation, which are dry type transformers.

2.4 Motors

Throughout the areas there are a number of motors, predominantly found on pumps. There are two primary types of pumps that are used for brine transport throughout the excavations; Siemens and TECO. During the motor survey process, the name plate information was collected, which included the horse power, motor speed (RPM), and efficiency. Motors that run periodically with minimal use have been excluded from this list. This includes compressors and hydraulic pumps. Using the motor efficiencies, the heat loss can be calculated using [2]:

$$\text{watts loss} = Hp \cdot 745.7 \cdot \left(\frac{100}{\eta} \right) \cdot \left(\frac{1 - \eta}{100} \right) \quad (6)$$

Calculations are made with a 100% utilization of the motors to calculate lost watts in the form of heat energy.

2.5 Settling tanks

Brine settling tanks are used to drop the larger pieces of debris out of flow suspension before advancing to the high pressure pumps. Large brine containment vessels with significant surface areas exposed to the excavation are used for the debris collection. In order to calculate the amount of heat removed through the settling process, the brine with the entrance and exit of the tanks was measured to find the temperature change. Additionally the volume and flow rate were measured. In order to calculate the change in heat energy, the heat capacity of saturated brine at 30°C was required. A heat capacity of 2979.88 J/kg°C was used to estimate the heat capacity of brine with a salt content of 260 g/kg.

In addition to the settling tanks, overflow and drainage systems are in place to collect leaking brine. These collection areas are irregular in flow and removal, which proves difficult to model in heat load analysis.

3. Instrumentation

3.1 Psychrometry

The data for analysis was collected with the use of Accutron Climatrax multi variable sensors and Onset HOBO data loggers. The Climatrax units are capable of measuring and displaying dew point, heat index, relative humidity, pressure, dry bulb temperature, wet bulb temperature, wet bulb globe temperature, and air density. The data was then collected using a HOBO four channel data logger. The four environmental factors monitored are dry bulb, wet bulb, relative humidity, pressure. Density was also manually collected and recorded during point surveys from the instrument. The monitoring units and data logger were mounted onto a 1.5m stand with its own power source and placed strategically throughout the circuit at the beginning and ending of the areas. Prior to placing the monitoring station throughout the circuit, a thorough investigation of adequate mixing due to turbulence in the air was conducted. Drift traverse point measurement surveys were taken to ensure homogenous environmental characteristics within the cross section of the drift. Once suitable locations were selected, the monitors were engaged.

3.2 Airflow

Airflow was monitored using hand held vane anemometers as well as Accutron metering systems placed in critical zones. Surveys were conducted regularly and checked against the stationary monitoring equipment. Airflow is consistent throughout much of study area due to the installation of bulkhead fans. Booster fans are located throughout the study area to promote adequate airflow and minimize leakages.

3.3 Rock heat absorption

The heat absorbed by the rock was monitored with Hukseflux HFP01 heat flux plates and MadgeTech dataloggers. The heat flux plate monitoring system was an adaptation of soil thermal conductivity testing equipment. Heat flux test sites included locations on the back and side walls where the Climatrax environmental monitors were placed. In order to ensure accuracy of the instrumentation, two heat flux plates were installed in close proximity to each other at each selected location. The surface for the instrumentation was prepared by grinding down the rock salt to provide a flat even surface within the rock strata. The site then had a thermally conductive adhesive applied as a medium between the heat flux plate and the rock surface. This assured complete contact between the plate and the site.

4. Results

To calculate the energy lost to the atmosphere as heat, the efficiency of the equipment was calculated at full load and continuous use. This was applied to all sources of heat with the exception of the electrical cables, which are based on 60% of full load. As a result

there are significant fluctuations in the total watts lost to the atmosphere based on equipment found within each zone. The primary sources of heat energy result from losses with transformers and pumping equipment. A typical 2500 kVA transformer results in a calculated 31,800W of lost power. There are a wide range of pumps used within the study area. The largest of these has a 597 kW motor, providing a calculated 28,100W of lost power. In contrast, there is a high diversity of electrical cable used. The largest losses occurring with the 4/0 cable are 15.35W/m. Individually, cables were a minimal source of lost energy, however the significant lengths proved to be an important source of losses.

In order to estimate the heat flow of the system (\dot{q}_r), enthalpies of the individual zones were calculated and applied to the mass flows. Measurements of the environmental conditions, including dry bulb, wet bulb, pressure, and density were collected from instrumentation and confirmed with surveys. The following equations were applied to account for the changes in the moisture content in the air [4]:

$$\dot{q}_r = \dot{M}_r (\Delta S + B) \quad (7)$$

$$S = h + 4.187 \cdot W + t_{wb} \quad (8)$$

$$h = 1.005 + t_{db} + W(2501.6 + 1.884 + t_{db}) \quad (9)$$

$$W = 0.622 \cdot \frac{P_v}{P_a - P_v} \quad (10)$$

$$\dot{M}_r = Q + w \quad (11)$$

Where \dot{M}_r is the mass flow (kg/s), ΔS is the sigma heat change (kJ/kg), B is a term which depend on the process involved and on the change in moisture content, h is the specific enthalpy (kJ/kg), W is the apparent specific humidity (kg/kg), P_v is the vapor pressure in the air (kPa), P_b is the barometric pressure (kPa), Q is the flow rate (m^3/s), and w is the air density (kg/m^3). The resultant flow of heat can be viewed in Table 1.

In addition to heat sources within the study area, there are heat sinks. The primary heat sinks are within the rock strata and brine tank locations. Potash and salt have relatively high thermal conductivity to transfer heat from the air into the rock strata. In order to evaluate the rock removal of heat, the calculated rock and sump removal in W/m^2 must be compared to the collected data. The trended data found in Figures 2 and 3 show a high degree of correlation between the measured rates and the calculated rock removal in zone 8, which does not have a settling tank or sump. When evaluating the calculated heat removal in all 14 zones, there are seven that fall within acceptable rates of less than $6.4W/m^2$. Furthermore there are three zones which are extraordinarily high. These can be attributed to the settling tanks and overflow sumps located within zones 6, 7, and 10. The high calculated removal rates may also be attributed to the assumed full utilization of the equipment. Although ideally there would be continuous operation of all the equipment for maximization of the pumping infrastructure, in practice this does not occur at a steady state.

Table 1. Summary of heat load study

Summary of Heat Load Study					
Area Number	Total Heat Loss (W)	Heat Flow (W)	Rock Heat Removal (W)	Room Area (m ²)	Rock and Sum Heat Removal per Unit Area (W/m ²)
1	187435.5	65.8	187369.8	12565.2	14.9
2	202534.2	171.1	202363.1	12440.7	16.3
3	35620.1	-540.8	36160.9	15995.2	2.3
4	82022.8	489.0	81533.8	7036.5	11.6
5	6710.6	39.4	6671.2	6561.1	1.0
6	129160.3	1308.2	127852.1	3962.0	32.3
7	224794.4	161.3	224633.1	7063.7	31.8
8	17166.5	98.2	17068.2	3952.1	4.3
9	150918.0	260.9	150657.1	7706.1	19.6
10	485040.9	1304.0	483736.9	6067.5	79.7
11	20239.0	-142.0	20381.0	3189.4	6.4
12	10212.1	141.0	10071.2	15039.8	0.7
13	10815.3	188.3	10627.0	4890.2	2.2
14	19789.0	20.6	19768.4	14237.7	1.4

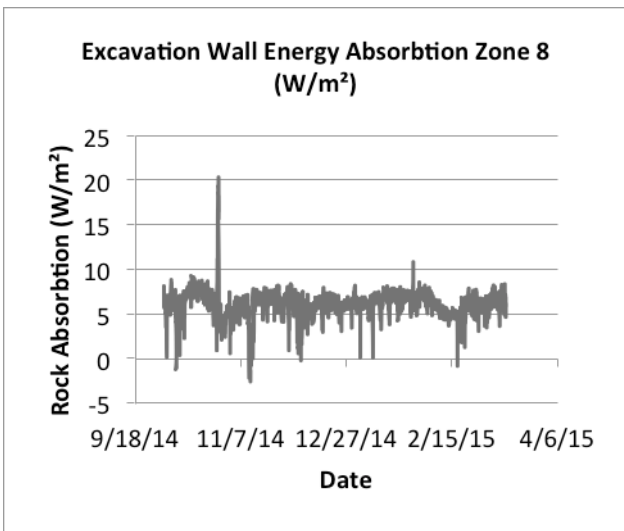


Fig. 2. Excavation wall energy absorption.

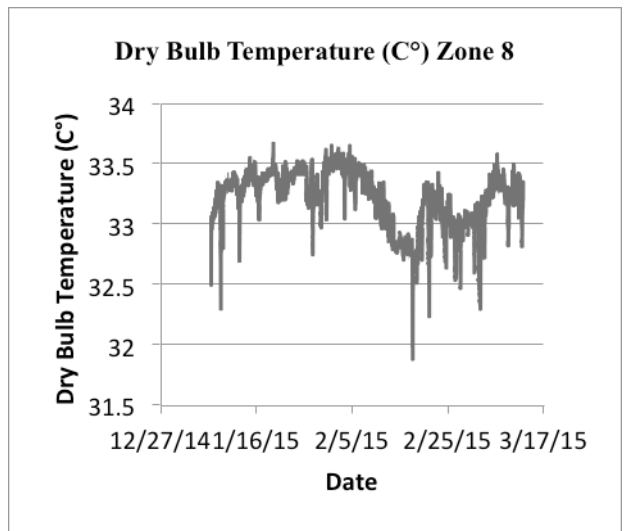


Fig. 4. Dry bulb temperature Zone 8.

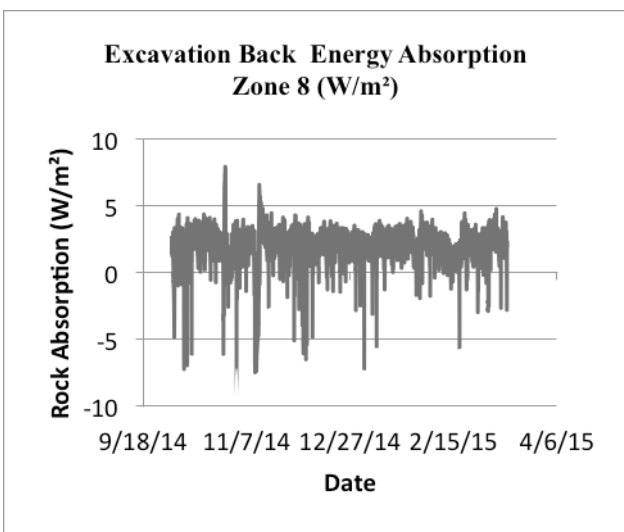


Fig. 3. Excavation back energy absorption.

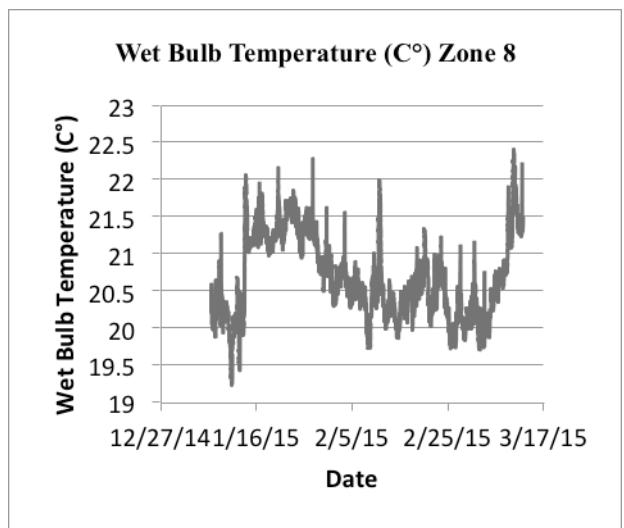


Fig. 5. Wet bulb temperature Zone 8.

Further investigation of the back and wall absorption shows periods of time when the rock strata moves from a heat source to a heat sink. This can be attributed to periods when the pumping infrastructure is shut down for maintenance or repair. With the reduction of the study area heat sources, the system maintains heat equilibrium as the heat moves from the rock back into the air minimizing big swings in heat environmental conditions. This is observed in data collected at the environmental monitoring stations in Figures 4 and 5 when compared to the data collected from the heat flux plates in Figures 2 and 3.

5. Conclusions

The initial results show high potential to effectively model heat loads based on equipment infrastructure within a potash mine. The methodology used to verify the calculated results in zone 8 must be applied to all the zones to ensure accuracy and validate the heat energy removal by both the rock and the brine throughout the entire study area. Further research into the virgin rock temperature is required and will be an essential tool into the continued development of heat management modeling techniques. The data collected from this research can be applied to reducing the temperature throughout the workings. Using the known heat removal rates in conjunction with the virgin rock temperature can assist ventilation engineers in building recirculation circuits to cool the air for reentry. Also, with the known

heat energy rate, as presented in Table 1, a cooling plant may be sized to remove heat generated by the equipment throughout the zones.

Acknowledgements

This paper was prepared with the research support from Mosaic Potash. A special thanks to Will Armstrong and Nicolette Bernardin for their assistance. This support is gratefully acknowledged.

References

- [1] McPherson, M.J., et al, CLIMSIM Version 2.0 for DOS User's Manual. Mine Ventilation Services, Inc., California. 1986.
- [2] White, W.N., Pahwa, A. and Cruz, C. Heat Loss from Electrical and Control Equipment in Industrial Plants: Part II - Results and Comparisons, 2004, ASHRAE.
- [3] NEMA TPI, Guide for Determining Energy Efficiency for Distribution Transformers. Virginia: National Electrical Manufacturers Association. 1996.
- [4] De Souza, E., Mine Ventilation Practitioners Guide. Kingston, Ontario. 2011

Ventilation Planning and Design

Applications of Modelling Software for Safety and Health Training in US Underground Coal Mines

Heather N Dougherty^a, Craig M Stewart^b

^aVirginia Tech, Blacksburg, VA, United States

^bUniversity of Queensland, St Lucia, QLD, Australia

After the Sago disaster and the mine improvement and new emergency response act of 2006 (MINER Act), emergency rules for mine operators were put into place requiring more aggressive and comprehensive training of underground miners. Mandatory MSHA federal training requirements increased from yearly to quarterly, and after the Upper Big Branch disaster in 2010, increased emphasis has been placed on miner training. Some examples of what companies and agencies have implemented are virtual training, mock mine emergency situations, and additional hands-on training to better prepare miners for emergency situations. The need for effective training while maintaining safety and production is vital. Software used for modeling and predicting mine ventilation has advanced to include dynamic changes to ventilation circuits resulting from emergency operational modifications and the introduction of contaminants and gas from fires. Visually informative and interactive software can assist miners in understanding ventilation hazards and opportunities during emergency situations, as well as assist in understanding of practical concepts of pressure, heat, dust, smoke and thermodynamics. An existing two-dimensional ventilation model will be evaluated and 3D models using Ventsim Visual. Basic ventilation training concepts will be developed to assist in understanding and visually convey basic ventilation information. Additional concepts of changes in ventilation resulting from smoke, fire, or circuit changes during emergencies will be considered and discussed.

Keywords: Ventilation modelling, Training, Emergency response

1. Introduction

Post-accident review of fatal accidents in the United States like Sago and Aracoma indicated that a lack of proper training - and possibly ventilation awareness - may have led to an increased loss of life. An understanding of the ventilation system during an emergency in some cases may have improved the chances of miners reaching safe areas such as refuge chambers, fresh air supplies or mine exits [1]. While ventilation design and circuits are generally discussed during mine induction and training, the presentation and conveyance of such information may limit the comprehension of information passed to employees.

Likewise, while technical staff are generally responsible for the competent planning and design of ventilation systems, the effective conveyance of this information to supervisors and management may be limited, particularly in a rapidly evolving emergency situation where time or access for gathering the required ventilation information is limited. Currently miner training in this technical area is limited to basic and regulatory standards.

2. Background

Training is an important part of any career in underground mining. A minimum of 40 hours of initial training is required to begin passage into the mining profession. From that point, regardless of position, a minimum of 8 hours of training including escapeway drills, ground control, ventilation, and expectation training is required annually. In recent years training for underground mining has progressed to include computer

based, “serious game”, and virtual reality that allows trainees to fully participate in their learning experience rather than a one-way transfer of information by lectures [2]. Mallett emphasizes the importance of computer-based learning for younger workers. However Mallett notes that when investigating this theory in a mine setting, group, hands-on, and simulations and drills were preferred as learning tools by the miners [3].

With the advancement of computer hardware and software, the use of 3D visualization has rapidly evolved in the past two decades, particularly in the field of mine planning and geology. In the last decade, mine ventilation software has increasingly adopted the use of 3D visualization and display to improve communication of ventilation concepts graphically showing air flows, with some software packages including advanced options like simulation and visualization of fire, smoke, and contaminants.

3. Computer Based Training

Computer based training is now common in many types of education and workplace instruction. Mining companies have adopted numerous computer-based techniques to create more interactive methods for miner training. Computers have allowed us to explore more ways to interact, master skills, and assess learned outcomes. Being able to take roles in virtual situations (digital role play) and make decisions that impact an outcome allows for a deeper understanding of concepts [2]. Virtual Reality (VR) has also recently become popular in underground training. VR allows participants to simulate dangerous situations or disasters without the

risk of working in those dangerous conditions. Simulation has also been used in training for emergency situations. By using simulation in training, a more real-time detailed information on what conditions a rescue group may encounter can be communicated, and realism of training can be increased [4,5].

4. Ventilation Software and Mining

Ventilation planning and implementation has always been a challenging job for the sections supervisor, mine foreman, and mining engineer. Ventilation modeling and planning software is an accepted standard in most underground mining operations. Computer modeling has empowered mines to better understand and validate their current ventilation while also projecting future mining ventilation schemes. Various software packages are offered on the market for underground mine ventilation and most are based on networks solved with the Hardy Cross approximation, but can differ in usability, interface, graphics and functionality of tasks. Zhang [6] compared five current popular ventilation software and found that each has strengths and weaknesses in various applications of ventilation design. As with any modeling software, the information gained from the tool is only as good as the information gathered and input to the software model.

As mines have become deeper and more extensive and complex in nature, using ventilation software for planning a ventilation system has become imperative in today's mining world. Pushing the mine extents further from primary fans leads to various issues that need to be known and planned for well in advance. The direct cost of ventilation in terms of power cost, infrastructure mining and, the indirect cost from the impact on mine safety and production requires extensive evaluation and justification to ensure costs remain reasonable while ventilation requirements are met. Even smaller mines with simple ventilation systems can usually benefit from a ventilation model to ensure safety, mine regulatory requirements and financial targets are met. Ventilation often forms a significant part of a feasibility study for new or expanded mines, and many specialist consultants and companies have been established to assist mines in this work. It is widely recognized that in addition to being a legislated requirement, effective ventilation can save money, reduce delays in mine development and production, and increase safety.

5. 2D vs 3D Ventilation Modeling

Before the advent of modern, graphics enabled computers, ventilation software was usually developed around a text interface, using spreadsheet type input and output entry methods as shown in Figure 1.

The screenshot shows a window titled 'H:\Business\VentSim\VENTSI-1\OTHERV-AIRNET\AIRNET.EXE'. The main area contains a table with columns: NO, NODE 1, NODE 2, RESIST, QUANTITY, AIRWAY, FAN, and PRESSURE. The data is as follows:

NO	NODE 1	NODE 2	RESIST	QUANTITY	AIRWAY	FAN	PRESSURE
1	09LP63	SURFACE	.0021	346.0		5	1366
2	10LM614B	11LM614B	.0184	281.3		0	825
3	11LM614B	10LM614B	.0080	281.3		0	67
4	11LM616D	11LP63	.0071	346.0		0	851
5	11LP63	09				0	75
6	11LM623E	09				0	47
7	11LM623E	SU				0	6
8	12L154	SU				0	1149
9	13L154	12				0	22
10	13LM614B	11				0	157
11	13LM616D	11				0	88
12	14AP614D	13LM614B	.0036	221.3		0	188
13	14AP614D	14AP614B	.0059	221.3		0	291
14	14AP614D	14AP616D	.0085	96.3		0	5
15	14AP616D	13LM616D	.0082	322.1		0	28
16	14AP613E	14AP614D	.0094	317.6		0	47
17	14AP604E	14AP605A	.0080	208.3		0	0
18	14AP613B	14AP613E	.0080	107.3		0	0
19	14AP605B	14AP613E	.0086	208.3		0	29

At the bottom of the window, it says 'File Name - UD30000' and 'Time - 11:03:52'. A 'Change Node' dialog box is also visible in the center of the table.

Fig 1: Text Interface from Mine Ventilation Software Airnet 2000 [7]

Modern graphical ventilation software is now generally offered as a two dimensional (2D) development and visualization environment, a 2D development combined with a three dimensional (3D) visualization environment, or a 3D development and visualization environment.

A 2D model will generally consist of nodes and lines representing the ventilation airways. The model is viewed as a colored branch network in either schematic layout or true coordinates as seen in Figure 2. Airway types will normally be identified as a defined color. For example, return airways in Figure 2 are red, with arrow heads indicating the airflow direction. Red numbers identify the pressure at a node, and blue numbers indicate the quantity of airflow in cubic feet per minute (cfm). Additional attributes are embedded within the model branches identifying the number of airways, type of airway, resistance, length, area, and if the quantity is limited.

Some disadvantages to this type of model is that not all of the entryways are shown by a physical branch, with grouping of common parallel airways into a single path to reduce model complexity common. Some airway information is input internally into the model, and cannot always be seen on the branch network. This can lead to misunderstanding or mistakes made to the visual aspects of the model, although detail and user-entered information may still produce a correct and verifiable model. This system is considered an expert system, designed for expert users to operate and interpret. Communicating the outcome of these ventilation simulations takes interpretation and additional work in the form of spreadsheets or additional AutoCAD drawings of key ventilation information to project to non-expert users including management, production, safety, and accounting personnel.

The difference between a 2D and a 3D model can be defined by more than just a representation of coordinates in three dimensions. True three dimensional models integrate more visually the dimensionality of the entry way, tunnels, boreholes, shafts and slopes, while closely resembling the size, shape and scale of a mine design in true coordinates (Figure 3). A 3D model can also extend to include the capability of viewing and moving internally within 3D tunnels as a virtual walk through the mine. This provides an important interface in future software design, particularly for knowledge transfer of information for training and presentation.

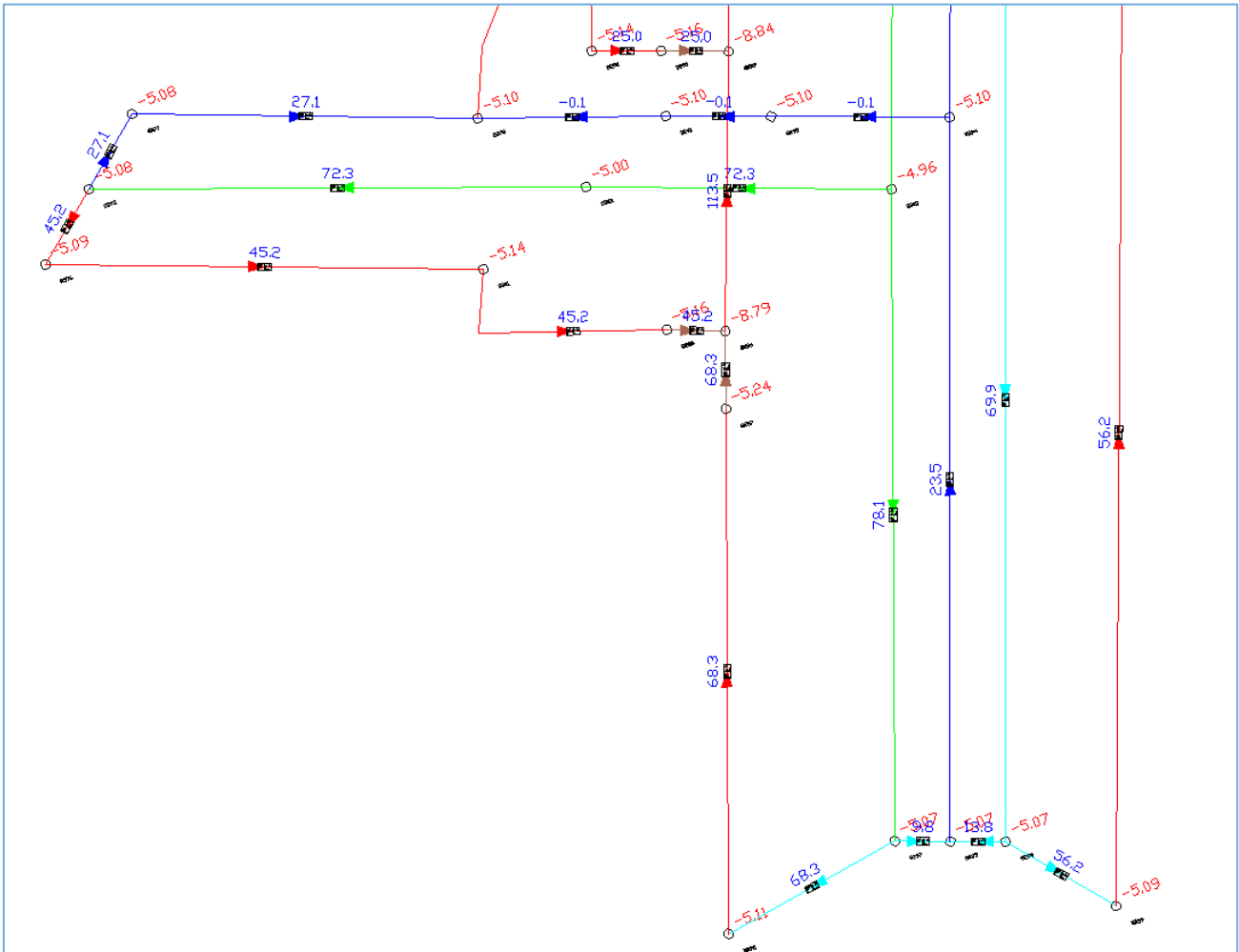


Fig. 2. 2D View of a Ventilation software output in a small area of an underground coal mine

Traditionally, early graphical ventilation software in the 1990s such as VnetPC and Ventsim (Classic) used simple lines to represent both 2D and 3D ventilation pathways. This approach limited the complexity of designs that could be displayed, and failed to represent airways of differing size and shapes. Much of the push to 3D has come from the need for communication across disciplines in the mining industry.

An earlier example of 3D ventilation visualization is Mivena, originally created in 1986 by the Department of earth resources engineering at Kyushu University in Japan[8] and later integrated a combined (hybrid) 2D data entry and display, with an Open-GL 3D hardware

accelerated visualization feature in 2002. Other hybrid 2D/3D ventilation software at the time, included Vuma from CSIR Miningtek and Bluhm Burton Engineering from South Africa.

Software offering both full 3D development and visualization environments appeared a number of years later, with Ventsim Visual in 2009, Vuma 3D in 2011, and most recently, VnetPC Pro in 2012. 3D graphics allows technical staff to more easily develop and communicate work to others including management, accounting, regulatory, political officials and the public [9].

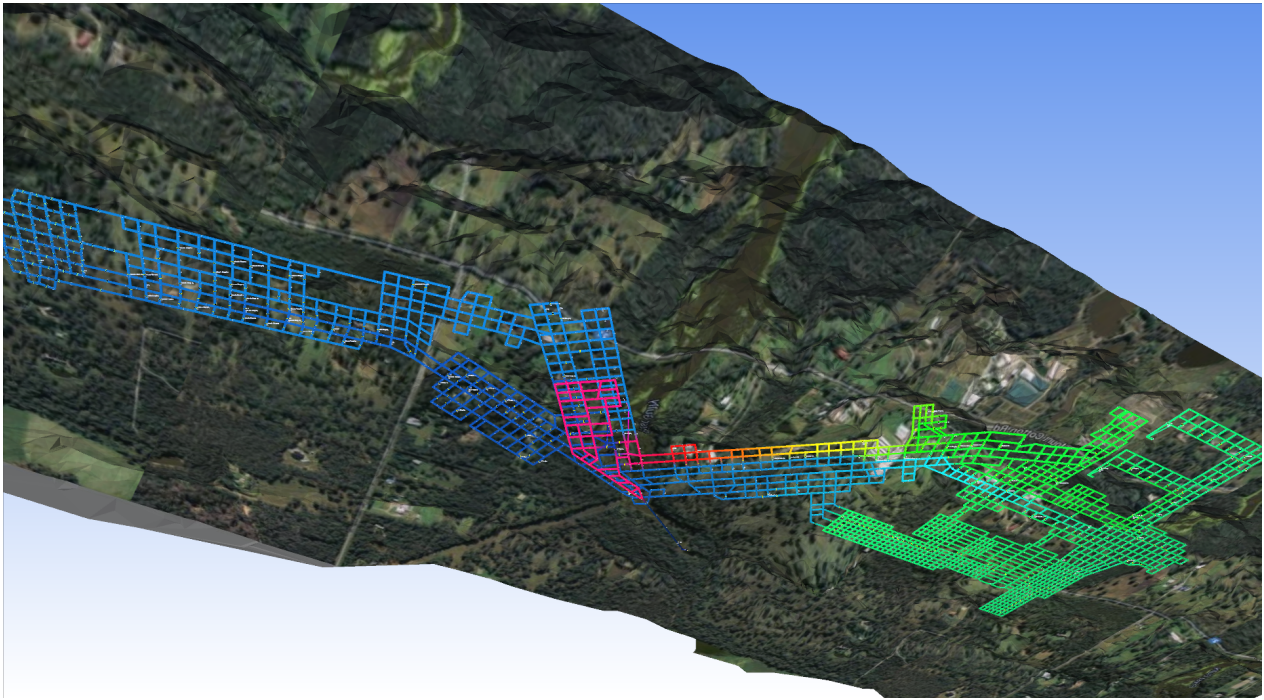


Fig 3: 3D example of a room and pillar coal mine with overlaying 3D topography and photography (Ventsim Visual)

6. Introduction to Underground Mine Ventilation

Training of ventilation normally consists of detailing the mines ventilation plan, examining the minimum airflow requirements at working faces and reviewing permissible levels of contaminants and dust. Basic ventilation concepts are commonly not discussed in training such as ventilation pressure, leakage, and dilution. These concepts are inherently hard to convey to miners or supporting staff. Ventilation concepts can be challenging and time consuming to describe and interpret to interested management and workers that have minimal or no experience with ventilation.

Using a 3D visual model of the mine the entire mine's ventilation flow can be shown which allows a greater assimilation and association with more common aspects of a mine map familiar to general mine personnel.

Figure 4 is an example of the use of 3D visualization of the mine entries and an overcast to convey location and understanding of the ventilation system. By using dynamic coloring, the model can convey how air is coursed through and flows within the mine tunnel system. Other variations in color may show pressure, temperature or gases.

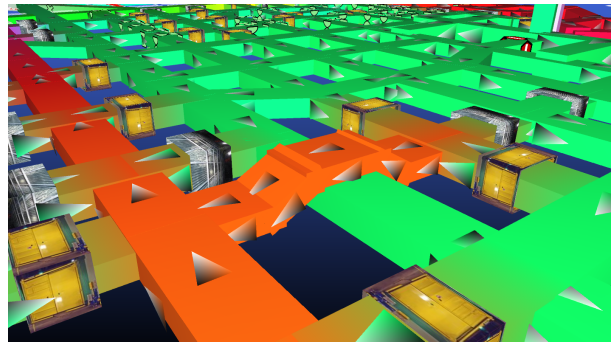


Fig. 4: 3D Visualization of mine entries and an overcast.

Figure 5 shows airflow using dynamic coloring to indicate how the air is coursed into and out of a three entry continuous miner section. Figure 5 and Figure 6 can help visually explain the concept of pressure and leakage. High intake airflows are seen in the center entry at the neck of the section by the bright red and pink colors, but not all of this air is coursed directly to the face when a long pathway is encountered. Depending on the pressure differences between the entries and the integrity of the wall or door separating the entries, there is a leakage between the entries from a higher pressure intake to a lower pressure entry. This leakage accumulates over the distance of the entryway and it can be seen in Figure 6 that the higher pressure of the intake entry in the center entry is leaking into the lower pressure entries of the return and belt entries gradually. Moving arrows within the model also indicates which direction and relative speed of the air movement.

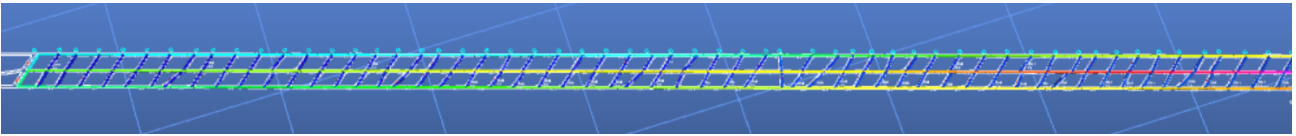


Fig 5: Dynamic coloring of airflow in a three entry gateroad section. Red showing the highest airflow, dark blue the lowest.

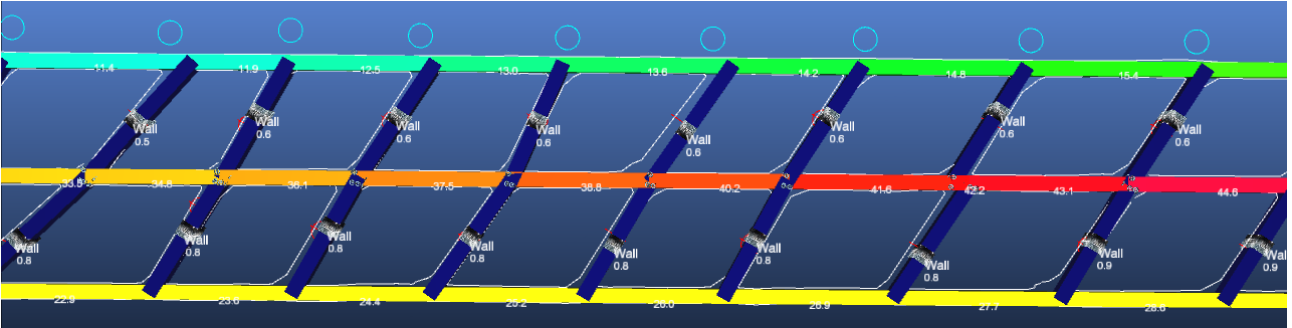


Fig 6: Close up of dynamic coloring of airflow in a three section gateroad.

7. Technical Engineering Staff and Management

Technical engineering staff and management typically have a more experienced and broader understanding of ventilation. Advanced issues like gas or contaminants movement can be more easily visualized by using contamination simulation. Dynamic (transient) simulation functions can display contaminant movement over time in critical areas. Figure 7 and Figure 8 show dynamic coloring for methane percent for an area of an underground room and pillar mine.

Additional contaminant spread can be shown using dynamic coloring or within a sensor time tracking function. This is can be used to determine the time it takes for harmful blast fumes to clear from the mining area. Gases such as Oxygen, CO₂, Nitrogen, CO, NO, Methane, DPM, and dust are a few contaminants that can be tracked and monitored within the software with proper input and parameters into the model.

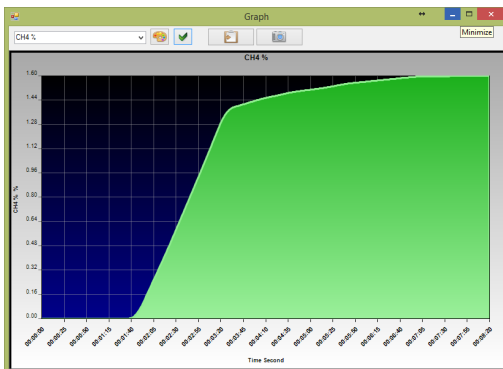


Fig 7: Graphing and time based information can be displayed at multiple chosen locations.

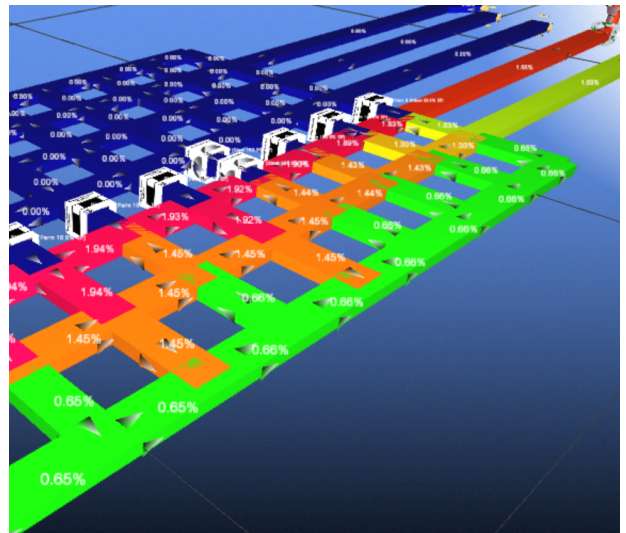


Fig 8: Example of a contaminant spread of methane on an intake and return side of a main entryway system (Ventsim Visual). Dynamic coloring and methane percentages are displayed along with airflow direction.

8. Additional Applications

Ventgraph and VentFIRE™ have been used to examine the impacts of escape and entrapment in various fire situations [10,11]. VentFIRE™ is a module that works within an existing Ventsim ventilation model, eliminating an additional step of creating a distinct model of a current operation to use for fire simulation and scenarios. This allows a mine that is utilizing this ventilation model to integrate a fire scenario for safety, training, or planning easily into their individual mine plan. The software also has the capability to examine multiple exercises of varied scenarios easily and quickly within the mines respective ventilation model. Videos of

these scenarios can be made within the program and shared, paused, and replayed for training.

A demonstration of a fire situation is shown in Figure 9. A graph of the airflow from a shaft location using the dynamic monitor function is shown. In this emergency situation, a fire is initiated in a wood lined intake shaft with a fan placed at the bottom of the shaft, this fan fails at approximately ten minutes into the emergency fire situation. It can be seen that the fire reverses the intake shaft and once the fan fails at approximately ten minutes into the simulation, the air flow to the fire increases from the lower mine level and contaminates other levels. Other contaminants can also be examined, like temperature, CO, CO₂, or visibility, either dynamically or graphically, it could be visually displayed how the dynamics of these entries change over time.

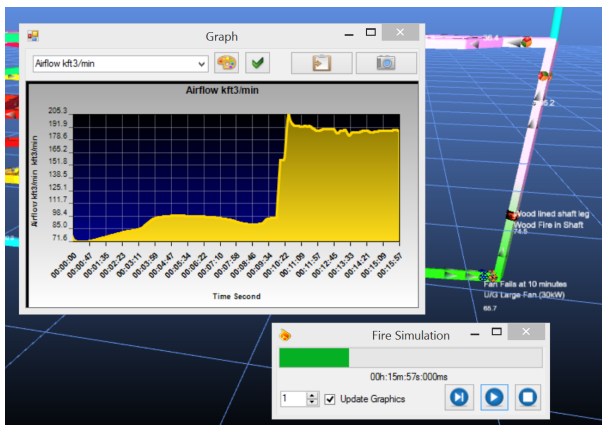


Fig 9: Fire simulation scenario, showing mine airflow dynamically, simulation time, and a graphical representation of airflow.

9. Conclusion

3D ventilation modelling can be a very useful tool to convey ventilation information, scenarios, and rescue situations due to its ease of use, situation variability, and interactive play and visualization. The next generation of miners and engineers have already been immersed in 3D computer generated environments through games and education from an early age. The effective conveyance of technical information via this visual interface is a natural progression of existing familiar environments.

Ventilation software providing visualization in 3D could potentially be considered overly elaborate for what is needed if purely for ventilation design, however it can also be utilized to more effectively convey information to non-expert persons, and to show detailed training concepts for standard situations, emergency, and escape scenarios to give more hands-on knowledge to miners. Although these examples are only a small portion of the functionality of the available software, having the ability to expand usability from a crucial planning engineering support such as a basic ventilation model can be of significant aid for other applications such as safety, training, and planning.

References

1. MSHA, *Report of Investigation fatal Underground Coal Mine Explosion January 2, 2006, Sago Mine, Wolf Run Mining Company*. 2007: MSHA. p. 190.
2. Mallett, L. and T. Orr. *Working in the Classroom-A Vision of Miner Training in the 21st Century*. in *The International Future Mining Conference & Exhibition*. 2008. Sydney, NSW.
3. Mallett, L., D. Reinke, and M.J. Brnich Jr, *Getting Through to Greenhorns: Do Old Training Styles Work with New Miners? Strategies For Improving Miners' Training*, 2002: p. 9.
4. Slaughter, C., J.C. Tien, and G.M. Meighen. *Practical Application of Mine Fire Simulation Software for Mine Emergency and Response*. in *SME Annual Meeting*. 2012. Seattle, WA: SME.
5. Wala, Andrzej M. "Teaching the principles of mine fire using an intelligent computer-aided instruction." *Frontiers in Education Conference, 1996. FIE'96. 26th Annual Conference., Proceedings of*. Vol. 3. IEEE, 1996.
6. Zhang, Y., Zhang X., Habibi A, Tien, J.C. *Comparison of Mine Ventilation Simulation Software*. in *SME Annual Meeting*. 2012. Seattle WA.
7. Airnet 2000, *In house mine ventilation simulation software, Mount Isa Mines, 1993, Queensland Australia*.
8. *Mine Ventilation Network Analysis Simulator MIVENA(ver.6.2c)*. [cited 2015 March 2015]; Available from: <http://reps.mine.kyushu-u.ac.jp/mivena/index-e.html>.
9. RS Ruddock, J.C. *Computer applications in mining - Business benefits*. in *New Zealand Minerals & Mining Conference*. 2000. AUSIMM.
10. Brake, D. *Fire Modelling in Underground Mines using Ventsim Visual VentFIRE Software*. 2013. Australian Mine Ventilation Conference/Adelaide, SA, Australia.
11. Gillies, A., Wu, H., & Wala, A. (2005). Australian mine emergency exercises aided by fire simulation. *Archives of Mining Sciences*, 50(1), 17-47.

Acoustic Directivity of Mine Ventilation Systems

Andrew Dobson*

HGC Engineering, Mississauga, Ontario, Canada

Manufacturer's or supplier's sound data for mine ventilation systems typically consists of only the near-field outlet/inlet sound levels, or the raw fan sound power levels, with little or no information about source directivity. The directivity factor of a source accounts for the proportion of sound being emitted in a specific direction, which is essential when predicting sound levels of mine ventilation equipment in the far-field to prevent underestimating sound levels in the surrounding vicinity. Recent sound level measurements of return air ventilation systems indicate that the in-situ directivities do not always coincide with the standard reference textbook values, thus making these factors difficult to predict. The end result of not considering the appropriate directivity factors can be the installation of equipment that causes annoyance to neighbors, sound levels exceeding regulatory limits, and the possible need for retrofit/replacement ventilation and/or noise control measures. This paper presents a case study highlighting the unique directivity characteristics associated with a mine ventilation system and emphasizes the importance of having directivity information provided by the manufacturers and suppliers.

Keywords: acoustic, noise, directivity, sound, ventilation, outlet

1. Introduction

In many jurisdictions, quantifying the sound emission levels of a mine is a regulatory requirement in situations where sound sensitive points of reception exist in the vicinity. This is achieved using a combination of in-situ sound power measurements, published sound level data from manufacturers, and acoustical modelling software to predict the sound levels in the far-field. Accordingly, a mine must either be designed to meet the applicable sound level limits prior to construction, or a noise abatement plan must be implemented to reduce the sound of an existing mine in situations where existing facilities do not meet the limits.

The ventilation systems used to circulate air through underground mines have the potential to be the greatest sources of environmental noise at mines. These fans tend to be high capacity axial or centrifugal fans, with direct exposure to the outdoors via the air intake or exhaust duct openings. The perceived audibility of this equipment can also be enhanced due to a pronounced tonal quality exhibited at the fan blade pass frequency.

The potential for disturbance due to the relatively high sound levels of mine ventilation fans is significant. Thus, it is important to consider the acoustic properties of the equipment when predicting far-field sound levels during the design phase of the mine, or when installing new ventilation equipment. These properties include the source sound power levels and corresponding acoustic signature of the fans in the system, and the acoustic directivity pattern of the system resulting from the physical arrangement of the equipment. Sound power level refers to the total rate at which a sound source emits acoustic energy into the surrounding environment. As such, this is a fundamental acoustical quantity, (analogous to a kW rating of a heat source) and it is independent of distance from the source, or the surroundings in which the source is placed. The acoustic directivity of a sound source represents the pattern in which the sound radiates from the acoustic center of the source. In essence, the directivity is a measure of the

difference in radiation with direction and is usually stated as a function of angular position around the acoustic center of the source [1]. Sound sources which are not acoustically directive radiate sound in a uniform or spherical pattern. The directivity pattern of a source such as a mine ventilation system is a function of the physical design, including the associated duct dimensions, the type and position of the fans, the rate of airflow, the frequency spectrum or acoustic signature of the fans, and the presence of physical noise control measures, such as a silencer. Manufacturers and suppliers provide accurate fan sound power level data; however, the associated acoustic directivity data is generally not provided.

A recent noise complaint investigation conducted by HGC Engineering concluded that a specific return air ventilation system was audible in a residential area, which was not considered during the initial acoustic assessment; given the orientation of the ventilation equipment, audibility in this location would generally be unexpected. The initial observations and measurements conducted in the subject residential area attributed the audibility to an atypical acoustic directivity pattern of the return air system. Accordingly, in-situ sound level measurements of this particular return air system, as well as a second return air system at another mine site, were conducted, specifically to quantify the respective directivity patterns. The results of these measurements confirmed that the directivity patterns of the equipment considered were not typical and were, in fact, different from the exhaust duct directivity patterns outlined in standard acoustical engineering textbooks.

The textbook directivities, and the directivity patterns resulting from the measurement of two ventilation systems are presented and discussed, below.

2. Textbook Directivity Factors

Standard acoustical engineering textbooks present methods for calculating acoustic directivity of exhaust

ducts, which account for the hydraulic diameter of the duct, the center band frequency in octave bands, and the composition of the gas exhausting from the duct. Table 1 lists the directivity indices calculated using the reference textbook methods, which have considered the variables (i.e. dimensions, exhaust gas, etc.) applicable to the specific mine ventilation exhaust ducts considered.

Table 1. Textbook [2] Directivity Indices, [dB]

Freq [Hz]	0°	15°	30°	45°	60°	75°	90°
31.5	0	0	0	0	0	0	0
63	4	3	1	0	0	-2	-4
125	6	4	2	0	-1	-4	-6
250	9	6	3	0	-2	-6	-10
500	10	6	3	-1	-4	-10	-15
1k	11	6	1	-4	-7	-12	-17
2k	11	5	-2	-8	-9	-13	-17
4k	11	3	-4	-12	-12	-15	-17
8k	11	3	-6	-14	-14	-16	-17

These values were input into a predictive computer model, Cadna/A version 4.4.145, and applied to the source sound power levels of the ventilation equipment measured for the purpose of this study (recall that the sound power level of a source is independent of the acoustical directivity, whereby sound power dictates the “total sound level”, and directivity dictates the direction in which the acoustic energy propagates through the atmosphere). The model is based on the methods from ISO Standard 9613-2 [3] which accounts for reduction in sound level with distance due to geometrical spreading, air absorption, ground attenuation and acoustical shielding by intervening structures.

Figure 1, below, provides the predicted sound pressure levels and the sound propagation pattern associated with the textbook directivity factors.

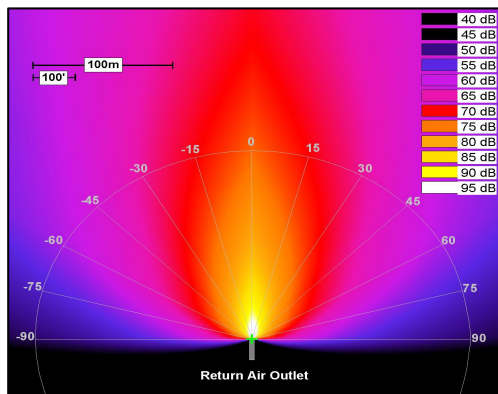


Fig. 1. Predicted Sound Pressure Levels [dBA] of Return Air Outlet with Directivities Calculated from Textbook [2]

This figure can also be used to derive the directivity indices shown in Table 1, above. From this, it is clear that the acoustic energy is concentrated in the on-axis (0°) direction, as would be anticipated.

3. In-Situ Measurements of Directivity

Sound level measurements of two individual exhaust duct outlets were conducted, at two separate mining facilities in Northern Ontario. The two systems utilized axial fans moving air at rates of approximately 150,000 cfm and 300,000 cfm. For both exhaust outlets, measurements were conducted in 1/3 octave bands using

a Brüel & Kjær Pulse Real-Time Analyzer, model 3560-B, equipped with a Brüel & Kjær model 3599 Sound Intensity Probe and model 4197 matched intensity microphone pair. Sound level measurements of the 150,000 cfm fan discharge outlet were conducted in the far-field, at a distance of 45 meters from the outlet, at 15° intervals relative to the on-axis position. Measurements of the 300,000 cfm fan were conducted at a distance of 50 meters from the discharge outlet, at 15° intervals relative to the on-axis position. These results were used to calculate the directivity indices associated with the exhaust outlets, summarized in Tables 2 and 3, below.

Table 2. Measured Directivity Indices, [dB] 150,000 cfm Fan

Freq [Hz]	0°	15°	30°	45°	60°	75°	90°
31.5	6	4	1	-3	5	8	10
63	0	9	9	8	8	-4	-16
125	5	8	7	6	7	5	3
250	6	3	6	9	8	3	-2
500	7	7	8	8	5	0	-5
1k	7	7	8	8	5	-6	-17
2k	7	8	8	8	4	-7	-18
4k	7	8	8	8	4	-3	-9
8k	6	8	8	7	6	-1	-7

Table 3. Measured Directivity Indices, [dB] 300,000 cfm Fan

Freq [Hz]	0°	15°	30°	45°	60°	75°	90°
31.5	9	7	6	4	3	4	4
63	7	8	7	6	5	2	-1
125	6	9	8	7	5	3	0
250	1	11	9	6	0	0	0
500	7	8	7	6	5	3	0
1k	3	11	9	6	1	-6	-12
2k	7	11	8	4	0	-5	-10
4k	7	10	7	4	0	-2	-3
8k	6	11	8	5	-1	-6	-11

Figures 2 and 3, below, show the predicted sound pressure levels and the sound propagation patterns associated with the 150,000 cfm fan and 300,000 cfm fan outlets, respectively. Again, these figures can be used to derive the directivity indices shown in Tables 2 and 3, above.

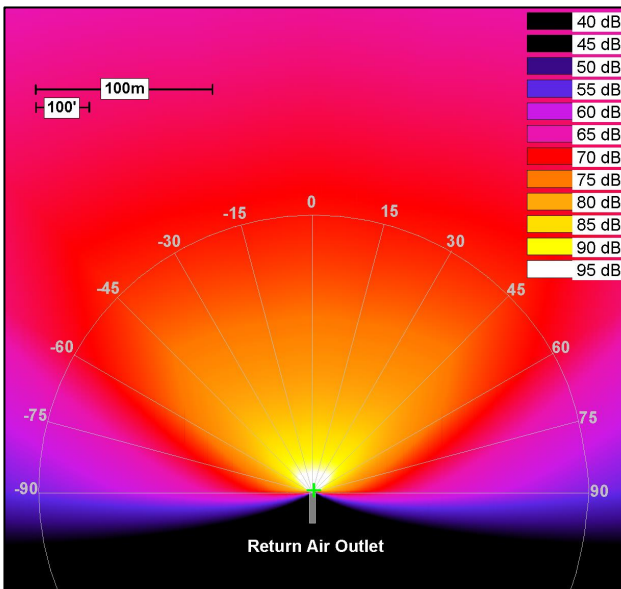


Fig. 2. Predicted Sound Pressure Levels [dBA] of Return Air Outlet with Measured Directivity Pattern – 150,000 cfm Fan

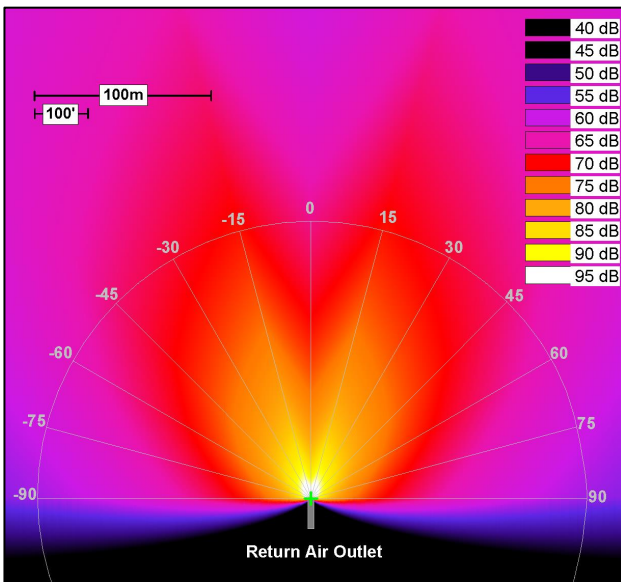


Fig. 3. Predicted Sound Pressure Levels [dBA] of Return Air Outlet with Measured Directivity Pattern – 300,000 cfm Fan

4. Discussion and Conclusions

Regarding the directivity patterns exhibited in Figures 2 and 3, the majority of acoustic energy is concentrated between the on-axis and 45° directions, which is expected and broadly similar to the reference textbook predictions. However, significant dissimilarities are realized at the specific angular positions.

The sound emanating from the 150,000 cfm fan outlet is relatively evenly spread between the 0° and 45° directions, and the sound from the 300,000 cfm fan outlet is heavily concentrated in the 15° direction. Comparing these to the pattern outlined in Figure 1, it is apparent that the application of the textbook directivity patterns to these sources, in a predictive scenario, would considerably underestimate the far-field sound levels in directions other than in the 0° direction.

These results are significant in the context of a new mine project, or when installing new ventilation equipment where the sound emission levels are a concern and governmental regulations apply. If accurate directivity data is not incorporated during the preliminary acoustical modelling phase, prior to construction, the offsite sound levels may be underestimated in some locations, and overestimated in other locations, in the offsite areas of concern surrounding the facility. The consequences of this can be the unforeseen annoyance of neighboring residents, sound levels which exceed the regulatory limits, and the unnecessary need for retrofit/replacement ventilation equipment and/or noise control measures.

While the textbook directivity information does provide estimations that can be applicable in some situations, this data should be used with caution when predicting the sound levels of mine ventilation systems. In addition, while the measured directivity data outlined herein accurately represents the ventilation systems considered, these may not be applicable to other systems. Nevertheless, collecting additional data, by conducting acoustical measurements in the manner outlined above, could provide additional insight regarding mine ventilation directivity patterns, and the factors contributing to the variations thereof.

Therefore, it is prudent that the manufacturer's and/or participants within the industry establish a method to accurately quantify the directivity pattern of a given system prior to the implementation at a mine site, to accompany the fan sound power levels, as this information is valuable in the context of assessing the sound levels of a mine.

Acknowledgments

The author wishes to thank Robert D. Stevens and Bill Gastmeier of HGC Engineering, for their technical expertise, oversight, and contributions.

References

- [1] Leo L. Beranek (Editor), *Noise and Vibration Control* (Revised Edition), Institute of Noise Control Engineering, Washington DC, 1988. p. 138.
- [2] David A. Bies and Colin H. Hansen, *Engineering Noise Control Theory and Practice*, (2nd Ed.) E & FN Spon, 1996.
- [3] International Organization for Standardization, *Acoustics – Attenuation of Sound during Propagation Outdoors – Part 2: General Method of Calculation*, ISO Standard 9613-2, Switzerland, 1996.

Development and Implementation of a Data Management Platform for Atmospheric Data in Underground Coal Mines

Zach Agioutantis^a, Kray Luxbacher^b, Heather Dougherty^b, Michael Karmis^b

^aUniversity of Kentucky, Lexington, Kentucky, USA
^bVirginia Tech, Blacksburg, Virginia, USA

As demand is growing for real-time monitoring and evaluation of mine parameters, there is an increasing need for appropriate data management in many mining applications. This includes atmospheric monitoring for underground coal and metal mines. Atmospheric monitoring in underground coal mines assists operators to determine whether conditions are safe for mining and allows them to operate ventilation systems more efficiently and effectively.

This paper presents a new database package that can manage, present and analyze data collected by multiple sensors in underground coal mines. This application follows the client/server paradigm, thus, allowing multiple users to access it at any given time and can support multiple projects (i.e., multiple mines, or multiple mine sections depending on the areal break down). It is fully parametric with respect to project definition, sensor/tag definition, data formatting and data grouping. Parameters can be defined and customized by each user. Sensor data can be directly imported, charted and correlated in any user-selected combination. In addition the user can view data through a map interface which is based on an actual mine map.

Keywords: data management, atmospheric monitoring, database, coal mining

1. Introduction

Today, large mining operations handle extensive volumes of mining related data generated by multiple sources that may or may not be compatible to one another. This data needs to be constantly managed, processed, evaluated and possibly cross-correlated. The only way that this can be accomplished in a user-friendly and efficient manner is using a centralized data management system.

Many operations have risen to the challenge and have developed specialized packages to handle large volumes of operational data in real time or near real time. These packages feature a user friendly interface through a desktop or web application. An example is the Visionlink System which is a web-based application that enables management of the maintenance, health, and utilization of heavy equipment. This is accomplished by using a combination of data monitoring hardware, Global Positioning System (GPS) technology, wireless communications, a central server, and a fleet database [1]. A drawback of such commercial or "closed" systems is, however, that their data cannot be cross-correlated with other data generated or collected at the same operation.

To fulfill the need of an integrated data management system at the company level, a new parametric system was designed and developed over a number of years for the monitoring time series data in mining operations [2]. One application of this system is the monitoring of atmospheric conditions in underground coal mines. This is an important task that helps mine personnel operate the ventilation systems in a more efficient manner and, therefore, ensure a safe environment for the workforce [2].

2. AMS monitoring in US coal mines

Atmospheric monitoring in US underground coal mines must be designed and implemented in accordance to federal laws and regulations, i.e., Title 30 of the Code of Federal Regulations (CFR). Furthermore, under current Atmospheric Monitoring System (AMS) regulations (CFR 30 §75.351), data archiving is not

required. Furthermore the equipment installed underground for AMS should be "permissible". The term permissible refers to equipment that meets the specifications by the US Mine Safety and Health Administration (MSHA) for the construction and maintenance of such equipment, to assure that such equipment will not cause a mine explosion or mine fire. Alert and alarm signals should be generated once certain gas concentrations are exceed.

According to the regulations, records must be kept regarding alert or alarm signals, AMS malfunctions, and seven-day tests of alert and alarm signals. These records must note the person that recorded the information, and the records must be kept in a secure book or electronic computer system that is not susceptible to alteration. In addition, these records must be kept for one year at a surface location at the mine made for inspection by miners and authorized representatives of the Secretary (CFR 30 §75.351(o)). The required records are limited to alert or alarm signals, malfunctions, system tests, and calibration.

Depending on the size and type of the underground operation, AMS should be able to gather data which cover several different components that may characterize the atmospheric conditions underground. Such parameters include, but are not limited to, the following: concentrations of various gases (CO, CO₂, CH₄, etc.), wet and dry temperature underground, temperature at the surface, humidity, barometric pressure, air flow, fan performance indicators (pressure, power, etc.), air velocity, total air pressure loss, etc. [2]

Although progress has been achieved in recent years because of the advent of electronics and data transmission systems, monitoring of atmospheric conditions still presents challenges due to current limitations in available technologies in terms of accuracy, response time, range, sensitivity, and survivability [2].

Proper monitoring becomes even more important in the case of coal mines, where high CH₄ concentrations present a definite hazard and/or high CO indicates development of a fire. In addition to everyday

operations, AMS can be used to detect incidents that have occurred, such as methane ignitions at the face, explosions behind seals, belt fires, etc. [2].

3. System architecture

Data management of an AMS should ensure that the current data are immediately available for visualization and processing, but it should also ensure the integrity and availability of historical data. AMS for underground mines that may employ many sensors, may generate large datasets on a daily basis, which presents a challenge for the development of AMS data management systems [2].

Based on experience gained through the development of other relational database applications [3, 4, 5] and using the available software infrastructure, a database system for the management of atmospheric data was developed by appropriate parameterization of the main database platform. This system comprises a relational database that can be accessed through a client/server protocol over a local area network (LAN) and a windows front end that can be executed on any windows computer (Figure 1). Depending on the utilization of the system, the database can either be hosted on a dedicated database server, or on server shared with other applications under a Windows or Linux environment. The backend database system was developed using Firebird 2.5 (an open source relational database system).

According to the specific design, data from a single or multiple distinct projects can be easily retrieved by grouping in many hierarchical levels. A project group can handle data from different areas which can be further subdivided into individual projects, different layouts or just simple instruments, sensor or station groups [2].

The system is designed as a stand-alone system which either can tie into a corporate network and automatically retrieve data by “listening” to data servers or data can be manually or automatically imported through excel or other common file formats. An example of the first option is presented in [4] while an example of the later is presented in [2].

Automated communication and data retrieval from data servers is accomplished by custom middleware modules as shown in Figure 2.

The system also features a user and role management subsystem. Users will need a username and password to access the data stored on the server. At the same time, based on their assigned role (e.g., admin, supervisor, operator, guest) they will have access to a specific subset of data and/or project setup options. This policy ensures

data integrity and provides security regarding data availability.

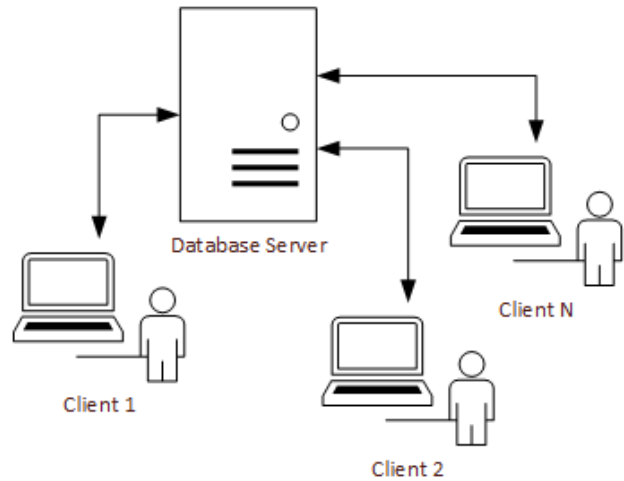


Fig. 1. Client – server system architecture

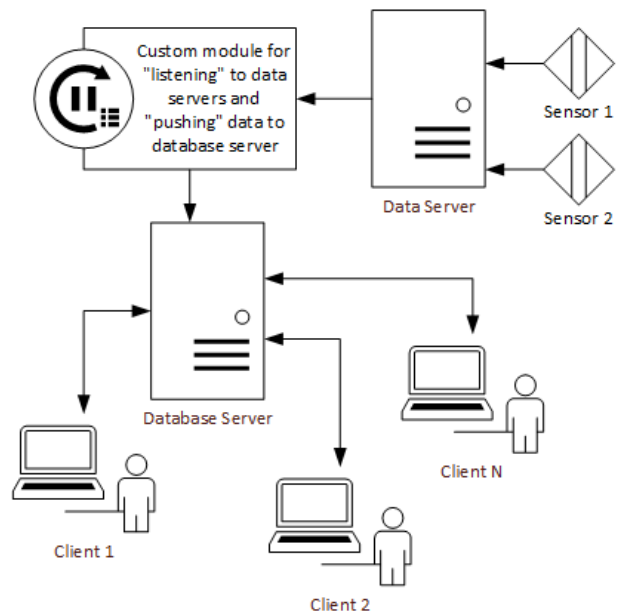


Fig. 2. Automated data retrieval system

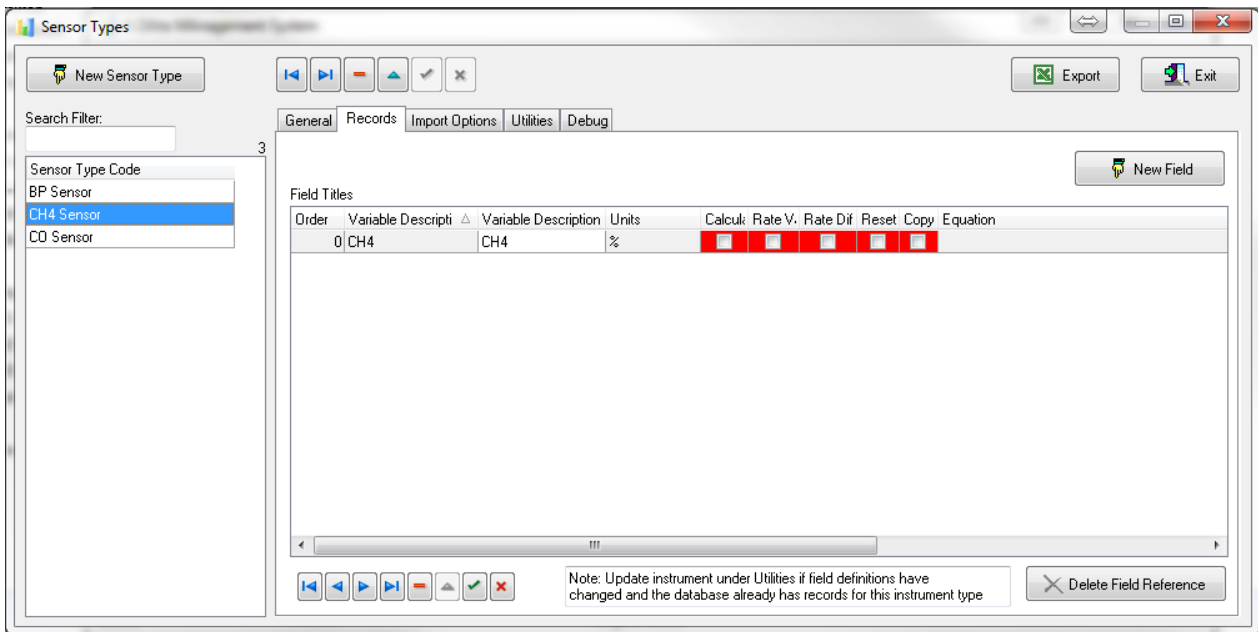


Fig. 3. Definition of custom sensor types – single variable sensor

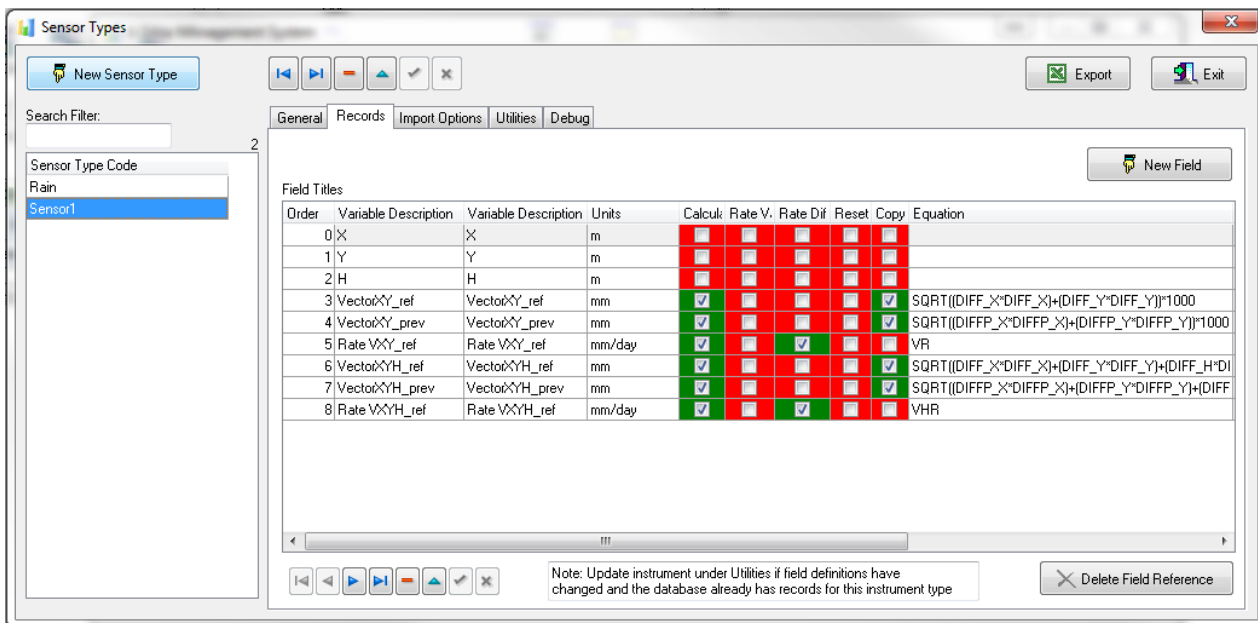


Fig. 4. Definition of custom sensor types – multiple variable sensor

The user can create any sensor configuration which could be either of a single variable, e.g., methane sensors for simple time series data (Figure 3), or of multiple primary and calculated variables measuring movements in three dimensions, such as 3D topo prisms (Figure 4).

Both the data that define the parameters of each project as well as the actual measurements from the AMS are stored in this integrated database environment (Figure 5).

For every sensor type, the system allows the user to create calculated fields, such as the rate of change. Sensors can be organized in groups or layouts within a specific project (Figure 6). A project can accommodate multiple layouts. This hierarchical system facilitates easier data management and analysis. Thus, large datasets can be easily managed, evaluated and critically correlated.

In this system, it is very easy to import data collected from external sources, i.e., weather data from an external weather station.

A simplified version of this database system has already been presented as the “Amanda” system [2, 6]. Amanda lacks all the enhancements that are presented here, since it was implemented only for single variable sensors.

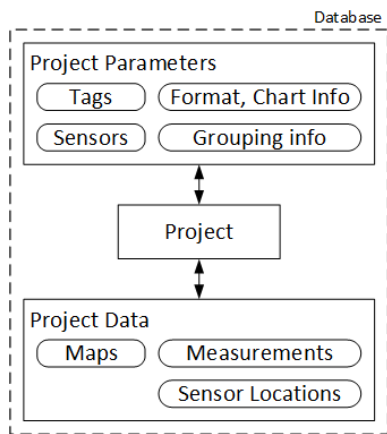


Fig. 5 Data stored in the database environment

Code	Aux Info
South	
CH4	CH4 Group
48PER	
Ch4 #42	outstation=4
Ch4 #50	outstation=4
Ch4 #50	outstation=1
Ch4 #52	outstation=1
CH4 #52	outstation=4
Ch4 #54	outstation=4
Ch4 #54	outstation=1
Ch4 #56	outstation=1
CH4 #58	outstation=1
CO	CO Group
CO #47	outstation=4
CO #55	outstation=1
O2	O2 Group
O2 #61	outstation=4
O2 #62	outstation=4

Fig. 6 Grouping of sensors in different levels

4. Application interface

4.1 Map interface

The application is designed to provide an intuitive interface for data visualization. One or more project view can be defined in each project group. The database

can store multiple AutoCAD files with different views of the study area. The windows application will then overlay sensor locations on the map based on the coordinates of their location. Furthermore, the user can select multiple points for display on the maps and then chart selected variables per instrument by just clicking one or multiple instruments.

Figure 7 shows an example of the map interface along with the sensors that are included in this project. The sensors are grouped in user-defined groups and are shown in a collapsible tree list.

Figure 8 is generated after the user double clicks on a sensor. The map display zooms in the area of the sensor and a chart appears on the right showing values for a pre-specified time interval.

4.2 Correlation of multiple time series

Multiple time series can be correlated either on the same chart (Figure 9) utilizing the left and right axis of the chart, or on stacked charts where each sensor type is plotted in a single sub charts (Figure 10). The example shown in Figure 10 includes the regional barometric pressure, methane concentrations from two methane sensors and the fan amps.

4.3 Statistical information

The database also provides statistical data for each project or project division, such as the total number of instruments, the total number of measurement records, the number of reference dates etc. Furthermore, all of the statistical information can be exported as Excel files. Currently the AMS database holds over 200 million records for multiple sensors including methane, CO and oxygen measurements, fan parameters (bearing temperature, amperes, etc.), regional barometric pressure values, etc.

5. Discussion

The advantages for using a database to manage, analyze and present data can be summarized as follows:

- A large dataset including over 200 million records measurements have been imported to date and are readily available for processing, evaluation and analysis. Using a database saves time and also reduces possible user errors and thus increases the confidence level of the presented results.

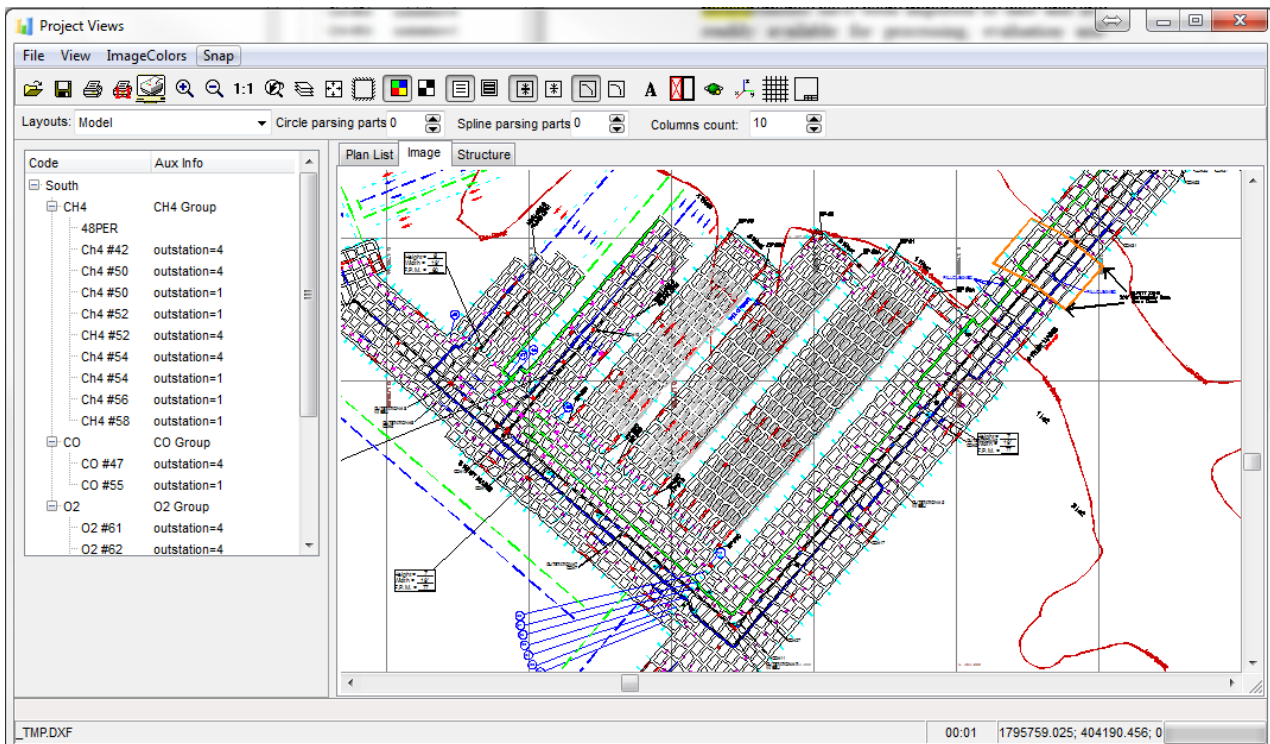


Fig. 7 Mine map and monitored sensors. Sensors are shown in a tree list in user defined groups

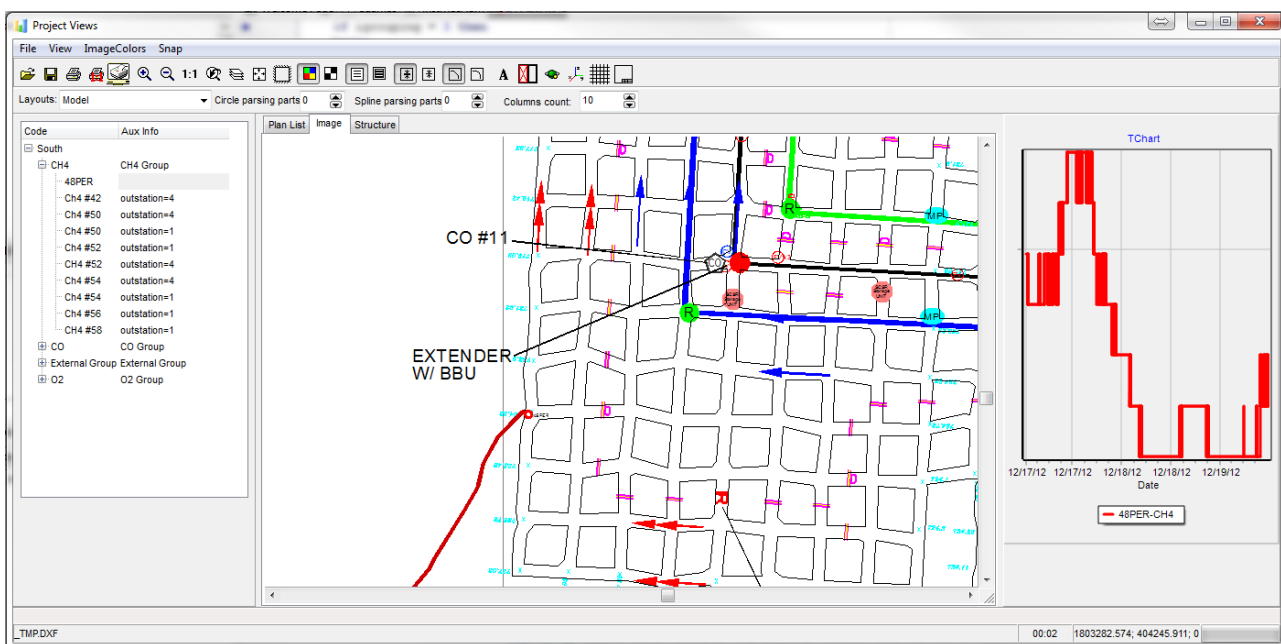


Fig. 8 Location and values for selected sensor

- This solution allows the user to collect, organize and store different types of data from many projects under a single interface, instead of dealing with multiple interrelated files.
- The presence of multiple grouping levels contribute to the functional management of data from multiple areas within a project and multiple projects within a project group.
- Measurements from different internal or external sensors can easily be plotted together and cross correlated. Figure 9 shows data from a methane

- sensor installed in the mine and barometric pressure data from a public weather station while Figure 10 presents data displayed in stacked time series charts.
- Sensor locations can easily be located on plan views that are stored developed as AutoCAD files, and thus, errors with respect to sensor positioning can easily be eliminated. This will help on going work for an intuitive interface to present AMS data to mine personnel are reported in [7].

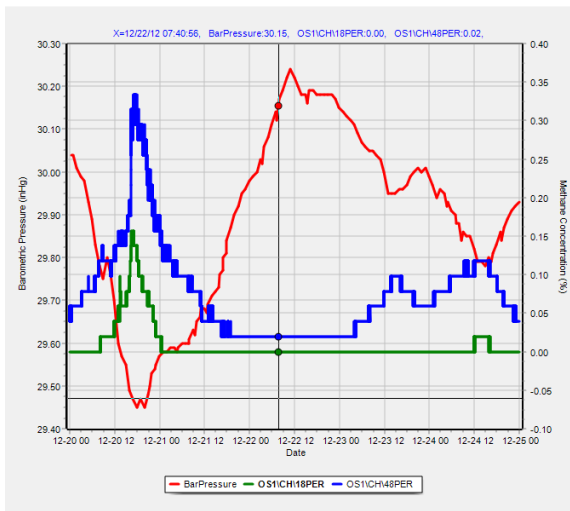


Fig. 9 Correlation of multiple time series utilizing the left and right chart axis. Similar sensors are grouped on the same axis

6. Summary and conclusions

This paper presents the basic features of a new database system that was developed for the management, processing and visualization of AMS data. This system was successfully used for the management of a large dataset with sensor measurements from an underground coal operation in the US. Barometric pressure data from a nearby public weather station were successfully imported into this database and cross-correlated with methane concentration values. The data were asynchronously imported into the database so as not to interfere with the mine systems.

This data management system significantly reduces the required processing and analysis time and at the same time provides alerts to the user when the predefined warning or alarm limits are exceeded. The user can easily correlate variables from multiple sensors for current and historical data. The database can archive data for multiple projects. Information can be easily retrieved in a consistent format for any project, providing valuable information for future studies.

References

- [1] http://www.cat.com/en_US/support/operations/technology/fleet-management-solutions/product-link/faqs.html (last accessed on May 15, 2015)
- [2] Agioutantis, Z., K. Luxbacher, M. Karmis, S. Schafrik, Development of an atmospheric data management system for underground coal mines, *The Journal of The Southern African Institute of Mining and Metallurgy*, 114, (December 2014), 1059-1063.
- [3] Agioutantis, Z., C. Steiakakis, G. Papavgeri and P. Schilizzi, Development of a geotechnical data management system for mining operations, Proceedings, 2015 SOMP Conference, Freiberg, Germany, 21-26 June, 2015.
- [4] Agioutantis, Z. and S. Papaterpos, A real-time event driven data management application for equipment monitoring in continuous surface mining operations, Proceedings, AIMS Conference, May 27-28, 2015, Aachen, Germany.
- [5] Agioutantis Z., G. Kaplanidis and C. Steiakakis, Development of a database system for geomechanical monitoring, Proceedings, 7th Panhellenic Geotechnical Congress, Athens, 5-7 November 2014, (in Greek).
- [6] Griffin, K. R., Utilization and Implementation of Atmospheric Monitoring Systems in United States Underground Coal Mines and Application of Risk Assessment, Doctoral Dissertation, 2013, Virginia Tech, Blacksburg, VA.
- [7] Dougherty, H., K. Luxbacher, M. Karmis and Z. Agioutantis, Design principles for a mining interface, Proceedings, APCOM 2015, May 23-27, 2015, Fairbanks, Alaska.

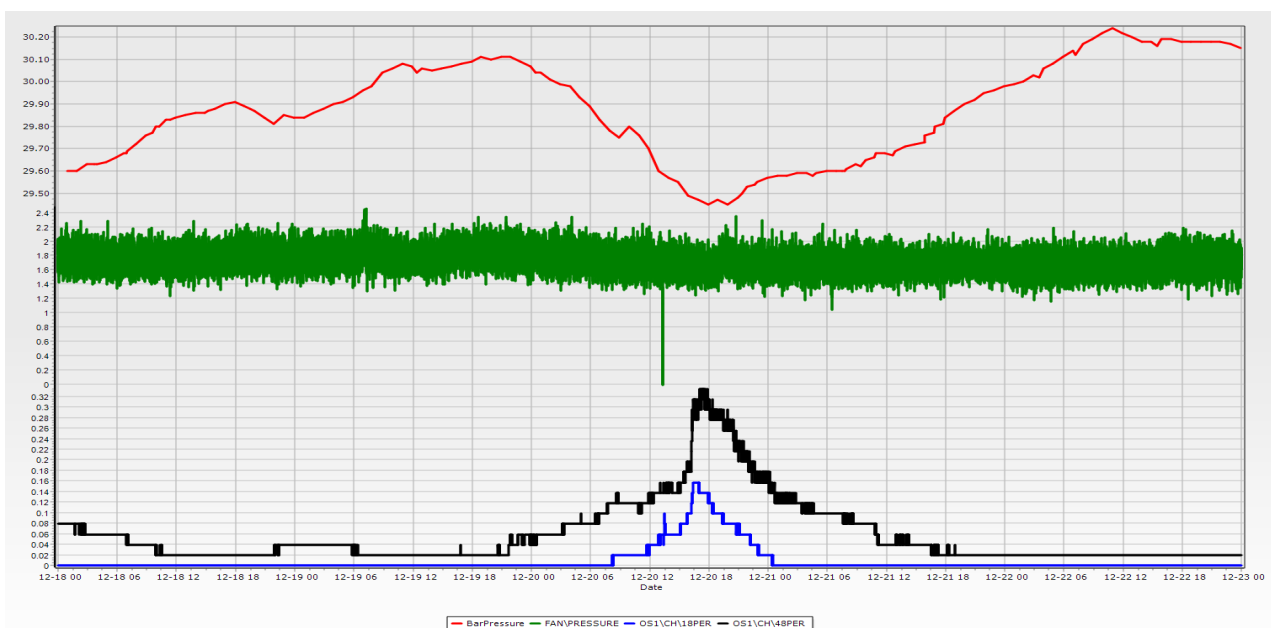


Fig. 10 Stacked time series charts of AMS data for a period of 5 days.

Reconciliation of Ventilation and Production Expansion in a Potash Mine

Kyle Penner^a, Euler De Souza^b

^a*PotashCorp, Rocanville Division, Saskatchewan, Canada*
^b*Queen's University, Kingston, Ontario, Canada*

Potash Corporation of Saskatchewan Inc. (PotashCorp) is developing an expansion of its Rocanville Division, a potash mine in southeastern Saskatchewan. The expansion is targeted to increase the sites output from the current 3.0 MMtpa to 5.7 MMtpa K₂O. In order to be compatible with the upgraded milling facilities, the current service shaft is being converted to a second production shaft. The increased milling and hoisting capacity has also meant an expansion of the mining fleet and mine footprint was required. The expansion also includes construction of a service shaft approximately 15 km from the existing site, meaning three shafts are available for mine ventilation. With an increased mine footprint and a much larger underground production fleet, the existing ventilation system had to be increased in capacity. This paper presents the many engineering innovations used to design an efficient and economic mine ventilation system. A completely new flow distribution was modeled, with the mine expanding from a two shaft system to a three shaft system. Extensive computer modeling was used to assist in fan selection and simulations were done to integrate production scheduling and ventilation requirements. Commissioning of the ventilation system upgrade is being implemented in phases to permit a controlled transfer of fresh air to the new shaft, and ramp up to full ventilation capacity with minimal disruption to mine operations.

Keywords: ventilation, primary fans, booster fans, circuit design

1. Introduction

Over the past decades, annual potassium intensive crop production has been driven upward by increases in world population, high rates of urbanization and decreases in arable land. Potash plays a central role in helping feed the world's growing population. Approximately 90% of world potash production is being used as fertilizer [5].

Rocanville Division, a potash mine in southeast Saskatchewan, is currently undergoing a major mine and mill expansion. The target site output for the expansion is 5.7 Million metric tonnes per annum (MMtpa) from the current 3.0 MMtpa K₂O. In order to feed the mill, an estimated 50,000 metric tonnes per day (approximately doubling the current production) will need to be mined and hoisted. The expansion consists of three components, doubling the mill capacity by building a new mill, doubling the hoist capacity by converting the existing service shaft into a production shaft, and doubling the mine output by increasing the mining machine fleet and mine footprint, along with the sinking of a new remote shaft to act as a service shaft.

The mine currently operates two shafts, #1 production shaft and #2 service shaft. Because retrofitting the hoist system in #1 Shaft to meet the planned feed rate would be impractical, the current service shaft is being converted to a production shaft containing two 46 metric tonne skips. In conjunction with the conversion of #2 Shaft to a production hoist, a third shaft (#3 Shaft) is currently being sunk 16 km from the Rocanville surface site. The #3 Shaft serves three significant purposes; it will act as a service shaft,

providing access for workers and materials to the mine, secondly, due to its location, it will provide shorter access to active mining areas, and finally provide a new source for fresh air to the mine.

To meet the planned mine production the production mining machine fleet and the mine footprint approximately doubled.

A major component of the expansion program includes the design, construction, and development of an upgraded ventilation system to reconcile ventilation with mine production expectations. This paper presents a description of the ventilation design study. The mine ventilation system was designed by analyzing the minimum requirements for effective production on a 'per machine' basis, and then scaled up to account for the entire fleet. Shaft capacities for airflow were also analyzed based on construction and shaft conveyances. Mine resistance was also estimated using ventilation engineering principles. Design parameters were verified through ventilation computer modelling. Design factors were then used to generate specifications for fan systems to be purchased and installed.

2. The current and future ventilation system

Rocanville ventilation has fresh air downcast into the mine through its service shaft, and exhaust upcast through the production shaft. With the conversion of #2 Shaft to a production shaft, #3 Shaft will act as the primary source of fresh air for the entire Rocanville Mine, and #2 Shaft will be converted to a second exhaust shaft.

In the new ventilation layout the airflow will enter the mine ventilation system at #3 Shaft, through use of surface primary fresh air fans. At the potash station of #3 Shaft, sets of underground booster fans will draw air from the shaft and boost it out to the mine workings. New shaft bottom underground booster fans will be installed to draw air from the workings and exhaust it up the #1 and newly converted #2 Shafts. Surface fans on both of these shafts will then draw the exhaust air from these shafts and ventilate it to atmosphere.

3. Estimation of flow requirements

Mining at Rocanville is done using electrically powered mining equipment, and the ore is conveyed to the shaft using electrically driven conveyor belts. However, development mining does utilize diesel powered Torkar ore haulers when conveyor belt installation is impractical. Also, the equipment used to support the mining activities (loaders, scoops, telehandlers, etc.) are diesel powered, and the vast majority of the personnel transport and maintenance support equipment are diesel powered trucks. The Saskatchewan Mines Regulations require 0.0633 m³/s of fresh air supplied for every diesel kilowatt underground [4].

One of current traits of the mine's ventilation circuit was that mining machines are independently ventilated in parallel, that is, each machine receives fresh air that has not been used by another machine. This feature guarantees a source of fresh air to each active face. Estimations of flow requirements are based on the support diesel equipment utilized at the face during the different phases of panel development and production.

Development mining utilizing Torkar and Loader mining is the most diesel intensive activity that takes place at the mine. Based on the diesel fleet and number of active mining machines, the current overall flow supply to the mine is 142 m³/s [1]. Through the process of expanding the mine, additional mining machines will enter production. Based on the number of active miners and production schedule, target underground airflow volumes for the mining machines has been estimated at 236 m³/s, not accounting for air leakage. Based on #3 Shaft ventilation capacity, the available fresh air flow volume at shaft bottom has been estimated at 254 m³/s. A schematic of the overall flow distribution is presented in Figure 1.

4. Ventilation design

The mine ventilation system was designed such that the creation of large differential pressures was avoided to minimize the potential for leakage and recirculation. The flow distribution was devised to attain lower resistance pressures and to minimize operating costs.

The selection and sizing of all ventilation fans required a detailed assessment of shaft resistances [2]. The surface fresh air and exhaust air fans were sized to overcome the plenum resistances and to slightly pressurize each shaft. Three underground booster fan installations were designed to serve the three shafts. The booster fans were sized to overcome shaft and underground circuit resistances [3]. An additional consideration for fan selection was that common sizes for fan components should be utilized whenever possible to reduce the required inventory of spare parts.

Approximate locations of the main fresh air and exhaust air underground booster fans are shown in Figure 1.

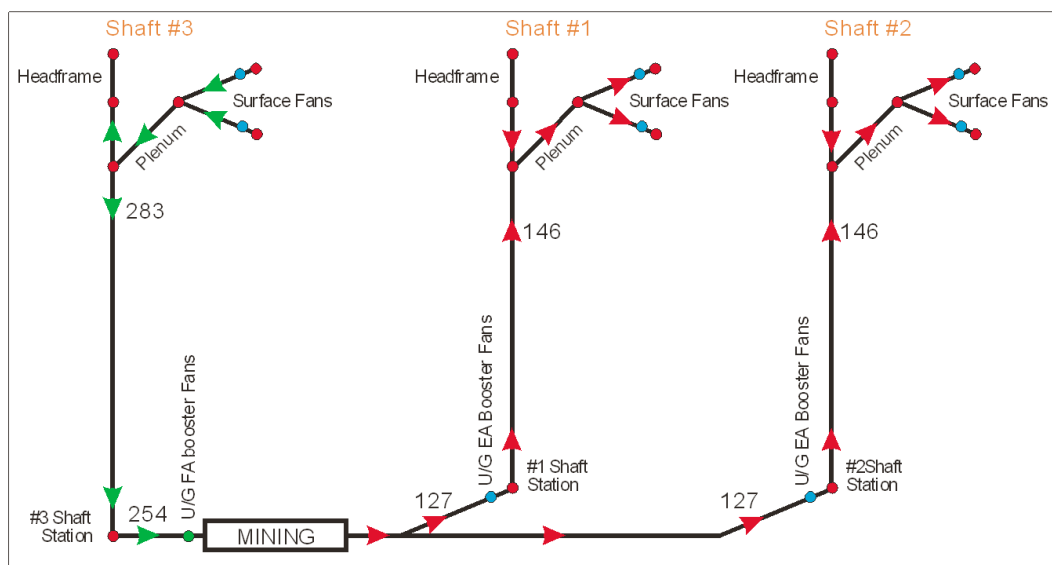


Fig. 1. Future overall mine flow distribution.

4.1 #3 Shaft surface fresh air fans

The surface fresh air fans were designed to bring heated fresh air from surface to the #3 Shaft. Sizing of the #3 Shaft main surface fresh air fans considered a horizontal assembly of two fans in parallel configuration. The design air flow rate was 153 m³/s. A fan total pressure 1 kPa was determined considering the plenum, heater and fan assemblage resistance pressures. Each fan will be fitted with a 225 kW motor and variable frequency drives (VFDs) will be installed to control the balance of pressures and distribution of flows.

Based on the fan design operating requirements vane axial fans, 2.6 m in diameter, with 1.27 m hub diameter, were selected.

4.2. #1 Shaft surface exhaust fans

The current #1 Shaft surface fans will continue to serve this exhaust airway in the future. The installation consists of two 2 m diameter, with 1.27 m hub diameter, vane axial fans, operating in parallel configuration. Each fan is fitted with a 112 kW motor. The surface exhaust fans were designed to draw exhaust air from the #1 Shaft via the plenum to the surface.

The design air flow rate was estimated at 85 m³/s. A fan total pressure 0.55 kPa was determined considering the plenum and fan assemblage resistance pressures.

4.3. #2 Shaft surface exhaust fans

Sizing of the #2 Shaft main surface exhaust air fans considered a horizontal assembly of two fans in parallel configuration. The surface exhaust fans were designed to draw exhaust air from the #2 Shaft via the plenum to the surface.

The design air flow rate was estimated at 83 m³/s. A fan total pressure 0.54 kPa was determined considering the plenum and fan assemblage resistance pressures. Each fan will be fitted with a 112 kW motor and VFDs will be installed to control the balance of pressures and distribution of flows.

Based on the fan design operating requirements vane axial fans, 2 m in diameter, with 0.76 m hub diameter, were selected.

4.4. #3 Shaft underground fresh air booster fans

The underground fresh air main booster fan installations were sized to overcome the #3 Shaft

resistance and the underground circuit resistance. The shaft resistance was determined based on detailed shaft ventilation surveys. The underground circuit resistance was estimated based on the current circuit and on ventilation modelling for the future layout.

Two underground fresh air fan stations will serve #3 Shaft. Each station will be comprised of two fans operating in parallel configuration. Each fan was sized based on a flow of 71 m³/s. A fan total pressure 1.5 kPa was determined considering the shaft, mine circuit and fan assemblage resistance pressures. VFDs will be installed to control the balance of pressures and distribution of flows.

Based on the fan design operating requirements, vane axial fans, 2 m in diameter, with 0.76 m hub diameter, were selected. Each fan will be fitted with a 150 kW motor.

4.5. #1 Shaft underground exhaust air booster fans

The underground exhaust air main booster fan installations were sized to overcome the #1 Shaft resistance and the underground circuit resistance. The shaft resistance was determined based on detailed shaft ventilation surveys.

The booster fan station will consist of two fans installed in parallel configuration. Each fan was sized based on a flow of 76 m³/s. A fan total pressure 1.1 kPa was determined considering the shaft, mine circuit and fan assemblage resistance pressures. Based on the fan design operating requirements vane axial fans, 2 m in diameter, with 0.76 m hub diameter, were selected. Each fan will be fitted with a 150 kW motor. VFDs will be installed to control the balance of pressures and distribution of flows.

4.6. #2 Shaft underground exhaust air booster fans

The underground exhaust air main booster fan installations were sized to overcome the #2 Shaft resistance and the underground circuit resistance. The boosters fan station will consist of two fans installed in parallel configuration.

Each fan was sized based on a flow of 76 m³/s. A fan total pressure 1.1 kPa was determined considering the shaft, mine circuit and fan assemblage resistance pressures.

Based on the fan design operating requirements vane axial fans, 2 m in diameter, with 0.76 m hub diameter, were selected. Each fan will be fitted with a 150 kW motor. VFDs will be installed to control the balance of pressures and distribution of flows.

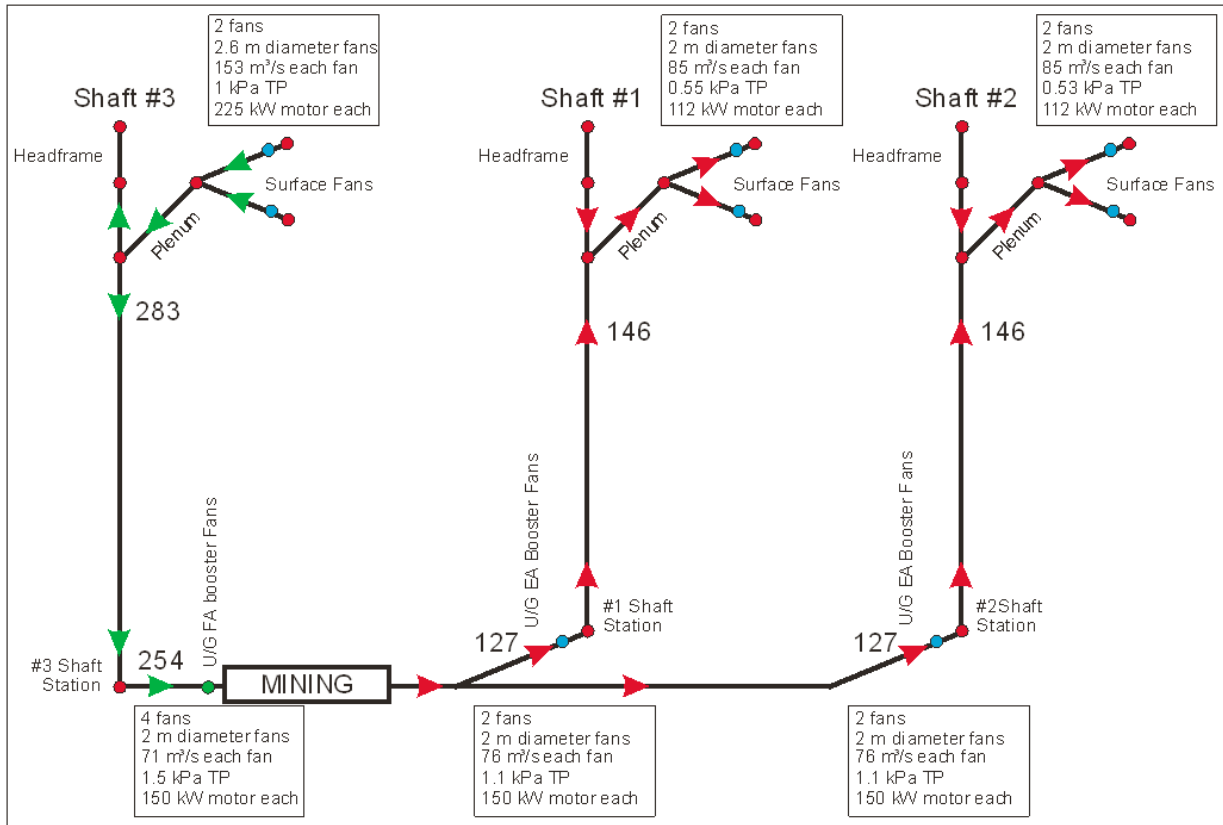


Fig. 2. Mine primary and main booster fan requirements.

4.7. Summary

Figure 2 presents a schematic for the main and booster fan design. A total of 6 main surface fans have been sized and selected with an installed brake power of 895 kW and a total of 8 underground booster fans have been sized with an installed brake power of 1194 kW. Overall, 14 fans have been sized and selected, with an installed brake power of 2089 kW. In addition, secondary underground booster fans will be necessary to achieve the required overall flow distribution. The goal of common fan sizing was also achieved, with all fans installed underground of the same size, make, manufacturer, and design. Only adjustments in blade angle were required to achieve design parameters for pressure and flow.

5. Design verification

Network modelling techniques were used to conduct simulations of the Rocanville mine ventilation system, and to verify the system design and fan requirements.

The computer model was updated to reflect current mine ventilation conditions (model verification) and checked for accuracy and correspondence with survey data (model calibration). Accurate verification and calibration of the ventilation network computer model developed by the mine are essential to produce models which provide a good representation of the current

mine ventilation system and which provide a reasonable representation of the mine ventilation system at each planned stage.

A series of ventilation scenarios were developed to verify the fan sizing and selection work, and to verify if the required local flow distribution can be achieved based on mine scheduling.

Model simulation results closely reflected the estimated individual system resistances and resistance pressures and also validated all fan system design recommendations.

In order to achieve the planned regional flow distribution, required regional booster fan stations were configured and modelled. All borers could be successfully supplied with the required flows.

6. Planned phased system implementation

Throughout the entire expansion, Rocanville mine was required to maintain a consistent supply of potash production. In order to facilitate production, and meet regulatory requirements for ventilation, a phased implementation was planned for the various systems.

6.1 Phase 1 - Pre-breakthrough readiness & production expansion

The mining machine fleet expansion was completed prior to the opening of Shaft #3. In order to facilitate an increased number of mining machines, zone cascade (series-parallel) ventilation was established to increase air volumes in the areas of the mine with heavy construction going on. This change was adopted, along with several necessary network adjustments in preparations for shaft breakthrough and the reversal of airflow in the fresh-air entries of the expanded mine. As well, all of the shaft-bottom underground booster fans were installed, and commissioned. The fans located underground at #1 Shaft were to be made fully operational prior to breakthrough of #3 Shaft. #1 Shaft was not to change in resistance, capacity, or flow, and therefore could be used to commission and test the first set of new fans. Through this phase, #2 Shaft will be supplying 142 m³/s of fresh air, and it will be exhausted up #1 Shaft.

6.2 Phase 2 - Breakthrough of Shaft #3

In order to start the transition process for the fresh air circuit, supply through #3 Shaft is to be slowly increased as the shaft becomes available and the circuit is tested. Congruently, supply from #2 Shaft is to be slowly reduced by using the VFD controls. #3 Shaft bottom is to be entirely air locked during the breakthrough process to prevent pressurized air from leaving the mine workings. The end goal for this phase is to supply up to 71 m³/s to the mine from #3 Shaft, and reduce supply from #2 Shaft to a similar volume (one quarter of the final system capacity). #1 Shaft will still be the only exhaust shaft, flowing 142 m³/s.

6.3 Phase 3 - Transition of fresh air supply to Shaft #3

The duty of servicing the mine with men and materials is planned to transfer to #3 Shaft as soon as the hoist is ready. When this happens, supply at #2 Shaft will cease, and flow at #3 Shaft will be increased (using VFD control) an additional 71 m³/s, to the original system capacity of 142 m³/s, and one half of the full system capacity. During Phase 3, #2 Shaft will be bulk-headed on the top and bottom to facilitate work replacing the headframe and hoist system on top, and the tie-in of the skip loadout system at the bottom. During this phase the current fresh air fans atop #2 Shaft will be removed and replaced with a new system, and the fresh air fans will be removed and relocated to mid-mine bulkheads, where they will provide pressure to supply mining blocks. #1 Shaft will still be the only exhaust shaft, flowing 142 m³/s.

6.4 Phase 4 - Re-opening of #2 Shaft/conversion to exhaust shaft & system ramp up

When the mechanical conversion of #2 Shaft into a production shaft is complete, the bulkheads will be removed, and ventilation system ramp-up can begin. Supply of fresh air at #3 Shaft will be increased, and the additional volume will be taken by the new underground and surface booster fans at #2 shaft. #1 Shaft will still be exhausting 142 m³/s. The goal for this phase is to ramp up the ventilation system to the full design capacity of 254 m³/s ventilating the mine workings.

6.5 Phase 5 - Final commissioning & optimization

Once the main flows have been established and the design capacity realized, the system will be optimized. The system will be tested by manipulating manual and network adjustable variable-frequency drives, and the effects will be catalogued. The test results, and effects from other inputs, like ambient surface conditions, will be used to build an automated control narrative for the main fans, having the system react automatically to various scenarios that may exist.

6.6 Summary

Throughout the process, Rocanville Mine plans to produce potash, and all mining machines will be effectively ventilated. The primary goal of reconciling the ventilation system with the production requirements is being effectively achieved.

7. Summary

An engineering assessment and design of the Rocanville Division mine ventilation system upgrade has been presented in this paper. Overall, 14 fans have been sized and selected, with an installed brake horsepower of 2089 kW, in order to achieve an overall flow of 254 m³/s.

An entirely new mine flow distribution was designed and modelled, with the mine expanding from a two shaft system to a three shaft system, and with the number of mining machines approximately doubling. Commissioning of the ventilation system is being successfully implemented in phases to permit a controlled ramp up to full ventilation capacity with minimal disruption to production and mine operations.

Computer model simulations demonstrated that the mine will, in the future, be able to meet all flow requirements, while meeting all regulatory and safety requirements.

References

- [1] AirFinders Inc. Rocanville Division Ventilation Engineering Design Study - Estimation of Airflow

Volume Requirements. 62 (2013).

- [2] AirFinders Inc. PotashCorp Rocanville Division Shaft Resistance and Airflow Characteristics Study. 51 (2009)
- [3] AirFinders Inc. Rocanville Division Ventilation Engineering Design Study - Mine Ventilation System Expansion Design. 83 (2013)
- [4] Saskatchewan Mines Regulations (2003)
- [5] PotashCorp – Markets & Industries (2015)

A Case Study of Optimization of Costs for Trackless Mining Ventilation and Cooling Systems

Pedram Rostami, PhD, CAPM^a, C. Alex Rawlins, PhD, RME^b,

^a*Stantec Consulting, Tempe, Arizona, USA*

^b*RME Consulting Canada, Toronto, Ontario, Canada*

Ventilation systems are not only an integral part of any underground mine design but are a significant contributor to the mine's capital and operating costs. The ventilation and cooling design systems presented in this paper were part of the prefeasibility evaluation of an underground platinum mine in South Africa. The mine will ultimately operate at the depth of 1,200 m below surface with a proposed 4 Mtpa production rate.

The proposed mining operation is a highly mechanized operation using diesel equipment. Significant daily production rate, large amount of equipment and expansive nature of the operation, contributed to challenging yet flexible ventilation design requirements.

This paper presents a case study of how to safely and efficiently optimize capital expenditure and operating costs associated with the mine air cooling and refrigeration system through practical ventilation design practices. Successful capital and operational savings by modulating installation and commissioning of refrigeration facilities can influence the economic realization of such systems. The adapted planning and design approach provided a cost-effective advantage while complying with design safety and regulations.

Keywords: Ventilation, Cooling, Cost Optimization, Refrigeration, Modeling, Design.

1. Introduction

This paper outlines a prefeasibility evaluation of the heat loads and related cooling system to be employed at the proposed platinum mine. The paper also provides appropriate details for a comprehensive understanding of the applied methodology. The proposed mine will be a trackless underground operation using a combination of mining methods. Initially, ore zones with vertical thicknesses greater than or equal to 18 m will be mined using the long-hole stoping (LHS) method, while thinner ore zones will be mined using mechanized drift-and-fill or drift-and-bench methods; hence, a highly mechanized operation with LHDs, trucks, drill rigs, personnel carriers, etc. is envisioned. Broken rock (ore and waste)

will be transported by the means of trucks to the main passes (ore and waste) and collection points.

Mining zones identified in the project occur at depths ranging between approximately 700 m to 1,600 m below surface.

Primary access to the mine will be via a 1,100 m deep, 10 m diameter production shaft (named Shaft No. 2), three additional shafts will be sunk to provide future ventilation and production support. Three main access levels are established as primary haulage levels and include a series of interconnecting ramps. Additional mining sublevels will be developed as necessary.

Figure 1 shows the proposed shaft locations and main access levels in a 3-D elevated view.

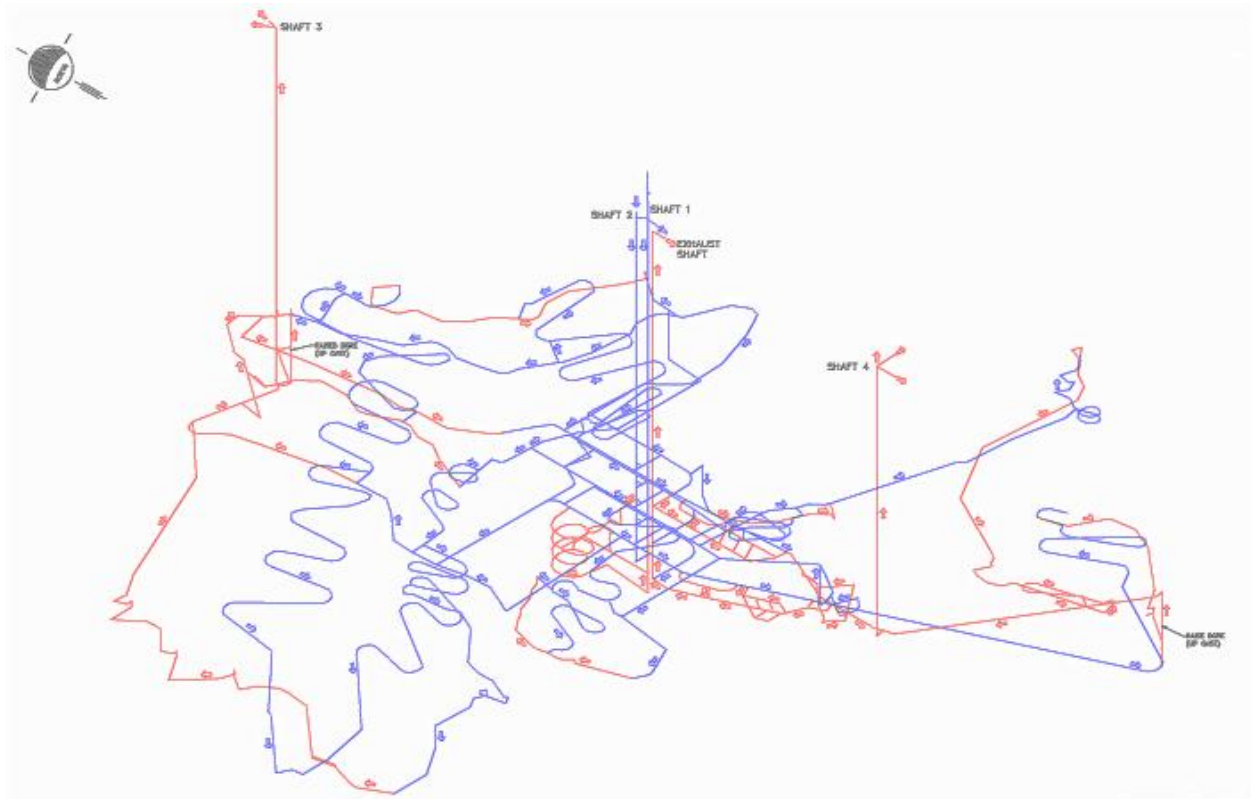


Figure 1. Proposed mine access layout.

Mining is performed using highly productive mechanized methods. For this reason, an annual ventilation estimate is based on requirements for mobile equipment (i.e., 0.06 m³/s/kW). The air requirements imposed on the underground operation is further influenced by equipment heat loads, auto compression, and virgin rock temperature, as the main sources of in-mine heat.

As a pull (exhaust) system arrangement, fresh air travels via the downcast shafts No.1 and No.2 and exhausted through a number of internal return air raises (RARs), serving each mining sublevel, through to the two main exhaust shafts (Shaft No. 3 and Shaft No. 4), each positioned on the opposite side of the ore body.

The mine is divided into smaller mining zones and subzones. For the project's ventilation study, these zones are further grouped into independent ventilation districts.

2. Ventilation Planning System

The planning methodology for this study includes the following typical steps in order to select the optimum planning strategy:

1. Determine mining method and rate of production.
2. Define acceptable environmental conditions.
3. Calculate heat load and impact from other contaminants such as gas emissions, dust, rock latent heat and fumes.
4. Calculate air and cooling requirements.
5. Optimize ventilation and refrigeration alternatives

6. Incorporate into the mine development and production plans.

Figure 2 shows a flow chart of the planning phase process.

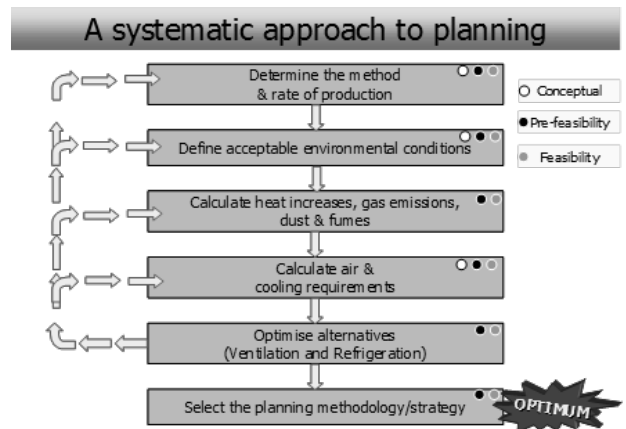


Figure 2. Planning phase flowchart

Table 1 presents the mine design parameters for the project.

Table 1. Indicative mine design parameters.

Description	Value and units
Mining method	Trackless
Drift dimensions	5 x 5 m
Lateral level intake dimensions	5 x 5 m
Production rate	4 Mtpa
Reject temperature at the main exhaust shafts	28.5°C
LHD machinery	242 kW
Loading trucks	550 kW
Description	Value and units

3. Ventilation Requirements and Design Criteria

The ventilation system is designed based on a primary exhaust system. The two main intake shafts (Shaft No.1 and Shaft No. 2) located at the center of the mining reserve provide fresh air to the underground operation, while Shaft No. 3 (North) and Shaft No. 4 (South) are the primary exhaust systems. Fresh air is distributed through a series of shaft stations, major ramps, and lateral haulages at the 750, 850, and 950 Levels. Regulators are used to distribute fresh air to the active mining areas and spent air then returns at either side of the mining sublevels.

Air quantities are based on a diesel emission dilution of 0.06 m³/s/kW of diesel engine power rating. The diesel engine ratings are based on technical specifications for major equipment.

An overall quantity of 923.85 m³/s was originally calculated due to the diesel fleet employed. This quantity was later adjusted to 1,157 m³/s for distribution (mining zone) requirements, cooling needs and in coordination with the mine development and production plan.

In order to address the health and safety of personnel, and as a general guideline in the design, air velocities in haulages are kept between 0.25 m/s as a minimum and 7.60 m/s as a maximum. Air velocities of 1 m/s in stoping areas and 2 m/s in sublevels are used as the criteria in which the former provided a minimum quantity of 25 m³/s.

Furthermore, the air velocity range between 7 m/s to 12 m/s (critical velocity range) are avoided in vertical upcast shafts or where condensation could occur, as this is the point at which water droplets will remain suspended in the airstream, increasing shaft resistance

and adding additional pressure (and possible fan failure) on surface fan installations.

4. Ventilation Modeling

Throughout this study, various ventilation models were developed; among them, four major stages of the mine design including (a) initial development, (b) preproduction, (c) full production, and (d) a future life of mine (LOM) were selected as specific study phases. The heat loads and related cooling requirements were tested and applied when applicable (reject temperature set at <28.5°C) during all four stages of the mine operation.

A cross-sectional area of 25 m² (5 x 5 m) was assigned to all haulages and sublevels. The surface fresh air intake temperature of 20/30°C (wet and dry bulb respectively) was determined from a five year average summer temperature statistical analysis for the region.

From best practice applications, practical experience, and ventilation simulation pressure distribution, it was concluded that it will be most suited to install the main exhaust fans on the surface. An emphasis was applied on the use of regulators rather than underground fan distribution systems.

To exhaust the air quantity of 1,157 m³/s, four main centrifugal type fans were selected, each with motor capability of 2,000 kW, operating at 5,000 kPa static pressure. Two fans, in bifurcated arrangement, are located on the surface at each exhaust shaft (Shaft No. 3 and No. 4).

5. Production Airflow Requirements

A large amount of development is initially required to facilitate the primary ore production. Figure 3 illustrates the annual production and development tonnage over the LOM and further illustrates the phased approach of the overall project. The required air quantity generally follows the production profile.

As indicated in Figure 3, a required total quantity of 1,157 m³/s at peak production was determined. The quantity buildup is in relation to the production and waste development fleet requirement.

Figure 4 shows the quantity and production profiles over Years -2 to 7. Note that the air quantities indicated are surface air quantities.

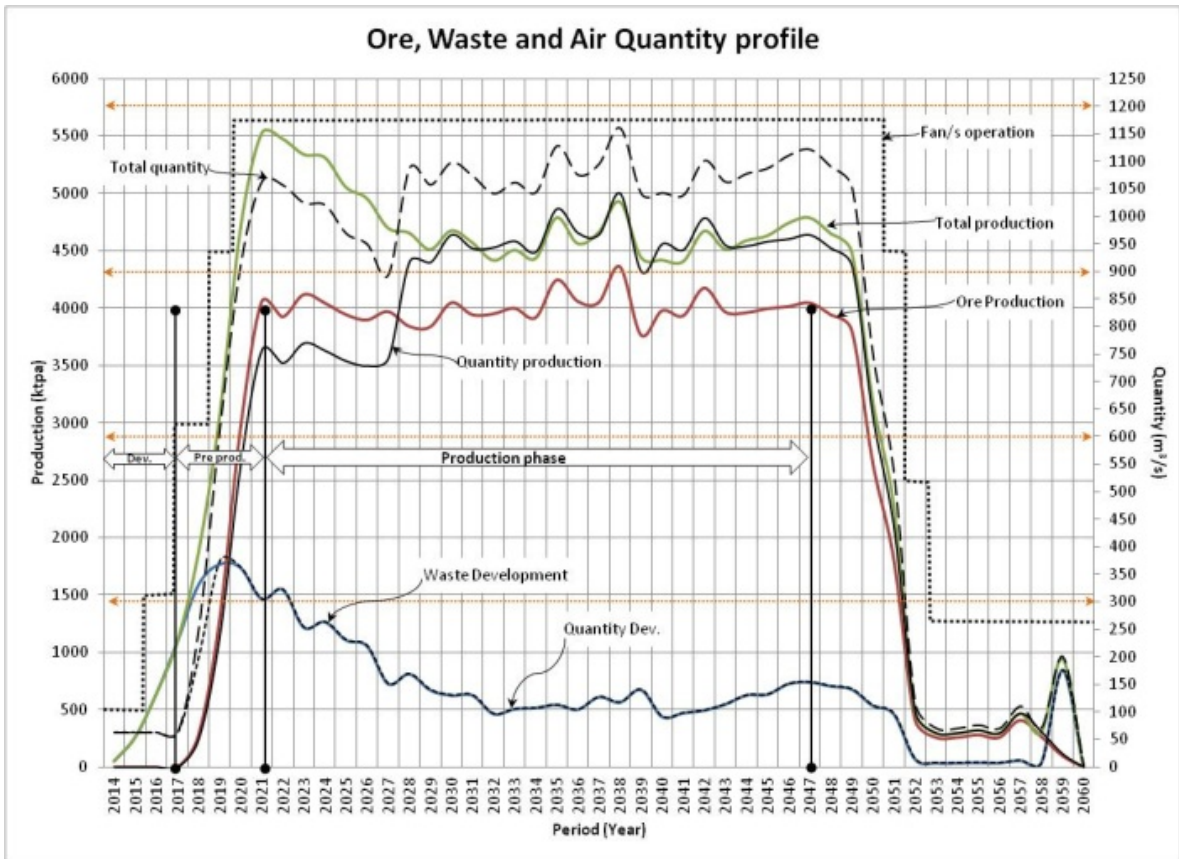


Fig. 3. Surface quantity illustrated in combination with production and waste development.

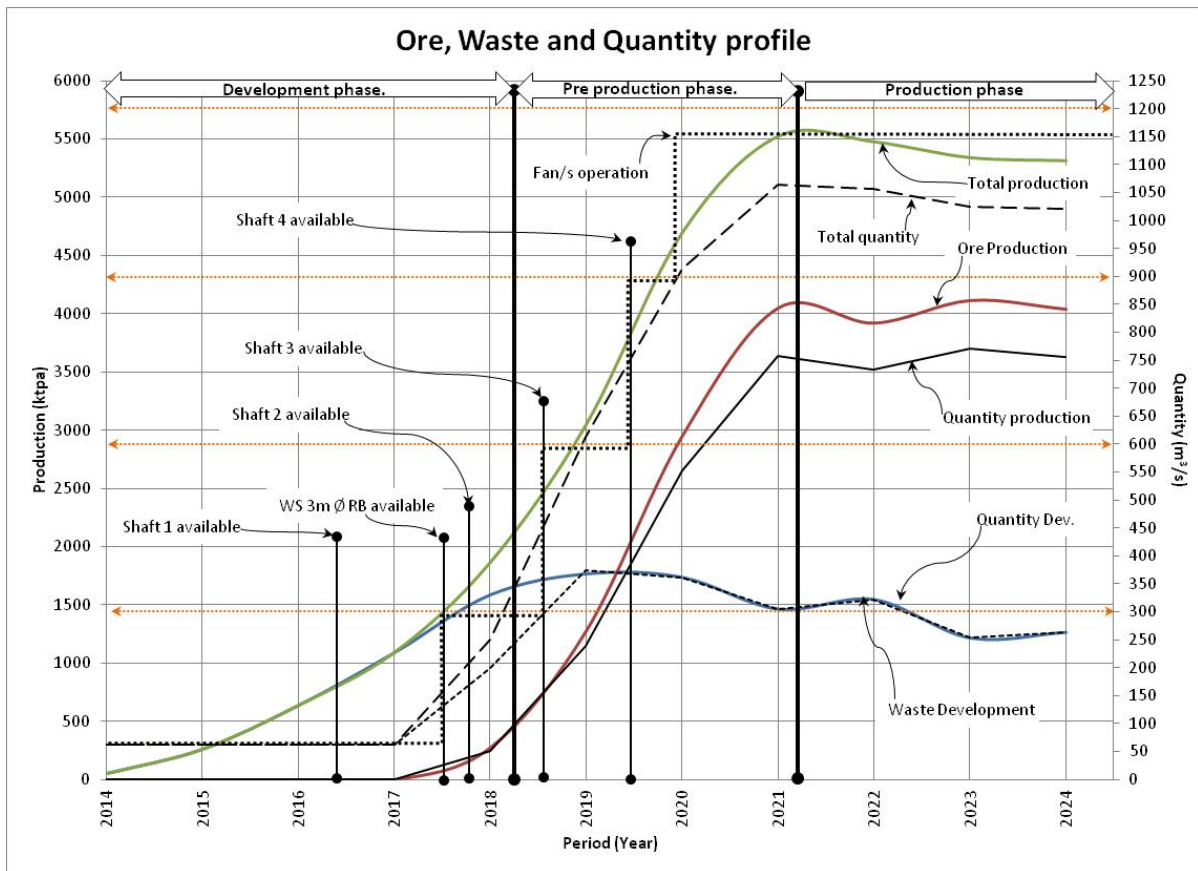


Fig. 4. Illustration indicating the first ten years of operation (quantity and production profiles included).

Figure 4 further shows the schedule of ventilation shafts as they are needed during the initial ramp-up period. It is important to note that from a ventilation shaft availability schedule, about one to two months are needed to install and commission the main surface fans. The orange-colored arrows are indicative of each fan capacity (300.00 m³/s each).

6. Mine Air Cooling and Refrigeration

Mine cooling evaluation consists of a large number of variables and geographical factors that govern the heat flow into mine airways. The cooling design for this project is based on achieving an average reject wet bulb temperature of 28.5°C and further applying a surface intake fresh air temperature of 20/30°C (wet and dry bulb, respectively).

As a first order comparison of alternative refrigeration systems included underground refrigeration installations and surface ice makers. It was determined that surface refrigeration using chilled water direct contact type (Bulk Air Cooling [BAC]) applications were the most practical and economical.

An ammonia refrigeration plant system was evaluated from a costing point of view and not considered further at the time due to surface spacing and legal requirements for such a system. Making use of small underground heat exchangers underground closer to the point of need is most efficient; however, piping and pumping compromise some of the energy and cost savings attained.

As a summary, the following contributors are given as in-mine heat-load sources.

- Geothermal gradient known as Virgin Rock Temperature (VRT).
- Backfill application and distribution system.
- Artificial heat load (e.g., trackless equipment, fissure water, broken rock, pumps, auxiliary fans, people, lighting).
- Ambient summer and winter surface fresh air intake temperatures.
- Mining depth and auto-compression.
- Energy exchange unit efficiencies.
- Energy recovery system efficiencies.
- Chilled water reticulation method.

Each one of the contributors and combinations thereof contribute either positively or negatively toward an underground mine's heat load and related cooling requirements.

Taking into consideration the location of this project and its mining system, detailed descriptions of some of the primary heat load contributors previously listed include the following and is summarized in Figure 5.

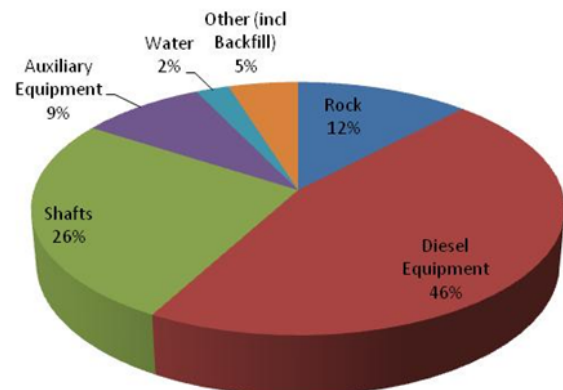


Fig. 5. Estimated breakdown of heat load contributors and their percentages.

- **VRT** – Thermal gradient is 18.3°C/km with a surface rock temperature of 25.5°C. At depth the rock temperature ranges between 47°C and 48°C. Heat load contribution was estimated at 6,292 kW. The VRT for other areas and specifically the mine region are shown in Figure 6 and Figure 7.
- **Trackless equipment** – Overall vehicle power is calculated to be 18,491 kW and the related heat load in conjunction with the use of all equipment is calculated as 31,084 kW.
- **Auto-compression air heat load** – From the surface to shaft depth auto-compression heat load is approximately 13,597 kW.
- **Service and fissure water heat load contribution through the mine** – It is estimated that about 100 L/s service water would be applied. An estimated 5,862 kW of heat could be applied to the underground mine environment. Additionally, due to the return water in a piping system, a conservative estimate of 20% is applied to heat load ingress, resulting in an approximate 1,200 kW heat load.
- **Backfill and other heat loads (e.g., people, lighting)** – This amounts to an approximate 2,531 kW heat load in the system.
- **Other in-mine heat loads** – Approximately 4,500 kW are introduced from auxiliary fans and pumping systems.

The overall heat load determined is calculated as 52,105 kW. The air cooling capacity is calculated at 32,853 kW; thus, the mechanical cooling required maintaining the reject temperature of 28.5°C is 19,252 kW, say 20 MW of refrigeration. Including approximately 10% as spare capacity for the Bulk Air Cooler (BAC) system, the final refrigeration plant capacity is designed to supply ±26,000 kW which includes about 20% energy losses over the distribution system.

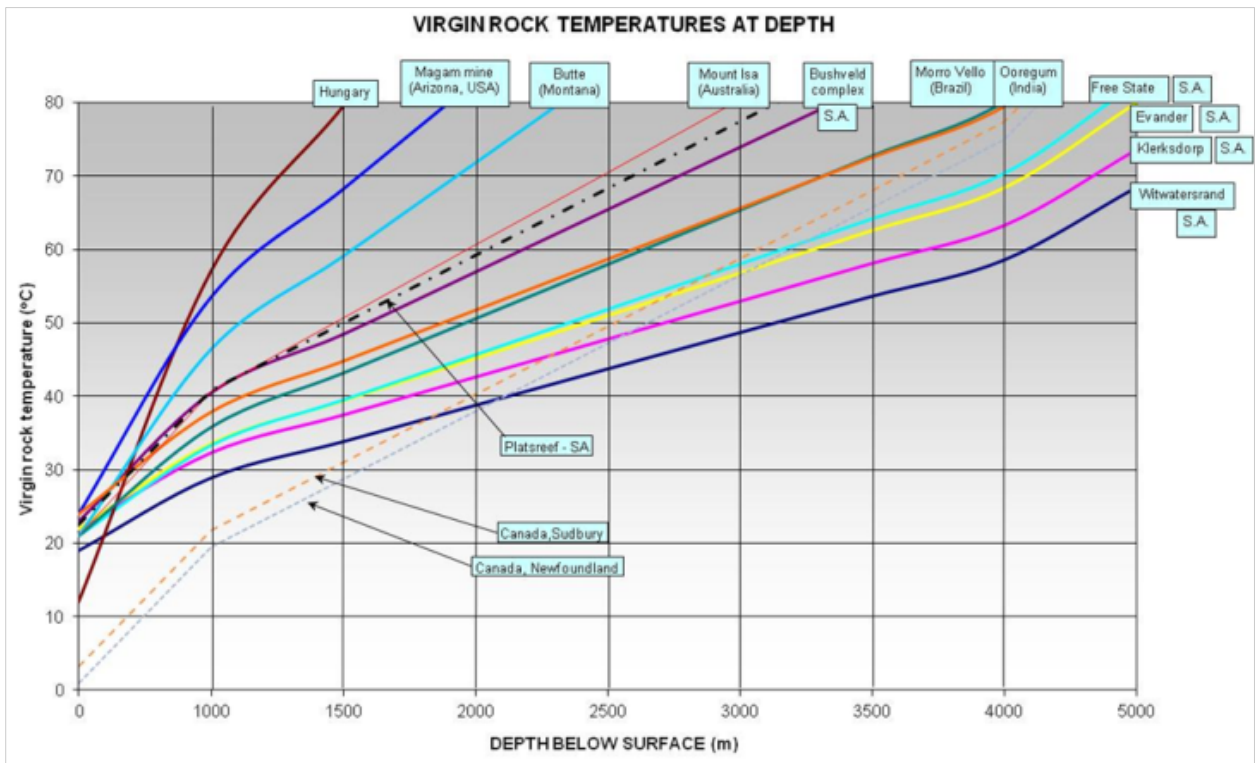


Fig. 6. Overall geothermal gradient for the mine and other world-wide areas.

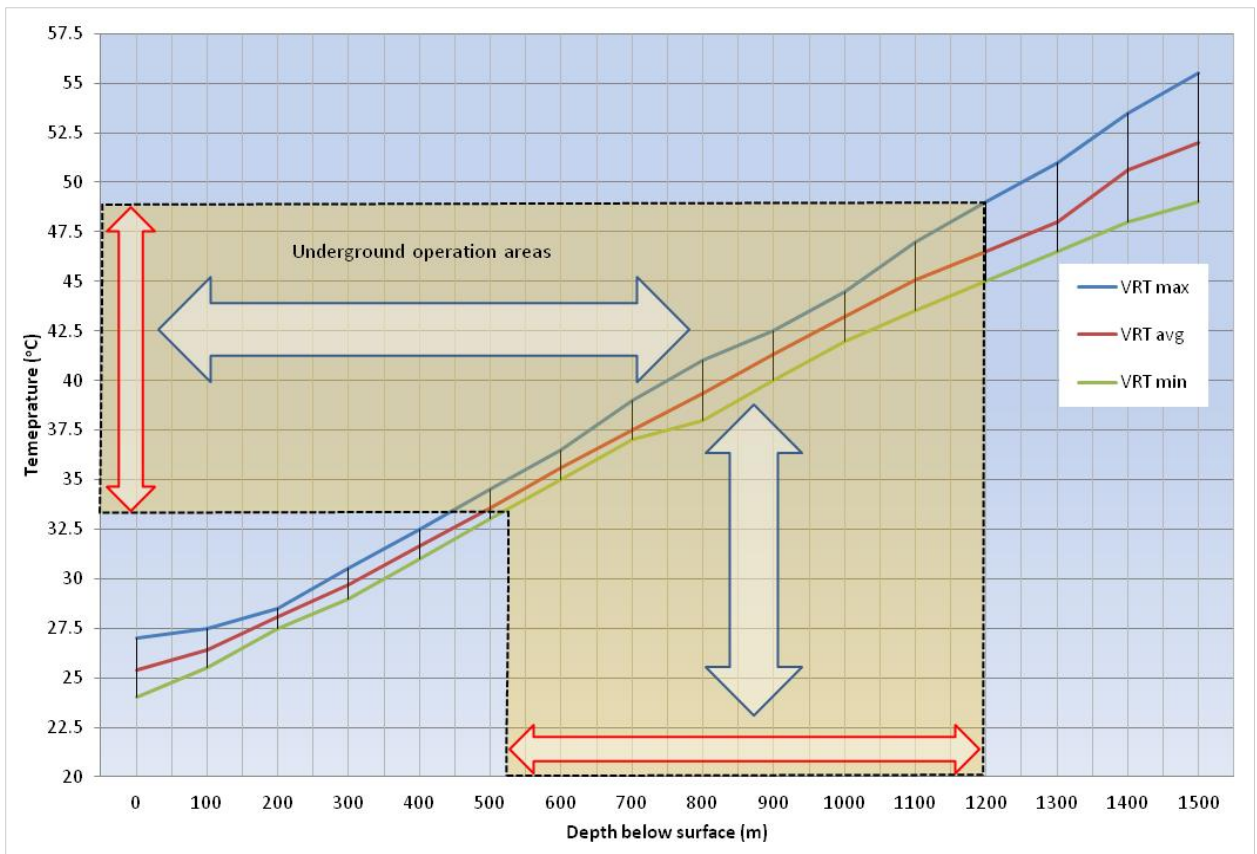


Fig. 7. Geothermal gradient profile for the mine location.

7. Mine Air Cooling Facilities and Cooling System Description

7.1 Bulk Air Cooler System

The single 20 MW BAC will be installed on surface at the Shaft No.1. The BAC system is a horizontal-type, counter flow, three stage heat exchanger. Fresh air is forced into the BAC chamber by means of three 200 m/s force fans positioned in parallel on the intake side of the BAC (600 m/s total). The intake mean summer wet bulb temperature is 20°C and the design outlet air temperature is 10°C saturated. Chilled water is sprayed into the moving air within the BAC chamber by means of spray nozzles separated in equal spacing along the chilled water pipes. The water droplets fall to the bottom of the chamber and are reticulated back to the refrigeration plant evaporator plate heat exchanger system where the system is repeated. Figure 8 illustrates a typical BAC system as described.

7.2 Refrigeration Plant

The surface refrigeration plant will comprise of four standard-packaged R134a centrifugal water chiller machines. Refrigerant R134a is non-toxic and therefore the refrigeration plant can be constructed adjacent to the BAC and close to the shaft. This type of compact

installation will have a relatively low capital cost and achieve a high system performance. The general layout of the refrigeration plant system is illustrated in Figure 9.

7.3 Condenser Cooling Tower (CCT)

Water from the refrigeration plant condenser unit is reticulated to the condenser cooling tower to cool the water and then circulates back to the plant where the process repeats. The condenser tower general layout is shown in Figure 10.

7.4 Overall Cooling System

Shaft No. 1 (7.25 m Ø) will be one of two fresh air downcast shafts and will be used exclusively for distribution of the chilled air from the surface to underground. An underbank chilled air distribution system will be constructed to provide a path for the chilled air transition from the BAC to the vertical shaft system. This underbank system connects the BAC to the vertical shaft via a typical airway, as shown in Figure 11.

An overall view of the refrigeration plant, the BAC, and the CCT is shown in Figure 12. The complete system will occupy an area of about 50 x 50 m.

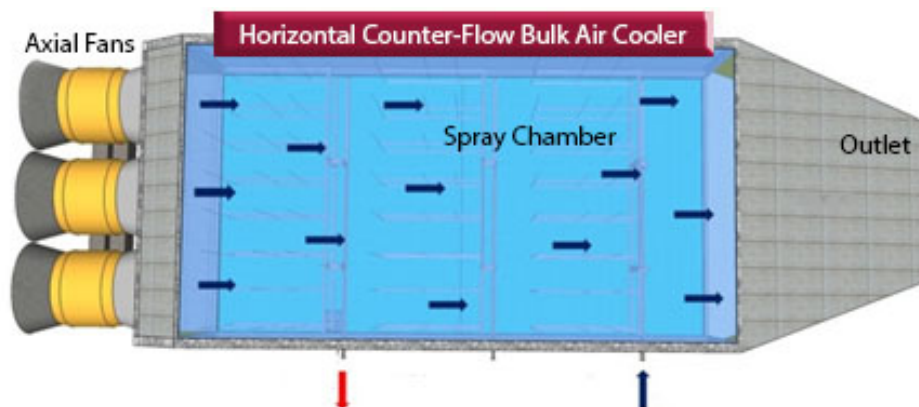


Fig. 8. Horizontal three-stage BAC general layout.

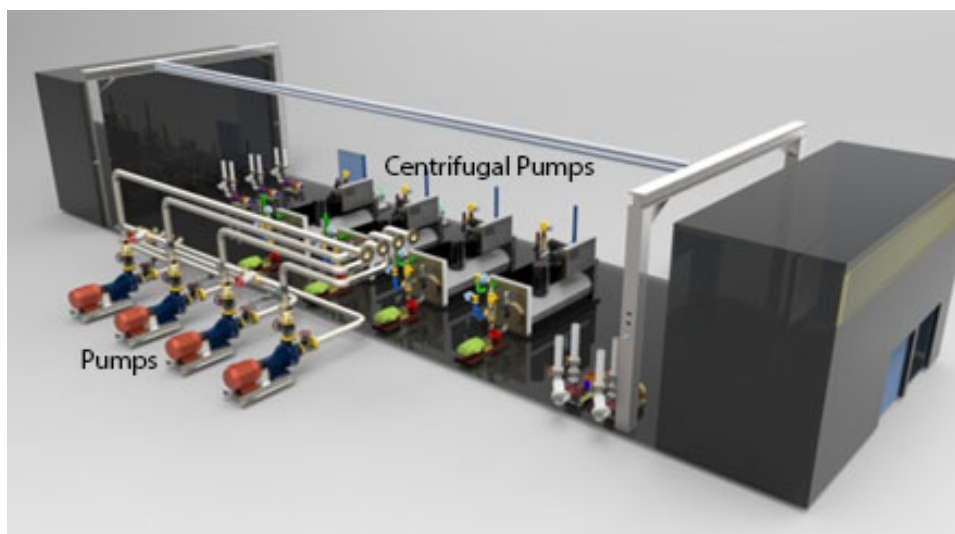


Fig. 9. Refrigeration plant illustration.

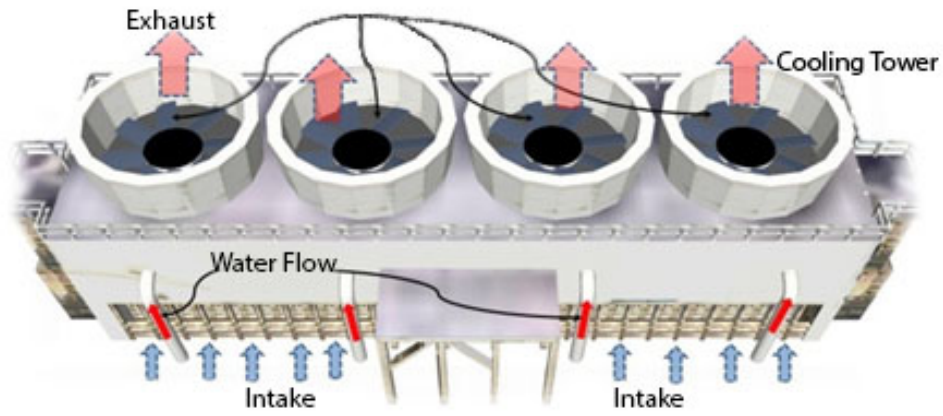


Fig. 10. Condenser cooling tower illustration.

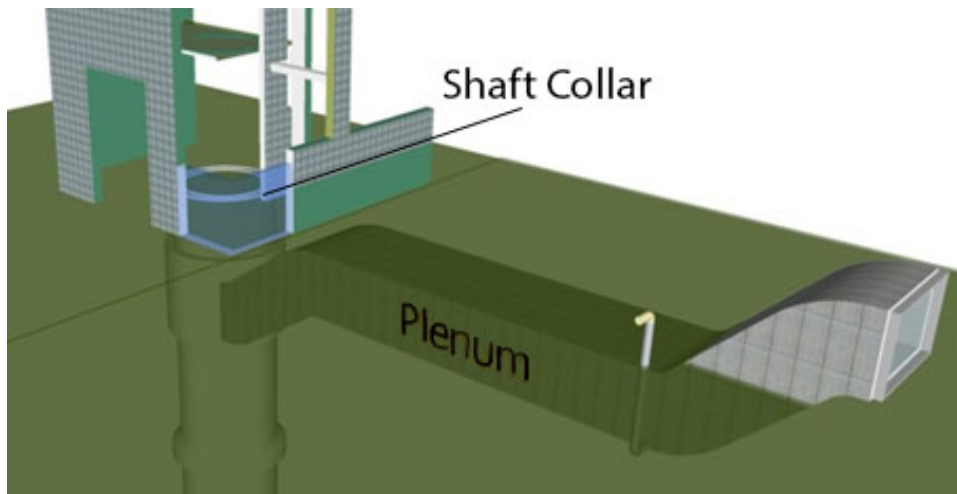


Fig. 11. Underbank fresh air intake system illustration.

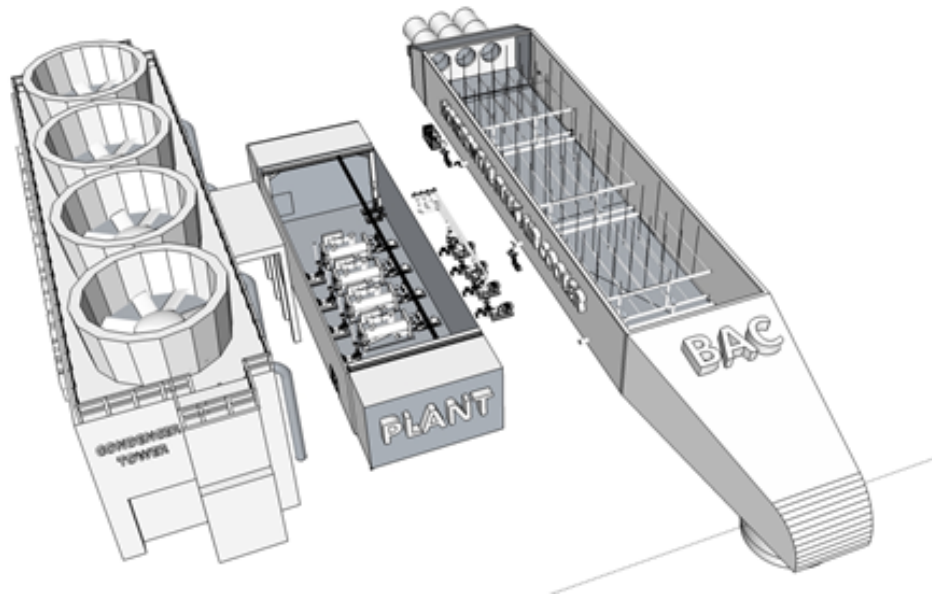


Fig. 12. Overall layout of the cooling system.

8. Capital and Operating Costs Savings of Modular Installation

8.1 Calculations

Considering the project's three-year ramp-up period along with the maximum cooling requirement only needed for the deeper mining operation of the mine, capital and operating cost savings are possible by modulating the installation and commissioning of the cooling system.

Figure 13 illustrates the step-loading of the cooling requirements for the production and development phases of the project, ultimately leading to full production.

The introduction of cooling could vary slightly depending on the actual location of development and production areas in the mine. The mining schedule will be monitored on a continuous basis and cooling introduction based on the production and development schedule.

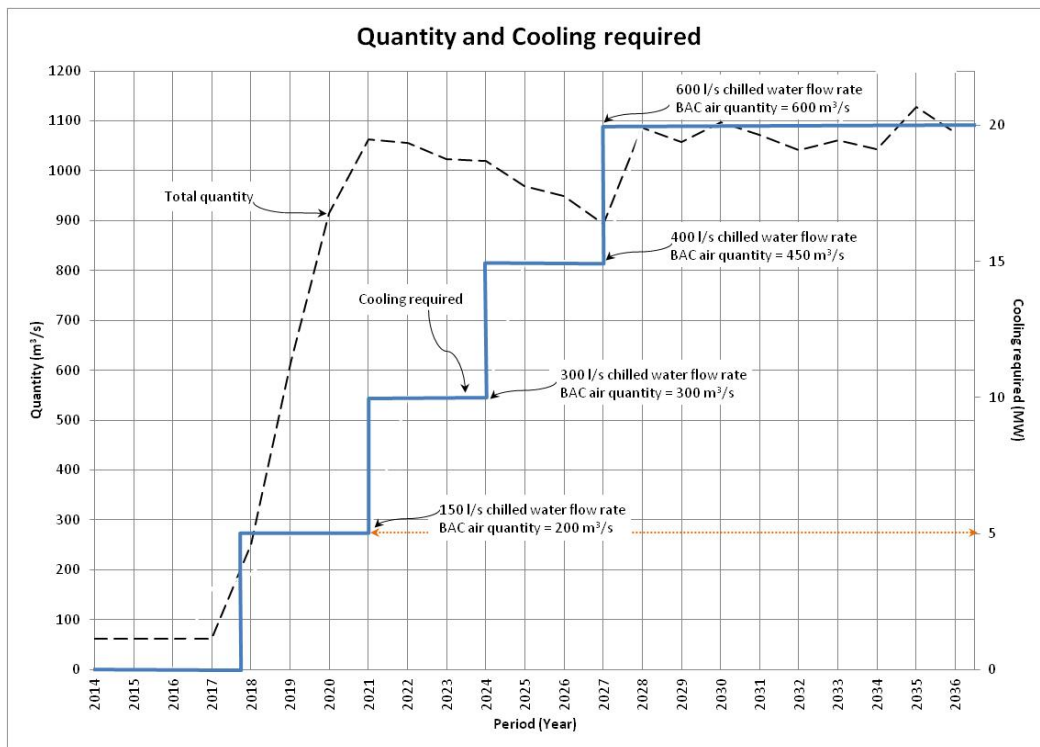


Fig. 13. BAC cooling, chilled water, and BAC quantity distribution schedule.

The first 5 MW cooling requirement was determined for initial development on the first four levels leading from the Shaft No.2. The remainder of the cooling schedule is based on a similar timeframe (with a slight reduction of three months per timeframe or stage) to ultimately implement the 20 MW cooling applied to the full production underground operation through the Shaft No. 1.

Per the contractor quota, the total capital cost of the full installed system is \$17.5 million. Such staged installation and associated purchasing every three years greatly helps with required up-front capital of only \$4.4 million and three installments of \$4.3 million on Year 4, Year 7 and Year 10, versus \$17.5 million up-front capital cost.

Assuming 10% interest rate over the time period, a straight NPV analysis will show a saving of \$5 million. Considering all the owner costs, EPCM, and site preparations, an additional \$1.19 million of savings after commissioning of the first module, \$790,909 by the second installation and \$400,000 after commissioning the third module can be achieved. The total possible savings will be about \$2.4 million on the capital cost alone.

Also this modular installation along with utilization of variable speed pumps, can contribute to significant savings on operating costs. In the winter time, when less cooling is required, reducing the number of pumps and flow rate can significantly reduce the power load.

9. Conclusions

Cooling is introduced over a time period of nine years where the first 5 MW BAC system is commissioned in the last quarter of Year -1 and the last unit commissioned in Year 10, giving a total of 20 MW cooling overall.

Using staged plant implementation over time greatly contributes toward reducing the capital and operating expenditures. In this project, the plant systems are phased in at one unit every three years after the first plant is installed and commissioned.

The resulted savings is estimated at about \$2.4 million benefit (14% savings) over a 30-year mine life, a substantial amount which cannot to be ignored considering the total capital cost of \$17.5 million. The cost savings was estimated using a sound economic cost evaluation.

This modular installation combined with variable speed pumping system can result in significant cost savings on operating costs over the life of mine as well.

Also the benefit of modularizing allows new operations to be producing cash flow to self-fund the modular expansions.

References

- [1] Danko, G.; Bahrami, D.; Rostami, P. "Seasonal Temperature Variations in Underground Tunnels." Paper presented at the 14th North American Mine Ventilation Symposium, UT, June 2012.
- [2] *Mine Ventilation and Refridgeration*. Prefeasibility Report, Ivanhoe Mines Limited, 2014.
- [3] Rawlins, C.A. Paper presented at the 11th

US/North American Mine Ventilation Symposium, PA, June 2006.

- [4] Rostami P.; Danko, G.; Bahrami, D. "Ventilation and Climate Simulation of Development Ends in Metal Mines." Paper presented at the Society for Mining Metallurgy, and Exploration Annual Meeting, Denver, CO, 2011.
- [5] Rostami, P. "Numerical Modeling of Contaminant Gas Transport in Underground Openings" Paper presented at the Society for Mining Metallurgy, and Exploration Annual Meeting, Denver, CO, 2013.

Mine Ventilation Model Calibration with Numerical Optimization

George L. Danko, Davood Bahrami, Chao Lu

University of Nevada, Reno, USA

Mine ventilation model calibration against ventilation survey data is difficult and labor intensive. Continuous re-calibration is necessary as the mine changes with operation. A calibrated and well-tuned ventilation model is key to applications such as safety, health and cost analysis and optimization. New technologies in ventilation monitoring and control further necessitate real-time ventilation model simulations in which the model must be kept calibrated.

New ventilation model calibration methods are emerging in which the resistances of the network elements are determined by numerical search algorithms for best fit between ventilation survey data and model simulation results. A least-square-fit (LSQ) numerical algorithm is described in the paper. The LSQ method optimally adjusts the network branch resistances until the simulated results of the ventilation network model best match the in situ mine surveying data of branch pressure differences and air flow rates. The algorithm may adjust all or only a selected set of air flow resistances of the ventilation network by minimizing the measured and simulated data in a least-square-fit sense according to availability of survey measurements.

A numerical example is given comparing the LSQ method with the branch-by-branch evaluation of the Atkinson's k -factor. The exercise shows that the algorithm has advantages over hand-calculations. The LSQ method uses the network model as a predictor simulator and always relates the results to a balanced network solution, obtaining better airway resistance results from measurements loaded with random as well as systematic measurement errors.

Keywords: ventilation model, calibration, numerical optimization

1. Introduction

Ventilating model calibration is an important recurring task as the mine is undergoing development in new areas, and closures in the mined-out sections. A calibrated ventilation model is a valuable numerical-analytical tool that can forward-predict mining environmental conditions under changing production or development scenarios. Ventilation simulations can be used to test solution options and predict likely outcomes, such as performed by Prosser et al. [1]. Model calculations may replace in situ measurements for checking what-if scenarios without actually modifying the conditions and interfering with operations. However, it is essential to trust the ventilation model and test its worthiness against in situ mine ventilation survey data, emphasized by MSHA [2], von Glehn et al. [3] and others. Several methods have been proposed for ventilation model calibration.

The classic method uses measurements of differential pressure with a gauge and tube, and branch air flow rate in each air branch under calibration described for example by McPherson [4], Prosser and Loomis [5]. The gauge and tube method provides direct access to the primary input parameters in the airway resistance formula. Other methods aim at simplifying the measurement task by eliminating the tube and use barometric pressure sensors. This method introduces potentially large pressure offset error components due to measurement sensor elevation differences found by Danko and Bahrami [6]. A genetic algorithm was tested and published for the solution by Liu et al. [7].

The aim of the paper is to test an inverse numerical algorithm that can evaluate the Atkinson's k -factors from in situ measurement data consisting of differential pressure and air flow rate readings in the airway branches of a ventilation network. The method is a variation of the evaluation procedure published

previously by Danko and Bahrami [6] for the same type of calibration task.

The new ventilation model calibration uses only a subset of the measurement data (pressures and air flow rates in air branches) consisting only the branches with significant energy loss. The mathematical method is based on the Jacobian sensitivity matrix of the ventilation system relative to airway resistance coefficients. The required adjustments on the k -factors are determined by the LSQ procedure by minimizing the Root-Mean-Square (RMS) error between measured and simulated results.

2. Method description

The goal of the LSQ procedure is to inverse-evaluate the Atkinson's k -factors from the measured pressure differences and flow rates of the air branches, ΔP_i , and branch flow rates, Q_i , respectively.

The objective function to be minimized is the RMS error between the values evaluated directly from measurements, $[k^M]$, and the simulated values, $[k^S]$ the later calculated from the ventilation model. In the LSQ algorithm, the air branch resistances, $[R^M]$ and $[R^S]$ are used, converted from the Atkinson k -factors. The objective function is:

$$\sum_{i=1}^N [\Delta P_i^S / (Q_i^S)^2 - \Delta P_i^M / (Q_i^M)^2]^2 = \min \quad (1)$$

where: $R_i = \Delta P_i^S / (Q_i^S)^2$ is an unknown, N -element vector, proportional to the of Atkinson's resistance factors;

ΔP_i^M and ΔP_i^S are measured and simulated N -element nodal pressures;

Q_i^M and Q_i^S are measured and simulated N -element branch flow rates.

The ΔP_i^S and Q_i^S values are calculated from the ventilation model using all trial values of R , $i=1\dots N$, simultaneously during the search for minimum error.

The Jacobian sensitivity matrix for the R , resistances is calculated from the ventilation network model as a response to the change in pressure loss and air flow rate in each branch. The ventilation network branch resistances are perturbed by changing the resistance coefficients multipliers, m , in the ventilation model systematically one-by-one by dm as follows

$$[J_R] = \begin{bmatrix} \frac{\partial(\Delta P_1/Q_1^2)}{\partial m_1} & \dots & \frac{\partial(\Delta P_1/Q_1^2)}{\partial m_N} \\ \vdots & \ddots & \vdots \\ \frac{\partial(\Delta P_M/Q_M^2)}{\partial m_1} & \dots & \frac{\partial(\Delta P_M/Q_M^2)}{\partial m_N} \end{bmatrix} \quad (2)$$

If all $dR_j = \Delta P_j^S / (Q_j^S)^2$, $j=1\dots M$ and dm , $i=1\dots N$, are arranged into a column vector, $[dR]$, and perturbation column vector, $[dm]$, respectively, the following matrix-vector equation can be written:

$$[dR] = [J_R][dm] \quad (3)$$

where $[dR]$ is an M -vector, $[dm]$ is an N -vector and $[J_R]$ is an $M \times N$ matrix.

The changes in Eq. (1) in branch pressure differences and air flow rates can be expressed with the Jacobian matrix in Eq. (2). First, the small differences in Eq. (1) are re-written:

$$\sum_{i=1}^N [d\Delta R_i]^2 = \min \quad (4)$$

where:

$$d\Delta R_i = \Delta P_i^S / (Q_i^S)^2 - \Delta P_i^M / (Q_i^M)^2 \quad (5)$$

Next, the square and summation in Eq. (4) is expressed as the scalar product of the difference vectors, using the vector transpose notation:

$$[d\Delta R]^T [d\Delta R] = \min \quad (6)$$

The Jacobian expressions from Eqs. (3) and (5) are substituted into Eq. (6):

$$[d\Delta P]^T [J_R][dm] = \min \quad (7)$$

Minimization for the LSQ solution is made by partial differentiation with respect to dm , $i=1\dots N$. Taking the partial derivatives of Eq. (7) for each row and re-arranging the partial differentials again as $[J_R]$, the following result is obtained:

$$[J_R]^T [J_R][dm] = -[J_R]^T [d\Delta R] \quad (8)$$

The $[dm]$ change vector for all m can be expressed from Eq. (8) to match vectors $[d\Delta R]$:

$$[dm] = -\{[J_R]^T [J_R]\}^{-1} [J_R]^T [d\Delta R] \quad (9)$$

Equation (9) is used iteratively by finding first the $[dm]$ change vector from the $[d\Delta R]$ vector calculated according to Eq. (5), an then modifying the multipliers for all branches of the ventilation model as an input vector $[m] = [m] + [dm]$ for a new simulation run. The iteration continues until no change is noticed in the $[m]$ vector. The Jacobian matrix is updated in every 10 iteration steps for compensating for the non-linearity of the ventilation model. The proof of concept and solution algorithm is shown in Figure 1.

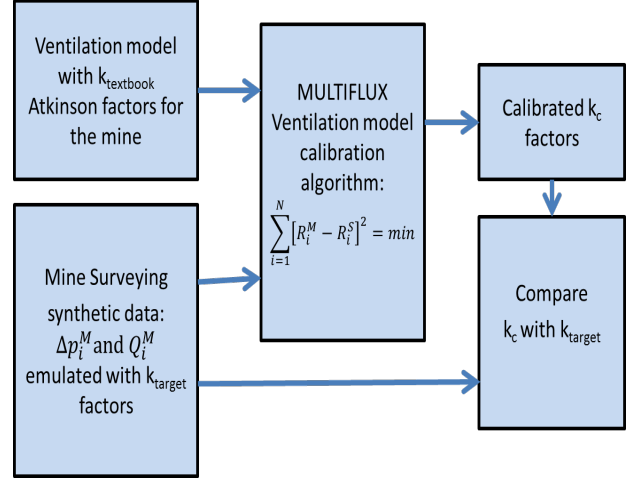


Figure 1. Proof of principle test diagram.

3. Numerical method verification

The method was tested for validation purposes. A mine ventilation network of a metal mine was used for testing the model calibration method shown in Figure 2. The set of Atkinson friction factors used in the model was considered as the reference true condition of the mine. The ventilation model was then solved by MULTIFLUX [8] in order to generate synthetic measurement data for pressure and flow rate assuming no measurement error for the reference case representing the average mine operating conditions.

In order to select the most significant airways, the airway power loss due to pressure losses was calculated. The histogram of the airway power loss is shown in Figure 3. Analysis of the power loss reveals that 42 of the most energy consuming airways represent 90% of the total power loss. The cumulative power loss is depicted in Figure 4. Only these 42 branches were subject for calibration.

Air branch pressure differences, $[\Delta P]$ and air flow rates, $[Q]$ were calculated from the model. Taking these calculated values as measurement results, $[\Delta P^M]$ and $[Q^M]$, the measured values for the mine were calculated as $R_i^M = \Delta P_i^M / (Q_i^M)^2$.

The iterative algorithm, starting with a trial set of $[R]$, was used to identify the “unknown” set of $[R]$ values from which the Atkinson’s k -factors were back calculated. The un-calibrated mine ventilation model results, called the “textbook mine” differ significantly in both pressure losses and branch flow rates, shown in Figs. 5 and 6. However, the LSQ calibration procedure is able to identify iteratively the unknown k -factors and modify the textbook mine model to match the target mine, identified only by its measurement results on pressures and air flow rates. The calibrated Atkinson friction factors perfectly match those for the target mine, shown in Fig. 7.

4. Application to data with measurement noise

Errors in the measurement are inevitable in an operating mine that is never really at steady-state. Errors

in the input data of the ventilation model in cross sections is another perturbation on the model output versus the in situ mine. Measurement sensor position errors further increase uncertainties. These all call for an evaluation method that can suppress random noise and match data with a ventilation model.

Reasonable measurement noises were added emulating in situ condition. Considering typical surveying conditions, a ± 10 Pa random error in pressure reading and $\pm 10\%$ error in air flow rate were considered. Two random noise realizations were made to check reproducibility of the matching results. A future investigation is planned using a true Monte-Carlo analysis. In addition to the white noise, 5 airways were selected to add more error such as human error of +10 Pa and 50% reduction of measured airflow rate as the emulation of one in situ data set, also executed in two random realizations.

The inverse-identified friction factor values from the iterative procedure matched reasonably well with the synthetic measured data, shown in Figures 8a, 8b and 9a, 9b for pressure loss, and flowrate, respectively, for the two different random realizations. Figures 10a, 10b and 11a, 11b show the inverse-identified Atkinson friction factors and the airway power loss, respectively, for the two random realizations.

The results from the branch-by-branch calculation, emulating the manual, gauge and tube evaluation are also shown for comparison. The gauge-and-tube method takes the network flow rate and pressure loss balances into account manually, node-by-node and loop-by-loop. However, manual network balance check is an impossibly expensive and time-consuming task. The proposed LSQ method ensures the balance of nodal air flow and pressure loops during calibration evaluation in spite of feeding it with measurement data with errors within reasonable error limits.

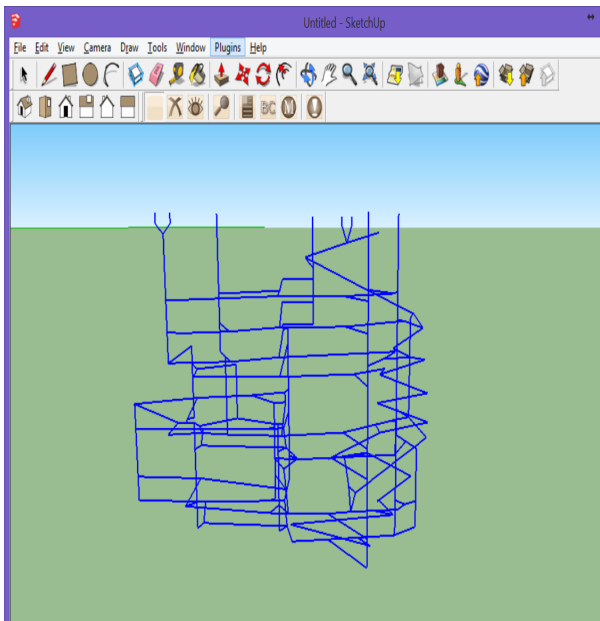


Figure 2. Schematic of a mine ventilation network.

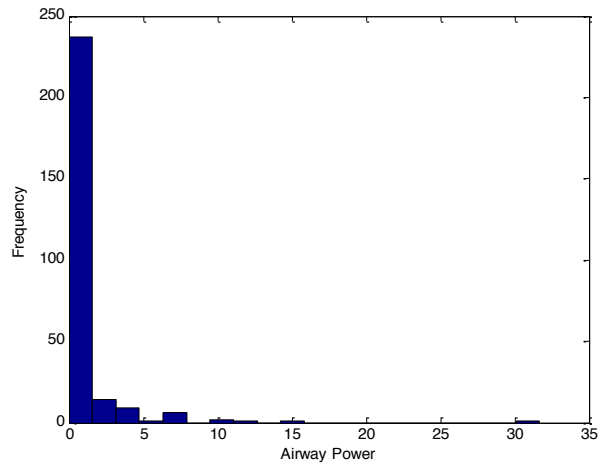


Figure 3. Histogram of the airway power loss.

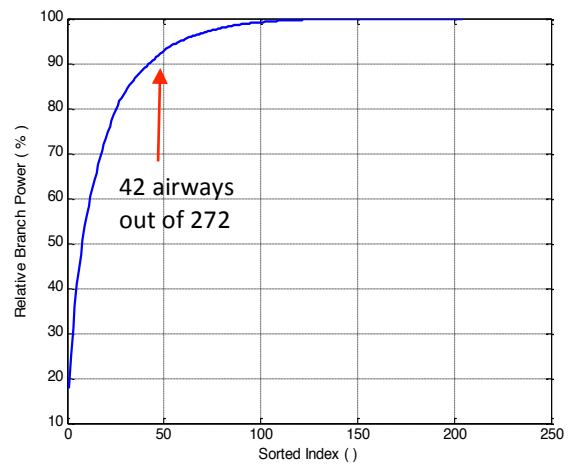


Figure 4. Cumulative airway relative power loss.

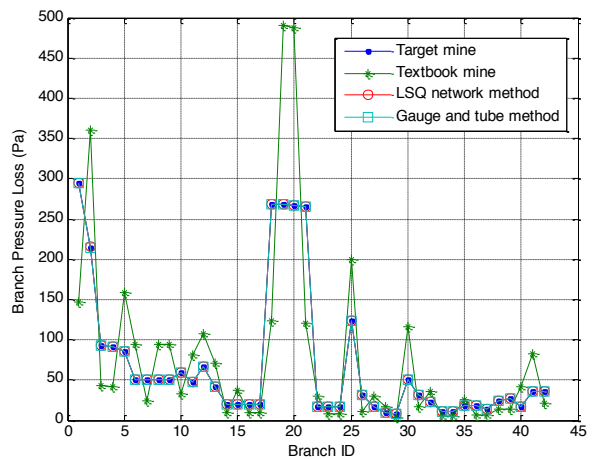


Figure 5. Pressure loss comparison (no noise).

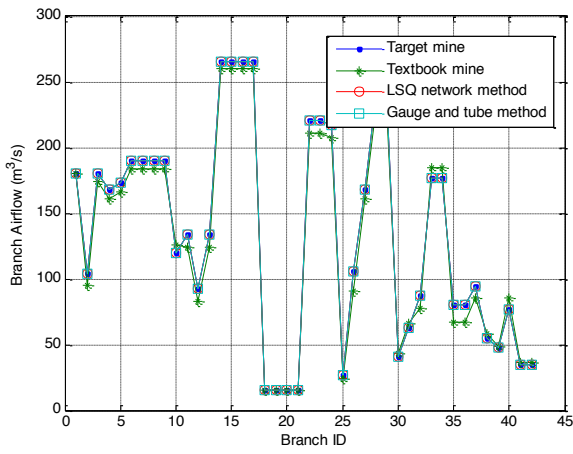


Figure 6. Branch flow rates comparison (no noise).

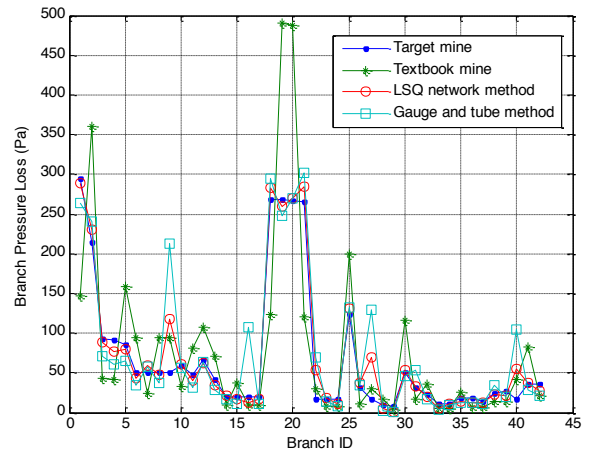


Figure 8b. Pressure loss comparison (with second noise realization).

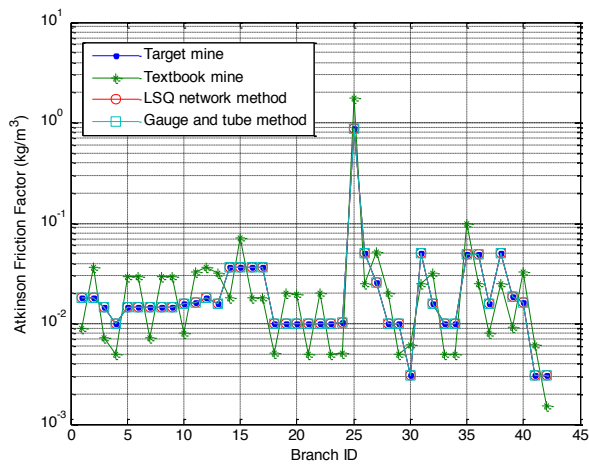


Figure 7. Atkinson friction factor comparison (no noise).

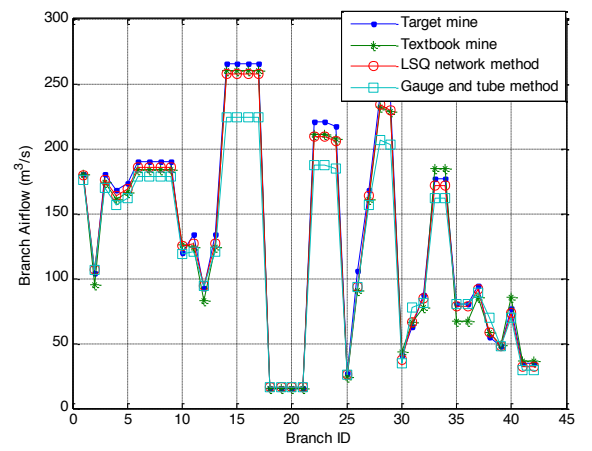


Figure 9a. Branch flow rates comparison (with first noise realization).

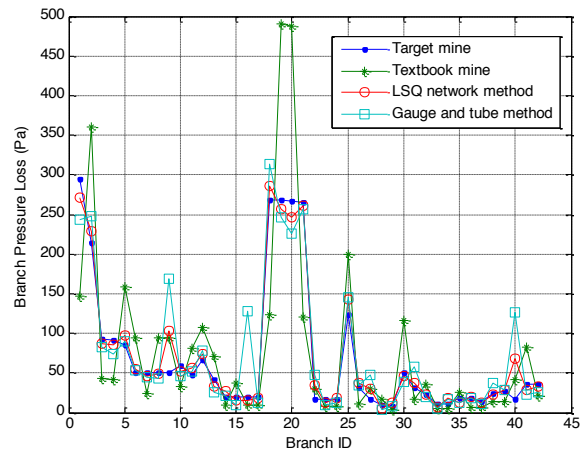


Figure 8a. Pressure loss comparison (with first noise realization).

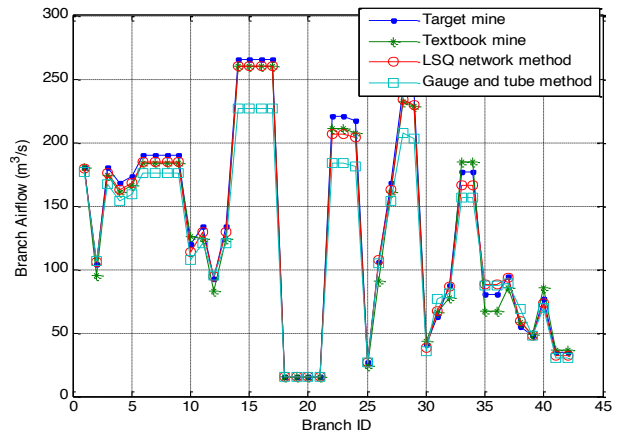


Figure 9b. Branch flow rates comparison (with second noise realization).

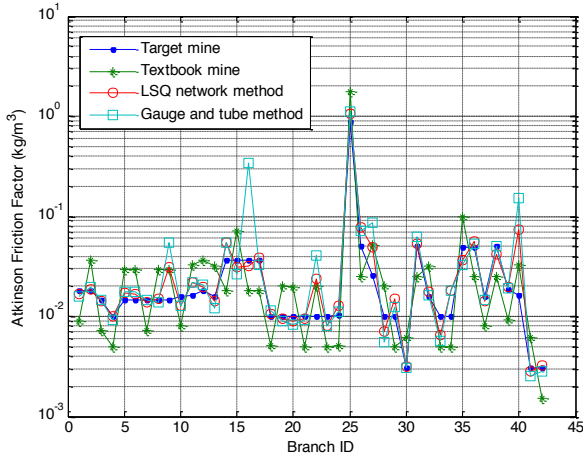


Figure 10a. Atkinson friction factor comparison (with first noise realization).

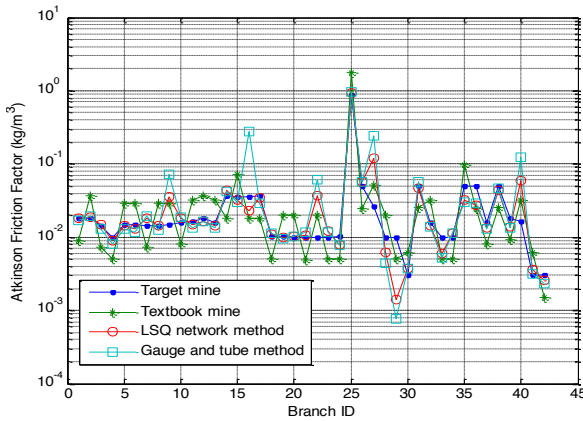


Figure 10b. Atkinson friction factor comparison (with second noise realization).

5. Discussion of the results

A calibration method is introduced and tested against numerical experiments, using controlled conditions with ‘synthetic’ data. Realistic, and even higher than typical ranges of measurement errors were used. The RMS errors of pressures, air flow rates, and Atkinson friction factor parameters were compared to the target mine. Two different noise realizations were used. The results are summarized in Table 1 for both noise realizations, the second shown below the first one.

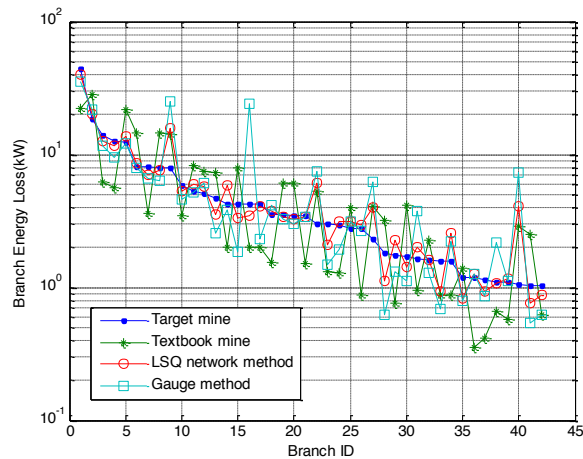


Figure 11a. Power loss comparison (with first noise realization).

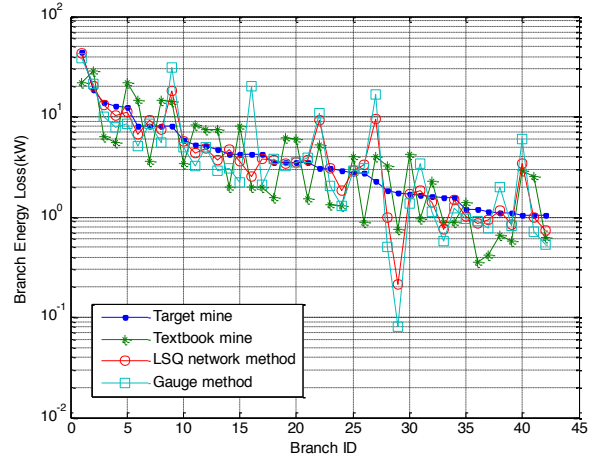


Figure 11b. Power loss comparison (with second noise realization).

Table 1. Comparison of the matching error from noisy data with two in situ measurement realizations.

Parameter	Un calibrated	Gauge and tube	LSQ
Pressure	105%	51%	21%
Loss		57%	25%
Flow Rate	6%	14%	4%
Atkinson'	341	15%	5%
		141%	50%

In the example, the relative RMS errors of the first noise realization in the airway pressure loss were 21% and 51% for the LSQ method and the gauge and tube method, respectively. The relative RMS errors in the airway flow rates are 4% and 14% for the LSQ method and the gauge and tube method, respectively. The relative RMS errors in the Atkinson k-factors were 72% and 161% for the LSQ method and the gauge and tube method, respectively. Similar RMS error values were obtained for the second noise realization.

The results show significant improvement using the LSQ method over individual branch-by-branch evaluation. The reason is that the LSQ method is based on matching the noisy measurement results with a mass-balanced and pressure-balanced ventilation network solution.

The balances of nodal air flow and pressure loops in the branch-by-branch evaluation typical to the gauge and tube must be manually maintained. This often tedious, manual task may be eliminated when using the network-based calibration method with an always balanced solution.

6. Conclusions

- The ventilation network model can be adequately calibrated against the measured pressure differences and branch flow rates by optimally adjusting the airway resistance characteristics in terms of the Atkinson k-factors.

- The LSQ method as an optimum solution is verified against numerical experiments, using controlled conditions with ‘synthetic’ data.
- The LSQ method predicts better results when compared to those obtained by the individual branch evaluations typical to the gauge-and-tube method.
- The LSQ fit optimization method always predicts balanced result and there is no need for manual checking of the pressure loops and air flow junctions of the networks.
- The proposed method uses the most significant airways with the highest pressure losses, reducing the number of measurements and the burden on the ventilation survey.

Acknowledgments

The financial support from NIOSH is gratefully acknowledged.

References

- [1] Prosser, B. S., Stinnette, J. D., and Paredes, J. (2002). "Ventilation Optimization at the La Camorra Mine." 9th U.S/North American Mine Ventilation Symposium. Proceedings, pp. 57-63.
- [2] MSHA. (2013). MSHA Handbook Series.
- [3] von Glehn, F. H., Marx, W. M., and Bluhm, S. J. (2008). "Verification and Calibration of Ventilation Network Models." 12th U.S/North American Mine Ventilation Symposium. Proceedings, pp. 275-279.
- [4] McPherson, M.J. (1993). Subsurface Ventilation and Environmental Engineering. New York, New York: Chapman & Hall. TIC: 215345. [ISBN 0 412 35300 8].
- [5] Prosser, B. S., & Loomis, I. M. (2004). "Measurement of Frictional Pressure Differentials during a Ventilation Survey." 10th U.S/North American Mine Ventilation Symposium. Proceedings, pp. 59-66.
- [6] Danko, G. and Bahrami, D. (2014). "Ventilation Model Calibration with Numerical Optimization." 10th Int. Mine Ventilation Congress, IMVC2014, pp. 379-387.
- [7] Liu, J., Deng, L., and Song, Y. (2013). "Inversion of Ventilation Resistance Coefficient of Mine Based on Genetic Algorithm." International Symposium on Mine Ventilation and Heat harm Prevention. Huludao-Liaoning-China. Proceedings, pp. 113-118.
- [8] Danko, G. (2013). "Subsurface Flow and Transport Process Model for Time dependent Mine Ventilation Simulations." Institute of Materials, Minerals and Mining, Mining Technology, Vol. 122, No. 3, pp. 134-144.

Behavior of Flow Through Mine Elbows and Louvers

Ali Haghghat¹, Stewart Gillies², Kray Luxbacher¹

¹Virginia Tech, Blacksburg, Virginia, USA

²Missouri University of Science and Technology, Rolla, Missouri, USA

Main mine fans are often connected to underground workings through ventilation control devices of ducting, damper controls, elbows or bends. An investigation was undertaken of a main mine surface fan system and associated elbow and louver. Leakage and shock losses in different parts of mine airways are of major concern. Comprehensive analyses was undertaken of these ventilation shock losses experimentally, numerically and computationally to increase understanding and optimize air flow through the mine. Pressure and air flow velocity across different parts of ventilation control devices set at different angles were measured experimentally. Two precision pressure transducers were used simultaneously to measure these pressure drops across the louver and the inlet and outlet of the elbow, and vane anemometers were utilized to measure velocity throughout the mine. Two approaches were used to determine shock loss factor across the elbow numerically. Losses associated with ventilation control devices were calculated numerically by using Bernoulli's equation for incompressible fluid. Calculations were compared with measured K loss factors for different angles and air power losses across the louver. Experimental results from measurements across ventilation control devices were compared to computational and numerical analysis. Pressure losses were investigated by computational fluid dynamics (CFD). The CFD exercises were conducted to gain understanding of flow behavior, for instance, various louver blade angles and elbow designs after comparison with measured results used to calibrate and verify the model. Research was undertaken to achieve the lowest shock loss elbow model and louver angles. Numerous models were compared with each other in order to achieve the optimal model. The model was used to predict possible locations and leakage flow rates for numerous boundary conditions and geometries over the elbow and inlet shaft. A series of simulations was performed for ideal design of main fan ductwork by reducing shock losses in that airway. The minimum shock loss and maximum velocity in the inlet shaft were determined as the best scenario for the ventilation network. Surface fan position was selected.

Keywords: CFD, Elbow, Shock Loss, Louver

1. Introduction

A comprehensive study was carried out to improve ducting systems at Missouri University of Science and Technology (MS&T) Experimental Mine by experimental, numerical and computational approaches. Two 765-16B Paroscientific pressure transducers with claimed accuracy of ± 8 Pa were used simultaneously to measure pressure drops across the louver, the inlet and outlet of elbows. Vane anemometers and Pitot tubes were utilized to measure velocity throughout the mine.

Pressure drop (total pressure or facing gauge) across the louver set at different angles and a 90° elbow was measured. Shock loss factors across the elbow were calculated using various dimensions and angles in order to achieve an acceptable design numerically. Two approaches were used to determine shock loss factor across the elbow numerically.

Atkinson's friction factor "k" for the mine elbow was determined. The Bernoulli Equation was used to calculate pressure loss across the louver at two discrete angles. An approach was used to determine 60° and 0° loss factors (K factors) across the louver numerically. Computational Fluid Dynamics (CFD) exercises were conducted to gain understanding of flow behavior at various louver blade angles and elbow design. Different parameters such as velocity inlet and outlet pressure drops were determined and ideal elbow and louver designs were selected according by use of three approaches. Experimental design was compared to the computational and numerical designs. The optimum position of main mine fan was determined from results of this study.

2. Current ventilation network

The MS&T Experimental Mine is accessed by two adits, three raises and two primary ventilation shafts. The mine has a 1.2 m diameter Joy axial vane fan with a 24 kW motor and an Alphair 4,500 axial vane fan with a 24 kW motor installed to move approximately 25 m/s of airflow at 1 kPa pressure through the underground working faces. Two 12 kW Spendrup booster fans have also been installed underground in series with the surface fans. The Joy axial surface main fan with two different speeds is connected to the 1.0 m diameter mine shaft inlet with a 90° elbow. The Alphair surface fan is installed vertically. Dimensions through the ducting system were measured in order to be used in numerical, experimental and computational designs. The mine's elbow is constructed of 1 mm thickness steel. Ducting with curved bend has width of 0.98 m as shown in Figure 1.

The louver controls airflow through the ducting attached to the Joy fan. Dimensions of louver blades were measured and are shown in Figure 2.

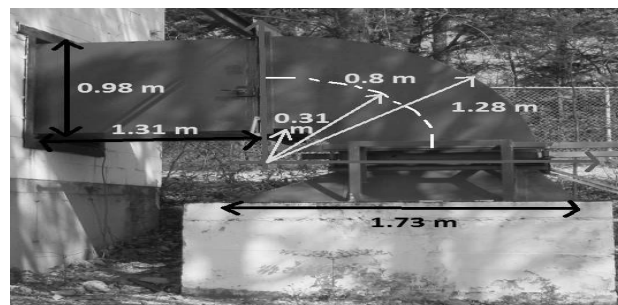


Figure 1. Dimensions of the 90° elbow.

Louver blades thickness and each blade's internal angle were measured at 2 mm and 120° respectively. The louver blades are controlled by a hydraulic pump in order to protect the surface fan from moisture or to use in emergency situations.

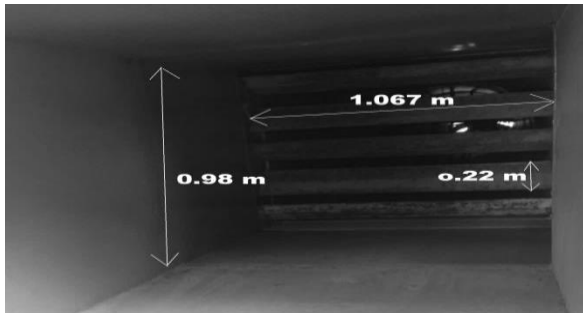


Figure 2. Dimensions of louver blades at 60° angle.

3. Experimental design

Although CFD has many advantages, it does not completely eliminate the need for experiments, which are needed to validate numerical solutions. For this reason, data collected during actual mine tests and CFD simulations are compared. This comparison allows a better understanding of the flow phenomena. Moreover, once the numerical solutions have been validated, CFD can be used with better confidence to predict the effect of changes in ductwork configurations on energy losses [5].

Pressure and air flow velocity across different parts of the elbow and louver set at different angles were measured experimentally in MS&T Experimental Mine. Five different stations were established along the duct. There is one within the surface atmosphere. In addition there is one underground, station 7 within the rock lined shaft of the mine as shown in Figure 3. Points 1, 2, 3, 4, 5, 6 and 7 were used for pressure measurements. Readings were repeated four times at each of the seven stations.

Two Paroscientific pressure transducers with Pitot tubes were used simultaneously to measure total pressure drops across the louver and at the inlet and outlet of the elbow. A hydraulic motor was used to change louver blade angles automatically. Louver blade angles of 60° and 0° to the horizontal were set for measurements. Percentage of pressure drop across the louver and the elbow was determined. Pressure at the surface and underground was measured by transducers. Because of lack of access through the duct only one station was used before the elbow.

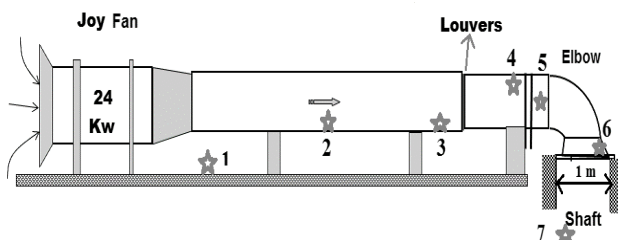


Figure 3. Joy surface fan and the position of stations.

3.1 Louver with a 60° blade angle

The Joy axial surface fan was set at its higher speed to produce an expected 1,000 Pa total pressure. The blade angle of the louver was fixed at 60° to the horizontal as shown in Figure 2. Measurements were taken in each station four times with four different lengths of Pitot tube (152 mm, 254 mm, 406 mm, and 560 mm) in the ducting in order to achieve accurate results from all parts of a section. The average total pressure and also the percentage of pressure drop across the elbow and the louver was calculated and plotted as shown in Table 1. With the exception of the surface and underground pressure readings all values are total pressure and take into account elevation and fan pressure. In this experiment velocity at the elbow's inlet was measured as 12.3 m/s. On account of 5 holes at that section, about 6.707 m³/s air quantity was leaked to the outside of the system. So by the change of louver's blade angle we could lead some air to the outside of the duct via series of holes at one side of the duct as shown in Figure 4.



Figure 4. Louvers holes on the duct surface

Table 1. Pressure drop at different stations with 60° angle of the louver.

Number	Location	P (kPa)	ΔP (Pa)	Loss (%)
1	Surface (absolute)	97.440	-	-
2	After fan	98.432	-	-
3	Before Louver	98.428	-	-
4	After Louver	97.583	845	85
5	Before Elbow	97.490	-	-
6	After Elbow	97.389	101	10
7	Underground (absolute)	97.534	-	-

The Joy axial fan can only deliver 992 Pa due to wear and tear. Through the louver system a pressure drop of 85% of 992 Pa has occurred. Not only the blades played key role to make the pressure drop in the ducting system, but also they guided some amount of air quantity to the outside of the system. In addition a second main pressure drop of 10 % has occurred across the elbow.

3.2 Louver with a 0° blade angle

As with the previous experiment the Joy axial surface fan was set at its higher speed to produce an expected 1,000 Pa pressure. The blade angle of the louver was fixed parallel to the ducting walls. All holes were covered with tape to hamper the leakage through

the holes. Measurements were repeated four times (the same as in the previous experiment) with four different lengths of Pitot tube at each station. The results were plotted in Table 2. Inlet velocity upstream of the elbow has been measured at 18.9 m/s.

Table 2. Pressure drop at different stations with 0° angle louver.

Number	Location	P (kPa)	ΔP (Pa)	Loss (%)
1	Surface (absolute)	97.440	-	-
2	After fan	98.432	-	-
3	Before Louver	98.425	-	-
4	After Louver	98.356	69	7
5	Before Elbow	98.137	-	-
6	After Elbow	97.900	237	23.8
7	Underground (absolute)	97.534	-	-

It is evident from the above table that the pressure produced by the Joy axial surface fan was the same as the previous experiment. According to the data shown in Table 2, the pressure drop across the louver decreased dramatically by the blade angles change from 60° to 0°. Pressure drop across 0° angle of the louver was measured at 69 Pa of the Joy axial fan total pressure. However the pressure drop across the elbow increased noticeably (about 24% of total pressure; the highest pressure drop measured in this experiment).

In summary, it is noteworthy that with the changes of the louver blade angles from 60° to 0°, the total pressure loss in the duct has decreased significantly. Louvers play a key role as airflow modulators. They do this by increasing or decreasing the pressure loss through the louvers and redirecting some amount of air quantity to the outside of the system. It is self-evident that if you change the angle of the louver, the pressure loss will be changed as will the airflow. Fan power is wasted due to air shock loss in passage through the louvers.

Fans may stall when a louver blade angle is set to give a high obstruction. With the reduction in pressure drop across the louver, the pressure drop across the elbow has proportionally increased. Available air quantity underground has been increased 64% by these experimental actions.

4. Numerical design

In this study different airflow parameters such as pressure drop, shock loss factor, equivalent Atkinson resistance, rational resistance with consideration of various blade angles and dimensions of the louver and elbow were calculated. Loss factors across the louver caused by different blade angles have also been calculated. The lowest pressure drop across elbows and louver resulting from all scenarios were selected as the ideal numerical design.

4.1 Pressure drop across elbows

The shock loss (X) factors may be expressed as a number of velocity pressures due to turbulence at any bend, variation in cross-sectional area, or any other cause of a change in the direction of airflow [2].

Equation 1 was utilized to calculate P_{shock} across an elbow with different angles and dimensions

$$P_{shock} = X (\rho/2) (Q^2/A^2) = R_{shock} Q^2 \text{ Pa} \quad (1)$$

where ρ is the density of air (kg/m³), Q is the air quantity (m³/s) and A is the area (m²) of cross section.

The relation between shock loss factor and equivalent Atkinson resistance has been defined by Equation 2.

$$R_{shock} = X (\rho / (2A^2)) \text{ N s}^2/\text{m}^5 \quad (2)$$

Equation 2 and rational resistance equation (Equation 3) were used in order to compare various scenarios [2].

$$R_{rational} = (X/(2A^2)) \text{ m}^2 \quad (3)$$

Shock loss factor for right angled bends of circular and rectangular cross sections for $\theta = 90^\circ$ are dependent on the height, width and radius of the bend [2]. The similar table for circular cross section from McPherson book was utilized for calculation of shock loss factor.

Correction factors for all shock loss factors other than 90° were considered in the calculations. The ratio of H/W and r/W for potential mine elbows of 60° and 45° were calculated as 1.0 and 0.8 in the same way as the actual mine elbow ratios which were calculated for the real mine elbow. The acceptable X factor for a 90° bend with r/W ratio approaches close to 2.0. Minor reductions in shock loss can be achieved for a bend by changing cross sectional dimensions (i.e. r/W). In the mine under study the height of cross section at the bottom of the shaft was measured to be 1.5 m and the width is 0.64 m. The ratios of H/W and r/W for an alternative elbow were calculated at 2.3 and 2. These changes improve the shock loss with reference to McPherson's book from 0.35 to 0.15. In all calculations air density of 1.23 kg/m³ and air velocity of 18.9 m/s were used. Calculated results of various conceivable situations are shown in Table 3 relying on information from McPherson [2] for circular and rectangular cross sections.

Table 3. Calculated results for elbows with different angles

Scenarios	X	R_{shock} (m ⁻²)	$R_{rational}$ (Ns ² /m ⁵)	P_{shock} (Pa)
Actual Mine Elbow 90°	0.35	0.19	0.233	76.7
Rectangular Elbow 90°	0.3	0.264	0.323	65.59
Circular Elbow 60°	0.28	0.152	0.186	61.23
Rectangular Elbow 45°	0.21	0.114	0.140	46.1
Rectangular Elbow 90° (new size)	0.15	0.08	0.098	32.26

It is apparent that the lowest-pressure design is the rectangular option. The pressure drop experiences only a moderate decrease with the change of cross section from rectangular to circular for 90° bends as is evident in Table 3. A related consideration is that circular ducts can withstand large pressure differences between the inside and the outside without undergoing any significant distortion, but noncircular ducts may not [1].

Noncircular ducts are often used in situations such as in major surface fans. Also every surface centrifugal fan has a circular to rectangular transition. The data in Table 3 shows that with a decreasing trend in bend angle of elbow from 90° to 45° the pressure drop is reduced while

the minimum pressure drop design was not achieved for MS&T experimental mine's shaft. The minimum pressure drop was achieved by the change of width and height of a smooth curved 90° elbow.

Analytical dependence of the local loss coefficient (ξ) on the geometric parameters of the fitting was found as follows:

$$\xi = C_1 (R/B)^{C_2} + C_3 \exp(C_4 (R/B)^{C_5}) \quad (4)$$

where

$$C_1 = (A/B) (-0.069 - 3.458 (A/B)^{C_6}) \quad (5)$$

$$C_2 = 0.092 (A/B)^{C_7} + 0.046 \quad (6)$$

$$C_3 = 1.247 + 0.177 \ln(A/B) \quad (7)$$

The radius of the inner and outer edges is characterized by the ratio R/B. The local pressure loss coefficient ξ is also affected by the ratio of the duct high and width A/B [7]. For the MS&T mine elbow the ratios of R/B and A/B were calculated 0.82 and 1. So the local pressure loss coefficient and P_{loss} were calculated as 0.29 and 63.5 Pa respectively.

Miller on 1990 explained that the loss factor for 90° bends varies considerably with Reynolds's number [3] although for fully developed turbulent flow characteristic of most mine airflow situations, the correction factor is constant. Loss coefficients from standard performance charts were modified by the application of Reynolds number correction factors.

Consistent with the calculated data from two different approaches, it is evident that the pressure loss difference between analytical approaches in comparison with table approach from McPherson book is 13.2 Pa. On account of lack of precision in determining the X factor from the table this pressure difference was observed.

4.2 Friction pressure loss across the louver

Friction loss (P_f) across a louver at two different angles were measured experimentally and then compared with the Bernoulli equation for incompressible fluid flow. The measured data from Table 4 were used to calculate P_f across the louver. 1.225 kg/m³ was used in the calculation as the density of air for 15° C.

Table 4. Measured data for louver pressure drop calculation.

Scenario	V	V	P_{in}	P_{out}
	No.3 (m/s)	No.4 (m/s)	No.3 kPa	No.4 kPa
60° louver	18.9	12.3	98.43	97.58
0° louver	18.9	18.9	98.43	98.36

Friction pressure loss for 60° and 0° of the louver was calculated as 961 Pa and 72 Pa respectively. In summary, it is noteworthy that a 60° blade angle has played a role as an impediment against airflow in the duct. The least pressure drop across the louver has been achieved with the change of blade angle to 0°. The pressure drop up to the elbow's inlet was improved to 89.6% numerically by changing the blade angle of the louver to 0°.

The louver loss factor (K factor) is a dimensionless value that indicates the aerodynamic resistance to airflow. This value describes the link between the

airflow through the louver and the pressure drop over it. During the experiments the static pressure difference was measured across a louver as calculated at distances in the upstream and downstream flow. The resulting K factor can be calculated using:

$$K = (\Delta P / P_i) \quad (8)$$

where ΔP_t is the total pressure difference across the duct and P_i is the velocity pressure loss in the duct calculated by using:

$$P_i = \rho V^2 / 2 \quad (9)$$

where ρ is the air density (i.e. 1.2 kg/m³ at STP) and V is the mean air velocity in the duct. Where the duct cross-sectional area is constant the total pressure difference ΔP_t is given as the static pressure difference ΔP_s , because the mean air velocity remains constant [4]. Velocity pressure and total pressure differences for two different blade angles of the louver were calculated and K factor was determined. Results are shown in Table 5.

Table 5. Calculated pressure drop and K factors across the louver.

Scenarios	60°	0°
	louver	louver
Total pressure difference (Pa)	845	69
Velocity pressure (Pa)	149.06	218.79
K factor	5.67	0.32

5. Computational design

5.1 CFD Model

To resolve engineering problems, one approach is to simplify the governing equations and boundary conditions. Another approach is to use numerical methods and algorithms, with the help of a computer, to get the approximate solutions [6]. The Experimental Mine elbow and louver geometric CFD model was built using AutoCAD 2012 software. The geometric model for various bend angles of elbow and louver blade angles was created. The geometry models were imported to Ansys Workbench to investigate the fluid flow in them. The geometry of elbow and louver was designed according to the measured dimensions.

Numerical modeling was run using FLUENT, the CFD module of ANSYS Workbench 14.0 software. The field measurement results were used to set up and initialize the simulation. The velocity inlet boundary condition was applied at the elbow and louver inlet. The pressure outlet boundary condition was applied at the outflow faces of elbows. The blades of the louver are symmetrical. These have been assigned as symmetry boundary condition. The outflow boundary condition was applied to the outlet and the holes at the side of louver. All the other surfaces have been treated using a no-slip boundary condition. The backflow turbulent intensity has been assumed to be 3% and the hydraulic diameter for every boundary condition was calculated.

5.2 Elbow scenarios

Four different scenarios were simulated to investigate airflow distribution through the elbow and compare the predicted pressure drop and velocity. The three dimensional continuity equations and time averaged Navier-Stokes along with the boundary conditions were solved using finite volume method. The geometries were imported to the Ansys fluent 14. The mesh was generated with meshing program using

approximately 64,000 to 126,000 tetrahedral control volumes. The average mesh quality was 0.82. The velocity and often temperature gradient normal to the wall is typically much larger than the gradient parallel to the wall. Hence the inflation layer control was designed to create thin elements that can capture the normal gradient with minimal elements near no-slip boundary condition as shown in Figure 5. The viscous model is set using standard k- ϵ realizable model with standard wall functions for near wall treatment. The physical properties of air are treated as constants with the density of 1.225 kg/m³ and viscosity of 1.7894e-05 kg/m-s. 18.9 m/s air velocity was applied to the velocity inlet as boundary condition and no slip boundary conditions are applied to all the wall boundaries. Pressure outlet boundary condition is imposed at the elbows outlet. Thickness of the wall has been set to 1 mm. 15.11 x10⁻⁶ m²/s has been used as the kinematic viscosity for Reynolds number calculation. The hydraulic diameter and Reynolds number were calculated for each scenario. The SIMPLE algorithm was used as the solution method for the pressure-velocity coupling. Second order upwind was considered for spatial discretization of momentum, turbulent kinetic energy, and turbulent dissipation rate. The convergence criterion was set at 10e-05 for continuity, kinetic energy (k) and turbulent dissipation (ϵ) equations. The calculation was run with 2500 iterations.

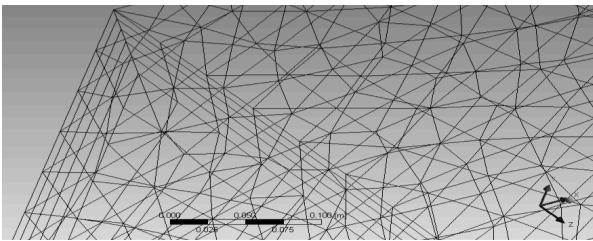


Figure 5. Inflation lines in generated mesh

5.2.1 Scenario 1, mine elbow

An attempt was made to simulate the airflow distribution inside the mine elbow. Two different inlet velocities were measured at the elbow inlet. Different air velocities were established by varying the lower blade angles. The velocities measured at the inlet were 18.9 and 12.3 m/s. The hydraulic diameter was calculated as 0.98.

Air entering the inlet duct is fully developed with Re numbers of 1,225,810 and 797,749 for two different velocities. In this scenario the mesh generated approximately 77,000 tetrahedral control volumes. Table 6 shows the results of this scenario.

Table 6. Correlation of experimental and CFD results across mine elbow with 90° bend angle.

Scenario	V _{Inlet} m/s	V _{outlet} m/s	ΔV m/s	P _{Drop} (Pa)
1A	18.9	14.3	4.6	217
Computational 1A	18.9	-	-	237
Experimental 1B	12.3	9.3	3	90.3
Computational 1B	12.3	-	-	101
Experimental	12.3	-	-	-

Simulated result for the pressure distributions is shown in Figure 6 for 18.9 m/s inlet velocity and blade angle of 90°.

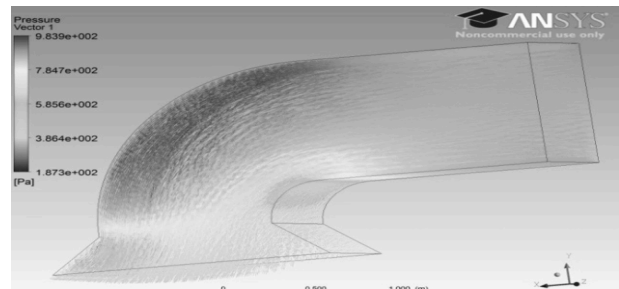


Figure 6. Pressure vectors through the mine elbow.

5.2.2 Scenario 2, 60° elbow

The same dimensions were used as the first scenario. Inlet velocity was set at 18.9 m/s. The mesh was generated for approximately 74,000 tetrahedral control volumes. The hydraulic diameter was calculated as 0.98. Air entering the inlet duct is fully developed with Reynolds number of 1,225,810. Pressure distributions were simulated and are illustrated in Figure 7.

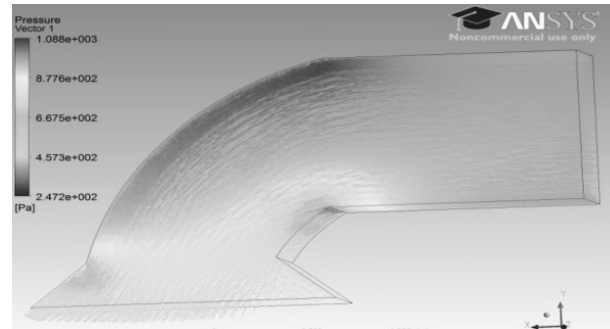


Figure 7. Pressure vectors through 60° elbow.

With the change of bend angle to 60° the outlet velocity increased to 15.3 m/s because of changes of the outlet dimension. The amount of pressure drop in comparison with 90° elbow decreased as shown in Table 7.

Table 7. 60° elbow CFD results.

Scenario	2
Velocity Inlet (m/s)	18.9
Velocity outlet (m/s)	15.3
Velocity Difference (m/s)	3.6
Pressure Drop (Pa)	181

5.2.3 Scenario 3, 45° elbow

Pressure distributions for this scenario were simulated and illustrated in Figure 8.

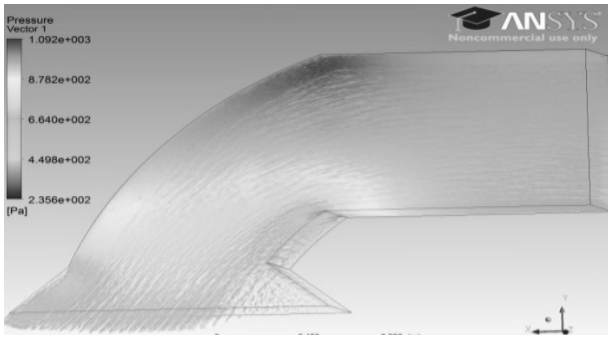


Figure 8. Pressure vectors through 45° elbow.

In this scenario the geometry of the elbow was designed with a 45° bend. The inlet velocity was embedded 18.9 m/s. The hydraulic diameter was calculated as 0.98. The mesh generated approximately 73,000 tetrahedral control volumes. Air entering the inlet duct was fully developed with Reynolds number of 1,225,810.

The result is shown in Table 8 for comparison with other scenarios. In this simulation the pressure drop in comparison with the mine 90° elbow increased. However the outlet velocity was improved.

Table 8. 45° elbow CFD results.

Scenario	3
Velocity Inlet (m/s)	18.9
Velocity outlet (m/s)	15.8
Velocity Difference (m/s)	3.1
Pressure Drop (Pa)	289

5.2.4 Scenario 4, ideal design

The Ideal numerical designed scenario was simulated according to the numerical approach. Height and width of the duct were calculated at 1.5 and 0.64m with a 90° bend angle. The hydraulic diameter and Reynolds number were calculated at 0.9 and 1,122,237. Inlet velocity for this scenario is similar to the previous scenarios and was embedded as 18.9 m/s. The mesh was generated approximately 64,000 tetrahedral control volumes. Pressure distribution is shown in Figure 9. The result of this scenario was summarized in Table 9.

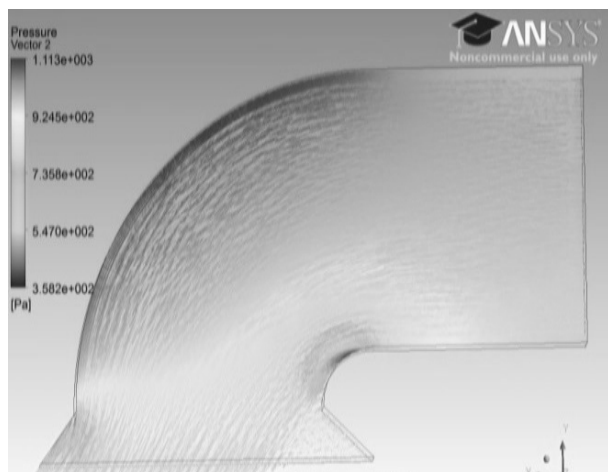


Figure 9. Pressure vectors through ideal elbow.

Table 9. Ideal elbow CFD results.

Scenario	4
Velocity Inlet (m/s)	18.9
Velocity outlet (m/s)	16.7
Velocity Difference (m/s)	2.2
Pressure Drop (Pa)	175.7

5.3 General Results and Discussion

It is noteworthy from all scenarios that a decrease in the bend angle has had an immense impact on the pressure drop. Consistent with the data from Table 6, pressure drop in the experimental results is more than the computational result. However the pressure drop differences for 12 m/s inlet velocity scenarios is 10.7 Pa. For an 18.9 m/s inlet velocity scenarios the pressure drop is calculated as 20 Pa. This study has shown that with just a change of elbow from 90° bend angle to 60° the pressure drop problem was improved. The outlet velocity was enhanced by changing the elbow 90° bend to 45° but this results in the pressure dropping significantly. An ideal design was not achieved just by changing the elbow's bend angle. The ideal design was accomplished when the height of the duct changed to 1.5m and the width to 0.64m with a smooth 90° bend angle. Due to formation of eddies at the end of the short bend angle in all scenarios; the diffuser form of the outlet should be changed as shown in Figure 10. Numerous CFD results are illustrated in Table 10.

Table 10. Various elbow's CFD results.

Scenario	V _{Inlet} m/s	V _{outlet} m/s	ΔV m/s	P _{Drop} (Pa)
90° Elbow Computational	18.9	12.12	6.78	217
60° Elbow Computational	18.9	15.3	3.6	181
45° Elbow Computational	18.9	15.8	3.1	189
Ideal Elbow Computational	18.9	16.7	2.2	175.7

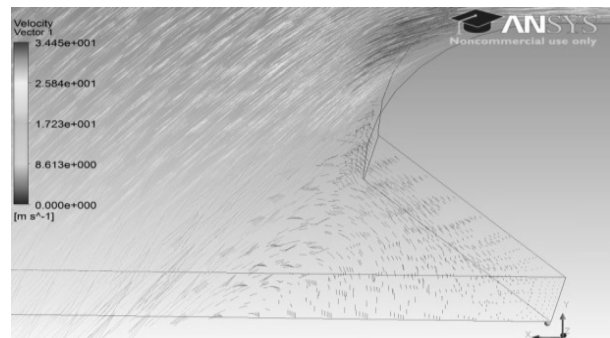


Figure 10. Eddies distribution vector at the elbow's outlet.

5.4 Louver Scenarios

Two different louver blade angles were designed in line with the mine's louver field measurements to investigate airflow behavior and compare the pressure drop and velocity with measured results. The geometries of all scenarios were simulated using AutoCAD and

imported into the Workbench 14. The computational domain was meshed and the grid generated with approximately 192,000 cells for the 60° blade angle and 200,000 tetrahedral control volumes for the 0° blade angle to the horizontal. The viscous model is set using the realizable k-ε model with standard wall functions for near wall treatment. Air physical properties are treated as constants with density of 1.225 kg/m³ and viscosity of 1.7894 e-05 kg/m-s.

A kinematic viscosity 15.11 x10-6 m²/s was used in the Reynolds number calculation. 18.9 m/s air velocity was applied to the velocity inlet as boundary condition and no slip boundary conditions are applied to all of the wall boundaries. The thickness of the wall was set to 1 mm. The blades of the louver were specified as symmetrical, and outflow boundary condition was imposed at the louver outlet and holes at the side of the louver. The hydraulic diameter was calculated 1.006. The SIMPLE algorithm was used as the solution method for the pressure-velocity coupling. The momentum was discretized using second order. The convergence criterion was set at 10e-05 for continuity, kinetic energy (k) and turbulent dissipation (ε) equations.

5.4.1 60° Angle louver

In this scenario blade angles of the louver were set to 60° and the geometry was simulated using AutoCAD according to the Experimental Mine louver dimensions. As shown in Figure 2 individual louver blades vary in angle. The geometry of 60° louver was simulated to match the field measurements. The inlet velocity and hydraulic diameter were set at 18.9 m/s and 1.02. The mesh was generated approximately 192,000 tetrahedral control volumes. Reynolds number for this simulation was calculated at 1,275,843. The pressure behavior of airflow across louver is shown in Figure 11.

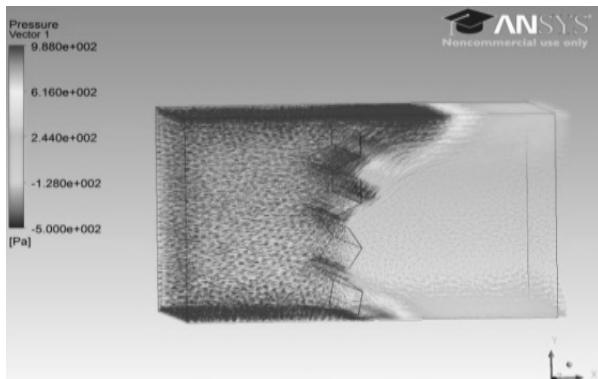


Figure 11. Pressure vectors across 60° angle louver.

It is evident from Figure 11 that eddies were created in the center of the duct and a large proportion of air has passed along the top and bottom parts of the duct. In addition on account of loss through the holes at the side of louver the velocity at the outlet decreased dramatically. This louver angle has had negative influence on the resulting airflow properties. Table 11 shows the result of this simulation according to 60° blade angle of the louver in comparison with experimental and numerical results when the Joy surface fan was set at high speed. The direction of airflow was along x axis left to right as shown Figure 11.

Table 11. Correlation of computational, experimental and numerical results across 60° angle louver.

Scenario	V _{inlet} m/s	V _{outlet} m/s	ΔV m/s	P _{Drop} (Pa)
60° Louver computational	18.9	12.77	6.13	762.4
60° Louver experimental	18.9	12.3	6.4	845
60° Louver numerical	18.9	12.3	6.4	961.36

5.4.2 Ideal louver

The geometry of a 0° angle louver was simulated by AutoCAD in line with measured dimensions as shown in Figure 2. The inlet velocity and hydraulic diameter were set at 18.9 m/s and 1.02. The generated mesh had approximately 200,000 tetrahedral control volumes. Reynolds number for this scenario was calculated at 1,275,843. The pressure behavior of airflow across the louver is shown in Figure 12. With the change of angle of louver blades to 0°, and closing the holes the pressure drop decreased noticeably and the outlet velocity approached close to the inlet velocity. Results of this study in comparison with the experimental and numerical studies are shown in Table 12. Consistent with the data in the Table 12, this scenario was selected as the best design for the position of the louver blades.



Figure 12. Pressure vectors across 0° angle louver.

Table 12. Correlation of computational, experimental and numerical results across 0° angle louver.

Scenario	V _{inlet} m/s	V _{outlet} m/s	ΔV m/s	P _{Drop} (Pa)
0° Louver computational	18.9	18.8	0.1	84
0° Louver experimental	18.9	18.9	0	69
0° Louver numerical	18.9	18.9	0	72.1

6. Conclusion

The least pressure drop across the examined elbows and louver has been achieved when the height and width of the elbow changed to 1.5m and 0.64m with a smooth 90° bend angle and with the change of louver blade angle to 0° to the horizontal. Differences in the experimental and computational results of pressure drop were calculated to be approximately 10% with the use of a 90° elbow and the 60° angle louver. An outlet velocity of 16.7 m/s has been achieved with use of the ideal elbow.

The pressure drop has decreased when the inlet velocity through the elbow has been decreased sharply. Computationally calculated pressure drop results with the 60° angle louver and a 90° mine elbow were determined as 979.4 Pa at the mine inlet shaft. With the change of louver blade angle to 0° and use of an ideal elbow the pressure drop was decreased to 259.7 Pa. With the employment of these changes the pressure drop was improved by 72.5% by the use of a CFD approach. The difference between experimental and numerical pressure drop results at a 0° angle louver is calculated as 4% while this difference for a 60° angle louver was 12%. The diffuser form of elbow at its outlet as shown in Figure 10 has produced eddies. The produced eddies have had a negative influence on airflow behavior through the elbow. Hence the mine elbow should be changed. This study has shown that both the louver and elbow can contribute to drop the produced pressure by a surface fan drastically. Various approaches were utilized to decrease the pressure drop across the louver and the elbow. However none of them have eradicated the amount of pressure drop in the ducting in a fully-fledged way. One approach for eliminating the pressure drop across ducts on surface is to mount the main mine fan vertically on the shaft. This study was carried out to allow a better understanding of flow behavior in surface ducting systems. It has also allowed the determination of the optimum operating conditions of the surface fan. As a result of these studies a vertical position was selected for the design of the main mine fan position at the MS&T Experimental Mine.

Acknowledgment

This paper was prepared with support from the National Institute of Occupational Health and Safety.

References

- [1] Çengel, Yunus. A. 2006. Introduction to thermodynamics and heat transfer, Second edition, The McGraw–Hill.
- [2] McPherson, Malcolm J. 1993. Subsurface ventilation and environmental engineering, online edition.
- [3] Miller, D. S. 1990. Internal flow systems, 2nd Ed. BHRA (Information services), Bedford.
- [4] Smith, S. J. 1998. Determination of k-factors of HVAC system components using measurement and CFD modelling, PhD dissertation, 27. University of Nottingham, UK.
- [5] Wala, A. M., Yingling, J. C., Zhang, J., and Ray, R. 1993. Validation study of computational fluid dynamics as a tool for mine ventilation design, SME annual meeting, 1997, 520-525.
- [6] Zheng Yi. 2011. Diesel particulate matter dispersion analysis in underground metal/nonmetal mines using computational fluid dynamics. PhD dissertation, 125. Missouri University of S&T. USA.
- [7] Zmrhal, V. and Schwarzer, J. 2009. Numerical simulation of local loss coefficients of ventilation duct fittings, Eleventh International IBPSA Conference, Glasgow, Scotland, 2009. 1761–1766.

Study of Ventilation in the Mine CERRO LINDA CIA. MINERA MILPO S.A to Increase Production from 15000 TPD to 18000 TPD

José Antonio Corimanya^a, Freddy Alvaro Herrera^b

^aUniversidad Nacional de Ingeniería, Lima, Peru
^bCia. Mina Milpo, Cerro Lindo, Peru

Cerro Lindo Mining Company, which is part of Votorantim – Milpo Group will increase its mining production from 15 000 tpd to 18 000 tpd. Then, a new study of ventilation is necessary in order to increase production in a safe way. The ventilation study is divided in three parts. The first part of the analysis involves the study of the current ventilation scenario at the study mine. The ventilation coverage in the mine is 92% and 1 305 390 CFM are pushed in the system at the intake. The air volume requirement for personnel is 35 880 CFM and 1 309 422 CFM for machinery. This first part of the study also included the modeling of the existing network of the mine by using the software Ventsim VISUAL PREMIUM. The air volume entering the mine was measured with an electronic device which allowed for the determining of the air volume at the mine intake. This device displayed a value of 1 305 390CFM as mentioned above. On the other hand a volume of 1 370 279 CFM was estimated with Ventsim so that the software approximated the reality in 95.2%. In the second project stage, the ventilation system was simulated with the software in order to determine the dimensions of fans for the new mining scenario (i.e., this includes the diesel equipment operating in the mine) Fans providing 250 000 CFM and 200 000 CFM were simulated under different pressures, and after some trials it was determine that the most suitable fans for the mine infrastructure, in terms of the ventilation system (i.e., optimizing the system), are fans of 200 000 CFM and 9.5 " H₂O total pressure. These fans should be able to allow 2 046 141 CFM to enter the mine, which would compensate for the expansion of production to 18 000 tpd. Economics were assessed within the third stage of the project. This economic assessment accounted for the necessary investments, such as for horizontal and vertical excavations, and ventilation energy costs (i.e. equipment and electricity). Energy costs associated with ventilation represent about 75% of the total costs. Two Raise boring (RB) machines with 3m in diameter are required to give support to the new production of 18 000 tpd, 5 969.6 ft (1 820 m) of vertical development, 3 673.6 ft (1120 m) of horizontal development and 3 additional air intake tunnels needs to be bored. In addition, 3 new fans with a capacity of 200 000 CFM and 9.5 " H₂O total pressure are required. The aforementioned investments have a cost of capital of \$4 524 801.

This analysis will be focused on the three stages in the primary ventilation system, since the secondary ventilation systems for each of the ore body are tied and dependent on the primary system.

Keywords: Sublevel stopping; Ventilation; Network; Energy efficiency

1. Introduction

Developing a mine in the production zones is usually performed without considering the support functions areas (i.e., Ventilation, retrofilling, utilities) in detail. The consideration of these supporting areas are necessary for the sustainability of the increase in production. If adjustments to this areas are not correctly considered a series of problems may advent creating difficulties to meet the required production. Then, the analysis for the increase of production should include the correct studies and designs for the support areas or activities. Special attention will be given to the ventilation of the time, since this is considered the main subject and constraint for the increase of the production of Cerro Lindo Mining Company Votorantim – Milpo from 15 000 tpd to 18 000 tpd. As part of a long term plan we will focus this study on the analysis of the primary ventilation system of the mine. The type of fans, its capacity and infrastructure issues will be addressed in order to increase the current coverage of the mine. In addition, a future expansion to 20 000 tpd will be factor in within this analysis.

2. Legal Part

Evaluations for production expansions in an underground mine in our country (Peru) are governed per the Supreme Decree 055-2010 EM [1]. The Supreme Decree defines standard patterns for the design of our ventilation system and for thermal environmental conditions. Field surveys and subsequent ventilation

designs will be evaluated and simulated by means of the ventilation software available in each mining company.

2.1 Flow required for workers

According to D.S. 055-2010-EM Regulations Occupational Safety and Health, the minimum amount of air required by man in underground mining is given as follows:

Up to 4 920 ft is 106 CFM / man.

From 4 920 - 9 840 ft is 141.2 CFM/ man.

From 9 840 - 13 120 ft is 176.4 CFM/ man.

From 13 120 ft to more is 212 CFM/ man.

2.2 Flow required for Diesel team

As established in Supreme Decree (SD) 055-2010-EM, air requirements for equipment are set to 3 m³ / min per HP (106 CFM per HP) to develop teams.

2.3 Flow required for dilution of pollutants

It is given by the relationship:

$$Q = A * V * N$$

Where:

A: average gallery ft²(m²) Section

N: number of levels in operation.

V: speed minimum airflow (m / min) (SD 055-2010-EM). In any case the air velocity will be less than twenty 20 m/min (65.6 ft/min) or more than two hundred fifty

250 m/min (820 ft/min) in the work of exploitation, including the development, preparation and everywhere where there are staff working. When explosive ANFO blasting or other agents are used, the air velocity of not less than twenty 25 m/min (82 ft/min).

3. Cerro Lindo Mine – Technical Description

3.1 Location

Cerro Lindo Mine is located in the south of Peru at 175 km south-east of Lima. The mine is located in Ica department, Chincha province, Chavin district, Huapunga zone and it is emplaced in an altitude of 5 969.6 ft (1820m). The main entrance to the mine is via the Panamerican Highway which goes until Jahuay creek into paved road and then by a road to the mine.

3.2 Exploitation Methods

The mine plan for Cerro Lindo is defined based on geological resources and geomechanical conditions of the deposit for an initial production of 7 490 tpd -10 000 tpd. The production was then ramped up to 15 000 tpd during the year 2013.

The method of exploitation is Sublevel Stopping [2] whose extractive sequence is shown in Figure 1.

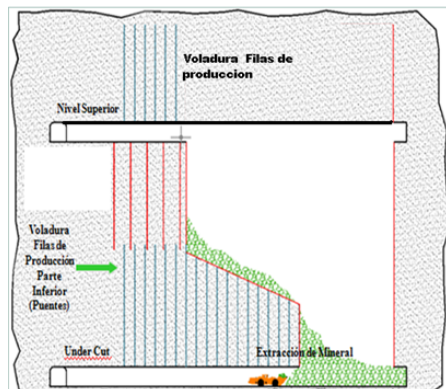


Fig 1. Negative drilling from top level and positive drilling from lower level.

3.2.1 Preparation infrastructure

The following infrastructure is required for the exploitation of a mineralized zone (stope) when using the method of sublevel stopping:

- Drilling level.
- Lower drilling and extraction level.
- Slot (Initial void for blasting)
- Shaft - Initial bore for the slot
- Drawpoints (loading points for blasted-fractured material)

3.2.2 Mining Cycle

Ore bodies are exploited applying the long holes drilling method by developing negative drillings from top level of 59 ft (18 m) in length and positive drilling from the lower level of 39.36 ft (12 m) in length. The diameter of the perforations lays between 2.5” and 3”.

Drillers are provided by Simba and Raptor. The drilling mesh is a 6.56 ft (2 m) – 7.21 ft (2.2 m) in burden and 6.56 ft (2 m) - 7.21 ft (2.2 m) in spacing. This characteristics are shown in detailed in Figure 11. Appendix 3.

Prior to blasting the executed holes are loaded with explosives. For the loading of the positive (+) holes (i.e., holes drilled upward from the drilling level) an Anfloader – also known as an ANFO Loader – is used. On the other hand, the negative holes (-) are manually loaded. In advance fronts an anfloader is used for the loading of the explosive charge. In both cases compressed air is used for the coupling of the ANFO.

SuperFan, Emulnor and HDP booster are the explosives used when setting off. Fanel, detonating cord (5D) and Carmex are accessories required for the detonation of the charge.

Mucking up and mineral loading is performed with two scooptrams. One is CAT-R1600G with a volumetric capacity of 6 yd^3 , and the second one is CAT-R2900G with capacity of 9.5 yd^3 . These pieces of equipment achieve in average 120 tph and 180 tph, respectively.. In addition, Hauling is performed with trucks of 25 and 35 ton of capacity. All hauling routes and trajectories remain strictly underground. A primary crusher is situated underground for comminution of the ore. Refusal and sterile material are transported to surface where it is contained in dumps.

Basically, the mining cycle for Cerro Lindo is comprised of drilling, explosive loading, blasting, mucking and hauling stages. A description of mineral loading and hauling is presented in Figure 3.

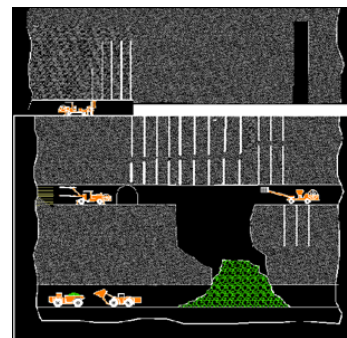


Figure 3. Scheme operations inside the mine.

4. First Stage: Diagnosis of Current Ventilation System for 15,000 t/day

Among the instruments used for airflow measurements our mine have the analog anemometer KESTREL that is used to measure speeds above 1 m/sec, while lower speeds are measured with use of anemometers DELTA OHM. In addition, pitot tubes are used to measure the air flow and total pressure (dynamic pressure and static pressure) among others. Measuring instruments must be calibrated and checked as indicated by the manufacturer since generally these instruments lose accuracy over time which could lead to erroneous input data. Each instrument should be used only used for the purpose it is intended to in order to avoid erroneous readings, for instance, anemometers are designed to operate in a speed range, the pitot tube to measure the air flow and total pressure, the smoke tube for the sense and direction of the air and others [3-5].

4.1 Control Stations

The control stations for the technical parameters of ventilation should be strategically located in the straightest part of the underground excavation in study and at a distant of 32.8 ft (10 m) before or after a change of section. It may be ensured that the ventilation parameters (e.g., air speed, temperature, absolute and relative pressure, section of the excavations, density of dry air and wet air density, presence of air pollutant (CO, CO₂, Sox) are kept constant within the section. The head of the ventilation area will determine the relevant parameters under consideration.. Data should be properly stored a database and the behavior of the considered variables is to be reviewed as time changes. The location of the control stations for the primary ventilation system is detailed in Table 1.

Table 1 Control stations for the primary system.

Level	Excavation	Air Condition and direction
1820	Bocamina 1820	Fresh aire intake
1800	Bocamina Rp.010	Fresh aire intake
1830	Bocamina Cx 010	Fresh aire intake
1875	Bocamina 1875	Fresh aire intake
1850	Old excavation	Fresh aire intake
1970	Bocamina 1970	Stale aire outflow
1970	Bocamina Bp 105	Stale aire outflow
1940	Bocamina 1940	Stale aire outflow
1945	Bocamina Faja N°3	Stale aire outflow

4.2 Air Balance

Air requirements for both personnel and vehicles fleet are factored into the air balance analysis. The current air balance prior simulation is displayed in Table 2.

Table 2 Current air balance

Air Requirement (CFM)	
For perssonel	35,880
For diesel equipment	1'390,422
For gases dilution	366,329

Details of the instruments used for the measurement of ventilation parameters in the main stations are presented in Table 6 of Appendix 1.

4.3 Current ventilation network simulation

4.3.1 Data feeding/input for the software

Data feeding is made from the main axes of the vertical, horizontal and oblique excavations data contained in 3D AUTOCAD 2014. The mine geometry is saved in this program as a DXF R12 file. It is recommended to have the information in several layers which means to have the vertical excavations in one layer, horizontal excavations in another so that data handling and its loading into the software Visual Ventsim 3D is done in a more efficient way (e.g., by reducing the chance of duplicate data). The ventilation Isometric shown in Figure 10 of Appendix 2.

Attention must be also given to importing the axes and excavations geometry from the R12 DXF file into the ventilation software. The model must be fed with characteristics as close as possible to reality. As a target, the simulation should represent the reality in a 95%. The Visual Ventsim software uses a graphical environment called DIRECTX for the processing and programming of the data. DIRECTX provides a lightweight graphical environmental, which makes possible to run the software in computer with low video capacity (i.e.m a video memory of 500 MB is taken as reference) Ventsim owes its efficiency and speed to the programming language in which it was structured. All algorithms are in VISUAL BASIC language, which makes the software agile and quite practical [8].

Figure 4 presents the input parameters assigned to each branch. If the software team determines that there are several branches inside the mine that have similar, or very similar characteristics, then these characteristics can be easily copied and loaded by using the copying features toolbar. The friction factor must be inputted from lookup tables or determined based on the type of rock located in each branch if available. It is recommended to calculate the friction factor in the field (i.e., by measures underground) and then to calculate the resistance for the different excavations. In a similar fashion it is possible to update stored attributes for the fans into the software as shown in Figure 5.

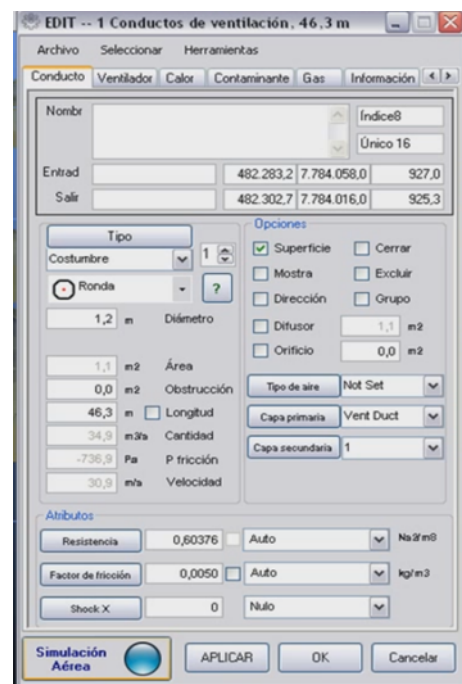


Figure 4. Ventsim Window for manually-entered data.

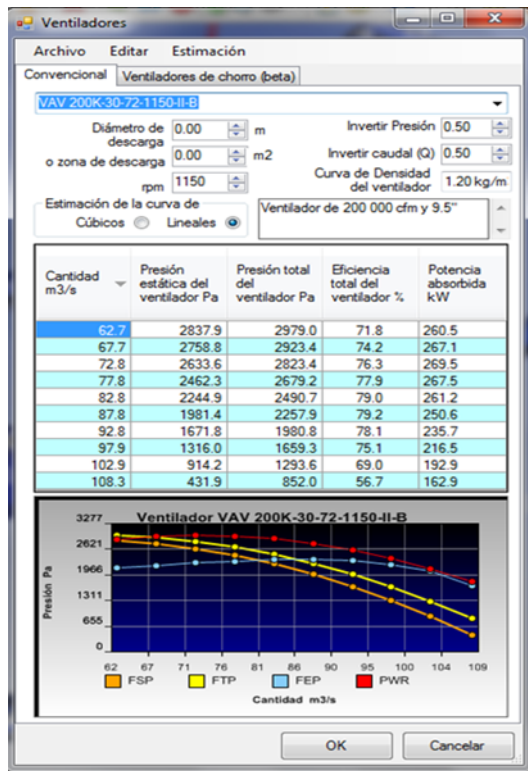


Figure 5. Points for the characteristic curve of a 200,000 CFM fan and dual-stage

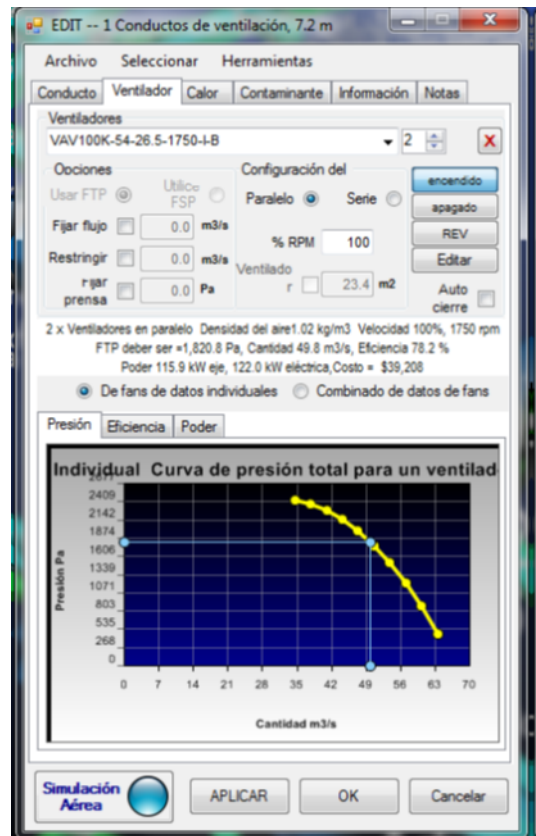


Figure 6. Operating point of a 100,000 CFM fan -d single stage.

4.3.2 Data feeding for Fans

The data input of the fans must be done according to the operating points that each manufacturer provide. This information is usually incorporated into the data sheet for the fan.

The operating point should be checked when performing the simulation runs so that it is within the characteristic curve of the fan. This information is shown in Figure 6.

4.3.3 Simulation results for the ventilation network

During the simulation of the current ventilation scenario some minor difficulties had to be addressed. This difficulties such as offline branches (i.e., branches without an ending or starting node) and some offline ventilation circuits were easily corrected. This issues were solved by using the software – Ventsim Visual – toolbar. The simulation report is presented in Table 3.

In order to check the state of the current network in the mine as well as checking our model it is first necessary to analyze ventilation sub-systems inside the mine. Indeed we have analyzed at the entry and exit of each ore body (i.e., at OB1, OB2, OB5, OB6A, OB6B and OB8). The simulation of the fans can be done by using the software FAN CURVE provided by AIRTEC.

Table 3. Ventsim simulation -software report.

OB	Level	Description	Q (cfm)	V (ft/s)
2	1680	Cx 020	29 876	2.30
2	1680	Cx 056	38 897	3.28
2	1680	Bp 131	36 869	2.95
2	1680	Cx 056	140 058	11.48
2	1680	Bp 131	37 504	2.95
2 y 5	1680	Bp 745A	7 204	0.66
2 y 5	1680	Bp 745 B	47 463	2.95
2 y 5	1680	Cx 019	29 029	3.28
2 y 5	1710	Bp 745 A	43 649	3.60
2 y 5	1710	Bp 745B	33 266	2.62
2 y 5	1710	Cx 019	25 427	1.97
2 y 5	1740	Bp 745 A	0.0	0.0
2 y 5	1740	Bp 745B	50 217	3.9
2 y 5	1740	Cx 019	49 370	3.9
5	1680	Bp 745 A	30 724	2.62
5	1680	Bp 745 B	63 143	5.25
5	1680	Cx 019	119 293	9.84
5	1710	Bp 105A	26 910	2.29
5	1710	Bp 105B	56 988	4.59
5	1710	Cx 005	119 293	9.84
5	1740	Bp 105A	0.0	0.0
5	1740	Bp 105B	37 292	2.95
5	1740	Cx 005	67 380	5.57

Table 4. Shafts construction projects.

Equipment	Air shaft	Crosscut	O B	Diam. (ft)	Length (ft)
RD 3250	RB705	705	6	9.84	459
RD 3250	RB705B	705	6	9.84	804
RD 3250	RB784	784	6	9.84	295
RD 3250	RB050	050	1	9.84	295
RD 3250	RB945	945	6 B	9.84	328
RD 3250	RB730	730	6 B	9.84	344
RD 3250	RB784B	784	6	9.84	951
71 RQ	RB932	935	2 B	9.84	328
71 RQ	RB953	953	2	9.84	197
71 RQ	RB745	745	6 B	9.84	459
71 RQ	RB936	936	2	9.84	951
71 RQ	RB785	785	2	9.84	558
				Total	5 970

This analysis was carried out corroborating speeds at the point of entry and exit of air of each ore body. The circuit will be adjusted dynamically according to each communication, advance, new stopes or others features that may affect the air velocity in an underground excavation. This adjustment is done due to the presence of sterile materials (i.e. refuse or non-grade rocks) which is represented as shock losses, inoperative equipment, cleaning in production zones, opening of shafts, fans movement, roughness adjustment excavations, fan performance adjustment, among others. After analyzing each sub ventilation system, and after the adjusting process it can be determined how well the model fits, or is in accordance, to reality. The simulation network results are calibrated within an error 4.8 %.

5. Design of the ventilation System for the projected 18,000 tpd production rate.

5.1. Construction of ventilation shafts

It's required to build 5 969.6 ft (1 820 m) of shafts with 10.2 ft (3.1m) in diameter as detailed in Table 4. A simulation for this situation is sketched in Figure 7.

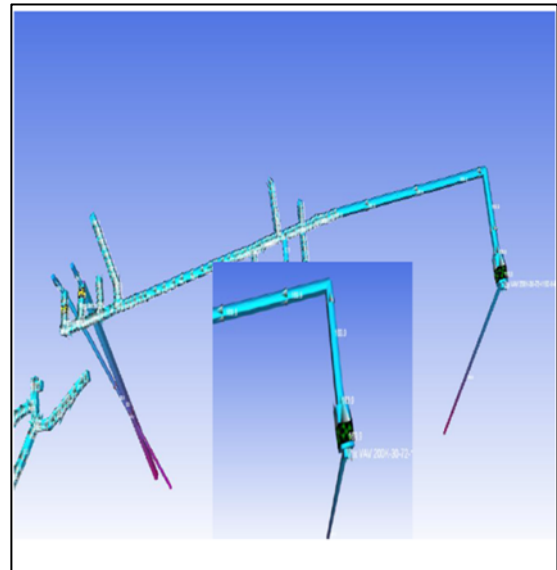


Figure 7. Simulation Ch-705 from the 1,820 level to the 1,925 level.

5.2 Selection of Fans

Exhaust ventilation is used in the mine, so to increase the amount of air in 600 000 CFM a series of main exhaust fans have to be used. For a typical excavation of dimensions 16.4 ft x 13.1 ft, 39 411 CFM can be exhausted if air speed is 1 m/s, then if the evacuation speed is 3 540 ft/min it would be possible to extract 709 407 CFM. This means that a new excavation to surface will be strictly necessary for extracting air. This excavation is represented in Figure 8. The simulation of

the ventilation system based on their resistance and other characteristics is shown in Figure 9.

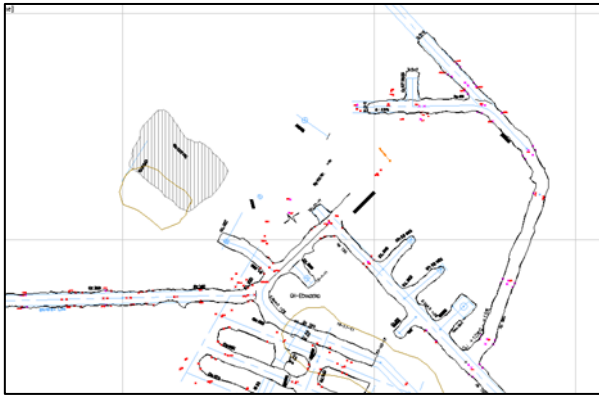


Figure 8. Adit entry, Rp. 950 which goes up to surface.

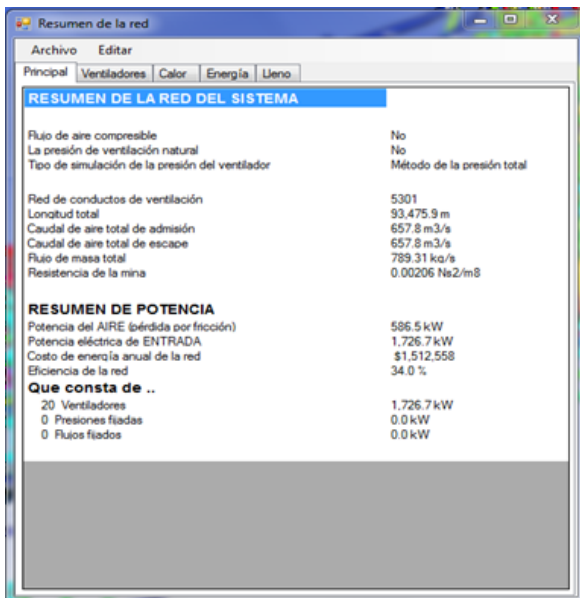


Figure 9. Summary of simulation including the total resistance

According to the second law of the fans by Fan Engineering - Buffalo Forge Company [6].

$$C_p = RQ^2 \quad (1)$$

$$R = \frac{k \cdot Per \cdot L}{A^3} \quad (2)$$

Where:

C_p: System pressure drop, Pa

A: Total resistance of the mine, Ns²/m⁸

Q: Total flow, m³/s

K: coefficient of friction, kg/m³

Per: Perimeter of the excavation, m

L: Length of the excavation, m

A: cross sectional area of the excavation, m²

Then:

$$R = 0.00209 \text{ Ns}^2/\text{m}^8$$

5.3 Simulation Results

To expand production to 18 000 tpd is necessary a flow of fresh air at the intake of 2 046 151 CFM therefore the air flow at the intake should be increased by 600 000 CFM to raise the mine coverage and to meet demand by 100 % . Different scenarios were analyzed and it was determined that for this purpose 3 fans with capacities of 200 000 CFM and 9.5"H₂O total pressure are required. These features enable future adjustments to the pallets of these fans so that future extension can be performed. This study also took into account the increase in the overall resistance of the mine for the next 7 years of operation.

$$Q = 665.3 \frac{\text{m}^3}{\text{s}}$$

$$249.1 \text{ Pa} = 1''\text{H}_2\text{O}$$

C_p = 3.70"H₂O, taking into account a loss factor of 40 %, a total of 5.18" H₂O.

Several simulations were performed in Ventsim with 300 000 CFM, 250 000 and 200 000 CFM fans. The equipment that optimized the stale air extraction, air systems inside the mine and power consumption were the 200 000 CFM fans with 9.5"H₂O total pressure at 1820 m.a.s.l.

The 200 000 CFM fans will be installed in parallel in the Rp. 950 Nv. 1970, which is connected to surface in order to extract the required amount of air.

The Operating point of the 200 000 CFM fan that optimize the ventilation system is shown in Figure10.

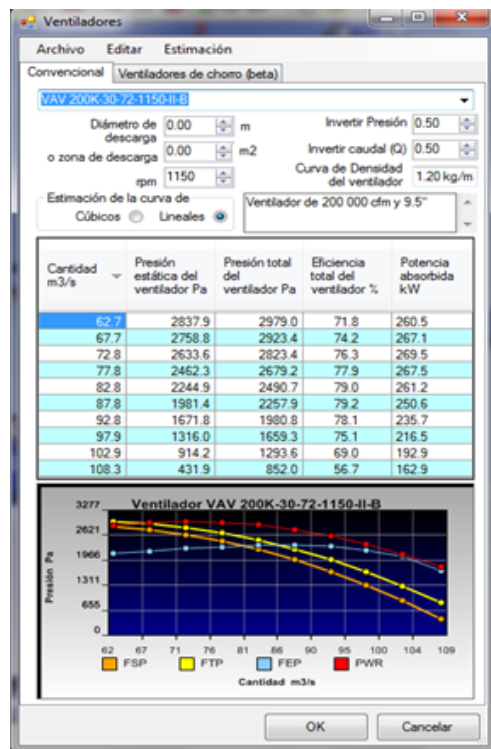


Figure 10. Operation point for a 200 000 CFM fan

Based on the modelling, these fans will be 72" of inside diameter, 1750 RPM single stage and type B.

While it is true that only 5.18"H2O total pressure are required according to modeling, our mine will grow and consequently the overall resistance of the mine will increase too. In addition, it should be considered that the main entries may be partially obstructed by trucks which generates a strong resistance to the main fans. For these reasons a fan of 9.5"H2O total pressure was chosen which may be subject to variations of 20% according to the vendors.

Simulation of these fans was also performed for the worst possible scenario. This would be the situation when the air entrances (intakes) are partially obstructed by trucks of 35 tons of capacity, which directly affects the main fans. This would affect the main fans by varying the operating points as a result of the increased resistance in the system. Then it becomes necessary to construct two additional mine entrances in order to optimize the performance of the main fans.

6. Economic Evaluation of the Project

It is required to have two RBs equipment for the construction of 10.16 ft in diameter shafts, and a crew strictly assigned to ventilation works. The cost for these jobs are summarized in Table 5.

Table 5. Costo de capital y costo operativo

Costo total de inversión			
Description	Quantity	Price	Sub total (\$)
Vertical Advance	5 969.6 ft	457.3 \$/ft	2 730 000
Horizontal Advance	3 676.6 ft	365.8 \$/ft	1 344 000
Fan94.39 m/s	03 und.	150 267\$/u	450 801
		Costo capital (\$)	4 524 801
		Costo operativo (\$)	1 809 920

Discussions and Conclusions

The primary ventilation system in CERRO LINDO MINE is governed by the major exhaust fans located in the upper levels for the extraction of stale air. At these levels are the mine adits for stale air extraction: Nv. 1940 mine entrance Bp. 105, Nv 1979 mine entrance Alimak and Nv 1970 main entrance Bp. 105. The vacuum created by these fans draws clear air into the main adits.

The vertical advance of 9.84 ft diameter shafts for the increase of production is 5 969.6 ft, this can only be done by renting an additional RB machine. Ventilation requirements per the DS 055 2010 EM cannot be met without this infrastructure.

The maximum air flow that can go through a typical excavation/adit of 16.4 ft x 13.1 ft to the characteristics of our unit is 710 000 CFM.

At the moment, the volume of fresh air entering the mine is 1 305 390CFM. For a production of 18 000 tpd the air volume shall be increased by 587 232CFM. In order to evacuate an additional air volume of 600 000 CFM a selection of fans should be done, and it should also forecast future production expansions (these expansions are restricted by the mine aerodynamic parameters) This design was covered by using axial fans with variable pallet angles. The pressure was determined so that the total pressure can be decreased and increased as well as the rate of extraction of each axial fan. This will be done in the curve of operation of each fan.

According to the software Ventsim Visual premium and to the software AIRTEC FANCURVE, the fans that fit better the reality of our mining operation are axial fans 200 000 CFM and 9.5"H2O total pressure at 1970 m.a.s.l.

If the Rp. 950 is connected with surface, clean air will get into this excavation and will be evacuated through the exhaust entries located at levels 1970 and 1940. This means that this air would not run no into the mine which would be very harmful to our mining operation. Based on the modelling results, the amount of air that would be wasted in this case would be 352 000 CFM.

The amount of clean air entering the main entrance adits is increased by increasing the capacity of extraction of stale air. Additionally, when increasing the air speed at the mine entrances (intakes) the average temperature becomes 16°C according to modeling and measures taken in the mine. This is not good for the health of those workers leaving work fronts that are at 30°C.

The cost of energy represents the 75% of the total cost of ventilation, which indicates that cost behavior is directly influenced by the consumption of electricity.

The optimal diameter for our mining unit containing all our aerodynamic characteristics, energy costs, operating costs and other parameters is 10.6 ft, our RB equipment build shafts of diameter 10.2 ft which is quite close to the designed optimal diameter.

The wind direction during the whole year needs to be inspected in order to define the most appropriate location of the entrance and/or exit adit. This information is provided by the environment area of the mine. The wind direction must be favorable to the direction of the exit or entry of air. This approach provides substantial energy savings. In addition it should be considered the way the fans will be power up and its operational parameters. Finally it should be also considered the type of rock where the infrastructure will be built.

Modelling results are directly affected by the level of approximation of the model to reality. An acceptable figure in Ventsim for the approximation is 95%. Adjustments to the model should be made constantly, periodically or whenever changes are made to the primary or secondary ventilation systems. The results of the modeling software should be corrected according to the experience of the modelling team and the reality of the mine.

It is necessary to make two more fresh air entrances in the mine so that the air speed at the air entries is not increased. An entry should be exclusively dedicated for the personnel of the mine.

In our mining unit, two of the three main entries (fresh air entrances) are dedicated to hauling purposes. The trucks occupy the 70% of the cross sectional area of

the mine entrance which leads to high resistance in the ventilation system. This high resistance is responsible for changes in the operating point of the fans. Modelling is important for this scenario because of the 15 of the 38 units that comprise the trucks fleet in the mine are constantly going in and out. This creates resistance in the fresh-air entrances.

References

- [1] Reglamento de seguridad y salud ocupacional en minería D.S. N°055(2010-EM) 119-127.
- [2] Howard L. Hartman, SME Mining Engineering Handbook – Society for Mining, Metallurgy, and Exploration, Inc. USA1992.
- [3] Malcom J.Mc Pherson, Subsurface Ventilation Engineering, California 2009
- [4] Pablo Jiménez Ascanio, Ventilación de Minas Subterráneas y Túneles, Lima 2011
- [5] José Corimanya, Capacitación de Ventilación de Minas en mina Cerro Lindo, Chincha Enero 2014.
- [6] Fan Engineering, Published by Buffalo Forge Company, New York 1961.
- [7] Howard L. Hartman, Mine Ventilation and air conditioning, Third edition Jhon Wiley & Sons, INC, New York 1997.730pp.
- [8] Craig Stewart, Manual Ventsim Visual Advanced, Australia 2014.

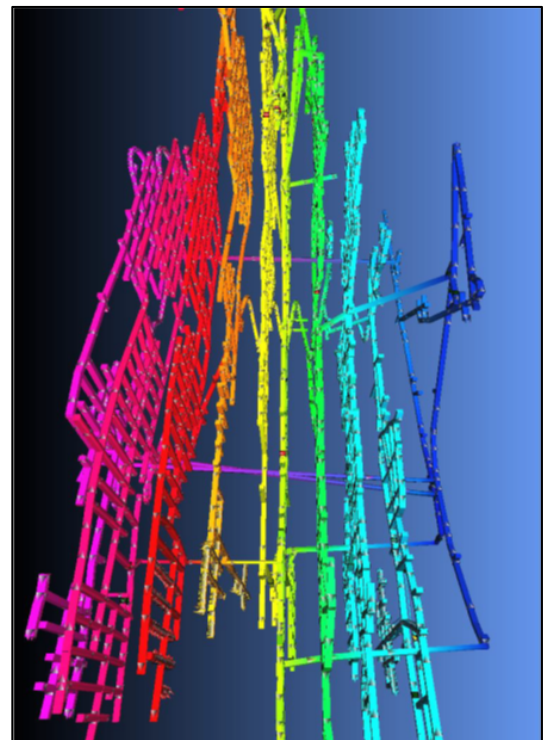


Figure 10. Isometric Cerro Lindo - mine ventilation system

Appendix 1

Table 6. Instrumentation for Ventilation

	Equipo	Marca	Modelo	Cantidad
1	Anemómetro	Kestrel	4500NV	1
2	Anemómetro	Kestrel	4000	2
3	Anemómetro	Delta OHM	HD 2103.1	2
4	Anemómetro	Trotec	TA300	1
5	Tubo de pitot	Dwyer	Serie 160	4
6	Bomba de Muestreo	MSA	Kwik Draw	6
7	Montajes para tubos de humo	MSA	---	6
8	Psicrómetro	---	---	2
9	Tubo de Humo	MSA	---	8
10	Manómetro	Dwyer	2025	1
11	Detector de gases	Drager	X-am 5600	1
12	Distanciómetro	Leica	D5	1
13	Sonómetro	AEMC	CA 832	1

Appendix 2

Slot Boring Building Negative
 Raptor team
 Centroid 4.9 ft (1.5 m)
 Drilling diameter drill (-): 3 "
 Mesh 7.2 ft (2.2 m) x 7.2 ft (2.2 m)
 Number of holes per section (-): 21
 Sectional drill meters or 820 ft (250 m)
 Drilling meters / 656 ft (200m / guard)

Centroid Raptor

Slot Boring Building Positive
 Raptor team
 Centroid 4.9ft (1.5m)
 Drilling diameter drill (-): 2.5 "
 Mesh 7.2ft x 7.2 ft (2.2 m x 2.2 m)
 Number of holes per section (-): 32
 Sectional drill meters or 1 426.8 ft (435 m)
 Drilling meters / 820 ft (250m / guard)

Centroid Raptor

Appendix 3

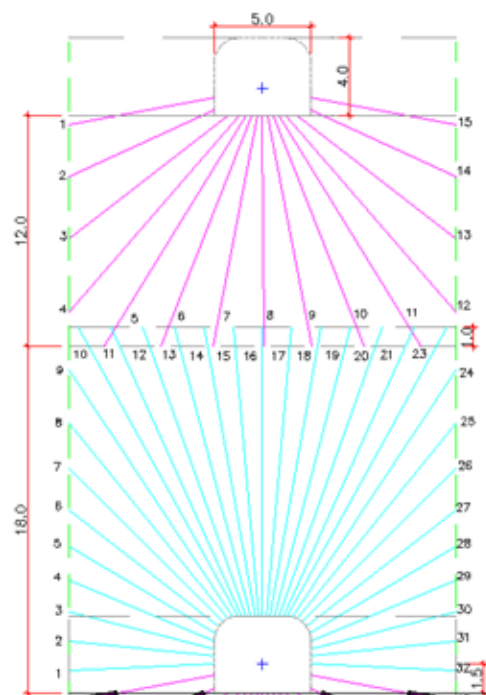


Figure 11. Typical drilling which has been used in Cerro Lindo.

Estudio de Ventilacion de la Mina Cerro Lindo CIA. Minera Milpo S.A. para Ampliar la Produccion de 15 000 a 18 000 TPD

J.A. Corimanya^a, F.A.Herrera^b

^aUniversidad Nacional de Ingenieria, Lima, Peru

^bCIA Mina Milpo, Cerro Lindo, Peru

La CIA Minera Cerro Lindo del grupo Votorantim - Milpo ampliara su producción de 15,000 tpd a 18,000 tpd por lo que requiere realizar un estudio de ventilación que pueda dar soporte a este nivel de producción. El presente estudio de ventilación se desarrollara en tres etapas. En la primera etapa se realiza un diagnóstico de la situación actual del sistema de ventilación de la mina, y se tiene una cobertura actual de 92% con un ingreso de aire medido con instrumento de 616.07 m/s (1'305,390 ft/min), de los cuales el requerimiento para todo el personal es 16.9 m/s (35,880 ft/min) y por equipos es 656.2 m/s (1'390,422 p/min). También se realizó el modelamiento de la red actual de la mina con el uso de software Ventsim visual premium, y nuestro modelo en el software obtuvo 646.69 m/s (1'370,279 ft/min) simulado, con lo cual nuestra aproximación con la realidad es de 95.2% y nuestro modelo queda validado. En una segunda etapa para estudiar el mejoramiento de la ventilación para la ampliación de la producción a 18,000 tpd se realizó la simulación con el software para la selección de ventiladores de acuerdo a las dimensiones de nuestros equipos diésel, para lo cual se realizaron corridas en el modelo con ventiladores de 117.98 m/s (250,000 ft/min) y 94.38 m/s (200,000 ft/min) de diversas presiones pero los ventiladores más adecuados de acuerdo a nuestra infraestructura de ventilación y que mejoran nuestro sistema de ventilación son ventiladores de 94.38 m/s (200,000 ft/min) y 2 346.45 Pa (9.5" de agua) de presión total y estos ventiladores deben ser capaces de permitir el ingreso de 965.67 m/s (2'046,141 ft/min) que son requeridos para la ampliación de producción a 18 000 tpd. En la tercera etapa se realizó la evaluación económica del proyecto, inversiones en excavaciones horizontales y verticales, equipos de ventilación y costo de energía de ventilación. Dentro de estos costos el costo de energía por ventilación representa el 75% del costo total del área. Para dar soporte a las 18,000 tpd es necesario tener dos equipos RB de 3 m de diámetro con una preparación vertical de 1,820 m, una preparación horizontal 1,120 m, construir 3 bocaminas adicionales de ingreso de aire fresco y una adquisición de 3 ventiladores de 94.38 m/s (200,000 ft/min) y 2,346.45 Pa (9.5" de agua) de presión total. Este trabajo representa aproximadamente \$ 4'524,801 en costo de capital.

El análisis en las tres etapas se centrara en el sistema primario de ventilación, dado que los sistemas de ventilación secundarios por cada cuerpo mineralizado son consecuencia del sistema primario de ventilación, la preparación en interior requerida y los equipos de ventilación son menores.

Palabras Clave: Tajeo por subniveles, Ventilación, Red, eficiencia energética.

1. Introducción

El presente estudio de ventilación tiene por objetivo dar soporte a la ampliación a corto plazo de la Cia. Minera Cerro Lindo Votorantim - Milpo de 15,000 tpd a 18,000 tpd y una posible ampliación en un plan a largo plazo, para poder llevar a cabo el incremento de la cobertura actual de mina y proyectándonos a una ampliación a 20,000 tpd.

Debido al crecimiento acelerado de la mina subterránea en sus niveles de producción se tienen problemas en las áreas de soporte técnico (Ventilación, relleno y servicios) y no se puede llevar de una forma sostenida la ampliación de esta producción.

2. Parte Legal

Las evaluaciones, ampliaciones de una mina subterránea en nuestro país (Perú) están regidas de acuerdo al Decreto Supremo 055 (2010 EM) [1], en el

cual se disponen estándares, patrones para el diseño de nuestros sistemas de ventilación y para las condiciones termo ambientales. Se realiza el levantamiento de campo de ventilación y su posterior diseño para evaluarlo y modelarlo en el software de ventilación que cuenta cada empresa minera.

2.1 Caudal necesario para el personal

Según el D.S. 055-2010-EM Reglamento de Seguridad y Salud Ocupacional, la cantidad mínima de aire necesario por hombre en minería subterránea esta dado de la siguiente manera:

- Hasta los 1,500 msnm es 3 m³/min por hombre.
- De 1,500 a 3,000 msnm es 4 m³/min por hombre.
- De 3,000 a 4,000 msnm es 5 m³/min por hombre.
- De 4,000 a mas es 6 m³/min por hombre.

2.2 Caudal necesario para equipo Diesel

Según lo establecido en el D.S. 055-2010-EM, los requerimientos de aire para los equipos están establecidos en 3 m³/min por cada HP que desarrollen los equipos.

3.2 Caudal necesario para la dilución de contaminantes

Esta dado por la relación:

$$Q = A \times V \times N$$

Dónde:

A: Sección promedio de la galería (m²)

N: número de niveles en operación.

V: Velocidad del flujo de aire mínimo (m/min) (D.S. 055-2010-EM). En ningún caso la velocidad del aire será menor de veinte (20) metros por minuto ni superior a doscientos cincuenta (250) metros por minuto en las labores de explotación, incluido el desarrollo, preparación y en todo lugar donde haya personal trabajando. Cuando se emplee explosivo ANFO u otros agentes de voladura, la velocidad del aire no será menor de veinticinco (25) metros por minuto.

3. Mina Cerro Lindo – Descripción Técnica

3.1 Ubicación

La Unidad Minera Cerro Lindo se ubica al Sur del Perú a 175 Km al sureste de Lima. En el Departamento de Ica, Provincia de Chincha, Distrito de Chavín, zona de Huapunga, esta Unidad se encuentra a una altitud de 1,820 msnm como entrada principal a la mina, el acceso es por la Panamericana Sur hasta la quebrada Jahuay en carretera asfaltada y luego por una carretera afirmada hacia la mina.

3.2 Método de Explotación

El plan de minado para Cerro Lindo está basado en los recursos geológicos definidos y las condiciones geomecánicas del yacimiento para una producción de 7,490 – 10,000 tpd inicial y luego ir estableciéndola hacia las 15,000 tpd durante el año 2013.

El método de explotación es tajeo por subniveles [2]. La secuencia se muestra en la Figura 1.

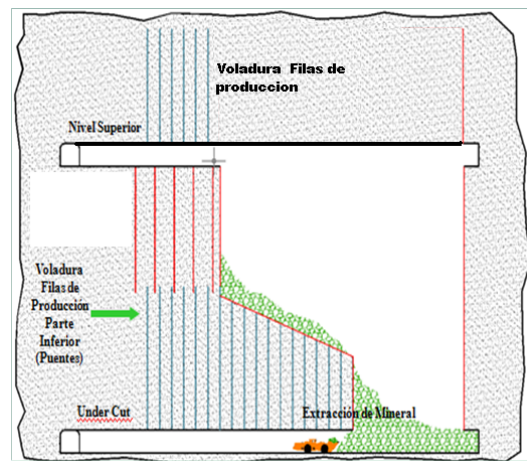


Figura 1. Perforaciones negativas del nivel superior y positivas del nivel inferior.

3.2.1 Preparación de Labores

Para poder explotar un tajeo por el método de Tajeos por subniveles se requiere tener la siguiente infraestructura de preparación:

- ✓ Nivel superior de perforación.
- ✓ Nivel inferior de perforación y extracción.
- ✓ Cara libre de las mallas de perforación.
- ✓ Chimenea de cara libre.
- ✓ Puntos de carguío para extracción de mineral.

3.2.2 Ciclo de Minado

La perforación empleada en la explotación de los cuerpos mineralizados es de taladros largos en forma radial; es decir se perfora en forma ascendente aproximadamente 18 m y en descendente 12 m. El diámetro de perforación es de 6.35 cm – 7.62 cm (2.5” - 3”) y los equipos utilizados son los simbas y raptor. La malla de perforación empleada es: burden 2 m - 2.2 m; espaciamiento 2m - 2.2m. El esquema de la perforación se muestra en la Figura 11 del Apéndice 3.

La voladura en nuestro caso para el carguío de los taladros (+) se utiliza como equipo de carguío el Cargador de Anfo y el carguío de los taladros (-) se realiza en forma manual. En los frentes de avance el equipo de carguío también es con Cargador de Anfo ambos equipos utilizan aire comprimido para el acoplamiento del ANFO. Explosivos: superfan, emulnor y booster HDP.

Accesorios: Fanel, Cordón Detonante (5P), Carmex.

Para la limpieza y transporte de mineral contamos con 02 modelos de palas cargadoras: LHD: CAT-R1600G de 4.6 m³ y CAT-R2900G de 7.3 m³ cuyos rendimientos alcanzados en promedio son de 120 ton/h para un CAT R1600G y 180 ton/h para un CAT R2900G. El transporte de mineral se realiza con camiones de 25 y 35 ton y todo el recorrido es en interior mina donde se tiene instalado una chancadora primaria, el desmonte generado en labores de avance es transportado a los botaderos en superficie.

La secuencia del sistema de limpieza y transporte de mineral se muestra en la Figura 3.

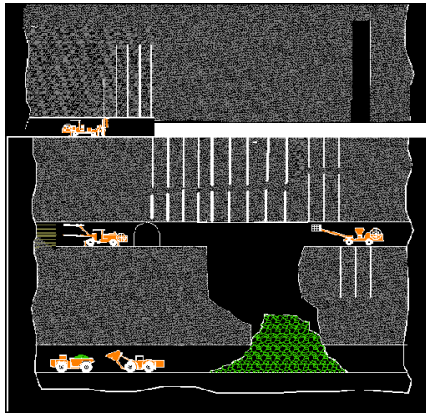


Figura. 3. Se muestra el esquema de las operaciones en interior mina.

4. Primera etapa: Diagnostico del Sistema de Ventilación Actual 15,000 tpd

Entre los instrumentos de medición de aire para el levantamiento de nuestra mina tenemos los anemómetros analógicos KESTREL para medir velocidades mayores a 1 m/s y para velocidades inferiores usamos los anemómetros DELTA OHM, los tubos de pitot para medir el flujo del aire y las presiones totales (presión estática y presión dinámica).

Los instrumentos de medición deben ser calibrados y revisarse su calibración de acuerdo a lo indicado por el fabricante pues generalmente con el tiempo estos equipos se descalibran y brindan datos erróneos. Se debe usar cada equipo para cada propósito para no tener lecturas erróneas con los equipos por ejemplo en los anemómetros estos vienen para trabajar en un rango de velocidades, el tubo de pitot para medir el flujo del aire y presión total, el tubo de humo para ver el sentido y dirección del aire entre otros [3-5].

4.1 Estaciones de Control

Las estaciones de control de los parámetros técnicos de ventilación deben estar estratégicamente ubicadas en la parte más recta en lo posible de la labor y a una distancia de 10 m antes o después de un cambio de sección cuidando siempre que no varíen los parámetros de ventilación como velocidad, temperatura, presión absoluta y relativa, sección de la labor, densidad del aire seco y densidad de aire húmedo, presencia de contaminante del aire (CO, CO₂, SO_x entre otros gases), entre otros que el jefe del área de ventilación crea conveniente. Estos datos deben ser debidamente registrados en una base de datos y se debe revisar el comportamiento de estas variables en el tiempo. El ingreso y salida de aire y las estaciones de control del sistema primario de ventilación se muestran en la Tabla 1.

Tabla 1. Estaciones de control de ventilación de la mina.

Nivel	Labor	Sentido y condicion del aire
1820	Bocamina 1820	Ingresa Aire Fresco
1800	Bocamina (Rp 010)	Ingresa Aire Fresco
1830	Bocamina Cx 010	Ingresa Aire Fresco
1875	Bocamina 1875	Ingresa Aire Fresco
1850	Labor antigua	Ingresa Aire Fresco
1970	Bocamina 1970	Sale Aire Viciado
1970	Bocamina Bp 0105	Sale Aire Viciado
1940	Bocamina 1940	Sale Aire Viciado
1945	Bocamina Faja N°3	Sale Aire Viciado

4.2 Balance de Aire

De acuerdo al parqueo de máquinas actual y de su requerimiento de aire por m³/s tanto para las máquinas y el personal se muestra el balance de aire actual (antes de la simulación). El balance de aire actual se muestra en la Tabla 2.

Tabla 2. Balance de aire actual.

BALANCE DE AIRE (m ³ /s)	
Caudal de ingreso	616.07
Caudal de salida de aire	619.25
Caudal requerido	673.10
COBERTURA	92%

Los detalles de los instrumentos usados para las mediciones de los parámetros de ventilación en las principales estaciones son presentados en la Tabla 6 del Apéndice 1.

4.3 Simulación de la Red Actual de ventilación

4.3.1 Alimentación de Data para las Labores

La alimentación de data se realiza a partir de los ejes principales de las labores verticales, horizontales y oblicuas en el programa AUTOCAD 2014 3D en el cual se guardan los ejes de las labores mencionadas en el formato R12 DXF, como recomendación se debe trabajar por capas en el AUTOCAD; es decir las labores verticales en una capa, las labores verticales en otra de tal manera que el manejo de datos al cargarlo al software Ventsim Visual 3D sea más eficiente y no se dupliquen los datos. El isométrico de ventilación se muestra en la Figura 10 del Apéndice 2.

Al momento de importar los ejes de las labores con el formato R12 DXF se debe tener especial cuidado en alimentar las características propias para que el modelamiento sea lo más cercano a la realidad; es decir la simulación debe representar un 95% de la realidad. El software Ventsim Visual usa un entorno gráfico DIRECTX para el procesamiento y programación de datos, este entorno gráfico es ligero lo que hace que el software no requiera de una computadora de gran capacidad de video para correr eficientemente (500 MB de referencia). Adicional a esto el software Ventsim debe su eficiencia y rapidez al lenguaje de programación en cual fue estructurado, todos sus algoritmos son en VISUAL BASIC, lo que hace al software ágil y bastante práctico [8]. La ventana de ingreso de información general al software Ventsim se muestra en la Figura 4.



Figura 4. Se muestra la ventana del Software Ventsim en la cual se cargan los datos manualmente.

La ventana de ingreso de puntos de curva característica para un modelo de ventilador al software Ventsim se muestra en la Figura 5.

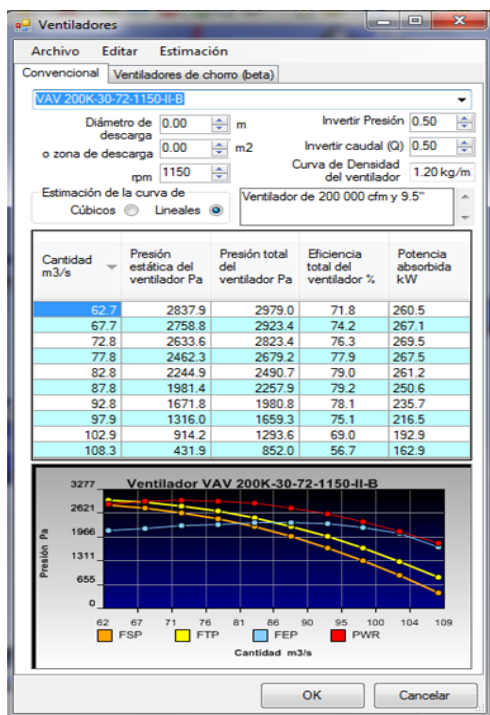


Figura 5. Puntos de curva característica de un ventilador de 94.39 m³/s (200,000 ft³/min) y de doble etapa.

En la imagen anterior se muestra los parámetros de entrada para cada ramal asignado, si de acuerdo al criterio del modelador existen varios ramales de interior mina que tienen similares o muy parecidas características se pueden cargar estas seleccionándolas todas y cargándolas de una sola vez o copiando las características en con el uso de la barra de herramientas del software. Para el ingreso de atributos se debe usar tablas de consulta para el uso del factor de fricción o se debe usar el tipo de roca que está en el campo de acuerdo a las herramientas disponibles se debe realizar el ingreso de datos. Lo recomendable es realizar el cálculo en el campo del factor de fricción y posteriormente el cálculo de resistencia de la labor.

4.3.2 Alimentación de Data para los Ventiladores

La selección de los ventiladores se debe realizar de acuerdo a la curva característica de ventiladores del fabricante debe entregar de cada equipo de ventilación es decir junto a la ficha técnica del ventilador y teniendo en cuenta el punto de operación de la mina. La ventana de ingreso selección de un modelo de ventilador con software Ventsim en el punto de operación de la mina se muestra en la Figura 6.

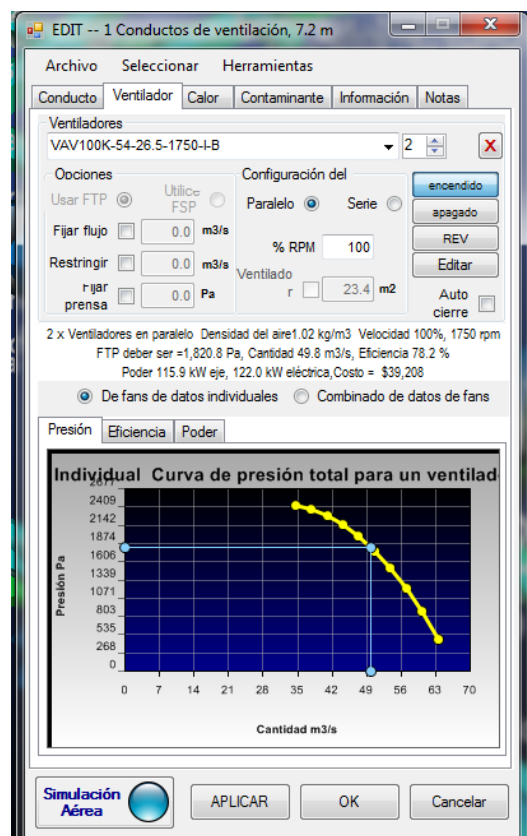


Figura 6. Punto de operación de un ventilador de 100,000 CFM y de una etapa.

Al realizar la corrida de simulación se debe revisar que el punto de operación (punto de trabajo del ventilador) se encuentre dentro de la curva de trabajo del ventilador.

4.3.3 Resultados de la Simulación de la red de Ventilación

Al realizar la simulación del panorama actual de toda la mina se presentaron algunos por menores fáciles de corregir como algunos cabos sueltos (ramales sin conexión) y algunos circuitos de ventilación sin conexión pero estos se pueden corregir fácilmente con la ayuda de la barra de herramientas del software Ventsim Visual.

Para revisar en qué estado se encuentra la red actual de mina y realizar la simulación respectiva se debe analizar cada sub sistema de aire en interior mina; por ejemplo nosotros hemos analizado el ingreso y salida de aire de cada cuerpo mineralizado a saber OB1, OB2, OB5 OB6 A y B y OB8.

Para la selección preliminar del modelo adecuado del ventilador de acuerdo a la altitud, caudal, presión y potencia requerida del motor, se utilizó el software de selección de Axiales Mineros de la fábrica de ventiladores peruana Airtec. Asimismo se obtuvo los puntos de la curva característica del ventilador seleccionado que fueron alimentados posteriormente al software Ventsim visual.

Luego de alimentar la información de los parámetros básicos al software Ventsim como la sección de la labor, longitud, resistencia a cada labor subterránea cuyo reporte de simulación se muestra en la Tabla 3.

Tabla3.Reporte simulación por el software Ventsim.

OB	Nivel	Labor	Q(m/s)	V(m/s)
2	1680	Cx 020	14.1	0.7
2	1680	Cx 056	18.4	1.0
2	1680	Bp 131	17.4	0.9
2	1680	Cx 056	66.1	3.5
2	1680	Bp 131	17.7	0.9
2 y 5	1680	Bp 745A	3.4	0.2
2 y 5	1680	Bp 745 B	22.4	0.9
2 y 5	1680	Cx 019	13.7	1
2 y 5	1710	Bp 745 A	20.6	1.1
2 y 5	1710	Bp 745B	15.7	0.8
2 y 5	1710	Cx 019	12.0	0.6
2 y 5	1740	Bp 745 A	0.0	0.0
2 y 5	1740	Bp 745B	23.7	1.2
2 y 5	1740	Cx 019	23.3	1.2
5	1680	Bp 745 A	14.5	0.8
5	1680	Bp 745 B	29.8	1.6
5	1680	Cx 019	56.3	3.0
5	1710	Bp 105A	12.7	0.7
5	1710	Bp 105B	26.9	1.4
5	1710	Cx 005	56.3	3.0
5	1740	Bp 105A	0	0
5	1740	Bp 105B	17.6	0.9

5	1740	Cx 005	31.8	1.7
---	------	--------	------	-----

Este análisis se realizará corroborando las velocidades en los puntos de ingreso de aire y salida de cada cuerpo mineralizado y el circuito se ira ajustando en forma dinámica de acuerdo a cada comunicación, avance, apertura de tajos u otros que afecten la velocidad del aire en una labor. Este ajuste se da por colocación de desmante que se representa como perdida por choque, equipos inoperativos, limpieza de tajos en producción apertura de chimeneas, movimiento de ventiladores, ajuste por rugosidad de las labores, ajuste por rendimiento del ventilador, entre otros principalmente. Luego de analizar cada sub sistema de ventilación por cuerpo realizado y ajustado brindara el ajuste del modelo en el software Ventsim visual.

Los resultados de la red de simulación se encuentran calibrados dentro de un rango de error del 4.8%.

5. Diseño del Sistema de Ventilación Proyectado a 18,000 tpd

5.1 Construcción de Chimeneas de Ventilación

Se requiere la construcción de 1,820 m de chimenea de 3.1 m de diámetro como se muestra en la tabla 4.

Tabla 4. Proyectos de construcción de chimeneas

Equipo	Chimenea	Cx	OB	Diam. (m)	Long. (m)
RD 3250	RB705	705	6	3	140
RD 3250	RB705B	705	6	3	245
RD 3250	RB784	784	6	3	90
RD 3250	RB050	050	1	3	90
RD 3250	RB945	945	6B	3	100
RD 3250	RB730	730	6B	3	105
RD 3250	RB784B	784	6	3	290
71 RQ	RB932	935	2B	3	100
71 RQ	RB953	953	2	3	60
71 RQ	RB745	745	6B	3	140
71 RQ	RB936	936	2	3	290
71 RQ	RB785	785	2	3	170
Total					1820

Luego de alimentar la información de las características aerodinámicas y luego de realizar la simulación de la simulación de ventilación de la Ch-705 desde el nivel 1820 al nivel 1925 con el software Ventsim el cual se muestra una vista en la Figura 7.

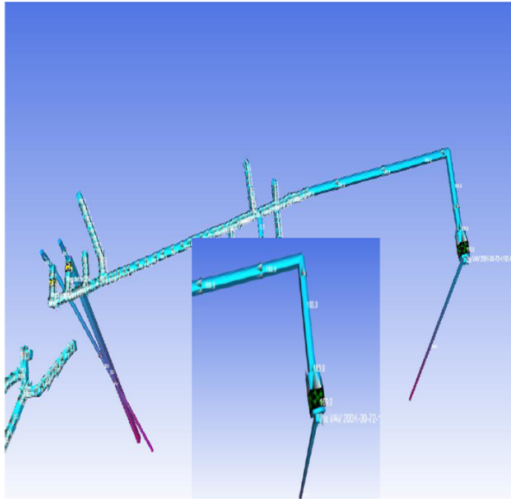


Figura 7. Simulación de la Ch-705 desde el nivel 1820 al nivel 1925.

5.2 Selección de Ventiladores

Nuestro sistema de ventilación es por succión por lo que para incrementar la cantidad de aire en 283.16 m/s (600,000 ft/min) debemos sacar 283.16 m/s (600,000 ft/min) mediante extractores principales. Considerando que por una labor de sección típica de 5m x 4m salen 18.6 m/s (39,411 ft/min) a una velocidad de 1m/s, y considerando una velocidad de evacuación de 18 m/s por una labor podemos extraer 334.8 m/s (709,407 ft/min), es decir se requerirá una bocamina adicional para la extracción estrictamente de aire, esta labor se muestra en la Figura 8.

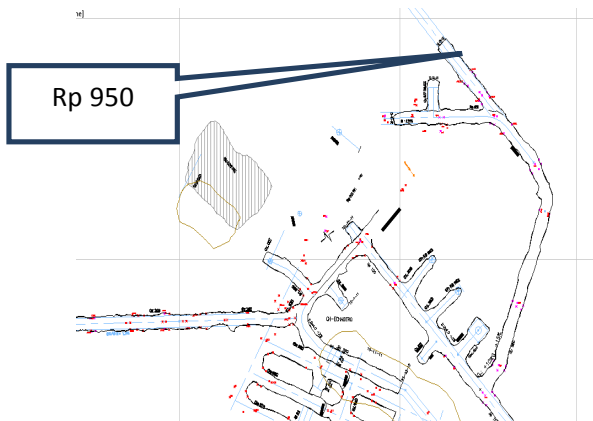


Figura 8. Bocamina Rp 950 que saldrá a superficie.

De acuerdo a la ley de los ventiladores se obtuvo las siguientes ecuaciones según el manual y diferentes textos sobre Ingeniería de Ventiladores [6-7].

$$Cp = RQ^2 \quad (1)$$

$$R = \frac{k \cdot Per \cdot L}{A^3} \quad (2)$$

Dónde:

Cp : Caída de presión del sistema, Pa

R : Resistencia total de la mina, NS/m⁸

Q : Caudal total, m/s

K : Coeficiente de fricción, kg/m

Per : Perímetro de la labor, m

L : Longitud de la labor, m

A : Área transversal de la labor, m²

Considerando:

$$R = 0.00209 NS^2/m^8$$

$$Q = 665.3 \frac{m^3}{s}$$

249.1 Pa = 1" de agua

$Cp=3.70$ Pulgadas de agua. Tomando en cuenta un factor de pérdidas de 40% un total de 5.18" de agua. Se realizaron varias simulaciones en el modelo de Ventsim con ventiladores de 141.58 m/s (300,000 ft/min), 117.98 m/s (250,000 ft/min) y ventiladores de 94.39 m/s (200,000 ft/min) los equipos que optimizaron las labores de extracción de aire viciado, los sistemas de aire en interior mina y el consumo de energía eléctrica fueron los ventiladores de 94.39 m/s (200,000 ft/min) y de 9.5" de agua de presión total a 1,820 msnm.

Los ventiladores de 94.39 m/s (200,000 ft/min) será instalados en paralelo en la Rp 950 Nv 1970 que conecta a superficie para poder extraer esta cantidad de aire requerido.

Los puntos de operación del ventilador de 94.39 m/s (200,000 ft/min) que optimizo el sistema de ventilación para la ampliación de la mina Cerro Lindo se muestra en la Figura 9.

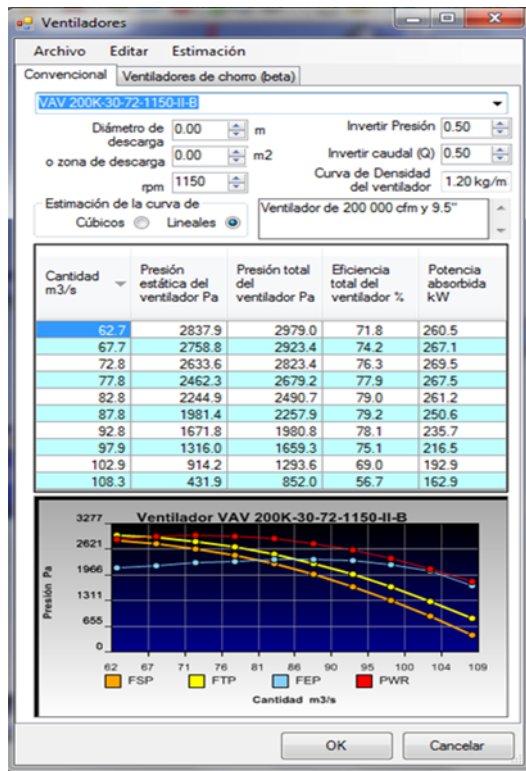


Figura 9. Puntos de operación del ventilador de 94.39 m/s (200,000 ft/min) que optimizo el sistema de ventilación.

Estos ventiladores de acuerdo al modelamiento serán de 182.88 cm de diámetro interno (72" de diámetro interno), 1,750 RPM de una sola etapa y tipo B.

Si bien es cierto solo se requieren de acuerdo al modelamiento 5.18" de presión total de agua, nuestra mina crecerá para lo cual la resistencia global de la mina también crecerá además se debe tener en cuenta que las bocaminas de ingreso de aire son obstruidas parcialmente por volquetes lo cual genera una fuerte resistencia a los ventiladores principales. Por estas razones se eligió un ventilador de 9.5" de agua de presión total de agua lo cual puede estar sujeto a variaciones de 20% de acuerdo a los proveedores. También se realizó la simulación de estos ventiladores en el peor escenario es decir cuando las bocaminas de ingreso de aire son parcialmente tapadas por volquetes de 35 toneladas de capacidad, lo cual afecta directamente a los ventiladores principales es decir sus puntos de operación varían de acuerdo a la variación de la resistencia del sistema, por lo que se hace necesario la construcción de dos bocaminas de ingreso de aire fresco para poder optimizar el rendimiento de los ventiladores principales.

5.3 Resultados Obtenidos de la Simulación

Para la ampliación a 18,000 tpd es necesario un caudal de ingreso de aire fresco de 965.67 m³/s (2,046 151 ft/min) con lo cual se hace necesario incrementar un caudal de ingreso de 283.17 m³/s (600,000 ft/min) para cubrir la demanda en más del 100% de cobertura, para este efecto se analizaron escenarios y se necesitan inicialmente 3 ventiladores de 94.39 m/s (200,000 ft/min) y 9.5" de agua de presión total, estas características permitirán en el futuro realizar ajustes a los alabes de estos ventiladores con lo cual se podrá realizar una ampliación del caudal de los mismos y también se tuvo en cuenta el incremento de la

resistencia global de la mina en el tiempo para los 7 años próximo de operación.

6. Evaluación Económica del Proyecto

Se requiere tener dos equipos RB que realicen construcción de chimeneas de 3.1 m de diámetro y una cuadrilla de preparación de labores estrictamente para ventilación.

El resumen de costos de capital tanto en avance vertical, el avance horizontal proyectado y la adquisición de tres (3) ventiladores principales axiales de 94.39 m/s cada uno y los costos operativos para ampliar la ventilación para una producción de 18,000 tpd se muestra en la Tabla 5.

Tabla 5. Costo de capital y costo operativo.

Costo total de inversión			
Descripción	Cantidad	Precio	Sub total (\$)
Avance vertical	1,820 m	1,500 \$/m	2'730,000
Avance horizontal	1,120 m	1,200 \$/m	1'344,000
Ventilador 94.39 m/s	3 und.	150,267\$/und.	450,801
		Costo capital (\$)	4'524,801
		Costo operativo (\$)	1'809,920

7. Discusión y Conclusiones

El sistema principal de ventilación en CERRO LINDO está gobernado por los extractores principales que están en los niveles superiores de extracción de aire viciado, en estos niveles se encuentran bocaminas de extracción de aire viciado Nv 1940 Bocamina Bp 105, Nv 1970 Bocamina Alimak y Nv 1970 Bocamina Bp 105, los vacíos que generan estos ventiladores hace que ingresen aire limpio por las bocaminas de ingreso de aire

El avance vertical para la ampliación es 1,820 m en chimeneas verticales de 3 m de diámetro, esto solo se podrá realizar con el alquiler de una máquina de RB adicional, sin esta infraestructura de ventilación no se podrá cubrir la necesidad de aire requerido de acuerdo al DS 055 2010 EM.

El máximo caudal que pueda pasar por una labor típica de 5m x 4m para las características de nuestra unidad es de 335 m³/s (710,000 ft/min).

El caudal de ingreso de aire fresco en la actualidad 1 305,390 CFM y para la ampliación a 18,000 tpd se requiere 587,232 CFM, es decir requerimos evacuar mínimamente 600,000 CFM adicionales, la selección de estos ventiladores debe considerar la ampliación posterior de la mina hasta donde los parámetros aerodinámicos lo permitan, este diseño se cubrió al usar ventiladores axiales de ángulos de alabe variable, la presión fue determinada de tal forma que pueda disminuirse la presión total y aumentar el caudal de

extracción de cada ventilador axial, esto se realizara en la curva de operación de cada ventilador.

De acuerdo al software de modelamiento Ventsim visual Premium y el software de selección preliminar de ventiladores auxiliares de la fábrica de ventiladores peruana AIRTEC; entonces los ventiladores más adecuados para la realidad de nuestra unidad minera son ventiladores axiales de 94.39 m/s (200.000 ft/min) y 9.5" de agua de presión total a 1,970 msnm.

Si se comunica la Rp 950 a superficie el aire de limpio ingresara por esta labor y será evacuado por las bocaminas de extracción de aire viciado que están en los niveles 1970 y 1940, es decir que este aire no recorrería interior mina lo cual sería muy perjudicial para nuestra unidad minera. El aire que ingresaría y se desperdiciaría según el modelamiento es de 166.12 m/s (352,000 ft/min).

Al incrementarse la capacidad de extracción de aire viciado se incrementa el ingreso de aire limpio por las bocaminas de ingreso de aire principales, con el aumento de la velocidad en estas bocaminas de ingreso de aire fresco la temperatura promedio sería de 16°C de acuerdo al modelamiento y medición en campo, lo cual no es bueno para la salud de los trabajadores que salen de los frentes de trabajo que están a 30 °C.

El costo de energía respecto al costo total de ventilación representa el 75% lo cual indica que el comportamiento del costo del área está influenciado directamente por el consumo de energía eléctrica.

El diámetro óptimo para nuestra unidad minera que contiene todas nuestras características aerodinámicas, costos de energía, costos de operación y otros parámetros es 3.24 m, nuestros equipos de RB realizan chimeneas de 3.1mts de diámetro lo cual es bastante cercano al diámetro optimo diseñado.

Para definir la ubicación más apropiada de la bocamina de entrada y/o salida de aire se debe revisar la dirección de los vientos durante el año, esta información la proporciona el are de medio ambiente de la unidad. Esta dirección de vientos siempre debe ser favorable a la dirección de salida o entrada de aire por estas bocaminas ya que se tiene un ahorro sustancial de costo de energía. Además se debe considerar como se alimentaran de energía los ventiladores y sus variadores, y el tipo de roca sobre el cual será construida esta infraestructura, en lo posible.

Los resultados del modelamiento son influenciados directamente por el grado de aproximación que tiene el modelo de ventilación en el software Ventsim a la realidad con una aceptación de 95% de error, este ajuste se debe realizar en forma constante, periódica o cada vez que se realice cambios en los sistemas de ventilación primarios o secundarios. Los resultados obtenidos en el software de modelamiento deben ser corregidos de acuerdo a la experiencia del modelador y la realidad de la mina un dato aceptable es incrementar el 20% del valor obtenido en la simulación.

Es necesario realizar dos bocaminas más de ingreso de aire fresco para no incrementar la velocidad de aire en las bocaminas de ingreso de personal actualmente, una bocamina debe ser estrictamente de ingreso de personal.

En nuestra unidad minera de las tres bocaminas de ingreso de aire fresco dos de ellas sirven de ingreso y salida de volquetes de 35 ton que ocupan un 70% del área transversal de la bocamina lo cual genera gran resistencia en el sistema de ventilación y hace que los ventiladores principales según el modelamiento trabajen en otro punto de operación, en este tipo de escenario es necesario realizar el modelamiento porque tenemos una flota de 38 volquetes de los cuales 15 salen y entran de interior mina creando resistencia en las bocaminas de ingreso de aire fresco.

Referencias

- [1] Reglamento de seguridad y salud ocupacional en minera D.S. N° 055 (2010-EM) 119-127.
- [2] Howard L. Hartman, SME Mining Engineering Handbook – Society for Mining, Metallurgy, and Exploration, Inc. USA 1992.
- [3] Malcom J. Mc Pherson, Subsurface Ventilation Engineering, California 2009.
- [4] Pablo Jiménez Ascanio, Ventilación de Minas Subterráneas y Túneles, Lima 2011
- [5] José Corimanya, Capacitación de Ventilación de Minas en mina Cerro Lindo, Chíncha Enero 2014.
- [6] Fan Engineering, Published by Buffalo Forge Company, New York 1961.
- [7] Howard L. Hartman, Mine Ventilation and air conditioning, Third edition Jhon Wiley & Sons, INC, New York 1997.
- [8] Craig Stewart, Manual de software para diseño y ventilación de minas subterráneas Ventsim visual advanced Enero 2014.

Apéndice 1

Tabla 6. Instrumentos de usados en la medición de parámetros de ventilación minera.

Inventario - Equipos de Medición				
	Equipo	Marca	Modelo	Cantidad
1	Anemómetro	Kestrel	4500 NV	1
2	Anemómetro	Kestrel	4000	2
3	Anemómetro	Delta OHM	HD 2103.1	2
4	Anemómetro	Trotec	TA300	1
5	Tubo de pitot	Dwyer	Serie 160	4
6	Bomba de Muestreo	MSA	Kwik Draw	6
7	Montajes para tubos de humo	MSA	---	6
8	Psicrómetro	---	---	2
9	Tubo de Humo	MSA	---	8
10	Manómetro	Dwyer	2025	1
11	Detector de gases	Drager	X-am 5600	1
12	Distanciómetro	Leica	D5	1
13	Sonómetro	AEMC	CA 832	1

Apéndice 2

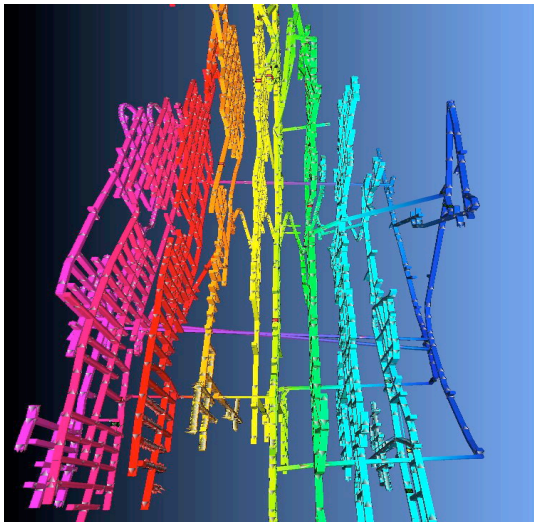


Figura 10. Isométrico de ventilación mina Cerro Lindo.

Apéndice 3

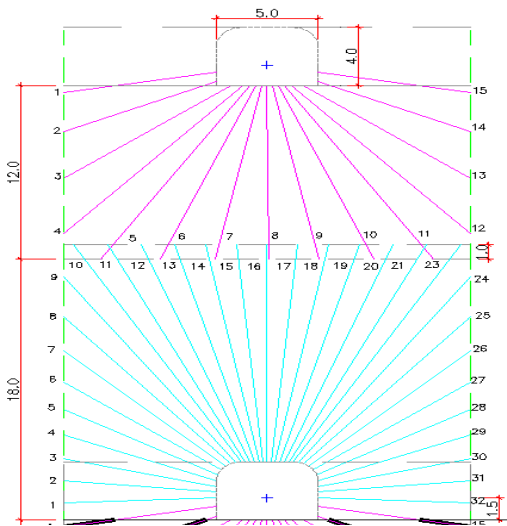


Figura 11. Perforación típica que se viene empleando en Cerro Lindo.

Effect of the Air Gap Associated with Cave Evolution on Cave Resistance

D. Eroglu^a, A. Baysal^a, K.M. Ajayi^b, P. Tukkaraja^c, K. Shahbazi^c, K. Katzenstein^c and D. Loring^d

^a M.S. Student, South Dakota School of Mines & Technology, Rapid City, USA.

^b Ph.D. Student, South Dakota School of Mines & Technology, Rapid City, USA.

^c Assistant Professor, South Dakota School of Mines & Technology, Rapid City, USA.

^d Chief Mine Engineer, Freeport-McMoRan, Inc.

Block caving is a large scale mining method, involving the undercutting and bulk extraction of ore through caving. This method is a feasible option for mining low grade, massive and disseminated mineral deposits that are too deep for conventional open-pit mining. As the rock breaks in the caving process, hazardous gases are released into the working areas of the mine that could create dangerous working conditions. Therefore, adequate precautions need to be taken to divert or dilute these gas concentrations to ensure the safety of mine personnel. Airflow is the primary method of controlling atmospheric conditions in underground mines. To design an effective ventilation system for a block cave mine, it is extremely helpful to predict the resistance of the cave area to airflow. Prediction of cave resistance is difficult due to the dynamic nature of the cave as it changes with respect to the cave propagation. Traditional measurement and ventilation modeling methods have been shown to provide imprecise results with respect to resistance of the caved area. Since cave resistance is related to the height of air gap associated with cave evolution, this research is focused on predicting a relationship between cave resistance and the height of air gap. Previous studies indicate that numerical modeling is a viable option to visualize the flow of incompressible fluids through porous rocks in a closed area. Hence, SC/Tetra, a Computational Fluid Dynamics (CFD) numerical simulation software package, is used to better understand the role of an air gap in the resistance of the evolving block cave area.

Keywords: block caving, air gap, cave resistance, CFD

1. Introduction

Caving methods are the preferred means of extracting large and low grade deep ore bodies that are present at depths that are not economic for traditional open-pit mining methods. This preference is due to the low cost and high productivity offered by caving. Many deep open-pit mines are switching to cave mining due to the increasing depth of the ore bodies. Currently, there are about 20 block or panel cave mines in operation all over the world. These include: Rio Tinto's Argyle diamond mine, Petra Diamond's Cullinan, Finsch and Kimberly diamond mines in South Africa, Codelco's three copper mines in Chile, DOZ copper mine in Indonesia, Northparkes and Ridgeway Deeps copper mines in Australia, Padcal, Palabora and Tongkuangyu copper mines in Philippines, South Africa and China respectively. Also, there is Newcrest Mining Company's Cadia East gold mine in Australia, New Gold Company's New Afton Gold mine in Canada, Shabani mine for asbestos in Zimbabwe and Freeport McMoRan's Henderson molybdenum mine in Colorado, USA. [1].

The caving process involves undercutting and extraction of broken rock from drawpoints located on

a production level. When the plan area of the mining footprint reaches a large enough dimension, a self-sustained propagating cave will develop as long as the broken and bulk ore continues to be withdrawn [2].

The block caving method includes multiple engineering challenges such as geotechnical risks in terms of ground control, and ventilation plans implemented to mitigate toxic gas concerns associated with rock fragmentation. During the caving process, different gases can be released into the mine working area or into the airstream. These gases might be dangerous to human health and adequate precautions should be taken to remove or dilute these gases.

Among the dangerous gases, radon is of major concern in block cave mines where uranium mineralization is present in the ore that is being mined.

Radon is a radioactive gas; it decays into polonium-218 (RaA) in 3.82 days, which then decays into lead-214 (RaB) in 3.05 minutes, which then decays into bismuth - 214 (RaC) in 26.8 minutes

which further decays into polonium - 214 (RaC') in 19.7 minutes and finally it decays into a stable element, lead - 210, in 164 micro-seconds. During the disintegration process radon and its daughters (RaA, RaB, RaC, RaC') release alpha, beta and gamma radiation which, if prolonged exposure occurs, are dangerous to human health [3].

During the caving process, as the rock breaks, radon and its daughters are generated and travel through the caved ore body to drawpoints on the production level [4].

This is an important concern with respect to the design and operation of the mine ventilation system. In the US, according to Mine Safety and Health Administration (MSHA) regulations, radon concentrations are to be maintained below 1.0 working level (WL) in all working areas of the mine. One of the approaches to reducing the radon concentrations in the mine is to optimize the ventilation system.

Optimization of ventilation system requires accurate estimation of gas emissions into the mine working areas and the prediction of cave resistance to the airflow. These parameters are difficult to predict in block caving mines, because of the dynamic nature of the caving method and the complex behavior of radon gas, as it decays into radon daughters. Furthermore, alterations in the height of air gap affect cave pressure and resistance. These variations make this issue even more multifaceted. However, traditional ventilation techniques cannot accurately estimate the gas emissions and the cave resistance values.

This paper presents a numerical approach for predicting a cave resistance to the airflow as cave evolves. Previous studies indicate that CFD simulation techniques were successfully used in predicting ventilation system design parameters, such as pressure drops, shock losses, and gas emissions in both coal and non-coal mines. Therefore, a CFD software package, SC/Tetra, is used in this study.

2. Cave Resistance

Accurate prediction of cave resistance to airflow is important in block caving mines with radon concerns. Due to the dynamic nature of an evolving cave, its resistance changes with respect to the cave propagation. There are several factors that affect the resistance as a cave evolves. However, the main factor is air gap. Since cave resistance is a function of air gap and air gap's height changes with respect to the cave propagation. Traditional pressure and quantity survey techniques cannot predict the cave resistance.

A conceptual model of the developing cave, described by Duplancic and Brady [5] consists of five main behavioral regions which are shown in Figure 1.

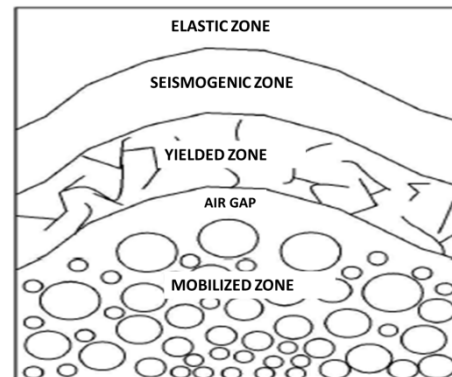


Fig. 1. Conceptual caving model after Duplancic and Brady [5].

The main behavioral zones are the elastic (pseudo-continuous domain), seismogenic, yield, air gap and caved zone. The caved zone is the region that has responded to production draw, while the yielded zone is a fractured region and has lost some or all of its cohesive strength and provides minimal support to the overlying rock mass [6].

2.1 Air Gap

In block caving method, the broken rock moves downwards when as rock is drawn from the drawpoint in the production drift. The rock in the yield zone doesn't break immediately as it retains some level of cohesion. There exists an air gap between the broken rock and the yield zone above it [6]. In the caving process this air gap is created intentionally to remove support from the caved rock mass, and to help improve the rock fragmentation [7].

The air gap directly affects the safety of block cave mining. So, the majority of caving operations monitor the size of the air gap through micro-seismic and/or time-domain reflectometry (TDR) cables to ensure that it does not reach an unsafe size. Production could be slowed or halted if the production outpaces the caving process and the air gap grows too large. The large air gap could create an air blast from a sudden collapse of the rock from the yield zone. Such an accident happened in the Northpakes Mine in November, 1999. This event led to the death of four people and underscores the importance of understanding the mechanics behind cave evolution.

Another reason to control the air gap is dilution. Hoek stated that the opening through which a group of particles can flow must be greater than three times the average particle size in order to overcome the

arching effect [8]. If the air gap is too small, fragmentation can be limited and arching can lead to difficulties in ore production.

The height of the air gap depends on two parameters: the extraction and rock breaking rates. Over extraction rates lead to larger heights of air gap that should be avoided in block cave mines to prevent air blasts.

Understanding the phenomenon of airflow through broken rock and the air gap is critical in designing an effective ventilation system for block cave mines. As the airflow reaches the cave, it faces dynamic and complex zones, in terms of airflow resistance. Hence, this study investigates the effect of changes in the air gap height on the resistance factor for a steady cave.

3. Methodology

A 2D cave geometry shown in Figure 2 was utilized for analyzing the effect of air gap height on the cave resistance. This geometrical model represents a typical block cave with caved zone, air gap, drawpoints and both production and undercut drifts.

The production level is a major concern for ventilation due to production of gases and dust from load, haul and dump activities [9]. On the other hand, the undercut level is of concern during the development stage of the cave as it is typically ventilated with positive pressure and some of this air moves through the air gap and broken rocks and could transport gases to the production level.

Existing literature indicates that the size of the air gap varies based on different scenarios. Carlson and Golden described a scenario at the Henderson Mine where the air gap is 9 m [10]. Nat and Tony described a scenario of high propagation, where the air gap ranges from 30-60 m [11]. In order to investigate these scenarios, eight different air gap heights: 4 m, 8 m, 10 m, 12 m, 18 m, 20 m, 23 m and 33 m were modeled, while keeping the remaining parameters of the cave geometry the same.

The velocity of airflow in the production and undercut drifts were modeled as 2.0 m/s and 1.276 m/s respectively. These values were based on the ventilation data from one of the panel cave mines.

Steady state, incompressible, and turbulent flow (Reynold's number = 136,449) conditions were assumed; Reynolds-Averaged Navier–Stokes and k-ε models were used for these simulations. It will be necessary to conduct analyses in the future to predict the best turbulent model applicable for block cave mining. However, in general, the k-ε model has been proven to be reliable for mining applications [12]. In summary, the conservation of mass, momentum, energy, and turbulence model equations were solved for analyzing airflow through the block cave.

SC/Tetra generates its mesh using the Unstructured Mesh Generator. Due to the complexity of the cave geometry, it is important to determine the mesh that would provide the most accurate representation of cave properties and therefore will provide reliable results. Mesh adaptation analyses were carried out for the geometry modeled.

Once the solution was converged, two planes were created on the intake and exhaust side of the cave to read the pressure values. Pressure drops were calculated based on the pressure values obtained from the CFD results. The air quantity was calculated using formula 1.

$$Q = V \times A \quad (m^3/s) \quad (1)$$

Where, Q is the air flow rate (quantity), A is the cross-sectional area of the drift (m²) and V is the velocity of the air (m/s).

Then the resistance of the cave was calculated using the square law given below.

$$\Delta p = R Q^2 \quad (Pa) \quad (2)$$

Where, Δp is the pressure drop (Pa) and R ($kL \frac{per}{A^3}$) is the Atkinson's resistance of the airway (Ns²/m⁸).

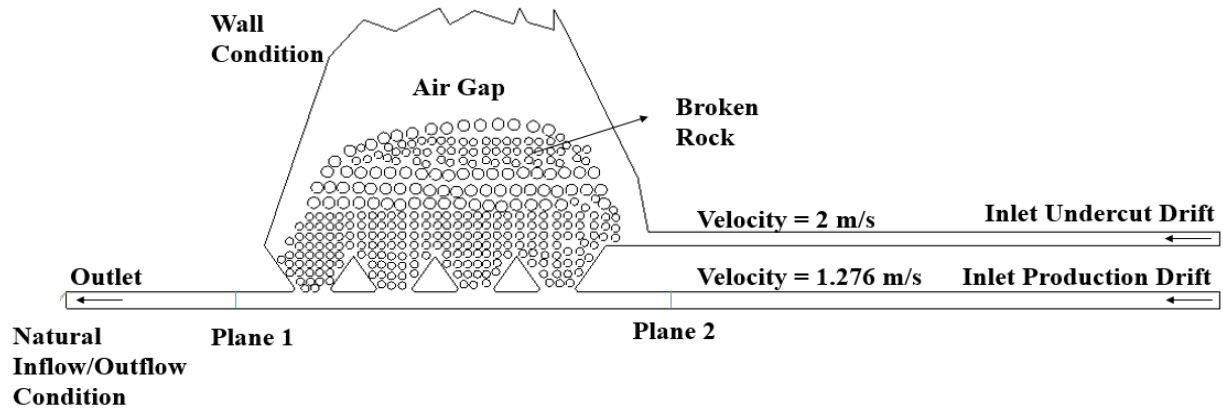


Fig. 2. 2D block cave model

As flow through a block cave is a complex phenomenon, typical flow assessment through porous media is not applicable here, as the cave's geometry is irregular. Also, flow through the cave is not similar to flow through a typical shock loss source (such as sharp bend, contraction, and expansion). Since the flow through the cave is a combination of both flow through porous medium and the shock loss source, the shock loss factor values were also calculated for the cave at eight different air gap heights.

Shock losses occur due to changes in airflow direction because of additional vortices initiated whenever there is a change of direction [3]. Several studies have been performed to analyze shock losses in different mine ventilation configurations. Jade and Sastry studied shock losses in two way splits and junctions of mine airway with CFD and experimental investigations [13], while Tukkaraja and Bandopadhyay studied shock losses at air crossings in a mine ventilation network using CFD techniques [14].

Shock losses across the cave at different air gap heights were calculated using the formula given below:

$$\Delta p_{shock} = X\rho \frac{u^2}{2} \quad (3)$$

Where X is the shock loss coefficient (dimensionless), u is the mean velocity of air (m/s), ρ is the air density (kg/m^3) and Δp_{shock} is the pressure drop across the cave.

4. Results and Conclusions

Airflow through the cave was analyzed for all eight different air gap heights; a steady state flow was developed for the optimized mesh elements.

To analyze the relationship between airflow and the pressure drop across the cave, CFD simulations were performed with six different inlet air velocities in the production drift for 33 m air gap height. Simulation results were shown in Table 1. Linear relationship was observed between the airflow and the pressure drop across the cave as shown in Figure 3.

Table 1. Cave resistance values

Air Velocity in the Production Drift (m/s)	Pressure Drop (Pa)	Air Quantity (m^3/s)	Resistance (Ns^2/m^8)
1.2760	9.6828	5.4868	0.3216
1.5760	12.9012	6.7768	0.2809
1.8760	16.8669	8.0668	0.2592
2.1760	23.3020	9.3568	0.2662
2.4760	29.1157	10.6468	0.2569
2.7760	31.9839	11.9368	0.2245

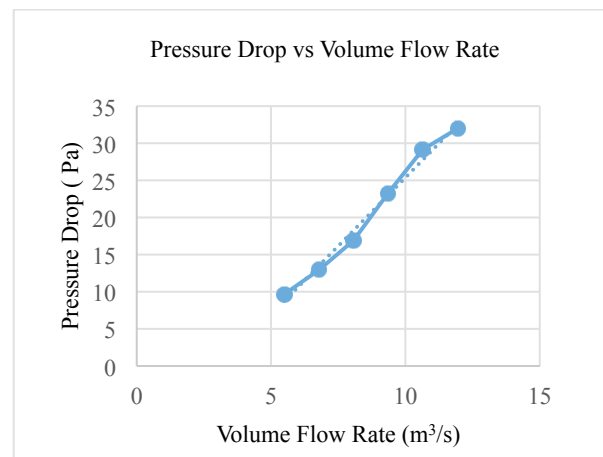


Fig. 3. Pressure drop vs volume flow rate

Velocity magnitudes and pressure contours of the cave with different air gap heights were obtained from the CFD results as shown in Figures 4 and 5.

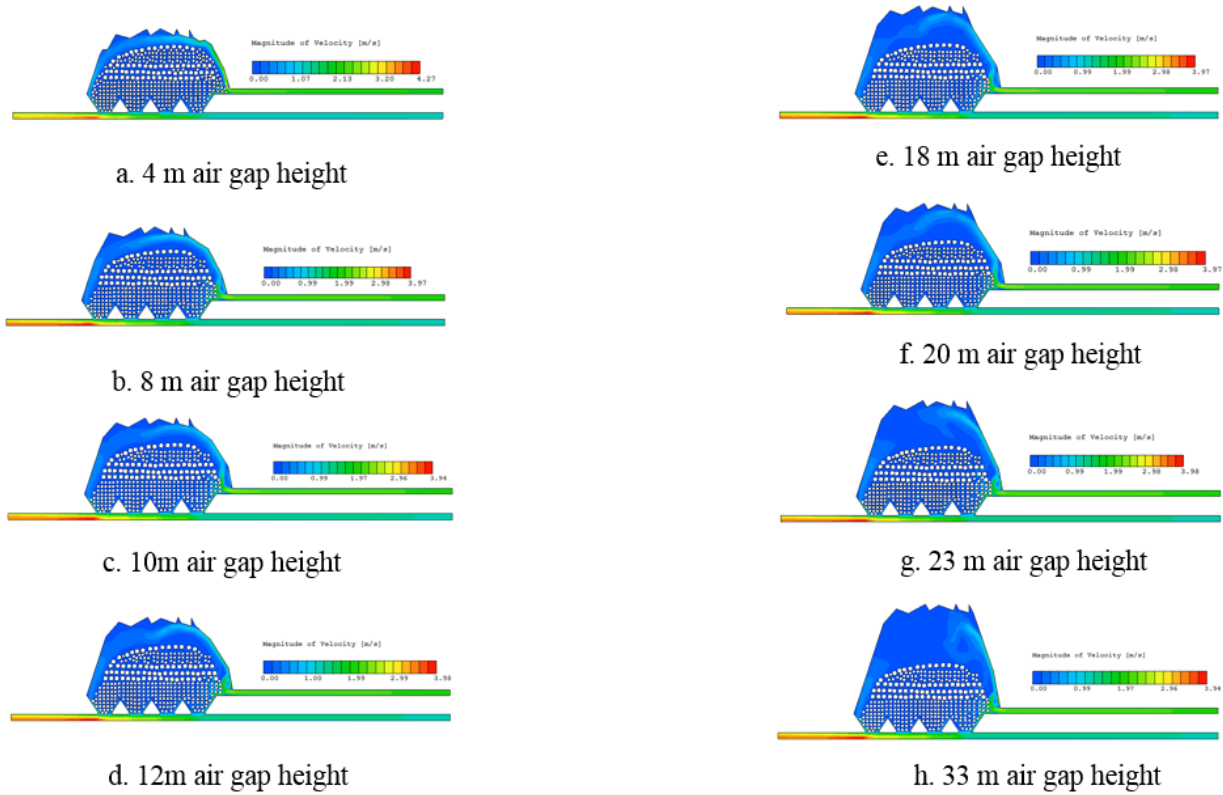


Fig. 4. Velocity magnitudes at 4 m to 33 m air gap height

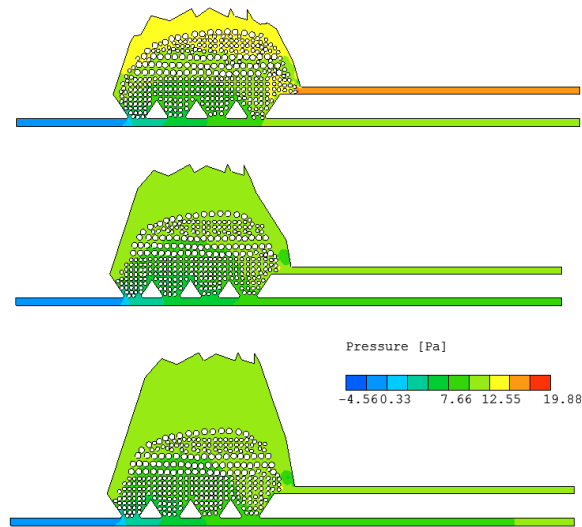


Fig. 5. Pressure contours for 4 m, 20 m and 33 m air gap heights respectively

It was observed that the size and intensity of the recirculation regions were reduced when the air gap height decreased from 33 m to 12 m; however, the opposite trend was noticed when the air gap height further reduced from 12 m to 4 m. This phenomenon was evident from the streak lines generated from the CFD results as shown in Figure 6.

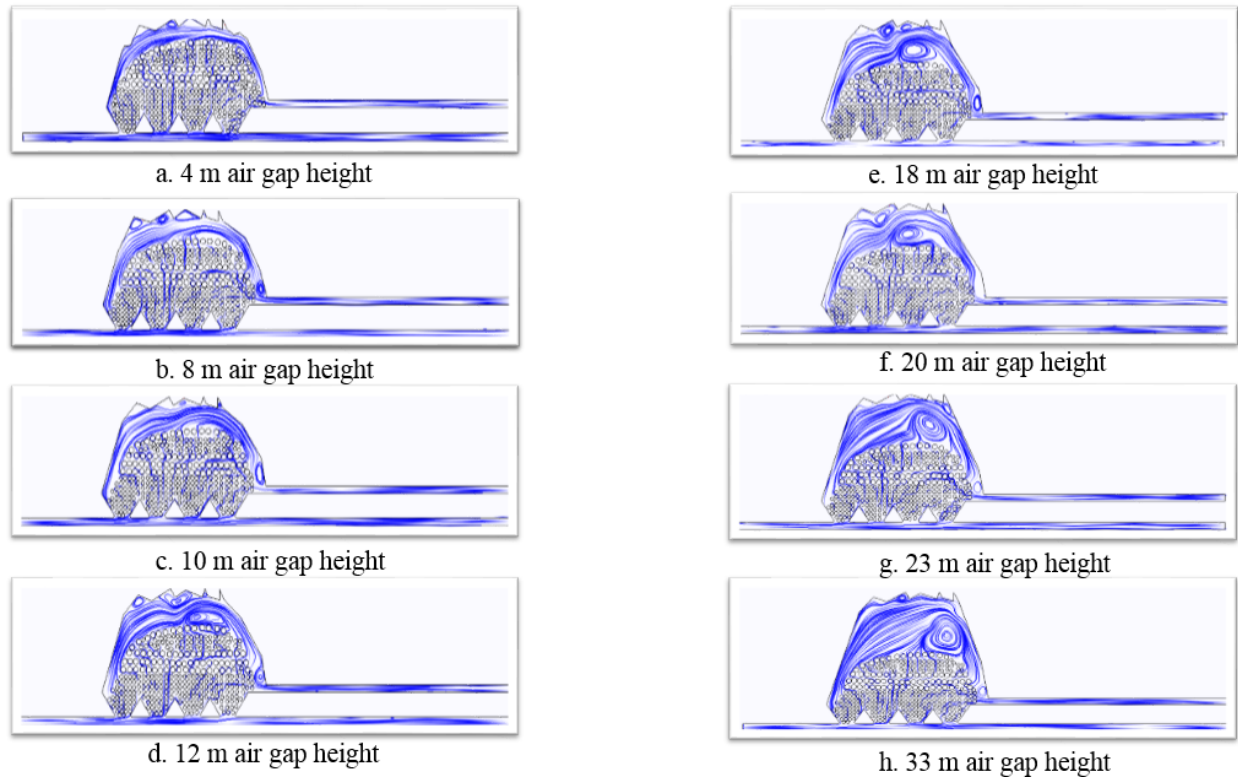


Fig. 6. Flow recirculation at 4 m to 33 m air gap height

Pressure drops across the cave were calculated from the pressure values measured at the planes that were created both on the inlet and outlet side of the cave in the CFD model. Then the resistance values were calculated using the square law (equation 2). Table 2 shows the pressure drops and resistance values of the cave for different air gap heights.

Table 2. Cave resistance values

Air Gap Height (m)	Air Quantity (m^3/s)	Pressure Drop (Pa)	Resistance (Ns^2/m^8)
33	5.4868	9.68275	0.3216
23	5.4868	9.7088	0.3225
20	5.4868	9.4375	0.3135
18	5.4868	9.4159	0.3128
12	5.4868	9.4016	0.3123
10	5.4868	9.498	0.3155
8	5.4868	9.6764	0.3214
4	5.4868	10.4569	0.3473

As shown in Figure 7, it was observed that the cave resistance value decreased when the air gap height increased from 4 m to 12 m; however, the opposite trend was noticed when the air gap height further increased from 20 m to 33 m with an exception of 12 m and 18 m air gap heights where almost the flat trend was observed. This resistance trend line indicates that, from the ventilation stand point, the optimum air gap height ranges from 12 m to 18 m.

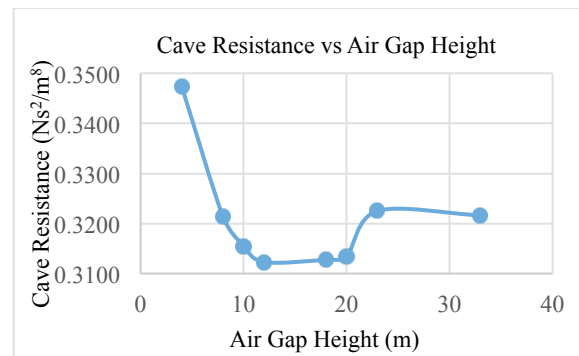


Fig. 7. Resistance vs air gap height

As it was mentioned before, since the flow through a typical block cave is a combination of flow phenomena that occurs at a porous medium, and at a shock loss source, shock loss factors were also calculated for all air gaps which are listed in Table 3. These shock loss factor values were plotted against air gap heights as shown in Figure 8. This plot depicts a similar trend that was observed with the resistance values.

Table 3. Shock loss factor values

Air Gap Height (m)	Pressure Drop (Pa)	Shock Loss Factor
33	9.6828	9.8623
23	9.7088	9.8889
20	9.4375	9.6125
18	9.4159	9.5905
12	9.4016	9.5760
10	9.4980	9.6742
8	9.6764	9.8559
4	10.4569	10.6509

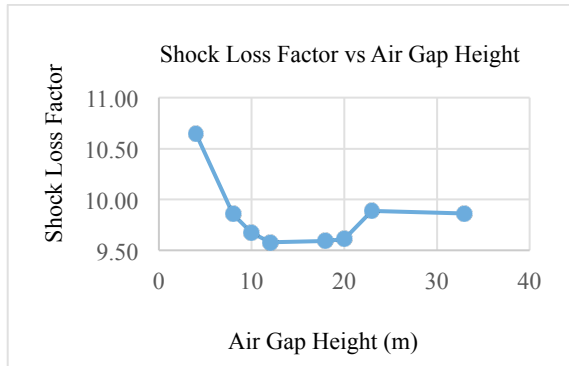


Fig. 8. Shock loss factor vs air gap

In conclusion, this study supports the hypothesis that the flow through the cave is a combination of flow phenomena that occurs at a porous medium and at a shock loss source.

5. Future Work

The cave resistance is a function of both the air gap and the porosity and permeability of the cave. Similar to the air gap, these geo-mechanical properties also change with respect to the cave propagation. Future work will involve the prediction of the cave propagation rate, the heights of different zones, and the porosity and permeability of a typical block cave particularly for caved and yield zones.

Acknowledgement

We greatly acknowledge the financial support of NIOSH (200-2014-59613), technical support from CFD software company (Cradle Co., Ltd.) and our industry partner.

References

- [1] S. Walker, "Block Caving: Mining Specialization," *E&MJ*, p. 34, 2014.
- [2] B. Sainsbury, D. Sainsbury and M. Pierce, "A historical review of the development of numerical cave," n.d.
- [3] M. J. McPherson, *Subsurface Ventilation and Environmental Engineering*, New York: Chapman and Hall, 1993.
- [4] D. Loring and E. Meisburg, "A discussion of radon and mitigation strategy at the Henderson Mine," Climax Molybdenum Company, Colorado, USA, n.d.
- [5] P. Duplancic and B. Brady, "Characterization of caving mechanisms by analysis of seismicity and rock stress. In: Proceedings of the Ninth International Congress on Rock Mechanics," Paris, France, 1999.
- [6] B. Sainsbury, "Sensitivities in the Numerical Assessment of Cave Propagation," in *Second International Symposium on Block and Sublevel Caving*, Perth, Australia, 2010.
- [7] M. H. Y. Potvin, "Interpreting Caving Mechanisms Using Microseismic Monitoring Data," in *5th International Conference and Exhibition on Mass Mining*, Lulea, Sweden, 2008.
- [8] H. Brown, *Practical Rock Engineering*, 2004.
- [9] J. P. Hurtado, O. Gutierrez and N. Moraga, "Numerical Simulation of Shock Losses at the Intake and Exhaust Raises of Block Caving Production Level," in *13th US/North American Mine Ventilation Symposium*, Sudbury, 2010.
- [10] G. Carlson and R. Golden, "Initiation, Growth, Monitoring and Management of the 7210 Cave at Henderson Mine- A case study," in *5th International Conference and Exhibition on Mass Mining*, Lulea, Sweden, 2008.
- [11] T. D. Nat Burgio, "Simulating Irregular Cave Propagation Using PCBC," in *5th International Conference and Exhibition on Mass Mining*, Lulea,

Sweden, 2008.

[12] Juan P. Hurtado, Nicolas Diaz, Enrique I. Acuna, Joaquin Fernandez, "Shock losses characterization of ventilation circuits for block caving production levels," *Tunnelling and underground space technology*, vol. 41, pp. 88-94, 2013.

[13] R. Jade and B. Sastry, "An Experimental and Numerical Study of Two-way Splits and Junctions in

Mine Airways," in *12th U.S./North American Mine Ventilation Symposium*, Nevada, 2008.

[14] P. Tukkaraja and S. Bandopadhyay, "Shock Loses at Air-crossing in a Mine Ventilatiom Network Using CFD Simulations," in *13th United States/North American Mine Ventilation Symposium*, Sudbury, 2010.

Assessment of Ventilation Circuit for Block Caving Production Level Drifts

J P Hurtado-Cruz ^a, E I Acuña-Duhart ^b, Y H San Martín-Lizana ^c, J P Vargas-Norambuena ^a

^aUniversidad de Santiago de Chile, Departamento de Ingeniería en Minas, Santiago, Chile

^bUniversidad del Desarrollo, Facultad de Ingeniería, Escuela de Minas, Chile

^cHatch, Minería y Metales Co. Chile

The current high production at block cave mines use significant numbers of diesel equipment. This equipment demands high ventilation rates of air to dilute these contaminants from the contribution of gases and dust from extracting, transporting and dumping the ore. As a result, production drifts have one of the largest airflow volume requirements in a block cave mine. The airflow to ventilate the production level is often from dedicated ventilation sublevels. Separate supply and exhaust raises are constructed to support production mining. Airflow coursing from the ventilation level to or from the production level is often coursed through a very tortuous route, with substantial head losses. These losses can result in significant energy consumption. This paper describes an analysis performed to improve geometric designs to minimize the energy consumption. Operational costs related to energy consumption are associated with design and changes were compared to optimize the result in order to increase power savings. In order to achieve this, the methodology of this study compares an experimental scale model and commercial package software of mine ventilation network, taking in account previous works about characterization of head loss to these geometries. The results shown here can be used to improve a production level mine ventilation systems to save energy while maintaining an acceptable underground mine environment for mine workers.

Keywords: block caving, mine ventilation, CFD, raises/shaft

1. Introduction

Block Cave is one of the more cost effective mining systems, which allows exploiting massive ore deposits. Their ventilation systems have evolved according to the technology state which has carried to adopt variants in the mine layout, some of that have been studied by Calizaya & Mutama [1]. Nowadays, the main production level in mechanized Block Cave systems use haul-load-dump vehicles (LHD) in the drifts production. These vehicles produce high rates of gases and dust, which must be diluted and removed with a higher airflow volume requirement according to the local law [2]. The air circuit follows from the fresh air intake to the exhaust is very tortuous, with singularities resulting in high shock losses, which are usually not properly accounted for in ventilation models resulting from a lack of available tabulated data for particular geometries [3]. Shock losses have been less studied in mine ventilation than in piping, although some previous works have given important information about shock losses for Block Cave mines.

Hurtado et al. [2-4] studied the intake and exhaust shock losses of production level drifts, mainly focused at El Teniente performance ventilation system (Figure 1), by mean of CFD techniques and laboratory modeling. This work helps to understand the turbulent behavior of airflow in a drift, developing experimental and CFD models which allow calibrating the shock losses values to a real scale size drift [3-5]. It is important to notice that secondary fans are located at fan chambers or inside of raises to supply enough airflow required and defeat head losses. Values of shock losses were obtained and also included the impact of a simple geometry modification to the curvature radius of the elbow-s, which was modelled using CFD [5-6]. The results of these studies were introduced in a commercial ventilation network program, proving an energy reduction of 25%.

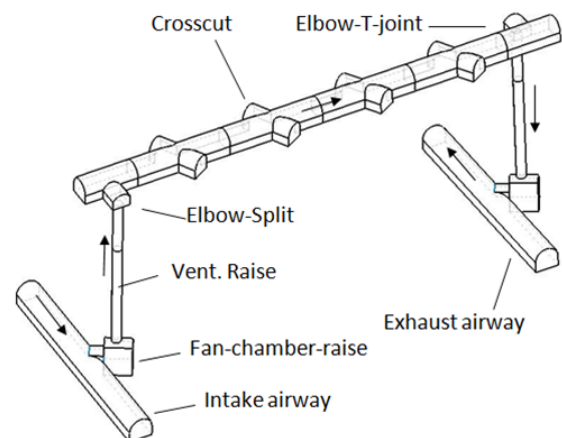


Fig. 1. General scheme of production drift ventilation system [6].

From previous mentioned works an experimental and numerical network models have been developed in a thesis work [7-8]. In this study is established a methodology to determine the operational cost per cubic meter of the circulating airflow, in terms of energy used by the ventilation system fans. That considers curvature radiuses at raises extremes and two additional diameters which were tested to ventilate a stretch of the production level according to El Teniente mine layout, using laboratory scale models. Studied geometries are shown in Figure 1 where the circuit has three main geometry singularities, namely elbow-split/T-joint, fan-chamber-raise and crosscut [6]. The stretch considers four crosscuts drifts (draw points) to ventilate from the inlet ventilation raise to the exhaust ventilation raise. Additionally it is necessary to include the fan chamber raises located in the intake and exhaust airways. The shock loss at the elbow-split/T-joint and fan chamber

raise depends on the direction of flow, which are studied separately by Hurtado *et al.* [5].

It is important to understand that this study impact on secondary ventilation. But in economic terms, the studied geometry (Figure 1) represents the most important circuit to study in block cave design systems at El Teniente layout nowadays, because it is repeated dozens or even hundreds of times.

2. Experimentation

2.1. Experimentation facilities

The singularities experimentally studied consider the geometries mentioned in the previous section. The fan-chamber-raise presents a geometric difference, in the experimental circuit it is opened, as presented in Figure 2, but in the previous works it was closed with an entrance only for the fan. It is important to take this aspect into account in the analysis because it reduces the shock loss in the geometry. Crosscut geometry is not considered in the scale circuit but it is considered further in the resistance estimation. Airway tunnel (intake and exhaust airways) has sections of 5.5 m x 5.5 m, production drifts 3.8 m x 4.0 m and raises 1.50 m diameter.

Figure 2 shows the experimental facilities. They are composed of a scale model (1:52), which was made with even wood, PVC split tubes and PVC tubes for raises; an “American Fan Company” fan model VP0404, with a TD – 5006 impeller model VP1 that was used to generate the airflow and pressure, as shown in Figure 2. A calibrated Venturi flow meter serves to measure the airflow in the system. Modifications in the curvature radius were molded with a heat gun in PVC. Figure 3 shows a modified raise with curvature radius (PVC tube) overlapped in a chamber's roof.

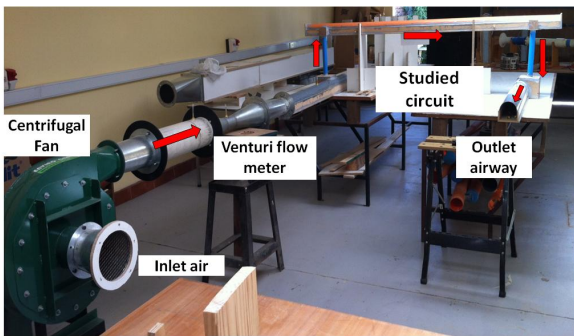


Fig. 2. Experimental facilities for the studied circuit.



Fig. 3. Modified raise with curvature radius at PVC tube.

Losses can be obtained from Equations (1) and (2), according to the static and dynamic pressures measured in the different stretches. The pressure loss and power are obtained from the square law Equation (3) and the power Equation (4), in Pascals, and kW. Figure 4 shows pressure taps that allows quantifying head losses to obtain the losses of the system [9-10].

$$P_v = Hx = X * \frac{\rho * V^2}{2} \quad (1)$$

$$X = \frac{Hx * 2}{\rho * V^2} \quad (2)$$

$$P = \frac{K * O * (L + L_e) * Q^2}{A^3} = R * Q^2 \quad (3)$$

$$\dot{W} = P * Q = R * Q^3 \quad (4)$$

Where:

\dot{W} = Power (Watts)

V = Average Velocity (m/s)

P = Pressure (Pa)

ρ = Density (kg/m³)

Re = Reynolds Number (dimensionless)

Q = Flow Rate (m³/s)

R = Resistance (Ns²/m⁸)

X = Shock Factor (dimensionless)

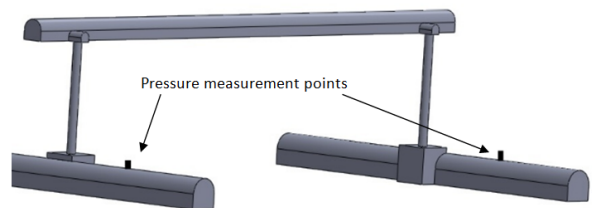


Fig. 4. Studied circuit diagram with measure points for pressure.

2.2. Raise modifications

First modification was conceived considering an operational and constructability point of view. It corresponds to the radius of curvature, which can be done with minor requirements of drilling and blasting. Diaz [6] obtained energy savings in the order of 25% with a curvature radius of 1.0 R (radius of raise), which

was found to be the optimum curvature radius. As a result, modified geometries correspond to a curvature radius of 1.0 R.

The second modification corresponds to increase of the raise diameter, which it is assumed would not generate an excessive extra cost or time to develop it. The actual diameter of raises is 1.50 m and the modifications consider 2.0 m and 2.5 m, an increment of 33.3% and 66.6% respectively. Scaled raise diameters are 28.4 mm, 36 mm and 48.2 mm, respectively. Figure 5 shows the raises modifications. It is important to highlight that including the tests for the different diameters and modifications to the radiuses for all the tested diameters, generates a total of six tests to be implemented.

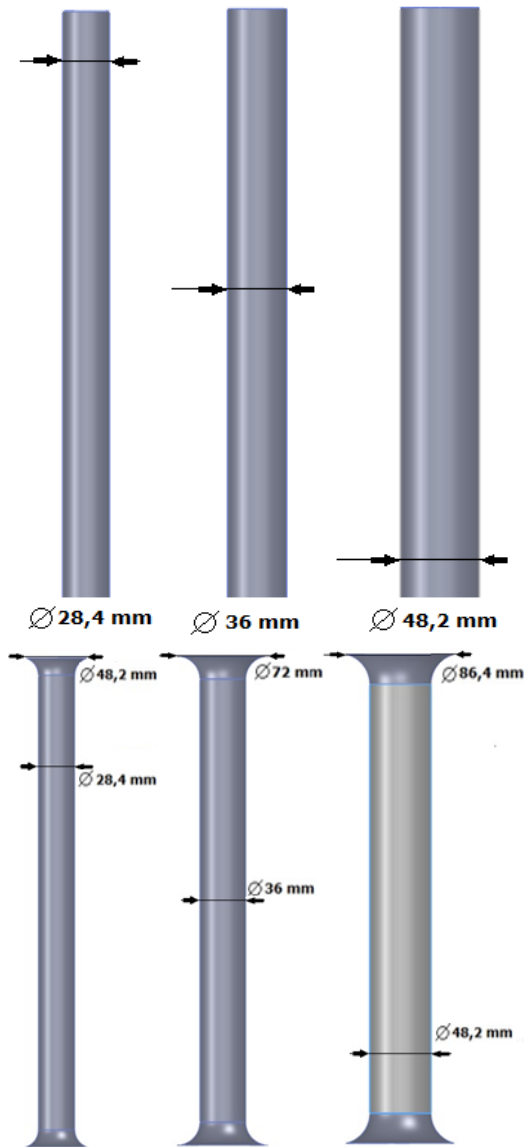


Fig. 5. Raise modification for diameter (upper figure) and diameter plus curvature radius (lower figure).

Hydraulic power can be understood as the power necessary to move the air, overcoming hydraulic losses, therefore its increment can be read as the hydraulic power which can give a fan when resistance of circuit diminishes. It is known that fans change their operational

point according to the circuit losses [9]. As expected, the carried out tests show different pressures, airflow rates and hydraulic power according to raise diameter and the modifications of curvature radius. Table 1 shows tested circuits and obtained results. Taking 1.50 m diameter as the base case and dividing by the hydraulic power to obtain an increment of hydraulic power of the system Figure 6 and 7 were obtained. Hydraulic power increment with diameter can reach approximately 90%. If increase in diameter and curvature radius is considered, the increment can reach almost 200% at maximum diameter of 2.5 m and 1.0 R curvature radius modification (2.5 m is equivalent to 48mm).

Table 1. Results obtained in the scale tested circuit.

Circuit	Pressure drop (Pa)	Flow rate (m ³ /s)	Resistance (Ns ² /m ⁸)	Hydraulic power (kW)
28.4 mm	3339	0.0263	4823894	0.088
36 mm	3269	0.0379	2271463	0.124
48.2 mm	3276	0.0503	1293536	0.165
28.4 mm Mod.	3326	0.0315	3361937	0.105
36 mm Mod.	3258	0.0539	1120777	0.176
48.2 mm Mod.	3234	0.0788	520574	0.255

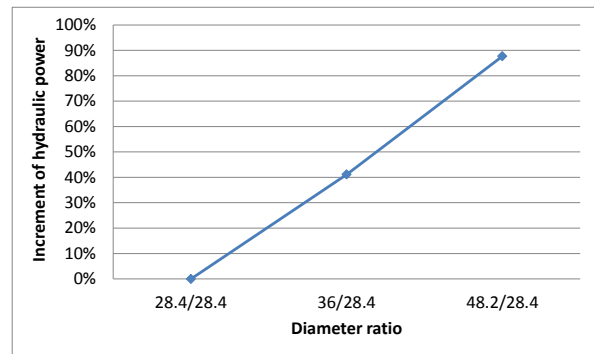


Fig. 6. System hydraulic increment for different diameters tested.

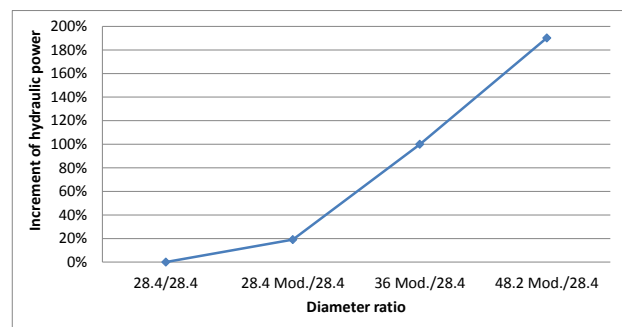


Fig. 7. Hydraulic power increment for different diameters and curvature radiuses tested.

3. Ventilation Modeling

3.1. Ventilation network program

The ventilation circuit was modeled with a commercial ventilation network software based on Hardy-Cross algorithm [12], commonly used in mine ventilation network modeling (VentSim). At present, one limitation of this type of ventilation network software is the incapability to assign shock losses

automatically, which must be added manually. Shock losses increase with complex geometry. In the case of known close singularities, the value of shock losses could not be predicted due to interference between them. That is the reason to determine them experimentally and with CFD techniques, as mentioned in the cited studies in previous sections.

The fan used for the ventilation network program simulations is an Alphaair 4500-VAX 1800 Full Blade with 30° blade angle, which operates at ranges of 20,000 to 80,000 cfm and 0 to 4 inches of water gage. Figure 8 presents the geometries implemented using the ventilation network program. The fans are located inside of raises (Figure 8).

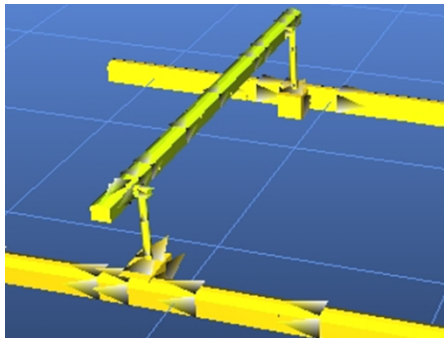


Fig. 8. Ventilation model of studied circuit.

The tested modifications have been selected from previous works which give the values necessary to estimate the total loss of the circuit. Table 2 shows the values of shock losses [7]. Once the circuit was simulated, the pressure drop, airflow rate and total resistance of the system at each circuit and its modifications were obtained and presented in Table 3.

Table 2. Values of shock losses [4] (Hurtado et al., 2012).

Circuit	X1	X2	X3	X4
	Fan/Chamber/Raise	Elbow/Split	Elbow/T-joint	Raise/Chamber/
Circuit 1 (Raise 1.5m)	2.0	1.5	1.0	1.5
Circuit 2 (Raise 2.0m)	2.0	1.5	1.0	1.5
Circuit 3 (Raise 2.5m)	2.0	1.5	1.0	1.5
Circuit 4 (Raise 1.5m Mod.)	1.2	1.2	0.9	1.2
Circuit 5 (Raise 2.0m Mod.)	1.15	1.15	0.9	1.15
Circuit 6 (Raise 2.5m Mod.)	1.2	1.2	0.9	1.2

Table 3. Results obtained from ventilation network program.

Circuit	Pressure drop (Pa)	Flow rate (m ³ /s)	Resistance (Ns ² /m ⁶)	Hydraulic power (kW)
1.5m (28.4mm)	602	31.9	0.59137	19.2
2.0m (36mm)	233	35.7	0.18286	8.3
2.5m (48.2mm)	104	36.8	0.0767	3.8
1.5m (28.4mm Mod.)	479	33.2	0.43466	15.9
2.5m (36mm Mod.)	170	36.2	0.13001	6.2
2.5m (48.2mm Mod.)	77	37.1	0.05576	2.9

3.2. Hydraulic power diminish

Table 3 shows resistance values for each case from the network software, similarly as Table 1 shows results obtained for the scale tested circuit. From resistance values, hydraulic power has been obtained from the pressure drop curve for different values of airflow. Consequently, the energy consumed is obtained introducing time which helps determining the energy per cubic meter for each resistance curve (kW-h). Figure 9 shows hydraulic power per hour in kW-h for the scale circuit and Figure 10 for the ventilation network program.

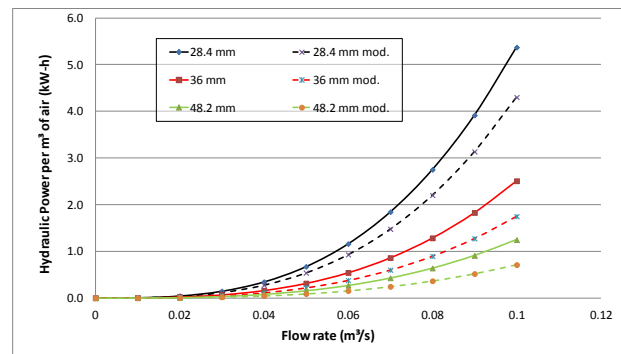


Fig. 9. Curve of kW-h per cubic meter supplied for the scale circuit.

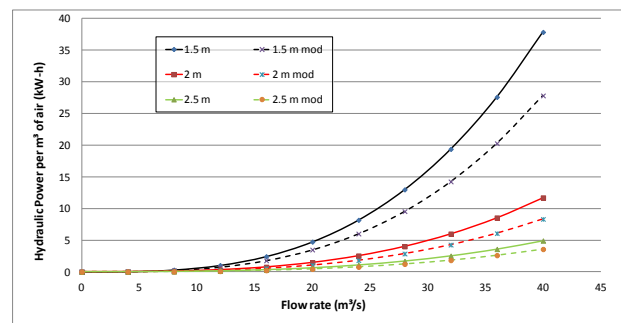


Fig. 10. Curve of kW-h per cubic meter supplied to network model.

4. Economic and design aspects

The graphs in the Figure 9 and 10 show the same behavior between the scale experimental circuit and the ventilation network program model. There is a magnitude difference in the scale that increases the expense of the air supply through the scale model because of the high resistance of the scaled circuit, due to flowing area is very tiny compared to the real size model. In this scale model, has been validated the improved applied to geometries of tested circuit and the used methodology.

However, in the case of mine circuit it is very important to notice that the results here exposed only are useful for the tested circuits. It is because ventilation circuits respond in different ways to the turbulence which depend mainly on velocities and the shape of geometry. Additionally, longitudes and dimensions of drifts and raises can vary according to the mine layout.

From the exposed results a notable difference can be appreciated for energy consumption when curvature radiuses are modified or diameter sizes changed. Concordantly, a larger radius or larger raise diameters diminish the energy consumption. In economic terms, assuming an energy price of 0.12 USD/kW-h, Figure 10 can be expressed in terms of cost, as shown Figure 11.

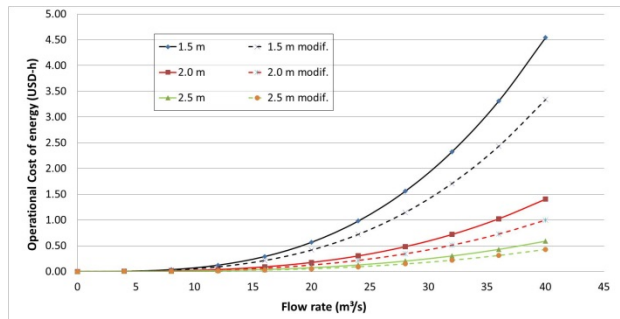


Fig. 11. Curve of USD-h per cubic meter supplied to network model.

For example, according to graph (Figure 11) airflow volume of 30 m³/s costs for the actual circuit 1.9 USD-h, but for modified rounded radius and diameter increased circuit only to 2.0 m it spends 0.4 USD-h. It is only 21% of the original consumption. In terms of annual consumption of energy, considering 70% fan efficiency, a fan active for 8 h per day and 360 days/year, creates a savings of $7817 - 1645 = 6172$ USD per year. If this value consider useful lifetime of the raise/shaft, can be obtained the total money saved, but it does not take into account marginal capital cost of drilling the extra diameter or curvature radius.

McPherson [10] exposes an economic analysis of shaft diameter as a function of present values of the capital cost of sinking the shaft and operating cost, so that to obtain the total cost function. From this it is possible to obtain the optimum (minimal) diameter. However, raise diameter depends on excavation method used, which could modify geometry of chambers. For example, raise drilling diameter is limited in blind hole method until 1.8 m, which gives the big chamber at intake and exhaust ventilation levels at present. But it is common with bigger diameters desirable to use the raise borer method, although it would increase the chambers at the production level drift because of the location of drill rigs. Also, this last can affect the ground support system because major caves diminish the base area of the crown pillar. Another alternative could be drilling and blasting (V.C.R.).

Among other aspects to take into account in the economic evaluation are useful lifetimes of the raises that range from 2-5 years or more, depending on the production rates, height of economic column, etc. But this lifetime could be extended if shaft/raise diameter is increased, so that they could be located with increased spacing including more drawpoints between them, due to less resistance of the circuit. In this way, a technical and economic analysis must be done to evaluate all these important issues which combine many aspects. These issues can be addressed in future works.

5. Conclusions

Laboratory scale model and ventilation network modelling was implemented in order to evaluate

geometric improvements in the design of ventilation circuit in a mechanized LHD block cave system. This allows estimating the cost per cubic meter of airflow supply. With these values it is possible to choose the most appropriate design or improvement to obtain cost effective mining designs to diminish operational cost. To reach these values it is necessary to calibrate and evaluate the specific layout of each mine in order to not misunderstand or make mistakes in the ventilation design input parameters. As shown in some previous works, each geometry must be assessed in order to obtain shock loss values. Capital cost of the showed modification should be evaluated in future works, including technical aspects which involve drilling method and ground support.

Acknowledgments

This research work has been supported by the Fondecyt Research Project 11085050 of Conicyt Chile and Dicyt Research Projects 051215HC and 051515HC of Universidad de Santiago de Chile.

References

- [1] F. Calizaya, K.R. Mutama, Comparative evaluation of Block Cave ventilation systems, Proc. 11th U.S./North American Mine Ventilation Symposium, Eds. In Ganguli & Bandopadhyay, Taylor & Francis Group Plc., (2004) 3-14. ISBN: 9058096335.
- [2] J.P. Hurtado, O. Gutiérrez, N.O. Moraga, Numerical Simulation of Shock Losses at the intake and exhaust Raises of Block Caving Production Level Drifts, proceedings of 13th US/North American Mine Ventilation Symposium, Sudbury. Vol1, (2010) 425-432.
- [3] J.P. Hurtado, N. Díaz, E. Acuña, 3D Characterization of Mine Ventilation Circuits for Block Caving Production Levels, MassMin2012: proceedings of sixth International Conference & Exhibition on Mass Mining, Sudbury, Ontario, Canada. June 10-14. (2012) Vol. 1, 896-911.
- [4] J.P. Hurtado, N. Díaz, C. Maya, E. Acuña, Caracterización numérica y experimental de pérdidas de carga en el nivel de producción en método Block Caving, Proceeding of 14th US/North American Mine Ventilation Symposium. Salt Lake City, Utah, United States of North America, June 17-20, Vol1, (2012) 553-559.
- [5] J.P. Hurtado, N. Díaz, E. Acuña, J. Fernández, Shock losses characterization of ventilation circuits for Block Caving production levels, Tunnelling and Underground Space Technology, Vol. 41, March 2014, 88-94, ISSN 0886-7798.
- [6] N. Díaz, Mejoramiento aerodinámico del sistema de ventilación de las calles de producción en mina El Teniente, Thesis of Universidad de Santiago de Chile, Santiago, Chile, 2011.
- [7] Y. San Martin-Lizana, Modelación experimental a escala de un circuito de ventilación aplicado a calles de producción de panel caving. Thesis of Universidad de Santiago de Chile, Santiago, Chile, 2013.
- [8] J.P. Hurtado-Cruz, Y.H. San Martin-Lizana. Analysis of geometric design in ventilation raises for Block Cave production level drifts. Caving2014, Third international

congress in Block Caving. Vol. 3. June 5-6. (2014). 638-646.

- [9] E.I. Acuña, I.S. Lowndes, A review of primary mine ventilation system optimization, INTERFACES, INFORMS, Vol. 44, No. 2, (2014), 163-175.
- [10] M.J. McPherson. Subsurface Ventilation and Environmental Engineering, Chapman & Hall, London, 1993.
- [11] E. Acuña, S. Hardcastle, L. Fava, S. Hall. The application of a MIP model to select the optimum auxiliary fan and operational settings for multiple period duties, INFOR, Vol. 48, No. 2, (2010) 89-96.

- [12] H. Cross. Analysis of flow in networks of conduits or conductors. Urbana. Univ. Ill. Bull., XXXIV (22) (1936), 29.

Ventilation and Mine Atmosphere Case Studies

An Engineer's Guide to Ventilation Surveys and Ventilation Modelling: A Case Study from a Large Underground Metal Mine

Casey Slaughter¹, Jerry Tien¹

1: Monash University, Melbourne, Australia

While there has been a decline in numbers of ventilation specialists with practical experience worldwide in the past couple of decades, the number of untrained young mining engineers freshly out of school has been increasing. Despite the best efforts of universities and professors many graduating mining engineers have only a passing knowledge of ventilation principles and practices. This leads to a much higher learning curve for new ventilation engineers entering the field. This paper aims to highlight some lessons learned from a 3-month ventilation survey and modelling project at a large underground metal mine in the US, and describe accurate steps in a survey and some of the subsequent procedures necessary for accurately analysing the survey results and the final output. The focus will be on steps to obtain accurate measurements with common instruments as well as paths to simplify survey procedures and ventilation models for complex networks, while still maintaining data resolution and fidelity.

Keywords: Ventilation surveys, Indirect base station method, Ventilation Modelling, Underground Metal Mines

1. Introduction

There are many reasons a mine should conduct ventilation surveys on a regular basis. The first and primary reason is to ensure that adequate air quantity with proper air quality is provided underground, to comply with safety standards and to provide a proper and productive working environment. Just as important is the creation and maintenance of a data bank to be used for future ventilation planning. At some mines this second purpose is sometimes lost in the day-to-day operations, often resulting in inaccurate models that don't accurately reflect the actual conditions underground because they are based upon inaccurate field data and/or inaccurate assumptions that do not apply to changing mining conditions. This became the case for one of the ventilation models used by mining engineers at a Large Underground Metal Mine (LUMM). To combat this the author was employed for a three-month period to conduct a primary ventilation survey and update and/or redo the computer model to better reflect the current ventilation conditions for accurate planning.

This paper will focus less on the instruments used and survey methods employed as those have been discussed ad nauseam in numerous other papers. Rather this paper will focus on the process of planning, implementing, analyzing, and modelling the data in this particular case study.

2. Ventilation Considerations at LUMM

LUMM is a large underground metal mine in North America. The ore is accessed via two shafts with a third under construction and extracted using a sublevel cut-and-fill method on multiple working levels. The mine is ventilated using an exhausting system where two fans are used in parallel. These 3.0 m (10 feet) fans pull approximately 750 m³/s (1.5 million cubic feet per minute or cfm) through the mine at 2,500 Pa (10 inch water gauge) pressure. In general the ventilating air was pulled underground through a 7.6m (25 feet) intake airshaft, then flows from the bottom of the mine upwards to a main exhaust level where the main fans are located, finally returning to the surface through a 6.0 m (20 feet) exhaust shaft. Due to the number of parallel splits which are also interconnected amongst each other the mine has a very complex network arrangement which also includes numerous booster fans used to ventilate specific levels (Figure 1). Due to the production and specific blending requirement a number of active mining areas with different deposit characteristics must be maintained (about 20-30 active headings) across the orebody on a variety of working levels.

3. Ventilation survey and modelling project

The primary author was hired in 2013 to work with the ventilation engineers on site to improve ventilation modelling through the development and implementation of

an additional field survey to supplement their standard monthly ventilation surveys.

3.1 Planning the Survey:

An undisputed fact that is not emphasized enough in literature is how critical it is to properly plan for a ventilation survey. Without a clear plan the data is often incomplete or muddled at best, or worse the survey is left incomplete. Michael Tuck, writing in the SME Mining Engineering Handbook section on mine ventilation gave the following advice: “Accuracy and required detail of the survey depend on the purpose of the survey [1].” The first step of the planning phase of any ventilation survey is to determine the ultimate goal of the survey: Is it to satisfy statutory requirements? Is it to identify and characterize leakage sources and inefficiencies within the ventilation system? Or is it to serve as the basis for a ventilation computer model as in this case? The goal helps determine the method and the desired level of accuracy needed from the survey data and by extension determines the required instruments.

When seeking advice on how to plan for a ventilation survey there are several resources available. The latest

in recent times [4-6]. However much of the recommendations and experience from the popular texts can be translated into a modern survey for straightforward ventilation networks. Other books on practical mine ventilation both go into much greater detail on survey procedures and techniques but are limited in terms of availability [7, 8]. However both have a more practical flair with the calculations and are somewhat easier to follow than the traditional texts. Lastly there have been a plethora of papers published on the subject of direct pressure surveys [9-18], and more modernly ones using high precision digital barometers [4-6], but none of these really address the surveys performed with enough detail. They mention the method and instruments but little information is usually provided into how they determined the detailed survey procedures or adapted the general method to the particular nuances of the mine in question. While helpful in terms of results obtained, they were generally not helpful for planning this survey.

The goal identified was to obtain “practical accuracy” for the survey and subsequent model. To this the indirect-base station method was chosen because it gives reasonable accuracy while allowing for flexibility to the survey teams and requires less time and manpower. The

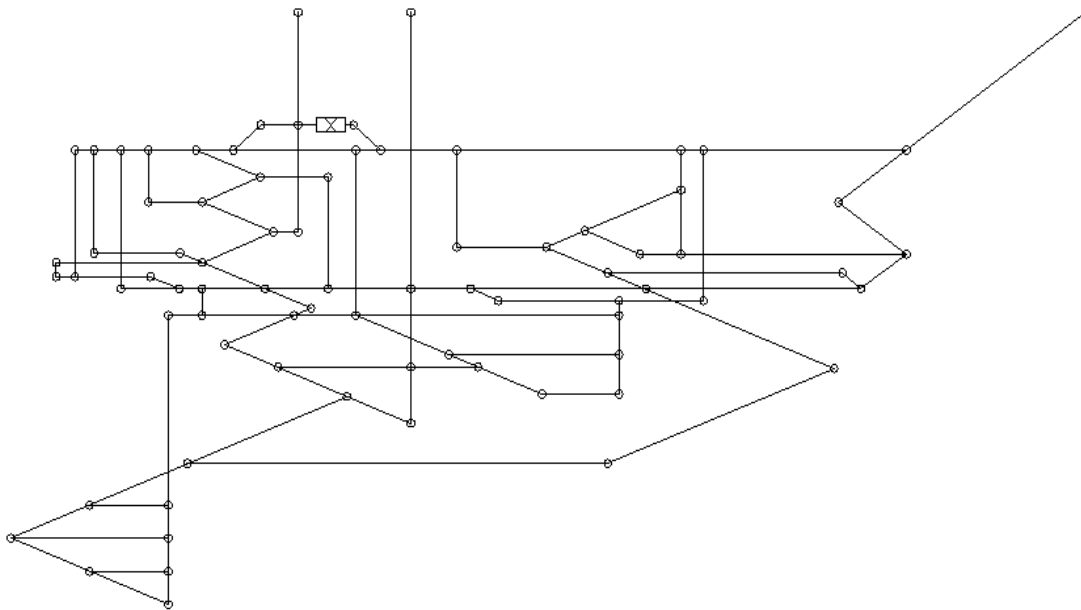


Fig. 1. LUMM Generalized Ventilation Schematic (not to scale)

edition of the SME Mining Engineering Handbook provides some general guidance however it lacks specifics [1]. The two main ventilation textbooks have more information on the different methods, yet both still reference old methods using analog instruments [2, 3], which have been mainly replaced with digital instruments

instruments chosen also satisfy the goal of “practical accuracy.” Davis and Testo 417 anemometers for measuring air velocities and GE DPI740 digital barometers used for the roving teams measuring absolute static pressure. Following Wala’s modified indirect base station method utilizing a continuous data-logger as a surface base

station, an Extech SD-700 barometric pressure/ humidity/ temperature data logger was acquired and used [19]. Psychrometric properties were taken using Kestrel 4000 units (Dry- and wet- bulb temperatures) and supplemented with a Bacharach sling psychrometer for verification purpose. Lastly some Magnehelic gauges were used for differential pressure measurements across stoppings, doors and regulators as needed. With the exception of the small continuous measuring unit, all instruments were on site prior to the start of this work and while none possess the highest precision or absolute accuracy they all were more than capable of returning data with acceptable accuracy for analysis and model construction.

Once the method and instruments had been selected the actual planning process could begin. Approximately two months before the survey was planned the nodes of the ventilation network were identified and labeled for easy reference. In this case they were isolated and systematically labeled according to the mining level with a unique identifier for each node or junction.

For LUMM over 150 nodes, where air branches would split or otherwise intersect, were identified. However the daunting task of tying these nodes together into coherent survey plans took several more hours of planning around the labeled mine maps using a “coding” system that was easy to recognize by the users. This system defined general survey “loops” that began at the main intake and followed major branches through the mine before travelling through the fans and exiting back to the surface. This method allows for a “closure check” that enables the engineer to validate their survey quickly using Kirchoff’s 2nd law.

Eight major survey loops were identified using this method. It also highlighted almost 30 sub-loops (alternate paths diverging from, and connecting back to, the main loop) which may not always be obvious but allowed for a more thorough understanding of the ventilation system. This system also allowed overlapping coverage of the shafts and fan areas to provide assurance of data accuracy for these critical areas. What should have been the most time-consuming portion of the planning process due to the complexity of the LUMM ventilation system was greatly simplified. This approach allowed for the systematic coverage of the major loops, many of which are not always readily apparent. With the identified loops and sub-loops the vast majority of the airways were able to have data collected and resistances calculated in a systematic way without leaving out any major branches.

3.2 Conducting the Survey

The survey was conducted in parallel with the other duties of the engineers involved. It was conducted during

the normal day shift over a three-week time period. The survey was constructed so that each loop be completed within a six- to eight-hour window, including preparation time and data entry following the survey. A small team of people (two to four) were involved at any given time and other engineers were rotated into the team periodically so that they were familiar with the new procedures used for this type of survey. Having more people involved also allowed for more peer review of the methods and data. However more personnel involved in the data collection also increases the chance of error. This was minimized by using a defined technique for the various instruments.



Fig. 2. Engineer Conducting Pressure Survey

To begin any particular survey loop, the involved personnel would look at the work schedule for operations so that key work areas could be avoided if possible and completed on another day with less activity. Barometrical data were reviewed so that problems with sudden barometric pressure variations could be potentially reconciled. Subsequent review of the barometrical data in the area shows pressure changes over the period were negligible and did not impact the survey results, they were left out in the calculation. This was also supported by additional sets of barometric surveys conducted prior to and following the ventilation surveys as well as analysis of historic National Oceanic and Atmospheric Administration data for the area [20].

Prior to each survey the personnel involved would discuss the plan of action for the particular loop and assign roles for the data collection to minimize user bias in the data collection, i.e. the same person would collect a particular type of data (pressure, flow, psychrometric for consistency) for each station of the survey loop.

To begin the surveys, pressure readings for both the continuous data logger and the roving barometer side by side at the intake shaft collar were taken simultaneously prior to going underground. It is essential the surface station be located at a secure location free from traffic to avoid any possible interference and disruption of measurements. In the Indirect Base Station method, the

surface monitoring station is used to primarily capture fluctuating barometric pressure. Using the Extech SD700 it was possible to also capture temperature and humidity trends for subsequent air density analysis.

They would then proceed to follow a pre-determined route of measurement stations, taking the required data along the survey loop: pressure, inlet air velocity(s), physical airway dimensions, and psychrometrics (Figure 2). The inlet air velocity refers to the air coming into each node or station. This was chosen just to be consistent in how the data was treated between nodes. Multiple measurements were taken at each station for accuracy and special care was taken to collect all data in similar circumstances with some adjustments to the stations needed to minimize possible measurement errors. For instance some planned velocity stations have irregular cross-sectional areas or near airway bends, or measurement stations were in high velocity areas. All adjustments and other items that could impact survey results were kept in the survey logbook for future reference.

The final set of pressure readings were taken at the exact same location where the very first set of readings were taken at the beginning of the survey: the intake shaft collar which is located in close proximity, about 30m (100 feet), to the exhaust shaft at the same elevation. The data from the data logger was downloaded and the small portable unit was recovered. This procedure was repeated for the remaining primary loops and included sub-loops. Barring any make-up measurements for missing information, this would conclude the field survey portion.

All data was entered into an Excel spreadsheet that was broken into three distinct parts: The first was for the surface base station information defined by the date and time which it was taken. The second was used to define the nodes and their relevant data such as elevation and a generic description to aid with locating the point underground. Lastly there was the main sheets for the various survey loops and their sub loops. For each survey the list of stations was arranged in order from intake to exhaust shaft along the air path. The primary data entered onto these sheets were the time the station was measured (to correlate to the surface base station readings), the air velocity (at least two readings within 10% of each other), the physical dimensions at the velocity measurement stations, dry and wet-bulb temperatures, and the static air pressure in terms of elevation to the nearest 0.3m (1 foot). Using the surface barometric pressure and the two temperatures, the air density can be calculated using standard psychrometric formula or charts. From the physical dimensions and average air velocities the flow quantity and velocity pressure can be calculated. The most important portion of the calculations was the resistance

determinations. After applying correction factors to the static pressure at each station to account for elevation, barometric and velocity corrections, the pressure differential between any two nodes can be calculated. Using this differential and the flow quantity the basic resistance can be calculated relatively easily using the Square Law [2, 3]. Measuring the distance and averaging the physical parameters (perimeter and cross sectional area) between these stations enables the conversion of the resistance to generic k-factors using Atkinson’s formula [2, 3]. The k-factors were then collated onto a single spreadsheet for final analysis and for computing averages for the main airway types.

While this type of spreadsheet was difficult to set up, it allowed a much quicker data entry and analysis for this survey and subsequent surveys. Care was taken to not discount any data until the resistances were calculated.

At this point it is worth noting that not all data collected yielded usable k-factors. This could have been due to conditions underground prohibiting the collection of the air velocity, due to small changes in the ventilation system such as doors being opened, or possibly due to minor human error in the data collection (data was collected by multiple groups in multiple days). Prior to the survey, instruments were verified to be within calibration and were routinely compared to ensure consistent results were obtained.

Of the 219 branches identified and measured, 137 (62%) k-factors were calculated. Closer analysis of these k-factors showed that roughly 45% were outside standard values and were subsequently discarded [21]. The remaining 75 k-factors (34% of all surveyed branches) were subdivided into four classes of airways and used to compute the relevant averages. By using more general classes there were a sufficient number of usable k-factors in each category to have meaningful averages. As more data is collected and analyzed in future surveys and added to the data bank, these k-factors can be better refined and more detailed classes of airways can be established. For instance the generic “raises” can be subdivided into Ventilation and Escape raises or even further based on the age or construction type.

Table 1: Calculated Friction Factors

Designation	Friction factor: kg/m ³ (k*10 ¹⁰)
Level	0.0280 (151)
Raise	0.0254 (137)
Ramp	0.0135 (73)
Shaft*	0.0425 (229)

Many of these k-factors were placed straight into the model under construction. Even with the lower percentage of the usable k-factors obtained the initial model showed good agreement with observations underground. However the “shaft” data was omitted due to some complex interactions that were observed with the multiple shaft landings and infrastructure surrounding the shaft stations which led to higher than expected resistance values. For modelling purposes data from older, more detailed shaft surveys were used. These provided good results with the rest of the calculated k factors.

3.3 Constructing and using the ventilation model:

The model was built using Ventsim Visual [22], but other ventilation modelling programs tend to follow a similar modelling plan [23]. Initially the general schematic of the mine was created using mine planning software and surveyed centerlines. Where possible the centerlines were simplified such that a representative skeleton of the mines ventilation system was created. This was done on the principle that starting with a simple model is best for comprehension and troubleshooting before adding the complexity necessary for advanced ventilation modelling tasks (heat and contaminant simulation etc.). This data was then saved in the .dxf file format which was then imported into Ventsim. This data was then readily converted into generic airways. At this point presets were created for levels, ramps raises, and shafts with generic friction factors and dimensions to give a rough model initially. Generic stoppings and other ventilation controls were added and the fans were copied from the existing model. At this point the generic skeleton model was created (Figure 3) and showed reasonable values for flows, flow directions, fan pressures and other relevant data. When comparing with the previous ventilation quantity survey there was good agreement between the model and observed flows.

With a simple calibration effort the accuracy could be improved. This typically involves referencing a second quantity survey and making adjustments to resistances starting at the intake shaft and moving systematically through the ventilation system slightly adjusting resistances until the flows in the model match those observed. The following formula provides the starting point for these adjustments:

$$R_{actual} = R_{model} * \left(\frac{Q_{model}}{Q_{actual}}\right)^2 \quad (1)$$

If desired these resistances can then be converted back into k factors using Atkinson’s Formula [2,3]

4. Conclusions:

Data generated during regular ventilation surveys, through proper modelling are essential to providing the most efficient ventilation system. While not complex in theory there are numerous issues that can arise and cause problems for less experienced ventilation engineers. First a solid foundation in ventilation theory is needed to plan complex ventilation surveys and analyze the results. Second, most of the references that we use from our university days, are often lacking on practical methods for complex system analysis and worse, are outdated when it comes to proper, modern instruments in use. Lastly is that ventilation modeling requires practice and experience that individual engineers today often lack. All of these can be mitigated using a team approach to design and planning.

The survey mentioned here was a successful trial of a new procedure to supplement the current ventilation surveys with an eye less on verification of the existing system parameters but more for future ventilation planning. While the data was more incomplete than the engineers would have preferred and yielded less than 35% usable friction factors due to various reasons, those friction factors combined can create a model with acceptable “practical accuracy” that could be readily improved through calibration and future surveys. In its current form this modeling effort would be considered a Base ventilation model that would form the framework for more detailed modeling.

The most common error that affected the friction factors were difficulty in acquiring all of the relevant data needed in Atkinson’s formula. Other issues that may have contributed to some of the outliers were interactions of infrastructure creating complex resistances that did not lend themselves well to modelling. A ready example is the safety barriers located on multiple shaft landings, each of which has multiple air outlets into the ventilation systems. These were difficult to assess in the survey and led to the use of older friction factors from a more detailed survey.

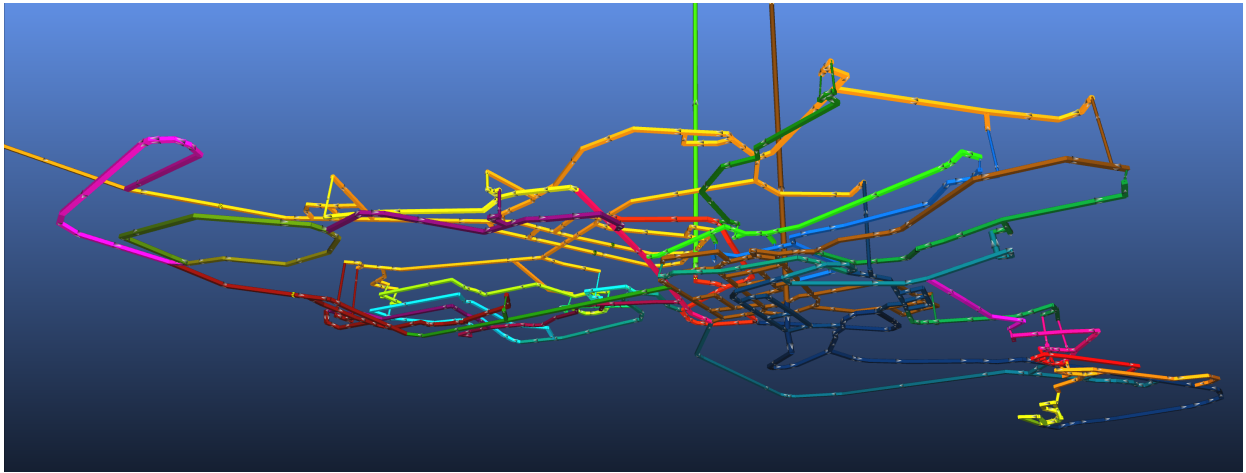


Fig. 3. LUMM Ventilation Model

Common complaints that are often mentioned about various instruments and survey methods (mainly the inherent “inaccuracy” of barometers or altimeters) are largely within the limits of practical accuracy required for most system modelling tasks. Common anemometers and digital barometers that are already on site are good enough to establish a basic ventilation model that can be used for future system planning with a simple calibration effort as the instrument accuracy is typically much smaller than the natural variations that are observed in a ventilations system, which are typically averaged out in the calculations and data analysis portions of the survey.

References

- [1] M. Tuck. “Chapter 15.3: Mine Ventilation “. *SME Mining Engineering Handbook 3rd Edition Vol 2*. Peter Darling (editor). Society of Mining Metallurgy and Exploration. 2011. pp. 1577-94
- [2] H. Hartman, J. Mutmanský, R. Ramani and Y.J. Wang. *Mine Ventilation and Air Conditioning 3rd Edition*. John Wiley and Sons 1997. pp 153 and 206-225
- [3] M. McPherson. *Subsurface Mine Ventilation*. Mine Ventilation Services. 2002. Accessed online <https://www.mvsengineering.com/index.php/download/publications> 17 Feb. 2015. pp. 6.17-24
- [4] A. Habibi, R. Kramer, and A. D. S. Gillies. “Comprehensive Pressure Quantity Survey for Investigating the Effects of Booster Fans in a Trona Mine.” SME, 2013.
- [5] J. Rowland. “Barometric Resistance Surveys A New Perspective.” 14th US/ North American Mine Ventilation Symposium, 2012.
- [6] J. Rowland. “Moving the Ventilation Report into the 21st Century.” Australian Coal Operators Conferences, 2009.
- [7] W.R. Kennedy. *Practical Mine Ventilation*. Intertec Publishing 1999. pp. 213-27
- [8] J. Tien. *Practical Mine Ventilation Engineering*. Intertec Publishing 1999. pp. 196-209
- [9] D. Adam, J. Hemenstall, and W. English. “Practical Ventilation Planning for the Mine Management Using a Digital Computer.” AusIMM Ventilation of Coal Mines Symposium, 1983.
- [10] D. Brake. “A Protocol and Standard for Mine Ventilation Studies.” 12th US/ North American Mine Ventilation Symposium, 2008.
- [11] D. Brunner, and M. McPherson. “Ventilation Planning Study of the El Teniente Block Caving Mine in Chile.” 4th International Mine Ventilation Congress, 1988.
- [12] I. Duckworth, K. Wallace, and R. Wise. “Ventilation Planning and Design of the Skyline Mines.” 7th US Mine Ventilation Symposium, 1998.
- [13] L. Frost. “Mine Ventilation from a Manager’s Standpoint.” Mining Society of Nova Scotia, 1941.
- [14] R.L. Grayson, R. Mishra, and Y. J. Wang. “Modeling the Ventilation Network for an Old Coal Mine.” 1st US Mine Ventilation Symposium, 1982.
- [15] E. Harris, R. Dalzell, R. Kline, and E. Miller. “A Method for Calculating Mine Ventilation Pressure Losses Using Computers and Desk-Top Calculators.” US Bureau of Mines, 1973.
- [16] P. Mitchell. “Mine Ventilation Planning of BHP Steel Division Collieries.” AusIMM Ventilation of Coal Mines Symposium, 1983.
- [17] N. Oswald, B. Prosser, and R. Ruckman. “Measured Values of Coal Mine Stopping Resistance.” 12th US/ North American Mine Ventilation Symposium, 2008.
- [18] A. Ralph, and T. Nixon. “Ventilation Survey Procedures and Database for Use with Computer Simulation Techniques.” AusIMM Ventilation of Coal Mines Symposium, 1983.
- [19] A. Wala. “A New Data Acquisition System for Mine Ventilation Surveys.” 6th US Mine Ventilation Symposium, 1993.
- [20] Anon. National Climatic Data Center: local station climate datasets. National Oceanic and Atmospheric Administration. Accessed online <http://www.ncdc.noaa.gov/> 17 Feb, 2015.
- [21] G.E. McElroy. “Engineering Factors in the Ventilation of Metal Mines.” US Bureau of Mines Bulletin 385, 1935.
- [22]

- [23] Chasm Consulting. "Ventsim-3D Mine Ventilation Simulation Software" Website <http://www.ventsim.com/> accessed 20 Feb 2015.
- [24] Y. Zhang, X. Zhang, A. Habibi, and J. Tien. "Comparison of Mine Ventilation Simulation Software." SME, 2012.

Primary Mine Ventilation Solution for the New Level Mine Project During the Construction Period 2015 – 2020

Enrique I. Acuña^a, Keith G. Wallace^b

^a*Proyecto Nuevo Nivel Mina, CODELCO, Rancagua, Chile*
^b*Mine Ventilation Services, Inc., Clovis, California USA*

The New Level Mine Project (NLMP) is the future underground expansion of the El Teniente mines near Rancagua, Chile. The maximum daily production rate is expected to be between 137 and 180 ktpd. Production is planned to start at the end of 2020. Construction is planned around two time phases, the initial development that started in 2012 and is scheduled to be completed in 2015 and a second phase from 2016 to 2020. Underground construction started three years ago from both surface and the current underground workings. New intake and exhaust adits are being constructed to the new mining horizon that will be the basis of a new independent ventilation system. These adits are scheduled for completion by the end of 2015 or early 2016. However, to support the extensive construction activities, it is necessary to use a portion of the current El Teniente mine ventilation system. This paper presents a study that was performed to achieve the airflow necessary to support the development of the mine during construction, between the years 2015 to 2020. The study describes the baseline ventilation model and the modifications performed to achieve the initial airflow objectives. Second, a sensitivity analysis was performed on the new intake and exhaust adits (numbers 74 and 75, respectively) to determine the maximum airflow possible in these adits in the event the airflow from the existing El Teniente mine is less than expected.

Keywords: Mine ventilation design, case studies

1. Introduction

In January, 2014, Mine Ventilation Services, Inc. (MVS) conducted a ventilation study of the proposed ventilation design for the construction of the CODELCO's New Level Mine Project (NLMP). This study consisted of measuring primary fans in the El Teniente mine, establishing a ventilation model of the existing system, modifying the model to reflect the proposed construction ventilation system for the NLMP, and deriving recommendations as to how much airflow could be obtained through the El Teniente mine and how much had to be provided through the NLMP ventilation adits to fulfill the airflow requirements for the construction phase between 2015 and 2020. The proposed ventilation system for the NLMP during construction is shown on Figure 1.

As presented in Figure 1, the NLMP is represented by a box, as the interest of this study is the first approximation to determine if the required airflow volumes could be achieved. As the NLMP mine is located at an altitude of 1800 meters above sea level, the main fresh and exhaust airways are inclined ramps called adits. In Figure 1 only Adits 74 and 75 are under construction and are part of the ventilation infrastructure of the NLMP, all the others belong to the El Teniente mine.

The design was based on providing 944 m/s (2,000,000 cfm) to NLMP. The initial aim was to achieve this flow, with 472 m/s (1,000,000 cfm) intaking through Adit 75 and the same amount provided from existing intake Adits 62, 63 and 65. Finally, fresh

air was also provided from the compressor station from Adit 61 to NLMP.

The exhaust for the mine is through a new parallel fan at the 58 Adit. Air from Reno presently going through 58 Adit would need to be diverted through raises to exhaust via Adits 51, 52 and 45. The new 58 fan capacity combined with Adit 74 exhaust will have a return capacity of 944 m/s (2,000,000 cfm).

During the establishment of the base model, it was noted that Adit 51 was not operating because of repairs to the airway and maintenance on the fan. The operating point for this fan was estimated from previous fan measurements taken by the El Teniente mine (historical data, [1] and [2]).

A second analysis was performed to evaluate and maximize the airflow that could be made available for the NLMP that did not involve the existing El Teniente mine infrastructure. This design was to increase the 74 and 75 fan duties to achieve the maximum flow possible while maintaining reasonable fan pressures and air velocities in these strategic airways.

2. Existing El Teniente mine ventilation system and "black box" ventilation model

The impacted adits, and their fan systems, for the proposed NLMP construction ventilation system are 45, 51, 52, 58, 61, 62, 63 and 65. Each adit had a main fan that was labeled per the adit number. For example the main fan on Adit 45 was V45. V is the first letter for the translation of fan in Spanish "ventilador". Each of these

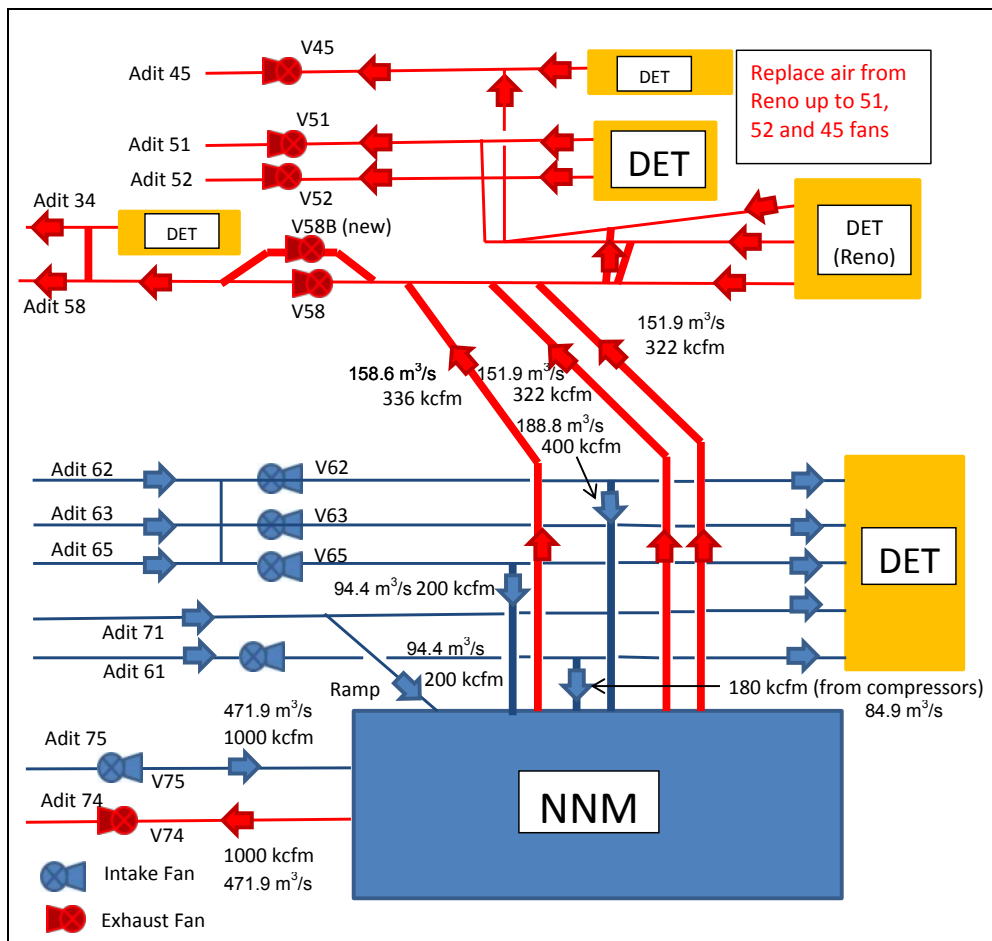


Fig. 1. Schematic of proposed ventilation system using air to/from existing El Teniente mine

fans was measured in the mine, for airflow and pressure loss across the fan, except V51, which was off for maintenance. During the survey it was not possible to collect any motor details, such as voltage, amperage, and power factor. During the survey it was highlighted as useful information in validating the fan operating point.

The resistance of the adits from surface to the primary fans was estimated using friction factors and airway sizes. The resistances were also estimated from the fans to the mine footprint. From the mine footprint, the model assumed a “black box” approach. Each branch connecting to the existing mine was assumed to be influenced either by a fan in that section of the mine or a resistance to flow. Therefore, after a base model was developed to give the flows into and out of the mine that roughly matched the measured data, those branches connecting the existing mine were adjusted to a fixed pressure (e.g. fan) or fixed resistance branch. In this way, any adjustments to the existing mine to simulate the changes necessary to increase the flow to the NLMP would somewhat reflect the expected condition from the existing mine [4].

Figure 2 shows the existing El Teniente mine and shows the areas that were modeled with a “black box” and shows the fans that are impacted by the NLMP ventilation design.

From the analyses performed it was observed that certain areas of the mine would need additional regulation in order to optimize the airflow to NLMP or to make space available for NLMP airflow. A simplified

model was developed based on the current ventilation system as shown on Figure 3. The ventilation model does not include details of the existing El Teniente mine, rather it shows primarily the intake and exhaust airways and the existing development of the NLMP. The model assumed airflows into O/P 14 and CH O/P 12/13 from other levels that were not measured, but must be flowing into the raise since two levels were measured. Some of these areas are hard to access or have no access at all, especially near O/P 14 raise which used to be an ore pass.

The model balanced reasonably well with the measured airflows and fan pressures (+/- 15%). Fan curves were estimated from information provided by El Teniente mine historical recent data. The validity and accuracy of these fan curves is unknown.

3. Model of NLMP with connections to existing mine

Figure 4 shows the ventilation model reflecting the required new raises to support future ventilation demands. To achieve the airflows shown on Figure 1, the primary intake fans V62, V63 and V65 were modeled as fixed pressure fans. Exhaust fans at V58 were modified to include a second fan in parallel and modeled with a fixed pressure. The V45 fan was also modeled as a fixed pressure fan. The V51 and V52 fans

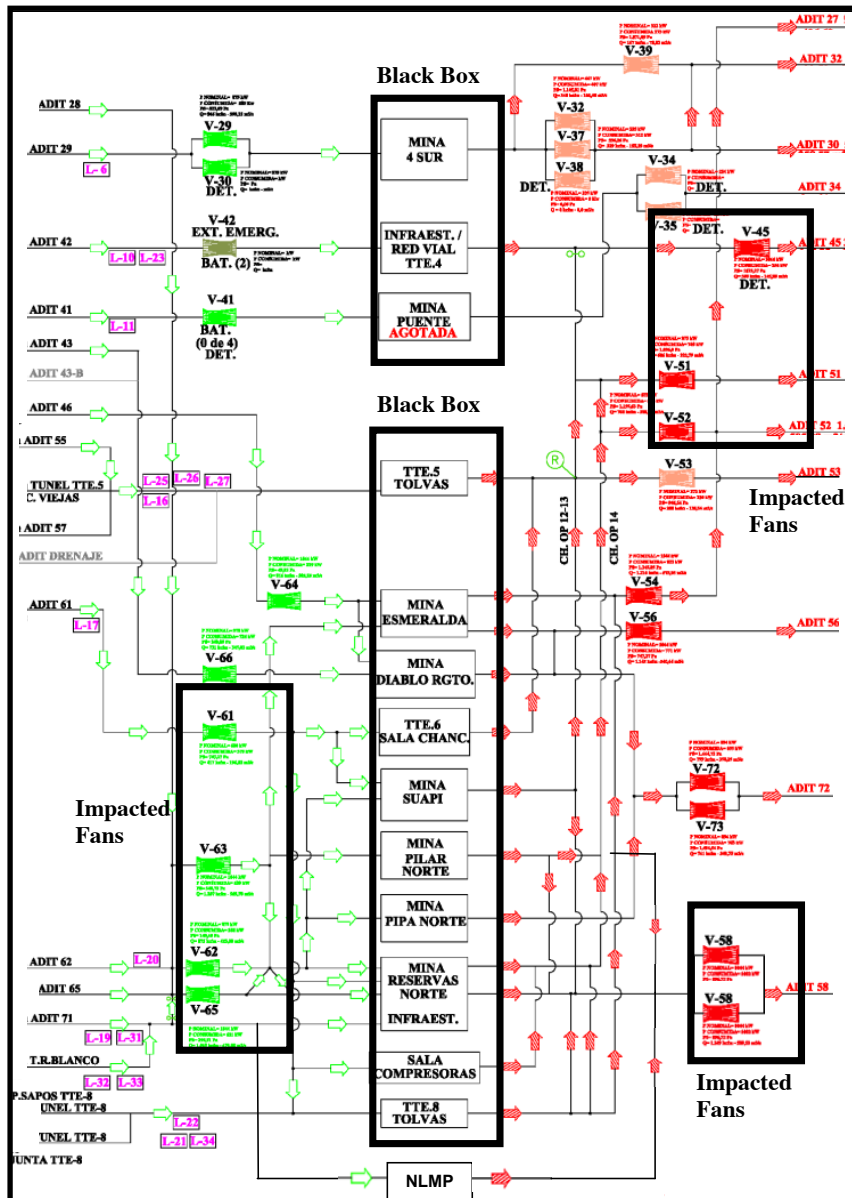


Fig. 2. Schematic of El Teniente mine ventilation system.

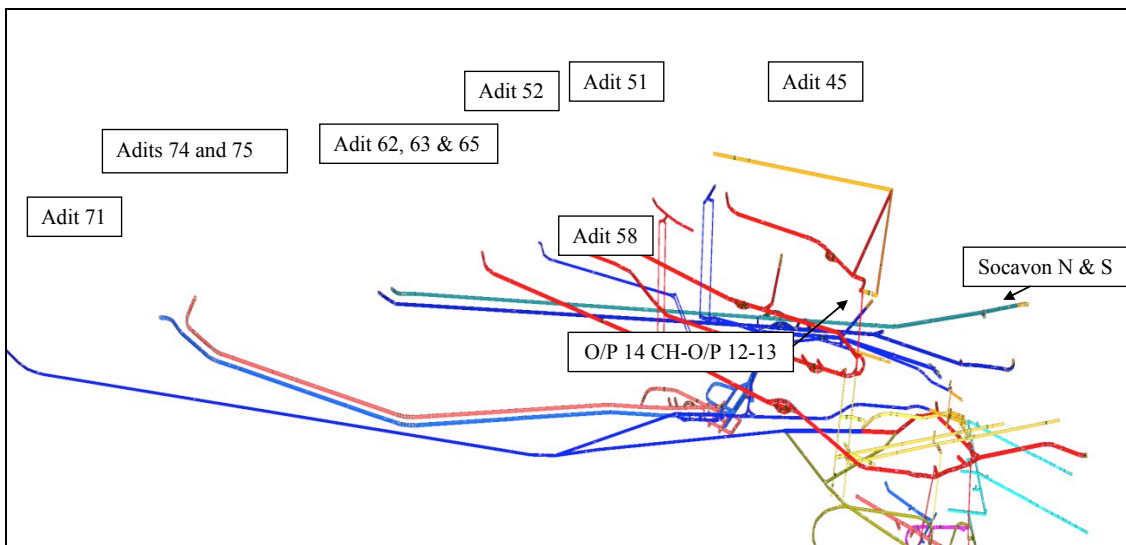


Fig. 3. VentSIM® model of existing ventilation system.

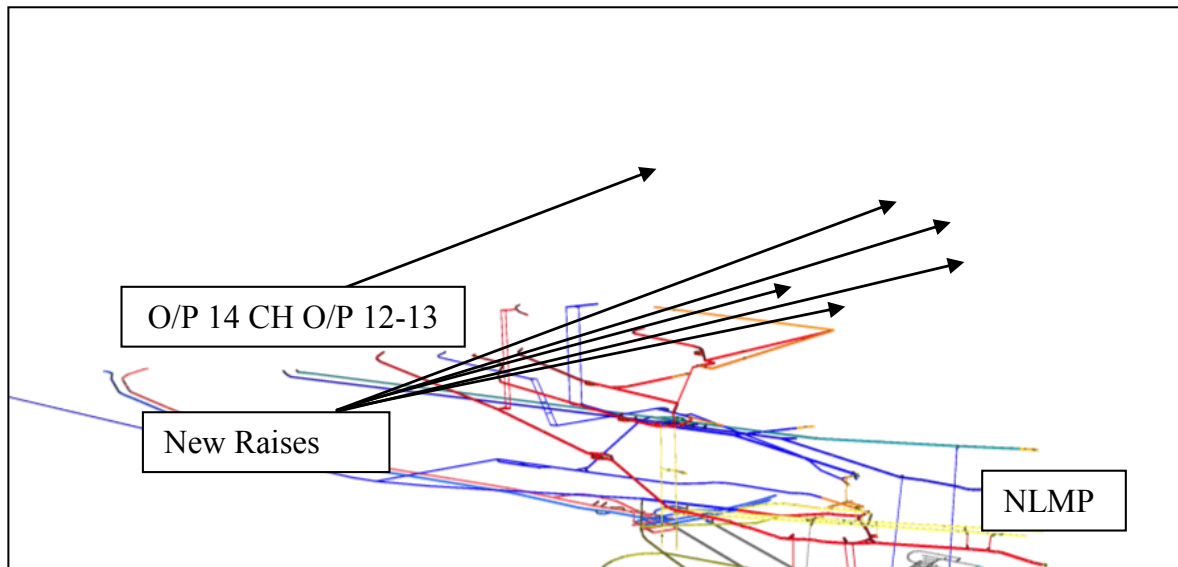


Fig. 4. VentSIM® model developed for using existing El Teniente Mine to supplement airflow to NLMP

were kept on their respective fan curves. The fans were based on a fixed pressure fan after using a fixed quantity branch at the fan location. This was the easiest way to determine the necessary fan pressure at each location. The operating points were compared with the fan curves to determine the new fan setting and ensure the fan would operate in a stable condition.

New exhaust raises were included that connected the Adit 58 drift to Socavon Norte and Sur. This allowed exhaust air from the El Teniente mine to flow towards V51, V52 and V45. New raises were also included in the model to maximize the exhaust air from the NLMP up to V58. Airflow was increased in O/P 14 and CH O/P 12-13 (that was opened to the 45 Adit). The model assumed clean connections from Socavon to O/P 14 and CH O/P 12-13 on the Socavon level, as presented in Figures 3 and 4.

The objective of this modeling was to keep the airflows in and out of the existing mine constant while increasing airflow in and out of NLMP. This was accomplished by trial and error with the model. The El Teniente intake and exhaust fans were adjusted to give a new flow regimen while checking the flows in and out of the existing El Teniente connections. The fans were adjusted in an attempt to increase airflow while maintaining the fan power within the current motor capacity.

4. Model results

Intake fans V62, V63 and V65 were adjusted to increase airflow in an attempt to provide 283 m/s (600,000 cfm) to the NLMP. New intake raises connected Adit 62 and Adit 65 to the NLMP. Booster fans were necessary to push air down to NLMP on these raises. A new duct system was modeled to take compressor air from Teniente Sub 6 down a ventilation raise to NLMP. This intake system is challenging as the flow across the compressors at 85 m/s (180,000 cfm) would result in a relatively high velocity in the compressor room. In addition, the compressor system requires two fans at the bottom of the raise that will

connect to the ducting to pass to the ventilation raise. Figure 5 shows the compressor air system.

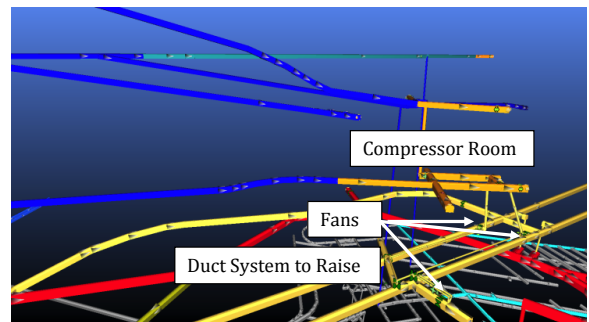


Fig. 5. Compressor room ventilation design

There is an inherent danger in using compressor room air as intake. This danger is if there is a fire in the room. A fail safe system of sensors and dampers was considered to turn off this system in the event of a fire and open the exhaust to Socavon Sur (airway where the ducting is to be installed) to exit the mine.

The final intake to NLMP is via the Adit 71 intake ramp. An initial design value was estimated at 94.2 m/s (200,000 cfm) intaking from this route.

Exhaust from the system was modeled with raises connecting NLMP with Adit 58. A second exhaust fan V58B was added in parallel to V58 to increase flow on this level [3]. In order to accommodate the air on Adit 58, additional exhaust raises were modeled that took air from Adit 58 to the Socavon level. From this point, the additional airflow would upcast O/P 14 and CH O/P 12-13 and exhaust the mine via fans V51, V52 and V45.

In reviewing the model results, the key elements were maintaining the airflows in and out of the existing El Teniente connections while keeping the existing fans operating within their motor capacities. The model included 472 m/s (1,000,000 cfm) intaking and exhausting Adit 74 and Adit 75 with new fans on these drives. The NLMP mine development at the time of this model was estimated around the 2017 time frame. No airflow controls were installed in NLMP to give a flow distribution, rather the connections were open to allow

maximum flow in this area of the mine. The objective of this study was to determine the maximum airflow capacity of the El Teniente mine ventilation system that could be available to the NLMP and not the airflow distribution in NLMP. The model results are described as follows:

1. The intake fans V62, V63 and V65 can be adjusted to give an increased flow of 270 m/s (570,000 cfm);
2. Air from the Teniente Sub 6 compressors was modeled at 75.5 m/s (160,000 cfm). This was limited from the design 85 m/s (180,000 cfm) because of velocity concerns in the compressor room and losses in the duct system to the intake raise to NNM;
3. The exhaust fan V58B in parallel at V58 appear to only be capable of 307 m/s (650,000 cfm) with each fan at a fan total pressure of 1.74 kPa (7.0 in. w.g.). This is a total flow through the two fans of 613.5 m/s (1,300,000 cfm). This value was limited more on fan pressure than volume, and was due to using the design cross sectional area instead of the measured area. Based on the measured dimensions, the modeling suggests this flow could be increased to 708 m/s (1,500,000 cfm);
4. The exhaust system up O/P 14 and CH O/P 12-13 had 293 m/s (620,000 cfm) at 1.6 kPa (6.3 in. w.g.) exhausting through V52, 290 m/s (615,000 cfm) at 1.5 kPa (5.9 in. w.g.) exhausting V51 and 300 m/s (640,000 cfm) at 1.5 kPa (6 in. w.g.) exhausting V45. On V45 the existing mine connections on these level needed regulators in order to limit exhaust air to this level and to pull air up the small exhaust raise from Adit 51;
5. The ramp flow downwards from Adit 71 was predicted to be 42 m/s (90,000 cfm). The ramp flow is a natural split of air since no fan is involved in this path. If the V58 fan can be increased because of a larger drift dimension, this split of air will increase to an estimated 70.8 to 94.4 m/s (150,000 to 200,000 cfm);
6. V74 fan was predicted at 0.9 kPa (3.5 in. w.g.) at an airflow of 472 m/s (1,000,000 cfm) with the V75 fan predicted duty of 1.7 kPa (6.7 in. w.g.) at a matching airflow of 472 m/s (1,000,000 cfm). The airflow in and out of V74/75 is contingent on the configuration of the NLMP to deliver and exhaust this airflow. The current model is still remains an estimate of the facility when these fans will be available. During the study, it was not clear yet how the NLMP ventilation system was going to be configured due to recent changes in the mine design, mainly due to new geomechanic constraints.

With this model all flows in and out of the existing mine were maintained reasonably close to current values. The limitation in total flow appears to be in what can be

exhausted from the mine. The intake has the capacity to supply additional airflow, but the exhaust is limited on the Adit 45 fan and in the Adit 58 parallel fans.

The total flow to NLMP, including the 472 m/s (1,000,000 cfm) from/to Adit 74 and 75 is predicted to be 779 m/s (1,650,000 cfm). This is approximately 18 % less than the desired airflow of 944 m/s (2,000,000 cfm). Table 1 shows the measured against predicted airflows for the scenarios analyzed.

The modeling was based on the design cross sectional area of Adit 58. It appears that the adit dimension is larger than estimated. If the larger area, partially measured in the field, is considered, then the airflow volume achievable increases 94.4 m/s (200,000 cfm) to 873 m/s (1,850,000 cfm). This airflow is still 7.5% lower than the desired 944 m/s (2,000,000 cfm). The area of the full Adit 58 needs to be field verified.

Adits 74 and 75 were also modeled considering a sampling of measured cross sectional areas that were larger than the design values used in the analysis. If this airway is larger, then modeling indicates an additional 70.8 m/s (150,000 cfm) may be achieved.

As a result, modeling by MVS and the NLMP engineers indicated that it may be possible to achieve a total airflow of 944 m/s (2,000,000 cfm). This total flow is contingent on Adits 58, 74 and 75 being of a larger area than their respective design values.

This study was performed in order to propose the new ventilation system to the Division El Teniente. Using air from the existing mine needs approval from the operators of the El Teniente ventilation system. This approval is pending and there is no guarantee that the solution presented in this paper will be approved by the division. Therefore, contingencies were planned to maximize the airflow through Adits 74 and 75.

5. Model of increased 74 and 75 fan duties

Models were developed increasing the airflow in Adits 74 and 75 without connecting to the existing mine (other than the existing exhaust raise and Adit 71 intake down the ramp). The existing flows in the ramp were maintained at 94.4 m/s (200,000 cfm). The V74 and V75 fans were modeled as fixed airflow fans with the model predicting the required fan pressure. The results of this analysis were:

1. The intake fan maximum duty point appears to be 708 m/s (1,500,000 cfm) at a fan total pressure of 2.4 kPa (9.7 in. w.g.);
2. The exhaust fan maximum duty point appears to be 708 m/s (1,500,000 cfm) at a fan total pressure of 3.3 kPa (13.3 in. w.g.). This higher pressure is due to twin raises that are in front of this fan;
3. The velocity in the mine entries approach 15.2 m/s (3,000 ft/min). This is very high and it is not recommended to exceed this value.

Table 1. Measured against predicted airflow and model results.

Location	Measured or Estimated Flow to/from El Teniente		Estimated Flow to/from El Teniente with V51 Fan Operational		Predicted Flow After Modifications for Air to NNM		Flow to/from NNM Included in Predicted Flow		Comment
	(m ³ /s)	(kcfm)	(m ³ /s)	(kcfm)	(m ³ /s)	(kcfm)	(m ³ /s)	(kcfm)	
Adit 61	212.8	451.0	226.5	480.0	236.0	500.0	80.2	170.0	Base model 33 m ³ /s (70 kcfm) to compressor
Adit 62	410.6	870.0	410.6	870.0	462.5	980.0	94.4	200.0	
Adit 63	552.2	1170.0	556.9	1180.0	648.9	1375.0	0.0	0.0	
Adit 65	422.4	895.0	411.5	872.0	549.8	1165.0	94.4	200.0	
Adit 71	129.8	275.0	136.9	290.0	136.9	290.0	42.5	90.0	Base model 80.2 m ³ /s (170 kcfm) to NNM
Intake Subtotal	1727.8	3661.0	1742.4	3692.0	2034.1	4310.0	311.5	660.0	
Different predicted less NNM less V51 base model:							-19.8	-42.0	
Adit 45*	165.2	350.0	198.2	420.0	296.4	628.0	0.0	0.0	
Adit 51	(Flow to 45 Rse)		299.2	634.0	269.5	571.0	0.0	0.0	Base model V51 off
Adit 52	345.9	733.0	309.1	655.0	284.1	602.0	0.0	0.0	
Adit 58	526.2	1115.0	488.5	1035.0	594.6	1260.0	310.5	658.0	Base model 80.2 m ³ /s (170 kcfm) from NNM
Socavon N/S	189.7	402.0	331.8	703.0	446.0	945.0	0.0	0.0	Predicted model 188.8 m ³ /s (400 kcfm) from DET
DET/TTE8**	146.3	310.0	250.1	530.0	216.6	459.0	0.0	0.0	
Exhaust Subtotal	1373.4	165.2	1876.9	3977.0	2107.2	4465.0	310.5	658.0	
Different predicted less NNM less V51 base model:							-80.2	-170.0	

* Measured model raise 51 to 45 open. V51 base model raise 51 to 45 closed. Predicted flow from NNM had raise open.

**connections to O/P 13 and CHIM 12/13

Note: 188 m³/s (400 kcfm) diverted from Reno to Socavon for air to enter Adit 58 from NNM.

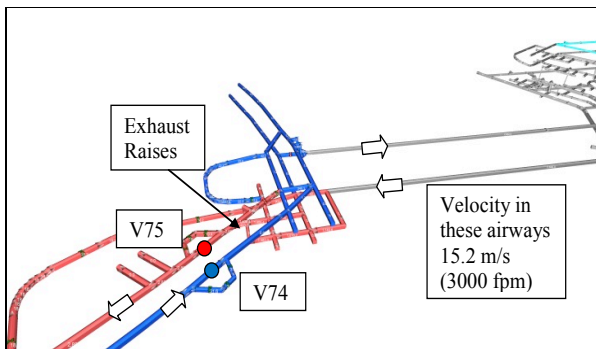


Fig. 6. Increased airflow through Adits V74 and V75.

If this scenario is to be implemented, then further modeling is required to ascertain how these new fans will fit with the final ventilation design for the NLMP. Currently, this design effort is outside the current scope of work. Figure 6 shows the results of this modeling.

6. Conclusions

The work MVS and NLMP engineers performed in this study involved measuring all primary fans impacted by proposed design changes and establishing an approximate ventilation model of the existing ventilation system. This model is a simplification of the current El Teniente mine without the details of the mine airflow distribution. The existing mine was modeled as a “black box” with airflow in and out based on the measured flow regime.

The results of the modeling showed that it does not appear feasible to achieve an extra 472 m³/s (1,000,000 cfm) from the existing El Teniente mine while maintaining existing airflows into the various mining zones in El Teniente. The preliminary calculations showed that the design could accommodate 778 m³/s (1,650,000 cfm). This was based on a limited capacity of the parallel Adit 58 fans. However, the calculations were based on drift dimensions of 5.5 m wide by 6.9 m high from the fan location into the mine. The drift dimensions

from the portal to the fan were measured at several locations as 7.2 m wide by 6.9 m high. If this dimension carries through to the mine, then it may be possible to increase flow through the 58 fans from 613.5 m³/s (1,300,000 cfm) to 708 m³/s (1,500,000 cfm). This is an increase of 94.4 m³/s (200,000 cfm) thereby increasing the total NLMP airflow to 873 m³/s (1,850,000 cfm).

These analyses assumed that the Adit 74 and 75 airflow is fixed at 472 m³/s (1,000,000 cfm). The model showed that to achieve these flows a fan total pressures of 1.74 kPa (7 in. w.g.) is required for the exhaust fan and 0.8 kPa (3.3 in. w.g.) for the intake fan. These fan pressures were based models with the 74 and 75 Adits at a cross-sectional area of 44.2 m². Subsequent measurements of actual cross-sectional area (at several locations) showed an average dimension of 54.2 m². Using this dimension and increasing the fan airflow through each fan to 542.7 m³/s (1,150,000 cfm) resulted in fan total pressures of 1.9 kPa (7.5 in. w.g.) for the exhaust fan and 1.07 kPa (4.3 in. w.g.) for the intake fan. These values indicate that if the 74 and 75 adits are larger than originally modeled that the 74 and 75 fans should be capable of increased flow. If Adit 58 and Adits 74 and 75 are larger in dimension, then modeling shows that it may be possible to achieve a total flow to NLMP of 944 m³/s (2,000,000 cfm)

A supplemental analysis was conducted to determine the fan requirements on Adit 74 and 75 if it is not possible to use the existing mine ventilation system. This analysis showed the maximum flow through Adit 74 and 75 would be approximately 826 m³/s (1,750,000 cfm). Flows higher than this would require fan pressures in excess of 2.5 kPa (10 in. w.g.) with velocities exceeding 15 m/s (3,000 ft/min). It is not recommended to exceed this velocity since Adits 74 and 75 will be travel ways.

Acknowledgements

The authors would like to express their gratitude to Codelco’s staff and management for their cooperation in

this work and their permission to present the findings. The authors would also like to thank Heriberto Soto and Roberto Alvarez for their cooperation and involvement in this work.

References

- [1] Informe plan quinquenal de ventilación 2014-2018, ADM-V-INF-145-2014 REV 0 [CODELCO, Chile]
- [2] Informe de control puntos operacionales ventiladores principales mina, ADM-V-INF-127-2013 REV 0 [CODELCO, Chile].
- [3] J.P. Hurtado and E.I. Acuña, “CFD Analysis of 58 Adit Main Fans Parallel Installation for the 2015-2019 Underground Developments of the New level Mine Project, Accepted at Applied Thermal Engineering, Especial Issue “Energy in Mining, 2015”.
- [4] McPherson, M.J., “Subsurface Ventilation Engineering” 824 pgs, copyright, Mine Ventilation Services, Inc., 2008 ISBN 978-0-692-00024-3

Sinking of Resolution No.10 Shaft in Extreme Heat Conditions

Frank von Glehn^a, Steven Bluhm^a, Tom Goodell^b, Dave Lunderstedt^c

^aBBE Consulting, South Africa

^bResolution Copper, USA

^cRSV USA, USA

Resolution Copper Mine in Arizona, USA, is planned to be a 2116m [6950ft] deep block cave mine with virgin rock temperatures exceeding 176°F [80°C]. The project has sunk an exploratory shaft to access the orebody for characterization studies. The 28ft [8.5m] diameter No.10 Shaft sink was ventilated from surface using a ducted ventilation/cooling system with flow reversal after the blast and reached the ultimate depth in November 2014. During the planning stages it was recognized that, because of the high virgin rock temperatures and a relatively high surface ambient condition, heat and ventilation issues will be very important in achieving targeted sinking rates. Heat load predictions were made on a regular basis to estimate cooling and ventilation requirements. The system included refrigeration machines that cooled a glycol/water mixture to about -4°C [25°F] which was pumped to cooling coils located underground at an intermediate level. The ventilation fans were selected for a varying duty as the sink progressed and included VSDs.

A ventilation monitoring system was set-up for day-to-day management as well as to verify the heat load predictions. The system recorded ambient pressure, dry-bulb temperature, humidity, air velocity, differential pressure at some 18 stations in the intake and return air streams, as well as flow rate and temperature in compressed air and machine water circuits. Provision was also made to monitor gas concentrations in the duct system to ensure that blast fumes were cleared before personnel re-entered the shaft after a blast.

This paper describes the heat load predictions and the details of the ventilation and cooling system for the shaft sink as well as the monitoring system and the valuable data that has been collected.

Keywords: Ventilation, cooling, shaft, virgin rock temperature, heat loads

1. Introduction

Resolution Copper Mine [RCM] is a joint venture owned by Rio Tinto and BHP Billiton formed to develop and operate an underground copper mine near Superior, Arizona, U.S. The project targets a deep-seated porphyry copper deposit located under the inactive Magma Mine. Rio Tinto has reported a known resource of 1.3 billion tons containing 1.5 percent copper and 0.037 percent molybdenum. The proposed mine is one of the largest copper resources in North America. The mine is planned to be a 2116m deep block cave operation with virgin rock temperatures exceeding 80°C, Pascoe *et al* [1], Bluhm *et al* [2].

The project has sunk the exploratory No.10 Shaft to access the orebody for characterization studies, Goodell [3]. The 8.5m diameter No.10 Shaft sink encountered severe inflows of hot ground water at depth, in almost overwhelming quantities, but reached the ultimate depth in Nov 2014. The final sinking work was carried out under extreme conditions of depth, hot water ingress and geothermal heat and this related to a very impressive mining engineering achievement. The fact that there was only one serious lost time injury recorded during the six years is an exceptional safety achievement under these severe conditions.

During the planning stages it was recognized that, due to the high virgin rock temperatures and relatively high surface summer temperatures, heat and ventilation issues would prove to be very important in achieving the targeted sinking rates.

The ventilation and cooling system went through a number of revisions and modifications as operational changes in the shaft sink were implemented. In addition, when the shaft sink had advanced to within about 150m of the ultimate depth, very significant quantities of hot ground water were encountered. Following all efforts to minimize the inflow by cementation and grouting, the hot ground water ingress dictated the need to increase in the refrigeration resources. The inflow of hot water reached values of 38 l/s [600gpm] with some of the water at temperatures exceeding 80°C [original design criteria had been set at much lower flows]. This necessitated the urgent increase in refrigeration capacity and eventually the refrigeration rating required to complete the sink rose to 10MW_s. This paper deals with some aspects of the initial system, but focuses mainly on the ultimate system, shown in Figure 1.

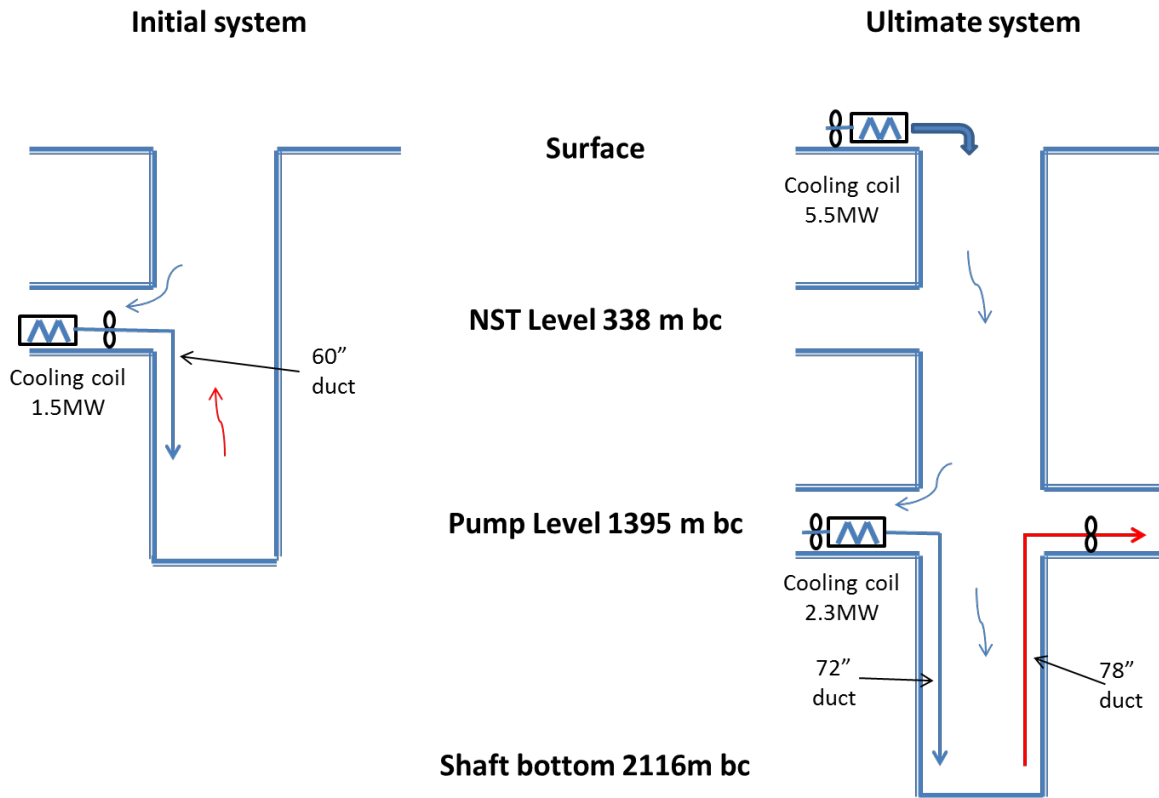


Fig. 1. Shaft and ventilation layout

The simplified layout is given in Figure 1 and some of the relevant project design criteria are:

- Summer surface temperature 21/37°Cwb/db
- Barometric pressure 88 kPa
- Max workspace temperature 7.5/37.5°Cwb/db
- Geothermal gradient / 100m 2.7°C
- Never Sweat [NST] level depth bc 338m
- Pump level depth bc 1395m
- Shaft bottom depth bc 2116m

The shaft sink was broken into two ventilation periods:

- Shaft sink from NST level to Pump level with fans and air cooler system on NST level.
- Shaft sink from Pump level to shaft bottom with fans and air coolers on surface and on Pump level

The initial system comprised free-standing air-cooled refrigeration machines located on surface near the bank providing cold water to underground. Figure 2 shows the first refrigeration unit at No.10 Shaft. The sinking fans and air cooling cars were initially located on NST level. The coolant [initially chilled water and later glycol] was circulated from the chiller to underground air cooling coils. The coolant remained in closed-circuit in an insulated supply and return 200mm pipe system.



Fig. 2. Air cooled refrigeration machines

The shaft sink ventilation was designed to normally operate in a forced ventilation mode. However, just before each blast, the flow was designed to be reversed and the system operated in an exhaust mode. Thus, at the blast and shortly thereafter, the blasting fumes, smoke, gases, dust, water vapour and heat were directly removed from the working environment. This approach was to assist with controlling the temperature conditions because heat and water vapour are removed directly from the system.

In the original design the cooling cars and main sink fans were planned to be relocated on Pump Level. However, with the encountering of hot ground water in

almost overwhelming quantities the refrigeration system had to be significantly upgraded. The ultimate system is described in the following sections.

2. Heat loads in ultimate scenario

An important feature of this work has been the simulation and monitoring of all the ventilation and heat flow components. The thermo dynamics of the overall system are complex because there are many interactive effects and analyses were carried out using specialist software. These programs interactively account for the effect of components such as ducts, pipes, surrounding rock, muck, machinery, density changes, duct leakage, water ingress and predict the air flow distribution and temperatures throughout the system. The monitoring has confirmed the accuracy of the models, and in this manner it has been possible to confidently predict and anticipate working conditions. The cooling and ventilation monitoring was a very important aspect. Measured data [temperatures, flows] were compared with predicted values and the predictions regularly calibrated to ensure predictions for future scenarios were accurate. The monitoring system is described in more detail in Section 6.

Figure 3 shows typical temperature variations at the measurement locations for a period in May 2013. The ‘Coil inlet’ reading is before the cooling coils on NST; ‘Force duct NST’ is after the cooling coils; ‘Set 116’ is halfway between NST and Pump Level; ‘Galloway duct’ is

the air delivered in the duct to the sinking stage and ‘Deck 5’ is the sinking stage deck closest to the bench. These measurements were taken during the period of increasing water inflow and show the effect of the additional heat in the bench area.

This extensive monitoring system allowed the calculation of the real heat loads [not theoretical] and allowed the models to be calibrated as conditions changed - this was an extremely useful tool to ensure sufficient ventilation resources were applied.

The various components of the heat loads are discussed below.

2.1 Fissure water

During the first part of the sink hot ground water encountered had averaged about 1 to 2 l/s but then at depth severe hot water was encountered and the inflow grew to 38 l/s [600gpm], see Figure 4.

The heat load from the water to the air environment is created by hot water being exposed to the atmosphere. The heat [and mass] transfer from the hot water surfaces to the air is dependent on the difference in vapour pressure between the water surface and the air mass as well as the temperature difference with convection and radiant components. The overall heat transfer from the exposed water will be rapid - it is a very efficient heat transfer mechanism with challenging consequences.

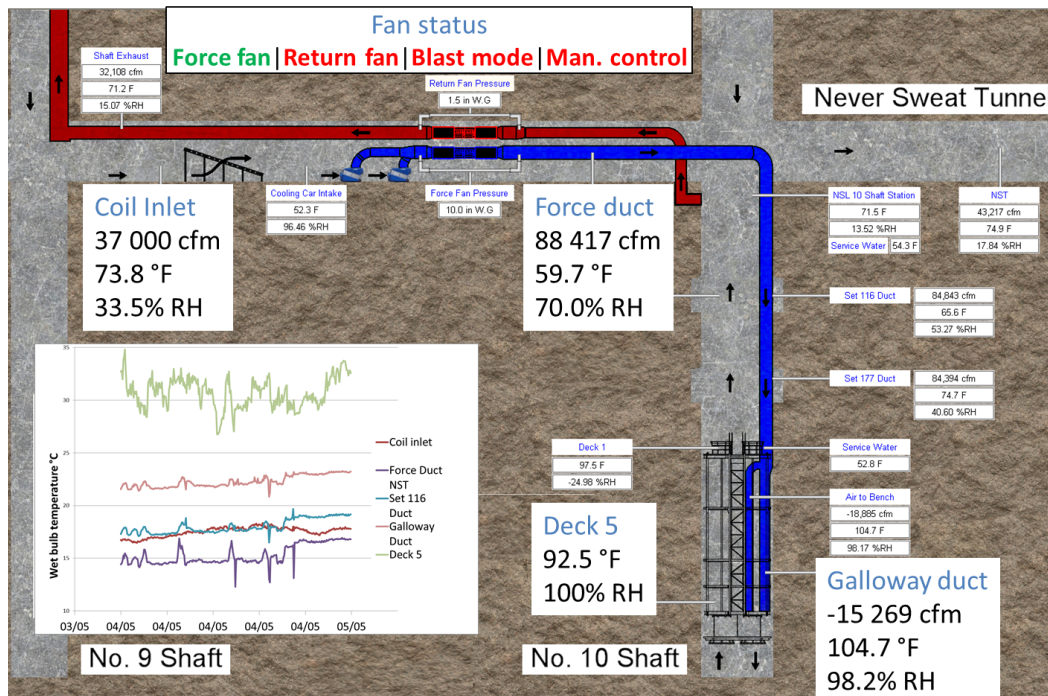


Fig. 3. Typical screen shot of monitoring system showing measured temperatures

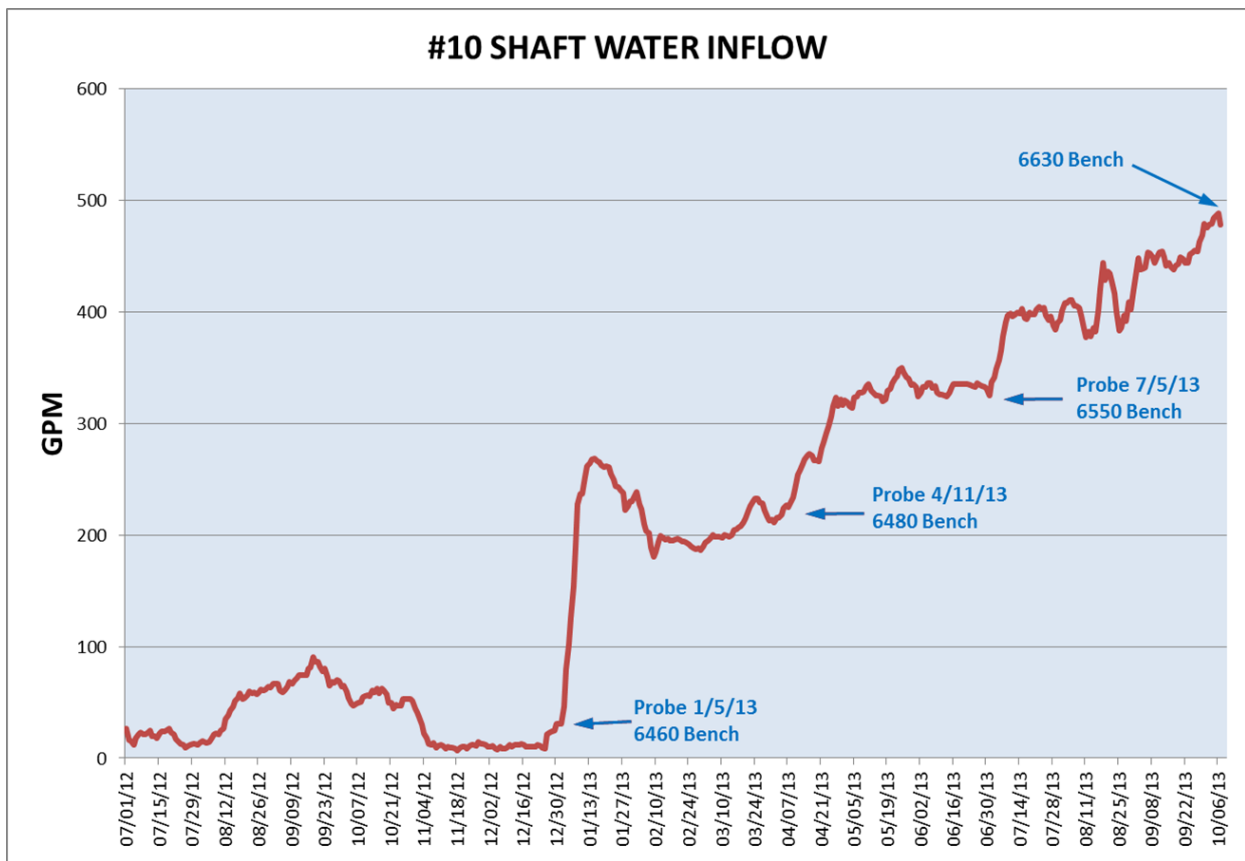


Fig. 4. Water inflow measurements

The water entered the ‘atmosphere’ at the virgin rock temperature or higher [this is common when fissure water is encountered]. The observed situation at No.10 Shaft was that water was ‘exposed’ and the partially flowed behind lining [coming out at joints and flowing down barrel]. It also flowed directly into the unlined barrel sections and the bench.

Figure 5 shows a thermal image of the conditions on the bench during the period of high water inflow.



Fig. 5 Thermal image of drilling through grout packer into hot water.

The water left the overall barrel workspace at an average of 43°C. Thus this ground water was cooled by 28°C, imparting this heat load of 4.4MW onto the underground work environment. The measured heat from the fissure water in the barrel and bench areas was as follows:

- Barrel to top of Galloway 3.1MW
- Bench area 1.3MW

Based on measurement of the water temperature at various locations, it was determined that the hot water entered an exposed position at an *average* temperature of about 71°C with certain areas near the bench in excess of 80°C. In order to appreciate the severity of this, Figure 6 shows conditions under which scolding will take place - the severity of the RCM temperatures is self-evident [this graphic was part of RCM’s safety considerations].

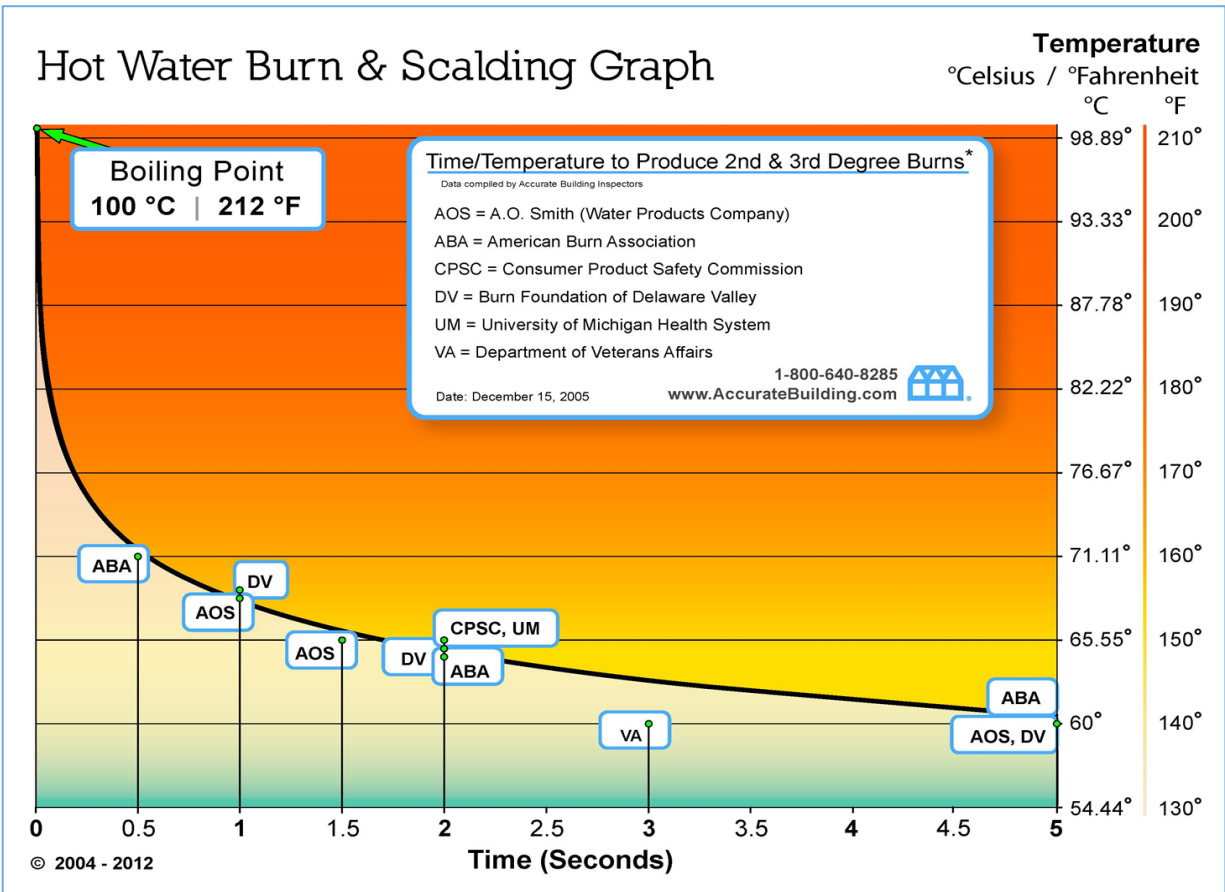


Fig. 6 Scalding potential due to expected hot water

3. Other heat loads

The mining operations at the face are cyclical with drilling, blasting and cleaning activities. The variations in heat flow within the cycle become repetitive and a pattern [re-occurring state] evolves. Furthermore, because of the thermal storage effects of the surrounding rock, broken rock and water at shaft bottom, the cyclical nature of the shaft sinking activities are damped-out [to a large extent]. The calculation methods determine the cyclical average heat flow based on the re-occurring state.

The analysis divided the sinking zone into a number of areas and determined the cyclical average heat flow [based on the re-occurring state]. The heat flow processes are complex and, in this work, the VUMA software was used. VUMA allows the thermodynamic and aerodynamic flow parameters to be predicted simultaneously. In this analysis, there was a further complication [requiring iterative calculation] because heat transfer occurred between the refrigerated air in the duct and the air in the shaft barrel and heat from exhaust duct. The ongoing measured data obtained during the sink assisted in checking the model and calibrating input parameters as necessary. The results of the air flow and heat load analysis are depicted in Figure 7 and the observations are as follows.

4. Heat cooling balances

4.1 Heat load in barrel - Pump Level to top of Galloway

The total heat flow into the barrel to top of Galloway was determined [and measured] as:

Heat from surrounding rock, autocompression	1.0MW
Heat from fissure water	3.1MW
Total heating to top of Galloway	4.1MW

Of this heat, some flowed to the downcast air in the upper barrel, some to the 72" duct, some to the 78" duct and the balance to the shaft bottom with the air in the barrel which ultimately entered the 78" duct.

Heat from barrel to 72" duct	0.7MW
Heat from barrel to 78" duct	0.1MW
Air in barrel into 78" duct	3.0MW
Downcast air in upper barrel	0.3MW
Total cooling to top of Galloway	4.1MW

4.2 Heat load at bench area

The ventilation air was delivered to the workspace [Galloway] at about 18/26°Cwb/db where it experienced complex heat and mass [water vapour] transfer processes. Heat flow components included surrounding rock, broken rock, fissure water, cement hydration, equipment, explosives, men, etc. The heat and mass transfer

components also included the effect of ‘resident’ water [on rock and shaft bottom] as well as the effect of applying fresh service water and the small effect of the compressed air exhaust from pneumatic equipment. The reject condition from the work space was 27.5/33°Cwb/db. Thus the net heat pick-up of the air flow was 1.8MW, which was 95% of the total heat load. The heat balance in the workspace relates to:

Heat from surrounding rock, broken rock 0.5MW
 Heat from fissure water 1.3MW

Heat from equipment, hydration, lights, men 0.2MW
Total heat 2.0MW
 Cooling from ventilation air 1.9MW
 Cooling from service water + comp air 0.1MW
Total cooling 2.0MW

Figure 7 shows the condition at shaft bottom and summarizes the heat balance.

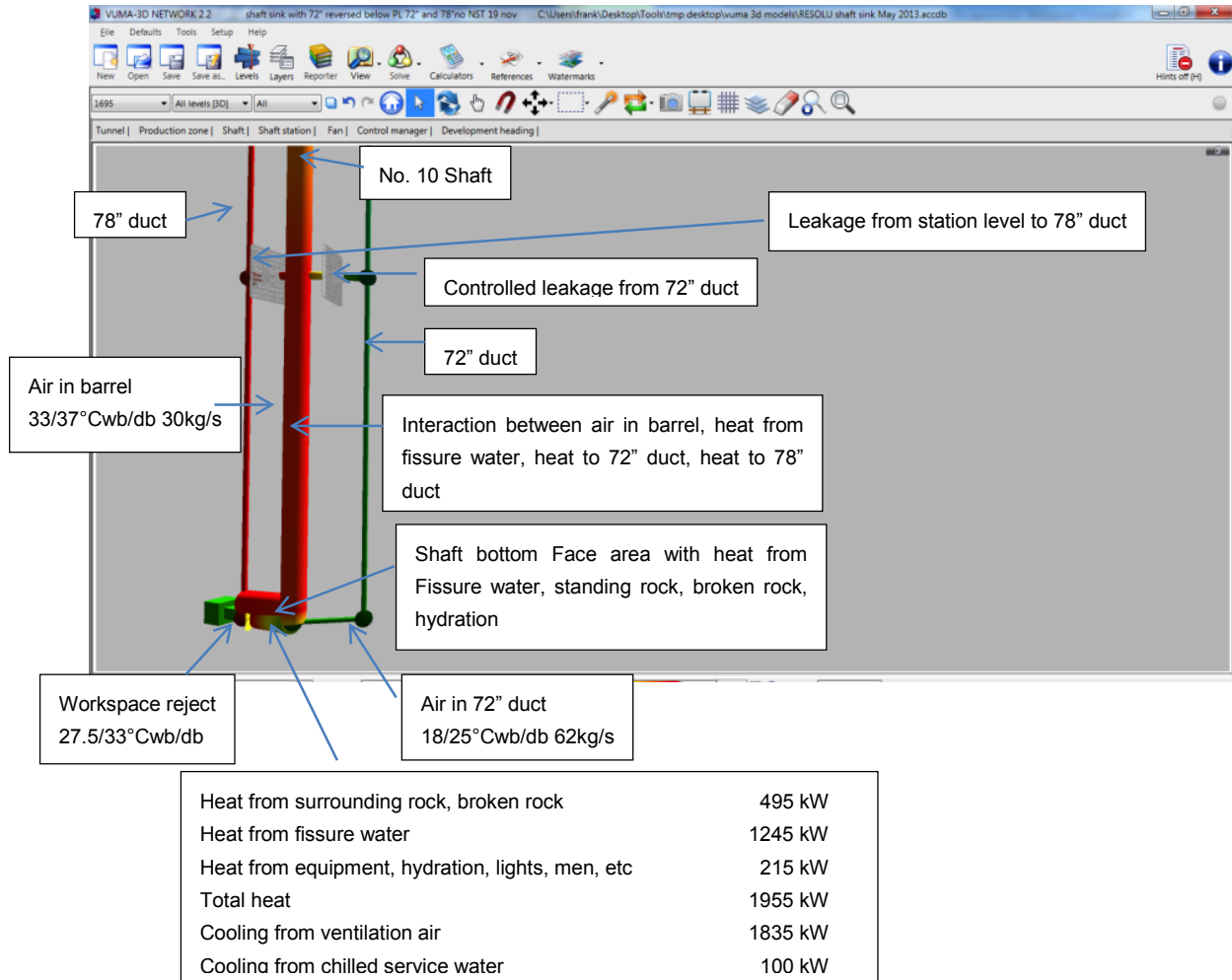


Fig. 7. Critical parameters at shaft bottom

5. Ultimate ventilation/cooling system

5.1 Ventilation

Figure 8 shows a process flow diagram of the ultimate ventilation and cooling system. The primary ventilation flow of 115kg/s was delivered to Pump Level in the No.10 Shaft barrel from surface. Of this, the ventilation rate delivered to the 72" ventilation duct on Pump Level was

80kg/s. This flowed through the main force fan with pressure rating 2.6kPa [10.3"] and then to the cooling coil banks. As it flowed down the duct, air leaked out of the 72" duct at joints and, in addition, butterfly dampers located below the main stations were used for controlled leakage to ensure acceptable conditions in the barrel of the shaft. There was also leakage from the barrel into the 78" exhaust duct.

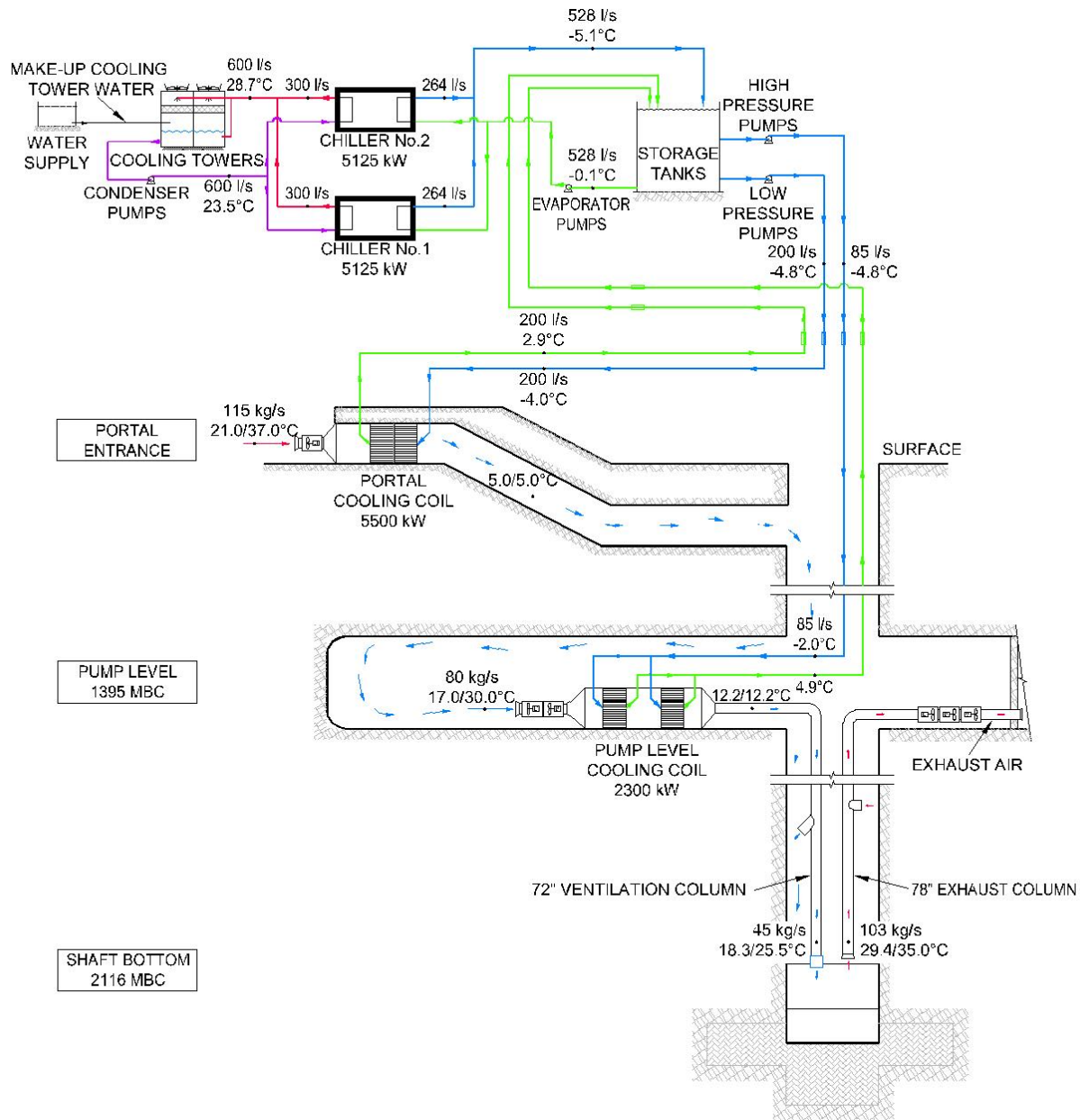


Fig. 8. Process flow diagram of ultimate system

The air flow delivered to the sinking stage was about 50kg/s. The ratings of the installed fans were as follows:

- Surface portal fresh air 1x250hp 115kg/s
- Pump level fresh air 2x250hp 80kg/s
- Pump level exhaust 3x250hp 115kg/s

5.2 Cooling capacity

Cooling stations were established on surface and on Pump Level. The pipes delivering coolant to and from the underground cooling coils on Pump Level were 200 mm

diameter. With the ingress of hot ground water, it was necessary to fully maximize the cooling carrying capacity of this pipe system. This included using a high pressure pump system to maximize flow at significantly higher-than-normal pipe flow speeds [maximum design flow of coolant that could be delivered to Pump Level was 85l/s]. The maximizing of the cooling carrying capacity also included converting the coolant to glycol and operating at sub-zero temperatures, and a 28% mixture of ethylene glycol and water solution was introduced. This allowed the chilled coolant to be operated down to -4°C. This low temperature coolant also helped in reducing the size of the

cooling coils on Pump Level where there was limited space available.



Fig. 9. Surface cooling coil and force fan

The ultimate cooling system had the following rated cooling coil air coolers:

- Surface portal air cooler 5.5MW_k
- Cooling coils on Pump Level 2.3MW_k
- Total available cooling capacity 7.9MW_k

Figure 9 shows the cooling coils on surface and Figure 10 shows the layout of the force and exhaust ducting on Pump Level. Figure 11 shows the Pump Level cooling coils under construction.

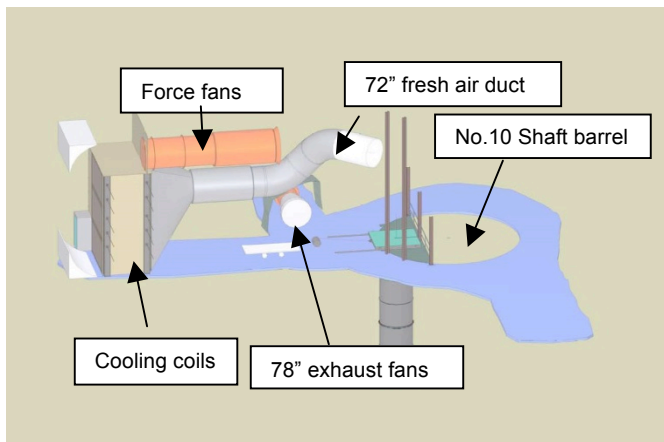


Fig. 10. Layout of force and exhaust ducting on Pump Level

The cooling provided to the cooling coils was delivered by two single-stage centrifugal refrigeration machines each rated at 5.2MW_k operating with glycol to give a total rating of 10.4MW_k. The system thus had some spare rated capacity which was an appropriate level of contingency planning considering the drastic effects of the hot ground water.



Fig. 11. Pump Level cooling coil under construction

Figures 12 and 13 show some of the refrigeration components, including the insulated pipe delivering the glycol/water mixture to the cooling coils.



Fig. 12. Glycol/water chiller in plant room

6. Monitoring system

The underground ventilation control activities comprised:

- PLC for system control sequences and interlocks
- MCC switch-gear for fans and duct gate actuators.
- Variable speed drives [VSD] for all fan units



Fig. 13. Plant room, condenser cooling towers and insulated piping

- Instrumentation and displays of:
 - all relevant information from Surface Control Centre [see below]
 - gas monitoring instrumentation
 - status of ventilation control gates
 - ventilation flow rates [in-duct air speed]
 - ventilation air temperatures
 - ventilation air pressures
 - water flow rates
 - water temperatures
 - water pressures [manual gauges only]
 - fan unit[s] vibration levels
 - fan motor[s] winding temperatures
 - electrical power information
 - fan units running indication

The underground-based PLC system was connected via fibre-optic back-bone to the surface-based control centre located in the hoist control room.

The Surface Control Centre comprised:

- MCC switch-gear for chilled water pumps and supply to refrigeration modules
- PLC for system control sequences and interlocks
- Display of I/O ex refrigeration machine proprietary embedded PLC and instrumentation
- Instrumentation and displays of information from Underground Control Centre [as above]

The ventilation monitoring instrumentation installed on the Galloway was kept practically minimalistic. The only instrumentation related to gas monitoring equipment [O₂, CO, NH₃] at the duct cassette assembly.

Manual measurement of shaft-bottom temperature conditions and air flow rates was by hand-held instruments and manually recorded and reported. While due consideration was given to more sophisticated systems, it was felt it was impractical to expect such systems to operate reliably in this environment.

The tool based on the comparisons between predicted and measured data will be used for the design of effective

‘calibrated’ ventilation/cooling systems for the future shaft sink operations at Resolution.

7. Conclusions

The 4.4MW heat load from the water made up 66% of the total heat load and almost overwhelmed the capacity to complete the sink. It was only through the application of a significant refrigeration system [the magnitude of which would normally be sufficient to cool an entire hot mine] that the heat load from the water was combatted.

The work has been carried out under extreme conditions of depth, hot water ingress and geothermal heat and will probably go down in the annals of shaft sinking history as one of the most difficult. In addition, the fact that there was only one serious lost time injury recorded during the six years is a phenomenal safety achievement under these very severe conditions.

An important feature of this work was the simulation and monitoring of all the ventilation and heat flow components. The thermo dynamics of the overall system are complex because there are many interactive effects and analyses were carried out using in-house computer programs. These programs interactively account for the effect of components such as ducts, pipes, surrounding rock, muck, machinery, density changes, duct leakage and predict the air flow distribution and temperatures throughout the system.

The monitoring has confirmed the accuracy of the models, and in this manner it has been possible to confidently ensure healthy and safe working conditions while at the same time minimizing both the capital and running costs and optimizing the timing of the capital expenses. Valuable lessons have been learnt, which will be applied during the design of the remaining shafts required for Resolution Copper mine.

Acknowledgements

The ventilation and cooling design was undertaken in close cooperation with RCM, RSV-USA and Cementation. The authors thank RCM for permission to present this paper.

References

- [1] Pascoe, C, Oddie, M & Edgar, I, 2008. Panel caving at the Resolution Copper project, in *Proceedings Fifth International Conference and Exhibition on Mass Mining*, Lulea, Sweden.
- [2] Bluhm, S, Moreby, R, von Glehn, F & Pascoe, C. 2013. Life-of-mine ventilation and refrigeration planning for Resolution Copper Mine, in *Proceedings Australian Mine Ventilation Conference*, Adelaide, Australia, July 2013.
- [3] Goodell, T. 2014. Sinking America’s deepest shaft, in *Proceedings of the 40th ISEE Conference on Explosives and Rock Blasting Techniques*. February 2014 Denver Colorado

Ventilation Analyses at the Waste Isolation Pilot Plant Post Radiological Event

Keith G. Wallace^a, Jill I. Farnsworth^b, Eric C. Rodriguez^b

^aMine Ventilation Services, Inc., Clovis California, USA
^bNuclear Waste Partnership, LLC, Carlsbad, New Mexico, USA

On the evening of February 14, 2014, radiological sensors underground at the Waste Isolation Pilot Plant (WIPP) facility detected a radiation release. This sensor triggered a reconfiguration of the ventilation system from a flow of 123 m³/s (260,000 cfm) to 28.3 m³/s (60,000 cfm) through two HEPA filtration trains. The ventilation system has been kept at a filtered flow of 28.3 m³/s (60,000 cfm) since the radiation event. Approximately two months after the event several of the high efficiency pre-filters in the filter trains were showing an increase in differential pressure, which is indicative of filter loading. This paper describes the analyses performed to engineer a “by-pass” inlet to the operating fan in order to maintain 28.3 m³/s (60,000 cfm) while taking one filter train off line. Once the train was off-line, the pre-filters could be changed out. Operating at the filtered flow rate also resulted in noticeable impacts from natural ventilation pressure, particularly in the winter months. This too is described in the paper along with the proposed modifications to the current ventilation configuration. Proposed modifications include the addition of fans and filter trains on surface in parallel with the existing system and the addition of an underground booster fan to increase flow to the “clean” side of the facility.

Keywords: Mine ventilation design, nuclear waste repositories.

1. Introduction

The Waste Isolation Pilot Plant (WIPP) facility is the only transuranic waste repository in the United States. The facility is located approximately 30 miles East of Carlsbad, New Mexico (Figure 1). The WIPP facility is a U.S. Department of Energy facility designed for the permanent disposal of transuranic radioactive waste. Transuranic waste typically consists of materials which have come in contact with radioactive substances. This can include gloves, tools, rags, and assorted machinery used in the production of nuclear fuel and weapons. The WIPP facility opened in 1999 and had completed emplacing waste in 6 of 8 panels. The repository horizon is 655 m (2,150 ft) below surface in the Salado geologic formation (salt).

In February 2014, two incidents occurred at WIPP. On February 5th, a salt haul truck caught fire. Workers were evacuated and the underground operations were shut down. Nine days later, on the evening of February 14th, a second, unrelated event occurred when a continuous air monitor (CAM) alarmed. The CAM measured airborne radioactivity close to the panel where active waste emplacement operations were occurring. The CAM alarmed in the evening and no personnel were underground at the time of the incident. Figure 2 is a drawing of the WIPP facility and shows the location of these two events. The CAM alarm triggered an automatic ventilation system switch from one primary unfiltered fan to filtration mode where all air exhausting the underground passes through high efficiency filter banks. The cause of the release is likely due to a container of waste self-heating in Panel 7, Room 7.

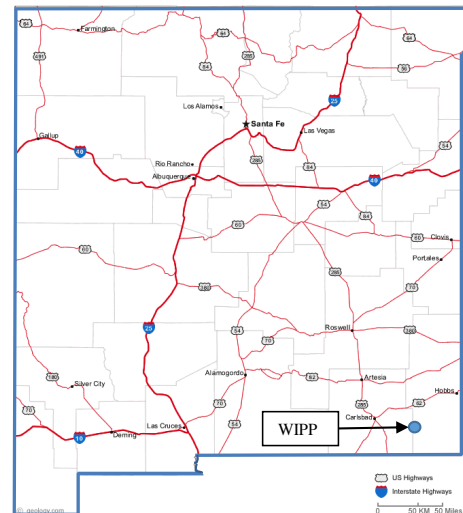


Fig. 1. Location of WIPP facility.

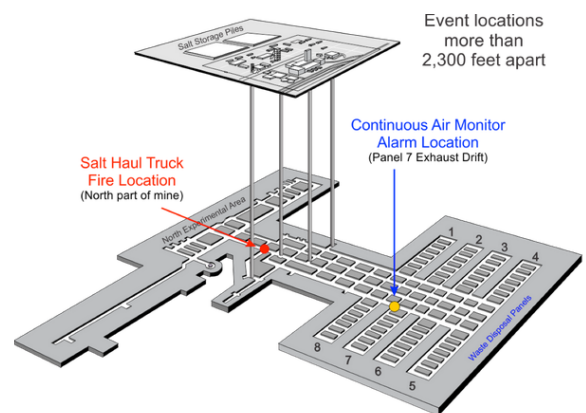


Fig. 2. WIPP facility and location of incidents.

The efforts at WIPP since the radiation event have included investigations into what caused the radiation event and establishing work areas in the underground for

ground control activities (e.g. rock bolting and scaling). From a ventilation perspective, the key work has been developing a methodology to replace air filters in the filtration building and concepts to increase total filtered exhaust capacity. In addition, understanding the impact of natural ventilation pressures (NVP) on the airflow distribution became more important while in filtration mode.

2. Ventilation and primary fan description

The underground ventilation system at WIPP is divided into four primary splits. These are the North area, the construction area, the disposal area and the waste shaft station area. Figure 3 shows these areas. The surface fans consist of three 445 kW (600 hp) “700” series centrifugal fans and three 175 kW (235 hp) “860” series centrifugal fans. Figure 4 shows the surface fan configuration along with the filtration building.

Prior to the radiologic event, in normal operation, the ventilation system discharged unfiltered air. One or two of the unfiltered 700 fans were typically operated. Two 700 fans will generate a volume of approximately 225 m³/s (475,000 cfm). One 700 fan in operation will generate a flow of 125 m³/s (265,000 cfm).

Since the radiologic event, the ventilation system has been maintained in filtration mode. In this mode, one of three filtration 860 fans operate to deliver 28.3 m³/s (60,000 cfm) to the underground and through the filter trains inside of the filtration building. Two filter trains are in parallel, each with a capacity of 14.2 m³/s (30,000 cfm). A filter train contains four filter banks in series; these are one moderate efficiency (60-65%) bank, one high efficiency (90-95%) bank, and two HEPA (High

Efficiency Particulate Air of 99.97% efficiency) banks of filters.

3. Operating the facility in filtration mode

In filtration mode only 28.3 m³/s (60,000 cfm) is exhausting the underground. Because the repository horizon is 2,150 ft below surface and the air expands as it courses up the Exhaust Shaft (ES), the actual airflow on the horizon is approximately 26.0 m³/s (55,000 cfm). This mode isolates portions of the underground by closing all connections between the construction circuit and the disposal circuit. In addition, air from the north circuit is isolated by closing a strategic door in the north circuit return. The primary circuit in this configuration is air intaking the Waste Shaft (WS) and coursing across to the ES. However, intake air is also provided by leakage across bulkheads separating the construction and north end to the disposal and waste shaft station circuits. In filtration mode the primary ventilation function is to maintain underground flow from the clean area to the disposal circuit and ensure all exhaust air from the disposal circuit and waste shaft station passes through the surface filtration system. Because the WIPP facility is constructed in a salt horizon, the ground predictably creeps. This action results in squeeze on bulkheads. A typical bulkhead with regulator is shown on Figure 5. As seen, the bulkhead consists of steel center section with conveyor belt material as flashing around the edges. The bulkhead steel supports are designed to slide both vertically and horizontally to allow for some relief to the squeeze. The design works well, but inevitably leads to some leakage across each bulkhead. This air leakage accounts for a significant amount of the total flow in filtration mode. The leakage is from the north and construction circuits (clean side) to the disposal circuit.

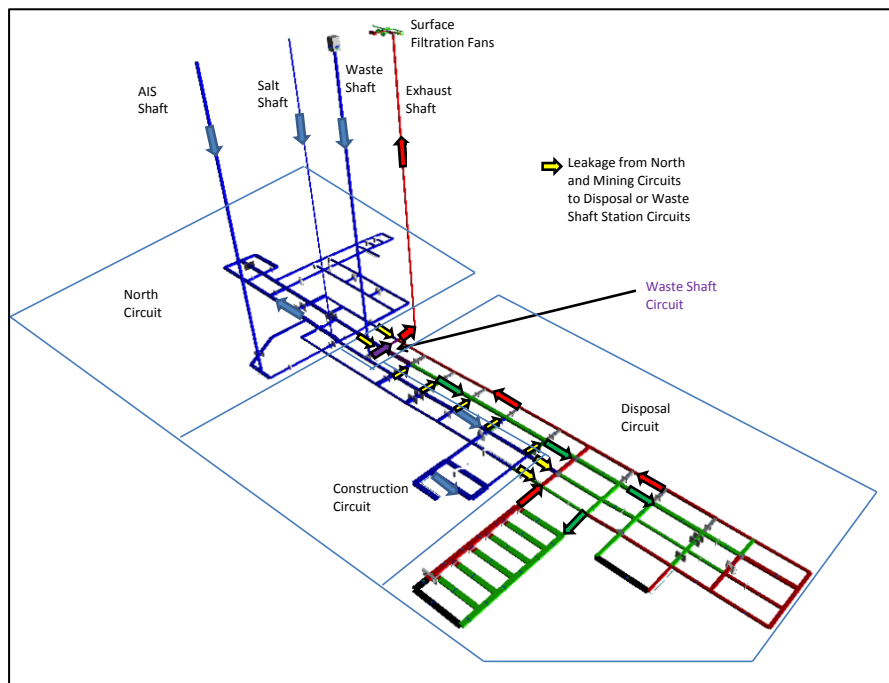


Fig. 3. Underground ventilation circuits at WIPP.

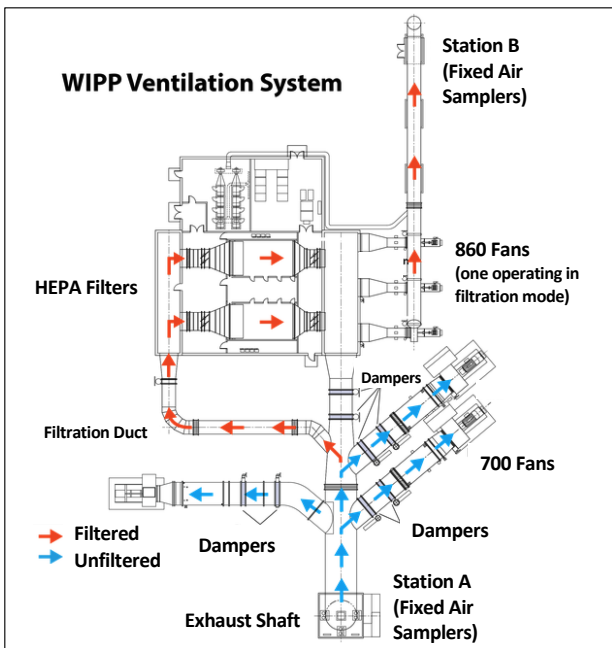


Fig. 4. WIPP surface fan configuration.



Fig. 5. Example of bulkhead with regulator at WIPP.

3.1 Ventilation configuration for filter change out

The 860 fans were originally designed at WIPP to provide 28.3 m/s (60,000 cfm) at very high operating pressures. The reason for this was in the mid-1980s these fans were going to be the only surface fans for the facility. All three would operate in parallel, bypassing the filter units and delivering about 85.0 m/s (180,000 cfm) with a fan total pressure of approximately 3.7 kPa (15 in. w.g.). Subsequently, the design changed to include the 700 fans and a third intake shaft (the Air Intake Shaft). The flow through each 860 fan can be adjusted using an inlet vane control (IVC). Because the fans were specified for high pressure, the IVC needs to be adjusted significantly to fix the airflow at 28.3 m/s (60,000 cfm). Figure 6 shows an 860 fan curve. To maintain the design flow the IVC is set to approximately 50% of full open.

After the radiation event, the differential pressures across the filters were continuously monitored. Engineers noted that the moderate and high efficiency filters in both filter trains were increasing in pressure while the HEPA filters maintained a steady pressure drop. Figure 7 shows the filter arrangement for each filter train. It was thought that the truck fire incident may

have resulted in some build up on the moderate and high efficiency filters of soot and smoke, causing these filters to load with moisture exhausting from the underground.

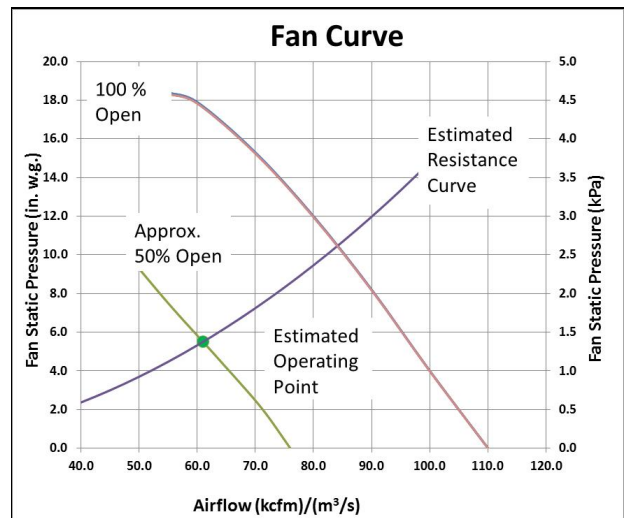


Fig. 6. 860 fan curve.

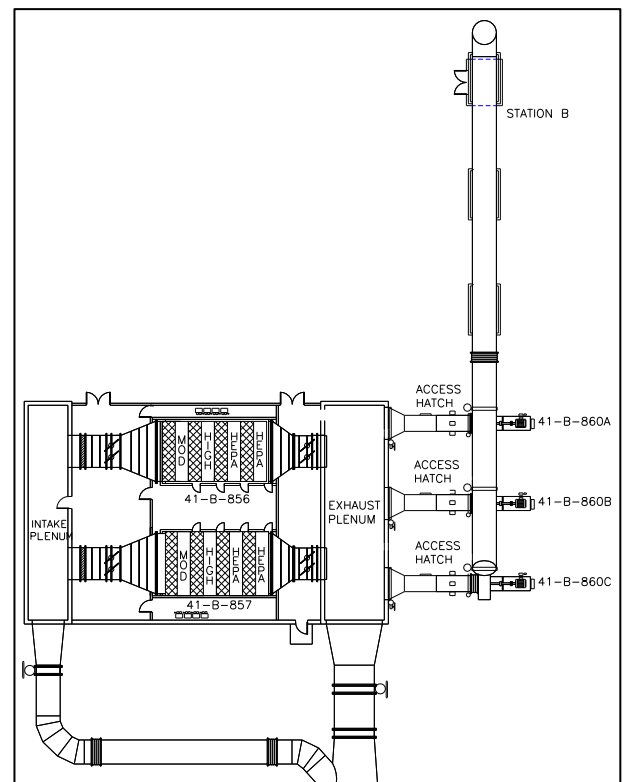


Fig. 7. Filter arrangement drawing.

Even though the differential pressure for these filters was well below the design limit values for filter failure, project management decided that it would be best to change out the moderate and high efficiency filters in each filter train. To do this one filter train needed to be taken off line while maintaining some flow to the underground. This would produce an underground airflow of only 14.2 m/s (30,000 cfm).

The site ventilation engineer became concerned that attempting to operate an 860 fan with an IVC setting capable of providing this low flow would result in

excessive vibration of the 860 fan. Vibration on the 860 fans was noted to be relatively high and the project did not wish to exacerbate the potential problem. Therefore, another option was required to maintain the 860 fan at 28.3 m³/s (60,000 cfm) but only allow 14.2 m³/s (30,000 cfm) through the single operating filter train.

Engineers investigated the 860 fan system and noticed an access hatch on the inlet side to each fan (see Figures 7 and 8). Opening this hatch on one of the non-operating fans and opening an isolation damper to the filter train exhaust plenum, air could be short-circuited into the adjacent operating fan while maintaining a nominal 14.2 m³/s (30,000 cfm) through the operating filter train.

The calculation used to verify the opening size of the hatch was to calculate the area from the following orifice equation (in imperial units):

$$A=CQ(\rho/p)^{0.5} \quad (1)$$

- Where
- A = Orifice Area (m² or ft²)
 - C = Constant (1.2 [SI] or 48.8924 [IMP])
 - Q = Airflow (m³/s or kcfm)
 - p = Differential Pressure (Pa or milli-in. w.g.)
 - ρ = Air Density (kg/m³ or lb/ft³)



Fig. 8. 860 fan access hatch with isolation damper.

This equation to compute the orifice area is in the ventilation simulation package VnetPC Pro+. Applying a fixed airflow to the hatch in the model resulted in an estimate of the required area to achieve the required flow through the hatch while maintaining flow through one filter train while the other filter train was being worked on. Modeling showed an area of 0.55 m² (6 ft²) would be sufficient to achieve the design flows. Field testing using hot wire anemometers and a digital manometer resulted in setting the regulator area to 0.72 m² (7.75 ft²). The model results were found to be a reasonable predictive tool in setting the regulator area. Field testing confirmed airflow through a single filter train at 14.2 m³/s (30,000 cfm) while maintaining at least 28.3 m³/s

(60,000 cfm) through the operating 860 fan. Vibration was not an issue during the filter change out.

To switch from one filter train to the other for changing the moderate and high efficiency filters, the process involved opening the filter train that had been changed out in parallel with the filter train to be changed. The by-pass regulator was opened fully during this process. Once both filter trains were open, the filter to be changed was isolated from the circuit and the by-pass regulator adjusted to deliver the desired flow distribution to limit flow through the single filter train to 14.2 m³/s (30,000 cfm).

4. Impact of natural ventilation pressure

Natural ventilation pressure (NVP) at WIPP can be significant. NVP is caused by an imbalance in air density between two columns of air. The WIPP site is at an elevation of approximately 1,000 m (3,200 ft) above sea level. It is in a high desert and diurnal variations cause temperatures to swing from 30 °C (86 °F) to -1 °C (30 °F). In addition, seasonal changes can record temperatures as low as -10 °C (14 °F) to as high as 41 °C (106 °F). These wide temperature swings result in NVPs that can assist or oppose flow into the underground. Calculations of NVP have shown during cold winter conditions, pressures as high as 0.6 kPa (2.4 in. w.g.) can be applied assisting airflow into the facility. In summer, a negative pressure (opposing flow to the underground) of -0.35 kPa (-1.4 in. w.g.) have been measured.

In filtration mode the impact of NVP is more pronounced. Therefore, to maintain flow at 28.3 m³/s (60,000 cfm), the 860 fan only needs about 1.5 kPa (6 in. w.g.) (see Figure 6). Of this delivered pressure the filter train pressure drop is approximately 1.0 kPa (4 in. w.g.) This means only 0.25 to 0.5 kPa (1.0 to 2.0 in. w.g.) is available to move air through the underground and through the surface ductwork. There can be times when the NVP is greater than the delivered fan pressure.

With high winter NVPs and three intake shafts, Air Intake Shaft (AIS), Salt Handling Shaft (SHS), and Waste Shaft (WS), if unchecked, air will downcast the larger diameter AIS and air will upcast the SHS and potentially upcast the WS (by pushing air through bulkheads and doors to the waste shaft station). When the radiologic event occurred in February, 2014 it was a relatively cold day. It was noted that after the shift to filtration that evening, air at that time was significantly downcasting the AIS and upcasting the SHS. The SHS was acting like a “relief valve” for the additional air entering the facility. This had no impact on maintaining air leakage from the “clean” side of the underground to the disposal circuit. In fact, the high NVP resulted in significant differential pressures across bulkheads separating the construction and north areas from the disposal circuit (forcing more air towards the disposal circuit). The excess air entering the AIS was simply upcasting the SHS.

To minimize the impact of NVP, site operators with engineering consent, have covered the top of the AIS with brattice. With the AIS covered, the primary intakes are the SHS and WS. This is the current configuration at the site and will likely continue until ventilation upgrades are complete.

5. Ventilation upgrades to support recovery

WIPP currently is working on recovering the underground from the radiologic event in order to resume normal activities. Recovering from this accident will require isolating the emplacement room where the accident occurred, decontaminating areas where there is contamination, conducting ground control operations, and installing an interim closure system for panel 6 (it was in the process of having a closure system installed at the time of the accident).

With the current 28.3 m/s (60,000 cfm) fan flow, it is challenging to do the recovery activities listed in a timely manner. Diverting the limited airflow to strategic areas in the underground will achieve this task, but parallel activities may not be possible because of the limited total airflow. Therefore, two ventilation modifications are to be installed at WIPP. The first, called Interim Ventilation System (IVS) installs additional filtration capacity to increase flow through the ES. The second is to install an underground booster fan to increase airflow to the construction and north air circuits. This is called the Supplemental Ventilation System (SVS). These systems are being brought on line until a permanent ventilation system upgrade is installed at WIPP.

5.1 Interim ventilation System

To support recovery efforts additional filtered air exhaust is required. This will be achieved by installing new surface filtration units. IVS will increase total surface filtration capacity by two more filter trains on the surface. Each new filter train will handle an additional 12.7 m/s (27,000 cfm). This will increase the total filtered air exhaust to 53.8 m/s (114,000 cfm). This total is comprised of 28.3 m/s (60,000 cfm) from the 860 fan plus 25.5 m/s (54,000 cfm) through the new filter units. The increase in flow will allow for recovery activities to be performed in the disposal circuit and will also allow for resumption of limited waste handling operations, once the clean-up and room and panel closure systems are installed.

Figure 9 depicts the proposed new surface filtration units. Each filter train will have a dedicated fan (called 960 fans). The intake side of the filter train will connect to one of the existing 700 fan ducts with the exhaust duct routed to the current exhaust duct to Station B. Station B is a monitoring point for air exhausting the underground and all air is designed to pass through this station (see Figure 7). The IVS is expected to be operational by mid to late 2015.

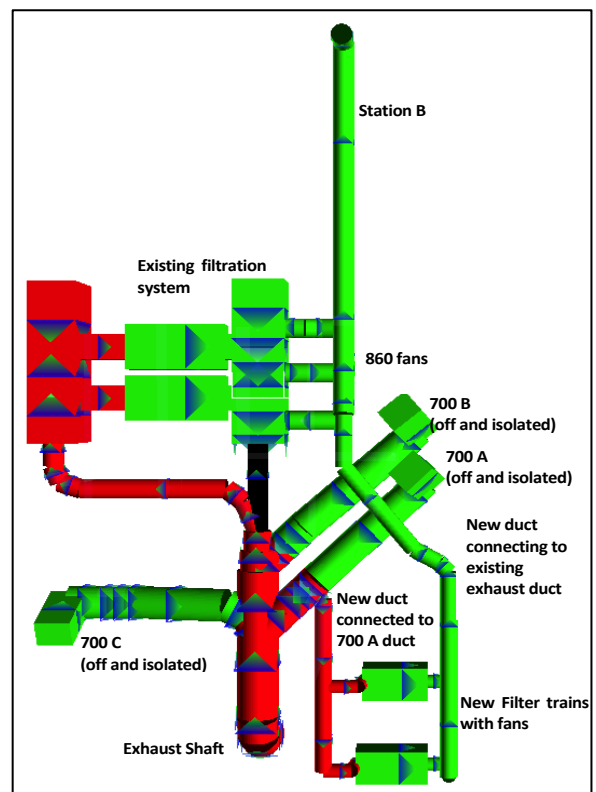


Fig. 9. Surface arrangement for IVS

5.2 Supplemental ventilation system

After the IVS is installed and operational the airflow exhausting the WIPP underground will be limited to 53.8 m/s (114,000 cfm). This is insufficient flow to support mining activity in the construction area and experimental work in the north areas of the mine (see Figure 3). Therefore, engineers have developed a system where a booster fan is installed in the underground that will pull air down the AIS and push air to the north area and construction area. The air downcasting the AIS will upcast the SHS and pass through to the disposal circuit to supplement the air downcasting the WS.

The booster fan will be located in the S-90 drift at the base of the AIS. The design is for 61.3 m/s (130,000 cfm) passing through the booster fan. Of this between 33 and 38 m/s (70,000 and 80,000 cfm) will upcast the SHS. The AIS was selected as the downcast shaft because of its greater capacity than the SHS. Pulling 61.3 m/s (130,000 cfm) through the 3.1 m (10 ft) diameter SHS (with fixed buntons and guide arrangements) would require significant fan pressure, particularly when the cage is stationed at the shaft collar. Figure 10 shows the location of the booster fan and predicted airflow distribution through the underground. A control bulkhead will be installed to the north of the SHS so intake air from S-90 can course north and return to the SHS from the east.

The S-90 fan motor will be equipped with a variable frequency drive (VFD) to maintain the flow at 61.3 m/s (130,000 cfm). A flow sensor will be installed in the booster fan for the purpose of automating the VFD setting. However, in very cold surface conditions, the NVP may apply a significant pressure that would cause the S-90 fan to behave more as a regulator than a fan.

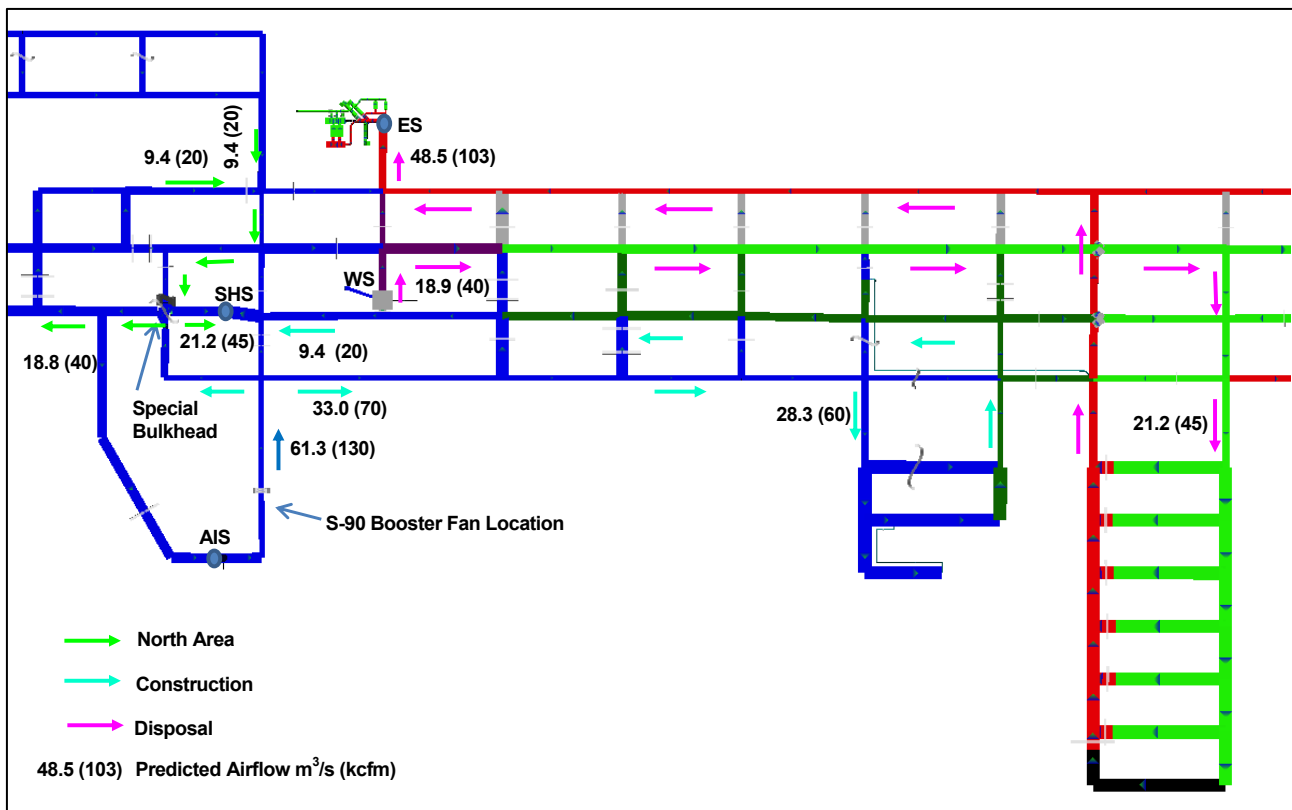


Fig. 10. Proposed IVS/SVS underground ventilation circuits at with predicted airflows at WIPP.

In order to maintain a constant flow through the fan, in addition to a VFD the outlet of the fan will have a louvered regulator that will be controlled by an electric actuator. In high winter NVP conditions the fan VFD will adjust to a low value then the regulator will begin to close to maintain the flow. This will allow the fan to operate in a stable range while controlling NVP impacts on the underground flow distribution. The S-90 fan was specified to handle the highest pressure predicted from the maximum summer conditions where the NVP can oppose flow to the underground. In this condition, the VFD will operate closer to full load with the regulator wide open.

5.3 Control logic for IVS and SVS system operation

After the IVS and SVS systems are installed at WIPP it will be necessary to understand how the two systems interact. The base analysis assumes all filtration fans are in operation along with the S-90 fan. Engineering modeled the ventilation system when one or more surface fans are off line. In this situation it is possible for the S-90 fan to push air into the disposal circuit and then drive air from the disposal return towards the WS. This is an undesirable consequence of operating an underground booster fan with a loss of surface fan operation. Therefore, control logic was developed that will automatically shut down the S-90 fan should flow reversal be monitored at the regulator separating the waste shaft station from the disposal return. This control will be hardwired from the differential pressure sensor on this regulator to the programmable logic controller for the S-90 fan.

Engineering also analyzed the impact of losing the S-90 fan while operating the IVS fans. The SVS brings air down the AIS and upcasts the SHS. Of the 48 m/s (103,000 cfm) entering the ES, only 19 m/s (40,000

cfm) is intake air from the WS. This results in 29 m/s (60,000 cfm) of intake air coming from the construction and north areas of the underground (leakage through bulkheads and controlled inlet through regulators). Concern was raised over the potential time delay, following the S-90 fan power loss, before the upcast column of air in the SHS reverses to provide airflow necessary to ventilate the disposal circuit.

To ensure flow is maintained through the AIS shaft to provide air to the disposal circuit, the S-90 fan upon loss of power will fail open (that is the damper will stay open allowing air to flow through the fan assembly). With this condition, modeling showed that there was a minimal impact on the overall ventilation system when the S-90 fan is turned off.

In addition to the underground control system monitoring differential pressure and the S-90 fan operational condition, all data from both the surface fans and underground will be transmitted to the Central Monitoring System (CMS) at WIPP. The CMS will also have the ability to stop any operating fan. Therefore, should an alarm be noted caused by a fan outage or other event, the CMS operator could manually turn off the underground fan.

With the SVS and IVS in place, the underground ventilation system at WIPP will be able to recover from the radiologic event and begin limited operation until a permanent upgrade to the WIPP ventilation system is installed

5.4 Permanent ventilation upgrades

At present the Department of Energy is evaluating numerous options to upgrade the permanent ventilation system at WIPP. These options may include a new shaft,

increased surface filtration capacity and other capital improvements. The recommended permanent ventilation system upgrades have not been determined at the time of preparing this paper.

Acknowledgments

The authors would like to acknowledge the management team of Nuclear Waste Partners, LLC for reviewing and allowing this paper to be published. Particular thanks are given to Mr. Rey Carrasco and Ms. Victoria Parker for their review of the manuscript.

References

- [1] Recovery Facts, U.S. Department of Energy, http://www.wipp.energy.gov/wipprecovery/fact_sheets.html

Arctic Mine Air Heating

Andrew M. Wilson^a, Euler De Souza^b

*Rio Tinto Diavik Diamond Mine, Lac de Gras, Northwest Territories, Canada
Queen's University, Kingston, Ontario, Canada*

Northern mines use robust mine air heaters that can withstand the rigors of operation in such a harsh environment. Today's mine air heaters are complex systems with fully automated PLC controls and remote communications. Innovative combustion and heat transfer technologies are normally employed to maximize efficiency and performance. Sizing and selection of such heat processing systems is based on safety, reliability, efficiency and serviceability.

In extreme environments such as the Canadian arctic, efficient operation of mine heaters can be quite complicated and even the most efficient system has the potential to burn through considerable energy inputs at significant cost. It is therefore prudent to optimize the heating system settings to eliminate business waste.

A scientific methodology for optimizing the operation of heat processing equipment is introduced in this paper. A psychrometry based model was developed as the method of effectively controlling the mine air supply state point. The theoretical limits of the mine air heaters are discussed in terms of psychrometry to propose an optimized system operating point. Some of the practical considerations and methods proposed to guarantee safety and to manage the operational risk in harsh arctic environments are considered. A method using climate normals and heating degree-days is introduced as a basis to evaluate the overall system performance. These tools show promise for forecasting and budgeting, considering the variable effects of the weather.

A case study is presented to demonstrate how system air heating performance can be maximized and heating costs reduced using the proposed methodology.

Keywords: Arctic, mine air heating, underground ventilation, ice, psychrometry

1. Introduction

Like many other facets in mining, the goal of mine air heating is to create a safe environment for the workers, the equipment, and facilitate an efficient extraction of the resource – in that order. Unlike a residence or an office building, the goal is not the comfort of the workforce.

The ultimate goal of optimizing the mine heating system is to reduce the energy consumption, which is a significant operating cost. Additionally this has significant environmental benefits: directly reducing the production of carbon dioxide and other contaminants that would have otherwise been released into the atmosphere.

A scientific methodology for optimizing the operation of heat processing equipment is introduced in this paper, and a case study is presented to demonstrate how the proposed methodology can be effectively used to maximize the system air heating and reduce heating costs.

2. Heating and psychrometry

The primary governing factor for mine air heating is to prevent the formation of ice in areas that would create a hazard or damage equipment and infrastructure.

2.1 Forming ice through autocompression

In some mine ventilation systems the air mass will create fog and start to deposit frost and ice on the walls. This can occur when warm humid air undergoes a process of autocompression as the air travels up a ramp, a shaft, or otherwise increases in elevation. The sensible heat and dry bulb temperature reduce to a point where the air mass reaches its water saturation limit, the excess

water is then precipitated as fog or airborne ice crystals. If there is a surface temperature below 0 °C (32 °F) present a deposit of frost and possibly thicker ice will start to develop.

Reduced visibility caused by the fog can create some significant issues for mobile equipment. Some mines have used track lighting systems to either mark the center of the travel way, or the side walls, as an aid to the drivers. Additionally traffic control lights can be used to minimize the potential for oncoming traffic in the affected areas. It is also common to disallow pedestrians in areas of low visibility.

Mines in a temperate climate will experience this issue in the most extreme cold months of the year at or near a portal and it can be generally managed without too much concern. Occasionally mines have managed these issues by seasonally reversing the ventilation direction.

This situation may also occur in an exhaust shaft near the surface, but it may be completely inaccessible and therefore undetected. In this situation a prudent control would be to monitor the exhaust shaft resistance using some differential pressure instrumentation.

Perhaps the most dangerous situation is when this occurs in a shaft during a sinking operation. The formation of ice on the walls, the Galloway, the collar, or inside the head frame presents a serious risk to any worker below. Therefore it is important to prevent ice forming conditions in this environment. If a fog begins to form, it becomes very important to monitor these locations for any potential ice.

In an arctic mine constructed in the permafrost zones, the potential for ice formation may be increased because it can occur at increasing depths. All of the principles discussed above are still the same. However, there is an

increased risk by developing ice and having it continue to grow from one year to the next.

Another situation that may present a serious safety hazard is if ice is allowed to form over a period of time and then the conditions rapidly warm. This may happen when a surface ventilation raise, constructed and unused for a period of time, is then commissioned, the ice present can warm up and begin to fall. It is conceivable to have tens of kilograms of ice falling over a few hundred meters, which will have very devastating consequences for anything in the line of fire. Raise camera surveys are an important tool to mitigate this hazard.

2.2 Forming ice in warmer temperatures

Under some very specific conditions, it is possible to form ice in an air stream that is above 0 °C (32 °F), which is typically thought of as non-freezing temperatures.

The air mass in an arctic environment is extremely dry. In the Lac de Gras region of the Northwest Territories, Canada the humidity ratio of the surface air is less than 1 g/kg of dry air for over 40% of the year. This corresponds to the saturated water vapor pressure at -15 °C (5 °F) dry bulb temperature. If that air is heated up to room temperature of 20 °C (68 °F) dry bulb temperature using a dry process, the air would be about 8% relative humidity. At a more reasonable mine air heater set-point temperature of 5 °C (41 °F) dry bulb temperature, the air would be approximately 20% relative humidity. Liquid water evaporates very quickly under these conditions.

The process of evaporation is a powerful form of heat transfer. The water surface evaporates which is driven by the forces of equilibrium. This is an energy transfer to the vapor phase (latent heat of vaporization) from the water that remains in the liquid state reducing its sensible heat, therefore creating a localized reduction in the water temperature. This evaporation process can be so significant that the liquid water is locally cooled to the point of freezing, which releases more energy (latent heat of fusion), which is also consumed by the evaporation.

This is the same effect that will be experienced using a damp towel on your neck while trekking through the Australian outback or possibly in an evaporative cooler (aka. swamp cooler) used in the Mojave Desert. In the arctic however this heat transfer has the power to locally cool the water to the point of creating ice. If this was a standing pool of water then it would eventually evaporate in such a dry air mass and not likely create a significant safety hazard. However if the water is dripping from fractures in the rock, this can be a progressive formation of ice that can present a serious hazard to equipment and personnel.

In many areas of the arctic, permafrost conditions exist only under exposed land and will not be found under lakes that do not completely freeze [1]. Therefore if the orebody extends under a lake or is hydraulically connected to the lake it is reasonable to assume that the mine will experience an inflow of water and would then be considered a wet mine. The experience of the mines in the Lac de Gras area, the permafrost can extend to approximately 200 m depth under the land, but there is a steep transition boundary to unfrozen ground which closely matches the original lake shore boundaries. In

the situations where the lake is pushed back using a water retention dyke, the permafrost is only superficial in the areas that were previously under the lake bed.

Only dry mines, which do not experience any water inflow, would be considered candidates for mining in freezing workplace conditions. That is unless measures were taken to artificially eliminate the inflow of water.

The theoretical limit to form ice using this evaporation driven process would be 0 °C (32 °F) wet bulb temperature. The surface effects will change the practical limits that include wall friction generating some sensible heat and counteract the evaporative cooling effects.

Based on experience the authors propose to use a design limit of ice forming potential at minus 1 °C (30 °F) in a location where there is known or a potential source of water.

In a typical mine ventilation network this would correspond to a location at the surface collar of a fresh air raise, some location inside that raise, or in the subsequent drifts that are immediately connected to the fresh air system. The sensible heat, as well as the wet bulb temperature increase as the air mass progresses through the mine ventilation system. That is unless the air experiences the autocompression cooling which was discussed in the earlier section, or the air is mixed with unconditioned air from surface.

Figure 1 shows the psychrometric regions for ice formation. The green zone is above 1 °C (34 °F) wet bulb temperature, where no ice is expected to form. The yellow zone is the transition where ice could begin to form and these locations should be actively monitored for ice. The red zone is everything below minus 1 °C (30 °F) wet temperature and below 0°C (32 °F) dry bulb temperature, where ice formation should be expected. This psychrometric chart has been developed for standard pressure of 101.325 kPa. This chart will be slightly different for locations operating under different pressure regimes.

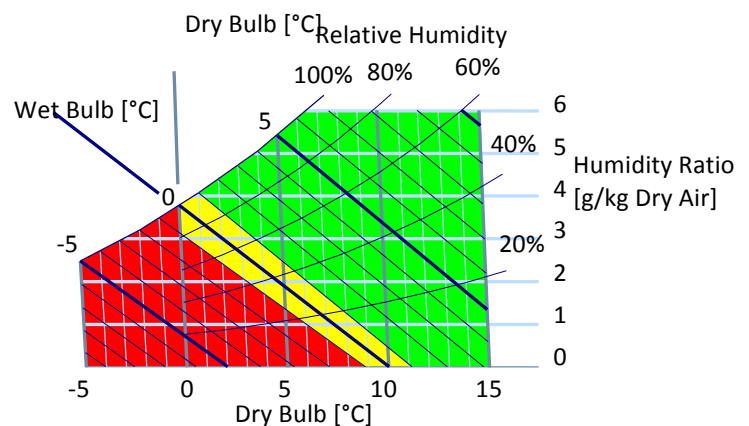


Fig. 1. Psychrometric ice forming regions (adapted from UIGI) [2].

3. Mine air heater technology

Mine air heating technology can be separated into two distinct categories: direct combustion, and indirect combustion.

3.1 Direct combustion mine air heaters

Most mines that require air heating use convenient and relatively clean burning fuels – typically natural gas or propane. This allows a direct combustion configuration. In this type of system the burner and the products of combustion are inside the air stream going underground. Typically these systems are efficient, simple, and reliable options if the appropriate fuel is readily available.

The efficiency of these systems can partly be attributed to the complete capture of all of the products of combustion. Typically contract maintenance is performed only a few times through the year, and few mines maintain the technical experience to completely support the combustion equipment. With the exception of a relatively small maintenance cost, the operation is often only aware of the total fuel costs.

One of the disadvantages of using a direct combustion mine air heater is a baseline of carbon monoxide (CO) as well as other products of combustion is present in the mine. The use of this type of heating system effectively lowers the amount of CO that can be produced by mining activities before reaching the acceptable threshold limit values for a workplace.

Often the only “optimization” of these systems is the result of infrequent tweaking. When a hazard or concern is identified, the set-point temperature is raised. When management focuses on reducing costs, the set-point is lowered and the cycle continues indefinitely.

The authors were unable to find any documented accounts of optimizing these systems using psychrometric principles.

3.2 Indirect combustion mine air heaters

In the Northwest Territories, Canada the operating mines are primarily supplied with bulk materials using a winter ice road which is only open for 8 to 10 weeks a year. These locations are off-grid and the primary source of energy is diesel, which is delivered by super B tankers fully loaded with up to 48,000 to 50,000 liters (12,700 to 13,200 US gal) at a time. Diesel is the preferred choice because it is stable, has a high energy density, and is generally safe to transport and handle.

Diesel fuel is not as clean burning as the alternatives used in the direct combustion mine air heaters. Therefore the burner products of combustion are contained inside a combustion chamber followed by a heat exchanger before being exhausted to atmosphere. The mine air is then passed over this combustion circuit and as a result it should not have any significant contaminants as it enters the mine. Therefore there is no baseline carbon monoxide content as you would have with a direct combustion mine air heater system.

Typically a primary fresh air fan on surface will move more air than a single heater module is capable of conditioning at the peak heating demands, therefore a heater is composed of several heater modules and a plenum building which is then connected to the fan. At Diavik there are five primary fresh air fans (450HP Alphair 10150-AMF-5500 FB 880 rpm), each with six ACI-Canefco mine air heater modules capable of producing approximately 1.65 MW (5.63 MMBTU/hr.) of output heat while consuming about 3.4 L/min (54 US gal/hr.) of diesel at full throttle per module.

The indirect combustion mine air heaters are significantly more complicated than their direct combustion counterparts. As a result the maintenance requirements are also significantly increased. Any operation with these types of heaters should have experienced industrial oil burner mechanic support available on site. Regular maintenance is critical to operating an efficient and reliable heating system.

4. Heat plant efficiency and heating costs

The air mass in the arctic, as discussed earlier, is extremely dry. As a result the specific heat capacity (C_p) of that air is very insensitive to the water vapor pressure. To illustrate this consider an air mass at minus 20 °C (minus 4 °F) at 101.325 kPa standard pressure. The C_p would be 1.0050 kJ/kg·K at 0% relative humidity, and only 1.0064 kJ/kg·K at 100% relative humidity; a difference of significantly less than 1%, which is well within the margin of error in measurement and forecasting. It therefore can be assumed that the energy required to heat the mine air is directly proportional to the mass and the temperature delta (ΔT) for a stable system. Heating-degree-days (K·day) can be used as the demand function for estimating the mine air heater energy requirements. Similar models are commonly used by heating oil delivery companies to estimate demand when contract residential and commercial clients require a refill. The same logic and principles hold that it should be a useful tool to estimate the demands on mine air heating.

The heating degree-day measurement is an integration of the difference between the input temperature (ambient), and the output temperature (raise set-point) over time. A limitation is placed on the integration to represent zero heating-degree-days for any time that the input is higher than the output temperature (negative ΔT). In other terms, if it's warm enough outside then no heat is required and there is no demand for heat.

For example if the average ambient temperature for a day is minus 20 °C (minus 4 °F) and the air is heated up to a set-point temperature of 5 °C (41 °F), then this would contribute 25 K·day to the heat demand function for the day. Similarly if the ambient temperature was above 5 °C (41 °F), then that would contribute zero K·day in demand.

Typically this calculation is performed on hourly data to accurately capture the periods where the temperature fluctuates above and below the set-point temperature. Heating-degree-day values can be calculated on a daily, weekly, monthly, or complete heating season basis.

Figure 2 demonstrates a strong linear relationship between the heating-degree-day and the fuel consumption. This data is from a single fuel pumping system delivering diesel to one of the primary fans equipped with six heater modules. The individual data points were generated on a daily basis over a period of 900 days.

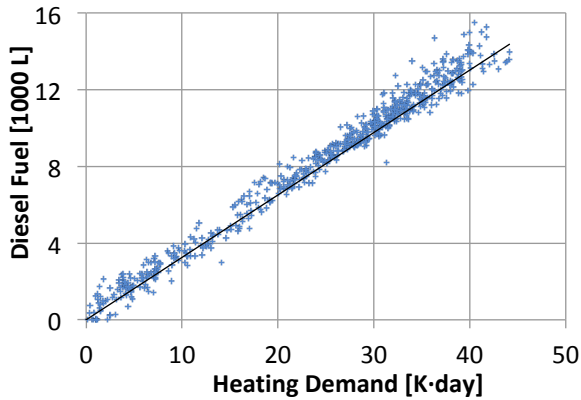


Fig. 2. Fuel to heating degree day relationship.

When heating-degree-days are being used in forecasting, they should be calculated on a climate normal, which represents the “average” year over a much longer period of time. The dataset that is required to calculate this should be high quality measurements of temperature on an hourly frequency over a period of 10 – 30 years, with very little missing observations. Obviously this is a difficult requirement especially in forecasting the heating demands at the feasibility stage of a new property.

Figure 3 shows a climate normal model in the form of a cumulative probability distribution for dry bulb temperature that was developed for the Lac de Gras, Northwest Territories area based on hourly weather observations over a period of 2000 through 2010.

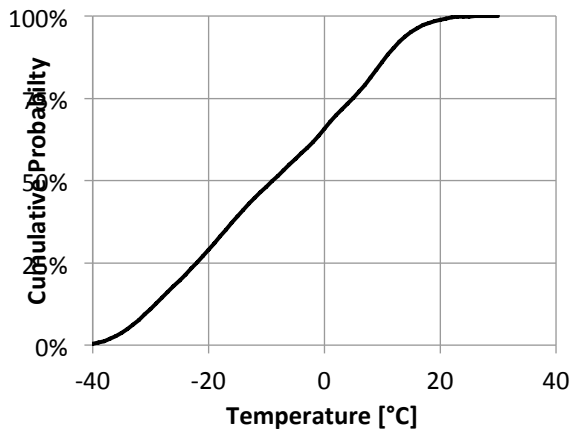


Fig. 3. Climate normal temperature - Lac de Gras.

A relationship of heating-degree-days to set-point temperature is produced as a result of analyzing the climate normal data. Often this kind of data is generated by government agencies for populated areas. An example of this presented in Table 1 for the Lac de Gras region in the Northwest Territories, Canada based on measurements at the Diavik mine site over the period of 2000 through 2010.

Table 1. Heating degree days by set-point.

Raise Set-point Temperature [°C]	Raise Set-point Temperature [°F]	Degree-days [K·day]
6	43	5946
5	41	5668
4	39	5397
3	37	5132
2	36	4874
1	34	4622
0	32	4378

The relationship between set-point and heating-degree-day suggests that the simple act of reducing the raise set-point temperature from 5 °C (41 °F) with a demand of 5668 K·day, down to 4 °C (39 °F) with a demand of 5397 K·day, would save approximately 4.8% a year. In this region a change of a couple of degrees Celsius in set-point temperature to an underground mine represents a significant potential savings (or loss) in over a year.

For the purposes of estimating the diesel fuel requirements, the authors have used a nominal 80% efficiency for indirect combustion mine air heaters using an arctic diesel product with a density of 0.85 kg/L at the standard temperature of 15 °C and a 42.76 MJ/kg net heat of combustion, which was provided by the fuel supplier Petro-Canada. This works out to be approximately 36.35 MJ/L (130,400 BTU/US Gal). The original burner design calculations were based on No.2 fuel oil, with a general heating content of 39.02 MJ/L (140,000 BTU/US Gal). The authors have used the fuel supplier values over the design documents in their analysis. Calculations based on No.2 fuel oil, where a mine is using an arctic diesel product with different properties, can under estimate the fuel requirements.

An estimate can be made of the fuel requirements for any new installation using this data on the fuel, heater efficiency, the required mass flow rate of a designed ventilation system, and an assumed specific heat capacity for the air.

5. Controlling the mine supply air set-point

The mine air heater system is controlled by a local programmable logic controller (PLC). It is advisable that the PLC be also connected to a larger supervisory control and data acquisition (SCADA) system. The value of the SCADA system is to remotely monitor the system performance and collect operating data that can be later analyzed to measure the effects of changes on system performance.

The most basic system control is based on a proportional-integral-derivative (PID) controller. The PID controller uses the process-variable (system temperature) as feedback to achieve a constant set-point value (target dry bulb temperature), by adjusting the control-variable (burner module throttle).

The system temperature is measured at the outlet of the heating plant, typically at the collar of the raise, by one or more long averaging Pt100 resistive temperature detectors (RTD) probes. These RTDs are installed inside perforated steel pipes across the raise for support. The steel structure also helps to smooth the signal measurement due a substantial increase in thermal capacity in comparison to the sensor directly exposed to the flow of the air. The result is a slower reacting signal

that is suitable as the process-variable input to a PID controller.

The control-variable is the burner module throttle, which is commonly a 4-20 mA encoded control signal that is transmitted from the PLC to an actuator in the burner. The actuator in turn connects to various valves by way of mechanical linkages to adjust the burner module heat output. The control system would then be able to modulate continuously between zero (4 mA) and 100% throttle (20 mA).

5.1 Turndown ratio control consideration

Each burner design has a lower limit of heat output, beyond which stable combustion cannot be sustained. This is referred to the turndown ratio, which is approximately 25:1 for natural gas or propane. This means that the minimum heat output at zero throttle is twenty five times smaller than the maximum heat output, hence 4% of the maximum.

Diesel particles need to be atomized into smaller droplets and ultimately vaporized and mixed with a controlled amount of combustion air before it can undergo an efficient combustion. This is commonly accomplished by one of two mechanisms: compressed air assisted atomization with a 10:1 turndown ratio, or a high-pressure fuel nozzle with a 3:1 turndown ratio. The resulting minimum heat production from these types of burners is 10% and 33.3% of the maximum heat output correspondingly.

In the Lac de Gras area most burner modules used in the mine air heating applications are selected to have a design ΔT of approximately 50 K (90 °R) such that they can heat the air from minus 45 °C (minus 49 °F) up to a set-point temperature of 5 °C (41 °F).

Assuming that the burner module is using a high-pressure fuel nozzle design with a turndown ratio of 33.3%, and maximum throttle perfectly heated the air from minus 45 °C to 5 °C. The minimum fire, or zero throttle, would correspond to a system ΔT of 16.7 K (30 °R). The system would not be able to modulate to achieve a set-point temperature when the incoming temperature is above minus 11.7 °C (10.9 °F).

For example, if the incoming air temperature was only minus 3.0 °C (26.6 °F), then the air would be wastefully heated up to 13.7 °C (56.7 °F). Although perhaps a more comfortable working environment, this would be considered a significant and avoidable waste of energy.

In a boiler heating system, or a residential / commercial space heating application, the burners could be controlled by cycling them on and off to control the temperature in the lower zone. Unfortunately by the nature of the burners and the demands of the underground mining environment, this is not a viable option.

Instead the PLC controlling the system needs to shut down some of the burner modules in the system – a process called staging. If the system in the above example had an incoming air temperature of minus 3.0 °C (26.6 °F), the system could shut down four of six heater modules connected to the system. Assuming the air flows across each heater module were equal, this would result in 33.3% of heated air from two modules at 13.7 °C (56.7 °F) mixing with 66.7% of unheated if the modules were at zero throttle. The result would be a

mixed air mass with temperature of approximately 2.6 °C (36.6 °F) at 0% throttle. This is below the set-point temperature given in this example of 5 °C (41 °F), but the burner module throttle on each of the two operating burners can easily be modulated by the PID loop to achieve the required set-point temperature.

Another one of the critical functions of the PLC system is to provide a series of protection systems of interlocks to increase safety to the workforce, and prevent unnecessary damage to the equipment and infrastructure. Perhaps the most important controls are the over-temperature sensors and the carbon monoxide sensors, both which are intended to shut-down the fresh air system in the event of a fire to minimize smoke and other contaminants from entering the mine fresh air system.

6. Proposed methodology for optimization

The process of optimizing a mine ventilation system is inherently a process of continuous improvement. A structured process: define, measure, analyze, improve, and control (DMAIC) can be a valuable tool to use when making improvements to the mine air heating system.

6.1 Define

The goal is to reduce the fuel quantities required to heat the mine air. The primary inputs are: incoming air temperature, the heating set-point temperature, the air flow quantity, and the system efficiency. The incoming air temperature is beyond control, and quantity of the air flow is considered out of the scope of this investigation. Only heating set-point temperature and changes to the system to improve efficiency can be made to optimize the arctic mine air heating system.

6.2 Measure

The mine air heating system is complex and variable. As a result it requires some effort to ensure that the process variables are being measured correctly. The airflow sensors require periodic calibration using a pitot traverse. Fuel flow sensors require calibration and require consistent configuration (eg. temperature / density corrected measurement or standard density). The ambient temperature probes must be shielded from the radiation effects of sunlight, and not buried in snow drifts. The raise air flow temperature sensors should be long averaging sensors to provide a reasonable cross section of the air flow. Ideally the output temperature sensor would be placed at some reasonable distance down-stream to allow for a nearly complete mixing of the heated air, but this is limited by physical access and other practicality considerations.

6.3 Analyze

The core of the analysis at a high level can focus on a measure of fuel consumption intensity. The authors would propose using the consumption rate in liters [L] and normalize that on air flow rate [m^3/s], and heating demand degree-days per day [$\text{K}\cdot\text{day}$]. The resulting units of intensity would be in [$\text{L}\cdot\text{s}/\text{K}\cdot\text{day}\cdot\text{m}^3$].

Assuming a standard density of 1.20 kg/m^3 , C_p of $1.0050 \text{ kJ/kg}\cdot\text{K}$, net heat of combustion of 36.35 MJ/L , and a nominal efficiency of 80%, and a constant 86400 seconds per day, the idealized fuel consumption intensity is calculated to be $3.58 \text{ L}\cdot\text{s}/\text{K}\cdot\text{day}\cdot\text{m}^3$.

The authors have found that using a measurement of fuel consumption intensity is more useful than back calculating an efficiency. The cumulative effect of assumptions and measurement errors makes the calculated efficiency differ from the true efficiency. The difference between true and calculated efficiency can create unnecessary confusion for those who are not familiar with the process.

Trends of the fuel consumption intensity have successfully been calculated on monthly, daily, and hourly intervals. The longer time intervals have the benefit of smoothing out the resulting data.

Although this is the preferred analysis to evaluate system changes, it does not provide meaningful insight into the effects of lowering the set-point temperature, which is also a significant system improvement. The value of the changes to the set-point can be inferred from the heating degree-days by set-point temperature basis discussed earlier.

6.4 Improve and control

As a result of the data analysis a list of potential improvements can be generated. This will typically include a mix of mechanical changes, maintenance strategies, and changes to the process controls. These will need to be evaluated and prioritized. Incrementally systematic improvements can be made. A process of continuous improvement is used where following the changes data is collected, analyzed, and this is repeated.

7. Areas for improvement

It has been the experience of the authors that areas for optimizing mine air heating fall into one of four categories, described below.

7.1 Obvious

These project areas include insulating ducting, and correcting other known issues with the system. Often these are not controversial and very obvious changes. Therefore they do not benefit from the aforementioned DMAIC process. One of the first goals to be addressed in this category is to improve the system stability. This specifically includes ensuring that the heating system does not have significant departures from the set-point temperature.

7.2 Process control

The most significant improvement that can be made to the process control is by optimizing the set-point temperature. This starts by identifying the critical locations in the ventilation system, and making system adjustments to reliably achieve the required heating, while eliminating the waste associated with overheating the air.

7.3 Combustion & mechanical

Improvements can be made to the combustion and mechanical operation of the heating plant. These are generally well understood and documented by the equipment manufacturer and other specialists.

One of the most significant changes that can be made is by reducing the amount of excess air provided by the combustion blower, and increasing the residency time of the products of combustion in the heat exchanger. It may be possible to reduce this enough to create a condensing environment inside the heat exchanger. The efficiency gained is by recovering the latent heat of vaporization from the exhaust water vapor that would have otherwise been lost. The condensate that develops inside the burner needs to be removed from the system through drains, collected and disposed of properly. Additionally there is now the possibility that some localized parts of the heat exchanger may start to develop ice, which could cause other inefficiencies and potential damage.

7.4 Preconditioning

There exists the possibility of harvesting energy from other sources and using that to precondition the incoming air in advance of the mine air heaters.

The Macassa mine in Kirkland Lake, Ontario, Canada pre-heated their mine air using energy recovered from the mine water and compressor systems. [3]

Other authors have proposed recovering heat from the mine exhaust systems. [4]

Remote arctic mines typically have a surplus of waste heat from the diesel electrical generation facility, especially in the summer months when there are few requirements to heat buildings. It might be economically feasible to create a borehole thermal energy storage facility and recover this for the mine air heating season.

There possibly exist many more site-specific novel sources of low grade energy that can be harvested. Based on the set-point heating degree-day relationship developed above, a few degrees are all it takes to create some significant potential energy savings. Some early design decisions before construction begins may create or eliminate these potential opportunities. It may be very lucrative to consider these opportunities early in the project design stages.

8. Case study

Over the past few years the Diavik Diamond Mine has been implementing various energy improvement projects in an effort to reduce the overall mine operating costs. The mine air heating system currently represents the largest consumer for diesel on site after the power generation facility.

A substantial list of deficiencies and opportunities was generated for the mine air heating facility. These were subsequently ranked and significant effort has been made in reducing the diesel consumption at this facility. This included insulating ducting, developing a burner hour-based maintenance strategy, improving instrumentation and control strategies.

Figure 4 shows the trend of the fuel intensity as calculated monthly for the mine-wide fresh air heating

facility. The majority of improvements occurred at the end of the 2013-2014 heating season, and before the start of the 2014-2015 heating season. Part of the change in this trend has been attributed to an improved instrumentation and as such would not be realized as savings.

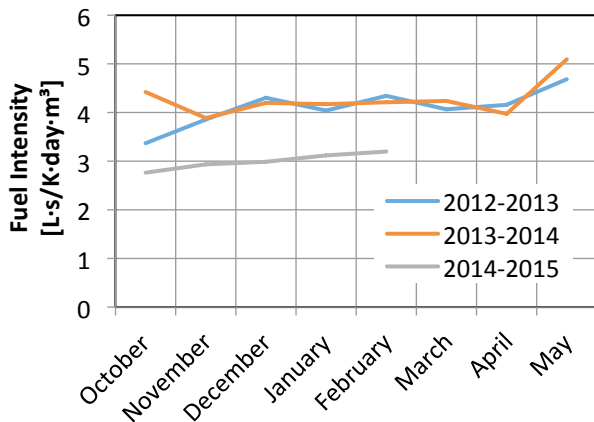


Fig. 4. Heating fuel intensity by month.

Additionally the raise set-point temperature has been systematically lowered from 6 °C (43 °F) down to 4 °C (39 °F) on three of the five primary fresh air fans. The remaining two fans require some control changes as a prerequisite before the set-point temperature can also be lowered. Preliminary data suggests that the savings are in agreement with the heating-degree-days predictions.

A monitoring program has been developed to identify any ice forming in the fresh air raises before it presents a significant risk to safety or damage equipment. This includes periodic inspections of the fresh air raises using a raise camera system, online monitoring of raise pressures. The critical location was identified near the bottom of the raise, where water is present. This location has been instrumented and is being monitored for wet bulb temperatures. Following the set-point temperature reduction, the temperature measured at this critical location fluctuates between 0 °C (32 °F) and minus 1 °C (30 °F) wet bulb temperature, which is at the limit of where the formation of ice can be expected.

To illustrate the potential savings associated with the set-point change, assume 125 m³/s (265 kcfm) air flow rate per primary fan. The fuel requirement can be predicted using idealized fuel consumption intensity is calculated to be 3.58 L·s/K·day·m³ that was developed earlier, and the heating-degree data in Table 1. For a 6 °C (43 °F) set-point base case, 2.66 million liters of fuel would be required over the course of an “average” year to heat the mine air per fan. Reducing the set-point to 4 °C (39 °F) would only require 2.42 million liters per fan, a 9.2% savings in fuel. At the time of writing this the price at the pump for diesel in Yellowknife, Northwest Territories, Canada is approximately 1.25 \$/L. Using that price, the savings would be in the order of \$300,000 annually per fan.

9. Conclusions

Arctic mine air heaters represent a significant cost to an operating mine. The heating-degree-day basis has been shown as a useful tool in predicting changes, and forecasting fuel consumption. Using the proposed systematic approach to improving the mine air heater system can generate significant savings. These savings can be realized by reducing the set-point temperature, and improving the system control. Other improvements can be made in the areas of mechanical, combustion, and potentially energy harvesting. The case study illustrates that small percentage point improvements can have significant financial and environmental impact for an operation.

Acknowledgements

Diavik’s burner mechanics Brett Cameron and Don Sanderson deserve much credit as they are critical to maintaining and operating the burners which keep the mine warm, safe, and functioning especially on the occasions when these two gentlemen are working in rather unhospitable conditions. The authors would also like to thank Diavik management, supervision, technical staff and all of the others involved in maintaining, and upgrading the mine air ventilation and related infrastructure. Additionally the authors would like to thank both ACI-Canefco and Murray Mechanical for their support in some of these initiatives.

References

- [1] X. Hu et al., Geomorphological, geotechnical and geothermal conditions at Diavik Mines, Proc. 8th International Conference on Permafrost (2003) 437-422.
- [2] Universal Industrial Gases Inc., SI Psychrometric Chart Barometric Pressure 760 mm of Mercury (accessed 2014) http://www.uigi.com/UIGI_SI.PDF.
- [3] H. de Ruiter, Energy Savings in Mining, Mining Magazine (October 1992) 240-245.
- [4] H. Dello Sbarba et al., Economics of exhaust air heat recovery systems for mine ventilation, International Journal of Mining, Reclamation and Environment Vol.26 Issue 3 (2012) 185-198.

A Discussion of the Automated Ventilation Systems at the Henderson Mine

D.M. Loring, R.D. Brokering, A. Rogers, B.P. Dhyne

Climax Molybdenum Company, Henderson Operations, Empire, Colorado, USA

Climax Molybdenum Company's Henderson Mine, owned by Freeport-McMoRan Inc., is a 32,000 tonne per day panel caving molybdenum mine located about 69 km west of Denver, Colorado. Over the years Henderson has installed a number of automated ventilation control systems for a variety of purposes. Among these are "ventilation on demand"-type systems to direct air where it is needed. As the footprint of the mine expands, with production coming from multiple panels on different levels of the mine, the efficient and effective use of air becomes essential in order to maintain or reduce ventilation energy costs. This paper describes the systems that are currently in use, including those that have been installed recently. The purpose of these systems will be discussed, as well as the design criteria, function, construction, and method of control.

Keywords: Automated Ventilation, Molybdenum, Caving

1. Introduction

The Henderson Mine is located 69 km west of Denver, Colorado, at an elevation of 3,170 m above sea level. The mill is located 24 km west of the mine, on the other side of the Continental Divide, at an elevation of 2,800 m above sea level. The ore body is located between 900 to 1,500 m below the surface, and is accessed through an 8.5 m diameter service shaft. Ore is crushed underground and transported to the mill site on three 1.2 m wide conveyor belts. An LHD panel-caving system has been used to extract approximately 240 million tonnes of molybdenum ore since production began in 1976.

Henderson Mine utilizes an exhaust ventilation system. Ventilation is supplied to the mine through the 7.0 m diameter No. 1 intake shaft, the 8.5 m diameter No. 2 service shaft, the 7 m diameter No. 3 intake shaft, and the 17 km long ore haulage tunnel. Air is exhausted solely through the 9.8 m diameter No. 5 exhaust shaft.

Throughout Henderson's mine life the ventilation system has been modified to change with the growing and deepening mine in order to improve working conditions for the employees, as well as to reduce risk and costs. The primary goal of the ventilation system is to supply sufficient fresh air to the working areas, minimize risk to employees, and do this all while minimizing costs.

Automated ventilated systems have come in a number of forms at Henderson. The first are automated fire protection systems, where the primary purpose is to minimize risk to employees in the highly unlikely event of a fire in a particular location. The second are remotely operated ventilation systems. The third are automated ventilation management systems, where the primary purpose is to move air from one location to another based on the location of equipment.

2. Henderson Industrial Health and Safety

2.1 Introduction

The Henderson management, safety programs, and ventilation engineering group are all committed to continuous improvement. At its core, the philosophy can be summed up by simply "zero" – the goal for zero injuries, accidents, or incidents, including health-related incidents.

A well-designed and strong-functioning ventilation system is critical to achieving "zero" in an underground mine. Recent advances in mine ventilation technologies and practices have played a major part in vast improvements in underground mine safety.

Significant resources have been committed to reduce exposures to radon, dust, diesel particulate matter (DPM), and gases underground on a continual basis at Henderson Mine. Automated ventilation systems take these IH factors into account during design and operation so that improvement can continue.

2.2 Ventilation-related concerns

The Freeport-McMoRan safety philosophy is applied to ventilation design, planning, and management at Henderson. The primary design concerns and constraints are:

- 1) Fire risk
- 2) Radon control
- 3) Silica dust
- 4) DPM reduction
- 5) Blasting and other gasses
- 6) Climate / work environment (both strata-related heat and winter conditions)

3.2 LA Ramp Fire System

The LA ramp serves as the primary personnel access to the lower production panel and the truck haulage level. The ramp is also an intake ventilation source for the haulage level and an intake ventilation source for the lower production panel. In the unlikely occurrence of an event on the ramp, a fire protection system was implemented to divert ramp air above the primary lower level workings. The system consists of three fire doors equipped with carbon monoxide sensors and one louver connecting the ramp system to the primary exhaust system (figure 3). If carbon monoxide is detected on the ramp, the following occurs:

- 1) The louver opens, drawing air flow from the ramp to main exhaust.
- 2) One set of haulage level booster fans reduces speed to 50%.
- 3) Warning lights and audible alarms trigger on the fire doors, then the doors close after 30 seconds.

With the system activated all personnel in the lower working areas will have a direct supply of fresh air from other sources.

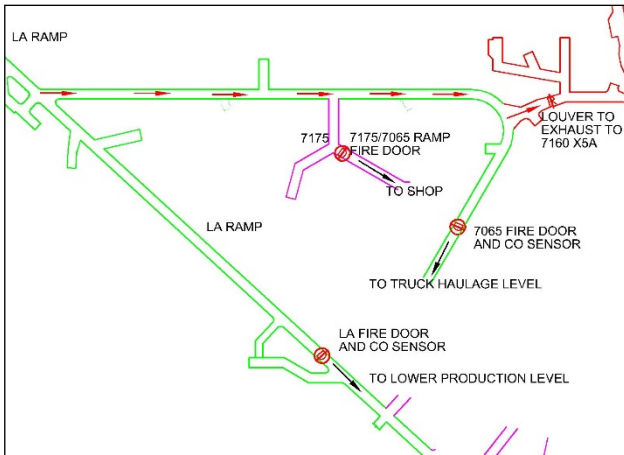


Fig. 3. LA Ramp Fire Protection Systems

4. Heading Fan Control

4.1 Development Headings

Development heading fan control is an event based system designed to allow employees to start and stop fans from remote locations when blasting. This eliminates the risk of entering a heading or an area that might contain products of combustion in the air stream after an end-of-shift blast. It is also intended to maximize ventilation utilization in headings as well as reduce power usage. Nearly all existing development fans are connected to the mine's human-machine interface program (HMI – figure 4). Either miners underground or a dispatcher on the surface can remotely start and stop these development fans. This permits fans to be started between shifts prior to employees checking work areas.



Fig. 4. HMI Fan Control Screen

5. Ventilation on Demand (VOD)

5.1 7065 Haulage VOD system

The 7065 level is a truck haulage level consisting of haulage loops containing four or five loading chutes connected by entry and exit hanging walls (see figure 5). Historically each chute would utilize an 11 kW fan exhausting approximately 5-7 m/s down a raise located at the back of the chute cutout. The southern-most chute in the loop utilized a 30 kW fan moving 16-19 m/s to maintain sufficient airflow throughout the entire truck loop.

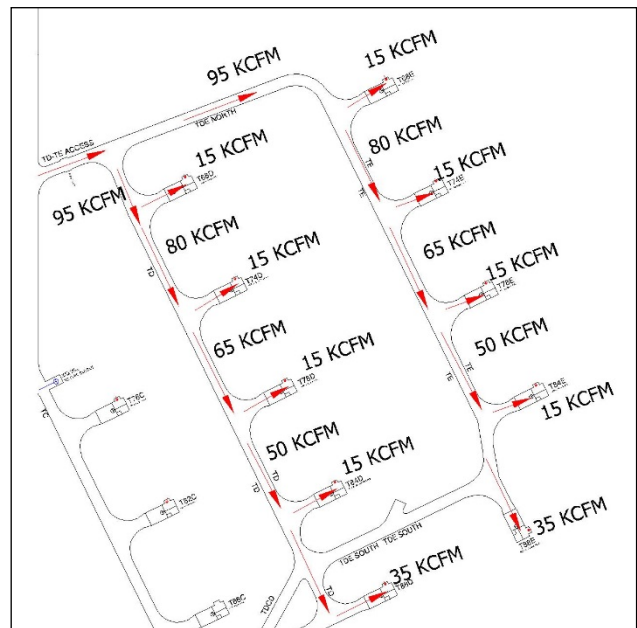


Fig. 5. 7065 D&E Haulage Loops: Original Design

The haulage loops exhaust from a raise located behind the truck chute to a drift located below, on the 7025 level, mirroring the development of the 7065 level. The 7025 level is ventilated through two areas, the first is a 2.4 m diameter raise connecting to the 7500 level with a 75 kW fan located on the 7500 level. The second means of exhausting the 7025 level are parallel 2.1 m diameter raises connecting to the 7160 level with each raise utilizing a 112 kW fan to pull exhaust air up from the level.

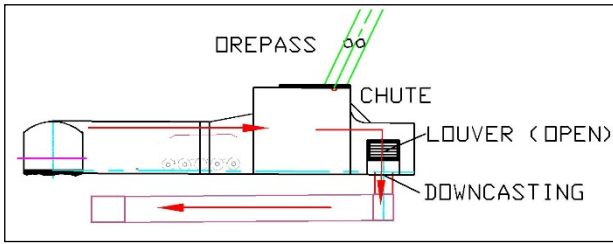


Fig. 6. General Chute Ventilation Arrangement

The VOD system installed on the 7065 level is a louver system utilizing negative pressure created from the 7025 level primary exhaust fans. All 11 kW and 30 kW fans from the original chute construction were removed and replaced with louvers (see figure 6). The louvers replacing the 30 kW fans on the southern chutes are set to default open, so as to consistently ventilate the loops (see figure 7). Louvers replacing the 11 kW fans are set to default closed. This configuration of louver settings allows for sustained overall air flow through haulage drifting, at approximately 19 to 28 m/s per loop. When an operator activates the chute, the louver opens. As that louver opens, the louver at the end of the loop closes. The ventilation from the entire loop then flushes through the active chute, resulting in faster dispersal of dust from the loading process (see figure 7).

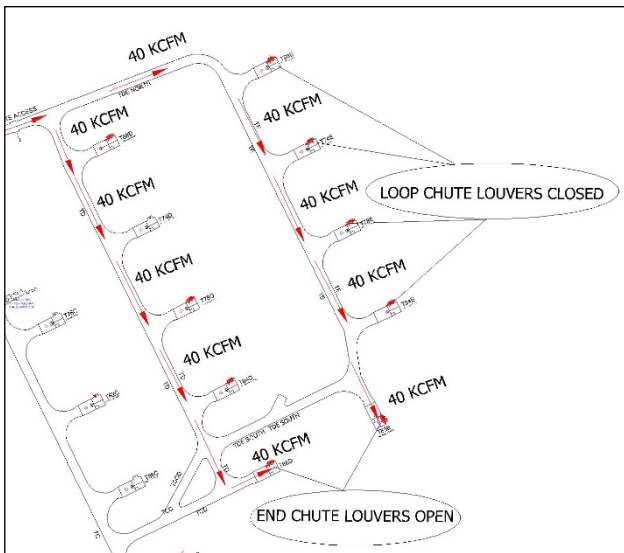


Fig. 7. 7065 D and E Haulage Loops VOD: normal mode

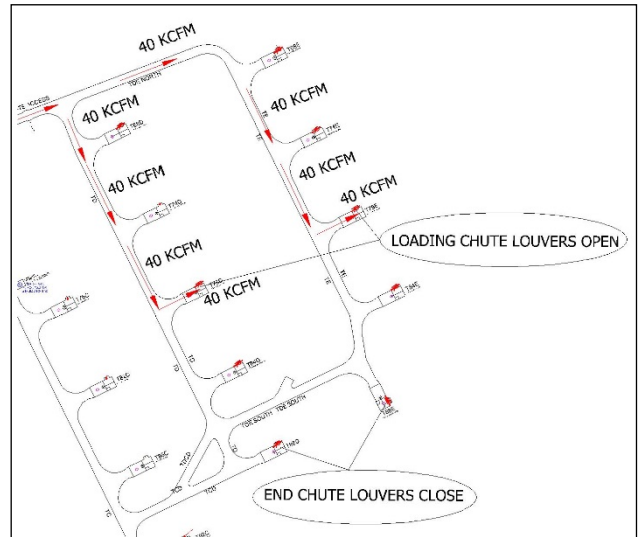


Fig. 8. 7065 D and E Haulage Loops VOD: truck loading mode

The benefits of converting to the 7065 VOD system have included:

- 1) Increased air velocity in chute loading area resulting in faster dilution of dust in loading chutes and in corresponding loops.
- 2) Removal of 490 hp of continuous running fan power (figure 9), and corresponding power savings.

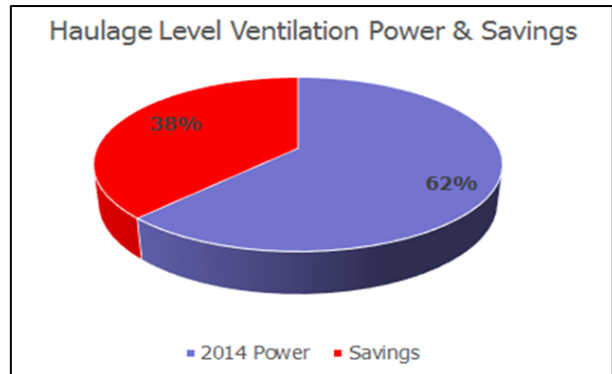


Fig. 9. 7065 Haulage Level VOD power reduction

6. Conclusion

The Henderson Mine has taken steps in utilizing automated systems throughout the mine. Health and safety is a significant part of the Henderson culture and includes direct ties to ventilation. The primary job of a ventilation engineer is to deliver fresh air to all employees. Utilizing automated systems has allowed for upgraded fire systems, faster removal of dust from work areas, and remote activation of fans to flush blast gasses and eliminate potential exposures.

Technical Ventilation Services of a Large Coal Mining Company

Bryan Boskovich, Raghuveer Reddy Thadisina, Brian Persinski

*Alpha Natural Resources
Engineering Methods and Standards – Ventilation Group
Kirby, PA, United States*

Ventilation is a key component for any underground coal mining operation. Alpha Natural Resources is a leading coal producer that currently has 40 underground operations that incorporate several different mining methods. Within the organization, Alpha has a three person ventilation engineering group which works in the Engineering Methods and Standards division. The ventilation group's primary focus is on ventilation efficiency, cost control, and safety and is tasked to provide ventilation knowledge, support and training to all affiliated underground mines. This is done by: communicating with mine engineering and operations personnel, performing surveys and analyzing field data, developing ventilation simulations based on data collected and requests from mine personnel, presenting results of surveys and simulations to engineering and mine personnel, and working with group leaders to develop ventilation standards and best practices as well as providing ventilation education for the company. To best service the mines with valuable technical information, it has been determined that the evaluation life cycle (from request to recommendation) should be completed before the next section belt move, i.e. within four days. This has been accomplished by standardizing methods, ensuring availability, realizing the true needs from operations management and developing proactive resources for ventilation evaluation including risk assessment. The results of these procedures have been positive during fan installations, various ventilation changes, and in future planning purposes.

Keywords: Coal, Ventilation Efficiency

1. Introduction

The ventilation group within Alpha Natural Resources currently provides service to underground operations in four states, Pennsylvania, West Virginia, Virginia and Kentucky. These operations utilize many underground mining methods including continuous mining, longwall mining and room and pillar mining. They also utilize several types of ventilation systems, such as blowing, exhaust, and push-pull. The operations vary in size with some mines having a single unit and a single fan to others with four mining units and multiple fans. Due to the broad range of mines within the company, there is no "one size fits all" solution to the many problems and questions that come about. Also, an expedited form of assistance is sometimes needed. When this happens, a reliance on knowledge from the mine management, determination of best practices, utilization of standardized procedures, and recollection of past experiences help to allow for fast, accurate results.

2. Request Process

Within the ventilation group there are two basic avenues that initiate the progression of work. One is a request from the operations to analyze a specific current issue and the other is a request to analyze the current system and then to project future changes or provide future analysis. The first request is typically a reactive process (something is going on that needs attention immediately) and the second request is a proactive process (aiming at sorting through issues before they occur.) With this in mind, the ventilation group has

developed several metrics to help assess the mines and determine when a mine would need assistance before a problem could arise. These include:

- Monthly ventilation metrics
- Ventilation violation tracking
- Mine ventilation rating system

The monthly ventilation metric requires specific ventilation readings to be taken by mine personnel each month and is distributed to the ventilation group. From this data, month to month trends can be evaluated and threshold values can be identified. If the trends move towards these threshold values, a pre-defined plan of action is followed to improve the trend before any issue occurs. Figure 1 shows a graph that compiles four months of data for a mine with two mining units. Figure 2 is a flowchart detailing the process and plan of action while analyzing the monthly data.

Ventilation violation tracking takes into account all of the company's CFR 75.300 violations and breaks the data down by mine or by specific violation. From this data, trends can also be inferred and appropriate action for remediation can be taken. Figure 3 is an example of 75.300 violations for each mine during a one month time period.

The mine ventilation rating system compares all mines in the company on a specific set of four parameters vs. the number of active units at each operation. This helps to categorize all of the mines in the company and create a ranking of which mines may need the most attention. Figure 4 is an example of the rating system matrix with low, medium and high categories to help prioritize where to provide attention.

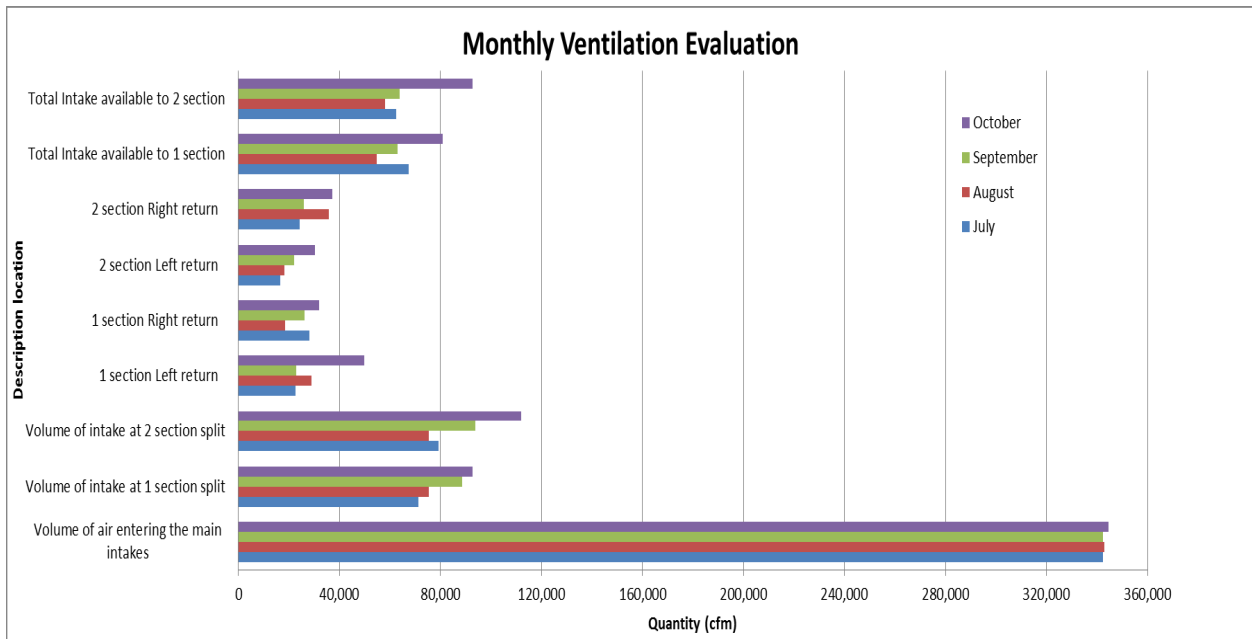


Fig. 1. Example of Monthly Ventilation Metric data

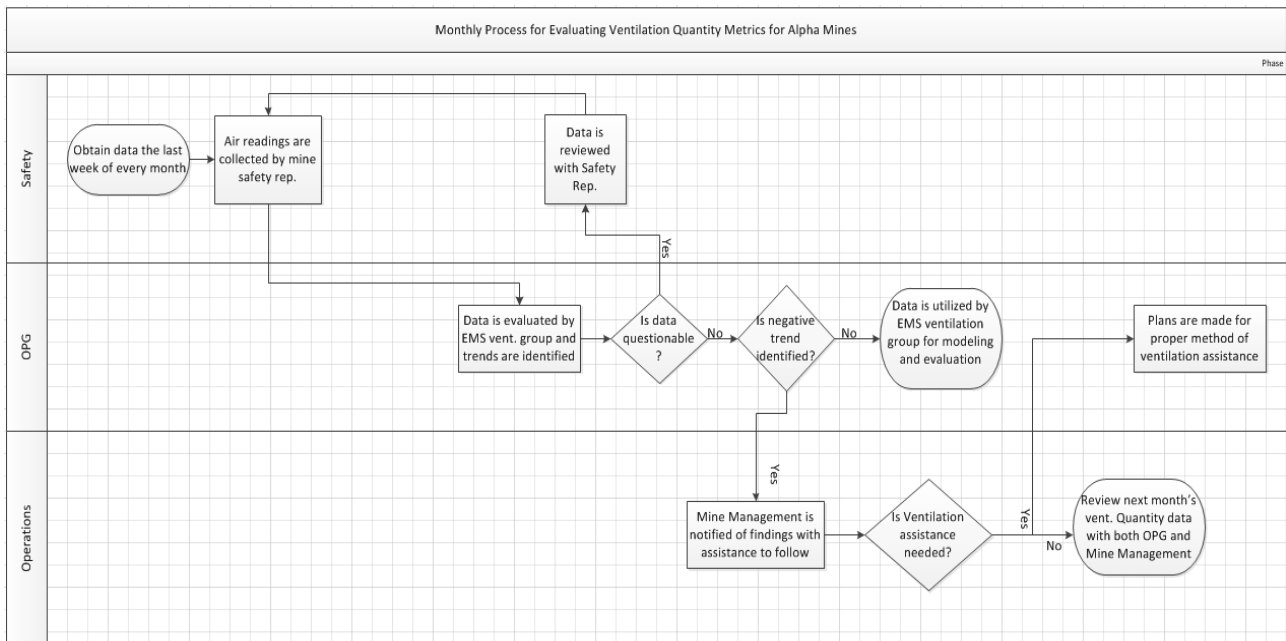


Fig. 2. Flowchart for evaluating monthly ventilation metrics

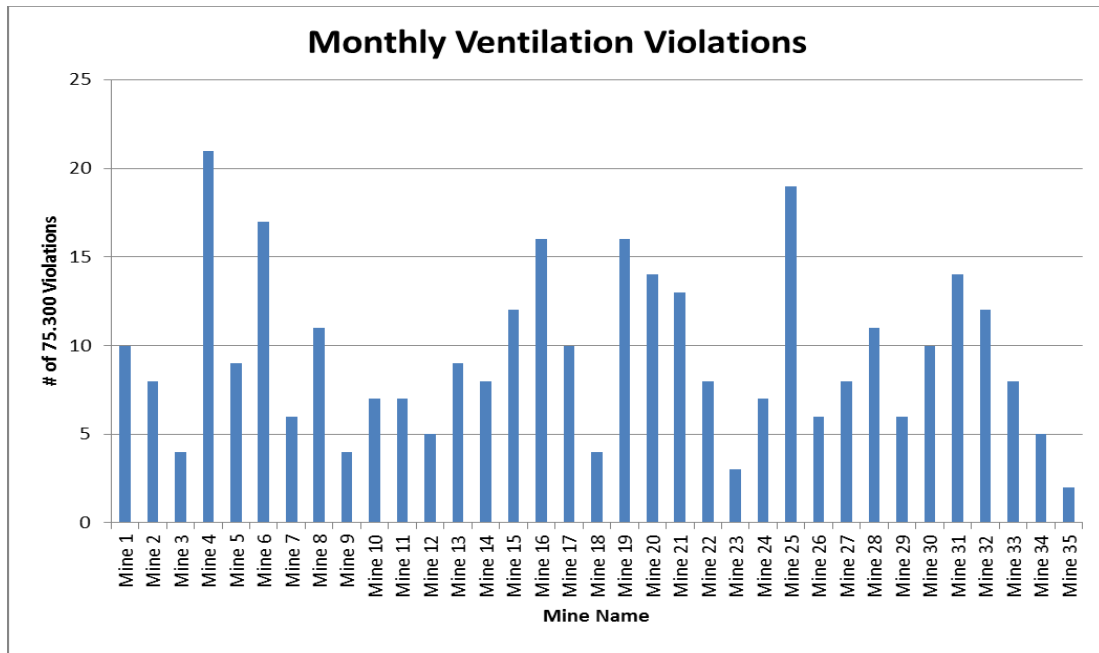


Fig. 3. Example of Monthly Ventilation Violation Tracking

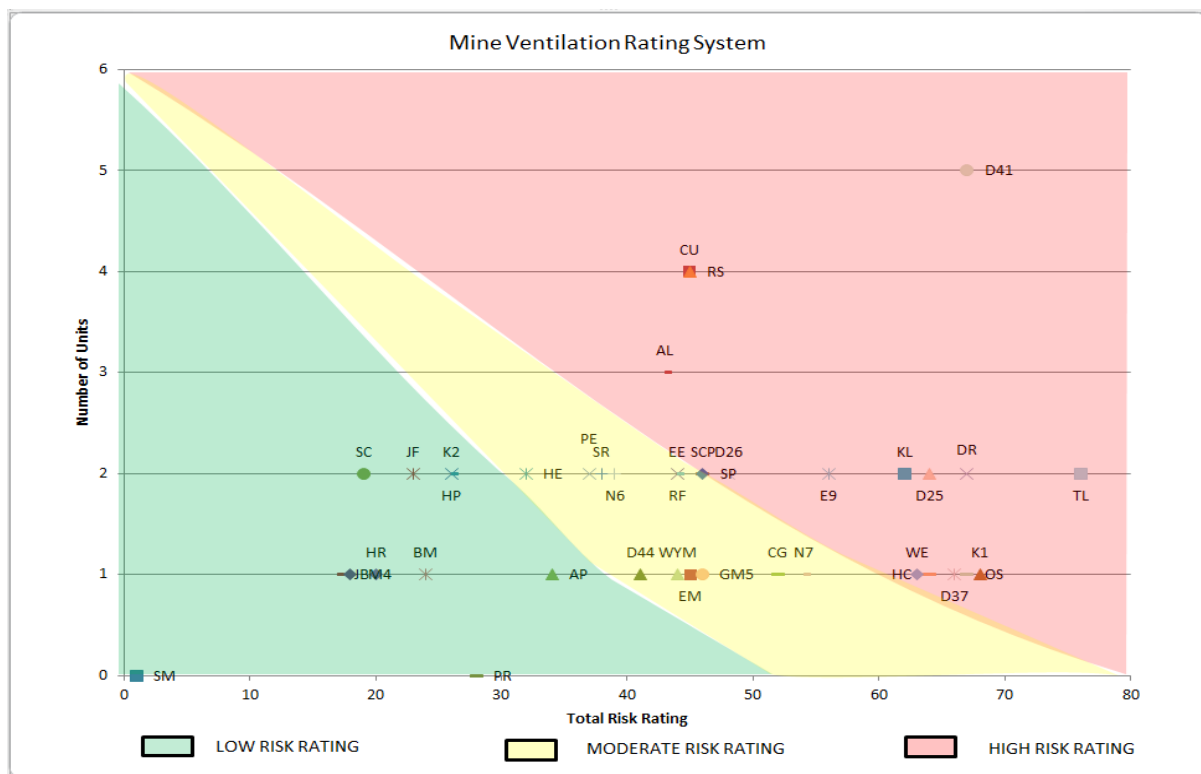


Fig. 4. Example of Mine Ventilation Rating System

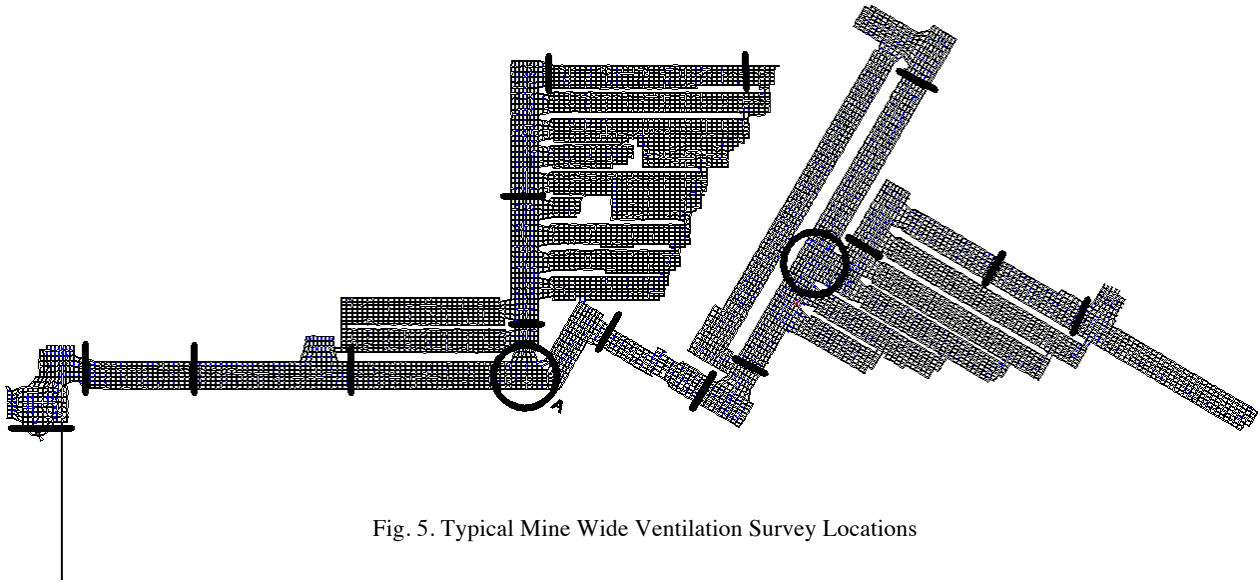


Fig. 5. Typical Mine Wide Ventilation Survey Locations

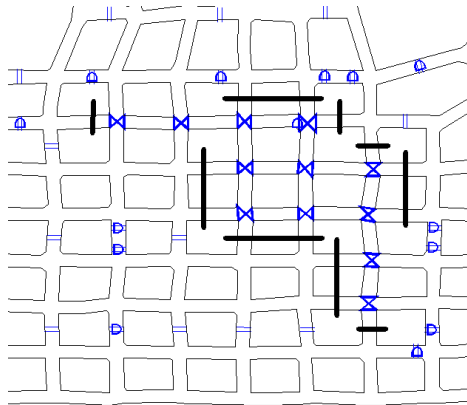


Fig. 6. Typical Survey Locations at close up of Section Split A (see Fig. 4)

3. Ventilation Survey

Once a request is made, regardless of the type, it has been determined that a mine wide survey is always necessary. Any recommendation made has the potential to affect the entire ventilation system. Every survey that the group performs follows a similar pattern and setup which allows the process of calculating and providing results to be accomplished in a timely manner [1-3].

When setting up the survey, an updated mine map is requested from engineering. Then the map is analyzed and line readings are placed at intervals based on the mine network and past experience to adequately capture any major restrictions or leakage areas. The spacing and placement is also based upon ease of input into the computer simulation to help decrease the time between

survey and delivering results. Figure 5 is an example of typical survey locations at an underground mine.

Along with the line readings, key areas such as overcasts, areas of high restriction and regulation are added. Figure 6 is an example of an area as described above at a section split.

During the survey, the ventilation group will divide the locations of the line readings into as many as three groups. To ensure accuracy, identical equipment is used for each team and standard procedures for taking each reading are practiced. At each marked location, air readings are taken in each entry, using an anemometer or smoke tube, and elevation readings, which are later converted to direct pressures, are taken with an altimeter in each set of common entries. A manometer is also used to record pressure differentials across man doors and regulators. In conjunction with the altimeter, a data logging surface barometer is used to track any barometric changes during the survey and is used in the calculation of the direct pressures.

In addition to measuring pressures and quantities, the mine map is also scrutinized to ensure that ventilation controls in the mine match what has been built underground. The ventilation controls themselves are also examined and any areas for immediate repair are noted. Aside from all underground ventilation controls, the fan(s) and fan housing(s) are measured for quantity and pressure and checked for leakage and damage. Also, the fan size and motor capacity are examined for adequate capacity.

After completing the survey, the data is reduced to a useable form and placed on the mine map at the locations where all of the readings were taken.

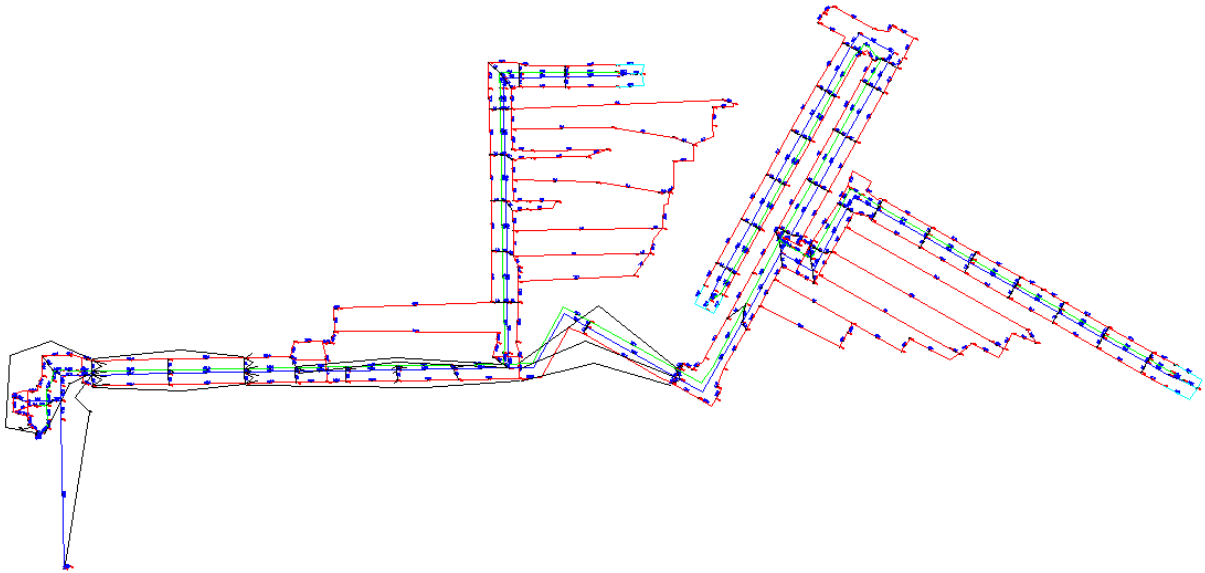


Fig. 7. Schematic of Base Ventilation Model

4. Base Ventilation Model

Once the data is compiled, the quantity and pressure data is entered into computer ventilation simulation software. The software essentially calculates the resistance of the airways for the entire mine network. In addition, fan and shaft information is also entered into the program. The goal is to develop a ventilation model that is within 10% of the survey results. The base model then becomes the platform for all recommendations and changes.

5. Results and Recommendations

Using both the survey results and the base model, a complete picture of the ventilation system is analyzed. Once all of the information has been compiled, a map with all survey readings, the base ventilation model, and a write-up detailing overall observations and immediate recommendations is sent out to mine management and engineering.

After the mine has time to digest this information, a follow up meeting is usually scheduled. At this point, any changes or projections they would like to see forecasted are then created as models built off of the base model. The changes are then tracked for both positive and negative effects to the overall system and placed into a table to easily identify which option is the best.

Scenario	DWG	Description	Fan Type & Blade Position	Fan Water Gauge	Section 1 (kcfm)				Section 2 (kcfm)			
					Left Return	Intake	Neutral	Right Return	Left Return	Intake	Neutral	Right Return
1	DWG.1	Base Model	M96-50-1180 @ x deg	W.G."	x	x	x	x	x	x	x	x
2	DWG.2	End 2015 Projection	M96-50-1180 @ x deg	W.G."	x	x	x	x	x	x	x	x
3	DWG.3	End 2016 Projection	M96-50-1180 @ x deg	W.G."	x	x	x	x	x	x	x	x
4	DWG.4	End 2017 Projection	M96-50-1180 @ x deg	W.G."	x	x	x	x	x	x	x	x

Fig. 8. Template of Results Spreadsheet

6. Company Growth/ Education

In order to improve the ventilation systems of Alpha's underground mines, the ventilation group is also focused on designing best ventilation practices, training its employees on better utilization of ventilation resources and informing its employees on new regulatory policies, mine trends, and procedures in ventilation.

During the ventilation group's visits to the mines and during conversations with mine management, a few important topics were identified. Upon researching these topics, the ventilation team designed best practices for those important topics and circulated to the mine

management. Topics of best practices designed are: face ventilation, line curtain, overcast construction, stopping construction, obtaining fan data, reading a fan chart, use of manometer, proper measurement of air readings, utilization of nine versus seven entries, and estimation of airflow through different sizes of boreholes. The group continuously looks for ventilation trends in the mines, and will design other best practices as needed.

The group understands the importance of involving mine management to acknowledge the team's goals. To better involve them in the process, the group recently conducted a ventilation short course titled 'Advanced Mine Ventilation: Theory, Analysis & Application'. For this, a 2 day course was designed to refresh ventilation basics, discuss flow and pressure measurements, explain pressure distribution with a scale model, review ventilation survey analysis, present case studies and perform exercises in a mine simulator. To conduct this class, the team utilized state of art Running Right Leadership Academy (RRLA). The class will be conducted a few times a year based on the needs of the operations. A continual focus on updating the course material as needed by the mine management is always considered.

The ventilation team is poised to continue its efforts in making all Alpha's mines safe, profitable and efficient to achieve its current goal of 0:50:5. The goal is to attain '0' fatalities and '50' percent reduction in injuries in '5' years. Alpha's ventilation team is also determined and well equipped to redefine itself to suit any new Alpha's goals and challenges.

7. Conclusion

Providing technical ventilation assistance for a large coal company has its challenges. The overall goal is to help each operation design and maintain a ventilation system that adequately dilutes, renders harmless, and carries away hazardous gases, dusts and fumes. This is accomplished by completing a full ventilation system analysis in a timely manner which allows for operations personnel to make quick, relevant decisions. Also, conveying a proactive approach to ventilation system analysis helps to identify issues before they occur. Finally, training, in the form of best practice documents and ventilation short courses, provides education to all levels of mine management.

References

- [1] H. Hartman, J. Mutmanský et al., Mine Ventilation and Air Conditioning, 1997, third edition. PP 207-225.
- [2] J. Rowland, "Barometric Resistance Surveys A New Perspective." 14th US/North American Mine Ventilation Symposium, 2012.
- [3] G.E. McElroy, D.S. Kingery "Making Ventilation Pressure Surveys with Altimeters" US Department of the Interior Information Circular 7809, 1957.

Modeling the ventilation network at NIOSH's Safety Research Coal Mine

Anthony Iannacchione^a, Aaron Jose^b, Timothy Horn^c, Gaetano Iannacchione^a, Stefano Iannacchione^a

^aUniversity of Pittsburgh, Pittsburgh, Pennsylvania, USA

^bAlpha Natural Resources, Waynesburg, Pennsylvania, USA

^cCONSOL Energy, Richlands, Virginia, USA

^dformerly with the University of Pittsburgh, Pittsburgh, Pennsylvania, USA

The University of Pittsburgh and the National Institute for Occupation Safety and Health (NIOSH) conducted a joint effort to better understand the ventilation network at the Safety Research Coal Mine (SRCM). The SRCM has an exhausting ventilation system with a Joy Axivane Series 1000, Model 54-26 ½ BD fan. According to the manufacturer's fan curve, the rated speed for the fan at the SRCM was 690-rpm. The fan, at a measured speed of 633-rpm, produced an air quantity of 34,427-ft³/min the base of the ventilation shaft.

A modified fan curve was used within VnetPro to simulate the performance of the SRCM fan under well-defined conditions. Under normal conditions, i.e. non-stall, the SRCM fan should operate with air flow between 28,000 and 37,000-ft³/min over a total pressure range of 1.1-in. w.g. At lower air quantities, the fans efficiency and stability may be compromised. Higher air quantities are not possible.

Three ventilation conditions were analyzed during this research. In all three conditions, measurements were conducted along a ventilation circuit formed by check curtains within several critical entries. Instruments were used to determine air velocity, relative humidity, temperature, size of the entry, and pressure drop throughout the mine. From these measurements, the SRCM operating point was determined.

Normal operating conditions (Condition 1) were modeled using a 165 branch VnetPro model. Gauge and trailing tube pressure drop surveys yielded entry k-factors ranging from 33.4 to 79-in.min.²/ft⁶. Parametric model runs were used to investigate the most appropriate resistances for various ventilation controls.

Condition 2 involved opening the mine entry doors to the atmosphere near the base of the fan shaft. With the portal doors opened, the air quantity measured at this location was 22% of the air entering the ventilation shaft. During Conditions 3, a curtain was installed inby the ventilation shaft. The air quantity entering the ventilation shaft dropped 29% and the static pressure rose from 0.34 to 0.51-in. w.g. These values suggest the fan was off its normal operating range as defined by the modified fan curve.

The SRCM has been a site of numerous important ventilation research projects over the last 50 years. Efforts to better understand the specific conditions that characterize the facility's ventilation system are needed to enhance future mine safety and health research projects. This research effort represents another step in this process.

Keywords: Safety Research Coal Mine, VnetPro, Fan Charts.

1. Introduction

The National Institute of Occupational Safety and Health (NIOSH) is currently working to model how fires affect underground ventilation systems. Some of this research is occurring at the Safety Research Coal Mine (SRCM) and would benefit from accurate ventilation modeling capabilities, preferably running under the VnetPro software platform. The University of Pittsburgh (Pitt) has undertaken an effort to assist in improving the accuracy of ventilation models of the NIOSH's SRCM.

1.2. Historical Context of the SRCM

The US Bureau of Mines (USBM) developed this research facility shortly after its creation by an act of Congress in 1910 (the Organic Act of 1910). The USBM acquired the mine property and some existing underground mines from the Consolidation Coal Company (now CONSOL Energy).

Sometime in the late 1960's to early 1970's, the Experimental Mine was separated into two coal mines, the SRCM and the Experimental Mine, each of which operate on their own independent ventilation circuit

(Figure 1). Two bulkhead doors act as the boundary between the two mines.

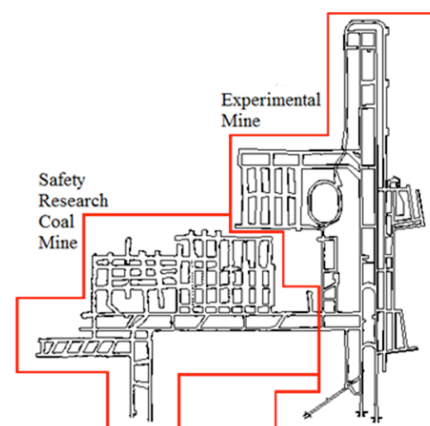


Fig. 1. A drawing showing the two NIOSH mines. To the right is the Experimental Mine, and to the left, the Safety Research Coal Mine (SRCM).

1.3 – SRCM Existing Ventilation Conditions

The NIOSH underground research facilities were visited twice during this project by the Pitt Team. The first visit occurred in July 2014 and collected preliminary information of existing ventilation controls including:

- Concrete block stoppings – Solid block walls built the whole width across the mine entry. Usually covered with a sealant on both sides to decrease air leakage. These stoppings can also be equipped with a man-door to provide passage through the stopping.
- Regulators – Used to restrict the amount of airflow through a concrete block stopping. Regulator doors can be adjusted to change the size of the opening. The larger the opening the more air is leaked through the stopping. Regulators provide a means of controlling the air flow through various areas in the mine.
- Steel bulkheads – Solid constructed similar to concrete block stoppings but are reinforced with steel in between block on either side. The man-door is also heavy duty steel. These are made to withstand large amounts of air pressure.
- Line Curtains – Thin workable reinforced tarp like material that acts like a curtain hung in the direction with the entry forcing air towards the end of the entries (faces).
- Check Curtains – Same material as line curtains only hung across the width of the entry to act as a stopping, blocking off the passage of air. Check curtains are not as efficient at stopping leakage as concrete block stoppings. The advantages of check curtains are their ability to be installed and removed with ease.
- Partially mined through crosscuts sealed with concrete block – When the continuous miner holes into a crosscut it leaves coal half way across the crosscut instead of removing all of the coal. This provides a natural barrier and allows a concrete block stopping to be built with half of the materials.
- Ventilation doors – Doors built into concrete block stoppings that are large enough for equipment to pass through.

1.4 – Data Collection Objectives

Data collected at the mine included measuring drops in pressure and altimeter changes between known points within the mines ventilation circuit, air velocities,

temperatures, relative humidity, and mine opening dimensions. Fan data was also collected and included static and velocity head readings. This data was used to calculate the resistance in the mine, fan performance curves, and changes in air quantity throughout the ventilation circuit. All data was analyzed and input into a VnetPro working model of the facility. Lastly, upset conditions were produced that dramatically changed the resistance of the mine circuit (portal doors were opened and a curtain was placed a few hundred feet from the fan).

1.5 - Principle Investigation Tool

All equipment used to characterize the SRCM ventilation system was supplied by NIOSH and included:

- Meters capable of reading pressure changes to the nearest 0.01 inches of water gage (in. w.g.)
- Vane anemometers
- Sling psychrometer
- Altimeter
- Pitot tubes
- Manometers
- Plastic tubing

The ventilation network simulation software developed by Dr. Malcom J. McPherson and sold by Mine Ventilation Services (MVS) under the name VnetPro [1].

2 - Data Collection and Analysis

On 10 October 2014 the SRCM ventilation system was temporarily altered to contain the majority of the air flow through a single entry of the underground facility (Figure 2). The green line represents the course of the air directed through the mine by an array of stoppings (blue) and curtains (red). The stoppings were permanent ventilation structures typically made of cement block and mortar some with man-doors and temporary curtain structures made of fire-resistant canvas. The curtains were hung from the roof and rib and supported with wood and metal members. Curtains typically leak more air than stoppings, even when doors are present. These changes in the ventilation system greatly simplified the SRCM ventilation circuit

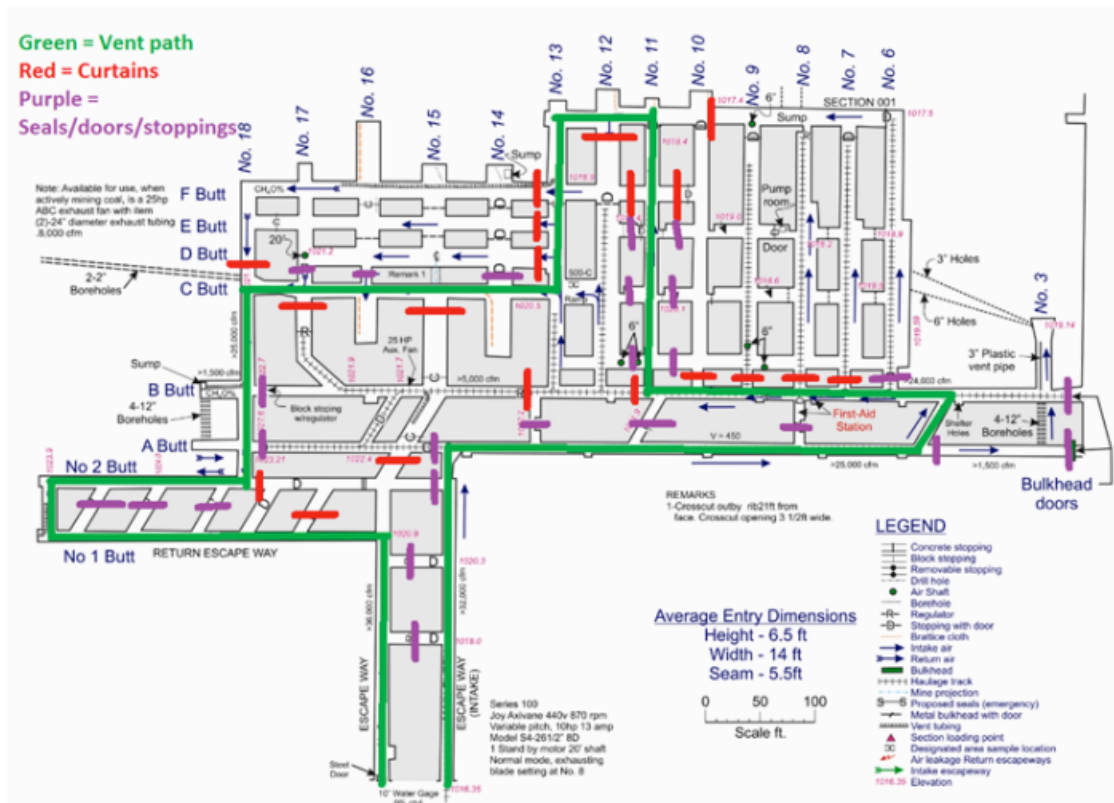


Fig. 2. Ventilation controls in-place during the 10 October 2014 field trip to the SRCM

The SRCM main fan is placed within a structure that contains three distinct parts: a) the 90° shaft top compartment, the fan blade and motor compartment, and the 90° exhaust elbow (Figure 3). The SRCM main fan is listed on the mine map (Figure 2) as a Joy Axivane Series 1000, 440 V, 870 rpm, Model 54-26 1/2 BD, normal blade mode set at #8, exhausting fan. The main fan information from the plate found within the fan compartment list it as a Joy Axivane Series 1000, 54-26 1/2 BD, Unit No. V1000-225, 690 rpm, EP110-8 GH motor (Figure 3).



Fig. 3. Three components of the SRCM fan structure.

On 10 October 2014, eight stations were located along the SRCM ventilation circuit. Numerous

conditions were measured at each station. A summary of the area, velocity, and quantity of air at each of these stations is shown in Table 1.

Table 1. Area, velocity, and quantity of air at each of the eight measurement stations.

Station Number	Circuit Position	Entry Area (ft ²)	Air Quantity (ft ³ /min)	Velocity (ft/min)
3	1	75	31,283	418
4	2	74	28,955	393
5	3	61	25,052	411
6	4	96	19,904	207
7	5	91	27,862	305
8	6	62	28,112	451
1	7	53	34,427	644
2	8	76	30,679	404

3.0 - Entry Resistance

There are generally two acceptable methods to measure the frictional pressure drop in mine entries: gauge and trailing tube method and barometer or altimeter method [2]. The gauge and trailing tube method is more accurate and is the preferred method when an entry can be traveled by foot, such as at the SRCM. The gauge and trailing tube method was the primary method used to measure frictional pressure drop along ventilation circuit. Additionally, altimeter measurements were used as a check; however, due to small differences in readings no useful information was obtained.

The primary purpose of conducting pressure surveys is to determine the frictional pressure drop, 'p', which

can then be used to calculate individual mine entry resistance and an appropriate resistance factor, k. The entry ventilation resistance, R, was determined using the formula [3]:

$$R = \frac{H_f}{Q^2} \quad (1)$$

The frictional head loss (H_f) is in inches of water gage (in. w.g.).

Note: It is standard practice to divide Q by 100,000 in the above formula to make the R , and k , more reasonable numbers.

The gauge and trailing tube survey instruments consisted of a magnahelic pressure gauge and 1/2-inch diameter plastic tubing. One end was stationed at the mouth or intake of the entry (Station 3) and this pressure reading was designated at zero. The tubing and pressure gauge were then advanced through the entry, stopping at designated positions. Pressure drops were measured at Stations 4 through 8. The recorded pressure drops are shown in the Table 2.

Table 2. Ventilation circuit recorded pressure drops and resistances.

Station	Length, ft	Flow, Q, 1000 ft ³ /min	SP Loss, H _f , in. w.g.	Resistance, R, P.U.
3 to 4	197	31.3 to 28.9	0.01	0.11
4 to 5	500	28.9 to 25.1	0.07	0.96
5 to 6	668	25.1 to 19.9	0.06	1.19
6 to 7	437	19.9 to 27.9	0.015	0.26
7 to 8	715	27.9 to 28.1	0.025	0.32

Another method to determine entry resistances is accomplished with the Atkinson's Equation [4]:

$$H_f = \frac{kO(L+L_e)Q^2}{5.2A^3} \quad (2)$$

Where:

Q = Air quantity, ft³/min

k = Empirical resistance factor, lbf·min²/ft⁴×10⁻¹⁰

O = Perimeter, ft

L = Entry length, ft

L_e = Effective length, ft

A = Area, ft²

In this equation, the head losses are a combination of the frictional resistance of the length of entry as well as the associated shock losses. Shock losses occur within the SRCM ventilation route whenever the air flow changes direction or when there is a contraction or expansion in the flow. The Atkinson's Equation (equation 2) compensates for these shock losses by assigning an effective length, L_e , for different shock producing conditions. The Hartman textbook provides a table (Table 5.3) for some of the most common shock loss conditions found within underground coal mines [4]. For example, a right-angle bend would add another

70-ft to the length of an entry while an acute sharp bend would add 150-ft. There were no bends between station 3 and 4; two 90-degree bends, and one acute bend between stations 4 and 5; three 90-degree bends between stations 5 and 6; one ninety between station 6 and 7, and five right angle bends between station 6 and 7.

The Resistance Factor, k , can be derived from equation 2 by using the measured resistances for various ventilation circuits within the SRCM:

$$k = \frac{5.2 \times R \times A^3}{(L+L_e) \times O} \quad (3)$$

Where:

k = Empirical resistance factor,

lbf·min²/ft⁴

$R = H_f/Q^2$, in·min²/ft⁶

O = Perimeter, ft

L = Entry length, ft

L_e = Effective length, ft

A = Area, ft²

Table 3 provides the measured Resistance Factors, k , for each of the segments within the SRCM ventilation circuit. Both the resistance, R , and the Resistance Factor, k , can be used within the VnetPro ventilation modeling program to define head losses along segments of the SRCM ventilation circuit.

Table 3. Resistance Factors, k , for each of the segments of the SRCM ventilation circuit.

Stations	Effective Length, L _e , ft	Perimeter, O, ft	Resistance Factor, k
3 to 4	0	36.6	33.4
4 to 5	290	32	79.0
5 to 6	210	44	36.3
6 to 7	70	41.6	57.4
7 to 8	350	33.4	35.6

4. - Fan Performance

Robert Krog provided the guidance for analyzing the SRCM fan [5]. The first step is to determine the Velocity Pressure (VP) and the Total Pressure (TP) for the SRCM fan based on the Model 54-26-690 fan curve. This is accomplished by applying the fan law and modifying the measured SRCM fan properties to fit within the manufactures parameters shown on the fan curve (Figure 4). The model 54-26-690 fan was tested by manufacture at 690 RPM. The SRCM RPM at 34,427-ft³/min is measured at 633. Therefore the adjusted air quantity (Q_{CHART}) is determined as follows:

$$Q_{\text{CHART}} = \left(\frac{\text{RPM}_{\text{CHART}}}{\text{RPM}_{\text{MEASURED}}} \right) \times 34,427 \quad (4)$$

$$Q_{\text{CHART}} = \left(\frac{690 \text{ RPM}}{633 \text{ RPM}} \right) \times 34,427$$

$$Q_{\text{CHART}} = 37,527\text{-ft}^3/\text{min}$$

The Q_{CHART} adjusted to the manufacture's fan curve is shown on Figure 4 (see black line).

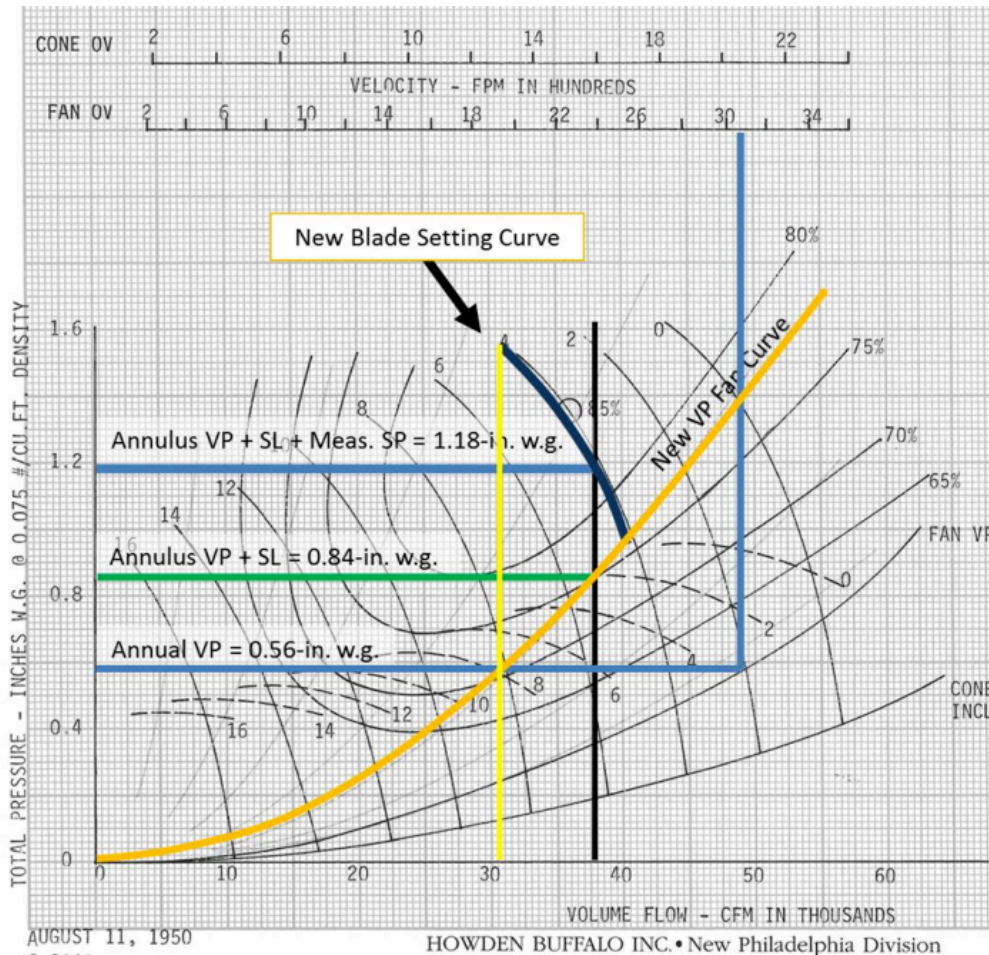


Fig. 4. Model 54-26-690 with various modifications.

The SRCM fan (Model 54-26-690) has a total area (Equation 5) of 15.9-ft² with an annulus area (Equation 6) equal to 3.7-ft². The effective fan area (Equation 7) is therefore equal to 12.2-ft².

$$Fan Area_{TOTAL} = \frac{\left(\frac{54in}{2}\right)^2 \times \pi}{144 \frac{in^2}{ft^2}} = 15.9 ft^2 \quad (5)$$

$$Fan Area_{ANNULUS} = \frac{\left(\frac{26in}{2}\right)^2 \times \pi}{144 \frac{in^2}{ft^2}} = 3.7 ft^2 \quad (6)$$

$$\frac{Fan Area_{EFFECTIVE}}{Fan Area_{ANNULUS}} = \frac{Fan Area_{TOTAL}}{12.2 ft^2} \quad (7)$$

The velocity of the air moving through the fan is calculated to be (Equation 8):

$$V_{FAN} = \frac{37,527 CFM}{12.2 ft^2} = 3,076 \frac{ft}{min} \quad (8)$$

The annulus Velocity Pressure (VP) loss is determined by connecting the scale on the top of Figure 4 at the 3,076 ft/min (Equation 8) mark with the Fan VP curve (vertical blue line on Figure 4). The horizontal blue line draw from this point intersects the y-axis at

0.56-in w.g. This is the annulus Velocity Pressure (VP) loss.

The shock loss (SL) from the SRCM fan housing and fan guarding is assumed to be 0.28-in. w.g. (0.56-in. w.g. multiplied by 0.5). When the shock loss is added to the annulus VP loss, a value of 0.84-in w.g. is calculated (Equation 9 and second upper green horizontal line on Figure 18). At this point, the fan is effectively 'not doing measurable work' on the air current. All the fan's work is going towards overcoming shock losses.

$$Annulus VP_{NEW} = Annulus VP + (Annulus VP \times Shock Loss) \quad (9)$$

$$Annulus VP_{NEW} = .56' + (0.56'' \times 0.5) = 0.84 in. w.g.$$

It is now possible to pass a curved line, starting at zero, and thru the intersection of the horizontal annulus VP + Shock Loss line and the vertical 37,527 air quantity line. The curve represents the new fan VP curve (orange line on Figure 3).

The last step is to add the annulus VP + Shock Loss values to the original static pressure (SP) of 0.34-in.w.g. measured at the SRCM fan.

$$0.84 + 0.34 = 1.18-in w.g.$$

The new SRCM fan curve (purple curve on Figure 4) is located between blade settings 4 and 5. The TP, VP, and SP for various points along the SRCM fan curve are measured (Table 4). The Fan Law is used to plot Q measured (Table 4) where Q from Chart is multiplied by the 633-RPM/690-RPM and TP, VP, and SP are multiplied by the square of 633-RPM/690-RPM. The VnetPro program requires the fan curve for SP (Fan TP minus the VP) versus Q.

Table 4. New TP, VP, and SP for versus Q for the SRCM fan.

Q from Chart	Q measured	Total Pressure, TP	Velocity Pressure, VP	Static Pressure, SP (TP - VP)
ft^3/min	ft^3/min	<i>in. w.g.</i>	<i>in. w.g.</i>	<i>in. w.g.</i>
30,500	27,980	1.30	0.47	0.83
34,000	31,191	1.18	0.58	0.59
37,527	34,427	0.99	0.71	0.29
40,500	37,154	0.81	0.81	0

5. VnetPro Simulation

The VnetPro program simulates ventilation systems by constructing branches, representing entries, and nodes, branch intersection points. Figure 5 shows how the VnetPro software organizes the ventilation data. Each branch is assigned a number and a connecting nodes, an appropriate area, and a resistance. The branch is also assigned a direction of flow represented by an arrow. If a ventilation control existed within the branch the following symbols were assigned:

- D Stopping with personnel/vehicle door (DD indicates double doors)
- || Permanent stopping
- | Check Curtain
- R Regulator

5.1 – Resistances and VnetPro

From Section 3, the resistance factors, k, for various SRCM entries was used to calculate resistances (practical units [P.U.] or $N \cdot s^2/m^8$). These unique k values (Table 3, last column) were applied to the 10 October 2014 ventilation circuit (Figure 5). The remaining entries, outside the 10 October 2014 ventilation circuit, were assigned a friction factor of k = 50.

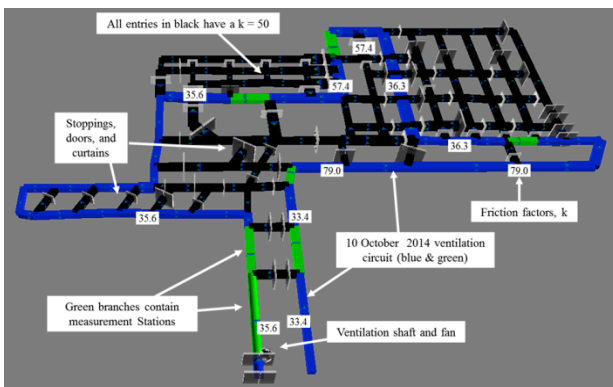


Fig. 5. Map showing the resistance factors, k, for the 10 October 2014 ventilation circuit.

The resistances values for various ventilation controls were altered in a series of VnetPro models. Air quantities, Q, from the eight measurement station were used to calibrate the models. The parametric analysis uses ventilation control resistances with the following ranges:

- Curtains = 1 to 5 P.U.
- Doors = 10 to 50 P.U.
- Stoppings = 25 to 100 P.U.

The most appropriate resistances were investigated by altering these values, one-ventilation control at-a-time. For example, Table 5 compares the measured versus modeled air quantities at six of the measurement stations. Test #1 is most closely aligned with the measured air quantities on 10 October 2014.

Table 5. A comparison between 10 October 2014 measured air quantities and the VnetPro model with the best fit (Test#1).

	Air Quantity, Q, 1000xft ³ /min						
	ST# 3	ST# 4	ST# 5	ST# 6	ST# 7	ST# 8	ST# 2
10 Oct.	31.3	29.0	25.1	19.9	27.9	28.1	30.7
Test #1	30.7	27.8	21.5	20.6	22.4	30.7	32.2

The parametric model runs found that the model best simulates measured conditions when curtain resistances, R = 1-P.U. The concrete Stoppings within the SRCM had much higher resistances, R = 50-P.U. The doors are more challenging to model because there can be a wide variation in their resistances, R. In general, a resistance, R, of 25-P.U. produced the most favorable results. There were two exceptions. The doors in the first two crosscuts between the intake and return entries experience the highest pressure drops. The SRCM has a double set of doors in both of these entries that increase the resistances of the crosscuts. As a result, these ventilation controls had higher resistances, R = 50-P.U. Another exception is the resistance, R, applied to the double doors at the return portal. Here, a resistance, R, or 25-P.U. was used to adequately model the measured leakage of 2,300-ft³/min.

There are 165 branches, 69 with ventilation controls, i.e. curtains, stoppings, doors, etc. Ninety-six branches have resistances calculated with k-factors. Fifty of these are along the 10 October 2014 ventilation circuits with resistances, R, between a low of 0.00054 and a high of 0.01991-P.U. The smallest resistances have the shortest branch lengths while the largest resistances have the longest lengths. A fixed quantity fan is placed within Branch #227 (vertical ventilation shaft), producing an air flow of 34,500-ft³/min.

All of the entries are rectangular in shape with the exception of Branches #1, #3, and #225. These entries are arched and concrete lined from the intake and return portal entries (Figure 5) to the first crosscut. Three branches (#1 – intake portal, #225 – exhaust portal, and #227 – vertical ventilation shaft) end in atmosphere.



Fig. 6. SRCM portals. a) the intake portal (no doors) is the start of Branch #1. b) the double door exhaust portal is the end of Branch #225.

5.2 – Fix versus Fan Curves, VnetPro Simulations

The precise SRCM fan curve developed in Section 4 was used in-place of fix fan condition. It is assumed that an accurate fan curve would allow for a more precise model of up-set conditions (see Section 6.0). To accomplish this task, the fan was moved to the top of a 20-ft, 5 by 5-ft rectangular shaft (Figure 7).

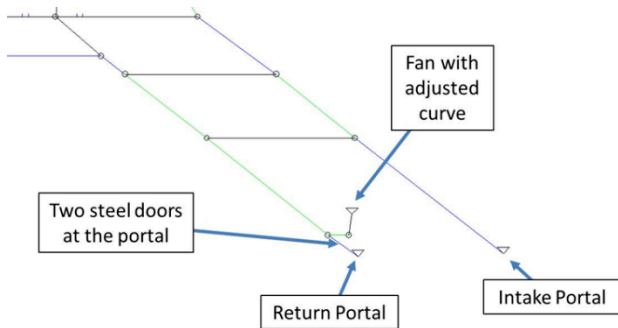


Fig. 7. Fan with adjusted fan curve added to the top of a 20-ft vertical shaft.

In these simulations, air quantity measurements from models with a fix fan and fan curved were run and compared to the 10 October 2014 measurements at the eight stations. The fix fan condition, Test #1 in Section 5.1, was found to have suitable resistance values for the various ventilation controls. A second condition (Test #2) was also simulated using the actual SRCM fan curve. All other conditions remain the same as with Test #1. The data in Table 6 demonstrates that the fan curve conditions produced a slightly less accurate ventilation circuit simulation than the fix fan. This was somewhat of a disappointment. There are several potential causes for this performance, i.e. incorrect resistances, errors in making air velocity measurements, inaccurate cross-sectional area for the entire mine. etc.

Table 6. Ventilation simulations with both the fix fan and fan curve conditions.

	Air Quantity, Q, 1000xft ³ /min							
	Station							
	1	2	3	4	5	6	7	8
Observed	34.4	30.7	31.3	29.0	25.1	19.9	27.9	28.1
Fix Fan, Test#1	34.5	32.2	30.7	27.8	20.1	20.6	22.4	30.7
Fan curve, Test#2	35.6	33.3	31.7	28.7	22.2	21.4	23.2	31.7

6.0 – Up-set Condition

Two up-set conditions were tested within the SRCM that deviated from normal ventilation configurations during 10 October 2014. In Test #3 both portal doors were opened, allowing air to short-circuit from the atmosphere to the fan without traveling through the facility beyond the portal area. In Test #4 both portal doors were closed and a curtain was installed completely across the entry just inby Station 2 (Figure 8).

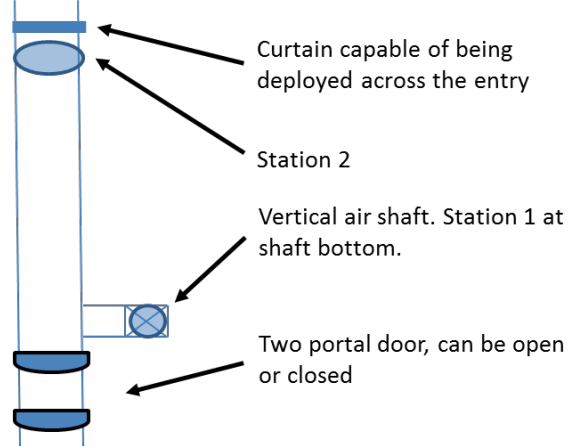


Fig. 8. Conditions during up-set testing showing a detailed view of the area where the tests were performed. Please note that Station 1 is within the vertical shaft leading directly to the in-let fan box.

Selected ventilation conditions during the up-set tests were monitored and are shown in Table 6. Let's examine the condition of the air (quantity and pressure) in and adjacent to the ventilation shaft (Station 1) during and prior to the up-set tests (Table 7).

Table 7. Upset conditions at the fan, Station 1, and Station 2 (Q, 10³ x ft³/min)

	Station 1				Station 2			
	Q measured	Vnet-Pro Model			Q measured	VnetPro Model		
		#2	#3	#4		#2	#3	#4
1	34.4	35.6	-	-	30.7	33.3	-	-
2	32.8	-	36.9	-	7.1	-	3.4	-
3	25.8	-	-	31.0	24.6	-	-	26.2

6.1 – Condition 1: Normal ventilation circuit for 10 October 2014

Condition 1 represents of operating point for the facility during 10 October 2014 (Figure 9). The measured and modeled operating point falls along the SRCM SP fan curve. The relationship between air quantity, Q, and pressure, SP, for the facility is defined by this curve. As the resistances within the facility are change, the corresponding air quantity, Q, will change. The SRCM fan curve suggest that its operating conditions range from a maximum pressure of ~ 1.1-in. w.g. to a minimum of ~ 0, while the air quantity should range from ~28,000 to ~37,000-ft³/min. Lower air flows are possible but these operating conditions may stall the fan.

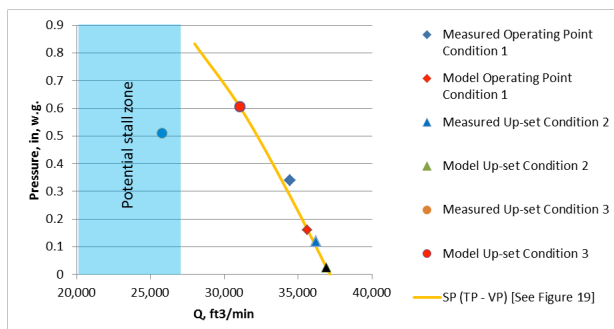


Fig. 9. SRCM SP fan curve with three distinct operating conditions.

The modeled operating point for condition 1 has a higher air flow and lower pressure than the measured operating point. This would suggest that the resistance values chosen for this study may be too low and should be raised to fall in-line with the measured values.

6.2 – Condition 2: Two portal doors opened

During Condition 2 the portal doors were opened, causing the air to short-circuit from the outside. When the portal doors are open, the fan does less work so the air quantity should increase and the resistance of the facility to the fan should be reduced (Figure 9).

When both portal doors were opened, the resistance on the fan was measured to be very low (0.12 in. w.g.), dropping the SP from 0.34 to 0.12-in. w.g. At this condition the TP air quantity (Q Chart) at the fan was calculated to be 39,490-ft³/min. The corresponding SRCM air quantity (Q estimated) was estimated to be 36,228-ft³/min (Q Chart x 633 RPM/690 RPM). This is very close to the maximum air quality for this fan configuration (~37,100-ft³/min, Table 5). The air quantity, Q measured, at Station 1 was 32,800-ft³/min and 7,100-ft³/min at Station 2. Seventy-eight percent of the air moving up the ventilation shaft came through the open double doors from outside of the facility. Here again, the model of condition 1 has a higher air flow and lower pressure than that measured within SRCM.

6.3 – Condition 3: Portal doors closed and curtain installed

For the third condition, the portal doors were closed and a curtain installed. The air quantity, Q measured, at Station 1 was 25,780-ft³/min and 24,600-ft³/min at Station 2. In this test, only 1,180-ft³/min of air came through the closed portal door or 95% of the air in the mine was coming through the entry with the curtain obstruction. The curtain reduced air quantity in the entry by 20 (24,600/30,679) to 29% (24,600/34,427). At the same time, the SP increased from 0.34-in. w.g., measured prior to the up-set tests, to 0.51-in. w.g. This represents a 50% increase in pressure. Clearly, this operating condition is outside of the normal operations for the SRCM fan. It is in a form of stall, causing the fan's efficiency and stability to be compromised. It is unlikely that the fan will experience vibrations since the blades are backward tipping and the fan blade conditions are typically used under higher pressure conditions (Robert Krog, personal communications). None-the-less, the efficiency and stability of the fan in the area of 'potential stall' are lessened and should be avoided when possible.

The model for Condition 3 wasn't able to simulate the SRCM fan in stall. Perhaps this is related to the resistance chosen for the curtain deployed near Station 2. A higher R would increase the pressure and potentially force the fan beyond the chart boundaries (Figure 8). When this happens, VnetPro halts its analysis and produces an error message for the user. It is also possible that entry resistances are higher than those used in the model.

7. Summary

The scope of the work in this ventilation survey included:

- Collecting basic mine ventilation information for NIOSH in their Safety Research Coal Mine, SRCM;
- Measuring the resistances of the selected mine entries;
- Characterizing the performance of the main fan; and
- Simulating the observed conditions within the VnetPro software platform.

This data collection effort is to assist NIOSH in modeling how fires affect underground ventilation systems.

The SRCM ventilation system is set up to exhaust. The main fan is a Joy Axivane Series 1000, 440-V, 870-rpm, Model 54-26 ½ BD. At the time of the ventilation survey the blade setting was observed to be set to #8 on the adjusting mechanism. According to the provided fan curve, the rated speed for the fan at the SRCM was 690-rpm. The fan was measured to 633-rpm using a strobe against the fan blades. The air flow across the fan was

measured at 34,427-ft³/min, measured at the base of the shaft.

The flows and pressures measurements were adjusted using the fan laws with an RPM ratio (actual and theoretical) and plotted against a 54-26-690 fan curve. Through a series of steps outlined by Robert Krog in a published paper and described in detail at one of the project team's classes, the actual SRCM fan curve was established with a blade setting more like a #4.5. The fan laws were used in reverse to achieve a plot of SP and air quantities, Q. This fan curve was used within VnetPro to simulate the performance of the SRCM fan under well-defined conditions.

Under normal conditions, i.e. non-stall, the SRCM fan should operate with air flow between 28,000 and 37,000-ft³/min over a range of 1.1-in. w.g. At lower air quantities, the fans efficiency and stability will be compromised. Higher air quantities are not possible. During the experiment, the dry bulb temperature was 53.6 degrees Fahrenheit. The relative humidity was 96 percent. The average entry dimensions are 91-ft². The length of the mine entry of the experiment is 2517-ft with a total SP of 0.18-in. w.g.

Several measurements were conducted along a predefined route through the SRCM. The main path of the ventilation circuit was formed by check curtains within several critical entries. Instruments were used to determine air velocity, relative humidity, temperature, and altitude, size of the entry, and pressure drop throughout the mine, as well as, pressure drop across the mine fan. From these measurements, and by utilizing the manufacturers fan curve, the SRCM operating point was determined.

Normal operating conditions during 10 October 2014 (Condition 1) were modeled using a VnetPro model with 165 branches. The model contained two kinds of resistances. The resistances produced by the ventilation circuit were calculated using the k-factor. These k-factors were based, in part, on pressure drop surveys conducted at the mine. Parametric model runs were used to find the most appropriate resistance, R, of the SRCM ventilation controls. The model contained three exits to the atmosphere. The SRCM fan was modeled with the 'fixed fan' parameters and compared with a fan curve specific to the facility. The fan curve was developed from a series of measurements made within the fan structure.

The Pitt team was particularly interested in conducting pressure surveys is to determine the frictional pressure drop, 'p'. This fundamental parameter can be used to calculate: a) individual mine entry resistance, b) total ventilation circuit resistance, and c) an appropriate resistance factor, k. The instruments used in the gauge and trailing tube survey consisted of a magnahelic pressure gauge and ½-inch diameter plastic tubing. The SP losses between stations 3 to 4, 4 to 5, 5 to 6, 6 to 7, and 7 to 8, yielded k-factors ranging from 33.4 to 79-in.min.²/ft⁶.

Condition 2 involved opening the mine entry doors to the atmosphere near the base of the fan shaft and the other test, Condition 3, involved installing a curtain about ~100-m inby the fan shaft. With the portal doors open, the air quantity measured at Station 1 was 32,800-ft³/min and 7,100-ft³/min at Station 2. The VnetPro models of this condition were somewhat inaccurate.

During the second up-set test, Conditions 3, a curtain was installed inby Station 2. The air quantity at Stations 1 and 2 were measured as 25,780 and 24,500-ft³/min, respectively, with pressures of 0.51-in. w.g. These values suggest the fan was off its normal operating range as defined by the fan curve. It is likely that the fan was in stall during much of this test.

Additional simulations will need to be run to determine if altering the resistance of the curtain might provide more accurate results. However, the quality of the velocity and pressure measurement at the fan made these up-set tests more difficult to analyze. Improving the quality of data associated with up-set test could yield better results and should be evaluated in future testing.

Acknowledgements

The Pitt project team would like to recognize the three undergraduates who assisted in the project; Vincent Denissen, James Helmig, John VanNess, and Jake Vitullo. In addition, the project team would like to thank the following individuals for the help during with this activity:

- Dan Alexander (NIOSH) for assistance in all phases of the project.
- Lihong Zhou (NIOSH) for reviewing the report.
- Paul Stefko (NIOSH) for arranging access to the SRCM and provided the necessary training for the team.
- Roy Grau (NIOSH) for providing various critical instruments and training on their use.
- James Addis (NIOSH) for assisting the project team with all aspects of the SRCM tests.
- Richard Thomas (NIOSH) for constructing the temporary curtains and provided critical instrumentation.
- Gerry Finfinger (NIOSH) for helping to arrange the approvals for the Pitt team.
- Robert Krog (West Virginia University) for providing extensive guidance in characterizing the SRCM fan and interpreting the data.

References

- [1] Anon, "VnetPro+ User's Manual & Tutorial," Mine Ventilation Services, Inc., 1625 Shaw Ave., Suite 103, Clovis, CA 93611, 2014, 117 p.
- [2] M.J. McPhersoio, Subsurface Ventilation Engineering, uploaded from the MVS Engineering website.

- [3] D.S. Kingery, "Introduction to Mine Ventilating Principles and Procedures," US Bureau of Mines Bulletin 589, 1960.
- [4] H. Hartman, J. Mutamansky, R.V. Ramani and Y.J. Wang, Mine Ventilation and Air Conditioning, Third Edition, 1997.
- [5] R.B. Krog, "Selection of Underground Booster Fans", Proceeding of the North American/Ninth US Mine Ventilation Symposium, Kingston, Ontario, Canada, 8-12 June 2002, Paper 136, pp. 153-158.

Air Temperature Inversions and its Impact on Natural Ventilation in Open pit Mines

K. V. Raj, G. J. Fochesatto and S. Bandopadhyay

University of Alaska Fairbanks, Fairbanks, AK 99775

In extreme climatic conditions, deep open pit mines trap pollutants as a result of the development of air temperature inversion. Management of the air quality becomes challenging with the disruption of natural ventilation cycles. Surface-based inversion (SBI) is formed as result of radiative cooling of the ground surface. The formation of this temperature inversion layer is common during the winter months in the Arctic and sub-Arctic. However, a temperature inversion can also develop above the SBI, depending on the synoptic meteorological conditions, commonly known as the elevated inversion (EI). Depending on the altitude, location and geometry of an open pit mine, different types of air inversion may occur. The growth of inversion descent is a function of sensible heat flux, atmospheric pressure, density of air, solar heat flux, and potential temperature.

Better understanding of the air inversion type, frequency and vertical structure of air inversion is important in order to design pollution mitigation measures in an open pit mine. In this paper, various types of inversion that can develop in open pit mines are discussed. Impacts of air inversions in open pit mines from various regions including mines from lower latitudes are analyzed.

Keywords: Air Inversion, Air Pollution, Open Pit Ventilation.

1. Introduction

The Arctic region contains vast mineral resources. Mining of these resources is a major activity in the Arctic regions in several countries, particularly the United States. With the advancement of open pit mining technology, the depth to which minerals can be profitably mined has increased, resulting in deeper pits than ever before. However, the increased operation depth carry several inherent challenges for mining operations. One of the challenges for deep open pit mining in cold climate is atmospheric air temperature inversion. A temperature inversion layer can be described as a positive upward thermal gradient that imposes a thermal stratification in the air layer surrounding the surface. This stratification severely restrict the vertical movement of trapped pollutants. By itself, inversion is not hazardous. However, due to the presence of source emission of gases and particulates during the mining process, the air within the pit can be severely and sometimes quickly contaminated, leading to serious health and safety consequences. To understand and analyze air inversions, it is necessary to understand the process by which such inversions and consequent entrappings of pollutants take place. Thus, an important area in open pit pollution dispersion modeling is the atmospheric boundary layer (ABL). The ABL experiences a diurnal cycle, generally evolving slowly during the day and night, but rapidly in the morning and sporadically during the evening transition. It is within the ABL that most release of pollutants take place and have the most significant direct impact on the health and safety of miners in an open pit mine. The mixing of pollution in the ABL is governed by the state of turbulence with different wind speeds, solar radiation

and surface heat fluxes resulting in different pollutant dispersion behaviors.

Stull [1] defines the ABL “as that part of the troposphere that is directly influenced by the presence of the earth’s surface, and responds to surface forcings with a timescale of about an hour or less (p. 2).” Surface forcings that are considered include frictional drag, evaporation and transpiration, heat transfer, pollutant emission, and terrain induced flow modification. Turbulent fluxes characterize the ABL state, and is generated as a result of both sensible heat fluxes (thermal forcing) and the wind shear (mechanical forcing). The length scale of turbulence in the atmosphere ranges from a millimeter to thousands of meters [1, 2].

The turbulent kinetic energy (TKE) rate equation describes the physical processes that generate turbulence. In the ABL, TKE production by buoyancy and shear approximately balance dissipation resulting in a small storage term, i.e., the intensity of the turbulence is changing slowly with time [1].

$$\text{TKE (Storage)} = \text{advection of TKE} + \text{Production /or loss by buoyancy} + \text{production/loss by shear} + \text{Turbulent transport} + \text{pressure correlation} - \text{dissipation} \quad (1)$$

Thus, turbulence is one of the important mechanisms dominating the transport processes in the atmospheric boundary layer. The turbulent eddy motions are generated by two mechanisms: wind shear and buoyancy. When a flow travels over rough surfaces such as trees, buildings, and terrain, cause the wind to develop shear turbulence and influences the temperature or any scalar field. Buoyancy on the other hand leads to the formation and rise of thermals.

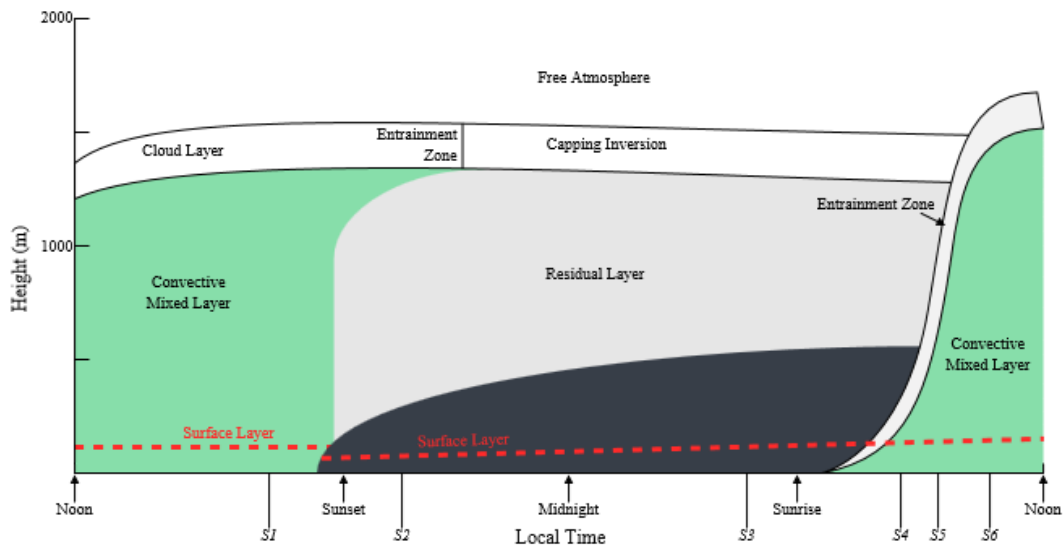


Fig. 1: The Boundary Layer in High Pressure Region over Land(Adapted from Stull) [1].

In Figure 1, the effects of diurnal cycles on the boundary layer structure over land surfaces in high pressure regions are presented. As it can be seen, the boundary layer structure has three major components: (1) a mixed layer, (2) a residual layer, and (3) a stable boundary layer.

A mixed layer evolves after the sunrise, mainly driven by convection. It is also called convective boundary layer (CBL). In the absence of clouds, the ground surface is heated by the incoming solar radiation. This causes the thermals to rise up, developing a turbulent motion in the atmosphere. The turbulent mixes the heat, momentum, moisture, and pollutants in the vertical direction reducing therefore the pollutant concentration. While at the same time, the atmospheric flow is in constant contact with the surface, and develops turbulence to maintain the progression of the ABL diurnal cycle.

In the absence of any cold air advection, the thermals generated during the day in fair weather conditions tend to cease just before the sunset. This allows the turbulence to decay in the formerly well-mixed layer [3]. This new layer formed is called the residual layer. The residual layer attains near-neutral stability under non-advective conditions [4, 5].

At night when the surface cools through the emission of longwave radiation, the ABL becomes stably stratified; i.e., the potential temperature of the air increases with height over the depth of the layer. In these conditions, the thermal stratification works to inhibit vertical motion, and any turbulence is generated mechanically through wind shear. This turbulence is much weaker than that of the CBL resulting in a much shallower boundary layer, with a depth of only few hundred meters. The ABL in this state is known as a stable boundary layer (SBL). The SBL formed during the night time is sometimes referred to as the nocturnal boundary layer.

The stable boundary layer prevails at night, but can also develop during the daytime in Arctic and sub-Arctic regions due to the lack of sunlight during the winter months. The SBL is characterized by statically stable air where the vertical stability suppresses the surface turbulence.

The SBL, can also be developed by warm air advection over a cooler surface [6]. In a majority of high pressure situations, air inversions are observed. Various studies have been conducted on the air inversion in Fairbanks, Alaska [7, 8] and more recently by Fochesatto and others [9], Mayfield and Fochesatto [6] and Malingowski and others [10]. Understanding the physics of the stable boundary layer is relevant to air flow and pollutant transport in deep open pit mines. Due to the suppressed vertical motion under the SBL, pollutants generated in an open pit mine primarily spread in the horizontal direction and do not leave the open pit [11].

Strong stable boundary layers can be prevalent in high latitudes in the winters when the air in the surface layer is confined to a cold-closed basin. The local and areal radiative forcing dominates the formation and breakup of the inversion, whereas, advection is limited by the geometry of the area. In these conditions, the flow in the cold pool is susceptible to developing strong stratified inversion layers [12, 13].

2. Processes Affecting the SBL

Several forces such as the radiation, the conduction, the turbulence, the subsidence, the advection and the local terrain configurations affect the formation and breakup of the SBL [1]. Among these forces, radiation plays a critical role both in the formation and destruction of the SBL. Conduction acts within few millimeters above the ground. For the purpose of modeling of pollutant transport in open pit mines, some of these forcings can be neglected depending upon the specific environmental conditions.

2.1 Radiation

In the absence of solar radiation and advective flows, the net radiation is dominated by long-wave radiation [1] which introduces the radiative cooling. There are generally four types of energy fluxes at an ideal surface: (1) the net radiation to and from surface, (2) the sensible, (3) latent heat fluxes to and from atmosphere, and (4) the heat flux into or out of the sub-medium [14]. The net radiation is the sum total of the incoming and out-going shortwave and longwave radiation. For a flat surface, the net radiation is illustrated in Figure 2, where $SW \downarrow$ is the

down-welling shortwave radiation; $SW \uparrow$ is the up-welling shortwave radiation; $LW \downarrow$ is the down-welling longwave radiation; and $LW \uparrow$ is the up-welling longwave radiation. The net radiation (R_n) is given as:

$$R_n = SW \downarrow - SW \uparrow + LW \downarrow - LW \uparrow \quad (2)$$

During the day in fair-weather conditions, the down-welling solar radiation is dominant. The surface gains energy from the solar heating, resulting in a net positive radiation. On the other hand, at night, in the absence of solar heating, the surface longwave radiation upwelling prevails, resulting in surface cooling, and net negative radiation. Due to the surface cooling a positive upward temperature profile near the ground is developed. Therefore, during the night, the longwave radiation balance plays a key role in determining the structure of the SBL. As can be seen in Figure 2, if pressure gradient forces can be neglected the incoming solar radiation is the major external surface forcing during the day.

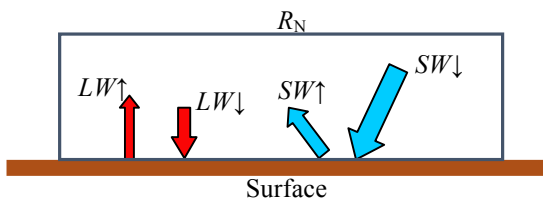


Fig. 2: An Illustration of Net Radiation Fluxes.

In response to the net radiation balance at the surface the sensible, latent, and ground heat fluxes are generated. Energy balance at the surface is given by:

$$R_n = H_s + H_l + H_g \quad (3)$$

Where, the terms H_s and H_l are the sensible and latent heat fluxes to and from the atmosphere, and the term H_g is the ground heat flux into or out of the sub-medium. Figure 3 shows a typical energy balance at the ground surface during the day and the night time. The heat loss due to the out-going radiation is balanced by the sensible and latent heat fluxes. The arrow represents the direction of heat fluxes.

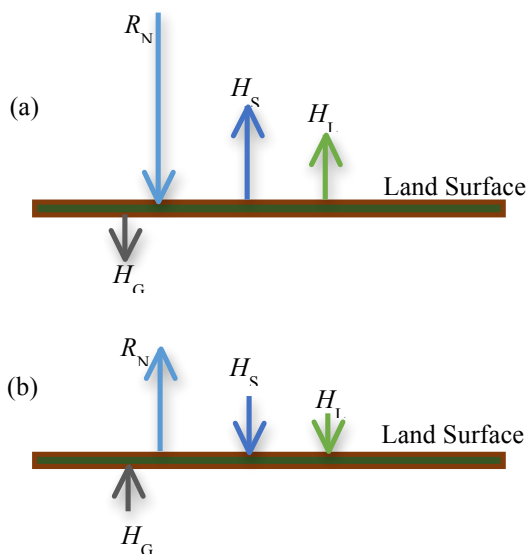


Fig. 3: A Typical Energy Balance during (a) Day-time (b) Night-time.

Figure 3(a) shows a typical day time scenario of energy balance, where the net radiation, R_n , is of the highest magnitude and pointing towards the ground surface. Sensible, H_s , and latent, H_l , heat fluxes are pointing away from the land surface into the atmosphere, whereas, the ground heat flux, H_g , also pointing away from land surface into the solid ground medium. Figure 3(b) shows a typical night time scenario of energy balance where direction of heat fluxes are opposite to the day time scenario.

The sensible heat flux is the result of temperature difference between the surface and the air above it. Whereas, the latent heat flux is represented by phase change, i.e., from ice to water and water to water vapor and vice versa. A small value of latent heat flux is observed in Arctic and sub-Arctic locations, such as Fairbanks during the mid-winter when the air is very dry [8, 9].

The ground heat flux into or out of a sub-medium is due to the exchange of heat through the ground. During the day in fair weather condition, the ground surface is heated by solar heating and the heat exchange into the ground is primarily due to conduction. During the night time and in the absence of solar radiation, the fluxes are directed out of the ground.

The actual magnitudes of the sensible, latent and ground heat fluxes depend on several factors such as the open pit surface (soil type) and its characteristics (moisture content, texture, vegetation, etc.), the season, the time of day, the weather conditions, and the geographical location.

2.2 SBL formation due to Subsidence and Advection

Formation of SBL is mainly attributed to the negative radiation balance. Subsidence and advection of warm air aloft, however, can also lead to the development of a SBL. Under a high pressure situation, and in the absence of warm air advection an upper layer subsidence causes warming of the upper layer of the ABL [15, 16].

As previously stated, SBL is also formed due to the advection of warm air over a cooler surface. During winters, the advection of warm air over a surface based inversion leads to the continuation of an existing inversion [17].

2.3 Air Inversions in Arctic and Sub-Arctic Region

As discussed previously, during the day, the ground surface is heated and the air mass rises as a result of solar heating. This results in a negative vertical temperature gradient as a function of elevation. Figure 4(a) shows the vertical temperature profile of National Weather Service upper air station at Fairbanks International Airport (FAI) in mid-summer under fair

weather conditions. It can be seen from the figure that the air temperature decreases with altitude.

On the other hand at night time and under the same high pressure situation, due to the radiative cooling of the earth surface leads to the lower air temperatures near the surface than at higher altitude, thus, forming a stable boundary layer Figure 4(b). The Earth's surface cools rapidly due to the radiative loss and the thermal properties of the surface. The lowest layers of the atmosphere cool more rapidly than the upper layers due to the cooling of the Earth's surface. Thus, a negative temperature gradient is established with its base on the surface.

Three distinct physical processes mainly govern the evolution and the structure of SBL: turbulence, radiative cooling, and the interaction of the SBL with the underlying sub-medium. Besides advection and thermodynamic processes, additional features such as katabatic flows, density currents, and downward transport of residual-layer turbulence also contribute to the formation of the SBL. One of the following three archetypes may occur, depending on the relative importance of radiation and turbulence: (1) fully turbulent, (2) intermittently turbulent and (3) radiative SBL. A stable boundary layer includes both intermittent and radiative archetypes.

In a weakly stratified boundary layer, the turbulence occurs continuously due to stronger wind and/or weaker

surface cooling. Whereas, in the case of a strong SBL, turbulence is weak and intermittent with small fluctuations [18]. A strong or very stable regime of boundary layers occurs under clear skies due to a large surface cooling rate and a weak mean wind velocity.

Surface-based inversion (SBI) is a common phenomenon during the winters in the Arctic and sub-Arctic regions [8, 19]. A typical winter temperature profile is presented in Figure 4 (b). The winters, in the Arctic and sub-Arctic regions under high pressure situation create a favorable condition for inversions to develop. Under such a condition, the stagnant air layers in contact with the ice and snow covered surfaces are cooled by the infrared radiation loss [20]. The inversion with its base at the surface is known as surface-based inversion [21].

The balance of various energy fluxes can be used to explain the change in surface temperature and development of inversions near the surface. Wendler and Jayaweera [8] showed that in the winter, in the absence of solar radiation, a decrease in cloudiness leads to a decrease in the surface temperature. The surface cooling rate in Fairbanks was observed to be more than 1°C per hour during the first 10 hours decreased cloudiness. They explained this is solely based on the negative radiation balance. During the winters in Fairbanks, the incoming shortwave radiation is negligible and therefore the net radiation is negative.

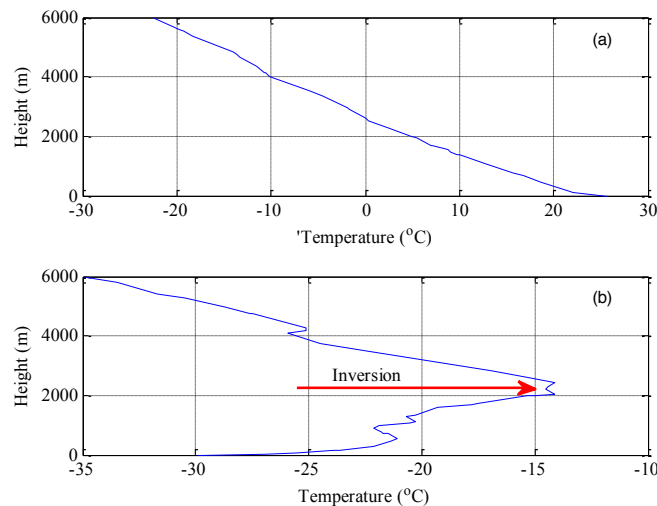


Fig. 4: Typical Vertical Temperature Profile at Fairbanks International Airport under Fair-Weather Conditions during (a) Mid-Summer and (b) Mid-Winter. (<http://weather.uwyo.edu/upperair/sounding.html>)

Wendler and Nicpon [19] characterized the inversions for Fairbanks, Alaska on a statistical basis. Using the hourly data from March, 1967 to February, 1968, they defined the occurrence of an inversion as higher temperatures at 200 m than at one meter above the ground surface. It was reported that, during the winter, statistically, an inversion occurred more than 95% of the time and more than 50% of the time for the whole study period. A more recent study comparing the radiosonde data from 1957 to 2004 was collected for the winter surface-based inversions in Fairbanks by Hartmann and Wendler [22]. They characterized the surface-based inversion in terms of temperature difference (ΔT) with altitude, pressure difference (ΔP), inversion depth (Δz), and by the ratio of the terms $\Delta T/\Delta z$. They reported a decrease of 212 m in the mean inversion depth (height) over the years. They also associated the surface wind direction with the events of

surface inversion and no surface inversion. The southerly winds are associated with both the inversion and no inversion conditions. No inversion events during southerly winds indicate that the advection of warmer and moist air accompanied by an increase in cloudiness restrains the formation of any surface-based inversion.

The air inversions, depending on their mode of development, height, and the processes that caused them, can be classified as surface-based and elevated inversions. A surface-based inversion (SBI) is an inversion with its base at the surface, whereas, an inversion developed over a surface-based inversion is called an elevated inversion (EI). Air inversions can either be surface-based, elevated, or both at the same time in the atmosphere depending on the meso-scale and micro-scale meteorology.

In the Arctic, apart from the surface-based inversion, another type of inversion has also been observed at higher elevations [6]. Depending upon synoptic conditions, the flow above the surface-based inversion may also develop elevated inversions. The elevated inversions are discontinuities in air density that occur between the surface-based inversion and the free troposphere, mainly as a function of specific synoptic large-scale flow. Known mechanisms [6] that give rise to elevated inversions in the atmospheric boundary layer flow are (1) warm-air advection flows or frontal inversions and (2) anti-cyclonic or subsidence inversions.

The warm air advection occurs when synoptic warm air flows over a stagnant low-level ABL flow or when warm air flows over large bodies of cold water. Elevated inversions during the anti-cyclone occur due to the subsidence of dry air which warms up the atmospheric layer above the surface-based inversion.

An example of a surface-based inversion along with an elevated inversion at FIA is presented in Figure 5. The data were collected on 12 UTC (Coordinated Universal Time) January 1st 2014. 12 UTC is 3:00 AM in Alaska Standard Time (AST) on January 1st 2014. The data at the Fairbanks International Airport are the radiosonde observational data taken every 0000 and 1200 UTC. The 0000 UTC represents 3:00 PM AST a day before and 1200 UTC is 3:00 AM AST on the same day. Figure 5 shows the base of an inversion starting at 0 m, i.e., the ground surface, making the first inversion, a surface-based inversion and another inversion starting to build up at around 1000 m above ground level (AGL). The inversion starting around 1000 m elevation is the base of the inversion known as the elevated inversion. A detailed discussion on various layers in the atmosphere in the Fairbanks area is presented by Mayfield and Fochesatto [6].

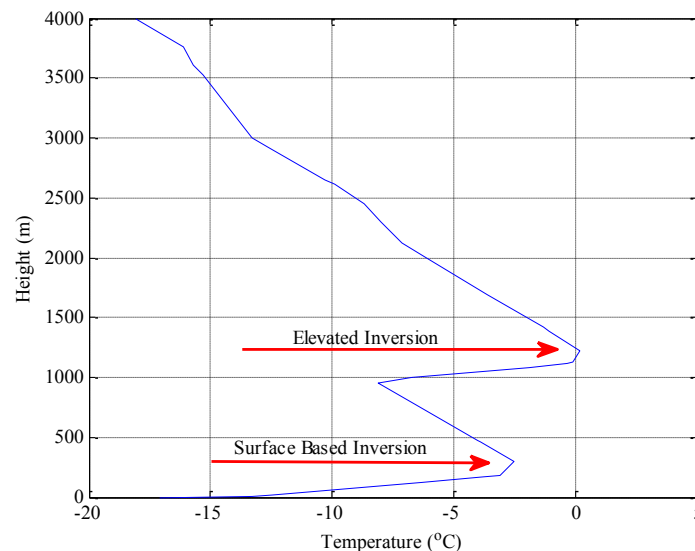


Fig. 5: An Example of a Temperature Profile with Multiple Inversion Layers

3. SBL of Open pit Mines

Open pit mines geometry is very much similar to mountain valleys in smaller scale with all sides closed. In order to understand the formation of SBL in open pit mines, a SBL of valley flow is presented here. Flows in mountain valleys are constrained due to the topographic configurations. Formation of inversions in the mountain valleys are attributed to the net negative radiation as well as in some cases subsidence and warm air advection. Several studies have been published on the SBL of valleys [8, 19, 23, 24].

Events of air inversion has been reported in various open pit mines in Arctic and sub-Arctic region. Several open pit mines such as, Kinross Fort Knox (Fairbanks) and Teck Cominco Red Dog mines in Alaska, BHP Billiton Ekati mine in Canada, Boliden Aitek mine in Sweden, and the Mirni and Udachini diamond open pit mines in Russia. Even Rio Tinto's Bingham Canyon mine in Utah has reported local air inversions from time

to time [25]. To illustrate the SBL regimes in Bingham Canyon Mine vertical structure of the temperature profile is presented in Figure 6. Figure 6(a) shows the night-time temperature profile, whereas, Figure 6(b) is for day-time temperature profile. Γ_d is the dry adiabatic lapse rate with a value of $9.8^\circ\text{C}/\text{km}$.

The occurrence of inversion at an open pit mine depends on the location. Figure 6 shows a strong inversion at the lower level of the pit. This inversion is mainly due to the cooling of the pit surface after the sunset. Apart from the surface-based inversion at the pit bottom, an elevated inversion can also be observed. The elevated inversion may have been formed due to the relatively faster cooling of the air mass near the Bingham pass and the advection of the cold air mass. During the daytime after solar radiation hits the pit walls, the stable stratification is weakened at the Bingham Canyon Mine.

In an open pit mine, the upward sensible heat flux also develops an unstable air mass layer over the pit surface, but, in contrast, the heated pit slopes causes warm air parcels to flow up-slope due to thermal buoyancy. These up-slope flows remove mass from the

base of the temperature inversion, resulting in a general subsiding motion over the center of the open pit [26].

In the Arctic and sub-Arctic region, during the winter months under high pressure system, the open pit mine surfaces start to cool continuously due to the radiative cooling (i.e., longwave radiation losses). The turbulent intensity is suppressed by the thermal stratification

(buoyancy suppression). Therefore, only the mechanical wind shear remains a source of turbulence. The atmospheric boundary layer (ABL), consequently becomes stably stratified and sometimes strongly-stratified. Under such conditions, the ABL is dominated by stably stratified layers during a large part of the winter months.

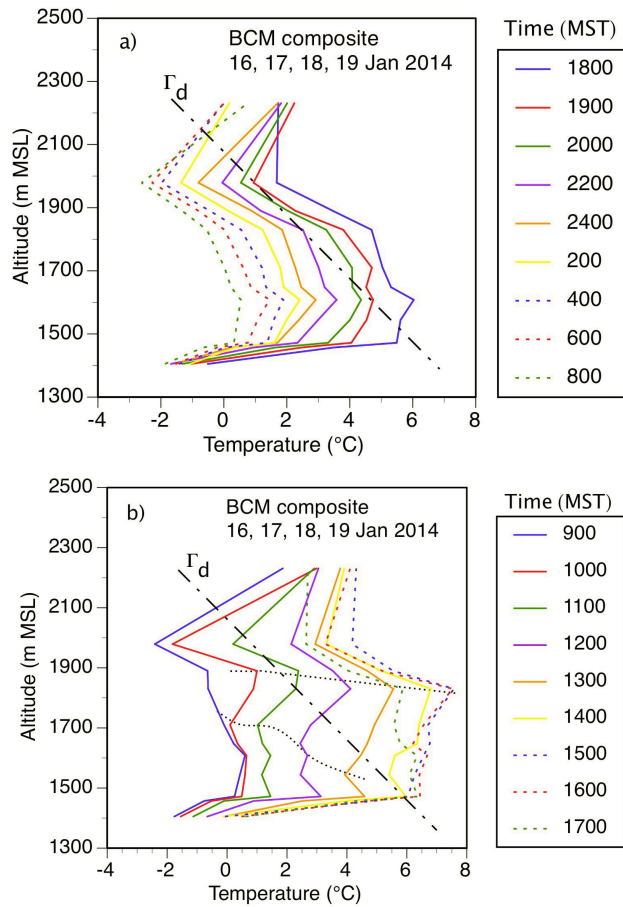


Fig. 6: Vertical Temperature Profile at Bingham Canyon Mine, Salt Lake City, Utah. a) Night-Time Temperature Profile, b) Day-Time Temperature Profile [25].

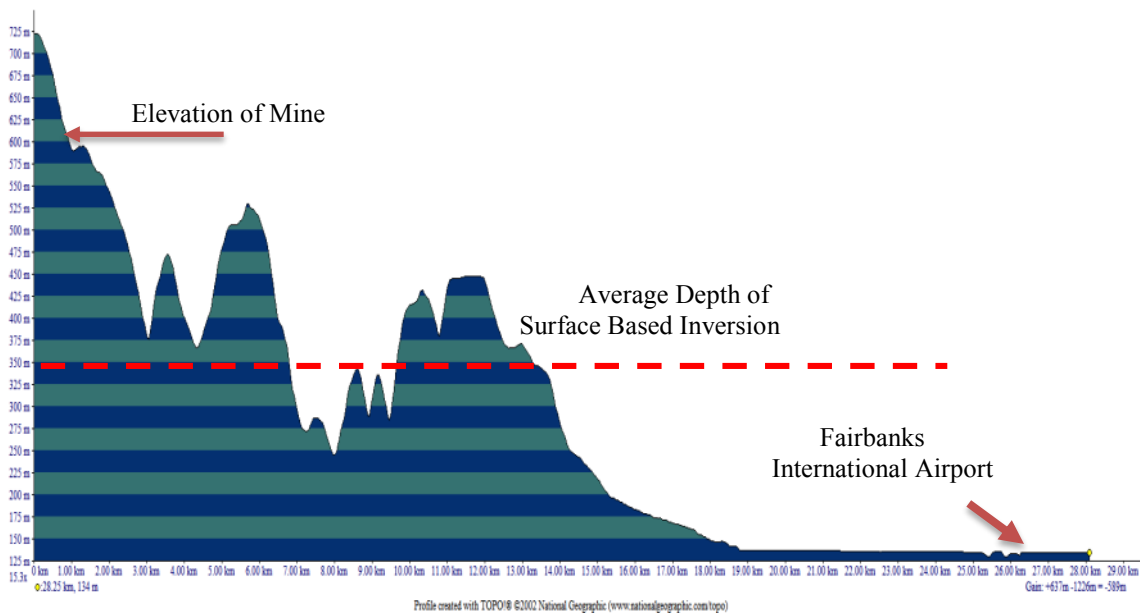


Fig. 7: Elevation Profile of the Local Topography from FAI to the Selected Mine.

From the recorded data of the frequencies of SBI and EI, it is possible to establish a correlation. To establish this correlation, a period of six months over the winters of 2013-2014 was selected. A number of inversions were observed at the selected open pit mine during 3rd through 6th December 2013 and 31st December 2013 through 2nd January 2014. For the same duration, the vertical temperature profiles at the Fairbanks International Airport are presented in Figure 8-10. These figures, indicate surface-based inversions at the Fairbanks area. During the same time frame, there were multiple instances of elevated inversions (Figure 8-10). It can be seen from these figures that, during the night time, there is a very strong surface-based inversion, whereas the elevated inversion is more prevalent during the evenings. On December 4th, 2013 at 0000 UTC, a SBI and EI are observed and continued to persist over the next twelve hours. It can be noted that SBI lead to colder temperature whereas EI occurs at warmer temperature. Elevated inversion can be seen around the 1000 m level in most cases. At the same time, there can be multiple layers of EI in the atmosphere. For the next couple of days multiple layers of elevated inversion were observed in the atmosphere which is likely caused by the synoptic forcing.

Analysis of the collected inversion data indicates that the inversions at the selected open pit mine is not consistent with the surface-based inversions in the Fairbanks area. This is due to the fact the surface-based inversions are locally driven while EIs are due to the synoptic forcings. A possible correlation may exist and therefore required further analysis. The Fairbanks International Airport (FAI) data are from a radiosonde which included temperature, pressure, dew point temperature, relative humidity, wind velocity and other variables at different elevations. Analysis of the collected temperature data indicates that SBI is common in Fairbanks area. On the other hand, the temperature data at the selected open pit suggest that the SBI is not common at the selected open pit mine. There is a direct qualitative correlation between the elevated inversions in the Fairbanks area and the inversions at the selected open pit. The selected open pit mine is located at a higher elevation than the Fairbanks area. The FIA is at an elevation of 134 m, whereas the selected open pit has an elevation of 600 m (Figure 7). The difference in elevation is significant since the selected mine is above the vertical extent of the surface-based inversion generally found in the Fairbanks area.

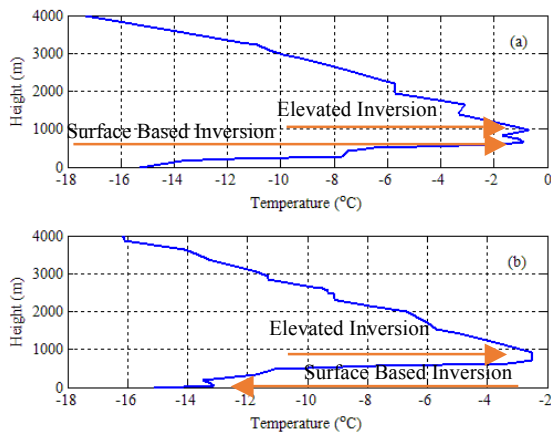


Fig. 8: Temperature Profile from FIA at (a) 0000 and (b) 1200 UTC December 4th 2013.

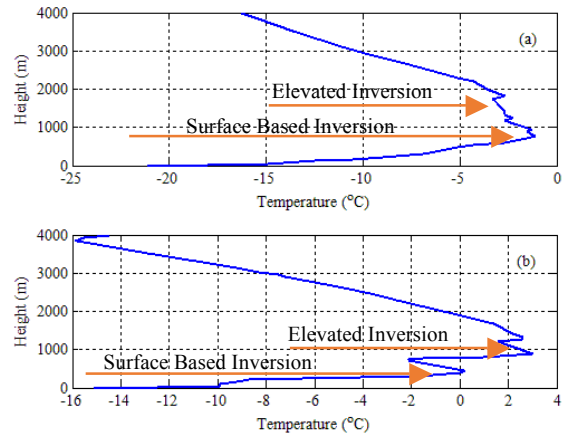


Fig. 9: Temperature Profile from FIA at (a) 0000 and (b) 1200 UTC December 5th 2013.

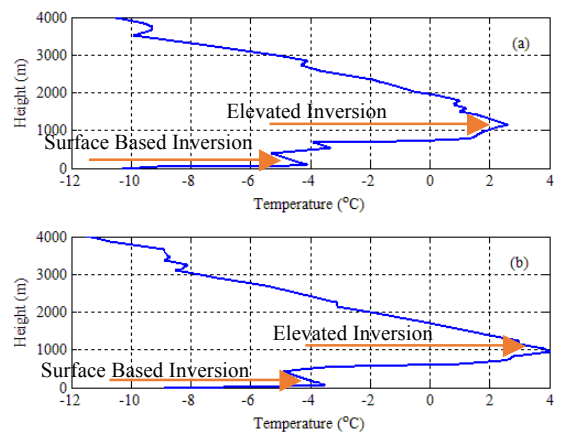


Fig. 10: Temperature Profile from FIA at (a) 0000 and (b) 1200 UTC December 6th 2013.

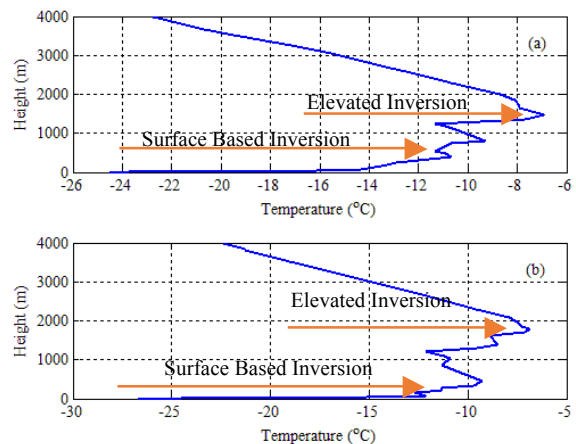


Fig. 11: Temperature Profile from FIA at (a) 0000 and (b) 1200 UTC December 31st 2013.

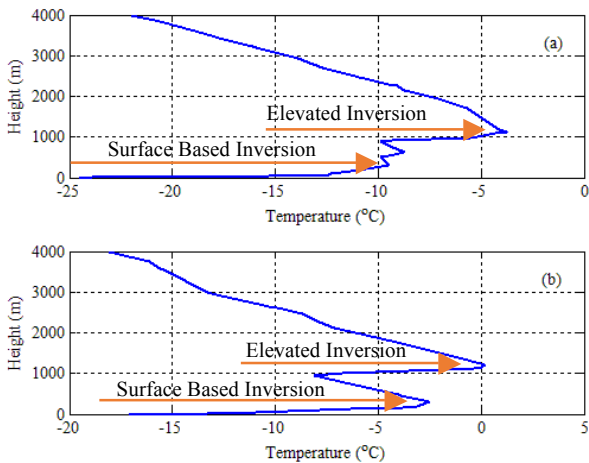


Fig. 12: Temperature Profile from FIA at (a) 0000 and (b) 1200 UTC January 1st 2014.

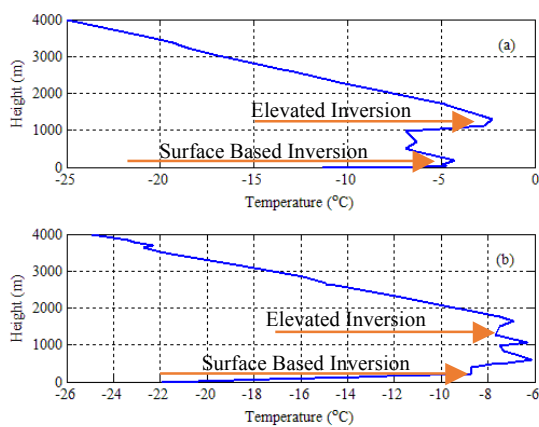


Fig. 13: Temperature Profile from FIA at (a) 0000 and (b) 1200 UTC January 2nd 2014.

In another instance, during December 31st, 2013 to January 2nd, 2014, there were inversions at the selected open pit mine as well as elevated inversions in the Fairbanks area. Figure 11-13 are the temperature profiles during the December 31st, 2013 to January 2nd, 2014 period. It is clearly seen from the figures that during the three days there were elevated inversions in the Fairbanks area as well as at the mine. Thus, it can be said that inversion at the selected open pit mine is strongly correlated to the elevated inversions and not influenced by the frequently occurring surface-based inversions in the Fairbanks area. It is also clear that, the altitude and the local topography of the selected open pit played an important role in the frequency of inversions.

4. Effect of Inversion on Natural Ventilation of Open Pit Mine

The turbulence in open pits under neutral condition is mostly due to a mechanical shear effect. Any turbulence that is generated in the stable boundary layer will be cancelled by the negative buoyancy near the surface whereas near the top of the stable layer turbulence is result of wind shear [27]. Once the inversion develops over the open pit, the pollutants accumulates in the pit over the time. Figure 14 shows the typical scenario at an open pit mine under air temperature inversion. The visible brown haze at the bottom portion of the figure is

due to the emissions from the diesel engines operating during the time of inversion [28]. The white snow cover benches are also clearly visible in the figure.

The air mass flowing within the pit loses energy in order to overcome the stably stratified layer and further energy loss occurs when the air comes in contact with the pit wall. As a result, the velocity decreases within the pit. The resulting wall-shear stress plays an important role in creating the recirculatory zones within the pit. Thus, it can be said that the buildup of the thermal stratification imposes an upper limits in the eddy-size in the turbulent field and leads to the accumulation of pollutants. On the other hand, air mass above the inversion layer, where turbulence is mainly due to the wind shear, is free of pollutants. Air flowing over the inversion layer advect the pollutants out of the pit.



Fig. 14: Pollutants Accumulated over the Open Pit under Inversion.

The ratio of the inlet velocity to the vertical velocity is important as the strength of the velocity in the vertical direction determines the dispersion of pollutants from the pit [11]. The change in the temperature and density directly impacts the flow regime within the pit. The air mass within the pit has an extremely low velocity compared with the less dense air out of the open-pit, and there is negligible impact on the air mass within the pit due to the inlet air velocity. These results in the accumulation of the pollutants within the pit [27].

The time scale of the turbulent structure in the stratified layers in an open pit is extremely small compared with the time-scale of the turbulent structure above the inversion layer.

Figure 15 illustrates the length scales for the eddies in a stably stratified layer. Eddies above the stably stratified layer is driven by large scale flows whereas the length scales within the stably stratified layer are restricted smaller scales.

As the inversion develops within the open pit, at the lower level or close to the surface, the air mass tends to sink because of the gravitational pull. Near the pit surface the air mass cools rapidly and its density increases with a decrease in temperature; thus, near the pit surface vertical velocity tends to be negative.

With the growth in strength of inversion and change in air density, the velocity of air within the pit significantly decreases. Thus, it can be said that the

change in the thermal regime in the pit affects the momentum and pollutants transfer within the pit.

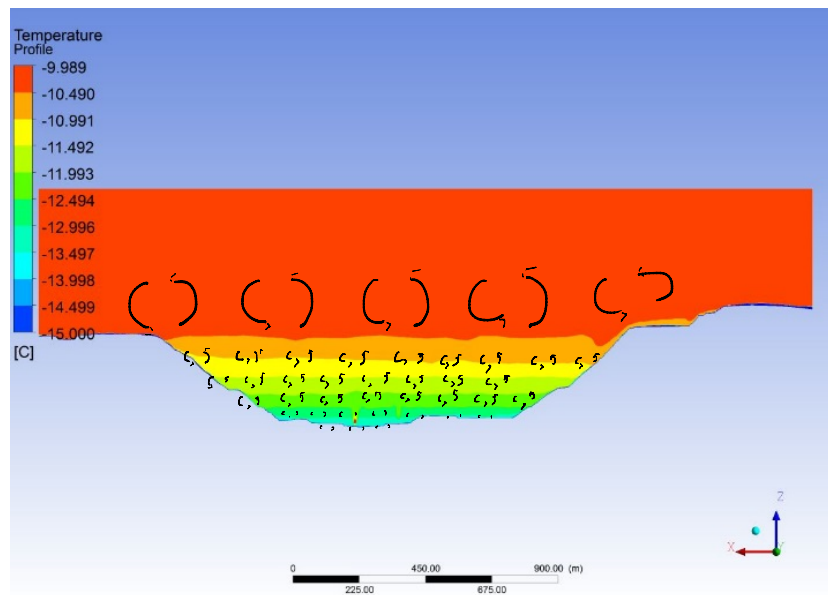


Fig. 15: Eddies of Different Length Scales

5. Summary and Conclusions

In extreme climatic conditions, deep open pit mines trap pollutants at pit bottom and management of the air quality can become challenging due to the disruption of natural ventilation cycles. It is within the ABL that most releases of pollutants take place and have the significant impact on the health and safety of miners in an open pit mine. Thus, an important ingredient in understanding open pit pollution dispersion modeling is the consideration of the local conditions of the atmospheric boundary layer. The mixing of pollutants in the ABL is governed by the state of turbulence and dynamics of the flow (i.e., wind speed and surface heat fluxes).

Surface-based inversion is a result of radiative cooling of the ground surface and are common in the development of nocturnal phase of the ABL diurnal cycle. And they become a common feature in the winter months in the Arctic and sub-Arctic regions due to the lack of sunlight. A temperature inversion can also develop above the SBI, depending upon the synoptic flow conditions, commonly known as the elevated inversion (EI). Depending on the altitude, location and geometry of an open pit mine, different types of air inversion can occur.

Air inversions in Fairbanks are mostly surface-based inversion (SBI). Whereas, the occurrence of air inversions at the open pit mine are affected by the elevated inversions. The location, topography, and altitude of the open pit mine also affects the event of inversions in open pit mines. The selected open pit mine is located at an elevation higher than the surface-based inversion occurring in Fairbanks, thus, the mine encounters inversion in form of elevated inversions.

The occurrence of turbulence over open pits under temperature inversion is mostly due to the effects of wind shear. Whereas, the thermal buoyancy is the cause of any turbulence generated within the inversion layer. The changes in the thermal regime of the air layers

directly impact the momentum transfer within the pit. In the absence of flow in the vertical direction from the base of the temperature inversion leads to serious accumulation of the pollutants over time.

Acknowledgments

The authors would like to acknowledge the National Institute for Occupational Safety and Health (NIOSH) for the financial support for this research. The authors would also like to acknowledge Mr. Chris Pritchard, NIOSH for his valuable suggestions and feedbacks on the current research work. The support of the ANSYS technical support staffs is gratefully acknowledged. The support of the staff mining engineers at the selected open pit mine in the Arctic is gratefully acknowledged.

References

- [1] Stull, R.B., *An Introduction to Boundary Layer Meteorology*. 1988, Netherlands: Kluwer Academic Publishers.
- [2] Garratt, J.R., *The Atmospheric Boundary Layer*. 1994: Cambridge university press.
- [3] Sorbjan, Z., *Structure of the Atmospheric Boundary Layer*. 1989, New Jersey: Prentice Hall. 317.
- [4] Fochesatto, G.J., P. Drobinski, C. Flamant, D. Guedalia, C. Sarrat, P.H. Flamant, and J. Pelon, *Evidence of Dynamical Coupling between the Residual Layer and the Developing Convective Boundary Layer*. *Boundary-Layer Meteorology*, 2001. **99**(3): p. 451-464.
- [5] Fochesatto, G.J., P. Drobinski, C. Flamant, D. Guedalia, C. Sarrat, P.H. Flamant, and J. Pelon, *Observational and Modeling of the Atmospheric Boundary Layer Nocturnal-Diurnal Transition during the ESQUIF Experiment*, in

- Advances in Laser Remote Sensing*, A. Dabas, C. Loth, and J. Pelon, Editors. 2001: Paris, France. p. 439-442.
- [6] Mayfield, J.A. and G.J. Fochesatto, *The Layered Structure of the Winter Atmospheric Boundary Layer in the Interior of Alaska*. Journal of Applied Meteorology and Climatology, 2012. **52**(4): p. 953-973.
- [7] Wendler, G., *Heat Balance Studies During an Ice-Fog Period in Fairbanks, Alaska*. Monthly Weather Review, 1969. **97**(7): p. 512-520.
- [8] Wendler, G. and K.O.L.F. Jayaweera, *Some Measurements of the Development of the Surface Inversion in Central Alaska During Winter*. Pure and Applied Geophysics, 1972. **99**(1): p. 209-221.
- [9] Fochesatto, G.J., J.A. Mayfield, D.P. Starkenburg, M.A. Gruber, and J. Conner, *Occurrence of Shallow Cold Flows in the Winter Atmospheric Boundary Layer of Interior of Alaska*. Meteorology and Atmospheric Physics, 2013: p. 1-14.
- [10] Malingowski, J., D. Atkinson, J. Fochesatto, J. Cherry, and E. Stevens, *An Observational Study of Radiation Temperature Inversions in Fairbanks, Alaska*. Polar Science, 2014. **8**(1): p. 24-39.
- [11] Raj, K.V., S. Bandopadhyay, and R.V. Ramani, *Turbulent Models for Pollutant Transport in Open Pit Mines under Stable Boundary Layer*, in *SME Annual Meeting*. 2015, Society for Mining, Metallurgy and Exploration: Denver, CO. p. Preprint# 15-026.
- [12] Lareau, N.P., E. Crosman, C.D. Whiteman, J.D. Horel, S.W. Hoch, W.O.J. Brown, and T.W. Horst, *The Persistent Cold-Air Pool Study*. Bulletin of the American Meteorological Society, 2013. **94**(1): p. 51-63.
- [13] Silcox, G.D., K.E. Kelly, E.T. Crosman, C.D. Whiteman, and B.L. Allen, *Wintertime PM_{2.5} Concentrations during Persistent, Multi-Day Cold-Air Pools in a Mountain Valley*. Atmospheric Environment, 2012. **46**(0): p. 17-24.
- [14] Arya, P.S., *Introduction to Micrometeorology*. Vol. 79. 2001: Academic press.
- [15] Carlson, M.A. and R.B. Stull, *Subsidence in the Nocturnal Boundary Layer*. Journal of Climate and Applied Meteorology, 1986. **25**(8): p. 1088-1099.
- [16] Bowling, S.A., T. Ohtake, and C.S. Benson, *Winter Pressure Systems and Ice Fog in Fairbanks, Alaska*. Journal of Applied Meteorology, 1968. **7**(6): p. 961-968.
- [17] Bradley, R.S., F.T. Keimig, and H.F. Diaz, *Climatology of surface-based inversions in the North American Arctic*. Journal of Geophysical Research: Atmospheres, 1992. **97**(D14): p. 15699-15712.
- [18] Mahrt, L., *Nocturnal Boundary-Layer Regimes*. Boundary-Layer Meteorology, 1998. **88**(2): p. 255-278.
- [19] Wendler, G. and P. Nicpon, *Low-Level Temperature Inversions in Fairbanks, Central Alaska*. Monthly Weather Review, 1975. **103**(1): p. 34-44.
- [20] Garratt, J.R. and R.A. Brost, *Radiative Cooling Effects within and above the Nocturnal Boundary Layer*. Journal of the Atmospheric Sciences, 1981. **38**(12): p. 2730-2746.
- [21] Bowling, S.A., *Climatology of High Latitude Air Pollution as Illustrated by Fairbanks and Anchorage, Alaska*. Journal of Climate and Applied Meteorology, 1986. **25**(1): p. 22-34.
- [22] Hartmann, B. and G. Wendler, *Climatology of the winter Surface Temperature Inversion in Fairbanks, Alaska*, in *8th Conference on Polar Meteorology and Oceanography*, V. Alexeev, Editor. 2005, American Meteorological Society: San Diego, CA. p. 1-7.
- [23] Whiteman, C.D., *Breakup of Temperature Inversions in Colorado Mountain Valleys*, in *Department of Atmospheric Science*. 1980, Colorado State University: Fort Collins, CO.
- [24] Whiteman, C.D., *Breakup of Temperature Inversions in Deep Mountain Valleys: Part I. Observations*. Journal of Applied Meteorology, 1982. **21**(3): p. 270-289.
- [25] Whiteman, C.D. and S.W. Hoch, *Bingham Mine Cold-Air Pool Structure and Evolution*. 2014, Department of Atmospheric Sciences, University of Utah: Salt Lake City, Utah.
- [26] Allwine, K.J., X. Bian, C.D. Whiteman, and H.W. Thistle, *VALDRIFT—A Valley Atmospheric Dispersion Model*. Journal of Applied Meteorology, 1997. **36**(8): p. 1076-1087.
- [27] Bandopadhyay, S., K.V. Raj, and R.V. Ramani, *A Three-Dimensional CFD Model of Pollutant Transport in a Deep Open-Pit Mine under Arctic Air Inversion*, in *Proceedings of the 10th International Mine Ventilation Congress*, F.v. Glehn and M. Biffi, Editors. 2014, The Mine Ventilation Society of South Africa: Sun City. p. 369-378.
- [28] Senaratne, I. and D. Shooter, *Elemental Composition in Source Identification of Brown Haze in Auckland, New Zealand*. Atmospheric Environment, 2004. **38**(19): p. 3049-3059.

Improving the Expected Cooling Capacity of the Conditioning System at Creighton Mine

Enrique I. Acuña^a, Cheryl Allen^a, Doug O'Connor^a

^aVale Canada Limited, Sudbury, Ontario, Canada
^aDoug O'Connor Consulting, Sudbury, Ontario, Canada

Creighton Mine has more than 100 years of production history and is continuing to develop deeper with the plan to reach 10,000 feet. The deeper levels of the mine have already reached 8000 ft level without the use of a mechanical refrigeration system. This has been achieved through the use of the Natural Heat Exchange Area (NHEA) implemented in the early 1960's. The NHEA is a remaining sublevel caving area mainly divided into 4 blocks with slusher trenches that were used to extract the ore. Today, it serves the purpose of conditioning the outside air temperature before being fed into the fresh air system of the mine. As Creighton mine progresses deeper, the temperature on the lowest levels will approach the limit of Vale's guidelines for working in heat. This paper presents the study developed to analyze the possibility of implementing modifications to the gathering area of the NHEA. The objective was to improve the distribution of the cooled air to the deeper levels and outline the impact that this change can have in terms of the additional levels that could be operated underground without the use of mechanical refrigeration. This study supports the efforts currently under development for energy conservation and to reduce the capital and operational costs of Creighton Mine while extending the expected life of the mine.

Keywords: Natural heat exchange, Critical Operational Depth

1. Introduction

The Natural Heat Exchange Area (NHEA) at Creighton Mine is an old sublevel cave area that is used to condition the incoming air from surface that goes into the three main fresh air systems of the mine. As presented by [1] the area is divided into trenches which are considered independent or parallel entrances for the airflow from surface. The air at ambient surface temperature passes through the fragmented rock mass sitting on the top of each trench where the heat exchange occurs. The airflow is transferred through ore passes and collected at the 800 level of the area where it is distributed into the three main ventilation systems of the mine. The airflow is collected in areas defined as Blocks, which are geographic aggregation of trenches. Six Blocks were initially identified, but only four are being used currently, as the middle two have been consumed by the cave. The current Blocks in use are 1, 2, 5 and 6.

The NHEA is currently manually operated whenever manpower is available and accesses to the blocks are available, following a protocol based on the trench temperature to achieve the coolest temperatures all year round. The operator enters the trench and opens or closes a control door at the end of each trench which controls the amount of airflow into the trench. Some restrictions apply as certain trenches cannot be open when the temperature of the air entering the trench drops below zero degrees Celsius, to avoid ice building up and sealing the airflow path. Also, a minimum number of trenches per Block must be kept open to avoid increasing the pressure requirement for the fan systems.

The problem faced by the operator of the area is to decide which doors to keep open and closed to maintain the lowest temperatures possible to benefit the deeper portions of the mine. Each trench contributes a certain amount of airflow at a specific temperature which combines to provide an air volume and temperature for each Block of the area. Therefore the goal is to keep the overall temperature of the airflow as low as possible. The NHEA has two main benefits, first it flattens the amplitude of the outside temperature range of -40°C to

+30°C to a range between 0°C to 7°C overall and also displaces the higher summer temperatures for two to three months of the year. Accordingly the hottest temperatures in the mine occur during the months of August to October depending on the year and the use of the NHEA. The main objective of the NHEA optimization problem is to identify the combination of doors that have to be open for each period, subject to the surface temperature, to minimize the highest temperature of the year.

The second problem after identifying the expected temperature at the 800 level is to be able to calculate the level at which the natural conditioning will no longer be enough to accommodate the needs of the operation. Considering the temperature of the airflows at the 800 level, the airflow distribution into the three main ventilation systems, and the expected heat load of the mine, the Critical Operational Depth (COD) can be calculated as indicated by [2]. The COD indicates how deep the mine activities can go without the use of mechanical refrigeration.

Through the initial modelling and optimization developed for the NHEA area, it was identified that there was an opportunity to improve the distribution of the airflow, as the coolest airflow gathered at the 800 level was not totally directed to the deeper levels of the mine. The objective of this paper is to present the initial and a proposed airflow distribution of the 800 level to quantify the benefit that could be obtained through this modification. This paper will detail the calculations required to determine the COD and examine the effect of 800 level airflow distributions on the COD.

2. 800 level airflow distribution

Currently the airflow of Blocks 1, 2, 5 and 6 is collected at the 800 level and then distributed to the three main ventilation systems of Creighton Mine as presented in Figure 1. As illustrated in Figure 1, the airflow coming from Block 1 goes into the 3rd system; the airflow from Block 2 goes into the 9 shaft system and the airflow coming from Blocks 5 and 6 goes into

the Main system. The incoming temperatures are used to calculate the COD which is the limit to start including mechanical refrigeration in order to avoid changes in the work and rest regimes as a result of increased wet bulb temperature in the working areas.

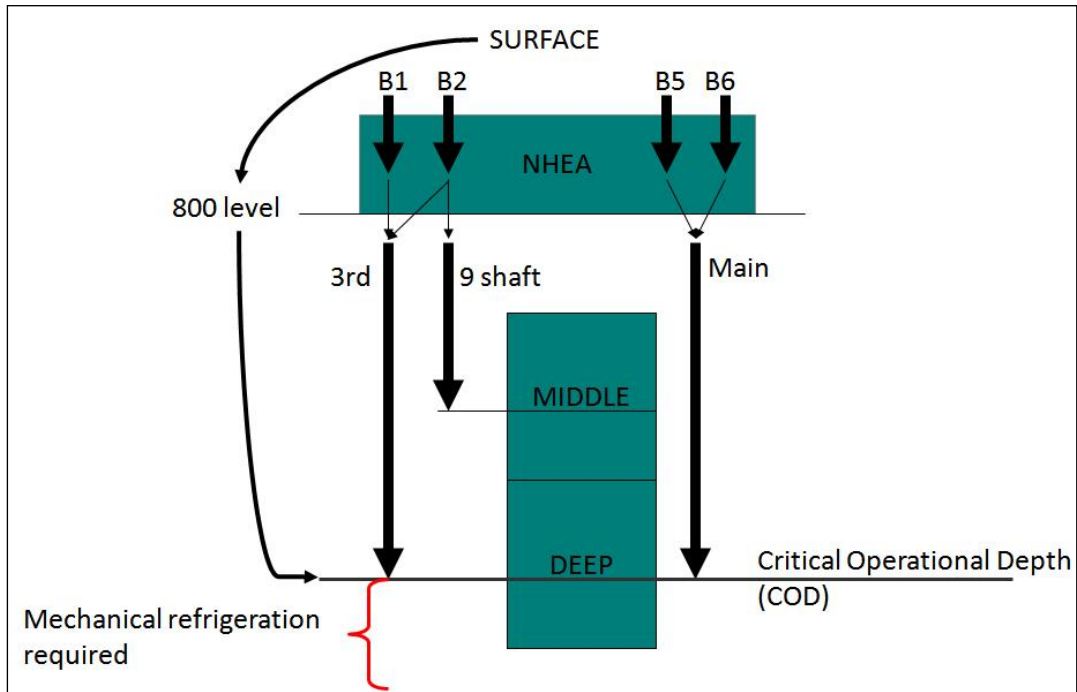


Fig. 1. Current fresh airflow distribution system at 800 level

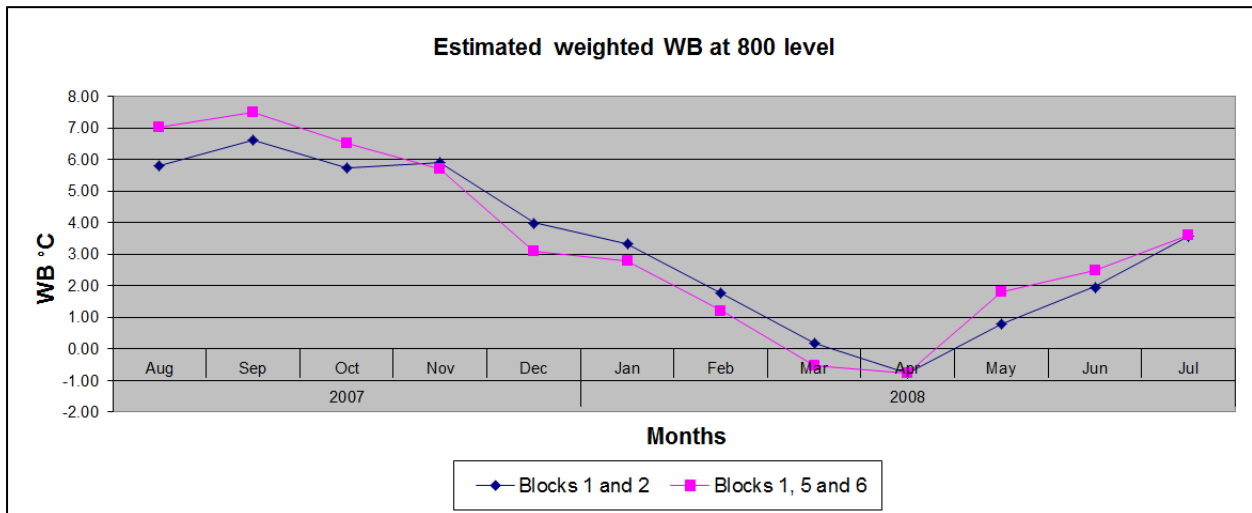


Fig. 2. Current fresh Estimated monthly average wet bulb temperature at 800 level

The dry bulb temperature sensors installed at the 800 level allow the measurement of the temperature for the total airflow contributed by each Blocks. Considering the high relative humidity of the 800 level, the wet bulb temperature was estimated and a weighted average calculated for the airflow coming from Blocks 1, 5 and 6, (Figure 2) which are the Blocks contributing airflow to the deeper portions of the mine. Additionally it was observed that Block 2 had a lower maximum temperature than Blocks 5 and 6, and the weighted average of Blocks 1 and 2 was also calculated and presented in Figure 2. It can be observed that the

maximum temperature at the 800 level over the year, registered in September can be lowered by almost 1°C if the airflow for the deep is provided by Blocks 1 and 2 instead of having the combined airflow of Blocks 1, 5 and 6. This observation is what motivated the work presented in this paper.

When working under heat conditions it is important to consider both wet bulb and dry bulb temperatures and the associated difference. The wet bulb temperature will command the evaporation process of sweat from the skin, which is the most effective mechanism the body

has to liberate heat from its core to cool down. The difference between wet and dry bulb temperature will determine how much ability the airflow has to absorb heat from a person's body and hence dictate how fast workers could get into a heat stress situation [4], [6]. If heat stress conditions are not met according to Vale's guidelines for working in heat, work/rest schedules are implemented. These work/rest schedules will impact the number of available working hours and could be avoided if the natural cooling capacity of the NHEA is used to its maximum.

Figure 3 presents the proposed distribution of airflow for 800 level where the Deep is fed with the airflow from Blocks 1 and 2 and the Middle portion of the mine is fed with the airflow of Blocks 5 and 6. The

main idea is that by directing the cooler airflow to the Deep, the expected COD will be the deepest possible.

3. Estimation of Critical Operational Depth

In order to build a preliminary estimation of the COD for Creighton Mine, three main parameters were taken into account: first, the airflow volume dedicated to the deep; second, the temperature at the 800 level and finally, the expected heat loads per level were defined and used to calculate the estimation of the depth at which the expected wet bulb temperature would go over the limit of Vale's guidelines for working in heat.

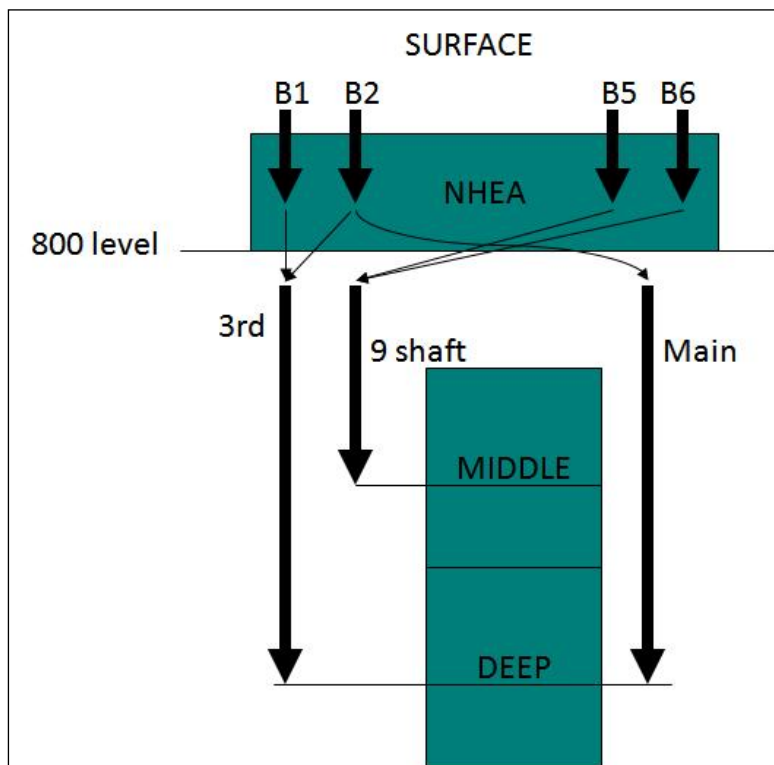


Fig. 3. Proposed fresh airflow distribution system at 800 level

For the airflow going to the Deep from 800 level, the initial wet bulb temperature, dry bulb temperature and barometric pressure estimations were used to calculate the measure of the energy contained in the airflow volume, when considering the airflow as a mix of dry air and water vapor [3]. The heat loads were estimated based on five contributing factors: auto compression, strata rock, broken rock, diesel equipment and electrical equipment. The most important contributing factor is auto compression followed by electrical and diesel equipment. The estimated heat load was determined and the energy content was calculated for each level of the deeper portion of the mine. With the new energy content and the estimated barometric pressure, the wet bulb temperature at the end of each level was calculated and then compared to the limit of Vale's Thermal Management Guideline [5] for working

in heat, to determine if the level had reached the limit and hence the COD. The obtained estimations of the temperatures for the different levels were compared to the available data from the audits and the heat loads were calibrated to better match the measured results. This exercise was developed for each month of the year, however only the hottest one was the one dictating the overall COD, as in any other case the estimated critical depth could be deeper.

Figure 4 presents the results of the calculation of the COD for the current airflow distribution at the 800 level, where the Deep is fed with the airflow coming from Blocks 1, 5 and 6. According to this estimation the COD for the mine was at the 8330 level, not too far from the levels that are currently being mined, but out in time far enough to develop and implement an appropriate solution.

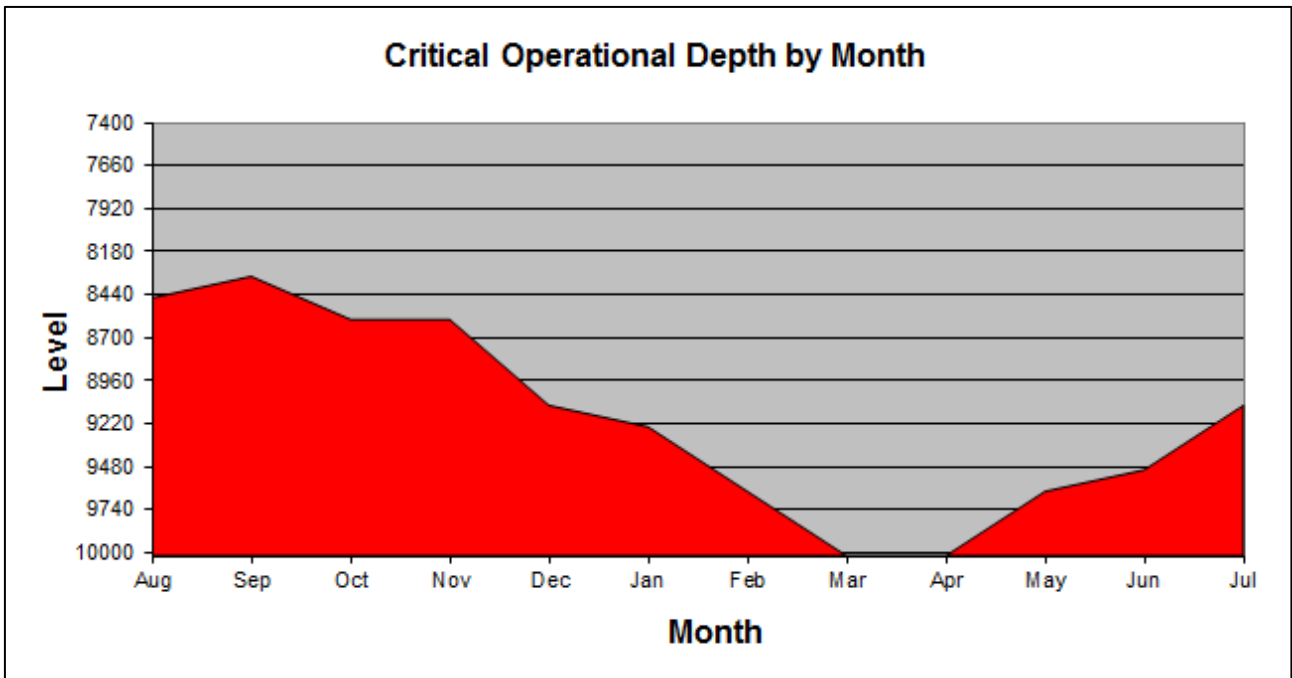


Fig. 4. Expected Critical Operational Depth

4. Results of proposed distribution of 800 level

Just as in the previous section, the calculations were generated to estimate the COD for every month, now considering the airflow coming from Blocks 1 and 2 instead of the airflow coming from Blocks 1, 5 and 6 only. This was based on the assumption that an arrangement could be designed and implemented at the 800 level, to assign the airflow of Block 2 to the Deep and the airflow of Blocks 5 and 6 to the Middle portion of the mine. Additionally, as presented by [2], the airflow temperature at the 800 level was improved (lowered) through the use of optimization techniques applied to the use of the trench doors to provide the coolest possible airflow temperature through the Blocks in both arrangements.

The COD was also determined using the optimized temperatures, with four possible alternatives being generated and displayed in Table 1. The first one, which is the current situation, using the airflow of Blocks 1, 5 and 6 for the deep, was used as the baseline. The second alternative is a modification to the distribution of 800 level to provide the deep with airflow from 1 and 2 Blocks only. The third and fourth options are respectively the first and second option but with the optimization approach applied resulting in a deeper COD. Table 1 also presents the improvement in terms of how many additional levels could be operated without the use of mechanical refrigeration all year round.

After observing the improvement between the current situation or baseline and the three additional alternatives, it is clear that changing the airflow distribution at the 800 level and optimizing the use of the NHEA is the option with the largest expected improvement. However, optimizing the NHEA is also the option which requires the largest investment as it implies the use of automation in the NHEA as well as the modification on 800 level.

Table 1 Results of COD analysis

Alternative	Airflow source	COD	Added levels
1	Blocks 1, 5 and 6	8330	0
2	Blocks 1 and 2	8460	1
3	Blocks 1, 5 and 6 optimized	8850	4
4	Blocks 1 and 2 optimized	8980	5

The proposed change in the airflow distribution at the 800 level, only reports the gain of an additional level, while the optimization of the use of the NHEA reports 4 additional levels according to the preliminary calculations. Considering that it takes on average 2 years to develop a new level, the expected delay in installing a refrigeration system could potentially be in the order of 10 years. Studies are currently being developed to estimate the cost and schedule for implementation of the alternative proposed in this paper. The results are encouraging and support the business case for automation of the NHEA.

5. Conclusions

The study developed in this paper was based on the previous findings of modeling and optimizing the NHEA at Creighton Mine and the estimation of the COD. According to these initial results, the possibility of changing the airflow distribution at the 800 level was evaluated with a positive impact in terms of delaying the COD of the mine. However with the expected improvement being only one additional level, it is unclear if the benefits will be enough to overcome the estimated costs. The validation of the estimation developed in this study will require the revision of the heat load calculation based on measurement of the wet

bulb temperatures in the deeper levels, to generate a more representative model and improve the confidence of the obtained results, which could be done with other commercial software such as ClimSim, VUMA or Ventsim. A positive outcome of this work was demonstrated by Creighton mine management starting the required engineering studies and determining a cost effective solution on time.

Acknowledgements

The authors would like to express their gratitude to Vale's staff and management for their cooperation in this work and their permission to present the findings. The study presented in this paper is the natural extension of the initial work developed by HATCH and particularly Kingsly Hortin, to estimate the COD.

References

- [1] Acuña, E., Tousignant, A., Bilal, N., Fava, L., Goforth, D., O'Connor, D. and Allen, C. A combined ventilation and thermodynamic model for dry surfaces to predict and optimize the NHEA cooling and heating capacity for Creighton mine. 13th US Mine Ventilation Symposium, Sudbury, Canada, June 14-16, 2010a, pp. 293-299.
- [2] Acuña, E. and O'Connor, D. A new approach to maximize the natural conditioning system at Creighton Mine. CIM MEMO Conference, Sudbury, Canada, October 25-27, 2010b.
- [3] Gatley, P.G. Understanding Psychrometrics, second edition, 2005. The American Society of Heating, Refrigeration and Air-Conditioning Engineers, Inc.
- [4] Hardcastle, S. and Butler, K. A comparison of globe, wet and dry temperature and humidity measuring devices available for heat stress assessment. 12th US Mine Ventilation Symposium, 2008, pp. 181-190.
- [5] Mines Technical Services. Thermal Management Guideline, Ontario Mines, 2008.
- [6] Payne, T. and Mitra, R. A review of heat issues in underground metalliferous mines. 12th US Mine Ventilation Symposium, 2008, pp. 197-201.

Diesel Exhaust and Other Contaminants

Diesel Oxidation Catalytic Converters for Underground Mining Applications

Aleksandar D. Bugarski, Jon A. Hummer, Gary M. Robb*

* National Institute for Occupational Safety and Health, Office of Mine Safety and Health Research, 626 Cochran Mill Rd., Pittsburgh, Pennsylvania 15236, U.S.A.

* AirFlow Catalyst Systems, Inc., 2144 Brighton-Henrietta Townline Rd. Suite 700, Rochester, NY 14623, U.S.A.

The diesel oxidation catalytic converter (DOC) has been extensively used by the underground mining industry to reduce exposure of workers to carbon monoxide (CO) and hydrocarbons (HC) emitted by diesel engines. The effects of those devices on the gaseous and diesel particulate matter emissions strongly depend on catalyst formulation. Recently, certain formulations of catalytic coatings used in DOCs marketed to underground mining were scrutinized for their potential to adversely affect emissions of the highly toxic compound, nitrogen dioxide (NO₂). This study was conducted to get a better understanding of the effects that contemporary and emerging DOC technologies have on gaseous emissions. For test purposes, an EPA certified Tier 2 engine was retrofitted with two DOCs, one with a catalytic coating traditionally marketed to the underground mining industry (DOC 1), and the other with a novel coating designed to minimize undesirable NO₂ emissions (DOC 2). The evaluation was done for various steady-state engine operating conditions, generating exhaust with temperatures between 200 °C and 400 °C and one mining related transient cycle. Despite differences in catalyst formulations, both evaluated DOCs similarly reduced CO (63 to 98 %) and HC (16-32%) emissions. However, for the majority of test conditions, the NO₂ emissions were found to be adversely affected by DOC 1. Dramatic increases in NO₂ emissions were observed at conditions that produced exhaust temperatures above 300 °C. Conversely, DOC 2 was found to favorably affect NO₂ emissions for all test conditions. The findings of this study suggests that DOC catalyst formulations and systems can be successfully designed and optimized for underground mining applications to provide the desired reductions in CO and HC emissions without de novo generation of NO₂ and in certain circumstances, provide a reduction in NO₂ emissions..

Keywords: Diesel Oxidation Catalyst, Nitrogen Dioxide, Underground Mining.

1. Introduction

Diesel-powered vehicles and equipment are the backbone of production and transportation in the underground mining industry. However, they are also one of the primary sources of miners' exposure to fresh submicron aerosols and noxious gases such as carbon monoxide (CO), nitric oxide (NO), nitrogen dioxide (NO₂), and hundreds of various hydrocarbons (HC) including potentially carcinogenic and mutagenic polycyclic aromatic hydrocarbons (PAHs) and nitrated-PAHs (n-PAH).

Over the past four decades DOCs have been extensively used in original equipment manufacturer (OEM) and retrofit applications to curtail some of the gaseous emissions from diesel powered equipment in underground mines [1-3]. Traditionally, the catalyst formulations and loadings used for underground mining DOCs have been optimized for effective curtailment of carbon monoxide (CO) and hydrocarbon (HC) emissions [4]. The major governing chemical reactions, oxidation of CO and HC are described by the equations 1 and 2.



Certain catalyst formulations, and primarily those containing Pt, promote the oxidation of nitric oxide (NO) to nitrogen dioxide (NO₂) while operated at temperatures typically observed for heavily loaded diesel engines [1,4-8]. That reaction is described by equation 3.



Under favorable conditions certain types of DOCs were shown to be effective in removing carcinogenic

and mutagenic poly aromatic hydrocarbons (PAHs) [9,10], and reducing both particle and vapor-phase-associated mutagenic activity of exhaust emitted by older technology engines [10,11]. Certain types of DOCs were even found to reduce the organic fraction of diesel particulate matter (DPM) [12]. The effectiveness of a DOC as a DPM control is primarily dependent on the fraction of organic carbon (OC) present in the engine exhaust because the total DPM reduction efficiency increases with an increase in OC content of the exhaust [13,14]. The simplified reaction of NO₂ with HC and DPM [4,6,15] is described by equation 4.



It is important to note that the performance of a catalyst can degrade with age. Katare et al. [6] showed that in presence of reductants (HC, CO, DPM), certain in-use DOCs with demonstrated low CO and HC conversion can be net consumers of NO₂.

The catalyst technologies gradually evolved to accommodate for advancements in diesel engine technologies, fuels, and exhaust aftertreatment technologies that resulted in generally lower CO, NO_x, HC, and DPM emissions. The DOCs found even new applications. Those with catalysts formulated to promote oxidation of NO to NO₂ have been extensively used in the diesel particulate filter (DPF) systems to increase the concentrations of NO₂ that is used in the DPF as a low-temperature DPM oxidizing agent [16,17] and in urea-based selective catalyst reduction (SCR) systems to increase the NO₂ concentration from engine levels to the levels needed to optimize the performance of the SCR catalyst [18]. Balancing the production and consumption of NO₂ in such systems over actual duty cycles, presents a major challenge. Without proper NO₂ slip control, these systems emit relatively high concentrations of NO₂.

and are considered unsuitable for underground mining applications. The use of similarly catalyzed exhaust aftertreatment devices increased the ratio of NO_x in NO_x in diesel emissions [3,8,19] and in the environment [2,7].

Nitrogen dioxide is a primary health concern because of its relatively high toxicity [20,21]. NO_x is also of concern because of its potential role in the formation of nitro-PAHs [22] and atmospheric ozone-forming chemistry [23]. Due to technical and economic issues related to ventilation of confined spaces, the NO_x emissions are of particular concern for the underground mining industry. The current regulations enforced by the Mine Safety and Health Administration (MSHA) in the U.S., limit NO_x exposure of underground coal [24] and metal/nonmetal (M/NM) miners [25] to a ceiling value (CE) of 5 ppm. That level was established on the basis of the 1972 and 1973 American Conference of Governmental Industrial Hygienists (ACGIH®) threshold limit values (TLV's), respectively. Certain states enforce the exposure limits for NO_x more stringent than those enforced by MSHA. E.g., the ambient concentration for NO_x in underground coal mines in West Virginia cannot exceed 3 ppm (CE) [26]. The ACGIH decision to reduce the TLV* for NO_x from 5 to 0.2 ppm [21] reinvigorated the discussion on the cost of controlling DPM emissions using catalyzed systems that adversely affect NO_x emissions.

The concern over de-novo formation of NO_x emissions motivated development and evaluation of alternative catalytic formulations [4,27,28]. At relevant diesel exhaust temperatures, Pd-based and base metal-Pd based formulations were found to have a low tendency to catalyze the oxidation of NO to NO₂, while being quite effective, comparably to Pt-based formulations, in catalyzing the oxidation of CO and HC to CO₂ and CO₂ and H₂O, respectively [4,27]. However, some of the recent laboratory studies [3,29] showed that a surprisingly high number of DOCs currently used in underground mining use the catalyst formulations that promote undesirable secondary NO₂ emissions.

Therefore, this study was conducted to demonstrate the fundamental differences in the effects of two types of contemporary catalyst formulations on emissions and emphasize the need for careful selection and the potential optimization of DOCs for specific underground mining applications.

2. Methodology and Materials

Two DOCs supplied by AirFlow Catalyst Systems Inc. (Rochester, NY) were evaluated during this study, EZDOC (DOC 1) and MinNoDOC (DOC 2). Both DOCs are using identical metal substrates sized for the test engine. The major difference between units was in the oxidation catalyst formulations. The washcoat of DOC 1 was impregnated with a catalyst formulation representative of the coatings traditionally used for DOCs marketed to the underground mining industry, to curtail CO and hydrocarbon emissions from traditional light- and medium-duty diesel engines operated in very well ventilated areas of underground mines. The catalyst used for DOC 2 was specifically formulated to allow for effective control of CO and hydrocarbon emissions from contemporary diesel engines, and to suppress the formation of secondary NO₂ emissions.

Testing took place at the diesel laboratory of the National Institute for Occupational Safety and Health

(NIOSH), Office of Mine Safety and Health Research (OMSHR). The DOCs were retrofitted to an electronically controlled, turbocharged, Mercedes Benz OM 904 LA rated at 174 hp. The emissions from this specific engine meet U.S. Environmental Protection Agency (EPA) Tier 2 standards. The engine was coupled to the SAJ AE400, 400 kW water-cooled eddy-current dynamometer. The testing was done using locally acquired ultralow sulfur diesel (ULSD). The test fuel was analyzed by Cashman Equipment Co. (Bentley Tribology Services, Sparks, NV). The results are summarized in Table 1.

Table 1. Fuel properties

Fuel Properties	ASTM	Value
	Test Method	
Aromatics [vol %]	D1319	24.2
Olefins [vol %]	D1319	1.6
Saturates [vol %]	D1319	74.2
Flash Point, [°C /°F]	D93	62.5 /144.5
Sulfur, by UV [ppm]	D5453	7.4
Cetane Number []	D613	44.5
API Gravity @ 15.6 °C [°API]	D1298	36.9
Heat of Combustion [BTU/gal]	D240	139945

The DOCs were tested for several steady-state engine operating conditions and one transient cycle. The first set of steady-state test conditions was selected to generate exhaust gases with temperatures ranging between 200 to 400 °C. That was achieved by maintaining the engine speed at 1800 rpm while gradually increasing engine load in steps from 136 to 610 Nm (Table 2, Fig. 1). A subset of four modes of the International Standards Organization for Standardization (ISO) 8-mode test cycle [30] was incorporated for the second set of steady state conditions (Table 2). The R100 (M1) and I100 (M5) modes are representative of heavy-duty engine operating conditions producing relatively high exhaust temperatures. The R50 (M3) and I50 (M7) modes are considered medium-duty engine operating conditions that produce low to medium exhaust temperatures (Fig. 1). The ISO 8178-C1 is used by MSHA for approval and certification of diesel engines for use in underground mines in the U.S. [31].

Table 2. Steady-state engine operating conditions

Engine Speed	Engine Load		ISO 8178 C1
	rpm	lb-ft Nm	
1800	100	136	N/A
800	200	271	N/A
1800	250	339	N/A
1800	300	407	N/A
1800	350	475	N/A
1800	400	542	N/A
1800	450	610	N/A
1400	235	319	M8 (I50)
1400	470	637	M6 (I100)
2200	190	258	M3 (R50)
2200	380	515	M1 (R100)

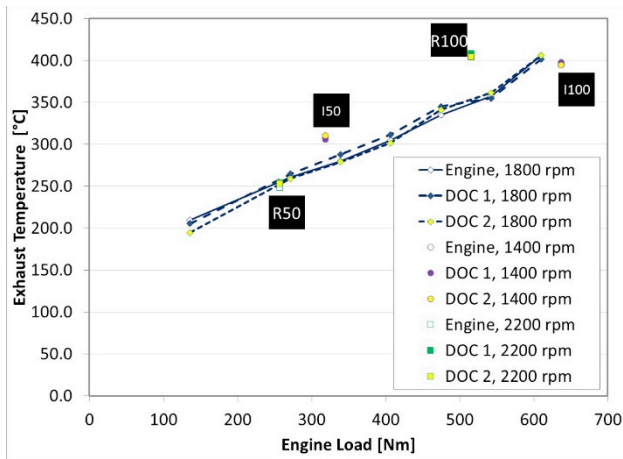


Fig. 1. Engine loads and corresponding exhaust temperatures at the inlet to DOC

In an attempt to quantify the effects of the DOCs for more production-representative conditions, the engine was operated over an 820-second transient mining cycle. This cycle has been recreated from field data to simulate operation of an engine in underground mining load-haul-dump vehicles.

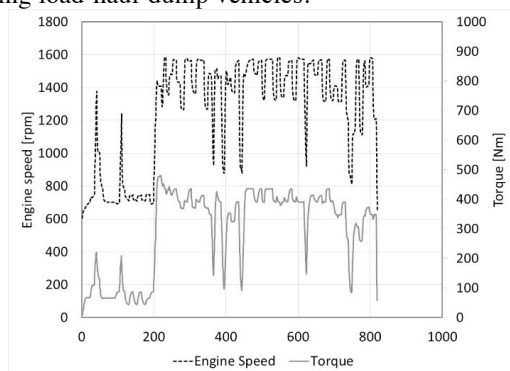


Fig. 2. Transient underground mining cycle

The concentrations of CO, CO₂, NO, NO₂, and hydrocarbons were measured upstream and downstream of the DOCs in undiluted exhaust using a Fourier transform infrared (FTIR) spectrometer (Gaset, DX-4000). The concentrations of the following hydrocarbons were combined to obtain total hydrocarbon concentrations (THC): ethane, propane, butane, pentane, hexane, octane, ethylene, acetylene, propene, 1,3-butadiene, formaldehyde, acetaldehyde, benzene, and toluene.

3. Results

Generally, the contributions of DOCs to CO₂ concentrations are negligible, and the results of CO₂ concentration measurements may be used to examine the consistency of the test procedure (Fig. 3). As indicated by the graphs given below, the variability in measured CO₂ concentrations for all steady-state tests conducted at the corresponding conditions was within ± 3 percent (Fig. 3b, Fig. 3c).

The results of steady-state and transient tests showed that both DOCs had favorable effects on CO emissions. For conditions that generated exhaust temperatures above 300 °C, the DOCs were found to be very efficient

in oxidizing CO (Fig. 4a). At those conditions, CO reduction was several percentages better for DOC 2 than for DOC 1 (Fig. 4b). At exhaust temperatures below 300 °C, DOC 1 was somewhat more efficient than DOC 2. For both DOCs, the highest efficiencies were observed during the heavy duty portion of the duty cycle (Fig. 4c). The reductions in cumulative CO emitted during the cycle for DOC 1 and DOC 2 were estimated to be 87 and 91 percent, respectively (Fig. 4d).

Both DOCs had a relatively minor effect on NO_x (NO_x=NO+NO₂) emissions (Fig. 5a). The presence of catalysts in DOCs affects processes such as oxidation of NO to NO₂ and the reduction of NO₂ to NO. However, since those reactions are reversible, the total sum of those compounds (NO_x) typically remains in equilibrium: Increases in NO₂ concentrations are typically offset by concurrent decreases in NO concentrations. For steady-state tests (I50, I100, R50, and R100), the effects of tested DOCs on NO_x were found to be within ± 5 percent (Fig. 5b).

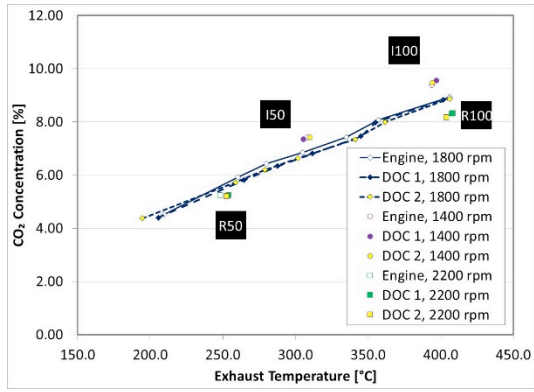


Figure 3A: CO₂ emissions for steady-state

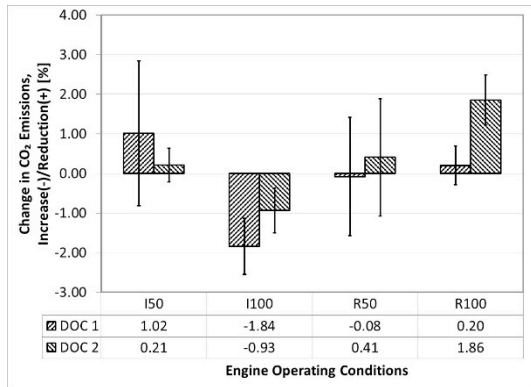


Figure 3B: changes in CO₂ emissions for I50, I100, R50 and R100 conditions

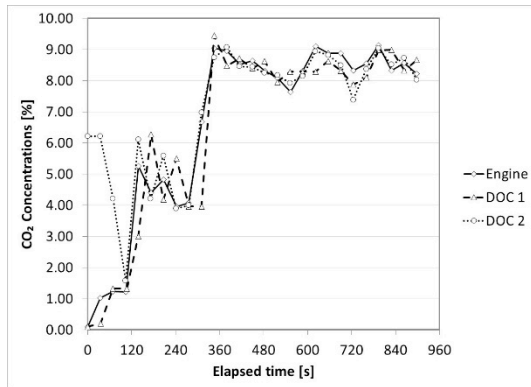


Figure 3C: CO₂ emissions for transient cycle

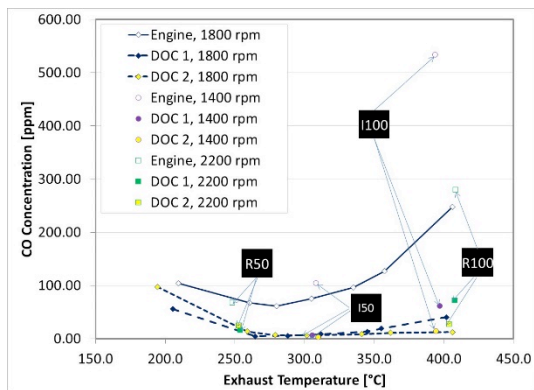


Figure 4A: CO emissions for steady-state conditions

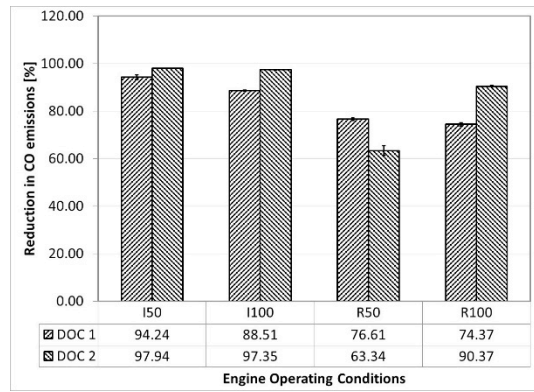


Figure 4B: reductions in CO emissions for I50, I100, R50, and R100 conditions

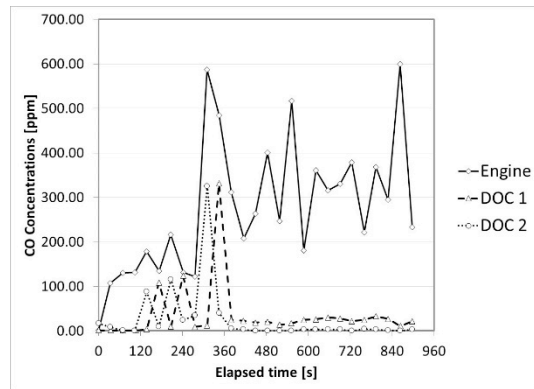


Figure 4C: CO emissions for transient duty cycle

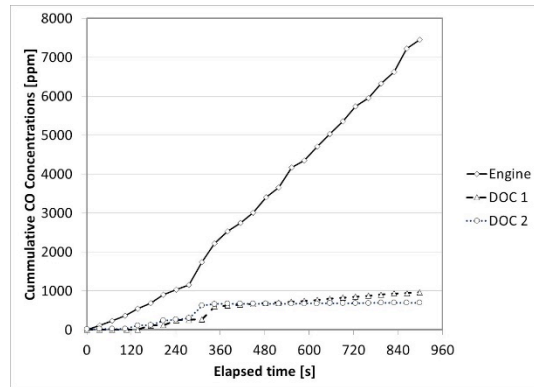


Figure 4D: cumulative CO emissions for transient duty cycle

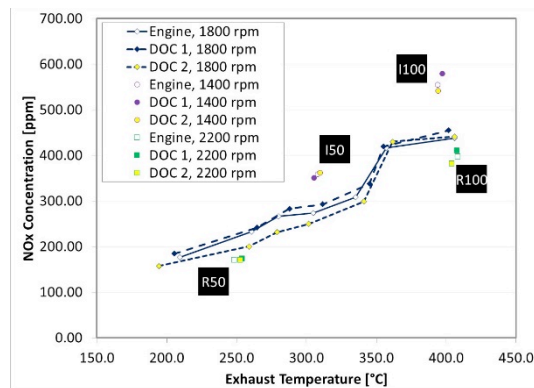


Figure 5A: NO_x emissions for steady-state conditions

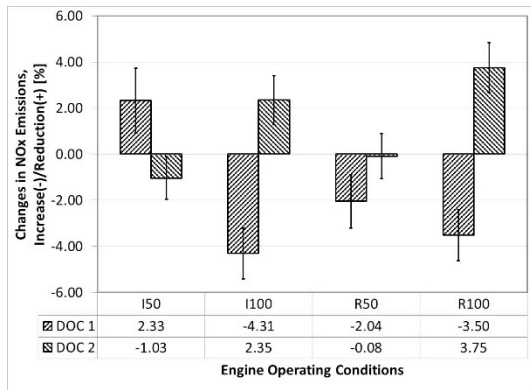


Figure 5B: Change in NO_x emissions for I50, I100, R50, and R100 conditions

In general, the NO₂ emissions were adversely affected by DOC 1, and favorably by DOC 2 (Fig. 6a, Fig. 6b). The effects of those DOCs on NO₂ emissions were found to be strongly dependent on exhaust temperature. In the case of DOC 1, the NO₂ emissions were above engine levels for exhaust temperatures exceeding 250 °C, exhibiting the highest values (up to 550 percent increase over engine emissions) at temperatures between 350 and 400 °C (Fig. 6a). The NO₂ emissions from DOC 2 were below engine levels for the entire examined range of exhaust temperatures (Fig. 6a). The cumulative emissions from the engine retrofitted with DOC 1 contained, approximately 129 percent more NO₂ than those from the engine alone, while the cumulative emissions from the engine equipped with DOC 2, contained approximately 77 percent less NO₂ than those from the engine alone (Fig. 6d). The NO₂ concentrations emitted from DOC 1 were higher throughout the cycle, but the bulk of NO₂ was emitted during the heavy-duty portion of the cycle (Fig. 6c). The NO₂ emissions from DOC 2 were relatively low and constant throughout the entire cycle (Fig. 6c).

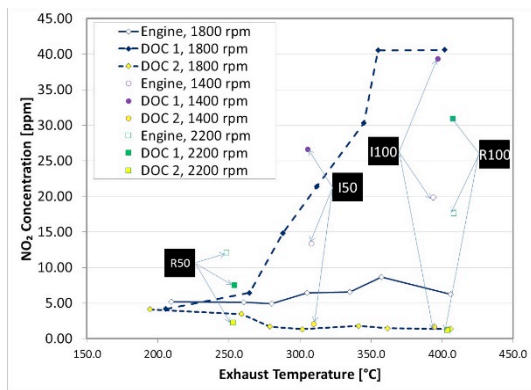


Figure 6A: NO₂ emissions for steady-state conditions

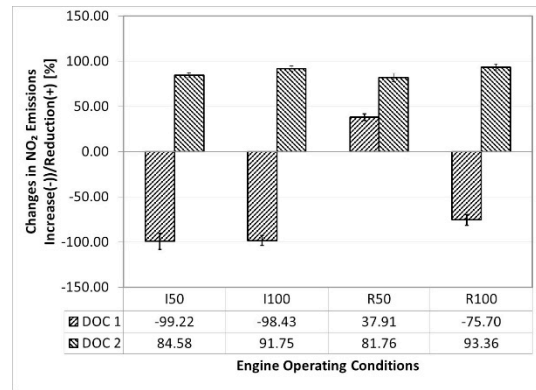


Figure 6B: changes in NO₂ emissions for I50, I100, R50, and R100 conditions

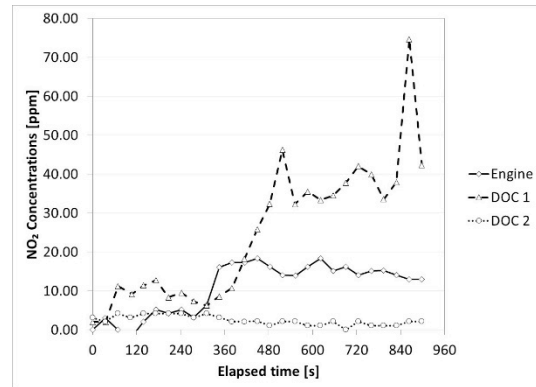


Figure 6C: NO₂ emissions for transient duty cycle

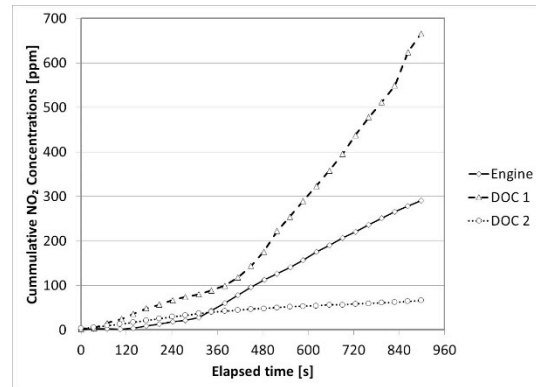


Figure 6D: cumulative NO₂ emissions for transient duty cycle

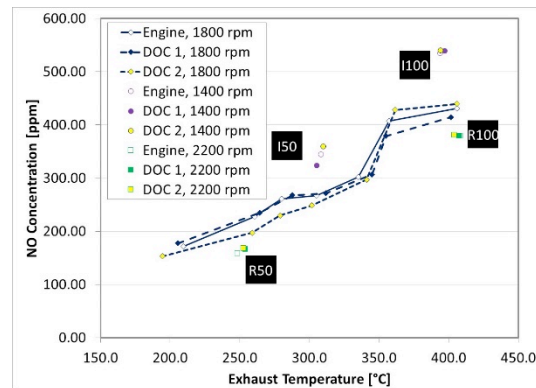


Figure 7A: NO emissions for steady-state conditions

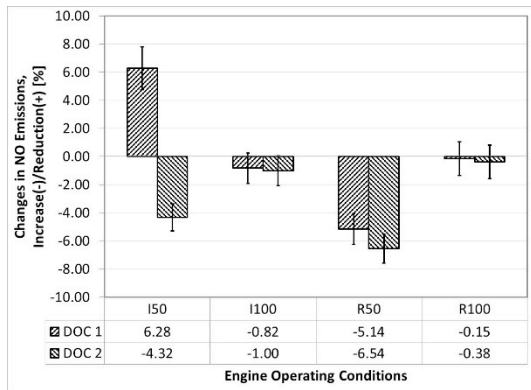


Figure 7B: changes in NO emissions for I50, I100, R50, and R100 conditions

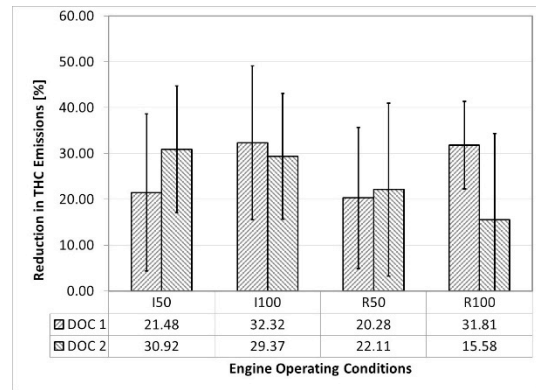


Figure 8B: changes in THC emissions for I50, I100, R50, and R100 conditions

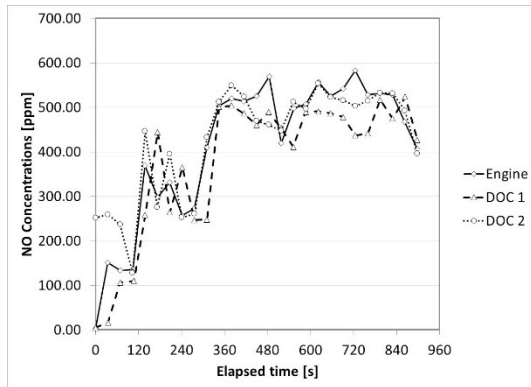


Figure 7C: NO emissions for transient duty cycle

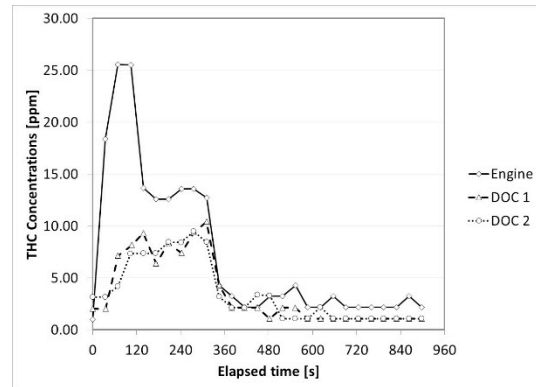


Figure 8C: THC emissions for transient duty cycle

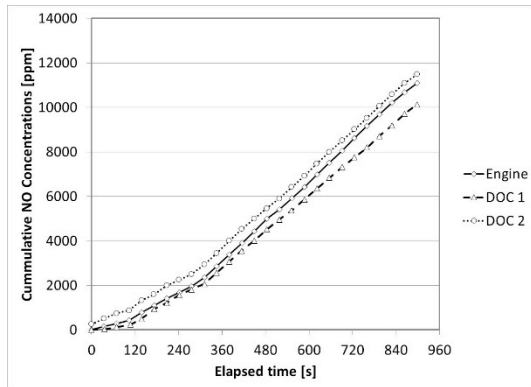


Figure 7D: cumulative NO emissions for transient duty cycle

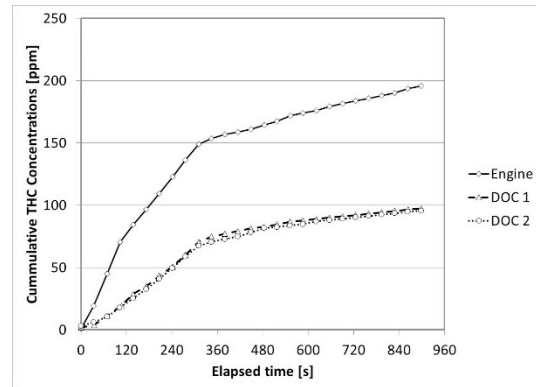


Figure 8D: cumulative THC emissions for transient duty cycle

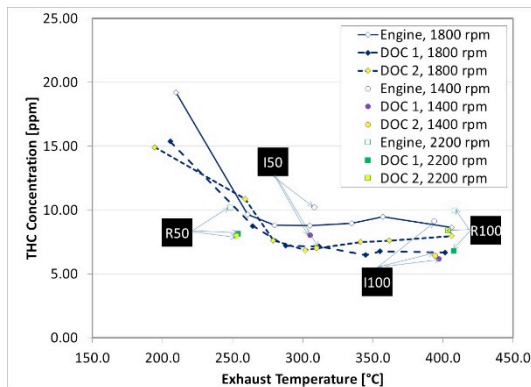


Figure 8A: THC emissions for steady-state conditions

NO comprised all but a few percent of the total NO_x emitted by the test engine and from DOC 2, and more than 90 percent of NO_x emitted from DOC 1. As a result, the major changes in NO_x emissions resulted in relatively minor changes in NO emissions (Fig 7a, Fig 7b). The effects of DOCs on NO emissions were within ± 7 percent (Fig. 7b). In the case of transient duty cycle, DOC 1 reduced the cumulative NO emissions by 9 percent and DOC 2 increased the cumulative NO emissions by 4 percent over levels recorded for the untreated exhaust (Fig. 7c and Fig. 7d).

Both DOCs were found to be fairly effective in controlling THC emissions (Fig. 8). The reductions in THC emissions were only slightly affected by exhaust temperatures (Fig. 8a). The average reductions observed during steady-state tests did not exceed 32 percent (Fig. 8b). Over the transient cycle, DOC 1 and DOC 2

reduced the cumulative THC concentrations by 50 and 51 percent, respectively (Fig. 8c, Fig. 8d).

4. Summary

The DOCs were found to be very effective in controlling CO emissions, and fairly effective in controlling THC emissions. The major difference was in the effects of those DOCs on NO_x emissions. Due to the adverse effects on NO_x emissions, DOC 1 appears not suitable for use on underground mining vehicles when operated over duty cycles where exhaust temperatures exceed 250 °C. DOC 2 appears to offer reasonable reductions in CO and THC emissions with a decrease in NO_x emissions for applications where exhaust temperatures are between 200 and 400 °C.

Due to the wide range of operating conditions, DOC catalyst formulations need to be optimized for specific applications by taking in account all targeted control parameters as well as exhaust physical properties and chemical composition. Properly optimized DOCs with catalyst formulations specifically designed for underground mining applications should provide the desired reductions in CO and HC emissions, while also reducing engine out NO_x emissions.

Disclaimer

The findings and conclusions in this manuscript are those of the authors and do not necessarily represent the views of NIOSH. Mention of company names or products does not constitute endorsement by the Centers for Disease Control and Prevention.

References

- [1] BT McClure et al., Effectiveness of catalytic converters on diesel engine used in underground mining. Bureau of Mines Information Circular 9197 (1999).
- [2] A.D. Bugarski et al., Isolated zone evaluation of the Tier 4i engine equipped with SCR system. Proceeding of 14th United States/North American Mine Ventilation Symposium, Salt Lake City, UT, June 17-20, 2012, 205-212.
- [3] J. Stachulak and M. Gangal, Effects of in-use DOCs on NO₂ emission in the underground operation. 20th Mining Diesel Emissions Council Conference, Toronto, Canada October 8-10, 2014.
- [4] A.W. Majewski et al., Nitrogen oxides reactions in diesel oxidation catalyst. SAE Technical Paper Series 950374 (1995).
- [5] J.L. Ambs and B.T. McClure, The influence of oxidation catalyst on NO₂ in diesel engine. SAE Technical Paper Series 932494 (1993).
- [6] S.R. Katare et al., Aged DOC is a net consumer of NO_x: Analyses of vehicle, engine-dynamometer and reactor data. SAE Technical Paper Series 2007-01-3984 (2007).
- [7] R. Alvares et al., Evidence of increase mass fraction of NO_x within real-world NO_x emissions of modern vehicles – derived from a reliable online measuring method. *Atmospheric Environment* 42 (2008), 4699-4707.
- [8] M.P. Keuken et al., Trends in primary NO_x and exhaust PM emissions from road traffic for the period 2000-2020 and implications for air quality and health in the Netherlands. *Atmospheric Environment* 54 (2012), 313-319.
- [9] G.M. Pataky et al., Effects of an oxidation catalytic converter on regulated and unregulated diesel emissions. SAE Technical Paper Series 940243 (1994).
- [10] S.T. Bagley et al., Effects of an oxidation catalytic converter and a biodiesel fuel on the chemical, mutagenic, and particle size characteristics of emissions from a diesel engine. *Environmental Science and Technology* 32 (1998), 1183-1191.
- [11] E.R. Kisin et al., Mutagenicity of biodiesel or diesel exhaust particles and the effects of engine operating conditions. *Journal of Environmental Engineering and Ecological Science* (2013). doi: 10.7243/2050-1323-2-3.
- [12] K. Vaarasmahti et al., Effects of oxidation catalyst on diesel soot particles. *Environmental Science and Technology* 40 (2006), 4776-4781.
- [13] S.D. Shah et al, Reduction of particulate matter emissions from diesel backup generators equipped with four different aftertreatment devices. *Environmental Science and Technology* 41 (2007), 5070-5076.
- [14] A.D. Bugarski et al., Effects of Diesel Exhaust Aftertreatment Devices on Concentrations and Size Distribution of Aerosols in Underground Mine Air. *Environmental Science and Technology* 43 (2009), 6737-6743.
- [15] C. Han et al., Role of organic carbon in heterogeneous reaction of NO₂ with soot. *Environmental Science and Technology* 47 (2013), 3174-3181.
- [16] R. Allansson et al., Optimizing the low temperature performance and regeneration efficiency of the continuously regenerating diesel particulate filter (Cr-Dpf) system. SAE Technical Paper 2002-01-0428 (2002).
- [17] C. Görsmann, Catalytic coatings for diesel particulate filter regeneration. In: Mayer A, ed. Particle filter retrofit for all diesel engines. Brill Ulrich, Haus der Technik Fachbuch Band 97 (2008), 137-160.
- [18] G. Madia et al., The effect of an oxidation precatalyst on the NO_x reduction by ammonia SCR. *Ind Eng Chem Res* 41 (2002), 3512-3517.
- [19] I.A. Khalek et al., Regulated and unregulated emissions from highway heavy-duty diesel engines complying with U.S. Environmental Protection Agency 2007 Emissions Standards. *Journal of Air and Waste Management Association* 61 (2011), 427-442.
- [20] NIOSH. Pocket Guide to Chemical Hazards. Department of Health and Human Services, Centers for Disease Control and Prevention, National Institute for Occupational Safety and Health, DHHS (NIOSH) Publication No. 2005-149 (2007), page 228.
- [21] ACGIH, Threshold Limit Values (TLVs) and Biological Exposure Indices (BEIs) - Nitrogen Dioxide. (2012).
- [22] N.V. Heeb et al., Secondary effects of catalytic diesel particulate filters: Conversion of PAHs versus formation of nitro-PAHs. *Environmental Science and Technology* 42 (2008), 3773-3779.
- [23] B. Zielinska, Atmospheric transformation of diesel

emissions. *Experimental and Toxicological Pathology* 57 (2005), 31-47.

- [24] 30 CFR 75.322, Mandatory Safety Standards. Underground coal mines. Harmful quantities of noxious gases. U.S. Department of Labor, Mine Safety and Health Administration, Code of Federal Regulations. Washington, DC: U.S. Government Printing Office, Office of the Federal Register.
- [25] 30 CFR 57.5001, Safety and Health Standards. Underground metal and nonmetal mines. Exposure limits for airborne contaminants. U.S. Department of Labor, Mine Safety and Health Administration, Code of Federal Regulations. Washington, DC: U.S. Government Printing Office, Office of the Federal Register.
- [26] WVDEC. Rules for operating diesel equipment in underground mines in West Virginia. West Virginia Diesel Equipment Commission. Title 196, Series 1 (2004).
- [27] K. Johansen et al., Novel base metal-palladium catalytic diesel filter coating with NO₂ reducing properties. SAE Technical Paper Series 2007-01-1921 (2007).
- [28] M. Khair et al., Catalytic formulation for NO₂ suppression and control. SAE Int. Journal of Fuels and Lubricants 1(1) (2009), 803-812, doi:10.4271/2008-01-1548.
- [29] L. Patts et al., Laboratory comparison of 2 DOCs used in mining industry: Effects on CO and NO₂. *Coal Age*, October 2013.
- [30] ISO, ISO 8178-1:1996: Reciprocating internal combustion engines. Exhaust emission measurement, Part 1: Test-bed measurement of gaseous and particulate exhaust emissions. International Organization for Standardization. Geneva, Switzerland (1996).
- [31] 61 Fed Reg. 55411, Mine Safety and Health Administration: 30 CFR Part 7. Approval, exhaust gas monitoring, and safety requirements for the use of diesel-powered equipment in underground coal mines; final rule. Code of Federal Regulations. Washington, DC: U.S. Government Printing Office, Office of the Federal Register.

Acronyms

ACGIH	American Conference of Governmental Industrial Hygienists
API	American Petroleum Institute
ASTM	ASTM International, an international standards organization that develops and publishes voluntary consensus technical standards
CE	celling value
CO	carbon monoxide
CO ₂	carbon dioxide
DOC	diesel oxidation catalytic converter
DPF	diesel particulate filter
DPM	diesel particulate matter
EZDOC	diesel oxidation catalytic converter supplied by AirFlow Catalyst Systems Inc.
FTIR	Fourier transform infra-red
HC	hydrocarbons
I50 (ISO M8)	intermediate speed 50 percent load
I100 (ISO M6)	intermediate speed 100 percent load
ISO	International Organization for Standardization
MinNoDOC	diesel oxidation catalytic converter supplied by AirFlow Catalyst Systems Inc.
M/NM	metal/nonmetal
MSHA	Mine Safety and Health Administration
NIOSH	National Institute for Occupational Safety and Health
nitro-PAHs	nitrated polycyclic aromatic hydrocarbons
NO	nitric oxide
NO ₂	nitrogen dioxides
NO _x	nitric oxides (NO _x =NO+NO ₂)
OEM	original equipment manufacturer
OMSHR	Office of Mine Safety and Health Research
PAH	polycyclic aromatic hydrocarbons
R50 (ISO M3)	rated speed 50 percent load
R100 (ISO M1)	rated speed 100 percent load
SAE	Society of Automotive Engineers
SCR	selective catalyst reduction
THC	total hydrocarbons
TLV	threshold limit values (ACGIH)
TR	transient
ULSD	ultralow sulfur diesel
U.S. EPA	U.S. Environmental Protection Agency

Simulation of DPM Dispersion for Different Mining Operations Inside a Dead-end Entry

Yi Zheng¹, Magesh Thiruvengadam², Hai Lan², Jerry C. Tien²

¹Department of Mining & Nuclear Engineering,
Missouri University of Science and Technology (MST), MO 65401, USA

²Clean Air Power Inc., Poway, CA 92064, USA

Division of Mining and Resources Engineering, Department of Civil Engineering, Monash University, Clayton Campus, Wellington Road, Clayton, VIC 3800, Australia

Diesel Particulate Matter (DPM) is considered carcinogenic after prolonged exposure. With more diesel-powered equipment used in underground mines, miners' exposure to DPM has become an increasing concern. This paper used computational fluid dynamics (CFD) methods to study DPM distribution inside a dead-end entry with different mining operations. The mining activities considered in this study include: Load-Haul-Dump (LHD) alone in mucking operation; drilling jumbo alone in drilling operation; LHD and truck in loading operation; and LHD and truck loading in one face area and a drill-jumbo drilling in another face area. It was assumed that all of the diesel vehicles were fitted with diesel particulate filter (DPF) and had minimum DPM emissions. A push-pull ventilation system was used to dilute and remove DPM inside the dead-end entry. A species transport model with buoyancy effect was then used to examine the DPM dispersion pattern. High DPM regions were identified in the face areas and dead-end entry. This can provide guidelines for good working practices. It can also be used for selection of DPM control strategies and DPM annual training for underground miners.

Keywords: diesel particulate matter, computational fluid dynamics, underground ventilation

1. Introduction

For underground mines, self-propelled diesel equipment that does not require a power cable or constant charging of batteries is preferred because working faces usually cover extensive areas where these facilities are not available. However, emissions from the tailpipe and its subsequent distribution in the underground mine are of growing concerns for miners.

Diesel particulate matter (DPM) is the particulate by-product of diesel exhaust and it can exist in different modes with different size distributions (5 nm to 10 μm). Due to its very small size and its ability to adsorb very complex (more than 1,800 different organic compounds were identified) [1] and potentially toxic hydrocarbons, it can be breathed into the alveolar region of the lungs of miners and cause from acute health problems such as asthma, eye and nose irritation, headaches and nausea [2-4] to long term carcinogenic effects [5-6]. Also due to the small size, once airborne, it is likely to remain airborne throughout the entire mine, affecting not only the workplace where it is produced but also areas downstream.

For underground coal mines, diesel engines used underground are divided into three categories under Mine Safety and Health Administration (MSHA) regulations: "permissible", "nonpermissible heavy-duty equipment, generators, and compressors" and "nonpermissible light-duty equipment." Equipment under each category is required to emit no more than a certain amount of DPM per hour [7]; otherwise, it will not be allowed to operate underground.

For underground metal/non-metal mines, MSHA regulations limit a miner's personal exposure to DPM to no more than 160 $\mu\text{g}/\text{m}^3$ of total carbon (TC) for an average eight-hour equivalent full shift (effective from May 20, 2008) [8]. Today, there are still mines that cannot meet this regulation limit.

To control DPM hazards, two types of strategies have been commonly used. One is DPM reduction and removal before it is released from the engine tailpipe, which includes proper diesel engine selection and maintenance [9-11], use of alternative fuels [12-13], and exhaust gas treatment devices [14-15], e.g., diesel particulate filters (DPF). The other is through control measures after DPM is discharged into the environment – mine ventilation systems, an enclosed equipment cab with filtered breathing air (environmental cab), personal protective equipment, and administrative controls [16-18].

Experience [19] showed that no single strategy can solve all DPM problems and a combination of several measures needs to be implemented in the field to attain compliance. Since none of the strategies are cost free, an effective, efficient, and economical control scheme for operations under different mining conditions is essential in order for a mining company to provide a safe working environment and to meet regulatory criteria. To achieve that, an understanding of DPM behaviour in mining environment can be very useful in selecting the control strategies and training the miners. Numerical simulations using CFD can be used for that purpose by visualizing DPM distribution based on laboratory experiments and field studies.

CFD simulations have been successfully used in mining research to detect spontaneous combustion and apply inertisation in gob areas [20-21], study airflow patterns and gas concentrations in continuous miner operations or heading development [22-26], investigate scrubber intake designs for longwall dust control [27], and estimate a mine's damage status by tracer gas and simulation after a disaster [28]. CFD modelling has been demonstrated as a powerful tool for understanding airflow movement and gas/dust behaviour in a complicated three dimensional environment. It can also provide useful information for initial concept testing of new ideas and equipment for environment control.

Simulation of DPM dispersion in underground mines was carried out by Zheng and Tien [29], in which DPM was considered to behave like a gas. Subsequent study showed that it gave good quantitative agreement with practical accuracy for the DPM distribution and successfully identified the DPM-affected areas above the threshold limit [30]. In the present study, DPM emission was also treated as a gas to examine its diffusion inside an underground single dead end entry.

In this study, several mining operations were taking place inside the dead-end entry of a typical underground mine. Depending on the mining operation, different types of diesel vehicles were used and each diesel vehicle emitted DPM from the tailpipe at different concentrations. The mining operations that were considered inside the face areas include 1) LHD working alone doing mucking operation, 2) drilling jumbo working alone doing drilling operation, 3) LHD and truck doing loading operation and 4) LHD and truck doing loading operation in one face area and a drill-jumbo doing drilling operation in another face area. It was assumed that all of the diesel vehicles were fitted with a DPF and had minimum DPM emissions from the tailpipe.

To provide effective ventilation in the deep dead-end entry, a push-pull system was used. The distributions of DPM concentration were presented along with area-weighted average DPM values inside the dead-end to study the effect of different mining operations on the DPM distribution pattern. This study can help mining

engineers to visualize the DPM plume under commonly encountered mining operations. The high DPM regions revealed by the simulation can also be used for selection of DPM control strategies and DPM annual training for underground miners.

2. Problem statement and CFD modeling

2.1 Statement of the problem

The schematic of the single dead-end entry with push-pull tube ventilation is shown in Figures 1 - 4 for different mining operations. The main entry measured 6 m in width, 5 m in height and 131 m in length, while the dead-end measured 6 m in width, 5 m in height, and 90 m in length. The three stub entries were evenly developed inside the dead-end entry and had the same cross-sectional dimensions as the main entry with 15 m in depth. The main entry had of 19.35 m/s (41,000 cfm) of fresh air flowing from the left to the right. The blower fan at the inlet of the push tubing was set to provide 8.02 m/s (17,000 cfm) of fresh air into the face area. The exhaust fan at the outlet of the pull tubing drew the diesel exhaust mixture at a rate of 9.44 m/s (20,000 cfm) from the face area and released it into the main entry. For all mining operations, with the exception of the combined drilling and loading activity, the push tubing extended into the dead-end entry for approximately 70 m while the pull tubing extended for approximately 81 m. The lengths of the push and pull tubing inside the main entry were 3.4 m and 22 m, respectively.

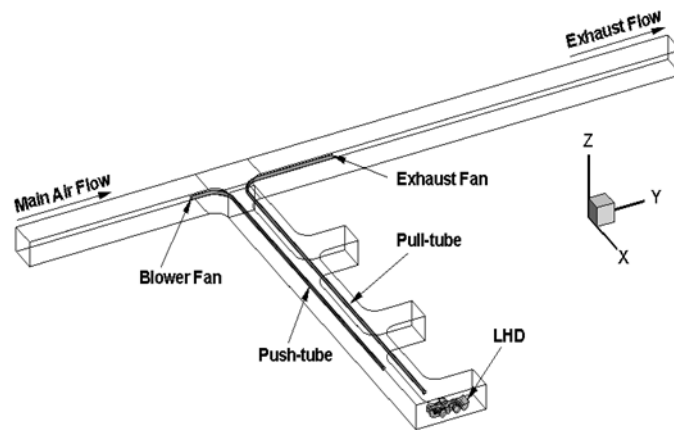


Fig. 1. Schematic of LHD mucking operation in dead-end entry with push-pull system.

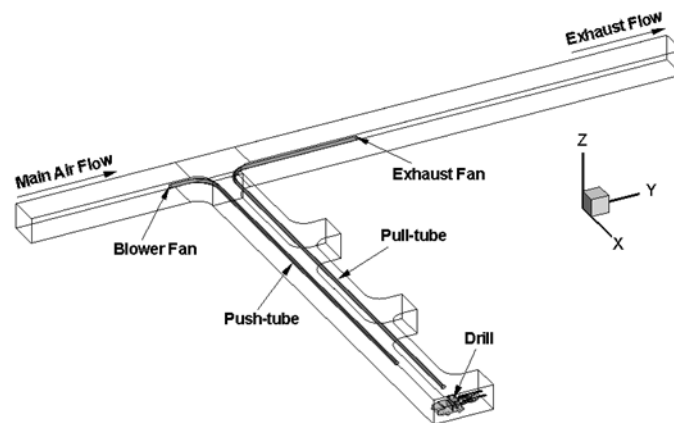


Fig. 2. Schematic of drill jumbo drilling operation in dead-end entry with push-pull system.

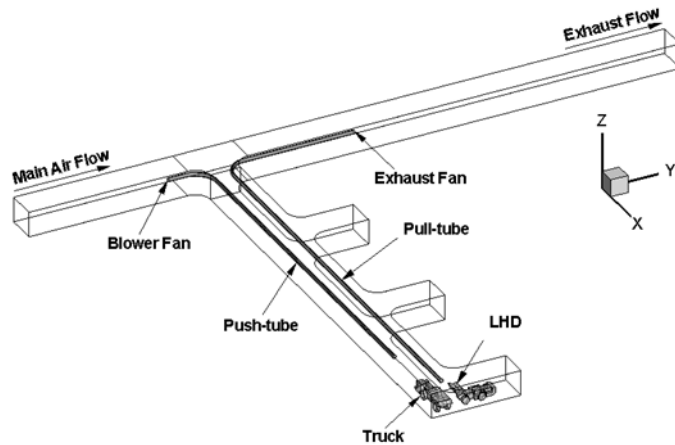


Fig. 3. Schematic of LHD and truck loading operation in dead-end entry with push-pull system.

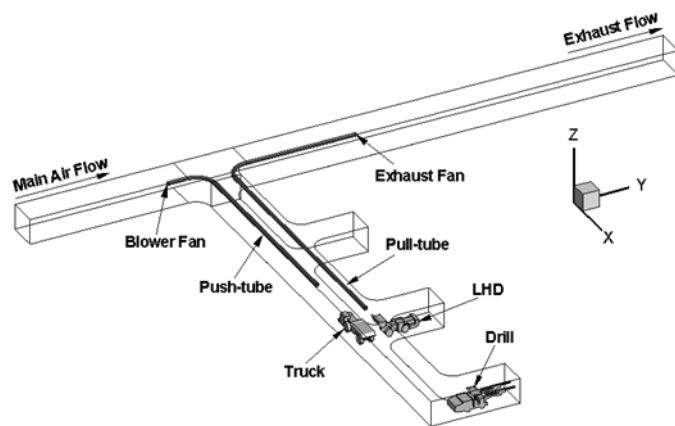


Fig. 4. Schematic of loading and drilling operation in dead-end entry with push-pull system.

The mining operations of LHD mucking, drilling, and LHD-truck loading were carried out in the inner-most face area of the dead-end. In the case of a combined operation, loading took place in the middle face area and drilling took place in the inner-most face area of the dead-end. All of the mining operations are set to take place for the time duration of 200 seconds. All diesel vehicles were fitted with a DPF and had minimum DPM emission from their tailpipes.

2.2 Assumptions

Based on Zheng's studies [29-30], this CFD simulation was conducted under the following assumptions: (1) DPM was treated as gas and the material selected as the representative for DPM was n-octane vapor (C₈H₁₈). The chemical reactions between species are not considered in this study; (2) both air and DPM are incompressible; (3) the flow in the domain is fully turbulent; (4) All the vehicles are stationary.

2.3 CFD modelling

Three-dimensional incompressible unsteady turbulent continuity, momentum, and energy equations, along with standard k- ϵ turbulent and non-reacting transport

equations (2 species, DPM and air) were solved using ANSYS FLUENT CFD software. The species transport model, available in FLUENT, was used to determine the DPM distribution pattern.

Due to the multiple cases covered in this study, all of the boundary conditions are summarized in Table 1. For the LHD, the tailpipe is located at the right rear of the vehicle and pointing backward; for the truck, the tailpipe is placed at the right front of the truck, pointing to the floor; for the drill jumbo, the tailpipe is placed at right rear of the vehicle and exhaust is discharged toward the floor. The parameters for the main ventilation and diesel vehicles are derived from Zheng's industrial field study [31-32] with only the low emission diesel engines. The detailed meanings of the boundary conditions can be found in the FLUENT manual [33].

In order to achieve accuracy in the simulation results, finer meshes were generated for the area close to diesel engines where high gradients existed. For all the models, about 1.5 million computational elements (cells) were generated. The unsteady flow calculations were made by using time step ($\Delta t = 0.1$ s) for the time period of 200 s (3 minutes and 20 seconds) for the different operations.

Table 1. Summary of boundary conditions.

	Boundary	Detailed settings
Main ventilation	Inlet	0.65 m/s, normal to boundary; DPM: 0 ppm.
	Exit	Pressure outlet (0 Pa).
Diesel equipment	LHD tailpipe	24.1 m/s, normal to boundary; 594 K; DPM, 1.73 ppm.
	Truck tailpipe	27.5 m/s, normal to boundary; 644 K; DPM, 2.0 ppm.
	Drill tailpipe	15 m/s, normal to boundary; 600 K; DPM, 2.0 ppm.
Walls		No slip, adiabatic walls.
Auxiliary Ventilation	Push-tube	Inlet: fan ($\Delta P = 481$ Pa); outlet: interior.
	Pull-tube	Inlet: interior; outlet: fan ($\Delta P = 800$ Pa).

3. Results and discussion

The general flow feature that arose in the single dead-end entry is shown in Figure 5 for the LHD and truck loading operation. Other mining operations have similar general airflow patterns. It shows the fresh air that entered the main entry and split into two parts. The first part flowed directly downstream to the exhaust section and exited the domain. The second part entered into the dead-end while the remaining part was drawn by the blower fan into the push tubing and delivered it to the working face area where the mining operation was taking place. This fresh air inside the dead-end flowed over the diesel vehicles and mixed with the emissions from their tailpipes creating a large recirculation flow region inside the working face area as shown in Figure 5. Due to the effect of buoyancy, this diffused mixture flowed upward towards the roof of the mine, reversed direction and started flowing upstream toward the main entry. A majority of this reversed flow was drawn by the exhaust fan through the pull tubing and drained into the main entry at high velocity. The remaining part reached the middle section of the main entry and divided into two parts. One part flowed upstream and reentered the push tubing while the other part flowed downstream and mixed with the exhaust flow from the pull tubing. This

complex flow behavior was due to the interaction between the high temperature tailpipe flow and the low temperature fresh air flow. The resulting DPM distributions inside the dead-end for each mining operation are discussed in detail below.

3.1 LHD-mucking (case 1)

The DPM distribution inside the dead-end during the LHD mucking operation is shown in Figure 6. From the colored DPM contours, it can be seen that, except for a very small region behind the tailpipe of the LHD, all other places in the single dead-end entry were in compliance with a DPM concentration of less than the prescribed regulatory limit of $160 \mu\text{g}/\text{m}^3$. It can be seen that the DPM distribution inside the dead-end attained a steady state condition within 10 seconds from the start of the operation. This was due to the low emission from the tailpipe of the LHD resulting from the installation of DPF. Similar DPM distribution results were obtained when only a blower fan was operating and the exhaust fan was turned off, or vice versa, to save cost and power. In this configuration, the LHD driver was not required to use enclosed cabs to provide protection from the harmful effects of DPM.

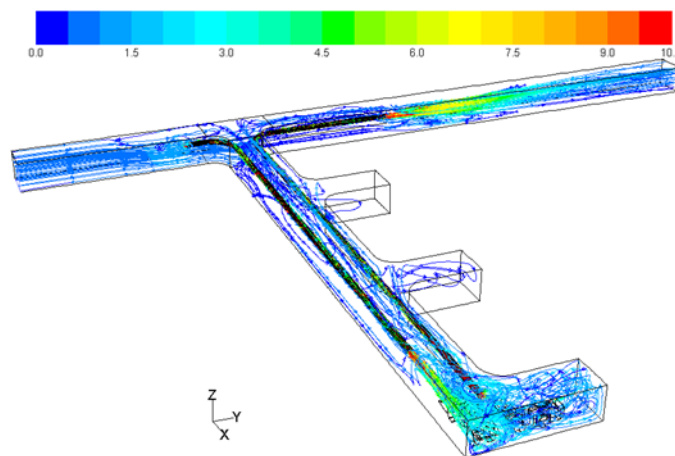


Fig. 5. Pathlines colored by velocity magnitude demonstrating general flow features for LHD and truck loading operation.

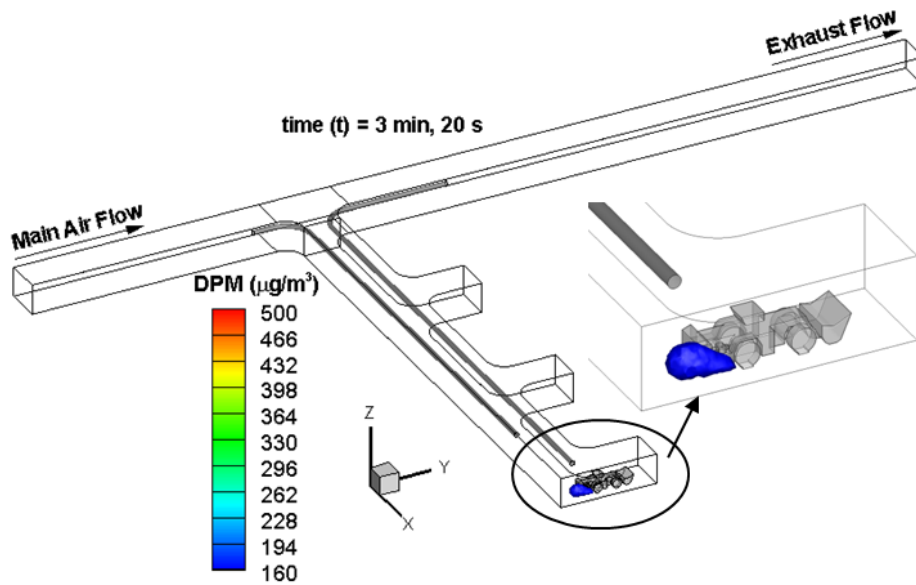


Fig. 6. DPM distribution ($>160\mu\text{g}/\text{m}^3$) from LHD mucking operation in the dead-end entry.

3.2 Drilling (case 2)

Figure 7 shows a drilling jumbo carrying out a drilling operation in the inner-most face area of the dead-end. From the colored contours, it can be clearly seen that, except for the immediate tailpipe regions of the drilling jumbo, all of the remaining areas were in compliance with a DPM concentration of less than 160 micrograms per cubic meter. It can also be seen that the DPM distribution during the drilling operation attained a steady state within 10 seconds from the start of the simulation. Similar to the mucking operation, there was a negligible difference in the DPM occupied areas inside the dead-end when either the blower fan or the exhaust fan was turned off to save power. Only a blower fan with push tubing, or an exhaust fan with pull tubing, was sufficient to obtain effective ventilation in the face area. During drilling, the operator of the drilling jumbo may not need to use enclosed cab to be protected from the harmful effects of DPM.

3.3 LHD-truck loading (case 3)

The DPM distribution in the same dead-end while the LHD-truck loading operation was occurring in the interior face area is shown in Figure 8. From the colored contours, it can be seen that DPM above the regulation limit occupied a small region behind the tailpipe of the LHD and a small region in the roof above the LHD. The DPM also covered small regions in front of the truck and in the roof area of the dead-end. From the distribution pattern, it can be seen that both blower and exhaust fans with push and pull tubing were necessary to effectively ventilate the face area. The LHD and the truck drivers may not require enclosed cabs to protect themselves from the harmful effects of DPM in this configuration. But if there is miner working around the colored region close to the tailpipes, he needs to wear personal protection equipment.

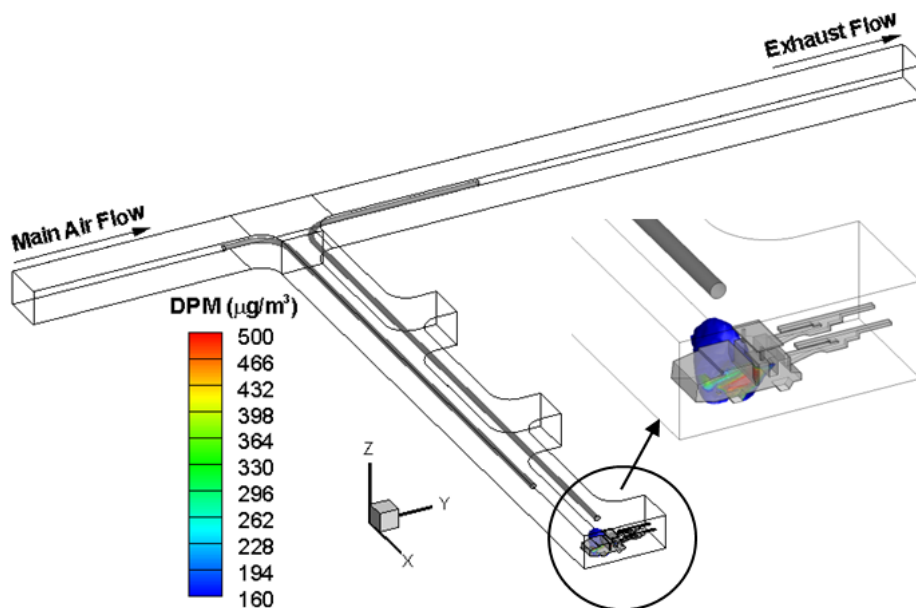


Fig. 7. DPM distribution ($>160\mu\text{g}/\text{m}^3$) from drilling operation in dead-end entry.

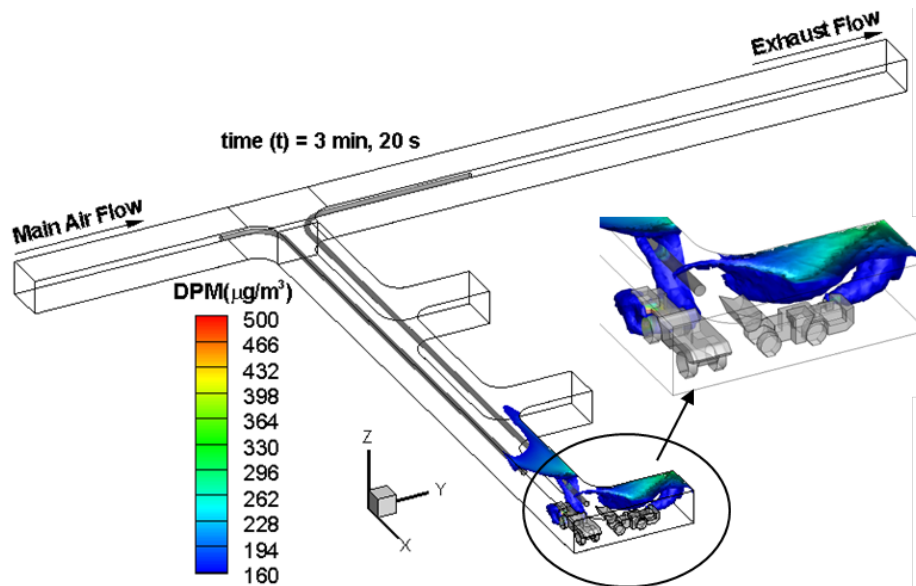


Fig. 8. DPM distribution ($>160\mu\text{g}/\text{m}^3$) from loading operation in dead-end entry.

3.4 Drilling and LHD-truck loading (case 4)

The DPM distribution, while both the loading and drilling operations were taking place inside the dead-end, is shown in Figure 9. The design of the push-pull tubing system was altered for this combined operation. Since most of the tail pipe emission was coming from the mid face area of the dead-end, the length of the push and pull tubing was shortened. In this case, the push tube extended for approximately 40 meters while the pull tubing extended for approximately 51 meters into the dead-end. The colored contours show the harmful diesel fumes that gradually filled the drilling and the loading face areas. From the colored contours, it can be clearly seen that the fan capacities of the push and pull tubing were not high enough to effectively ventilate the face areas. The operators of the LHD, the truck, and the drilling jumbo should use enclosed cabs in order to

safeguard themselves against the harmful effects of DPM.

4. Comparison of different mining operations

A comparison of the distribution of DPM inside the dead-end for different mining operations was made by plotting curves for different cross-sectional planes inside the dead-end. The cross-sectional planes of the mucking operation are shown in green color in Figure 10. Similar cut planes were also generated for other mining operations. The working face 1 was used when a single mining operation (mucking or drilling or loading) was taking place, but both working face 1 and working face 2 were used when two mining operations (drilling in work face 1 and loading in work face 2) were taking place. No mining operation took place in work place 3.

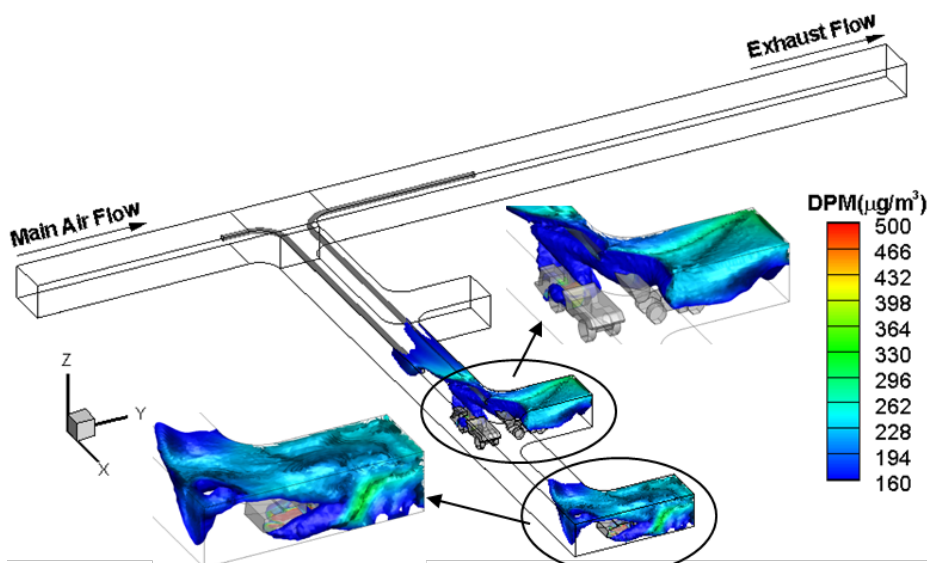


Fig. 9. DPM distribution ($>160\mu\text{g}/\text{m}^3$) from drilling and loading operation in dead-end entry.

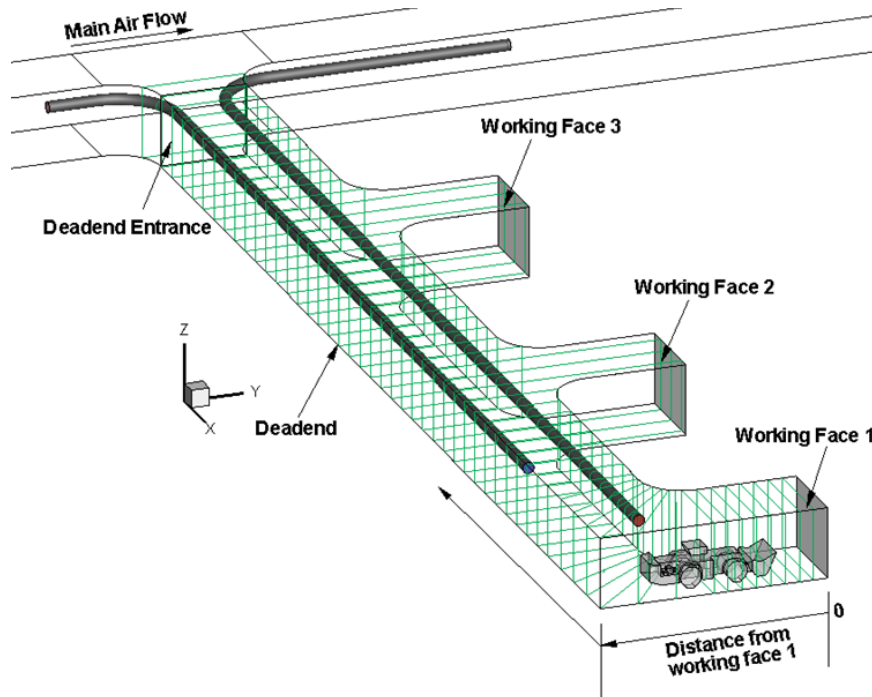


Fig. 10. Schematic of the cut cross-sectional planes inside the dead-end.

The area weighted averaged DPM values at these cross-sectional planes for different mining operations were plotted against the distance and compared, as shown in Fig. 11. The distance was measured from the working face 1, as shown in Figure 10. It can be clearly seen from the plot that the average DPM concentration was maximum for the combined drilling and loading operations, followed by the loading operation case.

This was expected because of the presence of more diesel vehicles inside the dead-end area. The minimum

average DPM concentration distribution occurred in the drilling jumbo operation, although the DPM mass fraction set at the tailpipe of the drill (2.0 ppm) was higher than the DPM mass fraction set at the tailpipe of the LHD (1.73 ppm). This was due to the total DPM emissions from the drilling jumbo being less. Another study [34] also suggested that the emission orientation can also help DPM dilution. The DPM from the drilling jumbo loses momentum by striking the ground and can be more easily mixed with the surrounding airflow.

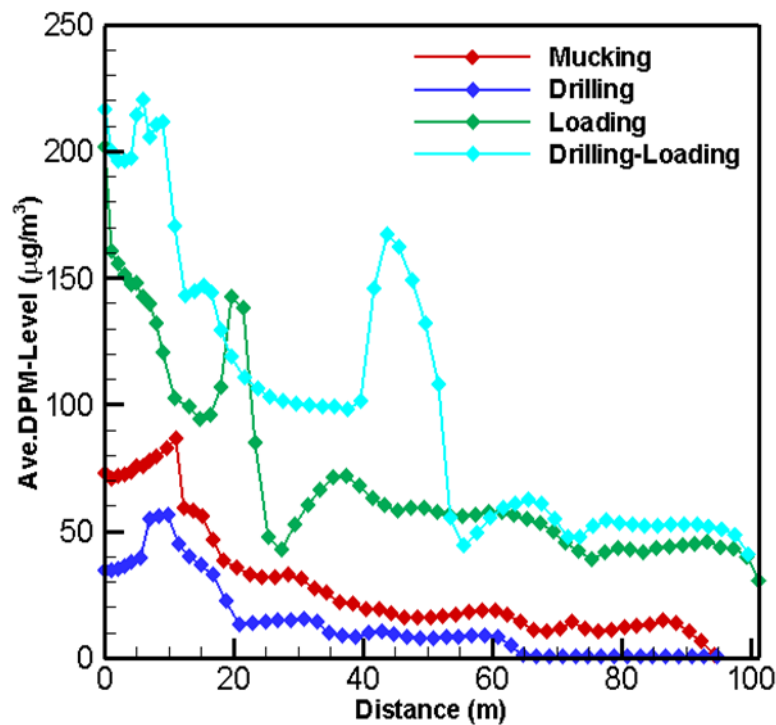


Fig. 11. Comparison of averaged DPM values at different cross-sectional planes inside the dead-end.

5. Conclusions

The effects of different mining operations inside the single dead-end entry were studied and are discussed in this paper. It can be clearly seen that the combination of two mining operations, or a mining operation that required two diesel vehicles inside the dead-end entry, increased the DPM production. The combined push-pull system was not required for single mining operations like drilling and LHD mucking. A blower fan with push tubing or an exhaust fan with pull tubing was sufficient to achieve effective ventilation in the face area. One of the fans could be shut down to save the amount of power required. During the LHD-truck loading operation, the short push and long pull tubing systems were both used to achieve effective ventilation in the face area. With the loading operation in one working face and the drilling operation in the other working face, the DPM production rate was large and the push-pull tube auxiliary ventilation system was ineffective for achieving the designed fresh air flow rates. The flow capacities of the blower and the exhaust fans need to be increased from their designed values to achieve better ventilation effect in the face area.

Acknowledgments

The authors wish to express their sincere gratitude to the financial support provided by the Western US Mining Safety and Health Training & Translation Center by the National Institute for Occupational Safety and Health (NIOSH) (Grant Number 1 R25 OH008319).

References

[1] CFR, Code of federal regulation, US Government Printing Office, Office the Federal Register, 2001.

<http://www.msha.gov/REGS/FEDREG/FINAL/2001finl/01-996.pdf>.

[2] G. Kahn and P. Orris, Acute overexposure to diesel exhaust: report of 13 cases, *Am J Ind Med* 13(3) (1988) 405-406.

[3] B. Rundell et al., Effects on symptoms and lung function in humans experimentally exposed to diesel exhaust, *Occup Environ Med* 53(10) (1996) 658-662.

[4] J.F. III Wade and L.S. Newman, Diesel asthma: reactive airways disease following overexposure to locomotive exhaust, *J Occup Med* 35(2) (1993) 149-154.

[5] NIOSH, Carcinogenic effects of exposure to diesel exhaust, National Institute for Occupational Safety and Health (NIOSH), Department of Health and Human Services, 1988. <http://www.cdc.gov/niosh/docs/88-116>.

[6] EPA, Health assessment document for diesel engine exhaust, U.S. Environmental Protection Agency, 2002. <http://cfpub.epa.gov/ncea/cfm/recordisplay.cfm?deid=29060>.

[7] 30CFR72.D, Diesel particulate matter—underground areas of underground coal mines, Code of Federal Regulations, Title 30, part 72, subpart D, (2014) 489-491. <http://www.gpo.gov/fdsys/pkg/CFR-2014-title30-vol1/pdf/CFR-2014-title30-vol1.pdf>.

[8] 30CFR57.5060, Limit on exposure to diesel particulate matter, Code of Federal Regulations, Title 30, part 57.5060, (2014) 370-371. <http://www.gpo.gov/fdsys/pkg/CFR-2014-title30-vol1/pdf/CFR-2014-title30-vol1.pdf>.

[9] S. McGinn, Maintenance guidelines and best practices for diesel engines, final report, Diesel emissions evaluation program (DEEP), 1999. http://www.camiro.org/DEEP/Project%20Reports/mtce_re

- port.pdf.
- [10] S. McGinn et al., Diesel emissions: mechanics' maintenance manual, Diesel emissions evaluation program (DEEP), 2010. <http://www.camiro.org/DEEP/Technology%20Sum%20A nd%20Reports/mechanicsman.pdf>.
- [11] P. Anyon, Managing diesel particle emissions through engine maintenance - an Australian perspective, Proceedings of the 12th U.S./North American Mine Ventilation Symposium, Reno, NV, USA, (2008) 521-526.
- [12] T.C. Zannis et al., Effects of fuel chemical structure and properties on diesel engine performance and pollutant emissions: review of the results of four European research programs, SAE SP 2185(2008) 1-36.
- [13] A.D. Bugarski et al., Aerosols emitted in underground mine air by diesel engine fueled with biodiesel, J Air Waste Manage Assoc 60(2) (2010) 237-244.
- [14] S.D. Shah et al., Reduction of particulate matter emissions from diesel backup generators equipped with four different aftertreatment devices, Env Sci Tech 41(14) (2007) 5070-5076.
- [15] A.D. Bugarski et al., Effects of diesel exhaust aftertreatment devices on concentrations and size distribution of aerosols in underground mine air, Env Sci Tech 43(17) (2009) 6737-6743.
- [16] A.B. Cecala et al., Reducing enclosed cab drill operator's respirable dust exposure with effective filtration and pressurization techniques, J Occup Environ Hyg 2(1) (2005) 54-63.
- [17] J.D. Noll et al., The effects of ventilation controls and environmental cabs on diesel particulate matter concentrations in some limestone mine. Proceedings of the 12th US/North American Mine Ventilation Symposium, Reno, NV, USA, (2008) 463-468.
- [18] MSHA, Practical ways to reduce exposure to diesel exhaust in mining—A toolbox, U.S. Department of Labor, Mine Safety and Health Administration, 2013. <http://www.msha.gov/S&HINFO/TOOLBOX/DTBFINAL .htm>.
- [19] A.D. Bugarski et al., Diesel aerosols and gases in underground mines: guide to exposure assessment and control. Department of Health and Human Services, Centers for Disease Control and Prevention, National Institute for Occupational Safety and Health, Office of Mine Safety and Health Research, Pittsburgh, PA and Spokane, WA, 2011.
- [20] L. Yuan and A.C. Smith, Computational fluid dynamics modeling of spontaneous heating in longwall gob areas, Trans Soc Min Metall Explor 322 (2007) 37-44.
- [21] T.X. Ren et al., Development of innovative goad inertisation practices to improve coal mine safety, COAL2005: Coal Operators' Conference, Brisbane, QLD, AU, (2005) 315-322.
- [22] P. Sullivan and J.V. Heerden, The simulation of environmental conditions in continuous miner developments using computational fluid dynamics, J Mine Vent Soc S Afr January (1993) 2-11.
- [23] D.M. Hargreaves and I.S. Lowndes, The computational modeling of the ventilation flows within a rapid development drive, Tunn Undergr Sp Tech 22(2) (2007) 150-160.
- [24] A.M. Wala et al., Mine face ventilation: a comparison against benchmark experiments for the CFD code validation, Min Eng 59(10) (2007) 49-55.
- [25] V.K. Kollipara et al., A CFD analysis of airflow patterns in face area for continuous miner making a right turn cut, 2012 SME Annual Meeting & Exhibit (preprint), (2012) 626-633.
- [26] S. Torno et al., Conventional and numerical models of blasting gas behavior in auxiliary ventilation of mining headings, Tunn Undergr Sp Tech 34(2013) 73-81.
- [27] T.X. Ren and R. Balusu, Innovative CFD modeling to improve dust control in longwalls, Coal 2008: Coal Operators' Conference, Wollongong, NSW, AU, (2008) 137-142.
- [28] G. Xu et al., Development of a remote analysis method for underground ventilation systems using tracer gas and CFD in a simplified laboratory apparatus, Tunn Undergr Sp Tech 33(2013) 1-11.
- [29] Y. Zheng and J.C. Tien, DPM dispersion study using CFD for underground metal/nonmetal mines, Proceedings of the 12th U.S./North America Mine ventilation Symposium, Reno, NV, USA, (2008) 487-493.
- [30] Y. Zheng et al., DPM dissipation at MST's experimental mine and comparison with simulation, J Coal Sci Eng (China) 17(3) (2011) 285-289.
- [31] Y. Zheng et al., Simulation of DPM distribution in a long single entry, 13th Mine Ventilation Symposium, Sudbury, Ontario, Canada, (2010) 149-156.
- [32] S. McGinn et al., Brunswick mine diesel particulate filter field study, Diesel emissions evaluation program (DEEP) final report of investigation, 2004. http://www.camiro.org/DEEP/Project_Reports/nordpf_fina l.pdf.
- [33] ANSYS, FLUENT user's guide, Release 15, ANSYS, Inc, 2014.
- [34] Y. Zheng et al., Simulation of DPM distribution in a long single entry with buoyancy effect, Int J Min Sci Tech, 25(1) (2015) 47-52.

Overview of DPM Control Strategies during Longwall Moves

Argyle Douglas Stewart Gillies^a, Hsin Wei Wu^b

^aMissouri University of Science and Technology, Rolla, Missouri, USA
^bGillies Wu Mining Technology Pty Ltd, Queensland, Australia

Occupational exposure limits for diesel particulate matter (DPM) are progressively being adopted in a number of countries. Many of these follow the lead of the US Mine Safety and Health Administration initiated in 2008. In line with adoption of best practice it is accepted that all exposures should be reduced to as low as reasonably achievable. Thus, the management of diesel emissions and occupational exposures to those emissions requires an integrated strategy incorporating efforts from all key and relevant mine production departments including management, production, maintenance, supply and occupational health and safety personnel. Coal mine longwall moves rely on use of high powered diesel equipment to transport and move the components that make up a longwall. This equipment in use often produces very high exhaust pollutants of exhaust gases and DPM. To reduce mine personnel exposure levels to diesel exhaust the hierarchy of controls should to be considered and followed. This can involve eliminating exposures by not using diesel equipment, isolation of miners from exposure – operator positioning in relation to exposure sources, and control by engineering methods – ventilation to reduce concentrations/dilution. Approaches generally adopted on longwalls currently rely on a combination of the strategies including optimization of ventilation, use of Diesel Tag Boards that minimize number of vehicles working installing and salvaging, and use of diesel particulate filters. A study has been undertaken into the mine ventilation systems currently in use during longwall moves within a number of modern longwall international mines. The paper reviews current longwall section ventilation systems and discusses evolving changes being adopted to address the more complex problems in dealing with diesel exhaust and particulate matter during phases of the operational moves. The effects of DPM on mine crew members as well as the diesel equipment operators within a longwall section are examined. Issues that should be considered in designing ventilation strategies during the moves are discussed.

Keywords: DPM, longwall move

1. Introduction

The invention of a compression ignition engine by Rudolph Diesel in the 1890s has contributed significantly to the productivity of many countries over the past 120 years, due to the widespread use of larger diesel powered equipment in most industrial activities. The use of diesel-powered plant in underground mining has steadily increased since the 1940s. During this time, diesel-driven mechanized machinery has replaced physical labor or pneumatically driven machines. Today there are a variety of mechanized diesel units for many underground operations.

The down side of use diesel machines in terms of occupational health has been the exposure of a large number of workers to the complex mixture of toxic gaseous, adsorbed organics and particulate components found in the raw exhaust emissions. The gaseous phase of diesel exhaust consists largely of the same gases found in air, such as nitrogen, oxygen, carbon dioxide and water vapor. The particulate fraction of the diesel exhaust aerosol consists of a solid carbon phase and ultra-fine droplets of a complex mix of semi-volatile organic compounds.

Exposure to the microscopic particles in diesel engine exhaust can lead to serious health problems including the incidence of cancers, heart disease and increased susceptibility to respiratory ailments of pneumonia, bronchitis, and asthma. The options for the treatment and reduction of diesel emissions have become a major area of concern for many mine operators. The basis for any complete DPM compliance strategy should be a comprehensive baseline study of the DPM present in the mine atmosphere including ambient air monitoring, analysis of monitored data, and development of a realistic plan for ambient DPM reduction. It is important that studies are taken on a real time basis to

allow important sources of DPM in the mine atmosphere to be prioritized.

NIOSH has been closely involved in development of instruments for measurement of airborne DPM for more than 20 years. The earliest approaches focused on shift average determinations with development of the SKC approach. Two real time DPM monitors have been developed since. The first, the real time Diesel version of Personal Dust Monitor (D-PDM) was developed on the base of the successful Personal Dust Monitor (PDM) unit. The heart of the PDM is a miniaturized direct mass measuring sensor that measures mine dust. Changes were undertaken to the PDM [1] to convert it to a DPM particulate submicrometer real time monitoring underground instrument which was named the D-PDM. The real time DPM unit continually reports levels of mine atmosphere submicrometer aerosol. The D-PDM results have been correlated with parallel SKC system DPM evaluations [2]. A phase of robustness and engineering testing has been undertaken to ensure the instrument can effectively assist mine management.

Another real time DPM measurement instrument, the FLIR Airtec, became commercially available in 2011 [3, 4]. It measures the Elemental Carbon (EC) component of DPM by a laser scattering approach. Both new instruments have been evaluated underground in robustness and reliability testing in coal and metal/non-metal mines.

Where diesel equipment is operating in confined areas such as underground mines there is a significant risk of exposure. Levels in Australian underground coal mines have been measured at up to 0.37 mg/m³ as EC [5, 6], although levels up to 2.2 mg/m³ have been measured, depending on job type and mining operation [7].

Levels in Australian underground metalliferous mines have been measured up to 0.42 mg/m³ EC [8]. Investigations in 2005 by SIMTARS also found elevated exposures in Queensland underground metalliferous mines [9]. For surface mining operations, forklift operators have been found to be the highest exposed group [10]. Levels up to 0.40 mg/m³ have been measured for forklift operators, with a median of 0.075 mg/m³ EC [11].

In recent years, occupational exposure limits for DPM are progressively being adopted in a number of countries. Many of these follow the lead of the US Mine Safety and Health Administration initiated in 2008. In line with adoption of best practice it is accepted that all exposures should be reduced to as low as reasonably achievable. There is currently no national exposure standard for DPM. However, a number of regulatory agencies in Australia have adopted the Australian Institute of Occupational Hygienists exposure limit recommendation of 0.1 mg/m³ as EC measured as a time-weighted average over eight hours (adjusted for extended work shifts). The management of diesel emissions and occupational exposures to those emissions requires an integrated strategy incorporating efforts from all key departments on a mine, including management, production, maintenance, supply and occupational health and safety.

Australian coal mine longwall moves rely on use of high powered diesel equipment of chariots and other machines that produces very high exhaust pollutants of gases and Diesel Particulate Matter (DPM). Many Australian coal mines have trouble meeting DPM "Target Limits" during all phases of the operational moves. "Target limits" used generally follow the NSW Guidelines for DPM: 0.1 mg/m³ of EC or 0.2 mg/m³ of Submicron Particulate.

The extensive use of diesel-powered equipment in underground mines makes it challenging to control workers' exposure to submicron aerosols and noxious gases emitted by those engines. In order to protect workers, mines need to establish a comprehensive program based on a multifaceted and integrated approach. To reduce mine personnel's exposure levels to DPM Bugarski et al [12] suggested that the hierarchy of controls should be considered and followed.

- Curtail emissions of the DPM and toxic gases at the source;
- Control pollutants after they are released in the underground mine environment; and
- Use administrative controls to reduce exposures of underground miners to pollutants.

1.1 Curtail Emissions or Elimination

Total elimination of the use of diesel powered machines in underground coal mines is generally impractical as electric options under current technology are not sufficiently versatile and are limited by range. It is possible to reduce diesel emissions with the uptake of tier 3 or better engine for the diesel machines used. However, within underground coal mines the majority of current diesel machines available are generally pre tier 3 and were designed in the 1950s.

The use of low sulphur or other low-emission fuels and low sulphur lubricants is a way of reducing diesel emissions. Low sulphur fuels with sulphur less than 500 ppm have been reduced even further. Some have been reduced to less than 5 ppm and are classified as Ultra

Low Sulphur Diesel. Fuel regulations in Australia mandate a maximum sulphur content of 10 ppm.

Another control that can be used is the use of emission control devices such as pleated diesel exhaust filters on diesel machines used to reduce diesel emissions by either removing solid fractions or converting pollutants into less harmful emissions. DPM filter systems can efficiently trap the solid fraction of diesel emissions and emerging technologies also suggest an ability to remove the fraction of nanoparticle size. Engine design, mine operating parameters and engine duty cycle should also be considered as part of the filter selection.

1.2 Isolation

It is possible to reduce the DPM exposure levels of workers by isolating workers from the source of the diesel emissions. This can be done as follows.

- Limiting size of crews working downstream or inbye of diesel equipment operations.
- Job rotation of miners employed on known heavy and intensive diesel use activities and
- Use of Diesel Tag Boards that limit the number of diesel machines in use relative to air quantities available in the ventilation split.

-

1.3 Administrative Controls

Various administrative or engineering controls can be applied to reduce workers exposure to DPM and some examples of these controls are as follows.

- Understand past and current personal exposure situations at operating sites through continuous personal DPM exposure monitoring programs under normal production, development and change out phases.
- Ventilation required as specified by regulations may not be adequate to protect against DPM as until recently limits have mainly been based only on gas dilution requirements.
- Quality of air supplied to the section.
- Quality and frequency of servicing of machines.
- Training and education of workers (particularly machine operators) about the impact of DPM controls and strategies that can be applied. This could include the following
 - Ensuring services are done.
 - Correcting use of machines for task.
 - Complying with Diesel Tag Board operations.
- Driving or operating machines according to conditions
- Understand impacts on workers positioned inbye of machines and direction of ventilation airflow.
- Hot machines perform poorly so radiator should be cleaned regularly to remove mud and dirt from exterior.
- Avoid leaving machines idling unnecessarily and avoid vehicle convoys.
- Air flow along working faces must comply with regulations.
- Personal Protective Equipment (PPE) must be available for use.

Approaches adopted in Australian coal mines currently rely on a combination of the following strategies

- Optimization of ventilation.
- Use of Diesel Tag Boards that minimize number of vehicles working in installation and salvage panels
- Use of Diesel particulate filters.
-

2.2 Examples of DPM control strategies at Mines

A number of examples are given illustrating DPM monitoring in Australian coal mines during longwall move operational activities. Results from DPM monitoring using real time DPM instruments are shown from three Australian coal mines with a particular emphasis given to the longwall panel ventilation arrangements and diesel vehicle travel routes. DPM control strategies utilized by these mines during their longwall move activities are also described.

2.1 Mine A

Mine A is a gassy highwall longwall mine a highwall mine with no underground Mains headings. Its face cutting heights range from 4.0 to 4.5 m and typical longwall panels are 320 m wide and about 2,100 m long with twin heading gate roads. Faces accommodate 184 two-leg chock shields. The main diesel activities were at the LW installation face. Figure 1 shows longwall panel ventilation arrangements and chock shield transport routes during Mine A surveys with final panel ventilation quantities.

DPM values in antitropical belt road show low average value (0.02 mg/m^3) as the air in belt road was not affected by the diesel activities in the travel road. Ventilation quantity in the LW installation panel was about $39 \text{ m}^3/\text{s}$ initially but increased to $50 \text{ m}^3/\text{s}$ as the panel exhaust fan operating condition changed. This Face quantity increase by about 30% and led to

reduction of DPM concentration levels (by additional dilution) of 30% as measured by the D-PDM units at both head gate (HG) and tail gate (TG) ends of the face as shown in the following figure. Diesel activities at face were at similar levels in the two different levels of panel air quantities. A total of six chock shields were installed during the 6.5 hours survey period with two chock shields installed in the first two hours with lower air quantity and four installed in the last 4 hours with higher air quantity.

2.2 Mine B

Mine B is a gassy underground longwall mine with mining heights from 2.8 to 3.1 m. Typical longwall panels are 300 m wide using 174 two-leg chock shields and about 3400 m long with twin heading gate roads. Mine B tests were undertaken over 3 days. These exercises monitored various ventilation arrangements of longwall face move during chock shield transport to the installation roadway. Figure 3 shows longwall ventilation arrangement for tests and the positions of the D-PDM monitors #106 and #108 during the tests. During the survey period loaded chock carriers travelled in and out through the TG. There was a total of $43 \text{ m}^3/\text{s}$ of air in the longwall installation panel with a back borehole downcasting about $11 \text{ m}^3/\text{s}$ and the rest from panel gateroads. Three chock shield carriers were available and a total of four chock shields were moved.

Mine B results were analyzed to identify sources and levels of DPM within the panel as shown in Table 1. By strategically placing the real time DPM monitors within the longwall panel various sources of the DPM could be identified.

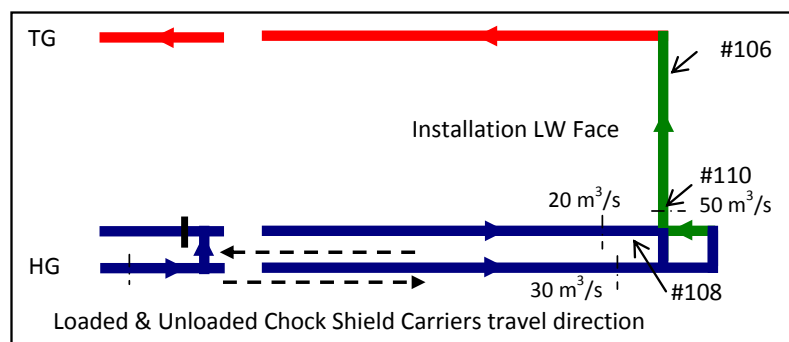


Fig. 1. Longwall panel ventilation and chock shields transport route arrangements of Mine A.

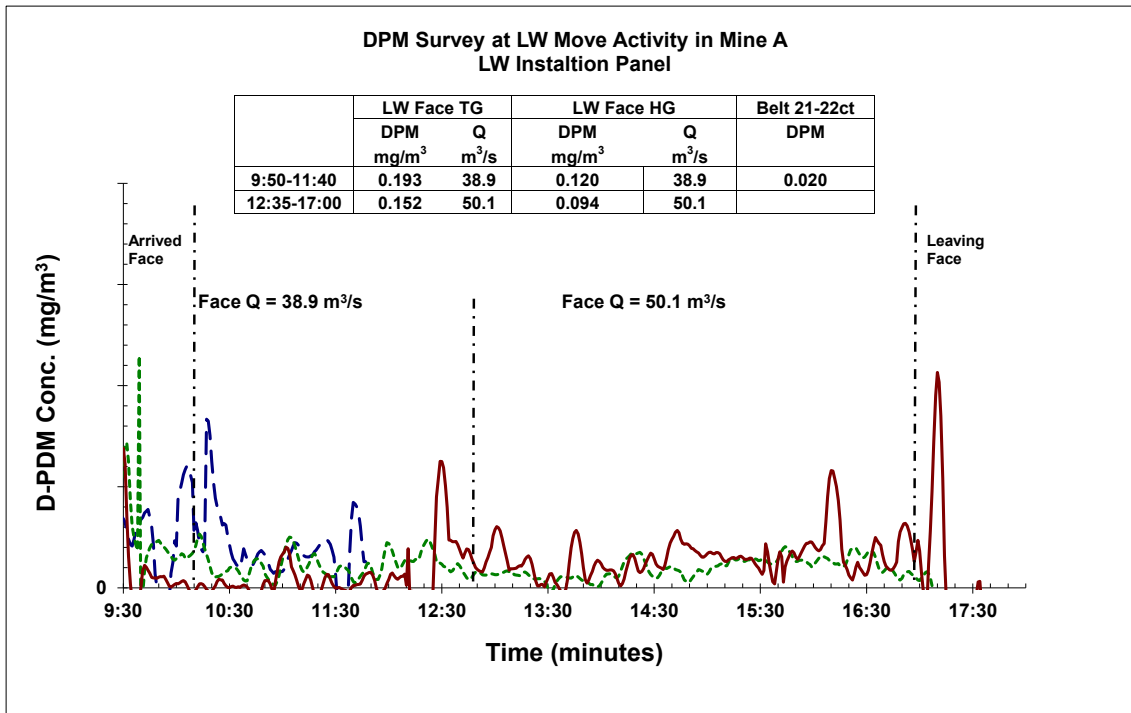


Fig. 2. Submicrometer DPM levels affected by the increase of panel ventilation quantities.

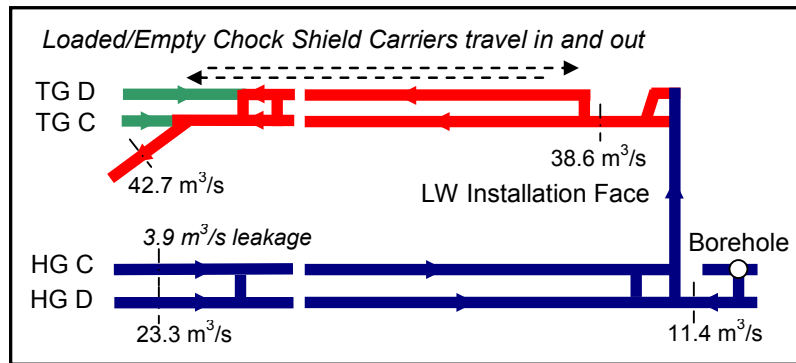


Fig. 3. Longwall panel ventilation and chock shields transport route arrangements of Mine B.

The DPM sources ($\mu\text{g/s}$) in Table 1 are calculated by knowing the air quantity (m^3/s) and the DPM concentration ($\mu\text{g}/\text{m}^3$) at various locations within the panel ventilation circuit.

There were significant DPM levels in TG Heading D due to outbye traffic and in particular the passage of chock shield carriers in the Mains intake air stream to the panel TG. There were also significant DPM levels added along the longwall face due to installation activities for chock shields by “shunting mules” or loaders. The largest source was from chock shield carriers that carried individual chock shields along the length of the TG to reach the face.

As discussed by Dabill [10] exposure of drivers of diesel vehicle to DPM can be limited by the vehicle traveling direction and the ventilation system. For vehicles travelling against the ventilation attempts should always be made to try to ensure the engine is trailing the driver. Under these conditions driver exposure to DPM will be low if no other vehicle are inbye. However, travelling against the ventilation flow with the engine forward can lead to very high driver

exposure and where possible this should be avoided or at the very least reduced to as short a time as possible.

Table 1. Sources of DPM identified in the longwall installation panel.

Location	Sources		Comments
	$\mu\text{g}/\text{s}$	%	
HG C/D Hdg	3.03	18.6	mains air at HG panel entrance
Borehole	0.00	0.0	intake at the back of panel
LW Face	4.77	29.2	shunting Mule or loaders
TG D Hdg	6.96	42.6	chock shield chariots travel way
TG C Hdg	0.00	0.0	no diesel activity
Leakages	1.57	9.6	via coffin seal & double doors
Total	16.32	100.0	

It is more difficult to minimize exposure when travelling with the airflow as no matter what speed the vehicle travels the driver is likely to be exposed. It is important for the vehicle not to travel at the same speed

as the ventilation air velocity as the vehicle driver will be operating in an ever increasing concentration of diesel exhaust emissions and consequently exposure could be very high. If the vehicle is likely to be travelling faster than the ventilation airflow then have the engine trailing and if the vehicle is slower than the ventilation have it orientated with the engine forward of the driver. By observing these practices or rules exposure to DPM will be kept to a minimum but will not be eliminated altogether. Table 2 demonstrates on vehicle speed and ventilation air velocity over a single travel route, Mine B TG Heading D, for chock shield delivery to the installation face.

Table 2. Data on chock shield carrier speeds and air velocities.

Time	Location	In/Out	Length (m)	Time (min)	Speed (m/s)	Air Vel (m/s)	Air Travel Time (min)
Chock Shield Carrier APS 1306							
09:53	TG 2ct	In	3,400	34	1.66	1.29	43.9
10:27	Face						
Against Air	Machine/Air Relative Velocity =					2.95	
10:31	Face	Out	3,400	26	2.18	1.29	43.9
10:57	TG 2ct						
With Air	Machine/Air Relative Velocity =					0.89	
Chock Shield Carrier CC 1112							
10:12	TG 2ct	In	3,250	28	1.93	1.29	41.9
10:40	TG 36ct						
Against Air	Machine/Air Relative Velocity =					3.22	
10:50	TG 36ct	Out	3,250	17	3.18	1.29	41.9
11:07	TG 2ct						
With Air	Machine/Air Relative Velocity =					1.89	

Points that can be established from Mine B data are as follows.

- In these specific tests chock shield carriers travel at higher average speed than air velocity.
- However on poor roads there could be slower machine travel speed than air velocity.
- The time difference and the peak concentration will depend on the air route, whether the air is travelling with or against the carrier direction, the air velocity as a function of the air quantity and chock shield carriers' travel speeds.
- In theory if the chock shield carrier travels with the air at the same speed as air velocity the peak concentration around the vehicle will be extremely high.
- A possible reduction in DPM driver exposure could have been achieved by consideration of the following.
- TG travel route panel air quantity could be increased.
- Alternatively TG could be re-routed, for instance air into panel up D Heading and return down C Heading.
- Increase in air velocity may result in relative air velocity and vehicle speed being very similar. This is to be avoided if vehicle travels with air as would have happened if vehicles came into the panel up D Heading.

- Best if vehicle travels against airflow direction.
- Best conditions would be achieved if air came into panel up D Heading and returned down C Heading and traffic was in the opposite direction and drove up C and down D Headings. In this configuration vehicles would always travel against air. If the vehicle exhaust outlet trails the driver then exhaust will pass away from the driver in both directions of travel.

2.3 Mine C

Mine C is also a gassy underground longwall mine with mining heights ranging from 4.1 to 4.5 m. Typical longwall panels are 250 m wide using 151 two-leg large and heavy chock shields and about 2500 m to 4000 m long with twin heading gate roads. The majority of diesel vehicles used for the longwall move at Mine C are fitted with exhaust filters. Electric and diesel powered dozers were used in the recovery face to pull chock shields off the face. However, only diesel powered dozers or loaders were used in the installation activities to reposition chock shields to their final positions. Diesel Tag Board systems were used at all major ventilation splits to manage and control diesel exhaust.

In order to assist in pre-planning and optimizing DPM control strategies, real time DPM surveys were undertaken prior to and during the longwall move at Mine C. Outbye DPM levels of the longwall recovery and installation panels were measured and ranged from 0.043 to 0.061 mg/m³. This is about 26% of the "Target Levels" of 0.2 mg/m³ and is within the ranges of normal outbye background levels that have been observed at various longwall mines over the years.

For one of the longwall installation panels observed in Mine C, a total of about 115 m³/s of air was available with 45 m³/s of fresh air was planned to be supplied via a back panel shaft, 30 m³/s from HG mid panel borehole and 40 m³/s from Mains. HG B Heading (Belt Road) and TG A Heading served as returns with 60 m³/s return via HG and 55 m³/s via TG as shown in Figure 4.

A list of possible travel routes for chock shield chariots that could be considered is as follows.

1. Loaded chariots in from TG A Heading and empty chariots out via HG A Heading.
2. Loaded chariots in from HG A Heading and empty chariots out via TG A Heading.
3. Loaded chariots in from HG A Heading and empty chariots out via HG A Heading.
4. Loaded chariots in from TG A Heading and empty chariots out via TG A Heading.

The availability of travel routes for chariots bringing in chock shields into longwall installation panels is subject to conditions of roadways and other activities that need to be undertaken in the roadways. Examples included possible requirements of installing secondary supports in TG roadway prior to longwall panel production commencing. From the viewpoint of the ventilation arrangement, traffic and diesel exhaust dilution; the preferred travel route would follow option number 1. Under this loaded chariots are traveling in from TG A Heading against airflow direction and empty chariots are traveling out via HG A Heading which is against airflow direction as well (as shown in Figure 5). In this option, chariots will be traveling in a loop with no chariots passing each other. While traveling in and out of the panel, chariots will be traveling against the airflow direction which will provide the maximum diesel

exhaust dilutions and reduce the exposure levels of the chariots operators.

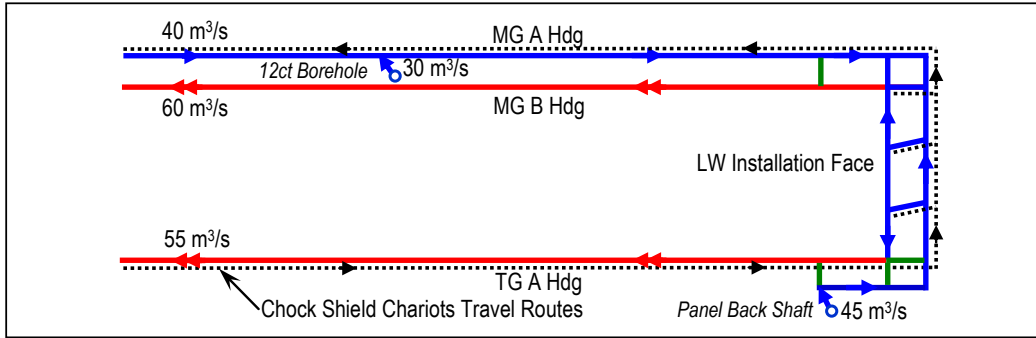


Fig. 4. Proposed ventilation arrangement in longwall installation panel of Mine C.

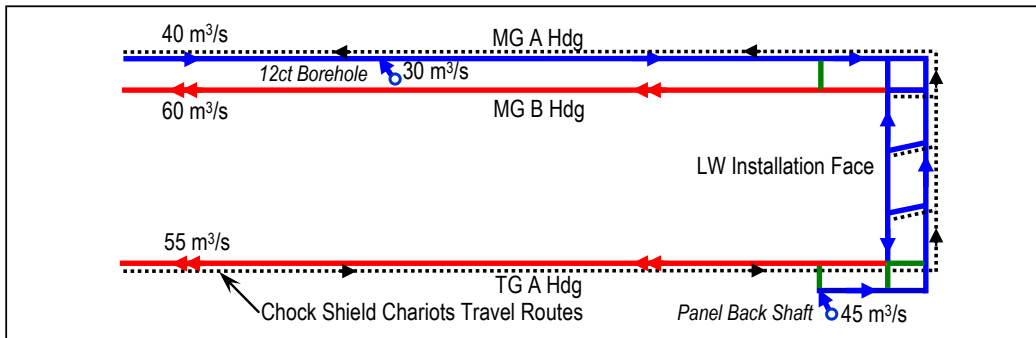


Fig. 5. Possible chariot travel route option No 1.

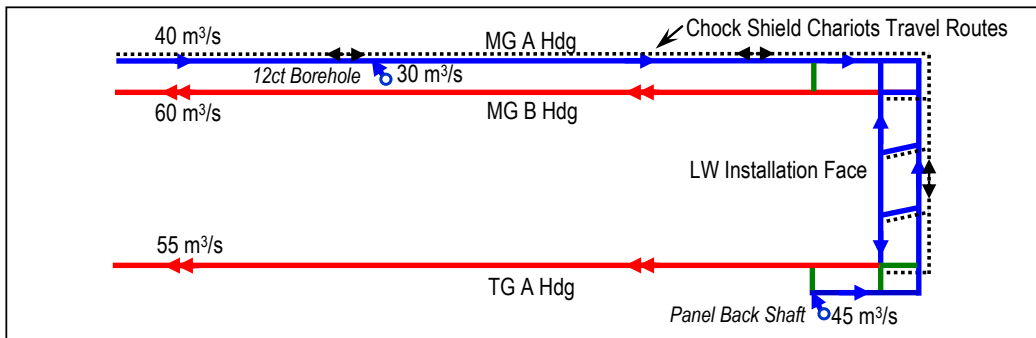


Fig. 6. Possible chariot travel route option No 3.

Possibly highest DPM contaminated air would be in TG A Heading with loaded chariots traveling in. However, this heavily contaminated air would not travel across the face road but exhaust directly into Mains returns. It should be noted that option No 1 and also travel route options, No 2 and No 4 will only be available if the roadway condition of TG A Heading is good enough to allow chariots traffic and there is no need for pre-installation of second supports in the TG A Heading prior to the new longwall production commencing.

If TG A Heading is not available, the only option left for the chariot travel route is option No 3 where loaded chariots traveling in from HG A Heading and empty chariots traveling out also in HG A Heading as shown in Figure 6. In this situation, chariot operators would be subjected to higher DPM exposures when traveling in in HG A Heading as it will travel in the same direction as ventilation airflow. This type of chariot travel route arrangement has been largely adopted in the previous

longwall moves at Mine C due to unavailability of the TG roadway for chariot travel.

As mentioned before the DPM exposure levels of operators will depend on vehicle speeds and air velocities. A large difference between vehicle speed and air velocity will result in lower exposure levels. In this option, the air in HG A Heading should be plentiful and if possible dump some air into HG B Heading before it reaches the installation face. Fresh air from panel back shaft will be less exposure to diesel activity as TG A Heading is not used for traffic in this case. Therefore, it is more favorable to use air from the panel back shaft to sweep across the installation face to provide lower DPM laden air to crew working at the face.

During Mine C longwall move real time DPM monitoring was undertaken over parts of four day shifts. It was found that results from D-PDM unit placed at mid-face of the installation face showed the average DPM levels at this position were only 60% to 75% of the "Target Limits". It was also noticed that at the

installation face crews were positioned working upstream of some hard working heavy diesel units such as ED40 repositioning chock shields and chock shield chariots unloading chock shields. Air quantities and ventilation circuit arrangements at the longwall installation panel appeared sufficient for diluting exhaust from diesel activities taking place during the survey period.

Data from the mine vehicle tracking system recorded for longwall installation panel at Diesel Tag Board location (HG A Heading 1-2ct) was examined as well. These vehicle movements in the travel road (HG A Heading) were plotted against the DPM recorded by D-PDM units and correlations were observed between vehicle movements and recorded DPM levels when possible DPM influence periods of vehicles traveling inbye and outbye were considered. Based on survey results, it was concluded that Diesel control strategies used in Mine C such as optimizing panel ventilation design and arrangement, the use of Diesel Tag Board and fitting exhaust filters for their diesel fleet during the longwall move were effective in reduction of DPM exposure levels of face crews and equipment operators when compared with other mining operations.

3. DPM control strategies during longwall moves

Longwall moves rely on use of high diesel powered equipment of chock shield movers (carriers or chariots) and other diesel powered machines that produces high levels of exhaust of gases and DPM. Many Australian coal mines find it a challenge to meet DPM “Target Limits” during all phases of longwall operational moves.

Over the last 8 years, 24 real time DPM surveys have been undertaken at nine Australian underground longwall mines during their longwall operational moves with 164 DPM sample point measurements identified for background DPM readings from outbye areas, longwall recovery face areas and longwall installation face areas. The following tables give a summary of DPM control strategies and ranges of DPM at various locations applied by these mines during their longwall moves.

Table 3. Summary of DPM controls used at Australian coal mines during longwall moves.

Mine	Type	DPM Control Strategies
A	LW Punch	Diesel tag boards, electric mule at recovery
B	LW	Diesel tag boards
C	LW Punch	Diesel tag boards, electric mule at recovery
D	LW	Diesel tag boards, electric mule at recovery, panel ventilation optimisation, back panel intake shaft
E	LW	Diesel tag boards, electric dozer, ventilation optimisation, panel intake shafts, exhaust filters
F	LW	Diesel tag boards, diesel & electric dozer at installation, back panel exhaust shaft
G	LW	Diesel tag boards, back panel intake boreholes
H	LW	Diesel tag boards, electric mule at recovery face
I	LW	Electric mule at installation, panel ventilation optimisation, back panel exhaust shaft

Approaches adopted in Australian coal mines rely as a first step on both ensuring there is enough air and optimization of the ventilation system design. Issues that should be considered in optimizing the longwall panel ventilation design include:

Table 4. Summary of ranges of DPM levels observed at Australian coal mines during longwall moves.

Mine	Outbye Background		Recovery Panels		Installation Panels	
	No of Samples	Range (mg/m ³)	No of Samples	Range (mg/m ³)	No of Samples	Range (mg/m ³)
A	3	0.020-0.024	2	0.035-0.052	3	0.137-0.176
B	3	0.067-0.103	2	0.175-0.812	5	0.137-0.447
C	0	-	2	0.113-0.121	3	0.119-0.209
D	8	0.057-0.089	9	0.087-0.183	8	0.125-0.583
E	12	0.025-0.099	16	0.118-0.289	24	0.102-0.256
F	0	-	0	-	17	0.136-0.695
G	4	0.037-0.069	8	0.153-0.272	15	0.150-0.409
H	2	0.108-0.126	3	0.160-0.295	5	0.208-1.076
I	2	0.067-0.076	4	0.076-0.289	4	0.190-0.452

- Maximize and maintain face air quantity where chock shield recovery, movement or installation activity is occurring to reduce DPM concentration level through dilution.
- Design panel ventilation arrangements to have all moving machinery (or at least loaded machinery) travelling in the opposite direction to ventilation air flow.
- Where machinery cannot be moved against airflow ensure that air velocity is significantly higher than machine speed to ensure that a plume of exhaust does not hang over the travelling equipment.
- Try to have parallel transport roadways so that movement occurs in a circuit with loaded machines travelling inbye on one road and outbye on a parallel adjacent road.
- Ensure face ventilation is designed in a way that face crews are working upstream of machinery and in particular machinery that is working on faces loading or unloading and positioning chock shields.
- Divide available air so that the majority is passing along the roadways in which loaded machinery travels that has to work hard.

Monitor DPM with real time instruments so that points where “Target” limits are not being met are readily identified and improvements are made during the current longwall move or in planning for the next longwall move. Divide available air so that the majority is passing along the headings in which loaded machinery travels.

Past experiences show that no one simple solution exists in managing and controlling DPM in mine atmosphere. An assessment of exposures to DPM levels in Australian coal mines has found that higher exposures generally occur where there are bad road or wet and difficult conditions, inadequate engine maintenance practices and excessively hardworking engines. Factors which results in lower DPM levels or exposures include use of low sulphur fuel, appropriate engine maintenance programs, positive and careful driving attitudes, good roadway conditions, good approaches to panel ventilation arrangement and control and effective control of diesel powered vehicles in the longwall panel. Reduction in the exposure of underground miners to diesel pollutants

requires the involvement of several key departments of mining companies, including those responsible for health and safety, engine or vehicle maintenance, mine ventilation, and production, as well as the departments responsible for acquiring vehicles, engines, exhaust after treatment systems, fuel, and lubricating oil. Coordination of efforts between various mine departments will need to be coordinated and attention to detail is necessary to sustain successful DPM control strategies.

4. Conclusions

Real time DPM Surveys have been undertaken at various Australian coal mines at points of expected high atmospheric DPM such as during longwall face moves over the last nine years. The paper has closely examined the influence of aspects of the mine ventilation system on underground DPM pollution within the underground mine environment in evaluations of longwall moves. Some observations have been made on the current state of longwall panel ventilation and various DPM control strategies used within the Australian coal mining industry. Issues could be considered in designing longwall panel ventilation arrangements in preparation of longwall moves have been presented.

There have been predictions for many years that mine operations are about to move dramatically towards the provision of a pleasant and comfortable work environment or put another way a mining environment based on quality of life. In the last five years there have been dramatic improvements in many aspects of mine ventilation in a substantial number of both coal and metalliferous mines. Awareness of DPM is receiving much emphasis at present. Newly emerging real time monitors will assist in the enhancement of health and safety within the underground mine environment. Improvements in productivity that result from raising of mine atmosphere quality are the most likely to receive financial priority.

Acknowledgments

The authors wish to acknowledge thanks to Australian coal mines’ personnel who have provided information that has assisted with the progression of this

study. Their efforts ensured that the principal aims of the studies were accomplished and a significant contribution made to future mine health and safety.

References

- [1] A. Gillies and H. Wu, Evaluation of a first mine real time diesel particulate matter (DPM) monitor, Australian Coal Association Research Program Grant C15028, Final Report, April (2008).
- [2] A. Gillies, Real time diesel particulate matter ambient monitoring in underground mines. *Journal of Coal Science and Engineering (China)*, 17(3), pp 225-231 (2011).
- [3] S. Janisko and J.D. Noll, Near real time monitoring of diesel particulate matter in underground mines. In *Proceedings of the 12th US/North American Mine Ventilation Symposium*, pp. 509-513 (2008), Reno, NV, Omnipress.
- [4] J.D. Noll and S. Janisko, Using laser absorption techniques to monitor diesel particulate matter exposure in underground stone mines. *International Society for Optics and Photonics*. In *Optics East* pp 67590 P-67590 (2007).
- [5] Joint Coal Board, Diesel Particulate in Coal Mines (1st Edition) – Questions & Answers. The Joint Coal Board NSW, Australia (1999).
- [6] A. Rogers, Exposure Measurement and Risk estimation from Diesel Particulate Exposures in Underground Coal Mines. Research Project No 20000, Joint Coal Board Health & Safety Trust (2005).
- [7] S. Pratt, A. Grainger, J Todd, G. Meena, A. Rogers and B. Davies, Evaluation and Control of Employee Exposure to Diesel Particulate at Several Australian Coal Mines, *Applied Occupational and Environmental Hygiene Journal* Vol. 12, No. 12, December (1997). Pp. 1032-1037.
- [8] B. Davies and A. Rogers, A guideline for the evaluation and control of diesel particulate in the occupational environment. Australian Institute of Occupational Hygienists, Inc. (2004).
- [9] K. Hedges, F. Djukic, G. Irving and T. Fisher, Diesel Particulate Matter in Underground Mines – Controlling the Risk, *Proceedings AusIMM New Leaders Conference*, 2-3 May (2007).
- [10] D. Dabill, Controlling and Monitoring Exposure to Diesel Engine Exhaust Emissions in Non-Coal Mines, Health and Safety Laboratory Research Report 252 for the UK HSE (2004).
- [11] J. Groves and J. Cain, A Survey of Exposure to Diesel Engine Exhaust Emission in the Workplace, *Ann Occup Hyg*, Vol 44, No 6, pp. 435-447 (2000).
- [12] A. Bugarski, S. Janisko, E. Cauda, J. Noll and S. Mischler, Diesel Aerosols and Gases in Underground Mines: Guide to Exposure Assessment and Control, Report of Investigations 9687, National Institute for Occupational Safety and Health, Pittsburgh, PA (2011).

Real-time monitoring of DPM, airborne Dust and correlating Elemental Carbon measured by two methods in underground mines in USA

Muhammad Usman Khan^a, Argyle Douglas Stewart Gillies^a

^aMissouri University of Science and Technology, Rolla MO, USA

In underground mines Diesel Particulate Matter (DPM) and airborne dust are considered to be the major causes of a large number of occupational diseases [1-3]. Long term and continuous exposure to DPM and respirable dust can result in severe health issues which include respiratory disease, lung cancer, reduced lung capacity and heart disease [1-4]. The US National Institute of Occupational Safety and Health (NIOSH), the US Mine Safety and Health Administration (MSHA) and others are working to improve understanding and measuring techniques for both DPM and mine dust. Most regulations consider shift average based exposure to define and determine Permissible Exposure Limits (PEL) for underground miners as MSHA relies on shift average based measurement for compliance determinations in underground mining. MSHA is currently reducing the shift averaged PEL regulation limit for respirable coal dust from 2.0 to 1.5 mg/m³ with final effect August, 2016. Continuous or real-time monitoring of DPM and dust is vital to gain understanding of fast and frequent changes in the mine atmosphere contamination levels due to the limitations of shift average based measurements. From March 2016 MSHA will require the use of Continuous Personal Dust Monitor (CPDM) to measure real-time respirable dust exposure under certain circumstances. Real-time monitors quantify the level of pollutants in the mine air and allow the implementation of control strategies at the time of high exposure. Real-time monitoring provides insights into the mine environment during different mine activities. The current study focuses on determinations of DPM and respirable dust levels in underground mines in the USA. The Personal Dust Monitor (PDM) was used for real-time dust determination whereas real-time DPM was measured by FLIR Airtec monitors. The shift average DPM level was determined by the NIOSH 5040 method. The relationship between shift average based Elemental Carbon (EC) from real-time and shift average instrumentation was established.

Keywords: Diesel particulate matter, Respirable dust, Permissible exposure limit, Pollutants, Personal dust monitor.

1. Introduction

Ventilation is a critical aspect of underground mining. The ventilation network in many modern mines changes as development is extended. Maintaining an understanding of the ventilation network is a big challenge for the ventilation engineer. An important task of underground mine ventilation engineer is to provide a clean and sufficient quantity of air. In most of non-gassy underground mines DPM and dust are the important sources of air pollution. Limitations involved with shift average measurement methods have promoted the concept of real-time monitoring of mine atmosphere. Continuous monitoring of dust and DPM is vital in understanding frequent changes in the mine atmosphere. Instrumentation development is allowing improved real-time monitoring of ventilation parameters with particular emphasis on gases, respirable dust, and DPM. Ventilation expenditure can also affect mine production as comfortable and pleasant work environments could return in increased miner productivity.

This paper principally focuses on the monitoring of dust and DPM in underground mines in the USA. Dust and

DPM measurements were taken in both metal and nonmetal mines. The personal dust monitor was used for continuous dust determinations. Real-time graphs of the dust concentrations were plotted during various mining activities. DPM was measured by two types of equipment. The FLIR Airtec DPM monitor was used to measure real-time component of DPM and SKC air sampling pumps were used for measuring MSHA approved NIOSH 5040 shift average DPM levels. The Airtec monitor also provides the time weighted average (TWA) value of elemental carbon. In order to compare DPM results using real-time monitoring with the NIOSH 5040 method approach both instruments were installed side by side at each measuring station. DPM samples were collected during performing various activities and the results from both measurement approaches were analyzed. A correlation equation was developed between shift average EC content measured by the two methods discussed and a very good correlation coefficient was obtained.

2. Respirable Dust Monitoring

The International Standardization Organization (ISO) describes dust as small solid particles which settle out under their own weight but which may remain suspended for some time [4]. Dust particles are usually in the size range from about 1 to 100 μm diameter and settle slowly under the influence of gravity [5]. However, in referring to particle size of airborne dust, the term "particle diameter" alone is an over simplification, since the geometric dimensions of a particle do not fully explain how it behaves in its airborne state [6]. Therefore, the most appropriate measure of particle size for many occupational hygiene situations is particle aerodynamic diameter. This can be defined as "the diameter of a hypothetical sphere of density 1 g/cm³ having the same terminal settling velocity in calm air as the particle in question, regardless of its geometric size, shape and true density" [4].

Miners are exposed to high level of mine dust and there are several factors which influence the effects of inhaled dust particles. Particle size is usually the critical factor that largely determines approximately where in the respiratory tract that particle may be deposited [4]. The settling of dust in the lungs could be increased by acute dust exposures and deep breaths. Miners suffer from a variety of illnesses caused by inhaled dust during work activities. For practical purposes some types of lung diseases caused by the inhalation and deposition of mineral dusts in the lungs are covered by the general term "pneumoconiosis." This term simply means "dusty lung [7]."

2.1 Personal Dust Monitor (PDM)

The PDM is a respirable dust sampler and a gravimetric equivalent analysis instrument. The main components of the device include a cap lamp and sample inlet located on the end of an umbilical cord, a belt-mounted enclosure containing the respirable dust cyclone, sampling, and mass measurement systems, and a charging and communication module used to transmit data between the monitor and a computer. The PDM gives real-time readings. The monitor internally measures the particle mass collected on its filter and results do not exhibit the same sensitivity to water spray droplets as optically based approaches [8-9]. The technology that forms the heart of the PDM is unique. It collects suspended particles on a filter while simultaneously determining the accumulated mass. The technique achieves microgram level mass resolution even in the hostile mine environment. The PDM is currently being adopted for statutory mine respirable dust determinations in the USA. By using this device miners and mine operators have the ability to view both cumulative and projected end-of-shift mass concentration values, as well as a short term 5, 15 or 30 minutes running averages. The instrument has particular application for determining high dust source locations and efficiency of engineering means of suppression and other approaches to

handling the mine dust. Being a personal dust monitor, the instrument measures the airborne dust from the breathing zone, so it has many advantages over instruments which measure from a fixed-point locations. It is also believed to be the first personal dust monitor instrument that reliably delivers a real-time reading [8]. The PDM is shown in Figure 1 below.



Figure 1. Personal Dust Monitor

2.1 Monitoring in Metal Mines

2.2.1 Measurement during mucking

As an illustration of the use of the PDM, dust sampling was conducted in a metal mine entry during normal mine operations. The PDM was placed in a particular mine entry during mucking activity over about six hours. The peak dust value based on 15 minutes concentration was 3.1 mg/m³ whereas, based on 30 minutes concentration the peak recorded value was 3.0 mg/m³. During monitoring over a shift, records were made of more than sixty diesel operated equipment units by maintaining a vehicle log at the recording passage. In the beginning of an activity the dust concentration was low, with the passage of time it started accumulating in the mine entry due to the less air flow at the face the concentration finally reached to its peak value at about 10:50am. From 10:55am to 11:55 am there was a gap in the activity which was followed by decrease in dust. This decrease in dust concentration can be seen in Figure 2. High dust concentration was observed with high vehicle frequency as initially four haul trucks were involved in dumping, after the gap one dumper was removed and only three dumpers were left for mucking. The dust concentration started accumulating again and it can be seen in Figure 2. Both 15 and 30 minutes dust concentrations were plotted against time and the graphs are shown in Figure 2.

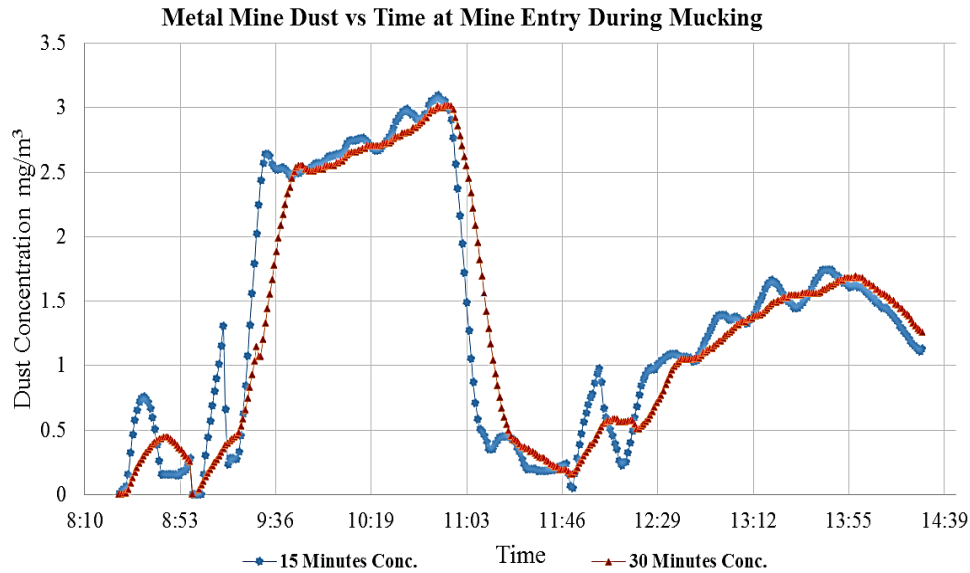


Fig 2. Real-time measured dust concentrations versus time over 15 and 30 minutes

2.2.2 Measurement at the face during loading

Another dust sample was collected in a metal mine. The PDM was hung at the face during loading operation where a front end loader (FEL) was loading the dumpers. One front end loader and three dumpers were involved in the activity. Total monitoring period was five hours and thirty minutes. This monitoring time includes a 90 minutes idle time (break time) near the middle. During the idle time the dust concentration was reduced, that reduction could be

observed in Figure 3. The peak recorded dust value based on 15 minutes concentration was 3.0 mg/m³ whereas based on 30 minutes concentration the peak recorded value was 2.9 mg/m³. The 30 minutes dust concentration graph is more consistent as compared to dust concentrations recorded at 15 minutes interval. During monitoring period forty dumpers were loaded by the FEL. Both 15 and 30 minutes dust concentrations were plotted against time. The real-time dust concentration graph is shown in the Figure 3 below.

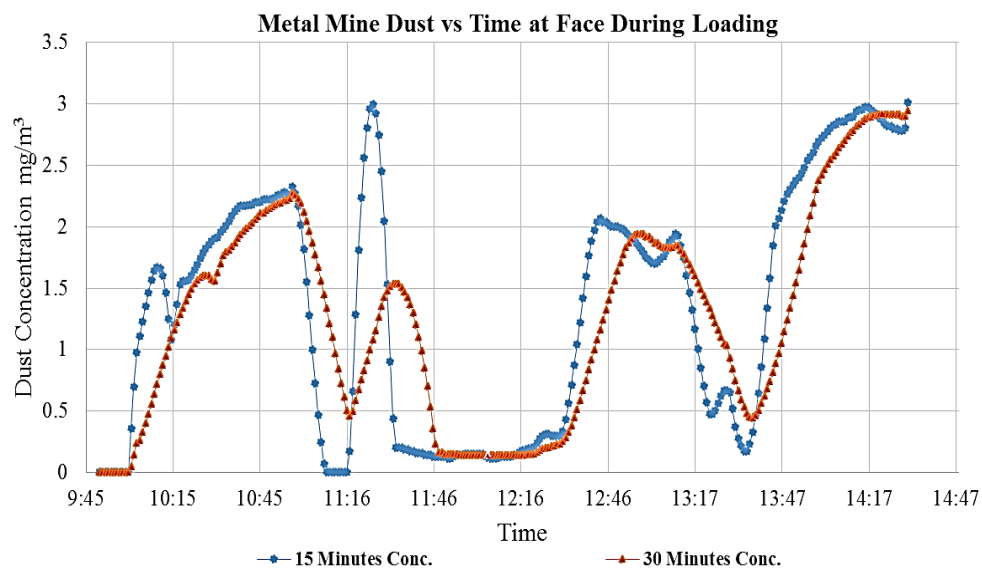


Fig 3. Real-time measured dust concentrations versus time over 15 and 30 minutes

2.2.3 Measurement during face drilling

Dust sample was also collected during drilling operation in another metal mine. The PDM was installed at the mine face where a 224kW jumbo drill was operating. Monitoring period was five hours and thirty minutes. The recorded peak dust value based on 15 minutes concentration was 2.9 mg/m³ and based on 30 minutes concentration the peak recorded value was 2.7 mg/m³. During the monitoring period all additional activities of vehicles or machinery in

the area of monitoring were observed and noted. One 97 kW diesel powered hydraulic mechanical scalar was also working during the whole monitoring time period at another face in a nearby entry. Low dust values were recorded at commencement of monitoring. At the face the air velocity was quite low so the dust started accumulating at the face with time. Both 15 and 30 minutes dust concentrations were plotted against time. The real-time graph of dust concentration is shown in Figure 4.

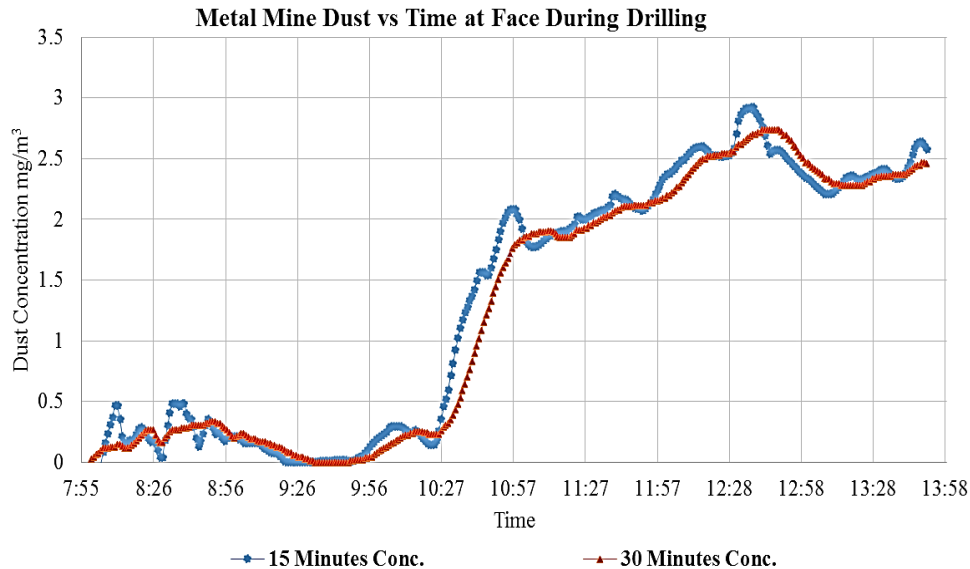


Fig 4. Real-time measured dust concentrations versus time over 15 and 30 minutes

2.3 Monitoring at Nonmetal Mine

2.3.1 Measurement in conveyor belt entry

Dust sampling was performed in a nonmetal mine entry of a long wall operation. PDM was installed in the conveyor belt entry. Monitoring continued for about eight hours. The peak dust value based on 15 and 30 minutes concentrations were 7.0

mg/m³ and 6.4 mg/m³ respectively. The belt was not in operation in the beginning of measurement so no dust concentration was recorded. The belt started at 9:45am and an exponential increase in dust concentration can be seen in Figure 5. The real-time dust concentrations for complete monitoring time is shown below in Figure 5.

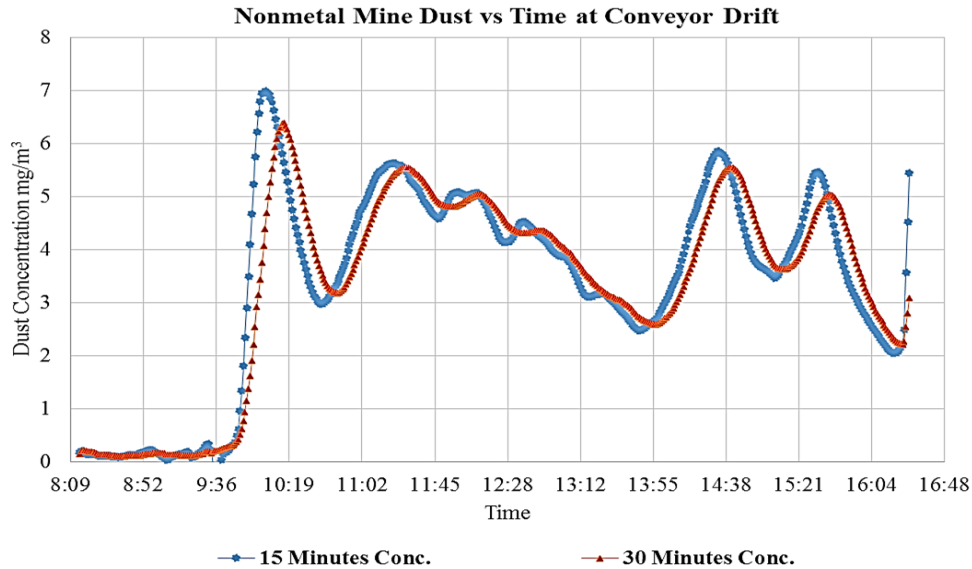


Fig 5. Real-time dust concentrations versus time over 15 and 30 minutes

3. Diesel Particulate Matter Monitoring

Diesel equipment has the ability to convert a large fraction of available energy into useable work. The diesel engine's high efficiency, ruggedness, economical operation and ease of maintenance makes it an attractive option for use in underground mines. It is very common for diesel engines in heavy duty trucks to have a life of 1,600,000 km [10]. Generally diesel equipment provides good maneuverability in underground mining operations. Diesel powered equipment offers more flexibility as compared to other available options, which makes it the first choice of underground mine operators. The underground mining industry is very likely to maintain its reliance on diesel powered equipment keeping in mind the recent developments in other energy alternatives [11].

Use of Diesel fuel is harmful to humans. Diesel particles are very small in size. The size of diesel particles is generally one order of magnitude smaller than the respirable dust aerosols in underground mines and predominantly less than one micron [12]. Force of gravity has less effect on DPM due to its small particle size. The phenomenon of less gravitational attraction increases the settling and residence time of DPM in the mine atmospheres. High residence time of DPM as compared to other mechanically generated particles increases its chances of deposition in the human respiratory tract. The small sized diesel aerosols penetrate deeply into regions of the human lung [13], which increase the health risks associated with long term exposure to diesel aerosols. Published studies documented the

adverse health effects of DPM exposure [14]. The NIOSH regarded diesel exhaust as carcinogenic and continuous and long term DPM exposure can result in several other occupational diseases including respiratory disease, reduced lung capacity, and heart disease. NIOSH also declared that the reductions in DPM exposure would reduce cancer risks [15].

DPM measurement is a challenging task and it is becoming a matter of serious concern due to the harmful health effects linked with the exposure of DPM. DPM is mainly composed of EC, Organic Carbon (OC) and Inorganics [16]. EC constitutes a large fraction of the diesel particulate mass and it can be used as a measure of DPM [17]. The NIOSH 5040 method is an established technique for measuring DPM and it can quantify DPM even at very low concentrations. MSHA employs NIOSH 5040 DPM sampling for compliance purpose in mines. The NIOSH 5040 sampling method requires that an exposure sample should be submitted to a laboratory for analysis. This process fundamentally involves a significant time lag before an accurate exposure determination can be made and during which time miners are potentially overexposed to airborne levels of DPM [9]. The issue of lag time can be addressed by using real-time DPM monitors. Various real-time DPM monitors are used in the mining industry [18, 19].

3.1 Results of DPM Monitoring

DPM data has been collected from different metal and nonmetal mines by employing two

different measuring methods, namely real-time and shift average method. The Airtec monitor which was used for real-time monitoring also provided shift averaged elemental carbon concentration measurements. The EC component of NIOSH 5040 method measurements were correlated with shift averaged EC values obtained from the Airtec monitors (Figure 6). A correlation equation with a very good value of coefficient of determination (R^2) was established. The developed correlation equation (I) is given as:

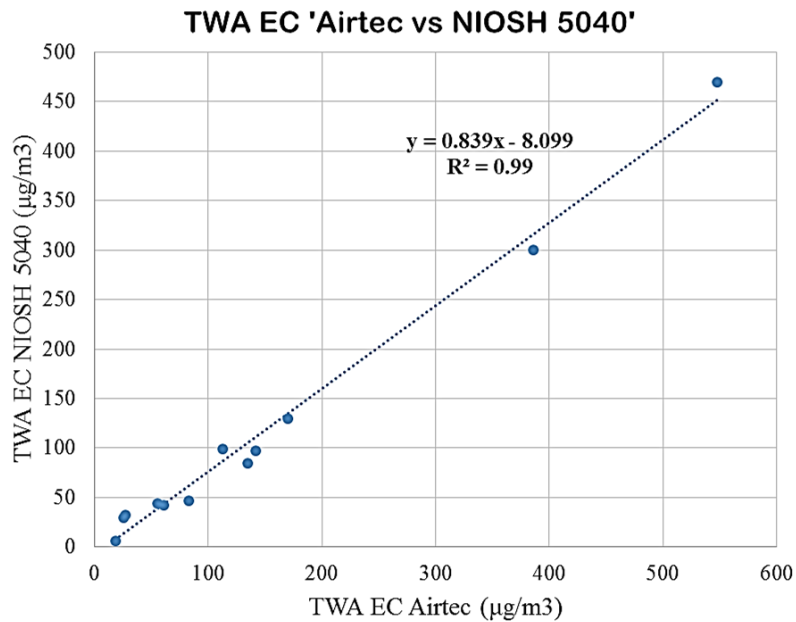
$$y = 0.839x - 8.099 \quad (I)$$

$$R^2 = 0.99$$

Where:

y = EC by NIOSH 5040 ($\mu\text{g}/\text{m}^3$)

x = EC by Airtec monitor ($\mu\text{g}/\text{m}^3$)



• TWA EC Airtec vs NIOSH 5040 Linear (TWA EC Airtec vs NIOSH 5040)

Fig 6. Correlation between shift average EC by Airtec and NIOSH 5040 method

4. Summary and Conclusions

Real-time monitoring of mine air pollutants is becoming popular in the mining industry as it allows the efficient implementation of dust and DPM control strategies. Real-time monitoring often highlights mine situations where the concentration of pollutants is relatively high for short but significant time periods. Relatively new and emerging real-time techniques were used for the determination of dust and DPM concentrations in metal and nonmetal mines in USA.

Higher dust concentrations were observed in a nonmetal mine as compared to the metal mines and belt conveyor was identified as the main source of dust in a nonmetal mine. The results of this study indicated that the TWA EC concentrations obtained

by the Airtec monitor were usually higher than the TWA EC concentrations obtained by NIOSH 5040 method.

A correlation equation was developed between shift average EC content measured by both, real-time and NIOSH 5040 methods. The established relationship could assist in the estimation of NIOSH 5040 EC content by using shift averaged EC concentration obtained from the Airtec monitor. The equation (I) could be used as a tool for determining the miners' DPM overexposures in metal and nonmetal mines, and it will also help in implementing the DPM control measures right at the time of high DPM concentrations in underground mine atmospheres. The correlation equation (I) may not be applicable to the coal mines because of environmental interferences.

5. Acknowledgement

The authors wish to acknowledge the Saudi Mining Polytechnic (SMP) institute for funding support, the University of Engineering and Technology, Lahore, Pakistan, the student participants from Missouri University of Science & Technology, Rolla, MO, USA, and the mines in US mining industry which participated in dust and DPM survey.

References

- [1] Federal Register, Department of Labor, Mine Safety and Health Administration, 30CFR part 57.
<http://www.msha.gov/REGS/FEDREG/FINAL/2006final/06-04497.pdf>, Web. 30 May 2015
- [2] Disease and Illness in U.S. Mining 1983-2001
<http://www.cdc.gov/niosh/mining/UserFiles/works/pdfs/daiiu.pdf>, May 30 2015.
- [3] Health Effects of Overexposure to Respirable silica dust.
<http://www.cdc.gov/niosh/mining/UserFiles/workshops/silicaMNM2010/1-Colinet-HealthEffects.pdf>, May 30 2015.
- [4] World Health Organization, Hazard prevention and control in the work environment: airborne dust, 1999.
- [5] Characterization of Air Quality. Glossary., ISO 4225-1994
- [6] Glossary of Atmospheric Chemistry Terms, 1990
<http://pac.iupac.org/publications/pac/pdf/1990/pdf/6211x2167.pdf>, June 7 2015.
- [7] A. D. Raed, J. M. Peter, Occupational Lung Disease.
<http://www.clevelandclinicmeded.com/medicalpubs/diseasemanagement/pulmonary/occupational-lung-disease/Default.htm>, May 30 2015.
- [8] A.D.S. Gillies, and H.W. Wu., Underground atmosphere realtime personal respirable dust and diesel particulate matter direct monitoring, 2008.
- [9] A.D.S. Gillies, The Magnitude of Diesel Particulate Matter in Underground Mine Workings: Advances in Real-Time Monitoring, 9th International Mine Ventilation Congress, 2009.
- [10] Anon, Diesel Emission Control Strategies Available to the Underground Mining Industry, ESI International, 1999.
- [11] Anon., Federal Register, Vol.66, No. 13, MSHA, 2001a.
- [12] D. B. Kittelson, Engines and nanoparticles: a review, *Journal of Aerosol Science*, 1998.
- [13] L. Morawska et al., Experimental Study of the Deposition of Combustion Aerosols in the Human Respiratory Tract, *Aerosol Sci*, 2005.
- [14] M.P. Walsh, Global trends in diesel emissions control-A 1999 update, No. 1999-01-0107. SAE Technical Paper, 1999.
- [15] National Institute of Occupational Safety and Health, Carcinogenic Effects of Exposure to Diesel Exhaust, CIB 50, 1988.
- [16] H.W. Wu and A.D.S. Gillies, Developments in Real Time Personal Diesel Particulate Monitoring in Mines, Proceedings of 12th US Mine Ventilation Symposium, 2008.
- [17] J.D. Noll et al., Relationship between elemental carbon, total carbon, and diesel particulate matter in several underground metal/non-metal mines, *Environmental science & technology*, 2007.
- [18] M.U. Khan and A.D.S. Gillies, Realtime Diesel Particulate Matter Monitoring in U.S. Underground Mines, SME Conference Proceedings 2015.
- [19] A.D.S. Gillies et al., Comparison of Diesel Particulate Matter Ambient Monitoring Practices in Underground Mines in Australia, the United States and South Africa, 10th International Mine Ventilation Congress, 2014.

DPM Monitoring in Underground Metal/Nonmetal Mines

E. McCullough^a, L. Rojas-Mendoza^a, E. Sarver^{a,*}

^a Virginia Polytechnic Institute and State University, Department of Mining and Minerals, Blacksburg, VA 24060, USA

The metal and nonmetal mining industries face increasingly stringent regulations regarding worker exposures to airborne particulates, including diesel particulate matter (DPM). Although significant progress has been achieved in reducing DPM exposures, mine operators still struggle to comply under a variety of conditions – particularly in large-opening mines where ventilation is challenging. One major issue in such environments is the inability to easily monitor DPM trends over long periods of time to determine factors influencing its buildup in areas of interest, as well as its response to mitigation strategies. At present, DPM measurements are limited to the NIOSH 5040 method (i.e., filter collection and external analysis) and the handheld Airtec DPM monitor (FLIR Systems, Inc., Albuquerque, NM), which provides quasi-real time data over relatively short time periods.

To transform the Airtec device to an autonomous area-monitoring unit, its basic components were modified by Nomadics, Inc. under NIOSH contract number 200-2010-36901. This resulted in a prototyped unit called the Airwatch DPM monitor, which does not require frequent filter replacement or battery re-charging; networking capabilities to connect multiple monitors were also achieved. While the prototyped monitor was successfully lab tested, field-testing was limited to just a few days underground. Further testing is needed to fully evaluate the monitor and ready it for commercial availability. Under a new Capacity Building in Ventilation project at Virginia Tech (CDC/NIOSH contract no. 200-2014-59646), we aim to demonstrate the capability of the Airwatch DPM monitor in high-priority areas of a stone mine over relatively long-term periods – and then use the monitors to investigate DPM response to ventilation conditions.

Keywords: Diesel Particulate Matter, Metal/non-Metal, Monitoring

1. Introduction

Diesel exhaust represents a ubiquitous occupational hazard in underground mine environments. The exhaust is a highly complex mixture of diesel particulate matter (DPM) and hydrocarbon gasses [1]. Since there is no technologically proven way to measure DPM directly, it is often quantified using elemental carbon (EC) measurements. [2]. Elemental carbon accounts for 23-100% of DPM, and is not generally affected by environmental interferences [3,4]. Historically, total carbon (TC) analysis was used which typically comprises over 80% of DPM [1]. TC is defined as the summation of elemental carbon and organic carbon (OC). However, cigarette smoke and mineral dust can interfere with TC readings, which has sometimes caused DPM measurements to report artificially high values [3].

DPM has a variable particulate size distribution. Particles are created within the micron and sub-micron scales [5]. Idealized size distribution is trimodal and related lognormally [1]. The smallest particulate mode is called the nuclei mode, which has particles diameters ranging from about 0.005 to 0.05 μ m. This mode represents less than 20% of DPM by mass, but greater than 90% of DPM by particle count [1]. Most DPM particulate mass is represented in the accumulation mode, with particle diameters on the order of about 0.05 to 1.0 μ m. The coarse mode represents particles with diameters greater than 1 μ m. All particles sizes are capable of suspension in air, and DPM is prone to clustering and reacting with other atmospheric components while suspended [1]. Such reactions may create synergies that are harmful to human health. DPM exposure in U.S. underground mines is regulated by the Mine Safety and Health Administration (MSHA). MSHA issued its Final Rule on DPM metal and nonmetal mine environments under 30 CFR Part 57 in 2008, mandating that a miner's personal exposure limit (PEL) to DPM cannot exceed 160 μ g/m³ of TC during an eight-hour work shift. MSHA requires that the standard National Institute for Occupational Safety and Health

(NIOSH) 5040 Method be used to measure DPM exposures to determine compliance [4]. This method employs a thermo-optical technique to analyze carbon particles in air samples collected on a 37 mm quartz fiber filter. It should be noted that this technique quantitates TC (by direct quantitation of EC and OC) or requires a site-specific conversion factor to convert EC into a TC equivalent [6,7]. These values should then be adjusted to an eight-hour time-weighted average.

1.1 DPM and Human Health

Underground miners are disproportionately exposed to DPM-related occupational hazards because heavy diesel-powered equipment runs regularly in tight spaces, with variable ventilation conditions. In spaces where airflow is limited, DPM does not disperse well, and due to its size can remain suspended in the air. Reported DPM concentrations in underground mine settings can be on the order of ten times higher than levels found in some other industrial settings, and more than 100 times higher than levels observed in urban areas [1]. NIOSH estimated in 2008 that 34,000 underground miners were at risk of exposure to DPM [1]. Human exposure to DPM presents many potential health complications. NIOSH estimated in 2008 that 34,000 underground miners were at risk of exposure to DPM [1]. Approximately 60,000 deaths in the United States per year are attributed to fine particulate exposure. Of these deaths, 21,000 are believed to be from DPM in particular [5]. The Clean Air Task Force reports that the estimated annual economic cost of particulate-related illness and death in the USA was \$139 billion [8]. Clearly, the social and economic impact caused by particulate-related illnesses should not go unaddressed.

2. DPM Monitoring

As noted above, for demonstrating compliance with DPM exposure limits in underground metal and

*Corresponding author: esarver@vt.edu

nonmetal mines, the NIOSH 5040 method must be used. While this method provides an accurate measurement of EC and OC concentrations (which can be translated into TC as proxy for DPM) over the short duration of sample collection, it is intended for determining personal exposures. Thus, it does not provide the ability to easily monitor DPM over long periods of time. For understanding DPM trends in the context of mine operation, and therefore mitigating exposure risks, monitoring capabilities are indeed critical. Recognizing this fact, a handheld, quasi real-time DPM monitor called the Airtec (FLIR Systems, Inc., Albuquerque, NM) was developed in collaboration with NIOSH. The Airtec is now commercially available as an engineering tool for mine operators. Another device, the Airwatch, has recently been prototyped. It is intended to meet the need for autonomous area monitoring, but is not yet ready for commercialization.

The following sections describe these three DPM monitoring options for underground metal and nonmetal mines, and their key characteristics are summarized in Table 1.

2.1 NIOSH 5040 Method

The most up to date version of the NIOSH 5040 method was published in 2003 [6]. The method incorporates thermo-optical analysis because of its selectivity and flexibility (e.g. can run manually and is programmable). The instrument was specifically developed for analysis of carbon-based aerosols (e.g., DPM) and is manufactured by Sunset Laboratories, Inc. (Tigard, OR). In general, the thermal analysis is completed in two phases. First, the sample is placed in an oven and heated to 850°C in inert atmosphere, causing the OC to become catalytically oxidized. This forms carbon dioxide, which can then be reduced to methane. The methane is then measured using a flame ionization detector (FID) [9]. Next, the sample is reheated up to about 900°C in an oxygen-rich atmosphere, such that the EC is also oxidized; again, the resulting carbon dioxide is reduced to methane, which is measured by FID. Since some char is produced by the OC during the first phase, which will oxidize in the second phase, the analyzer must also determine how much methane in the second phase is attributable to OC vs. EC. For this, it contains a pulsed diode laser and photodetector to monitor the sample for transmission of light. Effectively, once the transmittance is seen to increase (i.e., char production in first phase) and then decrease back to its original value (i.e., char oxidation in the second phase), all subsequent methane production is attributed to EC. For this optical analysis, the instrument requires a portion of the sample filter wider than the diameter of the laser [10,11].

To collect DPM samples for analysis by the 5040 method, a field sampling apparatus is used which consists of a small air pump, and a 37 mm quartz fiber filter that is held inside a plastic cassette. Often a device for removing relatively large particles from the DPM-laden airflow is also placed inline before the sample filter; generally, the oversized particles (i.e., > 0.8µm) are removed via an impactor filter. By using a size-selective sampler, airborne dust (i.e., which may include carbon-containing particles) is prevented from collecting on the DPM filter and creating a sample matrix interference for the analytical method [2]. When the impactor becomes full, DPM capture is no longer

efficient and the impactor must be replaced. SKC manufactures an all-in-one DPM cassette, which contains an impactor and quartz fiber DPM filter [12]. In very dusty environments, a cyclone may also be placed inline before the sampling cassette to exclude relatively large (i.e., > 5µm) particles before air reaches the impactor.

In an earlier design, the SKC DPM cassette was observed by Noll et al. to be problematic [2]. Specifically, DPM deposition on the filters was not uniform in regards to the surface area (i.e., surface areas over which DPM deposited were irregular and varied between cassettes.) Uniform deposition is critical for accurate calculation of aerosol EC, and then TC, concentrations since only a fraction of the filter is analyzed and must be assumed representative: the 5040-quantitated EC and TC masses are effectively converted to concentration values based on the fraction of sample surface area analyzed, the sampling time and the flowrate [2]. Once modification was made to improve the cassette design, they were determined to provide reliable measurements in laboratory and field environments [2].

Following promulgation of DPM rules in underground mines, the NIOSH 5040 method has provided a means for gathering a wealth of information, particularly about personal exposures; and improvements in the mine environment have undoubtedly resulted. However, this method, it is not a particularly practical engineering tool for mine operators aiming to conduct routine monitoring of DPM. Collected samples must be mailed to only a handful of equipped laboratories to perform the required analysis, which makes collecting results quite time consuming [5] – not to mention expensive. One test costs approximately \$100 for supplies and analysis, and this figure does not include mine labor [5]. Moreover, the lag period between sample collection and analysis makes it difficult to both recognize the conditions leading to overexposures and to gage the effectiveness of attempted DPM control mechanisms.

Beyond the issue with significant lag time between sample collection and result reporting, 5040 method results are also limited because they are associated with bulk samples (i.e., the final result is a time-weighted average concentration). This means that particular time segments within the sampling period cannot be isolated [5]. It would be helpful for mine operators to determine when peak exposures of DPM occur, ideally in real time, so that they can adjust ventilation controls accordingly.

2.2 In-mine DPM Monitoring

To address the need for in-mine monitoring, the Airtec DPM Monitor was developed. It is a handheld device and displays EC concentrations on a running 15-minute average – quasi real-time. The instrument meets NIOSH accuracy criteria and provides results with no statistical difference from the 5040 method [13]. It measures EC using a laser extinction technique, which works because EC concentrations are related to laser absorption [13]. The laser extinction is measured directly on a filter as it collects DPM, which is ideal for a small, portable device.

Mine operators may use the Airtec to “spot” check areas of interest in order to identify high DPM contributing sources, and also to evaluate personal

exposures to DPM. It has proven particularly useful for monitoring DPM in equipment cabs because it is not influenced by instantaneous pressure changes, such as those caused by opening and closing doors [7]. Researchers at NIOSH have observed that the Airtec is sensitive to cigarette smoke and will register it as a DPM reading [7], and so users should be aware of this potential for false-positive readings and not smoke while the monitor is being used. Being able to monitor DPM in near real-time allows mine operators to identify when levels are nearing compliance limits, as well as evaluate the effectiveness of engineering controls to abate it.

Functionally, the Airtec monitor has three main parts: a small air pump, a plastic cassette that holds a filter onto which DPM is collected, and a laser and sensor pair. As the DPM is collected, the laser is directed toward the filter and the sensor detects how much of the laser becomes blocked by EC (a primary component of DPM). The laser becomes increasingly “extinct” as more DPM is collected, and thus an effective measurement of EC is obtained. As is often the case with filter samples collected for the 5040 method, the Airtec can also use an impactor to keep dust from entering the device and depositing on the filter. (Previously, a “sharp cut” cyclone was also commercially available that could effectively remove particles > 0.8µm, but this model of cyclone is not being manufactured anymore.)

While the Airtec has afforded significant monitoring capabilities to mine operators, a new device developed under NIOSH contract number 200-2010-36901 called

the Airwatch DPM Monitor may provide even more utility in the way of long-term area monitoring. The Airwatch is currently in the prototype and demonstration phases. It is technologically similar to the Airtec, but includes several modifications that allow the device to operate autonomously over long periods of time. Most importantly, it can run on mine power (i.e., instead of batteries) and does not require frequent user attention or maintenance. The latter is possible because the Airwatch uses a self-advancing filter tape on which the DPM is collected [14]. The tape is similar in form to an audio or VHS cassette tape, wherein the clean filter media is rolled around one cylinder from one end and attached to another cylinder on the other end. DPM is collected via an air pump and deposited on a small area of tape between the two cylinders. Here, a laser and sensor pair similar to those used in the Airtec units is employed to track laser extinction, which can again be related to EC collected on the filter tape. When a given filter area is completely used (i.e., laser extinction is sufficiently high), the tape progresses forward to expose a clean area of filter to the laser and sensor. The exact life of this filter tape depends on the sampling environment and monitoring setup (i.e., concentration of DPM in the air, and frequency at which the Airwatch is programmed to collect data.) To avoid interference in laser extinction from dust particles, a sharp-cut cyclone is employed to prevent dust particles from depositing on the filter. As opposed to an impactor for this purpose, the cyclone does not need frequent replacement

Table 1. DPM Monitoring Options

Method	Analytical Technique	Primary Applications	Availability of Results	Sampling Unit
5040 Method	Thermo-optical with FID (quantitates EC and OC)	Personal exposures (required for compliance), short-term area monitoring	Lag time (days to weeks)	Portable
Airtec Monitor	Laser extinction (quantitates EC)	Personal exposures, short-term area monitoring, spot-checking	Quasi real-time	Portable
Airwatch Monitor	Laser extinction (quantitates EC)	Long-term, autonomous area monitoring, networking capabilities	Quasi real-time	Stationary

In its current design, the Airwatch can be programmed to transmit data to remote monitoring stations via hardwires (i.e., Ethernet or 4-20mA). Since a current-based signal is used, the signal transmitted does not degrade over distance. Where available, mining operations could certainly benefit from real-time DPM information that can be transferred quickly over wireless networks, and this capability is also envisioned for the Airwatch monitor. Long-term, operators might be able to

centrally process data and automatically incorporate them into other systems or decision-making schemes to alter mine parameters, such as ventilation [15]. Although the Airwatch has been successfully tested in the laboratory, extensive field testing has not been conducted to date

3. Research Approach

Under a new Capacity Building in Ventilation project sponsored by CDC/NIOSH through the Office of Mine Safety and Health Research (contract no. 200-2014-59646), the Airwatch technology will be demonstrated in an underground mining environment, and ultimately employed to monitor DPM under different ventilation scenarios.

The focus environment for this project is the large-opening mine. These mines experience airflow quantities so low that they are sometimes immeasurable with conventional equipment. In many, ventilation techniques are currently being employed to control DPM but they are still highly experimental, using trial-and-error approaches to gauge effectiveness [16]. These are notably costly, time-consuming, and less than optimal in terms of DPM control – certainly far from ideal. Some mines do not even have forced-ventilation systems in place. Rather, they depend on natural ventilation, which is uncontrolled and unreliable due to seasonal variations in temperatures that drive the movement of air [16]. Only a few research studies have been conducted regarding DPM in large-opening mines (e.g., see 16-18), but it is clear that effective, data-driven ventilation improvements require enhanced DPM monitoring networks.

3.1 Project and Task Description

Two main objectives related to DPM monitoring and ventilation have been established for this project: 1) to demonstrate the capability of the prototyped Airwatch devices to autonomously monitor DPM in high-priority areas of a study mine and 2) to determine DPM response to ventilation conditions in various areas of the mine. Work began during late 2014 and will be developed over the remainder of the five-year project. Table 2 displays the tasks that will be undertaken in order to fulfill the project objectives.

3.3 Progress to Date

Work is proceeding in cooperation with an industry partner (an underground stone mine) and to date, there has been progress towards Tasks 1 and 2. For Task 1, due to the very low air velocities in the study mine, it will be necessary to use an ultrasonic anemometer to collect accurate data. A UA6 (TSI Incorporated, Shoreview, MN) is currently being lab-tested and will be employed for spot ventilation surveys. The ventilation

data will be collected in concert with DPM data using the Airtec monitor. Survey points will be chosen together with the mine operator. A customized DPM cassette, designed and 3D-printed by NIOSH, will be used to reduce the DPM deposition area on the filters. This will effectively reduce the total surface area of the DPM filter so that the Airtec unit is much more sensitive and can provide faster EC readings (versus the 15-minute minimum sampling time that is normally required).

For Task 2, upgraded Airwatch monitors have been built (on a separate NIOSH contract). The new units have been modified to make them more rugged and user friendly. Comparative measurements are planned whereby the Airwatch and Airtec units will be employed simultaneously. Moreover, work is currently underway to design self-contained monitoring stations that couple a 2-axis ultrasonic anemometer that logs data cooperatively with an Airwatch unit to track air velocity. This future work will help determine how DPM responds to ventilation controls. Due to environmental conditions, the datalogger should be stowed inside some type of moisture-proof enclosure to protect it from atmospheric conditions.

4. Impact

Despite significant improvements over the past couple of decades, DPM is still a significant health concern for underground mine workers. Efforts to further reduce exposure risks require enhanced monitoring tools. Demonstration of the efficacy and utility of the Airwatch DPM monitor is expected to aid in progress toward its commercial availability. Ultimately, this tool should provide mine operators a means of tracking DPM with other environmental and operational conditions (e.g., ventilation) such that worker health can be adequately protected while optimizing other factors (e.g., energy usage, production, maintenance schedules, etc.).

Beyond these expected research outcomes of the Capacity Building in Ventilation project described here, development of expertise in the areas of mining engineering and occupational health is a primary objective. The project team includes multiple student researchers. Their current work will add to the scientific literature surrounding DPM monitoring and control; and the knowledge and experience they gain during this project will soon contribute to the broader mining community.

Table 2: Work tasks related to DPM monitoring and ventilation response

Task	Description
Initial Collection of Mine data (Year 1)	<ul style="list-style-type: none"> • Become familiar with operation and environmental conditions at the mine of study. • Conduct ventilation and DPM surveys by using: <ul style="list-style-type: none"> ○ Airtec real Time Monitors ○ Ultrasonic Anemometers
Receipt and lab resting of prototyped autonomous DPM monitors (Years 1-2)	<ul style="list-style-type: none"> • Receipt of prototyped autonomous DPM monitoring units from NIOSH • Becoming familiar with the units' design and operational requirements. • Units will be lab tested to confirm they are functioning properly <ul style="list-style-type: none"> ○ Capability to measure continually ○ Capability to log data ○ Accuracy and consistency amongst all units output. • Verification of autonomous DPM monitors' readiness for use underground.
Field-testing of autonomous DPM monitors (Years 2-4)	<ul style="list-style-type: none"> • Determining installation locations together with the mine operator. <ul style="list-style-type: none"> ○ High priority areas for monitoring of DPM ○ Safe and reliable for the operation of the testing equipment. • Installation of the prototyped monitors at the field site • Ensuring proper functioning in the mine environment and capability to record DPM data for long periods of time
Monitoring DPM responses to specific ventilation (Years 4-5)	<ul style="list-style-type: none"> • Tracking DPM response to different ventilation scenarios. • Scenarios will be determined in conjunction with the mine operator

Acknowledgements

The authors would like to thank CDC/NIOSH for support of this project (under contract no. 200-2014-59646). In particular, we thank Dr. James Noll for his technical guidance and advice.

References

- [1] K. Kimbal, Pahler, L., Larson, R. and J. VanDerslice, Monitoring diesel particulate matter and calculating diesel particulate densities using Grimm Model 1.109 real-time aerosol monitors in underground mines, *Journal of Occupational and Environmental Hygiene* (2012) 353-361.
- [2] J. Noll, Timko, R., McWilliams, L., Hall, P., and R. Haney, Sampling results of the improved SKC diesel particulate matter cassette, *Journal of Occupational and Environmental Hygiene* (2010) 29-37.
- [3] J. Noll, and S. Janisko, Using laser absorption techniques to monitor diesel particulate matter exposure in underground stone mines, *Proceedings from SPIE Vol. 6759* (2007).
- [4] "Diesel Particulate Matter Exposure of Underground Metal and Nonmetal Miners; Final Rule," *Federal Register* 30 CFR Part 57.
- [5] L. Takiff and G. Aiken, A real-time, wearable elemental carbon monitor for use in underground mines, 13th North American Mine Ventilation Symposium, (2010).
- [6] M. Birch, Method 5040 diesel particulate matter as elemental carbon, *NIOSH Manual of Analytical Methods Fourth Ed*, (2003).
- [7] J. Noll, Cecala, A., Organiscak, J., and S. Janisko, Real-time DPM monitoring: NIOSH develops a new tool for assessing and controlling exposure, *Engineering and Mining Journal*, June 2014, (2014) 78-81.
- [8] Clean Air Task Force (2005). Report, <http://catf.us/publications/view/83> accessed 9 March 2015.
- [9] M. Birch, Monitoring of diesel particulate exhaust in the workplace, *NIOSH Manual of Analytical Methods*, (2003).
- [10] J. Stinnette and K. Wallace, Jr. Conducting a comprehensive baseline study for diesel particulate matter, 10th North American Mine Ventilation Symposium (2004).
- [11] M. Peterson and M. Richards, Thermal-optical-transmittance analysis for organic, elemental, carbonate, total carbon, and OCX2 in PM2.5 by the EPA/NIOSH Method. (2002).
- [12] [SKC, Inc., Diesel particulate matter cassettes, Web, (2015).
- [13] J. Noll and S. Janisko, Evaluation of a wearable monitor for measuring real-time diesel particulate matter concentrations in several underground mines, *Journal of Occupational*

and Environmental Hygiene, (2013), p. 716-722.

- [14] Washington State Department of Health, The health of Washington State 2007: outdoor ambient air quality, p.8.5.5, (2008).
- [15] Nomadics Inc. Autonomous networked EC monitor. Final Report to Center of Disease Control and Prevention, N.D.
- [16] R. Krog, Grau III, R., Mucho, T., and S. Robertson, Ventilation planning layouts for large opening mines, National Institute for Occupational Safety and Health, (2008).
- [17] R. Grau III, S. Robertson, R. Krog, G. Chekan and T. Mucho, Raising the bar of ventilation for large-opening stone mines, National Institute for Occupational Safety and Health, 2008.
- [18] R. Grau III, T. Mucho, S. Robertson, A. Smith and F. Garcia, Practical techniques to improve the air quality in underground stone mines, National Institute for Occupational Safety and Health, N.D.

A Preliminary Investigation of DPM Scavenging by Water Sprays

L. Rojas-Mendoza ^a, E. McCullough ^a, E. Sarver ^{a,*}, J.R. Saylor ^b

^a Virginia Tech, Department of Mining and Minerals, Blacksburg, VA 24060, USA

^b Clemson University, Department of Mechanical Engineering, Clemson, SC 29634, USA

Diesel particulate matter (DPM) presents serious occupational health concerns, particularly in enclosed environments such as underground mines. Since 2002, DPM exposure in U.S. mines has been subject to regulations implemented by the Federal Mine Safety and Health Administration (MSHA). While current strategies to curb DPM exposures have been largely successful (e.g. improved ventilation and engine exhaust treatments), challenges still exist in some mine settings, particularly where relatively high airflows are not practicable. New technologies to remove DPM from such areas are needed. Water sprays have long been used in underground mine operations as part of comprehensive dust control programs. Indeed, significant research has been focused on the spray mechanisms for abating dust, with observations indicating that both material wetting and airborne-particle scavenging contribute to reductions in respirable dust concentrations. However, little attention has been given to the efficacy of spray droplets to scavenge DPM.

As part of a new Capacity Building in Ventilation project sponsored by the National Institute for Occupational Safety and Health (NIOSH), we aim to determine if and how water sprays might be used to control DPM in underground mines. This paper reviews DPM in the underground mine environment, airborne particle-water droplet interactions, and our research progress to date. The laboratory setup for experimental work is specifically described and several challenges are discussed, including dilution of the engine exhaust stream to achieve a steady supply of DPM under flow conditions compatible with analytical instruments.

Keywords: Diesel Particulate Matter, DPM, Water Sprays, Scavenging, Nanoparticles

1. Introduction

Diesel particulate matter (DPM) is a component of diesel exhaust that is hazardous to human health. It is classified by EPA and OSHA as a potential or suspected carcinogen [1, 2]. The type and severity of harm is dependent upon two factors: the amount of DPM to which a person is exposed, and the duration of the exposure [1]. Physical symptoms range from minor discomforts such as headaches and eye irritation under acute exposure, and major cardiovascular and pulmonary diseases (e.g., lung inflammation) under long term exposure [1-3]. Epidemiological studies demonstrate a relationship between DPM exposure and increased lung cancer rates. These increased lung cancer rates could be caused by polycyclic aromatic hydrocarbons (PAH) present in diesel exhaust [3]. However, specific mechanisms for health impacts from DPM exposures are not fully understood, particularly the adverse impacts of nanoparticles [3, 5]. Nanoparticle research is a significant priority because pulmonary deposition increases with decreasing particle sizes, and because some chemicals that are innocuous at larger sizes can be toxic at the nanoscale [4].

Underground miners represent a particularly high-risk population when it comes to DPM exposures [5], because of the heavy diesel powered equipment used in the enclosed environments where they work [6, 7]. In metal and nonmetal mines (M/NM), ventilation challenges (e.g., low air flows, leakage, recirculation) can make DPM so difficult to abate, that it becomes a restrictive variable for mining planning and operation [7-9].

In the US, issues related to occupational health of miners are covered by the Mine Safety and Health Administration (MSHA) [2, 6]. Regulation pertaining to permissible personal exposures in M/NM mines is found in the Code of Federal Regulation (CFR) from 30 CFR

57.5060 to 30 CFR 57.5075. DPM exposure limits have been regulated since 2002 [8], and the final personal exposure limit (PEL) became effective on May 20, 2008 [9]. It mandates that a miner's exposure to DPM must not exceed an average eight-hour equivalent full shift airborne concentration of $160 \mu\text{g}/\text{m}^3$ (on the basis of total carbon, TC) [10]. In general, noncompliance can be determined by use of a single sample collected and analyzed per the CFR [11]. The CFR also limits the amount of sulfur permitted in diesel fuel and the type of additives that can be used, and requires mine operators to monitor "as often as necessary" the concentration of DPM to protect miner health [13, 14].

1.1 DPM Characteristics

Diesel exhaust is composed of two phases, both of which contribute to occupational health risks: gas and solid particles [4, 5, 10]. The gaseous phase includes compounds such as CO, CO₂, NO_x, SO_x and a number of hydrocarbons [6, 15]. The solid phase is mainly composed of highly agglomerated carbonaceous material and ash, in addition to volatile sulfur and organic compounds [4]. The carbonaceous material is comprised of elemental carbon (EC) or soot and organic carbon (OC) [5]. TC is the sum of the EC and OC portions [6, 16]. The volatile organic fraction is the consequence of unburned fuel and lube oil, while sulfuric acid and sulfate particles are created from oxidation of SO₂ [5, 6].

Beyond classification by chemistry, DPM can be also be divided into size ranges based on aerodynamic diameter (AD), which is defined as the diameter of a $1\text{g}/\text{cm}^3$ density sphere of the same settling velocity (in air) as the particle of interest [4, 15]. Fine particles are generally those with $\text{AD} < 2.5 \mu\text{m}$, ultrafine particles are those with $\text{AD} < 0.1 \mu\text{m}$ (100nm), and nano-particles are those with $\text{AD} < 0.05 \mu\text{m}$ (50nm) [4, 5].

Based on size and formation mechanism, DPM particles can be classified in one of three typical modes: nuclei, accumulation, or coarse [4,15]. The nuclei mode is mostly composed of volatile organic and sulfur compounds residing in the nanoparticle range between about 0.003-0.03 μm (i.e., in the general region shown as “1” in Figure 1) [15]. These particles are formed in the engine during the exhaust dilution and cooling [14], which make their characteristics highly variable, depending on engine operation, dilution and sampling conditions [4, 5, 17]. These particles only account for 0.1 to 10% of the total mass, but around 90% of the total particle count [5, 15]. The accumulation mode includes submicron solids (carbonaceous agglomerates and adsorbed material) with diameters of roughly 0.030-0.5 μm (i.e., in the general region “2” in Figure 1). This mode spans from the upper end of the nanoparticle range, through the superfine range, to the lower end of the fine range [4]. The transition between the accumulation and coarse mode is somewhat fuzzy, but occurs between 0.5-1 μm . Finally, the coarse mode includes particles > 1 μm (i.e., in the general region “3” in Figure 1), which are generated as a consequence of deposition and following re-entrainment of particles in the engine walls and sampling systems. Relatively few particles actually fall into this mode by number, but they account for about 5-20% of the total mass [15]. Based on mass, most DPM resides in the accumulation mode, while from a number perspective, most DPM particles are found in the nuclei mode [5, 15]. This may present a safety concern because DPM is regulated on a mass basis – as is generally the case with all airborne particulates due to limitations of analytical methods – but some health effects may be strongly influenced by nanoparticle exposure [5].

1.2 DPM abatement in M/NM mines

Numerous efforts have been made to curb DPM exposure in underground M/NM mines (i.e., [7–10, 18, 19]). Both engineering and administrative controls exist. Administrative controls include modifications to operational procedures to decrease the DPM hazard. Limiting equipment speeds, restricting engine idling and identifying areas where no personal should be located are examples of such administrative controls [2, 6]. Engineering controls that are used consist of technical improvements that either reduce DPM generation (e.g., upgraded engine technologies, exhaust filters and preventative maintenance programs to minimize emissions) [2, 9], or reduce miner exposures (e.g., sealing equipment cabs, providing increased ventilation) [2, 6, 10, 11]. Indeed, increased ventilation is one of the simplest options for limiting DPM exposure in principle, however this is challenging in large-opening mines. In such environments, it may be impractical to significantly increase airflow or to introduce effective ventilation controls (i.e. permanent sealing, stoppings and curtains) [6]. NIOSH has conducted some research related to improved ventilation layouts for large-opening mines [e.g., 6–8, 18], but many operations will undoubtedly remain challenged to meet current (and any future) DPM exposure limits. Not only might these challenges result in instances of overexposures, but in many cases they may also constrain operational flexibility (e.g., in terms of production schedules, resource appropriation, etc.)

In light of the above, new technologies are needed for DPM abatement. Water sprays have long been used in mining environments to control airborne dusts [21, 22]. While few studies can be located in the published literature regarding the efficacy of sprays to reduce DPM, theory and very fundamental work on water droplet-particle interactions suggest that certain size ranges of DPM should be affected (i.e., [22–25]) .

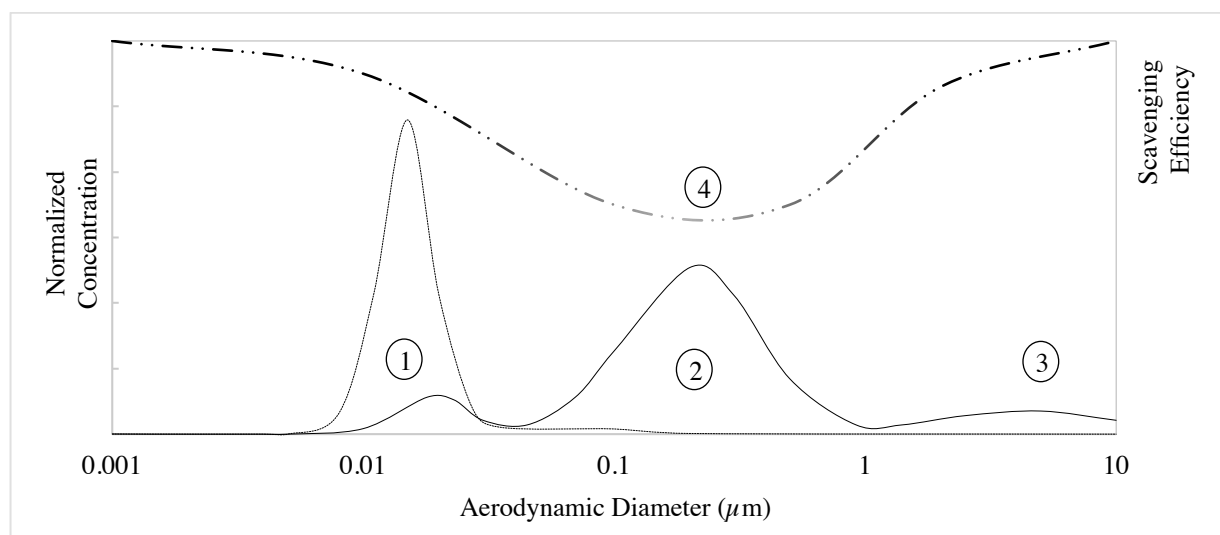


Fig 1. Illustrative depiction of DPM size distribution by number and by mass, and water droplet scavenging efficiency as a function of aerodynamic diameter. DPM size distribution (based on Kittelson (1997), [4]) exhibits three characteristic modes: Nuclei (shown as “1”), accumulation (shown as “2”), and coarse mode (shown as “3”) For the scavenging efficiency (based on and Kim et al. (2001), [17]) the zone shown as “4” corresponds to an area where the efficiency reaches a minimum.

2. Sprays in Underground Mining

The concentration of airborne particles in underground mines is conventionally controlled by ventilation (i.e., via dilution and/or displacement), dust

collector systems, and/or water sprays [22]. These techniques are ubiquitous in mining operations to control dust. Water sprays are often employed as part of a wet scrubber or as a local treatment by direct application to

the zone of interest (i.e., nearby production areas and mineral processing installations) [18, 20, 23].

Water sprays are effective through two major mechanisms: wetting suppression and particle scavenging [17, 18]. Wetting suppression is the most common method of dust control at mine operations, and the premise is that particles are prevented from becoming airborne in the workplace. Wetting may be functional when it is applied to bulk materials, or when it limits particles previously deposited on walls and equipment surfaces from being liberated [21]. Wetting effectiveness can be enhanced by increasing wetting uniformity and the number of water sprays [22]. On the other hand the role of particle scavenging, also called collection, is to remove particles from the air. Mechanistically, the idea is for particles to collide with water droplets, and then to fall out of the air [20, 21, 24].

The scavenging efficiency is related to the ability of a drop or group of drops to capture airborne particles [24, 27]. This efficiency can be quantified by the scavenging coefficient (E), which is defined as the number of particles scavenged relative to the total number of particles that could have been scavenged by the spray. Practically, a coefficient can be calculated for certain size ranges or modes [28], or even certain types of particles. The scavenging efficiency depends on several characteristics of the water drop (i.e., density, diameter, charge, surface tension and viscosity), the particle (i.e., density, diameter and electrical charge) and also on the airflow and spray characteristics. Spray characteristics include the type of nozzle (e.g., geometry), operating pressure and flow rate [29]. The most common nozzle designs employed for dust abatement in the mining industry include: hollow cone pattern, full-cone pattern, and flat spray patterns [29]. Each of them produces different water drop diameters and mean velocities.

A fair amount of research has been conducted on water sprays for dust particles in the respirable range. It is widely accepted that the capture efficiency is directly proportional to the relative velocity between the spray droplets and the dust particles, and inversely proportional to the droplet diameters [24, 29]. Smaller water droplets can be obtained by using atomizing or fog sprays, steam sprays, electrically-atomized sprays and sonically atomized sprays [22]. Research due to Saylor et al., (2014) demonstrated that the scavenging efficiency for particles within the sub-micron range (i.e., 0.1-10 μm) can be increased by using an ultrasonic standing-wave field [28]. However, it should be noted that the collection mechanism for dust particles might differ from the mechanism governing DPM scavenging since drop-particle interactions are size dependent.

2.1 DPM scavenging

There are four primary mechanisms of particle scavenging by water droplets: impaction; interception, Brownian diffusion and electrostatic attraction [22, 24, 30]. Impaction occurs when the path traveled by particles deviates from the flow streamlines due to particle inertia [26]. This mechanism depends on the Stokes number [26], and it plays an especially large role in spray scavenging of particles with diameters larger than 5 μm [17]. Thus, impaction is the governing mechanism for airborne dust scavenging, but is not expected to significantly affect DPM. Interception occurs when a particle stays on the flow streamline but because of its finite diameter, touches the water droplet. The efficiency of particle scavenging by interception is directly proportional to the particle diameter and inversely proportional to the droplet diameter [24, 25]. Brownian

diffusion, which refers to random motion of particles within a fluid, governs particle-droplet interactions for nanoparticles [25, 27, 30]. Indeed, the effect of interception and impaction are negligible for particles under 0.05 μm , where around 90% of the number of DPM particles reside [17]. Finally, electrostatic attraction might also be important under conditions where DPM, water droplets or both possess sufficient electrical charge [26].

DPM scavenging will be highly dependent on particle-drop interactions [28]. Under fixed conditions of droplet diameter and particle-drop velocity, E should be related to the particle diameter [17]. Figure 1 provides an illustrative depiction of the overall scavenging efficiency as a function of the AD. This plot was developed based on research by Kim et al., (2001) that addressed scavenging via diffusion, interception and impaction [17]. As seen in the figure, for ultrafine and smaller particles (i.e., < 0.1 μm) the scavenging efficiency increases as the particle diameter decreases, which is attributed to the growing influence of Brownian diffusion with decreasing particle diameter. For relatively large particles (i.e., > 1 μm) E increases as particle size increases, due to the increasing effect of particle inertia with increasing particle size. Accordingly, for a certain size range in the middle (i.e., in the zone “4” in Figure 1) scavenging is very inefficient since this is where neither diffusive effects nor inertia are very effective. This range is known as the Greenfield gap [31]

While the discussion above suggests that at least some fraction of DPM should be subject to significant scavenging by water sprays, little practical research has been carried out along these lines. In fact, a thorough search of the literature turned up only two related studies. These are summarized in Table 1.

3. New Research

Clearly there is limited published research regarding DPM scavenging by water sprays. However, the few available studies indicate that for certain cases (e.g., neutral drop-neutral DPM) a fraction of the DPM can be affected. Additionally, the fundamental fluid mechanics of scavenging suggest that both small and large particles can be collected through different mechanisms.

It should be noted that, to a certain extent, removal of DPM by sprays and abatement of DPM by ventilation, act in opposition to each other. Spray scavenging works best when the distance between a drop and a particle is small, i.e. at high particle concentrations. Ventilation, on the other hand, seeks to reduce particle concentrations. One way to address this tradeoff is to separate the spray scavenging and ventilation activities. This could be done, for example, by creating a spray scrubber in regions of high DPM loading and then subsequently diluting the output of the scrubber via ventilation. Another approach is to optimize the power dedicated to DPM abatement, dividing it between ventilation blower power and spray pump power to maximize DPM removal.

Under a new Capacity Building in Ventilation project sponsored by CDC/NIOSH (contract no. 200-2014-59646), research in this area and others will be carried out to determine the efficacy of water sprays for scavenging DPM. This project officially began in September 2014 and will be developed over 5 years. Project tasks related to DPM scavenging by water sprays are outlined in Table 2.

Table 1. Summary of previous practical research on scavenging of combustion particles by water sprays. This table summarizes the work and results obtained in two different studies. The first study was conducted at the Università degli Studi di Napoli “Federico II” by L. D. Addio et al. (2013), [24]. The second study was conducted at Kobe University – Japan by T. Ha Hong et al. (2009), [23].

Research Study	Methodology	Major findings
<p>“Removal of fine and ultrafine combustion derived particles in a wet electrostatic scrubber” [24]</p> <ul style="list-style-type: none"> Developed by the Università degli Studi di Napoli “Federico II” Determine the particle capture efficiency achieved in a wet electrostatic scrubber on particles ranging from 0.01-1μm. 	<ul style="list-style-type: none"> The source of particles was a naphtha lamp. Water droplets and particles were charged with opposite polarities. TSI 3910 and TSI 3340 were employed to determine particle concentration and distribution in the ranges 0.01-0.42μm and 0.09-0.74μm, respectively. Efficiency was evaluated for the next three cases: <ul style="list-style-type: none"> a) Uncharged sprays and uncharged particles b) Uncharged particles and charged drops. c) Particles and drops charged with opposite polarity. 	<ul style="list-style-type: none"> For experiment “a” the efficiency was above 10% for particles finer than 0.22μm and almost null for coarser particles. Overall particle removal efficiency for experiment “a” was around 5%. For experiment “b” the particle abatement reached an overall value of 35%, and for experiment “c” the overall efficiency reached 93%.
<p>“Simultaneous removal of NO_x and fine diesel particulate matter (DPM) by electrostatic water spraying” [23]</p> <ul style="list-style-type: none"> Developed by Kobe University – Japan. Evaluate the effectiveness of an electrostatic water spraying scrubber for the removal of NO_x and DPM emissions in marine exhaust gas. 	<ul style="list-style-type: none"> A diesel engine was used as a stationary DPM emission source. DPM was charged positive by using a corona power unity. Stainless electrodes were employed to charge water droplets by induction. An impactor (AS-500) was used to quantify DPM size distributions. Mass concentrations were obtained by weighting of filters. Scrubber efficiency was evaluated at different engine loads for the next scenarios: <ul style="list-style-type: none"> a) No water spray (NS) b) Neutral drop-neutral DPM (ND-NP) c) Charged drop-neutral DPM (CD-NP) d) Charged DPM-neutral drop (CP-ND) e) Charged drop-charged DPM (CD-CP) 	<ul style="list-style-type: none"> DPM mass concentration increased when engine load increased. ND-NP mass based scavenging efficiency roughly ranged from 10 to 20% for different engine loads. Mass based efficiency increased for the other scenarios. CD-NP < CP-ND < CD-CP. The mass-based scavenging efficiency showed to be directly proportional to the voltage applied for charged particles and drops.

3.1 Experimental setup and considerations

The experimental setup is shown in Figure 2 and consists of four main parts: A diesel engine as DPM source; a scavenging box (which includes the water spray system) to produce water droplets that can interact with DPM; particle counters on either side of the box to determine the efficiency of scavenging under different scenarios; and a number of devices allowing for system monitoring and control (e.g., pressure gauges, flowmeters). The most significant challenges to building and running the lab experimental system are environmental health and safety constraints, influence of dilution conditions on DPM concentration, protection of the particle counters (i.e., from overwhelming

concentrations or pressures) and control of the water spray parameters.

The DPM source employed for research purposes is a small diesel engine (component 1 in Figure 2). The main environmental concern regarding operation of a diesel engine indoors stems from the potential emissions into the laboratory space. Additionally, noise must be limited. The chosen engine creates low noise levels when run at 800 to 1000 rpm [32]; and an enclosure (the dashed lines in component 2 of Figure 2) with foam insulation material glued on the internal walls will provide additional assurance.

Table 2. Description of project tasks related to DPM scavenging by water sprays.

Task	Description and Variables
1) Construction of laboratory setup for spray/ventilation tests (Year 1)	<ul style="list-style-type: none"> • Design of the lab set up. • Identifying and acquiring the main components of the system: <ul style="list-style-type: none"> ○ Source of DPM -diesel engine. ○ Particle counters. ○ Scavenging box. ○ Water spray system. ○ Miscellaneous (i.e. flowmeters, filters) • Identifying and meeting environmental work space requirements. • Construction of lab set up. • Debugging and troubleshooting of lab set up.
2) Small-scale testing of water sprays on DPM scavenging (Year 2)	<ul style="list-style-type: none"> • Gathering data related to the overall scavenging efficiency of the water spray system. • Determining scavenging efficiency as a function of DPM diameter. • Testing on a small fraction of the engine exhaust (e.g., 1-10%) • Variables: <ul style="list-style-type: none"> ○ Spray atomization rate. ○ Dilution rate. ○ Airflow reaching the scavenging box (dilution rate & bleed-off fraction)
3) Large-scale testing of water sprays on DPM scavenging (Years 3-4)	<ul style="list-style-type: none"> • Adjusting lab set up for large-scale testing. • Experiments will be conducted on progressively larger fractions of the exhaust stream. • Determining the scavenging coefficient for the total amount of DPM for each particle diameter. • Additional Variables: <ul style="list-style-type: none"> ○ Engine operating load. ○ Flow temperature.
4) Field testing of water sprays (Year 4)	<ul style="list-style-type: none"> • The scavenging box will be decoupled from the DPM source and tested in an actual mining environment.

The enclosure will also serve to reduce vibrations and prevent accidental contact with the engine. A fan is located on top of the enclosure to guarantee enough air circulation to prevent overheating. A thermal insertion meter (18 in Figure 2) will also be employed to measure the total exhaust volume, which should fall between 30 and 40 CFM. The primary diesel exhaust (and the water-spray treated fraction of exhaust) will be piped out of the lab via a window (20 in Figure 2). DPM and CO monitors will be employed in several locations of the lab to monitor for exhaust leakage.

Dilution conditions influence the number of DPM particles in the system, especially for particles with AD lower than $0.1\mu\text{m}$ [18]. Conditions affecting the nucleation rate of DPM particles are dilution temperature, dilution ratio, residence time, relative humidity and sulfur content [5, 15, 17]. Sulfur content will be managed by use of a consistent fuel source and temperature through the installation of thermocouples (19 in Figure 2), however the other variables will require careful control and monitoring in order to guarantee repeatable conditions –

and therefore reproducibility of data. A fractional bleed-off will be taken from the main exhaust by using a dilution ejector (7 in Figure 2). A dilution ejector is a vacuum generator that serves two purposes: first to guarantee that DPM is drawn into the system and second to allow for the dilution of the DPM stream with compressed air. A set of on/off control valves will be installed downstream of the ejector diluter. The on/off valve (8 in Figure 2) will allow the control valve (9 in Figure 2) to remain fixed once the desired flow has been reached. Dilution will be primarily controlled by mixing high-purity dry air (3 in Figure 2) with the exhaust bleed-off. Additionally, a dilution “bridge” (11 in Figure 2) will be incorporated to drop the DPM concentration to readable levels for the particle counters. The bridge reduces concentration by selectively filtering a fraction of the bleed-off flow [33]. The dilution bridge will also operate as an open vent to keep the system pressure at, near, or only slightly over atmospheric pressure to prevent overpressure of the particle counters.

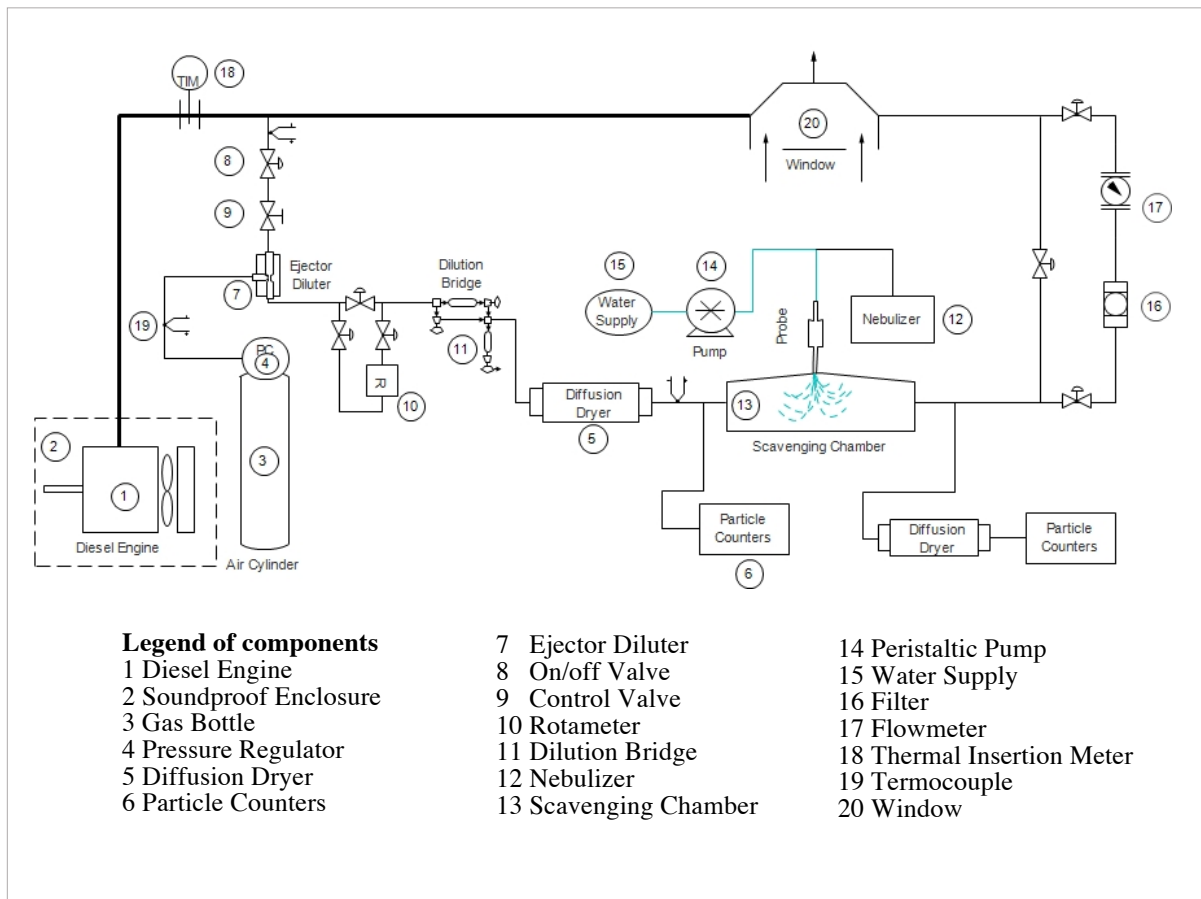


Fig 2. Preliminary design for DPM scavenging experiments using a water spray system and list of key components.

At the scavenging box, a tee will be used to direct one fraction of the diluted flow to the scavenging box while the remaining flow is directed to the upstream particle counters. In a similar way, the air leaving the scavenging box will also be split into two fractions. The major fraction will be directly exhausted from the lab, while the remaining fraction is sent to the downstream particle counters. The upstream and downstream particle counters will measure DPM concentration (i.e., by particle number as a function of size) entering and exiting the scavenging box as can be seen in Figure 2.

For the initial project stages, the scavenging box will be constructed of clear plastic, and will include a water drain. The spray source (12 in Figure 2) will be an ultrasonic nebulizer which converts high frequency electrical energy to mechanical vibrations, which are intensified by a probe to break water into micro-droplets. A 40 kHz atomizing probe will be used, providing atomization rates up to 30 mL/min and a median drop size of about 50 μ m [34]. The atomizer will be mounted on the top of the scavenging box, and the water (15 in Figure 2) entering this equipment will be regulated with a peristaltic pump (14 in Figure 2).

Key to the lab setup are the particle counters (6 in Figure 2). The TSI 3910 nanoparticle counter (NanoScan) will cover the size range 0.001-0.45 μ m (10-450nm) while the TSI 3330 optical particle sizer (OPS) will cover the range 0.3-10 μ m [35, 36]. Two diffusion dryers (5 in Figure 2) will be used to ensure that the particle counters only count DPM (and not water droplets). These pieces of equipment dry and remove water vapor from the gas flow by collecting large water droplets at the inlet and removing excess moisture by diffusional capture [37]. A

bypass line including a mass flowmeter (17 in Figure 2) with a filter upstream (16 in Figure 2) will be introduced into the piping design before the scavenging box exhaust (i.e., water spray treated air) is ducted out of the room. By having an accurate measure of the flow leaving the scavenging box, along with information about other flows in the system, an analytical balance should be possible.

The lab setup described here is currently under construction, and is expected to be completed by Fall 2015. At this time, work under Task 2 will begin. In the meantime, preliminary testing of specific components is underway.

4. Conclusions

DPM represents a serious concern for worker health in underground mines, and existing methods for ensuring that exposures are sufficiently limited may affect operational flexibility in many instances. Much work has been done to reduce DPM exposure by using a combination of administrative and engineering controls. However, the abatement of DPM is not trivial, and new technologies coupled with the existing methods are needed to optimize health protection and efficient operations. Water sprays, which have proven to be a useful tool in underground mining for the abatement of dust, represent a promising but scarcely studied engineering control. Evidence, including theory and some practical work in non-mining environments, suggests that a fraction of DPM might be scavenged by the use of water sprays.

Research conducted as part of a new Capacity Building in Ventilation project will provide fundamental insights into DPM-droplet interactions and specific conditions favoring the scavenging of certain DPM particle size ranges. This research will thus contribute to the scientific literature and address practical implications of water sprays as a novel DPM abatement technology in underground mine environments.

Acknowledgments

The authors thank the CDC/NIOSH Office of Mine Safety and Health Research (OMSHR) for funding this work (contract no. 200-2014-59646). We also want to thank Dr. James Noll in particular for his support and guidance. Views expressed here are those of the authors and do not necessarily represent those of any funding source.

References

- [1] United States Environmental Protection Agency, "Diesel Particulate Matter," January 4, 2014. [Online]. Available: <http://www.epa.gov/region1/eco/airtox/diesel.html>.
- [2] United States Department of Labor, "Diesel Exhaust/Diesel Particulate Matter," January, 2013. [Online]. Available: https://www.osha.gov/dts/hazardalerts/diesel_exhaust_hazard_alert.html.
- [3] Clean Air Task Force, "An analysis of diesel air pollution and public health in America," pp. 1–54, 2005.
- [4] D. Kittelson, "Engines and Nanaoparticles: A Review," *J. Aerosol Sci.*, vol. 29, no. 5, pp. 575–588, 1997.
- [5] The National Institute for Occupational Safety and Health (NIOSH), Diesel Aerosols and Gases in Underground Mines: Guide to Exposure Assessment and Control. 2011.
- [6] R. H. Grau, R. B. Krog, S. B. Obertson, J. M. Mutmansky, and R. V Ramani, "Maximizing the ventilation of large-opening mines," *Proc. 11th U.S./North Am. Mine Vent. Symp.*, pp. 53–60, 2006.
- [7] R. B. Krog, R. H. G. Iii, T. P. Mucho, and S. B. Robertson, "Ventilation Planning layouts for large opening mines," *SME Prepr. 04-187*, Littleton, CO Soc. Mining, Metall. Explor. Inc., pp. 1–9, 2011.
- [8] R. H. G. Iii, S. B. Robertson, R. B. Krog, G. J. Chekan, and T. P. Mucho, "Raising the Bar of Ventilation for Large-Opening Stone Mines," *Heal. (San Fr.)*, 2001.
- [9] J. D. Noll, L. Patts, and R. Grau, "The effects of ventilation controls and environmental cabs on diesel particulate matter concentrations in some limestone mines," 2007.
- [10] Code of Federal Regulations Title 30 Part 57 Section 5060 (30CFR57.5060), Limit on Exposure to diesel particulate matter. 2013.
- [11] Code of Federal Regulations Title 30 Part 57 Section 5061 (30CFR57.5061), Compliance Determinations. 2013.
- [12] Code of Federal Regulations Title 30 Part 57 Section 5065 (30CFR57.5065), Fueling Practices. 2013.[13] Code of Federal Regulations Title 30 Part 57 Section 5071 (30CFR57.5071), Exposure Monitoring. 2013.
- [14] DieselNet, "Diesel Exhaust Particle Size," 2007. [Online]. Available: <http://courses.washington.edu/cive494/DieselParticleSize.pdf>.
- [15] D. Kittelson, W. Watts, and J. Johnson, "Diesel Aerosol Sampling Methodology - CRC E-43: Final Report," 2002.
- [16] The National Institute for Occupational Safety and Health (NIOSH), "Elmental carbon (diesel particulate): METHOD 5040," 1999. .
- [17] H. T. Kim, C. H. Jung, S. N. Oh, and K. W. Lee, "Particle Removal Efficiency of Gravitational Wet Scrubber Considering Diffusion, Interception, and Impaction," *Environ. Eng. Sci.*, vol. 18, no. 2, pp. 125–136, 2001.
- [18] I. Abdul-khalek, D. Kittelson, and F. Brear, "The Influence of Dilution Conditions on Diesel Exhaust Particle Size Distribution easurements," *Soc. Automot. Eng.*, no. 724, 1999.
- [19] R. H. Grau, T. P. Mucho, S. B. Robertson, a C. Smith, and F. Garcia, "Practical techniques to improve the air quality in underground stone mines," *Proc. North Am. U.S. Mine Vent. Symp.*, pp. 123–129, 2002.
- [20] L. Takiff and G. Aiken, "A Real-Time, Wearable Elemental Carbon Monitor for Use in Underground Mines," *13th United States/North Am. Mine Vent. Symp.*, pp. 137–141, 2010.
- [21] H. Services, "Best Practices for Dust Control in Metal / Nonmetal Mining," 2010.
- [22] F. N. Kissell, "Handbook for Dust Control in Mining," pp. 1–131, 2003.
- [23] T. Ha Hong, O. Nishida, H. Fujita, and H. Wataru, "Simultaneous removal of NOx and fine diesel particulate matter (DPM) by electrostatic water spraying scrubber," *J. Mar. Eng. Technol.*, vol. A 15, pp. 45–53, 2009.
- [24] L. D. Addio, F. Di Natale, C. Carotenuto, G. Scoppa, and V. Dessy, "Removal of fine and ultrafine combustion derived particles in a wet electrostatic scrubber," *Proc. XXXVI Meet. Ital. Sect. Combust. Inst.*, 2013.
- [25] L. Cheng, "Collection of airborne dust by water sprays," *Ind. Eng. Chem. Process Des.*, vol. 12, no. 3, pp. 221–225, 1973.
- [26] H. H. Tran, N. Osami, F. Hirostugu, and H. Wataru, "Prediction for Diesel Particulate Matter (DPM) Collection Efficiency of Electrostatic Water Spraying Scrubber," vol. 44, no. 5, 2009.
- [27] C. Copeland, "Suppression and dispersion of airborne dust and nanoparticulates," *Michigan Technological Univesity*, 2007.
- [28] W. Ran, J. R. Saylor, and R. G. Holt, "Improved particle scavenging by a combination of ultrasonics and water sprays," *J. Aerosol Sci.*, vol. 67, pp. 104–118, 2014.
- [29] D. Pollock and J. Organiscak, "Airborne Dust Capture and Induced Airflow of Various Spray Nozzle Designs," *Aerosol Sci. Technol.*, vol. 41, pp. 711–720, 2007.
- [30] S. Calvert, "Scrubbing" in *Air Pollution*, 3d ed. New York, 1977.
- [31] S. M. Greenfield, "Rain Scavenging of Radioactive Particulate Matter from the Atmosphere," *J. Meteorol.*, vol. 14, pp. 115–125, 1957.
- [32] Kubota Global, "EA330-E3-NB1 Kubota EA series," 2015. [Online]. Available: <http://www.kubotaengine.com/products/engines/vertical-diesel/kubota-ea-series/ea330-e4-nb1>.
- [33] TSI, "Using the TSI Dilution Bridge with the SMPS," 2014.
- [34] Sonics & Materials Inc, "Ultrasonic Atomizers," 2015. [Online]. Available: <http://www.sonics.com/lp-atomizers.htm>.

- [35] TSI, "Optical Particle Sizer 3330," 2015. [Online]. Available: <http://www.tsi.com/optical-particle-sizer-3330/>.
- [36] TSI, "Nanoscan SMPS nanoparticle sizer 3910," 2015. [Online]. Available: http://www.tsi.com/nanoscan_smps_nanoparticle_sizer_3910/.
- [37] Air Techniques International (ATI), "DD 250 Diffusion Dryer," 2003. [Online]. Available: <http://www.atitest.com/html/products/details/dd250.html>.

Computational Fluid Dynamics Study of Radon Gas Migration in a Block Caving Mine

K.M. Ajayi^a, P. Tukkaraja^b, K. Shahbazi^b, K. Katzenstein^b and D. Loring^c

^a *PhD. Student, South Dakota School of Mines & Technology, Rapid City, SD 57701, USA.*

^b *Assistant Professor, South Dakota School of Mines & Technology, Rapid City, SD 57701, USA.*

^c *Chief Mine Engineer, Freeport-McMoRan Inc.*

Block caving is a viable method of mining massive, deep seated deposits. The process involves undermining an ore body and allowing the rock to fall under its own weight. Although the purpose of block caving is targeted at mining the ore, a by-product of the process can be the release of certain hazardous or potentially hazardous gases into the mine. Radon, a radioactive element, is one of the potentially hazardous gases released in some caving process. The generation of radon gas is not limited to the caving process but can also be from surrounding rock in an active mining area and is often emitted from old workings in the mine.

To design an effective ventilation system, in order to create a safe working environment in an underground block cave mine, it is necessary to understand the relationship between radon migration and the amount of airflow needed to keep the working areas safe. Several factors contribute to the migration of radon gas and emanation from the rock such as emanation power, temperature, pressure, rock size, annealing effects on emanation power, and porosity. This paper presents the methodology for developing a Computational Fluid Dynamics (CFD) model to study radon gas migration in a block caving mine. A typical block cave contains different zones; each zone has its own properties. Therefore, modelling of caving process will involve different analysis for different zones. However, the CFD model was developed assuming the mobilized, yield, seismogenic and elastic zones are porous media. The 3-dimensional model was used to investigate the relationship between airflow and radon gas migration with respect to space and time which seems to be a gap in the literature considering the effect of radon decay. SC/Tetra, a commercial CFD software, was used for this study as it allows for the simulation of gas migration through the cave and the mine openings. The study results showed the same trend as previous studies regarding the relationship between airflow and the corresponding radon concentrations in the working areas of a typical block cave mine. However, there were discrepancies in the values in both approaches. Future research will involve modelling the dynamic nature of the cave and validating the model with field data.

Keywords: Block caving, Radon gas, 3-dimensional model, Radioactive decay, Gas migration, CFD.

1. Introduction

Block caving is a mining method that involves the breaking of rock by the action of gravity after it has been undermined. It is regarded as a highly cost effective underground mass mining method [1]. With declining near-surface mineral deposits, it is one of the most cost effective methods to mine deep-seated deposits. However, caving and fracturing of the orebody often liberate radon from granitic ore [2].

2. Numerical modelling of gas emissions in underground mines

Gas migration and its interaction with the mine ventilation system is a complex process. To study this phenomenon, various researchers used multiple approaches: full scale underground measurements, scale

model studies with CFD and other numerical techniques [3]. CFD techniques were used to study this phenomenon in underground mines and they have been proven to be a reliable method of study. Mitev et al. studied airflow patterns in Bord and Pillar mining [4]. Several studies have been conducted to study the gob in longwall mining: Yuan and Smith investigated spontaneous heating in a longwall gob area [5], while Ren and Balusu studied goaf gas migration to control spontaneous combustion in a longwall mine [6], and Michael et al. studied inertization of a sealed mine area [7]. The investigation of the impact of face ventilation and nitrogen inertization in bleederless longwall gobs was performed by Mart et al.[8]. However, to the authors' knowledge, there is very little understanding on the phenomenon of gas migration in block cave mines. Despite the extensive geomechanical studies on block cave mines, there is limited detailed literature available on the prediction of porosity and

permeability of block cave which is critical for understanding the gas migration process in block cave mines. Board and Pierce suggested a porosity of 0.3 for caved rock [9] while Leonardi et al. suggested that the porosity of a steady cave with fine grains is less than 0.1 [10]. In this study, these values were used to model gas migration in a block cave mine.

3. Problem definition

According to Code of Federal Regulations (CFR), 30 CFR 57.5038, no person should be subjected to, a radon concentration, cumulative exposure of 4 Working Level Months (WLM) in one year with an upper limit of 2 WLM in two months. On average, the radiation level should not exceed 0.333 WLM per month to keep miners safe throughout the year. Due to its short half-life (3.82 days), it is important to develop control measures to reduce radon concentrations as low as possible in the mine air (ALARA Principle). In order to control the working level of radon in a mine, McPherson developed a relationship (Equation 1) to determine the quantity of air needed to achieve a desired working level at the exit of an airway supplied with uncontaminated air with constant radon emanation [11]. This equation predicts the radon level at the exit of an airway. However, prediction of radon migration with respect to space and time is not fully explored. This research is focused on developing a CFD model that can be used to predict radon level in a block cave mine with respect to space and time.

$$\frac{WL_1}{WL_2} = \left(\frac{Q_2}{Q_1}\right)^{1.8} \quad (1)$$

Where WL_1 is the working level corresponding to Q_1 (Air flow in m^3/s) and WL_2 corresponding to Q_2 (Air flow in m^3/s).

4. Radon gas

Rocks in the earth's crust contain uranium, a major source of radon, at a rate of about 4 grams per tonne on average [11]. Hence, the fracturing and breaking of these rocks leads to the release of radon gas in mines. Abumurad et al. predicted the average radon concentration in a crustal rock as 37 Bq/kg [12]. In the disintegration series of uranium, most of the decayed products are solids, unlike radon which is a gas. This facilitates its escape towards the atmosphere [11]. Radon is one decay product that has generated lots of concerns because it contributes significantly to human exposure to radioactivity. According to the U.S. surgeons, 20,000 Americans die from radon-related lung cancers every year [13]. There are several isotopes of radon but radon-222 is the most abundant. Radon (^{222}Rn) is an inert radioactive gas and a direct disintegration product from the decay of radium (^{226}Ra). During the disintegration process, radon releases

alpha, beta and gamma radiation which is very dangerous to human health [11]. Gamma radiation penetrates deeper into the body than alpha and beta radiation because it transfers high energy to atomic particles which can interact with tissues to form ions [13]. The radon daughters of concern are Polonium-218(RaA) with half-life of 3.1 minutes, Lead-214(RaB) with half-life of 26.8 minutes, Bismuth-214(RaC₁) with half-life of 19.7 minutes and Polonium-214(RaC₂) with half-life of 164 μs [11].

4.1 Radon gas emanation

Radon emanation is defined as the escape of a radon atom from a radium bearing grain into the pore space [14]. The actual emanation of radon from a rock surface can be measured or calculated from Equation 2 [11].

$$J = C_{\infty} \sqrt{\lambda D \theta} \quad (\text{pCi}/\text{m}^2\text{s}) \quad (2)$$

Where J is the radon gas emanation from rock surface ($\text{pCi}/\text{m}^2\text{s}$), θ is the rock porosity (fraction), C_{∞} is the radon concentration at infinite distance into rock (pCi/m^3) calculated as (B/λ) [15], B is the radon gas emanation from fragmented rock ($\text{pCi}/\text{m}^3\text{s}$); usually called emanating power, λ is radon decay constant (2.1×10^{-6} Bq), and D is the diffusion coefficient for rock (m^2/s).

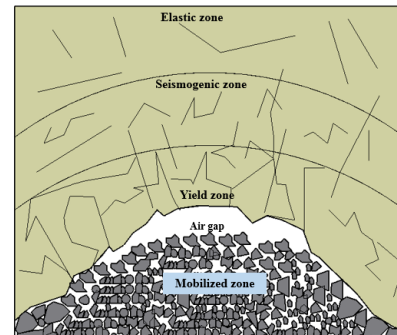


Fig. 1. Main regions of a propagating cave

To study the migration of radon in a mine, the emanating rate from an exposed surface J ($\text{pCi}/\text{m}^2\text{s}$) and emanating power B ($\text{pCi}/\text{m}^3\text{s}$) from drill cores or the samples must first be measured [11]. In the past, several experiments and surveys have been conducted to determine the emanating powers of different samples [12]. It is important to note that several factors such as radium distribution, grain size, moisture content, and temperature affect the emanation power of a given sample [14]. In block caving, it is complex to predict the emanation power because caving is a dynamic process. The rock surfaces in the drifts have the potential to emanate some quantity of radon gas into the mine environment. As the cave continues to propagate, the geometry of the cave changes

as shown in Figure 1. This change in geometry affects the porosity, which is another useful variable to predict the gas emanation. The extraction of ore from the draw points also changes the porosity of the cave. This dynamic nature of the cave complicates the study of radon gas migration in a block cave mine. The challenge in quantifying the release of radon gas into the mine is not only its mixing with the mine airstream, but also its disintegration into radon daughters with shorter half-lives. Hence, control measures should be taken to remove radon gas from the mine as soon as possible to reduce the residence time which affects the concentration (working level) of radon in the mine. McPherson stated that if an airway is supplied with uncontaminated air and the rate of radon emanation remains constant, then the exit working level of radon daughter is proportional to the residence time (t_r) raised to the power of 1.8 (Equation 3) [11]:

$$WL \propto (t_r)^{1.8} \quad (3)$$

4.2 Radon transport

The transport of radon gas is related to different factors. Most of these factors have been identified as advection, diffusion, radioactive decay, adsorption on solid grains, and the emanation as discussed above [16]. Being an inert element, it migrates through faults and fractured soils. Hence, it might sink into ground water, caves or rise in the atmosphere [16]. Existing literature indicates that several approaches have been used to model radon gas migration. Zakaria et al. utilized TOUGH2 software to study radon emanation and transport in the subsurface [16]. Urosevic et al. used a finite element method to simulate indoor radon and thoron distribution [17]. Kohl et al. used a coupled finite element code named FRACTure to study three different cases of radon transport (diffusion-advection-decay, diffusion-advection and diffusion decay) from subsurface to buildings. [18]. Dong et al. used FLUENT to study the dispersion of radon released from a uranium mine ventilation shaft [19]. In general, CFD has been used to simulate indoor distribution of radon [18][19]. However, there has been limited research in the applications of CFD to study radon gas migration in block cave mines.

5. Methodology

In this study, a preliminary 3-dimensional CFD modeling was developed by considering a steady cave condition without taking into account the effect of draw and other dynamic factors. The model assumes that the mobilized zone and draw points are filled with broken rocks. Hence, the draw points were considered as a part of the mobilized zone and treated as porous media. The yield, seismogenic and elastic zone were also treated as porous media based on properties discussed in section 5.1 below.

The air gap was modelled as open region between the mobilized and yield zone. A uniform radon emanation source was assumed for the model which is a limitation in

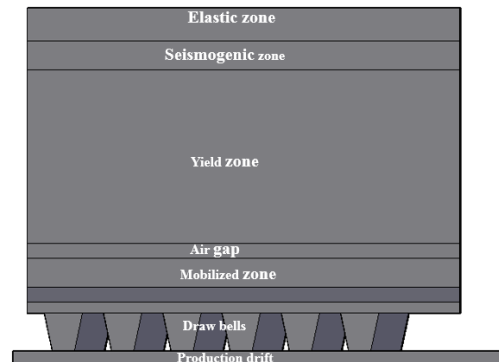


Fig. 2. Block cave layout (Front view of the geometry)

the model because the radon gas migration becomes steady after some time. The model considered radon decay; however, the modelling of radioactive decay is computationally expensive, to this effect, the radioactive decay simulation considered only radon 222 decay into polonium (^{218}Po). The basic unit conversions used for this simulation are: 1 Bq= 27 pCi [11], 1 WL = 100 pCi/L [11], 1 Bq= 1.75×10^{-19} kg [20].

5.1 Cave layout

This model considered a typical block cave mine that is fully developed. The model consists of a series of six draw points along two production drifts of a block caving mine as shown in Figures 2-4. The dimensions of the production drifts are modelled as 4.3 m wide and 4.3 m high, with an overall length of 170 m; the drawpoints are modelled as 4.3 m wide, and 4.3 m height. The cave is modelled as 150 m along the production drift, 30 m across the two drifts and 121.9 m high. The drawpoints are oriented at 56° to the production drifts, based on El-Teniente design. Duplancic and Brady investigated cave propagation phenomenon through numerical simulation studies and identified four main regions of a typical block cave [21]. However, another region, 'air gap' exists if the overlying yielded zone retains some level of cohesion [22]. Figure 1 shows a schematic diagram of the cave regions as presented by Sainsbury [22]. The mobilized zone consists of broken rock; properties of this zone are assumed to be similar to the draw columns. The air gap is the region between the yielded zone and the mobilized zone while the yielded zone is a region that is fractured and has lost all of its cohesive strength. The seismogenic zone is a region with the initiation of new fractures while the elastic zone is the region where the rock behaves like an elastic material [9]. The average thickness of the yield zone is estimated to

be usually 55-83 m [9]. However, this region is modelled as 60 m in height. The air gap is modelled as 5 m high, the seismogenic zone is modelled as 10 m, while the elastic zone is modelled as 20 m. The mobilized zone alongside with the drawpoints is modelled as 26.9 m in height.

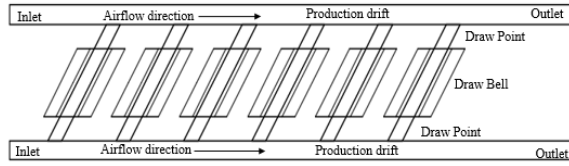


Fig. 3. Plan view of the cave showing the drawpoints, draw bells and drifts.

5.2 Porous media

As discussed above, all the cave zones were modelled as porous media except the air gap. SC/Tetra has a model for the porous media where a porosity of the given volume can be specified. The model has different types of porous media, however, the porous media packed bed filled with solid particles is used for this simulation. SC/Tetra does not consider the flow path in porous calculation configuration; an external force is applied in opposite direction to flow in order to induce pressure loss. The porosity of the broken rock in the drawpoints and mobilized zone is assumed as 30%, as discussed in Section 2 [9]. Fractured geological media are usually considered as porous media for the purpose of modelling [23]. Hence, the porosity of the yield zone is set as 5% and the seismologic zone set as 3% based on average values found in the literature for fractured rocks and the elastic zone is set as 1% based on the properties of intact rocks [24].

5.3 Radon diffusion and radioactive decay

Diffusion is one of the major factors that should be considered in the analysis of radon transport as discussed in section 4.2. The concentration of each diffusion species is treated as the ratio of the mass of a specific species to the total mass of all species present in the volume.

$$C_i = \frac{m_i}{M} \quad (5)$$

Where m_i the mass of a specific species and M is the total mass of all species. Important parameters for simulation of radon diffusion are diffusive coefficient or mass diffusivity, molar mass, specific heat at constant pressure and thermal conductivity. Radon diffusivity was set to $1.1 \times 10^{-5} \text{ m}^2/\text{s}$ [11]. The zones were modelled as volume

sources for radon gas emanation and the drift surfaces were modelled as sources of radon into the drift. Radon emanation from the volume of fragmented rock was computed as $600 \text{ pCi}/\text{m}^3\text{s}$ (B) while the radon gas emanation from the rock surface was computed as $10 \text{ pCi}/\text{m}^2\text{s}$ based on average values from literature. This assumes fragmented volume of rocks at different zone but different porosities. For this preliminary simulation, a uniform source of radon was considered. It is assumed that the radon emanation will be from the walls of the production drifts and volume sources from the mobilized, yield, seismic and elastic zones.

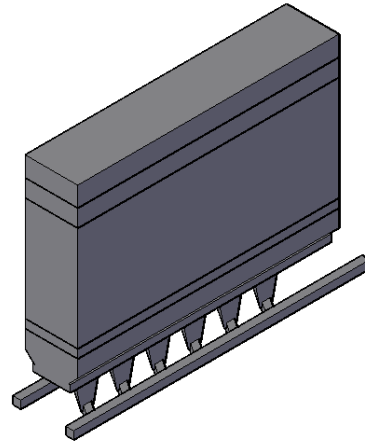


Fig. 4. Isometric view of the geometry.

Radioactive decay is considered in the analysis of radon transport as discussed in section 4.2. The model included the effect of radon decay on radon migration. Because decay simulation is computationally expensive, only the decay of radon (^{222}Rn) to polonium (^{218}Po) was simulated. In this case, the alpha particle was defined element to balance the mass equation as shown below. The reaction rate is defined as the decay constant of radon ($2.1 \times 10^{-6} \text{ Bq}$).



5.4 Boundary conditions

Obtaining a reliable result from a CFD model is highly dependent on the boundary conditions. The boundary condition used for the inlet is velocity condition with different values based on the quantity of airflow. The inlet temperature of the airflow is set as 20°C with no concentration of radon. A friction factor (k) for the walls of the production drifts is

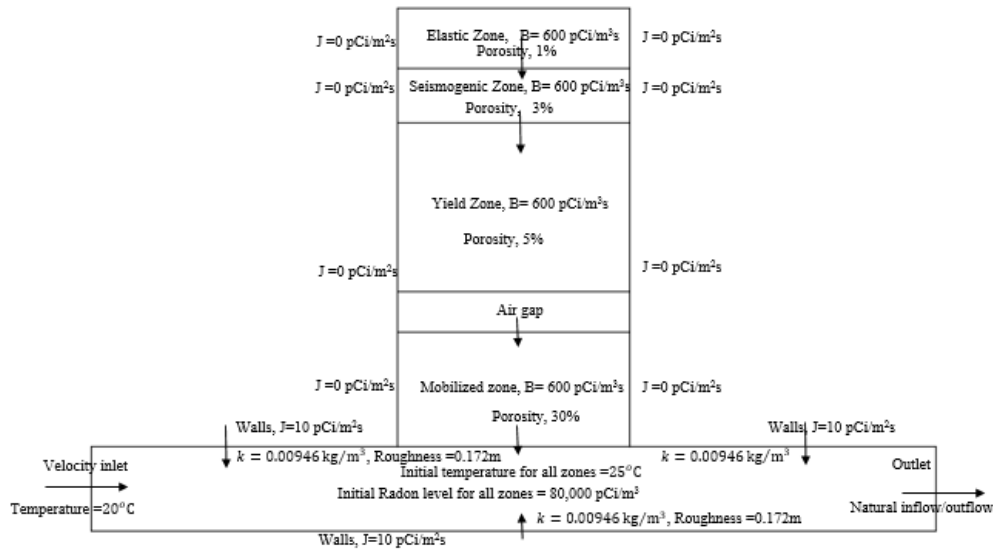


Fig.5. Schematic diagram of boundary conditions used for the CFD model

assigned as 0.00946 kg/m^3 . Natural inflow/outflow is used for the outlet conditions of both drifts; this condition assumes that velocity and pressure do not change in the normal direction. Therefore, the condition can be used if the flow does not really change near the boundary. It is used because the flow is assumed to continue into other sections of the mine. The wall condition was used for the walls of the production drift. Figure 5 shows a schematic diagram of the boundary conditions used for the simulation.

5.5 Solver settings

Airflow through the mine is assumed as incompressible and turbulent. A Courant number of 0.95 was used in this analysis to ensure accurate results and convergence criteria of 10^{-5} was considered for the radon gas diffusive species and velocity. Standard $k-\epsilon$ model was used for this simulation and was modified to ensure fully developed flow at the inlet of the airway. It will be necessary to do some analysis in the future to predict the best turbulent model applicable for block cave mining. However, in general, the $k-\epsilon$ model has been proven to be reliable for mining applications [1]. In summary, the conservation of mass, momentum, energy, turbulence model, diffusion and porous media equations were solved for analyzing radon migration in a block cave mine.

5.6 Grid independence study

It is important to ensure simulation results are grid independent. A grid independence study was carried out on the geometry to determine the mesh size that would give a reliable result due to the complex geometry of the cave. Results of mesh elements from a range of 1,028,256 to 18,123,158 were analyzed and it was observed that further increase from 10,517,955 mesh elements had no much effect on the result. Hence, the 10,517,955 mesh elements were used for this analysis.

6. Results

This preliminary analysis was performed to observe radon distribution in different zones of a block cave with airflow of $40,000 \text{ cfm}$ ($18.88 \text{ m}^3/\text{s}$) and the results were analyzed at steady state to understand study radon migration. Figure 6 shows the velocity magnitude through the production drifts, draw columns and drawpoints while Figure 7 shows the pressure distribution. The pressure distribution across a portion of the draw columns is shown in Figure 8. Radon distribution through the production drifts, draw columns and draw points are shown in Figure 9. From Figure 9, it was observed that the radon working level increased toward the end of the production drift due to drop in pressure as shown in Figures 7 and 8. This effect is clearly shown in Figure 8 by observing the pressure drop at the same position across the draw columns. It was observed that the

drawbells towards the end of the production drift has lower pressure which couldn't keep the radon deeper into the cave. Hence, the steady radon level at different zones can be obtained from the CFD results which could be helpful in understanding the concentration of radon in different zones; it is important in designing an optimum ventilation system for a block cave mine as the actual measurement of radon levels in different zones of block is difficult. Airflow is the primary method of controlling atmospheric conditions in underground mines. To investigate the phenomenon of airflow through block cave, a transient analysis was conducted to study the effect of different quantities of air flow in a production drift initially at 0.8 WL. The results were analyzed for 35,000 cfm (16.52 m³/s), 40,000 cfm (18.88 m³/s), 50,000 cfm (23.60 m³/s), 60,000 cfm (28.32 m³/s), 70,000 cfm (33.04 m³/s), 80,000 cfm (37.76 m³/s) and 85,000 cfm (40.12 m³/s) once the steady state flow condition was established. This is verified by the conservation of mass equation which infers a steady state condition if the radon concentration is steady with time [25]. A steady decrease was observed along the production drifts as the airflow increases. Towards the end of the drifts, the pressure of the airflow is decreased due to the effect of losses due to friction and shock losses as shown in Figures 8 and 9. This decrease in pressure through the drift makes the draw point toward the ends of the drift potentially dangerous due to higher concentration of radon gas. Figure 10 shows a modified range of radon working level to observe the potentially dangerous area with airflow of 40,000 cfm.

7. Verification

This is a preliminary study and has not been validated; however, the simulation results were compared with McPherson's relation of the airflow

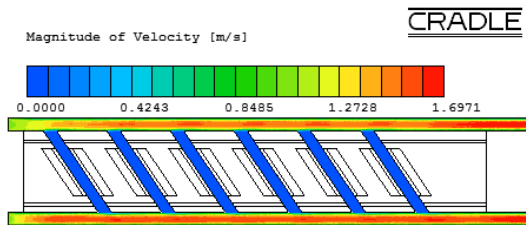


Fig. 6. Velocity magnitude with airflow of 40,000 cfm (18.88 m³/s)

and working level. McPherson developed a relationship (Equation 1) to determine the quantity of air needed to achieve a desired working level at the

exit of an airway supplied with uncontaminated air with constant radon emanation [11]. Equation 1 was

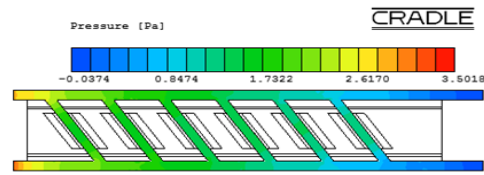


Fig. 7. Static gauge pressure distribution along the production drift ventilated with an airflow of 40,000 cfm (18.88 m³/s)

used to calculate the expected working level at the exit of the airway and compared with the simulation results (Figure 11). The initial simulation result for 35,000 cfm (16.52 m³/s) was used as the starting point to analyze the analytical solution. Result shows disparities in values but a close relationship was observed between both approaches. In general, there was a good agreement with the findings of Rock and Walker that the analytical results often underestimates the amount of air required to dilute the radon concentration [11]. However, it was observed that the radon level varies at different point of the of the airway outlet. Hence, the average radon level was used from the simulation results.

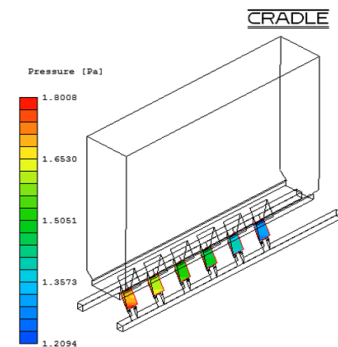


Fig. 8. Static gauge pressure distribution in the drawbells ventilated with an airflow of 40,000 cfm (18.88 m³/s) of fresh air.

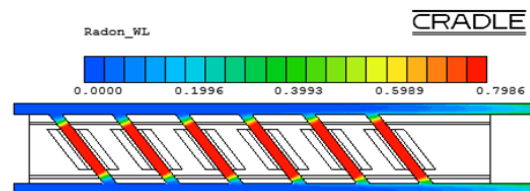


Fig. 9. Radon gas distribution in the mine initially at 0.8 WL ventilated with airflow of 40,000 cfm (18.88 m³/s) of fresh air

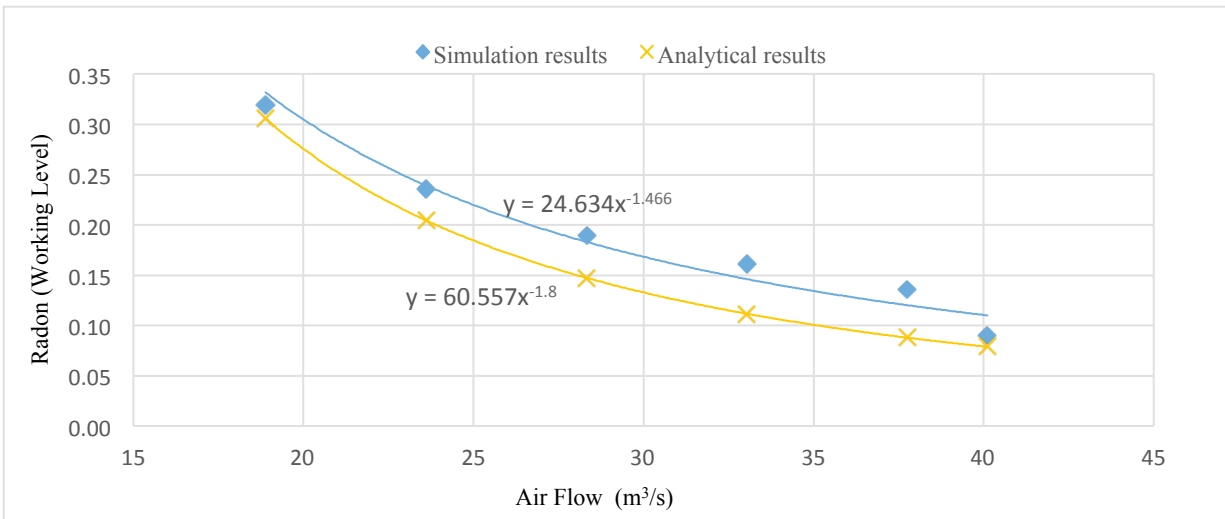


Fig. 11. Comparison plot of the Analytical formula [11] and simulation result

8. Future work

Future research will be focused on refining and validating these models with field data. It will involve developing a relationship between the airflow and working level with respect to space and time and studying the effects of different factors that affects radon gas concentration in the mine. Some of the identified factors are emanation power, temperature, pressure, rock size, annealing effects on emanation power and porosity [25]. These parameters will be studied to understand their effects on radon migration. Future research will also involve modelling of other abundant radon isotopes with shorter half-lives, and the migration of radon daughters in a block caving mine.

Acknowledgment

We greatly acknowledge the financial support of NIOSH (200-2014-59613), technical support from software Cradle Co., Ltd. and our industry partner.

References

- [1] Juan P. Hurtado, Nicolas Diaz, Enrique I. Acuna, Joaquin Fernandez, "Shock losses characterization of ventilation circuits for block caving production levels," *Tunnelling and underground space technology*, vol. 41, pp. 88-94, 2013.
- [2] D. M. Loring, E.P. Meisburger IV, "A discussion of radon and the mitigation strategy at the Henderson mine," in *13th United state/North American Mine ventilation symposium*, Sadbury, Ontario, 2010.
- [3] Adrian Kelsey, Christopher J Lea, Ian S Lowndes, David Whittles, Ting X Ren, "CFD modelling of methane movement in mine," in *International conference of safety in mine research institutes*, South African institute of mining and Metallurgy, 2003.
- [4] Mitev Ranjan, Karan Kumar, Subrata Kr. Ghosh, "Mine ventilation in a bord and pillar mines using CFD," *International Journal of Emerging technology and Advanced Engineering*, vol. 3, no. 3, pp. 389-393, 2013.
- [5] A.C Smith, L. Yuan, "Simulation of Spontaneous heating in longwall gob area with a bleederless ventilation system," *Mining Engineering*, pp. 61-66, 2008.
- [6] Ting Ren, R. Balusu, "CFD modelling of goaf gas migration to improve the control of spontaneous," in *Coal Operator's conference*, Aziz, 2005.
- [7] Michael A. Trevits, Liming Yuan, Michael Thibou, Guy Hatch, "Use of CFD modelling to study inert gas injection into a sealed mine," in *SME Annual meeting*, Phoenix, 2010.
- [8] J. Marts, J. Brune, R. Gilmore, D worall, J Grubb, "Impact of face ventilation and nitrogen inertisation on hazardous gas distribution in bleederless longwall mine," *Mining Engineering*, vol. 65, pp. 71-77, 2013.
- [9] Mark Board, M. E Pierce, "A review of recent experience in modelling of caving," in *Proceedings of the international workshop on numerical modelling for underground mine excavation*, 2009.
- [10] C.R Leonardi, D.R.J. Owen, Y.T Feng, W.J. Ferguson, "Computational modelling of fines migration in block caving operations," in *5th international conference and exhibition on mass mining*, Lulea, 2008.

- [11] M. J. McPherson, *Subsurface Ventilation and Environmental Engineering*, New York: Chapman and Hall, 1993.
- [12] K.M Abumurad, M.Al-Tamimi, "Emanation power of radon and its concentration in soil and rocks," *Radiation Measurements*, vol. 34, pp. 423-426, 2001.
- [13] D. M. Loring, "A study of radon regulation and pathology as it relates to underground hardrock mining," in *12th U.S./North American Mine ventilation symposium*, wallace, 2008.
- [14] Akihiro Sakoda, Yuu Ishimori, Kiyonori Yamaoka, "A comprehensive review of radon emanation measurements for mineral, rock, soil, mill tailing and fly ash," *Applied Radiation and isotopes*, vol. 69, pp. 1422-1435, 2011.
- [15] Robert C. Bates, John C. Edwards, "Mathematical modelling of time dependent radon flux problem," in *Second mine ventilation congress*, Reno, Nevada, 1980.
- [16] Zakaria Saadi, Didier Gay, Jerome Guillevic, Roselyne Ameen, "A new TOUGH2 module for simulation radon emanation and transport in the subsurface," in *TOUGH symposium*, Berkeley, 2012.
- [17] V. Urosevic, D. Nikezic, S. Vulovic, "A theoretical approach to indoor radon and thoron distribution," *Journal of Environmental Radioactivity*, vol. 99, pp. 1829-1833, 2008.
- [18] T. Kohl, F. Medici, L.Rybach, "Numerical simulation of radon transport from subsurface to buidings," *Journal of Applied Geophysics*, vol. 31, pp. 145-152, 1994.
- [19] Dong Xie, Hanqing Wang, Kimberlee J. Kerarfott, "Modelling and Experimental validation of dispersion of ^{222}Rn released from a uranium mine ventilation shaft," *Atmospheric Environment*, vol. 60, pp. 453-459, 2012.
- [20] Keramatollah Akbari, "Impact of Radon ventilation on indoor air quality abd buidling energy saving," *School of sustainable development of society and technology*, Keramatollah Akbari, 2009.
- [21] Duplancic P. and Brady, B H, "Characterization of caving mecahnisms by analysis of seismicity and rock stress,," in *9th International Congress on Rock Mechanics*, Paris, 1999.
- [22] B. Sainbury, "Sensitivities in the numerical assessment of cave propagation," in *Second international syposium on block and sublevel caving*, Perth, Australia, 2010.
- [23] M. J. Gordon, "Dependence of effective porosity on fracture continuity in fractured media," *Ground water*, vol. 24, no. 4, pp. 446-452, 1986.
- [24] "Rock Mechanics Laboratory LMR," [Online]. Available: http://lmrwww.epfl.ch/en/ensei/Rock_Mechanics/ENS_080312_EN_JZ_Notes_Chapter_4.pdf. [Accessed 10 February 2014].
- [25] Kazuichi Satomi, Paul Kruger, "Radon emanation mechanism from finely ground rocks," *Stanford geothermal program interdisciplinary research in Engineering and Earth sciences*, pp. 1-69, October 1982.

Economics of Diesel Fleet Replacement by Electric Mining Equipment

Julian Varaschin^a, Euler De Souza Ph.D^b

^aGoldcorp, Ontario, Canada

^bQueen's University, Kingston Ontario Canada

Over the past 10 to 15 years escalating energy costs, especially for diesel fuel, have helped erode the bottom lines of mining companies worldwide. At the same time, there is growing pressure to reduce the exposure of underground workers to diesel emissions. The persistence of these trends would seem to strongly favour electric mining equipment which could eliminate all air quality issues related to diesel engines and also provide a stably priced alternative to diesel equipment. Current conditions create an incentive for examining the economics of electric mining equipment as lower fuel costs and other savings could contribute to lower operating costs. Potential sources of cost savings include reduced ventilation costs, reduced fuel costs, reduced development costs and reduced CO₂ emissions. This paper shows how an engineering model can be developed to examine and compare the economics of diesel and electric equipment. The model examines both operating and capital costs for diesel and electric equipment, as well as the other sources for savings listed above.

Keywords: vent, ventilation, economic, evaluation, electric, diesel, equipment

1. Introduction and background

One of the largest input costs to a mining operation is the energy required to extract and process mineral ores. This demand for energy is typically met by diesel fuel, or electrical grid power.

Historically (starting in the mid 1980's), low and stable energy prices would have made it difficult to justify investing for increased energy efficiency [1]. However, increases in the cost of diesel fuel since the mid 2000's may now allow for a compelling case to be made for transitioning toward more efficient technologies and if possible away from diesel fuel.

The impact of diesel fuel in particular on input costs was identified in reports by industry analysts such as PricewaterhouseCoopers [2] and Ernst & Young [3]. In 2012 the latter specifically identified diesel fuel as the second biggest contributor to cost escalation in the South African mining sector after it had risen at a 15.7% annualized rate since 2007.

In an underground mining operation, the energy intensive extraction process is further exacerbated by the need for ventilating the work environment. In general ventilation is required in order to provide workers and diesel engines a source of fresh air and to dilute and clear away contaminants produced in the mining process. These include the following [4]:

- toxic equipment exhaust gases
- diesel particulate matter (DPM)
- heat
- dust (silica)
- and blasting fumes.

Although there are numerous reasons to ventilate a mine, it is likely that a majority of the costs incurred for ventilation are due in particular to the use of diesel

engines underground and the requirement in many mining jurisdictions to supply a given volume of air per bhp operating in the work place.

A 2005 report jointly published by the Canadian Industry Program for Energy Conservation (CIPEC), the Mining Association of Canada (MAC) and Natural Resources Canada (NRCan) looked in detail at how energy is consumed in underground mining operations and found that in a sample of 11 underground operations ventilation was by far the most energy intensive process before milling; accounting for about 50% of the energy consumed and between 1/3 to 2/5 of energy costs before milling. Dollar costs of ventilating the underground operations ranged from \$1.59 to \$4.18 (adjusted to 2014 US dollars) per tonne of ore [5].

In addition to the sustained increase in diesel fuel prices, the industry is also facing more rigorous standards for governing both the quality of the underground work environment and also the allowable levels of pollutants that can be emitted in diesel exhaust. In particular the industry is facing scrutiny of Diesel Particulate Matter (DPM), atmospheric Total Carbon (TC), atmospheric Elemental Carbon (EC) and Nitrogen Dioxide (NO₂). The industry is also facing a possible transition to a new engine standard, i.e. Tier 4, away from the current engine standard Tier 3. However, due to these changing standards and high fuel prices it is difficult to know what new or existing technologies will best serve the industry and provide the lowest costs in years to come.

2. Alternatives to diesel equipment

Over the years, several technologies have been proposed as alternatives to standard diesel equipment in an underground hard rock setting. These at least include the following:

- Tether and trolley-line electric equipment
- Battery powered electric equipment
- Hybrid diesel/electric equipment
- Hydrogen fuel cell equipment

In actuality, the only commercially available alternatives to underground diesel equipment are tether and trolley-line electric equipment, battery powered man carriers and small battery powered scoops and trucks.

3. The economics & price of diesel fuel

Since the mid 2000's the inflation adjusted cost (US\$ 2014) of sweet crude oil on world markets has increased from a ceiling of about \$40/bbl to a floor of between \$50/bbl and \$80/bbl. For a time it even peaked over \$140/bbl, a price over 3 and a half times more costly than at any point in the preceding two decades.

Unsurprisingly, movements in world oil prices during this period translated into higher retail prices for diesel fuel and gasoline. For example, between 2003 and 2014 the real retail price of diesel fuel in the US rose from an annual average of \$1.92/gal to an annual average of \$3.80/gal. This represents a 98% increase in the retail price of diesel fuel, or a 6% annualized increase over the 12 year period.

Conversely, movements in the price of oil were not followed by average market prices for electricity which instead remained relatively stable. During the same 12 year period the real retail price of electricity in the US grew from an annual average of 11.13¢/kW·hr in 2003 to an annual average of 12.39¢/kW·hr in 2014. This represents only an 11% increase in the price of electricity, or a 0.9% annualized increase over the period [1]. Real US retail prices for diesel fuel and electricity from 1999 – 2014 can be seen in Figure 1.

4. Evaluating capital & operating costs

4.1 LHD capital costs

Several recent publications agree that electric LHDs (eLHDs) have higher capital costs than traditional diesel LHDs [6] [7] [8].

The consensus among the sources is that the capital cost of an eLHD is approximately 20% higher than a diesel LHD, however, the differential seen for some smaller pieces of equipment ranged as high as 30% [7]. In addition to the initial premium for eLHDs, Moore notes in his article that a trailer with a diesel generator set could be required to move eLHDs beyond the range of the closest power take off and these could add an additional 10-20% to the purchase cost of an eLHD [6]. The full premium could then range 20to50% above the cost of a diesel LHD.

However, despite the stated premium for eLHDs, two papers suggest it may not be quite so large. For example, a 2014 paper suggests that for loaders of similar bucket capacities, "*capital costs ... for diesel and electric machines are similar*" [9]. Furthermore, a 2012 paper develops cost estimation formulae for both types of LHDs, and these do not exhibit the assumed premium for eLHDs when used to calculate costs for machines of equal bucket sizes [10].

For example, equations 1 and 2 were taken from the 2012 paper and they show two exponential relationships developed using single regression analysis (SRA) for estimating the capital cost of both diesel and electric LHDs. The paper indicates they have R² values of 0.923 and 0.953 respectively.

In order to compare the cost of diesel and electric LHDs, capital costs were calculated for varying bucket sizes and the difference between Equation 2 and Equation 1 were divided by Equation 1. The results can be seen in Figure 2 which shows that for bucket sizes larger than 3 cubic meters the premium for eLHDs is essentially not observable. Presumably if the premium existed the exponent in Equation 2 would have been much closer to the exponent in Equation 1. Regardless, even though the estimation formulae do not capture a persistent premium for eLHDs, it does not prove a premium doesn't exist. One possibility is that the premium could have just been lost within the margin of error of the estimation formulae.

$$\text{Diesel LHD Capital Cost} = 332,670x^{0.586} \quad (1)$$

$$\text{eLHD Capital Cost} = 400,060x^{0.484} \quad (2)$$

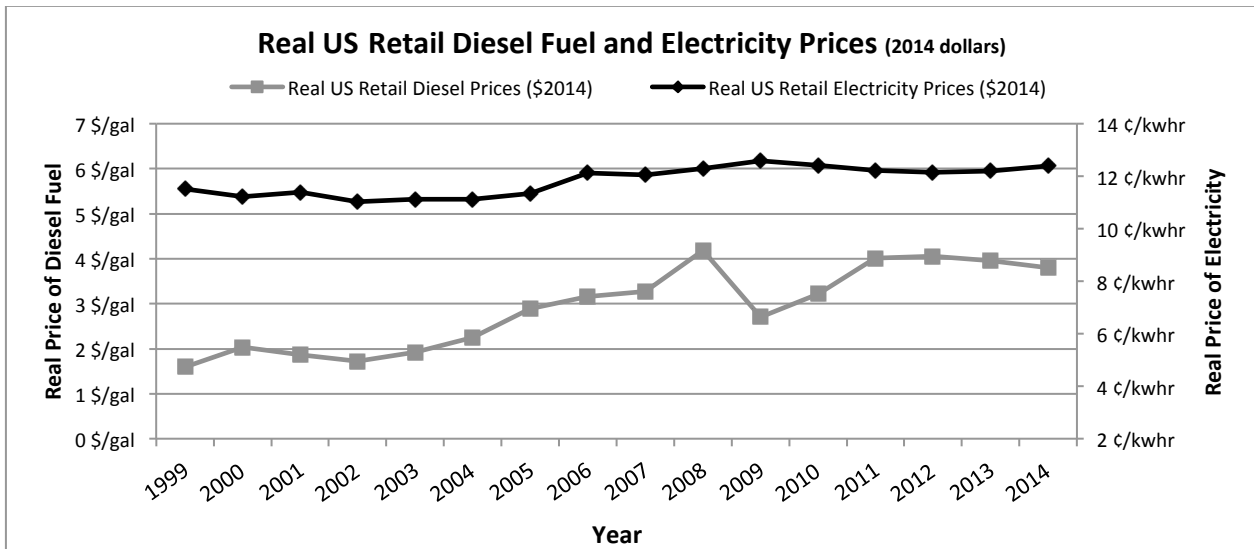


Fig. 1. Real US retail prices for diesel fuel and electricity from 1999 to 2014 in 2014 dollars. (Reprinted with permission)

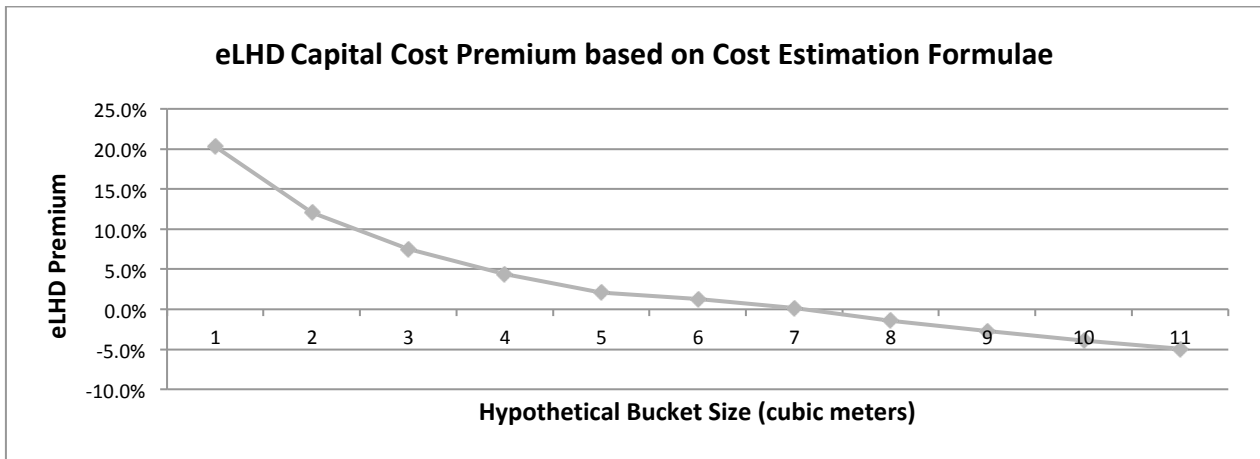


Fig. 2. Diesel and electric cost estimation formulae fail to show a premium for eLHDs. (Reprinted with permission)

4.2 LHD operating costs

Operating costs for eLHDs have been reported as being both lower and higher than their diesel counterparts [6] [7] [8] [9]. The reported differences in operating costs are usually attributed to the difference in cost between diesel fuel and electricity prices, and also to how expensive trailing cable maintenance is assumed to be. Although Paraszczak argues that operating costs for eLHDs must be lower under the right operating conditions due to their long and continued use in the Kiruna mine in Sweden [9], he also finds that according to a 2010 estimator's guide that operating costs for eLHDs are 15% higher than diesels.

Conversely, Jacobs finds in a 1993 Australian estimator's guide that maintenance costs for eLHDs are estimated to be approximately 30% lower than diesel LHDs [8]. However, he later inflates the hourly maintenance costs in his analysis by a significant 60%

to account for trailing cable replacement. Presumably to match the 15to20% premium reported in the 2010 estimator's guide used by Paraszczak.

Finally, in the 2012 paper by Sayadi et al. [10] it is possible to see how the operating costs (ignoring operator labour) for both diesel LHDs and eLHDs are broken into their component parts, Figure – 3.

The paper doesn't say which total hourly operating cost is higher or lower, however, if we assume that there is no difference in how diesel LHDs and eLHDs consume *Lubricants, Tires and Wear Parts*, it implies that the total hourly operating cost for eLHDs is lower as this would explain why the three categories appear proportionally larger. If the exercise is completed, the maintenance cost of the eLHD would come out 30% lower, the fuel costs would be approximately 50% lower and the total operating cost would be 30% lower

5. Economic evaluation of equipment using the average annual cost method

In general, the cost of labour should not be distinguished from other operating costs when comparing similar types of equipment. It is also true that maintenance costs are not separate from operating costs. In fact all maintenance costs, including the cost

of the labour to complete the maintenance, should be considered a subset of vehicle operating costs.

According to the *Average Annual Cost Method* [11], the average annual cost to run a piece of equipment is equal to the sum of depreciation, interest and operating costs.

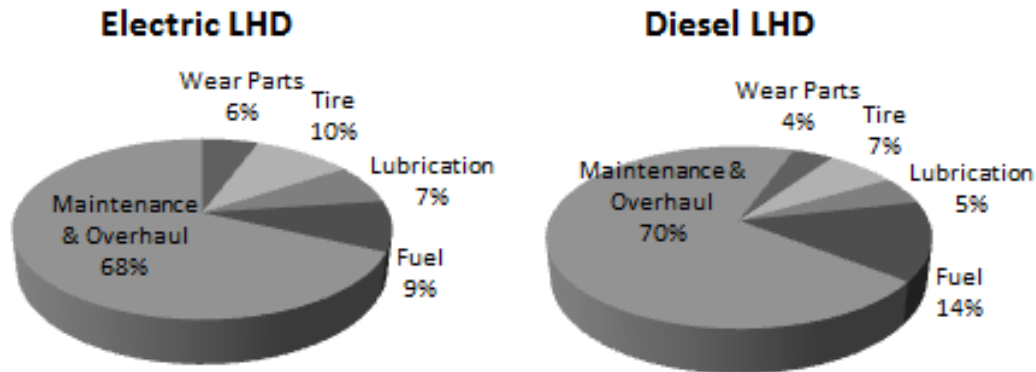


Fig. 3. Components of operating costs from Sayadi et al [10].

For example Equation 1 and its counterpart for operating costs, Equation 3, can be used to approximate an initial capital and operating cost for a 4.8m³ diesel LHD of \$833,333 and \$100/hr respectively. These estimates can then be combined with the assumptions listed in Table 1 in order to determine the average annual costs for each type of equipment, as seen in Table 2.

$$\text{Diesel LHD Op. Costs} = 36.19x^{0.638} \quad (3)$$

Table 1. Average annual cost assumptions.

Parameter	Value
LHD Bucket Size	4.8m ³
eLHD Cap. Ex. Premium	20%
eLHD Op. Ex. Premium	15%
Operating Hours per Year	6,000
Operator Salary per Year	\$100,000
Number of Operators	4
Service Life	4yr
Depreciation per Year	20%
Salvage Value	20%
Cost of Capital	8%

As can be seen from the average annual costs for each piece of equipment, even though eLHDs are assumed to cost 20% more than diesels to buy and 15% more than diesels to run (outside of labour costs), they are only 11% more costly to run each year on an all in basis.

Assuming the operating costs of electric equipment can vary based on their operating conditions, it is possible to use a range of operating costs to see how they impact the annual average cost.

Table 2. Average annual cost calculations.

Parameter	Diesel	Electric
Capital Cost	\$0.83 M	\$1.00 M
Salvage Value	\$0.17 M	\$0.20 M
Avg. Annual Investment	\$0.50 M	\$0.60 M
Avg. Annual Interest	\$0.04 M	\$0.05 M
Op. Ex. Less Labour	\$0.60 M	\$0.69 M
Annual Labour	\$0.40 M	\$0.40 M
Annual Depreciation	\$0.17 M	\$0.20 M
Average Annual Cost	\$1.21 M	\$1.34 M

Accordingly, Figure 4 shows the sensitivity of eLHD average annual costs to operating costs. It can be seen that despite an assumed 20% higher capital cost, if operating costs are assumed to be equal to a diesel LHD then the average annual cost of an eLHD is only 3% higher than a diesel LHD. As operating costs are assumed to be lower than diesel LHDs, it can be seen that eLHDs become less costly overall, again, despite the higher capital cost.

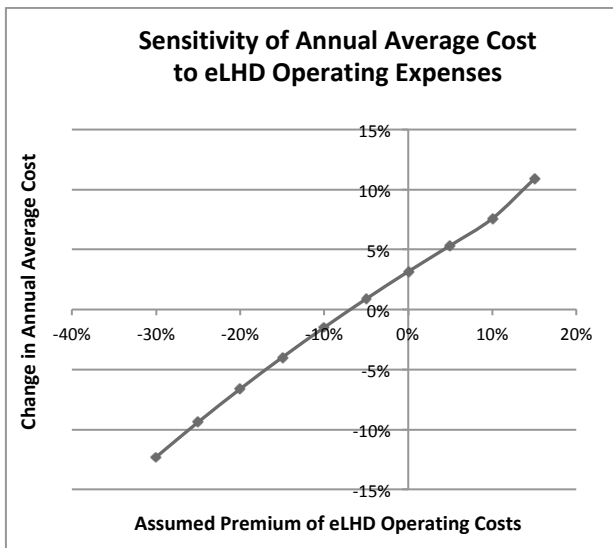


Fig. 4. Sensitivity of eLHD avg. annual cost to Op. Ex.

6. Estimating airflow requirements for electric equipment

Two recent papers address ventilation requirements for the dissipation of heat in an underground mine. The first addresses the heat produced by diesel equipment [4] and the other addresses the heat produced by electric equipment [12]. The first paper estimates the flow rate necessary to prevent the air temperature from increasing by more than 20°C for a specific engine size and its estimated consumption of diesel fuel. It found that a flow rate of 0.075m³/s per kW was necessary to prevent a temperature increase greater than 20°C. Making a basic assumption that electric motors produce 1/3 the heat for an equal amount of work [6] [9], perhaps this would suggest a flow rate of 0.025m³/s per kW for electric equipment.

The second paper assumed that the heat a piece of electric equipment contributed to the work environment was equivalent to its engine rating. It also assumed that an electric equipment fleet could be approximated by assuming vehicle motors were 70% as powerful as their diesel alternatives. It then used modelling software to determine how much airflow was required to prevent the deepest parts of various mine models from exceeding 30°C.

It was found that in a deep mine with little heat added from the host rock a flow rate of 0.04m³/s per kW could maintain the desired temperature. In a shallow mine, the necessary flow rate was found to be 0.03m³/s per kW.

Both of these approaches are helpful as they demonstrate the magnitude of air flow that could be expected to adequately supply electric equipment. However, it is likely that additional factors should be considered in order to determine how much airflows can be reduced in a mine fully benefitting from electric equipment.

For example, the following should also be considered:

- The above flows are calculated assuming each piece of equipment is operating at full load 100% of the time. In an operating mine, this is unlikely (even in the case of electric equipment, it should be considered how a changing load affects the Power Factors of the machine's motors).
- Adjustments were not made to auxiliary fans, and reducing aux. fan size could result in significant power savings (and also reduce heat loading underground).
- The ability to effectively exhaust blasting fumes in an acceptable amount of time should also be considered when discussing the lower limit to reducing airflows.

In order to determine **total** mine flowrates for electric equipment, it is proposed that the following steps be followed:

- 1) Determine the average heat loading of the equipment fleet, auxiliary fans and other sources during operation.
- 2) Consideration should then be given to adjusting total flow requirements according to estimations (or measurements) of equipment utilization rates.

For **drift** airflow requirements, the following steps are proposed:

- 1) Consider reducing the expected max heat loading (determined from the max number of kW's that will be operating in the heading at one time) by an engine/motor load factor.
- 2) Ensure auxiliary fans will provide a sufficient volume of air to
 - a. maintain an adequate flow velocity for working in the drift and
 - b. allow the drift to be quickly cleared of blasting fumes.

In order to estimate heat loading in a drift consider that a 300kW LHD on average throughout the shift might have an engine load factor of just over 50%. In this case, fuel consumption would be approximately 50L/hr as opposed to the ~90L/hr [4] that would be consumed under full load. This estimate might be considered reasonable as it happens to be proportional to the 40L/hr Jacobs used for a 256kW LHD in his cost/benefit analysis [8].

In this case it could be argued that the diesel LHD on average requires 0.0375m³/s per kW to dissipate heat. Assuming that on average an eLHD would do the same amount of mechanical work in a shift as an LHD and that each has a thermal efficiency of 35% and 90% respectively, then the 0.0375m³/s per kW can be factored by 0.4 (0.35/0.90 = 0.39) which results in a required airflow of 0.015m³/s per kW. To account for peak engine loading and to provide a factor of safety, this number could even be rounded up to 0.018, or

0.020 m³/s per kW (20-30%). This represents a 65% lower flowrate than the current regulation in Ontario.

7. Framework for evaluating total potential operational savings

7.1 Determining drift and level requirements

Due to issues that would arise in situations where lower airflow requirements would result in very low flow levels in a drift, the clearest example of savings on a local level are where flows would change from high to moderate. A good example would therefore be a level or drift where haul truck and LHD operation overlap (i.e. both operate at the same time).

For example, a 30t diesel haul truck with a 305 kW (410 hp) engine and a 6yd diesel LHD with a 200 kW (270 hp) engine typically would require 32 m³/s (68 kcfm) at 0.063 m³/s per kW. Assuming 25% leakage, a fan should supply 40 m³/s (85 kcfm).

Assuming these pieces of equipment were replaced by a 35t trolley-electric haul truck with a 72 kW diesel engine (400 kW main drive) and a 6yd eLHD with a 110 kW drive, then airflow requirements would be 4.5 m³/s for the haul truck at 0.063 m³/s per kW diesel and 2.2 m³/s for the eLHD at 0.02 m³/s per kW electric. The combined supply is then 6.7 m³/s (14 kcfm) or 8.5 m³/s (18 kcfm) with 25% leakage. Accordingly the velocity of air in a 4.5mWx4.5mH drift would drop significantly, but a final velocity of ~0.4m/s would not be unmanageable.

Table 3. Size reduction of auxiliary fans.

Parameter	Q ₁	Q ₂	Q ₃
Flow (cfm)	85,000	18,000	18,000
Duct Length (ft)	492	492	492
Duct k-factor	25	25	25
Duct Diameter (in)	60	60	36
Hs (in w.g.)	3.55	0.16	2.05
Fan Diameter (in)	48	48	36
Hv (in w.g.)	2.85	0.13	0.40
Ht	6.40	0.29	2.45
rpm	1780	n/a	1780
Motor hp	150	n/a	25
Blade ∠	28°	n/a	20.5°

By approximating a suitable fan according to the parameters in Table 3, it can be seen a 48" 150 hp fan would be required to supply 40 m³/s (85 kcfm) whereas only a 36" 25 hp fan can supply 8.5 m³/s (18 kcfm).

7.2 Determining total mine airflow

A base case scenario was imagined for a diesel fleet at a 3,000 tpd hard rock operation. Estimates for the total installed diesel power of different equipment types and their Utilization were combined in order to determine how much ventilation would be required for each type of equipment underground. Table 4 shows the original estimates for diesel power utilized in the

work place and the air required for ventilation at 0.063m³/s per kW.

Table 4. Estimating total mine airflows.

Equipment Type	Utilized kW	Base Q m ³ /s (kcfm)	New Q m ³ /s (kcfm)
Man Carriers	1,200	75 (160)	20 (40)
LHDs	1,350	85 (180)	15 (30)
Haul Trucks	3,000	190 (400)	80 (170)
Jumbos/Bolters	160	10 (20)	10 (20)
SLs/ANFO Loaders	320	20 (40)	20 (40)
Boom Trucks/Misc.	320	20 (40)	20 (40)
Auxiliary Fans		n/a	10 (30)
Total	6,350	400 (850)	175 (370)

To determine how the flow rate would change with electric equipment, the Utilized kW were factored by the differences in engine/motor power seen in the previous sub-section and then multiplied by the new rate of 0.02m³/s per kW. So, for example the 3,000 Utilized kW assumed for Haul Trucks was multiplied by (400/300) to get 4,000 Utilized kW and then 0.02m³/s per kW to get 80m³/s. eMan Carriers were assumed to have a motor power of 70 kW compared to 100 kW diesel Man Carriers. As seen in Table 4, flows decreased by ~60%.

7.3 Determining fuel savings

In order to calculate fuel use, assumptions (or measurements) must be made for the length of time equipment operates on average and how much fuel is consumed on average while it is operating.

For example the Effective Utilization of equipment could be multiplied by the shift length to determine how many hours on average that equipment operates each day. Then, from the on board computer (or some other form of data collection) the fuel consumption can be determined in liters or gallons per hour. The ratio of the actual fuel consumption to the maximum fuel consumption at full engine load could be considered the average engine load factor. For the purposes of demonstrating how fuel savings could be calculated, the following can be assumed:

- Diesel Engine Avg. Load Factor: 0.55
- Electric Motor Avg. Load Factor: 0.80
- Motor kW ≈ 70% of Diesel Engine kW

These values could be applied to the LHD Utilized kW from Table 4, for example, to calculate that both the LHDs (1,350 kW * 0.55 = 750 kW) and eLHDs (1,350 * 0.7 * 0.8 = 750 kW) complete roughly the same amount of work per hour of operation. However, assuming fuel consumption of 0.3 L/ kW·hr [4], the diesel engines will consume 225L of fuel per hour, or approximately \$180 in fuel at \$0.8/L. Whereas electrical power at \$0.07/ kW·hr would cost only \$53 for the same hour.

7.4 Direct cost savings

7.4.1 Main fan savings

Assuming there are 2 main fans for this mine and each supplies 200 m³/s at a total pressure set point of 3kPa (12" w.g.) and fan efficiencies of 83%, then using Equation 4 (metric) the power of the main fans can be calculated at 725kW each.

$$P_{fan} = \frac{H_T \cdot Q}{\eta} \quad (4)$$

Assuming no changes to the rest of the vent system, and fan diameters of 112", Equations 5 and 6 can be used to determine that a reduction in the flow rate to 175m³/s would result in a system total pressure of (0.57 kPa + 0.11 kPa) 0.68 kPa, a roughly 75% decrease. Again, using Equation 4 and assuming similar fan efficiencies, it is possible to see that the new system pressure would imply fan powers of 72kW each, a roughly 90% reduction in power.

$$H_{s_2} = \frac{H_{s_1} \cdot Q_2^2}{Q_1^2} \quad (5)$$

$$H_V = 0.6007 \cdot V^2 \quad (6)$$

Assuming the main fans ran 24 hours a day 360 days a year, at \$0.07/kW·hr the difference in operating cost would be \$790,000 per year.

7.4.2 Auxiliary fan savings

A similar analysis can be made for the local ventilation on a working level like the example described in Section 7.1. Assuming power costs of \$0.07/kW·hr and the auxiliary fan has a load factor of 0.85, a utilization of 0.75 and operates 365 days a year, it is possible to calculate that the 150hp fan would cost \$43,700 in power per year, whereas the 25hp fan would cost only \$7,300 per year. If 40 similar fan installations existed in an underground mine, the difference in power costs would be \$1.46M per year. Overall power requirements for the mine grid would drop by 3.7MW.

7.4.3 Fuel savings

Assuming that the same factors listed in Section 7.3 were applied to all of the equipment in Table 4, then the total fuel bill would be \$2.75M per year for diesel equipment versus only \$0.82M for electric. The difference in fuel costs would work out to \$1.93M each year.

8. Evaluation of potential economic benefits of electric equipment

Considering only the sources for cost savings already discussed it can be seen in Table 5 that these would total to \$4.2M per year. However, there are

additional sources of savings which could further reduce annual operating costs and these include the following:

- Mine air heating and/or cooling
- Smaller headings and raises
- And possibly in the future CO₂ credits

For example, assuming that the operation in question completes about 7,000m (20m/day * 350 days) of 5.5mWx5.5mH development per year, reducing the size of the duct used for ventilation from 60" to 36" in diameter could reduce the volume of material in each meter of development by 2.75 cubic meters (0.5m*5.5m). Assuming development costs of \$145 per cubic meter, over the course of the year development costs would be reduced by \$2.79M.

It is also possible to anticipate how a possible carbon credit or tax would add to the advantages offered by electric equipment. Assuming that each liter of diesel fuel emits 0.00269t of CO₂ and each MW·hr of electricity emits 0.133t of CO₂ (Ontario), it is possible to calculate that replacing diesel fuel reduces CO₂ emissions by approximately 7,750t per year and that reducing the power consumed by ventilation would further reduce CO₂ emissions by 4,275t per year. Assuming a similar price for carbon emissions as in the EU (€20/t ≈ \$27/t), these reductions would amount to an additional saving \$0.3M per year.

Table 5. Potential Economic Benefits of Equipment.

Operating Costs	Savings
Fuel	\$1.9M
Main Fan Power	\$0.8M
Aux. Fan Power	\$1.5M
Sub Total	\$4.2M
Reduced Propane Use	\$0.5M
Development	\$2.8M
Total Carbon Credits	\$0.3M
Total Potential Savings	\$7.8M

If these savings were realized by a gold mine which produced 200,000 oz of gold a year with *Cash Costs* of 700/oz, these cost savings would reduce its *Cash Costs* by ~\$39/oz which would equate to a ~5.6% reduction in operating costs. Alternatively, assuming an *All In Sustaining Cost* (AISC) of \$900/oz the savings would equate to a 4.3% reduction in operating cost.

As world oil prices have proven volatile, it is possible to consider how the reduction in *Cash Costs* will change as the price of diesel fuel changes. In Figure 5 it can be seen that with diesel prices ranging from 60 to 120 cents per liter the total potential reduction in *Cash Costs* ranges from 5.1% to 6.6%.

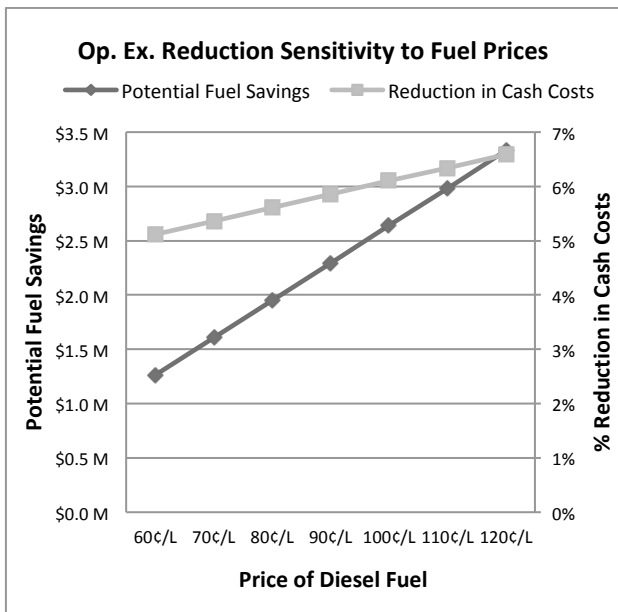


Figure 5. Op. Ex. Sensitivity to Fuel Price.

9. Summary, conclusions and future work

It is possible to see that the price of diesel fuel in particular provides a significant incentive to find alternative sources of power. However, it is also possible to see that there are a number of other factors which contribute to a mine's operating costs which could be reduced by transitioning away from traditional diesel equipment. In particular, the reduction in the power consumed not only by the main fans, but also by auxiliary fans and also the amount of development that currently needs to be done to support existing ventilation practices all contribute significantly to operating costs. Using reasonable approximations, this paper showed operating costs could be reduced on the order of 5% by optimizing power use and ventilation in underground hard rock mines. However, following a similar methodology with more refined numbers, perhaps using a real world case study, might reveal even more potential for the reduction of costs.

References

- [1] U.S. Energy Information Administration, Short-term Energy Outlook, Retrieved Feb 25, 2015 from Data - Real Prices Viewer: <http://www.eia.gov/forecasts/steo/realprices/>
- [2] PwC, Mine: The Growing Disconnect, Retrieved Nov 07, 2014, from Global mining publications, thought leadership and studies: https://www.pwc.ch/user_content/editor/files/publ_energy/pwc_mine_the_growing_disconnect_e.pdf
- [3] EY, Cost Control and Margin Protection in the South African Mining and Metals Industry (2013), Retrieved Nov 07, 2014, from Cost Control and Margin Protection in the South African Mining and Metals Industry: <http://emerging>

markets.ey.com/cost-control-south-african-mining-industry

- [4] J.D. Stinnette, Establishing Total Airflow Requirements for Underground Metal/Non-metal Mines based on the Diesel Equipment Fleet, Queen's University, Kingston, Ontario, Canada 2013.
- [5] Competitive Analysis Centre Inc., Benchmarking the Energy Consumption of Canadian Underground Bulk Mines, Canadian Industry Program for Energy Conservation (CIPEC), Ottawa, 2005.
- [6] P. Moore, Plugging the gap underground, Mining Magazine (Nov, 2010) 40-46.
- [7] J. Paraszczak et al., Electric load-haul-dump machines: real alternatives for diesels?, CIM Journal Vol. 4, No. 1 (2013).
- [8] W. Jacobs, Electric LHDs in Underground Hard Rock Mining: A Cost/Benefit Analysis, School of Mechanical and Chemical Engineering, University of Western Australia, Crawley, Western Australia (2013).
- [9] J. Paraszczak et al., Electrification of Loaders and Trucks - A Step Towards More Sustainable Underground Mining, International Conference on Renewable Energies and Power Quality, Renewable Energy and Power Quality Journal, Cordoba, Spain, 2014.
- [10] A. R. Sayadi et al., Hard-rock LHD cost estimation using single and multiple regressions based on principal component analysis, Tunnelling and Underground Space Technology (2012) 133-141.
- [11] P. L. McCarthy, Hard-Rock Equipment Selection and Sizing, in P. Darling, SME Mining Engineering Handbook (2011) 1143-1155, Society for Mining, Metallurgy & Exploration.
- [12] M. Kerai and A. Halim. Ventilation Requirement for Electric Vehicles in Underground Hard Rock Mines - A Conceptual Study, Journal of Research Projects Review (2012), 45-50.

Dust in the Underground Mine Environment

A New End-of-Shift Monitoring Approach for Respirable Crystalline Silica in Coal Mine Dust

Emanuele Cauda^a, Arthur Miller^b, Pamela Drake^c

^aOffice of Mine Safety and Health Research (OMSHR), Centers for Disease Control and Prevention (CDC) - National Institute for Occupational Safety and Health (NIOSH), Pittsburgh, PA, 15236 USA

^bOffice of Mine Safety and Health Research (OMSHR), Centers for Disease Control and Prevention (CDC) - National Institute for Occupational Safety and Health (NIOSH), Spokane, WA, 99207 USA

The exposure to respirable crystalline silica (RCS) in the coal mining industry is a recognized occupational hazard. Among other changes, the new coal mine dust regulation introduces a stand-alone exposure limit for RCS of 100 $\mu\text{g}/\text{m}^3$ for a full shift. The assessment and monitoring of the exposure to RCS is limited by two main factors: 1) variability of the silica percentage in the mining dust and 2) lengthy off-site laboratory analysis of collected samples. The monitoring of respirable dust containing silica via traditional or real-time techniques is not adequate. The Office of Mine Safety and Health Research (OMSHR) recently initiated the development of field-based End-of-Shift (EoS) silica monitoring solutions. The most promising approach includes the use of a portable Fourier Transform Infrared (FTIR) analyzer for the Direct-on-Filter (DoF) estimation of RCS in respirable samples immediately after the sampling event. The approach has been developed to be used with sampling media currently employed in coal mines for the collection of gravimetric samples. This manuscript presents and discusses the performance of the new DoF analytical approach used for samples collected in ten different U.S. coal mines. The performance has been evaluated in comparison with the current standard MSHA P7 method: linearity, bias, and standard error of the estimation are the metrics used for the comparison. The new on site silica monitoring solution will allow coal mine operators to perform self-assessment monitoring, assessment of high-risk tasks, and evaluation of dust control technologies.

Keywords: end-of-shift, respirable crystalline silica, monitoring, coal mine dust

1. Introduction

Exposure to airborne dust in many occupational environments can lead over time to debilitating respiratory diseases that can affect the health of workers. Workers employed in the mining industry can be exposed to high levels of respirable crystalline silica (hereafter RCS) and such exposure is associated with the development of silicosis [1], lung cancer [2, 3], other pulmonary tuberculosis, and airway diseases [4].

To control the exposure of coal miners to RCS, the U.S. Mine Safety and Health Administration (MSHA) sets daily permissible exposure limits on the most abundant RCS polymorph, α -quartz [5]. The exposure to RCS is currently quantified by collecting a filter sample with a respirable sampler and submitting the sample to an analytical laboratory, where it is analyzed by an established Fourier Transform Infrared (FTIR) analytical technique known as the P7 method [6]. The method entails the pretreatment of the sample by ashing the filter. The same monitoring approach adopted for enforcing the permissible exposure limit is used for activities of self-compliance assessment and engineering monitoring by the mining companies. Aside from the cost of the analysis of a single sample, the main limitation of the current approach is the lack of timely information provided to the health and safety responsible person on site. The time between sample collection and interpretation of the results at the mine site limits the possibility for operators to promptly address overexposures or to adjust the set-up of a control technology. In addition, the results could have little or no value if the RCS concentration varies frequently because of constantly changing geology and mining activities.

A more timely RCS monitoring approach in mining environments would overcome these issues. The National Institute for Occupational Safety and Health (NIOSH) Office of Mine Safety and Health Research

(OMSHR) is investigating technologies for field-based RCS monitoring solutions that would allow End-of-Shift (EoS) assessment of RCS. A technique using a portable FTIR has been investigated recently and showed promising results [7-9] for the estimation of RCS in dust samples aerosolized in a calm air chamber. Because of the potential application in the field, the technique requires the analysis of the respirable coal mine dust collected on a sampling filter without any preparation. This approach is generally called Direct-on-Filter (DoF) technique and it has been investigated and adopted by several researchers and agencies around the world [10, 11]. The uniqueness of the OMSHR approach is the intention of proposing the technique for on-site monitoring activities.

One of the issues for the analytical estimation of RCS in coal mine dust samples by FTIR is the presence of potential confounders. Dust in coal mines typically contains kaolinite, and the infra-red absorption of kaolinite significantly influences the mass of RCS estimated by spectrometry on filter samples. Correction methods to address the confounding effect of kaolinite are established for the standard MSHA P7 method [12]. A similar approach has been developed and tested for the DoF-FTIR technique developed by OMSHR [8]. The approach was evaluated for samples aerosolized in a dust chamber. The objective of the study here reported is to assess the performance of the DoF-FTIR technique in the estimation of RCS in dust samples collected in active coal mines in the United States.

2. Methodology

Respirable dust samples were collected in six different coal mines in the eastern United States, from five underground operations and one surface operation. Information on the counties and coal seams relative to

each mine are summarized in Table 1. Samples were collected in two different years at the surface operation and these samples were grouped in two datasets labeled Mine 6 and Mine 6a to show the identical geographical location but different sampling event.

Table 1. Information relatives to each sample set for this study.

Set	Operation	County	State	Seam
Mine 1	Underground	Raleigh County	WV	Upper Eagle Coal Seam
Mine 2	Underground	Harlan County	KY	Upper and Lower Harlan Seams
Mine 3	Underground	Wise County	VA	Upper Parsons Seam
Mine 4	Underground	Wayne County	WV	Coalburg seam
Mine 5	Underground	Randolph County	IL	Herrin No. 6 Seam
Mine 6	Surface	Kanawha	WV	
Mine 6a	Surface	Kanawha	WV	

Overall 91 samples collected in the six mines that were used in this study. The number of samples for each set is variable as is the range of respirable dust mass and RCS (Table 2); the variability is unavoidable considering that the samples were collected during normal operation at the mines. Airborne respirable dust samples were collected using sampling trains standardized for coal mines: a cyclone separator with a Dorr-Oliver design and operated at 2.0 l³min⁻¹ was used to separate the respirable dust fraction and the respirable particles that were deposited onto preweighed 37-mm PVC filters with a 5- μ m pore size. The filters were mounted in the coal dust sampling cassette.

After collection of the samples in the field, all filter samples were equilibrated, neutralized, and post-weighed in a controlled environment set at 22 \pm 0.7 $^{\circ}$ C and 50% \pm 2% relative humidity to determine the respirable dust mass. A gravimetric analysis of the samples was conducted with a micro balance (XP6, Mettler, Columbus, OH) with a precision better than 5 μ g. Overall the gravimetric analysis had an Limit of Quantification = 14 μ g in a single weighing [13]. Blank filters were used to correct the final mass determination.

Table 2. Respirable mass and RCS range for each dataset.

Set	N	Respirable mass		RCS	
		Min (mg)	Max (mg)	Min (μ g)	Max (μ g)
Mine 1	15	0.126	2.156	7.0	246.0
Mine 2	15	0.154	1.053	9.6	86.9
Mine 3	14	0.203	0.497	8.2	24.3
Mine 4	8	0.248	0.740	9.7	40.5
Mine 5	11	0.240	0.372	5.4	18.5
Mine 6	15	0.129	2.678	15.9	468.0
Mine 6a	15	0.191	1.159	23.1	152.0

After the determination of the respirable mass, the samples were analyzed via the DoF-FTIR technique developed by NIOSH OMSHR [7-9] for the estimation of RCS. The technique uses a portable battery operated FTIR spectrometer (Alpha, Bruker) in transmission mode (Figure 1). The method entails mounting the filter in a stainless steel holder placed so that the filter is centered between the horizontal IR source beam and the detector, where the beam has a 6-mm focal diameter. Spectra are collected in transmission mode at 2 cm⁻¹ resolution by averaging 40 scans. Each individual spectrum was saved in its raw form but was also ratioed against the spectrum of a blank filter to remove the filter background infrared signal.

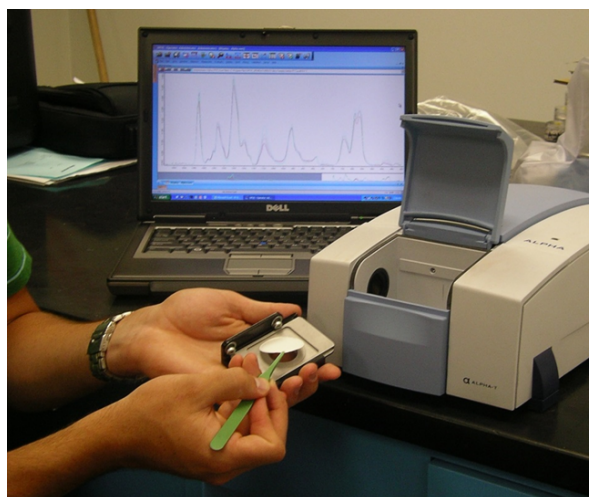


Fig. 1. Operator introducing a dust filter sample in the FTIR used for the DoF analysis of respirable crystalline silica (RCS)

The estimation of RCS entails using OPUS spectral analysis software (by Bruker Optics) to perform baseline correction and peak area integrations on IR spectra from each sample [8]. The estimation uses the integration of the α -quartz doublet in the range 767–816 cm⁻¹ and a calibration developed with standard quartz dust from U.S. Silica. A correction protocol for the interference of kaolinite is part of the method, which involves subtracting the potential contribution of kaolinite (the

band at 915-cm-1) to the doublet using a peak-ratio technique previously published [8, 12].

Finally, the samples were sent to an accredited laboratory (RJLee Group) for RCS quantification via the MSHA P7 method [6]. Because the DoF-FTIR technique is not destructive, the P7 analysis was conducted on the same sample. The estimation of RCS in each sample generated by the proposed DoF-FTIR technique was compared with the result of the standard analysis by using different approaches and metrics. The relationship between the estimation and standard analysis conducted on each sample was first investigated via regression analysis. Results on the quality of the linear correlation (R2) and characteristics of the regression analysis were selected as metrics of the comparison. The standard error of the estimate was also calculated for the entire dataset. This metric provides a single value characteristic of the error generated by using the DoF-FTIR technique instead of the standard laboratory analysis. Finally, the bias associated with the use of the proposed DoF-FTIR technique was calculated for each sample. For each dataset, the average bias and the confidence level (95%) were calculated.

3. Results and discussion

The results of the standard P7 analysis were used together with the gravimetric data to calculate the percent of RCS in the respirable dust for each sample and this information was grouped for each mine (Figure 2). The average percentage of RCS is different for each mine and there is a high variability within each set. The

percent of silica is substantially higher for the Mine6 and Mine6a samples that were collected in a surface operation, which is in line with recent analysis of the RCS percentage in dust present in mining operations [14, 15]. The results summarized in Figure 2 reinforce the need for a field-based silica monitoring solution and they highlight the inadequacy of respirable dust monitors to estimate the RCS level, being that the approach must assume constant silica content in the dust.

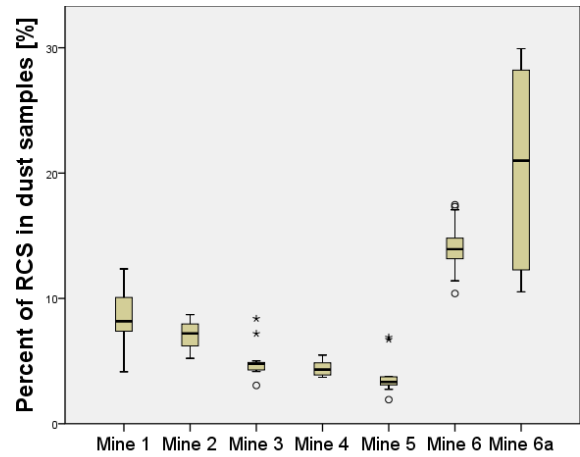


Fig. 2. Synopsis of RCS content in the seven mine sets

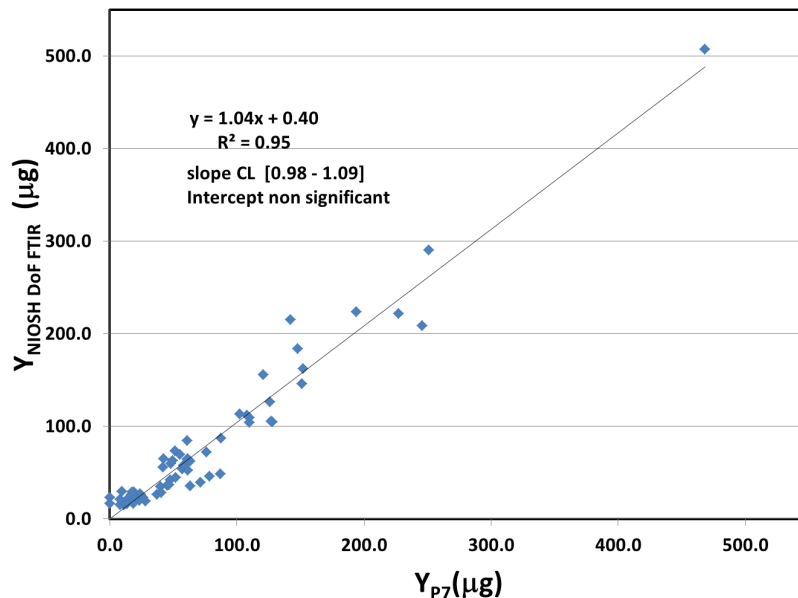


Fig. 3. Linear correlation of the results obtained via DoF-FTIR technique and P7 MSHA method.

The results of the DoF-FTIR estimation of RCS were then compared with the results of the P7 method for each sample. For comparing results of the DoF-FTIR estimation, the number of samples was reduced to 71, which was necessary to remove the samples below the limit of quantification (LOQ = 15 µg) for this new approach [16]. The results from both methods were very

highly correlated as shown by an R2 = 0.95 (Figure 3). A more accurate statistical analysis (alpha = 0.05) of the linear regression between the two sets of data indicated an average slope of 1.04 that is not significantly different from 1 (0.99; 1.10). In addition the intercept of 0.4 µg is nonsignificant (-5.4 ; 6.2).

The analysis of the standard error of the estimate showed an error associated with the DoF-FTIR technique of 18 μg . This value can be considered the uncertainty associated with the DoF-FTIR estimation, and it will be used in the future to compare the performance of the technique with dusts from different coal mine environments.

The analysis of the bias is a common approach to assess a new technique. The bias associated with the DoF-FTIR estimation was calculated for each sample (Figure 4). The average bias is 12.5% and this result is in line with a higher than 1 slope from the regression analysis. The cause for this average bias can be a non optimal kaolin correction for samples collected in active mines. A second finding is a high variability of the bias especially for samples with RCS less than 100 μg . Although a higher variability is expected for any analytical technique at low content, the samplers used in this study might have contributed to this result. In a recent study the estimation of RCS via DoF-FTIR technique on filters collected with the coal dust sampling cassettes was found affected by a 35% coefficient of variation [7]. The same variability is evident in Figure 4, and could also have contributed to the average bias. Another possibility is the effect of specific features in samples collected in active mines; these features could be carbonaceous confounders or characteristics of the infrared spectra for samples that were not ashed. The effect of the dust deposition could be assessed in the future by testing a different sampling cassette in the coal mine environment. If a substantial average bias is still present even if the variability is minimized, the consistency of this trend needs to be evaluated for samples collected in different mining environments. This could have two possible outcomes: 1) the bias is consistent for samples collected in different mining environments and a correction factor or approach needs to be developed; 2) the bias is mine-specific based on the geology and characteristics of the dust present in that mine, which would require a mine-specific correction factor. In both cases, the use of a more comprehensive analysis of infrared spectrum might be needed. Such an approach, based on partial least squares modeling, has been evaluated for the DoF-FTIR technique for samples collected in a noncoal environment [17] with excellent results.

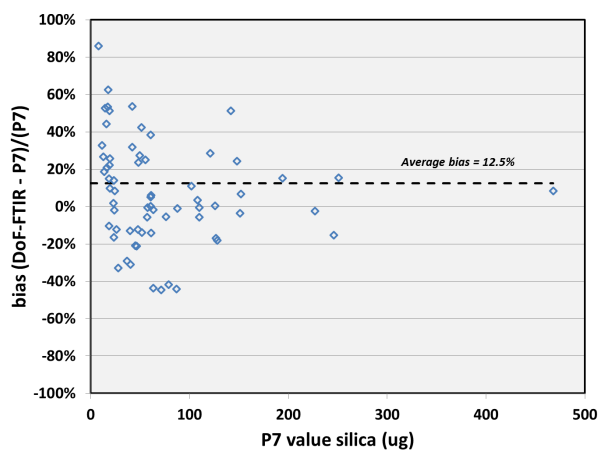


Fig. 4. Bias map generated by the DoF-FTIR estimation.

4. Summary

The manuscript presents a possible new monitoring approach for the End-of-Shift assessment of the miners exposure to respirable crystalline silica. The manuscript focuses on the evaluation of the new monitoring approach with dust samples collected in six different coal mines around the U.S. The results show that the percent of silica in the dust collected in the different mines is highly variable within and intra sets. This finding reinforces the need of a specific field-based silica monitoring solution.

The results of the new monitoring approach, based on the Direct-on-Filter estimation of silica, are well correlated with the results via the standard MSHA P7 method on the same samples. The slope of the regression and other statistical metrics used to assess the approach indicated a minimal overestimation compared to the standard analysis. The bias associated with the estimation is higher at low silica content in the dust samples and on average around 12%. This bias and its causes need to be further investigated. Possible causes are the variable deposition of the dust in the coal dust sampling cassette and the presence of other physical/geological confounders.

When optimized, the new silica monitoring approach will allow operators to conduct field-based self-assessment and engineering monitoring activities.

Disclaimer

The mention of any company or product does not constitute an endorsement by the Centers for Disease Control and Prevention. The findings and conclusions in this paper are those of the authors and do not necessarily represent the views of the National Institute for Occupational Safety and Health.

References

- [1]. Leung, C.C., I.T.S. Yu, and W.H. Chen, *Silicosis*. *Lancet*, 2012. **379**(9830): p. 2008-2018.
- [2]. IARC, *IARC monographs on the evaluation of carcinogenic risks to humans: silica, some silicates, coal dust and para-aramid fibrils. Vol 68*. Lyon, France: World Health Organization, International Agency for Research on Cancer. 1997.
- [3]. Straif, K., et al., *A review of human carcinogens-Part C: metals, arsenic, dusts, and fibres*. *Lancet Oncology*, 2009. **10**(5): p. 453-454.
- [4]. NIOSH, *NIOSH hazard review: health effects of occupational exposure to respirable crystalline silica*. Publication No. 2002-129. Cincinnati, OH: National Institute for Occupational Safety and Health., 2002.
- [5]. Register, F., *Vol. 79, No. 84 / Thursday, May 1, 2014 / Rules and Regulations, Lowering Miners' Exposure to Respirable Coal Mine Dust, Including Continuous Personal Dust Monitors; Final Rule*. 2014.
- [6]. Mine Safety Health Administration (MSHA), *Infrared Determination of Quartz in Respirable Coal Mine Dust - Method No. MSHA P7*. US Dept of Labor-MSHA-Pittsburgh Safety and Health Technology Center, 2008.
- [7]. Miller, A., et al., *Deposition uniformity of coal dust on filters and its effect on the accuracy of FTIR*

- analyses for silica*. Aerosol Science and Technology, 2013.
- [8]. Miller, A.L., et al., *Evaluating portable infrared spectrometers for measuring the silica content of coal dust*. Journal of Environmental Monitoring, 2012.
- [9]. Cauda, E., et al. *High-volume samplers for the assessment of respirable silica content in metal mine dust via direct-on-filter analysis*. in *10th International Mine Ventilation Congress*. 2014. Sun City, South Africa.
- [10]. HSE - Health and Safety Executive, *MDHS 101 - Crystalline silica in respirable airborne dusts Direct-on-filter analyses by infrared spectroscopy and X-ray diffraction*. 2005.
- [11]. Pretorius, C., *The Effect of Size-selective Samplers (Cyclones) on XRD Response*. Journal of the Mine Ventilation Society of South Africa, 2011.
- [12]. Ainsworth, S.M., P. Parobeck, and T. Tomb, *Determining the Quartz Content of Respirable Dust by FTIR, Informational Report 1189, U.S. Department of Labor, Mine Safety and Health Administration*. 1989.
- [13]. Page, S.J. and J.C. Volkwein, *A revised conversion factor relating respirable dust concentrations measured by 10 mm Dorr-Oliver nylon cyclones operated at 1.7 and 2.0 L min⁻¹*. Journal of Environmental Monitoring, 2009. **11**(3): p. 684-689.
- [14]. Cauda, E., et al., *Analysis of the silica percent in airborne respirable mine dust samples from U.S. operations*. ASTM STP1565 on Symposium on Silica and Associated Respirable Mineral Particles, October 25, 2012 - October 26, 2012, in Atlanta, GA., 2013.
- [15]. Joy, G.J., *Evaluation of the Approach to Respirable Quartz Exposure Control in U.S. Coal Mines*. Journal of Occupational and Environmental Hygiene, 2011. **9**(2): p. 65-68.
- [16]. Cauda, E., A. Miller, and P.L. Drake, *A new exposure monitoring approach for respirable crystalline silica: taking the laboratory to the mine site*. Journal of Occupational and Environmental Hygiene, 2015. **submitted**.
- [17]. Weakley, A., et al., *Quantifying silica in filter-deposited mine dusts using infrared spectra and partial least squares regression*. Analytical and Bioanalytical Chemistry, 2014: p. 1-10.

Ultrasonic Scrubber: Potential Applications in Dust Control

J.R. Saylor, W. Ran

Clemson University, Department of Mechanical Engineering, Clemson, SC 29634, USA

The ability to remove dust from the air in mining environments is a constant challenge. Significant research has been conducted on methods for controlling dust levels, including the use of sprays, ventilation, and methods for wetting cut and uncut material. Despite this research, dust levels remain difficult to control, particularly for micron scale particles. With regard to removing dust particles from the air using wet scrubbers, part of the challenge is the fact that for micron scale particles, water drops in the diameter range typical of industrial sprays will exhibit a minimum in scavenging coefficient for particles having a diameter on the order of one micron. This is because at about one micron, inertial effects are very weak, and yet Brownian motion is also not significant. In other words, micron scale particles inhabit a region of the parameter space where neither inertial nor diffusive mechanisms of particle-drop collision are strong. To enable better scavenging by scrubbers, a method is needed that would force micron scale dust particles to collide with water drops (and perhaps each other).

We have explored the use of the ultrasonic radiation force to help force dust particles and drops to collide. Specifically, we have developed a method whereby an ultrasonic standing wave field is established between an ultrasonic transducer and a passive reflector. Such standing waves exhibit pressure nodes where drops and particles can be made to accumulate. Such accumulation zones increase the chance of drop/particle collisions, thereby removing particles. We have developed a prototype, laboratory-scale implementation of this idea which we refer to as the "ultrasonic scrubber". Two inlets are directed into the ultrasonic standing wave field, one containing spray drops and the other containing micron-scale particles. Our experiments show that scavenging increases by as much as 140% in the presence of the ultrasonic standing wave field compared to scavenging with just the water spray and no ultrasonics. Results will be presented showing how the improvements engendered by ultrasonics vary with particle diameter, drop diameter, gas flow rate and spray flow rate. These results are all for a very small scale laboratory scrubber. Some ideas will be presented to suggest possible avenues for scale-up to an actual mining environment.

Keywords: dust, scrubber, ultrasonic, water spray

Considerations for an Automated SEM-EDX Routine for Characterizing Respirable Coal Mine Dust

Victoria Anne Johann*, Emily Allyn Sarver*

Virginia Tech, Blacksburg, Virginia, USA

Respirable dust in coal mining environments has long been a concern for occupational health. Over the past several decades, much effort has been devoted to reducing dust exposures in these environments, and rates of coal workers' pneumoconiosis (CWP) have dropped significantly. However, in some regions, including parts of Central Appalachia it appears that incidence of CWP has recently been on the rise. This trend is yet unexplained, but a possible factor might be changes in specific dust characteristics, such as particle composition, size or shape.

Prior work in our research group has developed a standardized methodology for analyzing coal mine dust particles on polycarbonate filter media using scanning electron microscopy with energy dispersive x-ray (SEM-EDX). While the method allows individual particles to be characterized, it is very time-intensive because the instrument user must interrogate each particle manually; this limits the number of particles that can practically be characterized per sample. Moreover, results may be somewhat user-dependent since classification of particle composition involves some interpretation of EDX spectra.

To overcome these problems, we aim to automate the current SEM-EDX method. The ability to analyze more particles without user bias should increase reproducibility of results as well as statistical confidence (i.e., in applying characteristics of the analyzed particles to the entire dust sample.) Some challenges do exist in creating an automated routine, which are primarily related to ensuring that the available software is programmed to differentiate individual particles from anomalies on the sample filter media, select and measure an appropriate number of particles across a sufficient surface area of the filter, and classify particle compositions similarly to a trained SEM-EDX user following a manual method. This paper discusses the benefits and challenges of an automated routine for coal mine dust characterization, and progress to date toward this effort.

Keywords: Coal workers' pneumoconiosis, Respirable dust, particle analysis, scanning electron microscopy, Automated SEM

1. Introduction

Coal mining operations generate dust which can be respired into the lungs of workers to cause occupational health diseases such as coal workers' pneumoconiosis (CWP). The mining industry saw dramatic reductions in CWP cases as dust standards and ventilation regulations in underground coal have improved over the past few decades under the Federal Coal Mine Health and Safety Act of 1969 [1]. The Act also established the Coal Workers' Health Surveillance Program through which NIOSH has witnessed first-hand the increase in CWP rates in the eastern United States, particularly Central Appalachia, since the mid-1990s [1-3]. This is of particular concern because the majority of cases have been reported in young coal miners and many of the cases are advanced [1-2]. Further research should be aimed toward determining the cause of increased incidence of CWP in Central Appalachia in order to improve miner health and safety [3]. Little is definitively known regarding the effects of specific dust characteristics (such as size, shape, and chemical composition) on lung disease occurrences in underground miners. Analyzing these dust particle characteristics using scanning electron microscopy (SEM) may be a good place to start. Automated SEM analysis could be particularly advantageous in collecting data from more dust samples at a faster rate.

Automated SEM-EDX analysis has historically been used for applications such as industrial process control and forensics [4]. However, SEM automated analysis hardware and software advancements have made it applicable to a variety of other applications, including mineral samples [4]. Automated SEM is able to analyze features such as inclusions in metals; porosity of geological samples, and samples containing wear debris from combustion engines [4]. Another application for mineral samples is the detection of an anomalous particle within a grouping of thousands of particles of other compositions [4]. This application might be particularly useful to the occupational health field for the analysis of dust samples containing atypical or hazardous particles.

Some work has been conducted in the realm of automated dust particle analysis. Deboudt et al. [5] performed automated SEM-EDX particle analysis on dust samples collected on the Atlantic coast of Africa. As in our project, this group collected airborne particulate samples on polycarbonate filters and ran an SEM at an accelerating voltage of 15kV. Using the Link ISIS Series 300 Microanalysis system developed by Oxford Instruments, this group was able to collect spectral data for individual particles with a 20 second acquisition time [5]. Even faster rates of data collection can be achieved though. Ritchie and Filip [6] recently undertook an effort to optimize the speed of automated particle analysis by

SEM-EDX and demonstrated data collection at approximately three particles per second. They employed a structured query language database that stores millions of particle records and is able to simultaneously classify multiple particles to multiple categories [6]. The authors' research group does not necessarily need to be analyzing particles at that rate, though aiming to speed up analysis time by a few seconds and perhaps creating a comprehensive particle database could be beneficial toward research efforts.

Other researchers have also worked on multi-frame particle analysis using the SEM. Fritz, Camus, and Rohde [7] have done work with automated microscope stage analysis that can cover hundreds of frames in one run to ensure total sample coverage. For applications in the mining industry, this ability is particularly attractive for particle sizing and the analysis of respirable dust particles. Collecting data for particles over the entire sample can be necessary for statistical significance [7]. The authors' research group also plans to employ automated multi-frame analysis.

2. Previously Developed Standard Dust Characterization Method

Prior work in the authors' research group has developed a standardized methodology for analyzing coal mine dust particles on a polycarbonate filter [8-10]. This method was developed using an FEI Quanta 600 FEG environmental scanning electron microscope (ESEM) (FEI, Hillsboro, OR) equipped with a Bruker Quantax 400 EDX spectroscope (Bruker, Ewing, NJ). The ESEM is operated under high vacuum conditions at a voltage of 15kV with a spot size of 5.0 μ m and at the optimal working distance of 12-13mm. Bruker Esprit software is used to collect spectra results for the classification of individual particles. The "spot" analysis function of the ESEM software is used in conjunction with the EDX software to generate elemental spectra.

Six compositional classification schemes were developed for coal mine dust particles based on peak elemental spectra heights of aluminum, calcium, carbon, copper, iron, magnesium, oxygen, potassium, silicon, sodium, sulfur, and titanium. The six classifications are "alumino-silicate," "carbonaceous," "carbonate," "heavy mineral," "mixed carbonaceous," and "quartz." Any particles that do not fit into these categories are termed "other." Data on particle size and shape is also collected in this dust characterization method. The long and intermediate dimensions of each particle are measured using the line measurement tool provided in the ESEM imaging software. The shape is qualitatively classified based on user interpretation as either "angular," "rounded," or "transitional."

The sample analysis routine begins by focusing the SEM at 10,000x magnification to provide optimal resolution for analyzing particles in the desired size range of 0.5-8.0 μ m in diameter. Two horizontal lines are drawn 2 μ m apart, centered on the screen and spanning the width of the screen, using a line measurement tool, as depicted in Figure 1.

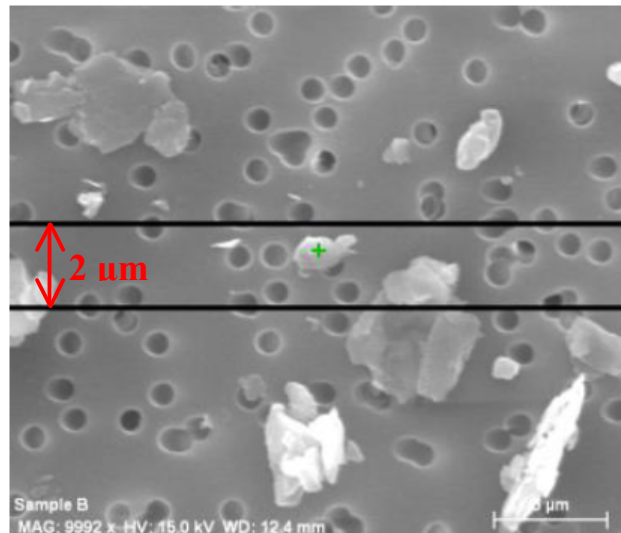


Fig. 1. Example of the horizontal lines drawn 2 μ m apart for particle selection. Only particles touching this region are to be selected for analysis [8].

The stage is moved so that the first field to be analyzed is three screen shifts from the outer, left edge of the filter, 2.25mm (one quarter of the filter diameter) down from the top of the filter. Moving from left to right and top to bottom each particle with a long dimension greater than 0.5 μ m intersecting the space between the two horizontal lines and falling completely within the field of view is analyzed. Up to ten particles meeting the specifications are characterized per field in order to ensure that at least ten fields are analyzed and increase the representativeness of the results. Figure 2 shows a backscatter detector image of a typical field of ten particles that would be analyzed.

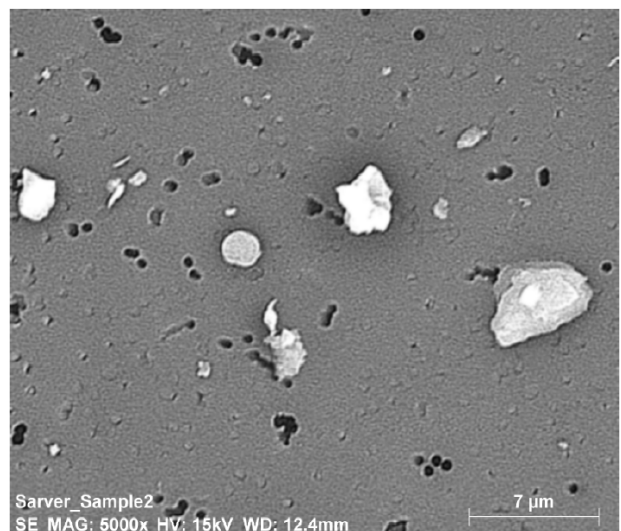


Fig. 2. Example of a typical field of particles to be analyzed (at 10,000x magnification).

Once the first field has been analyzed, the next field of view to the right is analyzed. If fewer than 100 particles have been analyzed upon reaching the edge of the first row, the stage is shifted so that the field of view is 4.5mm (one half of the filter diameter) from the top of the filter and the same procedure for the previous row is followed. If fewer than 100 particles have been analyzed upon reaching the edge of the second row, the stage is

shifted once more so that the field of view is 6.75mm (three quarters of the filter diameter) from the top of the filter, following the previous procedure. Figure 3 depicts this analysis routine in terms of filter navigation under the SEM.

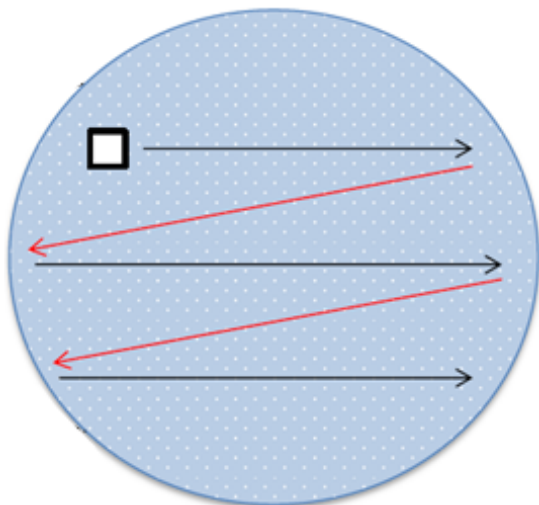


Fig. 3. Illustration of a 9 mm diameter polycarbonate filter and navigation routing for SEM-EDX analysis. The box represents the first frame in which particles are selected for characterization; the black arrows define the directions for successive screen shifts between characterization frames. When one horizontal line of analysis is complete (black arrows), the red arrows define shifting back to the left side of the filter to continue analysis on the next horizontal line [8].

The manual method has the capacity to analyze 100 particles on one sample in 75-90 minutes, depending on user experience and sample characteristics (e.g., particle density); despite the wealth of information that can be obtained, the method is clearly too time-consuming to be practical for a large number of samples.

3. Automation of the Standard Dust Characterization Method

Considering the need to significantly speed up particle characterization, efforts to automate the above routine have recently been initiated. This work is being developed using the same ESEM-EDX system previously mentioned, and several special features available for add-on to Bruker's Esprit software. A major benefit to automation is that the software can characterize particles at a magnification that is ten times lower than the magnification required for the standard dust characterization method. Figure 4 shows a backscatter detector image of a typical field of particles that would be analyzed using the automated routine.

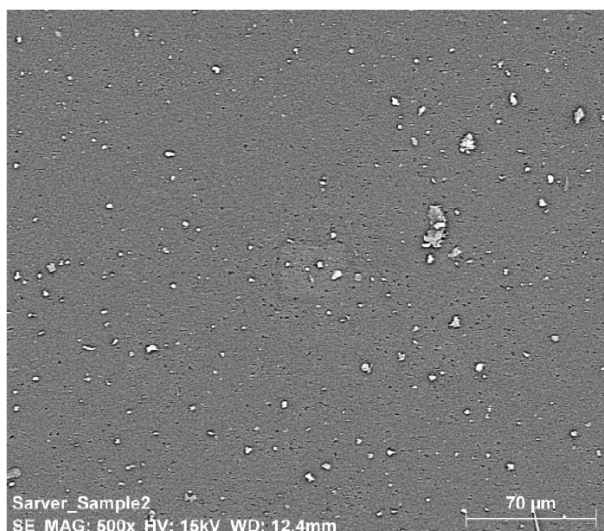


Fig. 4. Example of a typical field of particles (at 1,000x magnification).

This image comes from the same sample as Figure 2; however, by being able to analyze particles at 1,000x versus 10,000x magnification, many more particles can be analyzed per frame. Once the first frame is selected, the imaging tool in the Esprit software is used to pull the image of the frame from the SEM software and import it for analysis. A special feature in Esprit allows for rules and filters to be applied to the image so that the software is programmed to identify dust particles. Here, a binary image can be created and settings can be adjusted so that the software distinguishes particles as white and the filter as black. Figure 5 depicts the binary imaging process in Esprit.

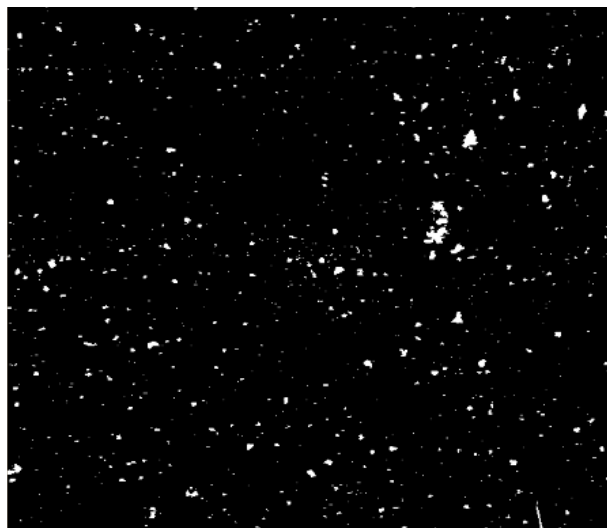


Fig. 5. Example of a binary image of a typical particle field (at 1,000x magnification). This is the same particle field as in Figure 4.

Once all settings have been adjusted for particle identification, particle sizing can be conducted. Figure 6 depicts the particle field once all the particles have been sized. The software outputs data such as length, width, and shape factor to characterize the particles by size and shape, as shown in Figure 7.

This single frame contains 171 particles that can be analyzed, 71 more particles than would have been analyzed in up to ten frames using the standard dust characterization method. This particle sizing routine minimizes user interpretation of the long and intermediate particle dimensions which was required for the standard dust characterization method.

Once sizing is completed, the particle classification scheme can be implemented. The Esprit software allows for particle classification based on the weight percent of elements detected in spectral analysis. Therefore, rules can be set for the maximum or minimum elemental weight percentages required for various particle classification categories. We have currently developed rudimentary rules and particle classification categories to demonstrate the utility of automated analysis and its potential for respirable dust particles from coal mining environments. The preliminary categories are based on typical elemental weight percentages observed for particles classified using the manual method. Figure 8 displays chemistry results for some particles identified in Figure 6, showing the weight percentages of specific elements considered by the classification rules. Figure 9 shows particle classification results in a bar chart as a useful visual tool.

It should be noted that the chemistry classification categories are not currently developed enough to accurately classify every particle (i.e., as it would be classified manually). This is especially true for carbonaceous particles because they can contain small weight percentages of elements other than carbon and oxygen. This does not allow them to be classified under the original carbonaceous category that only sets parameters for carbon and oxygen weight percentages. Therefore, in this preliminary work, a second

carbonaceous classification category was created with additional elemental weight percentage rules (i.e., "carbonaceous II" in Figure 9). By doing this, carbonaceous particles that were previously not classified are classified in the second carbonaceous category. A particle chemistry analysis feature in the Esprit software can classify each particle detected in the frame.

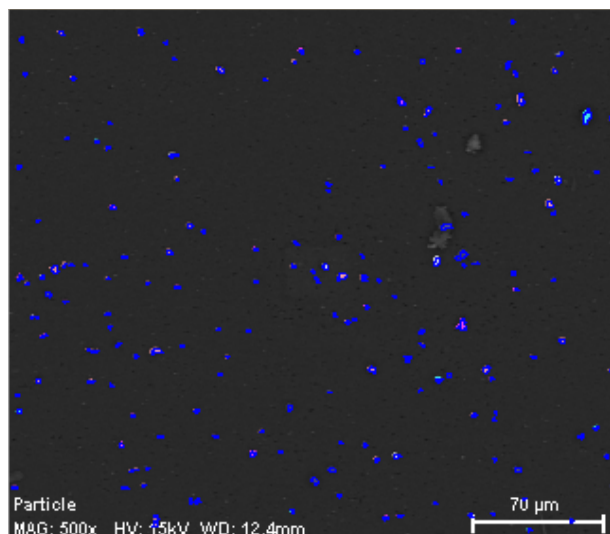


Fig. 6. Example of the particle sizing process in Esprit. This is the same particle field as in Figure 4. Each particle found that is accepted for analysis is outlined in blue while undergoing size classification.

Accepted	Area	Length	Width	Average Diameter	Pos X	Pos Y	Aspect Ratio	Feret Std Dev	Perimeter	Orientation	On Border	Shape Factor	Max Circle Rad
P162	3.4	2.88	1.78	2.54	3701	24858	1.62	0.28	8.1	2	0	0.661	1.02
P163	2.5	2.71	1.33	2.19	3808	24856	2.03	0.44	6.5	8	0	0.738	0.72
P164	2.7	3.69	0.89	2.73	3757	24855	4.15	0.88	8.2	176	0	0.511	0.51
P165	4.3	3.82	1.78	3.00	3796	24855	2.15	0.63	9.3	13	0	0.627	1.02
P166	4.1	3.69	1.78	2.96	3627	24854	2.07	0.62	9.0	11	0	0.632	1.02
P167	4.8	3.55	2.15	2.95	3751	24854	1.65	0.45	8.9	159	0	0.758	1.02
P168	3.4	2.71	2.05	2.45	3850	24852	1.32	0.17	7.5	58	0	0.757	1.02
P169	3.0	2.88	1.33	2.30	3876	24850	2.16	0.45	6.8	16	0	0.801	1.02
P170	7.5	4.75	3.12	3.88	3628	24850	1.52	0.51	12.7	145	0	0.590	1.14
P171	3.0	2.71	1.78	2.35	3827	24847	1.52	0.32	7.1	0	0	0.740	0.72
Min	2.3	2.35	0.89	1.98	3552	24847	1.09	0.08	5.8	0	0	0.364	0.51
Max	20.7	7.99	5.34	6.23	3876	25119	4.15	1.84	20.3	179	0	0.929	2.11
Average	5.0	3.62	2.06	2.98	3713	24973	1.86	0.50	9.2	83	0	0.701	1.04
Std Dev	3.3	1.13	0.76	0.88	96	75	0.53	0.27	3.0	74	0	0.119	0.30

Fig. 7. Example of the particle sizing results for some particles shown in Figures 4-6. The accepted particles are all numbered and listed in order in the first column. Other particle properties are provided for each particle in subsequent columns. At the bottom of the results page, minimum, maximum, average, and standard deviation values are provided for each particle property.

Alle	cps/eV	Results [Atom-% (norm.)]	Sort: Element
P1	0.06	Pd Au C O 92.27 Al 0.48 Si 1.43 Na 5.82	
P2	0.22	Pd Au C O 86.11 Al 7.85 Si 6.04	
P3	0.16	Pd Au C O 88.42 Al 6.33 Si 5.25	
P4	0.17	Pd Au C O 90.81 Al 0.42 Si 0.31 Ca 8.46	
P5	0.06	Pd Au C O 90.53 Al 4.63 Si 4.84	
P6	0.09	Pd Au C O 91.18 Al 1.53 Si 0.93 Ca 6.35	
P7	0.03	Pd Au C O 90.79 Al 3.34 Si 3.39 Fe 2.49	
P8	0.06	Pd Au C O 92.64 Al 1.24 Si 0.19 Ca 5.93	
P9	0.06	Pd Au C O 90.80 Al 2.57 Si 6.63	
P10	0.25	Pd Au C O 97.71 Al 1.23 Si 1.06	
P11	0.14	Pd Au C O 86.58 Al 6.62 Si 4.64 Ti 2.17	
P12	0.13	Pd Au C O 92.41 Al 3.12 Si 4.47	
P13	0.06	Pd Au C O 85.51 Al 7.23 Si 7.26	
P14	0.10	Pd Au C O 83.65 Al 7.98 Si 8.37	
P15	0.20	Pd Au C O 89.33 Al 6.66 Si 4.01	
P16	0.22	Pd Au C O 93.24 Al 1.50 Si 1.63 Fe 3.63	
P17	0.10	Pd Au C O 92.24 Al 1.36 Si 0.55 Ca 5.85	
P18	0.09	Pd Au C O 86.45 Al 7.39 Si 6.16	

Fig. 8. Example of the particle chemistry results for some particles shown in Figures 4-6. Each analyzed particle is listed in order in the first column. Information regarding the counts and weight percentages of detected elements are provided for each particle in subsequent columns.

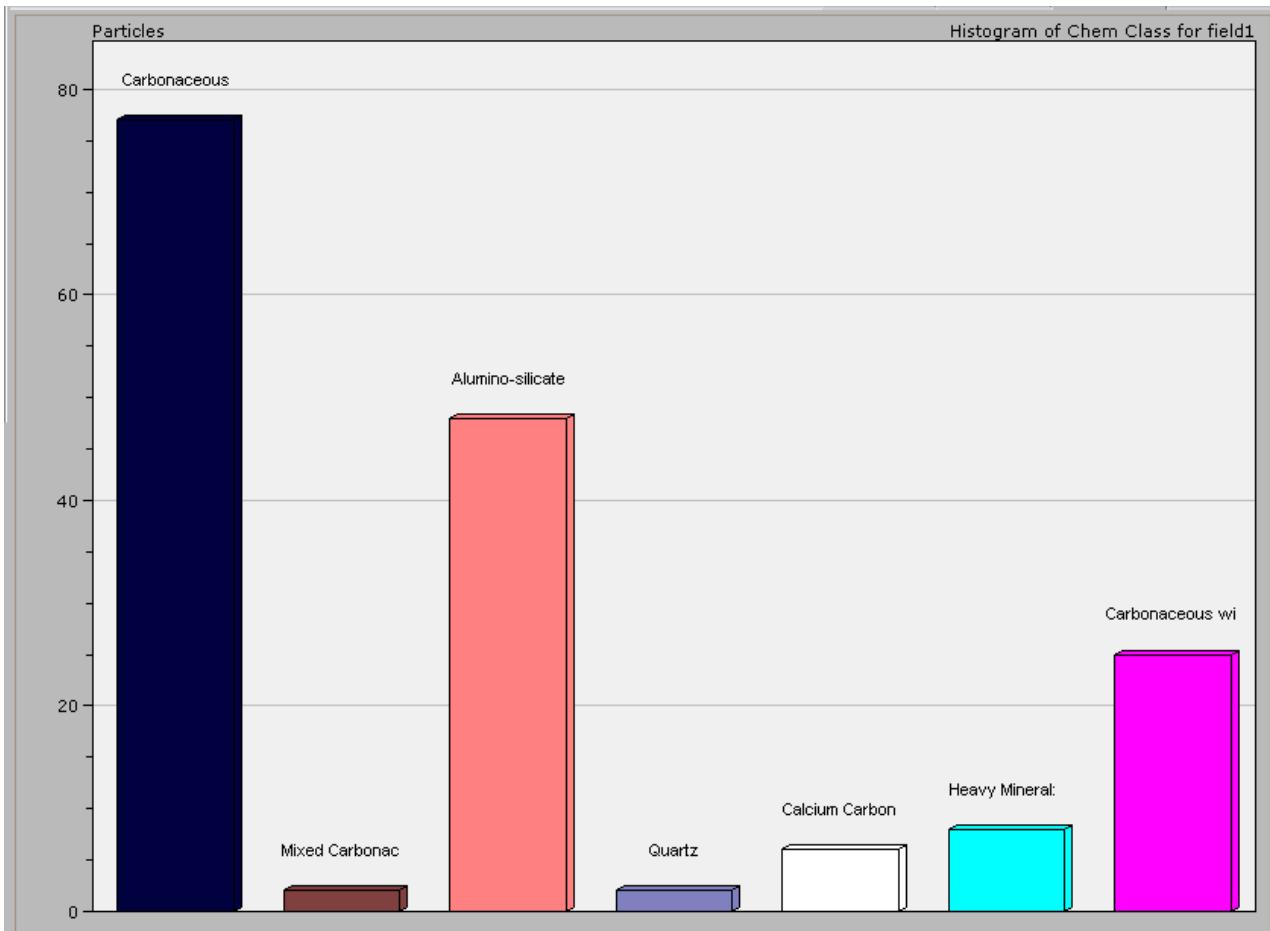


Fig. 9. Example of the particle classification results for particles shown in Figures 4-6. Once each particle is classified based on the specified chemical classification parameters, the Esprit software outputs a histogram with the particle frequency for each class (carbonaceous, mixed carbonaceous, alumino-silicate, quarts, carbonate, heavy mineral, and carbonaceous II)

The automated analysis at the particle density demonstrated in Figure 4 takes just over ten seconds per particle which allows for total analysis of this frame of 171 particles in approximately 30 minutes. At this rate,

171 dust particles are being analyzed two or three times faster than just 100 dust particles using the standard dust characterization method. It is expected that with several modifications in basic operating parameters of the SEM-

EDX system, the efficiency can be greatly increased. The majority of particles in this frame were classified as carbonaceous while many particles were classified as alumino-silicates and fewer were classified as heavy minerals, carbonates, mixed carbonaceous, and quartz.

Another special feature in the Esprit software allows for the automation of the microscope stage movement from frame to frame. The user is able to designate the starting frame position and the ending frame position along the sample filter. Once the entire area of the filter to be analyzed is determined, particle sizing and chemistry can be run frame by frame and the software will export the data after completion. This tool can even be used to run multiple samples consecutively so that up to 16 samples could be analyzed in one run.

4. Discussion

It seems as though developing an automated particle analysis routine is a step in the right direction for our research. The standard dust characterization method is too time-intensive for the amount of particles that can practically be analyzed per sample because the user must interrogate each particle manually. A major advantage to automated particle analysis is the amount of time saved in the lab due to quick, electronic characterization of particles. This is also applied to data entry where automated analysis automatically exports data into Microsoft Excel while data obtained from the standard method must be manually entered. Moreover, results from the standard dust characterization method may be somewhat user-dependent since classification of particle composition and shape currently involves some interpretation of EDX spectra. Other benefits of an automated particle analysis routine are a significant increase in the number of particles that can be analyzed per sample and minimization of user interpretation to acquire results. The ability to analyze more particles without user bias should increase reproducibility of results as well as statistical confidence in obtaining results from a representative portion of the sample.

However, some challenges do exist in creating an automated routine, including training the available software to appropriately make multiple decisions such as those involving differentiation of individual particles from anomalies on the filter media, selection of particles for analysis, and classification of particle composition. Another challenge arises due to the filter media being comprised of carbon and carbon being a key element in the classification of carbonaceous, mixed carbonaceous, and carbonate minerals. We are working to determine whether or not carbon should be deconvoluted for proper mineral identification and other key elements be used to classify these particles in its place. We have determined that gold and palladium should definitely be deconvoluted before spectral analysis because the sample coating is comprised of these elements and can interfere with the chemical identification of the dust particles.

5. Conclusion

There is much work still to be done to refine the particle classification parameters in order to properly automate the particle analysis. Our goal is to determine and implement the correct particle classification categories and their appropriate rules for our samples. To do this, we plan to:

- collect spectral data on many particles from our samples
- determine the appropriate elemental weight percentage thresholds for the classification parameters
- determine which elements should be deconvoluted
- modify the currently developed particle classification categories so that they are able to classify all particles encountered
- ensure that the software is properly classifying all particles

We aim to program the software to classify particles in the same manner that the user would classify them, but without the human error.

Acknowledgments

The authors acknowledge the Alpha Foundation for the Improvement of Mine Safety and Health for funding this work. We would also like to thank Steve McCartney of Virginia Tech ICTAS-NCFL for operational assistance with SEM-EDX analysis, Ted Juzwak of Bruker Corporation for assistance in learning the Esprit software capabilities, and Patrick Wynne for countless hours of SEM work. We are also grateful to Meredith Scaggs for her efforts to collect and prepare dust samples.

References

- [1] Centers for Disease Control (CDC). Advanced Cases of Coal Workers' Pneumoconiosis-Two Counties, Virginia. *MMWR*, 55.33 (2006) 909-913.
- [2] D. Blackley, C. Halldin, and A.S. Laney, Resurgence of a Debilitating and Entirely Preventable Respiratory Disease among Working Coal Miners. *American Journal of Respiratory and Critical Care Medicine* 190.6 (2014) 708-709.
- [3] E. Suarathana et al, Coal workers' pneumoconiosis in the United States: regional differences 40 years after implementation of the 1969 Federal Coal Mine Health and Safety Act, *Occupational and Environmental Medicine* 68.12 (2011) 908-913.
- [4] C. Lang et al., Automated SEM Analysis in Industrial Process Control and Scientific Research, *Microscopy Society of America*, 2014.
- [5] K. Deboudt et al., Mixing state of aerosols and direct observation of carbonaceous and marine coatings on African dust by individual particle analysis, *Journal of Geophysical Research* 115 (2010) 1-14.
- [6] N. Ritchie and V. Filip, SEMantics for High Speed Automated Particle Analysis by SEM/EDX, *Microscopy and Microanalysis* 17.S2 (2011) 896-897.[5] G. Fritz, P. Camus, and D. Rohde, Consideration for Automated Multi-Frame Particle Sizing in the SEM, *Microscopy and Microanalysis* 12.S02 (2006) 210-211.
- [7] R. Sellaro, Development and Demonstration of a Standard Methodology for Respirable Coal Mine

Dust Characterization Using SEM-EDX, Virginia Polytechnic Institute and State University, 2014.

- [8] R. Sellaro and E. Sarver, Preliminary investigation of SEM-EDX as a tool for characterization of coal mine dusts, *Mining Engineering* 66.8 (2014) 16-40.
- [9] R. Sellaro and E. Sarver, Characterization of respirable dust in an underground coal mine in Central Appalachia, *Transactions of the Society for Mining, Metallurgy & Exploration* 336 (2014) 457-466.

Considerations for TGA of Respirable Coal Mine Dust Samples

Meredith Scaggs^a, Emily Sarver, Cigdem Keles^a

^aVirginia Tech, Blacksburg, Virginia, USA

Respirable dust in underground coal mines has long been associated with occupational lung diseases, particularly coal workers' pneumoconiosis (CWP) and silicosis. Regular dust sampling is required for assessing occupational exposures, and compliance with federal regulations is determined on the basis of total respirable dust concentration and crystalline silica content by mass. In light of continued incidence of CWP amongst coal miners, additional information is needed to determine what role specific dust characteristics might play in health outcomes. While particle-level analysis is ideal, current time requirements and costs make this simply unfeasible for large numbers of samples. However, opportunities do exist for gleaning additional information from bulk analysis (i.e., beyond total mass and silica content) using relatively quick and inexpensive methods. Thermogravimetric analysis (TGA) may be a particularly attractive option. It involves precise sample weight measurement in a temperature controlled environment, such that weight changes over specific temperature ranges can be correlated to chemical changes of particular sample constituents. In principle, TGA offers the ability to determine the coal and total mineral mass fractions in respirable dust samples. Such analysis could conceivably be combined with standard methods currently used to measure total mass and silica content. Under some circumstances, TGA might also be extended to provide information on specific dust constituents of interest (such as calcite). In this paper, we consider the benefits and challenges of TGA of respirable coal mine dust samples, and provide preliminary results and observations from ongoing research on this topic.

Keywords: CWP, Occupational lung diseases, Thermogravimetric Analysis (TGA), Respirable dust, Silica.

1. Introduction

Over the past several decades, significant progress has been made toward improving worker health and safety at coal mining operations in the US [1,2,3]. However, respirable dust (i.e., particles less than about $5\mu\text{m}$ in aerodynamic diameter) is still a serious concern because exposures are associated with risks of occupational lung diseases, namely Coal Workers' Pneumoconiosis (CWP) and silicosis [4]. These diseases can severely decrease quality of life by limiting lung function, and in some cases may lead to progressive massive fibrosis (PMF), and can ultimately be fatal [4,5].

While federal regulation along with a variety of technological and operational advancements have resulted in a significant decline of such diseases, incidence remains unacceptably high – particularly in parts of Central Appalachia [6-8]. In some areas of this region, there appears to even be an increase in the incidence of CWP and silicosis [1,6-8]. While the reason(s) for this has yet to be definitively determined, some explanations point to unique mining conditions in this region. Indeed, these mines employ a smaller workforce operating in thinner seams of coal [3,6,7,9]. The reduced seam heights lead to mining of rock strata above and below the coal (i.e. the roof and floor), which may increase total dust exposures as well as exposures to specific types of particles based on their composition, size or shape. Moreover, the mining methods and mine sizes may also contribute to unique dust exposures. Continuous miners are generally employed with auxiliary support (e.g., roof bolting and shuttle car haulage), and most jobs have the potential for dust generation. Also, due to relatively small crews, many

miners can perform a variety of jobs and thus work in a variety of conditions.

1.1 Current Sampling and Analysis Methods for Respirable Coal Mine Dusts

In May 2014, the Mine Safety and Health Administration (MSHA) released a new rule regarding respirable coal mine dust exposures [10]. By August 2016, the permissible exposure limit (PEL) will be reduced from 2.0 to 1.5 mg/m^3 in production areas of mines; and from 1.0 to 0.5 mg/m^3 in entries used for ventilation and for "Part 90" miners (i.e., individuals already diagnosed with CWP). Moreover, in mines where respirable dust is comprised of greater than 5% quartz (by mass), the PEL is decreased to a mine-specific PEL in order to reduce health risks (see Ref) [1,10,11]. If a mine has silica content greater than 0.5 mg/m^3 , extended cuts with a continuous miner (i.e. production cuts greater than 20 feet prior to roof bolting) are also prohibited. [11]. To demonstrate compliance with the regulatory limits, personal dust monitoring is required for miners working in designated occupations which are identified by the increased risk for high dust exposure, such as the continuous miner or roof bolter operator [10,12,13]. Additionally, operators take samples in designated areas, including areas in the working face that are known for high dust generation for atmospheric concentrations and potential exposure for workers [10]. The new dust rule requires that compliance monitoring now be conducted when production is at least 80% of full production levels (i.e., as opposed to the 50% threshold that was required previously) [10].

Presently, dust monitoring involves collecting a full-shift sample with a permissible pump (i.e., certified intrinsically safe), sampling tube, and Dorr-Oliver cyclone (nylon, cut point of $\sim 4 \mu\text{m}$). Samples are collected onto polyvinyl chloride (PVC) filters of known weight housed in pre-assembled cassettes [12,14]. The pump is run at a flow rate of 1.7 L/min to mimic the rate of human respiration [12,14]; it is turned on when the miner enters the mine and left running until the miner returns to the surface. The sample is then shipped to a certified lab for analysis.

Analysis of respirable dust samples currently includes two results: the total sample weight, which can be converted to a mass concentration of exposure (mg/m^3), and the mass fraction of crystalline silica in the sample. The sample weight is determined gravimetrically (i.e., by difference between the filter weight before and after sample collection) [12,14,15], and the silica fraction is determined by infrared spectroscopy (IR) by either NIOSH Method 7603 or MSHA Method P7 [16,17]. For both methods, the PVC filters are ashed to remove organic matter (i.e. coal dust and the filter) and unoxidized material is redeposited on a vinyl acrylic copolymer filter, which can be scanned with IR [16,17].

As of February 1, 2016, compliance monitoring will also include use of the continuous personal dust monitor (CPDM) for miners working in high-dust areas [10]. The CPDM is a wearable unit that allows quasi real-time monitoring of total respirable dust exposures by measuring incremental changes in the weight of a filter as it collects dust over time. The idea is that miners can track their exposures during their work and make timely decisions to reduce their health risks. The CPDM does not allow for determination of silica content in respirable dust, and so silica must still be measured on samples collected and analyzed as described above. In order to provide more timely information regarding silica exposures, NIOSH is currently researching methods for direct-on-filter analysis that could be used immediately following sample collection (i.e., end of shift) [12,13,18-20]. While an ultimate goal would be real-time measurement of silica, end-of-shift results would certainly be an improvement over current methods.

1.2 Needs for Expanded Analysis

The field is indeed advancing toward faster capabilities for quantifying respirable coal mine dust exposures by total concentration and silica content, the two focal points of current regulation. But many other exposure aspects may be useful in understanding health risks and effects, particularly in light of apparent differences in lung disease rates between various coal mining regions [1,5,7]. Regarding the dust itself, characteristics such as particle shapes, sizes and chemistries may all be important. For instance, particle size and shape may play a role in the how well dust can penetrate and become embedded in lung

tissue [10,21], and a combination of size and chemistry may influence the relative reactivity of particles within the respiratory system [21,22]. Ideally, many individual particles could be analyzed to determine distributions of these characteristics. In reality, this is *possible* by methods such as scanning electron microscopy with energy-dispersive x-ray (SEM-EDX) – but far from *feasible* at large scale due to costs and time requirements [17]. However, there is potential to gather more data from dust samples than is currently done, without having to examine individual particles.

An objective of ongoing research by the authors is to develop efficient and relatively inexpensive methods for expanded analysis of respirable coal mine dust samples. Currently, we are focused on opportunities for using thermogravimetric analysis (TGA).

2. Thermogravimetric Analysis

TGA is used to monitor weight change of a sample as it is exposed to changing temperature in a given atmosphere [23]. Weight change is generally plotted as a function of temperature or time on a thermogram [23,24], and this information can be interpreted to understand chemical changes in the sample as it is heated. In some cases, TGA can be combined with additional analyses (e.g., to characterize the volatiles or reaction products that are generated as a sample decomposes) [23,25-28]. In the context of coal, TGA has long been used to conduct proximate analysis, in which the goal is to determine the ash content of the coal (i.e., the non-combustible mineral fraction) [29-31]. TGA has also been used for rank classification of coal samples [30].

The TGA instrument is comprised of two key components: the furnace and the balance. With tight control over the furnace chamber conditions (i.e., temperature and atmosphere) and a highly sensitive balance, experiments can be conducted with very good precision – for instance, allowing measurements of weight changes on the order of just a few μg . This ability has allowed proximate coal analysis to be done on very small sample sizes [29,30]. It also potentially provides an option for analysis of respirable dust samples from coal mines, which are typically on the order of tens to hundreds of μg .

2.1 Considering TGA for Respirable Dust Samples

At present, we are investigating the efficacy of TGA to estimate the mass fractions of coal (i.e., organic) and mineral (i.e., inorganic) content in respirable dust samples. For a very basic estimate, TGA of dust samples can be treated as analogous to proximate analysis of bulk coal samples: The coal content is oxidizable, and so is assumed to totally degrade (i.e., lose all of its mass) during the TGA process; whereas the mineral content does not appreciably degrade or react, and so the remaining residue

at the end of the TGA experiment is taken as the total mineral mass. Figure 1 illustrates hypothetical thermograms for this general example.

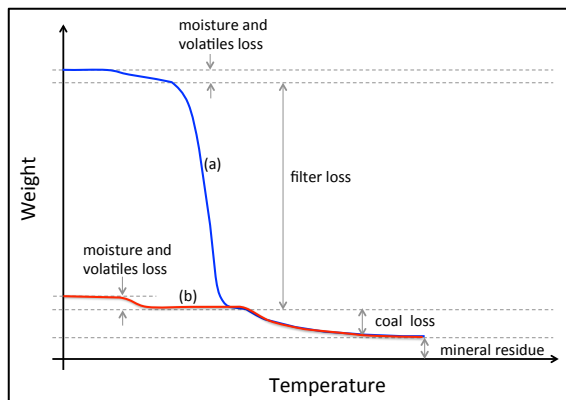


Fig. 1. Hypothetical thermograms for (a) direct-on-filter and (b) dust-only TGA of a respirable coal mine dust sample. For the direct-on-filter conceptualization, the filter media is assumed to decompose completely prior to coal oxidation.

In reality, the inorganic matter in a dust sample from a coal mine may include a number of different minerals from different sources. Minerals such as silica, silicates, or carbonates may be associated with shales or sandstones that make up roof or floor rock; and minerals such as pyrite or chloride salts may be ingrained in the coal seam. Of these, only carbonates are expected to react significantly within the same temperature range as coal. Carbonates can thermally decompose to mineral oxides and carbon dioxide, with the conversion of calcite (CaCO_3) to calcium oxide and carbon dioxide ($\text{CaO} + \text{CO}_2$) being a common example [18,25-28]. Thus, a more accurate estimate of coal and mineral fractions within a dust sample by TGA might necessitate separation of coal oxidation from carbonate decomposition.

The issue of carbonate content in coal mine dust samples is further complicated by “rock dusting” activities. Rock dust is primarily composed of calcite and/or dolomite ($\text{CaMg}(\text{CO}_3)_2$), and dusting is required in certain areas of mines to prevent propagation of coal dust explosions [32]. In areas with heavy rock dust applications, or when the rock dust product has a high proportion of very fine particles, rock dust might contribute significantly to the total respirable dust concentration [32]. TGA of samples from such areas should therefore consider calcite and/or dolomite, specifically; otherwise a simple proximate analysis approach as described above may overestimate the coal dust fraction.

The potential for using TGA to specifically estimate rock dust mass in a sample may also be of interest because it could allow operators to understand the influence of their rock dusting programs on respirable dust concentrations in the mine environment. As dust exposure limits are reduced with new regulation, understanding which activities are

contributing dust is critical for compliance efforts. While the main components of rock dust are not generally considered to adversely affect lung health, regulatory dust limits are currently aimed at total dust concentration (and silica mass content) – and so even innocuous dust particles are concerning.

3. Development of a TGA Method for Respirable Coal Mine Dust Samples

In principle, TGA of coal mine dust samples could be done as an intermediate step between current standard methods for assessing the total weight of a sample and its mass fraction of silica (i.e., NIOSH 7603 or MSHA P7) [16,17]. As illustrated in Figure 1, TGA might be done directly on the filter used to collect the dust sample, or on dust that has been removed from a filter. In either case, due to very small sample masses, a very sensitive TGA instrument is required.

For development of TGA method for respirable coal mine dust samples, we are using a Q500 Thermogravimetric Analyzer (TA Instruments, New Castle, DE). The Q500 employs a microbalance with $0.1\mu\text{g}$ resolution, and its vertical furnace eliminates some thermal influence on the balance [25,33]. The instrument is highly programmable, such that users can create precise methods that may be run without interference. Our instrument is also equipped with an autosampler, which provides the ability to run up to 16 separate samples in sequence. Platinum sample pans are used due to their inertness across a wide temperature range and because they are easy to clean.

To date, our method development work has focused on both direct-on-filter and dust-only TGA of respirable coal mine dust samples.

3.1 Direct-on-filter TGA

For a direct-on-filter method, the idea is simply to “ash” the entire sample filter in the TGA instrument. As such, an understanding of the filter media behavior as it is heated, and any potential interactions between it and the sample matrix, is needed. Ideally, the filter media: decomposes in a separate temperature range from the sample matrix; is highly uniform with respect to its ash content; and can be folded to fit in the TGA pans without significant mass loss. Considering the relative weight of filters (i.e., tens of mg) versus a typical dust sample (i.e., tens to hundreds of μg), decomposition of the filter at a different temperature than the coal (and other sample components such as calcite) is particularly important. Moreover, compatibility of the filter media with current dust sampling and analysis protocols should be considered.

Thus far, two filter media types have been evaluated: PVC and MCE (mixed cellulose ester). Both filter types are available in the 37 mm size commonly used for dust

sample collection in underground coal mines, and both can be used for respirable dust sampling, specifically [34,35]. Table 1 provides a comparison of key characteristics, with favorable characteristics denoted by a star.

Table 1. Comparison of PVC and MCE filter media characteristics.

PVC	MCE
★ Non-hygroscopic	Hygroscopic
Static charging possible	★ Low static charging
Some ash content	★ Virtually ashless
★ Pliable	Tears easily

PVC is currently used for respirable dust sampling in coal mines, and so is favorable from the perspective of utilizing TGA as an intermediate step between current gravimetric (i.e., total dust sample weight) and silica content analyses. However, PVC filters generally have ash content, which could complicate determination of mineral content in the dust sample matrix; and they also are subject to static charging issues [35]. MCE, on the other hand, is considered ashless and not susceptible to static buildup [34]. But the material is relatively hygroscopic, meaning it can easily absorb moisture, and this is problematic from the standpoint of current gravimetric analysis (i.e., accurately determining the dust sample weight is difficult) [34].

3.1.2 Summary of Experiments and Results

To test the suitability of PVC and MCE filters (37 mm, 5µm pore size) for direct-on-filter TGA of respirable coal mine dust samples, preliminary experiments were conducted (see [36] for more details). Blank filters of each type (n=20) were ashed under a variety of conditions to

observe their behavior; and several samples of pulverized raw coal (with varying mineral content) have also been ashed to simulate a dust sample that might be collected underground. Figure 2 shows typical thermograms for PVC, MCE and coal dust TGA experiments conducted in air (i.e., oxidizing environment). The main observations from these experiments were:

- Coal oxidation occurs above about 425°C; at lower temperatures, some moisture and volatiles are also lost.
- PVC filters weigh between about 15-18mg. They decompose in two primary stages (i.e., around 285°C, and then above about 450°C); the latter stage overlaps significantly with coal oxidation. The weight change ratio between these two stages of decomposition is not reproducible enough to predict the weight change in the coal oxidation region with sufficient accuracy. Ash in PVC filters tested is highly reproducible and accounts for about 0.13 ± 0.02% of total filter weight. Static charging was not observed to be a significant issue.
- MCE filters weigh between about 35-37mg. They decompose primarily below 425°C (i.e., losing about 98.5% of their weight), and the weight change ratio between decomposition before 425°C and after is highly reproducible. MCE ash content is also highly reproducible, and accounts for about 0.03 ± 0.01% of the total filter weight. Filter pliability can be increased misting the filters with high purity water during folding.

Based on these observations, further experiments were run where raw coal was pulverized and collected onto PVC and MCE filters. Because the PVC filters are non-hygroscopic, the dust sample weight could easily be determined by weighing the filter before and after dust collection. A Sartorius Cubis Microbalance (Bohemia, NY) was used for this.).

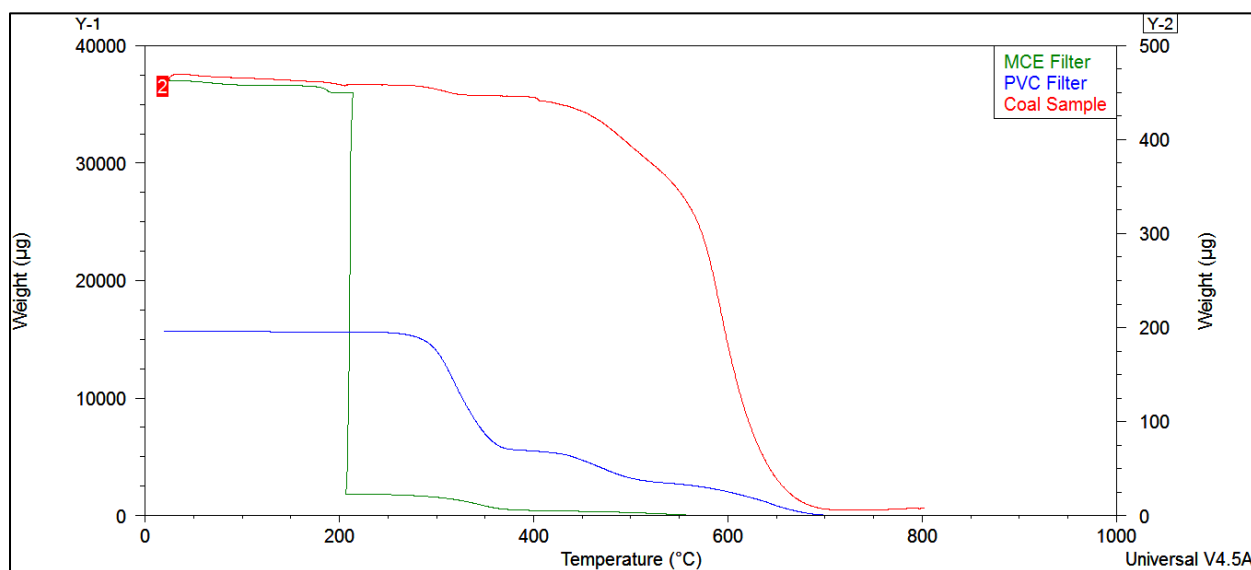


Fig. 2. Example thermograms for blank PVC and MCE filters (primary y-axis) and a raw coal sample (secondary y-axis). The PVC filter has two regions of weight loss, which span relatively wide temperature ranges, whereas the MCE filter losses most of its weight in one very narrow region. Coal oxidation is significant at temperatures above about 425°C.

For the MCE filters, pre- and post-weighing the filter may not provide an accurate sample weight due to moisture uptake, so the idea was to interpret the TGA results to determine the dry sample weight (i.e., by using the known filter decomposition rate and ash content as previously determined

For the dust on PVC filters, the coal and mineral fractions could be determined with good accuracy (i.e., as compared to the known ash content of the coal sample used to generate the dust). The coal and mineral fractions were determined using a simple proximate analysis approach: the dust sample weight was found as the difference between pre- and post-collection filter weight; the dust mineral weight was found as the difference between the final residue weight and the known ash content of the filter; and the dust coal weight was found as the difference between the dust sample weight and the dust mineral weight. Such analysis could certainly be conducted between current gravimetric and silica analyses for respirable dust samples; indeed, a sensitive TGA is not even needed for this, only the furnace and appropriate microbalance that are already used. However, this approach does not allow for determination of specific mineral components (e.g., calcite) of a dust sample.

Despite promising results from experiments on raw coal material and MCE separately, results from TGA of dust on these filters proved that direct-on-filter analysis is likely not possible. Figure 3 illustrates the reason for this. When the MCE begins to decompose just below 200°C, it appears that the coal particles immediately oxidize as well. As can be seen in the figure, the weight loss around this temperature associated with the dust-laden filter accounts for more than the filter weight; it also accounts for loss of most of the dust itself. This result was not initially expected, since in coal material-only experiments the primary weight loss did not occur until temperatures above 425°C. However, the result makes sense when considering that, although the furnace chamber temperature may only be around 200°C when the MCE filter decomposes, the local temperature where this reaction is happening should be much greater, and thus triggered spontaneous combustion of the coal particles. Considering the very fine size of the particles, and hence their large surface area, this result is not so surprising in retrospect. This explanation is supported by the small spike in furnace chamber temperature that can be seen Figure 3.

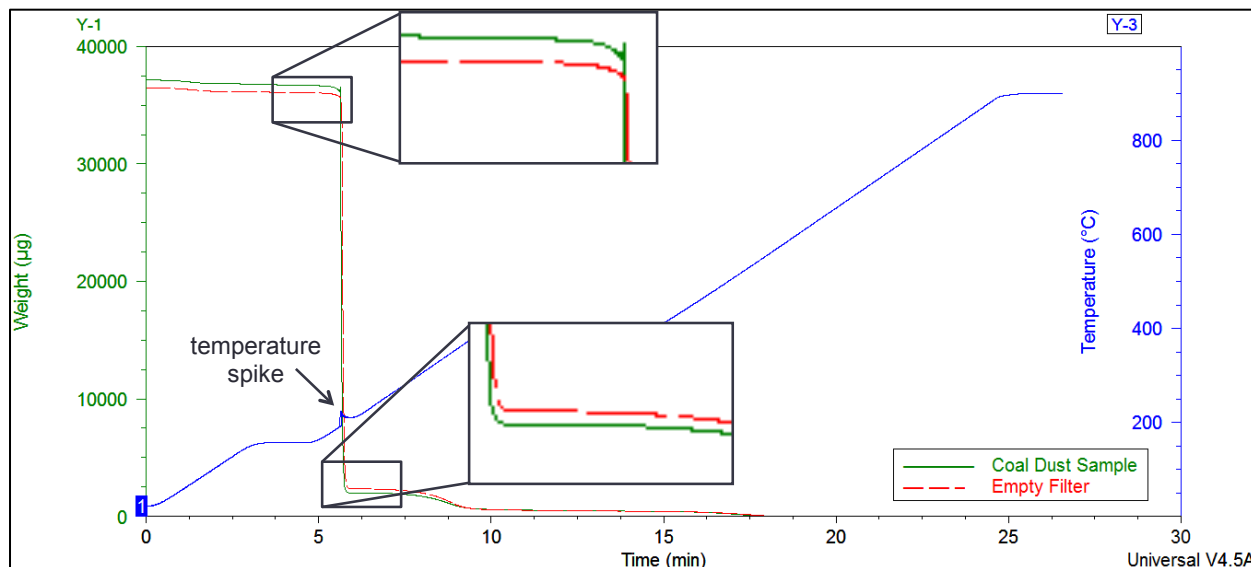


Fig. 3. Thermograms (weight on the primary y-axis vs. time) for a blank MCE filter and an MCE filter with dust generated from a raw coal sample; temperature is shown on the secondary y-axis. The difference in initial weights is about 80µg, with the dust-laden filter being heavier than the empty filter; the difference in filter weights after the significant decomposition just above 200°C is about 30µg, with the dust-laden filter now being lighter than the empty filter. This result indicates that the coal dust spontaneously combusted when the MCE filter decomposed. The furnace chamber temperature spike indicates that the MCE decomposition did indeed create significant heat.

In summary, direct-on-filter TGA using PVC filters is possible, but will not likely yield results that provide insights beyond a basic ratio of oxidizable to nonoxidizable content in a dust sample. Direct-on-filter TGA using MCE does not appear favorable at all, since the hygroscopic nature of the filters makes dust sample weight difficult to determine directly, and sample decomposition cannot be distinguished from filter decomposition during the TGA procedure.

Moreover, if determination of rock dust content in respirable coal mine dust samples is important, the sample will likely need to be removed from filters prior to TGA. This is because, similar to the effect that MCE filter decomposition has on spontaneous coal oxidation at relatively low furnace temperatures, calcite and dolomite may thermally degrade earlier than expected when in contact with the MCE material. Alternatively, an inert filter across the temperature range required to completely oxidize coal particles (e.g., glass fiber) might provide an option for direct-on-filter TGA with the opportunity to estimate rock dust content. However, this option could not be easily integrated between the current standard methods for gravimetric and silica content analyses.

3.2 Dust-only TGA

To increase resolution of TGA results and allow for evaluation of specific components of a respirable coal mine dust sample, particles may be removed from the filter on which they were collected. In principle, dust removal can be done on any filter – including perhaps the small glass fiber filters that are used in CPDMs. A procedure similar to that described in the sample preparation sections of the NIOSH 7603 or MSHA P7 can be used; in these methods, it is necessary to remove the silica-containing residue from a secondary filter following ashing of the PVC sample collection filter. In short, the filter is submerged in a tube of isopropanol, which is then briefly placed in an ultrasonic bath (or sonicator). The ultrasonic energy shakes the dust particles from the filter, which can then be removed from the tube, and the isopropanol is then evaporated. The residue in the tube then contains the dust particles. A fundamental assumption for a dust-only TGA method will of course be that the dust removed from the filter is representative of the entire sample on the filter.

3.2.1 Preliminary Observations Regarding Feasibility of Dust Removal

Preliminary experiments are underway to investigate the feasibility of removing respirable dust

from PVC and MCE filters (37 mm, 5 μ m pore size) that are compatible with approved dust sampling pumps for underground coal mines, and also the glass fiber filters that are specifically manufactured for use with the CPDM. Based on the interference between filter decomposition and coal dust oxidation observed during direct-on-filter TGA experiments, one major goal of the current work is to determine how to maximize dust particle removal while minimizing filter degradation that results in filter media particles being present in the removed dust sample.

To date, several important observations have been made regarding MCE and PVC filters:

- Isopropanol is not an appropriate medium for conducting the ultrasonic dust removal. In both cases, the filter media react with the isopropanol. Testing is ongoing with deionized water, which appears promising.
- For blank filters, sonication times of 0.5-3.0 minutes appear to have similar effects on filter degradation, meaning that similar amounts of filter residue result from these times. The residue is on the order of tens of μ g, which should dramatically reduce the tendency for filter decomposition to spur dust decomposition during TGA of removed dust samples. Sonication for longer periods of time results in the filters breaking down significantly, and thus a significant mass of filter residue may end up in dust samples removed from the filters.
- TGA of residue from sonication of blank filters shows similar results to TGA of the blank filters themselves. This indicates that filter particles present in removed dust samples should behave similarly
- Significant dust can be removed from filters. At present, it appears dust removal from the CPDM filters is more efficient than from PVC and MCE filters. This is likely due to the smaller surface area of the CPDM filters (i.e., 14 mm in diameter), which allows a thicker layer of dust to accumulate vs. the 37 mm filters.

While TGA experiments on dust removed from filters has not yet been completed, the above observations provide some promise that a method can be developed.

3.2.2 Determination of Rock Dust Fraction

Experiments are also underway to evaluate the feasibility of determining the rock dust fraction of a respirable dust sample collected in a coal mine. To date, reagent grade calcite and a real rock dust sample (raw limestone with calcite as the major

fraction and dolomite as a minor fraction) have been investigated. A TGA method has been developed which appears capable of distinguishing calcite and likely dolomite from coal dust

Figure 4 provides example thermograms of calcite, raw limestone and coal dust separately (top), and samples containing both the raw limestone and coal dust (bottom). The coal dust was generated from a raw coal sample as in other previous tests. The TGA method requires precise control over the furnace chamber. As noted on the figure, there are four primary phases of sample weight change during the method.

During the first phase of the TGA method only moisture and the small amount of volatiles from the coal are lost as the sample is heated to about 380°C. In the next phase, presumably the magnesium carbonate portion of the dolomite mineral lattice is converted to an oxide between about 380 and 400°C. In the third phase, the coal is oxidized as the temperature is ramped to about 500°C, and then the chamber is held isothermal for a relatively long period of time to ensure that coal oxidation is complete. The weight change in this phase is thus estimated to be the dry pure coal weight (i.e., non-volatile portion of the coal dust). In the final phase, the calcite is converted to calcium oxide as temperature is ramped to about 750°C, and held isothermal for some time again.

The residue (i.e., final weight) at the end of the experiment can be attributed to the calcium oxide and other mineral matter in the coal dust. Taking the weight change of the sample in the in the second and fourth phases of the method as the weight of carbon dioxide released during magnesium carbonate and calcite conversion, a stoichiometric relationship can be used to estimate the weight of these constituents in the sample, and also the weight of their resulting oxides. Finally, the difference between the experiment residue and the estimated oxide weights can be used to estimate the non-carbonate (i.e., inert) mineral weight in the coal.

As described, the developed method and determination of dust sample components (i.e., coal, carbonates, and all other mineral matter) does assume that rock dust is comprised completely of carbonates—which is not a practical assumption in many cases.

However, the method and calculations can easily be adjusted based on more accurate assumptions. We are currently developing a modified TGA method to allow for determination of magnesium carbonate, which is associated with rock dust products containing significant dolomite. And since rock dust products are often assayed to determine fractions of calcite, dolomite and minor minerals, such information can be used to come up with mine-specific calculations. Regardless, the fundamental TGA work appears very promising in this area.

4. Conclusions and Future Work

There are undoubtedly needs for enhanced understanding of respirable dust characteristics in coal mines. TGA provides great potential for very simple determination of coal to total mineral ratios – analogous to proximate analysis of bulk coal samples. Such information could help provide insights into the sources of respirable dusts, and allow an additional basis of comparison between dusts from different mines, different areas of the same mine, or generated under different conditions. As well, TGA may provide opportunities to estimate more specific mass fractions of dust samples – such as the fraction associated with rock dust products.

The preliminary results and observations presented here reveal that direct-on-filter TGA of samples collected on PVC filter media may provide at least some information about coal vs. mineral fractions of respirable dust. Moreover, such analysis could be easily integrated into current standard methods for gravimetric and silica content analyses. For more accurate estimation of coal and mineral fractions, as well as the rock dust fraction specifically, dust-only TGA appears promising.

Continuing research is focused on optimizing the efficiency of dust removal from multiple filter types, and determining detection limits with regards to dust sample weights. Work is also needed to further develop the TGA method(s) appropriate for calcite and dolomite estimation. Complementary analyses to TGA methods for respirable coal mine dusts samples are additionally being considered, such as examining residue from TGA experiments with SEM-EDX to allow identification of specific mineral particles.

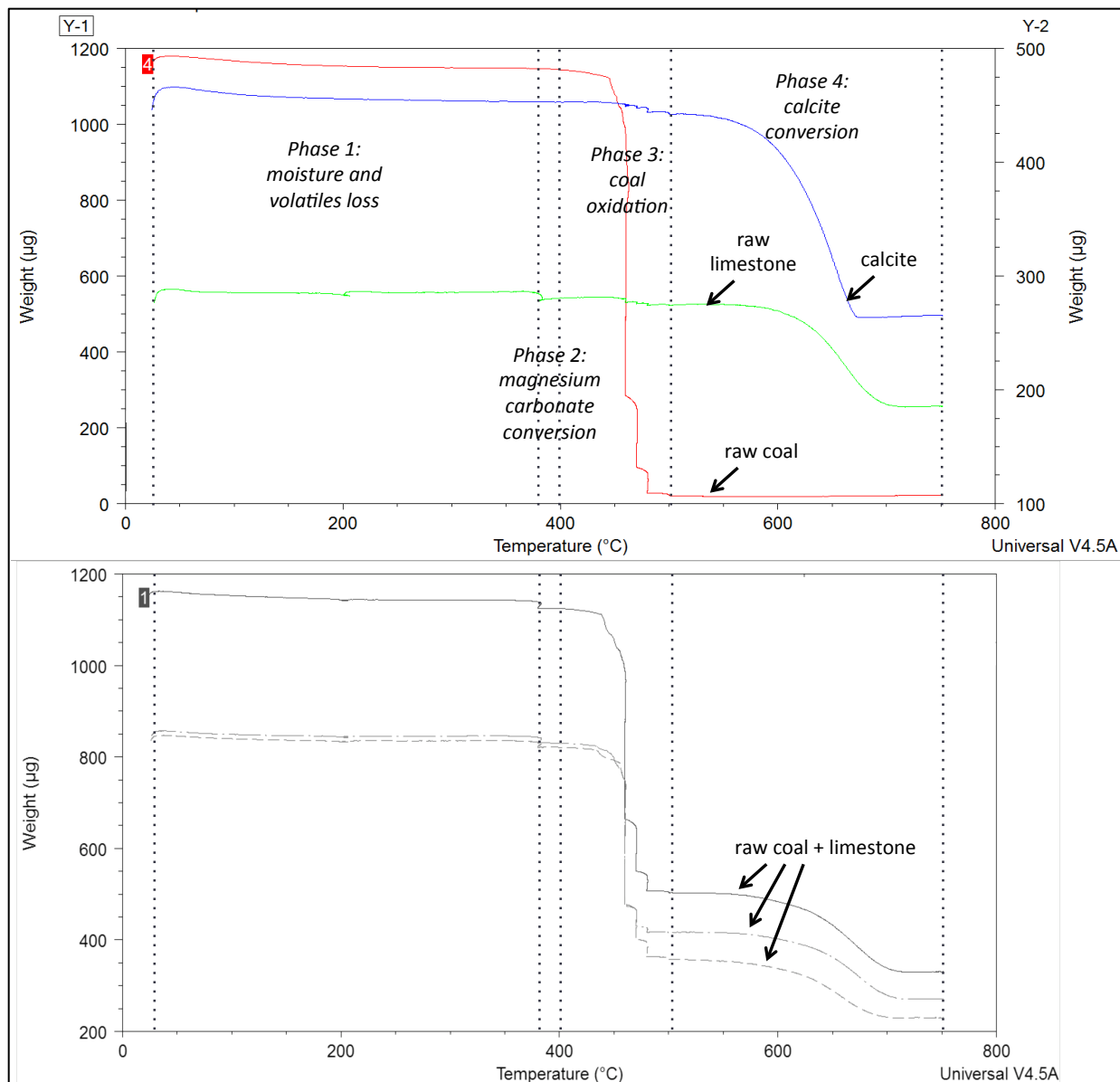


Fig. 4. Example thermograms for reagent grade calcite only, raw limestone only and raw coal dust only (top), and samples containing both raw coal and raw limestone dust (bottom). The TGA experiment method used here includes four major phases, which drive off moisture and volatiles at temperatures less than about 380°C, convert a minor fraction of the limestone to an oxide between about 380 and 400°C oxidize coal particles between about 400 and 500°C, and convert calcite to calcium oxide between about 500 and 750°C. The residue at the end of the experiments represents calcium oxide and/or inert mineral content in the raw coal.

Acknowledgements

We extend our gratitude to the Alpha Foundation for the Improvement of Mine Safety and Health for funding this work. We thank Dr. Charles Potter from TA Instruments for his guidance with the development of a method using TGA. We also thank all mine personnel in Central and Northern Appalachian mines that have provided access and assistance to collect dust samples, and those that have

shared their invaluable experience with our research team.

References

- [1] Suarathana, E., Laney, A. S., Storey, E., Hale, J. M., and Attfield, M. D. (2011). Coal workers' pneumoconiosis in the United States: regional differences 40 years after implementation of the 1969

- Federal Coal Mine Health and Safety Act. *Occupational and Environmental Medicine*, 68, 908-913.
- [2] National Institute for Occupational Safety and Health (1974). Criteria for a Recommended Standard – Occupational Exposure to Respirable Coal Mine Dust. DHEW (NIOSH), Publication No. 95-106.
- [3] World Health Organization. (1999). Hazard prevention and control in the work environment: airborne dust.
- [4] US Environmental Protection Agency (USEPA). (2013). Particulate Matter (PM) Research. Retrieved from <http://www.epa.gov/airsceience/air-particulatematter.htm>
- [5] Castranova, V., and Vallyathan, V. (2000). Silicosis and coal workers' pneumoconiosis. *Environmental Health Perspectives*, 108(Suppl 4), 675.
- [6] Laney, A. S., and Attfield, M. D. (2010). Coal workers' pneumoconiosis and progressive massive fibrosis are increasingly more prevalent among workers in small underground coal mines in the United States. *Occupational and environmental medicine*, 67(6), 428-431.
- [7] Centers for Disease Control (CDC) (2006). Advanced Cases of Coal Workers' Pneumoconiosis-Two Counties, Virginia. *MMWR*, 55(33).
- [8] dos S Antao, V. C., Petsonk, E. L., Sokolow, L. Z., Wolfe, A. L., Pinheiro, G. A., Hale, J. M., and Attfield, M. D. (2005). Rapidly progressive coal workers' pneumoconiosis in the United States: geographic clustering and other factors. *Occupational and environmental medicine*, 62(10), 670-674.
- [9] Schatzel, S. J. (2009). Identifying sources of respirable quartz and silica dust in underground coal mines in southern West Virginia, western Virginia, and eastern Kentucky. *International Journal of Coal Geology*, 78(2), 110-118.
- [10] Lowering Miners' Exposure to Respirable Coal Mine Dust, Including Continuous Personal Dust Monitors; Final Rule, 30 C.F.R. Parts 70, 71, 72, 75, and 90, (2014).
- [11] Maintenance of Incombustible Content of Rock Dust in Underground Coal Mines; Final Rule, 30 C.F.R. Part 75, (2011).
- [12] Colinet, J. F., Listak, J. M., Organiscak, J. A., Rider, J. P., and Wolfe, A. L. (2010). *Best practices for dust control in coal mining* (41-52). *DHHS*, Centers for Disease Control and Prevention, National Institute for Occupational Safety and Health, Office of Mine Safety and Health Research.
- [13] Reed, W. R., Listak, J. M., Page, S. J., and Organiscak, J. A. (2008). Summary of NIOSH Research Completed on Dust Control Methods for Surface and Underground Drilling. *Trans Soc Min Metall Explor*, 342:32-40.
- [14] Zefon. (2015). Coal Mine Dust Sampling System. Retrieved from <http://www.zefon.com/analytical/download/Coal-Mine-Equipment.pdf>
- [15] Bartley, D. L., and Feldman, R. (1998). NIOSH Manual of Analytical Methods (NMAM), 4th Edition, Particulates Not Otherwise Regulated: Method 0600, Issue 3, 1-6.
- [16] Schlecht, P., and Key-Schwartz, R. (2003). NIOSH Manual of Analytical Methods (NMAM), 4th Edition, QUARTZ in coal mine dust: Method 7603: Issue 3, 1-7.
- [17] Mine Safety and Health Administration (MSHA) (2014). Infrared Determination of Quartz in Respirable Coal Mine Dust, Method No.: P-7. US Department of Labor, Retrieved from: <http://www.msha.gov/Techsupp/pshtcweb/MSHA%20P7.pdf>
- [18] Sellaro, R. M. (2014). *Development and Demonstration of a Standard Methodology for Respirable Coal Mine Dust Characterization Using SEM-EDX*. Master's thesis, Virginia Polytechnic Institute and State University, Blacksburg, Virginia.
- [19] Tuchman, D. P. (1992). Research toward direct analysis of quartz dust on filters using FTIR spectroscopy. US Department of the Interior, Bureau of Mines.
- [20] Tuchman, D. P., Volkwein, J. C., and Vinson, R. P. (2008). Implementing infrared determination of quartz particulates on novel filters for a prototype dust monitor. *Journal of Environmental Monitoring*, 10(5), 671-678.
- [21] Mischler, Steven (2014) A Multistage Cyclone Array for the Collection of Size-segregated Silica Aerosols to Test the Hypothesis that Ultrafine Crystalline Silica Particles are More Efficient in Their Activation of Macrophages. Doctoral Dissertation, University of Pittsburgh.
- [22] National Institute for Occupational Safety and Health (NIOSH). (1991). Work-related lung disease surveillance report. Cincinnati, OH: U.S. Department of Health and Human Services, Public Health Service, Centers for Disease Control, *DHHS*, (NIOSH) Publication No. 91-113, Table 23, p. 38.
- [23] Coats, A. W., and Redfern, J. P. (1963). Thermogravimetric analysis. A review. *Analyst*, 88(1053), 906-924.
- [24] TA Instruments. (2006). TGA: Thermogravimetric Analyzer: Q Series Getting Started Guide.
- [25] Cheng, H., Liu, Q., Yang, J., and Frost, R. L. (2010). Thermogravimetric analysis of selected coal-bearing strata kaolinite. *Thermochimica Acta*, 507, 84-90.

- [26] Mu, J., and Perlmutter, D. D. (1981). Thermal decomposition of carbonates, carboxylates, oxalates, acetates, formates, and hydroxides. *Thermochimica Acta*, 49(2), 207-218.
- [27] Hills, A. W. D. (1968). The mechanism of the thermal decomposition of calcium carbonate. *Chemical Engineering Science*, 23(4), 297-320.
- [28] Gabor, M., Toth, M., Kristof, J., and Komaromi-Hiller, G. (1995). Thermal behavior and decomposition of intercalated kaolinite. *Clays and clay minerals*, 43(2), 223-228.
- [29] Annual Book of ASTM Standards (ASTM), Vol. 1994, Section 5, American Society of Testing Materials, Philadelphia, 1993, pp. D3172–D3189.
- [30] Mayoral, M. C., Izquierdo, M. T., Andres, J. M., and Rubio, B. (2001). Different approaches to proximate analysis by thermogravimetry analysis. *Thermochimica Acta*, 370(1), 91-97.
- [31] Li, Q., Zhao, C., Chen, X., Wu, W., and Li, Y. (2009). Comparison of pulverized coal combustion in air and in O₂/CO₂ mixtures by thermo-gravimetric analysis. *Journal of Analytical and Applied Pyrolysis*, 85(1), 521-528.
- [32] Combustible Materials and Rock Dusting; Final Rule, 30 C.F.R. Part 75 Subpart E, (2011).
- [33] Colinet, J. F. and Listak, J. M. (2012). Silica and Respirable Content in Rock Dust Samples. *Coal Age*.
- [34] Danley, R.L. and Schaefer, J.W. (2008). System and Method for a Thermogravimetric Analyzer Having Improved Dynamic Weight Baseline. United States Patent Application Publication, 16 pages.
- [35] Zefon. (2012). Material Safety Data Sheet: Nitocellulose Membrane Filters. <http://www.zefon.com/analytical/download/MSDS%20-%20Zefon%20MCE%20Membrane%20Filters.pdf>
- [36] Zefon. (2015). *PVC Membrane Filters*. Retrieved from <http://www.zefon.com/store/pvc-membrane-filter-gla-5000.html>
- [37] Keles, C., Scaggs, M., and Sarver, E., Preliminary Development of a TGA Method for Determining Coal to Mineral Ratios in Respirable Dust Samples, Proceedings of the 144th Annual Meeting and Exhibition of the Society of Mining, Metallurgy and Exploration Denver, CO February 15-18, 2015, preprints no. 15-137.

CFD Modeling of a Flooded-Bed Scrubber Concept for a Longwall Shearer Operating in a U.S. Coal Seam

William Chad Wedding*, Thomas Novak, Sampurna Arya, & Ashish Kumar

University of Kentucky, Lexington, KY, USA

The dust generated from mining activities remains a health and safety problem, particularly in underground coal mines. Coal Worker's pneumoconiosis (CWP), colloquially known as 'black lung', is a chronic respiratory disease resulting from extended exposure to respirable coal dust. Corrective actions to mitigate CWP, resulting from the Federal Coal Mine Health and Safety Act of 1969, have significantly reduced the incident rates over the last four decades. However, continuing efforts are needed to control this hazard and the newly mandated dust rule will increase the difficulty for mine operators to maintain compliance. A recent study by the National Institute for Occupational Safety and Health highlighted the ongoing health hazards that remain within the coal mining industry because respirable dust. This is especially true for mines using the longwall mining system due to its high production rates. Further, there are no commercially available dust scrubbers for longwall shearers as there are for continuous miner units. The problem of dust capture in underground coal mines utilizing the longwall mining system is being addressed in this paper.

A conceptual design for a flooded-bed scrubber built into a Joy 7LS longwall shearer is presented. Results from a computational fluid dynamics (CFD) study of the performance of a flooded-bed scrubber design are presented. The CFD study was aimed at maximizing the capture efficiency of the scrubber design while operating in a 2.1 meter (7 ft) coal seam under a variety of scrubber flow rates and mine ventilation conditions.

Keywords: longwall shearer, dust control, flooded bed scrubber, computational fluid dynamics

1. Introduction

Dust generated from mining activity is an inherent problem in mines, particularly for underground mines. Incidences of coal workers' pneumoconiosis, a debilitating respiratory ailment, have declined since the Federal Coal Mine Health and Safety Act of 1969, in the United States. Health hazards due to exposure to elevated dust concentrations of respirable dust still exist, according to the National Institute for Occupational Safety and Health (NIOSH) [1]. The problem with coal dust is not limited to health hazards.

The accumulation of coal dust can create a potentially catastrophic safety hazard. If the dust is not removed, it becomes airborne and will be advected downstream through the mine workings. This readily combustible coal dust must be diluted with rock dust to ensure that it remains inert in the event of a methane ignition. The blast wave from such an ignition can disturb this dust causing it to participate in and greatly enhance the resulting explosion. Such an event occurred at the Upper Big Branch Mine, according to the forensics report prepared by the Mine Safety and Health

Administration (MSHA) [2]. Numerous other incidents are documented in the literature.

In the United States, approximately half of the coal produced by underground mines utilize the longwall mining system. According to NIOSH, Longwall operators have historically had a difficult time meeting federal dust standards [3]. The difficulties meeting the dust standard will be aggravated by MSHA's new dust rule, which reduces the dust standard by one fourth. The primary means to deal with dust levels at the longwall face is through dilution with ventilation air, which have increased by about 65% since the mid-1990s [3]. There is a clear need for innovative ways to lower the dust level on longwall faces. This work is an effort to adapt flooded-bed scrubbers for use on a longwall shearer.

1.1 Previous efforts for longwall dust control

The United States Bureau of Mines began investigating the use of scrubbers for longwall dust control in the 1970s, though the efforts were abandoned by the 1980s [4]. This early research effort was performed under different conditions than is typical of today's longwall mine

operations. At the time, unidirectional cutting was common practice, and the quantity of air delivered across the face was much lower.

The research from this former period can be divided into three approaches: ventilated-drum [5] [6], ventilated-cowl (US Patent 4351567), water-powered scrubbers [7], and fan-powered flooded-bed scrubbers [8]. The first three methods relied on high pressure water sprays to move dust laden air into the scrubber inlets, while the last method used a vane-axial fan. High pressure water sprays are compact, allowing them to be mounted within the shearer drum and on the cowl. The main disadvantage of the sprays was the limited airflow capacity compared to fan-powered scrubbers. Their use was also confounded by excessive maintenance issues. For these reasons, water-powered scrubber research was abandoned at that time.

Designs that combined fan-powered flooded-bed scrubbers and longwall shearers were also attempted. Despite its dust reduction potential, the complexity of incorporating the ductwork into the shearer, size constraints, and lack of interest by the industry stalled research in this

area. The idea was revisited recently in Australia. Researchers working on a project funded by the Australian Coal Association Research Program developed a fan-powered dust scrubber for a longwall shearer working in a 5 m (16.4 ft) thick coal seam [9]. It was successfully tested at BHP Billiton's Broadmeadow Colliery in the Bowen Basin of North Queensland. Test results demonstrated an overall dust reduction potential of 14% to 56%, depending upon operating conditions and sampling methodology. The scrubber was mounted directly on the leading side of the ranging arm so that it was as close to the drum as possible. Because of its placement, one of the main challenges was developing a prototype that would stand the rigors of mining without being destroyed.

1.2 Flooded-bed scrubber use

In the U.S., the majority of room and pillar coal mines utilize fan-powered flooded-bed scrubbers in their dust control plans. They are considered effective in controlling dust generated at the face. The general arrangement of a fan-powered flooded-bed scrubber (U.S. Patent 4380353) can be seen in Figure 1.

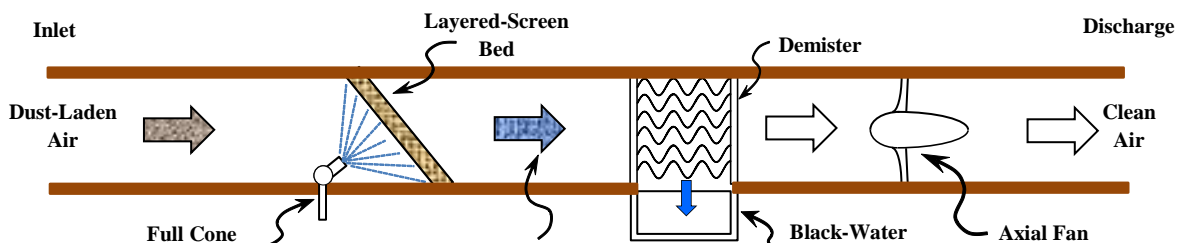


Fig. 1 General arrangement of fan-powered flooded-bed scrubbers

While operating, dust-laden air is drawn in through inlets near the cutting head and into ductwork within the miner. The air and dust passes through a layered-screen bed, typically consisting of 10 to 30 layers of woven steel mesh screens, with an 89 μm (0.0035 in.) wire diameter. An arrangement of one or more full cone nozzles keeps the layered-screen bed wetted with water. As the air and dust pass through the wetted screen, there is a high probability that the dust particles will become encased with water. Increasing the number of layers in the screen tends to increase the likelihood of dust becoming captured by the water, at the expense of increasing pressure drop across the layered-screen bed. The screens are typically installed at an angle to the flow, thereby increasing the available surface area of the bed.

After exiting the layered-screen bed, the air/dust/water mixture flows into the demister. This is an arrangement of parallel, sinuous layers of PVC material, which causes the airflow to make several changes in direction. Due to the mass and speed of the water droplets, their momentum causes them to collide with the layer of plastic. The water and dust then flow down the walls to a collection sump below and is pumped to the miner's discharge conveyor. Clean air exits through the fan, to the scrubber discharge.

The scrubber fan typically ranges in power from 9.7 kW to 30 kW (13 hp to 40 hp), with an airflow range of 1.7 m^3/s to 4.7 m^3/s (3.5 kcfm to 10 kcfm). In the U.S., the airflow through a scrubber is typically slightly lower than the quantity of ventilation air flowing to the face to minimize recirculation. The quantity of air flowing to the face must

be no lower than 1.4 m³/s (3 kcfm) in the U.S., to comply with Federal Law (30 CFR 75.325) and in practice it is usually higher to dilute methane and dust [10].

When considering scrubber systems, two operational characteristics describe the performance of the system as whole, *capture efficiency* and *cleaning efficiency* [4]. *Capture efficiency* is the measure of a system's ability to draw dust laden air into the scrubber; the percentage of dust in the air captured. *Cleaning efficiency* is the measure of a system's ability to remove dust from the air, once it has been captured. According to a study by NIOSH, a fan-powered flooded-bed scrubber, using a 30 layered-screen bed, can achieve a cleaning efficiency greater than 90% [11]. The challenge is capturing the dust laden air before it is diluted by ventilation air.

Longwall ventilation practices are not as conducive to the use of fan-powered flooded-bed scrubbers when compared to room and pillar operations. In a survey conducted by NIOSH in 2007, the average air velocity along a longwall face in the U.S. was found to be 3.38 m/s (665 fpm), with an airflow quantity of 31.6 m³/s (67 kcfm) [3]. The magnitude of the airflow precludes one from designing a system that matches the airflow quantity through the scrubber to the face quantity, as common with continuous miners. Since only a portion of the air will be captured by the scrubber, the placement of the inlet to the scrubber is critical in achieving a worthwhile capture efficiency. Thus, the inlet must be positioned close to the cutter drum, the principle source of dust on a longwall face [3]. This will allow the scrubber to capture the dust before it is diluted by the ventilation air. Care must be taken in the design to prevent larger coal particles from being ingested by the scrubber in order to prevent excessive clogging. The inlet and ducting must also be protected from spalling coal and rock. It must also not interfere with moving components, such as the ranging arm, cutter drum, or shields.

2. Current research approach

The research approach at the University of Kentucky is a site-specific application of a fan-powered flooded-bed scrubber to a typical U.S. longwall operation in a medium thickness coal seam. The average seam thickness at the mine is 2.1 m (7 ft) and is fairly consistent and flat which is

typical of the Pittsburgh coal seam. The longwall face employs a Joy 7LS shearer as seen in Figure 2, courtesy of computer-aided design data (CAD) provided by Joy Global. Although the mine utilizes a bidirectional cutting approach, this research project only addresses the headgate side of the shearer in this initial effort.

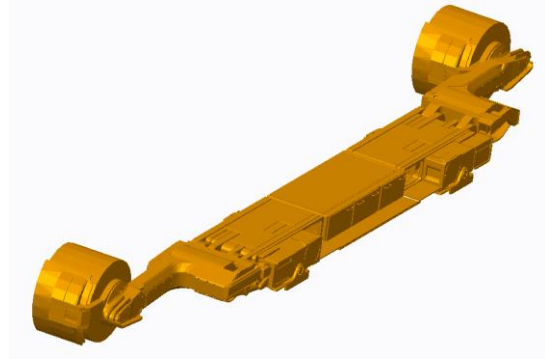


Fig. 2 Joy 7LS longwall shearer employed at the mine specific to the study

2.1 Details from the mine

A visit with the mine personnel yielded additional information to be included in the concept development. The mine operates three development sections utilizing continuous miners and one active longwall panel. The width of the longwall panel is 305 m (1,000 ft). The average longwall retreat rate per day is 34 m (112 ft).

Airflow quantity across the longwall face was controlled by a prescribed mean entry air velocity, according to their ventilation plan. An airflow velocity of no less than 2.5 m/s (500 fpm) at the head gate and a minimum of 2.0 m/s (400 fpm) within 30 m (100 ft) of the tail gate was maintained. This equals a minimum airflow quantity of 14 m³/s (30 kcfm) maintained in the last open break on the headgate. The ventilation plan included a provision requiring respiratory protection for any persons working more than 12 shields in by the shearer while cutting coal due to the expected, elevated concentrations of dust. A shearer air deflector was required to be installed and maintained on the headgate spray arm, which can be seen in Figure 3. This device extends past the head drum and serves to split the air flowing along the face, in an attempt to keep the dust-laden air clear of the walkway where miners are present.

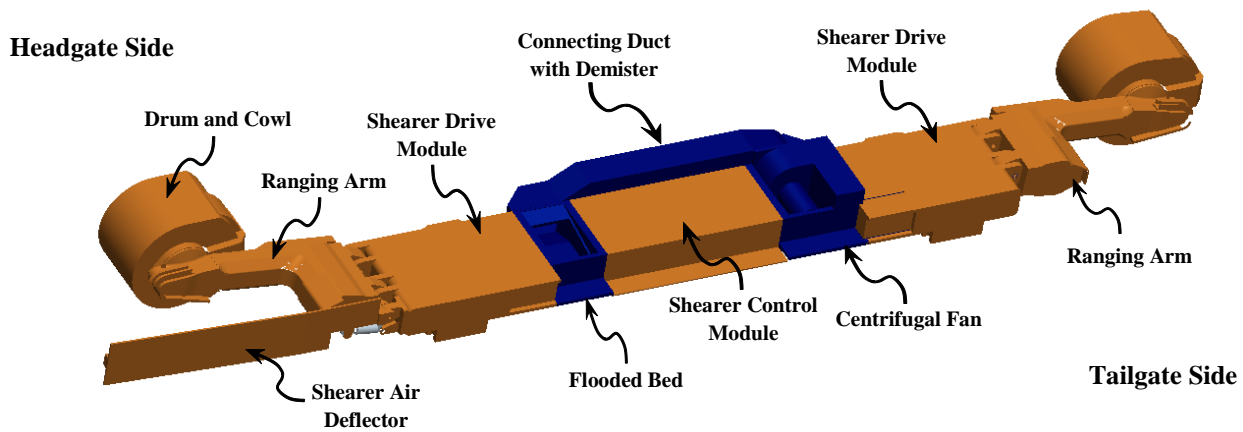


Fig. 3 Conceptual design for incorporating a fan-powered flooded-bed scrubber into a longwall shearer, with inlet and discharge ductwork removed for clarity

Observations of the shearer in operation highlighted several other concerns. The cutting actions of the headgate drum breaks the coal and sends it forward onto the armored face conveyor, or AFC. This spalled coal flowed out from the drum as it churns which brings a significant cloud of dust forward against the flow of air. A cloud of dust and mist close to the coal on the AFC was pulled along with the moving coal, as it heads to the stageloader. It does not advance far before being overcome by the ventilation air on the face and causing this dust to flow back over the shearer. The velocity of this spalled coal was assumed to depend upon the tangential velocity of the drum, which rotates at approximately 45 rpm. The average speed of the armored face conveyor was found to vary between 1.8 m/s and 2.0 m/s (355 fpm and 400 fpm). These were important observations to include in the CFD model as boundary conditions. This influence of the spalled coal has been included in the CAD model as shown in Figure 4, where the ranging arm can be seen cutting coal.

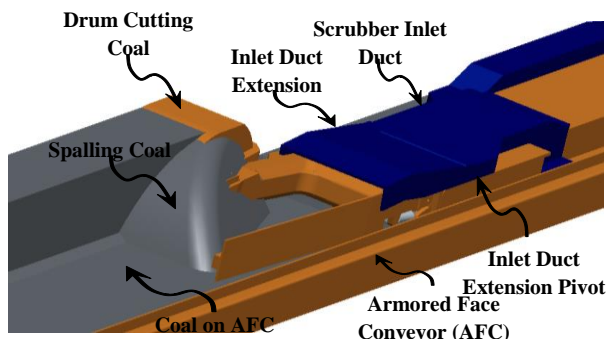


Fig. 4 Conceptual design of inlet duct arrangement and influence of spalling coal due to the actions of the headgate drum

2.2 Conceptual design

Discussions with the engineering team at Joy Global identified key constraints for developing the conceptual design. There is no more than 25 cm (10 in.) of space available above the body of the shearer before it is at risk of hitting a mobile roof support. This was the main constraint when examining where to place scrubber components. As shown in figure 1, there are three main components to a fan-powered flooded-bed scrubber, the flooded-bed, the demister, and the fan, before considering the ductwork. None of these components will fit within a 25 cm height envelope, if the quantity of air delivered to the scrubber is equal to or greater than the quantity of air employed by a continuous mine scrubber. This led to the addition of two new modules to the shearer body, as seen in Figure 3.

To make room for the scrubber components, two new modules were added to the shearer body between the control module and the drive modules. On the headgate side, a compartment for the flooded-bed screen and sprays was added. The screen was angled to maximize the available cross sectional area and its placement is readily accessible for maintenance. The fan was positioned between the control module and the tailgate drive section. Due to the arrangement of the flow, a centrifugal fan was chosen which can readily generate the necessary flow and pressure to power the scrubber. These can be observed in Figure 3. The flooded-bed module added 0.9 m (3 ft) to the length of the shearer, while the fan module added 1.2 m (4 ft). This increased the length of the shearer by 12.5%, from 16.8 m to 18.9 m (55 ft to 62 ft).

A section of ducting connecting the flooded-bed and centrifugal fan was added along the face side of the shearer body, as seen in Figure 3. This was positioned in the void left from the extraction of coal by the leading drum. It projected 0.4 m (1.25 ft) past the edge of the shearer towards the face. Within the duct, the demister and 95 liter (25 gal) black water sump were placed. As the duct is in close proximity to the face, it would be made from thick steel sections limiting the available area for airflow which was taken into account in the CFD model. Conversations with the mine staff indicated that the face side of the control module does not require frequent access for service, meaning the duct would not hamper such activities.

The inlet duct arrangement was critical to the success of the effort. As mentioned in Section 1.2, it is desirable to bring the inlet as close as possible to the dust source, in this case the headgate drum. Several iterations were testing before arriving at the configuration shown in Figure 4. The inlet duct extended up from the flooded-bed module and over the headgate drive module. This occupied the 25 cm (10 in) available height according to engineers at Joy. Like the connecting duct, this would be made of thick steel sections to ensure it survives the rigors of mining. This duct ended at the edge of the headgate drive module, which was insufficient for collecting the dust from the headgate drum. An adjustable extension was added to position the inlet just past the main portion of the ranging arm. It was designed to raise and lower separately so that it may be lowered to clear shields that might be in the way.

3. CFD modeling

CFD modeling is a numerical way of solving fluid dynamics problems. The equations used in this CFD model were the laws of conservation of mass and conservation of momentum. The software used for the simulations was Cradle SC / Tetra version 11, which includes its own preprocessor, solver, and post processor. SC / Tetra utilizes an unstructured mesh approach.

The geometry used for the CFD model was developed in CREO, a three-dimensional parametric modeling package, based upon the data provided by the mine and Joy Global. It includes the longwall shearer, armored face conveyor, the coal face, and a portion of the powered supports. The entire geometry of the powered roof supports was not used, in order to reduce the number of elements, resulting in the simplified geometry used for the domain, as shown in Figure 5. The region shown was approximately 25.5 m (83.7 ft) in length, 2 m tall (6.5 ft), and 4.7 m (15.4 ft) wide.

The boundary conditions for the model included a velocity inlet condition on the headgate side, thereby controlling the volume of air across the face. The tailgate

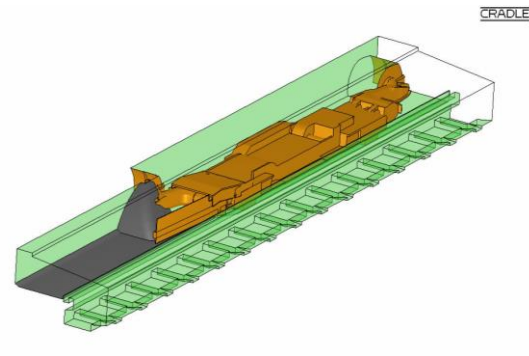


Fig. 5 CFD model computational domain

side was represented with a static pressure boundary condition of zero. The plane where the flooded-bed screen rests was chosen as the boundary for the scrubber inlet. In this way, the influence of the duct design was captured in the calculations. A volumetric flow was assigned to this region. The same magnitude of flow was assigned to the discharge of the centrifugal fan, representing the discharge of the scrubber system through that ductwork. The internal components of the scrubber, such as the flooded-bed screen and demister were not included in the computational domain. The coal on the AFC was given a translating boundary condition to mimic the influence of the moving conveyor. The spalled coal thrown up by the headgate drum was given a rotating wall condition, with the center of rotation at the axis of the drum. This gives that surface the appropriate tangential velocity observed at the mine. The remainder of the surfaces, such as the shearer body, AFC, and supports, were given a stationary wall boundary condition.

Within Cradle, multiple models are available to describe the influence of turbulence. In this study, two models of turbulence were tested: the standard $k - \epsilon$ model and a variation known as the RNG $k - \epsilon$ model. The RNG $k - \epsilon$ model differs from the standard model by adding an additional source term in the transport equation for the rate of kinetic energy dissipation. This allows it to describe the effects of rapid changes in strain rate and streamline curvatures.

In order to ensure that the mesh would not significantly impact the results of the simulation, it was necessary to establish grid independence. This was accomplished through progressive refinement of the size of the grid used in the model. Grid independence was established by monitoring velocity values near the inlet to the scrubber. The number of elements varied from 2.2 million elements to

8.1 million elements, with less than 3% variation observed in those velocity values. In each case, local refinement was required near the inlet and discharge of the scrubber, where high velocity and pressure gradients were present.

Steady state and transient state simulations were conducted at varying flowrates in the model in an attempt to find the optimum ratio between scrubber air volumes and face air volumes. Two different velocities were chosen for the headgate inlet, 2.5 m/s and 3.0 m/s (500 fpm and 600 fpm) and six scrubber flow volumes in equal increments from 3.0 m³/sec to 6.0 m³/sec (6,400 cfm to 12,700 cfm). Converged steady state solutions were used to establish the initial conditions for the transient simulation. Convergence was established by monitoring residuals RMS errors to a value less than 10⁻⁴ and domain mass imbalance to less than 0.1%. To represent dust in the system, 250 marker particles were generated at time zero, t=0.00 seconds, spread over the surface of the spalled coal in the model. The particles were then followed through the model as they are transported by the pattern of air at the faces, while influenced by the dust scrubber. The particles were counted when they reached the surface of the flooded-bed screen and are deemed to have been captured by the scrubber. After 20 seconds, the particles were either captured by the screen, or too far removed from the inlet to be captured. In this way, the *capture efficiency* of the scrubber design was estimated.

4. Results and discussion

A table of capture efficiency has been compiled with different airflows at the face and through the scrubber, as seen in Table 1. Reported capture efficiency values have converged to within 0.5% in each case.

From the table, it is clear that the scrubber and inlet design exhibits promise. It is achieving a 75% to 90% dust capture efficiency over the range of values tested, for dust generated at the headgate drum. As expected, as the volume of air through the scrubber increases, the dust capture efficiency increases, in general. In Figure 6, one can observe the predicted velocity contours along the face. The plane nearest the scrubber inlet exhibits a uniform flow pattern which would discourage mixing of the dust laden air prior to entering the scrubber inlet. This is thought to be the preferred flow pattern in this region, as the dust laden air should be contained on the face side of the shearer air deflector and away from the miners in the walkway. In these simulations, the spray nozzles have been excluded, in order to concentrate on the impact of the scrubber. Adding the spray nozzles will likely change the results, but the optimum

configuration of nozzles with an active scrubber is not known.

Table 1 Dust capture efficiency predicted by CFD simulation for varying scrubber volume flows and face velocities

Predicted Dust Capture Efficiency						
Mean Face	Scrubber Volume (m ³ /s)					
Velocity (m/s)	3.0	3.6	4.2	4.8	5.4	6.0
2.5	75.7%	85.1%	76.2%	80.3%	90.8%	88.3%
3	74.6%	81.4%	84.0%	88.8%	90.8%	88.0%

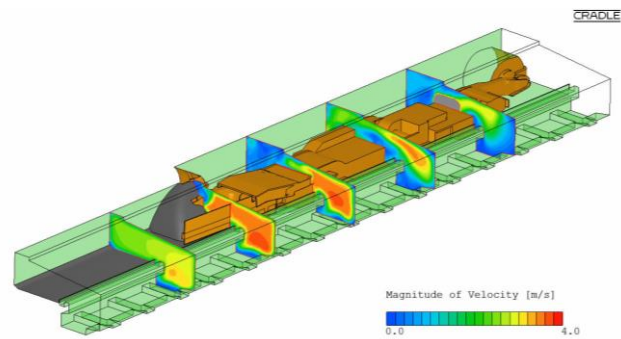


Fig. 6 Predicted velocity contours along the longwall face under the influence of a fan-powered flooded-bed scrubber, at 5.4 m³/s (11,400 cfm) through the scrubber with a mean face velocity of 2.5 m/s (500 fpm)

5. Ongoing and future work

The following CFD simulations are underway or planned. Individual components of the scrubber system will be characterized, including the flooded-bed and the demister. The discharge of the scrubber system needs to be examined to discover ways to take advantage of this energetic stream of clean air. The configuration of the spray nozzles on the shearer body will be examined in an attempt to optimize this system.

Aside from CFD modeling, a full scale, functional prototype of the scrubber system and a model of the longwall shearer is being built to be tested at the NIOSH facility in Pittsburgh, PA. A 1:20 reduced scale model is also being tested in the laboratory. These experiments are planned in order to validate the design and confirm the potential for this system to reduce dust concentrations at the longwall face and improve the working conditions and health of underground miners.

Acknowledgements

The authors would like to acknowledge the Alpha Foundation for funding this research effort. In addition, the

work was made possible by the contributions from the engineers at Joy Global and at Alliance Coal and through the cooperation of NIOSH.

Institute for Occupational Safety and Health, HID1, DHHS (NIOSH) Publication No. 97-147.

References

- [1] NIOSH (National Institute for Occupational Safety and Health), 2008, "Work-related lung disease surveillance report 2007, Volume 1 DHHS (NIOSH) Publication No. 2008-143a." Cincinnati, OH, National Institute for Occupational Safety and Health.
- [2] U.S. Department of Labor, Mine Safety and Health Administration, Coal Mine Safety and Health, (2011), "Report of Investigation, Fatal Underground Mine Explosion, April 5, 2010, Upper Big Branch Mine-South, Performance Coal Company, Montcoal, Raleigh County, West Virginia, ID No. 46-08436," Washington, D.C.
- [3] Rider, J.P., Colinet, J.F., 2010, "Chapter 3 – Controlling Respirable Dust on Longwall Mining Operations," Best Practices for Dust Control in Coal Mining, IC 9517, National Institute for Occupational Safety and Health, pp. 17-39.
- [4] Wirch, S. and R. Jankowski, 1991, "Shearer-Mounted Scrubbers, are They Viable and Cost Effective," *Proceedings of the 7th US Mine Ventilation Symposium*, pp. 319-325.
- [5] Divers, E. F., R. J. Jankowski, and J. S. Kelly, 1987, "Ventilated Drum Control Longwall Dust and Methane," *Proceedings of the 3rd US Mine Ventilation Symposium*, pp. 85-89.
- [6] French, A. G., 1983, "The Extraction of Respirable Dust from Machines Working on Longwall Faces," *Proceeding for the European Economic Communities Conference on Dust Control*, Luxembourg, 1983, pp. 57-73.
- [7] Kelly, J. S., 1982, "Shearer Mounted Dust Collector Laboratory Testing," Foster-Miller, Inc. Interim Final Report for US Bureau of Mines Contract J0387222, 168 pp.
- [8] Jayaraman, N. I., 1977, "Dust Control on a Longwall Face with a Shearer-Mounted Dust Collector," *U.S. Bureau of Mine Report of Investigation, RI 8248*, 13 pp.
- [9] Ren, T., R. Balusu, and B. Plush, 2009, "Dust control technology for longwall faces – Shearer scrubber development and field trials," ACARP Project C14036.
- [10] Listak, J. M., 2010, "Chapter 4 – Controlling Respirable Dust on Continuous Mining Operations," *Best Practices for Dust Control in Coal Mining*, IC 9517, National Institute for Occupational Safety and Health, pp. 41-64.
- [11] NIOSH (National Institute for Occupational Safety and Health), 1997, Hazard identification 1: Exposure to silica dust on continuous mining operations using flooded-bed scrubbers. Cincinnati, OH: U.S. Department of Health and Human Services, Centers for Disease Control and Prevention, National

Development of a Mine Dust Sampling Instrument for use in Underground Coal Mines

Benjamin Joseph Goertz^a, Jürgen Brune^a, Sean McDaniel^b, Tyler Rockley^a, Flavia Soares Barreto^a, Nicole Demontigny^a

Colorado School of Mines, Golden, Colorado, USA

Researchers at the Colorado School of Mines, under a project funded by the Alpha Foundation, have developed a working prototype of a dust sample collection device designed to determine if sufficient rock dust has been placed in an underground coal mine to prevent coal dust explosions. When used in conjunction with the Coal Dust Explosibility Meter (CDEM), the device will provide near instantaneous results on the quality of rock dusting at the tested location. The sampling device applies a pulse of air to a testing surface and collect a representative sample of mine dust based on the pneumatic entrainment process during a mine explosion.

The use of both physical testing and Computational Fluid Dynamics (CFD) modeling has allowed researchers to refine the design to accurately represent the particle entrainment and optimize the sample size collected for the CDEM. The prototype is being tested in a mine environment to produce information of usability and practical aspects of mine dust sampling. This paper is a progress report summarizing the current status of sampler development. Researchers expect to have a fully developed and tested sampler in early 2016.

Keywords: Mine Dust, Coal, Dust Sampling, Dust Testing

1. Introduction

Underground coal mines face the danger of methane and coal dust explosions. The disaster at Upper Big Branch Mine (2010) has demonstrated the impact of a violent coal dust explosion that fatally injured 29 miners. Reviewing the history of coal dust explosions, researchers found that that mine operators and mine inspectors do not have a reliable method of collecting dust samples to verify the inertness of the dust underground. This is a potential issue with small mines that do not have dedicated safety departments to track rock dusting work. The aim of this research is to develop a simple, portable Dust Sampling Device (DSD) that can help underground mine examiners collect dust samples from workings and test the explosibility of the sample near instantaneously.

Researchers determined that the current brush-and-pan sampling method required by MSHA [1] is flawed in several aspects: Mechanical sampling with a brush exerts forces on the mine dust that may differ significantly from those present during an explosion. Also, U.S Bureau of Mines research [2] has determined that only the top 0.125 inches of the mine dust layer will be entrained in a coal dust explosion. Using a handheld pan and brush, it is difficult to accurately and repeatedly sample a layer of this exact thickness.

The following will describe the CFD modeling and experimental testing for the development of the prototype sampler. Researchers analyze the accuracy and performance of the prototype during the course of the build process.

2. First Design Prototype of the DSD

2.1 Initial Nozzle Testing

To develop the initial prototype sampler, researchers tested various nozzle configurations to understand the scour patterns left when varying testing parameters including nozzle geometry, nozzle angle,

pneumatic pressure, duration of air pulse supplied to nozzle, nozzle height above the dust surface, nozzle orientation and sampler dimensions.

2.2 First Prototype Design

The first prototype was made using 1/8" thick pieces of ABS plastic, as shown in Figure 1. The nozzle is attached to the front wall of the sampler box and adjustable to the desired angle. A collection plate opposite the nozzles sits on the surface of the dust and is adjustable in length. This setup allowed researchers to change the width of the dust collection opening to optimize the collected sample mass for the CDEM.



Fig. 1. Side view (left) and bottom view (right) of first prototype with hose and nozzle system.

In order to deliver a defined air pulse to the sampler, researchers designed an air containment vessel with a charge-and-release valve configuration as shown in Figure 2. Researchers prime the air vessel to the desired pressure and then release the stored air through the hose and nozzle setup to create airflow into the sampler. This setup has been used with great success to supply a consistent and repeatable volume of pressurized air to the nozzles.



Fig. 2. Palm button charge and release valve system with air vessel.

Researchers tested with a large number of different air nozzles and an air knife to understand the interaction between nozzles and dust. Early results showed that, in order to achieve the 1/8" sample depth while collecting a mass of dust sufficient for a CDEM

test, two nozzles would need to be used in a horizontal pairing.

Different nozzle angles and vessel charging pressures were tried to understand the sensitivity of these parameters. To determine the scour depth, researchers used a metal caliper to gauge the maximum depth of the dust imprint against the original depth of the dust layer. This resulted in efficient and consistent measurements. The results of scour depth and dust mass collected vs. charge pressure are shown in Figures 3, 4 and 5 for different nozzle angles and with other key parameters varied. The data points represent the average values obtained from multiple tests.

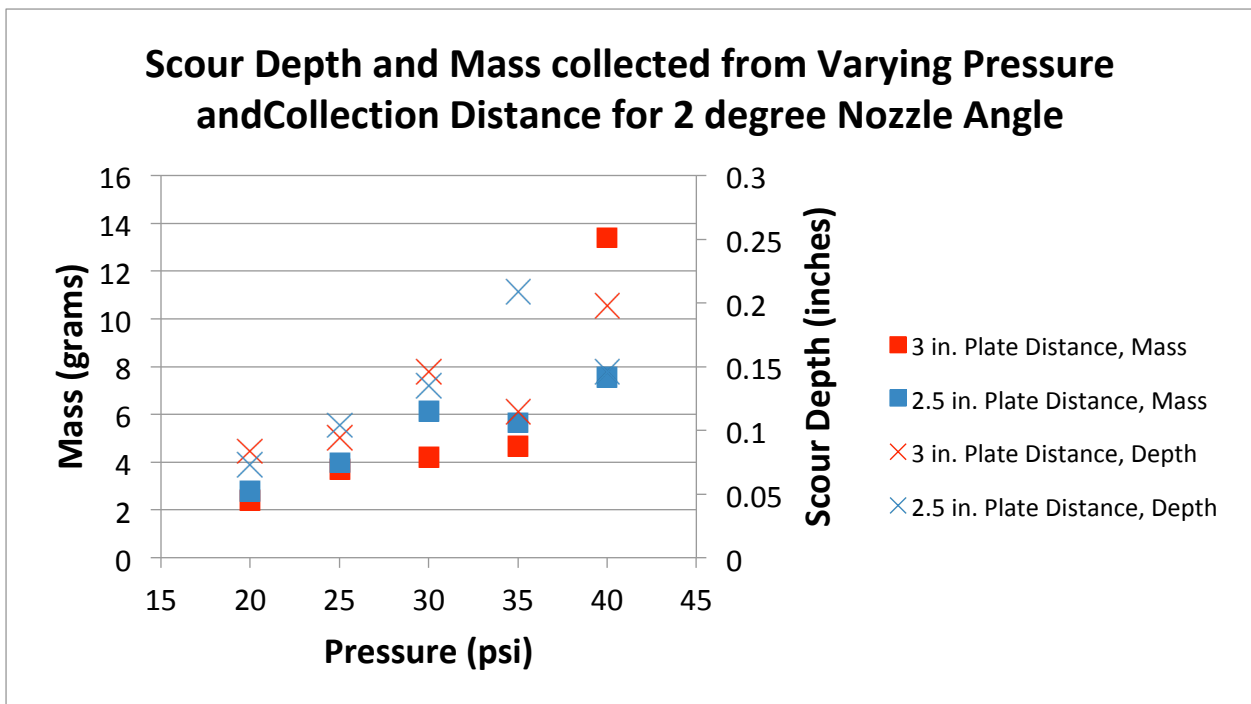


Fig. 3. Comparison of 3 inch and 2.5 inch Plate Distances for a 2-degree nozzle angle.

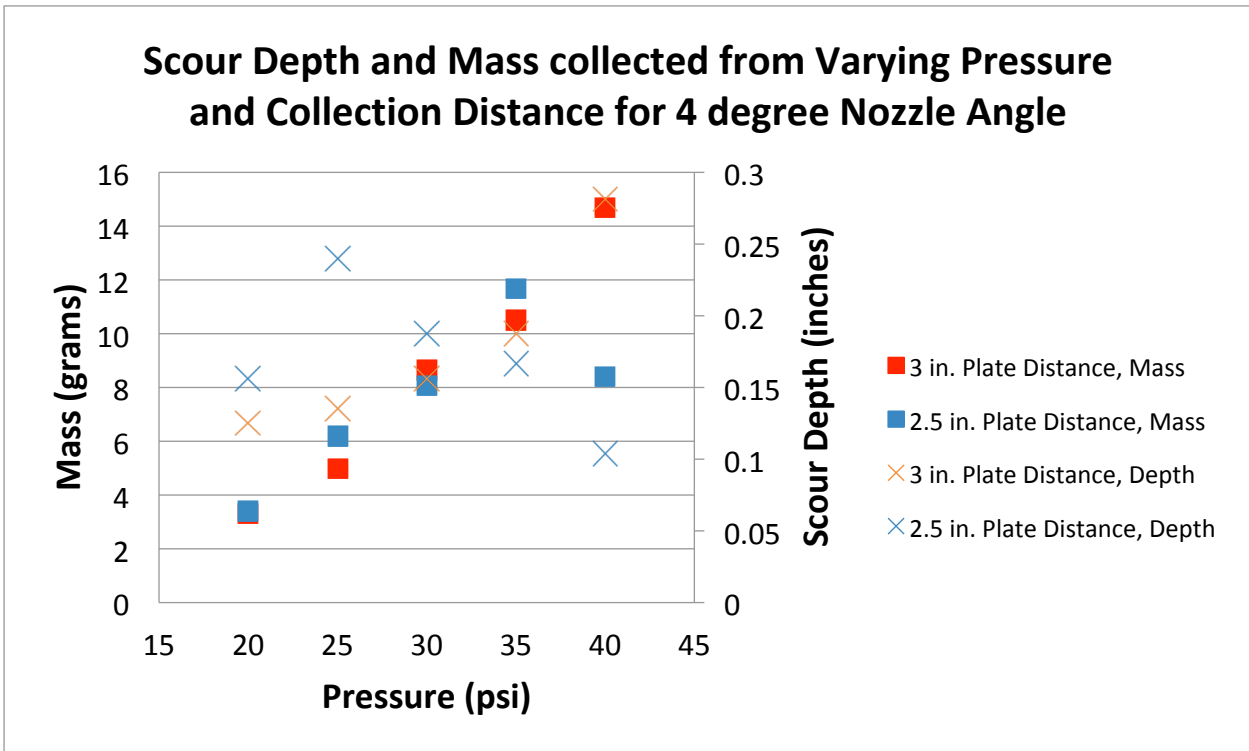


Fig. 4. Comparison of 3 inch and 2.5 inch Plate Distances for a 4 degree nozzle angle.

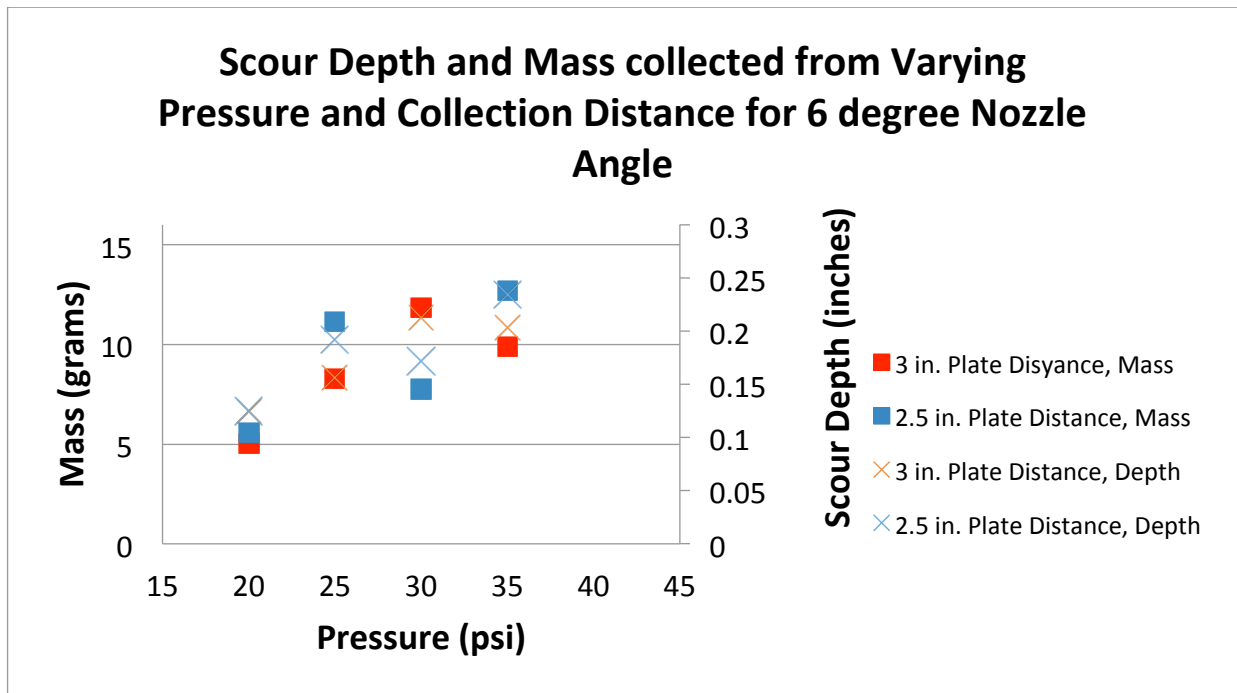


Fig. 5. Comparison of 3 inch and 2.5 inch Plate Distances for a 6 degree nozzle angle.

2.3 Effects of Dust Packing Density

Initial tests revealed that the packing density of the dust was inconsistent prior to sampling. Researchers developed a system to prepare an even, consistently packed layer of dust that represents a layer of freshly placed rock dust in the mine. The dust layering system consisted of a mesh screen mounted on a roller system in a box frame. Rock dust is loaded onto the screen and

then the box is moved forward and back to pass the rock dust through the screen, replicating the pneumatic spreading of rock dust in an underground coal mine. The system also allowed researchers to vary the thickness of the dust layer. Figure 6 shows the top box and screen assembly.



Fig. 6. Box screen-mesh assembly above dust layer.

3. Second Design Prototype of the DSD

3.1 Second Prototype Design

In the second prototyping phase, an improved sampler cavity design was developed based on previous test results and CFD modeling of dust movement in the device. Researchers determined that a flatter sampler cavity would better channel the airflow towards the collection area while reducing the amount of dust recirculation in the cavity. Researchers also determined that the previous method of dust collection from the sampler would be unsatisfactory for in-mine sampling. The new prototype had an open back with a plastic sample collection bag attached. Researchers also created inserts to vary the cavity height in the sampler. Figure 7 shows the second prototype with the nozzle and sample bag attached.



Fig. 7. Views of the second prototype with nozzle system.

To determine mass with the new collection method each bag would be weighed prior to being attached to the cavity and after the test was completed. Free dust on the exterior of the collection bag was brushed off to accurately determine the sample mass. Results for the scouring depth and sample mass for the second prototype are displayed in Figures 8 and 9, including error bars indicating the variability of test results.

3.2 Inconsistencies with Nozzle Height above Dust Layer

The data presented in the above figures shows inconsistencies between the test results. Though the averages appear reasonably close to the target, researchers recorded a number of outlying test results. Researchers found that the vertical distance from the nozzle to the dust surface was primarily responsible for these inconsistencies. A second series of tests at the 1.125 inch cavity height were conducted with researchers carefully placing the sampler so the nozzle ports remained at a consistent height directly above the dust layer. This improved sampling repeatability significantly. A comparison of the initial data and improved test data is provided in Table 1.

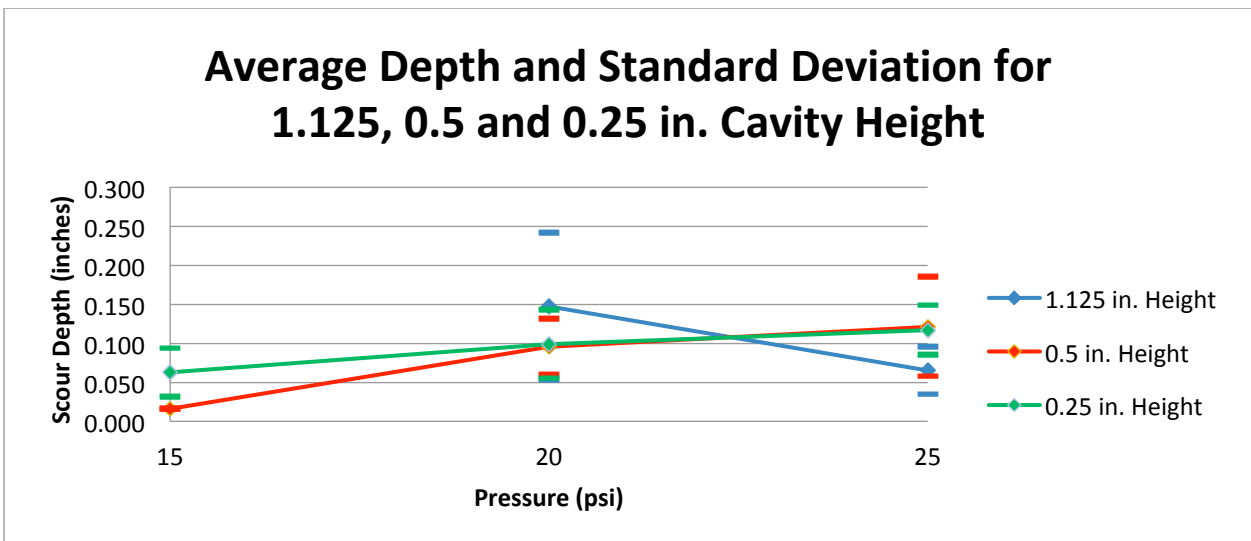


Fig. 8. Comparison of height and scour depth vs. pressure.

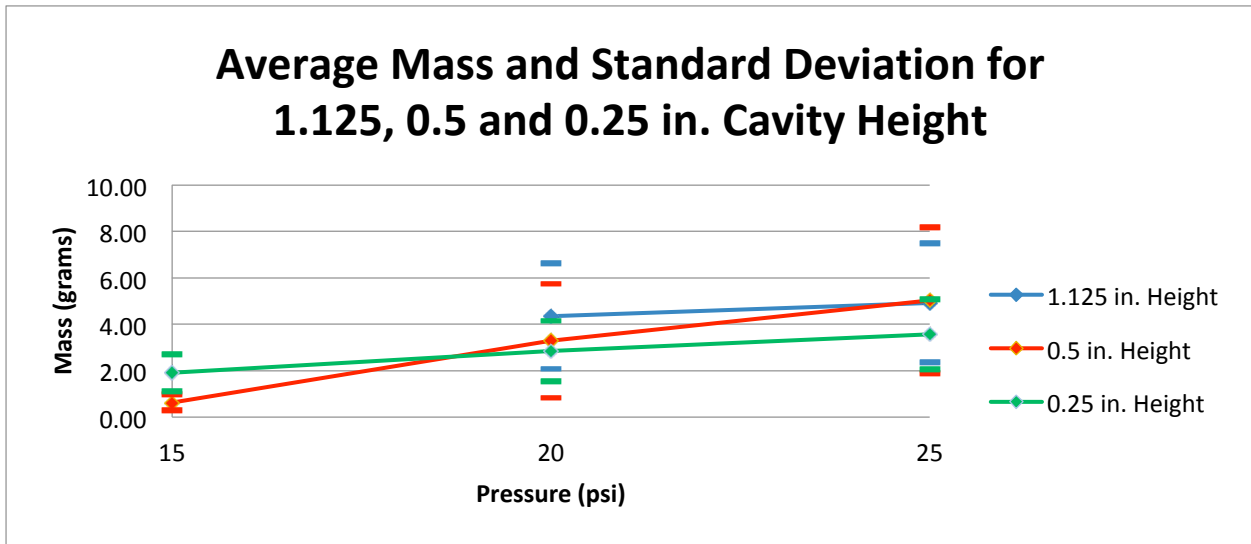


Fig. 9. Comparison of height to average and standard deviation of mass against pressure.

Table 1. Comparison of 1st run and 2nd run data for 1.125 inch cavity height.

Rock Dust Mass Weighed (grams)				
Pressure (psi)	Initial Test		Improved Test	
	Average	Standard Deviation	Average	Standard Deviation
20	4.35	2.27	2.35	0.47
25	4.92	2.57	3.08	0.56
Scour Depth Measured (inches)				
Pressure (psi)	Initial Test		Improved Test	
	Average	Standard Deviation	Average	Standard Deviation
20	0.148	0.094	0.094	0.028
25	0.065	0.030	0.109	0.026

4. Third Design Prototype of the DSD

Researchers have recently built a third design prototype which brought together the individual components into a unified hand-held device that could be used for in-mine testing. All of the system components have been compacted and attached to the main box design with some minor adjustments to the internal box dimensions made. This new prototype is also capable of testing from a compressed air-tank instead of a compressed air line which lends to the portability of the device when conducting sampling in a mine environment. Further testing of the components used in this new design and the overall functionality of the prototype is currently underway and will lead to the development of the final prototype design of the Dust Sampling Device later this summer.

5. CFD Modeling of Air and Dust Movement in DSD

Modeling of dust sampling device has been critical in correlating the optimum design with experimental results. The modeling activity involved 3

stages: designing the geometry, developing the mesh generation and defining boundary conditions.

The experimental design was replicated in CFD using ANSYS Fluent[®] as shown in Figure 10. The green layer represents the dust phase of the model while the pink section represents the sampler cavity.

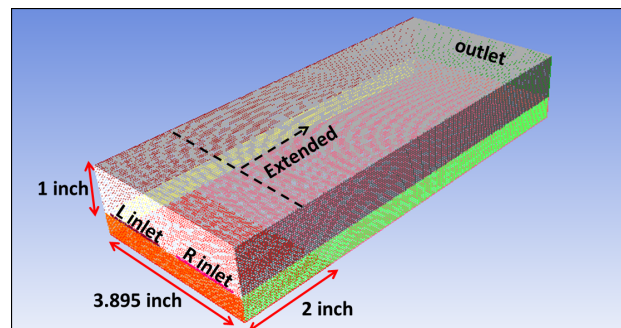


Fig. 10. CFD - Geometry design showing sections of red (air phase) and green (dust phase).

The quality of the CFD mesh has a significant impact on solvability and modeling results. The current mesh uses a cell size of 0.035 mm (x direction), 0.046 mm (y direction) and 0.042 mm in the z-direction. Mesh refinement and inflation were used near the interface between the dust and air phases. The mesh elements had the highest possible quality with no skewness as all cells were cuboid shaped. Reduction of the mesh size demonstrated mesh independence of the model.

The solver used for the analysis is the k-epsilon type with standard wall functions. Eulerian models with two phases (gas and solid) were used to replicate the expected interactions of the air and dust. Figure 11 shows a side view of the sampler and CFD dust entrainment model.

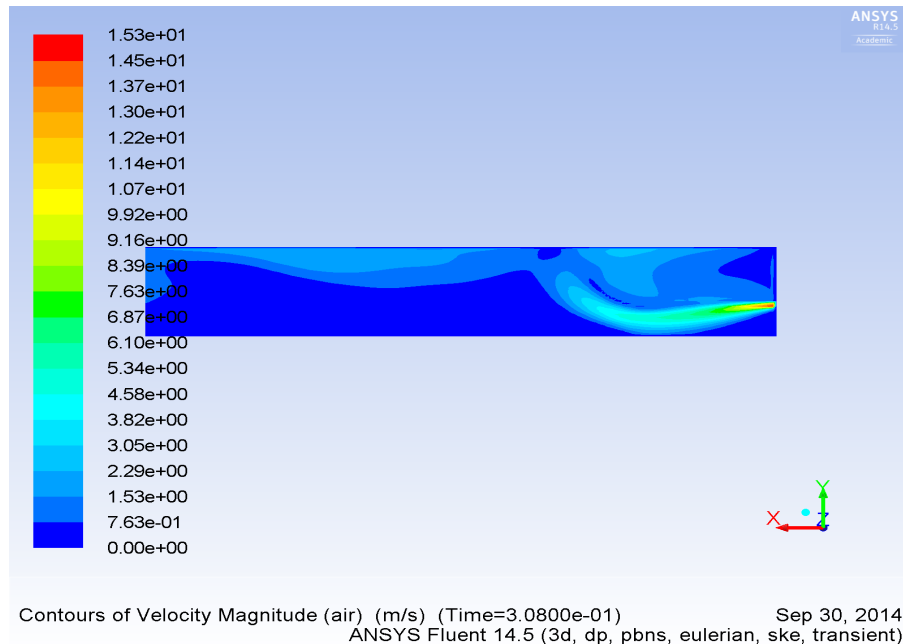


Fig. 11. Side view of CFD dust sampler model showing air injection movement through dust.

5.1 CFD Modeling Results

Researchers have confirmed laboratory testing results in the CFD model and are now using CFD modeling to further refine the second prototype. CFD modeling has indicated that using a staggered system of nozzles will increase the sample mass and improve the flow conditions inside the sampler. Researchers expect that this improvement, along with a wider lip to consistently place the nozzles above the dust surface, will result in further improvement in sample size and scouring accuracy.

6. Conclusions

Researchers at the Colorado School of Mines have developed a working prototype mine dust sampling instrument that will help mine operators and inspectors draw meaningful samples of mine dust, which can then be tested with a Coal Dust Explosibility Meter to verify that adequate amounts of rock dust have been placed in the mine to protect against coal dust explosions. Having the ability for a near instant measurements with a set of simple and relatively inexpensive sampling instruments is especially important for small mine operators who do not have a dedicated staff of mine safety and explosion control examiners. A final prototype is expected to be available in Q3 2015. Following in-mine testing, verification and approval by MSHA, researchers expect to engage with manufacturers to produce and market the sampler.

References

- [1] Mine Safety and Health Administration, Coal Mine Safety and Health General Inspection Procedures Handbook, Handbook Number: PH13-V-1 (February 2013) 276 p.
- [2] Nagy et al., Float Coal Hazard in Mines: A Progress Report, U.S. Bureau of Mines RI No. 6581, Pittsburgh (1965) 2 p.

Application of Box-Wilson Experimental Design Method for Underground Mine's Respiratory Coal Dust Studies

Yinping Chen, Guang Xu, Mahinda Kuruppu, Boris Albijanic

Western Australian School of Mines, Curtin University, Kalgoorlie, WA, Australia

Research on coal dust control in the laboratory has always been essential to better determine the optimal methods and solutions to improve underground air quality for health and safety reasons. This research aims at performing a comprehensive laboratory study to investigate factors (surfactant concentration, catalyzer concentration, water droplet size) involved in reducing respiratory coal dust. A designed experimental apparatus which composed of a wind tunnel, dust generators, water spray system, dust monitors, and a tail dust remover would be constructed to test the experimental variables related to coal dust control. Box-Wilson experimental design method (centre composite design) was employed to optimize these three significant factors for respiratory coal dust removal. Since the experiments are still in progress, the actual experimental data could not be present in this paper. Therefore, a set of hypothetical data was created for data analysis illustration to obtain a regression response for investigating the method to reach the maximum coal dust removal efficiency at the optimum conditions.

Key words: Respiratory coal dust, Box-Wilson experimental design, Surfactant, Catalyzer, Water droplet size

1. Introduction

Previous research has indicated that respiratory coal dust (particle size range $<10 \mu m$) makes up more than 60 percent of total airborne coal dusts [1], which poses a huge threat to miners who work in underground coal mines. Occupational exposure to respiratory coal dust could cause several adverse health consequences including coal workers' pneumoconiosis (CWP), silicosis, tuberculosis, emphysema and chronic renal disease [2]. These diseases have disabled numerous miners since the earliest history of coal mining, and imposed a heavy cost on coal miners' families as well as governments [3].

Water sprays is one of the oldest and most often used methods for coal dust reduction, and it has made significant contributions toward controlling average respiratory dust exposure of underground coal miners from over $6mg/m^3$ in 1969 to below $2mg/m^3$ in recent years [4]. However, using water alone cannot reduce the respiratory coal dust level due to its weaker wettability and stronger hydrophobicity [5] [6]. Therefore, improving the efficiency of water sprays on respiratory coal dust removal is necessary and crucial to coal mines and miners for an improved working environment.

Previous research has shown surfactant is crucial to improve the effectiveness of water spray systems on coal dust suppression. The use of varying amounts of surfactant added to sprayed water is a means to increase the efficiency to dust suppression [7]. Li, Lin [8] proved the wettability of coal dust could be greatly increased by adding surfactant in deionized water. Kilau and Pahlman [3] found using the same surfactant leads to different coal wettability due to varying degrees of natural wettability which can cause adverse

surfactant adsorption and resultant increased hydrophobicity. Glanville and Haley [9] concluded that the coal wettability is correlated over surfactant concentration and surfactant structures by performing the Walker Test and Draves Test. Cui, Baisheng [10] found magnetization surfactant solution has a great prospect in coal dust suppression by testing the surface tension and contact angle after surfactant solution was magnetized.

Some research indicated certain chemical additives such as sodium sulfate as a catalyzer could enhance the effectiveness of surfactant. WU and GU [11] confirmed that the combination of sodium sulfate and surfactant in low concentration could achieve the same effect of single surfactant with high concentration. A synergistic effect appears to take place in combination of nonionic along with anionic surfactant which permits the utilization of each individual surfactant at a certain concentration [12]. However, less experimental research on the impact of catalyzer on enhancing the function of surfactant relating to coal dust suppression has not been done. The application and mechanism of adding catalyzers to surfactant solution is not well established.

When using water spray systems for coal dust control, another primary consideration is the water droplet size. Based on laboratory experiments Pollock and Organiscak [4] put forward that increasing the water spray nozzles fluid pressure generally reduced droplet sizes with concurrent increase in dust capture. Since it is not easy to measure the droplet size, research on the droplet size always related to water spray fluid pressure and water spray velocity. In this study, the research on the water droplet size will be converted to the orifice of spray nozzles.

Most previous studies described the effectiveness of surfactant from measurements of parameters such as contact angle and surface tension. However, Nikitina and Taubman [13] have shown that static surface tension measurements of surfactant solution do not accurately characterize their dust wetting ability. Also, Copeland, Eisele [14] pointed out the effectiveness of dust suppression cannot be reliably predicted from measurements of these parameters. Thus, utilizing a wind tunnel laboratory apparatus can produce more reliable results to investigate coal dust suppression efficiency.

This paper aims at designing a laboratory apparatus with the function of investigating variables related to coal dust removal. The Box-Wilson statistical experimental design method (the centre composite rotatable design) will be used to study the combined effect of three independent factors (surfactant concentration, catalyzer concentration and water droplet size) on the coal dust removal instead of analysing each factor. Since the experiment is still in progress, the experimental data could not be present in this paper. Therefore, a set of hypothetical data will be created to obtain a regression response for investigating the method to reach the maximum coal dust removal efficiency at the optimum conditions.

2. Experiment

2.1 Central composite rotatable design

Experimental design technique is useful for analysis and modelling of problems in which a response of interest is influenced by factors. Full factorial, fractional factorial and central composite rotatable design are commonly used to study the relationship between the response and factors. The full factorial design usually requires multilevel experiments and it needs at least three levels per variable to obtain the coefficients of the quadratic terms in the response function. Thus for three independent variables in this study, the full factorial design requires 27 (3^3) runs plus replication. In addition, the coefficients of the quadratic terms in this model have relatively low precision [15]. Compared with full factorial design, the fractional factorial requires fewer tests while it is efficient when experimenter have already known there was no interaction among the certain factors [16].

In this study, the central composite rotatable design was employed to investigate the effects of major operating variables on coal dust removal rate and to seek an optimum combination of important variables resulting in the maximum coal dust removal. The central composite rotatable design was developed by Box and Wilson and improved by Box and Hunter [15, 17]. It is a response surface methodology that uses fewer tests than the full factorial design and also has desirable properties for fitting polynomial models.

The central composite rotatable design is based on the two-level factorial design with its origin at the centre, and it is axially added a fixed distance (α) from

the centre to provide the quadratic terms. The axial points ensures the variance of the model is constant at all points equidistant from the design centre [17]. Fig. 1 shows the central composite rotatable design and the coordinates for three factors ($k=3$).

The number of experiment runs needed for the central composite rotatable design consists of 2^k factorial points, $2k$ axial points and replicates tests at the centre.

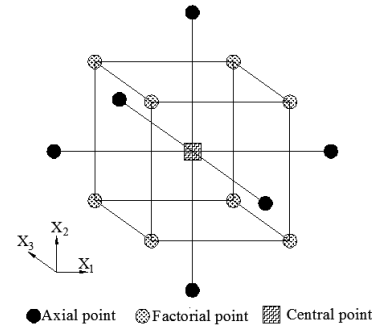


Fig. 1. Schematic diagram of central composite design for factors x_1 , x_2 and x_3

Replication of the central points is significant because it provides better estimates of experimental error and the constant value in polynomial models. Box and Hunter [17] recommend the number of tests at the central is 6 for three factors. Thus for experiments with three factors, applying the central composite rotatable design requires 20 experiment runs in total, including 8 (2^3) factorial points, 6 (2×3) axial points and one centre point with 6 replications.

In the central composite rotatable design, the ranges of values of the factors are coded to ± 1 for the factorial points, $\pm \alpha$ for the axial points and 0 for the central points. The relationship between coded values and actual values of factors is shown in Table 1.

The polynomial model for three factors as shown in Eq. (1):

$$y = b_0 + b_1x_1 + b_2x_2 + b_3x_3 + b_{12}x_1x_2 + b_{13}x_1x_3 + b_{23}x_2x_3 + b_{11}x_1^2 + b_{22}x_2^2 + b_{33}x_3^2 \quad (1)$$

Where y is the predicted response function, b_0 is the constant, b_1 , b_2 and b_3 are the linear coefficients, b_{12} , b_{13} and b_{23} are the cross product coefficients, and b_{11} , b_{22} and b_{33} are the quadratic coefficients.

2.2 Materials

In the experiment, the coal dust samples will be obtained from a coal mine, and will be crushed, screened, sieved through a 400 mesh (coal particles with size less than $38 \mu\text{m}$), divided, and oven dried prior to test. During preparation of coal dust samples, the bulk density, pH value, chemical composition and coal dust particle size distribution will be tested.

Table 1. Relationship between coded values and actual values of factors

Code	Actual value of factor
$-\alpha$	x_{\min}
-1	$\frac{(x_{\max} + x_{\min})}{2} - \frac{(x_{\max} - x_{\min})}{2\alpha}$
0	$\frac{(x_{\max} + x_{\min})}{2}$
+1	$\frac{(x_{\max} + x_{\min})}{2} + \frac{(x_{\max} - x_{\min})}{2\alpha}$
$+\alpha$	x_{\max}

Surfactant is one of the crucial factors affecting the efficiency of coal dust removal, and its concentration is the key to effective water spray control. A great deal of research about the influence of surfactant concentration on dust wettability has been done while the results were not consistent. For example, Li, Lin [8] proved concentration of surfactant was an important factor for dust wettability, and recommended 0.2% concentration of sodium dodecyl sulfonate (SDS) as the best choice for coal dust suppression application based on the laboratory experiment, and Chao, Peng [18] suggested that 0.6% concentration of surfactant of SDS can achieve good wetting performance while Wang, Tien [19] obtained a result that the effect of variation in surfactant concentration was insignificant. Thus, this research will further investigate this matter. In this study, SDS (sodium dodecyl sulfonic salt) is chosen due to its advantages, such as good performance of wetting, little pollution, low cost and easy preparation. Most research considered 0.1% as the minimum for surfactant concentration and the maximum always below 1% [8, 20, 21]. Therefore, the minimum and maximum concentration levels are determined to be 0.1% and 1%, respectively.

Sodium sulfate was chosen as a catalyzer to investigate the effect on coal dust removal as it is commonly used in chemical research. According to the research conducted by WU and GU [11], sodium sulfate effected the surface tension of SDS greatly when the concentration of sodium sulfate was under approximately 15mmol.L^{-1} . Thus, the concentration of sodium sulfate was set to be varied from 0.1mmol.L^{-1} to 15mmol.L^{-1} .

Nozzles used in this study are Type X FLUSH-FIT spray nozzles which can produce a precision uniform full cone spray and generally used in Longwall and Continuous Miner applications. The minimum and maximum orifice of this series nozzles are 0.6mm and 2.4mm , respectively.

2.3 Experimental design

In this research, the respiratory coal dust removal efficiency (y) is the response, and surfactant concentration (x_1), catalyzer concentration (x_2) and water droplet size (x_3) are chosen as three important independent variables. The surfactant concentration (x_1) is varied from 0.1% to 1%, catalyzer concentration (x_2) changes from 0.1mmol.L^{-1} to 15mmol.L^{-1} , and the

orifice of spray nozzles (x_3) is between 0.6mm and 2.4mm . The relationship between actual values and coded values of three factors was shown in Table 2. All these experiments will be conducted in a random order, and the factors, levels, coded values, actual values and response data are as shown in Table 3.

2.4 Experimental apparatus and procedures

All the experiments in this study will be performed in a laboratory apparatus. The apparatus consists of a wind tunnel (measures by $4000\text{mm} \times 500\text{mm} \times 500\text{mm}$), a dust generator, dust monitors, sprayers with various sizes (the spray nozzles chosen

Table 2. Actual values and coded values of three factors

Factors	Coded levels				
	$-\alpha$	-1	0	+1	$+\alpha$
Surfactant concentration (%)	0.1	0.28	0.55	0.82	1
Catalyzer concentration (mmol.L^{-1})	0.1	3.12	7.55	11.98	15
Water droplet size (mm)	0.6	1	1.5	2	2.4

for this research are all common in a fan, a water tank, and a tail dust remover. This laboratory wind tunnel has a function of simulating the process of coal dust suppression. The spraying water with surfactant and catalyzer is pumped from a water tank which is located outside of the wind tunnel. There is a sump designed to be connected to the wind tunnel to collect the used water. The pressure of spraying water can be regulated by a pressure meter. Water spray nozzles can be changed to different sizes to meet the experiment's need. Fig. 2 shows the schematic diagram of the laboratory wind tunnel apparatus. During the experiments, the air velocity of the fan will be set to a certain speed, and the prepared coal dust sample will be put into the dust generator. Water spray nozzles will be turned on before coal dust arrives. The time and water spray pressure for each run are kept the same. Dust monitors will be working over the whole process to record the dust concentration.

3. Data analysis method

3.1 Analysis of variance

Due to the limitation of time, all experiments have not been finished, so actual experimental data could not be represented in this paper. Thus, for the purpose of data analysis illustration, a set of 20 hypothetical experimental data is assumed for coal dust removal efficiency (y_i , $i=1\sim 20$) as shown in the last column of Table 3.

An analysis of variance for the linear, interaction and quadratic effects of variables on the response model were obtained in Table 4, which shows that the P-value of the model is very low which indicates that

the model is significant. The P-values of linear term, square term and interaction term are all less than 0.05, implying these terms are significant. The lack of fit P-value of 0.211 implies that lack of fit is not significant relative to pure error.

The coefficients of the polynomial model (Eq. (1)) and their significance are given in Table 5. It shows that in this study, the main effect of surfactant, Catalyzer, Drop size, Surfactant*Surfactant, Catalyzer*Catalyzer and Surfactant*Catalyzer are significant terms with P-values less than 0.05. Other insignificant terms with P-values that larger than 0.05 should not be in consideration in the polynomial model. The precision of the model can be judged by the determination coefficient R^2 , in this model, the R^2 -value is 97.06%, close to 1, that is to say only 2.94% of the variation cannot be explained by the model. The adjusted R^2 -value is 94.41% very close to the R^2 -value, indicating the model is at a high confidence level.

By applying regression analysis on the hypothetical experimental data, the equation with coded factors was obtained as in Eq. (2).

$$y = 79.55 + 5.10x_1 + 2.3x_2 - 3.75x_3 - 3.7x_1^2 - 3.35x_2^2 + 1.75x_1x_2 \quad (2)$$

3.2 Model adequacy checking

As analysed above, the regression equation was obtained based on the hypothetical experimental data. Model adequacy could be studied by residuals examination. The residuals should be structure-less if the model is adequate, which means residuals should contain no obvious patterns when the model is adequate. The analysis of residuals usually mainly includes check of the normality assumption, independence assumption and non-constant variance by plotting residual plots [22].

Table 3. Experimental conditions according Box-Wilson statistical experimental design

Std order	Run order	Coded levels of factors			Surfactant (%)	Catalyzer (mmol.L ⁻¹)	Water drop size (mm)	Dust removal efficiency (%)*	
		X ₁	X ₂	X ₃	X ₁	X ₂	X ₃	Y (hypothetical data)	
Factorial points	1	4	-1	-1	-1	0.28	3.12	1	y ₁ =68
	2	11	+1	-1	-1	0.82	3.12	1	y ₂ =75
	3	13	-1	+1	-1	0.28	11.98	1	y ₃ =71
	4	16	+1	+1	-1	0.82	11.98	1	y ₄ =85
	5	19	-1	-1	+1	0.28	3.12	2	y ₅ =65
	6	12	+1	-1	+1	0.82	3.12	2	y ₆ =69
	7	9	-1	+1	+1	0.28	11.98	2	y ₇ =64
	8	10	+1	+1	+1	0.82	11.98	2	y ₈ =75
Axial points	9	1	-α	0	0	0.1	7.55	1.5	y ₉ =60
	10	8	+α	0	0	1	7.55	1.5	y ₁₀ =80
	11	6	0	-α	0	0.55	0.1	1.5	y ₁₁ =67
	12	14	0	+α	0	0.55	15	1.5	y ₁₂ =75
	13	18	0	0	-α	0.55	7.55	0.6	y ₁₃ =87
	14	15	0	0	+α	0.55	7.55	2.4	y ₁₄ =72
Centre points	15	3	0	0	0	0.55	7.55	1.5	y ₁₅ =81
	16	20	0	0	0	0.55	7.55	1.5	y ₁₆ =80
	17	7	0	0	0	0.55	7.55	1.5	y ₁₇ =78
	18	17	0	0	0	0.55	7.55	1.5	y ₁₈ =81
	19	5	0	0	0	0.55	7.55	1.5	y ₁₉ =79
	20	2	0	0	0	0.55	7.55	1.5	y ₂₀ =78

*data of dust removal efficiency is hypothetical

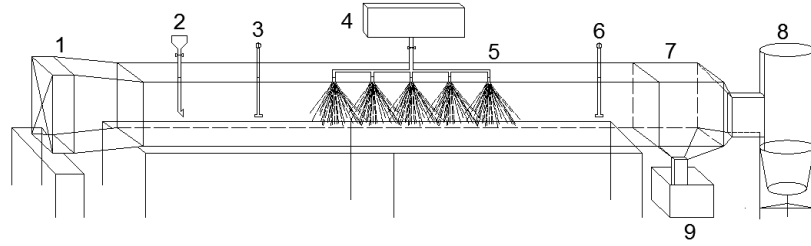


Fig. 2. Schematic diagram of the laboratory wind tunnel apparatus. 1. Axial Fan. 2. Dust Generator. 3. Dust Monitors. 4. Water Tank. 5. Sprayer Nozzles. 6. Dust Monitors. 7. Wind Tunnel. 8. Tail Dust Remover. 9. Sump.

Table 4. ANOVA table for regression

Source	DF	Adj SS	Adj MS	F	P
Model	9	985.12	109.458	36.63	0.000
Linear	3	619.67	206.556	69.13	0.000
Square	3	328.45	109.484	36.64	0.000
Interaction	3	37.00	12.333	4.13	0.038
Residual error	10	29.88	2.988	-	-
Lack-of-fit	5	20.38	4.076	2.15	0.211
Pure error	5	9.50	1.900	-	-
Total	19	1015.0	-	-	-

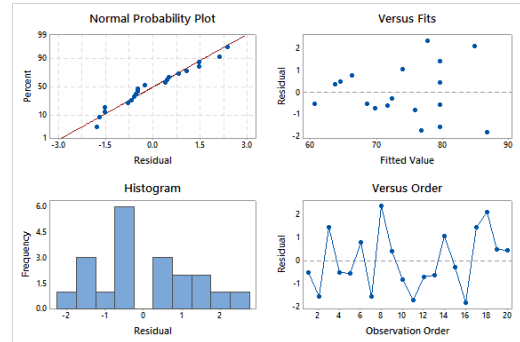


Fig. 3. Residual plots for coal dust removal efficiency

Thus, these residual plots for the response in this study were shown in Fig. 3. The plot of normal probability was utilized to check the normality assumption of the model, and this plot resembles an approximate line which indicates that the error distribution is relatively normal. The histogram of residuals was also applied to verify the normality assumption of the model. This plot should be like a sample from a normal distribution centred at zero when the $(0, \sigma^2)$ assumption on the error is normal. Due to the small sample, this plot of the histogram in this study showed fluctuation in the shape of the histogram, while it does not imply the normality assumption is abnormal. For checking the independence assumption, the plot of residuals in observation order was displayed in Fig. 3, and it does not show a tendency with runs of positive and negative residuals in a positive correlation which means the independence assumption is normal. In order to verify the non-constant variance, a plot of residuals versus fitted values was given in Fig. 3 with any obvious pattern, indicating the assumption is normal.

In terms of the results of residuals analysis, it could be concluded that the regression model obtained was normal.

3.3 Effects of variables on coal dust removal

Table 5. Regression coefficients and their significance

Term	Coef	SE Coef	T	P
Constant	79.553	0.705	112.84	0.000
Surfactant	5.099	0.468	10.90	0.000
Catalyzer	2.303	0.468	4.92	0.001
Drop size	-3.751	0.468	-8.02	0.000
Surfactant * Surfactant	-3.704	0.455	-8.13	0.000
Catalyzer * Catalyzer	-3.350	0.455	-7.36	0.000
Drop size* Drop size	-0.345	0.455	-0.76	0.466
Surfactant * Catalyzer	1.750	0.611	2.86	0.017
Surfactant * Drop size	-1.750	0.611	-1.23	0.248
Catalyzer * Drop size	-1.000	0.611	-1.64	0.133

$$S=1.72858, R^2=97.06\%, R^2(\text{adj})=94.41\%$$

In order to get a better understanding of the results based on the hypothetical experimental data, response surface methodology was employed to investigate the interactive effects of two factors on the response values, three-dimensional surface and contour plots were presented to study two variables at a time when another one kept at its central level.

Fig. 4 illustrates the combined effect of surfactant concentration and catalyzer concentration by keeping the water drop size at its centre level (1.5mm). As can be seen, the coal dust removal increases when the surfactant concentration and catalyzer concentration went up from 0.1% to about 0.7% and 0.1 mmol.L⁻¹ to approximately 8.5 mmol.L⁻¹ respectively, and the response value kept the same with further increase of surfactant concentration and catalyzer concentration, and then showed a slight decrease when both of surfactant concentration and catalyzer concentration reached the maximum. It could be concluded that surfactant concentration and catalyzer concentration had a great impact on the coal dust removal.

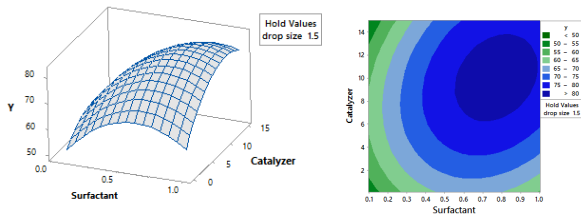


Fig. 4. Surface plot and contour plot of coal dust removal vs surfactant, catalyser

Fig. 5 indicates the relationship between coal dust removal and surfactant concentration and drop size when catalyzer concentration was at its centre level (7.55mmol.L⁻¹). It can be seen that the coal dust removal increased with the increase of surfactant concentration and drop size from 0.1% to around 0.6 % and 0.6mm to approximately 1.0mm respectively, and it showed a downward trend with the further increase of these two variables.

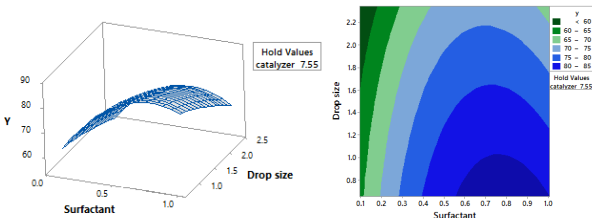


Fig. 5. Surface plot and contour plot of coal dust removal vs surfactant, drop size

Fig. 6 shows the effect on coal dust removal with the surfactant concentration keeping at its centre level (0.55%). When catalyzer concentration went up from 0.1mmol.L⁻¹ to about 8mmol.L⁻¹ and drop size increased from 0.6mm to around 0.8mm, the coal dust removal represented an upward trend; after that, it decreased when the catalyzer concentration and drop size kept increasing.

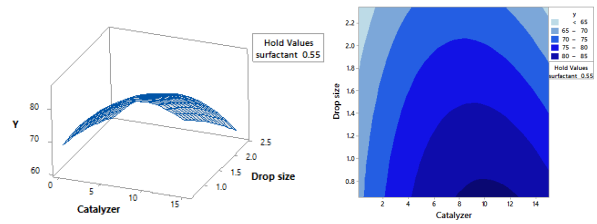


Fig. 6. Surface plot and contour plot of coal dust removal vs catalyzer, drop size

According to the Fig.4-6, the maximum value of response on any two variables could be found. Thus, the maximum coal dust removal could be obtained based on the regression model. According to the following Eq. (3) & (4) & (5) it is possible to obtain the optimization of y .

$$\frac{\partial y}{\partial x_1} = 0 \quad (3)$$

$$\frac{\partial y}{\partial x_2} = 0 \quad (4)$$

$$\frac{\partial y}{\partial x_3} = 0 \quad (5)$$

The response optimization results could be obtained as shown in Table 6.

Table 6. Factors' coded values and uncoded values in response optimization

Factors	Coded unit	Uncoded unit
Surfactant concentration x_1	0.82	0.77
Catalyzer concentration x_2	0.56	10
Water drop size x_3	-1.62	0.6

In terms of the regression equation of the model in this study, the maximum coal dust removal of 88.36% could be obtained with the condition of surfactant concentration 0.77%, catalyzer concentration 10mmol.L⁻¹ and a nozzle orifice of 0.6mm.

4. Conclusions

A set of experimental apparatus composed of a wind tunnel, dust generator, water spray system, dust monitors, and tail dust remover was designed to test the experimental variables related to coal dust control. One of the Box-Wilson experimental design methods, the central composite rotatable design was used to investigate the effect of surfactant concentration, catalyzer concentration and water drop size on coal dust removal. A regression equation of coal dust removal was derived by utilizing a set of hypothetical experimental data with statistical analyses, and it was fitted using the significant variable terms at greater than 95% confidence

level by variance analysis. Model adequacy was checked by residuals analysis, and it showed the model obtained in this study was approximately normal. Three-dimensional surface and contour plots were presented to better illustrate the combined effect of any two variables of coal dust removal. According to the method of analysing data, the maximum coal dust removal can be obtained based on the regression response.

5. Further work

Future work will aim at (1) the experiments will be conducted with laboratory experimental apparatuses according to the parameters shown in Table 3 (2) A new regression equation based on actual experimental data will be derived with statistical analyses and a further analysis on the model validation will be studied. In addition, comparison between the observed values and the predicted values will be made. (3) A detailed Analysis on the effect of three factors (surfactant concentration, catalyzer concentration and water drop size) on the response (coal dust removal rate) will be undertaken respectively. (4) The optimum value of each factor and maximum coal dust removal rate will be calculated by the regression equation based on experimental results.

References

- [1] Qin J, Ramani R, McPherson M. Generation and entrainment of coal dust in underground mines. Proceedings of the Fourth US Mine Ventilation Symposium, Berkeley, CA1989. p. 454-62.
- [2] Schulte PA RF, Key-Schwartz RJ, Bartley DL, Baron P, Schlecht PC, Gressel M, Echt AS. NOISH hazard review :health effects of occupational exposure to respirable crystalline silica. 2002.
- [3] Kilau HW, Pahlman JE. Coal wetting ability of surfactant solutions and the effect of multivalent anion additions. Colloids and surfaces. 1987;26:217-42.
- [4] Pollock D, Organiscak J. Airborne Dust Capture and Induced Airflow of Various Spray Nozzle Designs. Aerosol Science and Technology. 2007;41(7):711-20.
- [5] Organiscak JA, Page SJ, Jankowski RA. Sources and characteristics of quartz dust in coal mines: US Dept. of the Interior, Bureau of Mines; 1990.
- [6] Yang J, Wu X, Gao J, Li G. Surface characteristics and wetting mechanism of respirable coal dust. Mining Science and Technology (China). 2010;20(3):365-71.
- [7] Kim J, Tien JC. The effect of added base on coal wetting ability of nonionic surfactant solutions used for dust control. 1994.
- [8] Li Q, Lin B, Zhao S, Dai H. Surface physical properties and its effects on the wetting behaviors of respirable coal mine dust. Powder Technology. 2013;233:137-45.
- [9] Glanville JO, Haley LH. Studies of coal dust wetting by surfactant solutions. Colloids and Surfaces. 1982;4(3):209-12.
- [10] Cui D, Baisheng N, Hua Y, Linchao D, Caihong Z, Fei Z, et al. Experimental research on optimization and coal dust suppression performance of magnetized surfactant solution. Procedia Engineering. 2011;26:1314-21.
- [11] WU C, GU D-s. The improvement of addition of sodium sulfate on wettability of coal dust by anionic surfactant [J]. Journal of Safety and Environment. 2001;2:9.
- [12] Feldstein N. Surface Chemical Technology for Improved Wetting of Coal Dust: Bureau of Mines, US Department of the Interior, Minerals Health and Safety Technology; 1981.
- [13] Nikitina S, Taubman A. the role of adsorption kinetics in the effects of wetting dust particles by drops of solutions of surface active substances. Doklady akademii nauk sssr. 1957;116(1):113-6.
- [14] Copeland C, Eisele T, Kawatra S. Suppression of airborne particulates in iron ore processing facilities. International Journal of Mineral Processing. 2009;93(3):232-8.
- [15] Box GE, Wilson K. On the experimental attainment of optimum conditions. Journal of the Royal Statistical Society Series B (Methodological). 1951;13(1):1-45.
- [16] Box GE, Hunter JS. The 2 k-p Fractional Factorial Designs. Technometrics. 1961;3(3):311-51.
- [17] Box GE, Hunter JS. Multi-factor experimental designs for exploring response surfaces. The Annals of Mathematical Statistics. 1957:195-241.
- [18] Chao W, Peng X-l, Wu G-M. Wetting agent investigation for controlling dust of lead-zinc ores. Transactions of Nonferrous Metals Society of China. 2007;17(1):159-67.
- [19] Wang Y, Tien JC, Wilson JW, Erten M. Use of surfactants for dust control in mines. A laboratory study. 1991.
- [20] Tien JC, Kim J. Respirable coal dust control using surfactants. Applied occupational and environmental hygiene. 1997;12(12):957-63.
- [21] Wang K, Jiang S, Wu Z, Shao H, Pei X. Experimental study on complex wetting agent enhancing the dusting effect and its application.
- [22] Montgomery DC. Design and analysis of experiments: John Wiley & Sons; 2008.

Preliminary Laboratory Experiments Design for the Study of Bauxite Residue Dust Control

Xuhan Ding^a, Guang Xu^a, Mahinda Kuruppu^a, Boris Albijanic^a

^a*Western Australia School of Mines, Curtin University, Kalgoorlie, WA, Australia*

Bauxite residue sand is a by-product of aluminium processing. It is usually stored in a large-scale residue drying area (RDA). The bauxite residue is highly alkaline and contains a large percentage of metal oxides which are hazardous to the environment and human health. Therefore, fugitive dust generated from these RDAs is a major environmental concern that needs to be addressed and efficiently managed. The aim of this paper is to investigate the factors that influence the effectiveness of bauxite residue (red sand) dust control. As the first stage of the project, the major focus is laboratory experiments based on scientific experimental design which will be conducted using a wind tunnel. Factors such as wind speed, sand particulate size distribution, and the effectiveness of different chemical stabilizers will be studied, and these factors will be correlated to different dust control strategies. Photogrammetry technique will be used to monitor and identify dust generation areas, and calculate volume loss.

Key words: Bauxite Residue, Red Sand, Chemical Stabilizer, Wind Tunnel Test, Box-Behnken Design, 3D Model Reconstruction

1 Introduction

Modern production of aluminium is mainly extracted from bauxite ore through the Bayer process, with a product to by-product (bauxite residue) ratio of 0.7 to 2.5 [1]. Due to the huge aluminium commercial production, drastic bauxite residue is generated. As it is highly alkaline and contains large percentage of metal oxides which are hazardous to the environment and human health, fugitive dust generated from bauxite residue is becoming a major concern. In 2007, the global inventory of bauxite had reached 2.6 billion tonnes and it is predicated to be 4 billion tonnes by the end of 2015 [2]. As a result, bauxite residue dust control is now recognised to be an important issue in the bauxite mining industry.

Bauxite residue mainly consists of the insoluble fractions of bauxite that remains after aluminium-contained components were extracted, such as iron oxides, titanium dioxides, and some undissolved alumina. After the Bayer and refinery process, bauxite residue is separated into about 60% coarse sand fraction named red sand ($>150\mu\text{m}$) and 40% fine silt fraction named red mud ($<150\mu\text{m}$)[3]. However, due to ubiquitous incomplete separation, 10~15% red mud fraction remains in the sand and vice versa [4]. Because of the existence of alkaline sodium components after the Bayer process to extract alumina, and the washing process to extract caustic soda and dissolved alumina, the pH value of bauxite residue can range from 10~13, which indicate high alkalinity [1].

Dust can be generated from red sand fraction and red mud surface after dried. Due to its high pH value, strong alkalinity, amount of fine toxic heavy metal particles existing, and increased content of radioactive substance, inhalation of residue dust can irritate the human nose and throat. Even worse, if residue dust reaches to the lungs,

shortness of breath and chest tightness will take place [5]. Residue dust can also contaminate soil. Direct and long term contact between residue dust and soil will result in serious alkalization, which is addressed as an important environmental issue. One technique used for bauxite residue storage is "dry stacking", which uses much of the red sand fraction to construct the dyke walls for the red mud impoundments where the red mud is deposited and dried. This area is called the Residue Drying Area (RDA). In these practise, moisture loss of dyke walls after long-term exposure will induce unresisting to wind erosion. The threshold friction velocity (TFV) of dust emission in RDAs is generally 6.5m/s, while observed maximum natural wind velocity is up to 20m/s. As a result, if untreated, the amount of dust generated from red sand will migrate and contaminate the mine-site and the surrounding region on account of high alkalinity and large quantities.

While the physical and chemical properties for the red sand and red mud are different, this research only focuses on the dust issues related to the red sand. The study of red sand dust control has been highly concerned for several decades. One effective dust control method is the application of chemical stabilizers, which is the focus of this study. Via spread on red sand surface, stabilizer will enhance the cohesion between sand particles by constructing binding surface crust with certain hardness and strength, so as to conserve moisture and provide relative longer dust control [6]. The application of this method to other type of sand-like material is common, and the related studies can be found in the literature and relate to this study. Good performances were achieved when applying Dow Chemical M-167 Latex Binder and polyaspartic acid to enhance the anti-wind erosion ability and surface strength of coal particles and sand [7, 8]. Large scale applications of a variety of chemical

stabilizers on desert dust control also proved their high reliability and effectiveness [9]. These studies proved that applying chemical stabilizers on red sand will be an to be addressed. A large number of studies based on wind tunnel tests and computational fluid dynamics simulation (CFD) showed that natural factors such as wind speed, and inclination of sand surface also play significant roles in dust control [10-12]. The alteration of the value of each factor simultaneously or respectively can also result in different dust generation rate [12-15].

However, there are limited publications available in the literature which systematically study red sand dust control. The relationship between mechanical properties of crust generated by chemical stabilizers and red sand dust reduction rate is also rarely analysed. Effective dust control strategy by applying chemical stabilizers needs to be based on comprehensive analysis of interactions between each natural factor and crust mechanical properties, and systematic and completely randomized experimental design.

The aim of this research is to determine the most efficient and economical red sand dust control method using chemical stabilizers. To achieve this objective, the interactions between mechanical properties of chemical stabilizers and natural factors will be investigated, as well as their contributions to dust weight loss. The approaches used for the study are presented in the flowchart shown in

appropriate solution. However, in order to determine the most economical chemical stabilizer with the highest efficiency, the effect brought by natural factors also need Fig 1. Firstly, the physical properties of initial red sand samples, such as particle size distribution, moisture content and direct shear strength, will be analysed. Secondly, mechanical properties test will be conducted to measure the changes of mechanical properties of sand samples after applying chemical stabilizers. In this stage, the unconfined compressive strength and direct shear strength of sand will be tested by mixing sand sample with chemical stabilizers. Penetration resistance test and crust thickness measurement will be conducted by spraying chemical stabilizers on the red sand surface. Randomized block design is applied in this stage to eliminate the effect of different red sand sources. In the third stage, wind tunnel experiments will be conducted to measure dust weight loss and volume change under different chemical stabilizers treatments. Factorial design will be employed to determine the significance of each factor and their interactions and eliminate those factors with limited effect. After that, Box-Behnken Design is used to generate response surfaces for the optimal combination of each factor. Finally, whether optimum dust control performance can be correlated to mechanical properties can be found out. As the experiments are not finished yet, this paper will only present the framework of the experiments and research without experimental results.

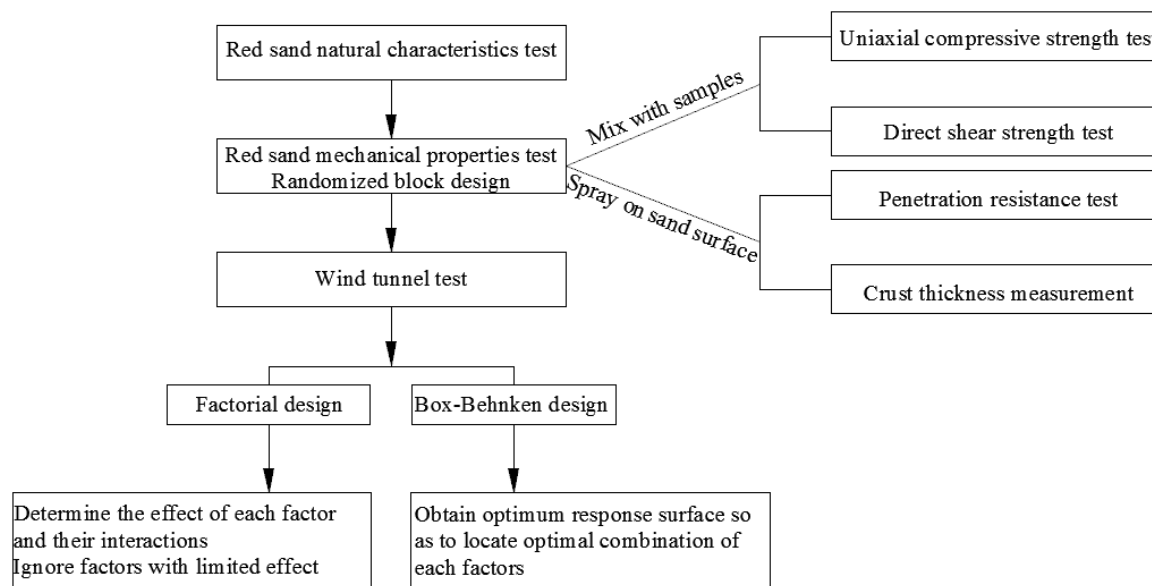


Fig 1. Flowchart of experiments

2 Red Sand Characteristics

2.1 Moisture Content

Moisture content tests are conducted using bauxite residue red sand obtained from one bauxite mine, denoted by M1. Six samples were separated by electronic divider and placed in an oven at 105°C for 24 hours to ensure entire drying. The weight of these samples before and after drying were measured in random order and recorded in

Table 1. The average moisture content of this sand is 10.73%.

Sample No.	1	2	3	4	5	6
Std.	3	1	4	6	5	2
Weight before drying m_1 (g)	276	323	340	299	271	325
Std.	5	2	1	6	3	4
Weight after drying m_2 (g)	250	292	306	270	245	293
Weight loss (g)	26	31	34	29	26	32
Moisture content (%)	10.4	10.6	11.1	10.7	10.6	10.9

2.2 Particle Size Distribution

After the moisture content test, particle size distribution tests are done by using these 6 dried samples. The order of tests is randomized and the size distribution curves are similar among samples. The result of particle size distribution analysis of this sand is shown in Fig 2. The P(80), which indicate the screen size for 80% particles to pass, is 0.425mm.

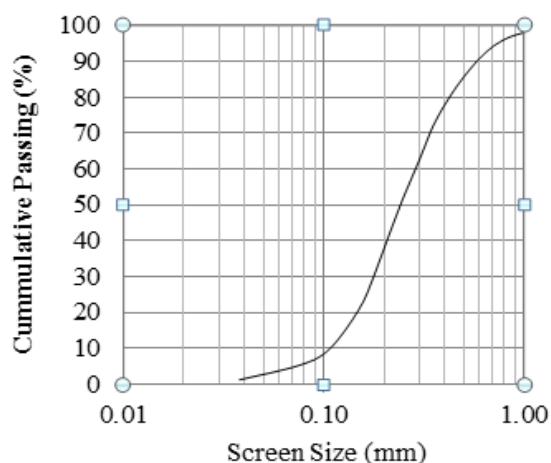


Fig 2. Particle Size Distribution of Red Sample

2.3 Shear Strength

Shear strength test are conducted using original red sand samples stored in sealed buckets. Hydraulic shear

stress setup is employed in this test where sand sample is filled in a cubic metal box with a dimension of 0.15m (L) \times 0.15m (W) \times 0.15m (H). The surface of sand sample is kept flat to ensure uniform normal load applies. Normal loads of 20KPa, 40KPa and 60KPa were applied in a random order, and the corresponding maximum shear stress values, which are the shear strengths were recorded. After each run, sand sample will be taken out and well mix with the rest of sand samples to eliminate the error brought by continually applied normal load. Shear strength is related to normal load σ on the failure plane by the equation 1, where φ is the friction angle and c is the cohesion.

$$\tau = \sigma \tan \varphi + c \quad (\text{Equation 1})$$

Table 2 provides shear strength data correspond to normal load. The friction angle of red sand is 38.27° and cohesion is 0.26 KPa.

Run Number	Random Order	Normal Load (KPa)	Shear Strength (KPa)
1	2	20	18.80
2	1	40	26.30
3	3	60	50.36
Friction Angle	38.27°	Cohesion	0.26

3 Mechanical Property Test

The mechanical characteristics of sand after chemical stabilizers are added will be analysed at the first stage to find out the relationship between each factor and mechanical properties. The variables of this test is the types of stabilizes and the solutions concentrations. Four types of chemical stabilizers, denoted as S1, S2, S3 and S4 will be tested to evaluate their mechanical properties. The upper and lower limits of solution concentration are 1% and 3%, which is recommended by the manufacture. Sources of red sand are blocked in a complete random design to eliminate its effect. Unconfined compressive strength, direct shear strength, penetration resistance and formed crust thickness are selected as main responses.

3.1 Unconfined Compressive Strength

For unconfined compressive strength test, specimens will be mixed with certain stabilizer solution (1/10 of specimen weight), and then prepared in cylindrical moulds with 5cm (diameter) \times 10cm (length) dimension by a load of 10N falling for 15 times [16]. After that, specimen will be taken out from mould left in ambient temperature for 24 hours and in the oven for another 24 hours under 70 °C, to achieve completed consolidation [16]. The vertical loading is strain-controlled at a strain rate of 0.5% to 2%, until the load start to decrease or 15% strain is reached.

Table 3 shows the entire inventory includes 4 types of stabilizers and 3 solution concentrations (e.g. 1%, 2%,

3%). For each combination of factor A and B, both of the two sources of sand will be tested to analysis the effect of each factor to UCS.

3.2 Direct Shear Strength

Cylindrical specimens used for direct shear strength test is 60mm in width and 20mm in thickness. The same procedures used in the UCS tests will be used for the preparation of the sand specimens in this test. Horizontal shear displacement is fixed as 0.2mm per minute until the stress reading start to decrease. This reading will be recorded as shear strength of specimen. Similarly, the arrangement of direct shear strength test is presented in Table 3.

3.3 Penetration Resistance - Crust Thickness

The unconfined compressive strength and direct shear strength of specimen introduced above are aimed at structure strength analysis after mix the sand sample with chemical stabilizers. However, in order to reflect the crust hardness and bonding strength between sand particles, penetration resistance and crust thickness will be measured. A plastic pipe with 70mm (internal diameter) ×35mm (depth) size is selected as specimen mould. Solutions with fixed volume will be sprayed uniformly on sand surface. Each specimen is laid up for 3 days for entire crust formation. The arrangement of this test is presented in Table 3. Resistance vs penetrating depth and crust thickness data will be measured by a penetrometer and a vernier caliper.

Table 3. Inventory of each combination of factors

Source No.	Factor A: Stabilizer	Factor B: Concentration (%)	Block 1: Sources of Sand	Order	Response 1 UCS (Pa)	Order	Response 2 Shear Strength (Pa)	Order	Response 3 Penetration Resistance
1	S1	1	K	20		10		13	
2	S1	1	P	10		8		19	
3	S2	1	K	2		9		15	
4	S2	1	P	21		5		12	
5	S3	1	K	24		15		4	
6	S3	1	P	17		1		2	
7	S4	1	K	6		19		20	
8	S4	1	P	1		12		16	
9	S1	2	K	9		6		22	
10	S1	2	P	23		11		9	
11	S2	2	K	12		14		23	
12	S2	2	P	15		24		18	
13	S3	2	K	5		22		5	
14	S3	2	P	4		4		8	
15	S4	2	K	19		16		21	
16	S4	2	P	13		21		3	
17	S1	3	K	3		23		1	
18	S1	3	P	22		13		11	
19	S2	3	K	8		18		7	
20	S2	3	P	18		3		10	
21	S3	3	K	16		17		24	
22	S3	3	P	14		2		6	
23	S4	3	K	11		20		17	
24	S4	3	P	7		7		14	

Note: As this is a preliminary study, the entire tests are not finished, so the response values are left empty.

4 Wind Tunnel Experiments

As natural occurrence of dust erosion under wind flow can hardly been evaluated [17, 18], a wind tunnel test is employed in this study. It refers to an aerodynamic experiment approach in accordance with the principal of the relativity of motion. By fixing samples in artificial environment with specified airflow, required data can be

achieved by simulating different operating scenarios. Wind tunnel test can provide more accurate control of experimental conditions than in-situ experiments, which improves test efficiency and accuracy.

4.1 Experimental Apparatus

The laboratory experiments use a wind tunnel with a dimension of 2.7m (L) × 0.24m (W) and 0.33m (H). A schematic diagram of this wind tunnel and the airflow velocity measurement system is shown in Fig 3. Head A is connected with 5.5KW, maximum 1460r/min ventilation

fan. Pitot tube connected to a calibrated manometer is used to measure airflow velocity. The regulation of airflow velocity is achieved by using a variable speed drive. Head B is connected to a cyclone dust collector to reduce the tail dust emission. The cross section area of segment 2 is reduced to 0.22m×0.225m to achieve higher wind velocity.

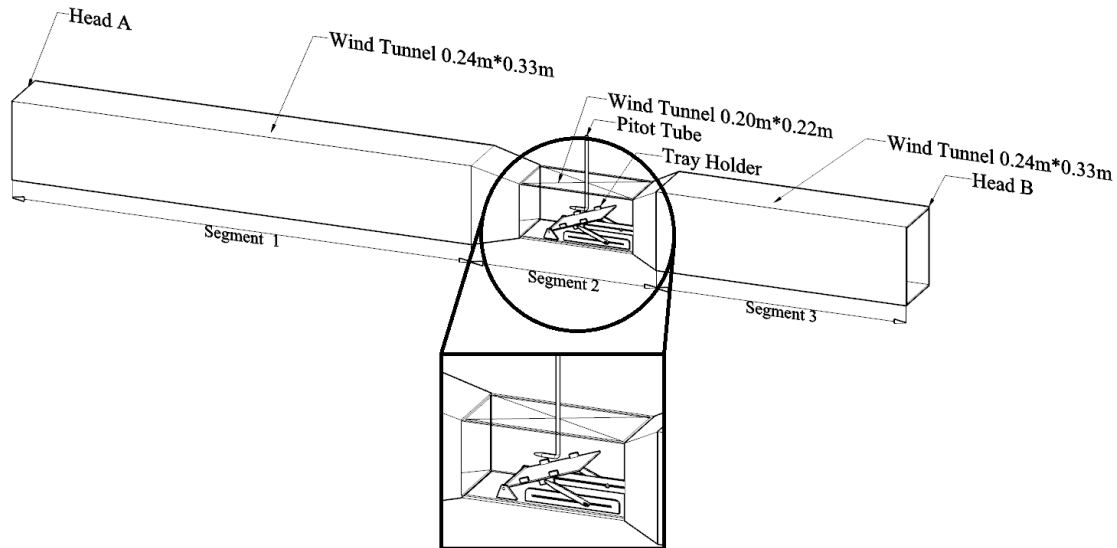


Fig 3. Schematic diagram of wind tunnel and airflow velocity measurement

Fig 4 shows the schematic diagram of the sand sample tray, which is made of steel material. The inner dimension is 0.150m (W) × 0.225m (L) × 0.028m (H). Two 0.012m×0.012m square aluminium bars having the length equal to the inner width of the tray were placed at the top edge of the tray to add weight and reduce the gap

generated on the top edge during the test. 4 pieces of metal having the width equal to the depth of the tray was placed against the tray's inner wall. General glue will be applied on the free face of metals to improve the adhesion with sand and prevent from generating gaps, so that reduce the impact of surround gaps.

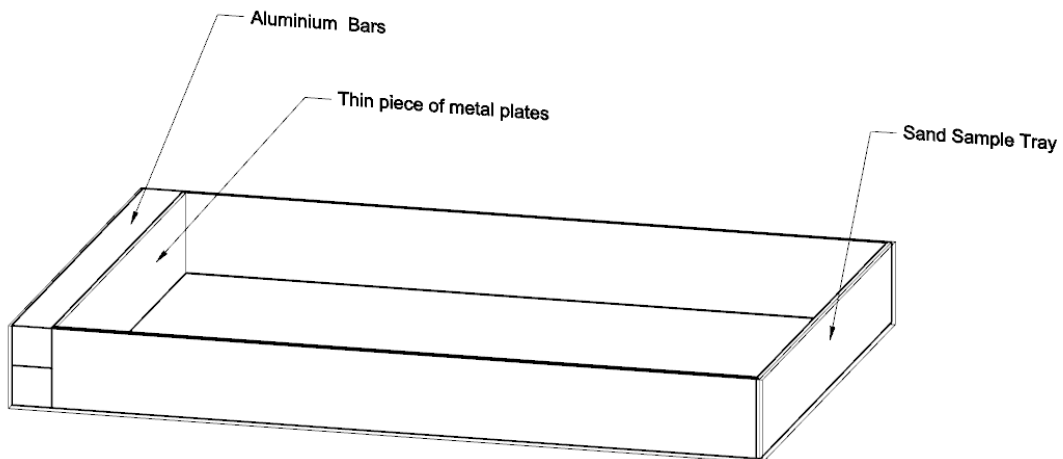


Fig 4. Schematic diagram of sand sample tray

4.2 Variables and Responses

Variables involved in this research are airflow velocity, sand surface inclination, types of chemical stabilizers and different concentrations of solutions. Ambient temperature and indoor humidity are setup as covariates and are

monitored as well in the experiments. The response is dust control efficiency after applying different chemical stabilizers. It can be quantified by monitoring sample weight loss and volume change. The lower of these two values, the higher dust control efficiency it indicates.

Another response, which is difficult to quantify, is dust generation area. This will be also monitored and analysed qualitatively.

Varying airflow velocity will be applied to provide different imposed force on sample surface to offer varying migration tendency. According to Sinclair Knight Merz (SKM) [19], dust emission from the waste dump will initiate at wind speed of approximately 6.5m/s. The observed maximum natural wind speed within residue drying area is 20m/s. Thus, this two are selected as the lower and upper limit of airflow velocity files. According to Stunder and Arya [11], another factor was pointed out which is the inclination of sand surface, and this was also agreed by Faria, Ferreira [12]. In order to evaluate the dust emission rate under varying angles between airflow and sand surface, different sample tray inclinations are applied. 15 and 45 degrees are used as the lower and upper limit of tray inclination values. 15 degrees is the minimum RDA slope inclination commonly used, while 45 degrees is the maximum angle that guarantees the slope stability [20]. Moreover, different types of chemical stabilizers and concentrations of solutions will influence the dust control capacity [21]. Therefore, these four variables together with different residue sample provided by M1 and M2 bauxite mine will be analysed, and related to the effectiveness of dust control.

4.3 Experimental Design

This research applies half fractional factorial design and Box-Behnken Design. Half fractional factorial design is used to determine the effect of each factor and their interactions, while Box-Behnken Design is to locate the

optimum combination of each factor with the highest dust control efficiency. As a preliminary study, only one randomly selected stabilizer will be tested in this section.

4.3.1 Half Fractional Factorial Design

There are four factors as described before. They are wind speed, sand surface inclination, solution concentrations and sources of sand samples. Thus, for a complete two-level factorial design, 2^4 runs are needed. However, because this is a preliminary study, two-level half fractional factorial design is used to reduce the number of runs. In general, a 2^{k-p} design is a $(1/2)^p$ fraction of a 2^k design using 2^{k-p} runs [22]. For the two-level half fractional factorial design, $p=1$, therefore 2^{4-1} fractional factorial design is formed. As illustrated in Table 4, the upper and lower limit of each factor are coded as “-1” and “+1”, respectively. Eight-run design is constructed beginning with a standard table of signs for a 2^3 design in the dummy factors a, b and c. The column of signs associated with the “abc” interaction is used to accommodate factor D. Thus, the main effect of factor D cannot be distinguished from the ABC interaction, which means the effects of D and ABC are confounded. The estimate of D can be written as $I_D \rightarrow D + ABC$. For the same reason, A, B, C is confounded with BCD, ACD, ABD, respectively.

The runs are made in random order to minimize the errors caused by unmeasured and uncontrolled disturbances and to ensure high accuracy. As the third and higher order interactions are small enough to be safely ignored, I_A , I_B , I_C and I_D can provide sufficient accuracy on the estimations of the four factors A, B, C, D.

Table 4. Arrangement of experiment processing

Run Number	a A	b B	c C	abc D	Random Order	Variable	-1	+1
1	-1	-1	-1	-1	3	A:Wind speed	6.5	20
2	+1	-1	-1	+1	6	B:Tray inclination	15	45
3	-1	+1	-1	+1	1	C:Concentration	1%	3%
4	+1	+1	-1	-1	5	D:Sand sample	K mine	P mine
5	-1	-1	+1	+1	2			
6	+1	-1	+1	-1	7			
7	-1	+1	+1	-1	8			
8	+1	+1	+1	+1	4			

4.3.2 Box-Behnken Design

There are two benefits of applying the Box-Behnken Design (BBD) to obtain the optimum combination of each factor.

1. Compared to other response surface methods, the lowest number of runs is required for BBD when there are 3 factors.
2. Levels of each factor selected in BBD are the same with standard mechanics experiments

discussed in section 3. Therefore, it is easy to correlate the conclusion of wind tunnel experiments with the findings of mechanicals property experiments with no additional test.

Box-Behnken Design, which belongs to a modern response surface method, is a compound rotatable or almost rotatable spherical design. The distance from each point within the experimental area to the central point of design is equivalent. In Box-Behnken Design, all tested points are located at the surface of a sphere with radius

equal to $\sqrt{2}$. Any point located at the apex of the cube created by the lower and upper limit of variables is not involved.

As the type of chemical stabilizers is categorical factor that cannot be simply coded, Box-Behnken Design will be applied to each chemical stabilizer separately. Thus, the types of chemical stabilizers are not treated as a factor in the following experiments. This means only three factors are setup in each Box-Behnken Design. The number of runs required for Box-Behnken Design is $N = k^2 + k + N_c$, where k is the number of factors and N_c is the replicate number of runs on the central point. As shown in Fig. 5, there are 12 surface points involved in three-factor Box-Behnken Design, while the number of centre points is recommended to be 5. Each point, which means one combination of each factor, request one test. Therefore, totally 17 tests should be conducted randomized to finalize the analysis of each type of chemical stabilizers.

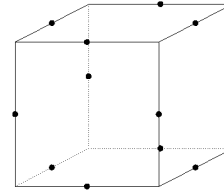


Fig 5. Surface testing point of three 3-level BBD

For the three-level three-factor Box-Behnken Design, a total of 17 randomized experimental runs, shown in Table 5, are needed. The mathematical relationship between responses and factors 1, 2, 3 defines a nonlinear second order polynomial involving 1 intercept, 3 squared terms, 3 first order terms and 3 second order interactions as shown below. Higher order interactions are eliminated due to their minor effects.

$$\text{Weight loss} = k_0 + k_a A + k_b B + k_c C + k_{aa} A^2 + k_{bb} B^2 + k_{cc} C^2 + k_{ab} AB + k_{ac} AC + k_{bc} BC$$

$$\text{Volume loss} = t_0 + t_a A + t_b B + t_c C + t_{aa} A^2 + t_{bb} B^2 + t_{cc} C^2 + t_{ab} AB + t_{ac} AC + t_{bc} BC$$

Table 5. Arrangement of Box-Behnken Design

Std.	Run	Factor 1 A : wind velocity (m/s)	Factor 2 B: tray inclination (°)	Factor 3 C: chemical concentration (%)	Response 1 Weight loss (g)	Response 2 Volume loss (cm ³)
6	1	20.00	30.00	1.00		
5	2	6.50	30.00	1.00		
10	3	13.25	45.00	1.00		
2	4	20.00	15.00	2.00		
9	5	13.25	15.00	1.00		
16	6	13.25	30.00	2.00		
3	7	6.50	45.00	2.00		
17	8	13.25	30.00	2.00		
15	9	13.25	30.00	2.00		
13	10	13.25	30.00	2.00		
7	11	6.50	30.00	3.00		
1	12	6.50	15.00	2.00		
4	13	20.00	45.00	2.00		
14	14	13.25	30.00	2.00		
11	15	13.25	15.00	3.00		
12	16	13.25	45.00	3.00		
8	17	20.00	30.00	3.00		

Note: As this is a preliminary study, the entire tests are not finished, so the response values are left empty.

Weight and volume data can be recorded via data acquiring procedures in the next section 4.4. Three replicates are recommended for each factor combination to obtain a mean value, and then fit into response 1 and response 2. Regression equations and response surfaces will be calculated by using Design-Expert software. These equations will be used to predicate and optimize the

values of each factor, and achieve the minimum dust weight loss and volume change. Ultimately, the best dust control strategy can be determined.

After the entire tests are finalised, ANOVA analysis will be conducted to evaluate achieved data and regression equations. Sum of squares (SS), degree of freedom (df),

mean square (MS), F value and lack of fit P value will be later calculated and analysed. Any variable with p(f) larger than 0.05 will be rejected. R-squared value will indicate the extent of the model fit data. Adjusted R-squared will determine how well the model fits data when the terms in the model need to be adjusted. Predicted R-squared will be calculated to evaluate how well the model can predict responses for new treatments. Adequate precision value measures the signal to noise ratio, which will assess whether the model can be used to navigate the design space.

4.4 Data Acquiring Procedures

In order to quantify dust loss and demonstrate dust generation area, an analytical scale and the 3D model reconstruction technique are used. One thing should be mentioned is the data and images introduced in the following procedures are from a trial test instead of the actual experiment. All their functions are to help demonstrate data acquiring procedures more visually. These procedures will be followed in the actual experiment.

Weight loss can be calculated through the subtraction of weight before and after wind tunnel test. After that, 3D model reconstruction technique will be used to measure volume change and demonstrate dust generation area.

Customized camera and Autodesk 123D catch software are applied to before and after wind tunnel test. 20~30 photos are taken to construct 3D models using the 123D catch software, as shown in Fig 6. This sample is placed on a flat matte board. Four cross marks are drawn at each corner for image processing calibration. Three reference points are marked at the centre of each cross marks to help rebuild the reference coordinate systems. The distance between each reference point is defined as 30cm, and this value will fit models into actual scale. These models will be exported to Mesh Mixer software afterwards for further processing. As displayed in Fig 7, the scope of bottom surface is cut using the reference points for comparison purpose. The clipped models will then be exported to Cloud Compare software for aligning and calibration. Sample (a) is setup as reference. The Z coordinate values from sample (b) subtract that from sample (a) will produce the contour diagram as shown in Fig 8. This can visually demonstrate dust erosion area.

Due to the non-uniformity of density distribution, volume change cannot be obtained directly through investigating weight loss. Therefore, Meshlab software will help to calculate sample volume change by computing geometric measurement of the 3D models generated from Mesh Mixer software.



(a) Before Test



(b) After Test

Fig 6. 3D model of one sand sample before and after wind tunnel test



(a) Before Test



(b) After Test

Fig 7. Point clouds of sample before and after test

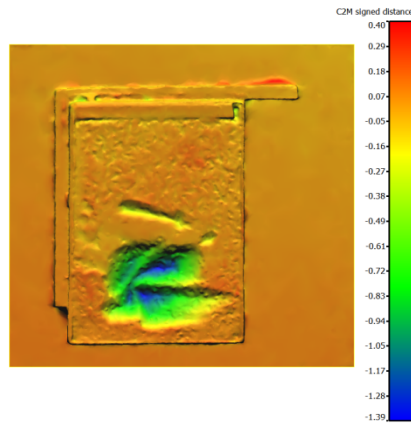


Fig 8. Contour diagram of coordinate to coordinate signed distance between two sample surfaces

5 Result Discussion

Result discussion after data acquired will focus on four aspects. The first one is how the different types of stabilizers and solution concentrations can change the mechanical property of red sand after applying chemical stabilizers. This can be done when mechanical property experiments finished.

After that, via wind tunnel experiments, the effect on red sand dust control brought by each single factor will be discussed through scatter and line charts, and then relates to generated nonlinear second order polynomials. Furthermore, the second order interactions between these factors will be analysed, especially the interactions between controllable factors, which are the type of stabilizers and solution concentration, and natural factors such as wind speed and sand surface inclination.

The third aspect is whether better crust mechanical properties can result in lower weight loss. This question can be answered by relate wind tunnel experiments to mechanical property tests, to evaluate is weight loss value simply related to crust mechanical properties or affiliated with the type of chemical stabilizers also.

Finally, whether the improvement of structure strength or surface crust viscosity is more significant in reducing weight loss will be analysed. As mentioned before, UCS and direct shear strength reflect the structure strength of red sand sample after mixed with chemical stabilizers, while penetration resistance represent the viscosity and tenacity of crust after spray chemical stabilizers on red sand surface. This analysis will provide the guideline for the selection of chemical stabilizers.

6 Conclusion and Future Work

This research aims at finding the most efficient and economical red sand dust control method using chemical stabilizers. Four types of commonly used chemical stabilizers will be studied in this paper. According to mechanics and wind tunnel experiments, and scientific experimental design methods, the impact to dust control brought by natural factors (e.g. wind speed, sand surface inclination) and the characteristics of chemical stabilizers

(e.g. types, solution concentration) can be evaluated comprehensively. The arrangement of experiments introduced in this paper is completely randomized to reduce error and avoid nuisance. The values selected for the factors in the mechanical property tests and wind tunnel experiments are the same so that no additional tests are required for result correlation. Based on this, future data analysis and conclusion will be adequate evidence-based and more reliable.

Due to limited study of chemical stabilizers focus on bauxite residue dust control, this research is conducted and will clearly illustrate the relationship of mechanical properties of red sand modified by chemical stabilizers and final dust reduction rate. Based on systematic experimental design, the effect of each single factor and two-level interaction will be found out. This research will contribute to better understand dust behaviour after addition of chemical stabilizers. These findings will establish a new dust control strategy on bauxite residue red sand dust control, which will benefit to the environmental friendly of bauxite mining industry and the reduction of the cost of environmental management.

In the future, chemical stabilizers and different sources of sand will be obtained from manufactures and bauxite mines. Actual experiments will be conducted afterwards to achieve real data for result analysis. The arrangement of experiments introduced in this paper may need adjustment based on initial test result.

Acknowledgements

This research is partially funded by Alcoa World Alumina Australia and Mining Education Australia Collaborative Research Fund. The authors also would like to acknowledge the in-kind support from Alcoa World Alumina Australia.

References

- [1] European aluminium a. Bauxite Residue Management : Best Practice. 2013(April):1-32.
- [2] Power G, Gräfe M, Klauber C. Review of current bauxite residue management, disposal and storage: practices,

- engineering and science. CSIPO Document DMR 3608, Australian Government. 2009;18.
- [3] Jones B, Haynes R, Phillips I. Effect of amendment of bauxite processing sand with organic materials on its chemical, physical and microbial properties. *Journal of Environmental Management*. 2010;91(11):2281-8.
- [4] Cooling D. Improving the sustainability of residue management practices—Alcoa World Alumina Australia. *Paste and Thickened Tailings: A Guide*. 2007:3-16.
- [5] European aluminium a. Background information on typical bauxite residue. 2012:1-3.
- [6] Liu J, Shi B, Jiang H, Bae S, Huang H. Improvement of water-stability of clay aggregates admixed with aqueous polymer soil stabilizers. *Catena*. 2009;77(3):175-9.
- [7] A. B, Davis W, Reinhold VN. *Air Pollution Engineering Manual*. New York 1992.
- [8] Yang J, Wang F, Fang L, Tan T. The effects of aging tests on a novel chemical sand-fixing agent – Polyaspartic acid. *Composites Science and Technology*. 2007;67(10):2160-4.
- [9] Han Z, Wang T, Dong Z, Hu Y, Yao Z. Chemical stabilization of mobile dunefields along a highway in the Taklimakan Desert of China. *Journal of arid environments*. 2007;68(2):260-70.
- [10] Keith DR. *Dust Control at Hazardous Waste Sites* 1985.
- [11] Stunder BB, Arya S. Windbreak effectiveness for storage pile fugitive dust control: a wind tunnel study. *JAPCA*. 1988;38(2):135-43.
- [12] Faria R, Ferreira AD, Sismeiro JL, Mendes JCF, Sousa ACM. Wind tunnel and computational study of the stoss slope effect on the aeolian erosion of transverse sand dunes. *Aeolian Research*. 2011;3(3):303-14.
- [13] Ferreira AD, Oliveira RA. Wind erosion of sand placed inside a rectangular box. *Journal of Wind Engineering and Industrial Aerodynamics*. 2009;97(1):1-10.
- [14] Turpin C, Harion JL. Numerical modeling of flow structures over various flat-topped stockpiles height: Implications on dust emissions. *Atmospheric Environment*. 2009;43(35):5579-87.
- [15] Badr T, Harion JL. Numerical modelling of flow over stockpiles: Implications on dust emissions. *Atmospheric Environment*. 2005;39(30):5576-84.
- [16] Lahalih SM, Ahmed N. Effect of new soil stabilizers on the compressive strength of dune sand. *Construction and building Materials*. 1998;12(6):321-8.
- [17] Goossens D. Wind tunnel calibration of the USGS dust deposition sampler: Sampling efficiency and grain size correction. *Aeolian Research*. 2010;2(2-3):159-70.
- [18] Zingg AW. A Portable Wind Tunnel and Dust Collector Developed to Evaluate the Erodibility of Field Surfaces. *AGRONOMY JOURNAL*. 1951:pp. 189-91.
- [19] Sinclair Knight Merz (SKM). *Dust Assessment - Pinjarra Bauxite Stockpile Area*. Report, Prepared for Alcoa of Australia, Pinjarra. 1997.
- [20] José CMF, Esteban Altabella J, García Darás F, Gallardo Izquierdo A. Influence of the design on slope stability in solid waste landfills. 2013.
- [21] Roe DC. Recent Innovations in Controlling Dust Emissions in the Bauxite/Alumina Industry. *GE Water & Process Technologies Technical Paper*. 2003:pp. 1-6.
- [22] George E. P. Box, J. Stuart Hunter, Hunter WG. *Statistics for Experimenters*. 2nd ed. United States of America 2005.

Mine Gases

Computational fluid dynamics modeling of methane distribution at a continuous miner face under various methane release conditions

Lihong Zhou^a, Christopher Pritchard^b, and Yi Zheng^a

*^aOffice of Mine Safety and Health Research (OMSHR)
National Institute for Occupational Safety and Health (NIOSH)
Pittsburgh, PA 15236, USA*

*^bSpokane Mining Research Division (SMRD) at NIOSH
Spokane WA 99207, USA*

Methane emissions can adversely affect both the safety and productivity of underground coal mines. The emission quantity and location of emissions at the continuous miner face, as well as ventilation quality and quantity applied to control coal mine methane, can contribute to the potential for methane accumulation. A good understanding of the impact of these emissions on the face methane distribution can be helpful to mine operators in effectively dealing with this serious problem. In this paper, both the methane emission rate and location were studied using the computational fluid dynamics (CFD) approach after models were validated against experimental tests conducted at a full-scale test facility. Five scenarios with various face methane emission rates and emission locations at a continuous miner face were modeled to demonstrate the impact on the methane distribution. Results showed that the maximum face methane concentration increased with the methane emission rate when the other ventilation conditions were kept constant. It was also shown that the change of methane emission location affected the size of the elevated methane zone but not the general location of where the methane ultimately accumulates.

Keywords: Mine Ventilation, Computational Fluid Dynamics, Continuous mining Face, Airflow Pattern, Methane Distribution, Methane monitoring

1. Introduction

Methane is a major concern in the safety of underground coal mining operations. Methane accumulations at a working face in underground coal mines can lead to a major explosion if not well managed. A good understanding of face methane distribution will be beneficial to mine operators in managing the face methane accumulation problem and improving methane control strategies. The quality of the ventilation and the liberation of methane at a working face are regarded as the major contributors to the accumulation of methane. The methane liberation at a working face from the mined coalbed and other adjacent gas-bearing strata is activated by the coal extraction activity, which disturbs the existing stress equilibrium in rock mass. The influx of gas to a working face area is defined by the geometry and size of the zone from which methane is emitted, the gas content of the strata, the degree of gas emission, and the intensity of mining activities [1]. In the United States, federal mining law stipulates that gas concentrations at the face be maintained at less than 1%. Ventilation has long been the primary means of controlling methane emissions in underground coal mines with the supplement means such as pre-degassing and gas drainage [2].

Many efforts have been made to address gas emission and gas control at the longwall face [2-5]. In contrast to the longwall face, a continuous miner face generally sees lower gas emission and smaller productivity; however, methane is still a major threat to the safety of miners [7]. At a continuous miner face, the ventilation is mainly affected by the method of

ventilation employed (blowing or exhausting), rib to curtain distance, curtain setback distance (distance from the deepest penetration of the face to the mouth of curtain), volume of air delivered to the face and auxiliary ventilation method. How the methane distribution is affected by various operating conditions at a continuous miner face has been widely researched [6-16]. Luxner [8] first developed airflow and methane distribution patterns in an equipment-free entry 2 m (6.5 ft) high and 3.7 m (12 ft) wide for various operating conditions, including blowing and exhausting curtain ventilation, tight rib distance, curtain setback distance, volume of air delivered by the curtain, and rate of methane released in the face area. Taylor et al. [7] recommended several practical guidelines for controlling and monitoring methane levels in the face areas of underground coal mines based on studies conducted for deep cutting (where cut depths exceed 6 m (20 ft)) at the Office of Mine Safety and Health Research (OMSHR) full-scale ventilation test gallery. The CFD approach was employed by Wala et al. [12] to investigate methane behavior in the empty face area with a blowing curtain and a 10.7 m (35 ft) curtain setback. The CFD model was validated for both airflows and methane concentrations in the face area against the experimental tests conducted at OMSHR's full-scale ventilation test gallery, showing that CFD techniques could be used for face ventilation system analysis and design after well-performed validations. Kollipara, et

al. [6] analyzed airflow patterns at a continuous miner face area when the continuous miner is making a straight initial cut.

As one of the critical factors affecting the methane distribution at a continuous miner face, the methane release conditions, including release quantity and location, have not been given sufficient attention in previous research. Methane emission at continuous miner faces varies considerably in volume as well as in location, affecting the resulting methane distribution at the face. Luxner [8] has studied the methane emission rates of 0.005-m³/s (10 cfm), 0.01 m³/s (20 cfm), and 0.014 m³/s (30 cfm) in an equipment-free face. His study indicated that both average and maximum methane concentrations were a function of the methane emission rate, and it was found that methane concentration generally increased with emission rate.

However, neither detailed test data nor the influence of the release location was interpreted in the research. Kurnia et al. [17] utilized CFD to simulate methane dispersion in a mine entry with discrete methane sources and various methods to handle these emissions. Simulation results indicated that methane dispersion inside the mine entry was influenced significantly by the number as well as location of the sources and quantity of methane released from each source. The examined mine's arc-shaped entry is not used in the U.S. coal mines and the ventilation method is different from that in US coal mines as well. In the current paper, the airflow behavior and methane distribution at a continuous miner face with various methane emission rates and emission locations are addressed. The objective of this study is to investigate how the quantity and locations of methane emissions affect the methane distribution pattern at a simulated continuous miner face utilizing a well-validated CFD model.

2. Validation Experiment

A series of experiments were conducted by the authors at the OMSHR full-scale ventilation test facility to validate the CFD model. The same gallery has been used by other OMSHR researchers, and its design and use are detailed in Taylor, et al. (2010). In these tests, the face was 4.0 m (13 ft) wide and 2.1 m (7 ft) high with a ventilation curtain offset of 0.6 m (2 ft) from the left rib to simulate a box cut. A full-scale model mining machine having approximately the same dimensions as a Joy CM-14 continuous miner without the rear-loading boom was positioned at the face. Ventilation air was drawn by the exhaust fan and adjusted to maintain the airflow at 4.6 m³/s (9,800 cfm). Blowing curtain ventilation was arranged by placing the curtain 0.6 m (2 ft) from the left side of the entry.

A uniform methane release at the face was simulated with a manifold consisting of four 3 m (10 ft) long horizontal copper pipes drilled on the top and bottom with 2 mm (1/16 in) diameter holes spaced 51 mm (2 in) apart. The four pipes were equally spaced and located 0.1 m (4 in) from the simulated face. Methane concentration measurements were made at 15 sampling locations (Fig. 1) with 12 of the sampling locations at the plane of 0.3 m (1 ft) below the roof and the other three (No. 11, 12, 13) at the half-plane which is 1.1 m (3.5 ft) below the roof.

It should be noted that neither a scrubber nor water sprays are applied in the tests and the CFD model of this paper. Only the most basic face ventilation configuration with a blowing ventilation curtain is set up for the tests. Machine-mounted water sprays and scrubbers have been extensively used in dust control in coal mines. It has also been widely accepted that they play an important role in reducing methane level at the face by directing additional intake air to the face especially in a deep cut face [14, 19]. At the current stage, this paper mainly focuses on examining the impact of methane release rate and location on the face methane distribution. The effect of scrubbers and water sprays can be very complicated [14]. It is hard to examine all of the scenarios that could exist in coal mine face ventilation. In this paper, we decided to simplify the face ventilation to the most basic configuration with only blowing curtain to avoid the interruption from water sprays and scrubbers and mainly concentrate on the gas emission condition. Further research, which will include the use of water sprays and scrubbers, has been planned for a future study.

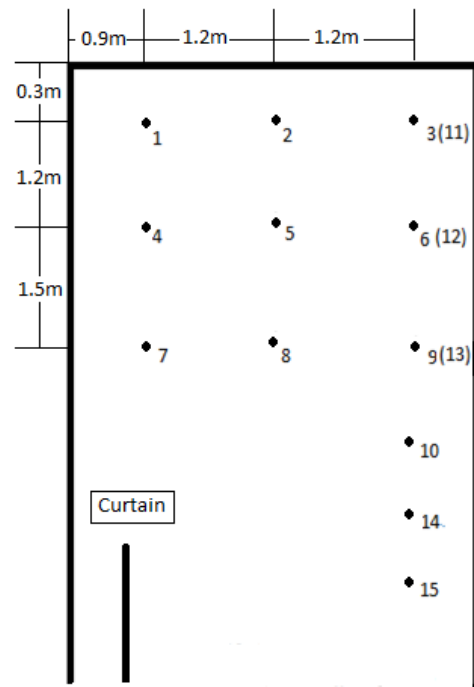


Fig. 1. Methane concentration sampling locations

3. CFD Models and Validation Study

The models were constructed, meshed, and post-processed with the commercial CFD software ANSYS Fluent 13.0. Fig. 2 shows a geometric 3-dimensional (3D) layout of the test face area as part of the test gallery. The fresh air was directed by the ventilation curtain on the left side of the working face. The methane was released from the gas manifold located at the face.

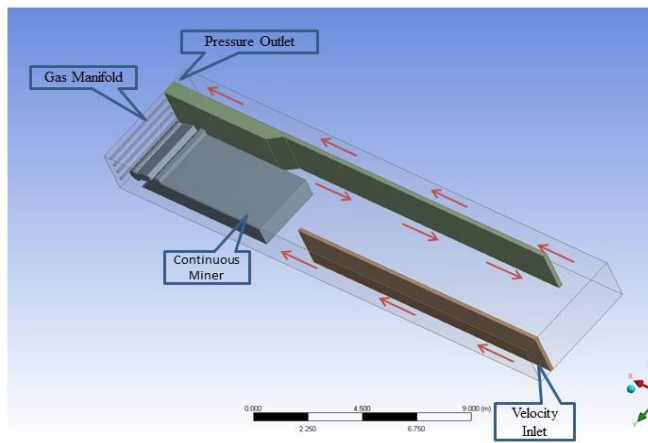


Fig. 2. Geometry of the face model

The most commonly used turbulence model in engineering, standard $k-\epsilon$, was used to model the turbulent flow in the face area. The species transportation model was employed to simulate methane transportation in the face air. Two velocity inlet boundary conditions were used at the mouth of the ventilation curtain and gas manifold (Fig. 2). The methane release model was simplified by assuming the gas was liberated from the outer surface of the tubes instead of through multiple holes. The detailed boundary conditions are:

- Velocity Inlet: 3.56 m/s (700 ft/min)
- Gas Inlet: 0.0085 m/s (18 cfm)
- Pressure Outlet: 0 Pa

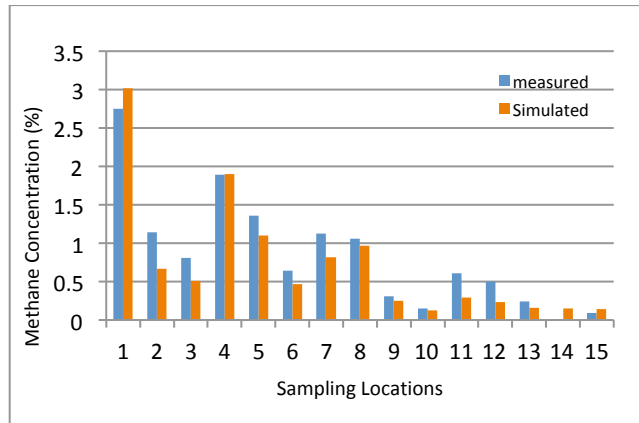


Fig. 3. Comparison of measured and simulated methane concentration at sampling locations

In the validation test, the methane was released evenly from four parallel pipes at the rate of 0.0085 m/s (18 cfm). The methane concentrations at each sampling location (Fig. 1) were extracted in the CFD computation domain and compared with the gallery experimental data. Fig. 3 displays the simulated and measured methane concentration at each of the sampling locations. The methane concentration measured experimentally at each location is well matched by the CFD simulation results. A good agreement between the simulated and measured methane concentration at the sampling locations suggests that this CFD model was well-

validated and could be used to examine other ventilation scenarios. No mesh independence study is conducted in this paper since the initial model was validated using experimental test data. Additionally, the modeling scenarios in this paper are executed by changing minor details thereby removing the need for a mesh independence study because of the similarity between the validated model and the scenarios.

As seen in Fig. 3, the maximum measured methane concentration for this test was approximately 2.8%. At these conditions, test personnel felt that the rate of 0.0085 m/s (18 cfm) was very close to the maximum that could be safely released in the ventilation gallery. This indicated that the continued tests with methane emission rates higher than 0.009 m/s (18 cfm) could not be conducted in the ventilation gallery under the current operation conditions. However, the overall U.S. peak methane emission average is around 0.008 m/s (17 cfm) with maximum rates of 0.02 m/s (40 cfm) [15]. To test larger methane emission cases, CFD modeling could be used effectively. In the real world, methane may be liberated at many locations in the working face. In order to investigate the impact of varying methane emission quantity and location on the face methane distribution, five scenarios with various methane emission rates and locations (Table 1) were simulated with the validated CFD model maintaining the same operation conditions and initial conditions.

Table 1. List of simulation scenarios

Case No.	Emission quantity m/s (cfm)	Emission location
1	0.0064 (13.5)	Top pipe
2	0.0085 (18)	Top pipe
3	0.017 (36)	Top pipe
4	0.017 (36)	All 4 pipes
5	0.017 (36)	Top two pipes

4. Results and Discussions

4.1 General airflow pattern

In the five examined scenarios, all the conditions that could affect the airflow behaviors are the same except for the methane emission. The influence of the released methane on the face airflow behavior can be disregarded because the rate of methane is several orders of magnitude lower than that of ventilation air. Fig. 4 illustrates the airflow pattern near the face as simulated for all scenarios developed by the CFD model. Two primary air currents are shown between the face and the mouth of the ventilation curtain. A flow separation occurs when one air current turns directly to the return side without sweeping through the face and the other air current reaches the face from the right side and flows over the continuous miner to the left side. The second air current flowing to the face creates a “Figure 8” pattern. This air current mainly contributes to the dilution of methane at the face. As shown in Fig.4, only a limited amount of air is reaching the face area and the majority of air is flowing back out of the face area.

The displayed airflow pattern in this 13 ft wide box cut face is consistent with some studies having been done by other peers. Very similar airflow patterns have been presented by Wala, et al. [12] in an equipment-free 13 ft wide box cut face. It was also indicated in Taylor et al.'s [13] tests that the ventilation flow created a "Figure 8" pattern that moved from the return to the intake side of the face in a continuous miner equipped box cut face with only a blowing curtain. The two above-mentioned airflow patterns [12,18] were obtained in faces that were very similar to those studied in this paper. However, the changes in face condition can greatly change the airflow behavior. Wala et al. [12] also described a case with a 16.5 ft wide slab cut face where the intake air flows from the left side to the right instead of making a "Figure 8" pattern like that in a box cut. Taylor and Zimmer's [18] study has demonstrated that the operation of either the scrubber or water sprays reversed the direction of the face flow, resulting in movement from the intake to the return side of the face. The airflow pattern at a face can vary with the face geometry, the ventilation curtain location, and the application of other ventilation controls.

In this studied case, the effectiveness of the ventilation to dilute methane gas relies highly on this second air current in the simulated scenarios. As shown in Fig. 4, the velocity of secondary air currents is lower than that of the primary airstream. Consequently, the elevated methane zone will most likely exist at the region of secondary airflow, which is at the front face area.

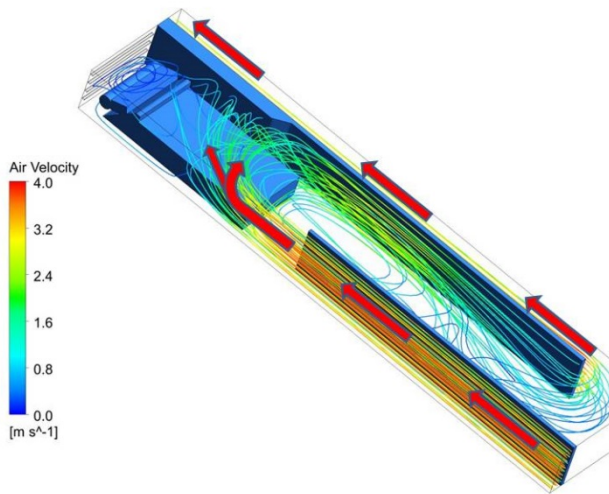


Fig. 4. Airflow path lines at the face

4.2 Comparisons of the simulated cases

Among the simulated scenarios, Scenario No. 1, 2, and 3 release methane from the top pipe. The only variable parameter is the methane emission rates which are 0.0064 m/s (13.5 cfm), 0.0085 m/s (18 cfm), and 0.017 m/s (36 cfm) respectively. Therefore, the comparisons among Scenario 1, 2, and 3 will indicate the impact of methane emission rate on the methane distribution at the face under the current operational conditions. Accordingly, the comparisons of Scenario No. 3, 4, and 5, which have a constant methane emission

rate but changing locations, illustrate how the various release locations affect the face methane distribution.

Fig. 5 shows the comparison of the elevated methane zones among Scenario No.1, 2, and 3 where methane was released from the top pipe only at the increasing rate of 0.0064 m/s (13.5 cfm), 0.0085 m/s (18 cfm), and 0.017 m/s (36 cfm) respectively. This illustration shows that the methane zone is concentrated mainly at the upper left corner of the face for all three scenarios as the methane is released constantly from the face. On the contrary, the methane accumulation at the right side of the face, except for the adjacent area of the top gas pipe, where the gas is released can be negligible, especially when the methane is released at a very low rate. The methane accumulates at the left side of the face can be well explained by the airflow behavior displayed in Fig. 4. At the front end of the face, the fresh airflow from the right side to the left which carries the released methane eventually accumulates at the left side of face. The location of the elevated methane zone at a continuous miner face largely relies on the airflow behavior. Any mining operation condition change will eventually change the methane distribution if it affects the airflow behavior at a continuous miner face.

As can be seen from Fig. 5, the size of the elevated methane zone is affected significantly by the methane emission rate. The increase in the methane release rate results in an apparent enlargement of the size of the methane zone. Comparing these three scenarios, it can be concluded that an escalation in the methane emission rate affects the size of the elevated zone but not the location of the methane zone.

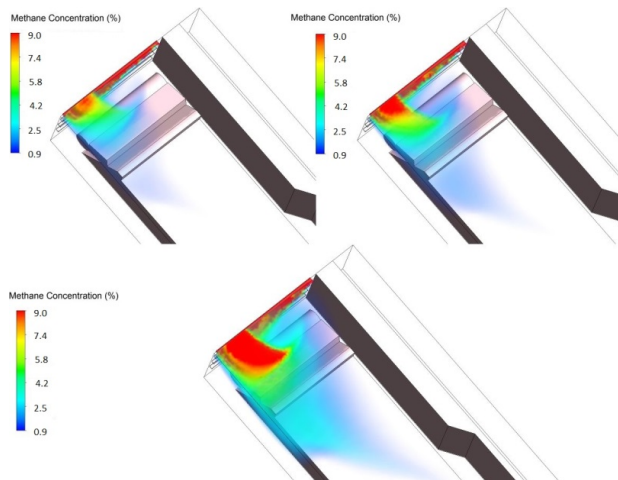


Fig. 5. Top view of elevated methane zone; top right: 0.0064 m/s (13.5 cfm); top left: 0.0085 m/s (18 cfm); bottom: 0.017 m/s (36 cfm)

A closer inspection of the methane concentration is made by plotting along a straight line parallel to the face and above the cutting drum of the continuous miner for each scenario. The simulated peak methane concentration along the plotting line appears to occur in the segment 0.6 m (2 ft) to 1.2 m (4 ft) from the left rib for each scenario. For each case, the methane concentration decreases along the face from left to right with a sharp drop occurring from 1.1 m (3.5 ft) to 1.5 m (5 ft). The highest methane level of 15% is observed in the scenario of 0.017 m/s (36 cfm) methane release rate and followed by 8% in the 0.0085 m/s (18 cfm) case. The lowest peak methane concentration of 5% arises from the scenario of 0.0064 m/s (13.5 cfm). Such a high methane concentration is barely seen in active coal mines or test facilities. The highest statistical methane release rate and the “worst” ventilation condition applied in this modeling contribute to the extremely high methane concentration obtained in this study.

Fig.6. shows that the highest methane concentration nearly doubles from 8% to 15% as the methane release rate doubles from 0.0085 m/s (18 cfm) to 0.017 m/s (36 cfm). Among the three scenarios, it shows that the highest methane emission rate yields the highest methane concentration and the highest methane concentration increase with the methane release rates, which has a good agreement with Luxner’s [8] observation that methane concentration in the immediate face area is a function of the volume of methane released.

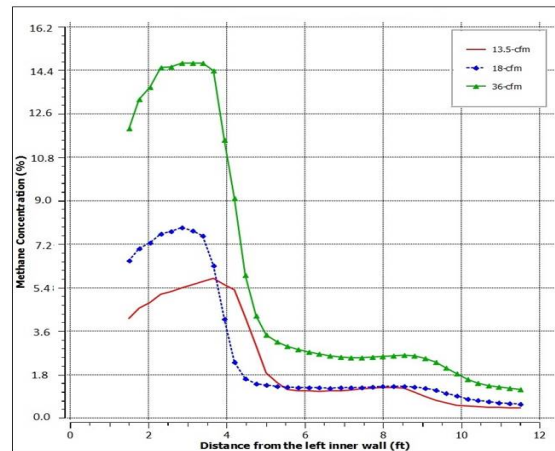
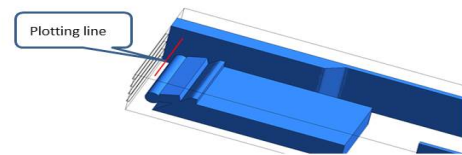


Fig. 6. Methane mass fraction along the line at the top of the face

In Scenario No. 3, 4, and 5 the methane is all released at the same rate of 0.017m/s (36 cfm) but from three different combinations of gas pipes. As shown in Table 1, Scenario No. 3 examines only the top pipe gas emission, whereas, Scenario No. 4 and No. 5 have the methane emitted from all the four pipes and the top two pipes respectively. The methane release rate at each release pipe is apparently different in the three scenarios as the numbers of involved release pipes are different in each scenario. Given the overall release rate is kept at 36 cfm, the methane is divided evenly to each assigned gas pipe for each case. Therefore, Scenario No. 3 has the largest methane release rate of 36 cfm, followed by Scenario No. 5 with 18 cfm, and Scenario No. 4 with 9 cfm per pipe. The variation in the methane release rate of each pipe results in different methane release velocities. The influence of the methane release velocity on the ventilation behavior can be negligible as the methane release velocity from the pipes is about several order-of-magnitude lower than that of ventilation air [17].

The comparison of methane distribution at the face for Scenario No. 3, 4, and 5 demonstrates the impact of methane release location on the face methane distribution as they have the same release rate. Fig. 7 illustrates the overview of the methane distribution at the face based on these scenarios where the elevated methane zone occurs at the left upper corner of the face as in all other simulations. Changing the location of methane release does not have significant impact on the general location of the elevated methane zone but only on the size of the zone.

Fig. 8 shows the methane contours at a vertical plane located 0.3 m (1 ft) from the left rib. The case with methane releasing from all four pipes has the largest zone, followed by the top two pipes, and then the top pipe. It appears that the “wider” emission source can

lead to the increased spread of methane at the face. The released methane barely reaches the lower parts of the release site as methane tends to rise and accumulate near the higher parts of face. On the vertical plane, it shows that the highest methane concentration mainly exists at the upper part of the face and also in the region near the release pipes.

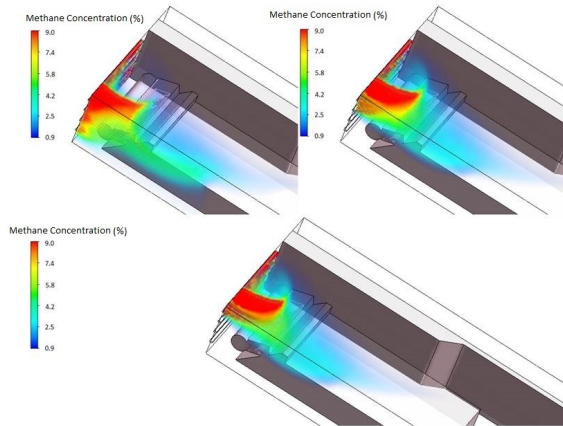


Fig. 7. Side view of methane elevated zones at the emission rate of 36 cfm released from the top pipe (top left); from the top two pipes (top right) and from all the pipes (bottom)

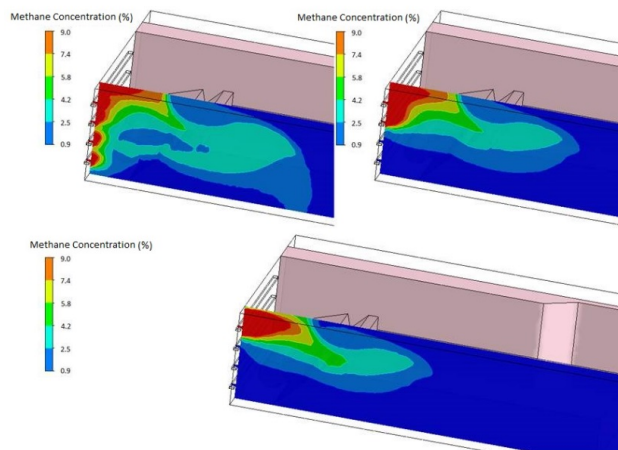


Fig. 8. Methane contours at the wall parallel plane 0.3 m (1 ft) inward from the left rib

5. Conclusions

The methane distribution at the continuous miner face can be determined by factors such as ventilation condition, face dimension and layout, and methane emission rate. In this research, validated experimental tests at a full-scale ventilation gallery and a series of computational fluid dynamics (CFD) simulations were carried out to investigate how methane emission rate and location affect the methane distribution at the continuous miner face.

The CFD model, representing a 13.5 ft wide continuous miner face with a continuous miner present, was constructed and validated with the full-scale methane test results. A very good agreement was obtained between the gallery test and simulated methane concentration. The simulations showed that CFD can provide a very good prediction of methane distribution at the continuous miner face.

Based upon five scenarios simulated with CFD, the impact of methane release rate and location were studied. The simulation results showed that the methane distribution at the continuous miner face was significantly affected by the variation of methane release rates. The peak methane concentration increased with the methane release rate. This study also demonstrated that changing the location of the methane emission does not have a significant impact on the general location of the elevated methane accumulation zone, but it does have an effect on the spread area of the zone.

It has to be noted that only the continuous miner faces with a blowing curtain were used in the tests and in the CFD models with no consideration of the influence of a scrubber and water sprays. The airflow behavior and methane accumulation scenarios differ from the scenarios that include the scrubber and water sprays. Future work will involve more complicated continuous miner face ventilation tests that will consider various face dimensions and more ventilation controls.

Acknowledgements

The authors sincerely thank Andrew L. Mazzella, Cynthia A. Hollerich and James D. Addis for their valuable work in conducting the experimental tests.

Disclaimer

The findings and conclusions in this report are those of the authors and do not necessarily represent the views of the National Institute for Occupational Safety and Health. Mention of any company or product does not constitute endorsement by NIOSH.

References

- [1] K. Noack, Control of gas emissions in underground coal mines, *International Journal of Coal geology* 35(1998)57-81.
- [2] W.P. Diamond, Methane control for underground coal mines. Bureau of Mines, Information Circular No. 9395 (1994) 51 pp.
- [3] T. Ren, and J. Edwards, Three-dimensional computational fluid dynamics modelling of methane flow through permeable strata around a longwall face. *Mining Technology*, 109(1) (2000) 41-48.
- [4] S. Schatzel, R. Krog, F. Garcia, J. Marshall, and J. Trackemas, Prediction of longwall methane emissions and the associated consequences of increasing longwall face lengths: a case study in the Pittsburgh coalbed, In: *Proceeding of 11th US/North American Mine Ventilation*

- Symposium, University Park, PA, (2006) 375-382.
- [5] C. Ö. Karacan, G. S. Esterhuizen, S. J. Schatzel, and W. P. Diamond, Reservoir simulation-based modeling for characterizing longwall methane emissions and gob gas venthole production. *International Journal of Coal Geology*, 71(2-3) (2007) 225-245.
- [6] V.K. Kollipara, D.D. Relangi, and Y.P. Chugh, A CFD analysis of air flow patterns in face area for continuous miner making a straight initial cut, In: *Proceeding of 14th United States/North American Mine ventilation Symposium*, Salt Lake City, UT, (2012) 265-272.
- [7] C.D. Taylor, J.E. Chilton, and G.V.R. Goodman, Guidelines for the control and monitoring of methane gas on continuous mining operations, *NIOSH Information Circular 9523* (2010) 85.
- [8] J. Luxner, Face Ventilation in Underground Bituminous Coal Mines-Airflow and Methane Distribution patterns in Immediate Face Area-Line Brattice, *Bureau of Mines Report of Investigation No. 7223* (1969) 20 .
- [9] C.F. Meyer and F.J. Van Zyl, Final project report: Reduce explosion risks and improve safety and health conditions by better ventilation practices in mechanical miner headings, *Safety in Mines Research Advisory Committee*, (1999) 62.
- [10] F.J. Van Zyl, and B.K. Belle, Final project report: quantification of methane behavior in continuous miner headings using a controlled environment, *Safety in Mines Research Advisory Committee*, (2000) 49.
- [11] A.M. Wala, J.C. Yingling, and J. Zhang, Evaluation of the face ventilation systems for extended cuts with remotely operated mining machines using three-dimensional numerical simulations, *SME pre-print*, 1998, *SME Annual Meeting*, Orlando, Florida. Print Number: 93-290.
- [12] A.M. Wala, S. Vytla, C.D. Taylor, and G. Huang, Mine face ventilation: a comparison of CFD results against benchmark experiments for the CFD code validation, *Mining Engineering*, (59)(2007) 49-55.
- [13] C.D. Taylor, E.D. Thimons, and J.A. Zimmer, Factors affecting the location of methanometers on mining equipment, In: *Proceeding of the 7th International Mine Ventilation Congress*, Krakow, Poland, June 17-22 (2001) 683-687.[
- [14] C.D. Taylor, J.E. Chilton, E. Hall, and R.J. Timko, Effect of scrubber operation on airflow and methane patterns at the mining face, In: *Proceeding of 11th U.S./North American Mine Ventilation Symposium*, University Park, PA, (2006)393-399.
- [15] F.N. Kissell, C.D. Taylor, and G. V. R. Goodman, Methane control at continuous miner sections in *Handbook for methane control in mining*, *NIOSH Information Circular 9486* (2006) 184.
- [16] D.M. Hargreaves, and I.S. Lowndes, The computational modeling of the ventilation flows within a rapid development drivage, *Tunneling and Underground Space Technology* 22 (2007) 150-160.
- [17] J.C. Kurnia, A.P. Sasmito, and A.S. Mujumdar, CFD simulation of methane dispersion and innovative methane management in underground mining faces. *Applied Mathematical Modelling*, 38(14) (2014) 3467-3484.
- [18] C.D. Taylor, and J.A. Zimmer, Effects of water sprays and scrubber exhaust on face methane concentrations. In S. Waselewski (ed.), *Proceedings, 7th Intl. Mine Ventilation Congress*, Krakow, Poland, June 17-2, Krakow 2001, EMAG.
- [19] J.C. Volkwein, and T.S. Wellman, Impact of Water Sprays on Scrubber Ventilation Effectiveness, *Bureau of Mines Report of Investigation No. 9259* (1989)12.

A Critical Look at Longwall Bleeder Ventilation

Jürgen F. Brune^a, John W. Grubb^a, Gregory E. Bogin, jr. ^a, R. Karl Zipf, jr. ^a, Jonathan A. Marts^a, Richard C. Gilmore^a, Sam Lolon^a and Saqib A. Saki^a

^aColorado School of Mines, Golden, Colorado, USA

Bleeder ventilation is common and legally required in underground longwall coal mines in the United States. This ventilation technique originated with room-and-pillar retreat mining and is intended to clear mined-out areas or gobs of any explosive methane-air mixtures. A system of bleeder ventilation entries surrounds the gob, intended to draw explosive methane accumulations directly towards a dedicated system of return airways and to a dedicated bleeder fan. Bleeder entries are traveled regularly for inspection purposes and the methane content within these travel ways is limited to 2%.

With the arrival of longwall mining in the United States in the 1970s, bleeder ventilation was extended to controlling methane in longwall gobs. Researchers at the Colorado School of Mines (CSM), under a research project funded by the CDC-NIOSH Office of Mine Safety and Health Research, have studied bleeder ventilated longwall gobs by examining gas compositions and gas flows using computational fluid dynamics (CFD) modeling techniques. Researchers found that bleeder ventilated gobs are surrounded by a fringe of methane-air mixtures in the explosive range. Investigations of numerous mine explosions indicate that these explosive mixtures may have either ignited within the gob or may have been pushed into the active mine workings.

This paper characterizes the explosion and fire hazards stemming from bleeder ventilated gobs and suggests improvements for ventilation practices that reduce or eliminate these hazards.

Keywords: Coal mining, longwall mining, explosion prevention, bleeder system, sealed gob, nitrogen inertization

1. Introduction

A coal mine ventilation system must control explosion hazards by diluting and carrying away potentially explosive mixtures of methane in air. In the United States, Title 30 CFR §75.334(b) [1] requires that, during and after pillar recovery, a bleeder system be used to ventilate the worked-out areas where pillars, including longwall panels, have been recovered, so that methane-air mixtures are continuously diluted and routed into a return air course. The mine operator must file and the U.S. Mine Safety and Health Administration (MSHA) approves a mine ventilation plan that must specify the “design and use of bleeder systems” as well as the “means to determine the effectiveness of bleeder systems.”

A concise definition of the terms “bleeder” and “gob” is given by Urosek et al. (2006) [2]:

Bleeder systems are the part of the mine ventilation network used to ventilate pillared areas in underground coal mines. Pillared areas are those in which pillars have been wholly or partially removed, including the areas where coal has been extracted by longwall mining. Bleeder systems protect miners from the hazards associated with methane and other gases, dusts and fumes, and oxygen deficiency that may occur in these mined-out areas. Effective bleeder systems control the air passing through the area and continuously dilute and move any methane-air mixtures and other gases, dusts, and fumes from the worked-out area away from active workings and into a return air course or to the surface of the mine. A bleeder

system includes the pillared area (including the internal airflow paths), bleeder entries, bleeder connections, and all associated ventilation control devices that control the air passing through the pillared area. Bleeder entries are special air courses designed and maintained as part of the mine ventilation system. It should be noted that a mined-out longwall panel is considered a “pillared area” in the context of this definition.

Stoltz (2007) [3] states that “effective bleeder systems control the air passing through the area and continuously dilute and move methane-air mixtures and other gases, dusts, and fumes from the worked-out area away from active workings, in an effective manner, preventing hazardous accumulations”.

Bleeder systems around longwall gobs are typically inspected by measuring air flow and methane content at key locations, the so-called Bleeder Evaluation Points (BEPs). Figure 1 (after Stoltz, 2007, [3]) indicates the points where air flows in to the bleeder system (yellow) and those where air flows out (red), usually, BEPs. An important part of the bleeder ventilation concept is that the gate road entries surrounding the gob panels are being kept open and free of obstructions such as roof falls and standing water (30 CFR §75.334(c)(3)) so that examiners can travel and inspect these airways. In this example, air can flow from the inlets in by the active longwall panel (right side in Figure 1) to the outlets at the left side. Similarly, air can flow from the inlets along the mains (bottom of Figure 1) to the outlets at the top left.

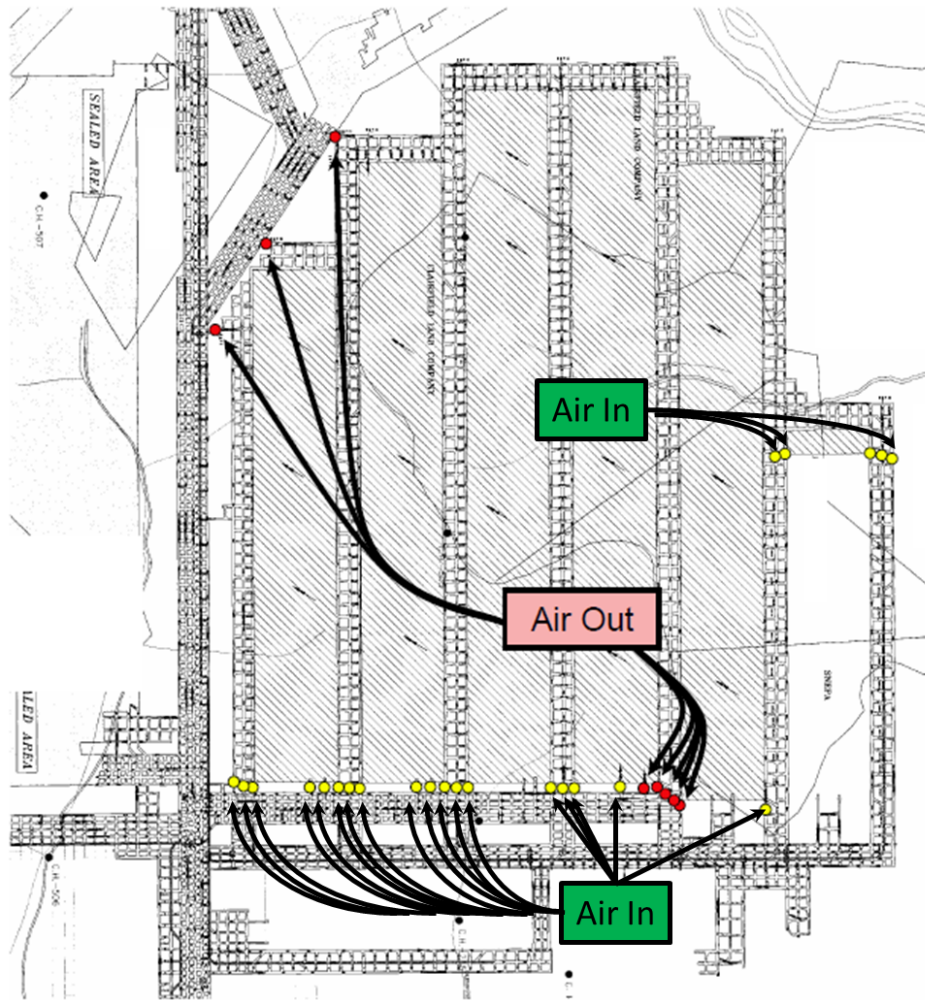


Fig. 1: System of bleeder ventilated longwall gobs with air inlets (yellow) and outlets (red), modified after Stoltz (2007) [3]

Bleeder entries that are being traveled for inspection and maintenance purposes may carry a maximum of 2% methane (30 CFR §75.323(e)). Likewise, the air exiting the bleeder outlets or BEPs may not contain more than 2% methane. Therefore, the mine operator must provide sufficient amount of fresh air entering the inlets to dilute the air exiting the BEPs to below 2%. Most recently, MSHA has provided guidance for the establishment and operation of bleeder ventilation systems in Program Policy Letter (PPL) No. P13-V-12 (Stricklin 2013) [4] to provide clarification and improvements to the way bleeder systems are being evaluated. This PPL was also issued to address concerns with the bleeder system at the Upper Big Branch mine.

If methane enters the gob from coal beds above or below the mined seam, there will be one or more regions with methane at higher concentrations in the center of the gob, and only the peripheral bleeder airways are being kept below 2%. This is evidenced by the function of gob ventilation boreholes (GVBs) which routinely carry over 80% methane and are typically shut down if the methane content drops below 50%. As documented by Brune (2013) [5], there exists a fringe explosive gas zone (EGZ) between the methane-rich center of the gob and the surrounding bleeder entries where the methane content lies within the explosive range. In fact, research appears to indicate that it is impossible to prevent the formation of EGZs in bleeder systems.

2. Brief Literature Review

Urosek and Watkins [6] examined different bleeder systems they deemed to be “safe” and “effective” by traveling the entire bleeder system in a series of case studies. They demonstrated that fresh air entered the gob areas and that the bleeder entries were maintained below 2% methane. However, they did not determine if higher concentrations of methane and/or explosive mixtures existed deep within the gobs.

Smith et al. (1994) [7] evaluated bleederless ventilation or progressively sealed gobs used around the world and recommended that bleeder systems be used if the coal is prone to spontaneous combustion and that gobs should be monitored for carbon monoxide as an indicator for spontaneous combustion. Smith et al., however, do not indicate that the absence of a bleeder system would result in explosion hazards.

Mucho et al. (2000) [8] conducted tracer gas studies to investigate gas flows in bleeder ventilated gobs that were equipped with GVBs. The tracer gas analysis demonstrated that the flow paths in the bleeder system were along the peripheral entries and that only minor amounts of tracer gas reported to the GVBs, indicating that a “sweeping” of the entire gob with bleeder air does not happen. Mucho et al. were unable to determine that fresh air injected into the bleeder system through the inlets was indeed able to dilute methane accumulations deep within the gob. This questions the intended function of a bleeder system. The findings by Mucho et al. were confirmed by the CFD modeling research conducted at CSM.

3. Explosion Hazards in Bleeder Systems

Beiter (2007) [9] summarized several other mine disasters where ventilation systems incorporating bleeders failed, including the fatal explosions at Farmington No. 9 in 1968 (78 fatalities), Greenwich Collieries in 1984 (3 fatalities), Pyro (William Station) No. 9 in 1989 (10 fatalities), Southmountain Coal Company No. 3 Mine in 1992 (8 fatalities), A.A.&W. Coal Co. Elmo #5 Mine (1 fatality) and several other cases where miners were injured or no injuries occurred.

Brune (2013) [5] describes a number of mine explosions or methane ignitions that occurred in or near bleeder ventilated gobs, including those at the Willow Creek mine 1998 and 2000 (two fatalities),

those at the Buchanan mine 2005 and 2007 and those at the Upper Big Branch mine in 1997 and in 2010, the latter explosion claiming 29 miners’ lives.

It appears that, in these documented cases, the bleeder systems were ineffective. However, based on the research at CSM, it is questionable whether it is at all possible to operate a bleeder system in a way where no EGZs exist, as all bleeder systems carry an EGZ fringe of explosive methane-air surrounding an interior gob that is filled with methane at concentrations above the explosive range, in a fuel-rich, inert state.

4. Modeling of Longwall Bleeder Systems and EGZs

Researchers at the Colorado School of Mines, under funding from the National Institute for Occupational Safety and Health (NIOSH) have conducted computational fluid dynamics modeling studies of bleeder ventilated and progressively sealed longwall gobs. Much of this work, including details on the CFD model calibration and verification, has been published in research papers by Gilmore et al., 2014 [10] and Gilmore et al., 2015 [11].

Figure 2 shows the EGZ fringe surrounding a bleeder ventilated gob. The color code follows the Coward triangle (Coward and Jones, 1952) [12] shown on the right, where EGZ mixtures are colored red, fresh air is colored blue, methane-rich inert mixtures in yellow and green representing both fuel-lean and low oxygen mixtures.

It should be noted that, in Figure 2, lower left inset, the bleeder entries that must be examined and traveled, have an atmosphere of at least 19.5% oxygen and <2% methane, satisfying U.S. mandatory safety standards.

Figure 3 shows a CFD simulation of EGZs in a bleeder system with slightly different regulator settings at the headgate side inlets to the longwall start-up rooms. The two regulators were changed from a total flow of 38,000 cfm (18 m³/s) to 17,000 cfm (9 m³/s) to fully closed. In all cases, the outside bleeder entries could be traveled from the headgate to the bleeder fan but the CFD model shows that, depending on these regulator settings, the EGZ changes dramatically in size and shape yet it is not possible to eliminate the EGZ. By closing the regulators in the start-up entries, more fresh air from the headgate is forced to enter the gob, where it creates rather large EGZs.

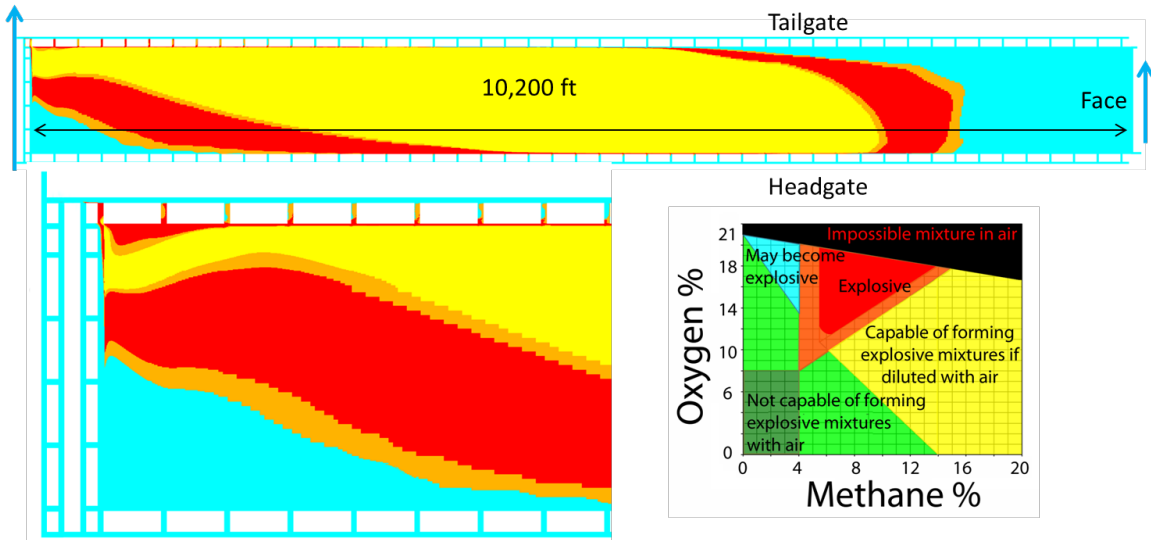


Fig. 2: EGZ surrounding a longwall gob. The image at bottom left shows detail near the start-up entries of the panel. Coward's triangle illustrates the color coding.

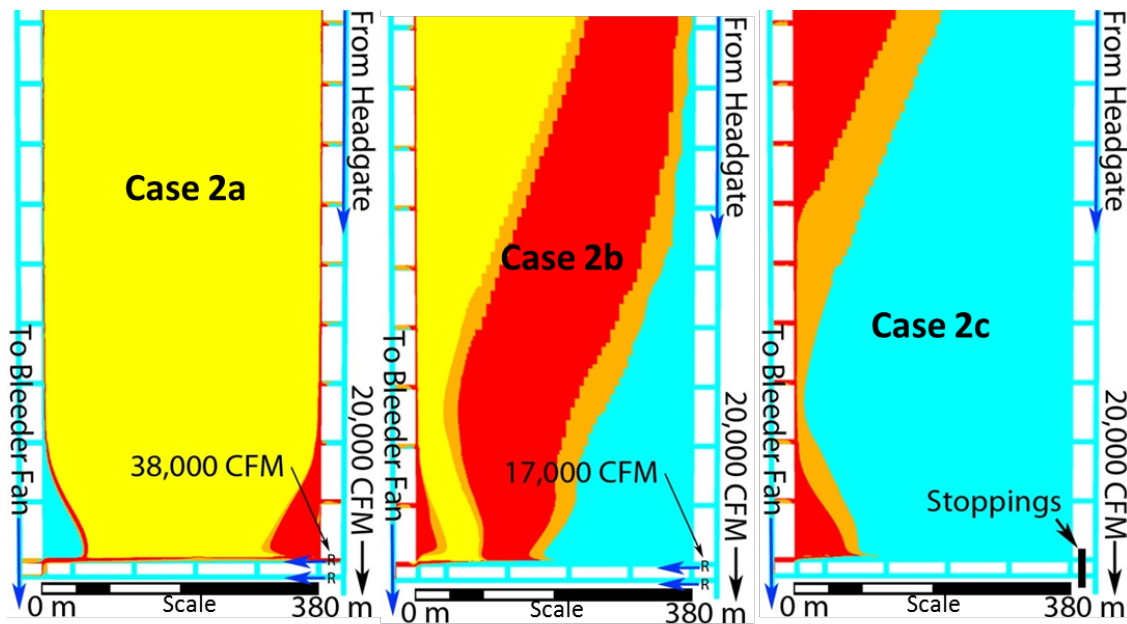


Fig. 3: Change of EGZ shape as a function of regulator settings

All simulations result in a contiguous EGZ fringe that surrounds the entire gob area. The CFD modeling research of bleeder ventilated gobs clearly demonstrates that the EGZ fringes exist and may pose significant explosion and fire hazards for miners working in or near the bleeder entries, for example, to examine these entries, operate pumps or maintain roof support.

5. Comparison of Bleeder Ventilated and Progressively Sealed Gobs

In the United States, coal mines may be permitted to operate progressively sealed gobs without a bleeder system. In progressively sealed gobs, stoppings are built in all headgate crosscuts once the headgate has passed. The sealed gob fills with methane, while all oxygen is consumed by slow oxidation reactions in the coal. This process eventually renders the gob

atmosphere inert. Permission to operate sealed gobs is granted by MSHA only on an exception basis – only a few U.S. mines are running progressively sealed gobs. Researchers at the Colorado School of Mines have documented with CFD modeling and measurements in operating mines that progressive sealing can significantly reduce and, in combination with nitrogen injection, practically eliminate EGZs in the gob. This was documented by Brune et al. (2015) [13] and Marts et al. (2015) [14]. Nitrogen injection from the headgate side can form a dynamic seal behind the longwall face that separates the methane-rich area deep inside the gob from the oxygen-rich atmosphere in the face, as shown in Figure 4. This dynamic seal effectively eliminates any EGZ fringe zone and the associated explosion and fire hazard. Researchers are still conducting parametric studies on dynamic seal formation to confirm that the EGZs can be eliminated, particularly during barometric pressure fluctuations. Studies also show that gob ventilation boreholes are effective and must be operated to drain excessive methane from the gob. If GVBs cannot extract sufficient methane from the gob, excessive methane will migrate to the tailgate exhaust where its concentration may exceed the statutory limit of 1%.

Progressively sealed gobs are common in European and Australian mines and have proven to be effective in the prevention of spontaneous combustion, especially in combination with nitrogen injection.

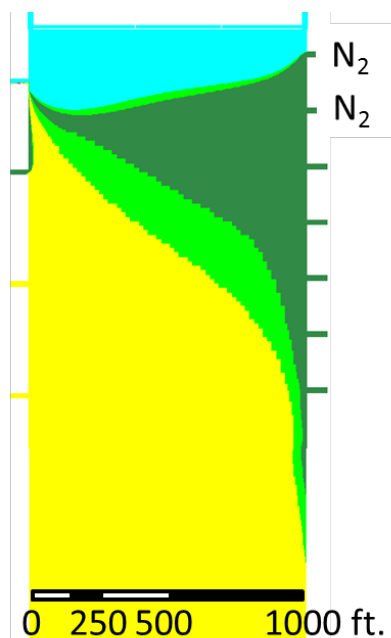


Fig. 4: Dynamic seal (green) formed in a progressively sealed gob (Marts et al., 2015) [14], separating the methane-rich interior of the gob (yellow) from the face air (blue).

6. Conclusions, Recommendations and Further Research

Researchers at the Colorado School of Mines (CSM), in a project funded by NIOSH, have documented that bleeder ventilated longwall gobs contain explosive gas zones (EGZs). These EGZs occur as complete fringes that surround the gob along the mixing zones between the face and bleeder entries that contain fresh air with a maximum of 2% methane and the center of the gob, where methane accumulates at concentrations high above the explosive range. CFD modeling shows that the EGZ fringes exist adjacent to bleeder entries that are traveled by miners regularly, exposing these miners to explosion and fire hazards. Numerous mine explosions and fires have occurred in and around bleeder ventilation systems, documenting that EGZ hazards in bleeder ventilated gobs exist and are real.

In a follow-up project, CSM researchers will determine how explosions and flames can propagate through EGZs in longwall gobs. CFD modeling, along with physical experiments, will serve to determine how far flames can travel through the rubble in the gob and how high explosion pressures become.

Acknowledgement

The authors gratefully acknowledge the sponsorship of the National Institute for Occupational Safety and Health (NIOSH), Office of Mine Safety and Health Research (OMSHR) that made this research possible.

References

- [1] United States Code of Federal Regulations, Title 30: Mineral Resources. U.S. Government Publishing Office (2015).
- [2] J.E. Urosek, W.J. Francart, and D.A. Beiter, Bleeder systems in underground coal mines, Handbook for Methane Control in Mining, F.N. Kissell (ed.), CDC NIOSH IC 9486 (2006).
- [3] R. Stoltz, Best practices - bleeder system evaluation, MSHA, Mine Ventilation Summit, Beckley WV (2007).
- [4] K.G. Stricklin, Examination, evaluation, and effectiveness of bleeder systems, U.S. Department of Labor, MSHA program policy letter no. P13-V-12 (2013).
- [5] J.F. Brune, The methane-air explosion hazard within coal mine gobs, SME Transactions, Vol. 334 (2013) 376-390.

- [6] J.E. Urosek and T.R. Watkins, Gob ventilation and bleeder systems in U.S. coal mines. Proc. 7th U.S. Mine Ventilation Symposium, (1995) 347-352.
- [7] A.C. Smith, W.P. Diamond, T.P. Mucho and J.A. Organiscak, Bleederless ventilation systems as a spontaneous combustion control measure in U.S. coal mines, U.S. Bureau of Mines IC 9377 (1994) 43.
- [8] T.P. Mucho, W.P. Diamond, F. Garcia, J.D. Byars, and S.L. Cario, Implications of recent NIOSH tracer gas studies on bleeder and gob gas ventilation design. Proceedings of the Society of Mining Engineers, Annual Meeting, Salt Lake City, UT, (2000) 1-17.
- [9] D. Beiter, Best practices - bleeder systems - internal airflow paths, MSHA Mine Ventilation Summit, Beckley WV (2007).
- [10] R.C. Gilmore, J.A. Marts, S.A. Saki, G.E. Bogin Jr., J.W. Grubb and J.F. Brune, CFD modeling of gas flows and explosion hazards in bleeder ventilated and progressively sealed longwall gobs, 10th International Mine Ventilation Congress, Sun City, South Africa (2014).
- [11] R.C. Gilmore, J.A. Marts, J.F. Brune, S.A. Saki, G.E. Bogin Jr. and J.W. Grubb, Impact of regulator settings on the formation of explosive gas zones in bleeder ventilated longwall gobs, SME Annual Meeting, Denver (2015) preprint 15-086.
- [12] H.F. Coward and G.W. Jones, Limits of flammability of gases and vapours, U.S.B.M. Bulletin No. 503 (1952).
- [13] J.F. Brune, J.W. Grubb, G.E. Bogin Jr., J.A. Marts, R.C. Gilmore, and S.A. Saki, Lessons learned from research about methane Explosive Gas Zones in coal mine gobs, SME Annual Meeting, Denver (2015) preprint 15-073.
- [14] J.A. Marts, R.C. Gilmore, J.F. Brune, S.A. Saki, G.E. Bogin Jr. and J.W. Grubb, Optimizing nitrogen injection for progressively sealed panels, SME Annual Meeting, Denver (2015) preprint 15-093.

Experimental Investigation of Using Thin Spray-on Liners as a Gas Management Tool in Underground Coal Mines

Zecheng Li^a, Duncan Chalmers^a, Serkan Saydam^a, Rudrajit Mitra^a, Furqan Hussain^b

^a*School of Mining Engineering, UNSW Australia, Sydney, Australia*
^b*School of Petroleum Engineering, UNSW Australia, Sydney, Australia*

Gas emissions can adversely affect the safety of underground coal mines, which may lead to dangerous gas accumulations and explosions. Every coal mine has to develop effective gas control strategies to control the gas concentration below the statutory requirements. A thin spray-on liner (TSL) is defined as a chemical based layer or coating (3-5 mm) that is sprayed onto the rock surface to support mining excavations. Since the introduction, TSLs have received some success as a ground support tool for underground mining. Besides ground support, TSLs also show some potential to be used as a gas management tool in underground coal mines due to their relative low permeability.

This paper presents an experimental study of the potential use of TSLs in underground coal mines as a gas management tool. Single phase gas permeability tests were conducted on intact and treated dry coal samples from an underground coal mine in New South Wales, Australia. The tested gases included methane (CH₄) and carbon dioxide (CO₂), as they are the common gases in coal seams, and helium (He) was used as a control gas. Experimental results show that the TSL tested can reduce the gas permeability of coal to a great magnitude. The results also indicate the potential benefit of using TSL as a gas management tool in underground coal mines.

Keywords: Thin spray-on liner (TSL), gas management, underground coal mine

1. Introduction

Coal seams contain mine gases in quantities which are functions of coalification degree and permeability of the overburdens [1]. When influenced by mining excavations, these gases can be emitted into the ventilation system and affect the safety of underground coal mines. Inadequate air quantities in the ventilation system may cause dangerous gas accumulations in the mine and may lead to gas explosions under certain circumstances and conditions [2]. Due to the risks, coal mine gases have always been regarded as a threat for underground coal mining [3].

A thin spray-on liner (TSL) is defined as a thin chemical based coating or layer that is applied onto the mining excavations with a thickness of 3 to 5 mm and is normally part of the support system [4]. They have been used as an alternative surface support system for underground rock support in hard rock mines [5-7]. However, their applications in coal mines have been slow [8, 9].

TSLs have a relatively low permeability which makes it a potential as a gas management tool in underground coal mines [10]. Archibald and De Souza [11] measured the radon gas blocking capacity and gas permeability of different TSL materials and thicknesses. They emphasised the potential use of TSLs in restricting hazardous gas inflows. Mass and Renken [12] assessed the effectiveness of different cementitious coatings as barriers to radon gas entry. Their results showed that the coatings tested all exhibited excellent permeability as they were 2 to 3 orders of magnitude smaller than the average concrete permeability. Further results indicated that any sealant placed on a highly permeable concrete would greatly reduce the permeability. Saghafi and Roberts [13] reported measurements of the permeability of a common TSL product for methane (CH₄), carbon dioxide (CO₂) and carbon monoxide (CO). Their results indicated that the permeability of TSLs were in the range of nanodarcies. They also pointed out that the permeability for CH₄ and CO₂ were very similar while the permeability for CO was a few times higher. Hussain

et al. [10] conducted permeability tests on coal samples coated with three different TSLs for CO₂ and nitrogen (N₂). This was the first test that had investigated the interaction between TSLs and coal. The experimental results showed that the TSLs tested can reduce gas permeability of coal by up to three orders of magnitude. However, their tests did not consider the permeability of CH₄ and the effect of gas adsorption during the test.

In this study, laboratory gas flow tests were conducted on intact and treated dry coal samples to study TSLs' potential for gas management in underground coal mines. The tested gases included CH₄ and CO₂, as they are the common gases in coal seams. In order to study the influence of gas adsorption on the permeability, helium was also used as a control gas. In this paper, the permeability test results are presented and analysed.

2. Test preparation and execution

2.1 Test apparatus

The permeability of a coal sample is measured by injecting dry gas through the sample and measuring the flowrate and differential pressure across the sample. A "Hassler" type core holder was used to conduct single phase gas flow tests on the samples. A schematic view of the permeability test apparatus is shown in Figure 1. A cylindrical coal sample was placed in a Viton sleeve attached to a core holder. Then a confining pressure of 1.72 MPa (250 psi) was applied on the sleeve with a water pump to make sure that the gas will only flow within the coal samples. A leakage test was also conducted to make sure that there was no leakage for both the confining part and injection part. The outlet was open to atmosphere and the flowrate of gas was measured by a flowmeter. After the pressure and flowrate were established, the values were recorded.

Using the following Darcy equation modified for compressible gas flow, the gas permeability is calculated:

$$k = \frac{2 \times 10^3 q_g \mu P_a}{A \Delta P^2} \quad (1)$$

k = coefficient of permeability (mD),

q_g = exit flowrate (cm³/s),

μ = viscosity of air at temperature of test (mPa·s),

L = length of sample (cm),

P_a = atmospheric pressure (bar),

A = cross section area of sample (cm²),

ΔP^2 = difference between injection and outlet pressures squared (bar²).

The Klinkenberg slippage correction [14] to the permeability was not applied in this study. To apply the Klinkenberg slippage correction, the permeability tests needs to be conducted under different pressures. However, coal permeability is pressure dependant due to different degrees of gas adsorption and stress effects under different pressure [15, 16]. Therefore, the pressure differential across the samples was constantly kept around 1 MPa (145 psi) for all tests in order to make reasonable comparisons between the measured results.

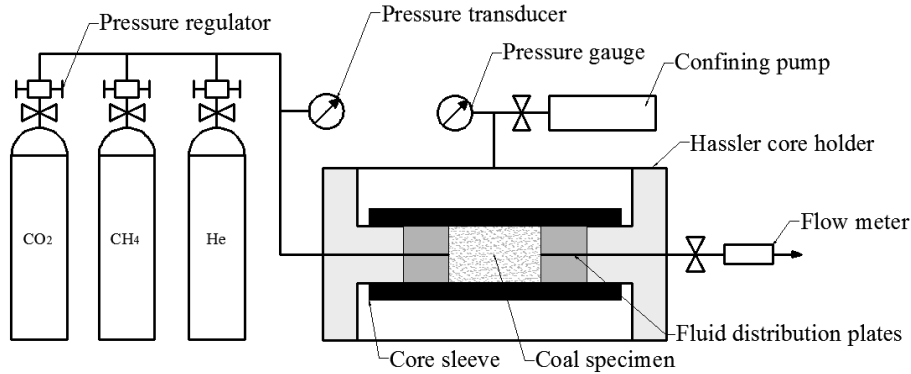


Fig. 1. Schematic view of permeability test apparatus.

2.2 Sample preparation

An adequate supply of homogeneous material is necessary for sample preparation. The selection of coal samples should provide a representative array of permeability values. In order to investigate the influence of bedding planes on the permeability results, two types of samples were prepared; parallel and normal to bedding planes. For each condition, three samples were used to conduct the permeability tests. The dimensions of the coal samples and TSL thicknesses can be seen in Table 1.

Table 1. Dimensions of coal samples for permeability tests.

Bedding planes	Sample No.	Length mm	Diameter mm	TSL thickness mm
Parallel	CP-1	60.79	26.10	4.84
	CP-2	57.87	26.04	5.25
	CP-3	49.56	26.08	5.13
Normal	CN-1	63.54	26.09	5.54
	CN-2	65.21	26.21	5.07
	CN-3	66.26	26.06	4.58

Under confining pressure, the coal is subjected to mechanical stress and this stress can affect the permeability significantly [17, 18]. The coal samples were covered by Araldite to minimise the effect of confining pressure. Figure 2 shows the coal samples before and after the TSL application. The test sample preparation process is summarised as follows:

- drill cylindrical core samples with 26 mm ID diameter coring bit;
- the end of the core samples should be cut with a diamond saw to be perpendicular to the axis;

- dry the sample in an oven under the temperature of 50°C for 48 hours;
- prepare a Perspex pipe (outer diameter = 38mm) which has the same length as the sample, then put the sample inside the pipe centrally;
- prepare araldite resin and pour it into the annular space between the pipe and sample, then allow to dry for 24 hours;
- cut both ends of the araldite-covered sample to make smooth surface;
- finished samples were evacuated at room temperature and stored in a fridge under the temperature of 5 °C to prevent contamination until testing.

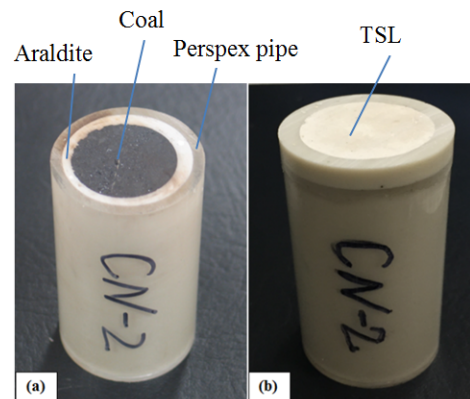


Fig. 2. Coal sample before (a) and after TSL application (b).

2.3 Test methodology

Carbon dioxide, methane and helium were chosen as the gas phases in the experiments. There are several

reasons for this. Firstly, coal seam gas is primarily composed of CH_4 and CO_2 , and they are main gases of concern in underground coal mines [10]. Therefore, permeability tests were carried out with both CO_2 and CH_4 to evaluate the effect of TSLs in reducing gas inflow. Secondly, the injection of CO_2 and CH_4 will reduce the permeability of coal, as CO_2 and CH_4 will adsorb onto the microscopic surfaces of the coal's molecular structure and swells the coal [19, 20]. Previous work also suggests that CO_2 has a higher tendency than CH_4 to adsorb onto the surface of coal [21]. In order to study the influence of gas adsorption on the permeability, helium was also used as a control gas.

A systematic procedure has been followed to evaluate the effect of TSLs on gas permeability. The coal

samples were firstly tested without TSL application. For each sample, helium was injected before and after the injection of CO_2 and CH_4 , with an injection order of He- CO_2 -He- CH_4 -He. In order to minimise the influence of adsorption and desorption on the permeability of CO_2 and CH_4 , the samples were saturated for 12 hours before the injection and vacuumed for 12 hours after the injection. In order to investigate the effect of TSLs on the gas permeability, the chosen TSL was applied on the outlet face of the cylindrical coal samples with a uniform thickness. Then the permeability test mentioned above was repeated to compare the permeability change for CO_2 , CH_4 and He

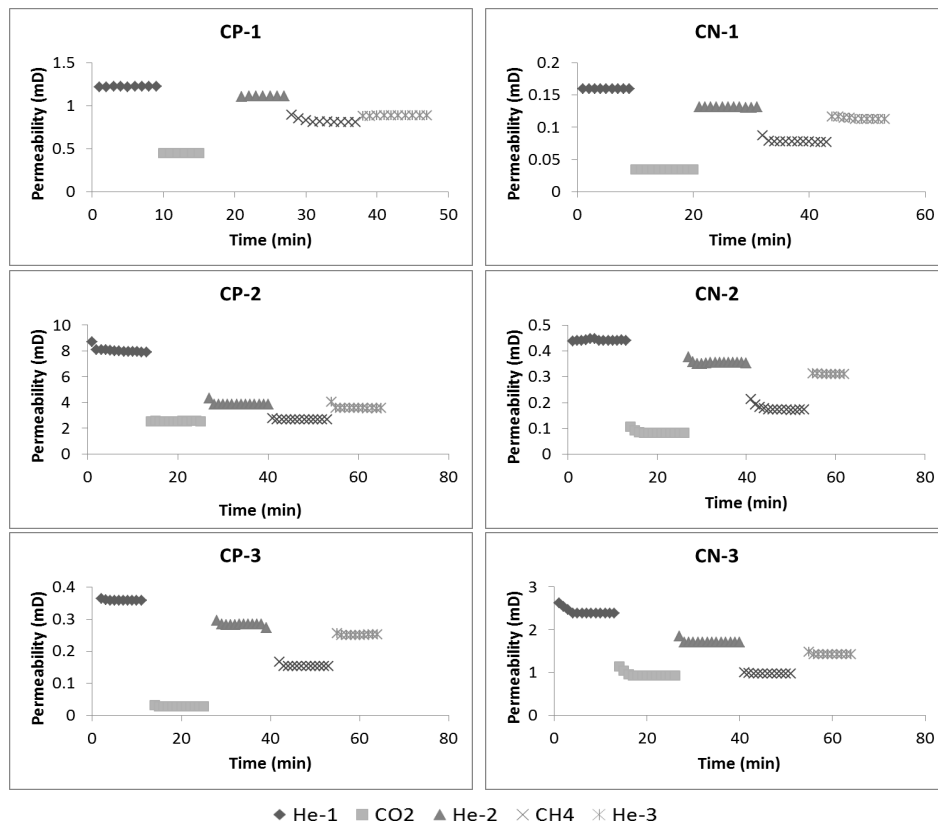


Fig. 3. Gas permeability test results before TSL application for samples parallel to bedding planes (CP 1-3) and normal to bedding planes (CN 1-3).

3. Permeability results before TSL application

The permeability test results before application of TSLs are shown in Figure 3. For each sample, the test includes one CO₂, one CH₄, and three He gas flow tests. Generally, all the samples show the following similar trends:

- the He injection gave the highest permeability, while the CO₂ injection gave the lowest permeability.
- the first injection of He provided the highest permeability; the injection of CO₂ reduced the He permeability; while CH₄ injection reduced the He permeability further.

Helium was used as a control gas to investigate the permeability drop after the injection of CO₂ and CH₄. By taking the first injection of He as the original permeability, the permeability drop is calculated as follows:

$$\text{Permeability drop} = \frac{k_i}{k_0} \quad (2)$$

k_0 = permeability for the first injection of He (mD),

k_i = permeability for the second or third injection of He (mD).

Based on the above equation, the permeability drop was calculated and is shown in Figure 4. Although the permeability drop varies from sample to sample, a general trend can be found that the injection of CO₂ and CH₄ decreases the permeability of He, with an average permeability drop around 75% after the tests with CO₂ and 64% after the tests with CH₄.

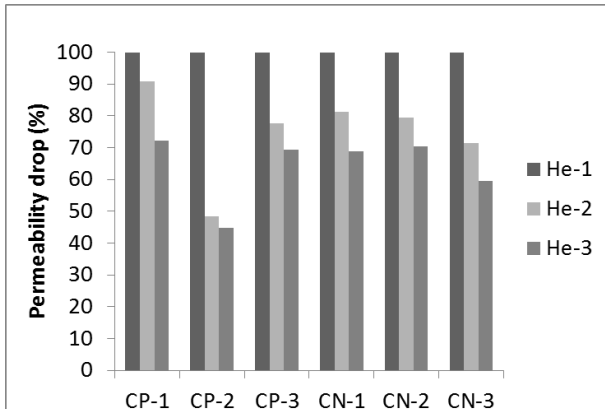


Fig. 4. Permeability drop after CO₂ and CH₄ injection.

The permeability results for CO₂ and CH₄ are listed in Table 2. Although the permeability of CH₄ is higher than CO₂, the permeability ratio between CH₄ and CO₂ varies significantly from sample to sample, with the value ranging from 1.05 to 5, as shown in Table 2. This may be due to the difference of mineral substance between different samples.

Table 2. Permeability results for CO₂ and CH₄.

Sample No.	k_{CO_2}	k_{CH_4}	k_{CH_4}/k_{CO_2}
CP-1	0.45	0.81	1.80
CP-2	2.54	2.66	1.05
CP-3	0.03	0.15	5.00
CN-1	0.03	0.08	2.67
CN-2	0.08	0.17	2.13
CN-3	0.92	0.97	1.05

Homogeneous, unfractured coal is relatively impermeable to gas. The permeability of larger coal masses is predominantly a result of the presence of the cleat [19]. As a natural fractured system, coal generally contains two distinct types of cleats (face and butt cleats), forming a continuous network structure containing individual blocks of coal matrix [22]. Face cleats are continuous and can extend for long distances while butt cleats, which are oriented perpendicular to the face cleat, are short and discontinuous [23]. Due to the nature of these cleat systems, face cleats are more permeable than butt cleats to gas and water. Therefore, coal seam permeability parallel to bedding planes is significantly higher than normal permeability, which is concluded as permeability anisotropy [24].

The average permeability results for parallel and normal to bedding planes are shown in Figure 5. For both CO₂ and CH₄, the permeability results parallel to bedding planes are much higher than normal to bedding planes. Specifically, the average CO₂ permeability parallel to bedding planes is 1.01 mD compared with 0.34 mD normal to bedding planes; while the CH₄ permeability results are 1.21 mD and 0.41 mD for parallel and normal to bedding planes, respectively.

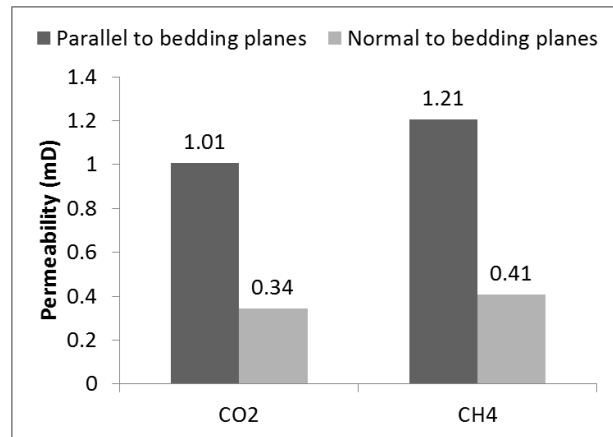


Fig. 5. Permeability results for samples parallel and normal to bedding planes.

4. Permeability results with TSL application

A polymer/cementitious TSL was applied on the outer side of the coal sample with an average thickness of 5 mm. This thickness is also a recommended thickness for applying TSL as a ground support tool [4]. After preparation, permeability tests mentioned above were repeated on these samples, and no gas flow was measured. With the current flowmeter used, it can be concluded that the flowrate is lower than 0.16 ml/min and the permeability results for all the samples are lower than 0.001 mD. The results indicate that the application of TSLs can reduce the permeability by at least 2-3 orders of magnitude.

5. Conclusions

Single phase gas permeability tests were conducted on coated coal samples to investigate the potential of using TSLs as a gas management tool in underground coal mines. Carbon dioxide, methane and helium were used for carrying out the permeability tests with/without TSL application.

The Helium permeability provided the highest value; the CO₂ permeability gave the lowest value and the CH₄ permeability is between CO₂ and He.

The injection of CO₂ and CH₄ decreased the permeability of He. After the injection of CO₂, the He permeability was about 74% of the original permeability; subsequently, after the injection of CH₄, the He permeability was further decreased to 63% of the original value.

The permeability of CH₄ is higher than CO₂; however, the permeability ratio between CH₄ and CO₂ varies significantly from sample to sample, with the value ranges from 1.05 to 5.

The permeability parallel to bedding planes is significantly higher than that normal to bedding planes. This conforms with previous research results. This is due to the nature of cleat systems inside coal: face cleats are more permeable than butt cleats.

After TSL application around 5 mm in thickness, no gas flow was measured through the coal samples. The chosen TSL can reduce the gas permeability by at least 2-3 orders of magnitude.

6. Recommendations

Permeability tests are recommended to be conducted with much higher accuracy flowmeter to determine the exact permeability of coal with TSL application. Different TSL materials are also recommended to be used for the permeability tests.

The experimental results from this study show that the TSL chosen is very efficient in controlling gas flow through coal. The results also indicate advantageous potentials for using TSL as a gas management tool in underground coal mines. In order for this technology to become a viable tool for gas management, research emphasis should be put on multiple field trials of TSLs under various conditions.

Apart from the benefits of using TSL as a gas management tool, the application of TSL could also bring many other benefits, such as ground support and

ventilation benefits. A model should be built to evaluate the cost benefits of TSLs for underground coal mines.

Acknowledgments

The authors would like to thank the TSL Company for providing the TSL material and the mine site for providing coal samples for testing. The first author would also like to thank China Scholarship Council (CSC) for supporting his study in Australia.

References

- [1] K. Noack, Control of gas emissions in underground coal mines, *International Journal of Coal Geology*, 35(1-4) (1998) 57-82.
- [2] L.W. Lunarzewski, Gas emission prediction and recovery in underground coal mines, *International Journal of Coal Geology*, 35(1-4) (1998) 117-145.
- [3] C.Ö. Karacan, F.A. Ruiz, M. Cotè, S. Phipps, Coal mine methane: a review of capture and utilization practices with benefits to mining safety and to greenhouse gas reduction, *International Journal of Coal Geology*, 86(2) (2011) 121-156.
- [4] S. Saydam, Y.S. Docrat, Evaluating the adhesion strength of different sealants on Kimberlite, in *Proceedings the 11th Congress of International Society of Rock Mechanics* (Lisbon, Portugal) (2007) 585-588.
- [5] D.D. Tannant, Thin spray-on liners for underground rock support testing and design issues, in *Proceedings the 1st International Seminar on Surface Support Liners: Membrane, Shotcrete and Mesh* (Perth, WA, Australia) (2001).
- [6] H. Yilmaz, S. Saydam, A.Z. Toper, Emerging support concept: thin spray-on liners, *Chamber of Mining Engineers of Turkey 18th International Mining Congress and Exhibition of Turkey* (Antalya, Turkey) (2003).
- [7] J.S. Kuijpers, E.J. Sellers, A.Z. Toper, T. Rangasamy, T. Ward, A.J. Rensburg, H. Yilmaz, D. Stacey, Required technical specifications and standard testing methodology for thin sprayed linings, Johannesburg, RSA, 2004.
- [8] S. Gilbert, S. Saydam, R. Mitra, Laboratory investigation of the potential use of thin spray-on liners in underground coal mines, *The symposium of extracting the science: a century of mining research* (Littleton, CO, USA) (2010) 225-234.
- [9] Z. Li, S. Saydam, R. Mitra, D. Chalmers, Investigation on adhesion strength of thin spray-on liners in an underground coal mine, in *Proceedings the Coal Operators' Conference 2015* (Wollongong, NSW, Australia) (2015) 192-198.
- [10] F. Hussain, S. Saydam, R. Mitra, Y. Cinar, Experimental study for reducing gas inflow by use of thin spray-on liners in underground coal mines, *Mining Technology*, 121(2) (2012) 61-67.
- [11] J.F. Archibald, E. De Souza, Mine support, radiation and ventilation control with spray-on barriers, *American Nuclear Society Symposium on High Level Nuclear Waste Management* (Las Vegas, NV, USA) (1993) 1770-1777.

- [12] J.J. Mass, K.J. Renken, Laboratory assessment of cementitious coatings as a barrier to radon gas entry, in *Proceedings the 1997 International Radon Symposium* (Cincinnati, OH, USA) (1997) 1.1-1.13.
- [13] A. Saghafi, D. Roberts, Study of the gas permeability of Tekflex used as a sealant in underground coal mines 2001.
- [14] L.J. Klinkenberg, The permeability of porous media to liquids and gases, *Drilling and production practice* (1941) 200-213.
- [15] F. Zhou, F. Hussain, Y. Cinar, Injecting pure N₂ and CO₂ to coal for enhanced coalbed methane: experimental observations and numerical simulation, *International Journal of Coal Geology*, 116 (2013) 53-62.
- [16] F. Zhou, F. Hussain, Z. Guo, S. Yanici, Y. Cinar, Adsorption/desorption characteristics for methane, nitrogen and carbon dioxide of coal samples from Southeast Qinshui Basin, China, *Energy, Exploration & Exploitation*, 31(4) (2013) 645-666.
- [17] W.H. Somerton, I.M. Söylemezoğlu, R.C. Dudley, Effect of stress on permeability of coal, *International Journal of Rock Mechanics and Mining Sciences & Geomechanics Abstracts*, 12(5-6) (1975) 129-145.
- [18] S. Durucan, J. Edwards, The effects of stress and fracturing on permeability of coal, *Mining Science and Technology*, 3(3) (1986) 205-216.
- [19] G.R. King, T. Ertekin, F.C. Schwerer, Numerical Simulation of the Transient Behavior of Coal-Seam Degasification Wells, *SPE Formation Evaluation* (1986) 165-183.
- [20] A. Saghafi, M. Faiz, D. Roberts, CO₂ storage and gas diffusivity properties of coals from Sydney Basin, Australia, *International Journal of Coal Geology*, 70(1-3) (2007) 240-254.
- [21] R. Pini, S. Ottiger, G. Storti, M. Mazzotti, Pure and competitive adsorption of CO₂, CH₄ and N₂ on coal for ECBM, *Energy Procedia*, 1(1) (2009) 1705-1710.
- [22] G.G. Wang, X. Zhang, X. Wei, X. Fu, B. Jiang, Y. Qin, A review on transport of coal seam gas and its impact on coalbed methane recovery, *Frontiers of Chemical Science and Engineering*, 5(2) (2011) 139-161.
- [23] J. Shi, S. Durucan, Gas storage and flow in coalbed reservoirs: Implementation of a bidisperse pore model for gas diffusion in coal matrix, *SPE Reservoir Evaluation and Engineering*, 8(2) (2005) 169-175.
- [24] S.J. Schatzel, C. Karacan, R. Krog, G. Esterhuizen, G. Goodman, Guidelines for the prediction and control of methane emissions on longwalls, Department of Health and Human Services, Centers for Disease Control and Prevention, National Institute for Occupational Safety and Health, Pittsburgh Research Laboratory, 2008.

Effect of Decreasing Barometric Pressure on Explosive Gas Zones in Bleeder Ventilated Longwall Gobs

Samuel A. Lolon^a, Richard C. Gilmore^a, Jürgen F. Brune^a, Gregory E. Bogin, Jr.^a, John W. Grubb^a, R. Karl Zipf, Jr.^a, Aditya Juganda^a, Saqib A. Saki^a.

^a *Colorado School of Mines, Golden, Colorado*

Mine explosions have long been known as a catastrophic risk in underground coal mining. Since 1970, the U.S. coal mine industry experienced 12 major disasters associated with methane explosions; most of which occurred during a significant drop in barometric pressure. Several of these disasters and numerous other explosions of lesser consequence suggest involvement of explosive gas zones (EGZs) or explosive methane-air mixture. Previous studies by researchers at the Colorado School of Mines (CSM) have been aimed at locating and reducing EGZs in longwall gobs but little work has been done to investigate the effect of barometric pressure on these EGZs.

In a new research project at CSM, funded by The National Institute for Occupational Safety and Health (NIOSH), the authors investigate how the locations and volumes of EGZs in bleeder ventilated longwall gobs change with decreasing barometric pressures. This work is being done using Computational Fluid Dynamics (CFD) modeling. In the simulated longwall panel, the authors found that the decreasing barometric pressure significantly affects EGZs size and shape. During barometer drops, explosive methane may expand and migrate from the gob into active working areas, exposing miners to potential hazards of explosion and fire. Research results suggest the need for thorough gas monitoring along the periphery of the longwall and in the bleeder entries.

Keywords: Barometric pressure, bleeder ventilation, methane explosion, longwall gob, computational fluid dynamics, explosive gas zone

1. Introduction

Methane gas explosions have long been a prevalent risk in underground coal mines. Many coal mine explosions including the Monongah mine disaster (December 1907), the deadliest in U.S. mining history, have occurred during fall and winter seasons of the year. Not only in the U.S., but also in other countries, the coal industry has experienced catastrophic explosions mostly during the colder season when abrupt barometric pressures changes are more frequent [1-3].

Fluctuations in barometric pressure can disturb the pressure balance between ventilated and sealed areas. For longwall mines, this will cause the gob to “breathe” in and out. A decreasing barometric pressure causes an outflow of contaminated air from the gob into the active mining area. Conversely, an increase in barometric pressure may result in fresh air ingress into the gob. The term “explosive gas zone (EGZ)” is used to describe zones of explosive methane-air mixtures within the gob. Brune [4] discussed evidence from numerous mine explosions that suggests that EGZs have formed within longwall gobs. EGZs can be ignited inside the gob or pushed out from the gob to active mine areas and explode there.

2. Natural causes of barometric pressure variation

Fauconnier [5] studied that pressure changes associated with cyclonic weather systems are the major contributing factor to gas explosions in mines. The diurnal and semidiurnal oscillations causes variations of surface barometric pressure. These oscillations are predominantly driven by the solar heating of the stratosphere and gravitational forces of the moon and sun that induces air movement and inhomogeneous temperature and pressure distribution over the earth [6]. Often, such events can result in a storm that causes a quick drop and rise in barometric pressure. Commonly the magnitude of changes due to a storm are higher than that due to normal diurnal cycles.

Figure 1 shows an example of yearly barometric pressure fluctuation near a mine site. The largest drop in this example was nearly 2000 Pa recorded over the course of 4 days. During a 12-month period, the fluctuation patterns are easily identifiable: mid-May through September and October through mid-May. Pressure changes appear more abrupt and intense during

the fall through winter seasons, gradually abate in spring, and are much steadier during the summer season. This is

a typical fluctuation trend in a yearly period [1-3, 5].

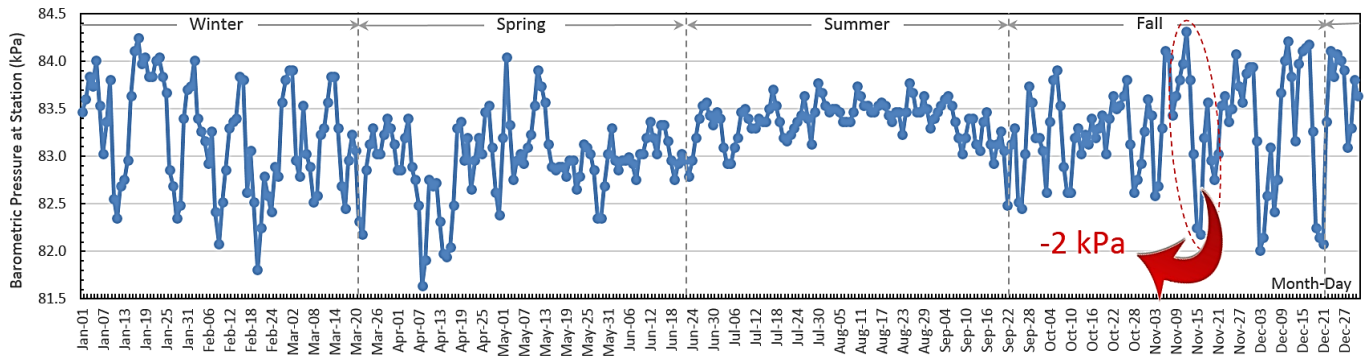


Fig. 1. Yearly profile of barometric pressure at a mine site.

Gob gases will expand or contract in response to these pressure changes. Field investigations have demonstrated a finding of higher methane emitted during drops in barometric pressure [1, 7-8].

3. U.S. coal mine explosions versus barometric pressure

Little work has been done to thoroughly study the gas inflow and outflow across longwall gob or sealed areas triggered by barometric pressure changes. However, a number of studies have related mine explosions to barometric pressure changes. Statistical analyses by Boyer, Kissel et al. and Hosler [2-3, 9] studied the impact of barometric drops on several major U.S. coal mine disasters prior to 1970. Similarly, Fauconnier [5] and Hemp [10] studied the effect of barometric pressure drops on gas explosions in South African mines.

In agreement with those earlier studies, most disastrous mine explosions in the U.S. since 1970 were also found to have occurred primarily from November through April (Table 1). Major disasters, as defined by the U.S. Mine Safety and Health Administration (MSHA), are accidents with five or more fatalities. Note that the table only includes such major disasters that are associated with methane explosion based on MSHA investigations [11]. Explosions caused by coal dust being ignited during blasting are excluded from the list such as those that happened at Finley Coal #15 and #16, Adkins #11, and at the RFH #1 mine.

Also shown in Table 1 are the average barometric pressure changes and number of preceding days (in parenthesis) of which these changes begin prior to the explosion. For example, a pressure drop of nearly 1600 Pa was recorded over the 2 days preceding the first explosion

at Scotia mine. For each explosion, daily barometric pressure records were obtained from three weather stations near the mine. Data are available from the National Weather Service database [12]. Barometric pressure values shown in Table 1 were selected from the station closest to the mine.

Table 1. U.S. major coal mine explosions associated with methane explosion from 1970 through 2014.

Mine	Date	Mine Type ¹⁾	Total Fatalities	Avg. Baro. Pres. Change, Pa (Preceding Days)
Itmann #3	12/16/72	RP	5	+508 (1)
Scotia ²⁾	3/9-11/76	RP	26	-1,591 (2)
Ferrel #17	11/7/80	RM	5	-779 (1)
Dutch Creek #1	4/15/81	LW	15	-34 (1)
Grundy #21	12/8/81	LW	13	-914 (3)
McClure #1	6/21/83	LW	7	+68 (3)
Pyro #9 Slope	9/13/89	LW	10	-237 (1)
Southmtn #3	12/7/92	RP	8	-609 (2)
JWR #5	9/23/01	LW	13	-203 (1)
Sago	1/2/06	RP	12	-440 (1)
Darby #1	5/20/06	RP	5	+576 (2)
UBB	4/5/10	LW	29	-271 (1)

Notes: ¹⁾ LW=longwall mine; RP=room and pillar; RM=retreat mine.
²⁾ Barometric pressure trend of the first explosion.

Most of the explosions listed in Table 1 occurred during and after a drop in barometric pressure in the fall and winter seasons including the Itmann #3 mine explosion. A nearby station recorded a barometric pressure drop of nearly 1422 Pa over a four-day period before it changed direction and went up by 508 Pa on the day prior to the explosion [12]. Interestingly, two explosions, McClure #1

and Darby #1, happened in the late spring and summer seasons. Slight barometric pressure increases were observed prior to the explosions in both mines. Investigations determined that the McClure #1 explosion was caused by inadequate ventilation to dilute methane, unrelated to a barometric pressure change. The Darby #1 mine explosion occurred near the seals of an abandoned area when miners were performing flame cutting outby one of the seals. As the barometric pressure had been rising for two days prior to the explosion, fresh air may have leaked into the sealed area, creating an explosive methane-air-atmosphere behind the seals. Despite increasing daily trends, hourly records indicated that the barometric pressure started to drop immediately before the explosion. This may have caused the explosive methane-air mixture to leak out from the sealed area. The explosion at the Sago mine is also considered independent of barometric pressure effects. MSHA investigators determined that a massive lightning strike was the most likely cause for this explosion [11] though barometric pressure drop was noted before the explosion.

As shown in Table 1, there are two characteristics of pressure changes that need further analysis in the follow-up research: the absolute magnitude and rate of change. It is understood that these characteristics play an important role in gob “breathing”. Their significance much depends on gob size and porosity, ventilation system, reservoir pressure of methane and many other factors. A certain magnitude of pressure change can increase explosion risk in a mine, but may be insignificant in other mines. For example, Belle [8] documented a notable increase of methane levels in the tailgate entry of a highly gassy mine for daily barometric pressure drop greater than 500 Pa. For non-gassy mines, this magnitude may result in negligible methane emissions.

Literature review indicates that mine explosions are complex events involving multiple factors. Therefore, it is sometimes difficult to isolate the impact of barometric pressure changes and their contribution to the event. Still, the analysis in Table 1 suggests that barometric pressure fluctuations have contributed to the events even if they were not the primary cause.

4. CFD modeling of barometric pressure variations

The use of computational modeling tools permits a more detailed analysis of barometric pressure effects on EGZs in longwall gobs that are largely inaccessible to direct measurements. In 1988, the U.S. Bureau of Mines

initiated a development of a computer program called Gob Assistant to analyze the gas flows into and out of gob areas due to barometric pressure changes [13]. More recently, Yuan and Smith [14] applied Computational Fluid Dynamics (CFD) to investigate barometric pressure influence on spontaneous heating in the gob. Researchers at CSM have used CFD to identify EGZ volumes and their locations in longwall gobs. With robust capabilities to handle fluid dynamic issues, CFD is a powerful tool to simulate mine ventilation condition changes associated with barometric pressure variations.

4.1 CFD longwall models and parameters

For this study, a 3-D bleeder ventilation model was developed using the Ansys Fluent[®] CFD software package. The model is a modification of a longwall panel developed by Marts et al. [15]. For simplification, this model does not include Gob Ventilation Boreholes (GVBs), nitrogen injection or other gob gas controls. The modeling objective was to isolate the gas flow communication between gob and the surrounding bleeder entries. The observations are focused on an area of 1,400 ft (430 m) inby the longwall face.

Figure 2 illustrates the layout of the panel and ventilation system used in this study. The simulated model block is 1000-ft (300-m) wide and 130-ft (40-m) high and includes a 40-ft (13-m) high, caved gob area, an 80-ft (24-m) high fractured zone and 6.5-ft (2-m) thick rider seam above the gob. The mine entries are typical 11-ft (3.3-m) by 20-ft (6-m) openings. Gob porosities of 14 to 40% were predicted from a FLAC 3D geomechanical model of the overlying strata and have previously been validated with actual mine subsidence data [16]. The gob permeability is calculated using the Carman-Kozeny relationship and ranges from 2×10^{-7} to $5.1 \times 10^{-6} \text{ m}^2$. Permeability and porosity distribution in the gob is shown in Figure 3.

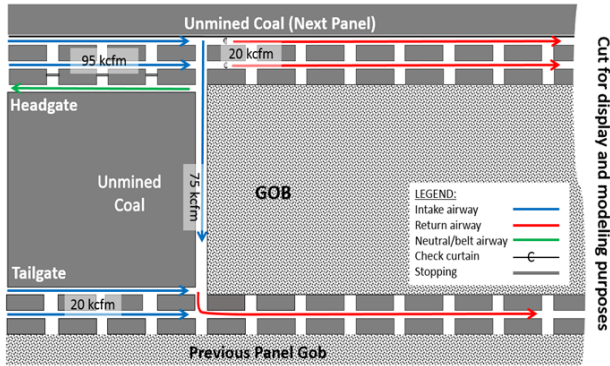


Fig. 2. Plan view of the simulated panel and ventilation arrangement.

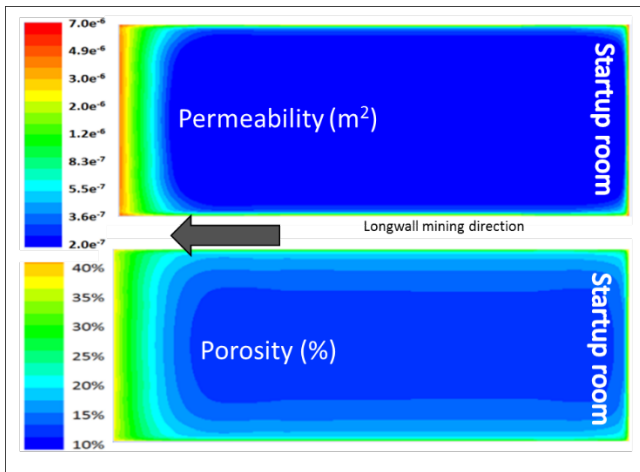


Fig. 3. Permeability and porosity distribution used in this study [16]. (Reprinted with permission)

Modeling parameters used in this study are shown in Table 2. A barometric pressure drop of 2,000 Pa, as shown in Figure 1, represents a significant atmospheric condition that a mine might experience. The simulated pressure drop rate is 17 Pa per hour. A user-defined function was developed to input this rate into the CFD model to simulate a time-dependent pressure profile. The pressure drop was superimposed to all ventilation inlet and return boundary conditions.

Table 2. Modeling parameters used in this study.

Parameter	Value
Pressure drop rate (Pa/hour)	17
Ventilation intake and return pressures range (Pa)	30 – 2,100
Avg. face ventilation (cfm)	75,000
Avg. face air velocity (m/s)	1.7

Inlet and outlet pressures were pre-estimated such that flow rate of ventilation air across the face reached 75,000

cfm at an average velocity of 1.7 m/s. Methane enters the model from the rider seam located above the fractured zone at an estimated pressure of 7,408 Pa. This is estimated twice as high as methane emission pressure used in a previous study by Gilmore et al. [16] to investigate the condition in the gob area near the face.

4.2 Modeling results

A base case was modeled at a steady, standard atmospheric pressure of 101 kPa. Subsequent cases of simulating barometric pressure change were compared to this base case. Time-step transient modeling was selected as opposed to a steady state run for these simulations. This allowed researchers to monitor and analyze changes in fluid flow, EGZ location and volume during the drop in barometric pressure.

Modeling produces visual diagrams of the explosibility characteristics of the gob atmosphere as shown in Figure 4. This diagram and details of this work have been published in a research paper by Marts et al [15] and Gilmore et al. [17]. The algorithm produces color codes to characterize the methane-air mixture based on the Coward's triangle [18]. EGZs are colored red, fresh air atmospheres blue, methane-rich inert gas mixtures yellow and methane- and oxygen-lean mixtures are colored green. Finally, the orange color denotes a zone with a near-explosive atmosphere.

Figure 5 shows the EGZ formation in the gob under base case conditions. A methane-rich zone is found in the center of the gob, while fresh air migrates into the gob behind the face and from the gate roads or bleeder entries. The permeability profile (see Figure 3) is a key factor for this methane distribution. EGZs, displayed in red, occur along the fringes between fresh air zones and the methane-rich center of the gob, where methane and air mix at explosive levels (i.e. 5-15% CH₄ and > 12% O₂).

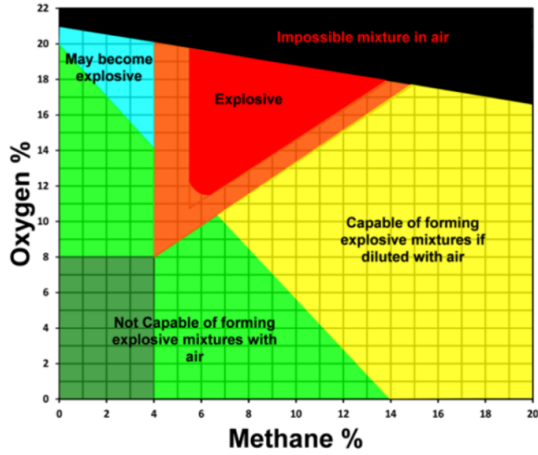


Fig. 4. Explosibility characterization – modified after Coward's triangle [15, 18] (Reprinted with permission).

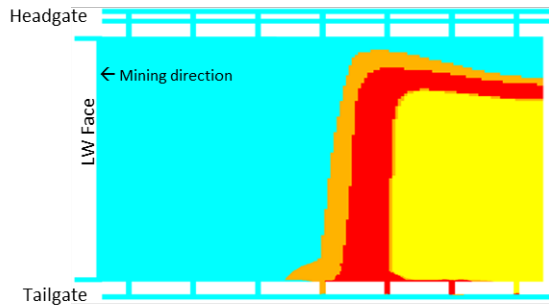


Fig. 5. Initial condition of EGZ in the gob. Colors refer to Fig. 4. The view plane is at 1.5 m above the gob floor.

As the barometric pressure drops, the EGZ volume in the gob increases. Figure 6a shows the red fringes that initially occur in the gob. These fringes are pushed out from the gob into the tailgate entry within hours following the pressure drop. Further decrease in barometric pressure causes the EGZ to expand towards the headgate entries. Figures 6c and 6d show EGZ fringes developing in the headgate bleeders. This condition exposes miners traveling these airways to explosion and fire hazards as well as asphyxiation due to lack of oxygen.

Figure 7 shows the normalized volume of EGZ modeled in the gob during the 24-hr downward trend of barometric pressure. As indicated in Figure 6, the EGZs expand significantly.

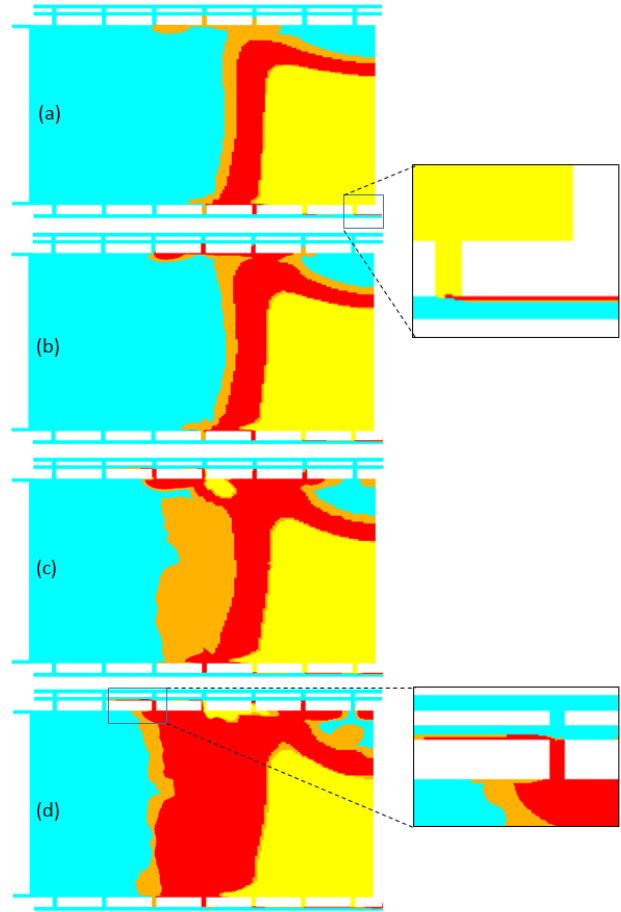


Fig. 6. EGZs in the gob after (a) 6 hours, (b) 12 hours, (c) 18 hours, and (d) 24 hours of barometric pressure fall. Colors refers to Fig. 4.

Brune [4] and Gilmore et al. [16] have predicted EGZ fringes in and around the gob through CFD simulation and from investigation reports of historical mine explosions and fires. This study shows that these fringes appear to be highly dependent on barometric pressure changes. Pressure changes cause them to move and expand from the gob into adjacent, active mine workings. CFD modeling shows the initial expansion towards the tailgate side. This is in agreement with longwall data analysis conducted by Belle [8] that concludes a significant role of barometric pressure changes on the tailgate gas levels.

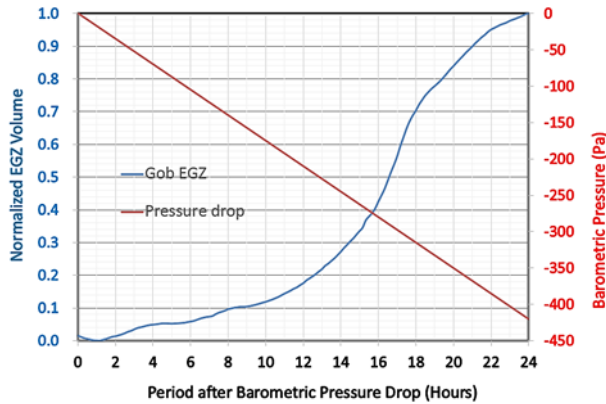


Fig. 7. Normalized EGZ volume in gob as a function of barometric pressure drop.

4.3 Conclusions and plans for future works

It is widely perceived that barometric pressure changes can affect the gas composition in longwall mine gobs. The fact that most of major mine explosions occurred during or after a sudden drop in barometric pressure supports this barometric effect on the mine atmosphere. CFD modeling demonstrates that the EGZs in the longwall gob can increase in size and are pushed out from the gob into active mine workings during barometric pressure drops, exposing miners to hazards of explosion, fire and asphyxiation. Initial modeling indicates that EGZs are more likely to be pushed towards the tailgate in bleeder ventilated gobs.

To better understand the barometric pressure variation effect on EGZs in longwall gobs, follow-up research will focus on the development of similar studies for progressively sealed longwall panels which are more common worldwide. Understanding barometric pressure effects will enable researchers to further develop safety practices for mine operation in response to barometric pressure changes. These practices may include atmospheric monitoring combined with early warning systems and ventilation strategies to prevent EGZ formation, including Gob Ventilation Boreholes (GVBs), nitrogen injection, and potentially, ventilation controls that can temporarily rebalance or increase the mine pressure.

Acknowledgements

The authors and researchers gratefully acknowledge the support from the National Institute for Occupational Safety and Health (NIOSH) under contract number 211-2014-60050 that made this research possible.

References

- [1] C.B. McIntosh, Atmospheric conditions and explosions in coal mines, *The Geographical Review* Vol.47 No.2 (1957) 156-174.
- [2] R.F. Boyer, Coal mine disasters: frequency by month, *Science* 19 Vol. 144 No. 3625 (1964) 1447-1449.
- [3] F.N. Kissell, A.E. Nagel, and M.G. Zabetakis, Coal mine explosions: seasonal trends", *Science* Vol. 179 No. 4076, (1973) 891-892.
- [4] J.F. Brune, The methane-air explosion hazard within coal mine gobs, *SME Transactions*, Vol. 334 (2013) 376-390.
- [5] C.J. Fauconnier, Fluctuations in barometric pressure as a contributory factor to gas explosions in South African mines, *Journal of the South African Institute of Mining and Metallurgy*, (1992) 131-147.
- [6] R.S. Lindzen, R.S. and S. Chapman, Atmospheric tides, *Space Science Reviews* 10.3-188, D. Reidel Publishing Co., Dordrecht-Holland.
- [7] S. Wasilewski, Influence of barometric pressure changes on ventilation conditions in deep mines, *Arch. Min. Sci.*, Vol. 59, No.3 (2014) 621-639.
- [8] B. Belle, Evaluation of barometric pressure (BP) and cage effect on longwall tailgate gas levels, *10th International Mine Ventilation* (2014).
- [9] C.L. Hosler, Atmospheric surface pressure related to coal mine explosions, *Trans. Am. Geophys. Union* Vol. 29 No.5 (1948) 607-612.
- [10] R. Hemp, The effect of changes in barometric pressure on mines in the highveld of South Africa, *Journal of the South African Institute of Mining and Metallurgy*, (1994) 133-146.
- [11] MSHA, Historical summary of mine disasters in the United States, Vol. II – Coal mines, U.S. Department of Labor, MSHA, Coal Mine Safety and Health, U.S. Department of Labor. Reprinted 2001 (1998). Also available at www.msha.gov.
- [12] National Climatic Data Center, National Oceanic and Atmospheric Administration (NOAA), accessed November 2014 through January 2015, <http://cdo.ncdc.noaa.gov/qcled/>
- [13] Foster-Miller, Inc., Final report for improved ventilation of sealed mine gob, Research Contract Report #J0308029, USBM Pittsburgh Research Center (1988), pp.1-21.
- [14] L. Yuan and A.C. Smith (2010), Modeling the effect of barometric pressure changes on spontaneous heating in bleederless longwall panels, *SME Annual Meeting and Exhibit* (2010).
- [15] J.A. Marts, R.C. Gilmore, J.F. Brune, G.E. Bogin Jr., J.W. Grubb, S. Saki, Dynamic gob response and

reservoir properties for active longwall coal mines, Mining Engineering Vol.66 No. 12 (2014), pp. 41-48.

- [16] R.C. Gilmore, J.A. Marts, J.F. Brune, S.A. Saki, G.E. Bogin Jr. and J.W. Grubb, Impact of regulator settings on the formation of explosive gas zones in bleeder ventilated longwall gobs, SME Annual Meeting, Denver (2015) preprint 15-086.
- [17] R.C. Gilmore, J.A. Marts, S.A. Saki, G.E. Bogin, J.W. Grubb and J.F. Brune, CFD modeling of gas flows and explosion hazards in bleeder ventilated and progressively sealed longwall gobs, 10th International Mine Ventilation Congress, Sun City, South Africa, (2014).
- [18] H.F. Coward and G.W. Jones, Limits of flammability of gases and vapors, U.S. Bureau of Mines Bulletin

Ventilation Air Methane Abatement Opportunities for the Coal Industry

Felicia Ruiz^a, Clark Talkington^b, Elizabeth Olson^b

^aUnited States Environmental Protection Agency, Washington, DC, USA

^bAdvanced Resources International, Inc., Arlington, Virginia, USA

Methane is a powerful greenhouse gas and the principal component of natural gas. Coal seams often contain significant quantities of methane. Underground coal mines must ensure that methane released into the mine during coal extraction does not build to dangerous levels. This is accomplished in part through the use of ventilation systems that remove methane from the mine and release it to the atmosphere. Although the methane concentration exhausted is quite low (typically ≤ 1 percent), the volume of air that ventilation systems move is so great that it actually constitutes the largest source of methane emissions from underground coal mines. Each year underground coal mines throughout the world emit more than 500 billion cubic feet of methane from their ventilation systems. In the United States, VAM accounts for 60 percent of total CMM emissions and around 75 percent of underground CMM emissions. Mines that choose to mitigate these emissions can obtain carbon credits as an additional revenue stream. The key drivers for wide-scale VAM project implementation are: (i) market conditions that generate sufficient economic incentives to install and operate VAM equipment; (ii) a sustainable and accessible resource base; and (iii) the legal, technical and policy factors that impact VAM design, installation and operation. Worldwide, the United States has become the most attractive market for VAM projects with the advent of the California Cap-and-Trade program and the acceptance of carbon emission reduction coal mine methane projects into the trading scheme as offsets. At the same time, two commercial projects in operation at active coal mines in the U.S. have provided a laboratory for encountering and overcoming obstacles in successfully deploying VAM abatement technology. The combination of market potential and early mover project experience present a solid foundation for wider acceptance of VAM as a carbon mitigation tool. This paper will examine the VAM resource potential in the U.S., outline the steps necessary to deliver a VAM project, discuss the current and future market conditions that could underwrite increased VAM development, review the current status of operating VAM projects in the United States, and analyze the challenges faced by the project sponsors and how they have overcome those challenges.

Keywords: Coal mine methane, Ventilation air methane, methane emission reductions, coal industry greenhouse gas emissions, methane capture and use

1. Introduction

Methane is the second largest source of anthropogenic greenhouse gases (GHGs), accounting for 16 percent of global GHG emissions [5]. Reduction of methane (CH₄) emissions has become a policy priority in recent years due to methane's high global warming potential (GWP) which is 28 to 34 times greater than that of CO₂ [5].

Underground coal mines are one of the leading sources of anthropogenic, or man-made, methane emissions in the United States. Methane is emitted during mining through mine ventilation and methane degasification systems for safety reasons. Coal mine methane (CMM), however, becomes a potent GHG upon emission to the atmosphere. But not every coal mine is a gassy mine. In the United States, about 30 percent of all active underground mines are considered to be gassy mines by the U.S. Environmental Protection Agency (USEPA), meaning they emit at least 100,000 cubic feet of methane per day [4]. The mining industry, the U.S.

Government and other stakeholders have made significant progress in reducing the industry's methane emissions over the last 35 years. USEPA's Coalbed Methane Outreach Program (CMOP) has led the U.S. Government's efforts to work voluntarily with industry to encourage greater CMM recovery and use. Ventilation Air Methane (VAM) has presented substantial technical and economic challenges due to the low concentration of methane in mine ventilation air. Mine Safety & Health Administration (MSHA) regulations limit shaft concentrations to a maximum of 1 percent in the ventilation circuit with the exception of bleeder shafts, which can have a maximum concentration of 2 percent. Although concentrations are low, the quantity of methane emitted is very high due to the large volumes of mine ventilation air emitted from exhaust shafts. Reducing VAM emissions will therefore have a significant impact on reducing total GHG emissions from the coal mining sector.

Analysis of USEPA data from the Greenhouse Gas Reporting Program (GHGRP) indicates that there are 50 mine shafts in the U.S. that could host a VAM destruction project. Two shafts have existing projects, leaving 48 shafts as prospective hosts for project opportunities. Abatement potential at current carbon prices could total 25 million metric tons of CO₂ equivalent.

The objective of this paper is to examine key drivers for successful project development that are necessary to experience wide-scale deployment of VAM mitigation in the United States. Now that a technology solution has been identified, attention is turning to the steps required to successfully develop projects, including the necessary market conditions to make them attractive investments. More specifically, we examine: (i) the VAM resource base in the U.S. to develop a realistic estimate of technical and economic potential; (ii) market drivers that generate sufficient economic incentives to install and operate VAM equipment; and (iii) the steps required to develop a successful VAM project including the legal, technical and policy factors that impact VAM design, installation and operation.

2. United States Environmental Protection Agency Programs to Promote CMM Recovery and Use

The U.S. Government has had a very active role in promoting CMM capture and use in the United States and in other countries. USEPA, in particular, has played a leading role through two established programs: the Coalbed Methane Outreach Program (CMOP) and the Global Methane Initiative (GMI). CMOP is a voluntary program whose mission is to promote the profitable recovery and use of CMM by working cooperatively with coal companies and related industries. Since its inception in 1994, CMOP has provided technical assistance to U.S. mines through pre-feasibility and feasibility studies evaluating the technical and economic merits of CMM and VAM projects, supporting policy analysis and development, and publishing tools to build the capacity of the coal industry and other stakeholders to implement CMM projects.

The GMI, launched in 2004, is a voluntary, international effort of 42 countries and the European Commission specifically targeting methane abatement, recovery, and use in five economic sectors, including coal. It promotes cost-effective, near-term methane recovery through partnerships between developed and developing countries, with participation from the private sector, development banks, and nongovernmental organizations. The Initiative reduces the informational, institutional, and other market barriers to project development through the development of tools and resources, training and international capacity building,

technology demonstration, and direct project support. Special emphasis is given to bringing together all of the actors necessary for project development, including governments, financial institutions, project developers, technology providers, and others.

CMOP has developed several tools to support reduction of VAM emissions including regular updates on VAM technology development, characterization of VAM emissions at gassy underground mines in the United States, an assessment of the world market for VAM, and grant support for a U.S. VAM demonstration project in partnership with the U.S. Department of Energy. These and other VAM resources may be found at <http://epa.gov/cmop/resources/vam.html>.

The GMI has also developed tools and contributed resources to encouraging greater VAM abatement worldwide. Notable among these are GMI's co-sponsorship of the United Nations *Best Practice Guidance for Effective Methane Drainage and Use in Coal Mines* which addresses good practice for VAM abatement and includes two cases studies of commercial VAM projects [9]. GMI also publishes and regularly updates country profiles of major coal mining countries worldwide with gas resource, VAM and methane drainage data at https://www.globalmethane.org/tools-resources/coal_addresses.aspx. Country-specific VAM studies for India, Russia, and Poland and mine-specific VAM pre-feasibility studies in India and China are available at <https://www.globalmethane.org/activities/indexact2.aspx?sector=coal>.

3. U.S. CMM Resources

There are two sources for publicly available CMM data in the United States: the Inventory of U.S. Greenhouse Gas Emissions and Sinks (the Inventory) and the Greenhouse Gas Reporting Program (GHGRP). USEPA produces the *Inventory of U.S. Greenhouse Gas Emissions and Sinks* (the Inventory) on an annual basis as part of its commitment to the United Nations Framework Convention on Climate Change (UNFCCC). The Inventory includes a summary of total U.S. CMM emissions, providing values for direct CH₄ emissions from underground mines and surface mines, post-mining emissions from underground and surface mines, methane utilization from underground mines and emissions from abandoned mines. While mine-specific data underpins the sector-wide totals presented in the Inventory, this data is not presented in the report or in associated annexes. Instead, detailed mine-specific data for gassy underground mines is available through the GHGRP, and is publicly available at <http://www.epa.gov/ghgreporting>.

There are two important distinctions between the Inventory and the GHGRP. The GHGRP collects data

only from active underground coal mines, and only from mines that liberate at least 36.5 million cubic feet (Mcf) in a calendar year. The second important difference is that the Inventory uses MSHA quarterly inspection reports to develop all VAM emission estimates, whereas the GHGRP allows reporters to use grab samples or a continuous emissions monitoring system (CEMS) in place of MSHA reports. Approximately 50% of reporters to the GHGRP use grab samples.

Data from both sources is used to develop reasonable estimates of total VAM emissions in the United States. VAM project potential at specific shafts is based on GHGRP data because reporters provide detailed information on volumetric air flow and CH₄ concentrations from for each exhaust shaft at individuals mines.

3.1 U.S. VAM emissions (U.S. Greenhouse Gas Inventory)

In 2013, methane accounted for 9.7 percent of all U.S. greenhouse gas emissions from human activities, with coal mines contributing 10 percent of total methane emissions [10]. Gas liberation at U.S. underground coal mines in 2013 totaled 125 billion cubic feet (Bcf) of methane with ventilation shafts accounting for 89 Bcf or 71 percent and gas drainage systems making up the remaining 36 Bcf (29 percent). Table 1 shows methane liberation at U.S. mines from 2008 through 2013.

The total annual volume of VAM liberation has declined as the number of underground mines has decreased. In 2008, for example, there were 583 operating underground coal mines in the U.S., but the number of underground mines had declined to 395 in 2013 [11]. However, the changes in mine population and VAM emissions are not proportional. During this period, the number of mines decreased by 32 percent, whereas total VAM emissions decreased just 11 percent. Many of the mines that are closing are smaller room-and-pillar mines rather than high-producing longwall mines, which contribute the largest share of VAM emissions. The important point here is that mine ventilation shafts will continue to be large sources of GHG emissions even as the number of underground mines declines.

Table 1. Underground Coal Mining CH₄ Emissions (Billion Cubic Feet) [10]

CMM Source	2008	2009	2010	2011	2012	2013
VAM	101	115	118	98	91	89
Degas	49	49	59	50	45	36
Total	150	163	177	147	137	125

3.2 U.S. VAM emissions (U.S. Greenhouse Gas Reporting Program)

USEPA issued the Mandatory Reporting of Greenhouse Gases Rule in 2010 (40 Code of Federal Regulations Part 98) in response to the FY2008 Consolidated Appropriations Act (H.R. 2764; Public Law 110-161), which requires reporting of greenhouse gas (GHG) data and other relevant information from large sources and suppliers in the United States. The purpose of the Reporting rule is to collect accurate and timely GHG data to inform future policy decisions. The collection of data required by the Reporting rule is carried out by the GHGRP. In 2013, 120 underground coal mines reported to the GHGRP. This represented 30 percent of the operating underground mines in the United States, but these mines accounted for 77 percent of all VAM liberated in 2013.

The chart in Figure 1 presents 2013 CH₄ emissions data from the GHGRP by basin. The Northern Appalachian basin holds the largest VAM resource with 35 Bcf of CH₄, but there are still substantial emissions in the Central and Southern Appalachian basins and in the Illinois basin, although Illinois basin mines have large volumetric throughput but lower CH₄ concentrations.

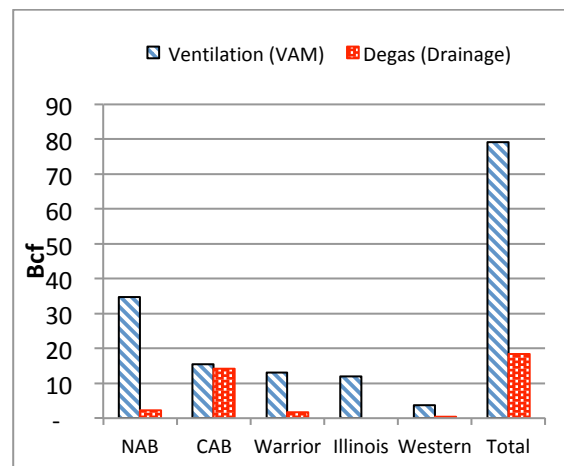


Figure 1. Underground coal mines sector – emissions by coal basin (2013) [3]

3.3 U.S. VAM project potential

A critical factor for successful VAM project development is access to shafts with sufficient methane throughput. Although the Inventory and the GHGRP provide a sound estimate of the total U.S. VAM emissions, total emissions do not equal VAM resource potential. This is because there are technical and economic limits for VAM abatement equipment. In contrast to the Inventory, the GHGRP provides an excellent source of mine-specific data to identify and prioritize ventilation shafts with the greatest potential for hosting a VAM project. Facilities reporting to the GHGRP must report the airflow and CH₄ concentration at each shaft. Figure 2 shows the number of U.S. shafts at CH₄ concentrations ranging from 0.40 percent to greater than 1 percent. The CH₄ concentration is calculated as a weighted average for the year since concentrations vary considerably.

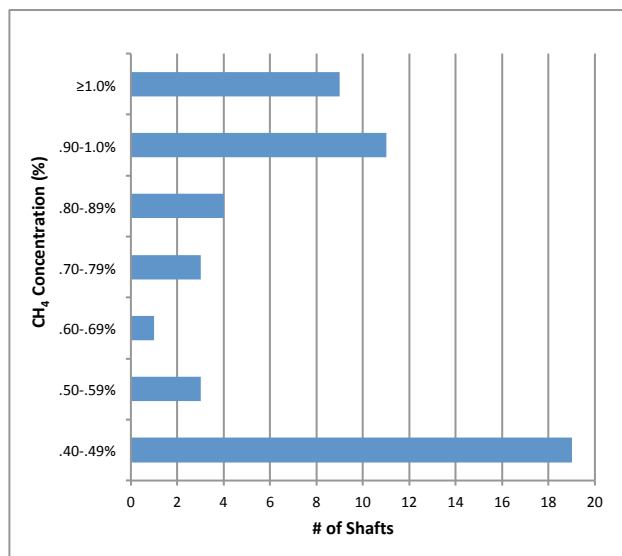


Figure 2: Number of mine shafts by CH₄ concentration [3]

Figure 3 plots the weighted annual average CH₄ concentration and the average annual volumetric air flow for individual shafts. Those shafts at CH₄ concentrations above 0.80 percent and volumetric air flow above 150,000 cfm present the most attractive opportunities for VAM projects from a technical and economic perspective. Additional factors such as location, site conditions, fan access and variation in CH₄ concentrations also impact whether a project is ultimately viable, but the first analysis, however, is the volume of methane to be oxidized versus the volume of air throughput.

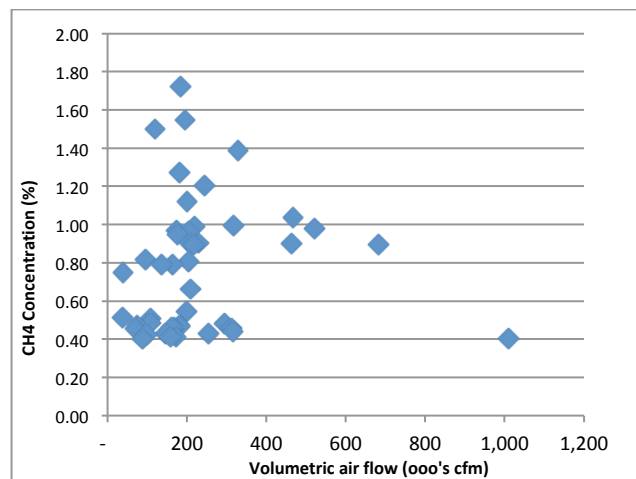


Figure 3. Shaft flows and CH₄ concentrations of individual mine shafts in the U.S. [3]

Initial projects in the U.S. have targeted these higher concentration shafts. Although many of the higher concentration shafts are shorter-lived bleeder shafts, the large quantities of methane emitted from these shafts make them attractive sites for VAM projects. In addition, new bleeders at a mine will open as mining progresses and old bleeders are shut in allowing for efficient remobilization of equipment.

4. Global VAM projects

Over time and with successful demonstration of commercial projects at active mines in three countries (Australia, China, United States), VAM project design using Regenerative Thermal Oxidizer (RTO) technology has become somewhat standardized. RTOs oxidize VAM at very high temperatures, ~ 1000 °C, and have been used in industrial processes for many years to oxidize volatile organic compounds (VOCs). The technology is now successfully adapted for VAM, and is positioned to be deployed more widely.

There are currently two operating VAM projects in the United States, and one project operating in Australia. In addition, several idled projects have previously operated at Chinese coal mines and one project is currently under development in China. Both the existing Australia project and the new China project include use of VAM for power production, whereas the U.S. projects are destruction only. All projects use RTO technology, but the power projects take steam from the RTO process to feed steam turbines for power generation.

4.1 Blue Creek No. 4 Mine – Biothermica Project (Alabama, USA)

The Blue Creek Mine No. 4, owned by Walter Energy, was the first active mine in the United States to host a VAM project. Biothermica, a Canadian company, is the financier and developer of the project and the manufacturer of the VAMOX® RTO used at the project.

site. The project was announced in May 2008, and the unit was installed on the Bleeder Shaft 4-9 fan in 2009. The nominal capacity of the RTO is 30,000 cubic feet per minute (cfm) or 14 Normal cubic meters per second (Nm³/s). According to Biothermica, the unit operated 27,000 hours as of November 2014 with an availability of 93 percent generating almost 81,000 carbon credits [6]. The success of the demonstration project has led to the design of a much larger RTO capable of handling 140,000 cfm, and plans are in place to install two of the larger units at a new bleeder shaft for a full-scale commercial project. The units will be able to handle CH₄ concentrations ranging from 0.30 percent to 1.2 percent. The new project is expected to generate around 400,000 carbon credits per year [6].

4.2 Marshall County Mine - Verdeo McElroy VAM Abatement Project (West Virginia, USA)

The project, announced in June 2010, was commissioned at Murray Energy's Marshall County Mine (formerly CONSOL Energy's McElroy Mine) in May 2012. Sindicatum Sustainable Resources (SSR) is the project financier and developer, and the RTOs are manufactured by DURR Systems. The project consists of 3 RTOs, each with a capacity of 53,330 cfm for a total throughput capacity of 160,000 cfm. The project is located at the 5 North 11-A Bleeder Fan. The VAM project is designed to take up to 80 percent of the shaft flow. The RTOs are capable of operating at CH₄ concentrations ranging from 0.30 percent to 1.2 percent, and the average shaft concentration during operation has been 1.03 percent. The project has thus far generated 197,411 carbon credits [7]. The project transferred to Murray Energy when the mine was purchased by Murray in December 2013.

4.3 Gaohe Mine (Shanxi Province, China)

The Chinese project is included in this paper because it relies solely on power sales revenue rather than a combination of carbon credits and power sales. The model could be transferred to the United States should power prices provide sufficient economic incentives by themselves or in concert with carbon credits, which will be discussed in more detail in Section 5.0. The Gaohe mine will host the largest VAM project in the world. The Shanxi LuAn Group, owner of the mine, is the project financier and developer. The project is close to completion and is expected to begin operation in 2015. Total throughput capacity will be 700,000 cfm utilizing 12 RTOs. The average methane concentration from the shaft is 0.30 percent, which is at the very low end of RTO technical capability. The project will enrich the VAM flow with drained gas averaging 25 percent CH₄ [8]. Heat produced by the oxidation process will be routed to a steam boiler which will generate sufficient steam for 30-MW of electricity. A similar project in

Australia has been generating 6 MW of power since 2007.

As previously noted, additional projects have operated in China, including one project with a throughput capacity of 210,000 cfm. The low price of carbon in global carbon markets has caused these projects to temporarily cease operations or in some cases to completely shut down.

5. Markets for VAM in the U.S.

The primary revenue driver for U.S. VAM projects today is carbon markets. The projects exist primarily to destroy methane emissions as a carbon abatement tool. Without carbon markets or subsidies to encourage greenhouse gas emission reductions, U.S. projects are unlikely to be economically viable until such time as industrial power prices are sufficiently high enough to provide an appropriate revenue stream. Until 2014, the market for emission reductions from CMM projects was limited to voluntary carbon markets. Although voluntary markets provide a real and valuable service ensuring that emission reductions meet rigorous criteria, the price of carbon credits in voluntary markets, generally below \$2.00 per metric ton of carbon dioxide (tCO₂e), has not been high enough to justify large scale investment in U.S. VAM projects. In 2014, this changed with the adoption of the Mine Methane Capture (MMC) Protocol by the California Air Resources Board (CARB) increasing carbon prices to \$8.00 initially. California is operating a regulatory compliance market, with a cap-and-trade program. CARB allows covered entities to purchase and trade California Compliant Offsets (CCOs) including offsets, or emission reductions, from CMM and VAM projects anywhere in the U.S. Thus, VAM projects at coal mines generating emission reductions may sell those emission reductions as CCOs to compliance buyers creating a revenue stream from VAM abatement. In turn, the compliance buyers may use those CCOs toward meeting their permitted CO₂ limit. To be recognized as CCOs, emission reductions from CMM and VAM projects must meet stringent criteria outlined in the MMC Protocol.

CCO prices are attractive and capable of generating cash flow to make the projects economically sustainable for projects that are currently operating or will be able to start in 2015 or even 2016. In February 2015, CCO prices ranged from \$9.50 for the most common offset with highest risk (8 years) to \$11.15 for Golden CCOs [1].

Although adoption of the MMC Protocol has generated new interest in U.S. VAM projects, the California cap-and-trade program is authorized only through 2020. The lead time for VAM projects is at least one year and often two years or more. This time is

necessary to design the site, fabricate and install the units, line up financing, and secure all permits and other authorizations. The capital and operating costs of VAM projects are high and payback can take 5 to 7 years. A project starting in 2015, with a commercial operation date of 2017, will have a very difficult time securing financing if there is no guarantee of revenue past 2020.

6. Developing a VAM project

Designing, developing and implementing a VAM project requires considerable research, data analysis, coordination with mine operations, and compliance with various regulatory regimes.

6.1 Development approach

The first step in project development is a thorough ventilation and gas audit of the mine operation, which should include use of a continuous emissions monitoring system to confirm existing methane concentrations and project future emissions with a reasonable degree of confidence. There should also be a good understanding of the gas drainage system and the role of the drainage system in the overarching gas management plan. High VAM concentrations today may be reduced significantly through a more aggressive drainage strategy potentially impacting the technical capability of a VAM destruction project, but certainly impacting the project economics. For example, D'Amico reported VAM concentrations fell from 0.90 percent CH₄ to 0.23 percent CH₄ at the Cumberland and Emerald mines in Pennsylvania, USA following deployment of surface pre-mine drainage [2]. If a VAM project was located at one of these mines, the reduction in methane concentration would translate to a 75 percent reduction in carbon credit revenue for the project.

The developer will work with a VAM equipment manufacturer and the mining company to size the project and produce specifications for the RTO plant, calculate power requirements, and secure necessary authorizations. Lessons learned by first movers in the VAM market provide important guidance for future development:

- (1) Accurate calculations of power consumption for fan operation necessary to pull VAM into the RTO plant and avoid back pressure on the fan are extremely important because power costs can comprise 20 to 50 percent of the project life cycle costs. A small increase in power consumption can have a major impact on costs considering that VAM units are generally designed to run continuously.
- (2) The major technical issue for RTOs has been overheating, particularly where methane

concentrations are especially rich, above 1 percent. Design modifications are ongoing, including refining hot-side bypasses and additional insulation.

- (3) In some cases, the underlying soils have not provided an adequate foundation for RTOs, requiring enhancements to the foundation in the form of pilings, which add significant cost and time delays.
- (4) Installation, start-up and commissioning can take many weeks as adjustments are often required, and these adjustments can continue during the first year of operation.

VAM RTOs are intended to be self-sustaining units after start-up. Once the project is turned over to the operator, whether a mine or 3rd party developer, operational requirements are limited with the exception of start-up adjustments. The project can be monitored remotely using a SCADA (Supervisory Control and Data Acquisition) system with a graphical interface using a computer, tablet or smart phone. For on-site operations, a walk-around once a day may be all that is required beyond a standard maintenance schedule recommended by the manufacturer and unscheduled maintenance.

6.2 Regulatory and policy framework

VAM abatement projects are developed and operated on a voluntary basis by the mine operator or a developer in partnership with the operator. An attractive investment framework coupled with an enabling regulatory policy framework will encourage wider VAM development.

Authorization to build and operate a VAM project requires amending the mine ventilation plan; therefore, it is critical that mine safety authorities be well informed about the role of a VAM project, the impact on mining operations, especially health and safety, the safety measures built into the projects, and the project operator's policies and practices. In the U.S., MSHA currently takes a neutral position with respect to VAM projects. The discretion to approve or deny a request is left to the judgment of the MSHA District Managers. But with two projects approved and several more under consideration, more MSHA districts are becoming familiar with VAM projects.

6.3 VAM project economics

VAM abatement projects entail significant capital (Capex) and operational (Opex) expenditures. Project costs vary depending on the size of the project (usually denoted as air throughput in Nm³/s or Nm³/hr), location, and power consumption requirements. Generally, costs increase with the size of a plant, although there are some

economies of scale. Revenues depend on CH₄ concentration and volumetric throughput – a higher concentration of CH₄ in a shaft flow will result in more CH₄ destroyed in the VAM plant generating more carbon credits. This drives project developers to prioritize shafts with higher CH₄ concentrations to maximize revenue.

Operations and maintenance expenses, other than power costs, are approximately 8-10 percent of Capex per year. Power consumption can be a large component of the life cycle costs of the project, especially in countries where industrial power prices are high. In the U.S., industrial power prices tend to be lower, especially in some coal producing regions, thus power costs can be expected to account for 15-25 percent of the total cost over the life of a U.S. project. Table 2 shows the economics for an example VAM project in the United States assuming a conservative projection of CCO prices for the California market and an average shaft concentration of 1 percent CH₄.

Table 2. Representative costs of a VAM project

VAM Project Costs (United States)	
Project life	10 Years
Shaft flow:	94 Nm ³ /s
CH ₄ %:	1.0
Power cost:	\$0.05/kWh
Discount rate:	12%
Availability:	91%
Carbon price Yr 1:	\$8.00 tCO ₂ e (Yr 1)
Carbon price Yr 10:	\$11.50 tCO ₂ e (Yr 10)
Capex:	\$6.4 million
Opex:	\$8.5 million
Total Cost:	\$14.9 million
IRR:	17.16%
NPV – 10 years:	\$1.39 million
Emission Reductions:	3,644,305 tCO₂

To assess how changes in carbon price will affect the project’s economic viability, Figure 4 charts the breakeven price (\$/tCO₂e) for the project at methane concentrations ranging from 0.40 percent to 1.1 percent.

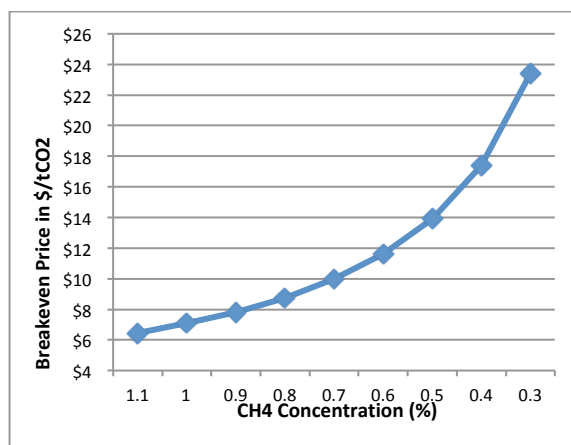


Figure 4. Breakeven price of example VAM project at different CH₄ concentrations

As the graph shows, CH₄ concentration is a major determinant of profitability with low concentrations requiring very high carbon credit prices. As the methane concentration decreases from 1.1 percent to 0.40 percent, the price of carbon credits required for the project to breakeven increases from just over \$6.00/tCO₂e to almost \$18.00/tCO₂e. A CH₄ concentration of 0.80 percent is required to meet current market prices which start at \$9.50/tCO₂e for a standard CCO. This concentration is found at 26 shafts in the U.S., meaning VAM projects at the majority of U.S. mine shafts remain subeconomic today. However, even a small increase in the price could result in substantially greater VAM potential as shafts with more marginal CH₄ concentrations become economic.

Figure 5 is a marginal abatement cost (MAC) curve that shows the cumulative VAM abatement potential at different carbon credit prices. Only mine shafts with at least 0.40 percent CH₄ concentration are included.

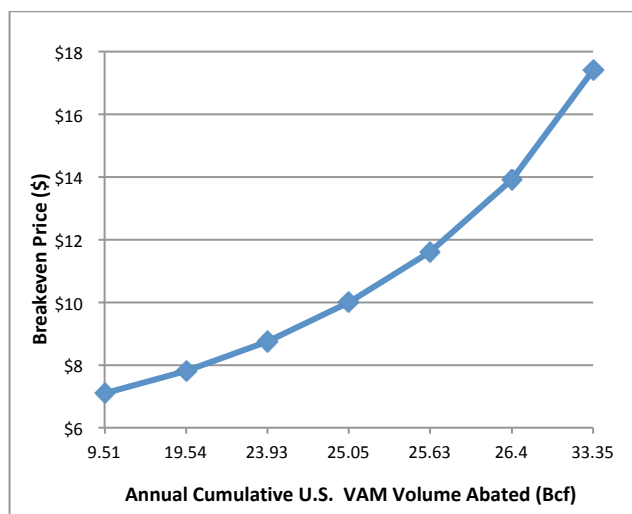


Figure 5. Marginal abatement cost curve for U.S. VAM projects

A carbon price of \$8.00/tCO₂e can result in 20 Bcf of VAM emission reductions per year equaling 22 percent of total U.S. VAM emissions. At \$12.00/tCO₂e, almost 26 Bcf can be destroyed economically. The chart shows that although it may not be possible to destroy all VAM emissions in the U.S., abatement of a large share of emissions is a realistic objective at favorable carbon credit prices.

7. Conclusions

The U.S. VAM resource is very large. Our analysis indicates that 50 mine shafts in the U.S. have average methane concentrations sufficient to host sustainable VAM projects, and 48 of those shafts are not associated with active VAM projects. Developing projects at these sites could reduce 20-40 percent of VAM emissions in the United States at a reasonable cost providing a great opportunity for incremental methane emission reductions in the coal sector. VAM also presents a potentially significant energy resource, and the recovery of heat from VAM units could support various heating applications, power generation, and even cooling.

VAM abatement technologies are available and in use today in commercial operations. Although small in number, they have demonstrated proof of concept and the industry is poised for wide-scale deployment. While it is unrealistic in the near term to assume that all VAM emissions can be abated, early movers have shown that RTO technology, and possibly other technologies, meet technical and economic objectives for VAM destruction.

Looking forward, several factors are critical for wide-scale deployment of VAM projects. First, the continued development of an enabling and predictable regulatory process that provides clear guidelines for authorization of VAM projects and ensures that those projects are installed and operated in line with mine health and safety standards must be maintained. In addition, a sustained carbon market with prices high enough to support VAM projects is required. Certainty in the California market after 2020 is especially critical at this time to provide investors with long-term confidence in the market. Local, state, and federal government agencies can also incentivize VAM abatement through other actions including expedited regulatory approvals, alternative royalty, fee and tax structures, and favorable power tariffs for energy generated by VAM projects.

More effective risk management by project developers is also important. In particular, understanding how the projects integrate with mine operations is fundamental to the long term sustainability of a VAM project. Proper due diligence in resource assessment and VAM characterization is also critical for the design of a VAM plant.

Finally, reducing capital and operating expenses is necessary to see more commercial development. Increased application of VAM technologies should result in economies of scale lowering production costs. Continued design improvement may also reduce Capex, although RTOs are subject to domestic and world markets for steel. Opex can be further lowered by reducing resistance in the RTO, which in turn will require less electric load – a major expense. Developing a safe direct easé connection is another long term goal of the industry because it will improve the capture efficiency of the plants, which now must take a slip stream.

EPA will continue to work with the U.S. coal industry and other stakeholders to reduce barriers to VAM development. CMOP has developed many tools for public use that help identify project opportunities and facilitate development of those projects. CMOP also performs significant outreach to the mining industry, investment community, and project developers to identify opportunities for regional or project level support.

References

- [1] California Carbon Info (2015). Market Report. February 6, 2015.
- [2] D'Amico, Joseph, 2010. Coal Mine Methane Recovery & Utilization Strategies. Presented at U.S. CMM Conference. Birmingham, AL. October 2010.
- [3] Envirofacts (2015) Envirofacts database. U.S. Environmental Protection Agency. Accessed March 2, 2015. <http://www.epa.gov/enviro/>
- [4] Greenhouse Gas Reporting Program (GHGRP), 2010. 40 CFR Part 98, Subpart FF.
- [5] IPCC, 2014: Climate Change 2014: Synthesis Report. Contribution of Working Groups I, II and III to the Fifth Assessment Report of the Intergovernmental Panel on Climate Change [Core Writing Team, R.K. Pachauri and L.A. Meyer (eds.)]. IPCC, Geneva, Switzerland, 151 pp.
- [6] Kay, Dominique (2014). Key Outcomes of VAM Abatement Demo Project at Walter Energy's Mine in Alabama. Delivered to the 2014 U.S. Coal Mine Methane Conference. Pittsburgh, PA USA November 2014. http://www.epa.gov/cmop/docs/cmm_conference_sep2014/2014USCMM_Kay.pdf
- [7] Savage, John (2014). Verdeo McElroy VAM Abatement Project. Delivered to 2014 U.S. Coal Mine Methane Conference. Pittsburgh, PA November 2014.
- [8] Schroeder, Jason and Karl Waltby (2014). Elevating VAM RTO Inlet Concentration Through CMM Blending for Power Generation. Delivered to

- the 2014 U.S. Coal Mine Methane Conference. Pittsburgh, PA USA November 2014.
- [9] United Nations Economic Commission for Europe (UNECE) 2010. Best Practice Guidance for Effective Methane Drainage and Use in Coal Mines. 2010. Geneva, Switzerland.
http://www.unece.org/fileadmin/DAM/energy/se/pdfs/cmm/pub/BestPractGuide_MethDrain_es31.pdf
- [10] U.S. Environmental Protection Agency (EPA), 2015. DRAFT Inventory of U.S. Greenhouse Gas Emissions and Sinks: 1990 – 2013. February 11, 2015.
<http://www.epa.gov/climatechange/ghgemissions/summary-report.html>
- [11] U.S. Energy Information Administration (EIA) 2015. Annual Coal Report 2013. Washington, DC. January 2015.

Gob Ventilation Boreholes Design Optimization for Longwall Coal Mining

Saqib A. Saki*, J.F. Brune^a, G.E. Bogin^a, R.C. Gilmore^a, J.W. Grubb^a, R.K. Zipf^a, J.A. Marts^a

^aColorado School of Mines (CSM), Golden, Colorado, USA

Gob ventilation boreholes (GVBs) are widely used in United States underground coal mines for longwall gob degasification purposes. GVBs can recover 30 to 50% of methane emissions from the longwall gob depending on geologic conditions [1]. Generally, GVBs are considered useful for reducing methane concentrations in working areas, explosion hazards and creating safer working conditions for the longwall section. Computational fluid dynamics (CFD) modeling efforts at the Colorado School of Mines (CSM) under a National Institute for Occupational Safety and Health (NIOSH) funded research project have confirmed that gob ventilation boreholes are helpful to reduce the methane concentrations at the face. However, they may also draw fresh air from the face into the gob, creating explosive gas zones (EGZs) within the gob. GVBs operation may thereby increase oxygen ingress into the gob and create explosive gas mixtures. It is important to identify the locations for GVBs placement to maximize the methane extraction and to minimize any explosion hazards. In this paper, CFD studies will be presented to analyze the effect of GVBs design and operating parameters on methane extraction, formation of EGZs in the gob and methane concentrations at the longwall face and tailgate. The distance of GVBs from the tailgate and the working face, the borehole diameter, the distance from the top of the coal seam being mined, the wellhead vacuum pressure and number of GVBs operating on the panel all have a significant effect on methane extraction, explosive gas mixtures volume and methane concentration in working areas. CFD studies at the CSM identified optimal GVBs design and operating parameters, which can maximize the benefits and minimize the risks.

Keywords: Longwall Mining; Computational Fluid Dynamics; Explosive Gas Zones; Gob Ventilation Boreholes

1. Introduction

Coal mines may be considered gassy based on the presence of hazardous gases like CH₄, CO and CO₂. Gases from rider seams above or below the mined coalbed can migrate into the gob and then move towards the working areas. In longwall coal mines with high methane emissions, sufficient ventilation and additional methane control measures are required to reduce the methane concentration in working areas to the statutory levels. Methane emissions may come from adjacent coal seams, the active longwall face, roof and floor strata, coal on the conveyers and remnant coal in the gob area. Several techniques or the combinations of techniques are utilized to control the methane hazard. These include coal bed degasification, ventilation, nitrogen injection into the gob and GVBs. Longwall face ventilation alone can only handle methane emissions up to a certain amount. When methane emissions exceed the face ventilation capacity, additional control measures are required. Drilling horizontal or vertical methane drainage holes into the coal seams or gob ventilation boreholes from the surface into the gob area to extract methane are common practices. GVBs are usually drilled from the surface above the longwall panel ahead of mining. When the GVBs are intercepted by the

advancing face and the gob begins to form, methane production starts from the boreholes. It is important to control the performance of GVBs to maintain a safe working environment in the mine. The performance of GVBs depends on multiple factors, including borehole location, length and diameter of slotted casing, setting depth of casing above the coal seam being mined, wellhead vacuum pressure, and permeability of caved-fractured zones.

GVBs remove the methane from the gob area and the fractured zone above the gob, as shown in Figure 1. GVBs are generally drilled to within 10 to 30 m above the top of the coal seam into the fractured zone, but not into the caved zone. This is done to avoid air ingress from the face and bleeder entries into the gob. GVBs are usually completed with a casing and 60 m of slotted pipe at the bottom [2]. Wellhead vacuum pressure is applied to these ventilation bore holes by installing vacuum pumps known as exhausters or blowers [2]. The vacuum creates a pressure sink to capture the methane and prevent it from entering into the underground workplace. For these GVBs to work effectively, they must be drilled close enough to the caved zone, as shown in the schematic representation of longwall coal mining and GVB operation over a longwall coal panel in Figure 1.

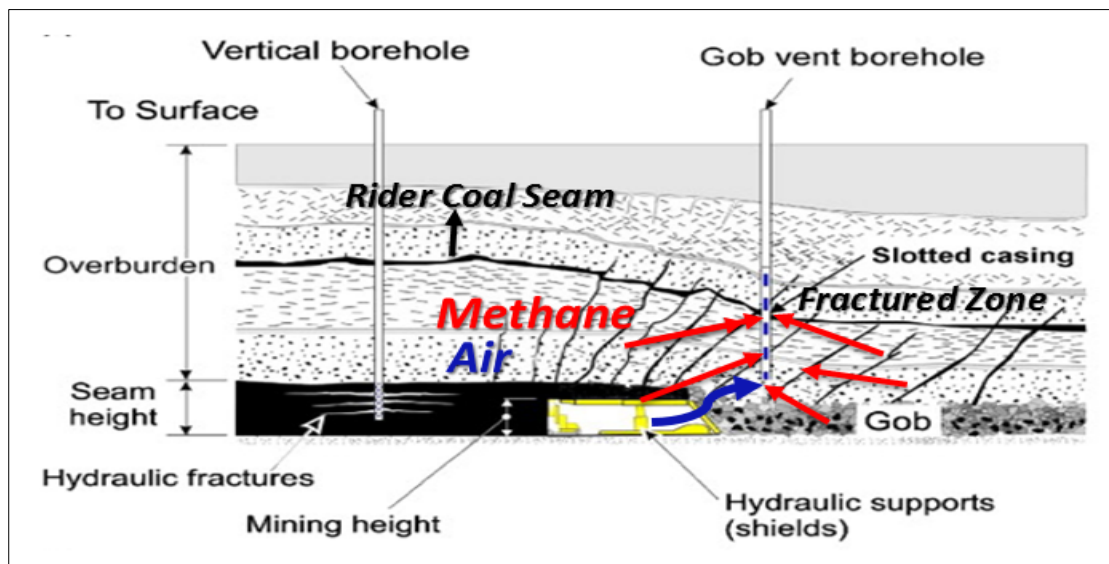


Fig. 1. Schematic representation of longwall mining with shearer, fractures extending the overlying strata, bedding plane separation, and possible methane flow paths (red arrows) and air leakage from the face into GVB [3].

2. Previous Research

Several experimental and numerical studies have been carried out to design, evaluate and optimize the performance of gob vent bore holes. The U.S. Bureau of Mines (USBM), the NIOSH Office of Mine Safety and Health Research (OMSHR), and several independent researches carried out studies on GVBs. The USBM evaluated the use of vertical boreholes to assist degasification of longwall gobs in the Kittanning coal bed at Bethlehem Mines Corporation's Mine No. 33, where methane was captured through surface boreholes using wellhead vacuum pumps [4]. An increase in daily coal production was reported due to reduced methane concentrations in the return airways [4]. Other longwall gob degasification experiments were conducted by the USBM [5] using surface ventilation boreholes in the Lower Kittanning coalbed in central Pennsylvania, where it was reported that the methane level in the return entries dropped by 75% after first drainage borehole was intercepted and started production. An experimental study to improve the performance of GVBs was conducted by USBM [6] in the Lower Kittanning coal bed. Researchers reported an 80% higher methane production for GVBs placed near the gate roads as compared to GVBs placed along the center line of the longwall panel [6].

Xue and Balusu [7] studied to capture gas from the longwall gobs in one of the gassiest mines in Australia. They monitored mine methane in real time and also conducted CFD modeling efforts of the gob. The methane emissions from the longwall panel were reduced from 1.5 m/s to 0.375 m/s with the help of GVBs. Xue and Balusu also recommended GVBs placement near the edges of the panels but keeping them a minimum distance away from the gate roads so that the GVBs would not draw ventilation air [7]. Balusu et al. presented findings on longwall gob gas drainage and control strategies for highly gassy mines, concluding that GVBs provide the highest capacity and lowest cost option for gob gas drainage. They recommended that the GVBs should be drilled at a distance of 30 to 70 m from the gate roads depending on the gob caving characteristics. Balusu et al. [8] also recommended that

ventilation system should be designed to minimize fresh air or oxygen ingress into the gob. This can be accomplished by immediately sealing-off all the cut-throughs behind the face, which improves overall gas drainage efficiency.

The mines in the Pittsburgh Coalbed have been the subject of extensive modeling studies for methane drainage and GVBs. Karacan [3] carried out an experimental study on longwall gob gas reservoirs and GVB production performance using well test analysis at multiple drawdown rates. In this study, wellhead gas production rates and pressures were monitored for six GVBs in adjacent longwall panels during and after mining. Karacan's study showed that well test and reservoir analysis methods can be used to calculate the permeability of the gob around the GVBs, determine their radius of influence and predict the GVBs' flow efficiencies [3]. A geomechanical study to determine the gob permeability distribution and its application to methane reservoir modeling of coal mine longwalls was done by Esterhuizen and Karacan [9]. Fast lagrangian analysis of continua in 3 dimensions (FLAC^{3D}) was used for Geomechanical modeling. A two-stage approach was used to simulate the complex process of methane emissions and flow by combining the output of geomechanical models with reservoir models [9]. Karacan et al. [10] applied reservoir modeling techniques to the evaluation and optimization of longwall methane control systems. Research results indicated that increasing the GVB casing diameter also increased the cumulative methane production though it resulted in a slight decrease in methane concentration. The research also demonstrated that longer lengths of slotted casing produced more methane. The setting depth of the casing played an important role relative to the concentration and volume of methane captured. Research indicated that, if the slotted casing protruded into the caved zone, the methane concentration of the GVB exhaust decreased by about 30%. Karacan et al. also reported that moving the GVB towards the centerline and away from the tailgate would reduce its gas drainage capability [11].

3. Gob and Strata Permeability and Porosity

3.1 Gob Parameters

Authors at CSM developed geo-mechanical models in FLAC^{3D}, following the approach originally developed by Esterhuizen and Karacan [9]. The geo-mechanical models were created using actual stratigraphic and rock mechanics data provided by the cooperating mines. The models were then calibrated with real time subsidence data as well as longwall shield loading data. The gob porosity was calculated as the difference between the initial porosity of the gob and the volumetric strain of the gob material as predicted by the model. The permeability was determined from the porosity model using the Carman-Kozeny relationship for flow through porous media, as shown below.

$$k_{gob} = \frac{k_{initial}}{0.241} \left(\frac{n^3}{(1-n)^2} \right) [md] \quad (1)$$

where k is the permeability in millidarcy and n is the porosity. Details about this geo-mechanical model can be found in a paper by Marts et al. [12]. The gob permeability is in the range of 2.0×10^{-7} to 5.1×10^{-6} m and the porosity ranges between 14 and 40%.

3.2 Strata and Fractured Zone

GVBs design, placement and performance depends on permeability distribution [6] in the fractured zone above the caved zone, where GVBs are terminated. In past research, permeability in the fractured zone has been simplified by using uniform values, which is not the actual case.

The permeability of coal-measure rocks is highly dependent on stress and stress redistribution after mining [13]. Insitu permeabilities depend on the rock type in stratigraphy but they get modified by stress changes. Durucan [14] presented following relationship in empirical equation form.

$$k = ae^{-b\sigma} \quad (2)$$

where k is the permeability, a and b are constants and σ is the applied stress.

Researchers at the University of Nottingham [15] have developed stress-permeability relationships by laboratory tests. These stress-permeability relationships were used to calculate the horizontal and vertical permeabilities of different rock layers in the fractured zone based on the predicted stresses from the geo-mechanical modeling. Initial permeabilities of different rocks were based on published sources [9, 12, 13, 15, 16]. The equations used to calculate the horizontal and vertical permeabilities are given below.

$$k_h = k_{ho} \times e^{-0.25(\sigma_{yy} - \sigma_{yyo})} \quad (3)$$

$$k_v = k_{vo} \times e^{-0.25(\sigma_{xx} - \sigma_{xxo})} \quad (4)$$

where k_h and k_v are modified horizontal and vertical permeabilities after mining induced stresses. σ_{xx} and σ_{yy} are horizontal and vertical stresses, while o indicates initial conditions.

The Carman-Kozeny equation was used to calculate porosity as shown below.

$$k \sim d^2 \phi^3 \quad d = 0.25 \text{ m} \quad (4)$$

where ϕ denotes porosity and d , grain size.

For the mine under consideration, the fractured zone is divided into five layers based on rock type and mining induced stress gradient as shown in Figure 2. The permeabilities of the strata layers are given in Table 1.

Table 1. Permeabilities of strata layers for the studied mine

Strata Layers #	Thickness(m)	Horizontal k (m ²)		Vertical k (m ²)	
		Min	Max	Min	Max
1	3.0	1.1E-12	1.4E-12	1.3E-12	1.6E-12
2	3.0	5.7E-13	6.8E-13	6.7E-13	7.8E-13
3	3.0	3.8E-13	4.5E-13	4.4E-13	5.2E-13
4	8.8	2.8E-13	3.4E-13	3.3E-13	3.9E-13
5	8.8	1.8E-13	2.1E-13	2.1E-13	2.5E-13

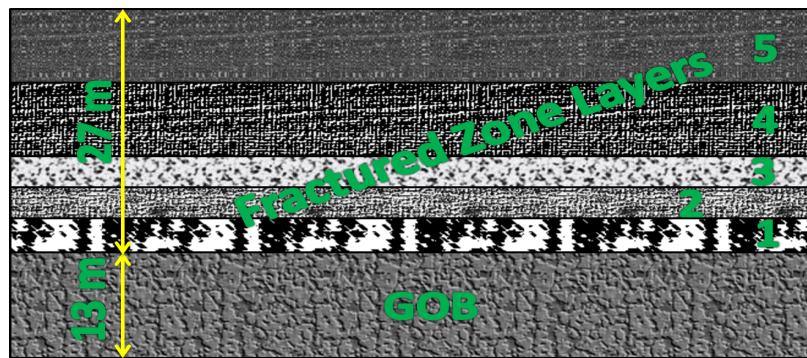


Fig. 2. Vertical cross section of gob and strata layers.

The strata layer#1 sits immediately above the caved zone as shown in Figure 2. The permeability data for each strata layer was used in the CFD model in the form of a user defined function (UDF).

4. Model and Ventilation Layout

The CFD model was created using ventilation and air quality data collected from a cooperating mine in the

western United States. The collected data consisted of mine layouts, geometric dimensions, lithology, overburden caving characteristics, ventilation operating conditions and gas concentration measurements. The CFD model panel is 314 m (1030 ft.) in width and 40 m (131 ft.) in height to account for the caved and fractured zone. The initial 13 m (42 ft.) are modeled as gob and remaining height is modeled as the fractured zone. At the top of the fractured zone there is a 2-m (6 ft.) rider coal

seam, which has been modeled as the methane inlet of the model. The fractured zone has been divided into layers based on rock type so that changes of permeability in the vertical direction can be accounted for. The effect of mining induced stresses and fracturing is negligible above the rider coal seam. A massive, low permeability

layer of shale is overlying the rider coal seam. This shale is not included in the model as its permeability is not expected to change significantly due to subsidence. The GVBs extend into the fractured zone and terminate above the caved zone. The length of the model is 460 m (1500 ft.). The CFD model is shown in Figure 3.

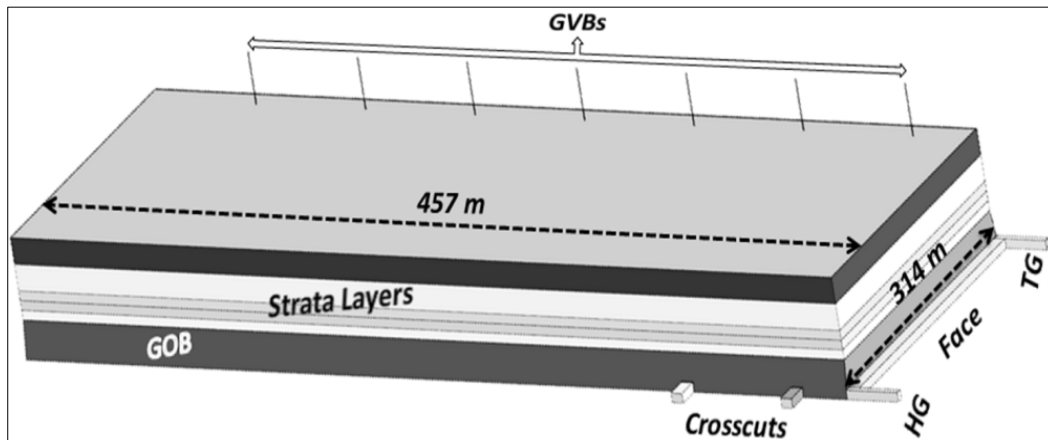


Fig. 3. Global CFD model geometry

The CFD model was constructed with a “U” ventilation design for a progressively sealed panel, as shown in Figure 4. In the United States, regulations normally require the use of a bleeder system [17]. Exceptions may be granted if the coal has a documented tendency to spontaneously combust. Many western United States coals are prone to spon com and several

mines in this area use progressive sealing (sometimes also referred to as bleederless panels) to reduce oxygen ingress into the gob. This is accomplished by progressively sealing the headgate side crosscuts in by the face as the panel advances. The fresh intake air enters the longwall face through the headgate, travels across the face and leaves through the tailgate.

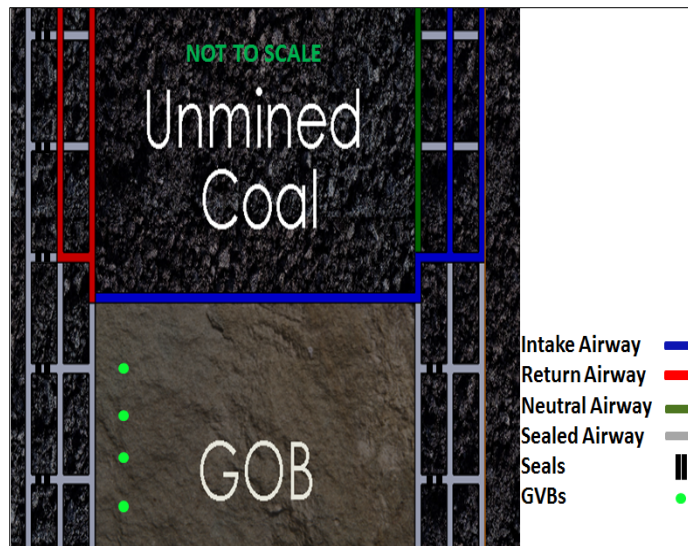


Fig. 4. Progressively sealed, U-Type ventilation

5. Explosion Hazard Characterization

The explosive potential for the mixtures of methane and air is presented using a coloring scheme based on Coward’s triangle [18] as depicted in Figure 5. There are four distinct regions: the explosive region (red), a fuel-rich inert region that can become explosive when fresh air or oxygen is added (yellow), an inert region where no

explosive composition is possible (green) and a fuel-lean inert, near fresh air region (blue). An orange fringe zone was added to denote atmospheres that are close to explosive.

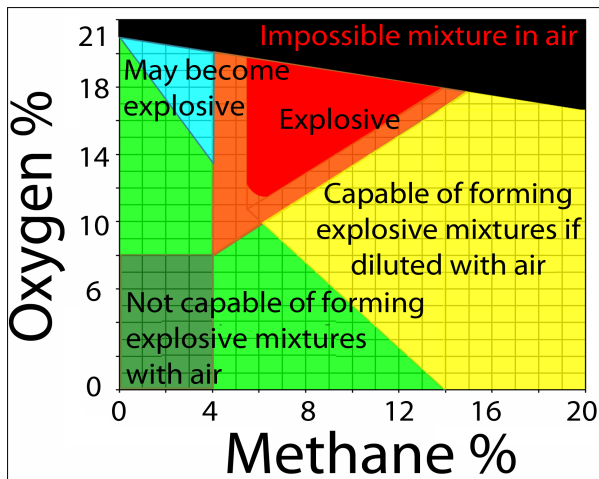


Fig. 5. Modified Coward's triangle [18], after Coward and Jones [20] (Reprinted with permission)

Worrall et al. [18] developed an algorithm as a UDF in FLUENT to correlate the methane-air mixtures in the CFD output plots with these colors. The contour plots for the plan view of the model are shown to visualize the EGZs in a plane at a height of 1.5 m (5 ft.) above the mine floor, which is approximately in the middle of the coal seam height. The risk of spontaneous combustion is qualitatively assessed by evaluating oxygen concentration and ingress distance in by the face. Spontaneous combustion of coal may be sustained by oxygen contents as low as 6% [19]. In the CFD modeling efforts, the longwall face ventilation air

quantity was 33 m/sec (70,000 cfm). The GVB wellhead vacuum pressure was 30 kPa (4 psi). The methane inlet amount for the model was determined from mine measurements of methane released by the ventilation systems and GVBs. The methane liberation rate used for the 460 m (1,500ft.) panel length is 0.5 m/s (1,000 cfm) and used as the base case. More information about CFD meshing, model setup, grid independence, turbulence, convergence and solution are discussed in a previous publication by Gilmore et al. [21].

6. GVB Location Optimization

The location of GVBs on longwall panel is important for the gob degasification effectiveness to reduce the methane concentration in the working areas. Diamond [6] demonstrated this in experimental field studies. In current study, GVBs location is optimized with respect to maximizing the methane reduction while minimizing the risks of losing the GVBs due to shear and gob compaction. Authors varied the distance of the GVBs from the gateroads and from the face and analyzed the effects. The base diameter of GVBs used in this study was 30 cm (12 in). The GVBs were operated independently of each other. The total width of the modeled fractured zone is 300 m (1,000 ft.). The results of the location studies, as shown in Figure 6 demonstrate that the GVB flow is maximized at a distance of 18 m (60 ft.) away from the tailgate and 44-88 m (100-200 ft.) in by the face. GVBs operating closer to the face pose a risk of drawing fresh air from the face into the gob which may support spontaneous combustion.

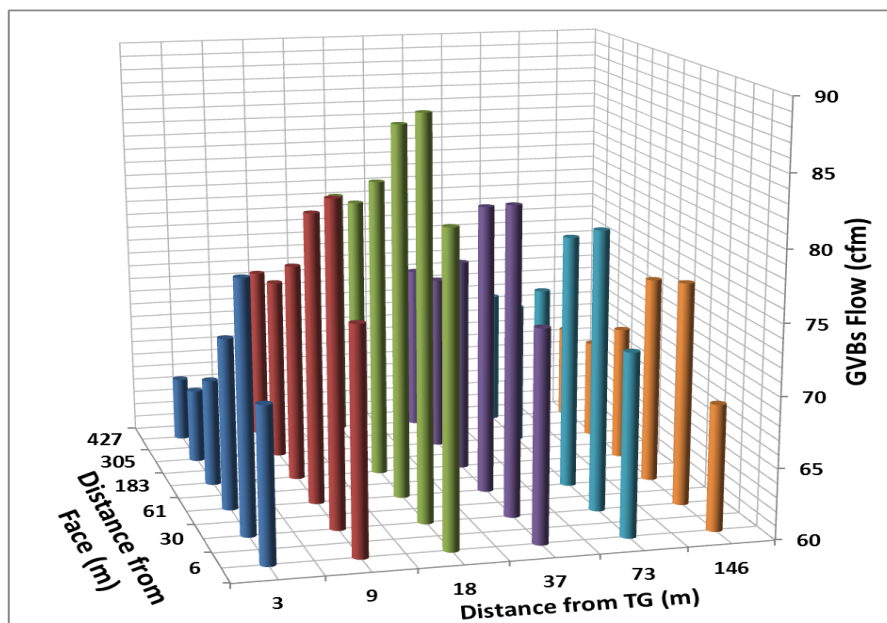


Fig. 6. GVBs Flow with respect to location

A second series of studies analyzed that what GVBs location is optimal to minimize EGZ volume and to reduce the tailgate methane concentration. Figure 7 shows relative EGZ volume as a function of GVBs location. EGZ volume is minimized at a distance of 18 m

(60 ft.) from the tailgate. GVBs near the center of the panel cause more fresh air ingress from headgate side, forming bigger EGZs. Figure 7 also shows that GVBs far in by the face cause the formation of larger EGZs because they pull fresh air deeper inside the gob.

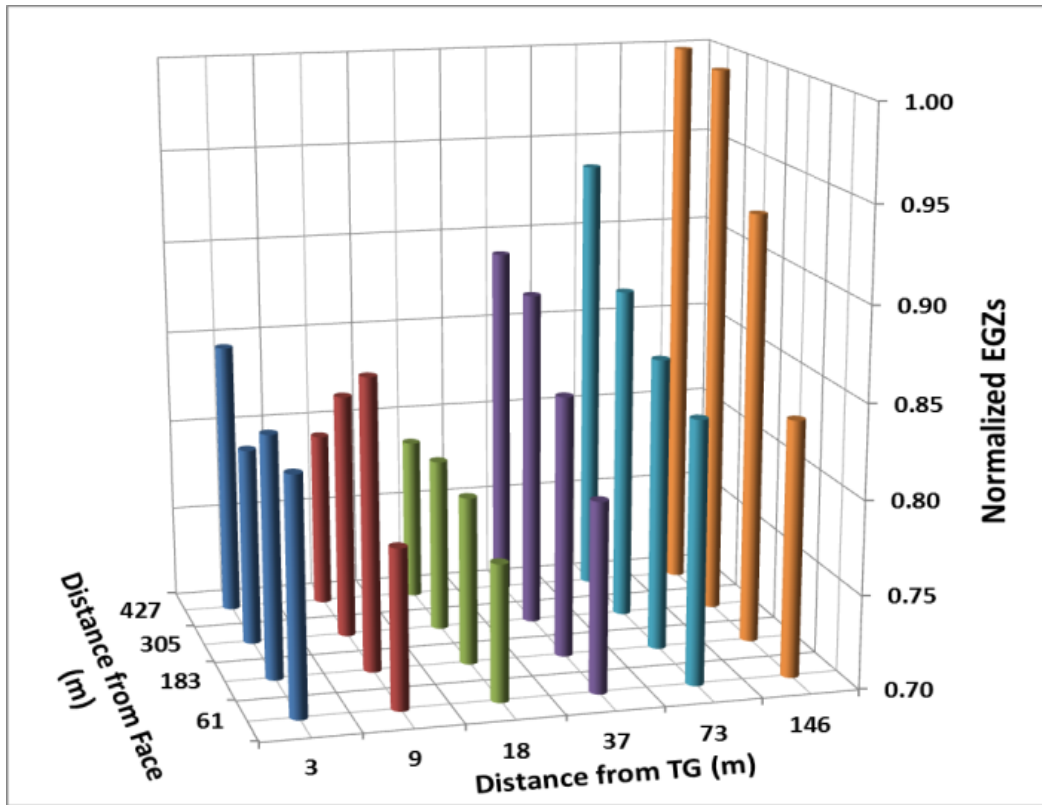


Fig. 7. EGZs comparison with respect to GVBs location

Figure 8 shows the contour plots of EGZs for two different GVB locations. The image on the left side shows the EGZ for a GVB operating at 18 m (60 ft.)

from the tailgate. The image on the right is for a GVB operating in the center of panel at a distance of 146 m (480 ft.) from tailgate and creating a slightly larger EGZ volume.

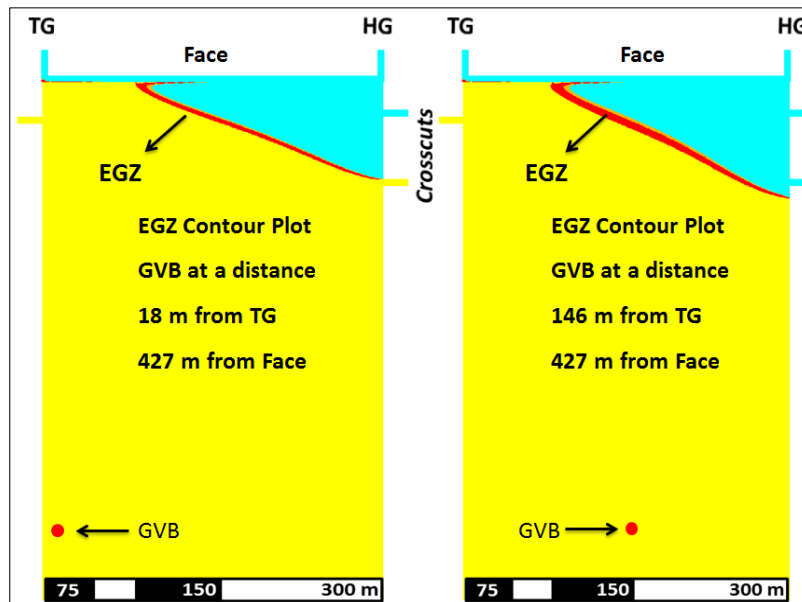


Fig. 8. EGZs contour plot comparison

Figure 9 shows a comparison of GVB effect to reduce methane concentration in the tailgate return air course. GVBs at a distance of 18 m (60 ft.) are also most

efficient in reducing methane concentrations in the return. The GVB setting depth impacts the quantity and quality of methane exhaust from GVBs, as reported by

Karacan [10]. Shear bands or horizontal shear zones in the gob can damage the casing and can partially or completely block the GVBs. Lowndes et al. [13] predicted that horizontal shear planes may develop within the immediate roof of the mined coal seam. To avoid the shearing of GVBs, the setting depth should lie above the caved zone. The permeability in or near the caved zone is higher than in the fractured zone. Therefore, if a GVB is set within the caved zone it will

draw more ventilation air through the gob and the methane concentration in the GVB exhaust will drop. It is recommended to terminate the GVBs above the caved zone to avoid the sharing of GVBs. It also helps to reduce the air ingress into the gob and hence reduces the risk of spontaneous combustion. Lower air ingress into gob may help to reduce the size of EGZs in the gob and hence the explosion hazard.

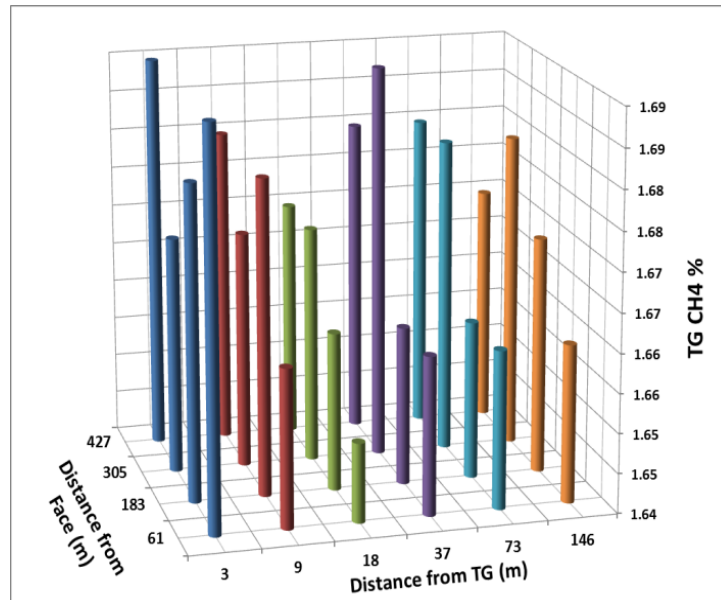


Fig. 9. Tailgate methane comparison with respect to GVBs location

7. Limitations of the Research

The results of CFD study are sensitive to the assumptions made for modeling. The permeability parameters of gob and fractured zone are based on geo-mechanical model predictions for a studied mine and can vary for any other mine. The amount of methane in the model is also based on the data provided by the studied mine and can vary for any other case. The assumptions are made due to the limited availability of data inside the gob. Sensitivity studies were run on the assumptions parameters. Increased methane in the model inertizes the gob and hence decreases the size and volume of EGZs, on the other hand it increases the methane concentration in the returns and GVBs exhaust. The modeling results are quite sensitive to the change in permeability of gob and fractured zone. Increase in permeability increases the methane coming into the model and hence decreases the size of EGZs due to inertization, while decrease in permeability reduces the amount of methane coming into the model and hence increases the size of EGZs. Increase in the permeability increases the flow through GVBs and vice versa. Increasing the permeability of gob and fractured zone by 10% reduced the volume of EGZ by 10%, it also increased the flow through the GVB by 11%. Decreasing the permeability of gob and fractured zone by 10% increase the volume of EGZ by 28%, it also reduced the flow through the GVB by 10%.

8. Summary and Conclusions

The following conclusions can be drawn from this research:

- The optimal GVBs location is at a distance of 18 m (60 ft.) from the tailgate for the studied mine with respect to GVBs flow, explosive gas zone formation and reducing methane concentrations in working areas.
- GVBs operating near the face have low methane concentration in the exhaust as they pull more ventilation air.
- GVBs operating at far distance from face cause deep air ingress into the gob.
- GVBs operating at far distance from face form larger EGZs and are less effective in reducing methane concentration in working areas.
- The setting depth of GVBs is an important factor determining the methane concentration in the GVBs exhaust.

Acknowledgments

Researchers at Colorado School of Mines gratefully acknowledge the financial support from NIOSH under contract number [200-2009-31409] and the cooperation of co-operating mines in the Western United States for providing the data for model construction and validation.

References

- [1] Economic decision making for methane drainage systems for underground coal mines, The Holmes Safety Association Bulletin, (1998) 3-9.
- [2] C.Ö. Karacan et al., Reservoir simulation-based modeling for characterizing longwall methane emissions and gob gas venthole production, *International Journal of Coal Geology* 71(2-3) (2007) 225-245.
- [3] Karacan. Degasification system selection for US longwall mines using an expert classification system. *Computers & Geosciences*, 35(3) (2009) 515-526.
- [4] C.H. Elder, Use of vertical boreholes for assisting ventilation of longwall gob areas, Bureau of Mines Methane Control Program, Technical Progress Report-13, 1969.
- [5] T. D. Moore et al., Longwall gob degasification with surface ventilation boreholes above the Lower Kittanning Coalbed, Report of Investigations 8195, 1976.
- [6] W. P. Diamond, Improving the Performance of Longwall Gob Gas Ventholes, USBM Report No. 448, United States Bureau of Mines, 1995.
- [7] S. Xue and R. Balusu, Capture gas from longwall goafs, The Commonwealth Scientific and Industrial Research Organisation (CSIRO), Exploration and Mining, 2002.
- [8] R. Balusu, N. Tuffs, R. Peace and S. Xue, Longwall Goaf Gas Drainage and Control Strategies for Highly Gassy Mines, 8th International Mine Ventilation Congress (2005) 201-209.
- [9] G.S. Esterhuizen, and C.Ö. Karacan, Development of Numerical Models to Investigate Permeability Changes and Gas Emission around Longwall Mining Panel, 40th U.S. Symposium on Rock Mechanics, 2005.
- [10] C.Ö. Karacan et al., Development and application of reservoir models for the evaluation and optimization of longwall methane control systems, National Institute for Occupational Safety and Health, Pittsburgh Research Laboratory, 2005.
- [11] C.Ö. Karacan., G.S. Esterhuizen, S.J. Schatzel, and W.P. Diamond, Numerical Analysis of the Impact of Longwall Panel Width on Methane Emissions and Performance of Gob Gas Ventholes, National Institute for Occupational Safety and Health, Pittsburgh Research Laboratory, 2007.
- [12] J.A. Marts, R.C. Gilmore, J.F. Brune, G.E. Bogin, J.W. Grubb and S.A. Saki, Dynamic gob response and reservoir properties for active longwall coal mines, *Mining Engineering*, 66(12) (2014) 59-66.
- [13] I.S. Lowndes, D.J. Reddish, T.X. Ren, D.N. Whittles, and D.M. Hargreaves, Improved modeling to support the prediction of gas migration and emission from active longwall panels, *Mine Ventilation*, eds. Euler De Souza, Balkema (2002) 267-272.
- [14] S. Durucan, An investigation into stress permeability relationships of coals and flow patterns around working longwall faces, PhD Thesis, university of Nottingham, 1981.
- [15] A. Kelsey, C.J. Lea, I.S. Lowndes, D. Whittles, T.X. Ren, CFD modeling of methane movement in mines, 30th International Conference of Safety in Mines Research Institutes, South African Institute of Mining and Metallurgy, 2003.
- [16] M.A. Lewis, C.S. Cheney and B.É. ÓDochartaigh, Guide to Permeability Indices, British Geological Survey, Open Report CR/06/160N. (2006) 29pp.
- [17] Mine Safety & Health Administration, Code of Federal Regulations - Title 30: Part 75.334-f.
- [18] D.M. Worrall, E.W. Wachel, U. Ozbay, D.R. Muñoz, and J.W. Grubb, Computational Fluid Dynamic Modeling of Sealed Longwall Gob in Underground Coal Mine – a Progress Report, 14th Annual North American Ventilation Conference, Salt Lake City, UT, 2012.
- [19] B. Beamish and R. Beamish, Experience with Using a Moist Coal Adiabatic Oven Testing Method for Spontaneous Combustion Assessment, 11th Underground Coal Operators' Conference, (2011) 380-384.
- [20] H.F. Coward and G. W. Jones, Limits of flammability of gases and vapor's, USBM Bull. No. 503, US Bureau of Mines, 1952.
- [21] R.C. Gilmore, J.A. Marts, J.F. Brune, S. Saki, G.E. Bogin, Jr., and J.W. Grubb, Simplifying CFD modeling of longwall gobs with a modular meshing approach, *Mining Engineering* 67(3) (2015) 68-72.

Effect of Discrete Fracture Network Representation of Gob on Airflow Distribution Near the Longwall Face

C. Özgen Karacan, Liming Yuan

NIOSH, Office of Mine Safety and Health Research, Pittsburgh, PA 15236, USA

Fluid transport properties of longwall gobs have a profound effect on methane control in mines, the formation of methane-air mixtures in certain regions within the caved and fractured zones, and inertization of gobs for spontaneous combustion control. In addition, gob permeability and its distribution, especially in the near-face region behind the shields, may have important consequences for face ventilation and air circulation behind the shields. In particular, in cases where the roof is competent and leaves a void behind the shields as a result of partial caving or hanging, air circulation may increase, causing face ventilation efficiency to decrease for the tailgate corner. Furthermore, this situation may create multiple locations of air exchange between the face and the gob, and may create local regions of methane accumulation that may prompt additional monitoring.

Despite the importance of the distribution of gob permeability, especially in the near-face area, the usual practice in design or in numerical modeling studies is to assume a gradually changing smooth permeability distribution by ignoring the fact that the gob is formed by discrete fractures and their networks. In fact, regardless of whether the gob is compacted or not, or what the value of permeability is, the only path for methane and air to move within the gob or near the gob is through fractures, which are random in nature, and the networks created by those fractures. Any fluid can move under the effect of pressure gradient only by following the fractures.

In this work, we present a comparative study to investigate non-smoothly distributed gob permeability and the permeability field created by discrete fractures for their effects on air movement near the face. For this study, discrete fracture networks were generated using controlled statistics. These networks along with the properties affected by their distribution were imported into a computational fluid dynamics (CFD) model of a longwall mine. The results of air movement along the face area were compared with those of smooth permeability distribution.

Keywords: Discrete fracture network, longwall gobs, ventilation, methane control, longwall face.

1. Introduction

Ventilation of coal mines is important not only for controlling particulates but also for controlling methane. Most methane-related accidents in longwall coal mines occur in areas with methane inflow from the floor or roof when methane degasification is limited or not practiced effectively, or in areas that are not ventilated adequately. When compared to other areas of an active mine, the ventilation at the working face and its vicinity is particularly important as there is always the possibility of an ignition source and high methane emissions during mining. This was evidenced, in part, by the occurrences of methane ignitions at the Upper Big Branch South Mine in 1997 and 2010, the latter of which led to a massive mine-wide explosion [1].

The longwall face has a direct exposure to newly cut coal, newly created gob behind the shields, and extensions to overlying and underlying strata where additional gas sources may exist. Worker safety at the longwall face requires control of methane concentrations, and thus adequate ventilation to control and eliminate potential accumulations of gas [2]. While increasing ventilation airflow quantity to dilute any increase in methane emissions is always an option, it may not always be possible especially if the operating longwall is at or near the practical airflow limits of the ventilation system. In this situation, particularly the tailgate corner can be a critical location as it is where the maximum amount of methane can accumulate and, yet, where the ventilation quantity may drop substantially due to leakage behind the shields and into the gob. In this regard, effective coal seam degasification and production management, as well as an understanding of airflow patterns in and around the longwall face, can be important to make the best use of available ventilation air [3,4].

Effective ventilation of longwall faces and the tailgate corner can be compromised by several factors. Over the years, enhancements in equipment have significantly improved the capability to effectively extract coal and have enabled longer faces. Longer faces, however, result in severe ventilation control issues due to complex airflow movements along the face and the increased potential for air exchanges between the immediate face area and the newly created gob just behind the shields [5,6]. This potential is especially exacerbated if the mine has a strong or cave-resistant roof that leaves large void spaces of various shapes and sizes behind the shields [7]. Unsupported roof may hang for a time until it caves, possibly in the form of large blocks—the immediate consequence of which is a large, non-uniform void space behind the shield line, creating variable parallel pathways for methane and airflow to move in by the shields.

The characteristics of the cave (block size, porosity, and permeability) will dictate the number of these pathways and their continuity for providing an access for air and gas to flow from the gob to the face. Such airflow movements are more likely within large and highly permeable openings, and have unpredictable dynamics due to the random packing of large blocks of roof rock that control movement and direction of airflow in the zone behind the shields. Voids of an irregular nature behind the shields cause ventilation losses at the face, cause leaking air to pick up gases from the gob and potentially return them to the near-face area, connect to gas sources within the roof and floor, and may necessitate additional ventilation monitoring.

Gob formation and gob structure behind the shields affect the behavior of methane-air mixtures behind the shields and in the near-face area. Fluid transport properties of the gob in relation to porosity and permeability have been addressed in previous research.

Karacan et al. [8] and Esterhuizen and Karacan [9] used a geo-mechanical approach to convert calculated stresses in the horizontal and vertical directions to local porosities. Each porosity determination was subsequently converted to a permeability value using empirical equations. Gob porosities and permeabilities generated using this method change their values gradually with the gob dimensions and are considered as ideal and smooth distributions. Smith and Yuan [10] used smoothly distributed permeability values within the gob region of a CFD model to study airflow and spontaneous heating in the gob. Likewise, Marts et al. [11] estimated reservoir properties of gob using a similar approach and to predict where explosive zones could be. Karacan [7], on the other hand, used sizes, shapes, and distributions of the rock blocks that could be determined from digital images to estimate gob porosity and permeability under different loadings.

The distributions of the properties and their values in the gob and in the near-face region are important in assessing their effects on the movement and retention of gas in a porous body. They are also important for evaluating exchanges of ventilation air, methane, and other gases between longwall faces and void areas behind shield lines. Theoretical modeling of flow based on the highly idealized situation of smooth permeability shows a very smooth air movement, as an arch, within the immediate gob as the result of smooth permeability and pressure gradient within the gob [10-12]. In reality, however, this is not always the case, and air movement in the gob and behind the shields is complex and controlled by the discrete nature of the fractures and the fracture network. Therefore, a more realistic representation of the distribution of gob properties is needed to better qualify and quantify the air and gas flow and the mixing process that occurs within the gob.

In this work, we present a comparative study to investigate smoothly distributed gob permeability and the permeability field created by discrete fractures for their effects on air movement near the face. For this study, we generated discrete fracture networks using controlled statistics on fracture directions, spacing, and aperture, as well as their termination. These networks along with porosity and permeability data were imported into a CFD model of a longwall mine panel described in Smith and Yuan [12] (2010). The results of air movement along the face area were compared with those of uniform permeability reported in the same study.

2. Gob and ventilation layout

This work uses the CFD model described in Smith and Yuan (2010) with the same boundary conditions. The CFD model developed for that work was only for an active panel and simulated a Y-type bleederless ventilation system.

A commercial CFD program, FLUENT, from Ansys, Inc., was used in this study to simulate the gas flow. The layout of the panel and the ventilation system are shown in Figure 1. The simulated gob area is 1,000 m long, 300 m wide, and 10 m high (as 5 separate mesh layers) starting from the bottom of the coal seam. The model was constructed using meshes of 2 m in size. The ventilation airways are 2 m high and 5 m wide. In the model, the headgate entry is ventilated and eventually goes to return after passing the back end of the panel. The simulations were conducted using the steady-state

solution as the initial conditions. The face is assumed to be stationary during the simulations.

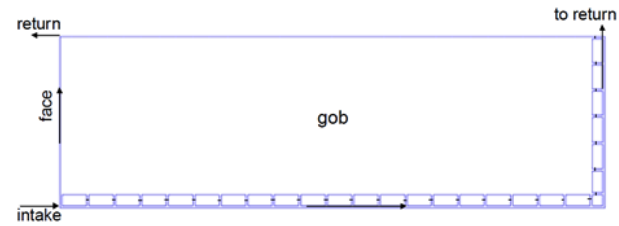


Fig. 1. Layout of longwall panel and ventilation system used in simulations.

Typical ventilation pressures for the bleederless ventilation system were used in the simulations. The pressure was -3.0 inches water gauge at the intake inlet and -3.5 inches water gauge at the return outlet. To control the airflow quantity to the longwall face, the wall roughness was adjusted to have a realistic intake airflow rate of 30 m/s (64,000 cfm). The gas flow in the longwall gob area was treated as laminar flow in a porous media using Darcy's law, while the gas flow in the ventilation airways was simulated as fully developed turbulent flow.

In this paper, our aim is to compare airflow in the gob and around the face area with respect to formation of the gob and distribution of its properties. In Smith and Yuan [10,12] permeability and porosity distributions of the gob area were based on geotechnical modeling [9], where translation of calculated stresses to permeability resulted in values varying between 3.0×10^{-4} to 8.5×10^{-4} millidarcies (md), and in porosity values varying between 0.17 and 0.41. Around the perimeter of the gob and immediately behind the face shields, the permeability and porosity values were the largest, while near the center of the gob, these values were the smallest due to compaction. One consequence of this treatment was the formation of continuous and symmetric zones of permeability and porosity, smoothly distributed over a large area and changing gradually with physical dimensions. A further and natural consequence of this treatment was on the gas movement; in such a porous medium (gob) flow profiles are continuous and smooth, which rarely happens in a fractured medium that is formed by disorderly assemblage of broken rocks with varying sizes and shapes.

In order to be able to reflect the random and discrete nature of the gob and to compare characteristics of the flow with those of the smooth profiles, we replaced the gob area of the CFD model with a discrete fracture network (DFN) model. In this process, in order to keep the value range the same, we scaled the original range of permeability and porosity values to fracture aperture and assigned the values to CFD mesh.

3. Discrete fracture network representation of gob

3.1 Generation of discrete fracture networks (DFN)

The discrete fracture network was generated using FracGen [13]. FracGen generates stochastic networks of lines that represent naturally occurring fractures in strata-bound reservoirs or aquifers. The fracture patterns generated by FracGen range from regular to random, or clustered, depending on the expected or observed

fractures in reality, and these features are controlled by the selected model. Since it is reasonable to expect that the fractures are random in a gob environment, the random fracture model was used.

In this work, 5 layers of fracture networks to represent the lower gob (caved zone) were generated. Each layer was 2 m thick, 300 m wide, and 1000 m long. The intensity of fracturing was decreased gradually from bottom (layer-1) to top (layer-5) to mimic the variation of intensity of fractures with gob height and also to change the fracture network and the vertical connections.

Each gob layer was generated by using two sets of fractures. A set is a series of fractures oriented in a certain direction. Of these two sets, set-1 was the master fracture set, which distributed the centers of the fractures in a set over the entire gob using a uniform probability distribution. Set-2 fractures were the regional fractures and they connected to the fractures of set-1.

Set-1 was controlled with Gaussian probability distribution and its direction was set with a mean of 90 degrees from north and a standard deviation of 45 degrees. In this set, the minimum fracture length was 3 m and the maximum length was 76 m, with fractures distributed following a uniform probability distribution to generate a 0.0097 fracture center point in each meter square (m²) of the area. In other words, this parameter controlled the fracture intensity. Fracture apertures were set with a mean of 0.6 m and a standard deviation of 0.15 m. In addition to the basic fracture attributes, how fractures should terminate was defined. Fractures may terminate at another fracture (T1) or at two different fractures (T2). Fracture terminations were controlled by a process called synthetic annealing, which was used to match the given intersection frequencies to a frequency

histogram for the set of fractures. During this process, fracture orientation was changed, endpoints were moved, densities were adjusted, and lengths were varied to be able to be consistent with the fracture densities. In layer-1, set-2 fractures had the same properties as those of set-1, but fracture orientations were defined with mean and standard deviation of 0 and 45 degrees, respectively.

Layers 2 to 5 of the gob were generated the same way. However, in order to decrease the intensity and continuity of fractures with gob height, and also to decrease the variation in orientation, maximum fracture length was decreased by 7.6 m, standard deviation of fracture orientation was decreased by 10 degrees, and fracture density was decreased by 0.0015 fracture center points per meter square for both set-1 and set-2 at each layer moving up. Figure 2 shows the aperture plot of the DFN generated for layer-1 and layer-5 of the gob.

3.2 Mapping and importing DFN values into CFD

The next step was to import DFNs of different gob layers with their permeability and porosity values into the CFD model.

CFD simulation models are based on grids (meshes). Therefore, assigning fracture centers to that system would not be helpful in assigning values and their continuity in each grid of known size and position in the gob. In order to tackle this problem, a DFN aperture map of each layer was mapped onto a grid of the same size as the CFD's grid area (500 x 150). For this purpose a gridding method with bi-linear interpolation—so that the generated grid would be equal to the CFD grid—was used.

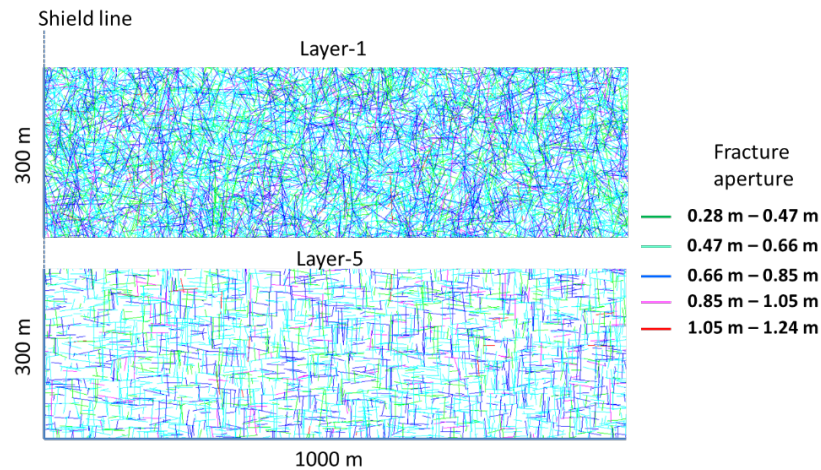


Fig. 2. Aperture plots of the DFN generated for layer-1 and layer-5 of the gob area.

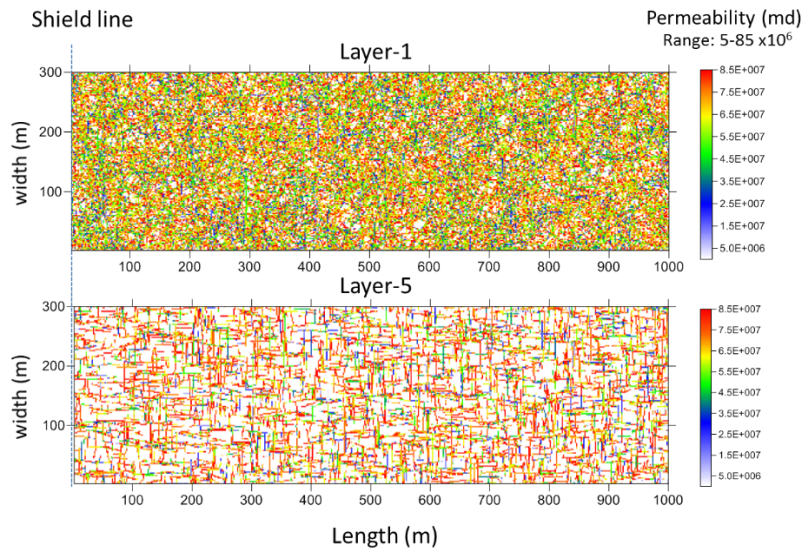


Fig. 3. Permeability maps of layer-1 and layer-5.

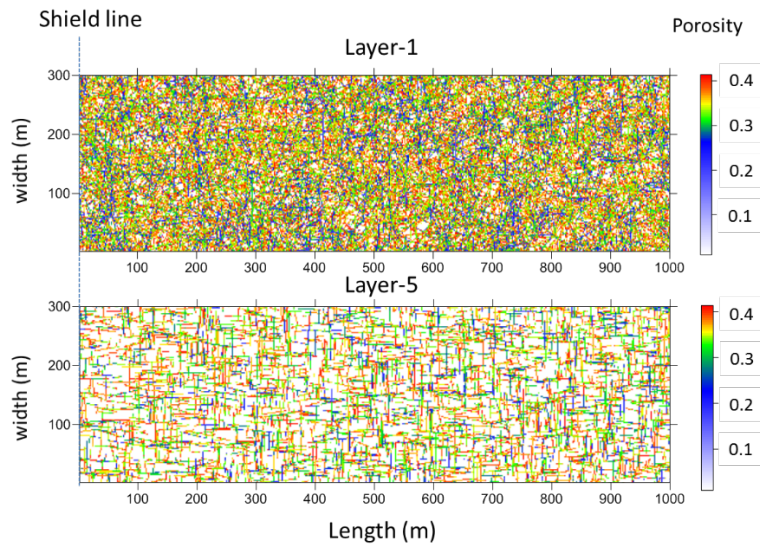


Fig. 4. Porosity maps of layer-1 and layer-5

After gridding the DFN maps, the fracture permeability and porosity ranges—i.e. 3.0×10^0 to 8.5×10^7 md, and 0.17 and 0.41—were scaled and mapped onto the grid based on the aperture distributions. This approach was taken to be consistent in the range of values that was used in the CFD model. The properties of those areas that were outside of any fracture grid, however, were assigned 1000 md and 0.01, as permeability and porosity, respectively, to represent less permeable areas, such as rocks and rock piles with no apparent property for gas transport. Such definition of the gob enabled the representation of a stochastically formed gob with its impermeable areas as well as fractures of various levels of randomly distributed transport and storage properties.

Next, permeability and porosity maps of all 5 layers were imported into the CFD code. Figure 3 and 4 show layer-1 and layer-5 with permeability and porosity fields, respectively.

The permeability and porosity maps of different layers of caved gob (Figures 3 and 4 for layer-1 and layer-5) were for the entire gob area and fractures begin immediately behind the shield line. While this may be the situation for weak roof materials where coal-measure strata cave immediately behind the shields, it is certainly not the case where roof rocks are competent and may hang for a while before they cave behind the shields. In such a situation, voids behind the shields can be larger, creating parallel airways for large amounts of air to leak behind the shields and into the gob. The immediate consequence of this is a decrease in the face air quantity and also a decrease in the air quantity needed for the tailgate corner. Furthermore, the rugged interface between the caved rocks and the void behind the shields may change the airflow pattern for air to recirculate to the face by picking up hazardous gases from the gob through connecting fractures. Therefore, strong roof conditions and the void behind the shields are of

theoretical and practical importance for longwall face ventilation.

In order to investigate this problem for airflow and the consequences for face ventilation using the CFD model, the grids of layer-1 (the first 2-m height of the gob) behind the shield line were modified in two additional models at a random pattern to create a zone of high permeability (1.0×10^{-10} md) and porosity (0.99). The average thickness of this zone was around 3 m in one case and 7 m in the other. These models were also imported into the CFD model as comparison cases, and they are shown in Figure 5 on the first 100-m section of the gob for easy visualization.

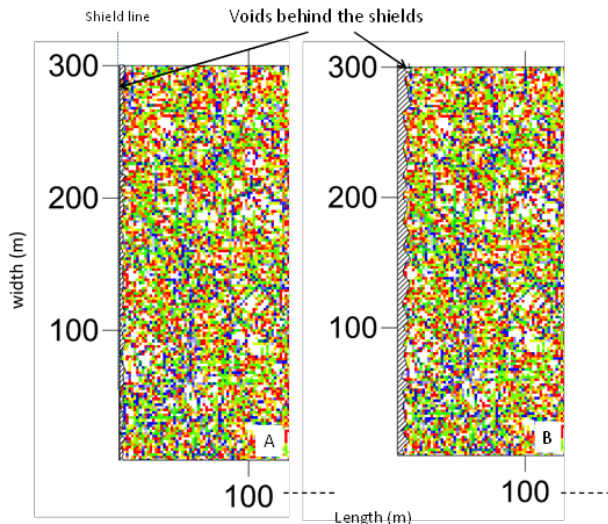


Fig. 5. Gob models (permeability shown) with varying-thickness void space behind the shields. A: 3-m average thickness, B: 7-m average thickness.

4. Results and discussion

CFD simulations were performed using the following flow and pressure boundary conditions: inlet airflow, 30 m/s (64,000 cfm); pressure at intake, -3.0 in. wg; pressure at return, -3.5 in. wg. In models, each of the gob permeability and porosity cases discussed in the previous section were used for comparison of airflow distribution around the face. For comparison purposes, these cases are described and are named as:

- Base case: the base model that used gob permeability and porosity distributed smoothly following a parabolic surface [9,10] (Smith and Yuan, 2008; Esterhuizen and Karacan, 2007).
- DFN: Discrete fracture network representation of gob and permeability and porosity distribution. This is the case where gob fractures are immediately behind the shields for direct comparison to the base case for flow distribution.
- DFN-void3: Discrete fracture network representation of the gob as in the DFN-full, but having a randomly generated void space with an average thickness of 3 m behind the shield. This case is to investigate the potential effect of the DFN and strong roof conditions that leave

large openings when caved. This model is illustrated in Figure 5-A.

- DFN-void7: Discrete fracture network representation of the gob as in the DFN-full, but having a randomly generated void space with an average thickness of 7 m behind the shield. This case is to investigate the potential effect of the DFN and strong roof conditions that hang before caving and leave a large opening behind the shields. This model is illustrated in Figure 5-B.

The flow patterns of air inside a gob have a profound effect on the spontaneous heating, methane distribution, and thus the formation of explosive zones and performance of gob gas ventholes. In order to visualize the flow patterns inside the gob, a virtual horizontal reference surface was created 1 m from the bottom of the mined coal seam floor to compare the results with respect to this horizontal reference surface. Therefore, the flow patterns that will be presented are within the first layer of the gob in the model. However, bearing in mind that the flow field is 3-D, although the vertical component of flow can be minimal due to weak pressure gradients in that direction, this layer is not independent of the other layers and still carries the signatures of interactions.

Figures 6 and 7 show velocity contours and flow-path lines, respectively, in the gob area to compare the base case with the DFN. The flow-path lines were generated by releasing 300 massless particles evenly distributed along a line that is 2 m away and parallel to the face shields. The color of the flow-path lines represents the velocity magnitude, while the numbers of flow-path lines in a certain area represent the amount of the airflow in that area. The single flow line some distance into the gob indicates that the quantity of airflow there is low.

The contour plots in Figure 6 show that the base case (A) has higher diverging and converging velocities (0.005-0.008 m/s) near the headgate and tailgate compared to the rest of the velocities observed. The results show that the near-gob zone behind the shields has a very smooth flow field with velocities around 0.001 m/s. These results suggest that permeability and pressure fields are changing gradually behind the shields, which is probably not true in reality. This is an expected consequence of smooth permeability and porosity fields being assigned to the gob. In comparison to the base case, Figure 6-B shows that the velocity contours of the DFN are more irregular and localized, and are distributed in the near-gob area behind the shields as well as at the tailgate and headgate corners. Within these contour areas, the velocity is variable and does not form gradually changing zones or values as the result of effective heterogeneity and connectedness of high and low permeability fractures as well as pressure field, as expected from flow in a fractured rock mass.

Figure 7-A and B show the flow-paths obtained for the base case and the DFN. The path lines in Figure 7-A show that flow through the gob was mainly concentrated behind the shields. At the headgate side, air leaked through the shields but some flowed back into the face again through the shields near the tailgate side. The air velocity ranged between 0.002 to 0.006 m/s in the gob, near the shields. The most notable result, though, is that much of the flow lines concentrate immediately behind the shields and that the flow lines are always continuous

and very smooth, indicating no heterogeneity and no aspect of the fractured medium disrupting flow lines (Figure 7A).

Contrary to the case of smoothly distributed properties, the flow lines resulting from the DFN are more tortuous, discontinuous, and localized based on the connectedness of fractures, continuity of permeable paths, and distribution of pressure differentials within those (Figure 7B). This figure also shows that some flow lines terminate in the gob, indicating that flow meets a dead end in the fractured medium, as well as local areas of faster flow. These are natural and expected consequences of dynamic challenging in flow in strongly heterogeneous fractured medium. Dynamic channeling and transport gives rise to fast and localized flow-paths, which are dependent on the permeability, its spatial distribution, and the pressure field [14]. The fast flow-paths occur not exclusively, but in addition to the existing fast flow associated with the presence of connected high-permeability zones, like a series of connected fractures or open channels within the gob. This also can be observed in Figure 7B following some of the flow lines. The effect of channeling on flow may also occur if there are saturation variations, i.e. if the gob is accumulating water.

The results presented in Figures 6 and 7 have important implications in terms of formation of explosive zones in the gob, spontaneous combustion, methane management, and predicting the performance of bleeder systems. The base case suggests that the formation of such zones will be continuous and smoothly distributed, whereas the results from the DFN suggest localized and discontinuous areas that may require attention in terms of improving predictive capabilities and control measures. Therefore, it is essential to conceptualize and formulate the gob by honoring its stochastic nature and the heterogeneity of flow.

In addition to the flow within the gob, the percentage of air flowing in the face area in relation to the inlet flow was also computed at the middle-point of the face. These computations showed that the base case had 98.1% of the inlet amount flowing in the face as opposed to 98.7% in the DFN. These numbers are comparable and suggest that although heterogeneous gob significantly affects the flow and related processes, it may not change the air quantity in the middle of the face as long as there is no void behind the shields.

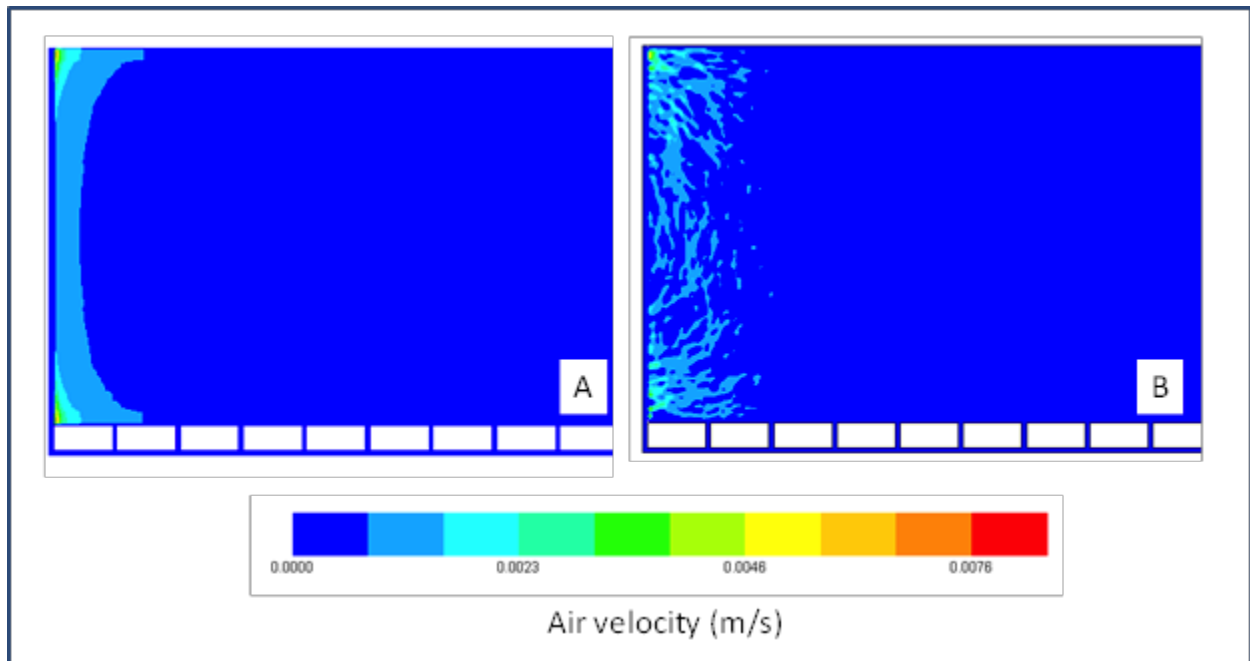


Fig. 6. Velocity contours behind the shields in the near-face region of the gob. A-base case, B-DFN.

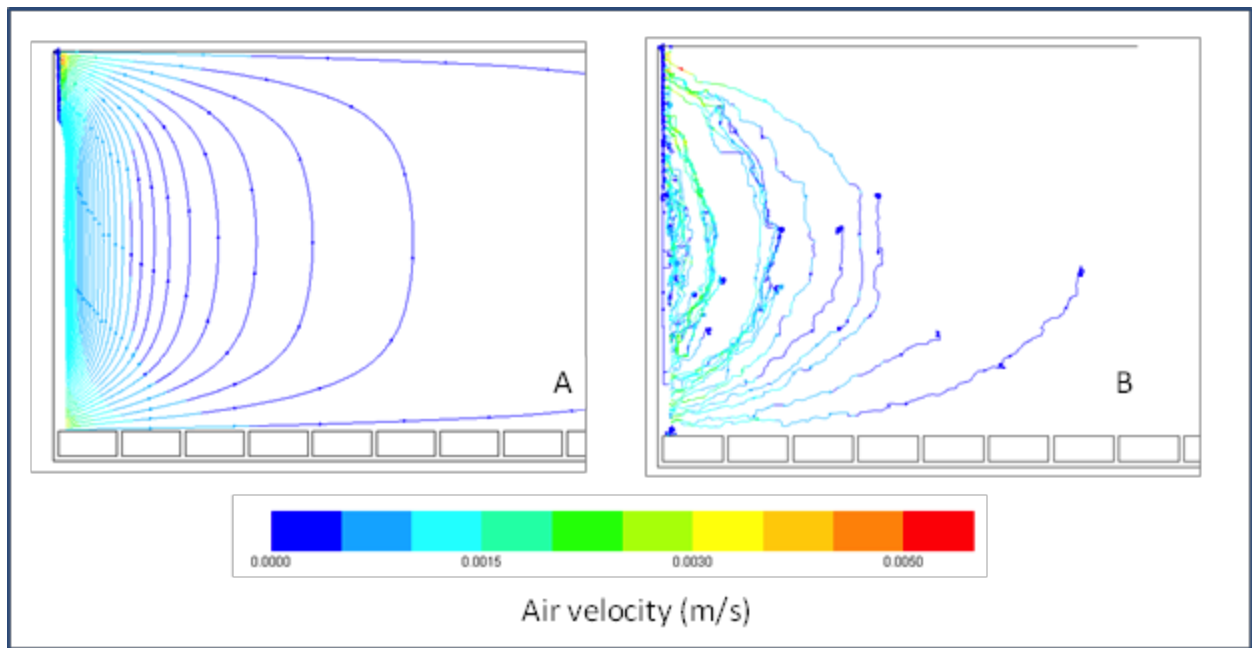


Fig. 7. Flow lines behind the shields and in the gob. A-base case, B-DFN.

Figure 8-A and B show the flow lines that result from another case of practical importance, especially in the case of competent roof conditions that leave voids behind the shields. Such voids usually are of varying thickness from the shield line and therefore are of different flow cross section and roughness. To investigate these situations, models DFN-void7 and DFN-void3, presented earlier in this paper, were simulated. Figure 8-A, DFN-void7, shows that most of the flow at the headgate travels behind the shields with a minimum amount of flow circulating back in to the gob.

In the case of a narrower void (DFN-void3) shown in Figure 8-B, on the other hand, although there is still a lot of air passing behind the shields, a larger amount of flow circulates back into the gob and to the face following the tortuous paths and heterogeneity in the gob. The air velocities within the observed flow lines are in the range of 0.0005 to 0.0015 m/s. This may be due to the obstructions to flow along the path behind the shields.

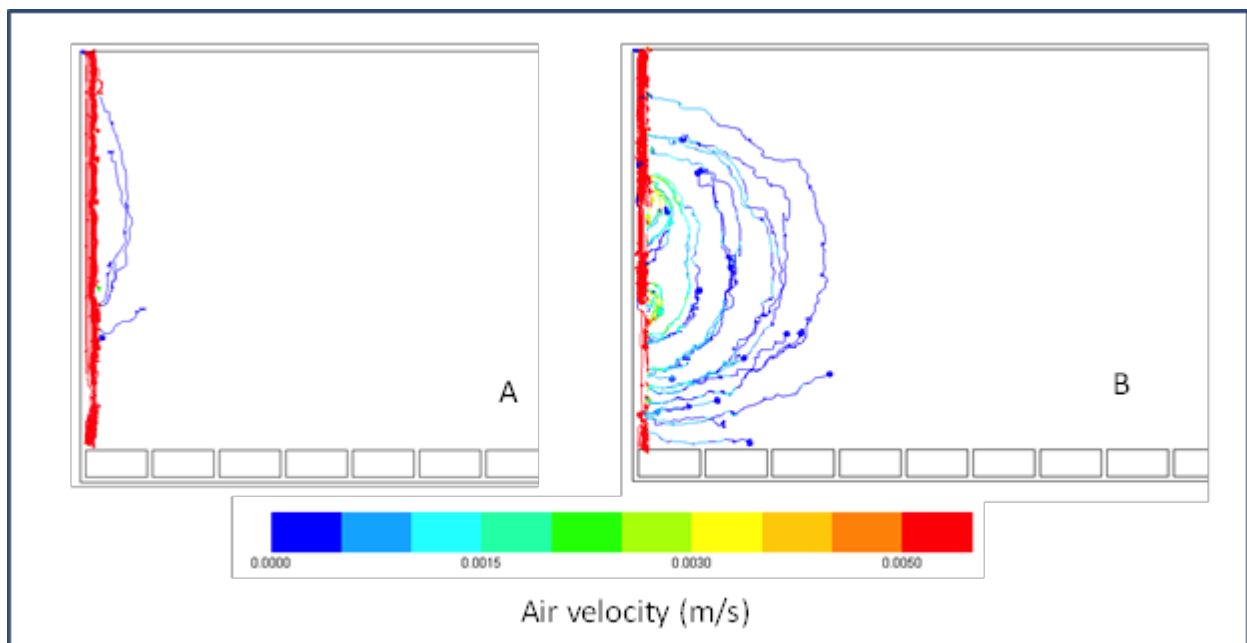


Fig. 8. Flow lines behind the shields and in the gob. A-DFN-void7, B-DFN-void3.

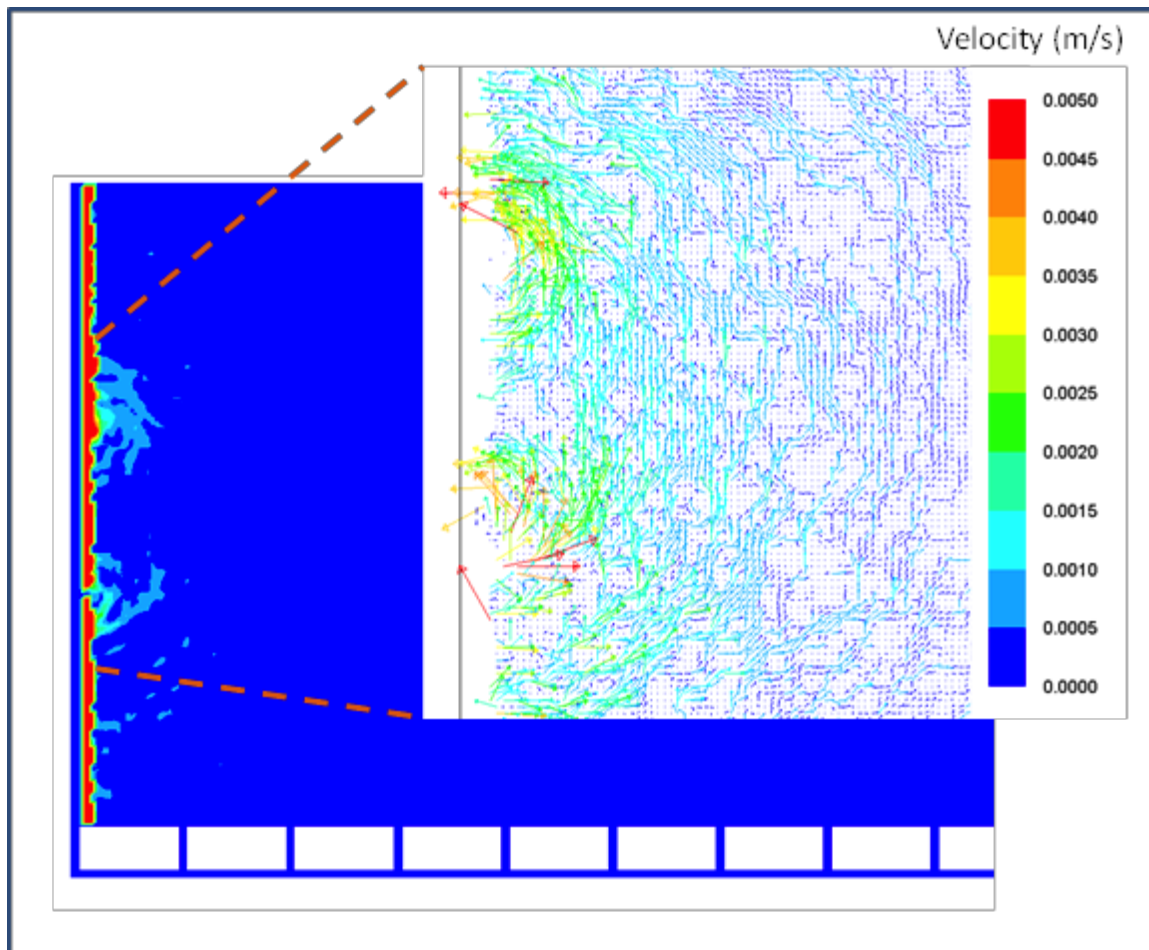


Fig. 9. Velocity contour and velocity vectors of the flow behind the shields in DFN-void3.

Moreover, it is also very important to note the presence of zones of higher-velocity air circulation in the middle section of the gob (Figure 8-B). These zones can be of significant importance for ventilation and monitoring as these are localized regions of flow rate increases and where hazardous gases, i.e. methane, may be entering back into the face area from the gob. These areas are shown in a contour map of DFN-void3 and flow vectors of the recirculation in Figure 9. In this figure, it is clear that the airflow enters into the gob via fractures and then circulates back to the void space with even higher velocities in some vectors. A closer examination of the surrounding boundary in which this flow pattern occurs suggests that the rougher locations where there are abrupt changes in the geometry of the boundary and of the width of the void space serve as the “nucleation areas”. Such behavior was observed in flow over rough surfaces where what were considered as small-scale effects, such as an abrupt change in apertures, may result in significant change in velocity streamlines and potential secondary flows [15,16]. Their studies compared streamlines calculated at two different locations along the same fracture at three different Reynolds numbers. The first location was an area of a large change in aperture while the second location was of a small depression in the fracture. The results showed that even at low Reynolds numbers, the flow developed zones of recirculation, creating areas of the fluid that do not actively contribute to bulk flow. As the Reynolds number is increased, however, the recirculation zones

become larger and appear in more places. These results demonstrated that roughness of a surface can affect fluid flow even at low Reynolds numbers (low velocities).

The results presented in Figures 8 and 9 have additional implications to what were already discussed in relation to flow and the importance of capturing heterogeneity of the gob in order to be able to predict formation of zones of explosive mixtures, spontaneous combustion, and methane flow behavior. These results indicate that void space behind the shields and its morphology causes local areas of recirculation as well as abrupt changes in flow direction and its velocity within the gob and behind the shields. Therefore, it is imperative to monitor these locations for the amount of flow, for ventilation purposes, as well as for the concentrations in order to be able to prevent accidents that may stem from local accumulations of gases.

The presence of voids behind the shields also affects the amount of airflow in the face. The base case and the DFN model had 98.1% and 98.7% of the inlet flow in the middle of the face, respectively. However, when there is void space of varying thickness behind the shields, these quantities drop significantly. The percentage of the inlet airflow in the middle of the face was 41.9% and 22.4% in the case of DFN-void3 and DFN-void7, respectively.

5. Conclusions

Properties of the gob and how they are distributed spatially significantly affect airflow distribution and patterns within the gob and around the face. The flow patterns of air inside a gob in turn have a profound effect on the spontaneous heating, methane distribution, and thus the formation of explosive zones, performance of gob gas ventholes, and ventilation efficiency around the face. This study compared the effects of discrete fracture network representation of gob properties with those of smoothly distributed properties. This work also demonstrated the effects of voids behind the shields on face ventilation and airflow patterns in the gob.

Results showed that smoothly distributed gob properties result in smooth and continuous flow lines, and thus large areas of well-mixed explosiveness, for instance. This situation is highly idealized and may not occur in most longwalls, as gobs are highly heterogeneous. The flow lines resulting from the DFN, however, are more tortuous, discontinuous, and localized based on the connectedness of fractures, as expected in naturally occurring heterogeneous media. The heterogeneous nature of the gob represented as the DFN shows dynamic channeling and transport, as well as fast flow-paths with the presence of connected high-permeability zones. Therefore, the DFN can better indicate localized and discontinuous areas that may require attention in terms of control measures.

Voids behind the shields allow significant air bypass and recirculation. When the void behind the shields is narrower, more air may leak into the gob due to higher resistance or potential obstructions to flow along the path behind the shields. In the case of wider voids, flow bypass is larger but recirculation is less. Furthermore, the rough interface between the void and the gob creates localized regions of flow rate increases. These regions are associated with abrupt changes in the geometry of the boundary and of the width of the void space. Therefore, it is important to monitor these locations for the amount of flow, for ventilation purposes, as well as for the concentrations in order to be able to prevent accidents that may stem from local accumulations of gases.

Disclaimer: The findings and conclusions in this paper are those of the author and do not necessarily represent the views of the National Institute for Occupational Safety and Health (NIOSH). Mention of any company name, product, or software does not constitute endorsement by NIOSH.

References

- [1] JD McAteer et al., Upper Big Branch - The April 5, 2010, explosion: a failure of basic coal mine safety practices. Report to the Governor, Governor's Independent Investigation Panel, May, (2011) 121 pp.
- [2] CÖ Karacan et al., Coal mine methane: A review of capture and utilization practices with benefits to mining safety and to greenhouse gas reduction. *Int. J. Coal Geology*, 86 (2011) 121-156.
- [3] RB Krog et al., Airflow distribution patterns at a longwall mine depicted by CFD analysis and calibrated by a tracer gas field study. Preprint 11-067, Annual Mtg, Society for Mining, Metallurgy, and Exploration, Denver, CO (2011).
- [4] CÖ Karacan and G Goodman. A CART technique to adjust production from longwall coal operations under ventilation constraints. *Safety Science*, 50 (2012) 510-522.
- [5] R Balusu et al., Goaf gas flow mechanics and development of gas and sponcom control strategies at a highly gassy coal mine. Proceedings, Australia-Japan Technology Exchange Workshop, Dec. 2-4, Hunter Valley (2001).
- [6] SJ Schatzel et al., Prediction of longwall methane emissions and the associated consequences of increasing longwall face lengths: A case study in the Pittsburgh coalbed. In: Mutmansky JM, Ramani RV, eds., Proceedings 11th U.S./North American Mine Ventilation Symposium, Penn State University, University Park, PA, (2006) 375-382.
- [7] CÖ Karacan, Prediction of porosity and permeability of caved zone in longwall gobs. *Transport in Porous Media*, 82 (2010) 413-439.
- [8] CÖ Karacan et al., Reservoir-simulation based modeling for characterizing longwall methane emissions and gob gas venthole production. *International Journal of Coal Geology*, 71 (2-3) (2007) 225-245.
- [9] GS Esterhuizen and CÖ Karacan, A methodology for determining gob permeability distributions and its application to reservoir modeling of coal mine longwalls, SME Annual Meeting, 25-26 February, Denver, CO. (2007)
- [10] AC Smith and L Yuan, Simulation of spontaneous heating in longwall gob area with a bleederless ventilation system. *Mining Engineering*, August, (2008) 61-66.
- [11] JA Marts et al., Dynamic Gob Response and Reservoir Properties for Active Longwall Coal Mines, SME preprint no. 14-114 (2014).
- [12] AC Smith and L Yuan, Modeling the effect of seal leakage on spontaneous heating in a longwall gob area. In: Proceedings of 13th United States/North American Mine Ventilation Symposium, Hardcastle S and McKinnon K (Eds.). (2010) 479-484.
- [13] DOE, FracGen & NFlow. Naturally-Fractured Natural Gas Reservoir Simulator. National Energy Technology Laboratory, Morgantown, West Virginia (2010).
- [14] C-F Tsang et al., Dynamic channeling of flow and transport in saturated and unsaturated heterogeneous media. In: Flow and Transport through Unsaturated Fractured Rock. Evans D.D., Nicholson, T.J., Rasmussen, T.C. (eds). Geophysical Monograph 42, American Geophysical Union, (2001) 33-44.
- [15] K Suga et al., An analytical wall-function for turbulent flows and heat transfer over rough walls. *International Journal of Heat and Fluid Flow* 27, (2006) 852-866.
- [16] S Briggs et al., Numerical modelling of flow and transport in rough fractures, *Journal of Rock Mechanics and Geotechnical Engineering* 6 (2014) 535-545.

Ventilation Methane Emissions of Underground Coal Mines in Zonguldak Coal Basin-Turkey

Abdullah Fişne*, Samet Can Özer, Olgun Esen*

Istanbul Technical University, Mining Engineering Department, Istanbul, TURKEY

Methane emission from ventilation system of an underground coal mine is an important indicator of how much methane is producing and how much air should be provided to keep the methane levels under statutory limits. Knowing the amount of ventilation methane emission is also important for environmental considerations and for identifying opportunities to capture and utilize the methane for energy production. This study was conducted to determine the magnitude of the methane emission and control problem in Turkish bituminous coal mines in Zonguldak Coal Basin. The Basin, located on the Black Sea coast, is the only bituminous coal basin of Turkey. Mining activities in the basin started in 1848 and have been carried out in the region for over 160 years. Several national and international companies operated various coal mines in the basin. The five mines namely Armutçuk, Kozlu, Üzülmez, Karadon, and Amasra in the basin have been operated by Turkish Hardcoal Enterprise which is a state-owned agency, and occupies an area of 6885 km². The historical ventilation methane emission data indicate that the emission rate for the coal mines in Zonguldak Coal Basin depends primarily on the coal production rate and mine depth during the period 1990 to 2013. The results also indicate a general decrease in ventilation methane emission over the last 23 years corresponding to a downward trend in coal production. The average daily methane emissions in thousand cubic meter per day in Turkish bituminous coal mines were obtained as 45.9 m³/d for Kozlu, 50.7 m³/d for Karadon, 25.5 m³/d for Üzülmez, 24.5 m³/d for Armutçuk, and 6.6 m³/d for Amasra. A good correlation was found between the methane emission rate and coal production rate and mine depth for the mines in Zonguldak Coal Basin.

Keywords: coal mine, mine ventilation, methane emission

1. Introduction

Methane emissions can adversely affect both the safety and the productivity of underground coal mines due to its explosion risk. Ventilation has long been the primary means of controlling methane emissions in underground coal mines to keep methane levels well below the explosive limit by diluting methane emissions that occur during mining.

Methane emissions in an underground coal mine ventilation system are an important indicator of how much methane is being produced and how much air should be provided to keep the methane levels under statutory limits. Knowing the amount of methane in the ventilation stream is also important for environmental considerations and for identifying opportunities to capture and utilize the methane for energy production [1]. This preliminary evaluation was conducted to determine the magnitude of the methane emission and control problem in Turkish bituminous coal mines in Zonguldak Coal Basin.

Turkey is an important coal producer in world. Its total coal production is 70.4 million tons in 2012 (2.3 million tons of hard coal and 68.1 million tons of lignite). Most of the lignite reserve is operated by surface mining method. Zonguldak Coal Basin, located on the Black Sea coast is the only bituminous coal basin of Turkey. Mining activities in the basin started in 1848 and has been carried out in the region for over 160 years. Several national and international companies operated various coal mines in the basin. In 1938, the basin was acquired by Ereğli Coal Enterprise which operated these mines until 1983, when the Turkish Hardcoal Enterprise (TTK) was founded [2, 3]. Since then the mines in the basin have been operated by Turkish Hardcoal

Enterprise. This State owned agency occupies an area of 6885 km².

2. Description of Zonguldak Coal Basin

Zonguldak Coal Basin, located on the Black Sea coast, is the main part of the Upper Carboniferous bituminous coal basin of Turkey. Much of the bituminous coal mining has thus been concentrated in the Zonguldak Basin. The coal seams are located in a Carboniferous deltaic sequence of Westphalian-A age. The coal field has been disturbed by tectonic activity, first by Hercynian and later by Alpine orogenesis resulting in folding and faulting of strata [2]. The Carboniferous coal-bearing sequence of Zonguldak basin contains the Namurian Alacağzı Formation, Westphalian A Kozlu Formation and Westphalian B-D Karadon Formation [4]. The geological map of the basin is given in Figure 1.

Namurian-aged Alacağzı Formation consists predominantly of light-colored fine to medium-grained, cross bedded sandstones and siltstones interbedded with shale. Alacağzı Formation is conformably overlain by Kozlu Formation which contains of mostly coal seams. Westphalian-A aged Kozlu Formation is formed by interbedded sandstones, siltstones, mudstones, conglomerates and coals. The overlying Westphalian B-C aged Karadon Formation bears a similar succession as the Kozlu formation, however with less number of coal

seams. They exist more than twenty coal seams such as Mileopera, Çay, and Acılık within the Kozlu formation. Net coal thickness for this stratigraphic sequence ranges from 30 to 32 m across the Kozlu region [6].

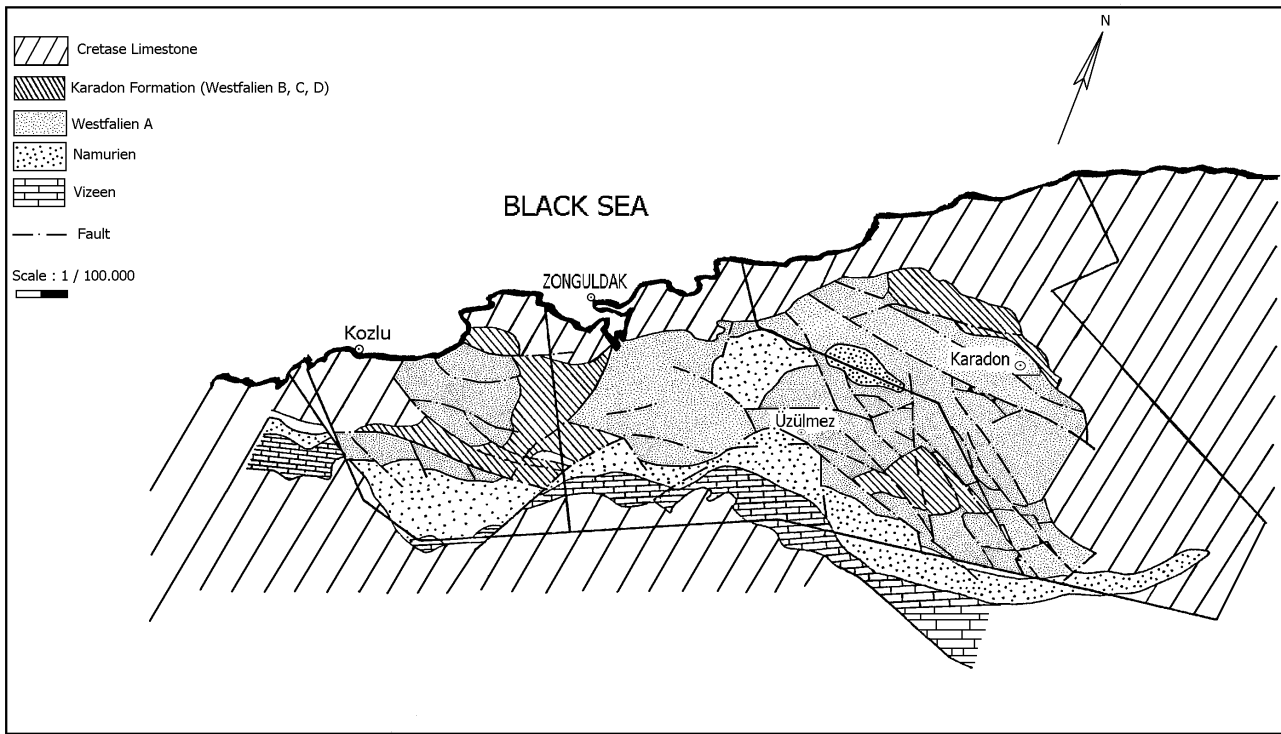


Fig. 1. Geological map of Zonguldak Coal Basin, Turkey [5].

Table 1. Description of underground coal mines in Zonguldak Coal Basin

Colliery	Reserve (x10 ⁶ ton)	Production (x10 ³ ton)	Number of Workers	Max. Depth (m)	Coal Type	Principal Mining Method
Amasra	407	250	774	400	Non Coking	Advancing and Retreating Manual Extraction Longwall with Caving
Armutçuk	33	252	1283	550	Semi Coking	Retreating Manual Extraction Longwall with Caving
Karadon	412	806	3590	540	Coking	Advancing and Retreating Manual Extraction Longwall with Caving
Kozlu	159	647	1990	630	Coking	Advancing and Retreating Manual Extraction Longwall with Caving
Üzülmez	305	486	1884	320	Coking	Retreating Manual Extraction Longwall with Caving

3. Mine Characteristics

Description of coal mines in Zonguldak Coal Basin is given in Table 1. The estimated coal reserve, carried to 1200 m under sea level, is about 1.32×10^6 tons of coal in this basin. 57 coal seams have been identified and 38 are workable with their thickness varying from 0.7 - 10 m and dips from 0 - 90°. The most important coal seams are the Cay and Acilik seams having average thickness of 6 and 4.5 m, respectively. Furthermore, the Sulu, Hacimemis, Domuzcu and Buyuk seams having an average thickness ranging from 1.5 m to 2.5 m are the other coal seams which are regarded as important for coal production. The coal has been produced by five collieries, namely, Armutçuk, Kozlu, Üzülmez, Karadon and Amasra from west to east. The Run-of-mine production in 2012 is about 2.44 million tons, using a labor force of workers 10490 of which 8637 was in underground.

It can be seen from Table 1 that the principal mining method in the basin is advancing and retreating long wall mining with back-caving. The folded and faulted geological condition in the basin prevents application of mechanized extraction; therefore, coal production is carried out only with the use of pneumatic hand picks and explosives. Also, high pressure air blasting technology is practiced in some seams which have a thickness of above 2 m and inclination above 45°. In the region, mining is extremely labour intensive because of limited application of mechanization in mining. Timber is exclusively used in coal face support. Galleries and gate roads are driven by drilling and blasting techniques and supported by steel arches. Underground transportation and haulage are carried out by belt conveyors and railways along the galleries, and then coal hoisted out to surface with the help of cages or skips operating within the shafts [7].

Average mining depths, annual production rates and average specific methane emissions data were analyzed from 1990 to 2013 for the coal mines in TTK. Specific methane emissions were calculated by the air velocity measurements and methane concentrations from return air shafts. Figure 2 shows the variation of production rates from 1990 to 2013 in the Zonguldak coal basin. It can be seen from the figure that the production rates show a continuous decline at Amasra, Armutçuk, Karadon, Kozlu and Üzülmöz Collieries.

Because of the difficult mining conditions imposed by the geology's structural complexity, mechanized mining methods cannot be used. Instead, labor intensive methods are in use (e.g., retreating short wall method with back caving is common). The high pressure air breaking method is used in the steep coal seams with a dip greater than 45 degrees and a seam thickness greater than two meters. Saleable production is approximately 80% of the mine production. Although coal production is declining, infrastructure projects including gallery and deep shaft development are underway with the goal of increasing production to 5 million tons per year from TTK's five mines. TTK has also opened approximately 40% of its resources to private sector miners under a royalty agreement. Currently, the private sector companies are producing about 1 million tons per year,

but are expected to increase production to 5 million tons per year in the midterm.

Figure 3 shows the variation of average mining depths from 1990 to 2013 in the Zonguldak coal basin. 38 coal seams are mineable for production out of 52 coal seam. The coal seam thicknesses change between 0.7 and 30 meters and the inclinations vary from 0° to 90°. Depth of mining has increased through time as shown in Figure 3. Currently, Armutçuk and Kozlu are the deepest at about -500 meters with Karadon at about -350 meters. At the Kozlu mine, significant reserves remain for many decades of coal production with the possibility of mining below -1000 meters in the future. TTK management expects the trend of mining deeper levels will continue. Under current practices, the number and severity of outbursts will increase as will methane emissions at the coal face as mining at deeper levels occur.

Due to nature of steep coal seams, the depth of mining were changed rapidly and getting deeper in the coal basin. The average mining depth increases approximately 12 meters for each year. The production and development operations have continued at the depths such as -540 and -630 meters in Karadon and Kozlu Collieries respectively. In these collieries, mining operations are prepared for deep coal mining at -1000 m.

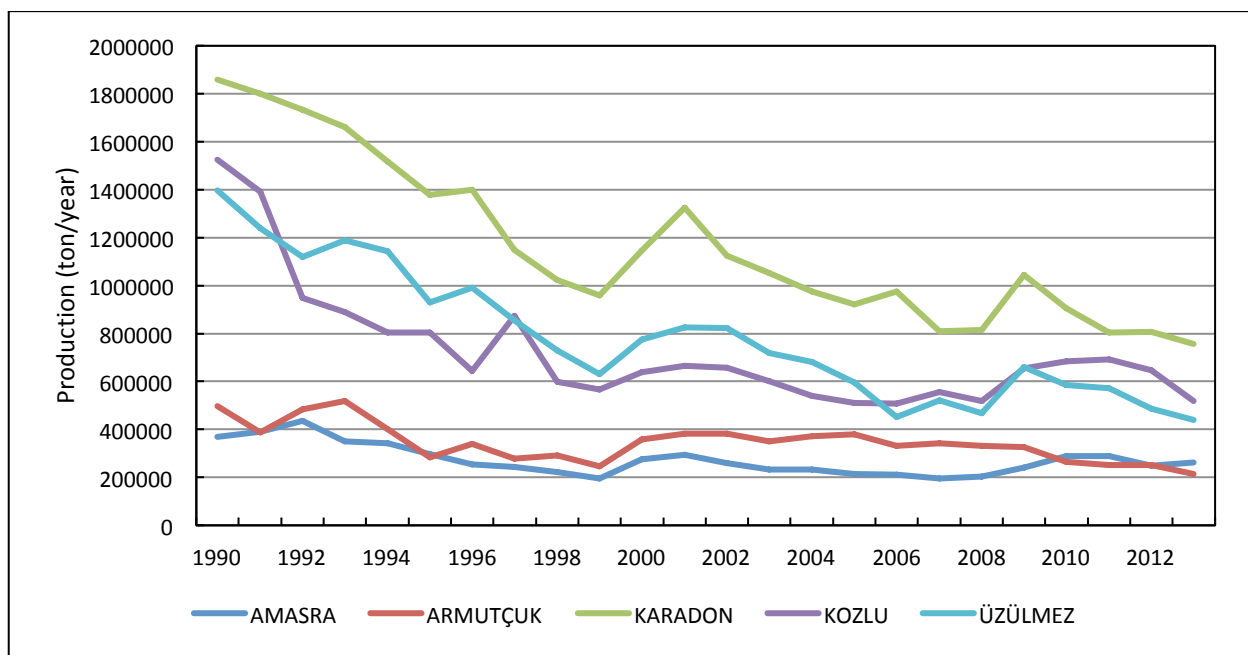


Fig. 2. Variation of production rates from 1990 to 2013 in the Zonguldak Coal Basin.

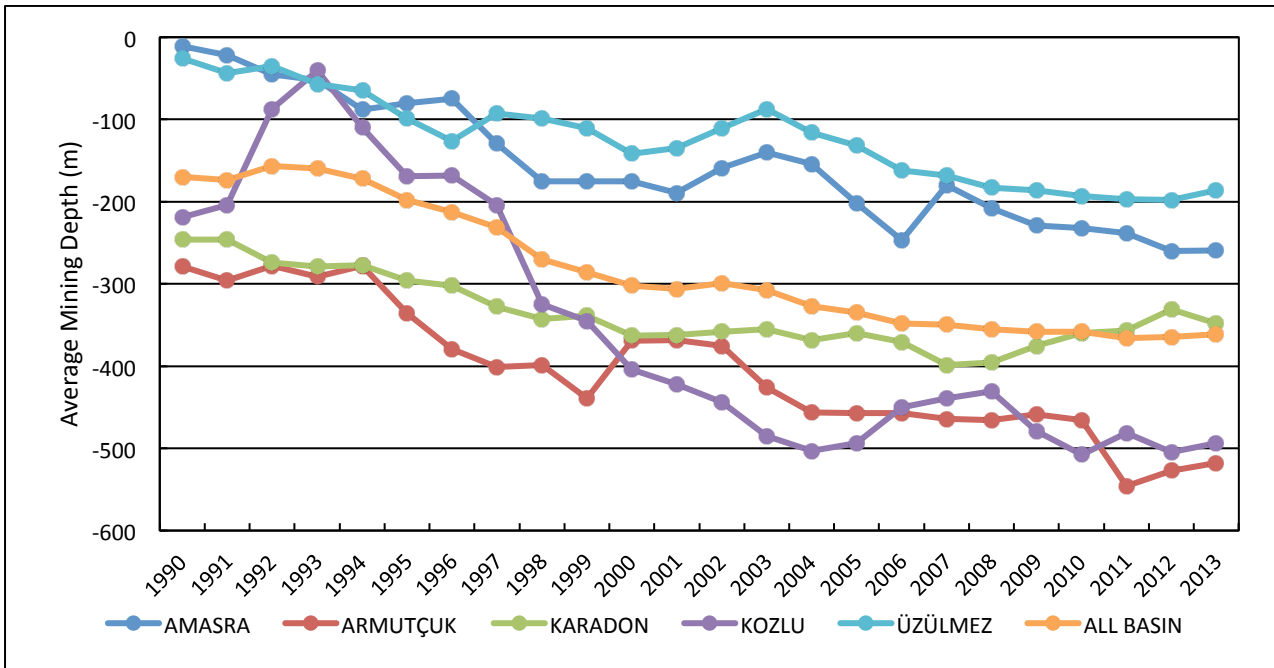


Fig. 3. Variation of average mining depths from 1990 to 2013 in the Zonguldak Coal Basin.

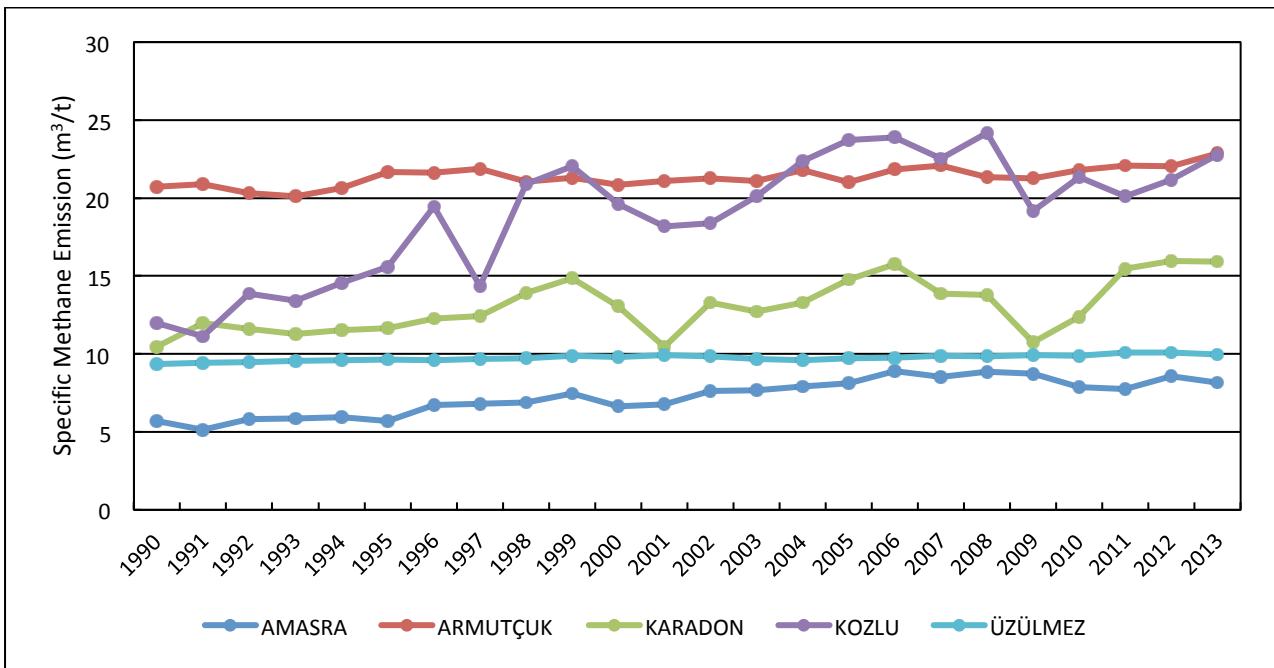


Fig. 4. Variation of specific emissions from 1990 to 2013 in Zonguldak Coal Basin.

4. Methane Emission

There are various geological and operational factors affecting a mine's methane emissions while coal is being extracted. The individual contributions of each of these factors to the total amount of emissions vary and, in most cases, may be difficult to distinguish from each other. Therefore, a relative term called "specific emissions" is used, quantified as a lumped parameter to designate the gassiness of a mine [8].

Specific emission is described as the amount of methane generated per unit amount of coal that is mined

[9]. This parameter is used to determine the ventilation and drainage requirements of a coal mine.

Methane emissions from TTK mines are reported as specific emissions, expressed in cubic meters of methane per tonne ($m^3/tonne$) of coal produced. Figure 4 shows the historical specific emissions by mine.

The specific emissions from an active mine will always be greater than the measured gas content of the mined coals. This is because additional methane is released from coals not mined as well as from other

gas-bearing strata that have been disturbed by the mining process. The Üzülmöz and Amasra mines are the shallowest and have the correspondingly lowest specific

emissions, while the Armutçuk, Karadon and Kozlu mines are among the deepest and have correspondingly higher specific emissions.

Table 2. Average values of mining depths, annual production rates and specific methane emissions at the collieries from 1990 to 2013.

Colliery	Mining Depth (m)	Production (ton/y)	Specific Methane Emission (m ³ /t)	Methane Emission Rate (10 ³ m ³ /d)	In-Situ Gas Content (m ³ /t)
Amasra	155	273245	7.26	6.61	5.37
Armutçuk	405	344512	21.36	24.53	6.87
Karadon	335	1164191	13.06	50.69	7.21
Kozlu	350	726370	18.95	45.88	8.73
Üzülmöz	123	784461	9.75	25.49	4.91

The average values of mining depths, annual production rates and specific methane emissions from 1990 to 2013 were given in Table 2 to assess the gassiness of Amasra, Armutçuk, Karadon, Kozlu and Üzülmöz Collieries. In-situ gas content values were obtained for each colliery by the limited number of gas content measurement studies in the basin [10]. These gas content values are also given in Table 2.

Armutçuk Colliery has the deepest production level in the coal basin with the depth of 405 meters and it is followed by the Kozlu and Karadon Collieries with the depth of 350 and 335 meters respectively. The shallowest mine are Amasra and Üzülmöz Collieries with the depths of 155 and 123 meters respectively. The highest annual production rate is in the Karadon Colliery with a production rate of 1 million tons of coal in the coal basin and it is followed by Üzülmöz and Kozlu Collieries in terms of highest production levels. The lowest coal production rates are in Amasra and Armutçuk Collieries. The most gassy coal mines in terms of specific emissions are Armutçuk and Kozlu Collieries in the coal basin. The specific methane emissions for these two collieries were determined as 21.36 m³/t and 18.95 m³/t respectively. Karadon follows these colliers with 13.06 m³/t specific methane emissions. Üzülmöz and Amasra Collieries have the lowest specific methane emissions with 9.75 m³/t and 7.26 m³/t respectively. According to Öztürk [10] in-situ gas content results are varied between 4.91 and 8.73 m³/t.

5. Analysis and Discussion

The influence of average mining depth on specific methane emission was investigated for the collieries in the basin and results were given in Figure 5. It can be seen from the figure that there is a good correlation between average mining depths and specific methane emissions. The methane emission rate rises in direct proportion to increasing mining depth.

The influence of average daily coal production on methane emission rate was investigated for collieries and the results were given in Figure 6. Most of parameters that influence on methane emission rate are also influence on production rates in underground coal mining. Field practices show the methane emission is directly related with coal production and increases with highest coal production rate [1, 11]. The methane

emission is increased by increasing the coal production and it is shown in Figure 6.

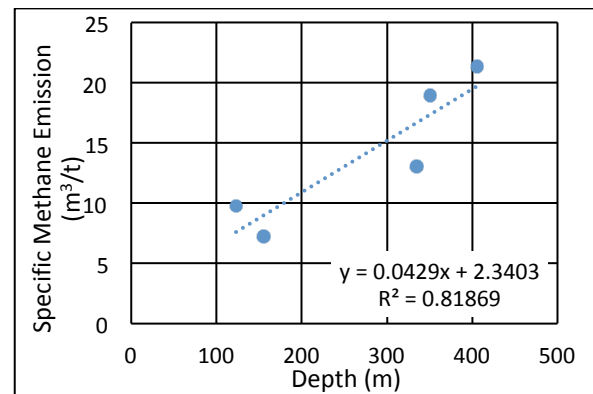


Fig. 5. Specific methane emission versus average mining depths for the mines in Zonguldak Coal Basin.

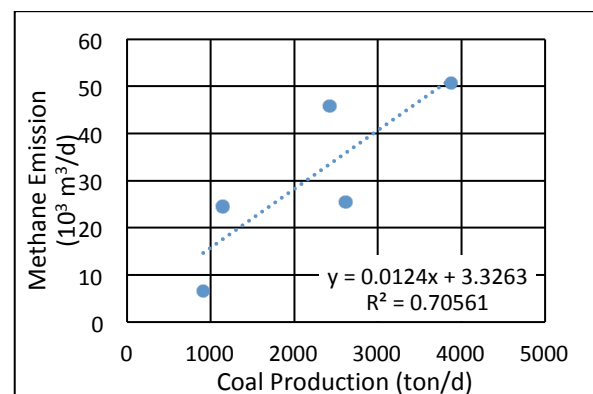


Fig. 6. Methane emission rate versus average coal production for the mines in Zonguldak Coal Basin.

As stated previously, methane emission rate for the coal mines in Zonguldak Coal Basin depends primarily on the coal production rate and mining depth. The influence of these two parameters are shown in Figure 7.

It can be seen from Figure 7, 89 % of the variation in methane emission could be explained by the variation of depth and production parameters. Irani et.al. [12] observed similar results for US underground coal mines.

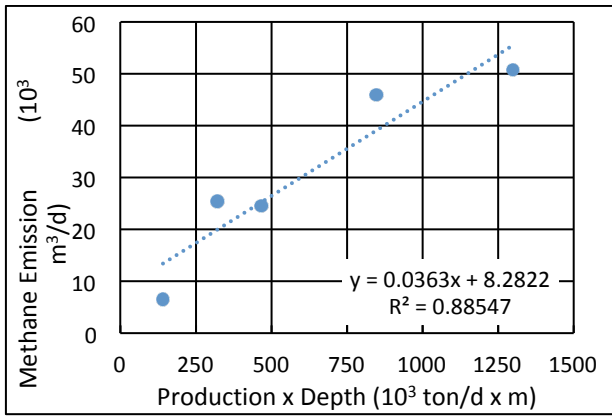


Fig. 7. Methane emission rate versus coal production rate times average mining depths for the mines in Zonguldak Coal Basin.

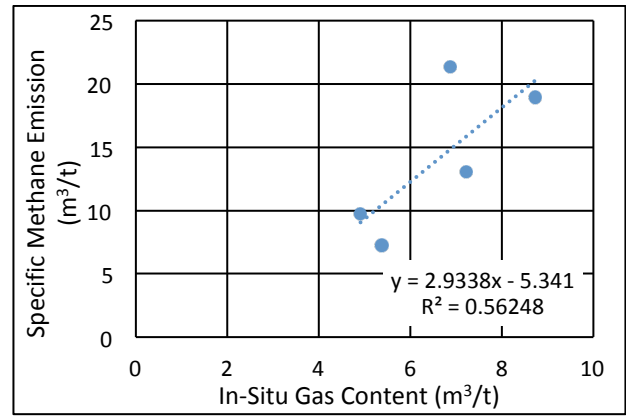


Fig. 9. The relationship between specific methane emissions and average in-situ gas content for the mines in Zonguldak Coal Basin.

Saghafi et.al. [13] investigated the relationship between production x in-situ gas content and methane emissions in Australian coal mines. They determined the methane emission is 4 times greater than production x in-situ gas content. In this paper, similar investigation was performed for coal mines in the Zonguldak coal basin and the result was given in Figure 8.

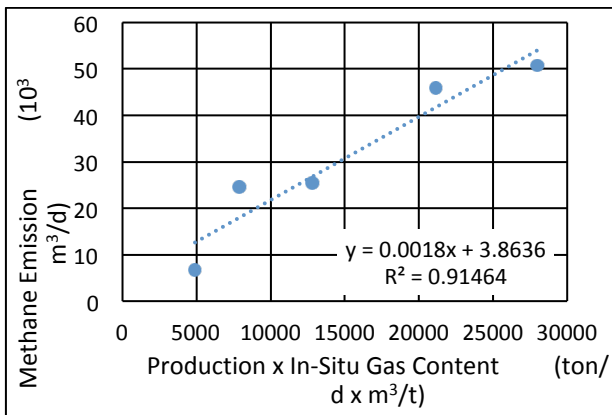


Fig. 8. Methane emission rate versus coal production rate times in-situ gas content for the mines in Zonguldak Coal Basin.

The relationship between specific methane emissions and average in-situ gas content values were investigated and the result was given in Figure 9. It is determined that the specific methane emission values are 3 times greater than the coal seams' gas contents. Kissell et.al. [14] were performed the similar investigations for US coal mines and they found that the specific methane emission values are 7 times greater than the coal seams' gas contents. The difference between the collieries of Zonguldak coal basin and US coal mines is distinct mining method application in each country and different geological condition.

6. Conclusion

Turkey's hard coal resource is restricted to a relatively small area along its northwest coast of the Black Sea. The coal measures are composed of numerous seams with high gas content. Mining conditions are extremely difficult because of intense faulting and folding of the strata with inclinations of up to 90 degrees. Difficult mining conditions, together with high gas contents and low permeability, have led to numerous coal outbursts, many of which have been catastrophic. Because of the complex nature of the geology, mechanized mining methods cannot be used so the mining is very labor intensive, exposing many miners to the hazards posed by the outburst conditions.

The objective of this preliminary study is to determine the magnitude of the methane emission and control problem in Turkish bituminous coal mines in Zonguldak Coal Basin. The historical ventilation methane emission data indicate that the emission rate for the coal mines in Zonguldak Coal Basin depends primarily on the coal production rate and mine depth during the period 1990 to 2013. The average daily methane emissions in thousand cubic meter per day in Turkish bituminous coal mines were obtained as 45.9 m³/d for Kozlu, 50.7 m³/d for Karadon, 25.5 m³/d for Üzülmöz, 24.5 m³/d for Armutçuk, and 6.6 m³/d for Amasra. The methane emission is increased by increasing the coal production. There is a good correlation between average mining depths and specific methane emissions. The specific methane emission values are 3 times greater than the coal seams' gas contents.

Acknowledgments

This study was carried out as part of Scientific and Technological Research Council of Turkey (TUBITAK) founded project "Determination of the Gas Contents and Gas Desorption Characteristics of the Coal Seams in Zonguldak Hardcoal Basin", Grant No. 113M460. The authors would like to express their gratitude to the Scientific and Technological Research Council of Turkey (TUBITAK) for funding this research.

References

- [1] C.Ö. Karacan, Modeling and prediction of ventilation methane emissions of US longwall mines using supervised artificial neural networks, *International Journal of Coal Geology*, 73 (2008) 371-387.
- [2] G. Okten, C. Biron, S. Saltoglu, Gas and coal outburst of Zonguldak coalfield of Turkey and preventive measures. *International Symp.-Cum-Workshop on Management and Control of High Gas Emissions and Outbursts in Underground Coal Mines*. Wollongong, Australia, 20-24 March (1995) 451-458.
- [3] A. Cakır, K. Baris, Assessment of an underground coal mine fire: a case study from Zonguldak, Turkey. *Underground Coal Operators'*, (2009) Conference Paper 108.
- [4] G. Gurdal, M.N. Yalcin, Gas adsorption capacity of Carboniferous coals in Zonguldak basin (NW Turkey) and its controlling factors, *Fuel*, 79 (2000) 1913-1924.
- [5] Şahin, A.N., 1997. Briquetting of Zonguldak Coals, MSc Thesis, Karaelmas University of Zonguldak-Turkey (in Turkish).
- [6] S. Toprak, Petrographic properties of major coal seams in Turkey and their formation, *International Journal of Coal Geology*, 78 (2009) 263-275.
- [7] H. Aydın, Evaluation of the risk of coal workers pneumoconiosis (CWP): A case study for the Turkish hardcoal mining, *Scientific Research and Essays*, 5 (2010) 3289-3297.
- [8] C.Ö. Karacan, F.A. Ruiz, M. Cote, S. Phipps, Coal mine methane: A review of capture and utilization practices with benefits to mining safety and to greenhouse gas reduction, *International Journal of Coal Geology*, 86 (2011) 121-156.
- [9] United Nations, Best practice guidance for effective methane drainage and use in coal mines. *Economic Commission for Europe Methane to Markets Partnership: ECE Energy Series*, 31, 2010.
- [10] M. Öztürk, Taşkömürü Havzası Damar Gaz İçerikleri Tespit Çalışmaları (Vol. 71). Zonguldak: Türkiye Taşkömürü Kurumu İş Sağlığı Güvenliği ve Eğitim Daire Başkanlığı, (2014).
- [11] L.W. Lunarzewski, Gas emission prediction and recovery in underground coal mines. *International Journal of Coal Geology*, 35 (1998) 117-145.
- [12] M.C. Irani, P. Jeran, M. Deul, Methane Emission from US Coal Mines: A Survey: US Department of the Interior, Bureau of Mines, (1972).
- [13] A. Saghafi, D.J. Williams, R.D. Lama, Worldwide methane emissions from underground coalmining. Paper presented at the Proceedings of the 6th International Mine Ventilation Congress, Pittsburgh, PA, (1997).
- [14] F.N. Kissell, C.M. McCulloch, C.H. Elder, C.H., The direct method of determining methane content of coal beds for ventilation design. Report of Investigations, 7767, (1973), US Bureau of Mines, Pittsburgh, PA.

Evaluation of Coal Seam Gas Content in Kozlu Colliery, Zonguldak/Turkey

Samet Can Özer, Olgun Esen, Abdullah Fişne

Istanbul Technical University, Mining Engineering Department, Istanbul, Turkey

Methane occurrence in coal mines has consistently been a causal factor in fatal occupational accidents like explosions, fires and suffocations throughout the history of mining. The gas content of coal seams plays an important role in mine safety and mine planning. This study is primarily focused on determining the gas content of coal seams in the Kozlu Colliery in the Zonguldak Coal Basin to quantify the magnitude of gas emissions into underground working areas and to support appropriate ventilation design. Zonguldak Coal Basin is the only bituminous coal basin of Turkey. Mining activities in the basin started in 1848 and have been carried out in the region for over 160 years. There are 38 mineable coal seams in the basin, and the coal has been produced by five collieries, from west to east: Armutçuk, Kozlu, Üzülmöz, Karadon and Amasra. Kozlu Colliery is one of the largest and gassiest collieries in terms of coal production and mining activities, and is the only mine utilizing undersea mining in some panels in Turkey. The most important coal seams are the Çay and Acılık seams having average thickness of 6 and 4.5 m, respectively. Also, the Sulu, Hacimemis, Domuzcu and Büyük seams are regarded as important for coal production. These coal seams have an average thickness ranging from 1.5 m to 2.5 m. Gas content of coal seams was measured using the so-called "direct method" developed by Bertard in the late 1960's.

Keywords: Gas Content, Direct method, Gas Storage Capacity

1. Introduction

The coalification process is described by the prehistoric transformation of vegetation to peat, lignite and hard coal. During this transformation massive amounts of gas is produced, most of which is stored in coal and surrounding strata. Although this gas includes carbon dioxide, nitrogen and other hydrocarbons, methane comprises approximately 90-95% of the gas stored within coal [1-2].

The presence of methane in coal mines has caused significant loss of life through explosions, fires and suffocations. Although improved methods, equipment, standards and planning have resulted in better ventilation systems, accidents are still happening due to excessive methane emissions. Deeper and increasingly mechanized coal mines increases the risk of excessive methane emissions. Methane related issues are an important topic of occupational accidents of underground coal mining in Turkey.

Gas is stored in coal through a number of mechanisms including: a) adsorbed molecules within micropores, b) trapped gas within matrix porosity, c) free gas in excess of that which can be adsorbed in cleat and fractures, and d) as a solute in ground water within coal fractures. Methane in coal pores and cleats desorbs to the mine atmosphere due to the reduction of pressure caused by excavation. Also, in some underground mines, the methane stored in coalbed under high pressure can exceed the strength of the face, causing bursts and large volumes of methane emissions into the mine [3]. The sudden outburst of gas and coal is one of the most important occupational safety problems in underground mines.

Methane control in underground coal mines is accomplished by "Methane Drainage and Ventilation"

methods. The effective implementation of these methods requires accurate predictions of methane emissions related to production. There are several techniques have been developed for this particular purpose. The most important and basic parameter of these techniques is to determine the gas content of coal seams accurately and reliably [2-4].

Methane related problems in the mines of the Zonguldak Coal Basin are related to extreme geological and tectonic conditions. In recent years, coal production in progressively deeper environments has been associated with increased frequency of methane-related accidents, caused by increased levels of gas content in coal. Methane emission is primarily controlling by ventilation in Zonguldak Coal Basin. Therefore ventilation will not be enough for controlling methane emissions. Methane drainage is going to be a necessity for the basin so continuous gas content determination studies are going to be the most important parameter of this application.

Systematic studies related to the gas content and gas emission characteristics of the minable coal seams in the basin are negligible.

The aim of this study is to determine the gas content of coal seams at the main development cross-cuts and/or panel headings of the Turkish Hardcoal Enterprise (TTK) Kozlu Mine.

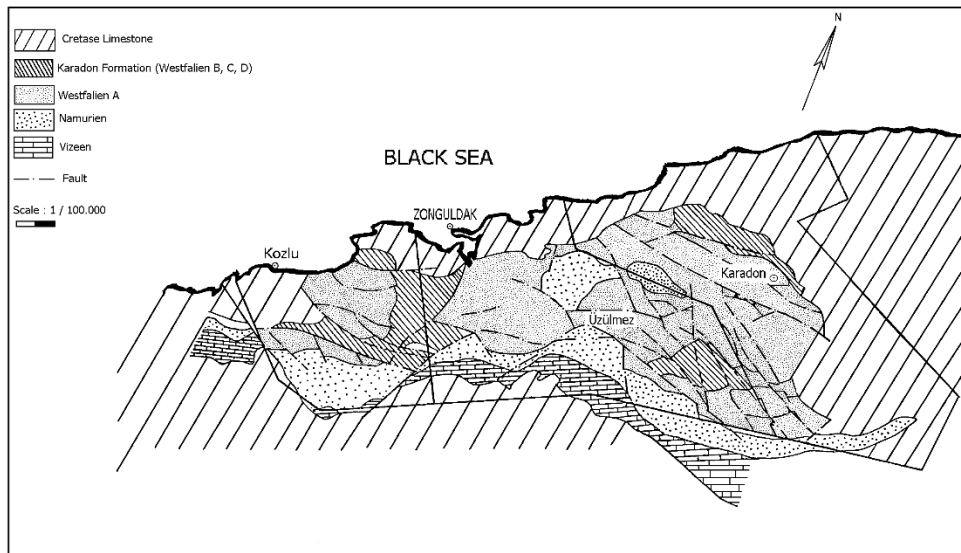


Fig. 1. Geological map of Zonguldak Coal Basin, Turkey [6]

2. Description of Zonguldak Coal Basin

The Zonguldak Coal Basin is the only basin in Turkey with minable hard coal deposits. There are two types of hard coal in the basin: coking and non-coking. Metallurgical coke is produced at Kozlu, Üzülmüş and Karadon collieries [5].

The coal seams are located in a Carboniferous deltaic sequence of Westphalian A age. The coalfield has been disturbed by tectonic activity, first by Hercynian and later by Alpine orogenesis resulting in folding and faulting of strata [7]. The Carboniferous coal-bearing sequence of Zonguldak Basin contains the Namurien Alacaagzı Formation, Westphalian A Kozlu Formation, and Westphalian B–D Karadon Formation [8]. The geological map of the basin is given in Figure 1 [6]. The estimated coal reserves, carried to 1,200 m under sea level, is about 1.3 billion tons of coal in this basin.

About 57 coal seams have been identified and, of which, 38 are workable with thickness varying from 0.7 to 10 m and dips from 0 to 90 degrees. The most important coal seams are the Çay and Acılık seams, with average thicknesses of 6 and 4.5 m, respectively. The Sulu, Hacimemiş, Domuzcu, and Büyük seams have average thicknesses ranging from 1.5 to 2.5 m and are regarded as important for coal production. The coal has been produced by five collieries, from west to east: Armutçuk, Kozlu, Üzülmüş, Karadon, and Amasra.

3. Gas Content Determination Studies

Developed methods used to determine gas content can be grouped under two headings: "Direct Method" and "Indirect Method". It also is possible to estimate the gas content of coal through "Empirical Equations" developed by many researchers [9].

There are many direct methods that have been developed for determining gas content. In most of these methods, the gas content of coal is divided into three main components: lost gas, desorbed gas and residual gas. Each of the components of the total gas content of coal is determined by direct measurements or predictions [10-11]. The methods are based on the same principal but have different applications. The core of such methods

involves taking the samples from the coalbed with the lowest possible gas loss and determining the amount of gas released from the sample.

The method developed by Bertard and his colleagues [12] in French Coal Research Center (CERCHAR) is considered the most fundamental approach ever developed. The study above assumes the amount of the lost gas is proportional to the square root of time in the early stage of desorption process.

In the mentioned method, the amount of desorbed gas during the time between taking a sample from the coalbed and sealing it in a sealed canister (Q_1) is determined by the extrapolation of the data obtained from methane desorption measurements. Total gas content of the coal is determined by adding this value to the values obtained during the transport of the canister to the laboratory and until the end of desorption (Q_2) and residual gas determined by grinding in a gas-tight mill (Q_3).

Coal samples were collected from Kozlu Colliery of TTK. Of all the TTK collieries, Kozlu Colliery has the deepest production and development levels. Correspondingly, it is one of the gassiest mines in Zonguldak Coal Basin. Sixty (60) samples from 6 different coal seams at Kozlu Colliery have been successfully taken from main development galleries and gateroads with horizontal drilling. Locations of the samples taken are given in Table 1.

A drilling machine with a vacuum ejector and hollow rods is used for the sampling, and seen in Figure 2. The most important advantage of this equipment is reducing the lost gas time as much as possible and retrieving the sample exactly from the intended depth.

Table 1. Locations of samples taken

Coal Seam	Number of Samples	Colliery	Depth (m)
Acılık	7	Kozlu	630
Çay	13	Kozlu	560 630
Sulu	17	Kozlu	560 630
Büyük	3	Kozlu	560
Domuzcu	9	Kozlu	425
			485 560
Hacımemiş	11	Kozlu	560 630



Fig. 2. Ejector and drilling machine for sampling

Studies to determine the gas content of a coal seam begin with specifying the exact sample point for drilling. Then, the drilling machine is connected to the compressed air system followed by preparation of the sample environment. According to dip and strike of the seam, drilling is oriented and the operation begins. The length of the drilling rods is 2 m. Samples were taken every 2 m, followed by the insertion of a new drilling rod. To take samples from the end of borehole by vacuum, the direction of compressed air is being changed by the valves over the ejector. The ejector is given in Figure 3. The sample is vacuumed along the hollow rods from the cutting point to the ejector's trap. Then whole organization is being stopped, one team screens the samples and took the oversize (< 2mm) samples into the tight containers, the other team adds the new 2 m rod to the drill. Times that cutting the sample and sealing it into the container are being noted.

After the sampling process is completed underground, samples are brought to the laboratory. Tight containers are connected to the analyzer for measuring the methane concentration which sample emitted into the container. Figure 4 shows the gas analyzer used for gas concentration measurements. This process is then repeated the next day and samples are ground using a sealed vibrating cup mill. A burette is connected to the mill to determine the volume of released gas, as shown in Figure 5. Proximate analysis is

performed on the ground sample to determine moisture, ash and volatile matter contents.

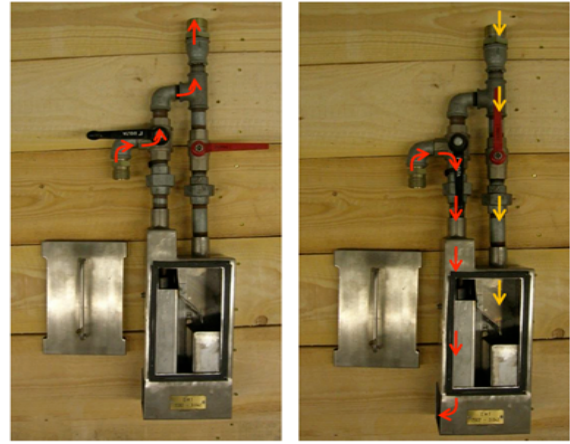


Fig. 3. Ejector box for sampling via vacuum



Fig. 4. Gas analyzer used for gas concentration measurements.



Fig. 5. Ring mill and burette assembly

4. Results and Discussion

All coal samples were taken by the horizontal drilling equipment from the coal seams. Sixty (60) samples were successfully taken by horizontal drilling 6 different coal seams at Kozlu Colliery. Coal samples were collected

from every 2 meters in drill hole with a maximum borehole length of 24 meters. Gas content measurement and proximate analysis was performed on each sample.

Proximate analyses of coal samples were determined to assess the clean coal gas content of samples. The ash, moisture, volatile matter and fixed carbon values of the coal samples have been determined to correct the gas content values. The proximate analyses were performed according to the ASTM D-3172 [13]. The results are given in Table 2. According to ASTM standard; coal samples are high volatile-B and high volatile-A bituminous coal. According to DIN standard, coal samples are in "gassy coal" and "gas flame coal" classifications.

In this study, the gas content determination studies were carried out in the coal seams of Acılık, Çay, Sulu, Büyük, Domuzcu and Hacımemiş in Kozlu Colliery. The obtained results are summarized and given in Table 3.

The average gas contents of coal seams vary between 5.48 m³/t and 10.28 m³/t on an as-received basis. Currently, most of the coal production in Kozlu Colliery is in the Acılık, Çay and Sulu coal seams. The average gas contents of these coal seams are 9.26 m³/t, 5.96 m³/t and 8.50 m³/t on an as-received basis and 10.44 m³/t, 7.05m³/t and 9.63 m³/t on a dry ash free basis respectively. The gas content of the Büyük seam was determined at as-received and dry ash free basis such as 5.48 m³/t and 6.37 m³/t respectively. The average gas contents of the Çay and Büyük seams are lower due to sample location. The coal sample of Çay seam was taken

from a development gallery which was excavated a long time ago. The coal sample from Domuzcu seam was taken from the panel which was located in the depths between 425 and -485 m with a gas content on an as-received basis is 6.73 m³/t and 8.01m³/t on a dry ash free basis.

Due to more intensive coal production, more coal samples were taken from Sulu seam. The average coal seam gas content of Sulu seam on an as-received basis was determined as 6.81 m³/t at -560 meters and as 8.87 m³/t at -630 meters below surface. The results demonstrate the gas content of the coal seams are higher in virgin and deeper coal seams.

Generally, the drilling distance is limited because of the coal seam structure. Studies have shown that the drilling should reach at least 10 m depth. The depth of sampling depends on several factors as time since exposure of the coal seam, permeability, gas pressure and stress regime. The minimum depth can be established only by testing. As soon as the laboratory test show that the gas contents remain on a stable level from a certain depth, the minimum depth of drilling is sure. It must be pointed out that, samples for determining the gas content of the coal seams should be collected from virgin coal areas. Otherwise, the gas content values will be lower and the results will not be representative.

Gas contents over 10 m³/ton are considered to be very high. Considering the average values for Kozlu, the Hacımemiş seam is very gassy, and Acılık and Sulu seams are also relatively high.

Table 2. The proximate analysis of the coal samples.

Coal Seam	Original Basis (%)				Dry Ash Free Basis (%)	
	Moisture	Ash	VM	FC	VM	FC
Acılık	0.61 - 1.44	7.24 - 13.53	18.86 - 27.71	58.81 - 69.22	21.42 - 32.03	67.97 - 78.58
Çay	0.87 - 1.21	8.09 - 26.09	23.28 - 25.22	49.55 - 66.34	27.05 - 32.94	67.06 - 72.95
Sulu	0.86 - 1.46	3.83 - 20.74	22.61 - 26.23	52.58 - 68.83	25.25 - 33.02	66.98 - 74.75
Büyük	1.05 - 1.18	5.14 - 19.08	24.80 - 31.52	54.01 - 62.16	31.05 - 36.85	63.15 - 68.95
Domuzcu	0.96 - 1.61	7.73 - 22.84	23.62 - 31.68	48.01 - 67.04	26.05 - 39.75	60.25 - 73.95
Hacımemiş	0.91 - 1.43	5.22 - 22.94	21.71 - 28.97	54.25 - 67.50	27.35 - 32.86	67.14 - 72.65

Table 3. The gas content results of coal seams at Zonguldak coal basin.

Coal Seam	Gas Content (m ³ /ton)							
	Original Basis				Dry Ash Free Basis			
	Min.	Max.	Ort.	Std.	Min.	Max.	Ort.	Std.
Acılık	6.55	11.54	9.26	1.70	7.57	13.11	10.44	1.98
Çay	3.71	8.76	5.96	1.61	4.96	9.63	7.05	1.68
Sulu	4.58	10.49	8.50	1.42	5.13	11.91	9.63	1.55
Büyük	5.31	5.61	5.48	0.15	5.99	6.65	6.37	0.34
Domuzcu	4.32	7.88	6.73	1.11	4.77	9.07	8.01	1.37
Hacımemiş	6.77	14.66	10.28	2.08	8.21	16.98	11.77	2.43

5. Conclusion

This study is primarily focused on determining the gas content of coal seams in Kozlu Colliery in Zonguldak Coal Basin to quantify the magnitude of gas emissions into underground working areas and to support appropriate ventilation design. Kozlu Colliery is one of the biggest and gassiest collieries in terms of coal

production and mining activities. Gas content of coal seams was measured using the so-called "direct method" developed by Bertard in the late 60's. The average gas contents of coal seams vary between 5.48 m³/t and 10.28 m³/t on an as-received basis. The average gas content of Acılık, Çay and Sulu coal seams are 9.26 m³/t, 5.96 m³/t and 8.50 m³/t on an as-received basis and 10.44 m³/t, 7.05m³/t and 9.63 m³/t on a dry ash free basis

respectively. The gas content of the Büyük seam was determined at as-received and dry ash free basis such as 5.48 m³/t and 6.37 m³/t respectively. This study show that the minimum depth of drilling is 10 m for Kozlu Colliery, and samples for determining the gas content of the coal seams should be collected from virgin coal areas. Otherwise, the gas content values will be lower and the results will not be representative. Gas contents over 10 m³/ton are considered to be very high. Considering the average values for Kozlu, the Hacimemis seam is very gassy, and Acılık and Sulu seams are also relatively high. The gas content data contained in this study, when combined with geologic and engineering studies, can be used as a basis for a preliminary estimate of mine ventilation requirements, and to determine if methane drainage in advance of mining should be considered.

Acknowledgments

This study was carried out as part of Scientific and Technological Research Council of Turkey (TUBITAK) founded project "Determination of the Gas Contents and Gas Desorption Characteristics of the Coal Seams in Zonguldak Hardcoal Basin", Grant No. 113M460. The authors would like to express their gratitude to the Scientific and Technological Research Council of Turkey (TUBITAK) for funding this research.

References

- [1] A. G. Kim, The composition of coalbed gas: U.S. Dept. of Interior, Bureau of Mines. (1973).
- [2] V. Didari, Metan Denetimi Gereksinimlerinin Ampirik Tekniklerle Belirlenmesi. Paper presented at the Türkiye 6. Coal Congress, Zonguldak. (1988).
- [3] G. Ökten, Zonguldak Taşkömür Havzasındaki Ani Gaz ve Kömür Püskürmesi Olaylarının İncelenmesi ve Olaya Eğilimli Zonların Belirlenebilirliğinin Araştırılması. (Doktora), İstanbul Teknik Üniversitesi, İstanbul, (1983).
- [4] F.N. Kissell, C.M. McCulloch, C.H. Elder, C.H., The direct method of determining methane content of coal beds for ventilation design. Report of Investigations, 7767, (1973), US Bureau of Mines, Pittsburgh, PA.
- [5] M. Öztürk, Taşkömürü Havzası Damar Gaz İçerikleri Tespit Çalışmaları (Vol. 71). Zonguldak: Türkiye Taşkömürü Kurumu İş Sağlığı Güvenliği ve Eğitim Daire Başkanlığı, (2014).
- [6] Şahin, A.N., 1997. Briquetting of Zonguldak Coals, MSc Thesis, Karaelmas University of Zonguldak-Turkey (in Turkish).
- [7] G. Okten, C. Biron, S. Saltoglu, Gas and coal outburst of Zonguldak coalfield of Turkey and preventive measures. International Symp.-Cum-Workshop on Management and Control of High Gas Emissions and Outbursts in Underground Coal Mines. Wollongong, Australia, 20–24 March (1995) 451–458.
- [8] G. Gurdal, M.N. Yalcin, Gas adsorption capacity of Carboniferous coals in Zonguldak basin (NW Turkey) and its controlling factors, Fuel, 79 (2000) 1913-1924.
- [9] A.G. Kim, Estimating methane content of bituminous coalbeds from adsorption data: Department of the Interior, Bureau of Mines, (1977).
- [10] W. P. Diamond & J. R. Levine, Direct method determination of the gas content of coal: procedures and results (pp. 36): US Bureau of Mines (1981) .
- [11] W. P. Diamond & S. J. Schatzel, Measuring the gas content of coal: a review. International Journal of Coal Geology, 35(1), 311-331 (1998).
- [12] C. Bertard, B. Bruyet & J. Gunther, Determination of Desorbable Gas Concentration of Coal (Direct Method). International Journal of Rock Mechanics and Mining Sciences, (1970) 7(1), 43-&.
- [13] ASTM D3172-13, (2013). Standard Practice for Proximate Analysis of Coal and Coke, ASTM International.

Mine Fires

Analysis of all reported Mine Fire Incidents: 2000-2013 in all types of United States mines

Casey Slaughter^a, Jerry Tien^a, Yingjiazi Cao^a

^a Monash University, Melbourne, Australia

This paper is a look at recent trends in mine fires in the United States from 2000-2013, following the works of De Rosa (2004a, 2004b, 2004c), Pomroy and Carigiet (1994), Butani and Pomroy (1988), and McDonald and Pomroy (1980). The data was obtained from the Mine Safety and Health Administration through their accident and employment reports available online. This paper will look at fires at underground metal/ nonmetal mines (120), at underground coal mines (157), fires at surface coal mines (452) and fires at surface metal/nonmetal mines (585). Additionally the number that cause injury (about 25%), the equipment involved (about 55% of fires), and other reported information will be investigated for potential trends.

Keywords (max 6): Mine Fires, Health and Safety

1 Introduction

Fire is a serious and significant danger that threatens not only the lives of miners but also the livelihood of their communities as well. Since the 1950's there has been a trend of central reporting of fires in mines with legal requirements coming in with the Mine Health and Safety Act of 1977 and further expansion with the Mine Improvement and New Emergency Response Act of 2006. Since the data has been collected, there have been analysis performed by groups looking at the statistical significance of the various points found therein.

The first of these looked at fires from 1950-1977 in coal mines [1]. The second looked at metal/nonmetal mines from 1950-1988 [2]. Both looked at both surface and underground fires in detail, specifically the duration of the fires (including non-reportable fires by interviewing various industry safety personnel), the extinguishment method and involved statistical analysis of the trends observed. A follow-up study of underground coal mines from 1978-1994 was subsequently completed [3]. From one of the same authors of the previous two studies, similar analysis was conducted including detailed looks at the ignition source, fuel involved, location underground, method of detection and extinguishment method. Later three studies were completed that focused on different aspects of the mine fire data roughly covering the 1990's: Coal Mine Fires [4], Metal/ Nonmetal Mines [5], and Fires Involving Mobile Equipment [6]. Again similar analysis was performed, looking at the risk rates, the equipment involved, method of detection, ignition source etc. All of these reports are singular in that they looked at similar data sets and came to similar conclusions, with few gaps in the records. This provides a comprehensive record of fires in the US to be compiled for comparison, including more recent data from Mine Safety and Health

Administration (MSHA) records used in this analysis shown in Fig. 1.

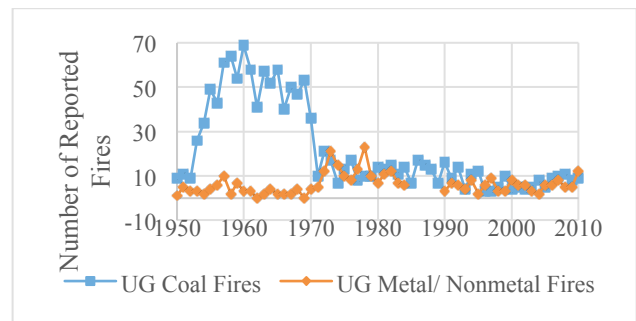


Fig. 1. Reported Underground Mine Fires by year 1950-2010

2 Data Access

In Jan 2009, a new initiative in open and transparent government was advanced in the United States. To that end a new web domain was established: www.data.gov. This portal was linked to many government agencies across the nation and eventually some other world agencies. In compliance with this initiative MSHA made available the part 50 data (accident, injury, citations, general production information, etc.) in easily accessible data formats. One change that MSHA made for this initiative is that from 2000 onward, the data sets include translations of many of the numeric codes that had been used previously and required reference to several handbooks for analysis. These changes make it very easy to access and utilize the data. In addition to the Part 50 data, data on citations, inspections, noise and dust sampling are also available. This paper is not intended to be exhaustive of the wealth of information contained in these databases, merely a representative sampling.

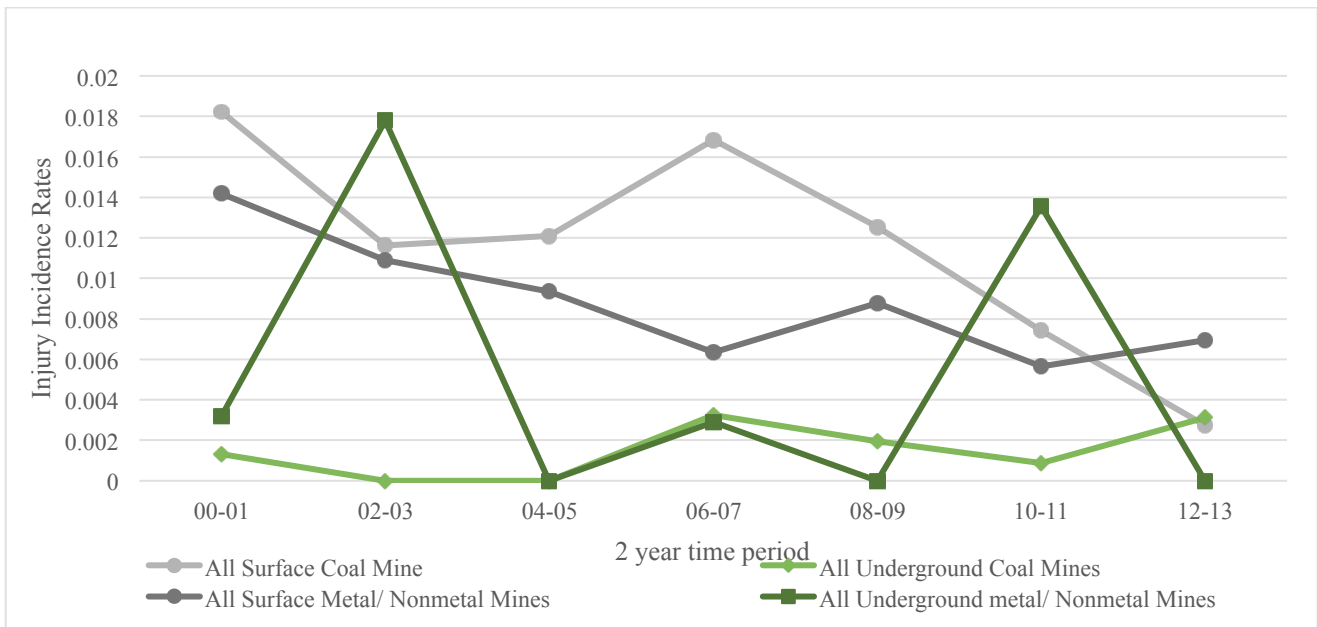


Fig. 2. Injury Incidence Rates for major mining categories

3 Methodology/ Data handling

In preparation several data files were obtained for analysis. These included the “mines”, “employment/production (yearly)”, “accident injuries”, and the “violations” data sets [7]. Functionality in Excel was used to link the various data sets together using the unique mine id value. This allowed for general information about the mines (commodity type, active status etc.) to be extracted for comparison which may not be fully possible within individual data sets. Some new columns and distinctions were made in order the ease analysis: dividing into two year categories, translation of accident time into general time of day, general classification of equipment involved, etc. Following the methodologies in earlier works [1-6], Fire Risk Rates (FRR) for coal mines, the number of fires per coal production, and Injury Risk Rates (IRR), the number of injuries times 200,000 per annual employee hours, were calculated for all categories in Fig. 2. Note that metal mines are not required to report production rates and so FRR cannot be calculated.

4 Data Analysis

The following data will be presented in two ways. The first will be a combined look at fires over time and appropriate risk rates for each major mining category. Next some subparts of the data set will be analyzed for the major categories over the whole time period (2000-2013). Reference will be made to the “previous time period,” this indicates comparisons made to previous works looking at fire data from the period of the 1990’s [4-6].

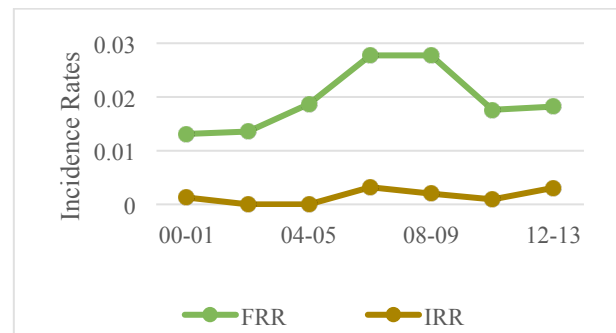


Fig. 3. Underground Coal Mine Incidence Rates

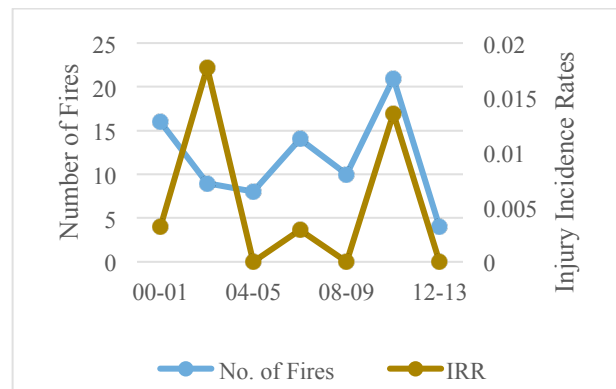


Fig. 4. Underground Metal/ Nonmetal Mine Fires and Injury Incidence rates

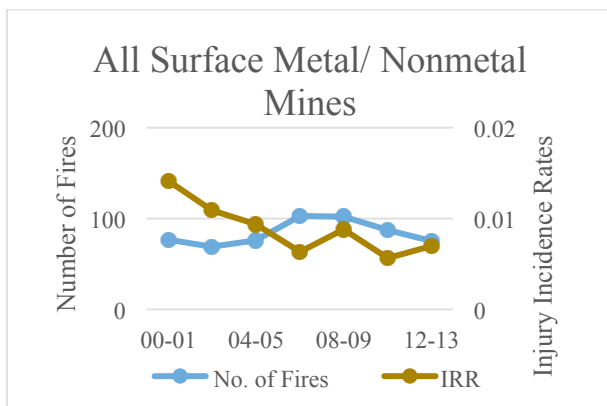


Fig. 5. Surface Metal/ Nonmetal Fires and Injuries Incidence Rates

4.1 Underground Coal Mines

Over the time period the fire risk rates nearly doubled by the middle of the time period before falling again as shown in Fig. 3. The simplest explanation is that increased reporting requirements were enacted in 2006 which required mines to report fires that burned more than 10 minutes before extinguished, previously 30 minutes [8]. These same regulations also contained other fire protection regulations that may have also contributed to the decline following the '08-09 time period. However this is a very simplistic solutions and does not seem to account for all of the increase, notable that occurring before 2006.

The injury incidence rates tended to be lower than the previous 10 year time period [4]. This is most likely a product of increased safety awareness and attention to fire protection. There is a spike in the '06-07 time period due to the notable fire accident that occurred that year, the Aracoma Mine Fire. However there is a possible uptick in the IRR in the '12-13 time period.

4.2 Underground Metal/ Nonmetal Mines

Similar results were obtained for the time period as for the previous time period [5], namely fluctuations in the number of fires which do not necessarily correlate to greater risk of injury as shown in Fig. 4. Looking deeper into the data reveals that the apparently large spikes in the IRR corresponds to five total injuries from a single fire in the '02-03 period and 4 separate incidents causing a single injury in the '10-11 period. This data suffers from a small sample size that hampers the ability to perform statistical analysis as evidenced by the wild trends.

4.3 Surface Coal Mines

The following data set includes various surface facilities and other non-traditional surface mines in with traditional surface mines. The FRR continues to fluctuate along a general increasing trend as shown in Fig. 6, contrasting the previous time period [4]. However the IRR continues a general decline which seems to indicate that if there is a greater risk of fire it poses less of a risk to miners.

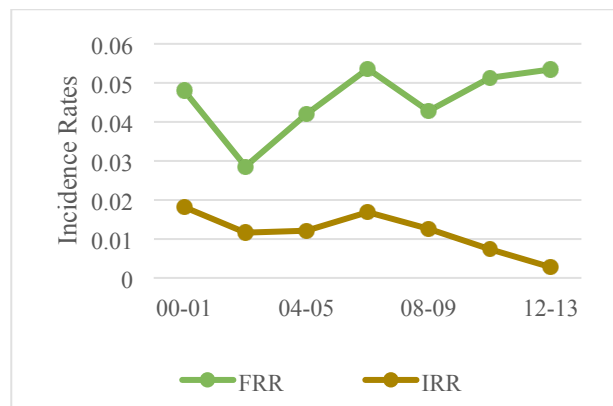


Fig. 6. Surface Coal Mines Incidence Rates

4.4 Surface Metal/ Nonmetal Mines

The number of mine fires in surface metal/ nonmetal mines behaved in an inconsistent way similar to other categories. There was a definite increase and peak between 2006 and 2009 before returning to pre-peak numbers. This contrasts the previous time period where a general decreasing trend was observed [5]. However the IRR tended to decrease over the time period as shown in Fig. 5.

4.5 Equipment involved Fires

Mining equipment is important to note because during the 2000-2013 time period mining equipment accounted for 55% of all fires in mines. When you cross reference this with fires that cause injury, the number increases to 65%. The data presents a wide variety of equipment types and codes so it can be somewhat difficult to identify general types that cause a higher proportion of fires, with many of the reported categories accounting for less than 1% of the total fires. However there are a few standout categories shown in Figure 7. The top three are conveyor belts, cutting and welding equipment and off-highway haulage trucks. For the most part these provide the largest proportion of equipment fires across all type of mining, the exception is haul trucks in underground coal mines which are more likely to have LHD/ scoops and personnel carrier fires. When only looking at fires that cause injury nearly 25% of those fires are due to cutting and welding operations, highlighting the importance of robust hot-work safety procedures.

4.6 Fire Injuries

In the whole, fires in mines are only responsible for a small percentage of injuries. However past experience has shown that they can cause widespread damage and injury if not properly controlled. From 2000-2013, 317 of the 1314 fires caused some degree of injury shown in Figure 8. Very few fires resulted in fatalities but a large proportion resulted in days restricted or days lost at an average of 10 days restricted and 35 days lost. When looking at the nature of

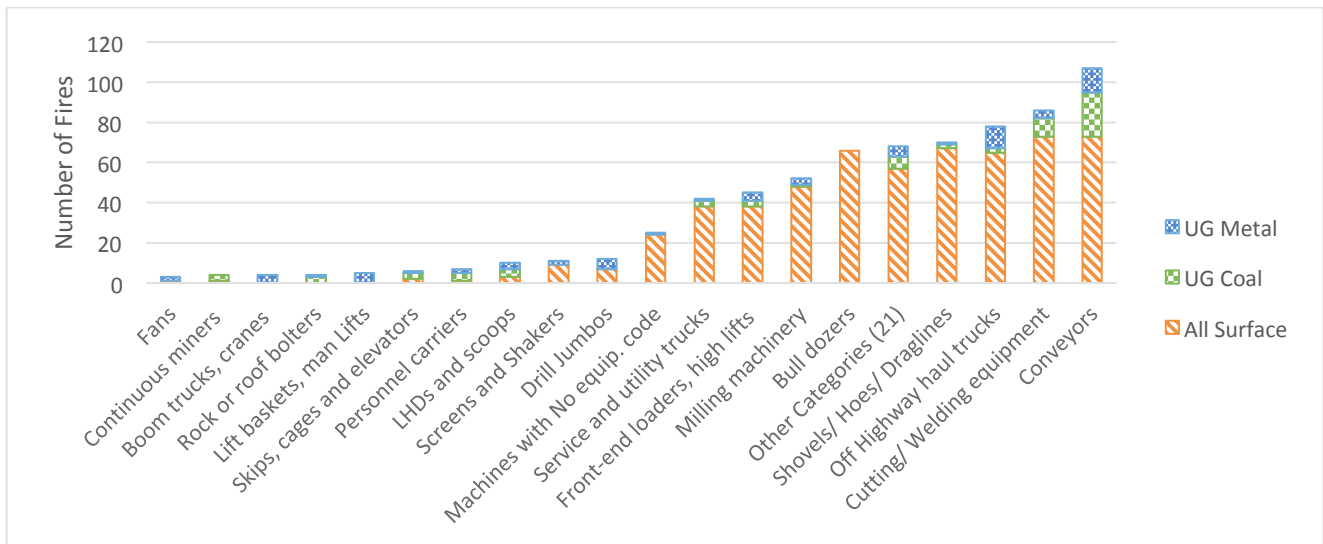


Fig. 7. Fires Involving Mobile Equipment

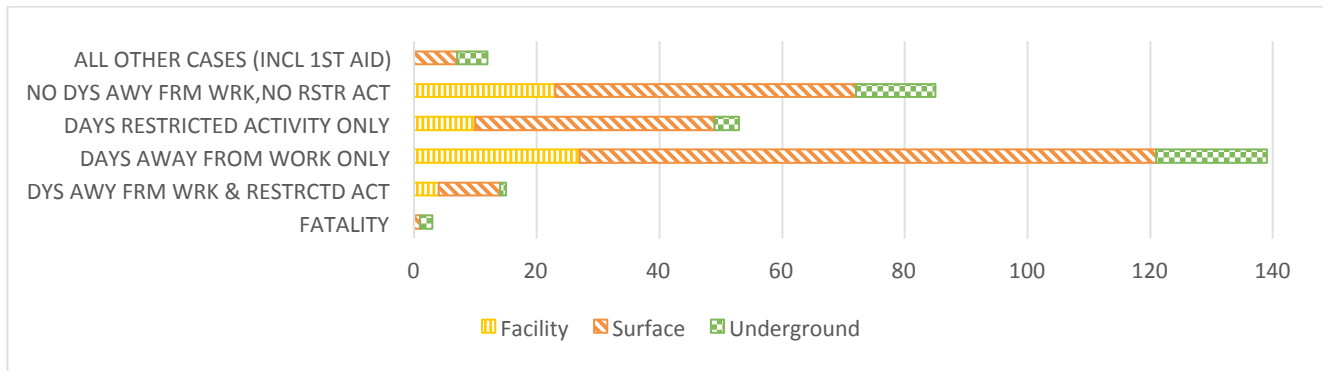


Fig. 8. Injuries caused by Fires

the injuries the vast majority of injuries for surface mines are burns or scalds (73%) with smoke inhalation a distant second (12%) and a wide array of other physical injuries such as sprains, bruises, lacerations etc. that imply some injuries sustained during fire evacuation. For underground mines burns are still the top injury mechanism (53%) but smoke inhalation is a much closer second (30%) with very few injuries due to other causes, possibly indicating a calmer evacuation or that fires have a larger reach in terms of possible injury to miners. Facilities also have a large portions of injuries due to burns (70%) and a sizable portion due to smoke inhalation as well (23%).

4.7 Time of day of fire

Several interesting trends emerge when looking at when the fire occurs during the day. For this the fires were sorted based on the time reported for the accident into 4 general, 6 hour time slots: night morning, afternoon, and evening. For surface mines and facilities the majority of

the fires occurred during the morning and afternoon times. For underground mines it appears that fires were more likely in the morning and evening times shown in Figure 9.

When trying to diagnose the reason behind this interesting trends begin to appear. First it is necessary to see to try and find out how many shifts are at each mine. This data can be found in the reported data. For active mines about 5,000 operate only a single production shift, about 1,000 operate two production shifts and less than 400 operate three production shifts. Next we can cross reference the fires that occurred in active mines with their number of production shifts. Here one can see that over half of the fires in active mines (487) are in mines with 2 production shifts. Looking again at the accident times and comparing to the number of production shifts approximately one third of the fires occur during the “Night” and “Evening” times, presumably outside of production shift times. Compared with mines that operate only one shift per day (25%) and

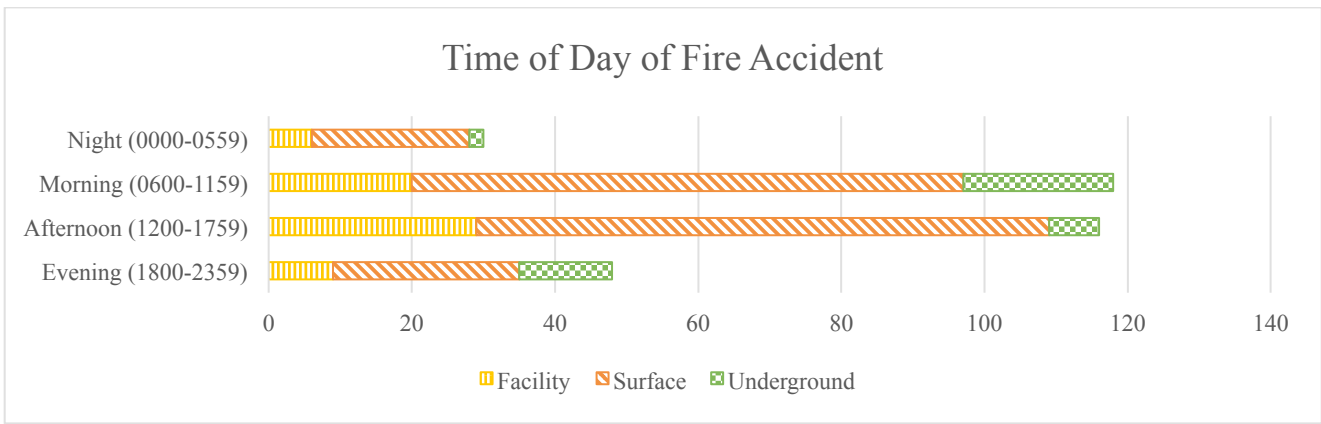


Fig. 9. Time of Day Fires Occurred

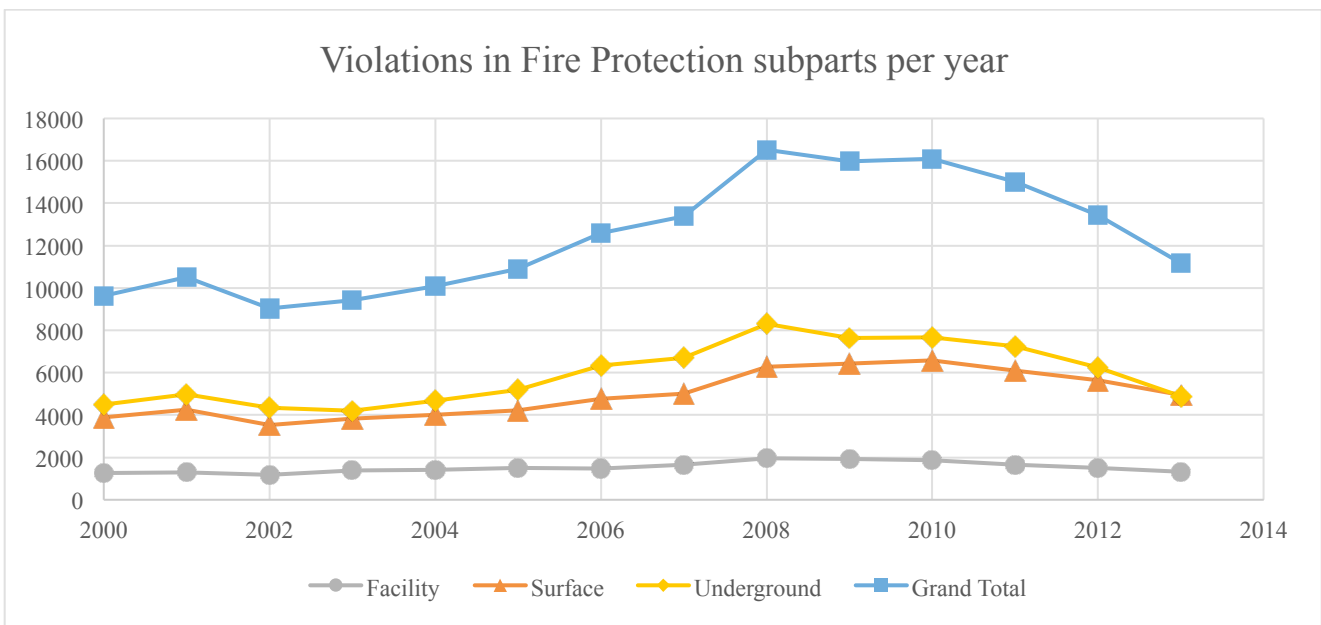


Fig. 10. Violations of Fire Protection Subparts per year

mines with three shifts per day (roughly equal distribution). It is not immediately clear why these trends. One possible explanation is that mines operating two production shifts often have a single maintenance shift. It has been shown that cutting and welding operations account for a sizable portion of fires. Maybe the combination of increased maintenance activity on a shift with a reduced workforce (less visual detection capability) can account for the higher proportion of fires? Further study is necessary if this is to be reasonably explained.

4.8 Citations for Fire Protection Violation

Being the leading enforcement agency, MSHA also keeps fairly detailed statistics of citations given over a wide range of health and safety standards. While the citations are located in different standards for different

mine types and mined commodity, the basic regulations governing fire protection are similar [9]. For analysis the number of citations regarding sections 56.4, 57.4, 75.11 and 77.11 were analyzed over time to attempt to spot any trends shown in Figure 10.

From 2000 to a peak in 2008 the number of citations issued rose more than 50%. The majority of these were issued to underground coal mines. Conversely for metal operations, it is typically surface mines that receive more citations. Now the number of citations issued usually has little to do with how “safe” a mine is from fire, but the trends can indicate regulator’s priorities in enforcing violations. More interesting is the increase in the proposed penalty amounts. In 2005 the total amount of proposed penalties for fire protection violations was \$1.2 million. By 2007 this number increased to \$5.6 million. This is

almost certainly due to the changes in federal regulations and proposed penalty amounts in 2006.

5 Conclusions

A variety of trends can be observed in the data contained with the MSHA open data sets. This paper focused entirely on mine fire related data in US mines from 2000-2013. The majority of these fires caused no injuries and the IRR's for all but underground coal mines trended down over the time period even though the number of fires or FRR trended upward. In 2011 the IRR for fires was below 0.015 for all categories of mines. For comparison in 2011 the IRR for all injuries was 2.73 [10].

Even though fires seem to be causing fewer injuries their numbers have been trending upward and offer severe consequences. Many of the injuries were days lost or days restricted and caused 3 fatalities. Also with changes in federal law, penalties for citations have increased significantly. While the law changes also decreased the minimum fire duration for required reporting, the increasing trend in the number of fires and FRR started before the changes took effect in the '06-07 time period indicating that these changes may not account for the increases in the number of fires reported.

The trends in the amount of fires involving mobile equipment were illuminating as well. Even in coal mines, where the mined material is itself volatile, a greater proportions of fires involved mobile or stationary equipment; predominantly conveyor belts or cutting and welding equipment. These fires also accounted for many of the injuries (64%). For surface mines injuries were mainly from burns and scalds. This was similar for underground mines and facilities however they both also had a large proportion due to smoke inhalation.

Many other trends were observed that raise questions that warrant further analysis. First is the trend for mines operating on two production shifts to have a greater proportion of fires than the more numerous mines operating on one production shift or the (presumably) more mechanized and productive mines operating three production shifts. Next is when the fires tend to occur. Even though most mines only operate a single shift many of the fires also occur during what may be off-shift times. Lastly is that this data set is in some ways not as complete as previous works have reported. Little in the way of fire data is presented, such as ignition source, suppression method, fuel involved, or the fire duration.

However using these data sets allowed for some new analysis in the nature and degree of injuries caused by fires. Also new is the analysis of the trend in citations for fire protection violations and the consequent increases in proposed penalties. It is especially comforting to look at the historic trend and see the great progress mines have made for fire safety.

Acknowledgements

The authors would like to thank the previous authors of works done in this area: Maria De Rosa, Bill Pomroy, L. Bruce McDonald, Shail Butani, and Annie Cargiet. Their hard work provided inspiration for this analysis and the ability to take a complete look at the history of mine fires in the US since the 1950s. The men and women of the Mine Safety and health Administration were also invaluable with the amount of data they have made available under data transparency efforts. To obtain and analyze this amount of data previously would have required visiting the various MSHA district offices. Now engineers and educators can analyze this data themselves on their own computers.

References

- [1] B. McDonald, and W. Pomroy. "A Statistical Analysis of Coal Mine Fire Incidents in the US from 1950 to 1977." US Bureau of Mines, 1980.
- [2] S. Butani, and W. Pomroy. "Statistical Analysis of Metal and Nonmetal Mine Fire Incidents in the United States from 1950-1984." In *Recent Developments in Metal and Nonmetal Mine Fire Protection*. Information Circular 9206. US Bureau of Mines, 1988.
- [3] W. Pomroy, and A. Cargiet. "Analysis of Underground Coal Mine Fire Incidents in the United States From 1978 Through 1992." US Bureau of Mines, 1995.
- [4] M. De Rosa. "Analysis of Mine Fires for All U.S. Underground and Surface Coal Mining Categories 1990-1999." National Institute for Occupational Safety and Health, 2004a.
- [5] M. De Rosa. "Analysis of Mine Fires for All U.S. Metal/ Nonmetal Mining Categories, 1990-2001." National Institute for Occupational Safety and Health, 2004b.
- [6] M. De Rosa. "Analysis of All Mobile Equipment Fires 1990-1999." National Institute for Occupational Safety and Health, 2004c.
- [7] "MSHA Open Government Data Sets." *MSHA-Open Government Initiative Portal*. Accessed December 8, 2014. <http://www.msha.gov/OpenGovernmentData/OGIMSHA.aspx>
- [8] *Mine Improvement and New Emergency Response Act of 2006*, PL 109-236 (S 2803), 109th Congress. 2006.
- [9] US Government Printing Office. *Code of Federal Regulations: Title 30*. Sections 56.4, 57.4, 75.11, and 77.11. 2012
- [10] "MSHA Fact Sheets-Injury Trends in Mining." Accessed March 17, 2015. <http://www.msha.gov/MSHAINFO/FactSheets/MSHAFACT2.HTM>

Principle Roles of Mine Fire Simulation in Mine Management and Emergency Planning

Jon Fox^a, John Bowling^a, Steven Schafrik^b

^a Mine Ventilation Services, Clovis, California, USA

^b Virginia Center for Coal and Energy Research, Virginia Tech, Blacksburg, Virginia, USA

Safety personnel and ventilation engineers need a tool for the design of credible fire scenarios and appropriate emergency response procedures. A validated ventilation network model with measured site-specific parameters is a necessary starting point for development of underground fire simulations. MineFire, based on the NIOSH MFIRE program, is an engineering tool used to simulate fire dangers. The MineFire tool combines the visualization and network editing tools familiar to ventilation engineers with fire simulation capabilities and result visualizations. Employing the evaluation tools one can develop realistic emergency procedures, including escape route planning and emergency response to maintain the health and safety of the underground workforce. This paper covers the three principle roles of mine fire simulations: 1. ventilation system design and evaluation, 2. operator training and 3. Emergency preparedness planning. Practical working knowledge contained in the MineFire program will be great for planning mining ventilation networks and the dynamic responses to fire events that will greatly improve emergency preparedness.

Keywords: Mine Design, Training, Emergency Preparedness, Mine Rescue, Mine Fire

1. Introduction

Most of the major mine disasters throughout the history of mining have been caused by explosions and/or fires and both causes remain among the greatest potential hazards in mining. The greatest hazard of mine fires is the poisonous and sometimes explosive combustion products which are carried through the mines by the ventilation airflow. Additional hazards occur due to interaction of the source fire with the airflow passing through the ventilation network. The volume expansion of the air as it passes through the fire has a constriction or throttle effect [1]. Density differences in non-horizontal communicating airways create buoyancy effects similar to chimney drafts. In order to educate mine ventilation engineers about these non-steady state interactive effects, the United States Bureau of Mines (USBM) undertook a software development project known as MFIRE [2].

The MFIRE program was developed in FORTRAN at the Michigan Technological University, under a contract from the former USBM. MFIRE performs normal ventilation network planning calculations, and dynamic transient state simulation of ventilation networks under a variety of conditions. MFIRE simulates a mine's ventilation system and its response to altered ventilation parameters such as the development of new mine workings or changes in ventilation control structures, external influences such as varying outside temperatures, and internal influences such as fires. The original version of MFIRE allowed ventilation networks of up to 500 branches and 10 fans.

MFIRE performs the transient-state simulation of a mine ventilation system as a stepped series of short-duration steady-state calculations with output from the initial step becoming the input for the next time step.

The heat transfer model is constructed on the basis of the energy balance of airflow to pre-calculate time-dependent air temperatures at different locations. Given data that describes the geometry of the mine network, airway resistances, dimensions, characteristic curves of fans and characteristics of the fire or thermal event, the program will provide tabular representations of various predicted ventilation, contaminant, and temperature parameters as well as graphical representation of the ventilation system and fume front propagation over selected time increments.

Following the disbanding of the USBM, the National Institute of Occupational Safety and Health (NIOSH) took over the project and contracted a software developer to rewrite the FORTRAN into C++ code that handles all input and output operations. Currently with release at version 3.0.2.0, the NIOSH software does not provide graphical interpretation of simulation results [3].

Mine Ventilation Services, Inc. (MVS) began development of MineFire in 2003 using the source code from MFIRE version 2.2, which was modified by MVS solely to increase the number of junctions and fans available and to run in the Windows operating environment [4]. This calculation kernel was then adapted into the user-friendly interface of MVS' VnetPC ventilation network software package. MineFire is designed to assist with the prediction of spread of contaminants, heat, or other changes in air density. The latest version has removed all network boundaries for ventilation models. The only limitation now is a maximum of 20 data points for a fan curve definition.

2. Program Description

MineFire performs steady-state ventilation network simulation and dynamic-transient-state modeling of ventilation networks under a variety of conditions. The program simulates a system's response to altered ventilation parameters such as: the introduction of fire to the system, varying outside temperatures, changing ventilation control structures, and development access for new mine workings.

MineFire requires a number of parameters in addition to those input into the VnetPC model. The modeler uses the k-factor resistance type for setting up the ventilation network, or assigns calculated resistance values for each branch. Length, perimeter, and area parameters must be defined for each branch of the model in order for the transient-time utilities in MineFire to function properly.

Not all MineFire parameters must be entered for successful simulations. In a fire simulation, conductivity, diffusivity, and rock temperature are recommended parameters for each branch in the model and may be defined as average values (Fig. 1).

The screenshot shows the 'Simulation Parameters' tab with the following sections:

- Select Calculations:** A dropdown menu set to 'Stop After Steady State Temp and Concentration Calcs'.
- MineFire Output:** A dropdown menu set to 'More Detailed'.
- Time Span to Assume Quasi-equilibrium:** An input field for hours.
- Simulation Metrics:**
 - Max Iterations in Temperature Part: []
 - Max Iterations in Dynamic Part: []
 - Time Increment in Dynamic Part: [] sec.
 - Time Span of Dynamic Simulation: [] min.
 - Time Interval for Output: [] min.
 - Allowable Residual Error: [] %
- Atmospheric Conditions:**
 - Reference Temperature of Air: [] (°F)
 - Reference Density: [] (lb/ft³)
 - Ambient Atmosphere Temperature: [] (°F)
- Average Values:**
 - Thermal Diffusivity of Rock: [] (ft²/hr)
 - Thermal Conductivity of Rock: [] (BTU/Hr-ft-°F)
 - Friction Factor: [] (lbf-min²/ft⁴)
- Use Average Values in MineFire Simulation
- Buttons:** 'Apply', 'Reject Changes', and 'Set Defaults'.

Fig. 1. Contaminant Data - Simulation Parameters Tab

Variable parameters and modeling boundary conditions required for model execution must be defined. A range of acceptable values are entered with validation rules applied to help maintain accuracy of simulation results.

2.1 Conductivity

This variable is the thermal conductivity for the rock mass. The number is used by the program to define the thermal transfer to or from the air mass as it travels through the airway. This will affect airflows in the mine.

An understanding of which rock type defines a branch is needed for detailed models. A theoretical average or general value for the rock mass may also suffice. Where the rock type in the model is uniform, large numbers of branches will have the same value. The units for conductivity are Btu/hr×ft×°F or W/m×°C.

2.2 Diffusivity

Rock diffusivity is obtained through laboratory testing of core samples, or from tables. It defines how quickly heat moves between the rock mass and the air as air moves through a branch. The units for diffusivity are ft²/hr. or m²/sec.

2.3 Rock Temperature

This variable uses the average temperature of the rock at a given network location and is based upon local borehole measurements or derived through known regional geothermal gradients. Sample measurements are taken in numerous key locations throughout the mine and this data is applied to those network junctions respectively. This data may be averaged as necessary.

2.4 Fan Data

Fan characteristic curves are defined by entering between two and twenty pairs of pressure - airflow quantity points. Fan characteristic curves must be defined by at least two points for the MineFire program to provide accurate results. This allows the program to correctly apply the effects of the changing natural ventilation pressure (NVP) with respect to the fan characteristic curves.

Model domain parameters are defined that control the simulation execution. These parameters govern iterative calculation characteristics, the fan curve fitting algorithm, and simulation timing conditions. Additional atmospheric parameters are defined to provide boundary conditions for temperature and reference density. The modeler determines parameters for time span, time step increment and allowable error between calculation iterations in order for the simulation to properly converge.

Contaminant source parameters are established for each proposed fire location for simulation. The airflow quantity for the fire source airway is used together with the mass of combustible materials to calculate contaminant production and heat generation from the fire. Diligent estimation of each fire source includes characteristics for both oxygen-rich and fuel-rich fire propagation.

A timeline is developed which most realistically represents the anticipated sequence of an underground mine fire. Time table events simulate conditions and actions which could be expected to occur during a mine fire. These discrete events describe changes to the ventilation network such as reversal of main fans,

closing of fire doors or the introduction of an emergency fan. The modeler decides the starting time and event duration, entering these discrete events sequentially into the time table (Fig. 2) tab of .

The screenshot shows the 'Time Table' tab of a simulation software. It features three main configuration sections:

- Branch Condition Change:** Includes a dropdown menu for 'Change to ordinary branch & modify branch resistance', a 'Branch ID' field, and options to 'Change to Ordinary Branch' with 'At Time' (minutes after time zero) and 'Resistance' (PU) fields.
- Change to Fan Branch:** Includes 'Fixed Pressure' (in.w.g.), a 'Fan Curve...' button, 'Fan Is On' checkbox, 'Fans In Parallel' and 'Fans In Series' dropdowns, and an 'NVP' checkbox.
- Change to Fire Branch:** Includes 'Flow Rate' (kcfm), 'Contaminate Concentration' (/(ft³ of O₂)), 'Concentration' (%), 'Heat Production' (%), 'Heat Transfer' (btu/min.), 'Reference Q' (kcfm), 'O₂ Concentration' (%), and 'Lead Time' (min.) fields.

Below these sections is a table with columns for 'Time', 'Branch ID', and 'Condition Change'. At the bottom, there are buttons for 'Add', 'Delete', 'Apply', and 'Reject Changes'.

Fig. 2 Contaminant Data - Time Table Tab

Important simulation results such as changes to fume front propagation, temperature rise and contaminant concentrations over the simulation timespan are displayed graphically in VnetPC. Subsequent analyses of the simulation reveal district locations susceptible to airflow reversal and/or recirculation. Visual display of simulation results allows mining engineers to optimize design of escape routes, plan locations of refuge chambers as mining production changes and effectively communicate those requirements to key safety personnel.

3. Program Assumptions

Sound risk assessment is essential to developing credible scenarios for fire simulations. Hazard analyses are conducted to identify the potential frequency of the hazard, number of people affected, potential spread of contaminants, cost of damage, and seriousness of each hazard. Accounting for actual and estimated fire source materials reflects the worst-case scenario. Once potential sources are identified, the magnitude of associated risks are evaluated to determine if they are tolerable or not. Each intolerable hazard is simulated using a realistic ventilation model, developed for a typical mining layout or for the development stage of worst-case ventilation.

Development of a ventilation model that uses realistic resistance values, in either k-factor or practical resistances calculated from measured field data is

required for MineFire. All fixed quantities are removed and all fans have curves to sufficiently represent anticipated operating points. The modeler takes into account the surface atmospheric conditions and incorporates them into the models.

A solid understanding of the NVP being applied to the ventilation network is also a requisite. Worst-case scenarios reflect maximum driving (or retarding) NVP and account for those forces appropriately in the model's respective airways. The effects of NVP are handled in MineFire with the insertion of an effective fixed pressure fan in the relevant airway. In this way, the effect of the conversion of thermal energy to mechanical work is represented as an effective fan pressure that is independent of airflow rate.

Development of a representative mine ventilation network model involves a considerable amount of effort. It is suggested the ventilation model being used as the basis for the fire model be developed from a ventilation survey of the mine workings. This is accomplished by using data from ventilation surveys together with information determined from known airway dimensions and characteristics. MVS has attempted to provide the user with explanations, reference material and sources, along with procedures for determining some of the input parameters. It is up to the user to envision credible scenarios according to specifics of the ventilation system or design in question.

4. Program Limitations

Fire behavior is very difficult to predict and nondeterministic; fire is energetic chemical reaction(s) with very chaotic inputs. The results of a simulation will only be as good as the inputs. Input data relating to fires is more complex. Heat release rates are calculated based upon which type(s) of fuel is (are) burning and available oxygen in the airflow at the hazard's location. The location of the fire in a main intake/exhaust airway or area of low flow is important in determining whether to assume an oxygen-rich or fuel-rich fire [5], which helps the user determine which parameters to use in the fire simulation. Contaminants are determined based on the stoichiometric reaction of the combustible materials.

MineFire does have several limitations. One of the most important of these is that it treats airways as one-dimensional: MineFire assumes instantaneous and complete mixing of airstreams at junctions and assumes uniform distribution of contaminants within a given transverse cross-section of the airway (e.g., no smoke layering). Additionally, the program assumes the fuel source burns indefinitely after ignition and ramp-up time: there are no time table events for ramp-down or burn-out of the fire. The program also does not directly deal with the impacts of a combustible ore, such as coal, adding fuel to the fire; nor does it deal with issues surrounding burn-through of stoppings or doors. These conditions are characterized by adding time table events to simulate the fire moving to adjacent entries or change

in fuel type. Localized thermodynamics of the fire and associated chemical reactions are also ignored. Thus, it does not contend with the issues of stratified (laminar) flow, either in the direction of bulk flow or reverse flow.

As with any time-based numerical modeling, the MineFire solution kernel uses results from the preceding time step to compute the following time step solution. Improper simulation parameters for time span, time step increment and allowable error between iterations lead to solution divergence. Very small errors in accuracy introduce compounded errors in the final stages of the simulation [6].

Successful fire simulation requires a series of interdependent decisions from the user in order to converge as expected. These decisions govern the simulation algorithms, and hence the quality of results. Understanding the model time domain conditions and applying sound judgment to those conditions requires considerable experience. Experience of the modeler ultimately limits the development of a fire simulation with credible results.

5. Program Additions

In order to balance ventilation network meshes, the summation of all pressure drops around a closed circuit will equal zero [7]. Synchronized psychrometric and pressure measurements along loop boundaries with surface readings will help the engineer account for NVP and accurately balance meshes. MineFire allows the user to introduce a differential NVP at any junction where these adjustments are accounted for in the model to balance individual circuits. In this way, balanced mesh loops will better handle the dynamic nature of fire modeling while allowing for airflow reversal and adjusting associated upstream airflow perturbances.

MineFire also adds two new curve fitting algorithms to better simulate changes to fan operating points during

fire events, Gaussian and constant pressure fan [4]. The MFIRE program has had two fan curve fitting methods built in with an optional parameter. The program includes the Least Squares method and a Spline method of curve fitting. These methods are used for interpolation of data points between the data points entered by the user. The optional parameter defines how to handle points that are beyond the extents of the user entered points, referred to here as the projection points. The projection points can be calculated using one of these three rules:

1. The end point slopes are continued indefinitely
2. Right most value is held constant
3. Left most and right most values are held constant.

Fan curve fitting method must be specified for individual fans, but the projected points method is consistent for all fans.

Experience shows that the most useful fitting method is the Least Squares method with projection points using the option to extend the fitted slope indefinitely. However, when the models are increasing in size and complexity, this combination of methods can yield data results that are beyond a reasonably fitted fan curve. An example graph of the internal calculations is show in Fig. 3.

In this case, the constant slope moving away from the inputted data allows the simulation routine to ask for unreasonable data from the fan curve. This example includes all data requests, including those in intermediate iterations. A new data table report was added to the program that will report all requested flowrates for each fan calculation and the pressure that was determined via the fitting method. Considering this data for very large and complex models it was determined that a new fitting method should be developed.

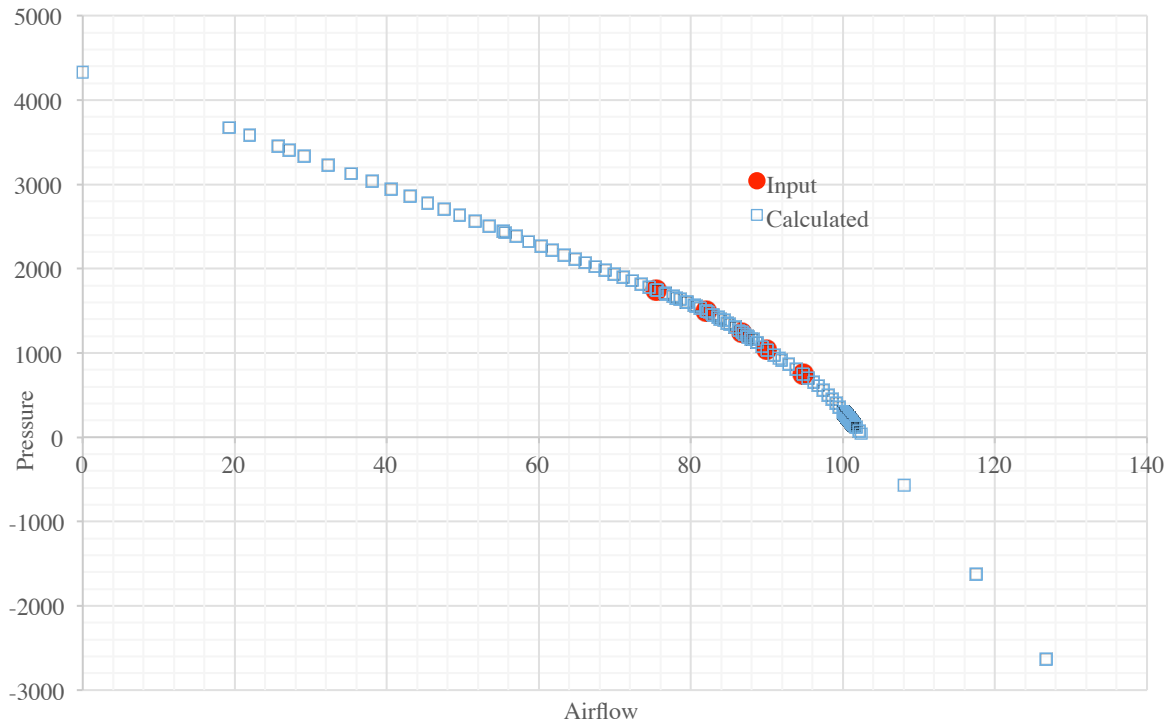


Fig. 3 Example of Fan Curve Fit with inputted data points and calculated data from MineFire simulation

Using the Polynomial fit method established in R. Sedgewick's "Algorithms in C", a new regression model was added [8]. There were several adaptations to the Sedgwick example to make the fit work faster by parallelizing the execution of the code. In addition, the three optional parameters are not necessary for the new curve fit. For values going to the right, they are not allowed to intersect the X axis and are not allowed to

return a Y value that is larger than the previous Y value. For values going to the right, the X axis intercept is the furthest value allowed providing that all Y values calculated are increasing. This provides for an inconsistent slope beyond the inputted values, but does not include data that can easily be regarded as unreasonable.

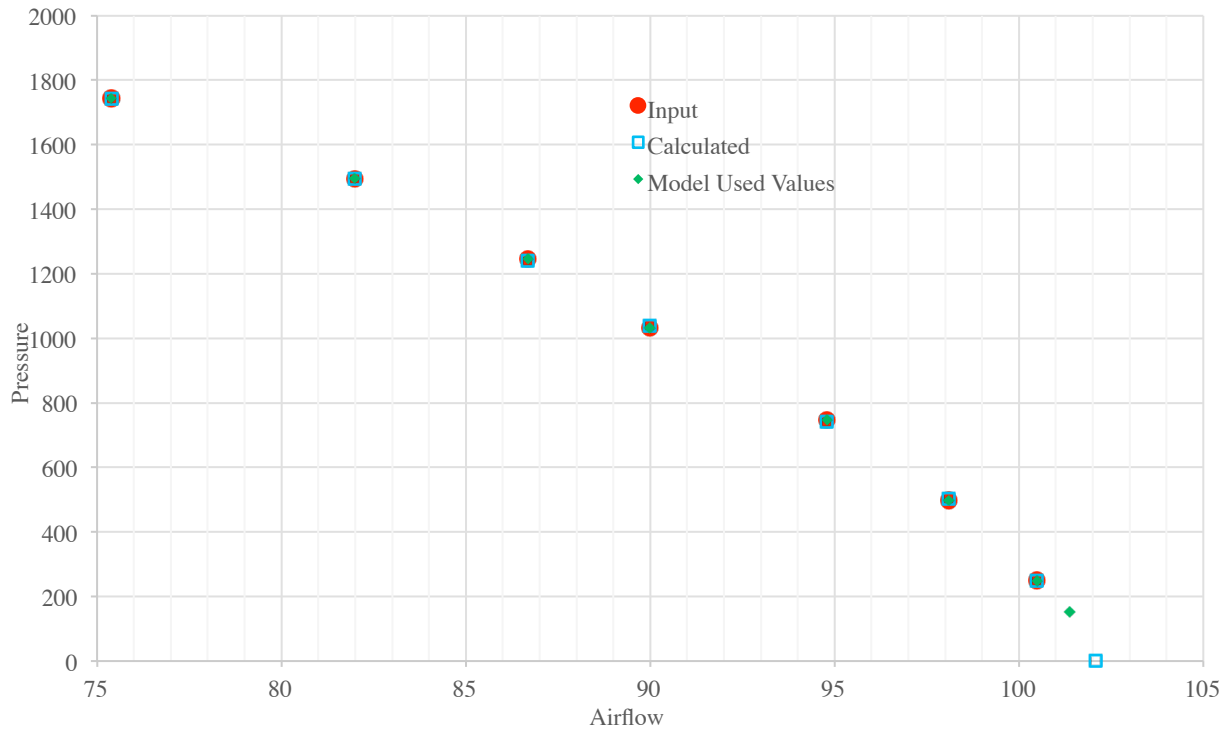


Fig. 4 Example of New Fan Curve Fit

Fig. 4 shows an example of this new fan curve fit. In this example, the user inputted points are shown

along with points that are calculated specifically to demonstrate the difference between the fitted curve and

the inputted data. The equation governing this fit is reported to the user and in future versions of the software the user will be able to input or override the equation.

Calculated points are also shown that is on the right hand most side of the curve, as well as one of the data points that was used in a solution to the model and is outside of the user inputted points. We have found that this fitting method will not work for all fans, but the new data that is available to the user will allow the expert to make better decisions about the fitting method that works best for their model.

6. Practical Applications

MineFire is a comprehensive engineering tool for ventilation engineers, upper management and emergency responders to evaluate the effects of fires on a mine ventilation network. MineFire is employed in three principle roles:

1. System design and evaluation – design stage efforts, in which potential fire hazards and fuel sources are known, such as maintenance shops and fuel bays. This allows mine safety and engineering personnel to consider the overall impacts of fire control procedures on the mine ventilation system for planning efforts, procedure development and training purposes.
2. Operator training – graphical display of simulation results provides immediate feedback necessary for miners to visualize effects of fire spread. The effects of a credible fire scenario and fire control measures are evaluated interactively.
3. Emergency preparedness – development of effective emergency response plans involves careful examination of potential risks and effective response to terminal hazards. Evaluating an existing mine plan for likely shortcomings in egress will be improved with the use of comprehensive fire modeling.

7. Modeling Fire Scenarios for Emergency Preparedness Plans

Ventilation engineers and officers should consider integral participation in their emergency preparedness planning team, alongside delegates from upper management. Development of emergency preparedness plans should include dressed rehearsals of simulated fire hazard mockups to give the planning team a tangible event to design around. The ability to quickly communicate the tasks required to control underground fire shows the necessary steps, the c
5
in which these steps need to occur and an efficient timeline for these tasks. Describing accepted firefighting efforts in sufficiently granular detail, along an acceptable timeline, is paramount when gathering “buy-in” from first responders and upper management to a credible fire simulation.

Miners play an important role in developing the mine-related aspects of the plan. Including a diverse team during the initial review stages of an emergency preparedness plan provides a broad perspective on those issues relevant to each person’s department or function. Problem solving is quantitatively better since people with different backgrounds, experience and expertise view problems from different perspectives.

Representatives from upper and middle management need to set aside sufficient budget and sit alongside rescue team members during the early phases so that all team members understand the benefits of mock emergency response exercises. If a mine does not have a fire brigade, the mining company should consider additional, more in-depth firefighting training for their rescue team members.

Training in fighting conveyor belt and other large equipment fires using fire hoses, nozzles and other related equipment [9]. Should a mine operator want to conduct this more intense training, they will need to equip rescue team members with appropriate personal protective equipment including fire fighter turnout gear, hoods, gloves and other related items.

Understanding necessary changes to ventilation controls and the timing of early responses to fire events greatly improves emergency preparedness. First responder teams benefit greatly from the use of MineFire as a prediction tool in training exercises. Animated playback of a fire simulation can be invaluable during emergency training.

Development of fire models for each working section gives each production team a sense of stewardship when reviewing firefighting procedures. Displaying animated results of the advance of noxious fumes from a simulated fire event to crew members will impart the urgency of response required to minimize the growth rate of a fire.

Working section firefighting brigades, and particularly production foremen, should become involved during review of fire simulation results amongst the emergency response team. Since many early firefighting response actions depend upon managing ventilation controls, section foremen need to understand the appropriate order of events for optimum mitigation.

Miners that are well informed of supplies necessary to fight a fire are more likely to keep those supplies in order and readily available in their section. Once the foreman understands the sequence of events to effectively modify the existing ventilation network in a firefighting exercise, critical supplies are more likely to remain at the ready [10].

8. Conclusion

This paper presented a use case for the NIOSH update MFIRE program with MVS’s modifications and a robust graphical interface. Ventilation experts using this program will be able to build and analyze credible

fire scenarios. This can be done in conjunction with regular mine ventilation modeling and analysis work in the same frontend program.

MVS has made several modifications to the NIOSH MFIRE program. They allow the user to make modifications to the NVP at various points in the model. This is a very nice feature for overcoming some limitations in the Hardy-Cross solver. The user also has a new fan curve fit method that is very accurate. To improve the accuracy, the internal fan curve calculations are now made available to the modeler in an intuitive manner allowing the expert to make better decisions about the fans that are deployed in the mine. New reporting capabilities have been added that put more data into the model mesh available to view and in table views.

While adding features to the MineFire program, it was of great concern to MVS that the additional features not preclude a user from running the model in current or future version of the NIOSH produced MFIRE. As long as a user does not take advantage of new features such as the new fan curve fit or the NVP editor, an XML file that is compatible with the NIOSH version of the program can be created. Other differences between the two programs are model size and number of fan curve points.

An example mine was presented that shows how all of these proven features of MFIRE have been incorporated into MineFire and how the new features can be utilized. This was also performed with a significant speed-up of the execution time. With proper planning and appropriate usage of MineFire, mine emergencies can be mitigated altogether or can be responded to in an efficient manner.

Acknowledgments

The work described in this paper would not be possible without the dozens of mining engineers, scientists and programmers who have modified and improved the operation and accuracy of the MFIRE program over the years. A special thanks goes out to all the civil servants involved with carrying forward the vision of comprehensive scientific research and continued software development necessary to educate those responsible for the health and safety of the underground workforce through better understanding in the dynamic nature of mine fires.

References

- [1] D.W. Mitchell, P.E., Mine Fires, Maclean Hunter, Chicago, IL (1990) 6-13.
- [2] Chang, Xintan, L.W. Laage, and R.E. Greuer. A user's manual for MFIRE: a computer simulation program for mine ventilation and fire modeling. Vol. 9245. US Dept. of the Interior, Bureau of Mines (1990).
- [3] NIOSHTIC2 Number: 20040441, Technology News 549, MFIRE 3.0 - NIOSH Brings MFIRE into 21st Century, National Institute for Occupational Safety and Health, DHHS (NIOSH) Publication No. 2012-127, TN 549, Pittsburgh, PA (2012).
- [4] K.W. Wallace, et. al., MineFire Pro+ User's Manual and Tutorial, Mine Ventilation Services, Inc., Clovis, CA (2014) 11, 24.
- [5] S.J. Schafrik and R. Ruckman, Expanding the Limitations of the MFIRE Simulation Model, Society for Mining, Metallurgy, and Exploration, Inc., Littleton, CO (2011).
- [6] J.E. Fox, G. Danko and D. Bahrami, Development End Characterization through Response Curves, SME Annual Meeting, Seattle, WA (2012).
- [7] M.J. McPherson, Subsurface Ventilation Engineering, Mine Ventilation Services, Inc., Clovis, CA (2009) 236.
- [8] R. Sedgewick, Algorithms in C, Addison-Wesley (1990) 545-555.
- [9] R. Shackelford, Fire Behavior and Combustion Processes, Delmar, Clifton Park, NY (2009) 13.
- [10] J. Strang, P. Mackenzie-Wood, A Manual on Mine Rescue Safety and Gas Detection, Weston & Co., Sydney, NSW (1985) 79.

Spontaneous combustion prediction and remediation techniques

Ankit Jha, Felipe Calizaya, Michael G Nelson

University of Utah, Salt Lake City, Utah, U.S.A

Methods for predicting spontaneous combustion include examining coal properties and observing coal-oxygen interactions. Accurate predictions in mines are difficult because of variations encountered in actual conditions which change coal behavior considerably. The most common remediation techniques for control of spontaneous combustion are isolation and inertization, and pressure balancing. When isolation and inertization are used, there can be considerable leakage of air from stoppings, which can dilute the whole process and increase nitrogen consumption. The pressure balancing approach can provide a solution that is not so susceptible to leakage problems.

A series of experiments were conducted at University of Utah mine ventilation laboratory to ascertain the variation of pressure across a simulated mine gob with an adjacent pressure chamber. Experiments were conducted at different conditions, including variations in the pressure build-up and decay rates at the chamber, in an attempt to reduce the ingress of air to the gob. Results of these experiments are reported in this paper.

Keywords: Spontaneous combustion, Inertization, Pressure balancing

1. Introduction

Certain materials such as coal and pyrites have the characteristics of self-heating upon interaction with the mine air. If the heat liberated is greater than the rate of dissipation, it may result in a chain reaction known as spontaneous combustion or endogenous fire. The risk from such fires may accrue at a temperature much lower than the corresponding ignition temperature of the material, depending on extraneous conditions such as coal quality, geological conditions, and mining practice.

Seals used to separate the working areas from the gob are not airtight, and they tend to “breathe in and breathe out” with changes in barometric pressure. In mines ventilated by a U-tube exhaust system, the gob is often kept under negative pressure. Under these circumstances, an increase in barometric pressure may cause an influx of fresh air into the gob. This quantity may be sufficient to start the self-heating of coal.

1.1 Factors influencing spontaneous combustion

The interaction of coal with oxygen is an exothermic process. Some of the important factors that contribute to the generation of heat are coal properties, geological conditions, and mining method. A number of different estimation and prediction methods are available to predict the propensity of coal for spontaneous combustion. Different methods used to predict the heating of coal on the basis of coal-oxygen interactions include crossing point temperature, differential thermal analysis, and adiabatic calorimetry technique [1, 2]. Adiabatic calorimetry is used to simulate conditions close to those that occur during mining, and is based on the fact that spontaneous combustion is an adiabatic phenomena. Each method has its own limitations, and accurate prediction of spontaneous combustion with any of them is difficult.

Moreover, the interaction of each of the key factors to generate spontaneous combustion is complex. Control measures in the form of remediation techniques should be

practiced to prevent any spontaneous combustion and unwanted subsequent events.

1.2 Remediation techniques

The techniques used to control spontaneous combustion include caved area inertization and pressure balancing. Inertization refers to injection of an inert gas into the gob atmosphere to reduce the concentration of oxygen and render the atmosphere inert in relation to methane content. Inertization also helps reduce the oxygen concentration in and around the heated area, and to reduce the intensity and spread of secondary combustion. Pressure balancing is a technique in which the pressure across the gob area is minimized to control the ingress of air. There are two types of pressure balancing techniques which can be used: passive and active techniques.

1.2.1 Passive pressure balancing

Using this method, pressure balancing is achieved by adjusting the flow in the affected area using regulators and fans, or by judicious adjustment of the air flow rate. The adjustment takes place first through the different branches of primary ventilation network, and second through pipes and pressure chambers designed for the purpose [3]. A pressure chamber is constructed by first building an isolation stopping in front of the isolation seal and then equipping it with a set of air sampling and flow control devices. Two pipes are laid out connecting the pressure chamber to the main intake and return airways. Air sampling pipes through the isolation stoppings are used to measure the pressure differential across the stoppings. When the pressure differential across the isolation stopping is greater than an allowable value, this is balanced by adjusting the airflow rates through these pipes.

Figure. 1 shows a schematic of a passive pressure balancing arrangement. The seals used to isolate the gob are not usually airtight and the pressure differential between the intake and gob side can be high enough to cause an ingress of air in the gob. A passive pressure

chamber can be installed by making another seal adjacent to the original seal and connecting it to the intake and return airway using pipes. Once these connections are made, the air flowing in the mine is used to pressurize the chambers using control valves. These valves regulate the quantity of air that enters the chamber, to attain the desired pressure. Once the pressure inside the chamber equals that of the gob, pressure balancing is said to be achieved.

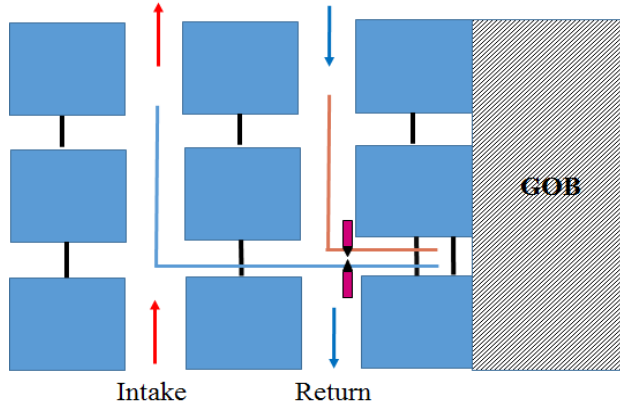


Fig. 1. Schematic of passive pressure balancing arrangement.

1.2.2 Active pressure balancing

This is a preferred choice when passive pressure balancing is difficult to implement. In this method pressure chambers are built in a manner similar to the previous method, except that here the chamber is connected to a source of inert gas. The chamber is equipped with a differential pressure sensor and a microprocessor, which are the active components of a control loop that ensures an adequate flow of inert gas to the chamber [6].

When the chamber is pressurized and maintained at a pressure slightly higher than that of the gob area, minimal leakage of inert gas (usually nitrogen) occurs from the chamber to the gob side. Inert gas leakage from chamber to the gob does not affect its atmosphere. In this way the

ingress of oxygen can be contained and spontaneous combustion can be mitigated. In addition, gob air is prevented from flowing towards the face when barometric pressure variations occur. There are several sources of inert gas that can be used with this method, depending on local conditions and quantity requirements.

Figure. 2 shows a schematic of an active pressure balancing chamber. The chamber is isolated from mine openings by two seals. Placing a more substantial seal on the outer end of the chamber will ensure that the leakage from the gob to the workings is reduced when the pressure differential across the seal is positive [4, 5].

A central pipeline carrying inert gas is used to pressurize the chamber. Differential pressure sensors are used to monitor the gage pressures in the chamber and the gob. If the pressure in the gob is higher than the mine side, a microprocessor controller will open the valves and pressurize the chamber. The chamber is pressurized so that its pressure is slightly higher than the gob pressure.

2. University of Utah mine ventilation model

Laboratory models are helpful in simulating real life problems. Experiments can be performed to come up with meaningful conclusions, which may not be possible in active mines. The University of Utah laboratory ventilation model (Figure 3) is constructed of 0.15-m (5.75-in.) diameter pipe and equipped with two fans and an atmospheric monitoring system.

The pipes are configured in a standard U-shaped ventilation network with one intake and two return airways. Crosscuts are constructed of 0.06-m (2.5-in.) diameter pipes, which act as leakage paths between the intake and the return airways. Two airways, one each designated as continuous miner face and longwall face, are used to simulate two active workings. The model is equipped with a main blower fan and a bleeder fan. Each fan is equipped with a variable frequency drive to allow changing the fan duty for different experimental conditions.

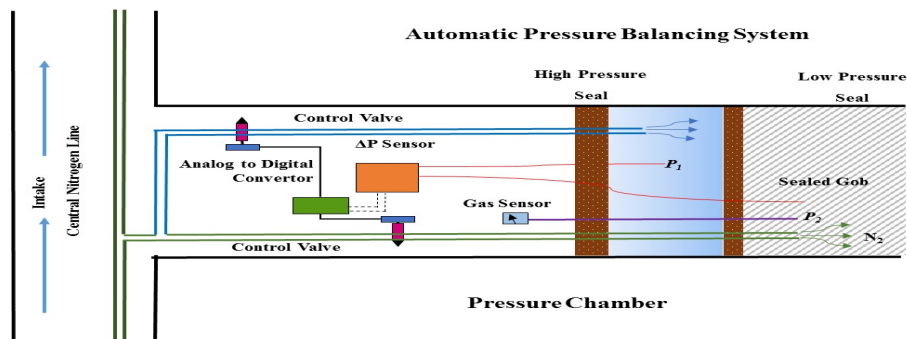


Fig. 2. Schematic of active pressure balancing chamber



Fig.3 University of Utah laboratory model

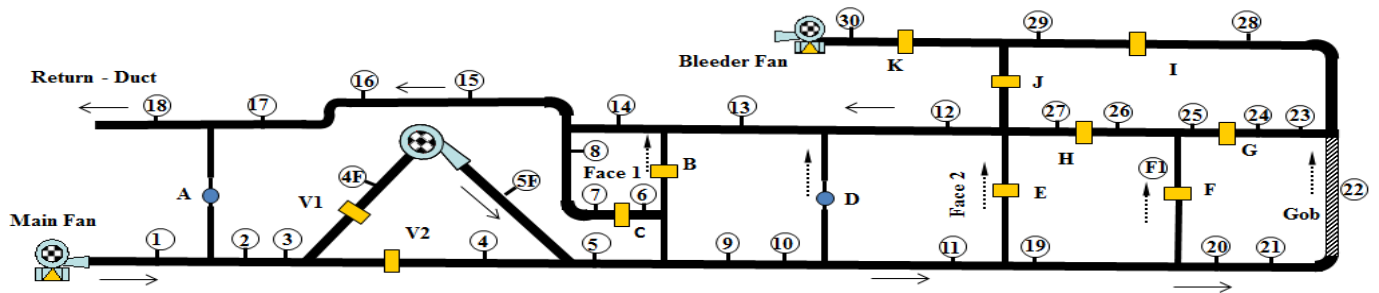


Fig. 4. Schematic of laboratory model

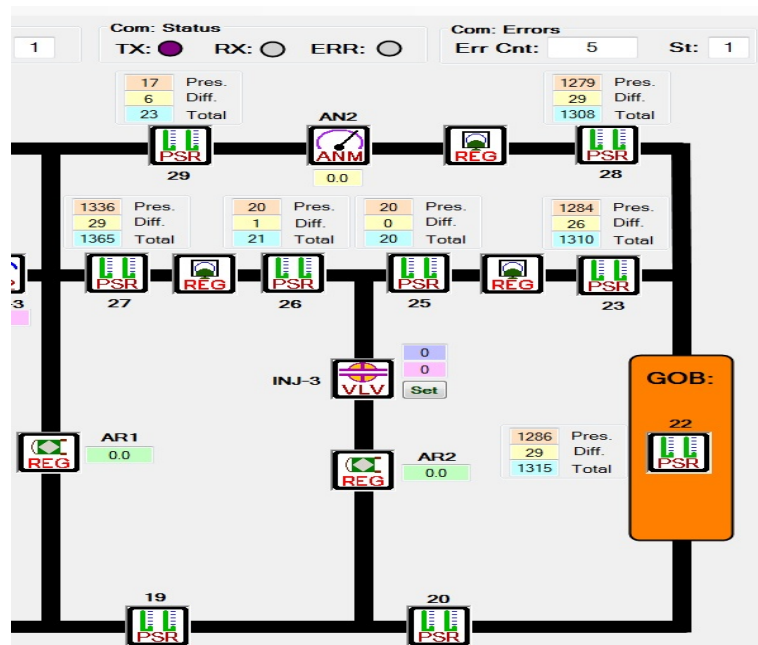


Fig. 5. Gob section of University of Utah atmospheric monitoring and control system

Figure. 4 is a schematic of the laboratory model showing the intake and return airways, the simulated workings (Faces 1 and 2), and the locations of fans, regulators, and pressure-quantity measuring stations.

The model was used to conduct several pressure balancing experiments. In each experiment, the main fan was used as the pressure source. Perforated gate valves of variable resistances were used as regulators to control the flow of air and achieve the desired quantities at the simulated working faces. A container, filled with broken rock (shaded area in Figure 4) was used to simulate the

mine gob. This section was equipped with a bleeder fan and a set of regulators to allow simulation of different gob ventilation scenarios.

3. Continuous monitoring system

The University of Utah laboratory model is equipped with a micro-processor based atmospheric monitoring and control system. The monitoring system consists of a host PC attached to a communication network and a set of air velocity and pressure transducers and a CO₂ gas injection-system.

Figure 5 shows gob section of the model. The pressure recorded by these transducers are mentioned against them. Each transducer is equipped with its own microprocessor controlled by a host PC. Typical functions performed by the microprocessor include scaling, averaging, filtering, and verification of signals throughout the system. All communication in the system uses RS 485 standard interface hardware. Each module draws a small amount of power (~ 30 milliamps) from 12-V DC bus for its internal digital and analog circuitry. Each module has a unique address and responds to control and query commands sent across the network.

Following is a summary of the components currently used with this system:

- Pressure transducers are used to monitor the static, velocity, and total pressure across the system. In total 25 pressure transducers are installed.
- CO₂ gas injection and sampling system is used to control the flow of carbon dioxide in the model and to determine its concentration at three strategic locations.
- Fan control devices are used to change the fan speeds for different experimental conditions.

This system was used to continuously monitor and record data for a set of laboratory tests. The data was recorded every second and stored in an Excel file. The data in this file was processed to analyze and evaluate the effect of variations of fan pressures and regulator resistances on airflow distribution across the gob.

4. Laboratory experiments

Three experimental conditions were set up by changing the main fan duty and regulator resistances in the model. Two of these were set up for passive pressure balancing, and one for active pressure balancing.

4.1 Experiment 1

The aim of this experiment was to minimize the pressure differentials across the gob by changing regulator resistances in the model.

Two gob ventilation scenarios were set up, one for a punch-out bleeder ventilation system, the other for wrap-around ventilation system. For the former, the regulator in the punch-out airway (regulator K in Figure 6) was partially blocked so that only 28% of its total area was open. This allowed a fraction of the gas generated in the gob to be vented to the surface. For the latter, this regulator was fully closed and regulator J was partially open. In each case, the blower fan was the only source of pressure for the system. The initial conditions and the results of each test are presented below.

Case 1- Punch-out bleeder system

Initial conditions. These are given by:

- Main fan pressure: 1635 Pa.
- Regulator settings: regulators A, B, and D, with 5% total open area, represent high quality stoppings with almost zero leakage flow, and the other regulators (C at 28% open area, F at 50%, G at 8%, H at 28%, J at 8%, and K at 28%) represent leakage paths.

Results. Air pressure–quantity measurements were taken using a barometer, manometers, Pitot tubes, and a thermometer. Pressure differentials were measured using micro-manometers. The results of these measurements were used to determine the fan duty and plot pressure gradients. Figure. 7(a) shows the static pressure profile for this model. In this case, the blower fan supplied 0.45 m/s of air at 1635 Pa of static pressure. In this Figure, the blue line indicates pressure profile in the intake airway and the red line, the pressure profile in the return side. Under these conditions, the differential pressure across the gob area was about 100 Pa.

Case 2. Wrap-around bleeder system

In this case, the mine gob was ventilated by a set of airways arranged in a wrap-around ventilation system. The pressure differentials across the gob were controlled using regulators placed between the cross-cuts and the simulated mine gob. The system imitates a longwall section in which the regulator in the bleeder entry (regulator K in Figure 7) is fully closed, and the regulator in the inby cross-cut (J) is partially open. This arrangement was used to minimize the pressure differential across the gob.

The initial conditions and the results achieved are presented below.

Initial condition. These are given by:

- Main fan pressure: 1740 Pa.
- Regulator settings: the regulator in bleeder entry (K) was fully closed, and the regulator in the in-by cross-cut (J), partially open. Settings of other regulators were the same as in case 1.

Results. Figure 7(b) shows the static pressure profile for this case. The pressure generated by the main fan was 1740 Pa, slightly higher than that recorded in the previous case. This pressure decreased as the air moved towards the longwall face. The pressure differentials across the gob were practically nil, indicating that the gob air was stagnant. This can be observed by comparing the pressure profiles around the simulated mine gob, indicated in Figures 7(a) and 7(b) by the dashed vertical lines.

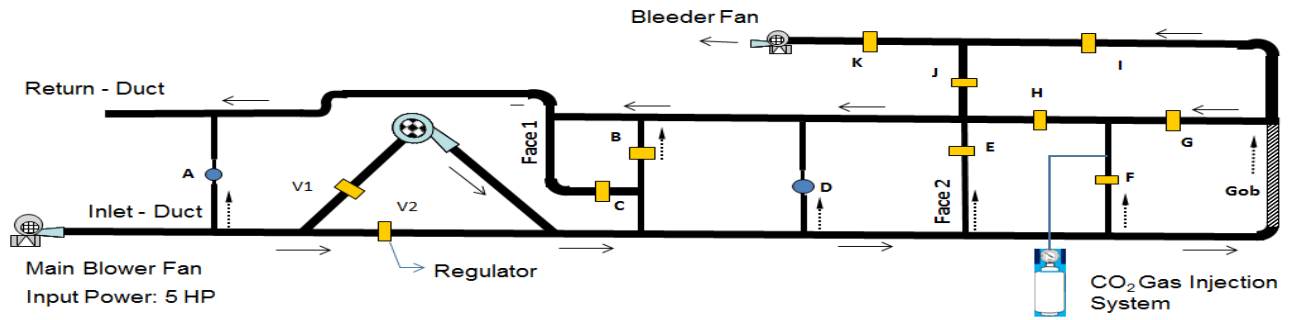


Fig. 6. Schematic of model and corresponding pressure profile

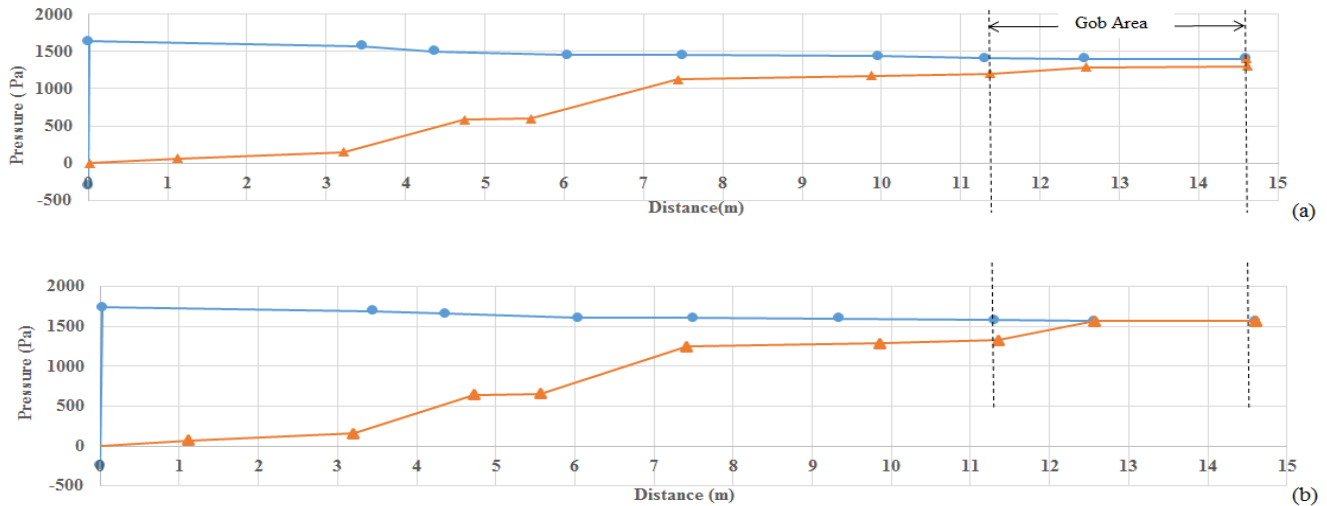


Fig. 7. Pressure profiles for two longwall bleeder ventilation systems: (a) Punch-out system, and (b) wrap-around system.

4.2 Experiment 2

The aim of this experiment was to test a passive pressure balancing system in the simulated gob model. The University of Utah ventilation model was modified to include a pressure chamber and two flow control pipes, connecting the chamber to the main intake and return airways (Figure 8). The chamber was built by isolating a section of the gob using three fully-closed stoppings, F, G and H. Tubing were used such that the existing airflow in the intake and return can be used to raise the pressure in chamber. Two 3-mm-diameter silicon tubes were used to connect the chamber to the intake and return airways. These tubes were equipped with pressure gages and flow control valves.

A test was conducted under the following conditions:

- Main fan pressure: 1620 Pa.
- Regulator settings: Regulators A, D, I, and J were partially closed, with 5 % of total area open; regulators C and K had 28% of total area.

During the experiment the pressure differential between the chamber and the gob was monitored continuously. When this difference was deemed to be significant, the pressure in the chamber was balanced by manually opening one of the flow control valves (C1 or C2), depending upon the relative pressure in the chamber. Figure. 9. shows the pressure profile obtained before and after the opening the control valve C2, used to balance the pressure in the chamber.

A comparison of the pressure profiles shown in Figure 9 (a) and (b) shows that when the control valve C2 was opened, the pressure difference across the regulator G, which separates the intake and gob, dropped from 545 Pa to 55 Pa. Based on these results it was concluded that a pressure chamber equipped with flow control pipes can be used to reduce or balance the pressure across the gob, thus reducing the possibility of a spontaneous combustion event.

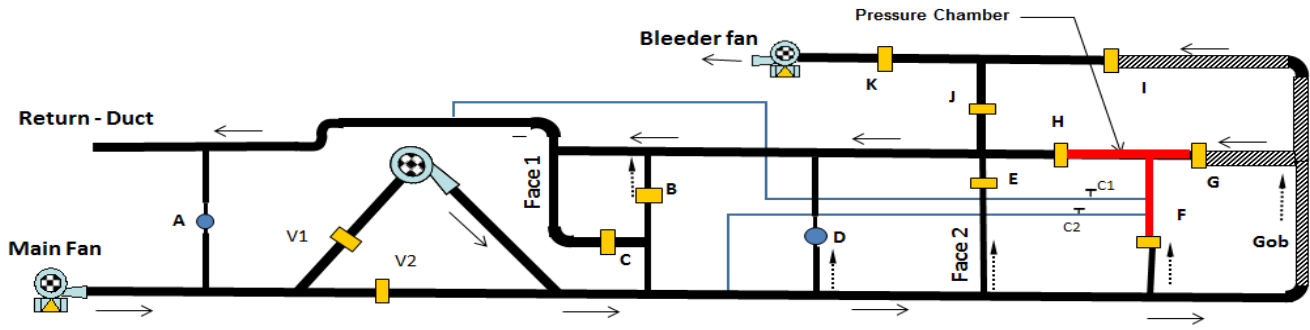


Fig. 8. Schematic of the model for passive pressure balancing system

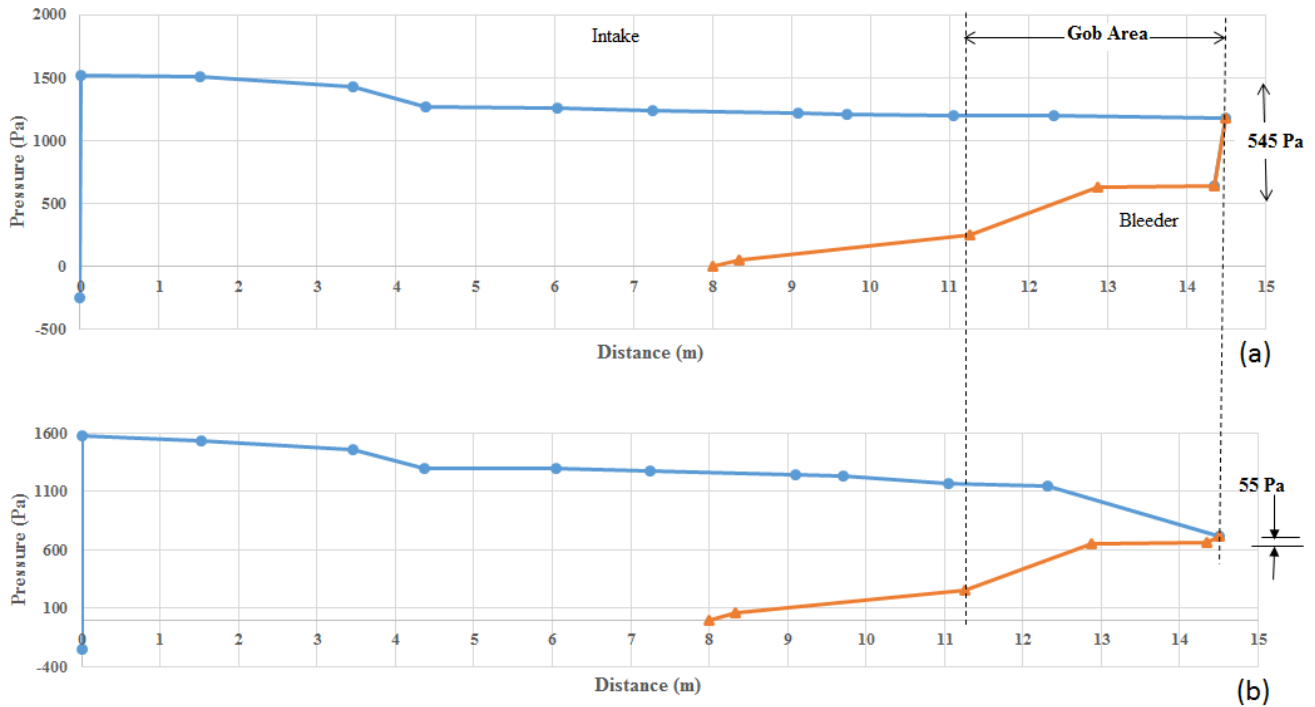


Fig. 9. Pressure profiles with pressure chamber in place; (a) when control valves C1 and C2 were both closed, and (b) after control valve C2 was open.

4.3 Experiment 3

This section describes an active pressure balancing experiment carried out with the University of Utah ventilation model. The aim of this experiment was to use an external automated CO₂ injection system to pressurize the chamber. Pressure transducers and gas sampling monitors were used to monitor pressure differentials across the gob and gas concentrations in the return airway.

As in the previous experiment, the pressure chamber was established by using three regulators (G, F and H), of which two were fully closed and the third (G) had 0.05 % of its total area open. The chamber volume was 0.03 m³ (1.2 ft³). Two pressure transducers (PS 26 and PS 23 in Figure 10) were used to monitor pressure differentials across and around the gob.

The experiment was initiated by operating the main fan at full speed and monitoring the gage pressures along the ductwork and pressure differentials around the simulated gob (stage 1). The gas injection system was then opened to reach a pre-established flowrate, held for few seconds, and shut off (stage 2). This caused the chamber to be pressurized and a new steady-state level reached. When the gas injection system was shut off, the chamber pressure returned to its initial level due to reverse leakage from the chamber to the gob.

When the chamber is pressurized the leakage from the intake towards the gob can be reduced or eliminated. This process was repeated to observe the variations of pressure build up and decay. The initial conditions and the results achieved are presented below.

Initial conditions:

- Main fan duty: Pressure 1790 Pa, quantity 0.4 m³/sec and frequency 60 Hz.
- Regulator settings: Regulators B, F, G and K fully closed; H, 0.05 % open, and the rest as in experiment 1.

Results. When the experiment was initiated (stage 1), the differential pressure across the stopping separating the chamber from the gob (regulator G in Figure 8) was -150 Pa. This was created by the back pressure caused by closing the regulator K and using a wrap-around ventilation system. Under this condition, the chamber was held under negative pressure. This pressure difference is sufficient to cause the ingress of gob gas into the face. To mitigate the problem, carbon dioxide

was injected to the chamber at the rate of 10 L/min (stage 2).

This inflow of gas pressurized the chamber to a maximum of 1,860 Pa, and reversed the pressure difference across the stopping (regulator G) from -150 Pa to 450 Pa, causing part of the pressurized gas to migrate from the chamber into the gob. This flow reversal was sustained as long as the gas injection rate was kept constant. When the gas injection was stopped, the pressure in the chamber returned to its initial level. Figure 11 shows the pressure differences between the chamber and the gob for the two conditions, without and with gas injection into the chamber. Based on these results it was concluded that the pressure chamber can be used to stop the gas flow from the gob into the face.

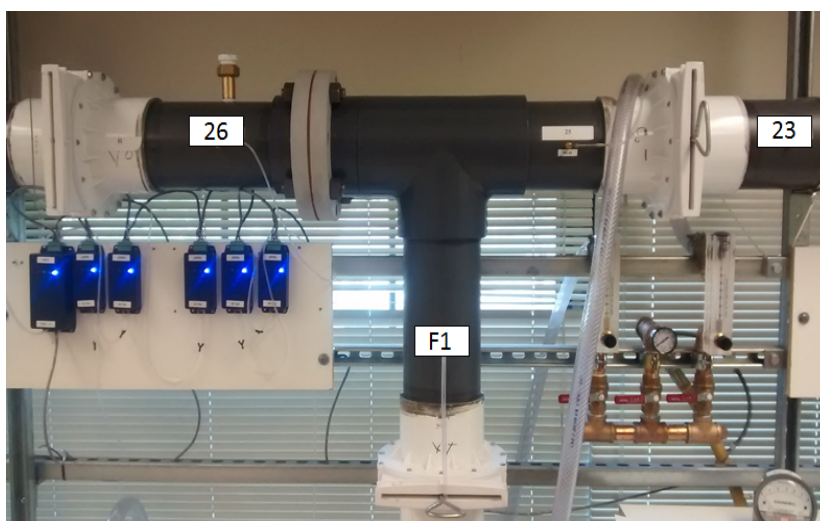


Fig. 10. Automated pressure transducers for monitoring pressure at the chamber and gob.

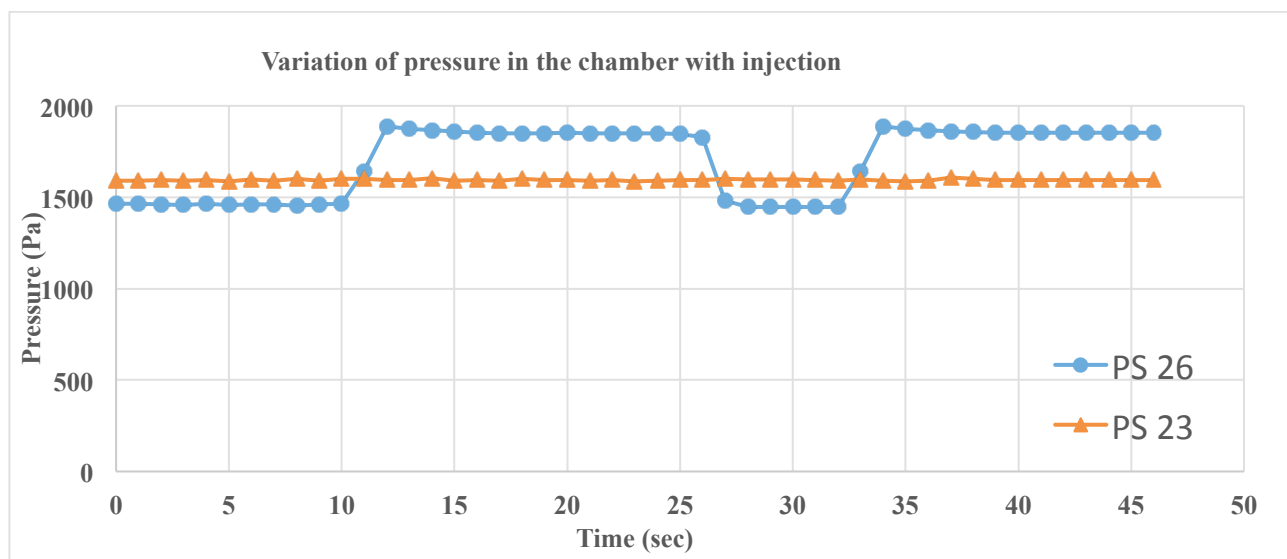


Fig. 11. Pressure build-up and decay in the chamber with changes in gas injection rate

5. Conclusions

Pressure balancing is an effective technique to control spontaneous combustion in underground coal mines. There are two types: passive and active. Passive pressure balancing is used when large pressure differences across the gob are expected. It is desirable because it does not require any external pressure source. Active pressure balancing requires an external pressure source. It can be used where passive pressure balancing is not effective.

The University of Utah's ventilation laboratory model was upgraded to include a longwall section, a pressure chamber, and a bleeder ventilation system. Three experimental conditions were set up in this model, two to investigate the effects of passive pressure balancing on the flow distribution in the gob, and one for active pressure balancing.

When a longwall gob is ventilated by bleeder entries, the wrap-around system is more effective in controlling the pressure differential across the gob than the punch-out system. The results of experiment 1 demonstrated this fact.

A pressure chamber together with two flow control pipes connecting the chamber to the main intake or return airways can be used to minimize the pressure difference across the gob. Experiment 2 showed that when the intake pipe flow control valve was opened, the pressure difference across the gob dropped from 545 Pa to 55 Pa, thus reducing the ingress of air to the simulated gob.

In experiment 3, a pressure chamber was created near the gob by isolating a crosscut using three gate valves, two that were fully closed and one that had a pinhole to simulate leakage path. The fan was operated at 1,790 Pa and the CO₂ gas injected to the chamber at fixed rate (10 L/min). This action allowed the pressure build-up in the chamber. Once the targeted pressure was reached, the gas control valve was switched off and the chamber depressurized. This experiment demonstrated that an external, automated CO₂ injection system could be used to pressurize the chamber and control gas flow into the gob.

Disclosure

This study was sponsored by the Alpha Foundation for the Improvement of Mine Safety and Health, Inc. (ALPHA FOUNDATION). The views, opinions and recommendations expressed herein are solely those of the authors and do not imply any endorsement by the ALPHA FOUNDATION, its Directors and staff.

References

- [1] S.C. Banerjee 2000. Prevention and Combating Mine Fires. Rotterdam: A. A Balkema.
- [2] A.C Smith., W.P Rumancik., and C.P Lazzara. SPONCOM, A computer program for the underground mines. In Proceeding of 5th Conference of use of computer in coal industry 1996. Morgantown, WV, January 1996
- [3] S.K Ray, and R.P Singh, 2007. Recent Development and Practices to Control Fire in Underground Coal Mines. Fire Technology, 43, 285-300, 2007.
- [4] D.R Chalmers, 2008. Sealing Design. In Proceedings of 12th U.S. North American Mine Ventilation Symposium 2008. Reno, NV, June 2008.
- [5] Brady, J.P., Burra, S., and Calderwood, B.R., 2008. The positive pressure chamber. In Proceedings of 12th U.S. North American Mine Ventilation Symposium, Reno, NV, June 2008.
- [6] S.K Ray., L. K Bandopadhyay., N. Sahay., R.P Singh., I Ahmad., and B.C Bhowmick. Microprocessor based dynamic pressure neutralizing system for control of fire in sealed off area in underground mines. Journal of Scientific and Industrial Research. Vol 63, page 297-304. March 2004.

Fire Behavior Analysis of a Mine Future Plan

Ali Haghghat¹, Stewart Gillies²

¹Virginia Tech, Blacksburg, Virginia, USA

²Missouri University of Science and Technology, Rolla, Missouri, USA

No underground peril has the greater potential for the large loss of life than a mine fire or explosion. A study was carried out at the Missouri University of Science and Technology MS&T Experimental Mine to better understand fire behavior in unpredictable incidents. MS&T Experimental Mine is a limestone underground mine. Ventsim Visual software modeling was used to investigate fire behavior through airways of the mine ventilation network planned for the future. Both naturally and mechanically induced ventilation pressures were taken into account. Within different parts of the mine two different scenarios were determined. In all scenarios examined the fire source was a burning Bobcat vehicle. The effect of usage of two different kinds of tires were investigated in all scenarios. Numerous parameters such as levels of CO, CO₂ and psychrometric behavior, visibility and airflow direction were investigated during the study time. Four stations were chosen as the target points to monitor predetermined factors. Various options were considered to confine the fire in a part of the mine. The effect of tires on fire intensity was considered as one of the most important factors for fire control. High risk parts of the mine were identified. An approach to control the fire at different time increments focusing on selected key parameters of lowest levels of toxic gases and dry bulb temperature and high visibility was adopted. Procedures to control fires in two main sections of the mine from external to excavations were proposed. This study has been undertaken to show that the development of an emergency plan ahead of any incident is vital in fire events for all mines.

Keywords: Fire Analysis, Ventism, Visibility, Psychrometric Behavior, Species

1. Introduction

The smoke and gases produced by a fire in a confined space may quickly create a lethal atmosphere for underground workers exposed to the event. For this reason there is a need to predict the effects of underground fires and utilize the results to establish emergency response procedures and systems to ensure the safety of people working underground (Ventsim manual). A study has been carried out to simulate a fire event in the MS&T Experimental Mine future layout using Ventsim Visual software in order to investigate produced noxious gases and select the fastest and safest design to mitigate the percentage of hazard in the mine. Heat simulation and dynamic simulation have been calibrated for fire simulation commencement. All psychrometric data has been put in to the simulator according to the latest field survey. Two scenarios have been considered to investigate numerous parameters such as CO, CO₂, airflow, and dry bulb temperature at stations. Four different stations have been determined as the target points to monitor fire behavior. Four hours was set as the simulation time for all scenarios. Fire events in all scenarios have been set to 20% diesel and 80% rubber in four main steps. Natural and mechanical ventilation pressures have been considered in all scenarios. The direction of airflow has been investigated in each scenario.

Surface fan operation has been controlled according to the least amount of hazard accomplishment. After three minutes of fire event both booster fans was turned off. Various options have been considered to reduce the amount of dangerous gases at monitored stations in all scenarios. Tire selection has been considered in all simulations. Confining the fire in a limited area and the lowest monitored amount of CO, CO₂, and dry bulb temperature at determined stations and high amount of O₂ in safe areas of the mine have been determined as the key criteria amongst all scenarios for selecting the optimal scheme in emergency situations. The ideal long distance control of fire for mitigation of hazards,

temperature and toxic gases has been selected as the most advantageous plan in each scenario.

2. Scenarios specification

The main problem with many mines today is that they are complex often with multiple shafts, ramps and drifts making it difficult to control the way the smoke and heat spread in the instance of a fire. Ventsim Visual program was used to investigate fire behavior in monitored stations of the mine.

VentFIRE in Ventsim Visual program uses a discrete sub-cell transport and node mixing method to simulate moving parcels of heat and gas around a mine. To dynamically model mine ventilation and accurately take into account continual changes in atmospheric concentrations of gases and heat including recirculation, VentFIRE breaks the model into small independent 'cells' which move freely around a model, mixing with other cells at junctions. Heat transfer to and from each cell from rock strata is calculated by the radial heat transfer method, but with strata heat transfer modified by the assumption of exposed rock boundary temperatures at a long term aged average, coupled with a very short time Gibson's algorithm constant to accelerate heat transfer to and from the immediate rock boundaries during the fire simulation as described in Ventsim Manual [9].

Risk analysis may be done in many different ways both qualitatively and quantitatively [5]. To be effective, addressing risk at mines or industry-wide requires such a targeted and systematic approach that is capable of solving the problems permanently, thereby precluding a potential reoccurrence of them [4].

Fire simulations have been designed according to the designed air simulation of experimental mine future ventilation network. In all scenarios main surface fans have been set to the pull system. Heat and dynamic simulation as prerequisite of fire simulation have been designed appropriately. Dynamic increment has been set

to 0.5 seconds for all simulations. Both natural and mechanical induced ventilation pressures have been taken into account in all scenarios.

Two different scenarios were considered to investigate airflow behavior and numerous characteristics in predetermined parts of the mine. Rock type has been set to limestone in all scenarios with 1.3 W/m °C thermal conductivity, 1.2 m/s 10⁻⁶ Thermal diffusivity, 840 j/kg °C Specific heat and 1.290 kg/m³ as density. In all simulations, 25° C was assigned to the rock temperature. According to the latest pressure and quantity survey, 18.5° C and 22° C were put in the simulation for surface wet bulb and dry bulb temperatures. The amount of 20% diesel and 80% rubber were put into the program as the fuel type for burning. Four main events with different start and end time periods and initial and ending burning rates have been set as the dynamic events for the creation of the fire simulation. Dynamic event data for the design of a Bobcat burning is shown in Table 1. The smoothing factor for the simulation result has been set to 500. Four monitors as shown in Figure 1, were established to investigate different airflow parameters at those stations. For all scenarios, the amounts of CO₂, CO, and O₂, psychrometric properties, visibility, and airflow were monitored at the four predetermined stations. Numerous procedures have been investigated to control produced fire at selected working face. An optimum way was proposed to reduce hazards in perilous situations at three main spots of the mine. In all scenarios the threshold limit values (TLV) for CO and CO₂ were considered 25 ppm and 0.5% respectively.

Table 1. Bob cat with EarthForce™ compact tires burning event information through 4 hours.

Events	Time Range (sec)		Burn Rate (Kg/hour)	
	Start	End	Initial	Final
Name starts	0	1800	0	200
escalates	1800	3600	200	480
maximum	3600	13800	480	480
ends	13800	14400	480	0

Twenty percent diesel and eighty percent rubber have been assigned to be burnt. During the first 30 minutes, 2500 kW energy has been produced by burning of that fuel. The second step of the fire event is when it escalates. The period of this step was set to 1 hour. The amount of energy has increased to 6000 kW. During the third step of the fire event (fire maximum) 6000 kW has been produced by the fire. The period of this step was set to two hours and fifty minutes. During the fire termination step, 6000 kW has reduced to zero in the last 10 minutes.

The intensity of a fire or heat release rate is largely determined by the rate at which oxygen can reach the fire and the surface area and type of fuel available for burning. Within certain limits, if more oxygen reaches the fire, the intensity of the fire increases and vice versa [2].

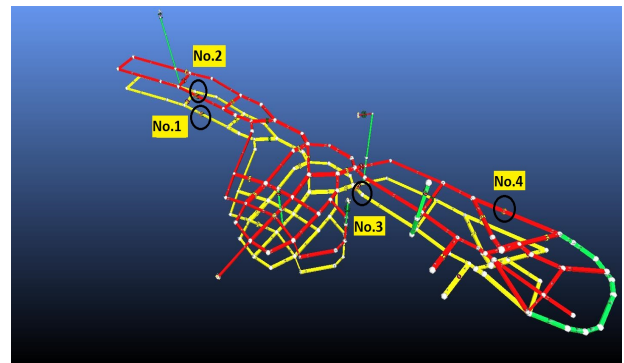


Figure 1. Monitors position through airways.

3. Tire specifications in the mine

The Bobcats in MS&T Experimental Mine have been using two different types of solid tires. All Scenarios have been simulated according to the EarthForce™ solid press-on tire. The use of standard duty pneumatic tires were compared to the EarthForce™ solid tires too.

3.1 EarthForce™ solid press-on tires

These kinds of tires with their sidewalls are designed to prevent cuts and cracks in aggressive terrain. They are made of heavy duty rubber compounds for increased service life and have advantages as following:

- Deep lug treads provide traction in an assortment of terrains
- Great shock absorption for machine longevity and operator comfort
- Super smooth tires also feature air-cushioned design

The use of this tire in the Experimental Mine is shown in Figure 2.



Figure 2. EarthForce™ solid press-on tire.

By the use of this kind of tire, the money spent due to flat tires has been eliminated and the longer tire life time has been achieved. Specification of this kind of tire has been shown in Table 2.

Table 2. EarthForce™ solid press-on tire specifications in experimental mine.

Model	EarthForce™
Style	Dirt Terrain with Rim
Outside Dia. (mm)	838
Tire Width (mm)	305
Rim Dia. (mm)	406
Tread Depth (mm)	51
Weight (kg)	113

3.2 Standard duty pneumatic tires

These tires are created for long wear during normal machine-hour applications. The use of this tire in the Experimental Mine is shown in Figure 3.

The special rim guard and thick sidewalls provide protection against punctures. They're constructed with natural and synthetic rubber. Specification of Standard Duty Tires is shown in Table 3.



Figure 3. Standard Duty pneumatic tires.

Table 3. Standard Duty pneumatic tire specifications.

Model	Skid-Steer Loader
Style	Standard
Outside Dia. (mm)	787
Tire Width (mm)	254
Rim Dia. (mm)	419
Tread Depth (mm)	14
Weight (kg)	36

As Thyer in 2002 [8] explained, the key principles of fire management in an underground mine are as following

- Prevention of the fire commencement by the usage of appropriate suppression materials or systems
- Early detection of fire and provision of effective system to isolate/reduce the impact of fire.
- Providing warning for persons underground and applying the effective egress and refuge systems

The identification of potential fire locations and fire types and the associated consequences are the main focus of every fire study. In order to do this a hazard analysis is necessary. To conduct fire modeling, it is necessary to evaluate the risk of a fire in the mine and its consequence [6]. According to the conducted hazard analysis study, two main locations have been selected for fire analysis in the MS&T Experimental Mine.

4. Scenarios

4.1 Scenario 1, fire at the west working face (down level).

Fires rarely start in shafts, because these are generally damp or wet. In slopes or drift entrances fire are as likely to occur as in any mine passage or level [7].

In this scenario, fire has been set at the west working face on the lower level. The pull system of surface fans has been considered to investigate the behavior of fire and different characteristics through the airways in four hours real time. The fire event has been set to act as shown in Table 1. EarthForce™ solid tires have been used in the Bobcat burning simulation. Six minutes after fire event commencement, the east surface fan has been set off. Three minutes after initiation of the fire event, booster fans in lower and upper levels have been turned off. Two blocked raises at the center and the east part of the network and two closed adits at the east panel of the experimental mine, as shown in Figure 4, have been opened after ten minutes in simulation. The west portal was closed 10 minutes after the fire started. All of the times for this scenario were selected according to the distance and the action of the mine's work force. The distribution of noxious gases through the airways after 1 hour is shown in Figure 5.

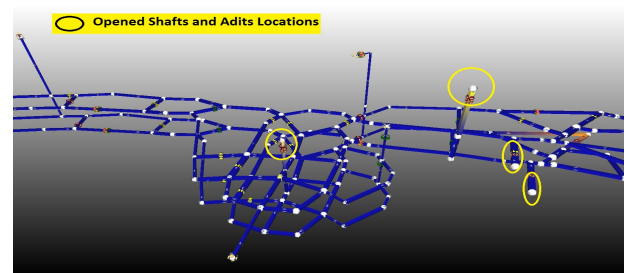


Figure 4. Opened adits and shafts 10 minutes after fire starts.

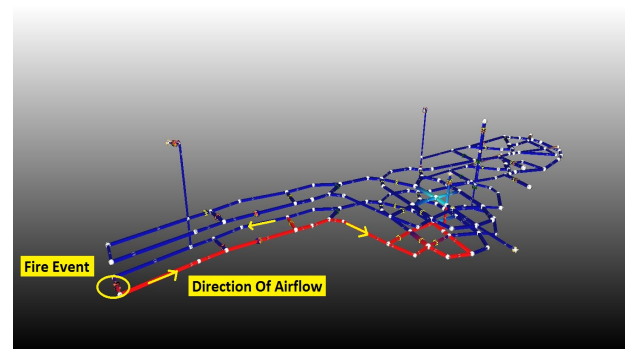


Figure 5. Fire distribution, 1 hour after fire initiation (pull system).

The slope of the tunnel, combined with its reduced height, causes a predominant propagation of the smoke in the ascending direction. Thus, the exhaust openings placed in the descending direction with respect to the fire location do not aspirate smoke, but clean air. In the case of an emergency, the individual operation of the exhaust openings should be allowed. Also, their number should be increased, in order to open more exhaust openings located in the ascending direction from the fire location [1].

4.1.1 Airflow and O₂ behavior at monitored stations

Fires produce large amounts of very hot, very low-density gas. This results in four main effects on the ventilation system as following [3]:

- Throttling or choking effect
- Chimney or natural draft or natural ventilation effect
- Flow reversal
- Roll back

Natural ventilation pressure, opened adits, shafts, and fire affected the direction of airflow at all stations. The airflow direction has been changed at station 1 about 1 hour after the fire began. The airflow result at station 1 during the whole burning time is shown in Figure 6.

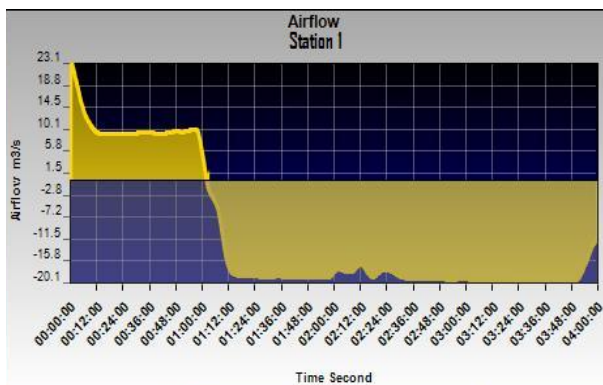


Figure 6. Air flow behavior at station 1.

It is evident from Figure 6 that the maximum amount of airflow at station 1 in the reversed direction was 20.1 m/s. As it can be seen in this figure, the graph exhibits sharp drop during the first 12 minutes when booster fans and east surface fan have been turned off and the adits and raises have been opened completely at 10 minutes and then remained constant up to 1 hour. The airflow has been decreased dramatically at that time because airflow has been reversed and it almost leveled off up to the last 10 minutes. The last drop happened in the last 10 minutes of the fire event. The graph under the zero line is showing the reversed direction of airflow at that station through the time. The airflow decreased near the end of the fire.

Airflow at stations 3 and 4 behaved the same. The least amount of airflow has been recorded at 8.1 m/s at station 4 (furthest monitor to the fire source) in the reversed direction. An airflow diagram at station 4 is plotted in Figure 7. At 10 minutes, the airflow direction at station 4 has been changed and then increased marginally to 8.1 m/s up to the end of 1 hour and almost remained constant up to the end of simulation. The minimum and maximum amount of airflow at station 3 has been recorded as 26.3 and 26.7 m/s.

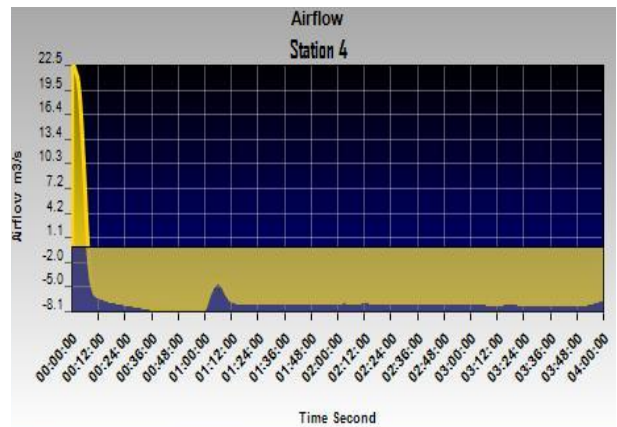


Figure 7. Airflow distribution in 4 hours at station 4.

According to the airflow data at station number 2, it is evident that the airflow graph decreased when the fans were turned off. Then the airflow increased conspicuously, across the period from 10 minutes to 1 hour, to 22.4 m/s. Because of the fire behavior, the direction has been changed again at 1 hour after fire initiation and reached to 5.5 m/s at which it remained constant up to the end of event. The results are illustrated in Figure 8.

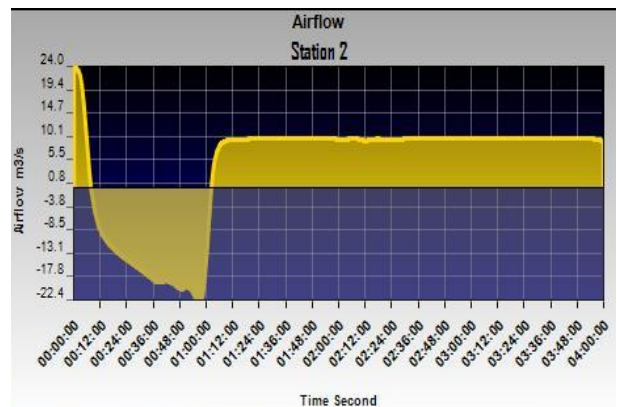


Figure 8. Airflow distribution at station 2.

It is evident from the above figures that natural ventilation pressure, effects of opened adits and shaft and fire effect have had a large effect on the direction of airflow at all part of the mine.

Before the fire event, the amount of O₂ ranges from 21.1% to 21.7% in all scenarios. The least amount of O₂ that has been monitored was 18.8% at the closest station to the fire when the fire has been simulated for 4 hours. The closest station to the fire was station 1. The range of O₂ in all stations is shown in Table 4.

Table 4. Oxygen percentage in all stations through 4 hours.

Station	Min O ₂ %	Max O ₂ %
1	18.8	21.3
2	20.5	21.4
3	21.6	21.7
4	21.0	21.1

4.1.2 CO and CO₂ behavior at stations

At all stations, the amount of CO and CO₂ has been recorded in order to get a better understanding of fire behavior through the airways. At station 1, the amount of CO has increased dramatically and approached 2200 ppm as the peak point after 1 hour and then it remained constant up to the last 10 minutes. The graph exhibits a sharp decrease during fire termination period. The amount of CO at the end of the fire event after 4 hours was approximately 700 ppm.

By briefly glancing at the CO₂ graph from this station, it is evident that the CO₂ is behaving the same as CO behaved in the period of the fire. The highest amount of CO₂ at this station was 1.86 % and at the end of 4 hours this amount has been diminished to 0.220% conspicuously. The highest amount of CO and CO₂ were recorded in this station.

The amount of CO has escalated dramatically in the first 72 minutes of the event at station number 2. The highest concentration during the fire was 1427 ppm and then it decreased sharply to 714 ppm. A direction change has been determined to be the main reason for the great change in the amount of CO between 60 and 72 minutes. After 72 minutes, the amount of CO has decreased sharply to 714 ppm and then almost leveled off until the last 10 minutes. A sharp decrease happened during the last 10 minutes. The amount of CO at the end of 4 hours was 350 ppm. The results are gathered in Figure 9.

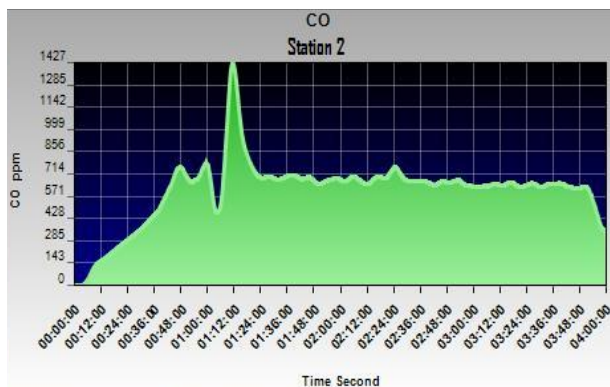


Figure 9. Amount of CO at station 2.

When the CO₂ graph at this station was studied, it was discerned that the behavior of CO₂ was the same as CO at this station. The maximum amount of CO₂ at station 2 was 0.438% as shown in Figure 10.

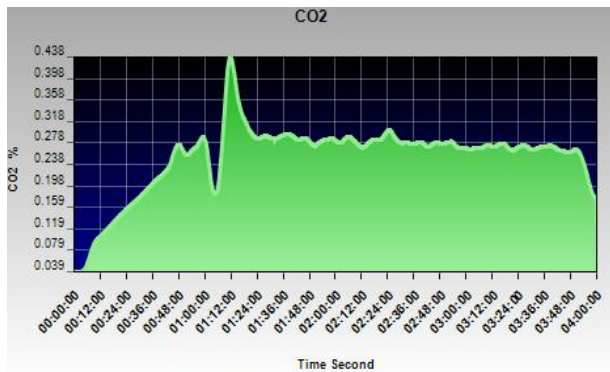


Figure 10. CO₂ behavior at station 2.

It is clear that the furthest station had the least amount of toxic gases compared to the other stations.

Due to its distance, the least amount has been recorded at station 4. The monitored amount of CO and CO₂ at the east part of the mine was not considerable. Stations 3 and 4 have been determined to be the safest place amongst all determined stations in this scenario. At these stations, the amount of CO and CO₂ has been kept less than TLV. As has been seen at the previous stations, the graph behavior of CO and CO₂ were the same as each other at both 3 and 4 stations. The result of CO and CO₂ at stations 3 and 4 are shown in Table 5.

Table 5. CO and CO₂ results at stations 3 and 4.

Station	3	4
Min CO (ppm)	0	0
Max CO (ppm)	7	4
Min CO ₂ %	0.039	0.038
Max CO ₂ %	0.063	0.054

4.1.3 Psychrometric behavior at stations

In this study, all dry and wet bulb temperatures and the rock temperature have been investigated at all stations. The highest temperature was recorded at station 1. The temperature changes during the 4 hour fire event at stations 3 and 4 were not considerable. During the first hour, the dry bulb temperature graph remained at its lowest amount. During the next 12 minutes, the temperature reached its highest point at 201 °C at station 1. Then it decreased to 183.4 °C and it plateaued until the last 10 minutes of the simulation. During the last 10 minutes, the graph has decreased noticeably to 78 °C at the end of the 4 hour simulation. The result of dry bulb temperature at station 1 is plotted in Figure 11. The wet bulb temperature behaved the same as the dry bulb temperature. The minimum and maximum wet bulb temperatures were 19.8 °C and 52.7 °C.

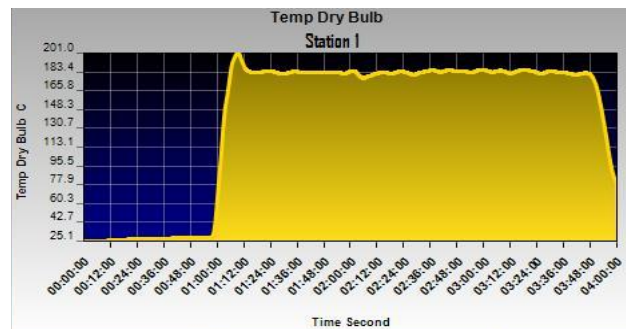


Figure 11. Dry bulb temperature graph at station 1 in 4 hours fire event.

The rock temperature continued to increase from the beginning of the fire event until the end. The highest rock temperature amongst all of the stations was 67.4 °C at station 1. The result of rock temperature at station 1 has been shown in Figure 12.

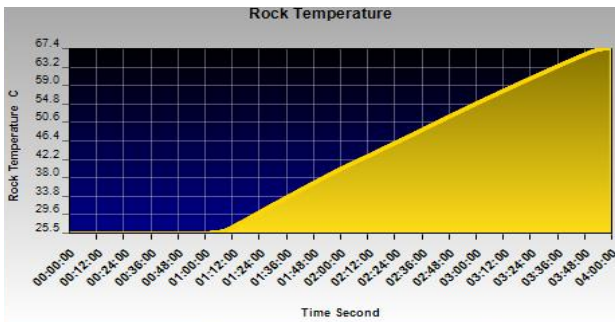


Figure 12. Rock temperature changes at station 1.

The range of psychrometric behavior at the other stations has been recorded and is illustrated in Table 6.

Table 6. Various temperature result at stations 2, 3 and 4.

Station	2	3	4
Min DB Temp °C	24.8	25.1	24.5
Max DB Temp °C	77.2	28.8	26.1
Min WB Temp °C	19.6	19.9	19.6
Max WB Temp °C	34.8	20.0	20.6
Min Rock Temp °C	25.1	21.5	24.6
Max Rock Temp °C	28.4	25.2	24.6

It is evident from Table 6 that the fire has not had a significant impact on temperature changes at the eastern part of the mine.

4.1.4 Visibility at stations

With the exception of stations 1 and 2, all of the stations' visibility have not been affected by the fire. This was evident from the fact that the eastern part of the mine was devoid of smoke. Visibility at station 1 decreased from 25 m to 0.1 m during the first hour and then it remained the same until the last 10 minutes. During the final step of the fire, the visibility at that station increased to 2.6 m. The visibility graph is plotted in Figure 13.

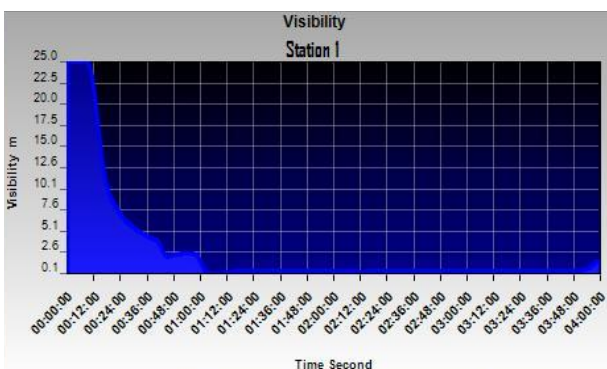


Figure 13. Visibility graph at station 1.

The visibility graph at station 2 was recorded the same as it was at station 1. The visibility was 25 m before the fire event and it decreased spectacularly to 0.6 m where it remained constant until the last 10 minutes. Visibility increased to 3 m during the fire termination step.

In summary, it is noteworthy that the fire was controlled in the western part of the mine by opening the specified adits and shafts. By this action, half of the mine was saved from noxious gases. The other options were examined in order to get the safest atmosphere throughout the mine. It is not recommended to turn all of the fans off. The amount of toxic gases were too high when all of the fans were turned off. The following procedure was determined as the best approach to diminish the hazard level in emergency situations at that working face:

- (a) East surface fan has been turned off.
- (b) Booster fans in lower and upper levels have been turned off.
- (c) The two blocked raises at the center and eastern parts of the network and the two closed adits at the eastern panel have been opened.
- (d) West portal has been closed.

This approach has been determined as the optimum reaction to decrease the hazards of the fire at the bottom west panel in an emergency situation.

By changing the EarthForce™ compact tires to standard duty pneumatic tires in the simulation, the amount of burning has decreased and also hazards have decreased respectively. The results are shown in Tables 7 and 8.

Table 7. Average CO according to 2 different tires at all stations.

Tire Type	EarthForce™	Standard Duty
Property	Average CO (ppm)	Average CO (ppm)
Station 1	1100	308
Station 2	350	174
Station 3	3.5	1
Station 4	2	0.5

Table 8. Average DB temperature according to 2 different tires at all stations.

Tire Type	EarthForce™	Standard Duty
Property	Average DB Temp °C	Average DB Temp °C
Station 1	113	48
Station 2	51	40
Station 3	27	25.7
Station 4	25.3	24.6

4.2 Scenario 2, fire at the east working face

The fire has been set at the ramp on the east part of the mine. Surface fans pulling air have been considered in this investigation of fire behavior and different characteristics through the airways for, four hours real time. Six minutes after fire event commencement, the west surface fan has been turned off while the east surface fan has not. Booster fans on the surface and lower levels were not deactivated during the whole time of the fire event. Both of shafts at the central part of the network have been opened 10 minutes into the fire event. The east adit, drainage adit, and shaft have been opened 10 minutes after the fire initiation time too. All times for this scenario have been selected according to the distance and reaction of the mine's staff. The

distribution of fire and the determined adits and shafts for the pull system of the surface fans through the airways is shown in Figure 14.

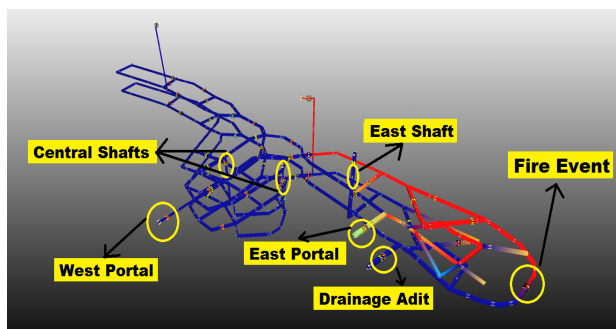


Figure 14. Fire distribution and effective mine's component on airflow direction.

4.2.1 Airflow and O₂ behavior at stations

Because of the east surface fan and two booster fans' pressure, natural ventilation pressure has not influenced airflow direction at any of stations. The maximum airflow changes in the period of the fire event were monitored at station 3. The airflow results during the four hours at station 3 are shown in Figure 15. The amount of airflow through the west part of the mine decreased by turning the west surface fan off. The amount of airflow at the east part of the mine increased noticeably and then it remained constant. The maximum amount of airflow at station 3 was 40.5 m/s. The amount of airflow was constant from 15 minutes until the end step of the fire event.

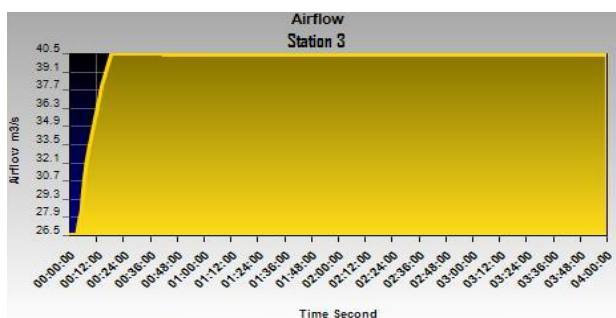


Figure 15. Airflow distribution at station 3.

The direction of airflow at stations 1 and 2 was not changed. During the first 6 minutes, the amount of airflow decreased to 20.0 m/s and then started to increase sharply to 21.7 m/s in the first 15 minutes and then it leveled off until the end of event. It is evident from airflow diagrams at all stations that the behavior of airflow at the two stations in the west part of the mine and two stations in the east part of the mine are the same.

Before the fire event, the amount of O₂ ranged from 21.1% - 21.6% in all scenarios. The highest change was 1% at station 4. The percentage of O₂ at the other stations did not change considerably. The ranges of O₂ from all stations are shown in Table 9. The amount of O₂ decreased conspicuously at the closest station to the fire, however the TLV was not reached, as illustrated in Figure 16.

Table 9. Oxygen percentage at all stations.

Stations	Min O ₂ %	Max O ₂ %
Station 1	20,9	21,3
Station 2	21	21,4
Station 3	21,1	21,6
Station 4	20,1	21,1

When the west surface fan was turned off, the amount of airflow decreased. The level of O₂ did not go below the O₂ TLV.

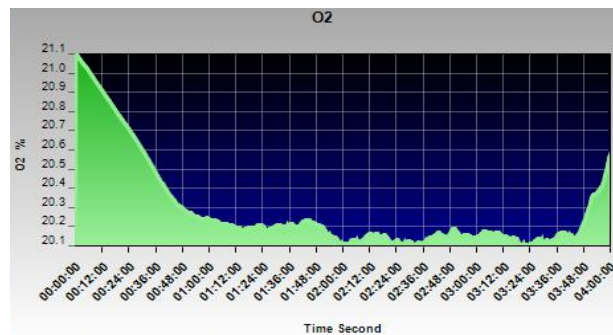


Figure 16. O₂ percentage at station 4 during the fire event.

The direction of airflow changed when all of the fans were turned off. The direction of airflow when the fans have been turned off is plotted in Figure 17.

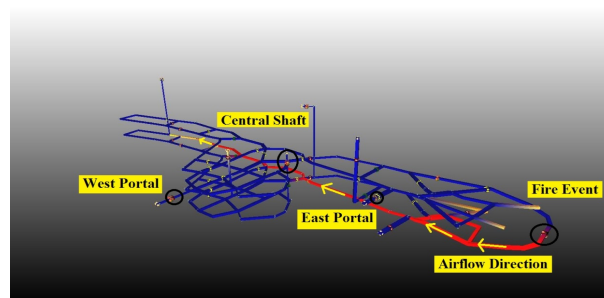


Figure 17. Direction of airflow when all fans are off.

4.2.2 CO and CO₂ behavior at stations in scenario 2

At all of the stations, the amount of CO and CO₂ was recorded in order to determine the toxic atmosphere and fire behavior through the airways. At station 4, the amount of CO increased to 809 ppm dramatically when the west surface fan was turned off. The graph reached the highest point at 2 hours and then remained almost constant until the last 10 minutes, at which point the concentration dropped to 490 ppm. If all of the surface and booster fans would be turned off, the amount of CO would be increased in the mine and also the direction of fire would be changed. The monitored result for CO at station 4 is shown in Figure 18. The highest amount of CO was recorded at station 4. When the amount of CO is high at station 4, the amount of CO at the other parts of the mine were zero.

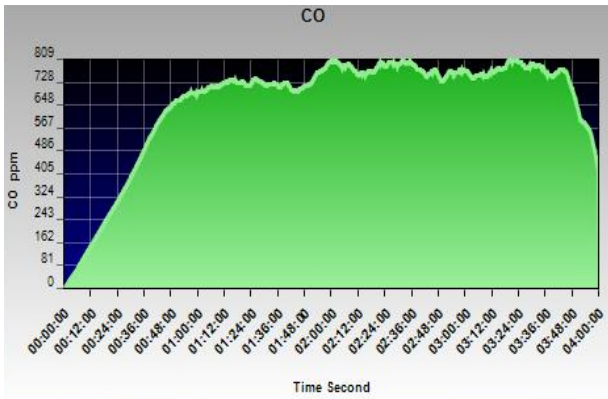


Figure 18. CO distribution at station 4.

By this action the fire was controlled at the east part of the mine without any hazardous effect on the other parts of the mine.

If we take a closer look at CO₂ graphs from all of the stations it is evident that CO₂ is behaving as CO behaved in the period of the fire event. The highest amount of CO₂ was 0.36 % at station 4. The highest amount of CO and CO₂ were at that station. The results of CO and CO₂ at stations are shown in Table 10.

Table 10. CO and CO₂ results at all stations.

Station	1	2	3	4
Min CO (ppm)	0	0	0	0
Max CO (ppm)	1	1	1	809
Min CO ₂ %	0.038	0.038	0.039	0.038
Max CO ₂ %	0.039	0.039	0.04	0.359

Consistent with the data in Table 10, it is seen that the TLV for CO₂ and CO at the central and eastern part of the mine has not been reached. Hence those parts of the mine were selected as the safe parts in an emergency situation. The result of CO₂ at station 4 is shown in Figure 19.

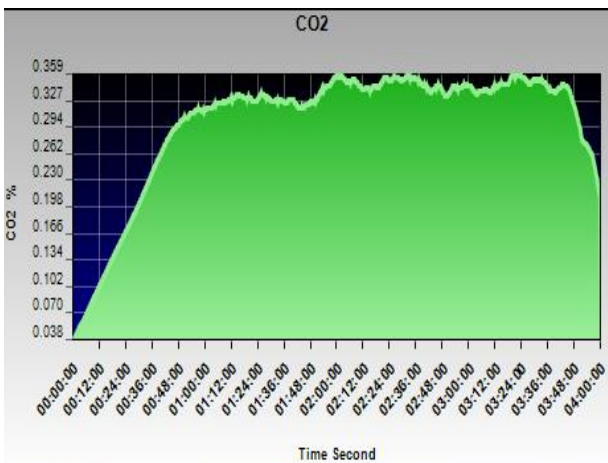


Figure 19. CO₂ distribution at station 4.

When all of the fans were turned off, the amount of CO at station 4, increased dramatically. The approximate amount of CO at that station had reached 2750 ppm. The amount of CO at the other stations was inconsequential. The average amount of CO and CO₂ at station 4, is shown in Table 11.

Table 11. CO and CO₂ amount at station 4, when all fans are off.

Station	4
Average DB °C	120
Visibility (m)	0.3
Average CO ₂ (%)	1.2
Average CO (ppm)	2750

4.2.3 Psychrometric behavior at stations

In this study, all dry and wet bulb temperatures and rock temperature were investigated at all stations. Obviously, the highest temperature was monitored at station 4. Temperature changes during the 4 hour fire event at other stations were not considerable. After 2 hours, the dry bulb temperature reached its peak point at 112.3° C at station 4 and then it remained constant during the next 1 hour and 50 minutes. The graph is exhibiting a sharp decrease in the last 12 minutes of the fire event. The dry bulb temperatures at station 4 are shown in Figure 20.

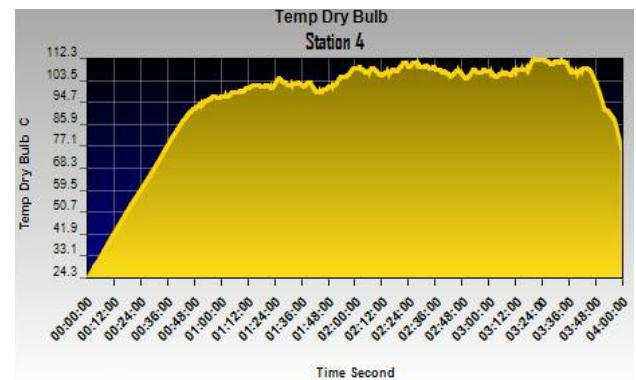


Figure 20. Dry bulb temperature at station 4.

The wet and dry bulb temperatures behaved the same at all stations, just as they did in previous scenarios. The minimum and maximum wet bulb temperatures at station 4 were 19.9° and 39.8° C. The highest rock temperature amongst all stations was 38.5° C at that station. The rock temperature at station 4 is illustrated in Figure 21. The rock temperature increased dramatically up to the termination time of the simulation.

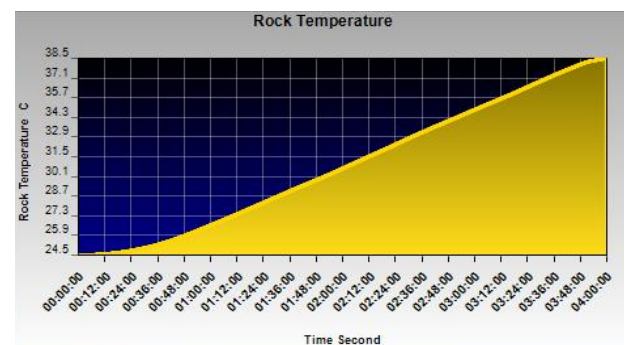


Figure 21. Rock temperature behavior at station 4.

The dry and wet bulb temperatures did not experience any important changes at stations 1, 2, or 3.

The fire did not have any impression on the rock temperature at those stations either. The changes in temperature at other stations are illustrated in Table 12.

Table 12. Various monitored temperatures at stations 1, 2 and 3.

Station	1	2	3
Min DB °C	25.2	24.8	24.8
Max DB °C	25.4	25	24.9
Min WB °C	19.9	19.6	19.9
Max WB °C	20	19.7	20.1
Min Rock °C	25.4	25.0	24.8
Max Rock °C	25.4	25.1	25.1

From Table 12 data it can be seen that the fire has not changed temperatures at those stations significantly.

4.2.4 Visibility at stations

With the exception of station 4, none of the stations' visibility were affected by the fire. Visibility at station 4 decreased from 25 m to 1 m during the first 30 minutes and then it remained the same until the last 10 minutes. During the final step of the fire, the visibility at that station increased to 3.4 m. The visibility graph is plotted in Figure 22.

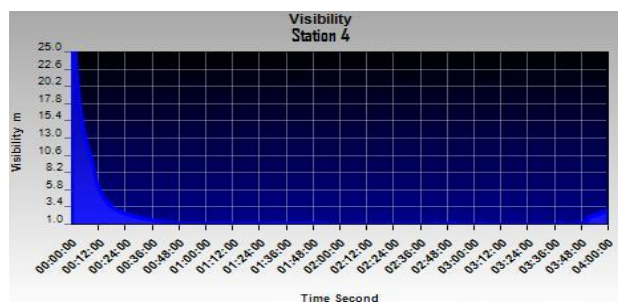


Figure 22. Visibility graph at station 4.

The amount of burning and hazards were decreased respectively by the change of EarthForce™ compact solid tires to standard duty pneumatic tires in simulation. Results. The average CO was monitored 400 ppm at station 4 when EarthForce™ tire was used while with the usage of Standard Duty tire, CO decreased to 170 ppm. Besides, the DB temperature at station 4 decreased from 68.3°C to 45.2°C when the Standard Duty was used.

All in all, the fire was controlled by turning the west surface fan on. Although by this action east and central parts of the mine have been saved from noxious gases, the effect of opened adits and shafts and also fan management in emergency situations cannot be ignored. The other options, like opening closed shafts and adits, or turning the east surface fan off, have been examined in order to get the safest atmosphere through the mine. If all of the fans have been turned off, the direction of fire does not change and the amount of toxic gases and temperature increase considerably in all parts of the mine. The following procedure should be considered for mitigation of hazards when the fire happens at the decline in an emergency situation:

- (a) West surface fan should be off.
- (b) East surface fan and booster fans should be turned on.
- (c) All adits and shafts should be opened.

5. Conclusion

It is noteworthy that distance and airflow direction have played key roles in the amount of CO and CO₂ and temperature changes. Unfortunately, the anticipation of a fire before the event is extremely difficult, not only the location (which to some degree may be predicted using risk assessment techniques on possible combustible sources), but also to the nature, size and behavior of the fire. This study was carried out for better understanding of airflow behavior and fire behavior when a Bobcat vehicle began burning at working faces. The highest amount of toxic CO gas was 3000 ppm at the closest station to the fire when all fans have been turned off.

The west working face at the bottom level was determined as the most perilous part of the mine for executing more safety issues. It is very hard to control the fire when it happens at that part of the mine. By turning all of the fans off, noxious gases have been trapped in the mine. So turning all of the surface and booster fans off wasn't selected as the ideal approach to control the fire. The highest temperature was 200° C at station 1 in scenario 1. CO and CO₂ behaved the same as one another at every station. Numerous applications (such as closing or opening different doors and shafts and turning on or off of different fans) were investigated to discern the optimum procedure for controlling the fire.

However, the best approach was achieved in each scenario by the proposed procedures. This study has shown that tires of vehicles are one of the most important factors in a fire event. Despite this fact, the least consideration has been employed for choosing the tires of vehicles in the mines. The lifetime of tires always pulled the focus of purchasers in industry while burning hazards were neglected. Standard duty pneumatic tires were selected as the Experimental Mine Bobcats' tires for working in underground. The reversed direction of surface fans was considered in this study while in real mines it is very hard to employ this application. In addition, mismanagement and lack of emergency layout in emergency situations can lead to malignant consequences for a mine. This study was carried out to show that the emergency plans for fire events ahead of any emergency are needed for every mine and also underground fires which have been initiated by mobile equipment are still relatively common and likely to be underestimated.

Acknowledgment

This paper was prepared with support from the National Institute of Occupational Health and Safety.

References

- [1] Ballesteros-Tajadura, R., Santolaria-Morros, C., Blanco-Marigorta, E. Influence of the slope in the ventilation semi-transversal system of an urban tunnel, Universidad de Oviedo, A ´ rea de Mecanica de Fluidos, Spain.
- [2] Tunnelling and Underground Space Technology 21 (2006) 21–28R. Anderl et al., Hydrogen isotope retention in beryllium for tokamak plasma-facing applications, Journal of Nuclear Materials 273 (1) (1999) 1-26.

- [3] Brake, D. J., Fire Modelling in Underground Mines using Ventsim Visual VentFIRE Software, Australian Mine Ventilation Conference / Adelaide, SA, Australia, (2013).
- [4] Gillies, A. D. S, Wu, H, Reece, D and Hosking, R., Use of Mine Fire Simulation for Emergency Preparedness, Proceedings Qld Mining Industry Health and Safety Conference (2004), pp 13-20 (Qld Resources Council).
- [5] Grayson, T. L., Kinilakodi, H., Kecojevic, V., Pilot sample risk analysis for underground coal mine fires and explosions using MSHA citation data” Safety Science 47 (2009) 1371–1378.
- [6] Joy, J., Griffiths, D., National Industry Safety and Health Risk Assessment Guideline, Version No. 7, Minerals Industry Safety and Health Centre (MISHC), University of Queensland, Australia, p. 157 (2007).
- [7] Prosser, B., Ruckman, R. Conducting a fire modeling study, 13th United States/North American Mine Ventilation Symposium, (2010) – Hardcastle & McKinnon 365–370.
- [8] Rice, S. George, Mine fires: a preliminary study. Dept of Interior, Bureau of mines. (1912).
- [9] Thyer, A., Development of a fire and explosion risk assessment methodology for underground mines [online], Science Group (Fire and Explosion), Health and Safety Laboratory. Report HSL, (2002). 24. 61 pp.
- [10] Ventsim Visual™ 3, 2014, Ventsim Visual Tm User Guide, Ventsim Company.

Underground Fire Rollback Simulation in Large Scale Ventilation Models

Craig M Stewart^{a,b}, Saïed M. Aminossadati^a, Mehmet S. Kizil^b

^aThe University of Queensland, Brisbane, Australia

^bChasm Consulting, Brisbane Australia

Fire in an underground mine poses a serious threat to health and safety of personnel due to the spread of heat, smoke and noxious gases throughout the ventilation system. Predicting the behavior and likely spread of combustion products is important in understanding the potential risk to personnel and assists in developing suitable emergency response plans.

One aspect of fire effects on ventilation that is difficult to predict is a phenomenon known as rollback. Fire rollback causes hot combustion products (smoke and gas) to move along the roof of tunnels in the opposite direction to primary ventilation flow, potentially circulating combustion products into areas upstream from the fire source.

Modelling of fire rollback behavior has been achieved with computational fluid dynamics (CFD) methods, however CFD is not currently practical for mine wide simulation due to model size and speed constraints. Empirical prediction that considers airway size, slope, and air velocity can also be used but it is not ideal for automatic integration into large scale ventilation models.

A feasible solution is to create a single network model to simulate both the large scale ventilation model and the smaller scale rollback behavior. This can potentially be achieved by creating a detailed high density three-dimensional mesh of pathways bounded by the airway around a fire which then feeds into the simpler network of a large scale ventilation model. The high density mesh allows a transient mass balanced Hardy Cross method to simulate air currents independently in three dimensions within the fire region, based on heat and natural buoyancy within each pathway. This paper explores the method, compares with empirical methods, and demonstrates the potential of full integration into conventional whole mine network analysis simulation without the complexity of CFD analysis or empirical equation assumptions.

Keywords: Fire Simulation, Rollback, CFD

1. Introduction

Mine fires present one of the most serious hazards for underground personnel. Few hazards have such potential for substantial loss of life or damage to property, and the prevention and control of fire is at the foremost of most mine safety management and emergency response plans.

Mine fires generate enormous media scrutiny due to the tragic history of mine disasters and the devastating effects on the surrounding community. Mining history is littered with mine fire incidents and disasters with outcomes varying from massive loss of life to success stories of mine rescue and fire control.

For example, in 2014 an explosion at the Soma coal mine in Turkey caused an underground mine fire resulting in the deaths of 301 people, mostly from carbon monoxide poisoning [1]. In the same year, South Africa's Kusasalethu mine, 486 miners were trapped underground following a fire that occurred about 2.3 km (1.43 miles) underground during maintenance on an air cooler. Fortunately in this case all miners were eventually rescued unharmed [2].

Coal mines, metaliferous mines and civil tunnels are highly exposed to the dangers of mine fires, and while the mechanisms of ignition and resulting fire behavior may differ in some circumstances, the hazards to human life created by heat, smoke and noxious gases are the same.

2. Modelling Fire Behavior

2.1 History

Modelling the behavior of a fire and the spread of noxious gases through a mine has long been recognized as an important tool in assisting with emergency preparedness for mines and tunnels [3]. In particular the ability to predict the spread of smoke and fumes can assist in many aspects of mine fire hazard mitigation and control. For example, mine ventilation designs can be improved to be more resilient to fire outbreak with smoke and fumes directed away from work areas, and the operation of vent controls and fans potentially modified in the event of a fire. Emergency refuge stations and fresh air emergency bases can be located in areas that ensure maximum availability and access to mine personnel. In the event of a fire outbreak, fire modeling software may even assist in the real time understanding the spread of gases and changes in ventilation flows and directions.

Mine ventilation software has rapidly developed since the introduction of digital computers in the 1950s, however the advent of more powerful computers in the 1980s, prompted efforts to develop software specifically to evaluate and understand the behavior of fires in mines, as well as the contamination and spread of fire fumes and smoke throughout mines and tunnels. [4]. Fire modeling software can be broadly divided into two categories.

2.2 Computational Fluid Dynamics Methods

Detailed fire modelling in three dimensions in tunnels is usually attempted by computational fluid

dynamics (CFD) analysis [5]. This approach focuses on the behavior of airflow, heat, smoke and gas fumes in the immediate vicinity of the fire, and works from a finely constructed numerical grid that defines the boundary conditions of the three dimensional environment and the interaction of the air movement to the boundaries and itself. CFD modelling is generally considered for simulation of the area around the immediate fire, but is poorly suited to larger models because of speed and model complexity constraints [6].

The Fire Dynamics Simulator (FDS) is a popular software code in this category, and was released to the public in 2000 by National Institute of Standards and Technology (NIST). It has been used extensively in tunnel fire modeling [5]. An extension to this software is PyroSim™, developed by Thunderhead Engineering Consultants, which adds a graphical user interface to FDS allowing improved integration into CAD software [7].

2.3 Network Analysis Simulation Methods

A flow network consists of a series of nodes or junctions connected by pathways defining the potential movement of airflow. The mesh of connecting pathways between nodes is analyzed by considering the pressure or energy balance between closed loops of connecting nodes, using an iterative solver approach. The fundamentals of many popular modern network solving methods were originally conceived in the mid-1800s with Kirchhoff's Law and further refined in the 1920s for rapid solving of fluid flow networks with the Hardy Cross algorithm.

Unlike CFD, network analysis only considers the possibility of movement of air along one pathway between nodes, and therefore restricts flow to only the one dimension. The natural ventilation pressures along the pathways resulting from heat affected air densities are included in the pressure or energy balance equations to predict the change in airflow volumes and directions from the fire heat.

Contaminants released by the fire are added to airflow volumes and transported through the mine network using transient time based simulation techniques. The behavior and gas released from the fire can be modified during the simulation based on the fuel source and the amount of oxygen available for the fire. The resultant simulation can provide a complete time based spread of heat and contaminants, together with identification and timing of any ventilation direction and flow changes,

Numerous fire simulators have been developed since the 1980s, however examples of software currently in common use includes MFIRE (originally developed by US Bureau of Mines) [4], Ventgraph (developed by the Polish Academy of Sciences [8]) and Ventsim VentFire (developed by Chasm Consulting [9]).

2.4 Rollback Considerations

A significant complication of fire modelling in a confined tunnel is a phenomena called 'rollback'. Rollback occurs when hot gases and vaporized burning fuel from the fire rises to the roof due to heat driven natural ventilation pressures. The combustion products are then forced along the roof and if insufficient forward velocity of ventilation is available, then the gases may

spread in either direction, both upstream and downstream from the fire. The heated rollback gases may continue to propagate further (possibly spreading the fire elsewhere) until they have cooled sufficiently to lose natural ventilation buoyancy and re-enter and mix with the lower airstream. The rollback of combustion products in a Swedish fire tunnel test is shown in Figure 1.



Fig. 1. Rollback occurring in a Swedish fire tunnel test [10].

The spread of rollback products effectively creates a bi-directional flow in the same tunnel and may inundate firefighting or mine rescues crews approaching from the upstream direction placing them in potential danger. In addition, the rollback may push back into other intersections that would normally be predicted to be in fresh air in a one dimensional simulation.

Researchers determined that smoke rollback is dependent on the tunnel dimension, the fire intensity, and the air velocity [11], and rollback modeling must at a minimum consider these factors if modeling of the process is to be successfully achieved.

3. Analysis of Rollback

3.1 Computational Fluid Dynamics

Detailed modeling of rollback behavior is generally accepted as requiring a CFD software approach, which predicts the three dimensional movement of hot gases in a confined space. However CFD models can be time consuming to develop and coupled with lengthy simulation time, this limits the size and complexity of the modeling environment. The method is therefore suitable for only small areas, and cannot currently be used for modeling fire in large whole mine ventilation systems [6].

Figure 2 shows the 3D modeling results of a small diesel fire with a limited velocity of air travelling right to left. Modelling was performed with the Fire Dynamics Simulator (FDS) using the software PyroSim™ for the graphical front end [6]. The model clearly shows the rollback of a heated layer of air and smoke travelling in the opposite direction to the main airflow.

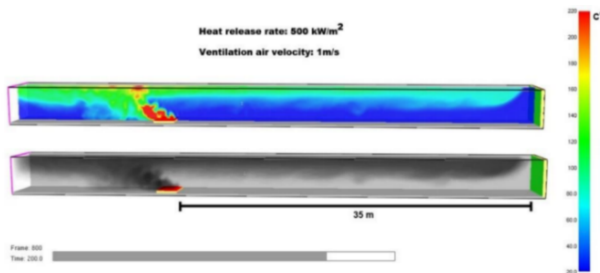


Fig. 2. Example of CFD modeling in PyroSim™ showing smoke and heat [6]

3.2 Empirical Analysis of Rollback

Adjiski [6] suggests network analysis methods are considered limited in capability to simulate rollback because tunnels and shafts are only considered as a single uni-directional pathway, and therefore bi-directional airflow movement such as rollback cannot be modeled. Airflows are either fully one direction or the other.

One method proposed by Lihong and Smith [12] is to consider rollback within a network analysis model by incorporating semi-empirical equations to predict the circumstances in which rollback may occur. The method was implemented into the US Bureau of Mines MFIRE program in 2011 and validated in fire tunnel tests.

Lihong and Smith proposed using a method incorporating the tunnel hydraulic height, fire temperature, heat release rate, and tunnel inclination into a formula that establishes the critical velocity under which rollback will be likely to occur during an MFIRE simulation. In the event of rollback, a further formula can then be used to predict and report the length of rollback.

A limitation of this method is that rollback occurrence is only reported during simulation and not used or simulated within the greater model. In addition, complex geometry such as changing airway inclinations, nearby intersections and variations in rock properties are not considered by the calculations.

4. Rollback Modelling with Network Analysis Simulation

Network analysis is generally considered only suitable for representing models with unidirectional pathway. This study was conducted to test whether unidirectional pathways could be split within a network model to allow bi-directional airflow along the upper and lower regions of the airway. Danko [13] proposed a similar concept for energy and moisture flow movement within large cavities and development headings using a network model, but restricted the use for non-fire related heat flow and moisture distribution.

The use of an interconnected mesh of horizontal and vertical airway paths within a large bounded airway allows two or three dimensional natural pressure driven movement of airflow within the larger volume. The properties of the split airways are maintained such that the combined boundary and resistance parameters of the pathways still mimic the original airway path for unidirectional flow.

4.1 Overview

The method of using a high density mesh of pathways within defined airways in a network was explored using an unmodified version of the Ventsim Visual™ VentFire™ module [9], however it may be possible that other network simulation software incorporating fire heat and natural ventilation may also be able to utilize this method. VentFire™ is a module integrated into Ventsim Visual™ mine ventilation software that uses network analysis for large scale mine simulation of the effects of a defined fire situation. The software uses heat driven natural ventilation pressures, and transient simulation of fire heat and gases to predict fire behavior in a mine [14].

4.2 Constructing the Pathways

To create a high density three dimensional mesh within a defined airway, an algorithm was developed to automatically split the airway both lengthways and vertically to create an upper and lower pathways, interconnected by regular vertical pathways. This allows the user to manually select a region immediately around the fire location to split before the simulation.

Figure 3 shows a single airway that has been split to upper and lower horizontal pathways. These pathways were sized exactly half the height of the original airway. Using Ventsim Visual™ wall exclusion option, the facing boundaries of the upper and lower boundaries were removed from the airway resistance and heat transfer calculations. This created an overall combined parallel resistance nearly identical to the original single airway, and limits heat transfer from fire to only the immediate rock surface surrounding the upper and lower airways. Simulating airflow *without* fire, therefore gives identical airflow results to the original single linear path.

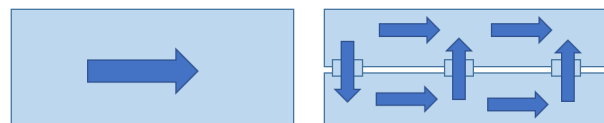


Fig. 3. Splitting single airway into bidirectional flow meshes

To facilitate the buoyancy driven air transfer between the upper and lower horizontal pathways, vertical pathway connections at a frequency of a minimum 4 m were created, although higher frequency could be used for more detailed analysis. The vertical airways are established at minimal size, assume no boundary resistance or heat transfer, and have a fixed resistance of 0.001 Ns/m² to allow relatively low resistance movement of air between upper and lower layers. Further testing found that resistance values for the vertical connections were reasonably insensitive providing they were a magnitude lower or more than the horizontal resistances.

4.3 Applying Fire Heat

The heat generated from fires can be calculated by considering the heat of combustion properties and burning rates of the fuel. The heat release rate (HRR) and moisture calculated can then be applied to the energy content (as sensible and latent heat) of the air surrounding the fire to calculate the temperature and the resulting air density calculated from a modified ideal gas law equation (Equation 1)

$$\rho(\text{humid}) = \frac{p_d M_d + p_v M_v}{RT} \quad (1)$$

Where:

$\rho(\text{humid})$ = Density of the humid air (kg/m³)

p_d = Partial pressure of dry air (Pa)

p_v = Pressure of water vapor (Pa)

R = Universal gas constant, 8.314 J/(K·mol)

T = Temperature (K)

M_d = Molar mass of dry air, 0.028964 kg/mol

M_v = Molar mass of water vapor, 0.018016 kg/mol

$$NVP = \Delta\rho gh \quad (2)$$

Where:

NVP = natural ventilation pressure

$\Delta\rho$ = air density difference between networked column and reference column, kg/m³

h = height of airway column, m

The NVP calculation can be applied to every networked branch with a vertical variation (including the interconnecting vertical rollback branches) to calculate the flow within a pressure balanced Hardy Cross network approximation of flow quantity and direction.

4.4 Transient (Dynamic) Simulation

Flow direction and volumes can be initially calculated by a steady state Hardy Cross simulation, and the resulting airflow velocities can be used to calculate the average speed of movement of gas and heat through the model.

Ventsim Visual™ uses a sub-cell transport method for transient modelling (labelled dynamic simulation in Ventsim Visual™), where airway pathways are split into smaller cells, each carrying a portion of the airway products through the model and over the fire.

Oxygen within cells that pass over the fire is consumed and replaced with combustion gases. The cells continue to move through the model, distributing heat and gases to pathways away from the fire.

The combined temperature and density of each group of cells in a branch airway is then used to recalculate NVP for the model, and further steady state flow balance simulations are periodically performed. Transient cell movement periods were set to every 0.1 s during

simulation, and steady state flow simulations were set to every 1.0 s to assess changes in flow direction and volume.

Cells entering junctions between branches are mass balanced and mixed uniformly with other cells entering the junction and the combined heat and gas is delivered into cells downstream from the junction (Figure 4).

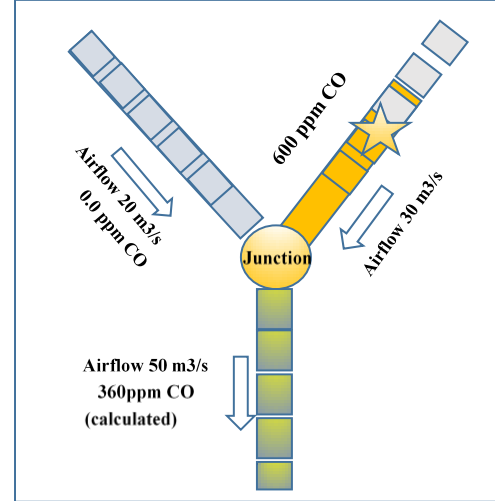


Fig. 4. Plan section showing transient flow and mixing simulation using sub cells

The results of the steady state simulation are transferred back into the transient simulation to alter the speed and direction of the cell movements. The global mine model joins seamlessly with the high density meshed part of the model where the fire is located, and mixed cells are free to move around the upper rollback layer, as well as in and out of the fire zone (Figure 5).

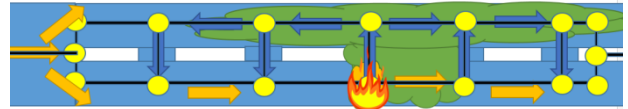


Fig. 5. Vertical section showing possible transient flow and rollback simulation around fire zone

5. Model Validation

5.1 Overview

An MFIRE model developed by Lihong and Smith [12] was used to validate the empirical rollback equation implementation in MFIRE. This model (Figure 6) is the basis for the high density network simulation in Ventsim Visual™.

The model incorporated a simplified representation of a number of connecting panels of an experimental mine, where a small diesel fire was ignited, producing a heat release rate (HRR) of approximately 520 kW (equivalent to around 50 l/hr burn rate of diesel fuel). The model was validated comparing actual rollback observations in the real mine fire versus MFIRE simulated results and the empirical rollback equations.

The Ventsim Visual™ model (Figure 7) was developed used identical sizes, resistances and lengths to

the MFIRE model and a fix flow in the C-Butt exhaust was used to duplicate the initial flow velocities.

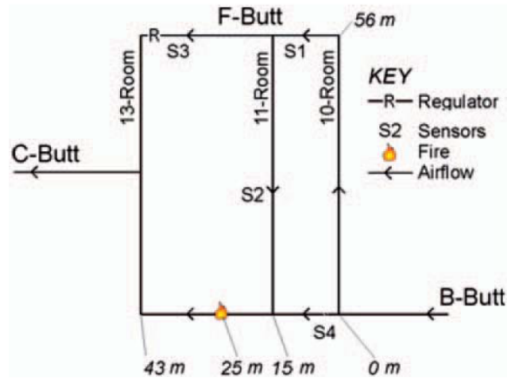


Fig. 6. MFIRE Validation Model [12]

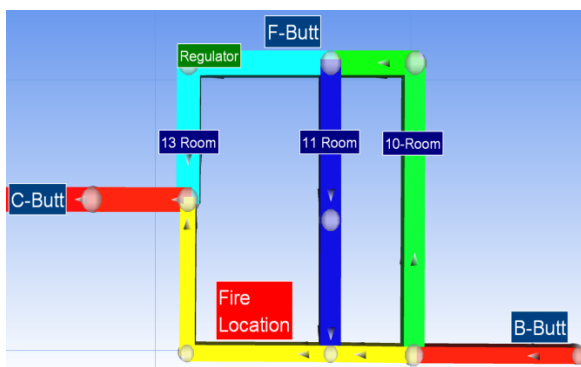


Fig. 7. Ventsim Visual™ model equivalent

5.2 Splitting Airways

Once the model is created, the airway splitting algorithm is used to manually select and split the pathways around the fire region into upper and lower pathways with vertical connection between. Approximately 40 m of airways each side of the fire were split to allow rollback (Figure 8).

The split length varies between 5 and 10 m depending on the length of the original branch. Finer splits can be specified however did not necessarily produce better results. Arguably, the splits create only a two dimensional flow network along the airways, however given the exact position of the fire across a tunnel may be unknown and rollback tends to be uniformly spread across the roof of a tunnel, this approach is seen as valid, and a three dimensional mesh (longitudinal, height and width pathways) would unlikely create additional value.

A current limitation of Ventsim Visual™ VentFire™ is that smaller lengths require a smaller dynamic time increment to allow creation of sufficient sub cells for accurate simulation and therefore the size of the split will adversely impact simulation time, particularly for large models.

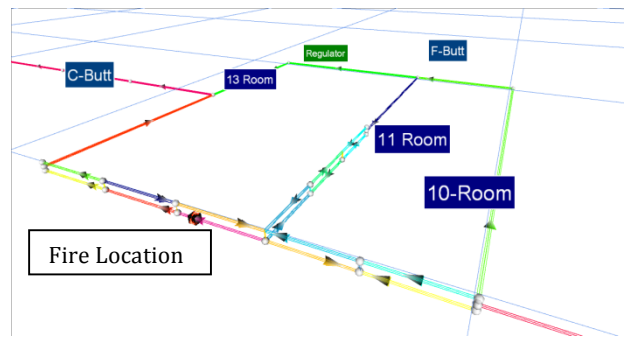


Fig. 8. Airway branches split into bi-directional upper/lower layers with vertical joins.

5.3 Varying Model Parameters

Three different flow velocities were specified to test against the MFIRE model validation results. In addition, the effect of slope was analyzed in the model by sloping all airways at 12% from left to right, and then from right to left.

Finally, a test example was done on a full mine model. While this example wasn't validated, the technique and outcomes were observed for relevance in a real mine simulation or emergency analysis.

6. Comparison with MFIRE Empirical Approach

The simulations demonstrated results broadly consistent with the MFIRE empirical equations. It was difficult to directly compare results as the empirical equations suggest a definite exact critical velocity at which reversal will occur, whereas the VentFire™ simulation with the bi-directional airways created different upper and lower velocity flows, as well as a slightly chaotic simulation output where airflows directions oscillated as natural ventilation pressures and heat was dynamically balanced. Only a few units (Pa) of pressure difference may exist in natural ventilation during simulation, and the oscillating reversal of individual airways and vertical joins may result because of this changing small variance.

It was also observed in the Swedish train fire tunnel test [10], that fire and rollback simulation in real life can also be chaotic and unpredictable due to the direct behavior of the fire and inconsistent supply of oxygen to the fire in the event of low airflow. It must be noted that VentFire™ will deliberately throttle back a fire if insufficient oxygen is temporarily available to the fire, resulting in a 'flaring' of the fire as new oxygen enters, and an uneven application of heat and NVP to the air.

6.1 Simulation Observations

The initial MFIRE study [12] suggested a critical velocity of 0.88 m/s of airflow velocity towards the fire under which rollback would occur. Actual observations showed smoke rollback into 11-Room and some evenly mixed smoke present back to 10-Room.

The VentFire™ simulation with an initial airflow of 0.68 m/s (decreasing by volumetric expansion during the simulation to around 0.35 m/s) showed a clear rollback situation into the proceeding junction and then into 11

Room, however smoke did not penetrate fully back to 10-Room. The discrepancy can perhaps be explained by the more even distribution of fire heat applied in VentFire across the full tunnel section which may have reduced the peak temperature in the rollback layer. This potentially could be resolved by increasing network mesh density or rollback thickness but was not tested during the project.

Without the rollback function, it would have been assumed that all heat and gases from the fire would have continued to travel out towards C-Butt, and no contamination of 11-Room would have occurred. Figure 9 shows rollback past into and past 11-Room junction.

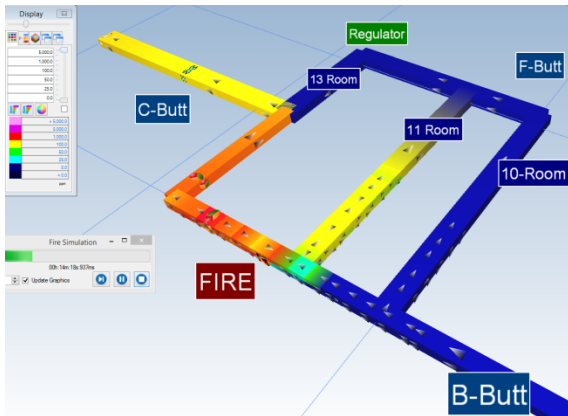


Fig. 9. Air velocity initially 0.68 m/s into fire (colors represent carbon monoxide level estimation, red=high, blue = low), rollback occurs.

A further test increasing the velocity of flow into the fire was performed with the VentFire™ simulation. The initial airflow was increased to 1.0m/s (again this decreased during simulation due to air expansion) and showed partial rollback immediately around the fire, but ultimately no contamination of 11-Room (Figure 10).

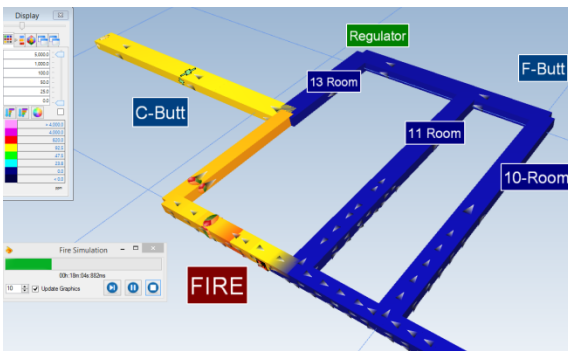


Fig. 10. Air velocity initially 1.0m/s into fire, partial rollback

A VentFire™ simulation with an initial airflow of 1.5 m/s showed no evidence of rollback, and no contamination of 11-Room (Fig. 11).

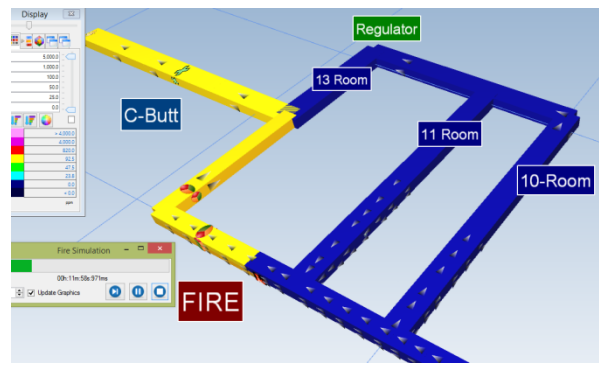


Fig. 11. Air velocity initially 1.5 m/s into fire, no rollback

6.2 Inclining the model

No validation of the inclined results could be made because the actual validation test work was not performed on inclined airways. Nonetheless, Equation (1) from the MFIRE empirical equation suggest that slope should have a clear effect on the rollback critical velocity, and therefore the occurrence of rollback, and this was tested in the VentFire™ model.

Figure 12 shows that inclining the model at 12% away from the fire, resulted in the smoke and heat travelling away from the fire with no rollback occurring. For rollback to occur, sufficient pressure would have had to be available to force the heated air downwards against its own natural ventilation pressure, and into the oncoming air velocity.

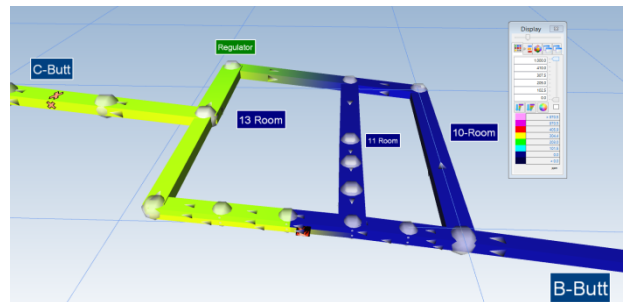


Fig. 12. Inclined at 12% to the left (0.68 m/s initial)

Figure 13 shows that inclining the model at 12% towards the fire causes rollback and reversal to occur all the way to the 10-Room intersection and into 10-Room, as the natural ventilation pressure of the heated air can now be used to assist in the rollback direction.

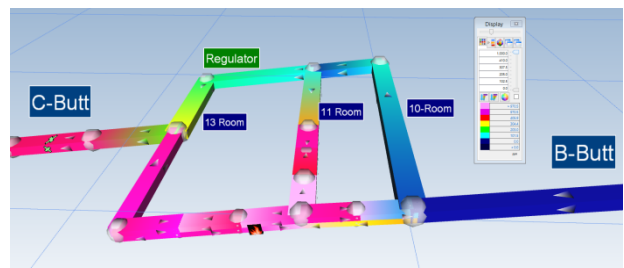


Fig. 13. Inclined at 12% to the right (0.68 m/s initial)

7. Comparison with CFD Approach

The opportunity was also taken to compare the results of a CFD study of a 3000 kW fire in a tunnel by Goce Delchev University [6]. The tunnel was modeled in CFD at 4 m wide by 3 m high, with a length of 50 m. A diesel pool fire was assumed generating a heat release rate of 500 kW/m² over a 6m² area.

An equivalent 3000 kW HRR diesel fire was built in an identical size tunnel in Ventsim Visual™ VentFire™ to compare results.

7.1 CFD Results

The CFD study compared fire rollback with three (3) different air velocities at 1.0 m/s, 1.5 m/s and 2.0 m/s (Figure 14). The CFD results suggested extensive (30 m+) rollback would occur in the 1.0 m/s case, partial rollback (9 m) in the 1.5 m/s case, and no rollback in the 2.0 m/s case.

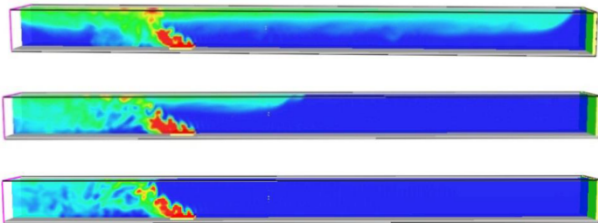


Fig. 14. CFD Modelling of 1.0 m/s (top), 1.5 m/s (mid) and 2.0 m/s (bottom). [6]

7.2 Ventsim Visual™ VentFire™ Results

The equivalent Ventsim VentFire™ simulation showed broadly consistent results, although considerable variability was observed during simulation (Figure 15). The 1.0m/s case generated rollback ranging from 20-40 m in length, the 1.5 m/s case generated rollback ranging from 10-15 m in length, and the 2.0 m/s case generated only minor rollback directly above the fire, with occasional 5 m extensions into the wind.

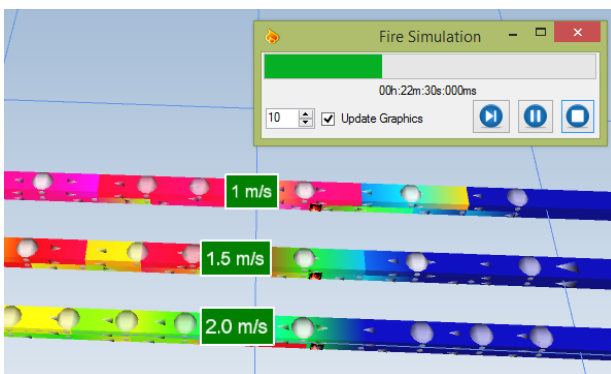


Fig. 15. VentFire™ Modelling: 1.0 m/s (top), 1.5 m/s (mid) and 2.0 m/s (bottom).

8. Full Complexity Model Testing

The method presented was tested on a full mine ventilation model. Although not validated, the speed at which the method could be applied and the rapid results that can be obtained, gives credence that this method may be suitable for real time emergency evaluation, instead of the usual post-event analysis of a fire

outcome. Ventsim VentFire™ shows results graphically as it progresses allowing visual inspection during the simulation.

Figure 16 shows a mine ventilation model where a truck fire was assumed on a main ramp. The combustibles on the truck were assumed burned over four (4) hours, and the ventilation model observed for changes during the simulation.

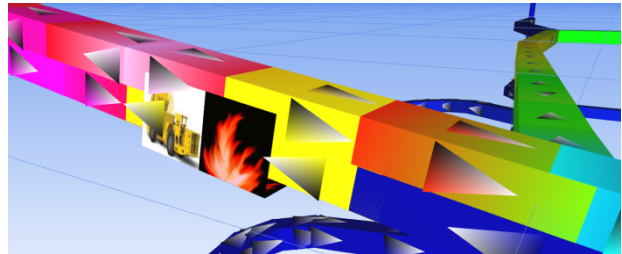


Fig. 16. Full Scale Mine Ventilation Model

8.1 Results

It was immediately observed that rollback of fumes occurred uphill on the ramp approximately 40 m above the truck against the main ventilation flow (Figure 17). Later in the simulation, complete reversal of the main ramp flow occurs, directing smoke and fumes into previously clear areas. Even after complete reversal occurs in the ramp, rollback *against* the reversed flows directed fumes unexpectedly into an area just downhill from the fire.

The complexity of results of this simulation suggest that a variety of unexpected conditions could occur should this have been a real fire. In the event of trapped personnel or a mine rescue excursion into the area, these conditions may have placed personnel in further danger, and would have been well worth considering during the planning phase of any rescue or evacuation scenario.

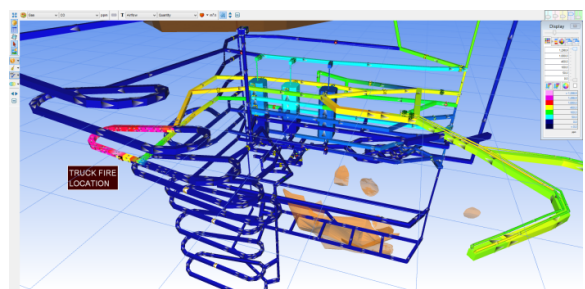


Fig. 17. Rollback then flow reversal uphill from the truck fire location.

Assuming a valid ventilation model is already available, a Vent Fire Location simulation can be quickly constructed with initial results from the simulation achieved within minutes.

9. Conclusions

Utilizing a high density mesh of rollback branches within a broader network analysis model to simulate rollback zones appears to be a useful method for rapid rollback simulation and integration within a global mine ventilation fire model. Despite the time based variability

of the VentFire™ results, the method provides results which are broadly consistent (but not exactly the same) as empirical and CFD analysis.

The method must be recognized as a highly simplified simulation that ignores much of the detail of a real fire such as radiant heat and convection within the 3D space. However while the method does not provide the accuracy or detail of CFD modelling, neither does it require the extensive inputs and assumptions of CFD methods, and given the amount of uncertainty in the estimation or measurement of fire variables, this may provide a perfectly acceptable initial analysis of the situation.

While CFD analysis promises detailed results around the immediate fire zone, the limited area possible to simulate, and the time taken to create and simulate models rule this method out for larger simulations or when quick results are required. Empirical analysis (with MFIRE for example) only provides an indication of the possibility of occurrence of rollback, but does not provide any additional analysis of the effects of the rollback on the remainder of simulation model.

In the event that results must quickly be known or estimated, the proposed integrated network analysis method has the potential to provide one of the most rapid ways to integrate and obtain results of rollback simulation details into a broad and extensive mine ventilation model. Ultimately, the effective use of such a method relies on a mine having an accurate model of the ventilation system, however most mines now have these models for ongoing planning and design purposes.

References

- [1] ABC/wires, *Turkish coalmine disaster*., in *Final death toll from Soma accident stands at 301*, ABC/wires, Editor. 2014, ABC.
- [2] Reuters, *South African gold miners rescued after a fire at Harmony Gold*. 2015.
- [3] McPherson, M.J. and F.B. Hinsley, *Subsurface ventilation and environmental engineering*. Vol. 131. 1993: Chapman & Hall London.
- [4] Cheng, L.H., T.H. Ueng, and C.W. Liu, *Simulation of ventilation and fire in the underground facilities*. Fire Safety Journal, 2001. **36**(6): p. 597-619.
- [5] Weisenpacher, P., L. Halada, and J. Glasa. *Computer simulation of fire in a tunnel using parallel version of FDS*. in *Proc. of the 7th Mediterranean Combustion Symp., Assoc. Sezione Italiana del Comb. Inst.* 2011.
- [6] Adjiski, V., *Possibilities For Simulating The Smoke Rollback Effect In Underground Mines Using Cfd Software/Možnosti Simulace Zpětného Proudění Kouře V Hlubinných Dolech Pomocí Cfd Softwaru*. GeoScience Engineering, 2014. **60**(2): p. 8-16.
- [7] Thunderhead Engineering Consultants, *PyroSim User Manual-PyroSim*. Inc. Manhattan, KS: p. 66502-6081.
- [8] Krawczyk, J. and W. Dziurzyński, *Modelling propagation of gas contaminants in tunnels during normal operation and fires with mine ventilation software VENTGRAPH*. Budownictwo Górnicze i Tunelowe, 2012: p. 11-14.
- [9] Stewart, C.M., *Ventsim Version 3.0 with VentFire*. 2012, Chasm Consulting: Brisbane. p. Ventfire Fire Simulation Module.
- [10] METRO project, A., Sweden. *Full Scale Fire Tunnel Test*. Full-scale fire test in train tunnel 2011-09-07, METRO project, Arvika, Sweden 2011; Available from: <https://www.youtube.com/watch?v=sKgPIUs-SF0>.
- [11] Hwang, C.C. and J.C. Edwards, *The critical ventilation velocity in tunnel fires—a computer simulation*. Fire Safety Journal, 2005. **40**(3): p. 213-244.
- [12] Lihong, Z. and A. Smith, *Improvement of a mine fire simulation program—incorporation of smoke rollback into MFIRE 3.0*. Office of Mine Safety and Health Research, National Institute for Occupational Safety and Health, Pittsburgh, PA, 2011: p. 78-85.
- [13] G. Danko, D.B., *Application of MULTIFLUX for air, heat and moisture flow simulations*, in *12th U.S./North American Mine Ventilation Symposium 2008*, Wallace, Editor. 2008: Reno, NV.
- [14] Brake, D. *Fire Modelling in Underground Mines using Ventsim Visual VentFIRE Software*. 2013. Australian Mine Ventilation Conference/Adelaide, SA, Australia.

Numerical Study on the Effects of Water Spray Characteristics on Suppression of Conveyor Belt Fires

Liming Yuan, Alex C. Smith

*National Institute for Occupational Safety and Health
Office of Mine Safety and Health Research
Pittsburgh, PA 15236, USA*

Conveyor belt fires in an underground mine pose a serious life threat to the workers. Water sprinkler systems are usually used to extinguish underground conveyor belt fires; however, the suppression process is complex due to the potential for flame spread and its interaction with airflow in the entry. In this paper, computational fluid dynamics (CFD) simulations were conducted to investigate the effects of water spray characteristics on the suppression of conveyor belt fires in a mine entry. The CFD model was developed in a previous study and was calibrated using large-scale experimental results. The model was able to simulate the interaction between the ventilation airflow, the flame spread over the belt, and the water spray in the mine entry. The studied water spray characteristics included water droplet size, initial droplet velocity, and spray angles, and the influence of each of these on the suppression of conveyor belt fires was examined. The results showed that the conveyor belt fire was mainly suppressed by fuel surface cooling. Flame cooling (gas-phase cooling from water droplet evaporation) had an insignificant effect on the suppression. Simulation results from this study can be used to develop more effective engineering design for installation of fire suppression systems for underground coal mines.

Keywords: Conveyor belt fire, computational fluid dynamics, water spray, suppression.

1. Introduction

A conveyor belt fire in an underground mine is a life threat for underground miners. On January 19, 2006, two miners were fatally injured in an underground conveyor belt fire at the Aracoma Alma No. 1 mine, located in Logan County, West Virginia, when they became separated from their crew while trying to escape from the fire. When the underground conveyor belt fire occurred, the gaseous combustion products and smoke produced from the burning of the belt were carried throughout the entire ventilation system, exposing underground miners to potentially hazardous levels of toxic gases. As confirmed later by the accident investigation team, those two miners died of carbon monoxide (CO) poisoning [1]. The smoke produced from the burning belt also limited visibility for the miners, making it much more difficult to escape from the mine. As this example demonstrates, it is important to suppress and control belt fires in a timely manner in order to prevent the fire from causing any injury to the miners and ensure they can evacuate safely from the mine.

Water spray systems are commonly installed in the belt entry to extinguish a belt fire. However, the suppression process of a belt fire is complicated by the flame spread along the belt and the airflow in the entry. Large-scale experiments were conducted by NIOSH to evaluate the effects of air velocity, water sprinkler activation temperature, and a limited water application time on the effectiveness of water sprinkler fire suppression systems to extinguish conveyor belt fires [2-4]. Several novel fire suppression agents, such as fire-fighting foams and gels, as well as water mist systems were also evaluated for their ability to suppress conveyor belt fires in underground coal mines [5]. As stressed by past study findings, to develop a more effective fire protection system for the conveyor belt entry in an underground mine, more systematic engineering data are needed. Although full-scale experiments can be conducted to obtain engineering data to develop guidelines for performance-based designs for the installation of mine fire suppression systems, these tests

cannot address all issues. In addition, the tests are both expensive and time-consuming.

Computational fluid dynamics (CFD) modeling has been widely used in simulating the interaction between water spray/mist and a fire and can provide insights into the complicated interaction between conveyor belt fires and the mine ventilation airflow [6, 7]. In this paper, a series of CFD simulations were conducted to investigate the effects of water sprinkler droplet size, droplet initial velocity, and spray angles on the suppression of conveyor belt fires in a mine entry. The CFD model was calibrated using large-scale conveyor belt fire test results from a previous study [8]. The simulation results in this study can be used to design more effective fire protection systems for conveyor belt entries in underground coal mines.

2. Modeling of water spray

In our previous study, a CFD model was developed to simulate the flame spread over the conveyor belt in a large-scale tunnel using the NIST Fire Dynamics Simulator version 5 (FDS) [8]. In the model, thermogravimetric analysis (TGA) data for the conveyor belt were used to calculate the kinetic properties for modeling the pyrolysis process of the conveyor belt. The CFD model was calibrated using the large-scale conveyor belt fire test results [8]. The comparison between simulation and test results showed that the CFD model was able to capture the major features of the flame spread over the conveyor belt. A detailed description of the modeling is provided in that publication.

In the current study, the modeling of water spray and its interaction with the flame was added to the CFD model to simulate the water suppression of conveyor belt fires using FDS. To simulate water spray suppression of belt fires, some spray characteristics need to be specified as input for the simulations. Those characteristics include sprinkler activation temperature, sprinkler response time index (RTI), water flow rate, droplet

diameter, droplet initial velocity, and spray angles. The sprinkler activation temperature and RTI value were obtained from the sprinkler manufacturer. The water flow rate was calculated based on the K-factor value of the sprinkler and the operating pressure of the sprinkler system using the equation:

$$\dot{m} = K\sqrt{P} \quad (1)$$

where \dot{m} is the water flow rate, K is the K-factor for the sprinkler, and P is the operating pressure. A water spray usually consists of various-sized spherical droplets. The size distribution of the water droplets can be expressed in terms of its Cumulative volume fraction (CVF), a function that relates the fraction of the liquid volume transported by droplets less than a given diameter. The CVF for water droplets from a sprinkler may be represented by a combination of log-normal and Rosin-Rammler distributions [9]:

$$F(d) = \begin{cases} \frac{1}{\sqrt{2\pi}} \int_0^d \frac{1}{\sqrt{2\pi}} e^{-\frac{[\ln(d'/d_m)]^2}{2\sigma^2}} dd' & (d \leq d_m) \\ 1 - e^{-0.693\left(\frac{d}{d_m}\right)^\gamma} & (d > d_m) \end{cases} \quad (2)$$

where d_m is the median droplet diameter defined as the diameter of a droplet for which half of the droplets have a larger diameter and half a smaller diameter, and γ and σ are empirical constants equal to 2.4 and 0.6, respectively. The median droplet diameter is a function of the sprinkler orifice diameter, operating pressure, and geometry. Research has found a correlation for the median droplet diameter [10]:

$$\frac{d_m}{D} = cWe^{-1/3} \quad (3)$$

where D is the orifice diameter of the sprinkler and c is a constant. The Weber number, We , defined as the ratio of inertial forces to surface tension forces is given by:

$$We = \frac{\rho_d u_d^2 D}{\sigma_d} \quad (4)$$

where ρ_d is the density of liquid, u_d is the droplet initial velocity, and σ_d is the liquid surface tension. The initial velocity can be computed from the mass flow rate and the orifice diameter. The constant c appears to be independent of flow rate and operating pressure. Sheppard conducted an extensive experimental study to measure the water spray characteristics for fire sprinklers [11]. The value for the constant c measured in his study ranged from 0.72 to 2.48 with an average of 1.53. The calculated median droplet diameter for the sprinkler used in the simulation, based on the Sheppard study average value, was 503 μm .

3. Numerical details

Figure 1 shows the physical model of the simulated tunnel and the conveyor belt. The physical dimensions and the belt setup are based on the large-scale conveyor belt fire test conducted in a previous study to calibrate the CFD model [8]. The dimensions for the actual tunnel are 46.6 m long, 5.5 m wide, and 2.2 m high. For the simulation the tunnel length was limited to 20 m. The conveyor belt used in this study is styrene-butadiene rubber (SBR) with dimensions of 11 m long, 1.8 m wide, and 15 mm thick. The metal shields used in the test to prevent the blowout of the ignition flame were modeled as the real sizes. The airflow velocity at the inlet of the

tunnel was set at 1.5 m/s as in the test. In the simulation, a burner is used to ignite the belt as in the large-scale conveyor belt fire test. The burner is located on the floor between the shields and a vertical obstruction which acts to prevent the burner flame to reach the bottom of the belt. The average value of the measured heat release rate (HRR) during the duration of the burner in the test is used as the heat output for the burner that is turned on for 10 minutes as in the test.

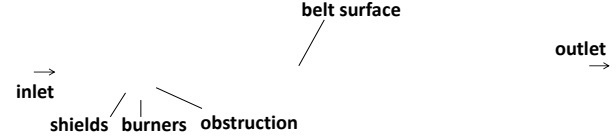


Fig. 1. Physical model of simulated tunnel and conveyor belt.

Eight water sprinklers were placed below the roof of the tunnel with the center distance of 2.4 m to protect the conveyor belt along the centerline of the belt. Each water sprinkler has an activation temperature of 140 °C and a discharge coefficient of $K = 80.6 \text{ Lpm/bar}^{0.5}$. With the conditions studied in this work, the first sprinkler was activated 304 seconds after the ignition.

It has been well known that grid size can affect the FDS simulation results. Therefore, it is important to determine an appropriate grid size to achieve the desired reliability. As suggested by McGrattan et al. [12], the grid size near the fire source should be no larger than 0.1 D^* to ensure reliable simulation results. D^* represents the characteristic length scale for a fire source and is written as:

$$D^* = \left(\frac{Q}{\rho_c p T_0 \sqrt{g}} \right)^{2/5} \quad (5)$$

where Q is the HRR of fire, ρ_c is air density, C_p is specific heat of air, T_0 is ambient temperature, and g is gravity acceleration. In our large-scale conveyor belt fire test, the measured HRR, Q , was between 2 and 7 MW. The corresponding value for D^* is between 1.3 and 2.1 m. Therefore, a grid size of 0.1 m was selected in this study.

4. Results and discussion

4.1 Effect of water droplet size

To investigate the effect of water droplet size on the suppression of conveyor belt fires, six different water droplet diameters between 200 and 900 μm were used in the simulations. Simulation results based on different droplet diameters are shown in Figures 2 to 5. The centerline belt surface temperatures 5 m from the belt leading edge with different water droplet sizes are plotted in Figure 2. Although the belt fire was suppressed with different water droplet sizes, 900- μm -diameter droplets had the lowest surface temperature at this location, indicating that more water droplets with larger size reached this location. With the droplet size decreased from 900 to 300 μm , the surface temperature increased. However, the surface temperature decreased when the droplet size was decreased from 300 to 250 μm , then to 200 μm . This can be seen clearly in Figure 3 showing the surface centerline temperature 5 m from the belt leading edge two minutes after the sprinkler was activated. This is probably because the flame cooling

effect became more significant with the finer water droplets.

The belt surface temperature is determined by the heat received at the surface from the flame and the heat removed by the water. In order to cool the belt surface, the water spray must penetrate the flame to reach the surface. Therefore, it is easier to suppress the belt fire using larger droplets. On the other hand, smaller water droplets from the spray can easily evaporate and absorb the heat from the flame, leading to the cooling of the flame that also results in lower surface temperature. This explains why 300- μm -diameter droplets produce the highest belt surface temperature compared to other droplet diameters.

The centerline surface temperatures 7 m from the belt leading edge for different water droplet sizes are shown in Figure 4. As the droplet size decreased from 900 to 200 μm , the surface temperature also decreased. This is because more water droplets reached this location as the droplet size decreased due to the effect of ventilation

airflow. Smaller droplets were affected more by the ventilation airflow than larger droplets. Figure 5 shows the smoke temperatures 15 cm below the roof downstream of the belt for different water droplet sizes. The smoke temperature also decreased as the droplet diameter decreased, probably because of the increased flame cooling effect.

These simulation results indicate that smaller water droplets are more effective at cooling the belt surface downstream and at reducing the smoke temperature, while larger water droplets are more effective at cooling the belt surface beneath the flame. Under conditions studied here, 200 μm -diameter water droplets are the most effective droplet size to cool both the surface temperature and smoke temperature.

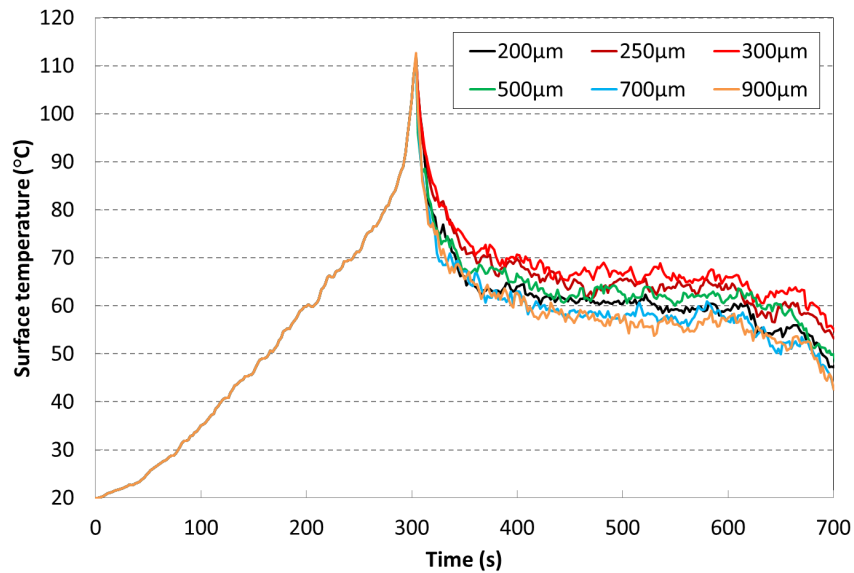


Fig. 2. Belt surface temperatures 5 m from belt leading edge for different water droplet sizes.

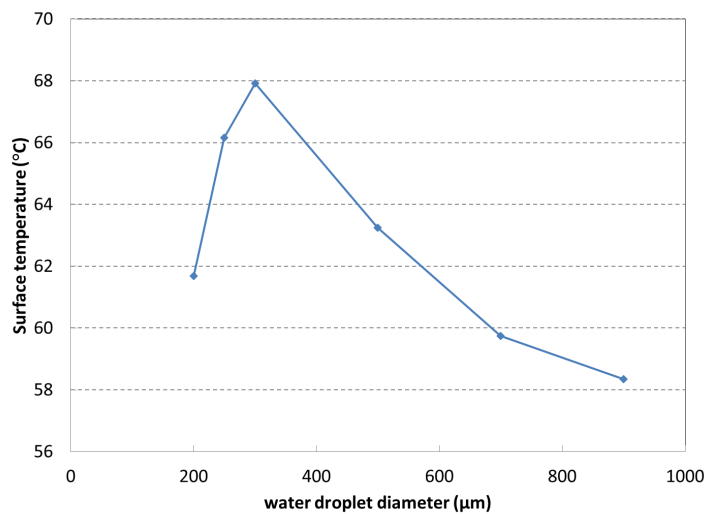


Fig. 3. Belt surface centerline temperatures versus water droplet diameters: 5 m from leading edge at two minutes from sprinkler activation.

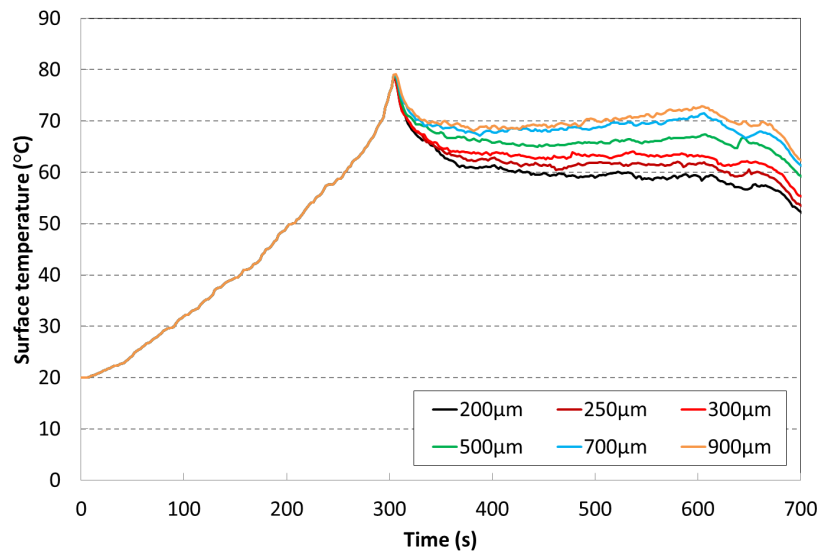


Fig. 4. Belt surface temperatures 7 m from belt leading edge for different water droplet sizes.

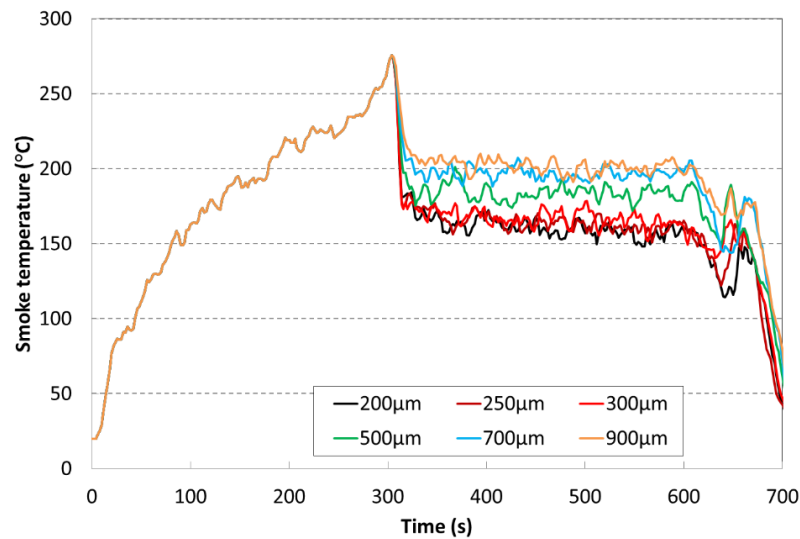


Fig. 5. Downstream smoke temperatures 15 cm below roof for different water droplet sizes.

4.2 Effect of initial velocity

CFD simulations were conducted with water droplet initial velocities ranging from 2 to 30 m/s to examine the effect of droplet initial velocity on the suppression of conveyor belt fires. Figure 6 shows the centerline belt surface temperatures 5 m from the belt leading edge with different droplet initial velocities. As the initial velocity increased from 2 to 10 m/s, the surface temperature decreased gradually. When the initial velocity increased to 20 m/s, the surface temperature decreased sharply. With the initial velocity further increased to 30 m/s, the surface temperature was nearly the same as that of 20 m/s initial velocity. The centerline belt surface temperatures 7 m from the belt leading edge with different droplet initial velocities are shown in Figure 7.

The surface temperature decreased as the initial velocity increased from 2 to 10 m/s. Further increase of initial velocity resulted in no apparent difference on the surface temperatures. The droplet initial velocity seemed to have insignificant effect on the smoke temperature downstream of the burning belt as shown in Figure 8. Only the initial velocity of 2 m/s produced slightly higher smoke temperature.

These results indicate that the higher the initial velocity, the lower the surface temperature was up to 20 m/s. Initial velocities higher than 20 m/s did not produce any difference on the belt temperature. The initial velocity had an insignificant effect on the downstream smoke temperature.

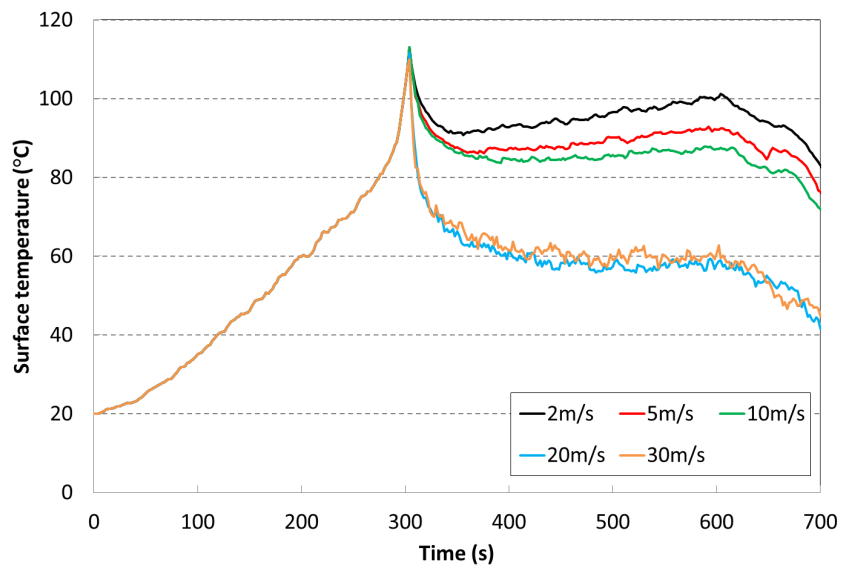


Fig. 6. Belt surface temperatures for different initial velocities: 5 m from belt leading edge.

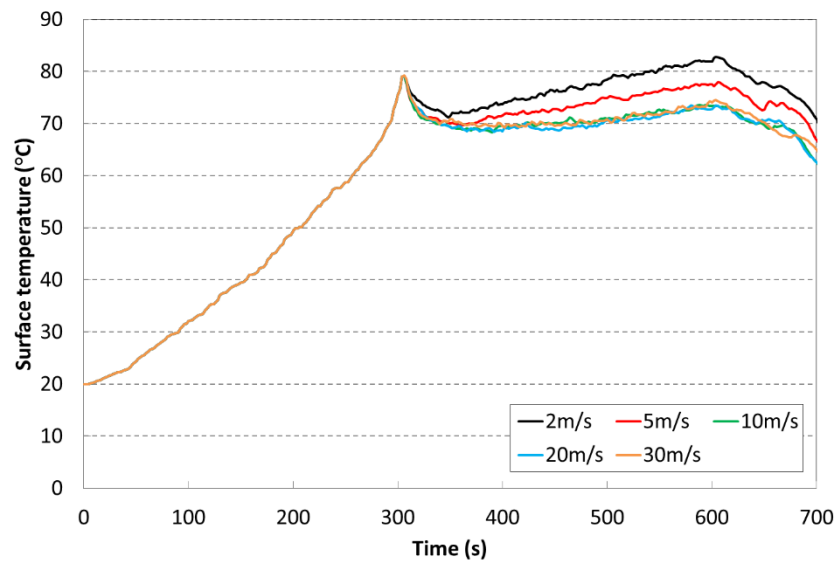


Fig. 7. Belt surface temperatures for different initial velocities: 7 m from belt leading edge.

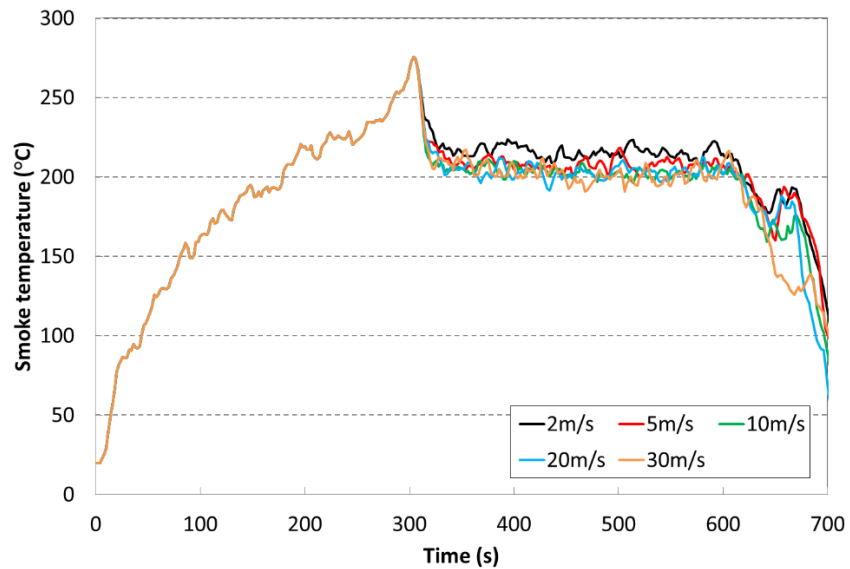


Fig. 8. Downstream smoke temperatures 15 cm below roof for different initial velocities.

4.3 Effect of spray angles

Spray angles can also impact the effectiveness of the water spray suppression of conveyor belt fires. Spray angles include the inner spray angle and the outer spray angle. The inner spray angle is the boundary of the area inside the spray where there is no water, while the outer spray angle is the angle of the outer boundaries of the spray. In this study, one full-cone and three hollow-cone sprays were examined in the CFD simulations. The full-cone spray has spray angles of 0 to 72 degrees, while three hollow-cone sprays have spray angles of 30 to 90, 30 to 78, and 50 to 75 degrees, respectively. Figure 9 shows the centerline belt surface temperatures 5 m from the belt leading edge with different spray angles. The full-cone spray produced the highest surface temperature at this location, while the hollow cone sprays produced much lower surface temperatures compared to the full-cone spray. The full-cone spray also produced the highest surface temperature 7 m from the belt leading edge compared to those hollow-cone sprays, as shown in Figure 10. Although all three hollow-cone sprays produced lower surface temperature compared to the full-cone spray, the hollow-cone spray with the angles of 30 to 90 degrees produced the lowest surface temperature at this location. However, there is no significant difference between the smoke temperatures for the full-cone and hollow-cone sprays, as shown in Figure 11, even though the hollow-cone spray with the angles of 30 to 90 degree still produced the lowest smoke temperature.

These results indicate that the full-cone spray is least effective and the hollow-cone spray with the angles of 30 to 90 degrees is most effective to suppress the conveyor belt fires under conditions studied in this work.

5. Conclusions

CFD simulations were conducted to investigate the effects of water droplet size, droplet initial velocity and spray angles on the effectiveness of water spray suppression of conveyor belt fires in a large-scale tunnel. Simulation results demonstrate that under the conditions in this study, smaller water droplets are more effective for cooling the belt surface downstream and reducing the smoke temperature, while larger water droplets are more effective for cooling the belt surface beneath the flame. The appropriate water droplet diameter to reduce both the belt surface temperature and smoke temperature was 200 μm . The initial velocity of 20 m/s was the most effective to reduce the belt surface temperatures. The most effective spray cone angles to suppress the conveyor belt fires are the hollow-cone spray angles of 30 to 90 degrees.

The water droplet size had an important effect on the downstream smoke temperature, while the droplet initial velocity and spray angles had insignificant effect on the smoke temperature.

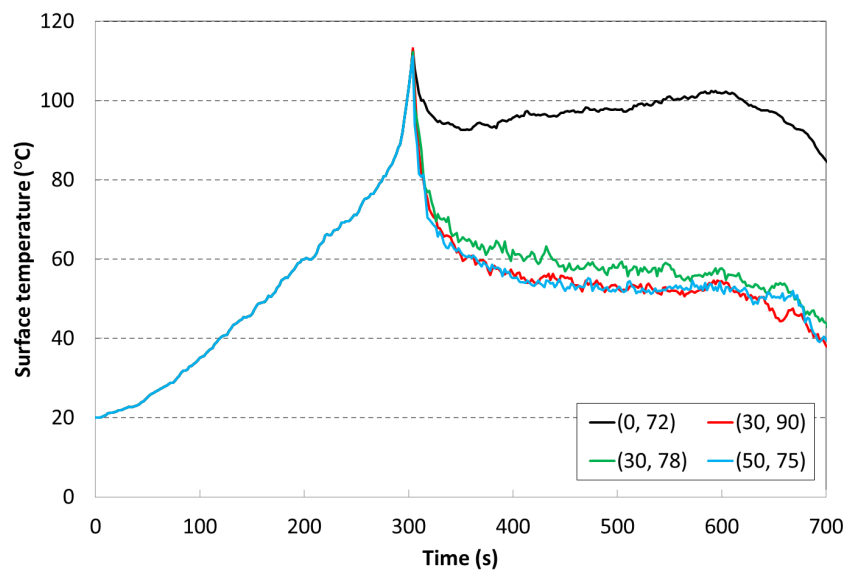


Fig. 9. Belt surface temperatures 5 m from belt leading edge for different spray angles.

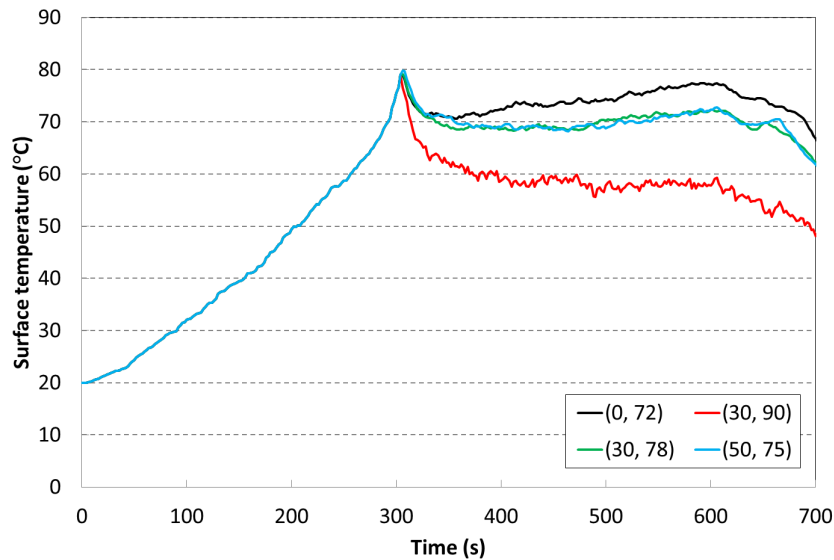


Fig. 10. Belt surface temperatures 7 m from belt leading edge for different spray angles.

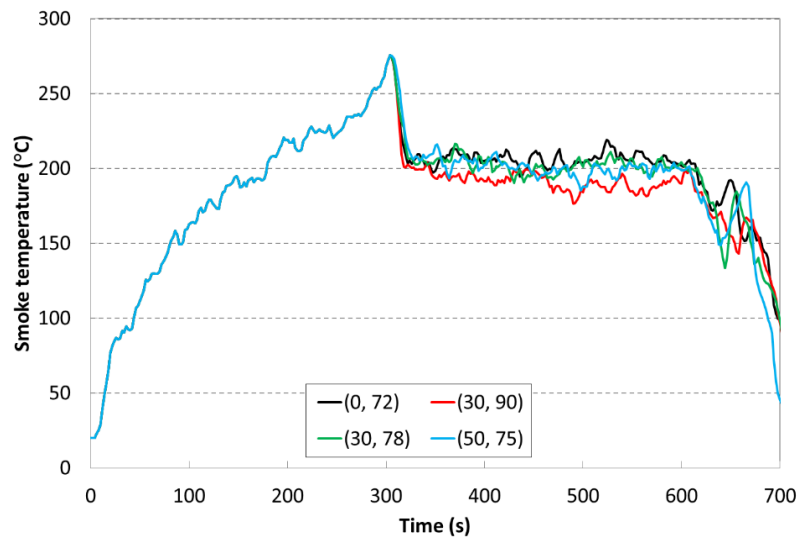


Fig. 11. Downstream smoke temperatures 15 cm below roof for different spray angles.

Disclaimer

The findings and conclusions in this report are those of the authors and do not necessarily represent the views of the National Institute for Occupational Safety and Health.

References

- [1] Mine Safety and Health Administration, Report of Investigation: Fatal underground coal mine fire - Aracoma Alma Mine #1, 2007.
- [2] A.C. Smith, R. W. Pro, and C. P. Lazzara, Performance of automatic Sprinkler systems for extinguishing incipient and propagating conveyor belt fires under ventilated conditions, USBM RI 9538, 1995.
- [3] J.H. Rowland, H. Verakis, M.A. Hockenberry, A.C. Smith, Effect of air velocity on conveyor belt fire suppression systems, Transactions of Society for Mining, Metallurgy, and Exploration 328 (2011) 493-501.
- [4] K.A. Teacoach, J.H. Rowland, A.C. Smith, Improvements in conveyor belt fire suppression systems for U.S. coal mines, Transactions of Society for Mining, Metallurgy, and Exploration 328 (2011) 502-506.
- [5] K.A. Teacoach, R.A. Thomas, Evaluation of novel fire suppression systems for conveyor belt fires in underground coal mines, Proceeding of the Seventh International Seminar on Fire & Explosion Hazards (2013) pp. 453-462.
- [6] E. Blanchard, P. Fromy, P. Carlotti, P. Boulet, S. Desanghere, J.P. Vantelon, J.P. Garo, Experimental and numerical study of the interaction between water mist and fire in an intermediate test tunnel, Fire Technology 50 (2013) 565-587.
- [7] A. Jenft, A. Collin, P. Boulet, G. Pianet, A. Breton, A. Muller, Experimental and numerical study of pool fire suppression using water mist, Fire Safety Journal 67 (2014) 1-12.
- [8] L. Yuan, R.J. Mainiero, J.H. Rowland, R.A. Thomas, A.C. Smith, Numerical and experimental study on

flame spread over conveyor belts in a large-scale tunnel, *Journal of Loss prevention in Process Industries* 30 (2014) 55-62.

- [9] K.B. McGrattan, S. Hostikka, J.E. Floyd, H. Baum, R. Rehm, W. Mell, R. McDermott, *Fire Dynamics Simulator (version 5.5): Technical Reference Guide*, National Institute of Standards and Technology, NIST Special Publication 1018-5, 2010.
- [10] J.R. Lawson, W.D. Walton, D.D. Evans, *Measurement of droplet size in sprinkler sprays*, National Bureau of Standards, NBSIR 88-3715, 1988.
- [11] D.T. Sheppard, *Spray characteristics of fire sprinklers*, National Institute of Standards and Technology, NIST GCR 02-838, 2002.
- [12] K.B. McGrattan, H. Baum, R. Rehm, *Large eddy simulation of smoke movement*, *Fire Safety Journal* 30 (1998) 161–178.

Modeling and Simulation of Multiple Underground Mine Fire Scenarios at Freeport Indonesia

Rick Brake^a, Alex Hatt^{b,c}, Riza Sani^d

^a*Mine Ventilation Australia, Queensland, Australia*

^b*Freeport-McMoRan, Phoenix, Arizona, USA*

^c*University of Nevada, Reno, USA*

^d*PT Freeport Indonesia, Tembagapura, Papua, Indonesia*

Mine fires remain one of the most potentially devastating underground incidents due to the prospect of multiple fatalities from the toxic products of combustion, the costly and time-consuming damage to critical underground infrastructure, and the damage to corporate standing and the 'social license' to operate. The behavior of mine fires is difficult to predict and often counter-intuitive, especially for intense fires where the amount of energy released by the fire in terms of natural ventilation pressures can dramatically change the volume and direction of airflow in ventilation circuits. This can have major and unexpected impacts on egress and entrapment, firefighting strategies, and the need for and design of fire protection systems.

This paper describes a technical study of the potential impacts of mine fires at the Freeport-McMoRan underground mining complex in Indonesia, examining seventeen potentially critical fire scenarios at PTFI as identified by a risk assessment. The range of fires examined includes mine mobile equipment fires, magazine fires, fuel bay fires, fire involving multiple light vehicles in a parking area, a compressor fire, an electrical sub-station fire, a conveyor fire, fire on an bus transporting personnel, spontaneous combustion fires, and fire in a long 'naturally ventilated' tunnel used by all vehicles to access the mine surface facilities, but physically unconnected to the mine.

A comprehensive review of available technical data from civil and mining sources in terms of the peak heat release rate (HRR) and HRR-time growth/decay curves was undertaken, as well as a careful review of existing data on human survivability limits. This led to the adoption of new design criteria for the modelling of fires as well as survivability limits. Modelling of each scenario was performed in VentSim Visual. To assist in communication of the complex fire behavior to management and workers, "real-time" animations showing direction, flow, and toxic gas concentrations were produced. The implications of the study in terms of egress and entrapment systems, incident management systems, and fire protection systems are also discussed.

Keywords: Fire, Underground, Mine, Modeling, Simulation, Freeport.

1. Introduction

P.T. Freeport Indonesia (PTFI) operates a complex of surface and underground mines in the Grasberg Minerals District located in the highlands of Papua, Indonesia. Currently the mining complex is producing ore from the Grasberg Open Pit (GRS), the Deep Ore Zone (DOZ), and Big Gossan (BG) mines. As surface operations at the GRS end (currently forecasted in 2017) plans call for a transition to underground mining to replace GRS pit feed to the mill. With this in mind PTFI has initiated development of two block cave mines.

The Grasberg Block Cave (GBC) is a continuation of the mining of the Grasberg Deposit from beneath the current pit. The Deep Mill Level Zone (DMLZ) is the next lift in the East Ertsberg Skarn System (EES) and lies below the footprint of the DOZ Mine. In aggregate the planned underground expansion represents a reserve of approximately 1.5 billion metric tons and will support a processing rate of 240 ktpd through the end of the current Contract of Work in 2041.

2. PTFI Underground Expansion

With the planned end of surface mining from the Grasberg Open Pit in 2017, PTFI will transition to an entirely underground mining operation. This transition requires substantial additions to the current underground operations, with major expansions in underground shops, electrical systems, crush/convey operations, and fleet size to support the increased mining rates. These facilities are large enough to support the operations of

each mine along with offsetting the loss of surface maintenance facilities due to caving and construction.

In light of the expansion of the underground facilities an 'Underground Fire Risk Assessment' was completed in November 2013. This assessment generated 17 scenarios that were considered to be credible fire risks based on the knowledge of site engineering and safety groups, as well as external consultants. These were not the 17 "highest risk" scenarios, but were chosen to capture a broad range of types of fires underground as well as some of the highest risk scenarios.

3. Revisiting Fire Modeling

3.1 Scenarios

Subsequent to the risk assessment a decision was made to pursue computer modeling of the 17 scenarios identified. The scenarios considered can be generally described as mobile equipment fires, conveyor belt fires, electrical transformer fires, explosives fires, and spontaneous combustion events. Past fire events at PTFI as described in Duckworth [6] were updated with additional to-date information from safety groups. This reinforced the belief that the most frequent risks for fires in the underground were presented by mobile equipment, and that the ongoing expansion of the underground fleet since the last evaluation would increase this risk.

The planned increases in staffing and extents of the operation presented a number of challenges on how best to communicate the risk from fire to stakeholders. Given the advances in computer graphics in the last 5 to 10

years the decision was made to use the VentFire package within VentSim Visual to generate video animations for each scenario. These videos would in turn be used to visually convey the potential risks from fires to stakeholders.

3.2 Determining Design Fires

The 17 scenarios generated from the risk assessment are listed below in Table 1.

Table 1. PTFI Fire Modeling Scenarios

Scenario Number	Scenario Short Title	Type of Fire	Operations Affected
1	AB Tunnels Intakes	AD55 truck	GBC, Big Gossan, DMLZ
2	DOZ Intakes	Iveco bus	DOZ
3	ARD Portals Intakes	AD55 truck	GBC, Big Gossan
4	DOZ Intake Fuel/Lube	R1700 LHD	DOZ
5	DOZ Magazine	ANFO	DOZ
6	GRS 34 Conveyor	Conveyor	DOZ
7	GVD Intake	AD55 truck	GBC
8	Kasuang Magazine	ANFO	Big Gossan
9	CI3 Compressor	Compressor	GBC
10	Kasuang Intake	AD55 truck	Big Gossan
11	Intake 3, XC11	Electrical Substation	DOZ
12	Big Gossan Workshop	R1700 LHD	Big Gossan
13	DOZ Parking Lot	5 light vehicles	DOZ
14	DOZ Spontaneous Combustion	Spontaneous combustion	DOZ
15	GRS OP Spontaneous Combustion	Spontaneous combustion	DOZ
16	Zaaghams Tunnel	Iveco bus	Zaaghams tunnel
17	GVD 3 Access	AD55 truck	DOZ, GBC, Big Gossan, DMLZ

While the majority of the scenarios considered fires involving mobile equipment a selection of fires related to conveyors, electrical substations, underground compressors, and spontaneous combustion were also chosen to better understand their potential impact.

With the large number of scenarios to be considered the fires were reduced down to a series of ‘design fires’ that could then be shared between scenarios to reduce the amount of work required in setting up the models. This in turn made more time available for analyzing and understanding the results as well as making improvements in how the final information was presented. For mobile equipment fires fuel inventories were created for each of the four mobile equipment scenarios (AD55 haul truck, Iveco Bus, R1700 LHD, Five Toyota Light Vehicles) based on manufacturer specification and equipment data sheets. Calorific values were assigned for each fuel item based on a literature search of fuel values from differing sources including the power generation industry [1], past studies completed by the USBM [9], and the European Thematic Network Fire in Tunnels [10] as shown in Table 2. This was reduced to the inputs for the fire simulation, namely the Peak Heat Release Rate (HRR) and durations of the three phases of the fire as shown in Table 3. Similar inventories were completed for the remaining non-equipment fire scenarios.

fire. Also, note that the dividing line between “fully developed” and “decay” is rather arbitrary.

4. Heat Release Rate (HRR) Curves

4.1 Concept and Recent Developments

The heat output (“heat release rate” or HRR) from the fire at any time governs most of the behavior of the fire and is therefore critical to any fire modelling.

The stages of a fire and the true HRR of a fire are generally said to follow the type of curve shown in Figure 1.

In Figure 1, note that the peak HRR is only an instantaneous value. The peak HRR is not the average HRR during the peak (or fully developed) phase of the

Table 2. Fuel Inventories for Mobile Equipment

	Heating Value (kJ/kg)	Combustible Mass (kg)			
		AD55 Truck	Iveco Bus	R170 LHD	Five light vehicles
Tires	32,599	4,663	435	3,520	472
Diesel fuel	45,101	960	300	990	871
Hydraulic oil	31,168	258	-	125	108
Equiv. diesel for interior	45,101	-	15	-	-
Hoses and flammables	32,599	466	44	352	47

Table 3. Calculated Fire Parameters Based on Fuel Load and Peak HRR

		AD55 Truck	Iveco Bus	R1700 LHD	Five light vehicles
Total heat of combustion	GJ	217	29	174	59
Total mass fuel	kg	6,319	786	4,961	1,475
Weighted average	MJ/kg mixed fuel	34.4	37.5	35.0	39.7
Peak HRR mass	Mass kg/hr	6,825	849	5,358	1,593
Tires & hoses	% by mass	81%	61%	78%	35%
Diesel fuel	% by mass	15%	38%	20%	59%
Hydraulic oil	% by mass	4%	0%	3%	7%
Equiv. diesel for interior	% by mass	0%	2%	0%	0%
Peak HRR/GJ ratio	ratio	0.3	0.3	0.3	0.3
Peak HRR	MW	65	9	52	18
Growth phase	mins	5.6	5.6	5.6	5.6
Peak phase	mins	30.6	30.6	30.6	30.6
Decay phase	mins	44.4	44.4	44.4	44.4
Total fire duration	mins	81	81	81	81

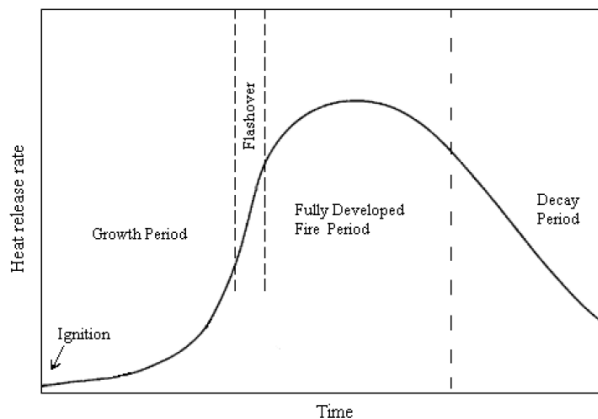


Fig. 1. Idealized stages of a fire [18]

0.3 m/s (low) and increased during the fire to 2.2 m/s due to natural ventilation pressure (NVP).

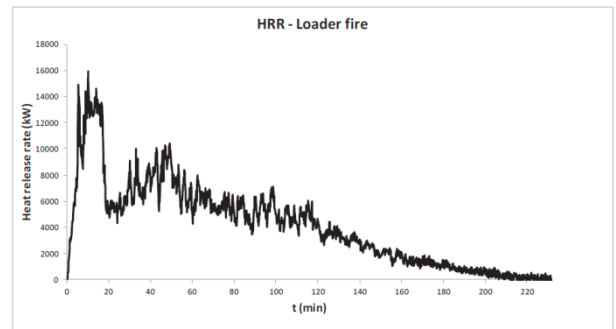


Fig. 2. HRR-time curve for 14 tonne payload Toro 501DL LHD fire [11]

Despite the above conceptual curve there are many ways a fire can start and progress which can alter the peak HRR and the duration of a fire. For example, Hansen [11] conducted a full-scale underground fire on a 14 tonne payload Toro 501 LHD (total calorific value on board of 76 GJ) and obtained the HRR-time curve in Figure 2. In this fire the front two tires did not catch fire so the total heat produced was estimated at 50.5 GJ. If the tires had burnt the peak HRR and fire duration would have increased somewhat. The peak HRR was 16 MW although this is an instantaneous spike; if averaged over 10 minutes, the peak could also be interpreted as closer to 13 MW. The peak occurred within only a few minutes of ignition.

The total fire duration was more than three hours although there was a pronounced decay after two hours. Note that the ratio of peak (16 MW) to average (7 MW) HRR was about two during the first two hours and the ratio of peak HRR (MW) to calorific value burnt (50.5 GJ) was about 0.3. Wind speed over the fire started at

Hansen also conducted a full-scale underground fire on a drill rig (total calorific value 32.5 GJ) and obtained the HRR-time curve shown in Figure 3. The peak HRR was measured at 29 MW although, like the LHD, this is an instantaneous spike. The peak could also be interpreted as closer to 25 MW over 3 or 4 minutes (still roughly double that of the LHD) or even lower at about 18 MW if the “peak” is defined as a 10 minute period. The peak HRR in this case occurred approximately 20 minutes after ignition. The total fire duration was approximately 70 minutes (average HRR 9 MW) although there was a pronounced decay immediately after the peak was reached. Note that the ratio of peak to average HRR was also about 2 (18/9) and the ratio of peak HRR (MW) to calorific value burnt was about 0.55 (18/32.5). Wind speed over the fire started at 1.3 m/s and increased during the fire to about 2.6 m/s at the peak HRR. Minimum oxygen downwind was 17.2% and maximum CO₂ was 2.37%. The CO was not measured during to an instrumentation problem.

Note that both the Hansen tests were conducted under relatively low wind speeds (2.2 to 2.6 m/s at the peak HRRs).

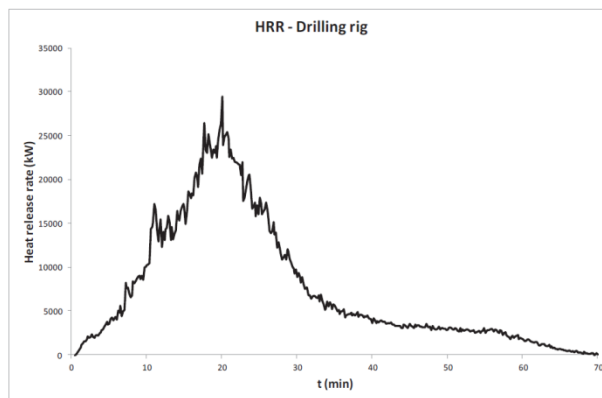


Fig. 3. HRR-time curve for drill rig fire [11]

Further measured data on large single vehicle fires was obtained from the Handbook of Tunnel Fire Safety [2] and is shown in Table 3 which is also in line with data presented by Duckworth [7].

Table 3 Measured fire data on heavy goods vehicle (HGV) fires in tunnels [2]

Tunnel Cross Section (m ²)	GJ	Wind Speed (m/s)	Peak HRR (MW)	Time to Peak HRR (min)	Peak HRR /GJ
32	240	3	202	18	0.84
32	129	3	157	14	1.22
30	87	3 to 6	128	18	1.47
32	152	3	119	10	0.78
32	67	3	67	14	1.00
50	19	1 to 2	26	12	1.37
50	10	1.5	13	16	1.30
50	10	5.3	19	8	1.90
50	10	5	16	8	1.60
30	63	0.7	17	15	0.27
50	35	unknown	23	48	0.66
Avg				16.4	1.1
Max					1.90
Min					0.27

Wind speed has an effect on the intensity (HRR) of a fire, particularly during its growth phase (increasing how fast the fire grows). Very high wind speeds can potentially increase the duration of the growth phase (i.e. slow down the growth of the fire) by taking heat away from the fire. During the peak phase, the peak HRR values increase as wind speed increases up to about 3 to 5 m/s, beyond which the HRR does not further increase. See Figure 4 where “k” is the ratio of HRR in the actual fire to the HRR that the same fire would produce in the open (i.e. on surface) with no artificial airflow over it.

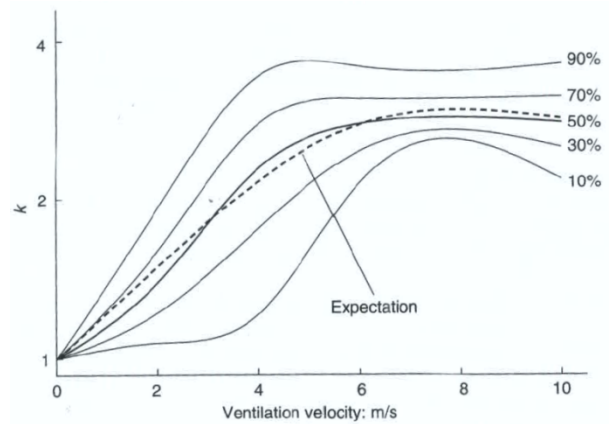


Fig. 4. Influence of wind speed on peak HRR values in a tunnel fire [2]

Although experimental work has shown that there is an interdependency between velocity over the fire, the HRR, and NVP much of the discussion in the literature assumes NVP developed by an underground fire is small, overall airflow in the tunnel remains relatively constant, and that it does not change direction over the fire. This is frequently not the case in underground metal mines where the geometry of the deposit typically required operation over a range of elevations that are interconnected via travel ways. This geometry allows for conditions to develop that would otherwise not be experienced in a controlled lab test setting, and which increase the difficulty of accurately modeling the behavior of the fire. Brake [3] notes:

“In some cases, the NVP produced by the fire results in choking to the point where further development of the fire is oxygen constrained; however, not enough NVP may be produced to actually reverse the flow over the fire.”

Where a fire does reverse direction, the low oxygen content of the products of combustion (POCs) now being drawn back over the fire decreases the heat output from the fire which reduces the NVP that the fire is producing. In some cases, this loss of NVP causes the flow over the fire to revert to its original direction. In certain circumstances an unstable situation may develop where the airflow reverses back and forth. In practice, rollback could potentially develop in such a scenario drawing fresh air to the fire and potentially restarting the sequence.

This highlights one of the more important limitations of computerized modeling of fires. The model is an approximation of the behaviors of a more complex system, and that the model has limitations (e.g. one-dimensional flow) that give the results a degree of uncertainty.

4.2 Variations on HRR Curves

Due to the inherent variability in the exact behavior of tunnel fires, different simplifications of the HRR curve are used in practice. These are intended to give a numerical representation of the fire for a single set of assumed parameters.

4.2.1 “Traditional” Method

In this approach the calorific value of each of the combustibles in the fire are summed, and an average heat release rate is calculated depending on the duration of the fire. The important thing to note is that in this technique the HRR is constant through the duration of the fire. See Figure 5.

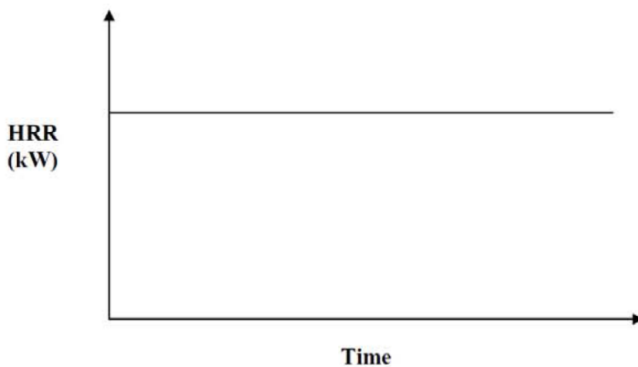


Fig. 5. “Traditional” HRR model [14]

4.2.2 Duggan Method

This method superimposes together the heat release rate of each individual fuel type (based on the exposed area for that fuel and its ‘measured’ HRR per exposed surface area). It is assumed that all these materials ignite at the same time. See Figure 6.

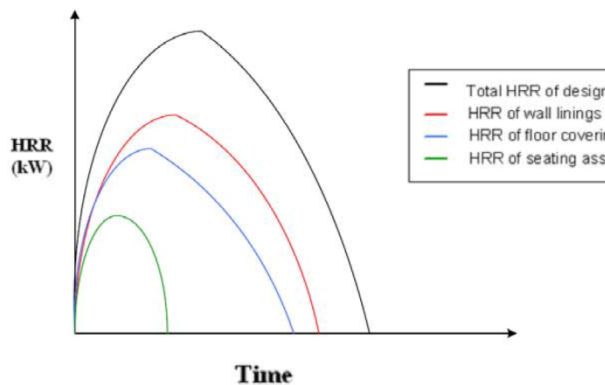


Fig. 6. Duggan HRR model [14] (Sic)

4.2.3 “Realistic” Method

The “Realistic” method is similar to the Duggan method but allows the various fuels to commence burning at different times. This results in a HRR as shown in Figure 7. Note that this is approaching the “true” HRR shape of Figure 1.

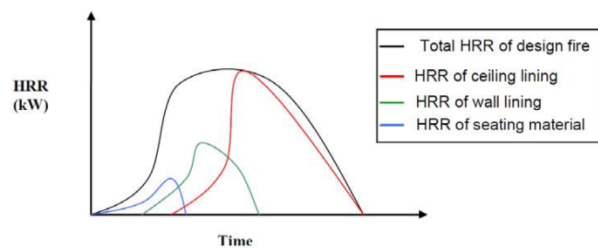


Figure 7 “Realistic” HRR model [14] (Sic)

4.2.4 “t-squared” Method

In the “t-squared” method the HRR in both the growth period (from t_0 to t_1) and the decay period (from t_2

to t_3) increase and decrease as square of the time respectively as shown in Figure 8. This is the type of curve used by MFIRE 2.30 [18].

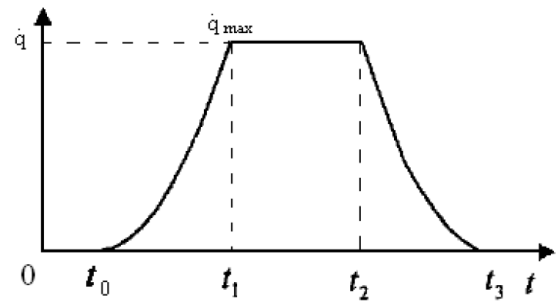


Figure 8 “t-squared” HRR model [18]

4.2 Critical Points of Understanding

Some important points can be noted from the discussion in section 4.1, with respect to underground mine fire scenarios:

- The duration of the growth phase can range from a few minutes to 20 minutes.
- There is usually only a small quantity of the total fuel on board that is consumed in the growth phase (before flashover).
- Unless the fire is manually extinguished, most fires have a long tail (decay period) in which a substantial fraction of the total fuel is burnt.
- The ratio of peak HRR to total calorific content in mobile equipment fire varies from 0.3 to 1.9 (LHD) and 0.3 to 0.77 (drill rig) for the underground mine fires measured by Hansen.
- This ratio will be higher where there is more surface area for fuel to burn (e.g. 4 separate tires plus diesel fuel plus hydraulic fuel) compared to less surface area to burn (e.g. ANFO stacked in pallets).
- The peak HRR is just a very short duration spike which is to be expected in underground mine fires which, after flashover, are usually (but not always) limited by available fuel rather than airflow (oxygen).
- A more representative value is probably the “average” HRR during the “fully-developed” phase of the fire.
- The shape of the HRR in the “fully developed” phase can vary significantly.
- The “dividing line” between “fully developed” and “decay” phases can be rather arbitrary.
- The peak HRR increases with increasing wind speed up to about 3 to 5 m/s.
- The HRR-time curve can change very significantly if natural ventilation pressures make dramatic changes to airflow over the fire, or cause airflow reversals at the site of the fire.

4.3 Modified t-squared method

Based on the information gathered from a review of the different methods of constructing HRR curves a new approach was implemented for this study. The main item of focus was the relationship between the ‘peak’ HRR and the total energy content of the fuel. The following parameters were used in defining the HRR curves for heavy equipment in the modeling conducted.

- A growth phase in which 5% of the fuel is consumed
- A peak phase in which 55% of the fuel is consumed
- A decay phase in which 40% of the fuel is consumed
- A peak HRR (MW) of 0.3 x calorific content (GJ)

These parameters were selected based on representation of the phenomena observed in more recent full scale experiments reviewed in the literature, however they could be adjusted. The definition of the peak HRR as a function of the total fuel content implies that the intensity of the fire is limited by the mass of the objects burning. This agrees with intuitive notions and research observations of burning objects. The more massive the burning object is, and implicitly the greater the surface area, the greater the potential intensity (maximum HRR) of the fire.

By linking each phase to a fraction of the total fuel load the development and decline of the fire can be adjusted by the modification of the mass fractions. This again agrees with intuitive notions of burning objects. An object that catches fire and rapidly increases in intensity will have little time to burn fuel as compared to the same object taking a longer time to reach the 'fully developed' phase.

No manual 'throttling' of the fire is required in HRR curve itself. Based on the oxygen consumption rates of the fuels input into VentFire, the software calculates the amount of oxygen 'consumed' by the fire and reduces the heat output when insufficient oxygen is available (e.g. air passing back over the fire during a flow reversal). What constitutes insufficient can be adjusted by the user from the default values should it be desired or necessary.

This method is similar to the "t-squared" approach but modified so that the growth and decay phases are linear increases and decreases in HRR making them more directly compatible with the VentFire software package. This is the approach used in the modelling reported in this paper. See Figure 9.

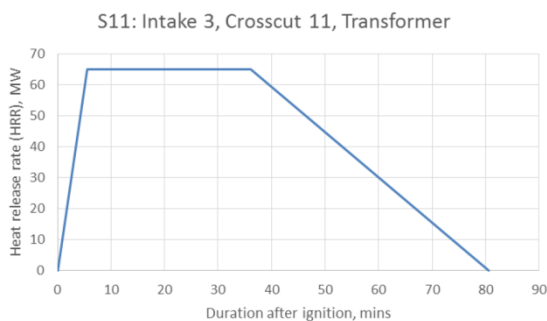


Figure 9 Modified "t-squared" HRR mode

This approach addresses some of the challenges and known limitations associated with the implementation of other HRR curves:

- The use of a linearized HRR rather than smooth curves, thereby simplifying the input to the model.
- The definition of phases by the amount of fuel consumed rather than a time phase. While the two are inherently linked the definition by fuel consumption appears to lead to greater understanding by personnel.

- The definition of the peak HRR as a plateau in the HRR rather than a point value. While the peak HRR is in fact a point value in a real fire the use of a period of constant output better defines the general behavior of the fire.
- Boundaries between phases (while still arbitrary) are well defined.
- No manual throttling of the fire for insufficient oxygen. In other words, Ventfire would automatically adjust the HRR "design fire" curves where there was insufficient oxygen to support the HRR.
- No assumptions required about the times of ignition for various fuel components of a fire, which can vary widely depending on the actual conditions and flame spread.

5. Building the Models

The DOZ mine has undergone numerous expansions in production capacity, initially starting at 25 ktpd and expanding to the current 80 ktpd operation. With each of these expansions in production capacity the primary ventilation system has been added to accordingly, increasing from an original design flow of approximately 970 m³/s [5] to the present system specification of approximately 2,300 m³/s. During this 6 year period of production expansion, 5 ventilation surveys of the combined DOZ and MLA ventilation systems were completed.

In addition to the DOZ ventilation surveys, ventilation surveys have been completed in the other underground mines to verify design values, system operating points, and provide models for planning. In total, 11 ventilation surveys of the underground workings were completed in roughly a 10 year span with notable overlap as drift dimensions and primary fan arrangements were changed. This presented a large amount of relevant data to review before being integrated into a model that was suitable for modeling fires.

With the long history of ventilation surveys and modeling at PTFI site engineers have traditionally used resistance per length (R/L) values and incompressible flow models for day to day operations. While this is adequate for the vast majority of work, incompressible flow does not work with the thermodynamic calculations that are used in fire modeling. Additionally, the use of R/L data for resulted in many drifts being modeled as 1 m diameter 'pipes' with dimension specific R/L values rather than rectangular drifts. This presented an issue for the correct calculation of velocities and spread times, as well as giving incorrect area/perimeter data for thermodynamic modelling.

Resistance data from past ventilation surveys was checked against mine survey pickups from the period to determine the correct drift dimensions and corrected to standard density from the mine density. Where drift dimensions had changed and new pressure/volume (P/Q) survey data was not available (such as the benching of intake drifts), as-built dimensions with k-factors suggested by historic data [8] were used.

Because of the large extent of the existing underground workings it was not considered feasible or cost effective to conduct a complete P/Q survey of all areas. The ventilation department at PTFI undertakes monthly volumetric surveys of the working areas in the

mines as well as primary fan operating points. Measured resistances were compiled into a VentSim model that was then checked against fan operating points, monthly volumetric surveys, and field P/Q data at critical points. These checks were used to further refine the model to more closely represent current operating conditions at the mine. Issues were encountered with respect to pressure closure in the models, however flows in primary ventilation and access drifts correlated well with recent measurements. This was considered an acceptable trade-off, with the goal of accurately modeling the spread of contaminants in primary infrastructure rather than focusing on complete model closure.

6. Survivability Criteria

In addition to the computer modeling of the fire itself, basic survivability criteria was also evaluated with consideration of the altitude above sea level and parameters that could be reasonably modeled with the software. It is important to note that the survivability criteria excludes persons caught directly in the fire (i.e. passengers on a bus that catches fire), persons trapped in by a fire, and rescue personnel who have special training and equipment.

Factors that were considered in the development of survivability criteria included the concentration of toxic gasses, low oxygen, high temperatures, and reductions in visibility which could impede safe egress. Factors specific to the PTFI mines include high altitude, prevalence of smoking with the underground workforce, and use of oxygen generating SCSRs.

Underground workings at PTFI extend from 2500 to 4000 m above sea level as a result of the multiple lifts of caving that have occurred and the interconnection of existing ventilation infrastructure to new workings. Studies have shown that preferential bonding between carbon monoxide and hemoglobin may be made worse by increased altitude [15]. Additionally, the prevalence of smoking in the underground workforce increases the likelihood that workers will already have an increased concentration of carbon monoxide in their blood compared to a non-smoking counterpart.

With the increased perceived risk to workers, the dosage limit for carbon monoxide in this study was reduced to 18,000 ppm-minutes, or the equivalent of an average exposure of 600 ppm for 30 minutes (a Fractional Effective Dose (FED) of 0.5 [16]). This is half of the NIOSH Immediate Danger to Life and Health (IDLH) value of 1200 ppm over 30 minutes or 36,000 ppm-minutes at sea level [13].

While the reduction of the partial pressure of oxygen at altitude due to low barometric pressure is effectively the same as a reduction in the concentration of oxygen at sea level, in this fire scenario modelling the controlling toxic gas will be either carbon monoxide or carbon dioxide. Therefore a nominal limit of 18% oxygen was chosen without introducing any additional complications.

PTFI makes use of SAVOX 30 minute oxygen generating self-rescuers. These units are rated by the manufacturer at 30 minutes for a person of roughly 75 kg who is calm. Testing has shown that the capacity of the unit can be used up in as little as 15 minutes depending on the size and duress of the individual. In line with best practice, the de-rated capacity of 15 minutes was assumed for tenability. This would be in addition to the time that a person could travel safely after the SCSR was consumed, before the potential exposure to other hazards would become debilitating.

Poor visibility during egress reduces travel speed, makes it difficult to locate the egress, increases the hazards during egress (e.g. vertical openings or tripping) and has a major psychological impact. Paveley [14] notes that at visibility of 7 m egress is relatively unhindered, but at 3 m most persons will not enter smoke. Travel speeds and distances under self-rescuer have been reported earlier by Brake and Bates [4] and these were used in this study. WB and DB limits were from an examination of the Oxford index by Leithead and Lind [12] and from British Coal work on mine rescue brigadesmen as reported by Varley [17].

7. Analysis of Results

With the large number of scenarios a concise method of evaluating and communicating the results of each simulation was required. For reporting purposes a table approach was used, where each of the potentially toxic agents were listed along with the accepted "Safe" limit for egress. Values that approached or exceeded the applicable limit were flagged for review. This is shown in Table 4. Obviously gas toxicity is only relevant where the person is not wearing a self-rescuer, the self-rescuer is not operating properly, or the duration of exposure exceeds the self-rescuer time limit. In some instances the toxic concentration was still increasing when the model was terminated for practical reasons, but in most cases the peak value was reached (PVR).

In addition to the table approach video animations were generated using the Dynamic Simulation tool in VentSim. These illustrated the time dependent spread of POCs using color coding of branches as well as annotative values at key monitoring points. Emphasis was placed during presentation on the fact that these scenarios were only potential outcomes based on probable estimates, and that given the number of unknowns about actual fires there was no way to predict exactly how smoke would spread through the underground workings. Of course, an advantage of modelling is that once a fire is "set up", then running the simulation with different assumptions is a straightforward exercise.

Both the tabular and video forms of presentation were well received by site personnel and in many cases either reinforced existing thoughts on the risks presented by fire or clarified the potential extents of contaminant spread throughout the underground complex.

Table 4. Example Summary Fire Modeling Results¹

	“Safe” limit for egress	Monitoring Point Peak Values					
		Fire: Iveco Bus in DOZ Intakes	MP02: XC 11 Shop	MP11: DOZ Magazine	MP05: DOZ Lunchroom	MP19: DOZ Intake Fuel/Lube Shop	MP30: DOZ Haulage
Critical Agent	Peak Value Reached?	PVR	PVR	PVR	PVR	PVR	PVR
Carbon Monoxide	600 ppm by volume	153	Nil	90	2	88	2
Oxygen	18% by volume	20.8	Normal	20.9	Normal	21.0	21.0
Carbon Dioxide	40,000 ppm (4%)	131	Normal	930	390	920	390
Visibility	10 m	4.8	Normal	8.2	25	8.4	25
Temperature, WB	32° C	18.8	Normal	11.4	10.5	11.1	11.0
Temperature, DB	60° C	35.7	Normal	11.4	10.7	11.12	11.2
Comments ²	Safe	Safe	Safe	Safe	Safe	Safe	Safe

¹ Note that these are based on 30 minute exposures, and therefore (with exception of visibility, WB and DB) are only relevant where the exposure is longer than 30 minutes AND the individual is not wearing a SCSR or is inside a refuge. Visibility, WB and DB will impact on survivability even if wearing SCSRs.

² Locations labeled as “Safe” imply that there is no information collected from the simulation which exceeded the established limits, and that it is likely that a person could safely egress the area indicated without suffering long term effects from exposure to the conditions shown.

8. Outcomes at Site

With the renewed focus on the risk presented by underground fires PTFI has established an Underground Fire Risk Control and Response Management Committee. This committee consists of individuals from industrial hygiene, mine rescue, ventilation, safety, ore flow, electrical maintenance, and underground maintenance along with subject matter experts from other departments who are tasked with updating standard operating procedures, policies, standards, and emergency response plans. In addition, the group performs work area audits for compliance with internal standards and applicable regulations.

Acknowledgements

The authors would like to acknowledge the numerous individuals at PTFI who participated in the risk assessments, underground inspections, and data collection that supported this work. The authors would also like to thank management at Freeport-McMoRan and PTFI for supporting the publication of this paper.

References

- [1] Bajus M and Olahová N, 2011. Thermal Conversion of Scrap Tyres. *Petroleum & Coal* 53 (2).
- [2] Beard A and Carvel R, 2011. *Handbook of Tunnel Fire Safety*. ICE Publishing, 2nd ed.
- [3] Brake, D J, 2013. Fire Modelling in Underground Mines using Ventsim Visual VentFIRE Software. Proc 2nd Australian Mine Vent conf (Chalmers D, ed). Adelaide. The AusIMM, pp 265-276.
- [4] Brake, D J and Bates G P, 1999. Criteria for the design of emergency refuge stations for an underground metal mine. Proc AusIMM 304(2):1-8.
- [5] Calizaya F and Mulyadi A, 1998. A New P.T. Freeport Mine Ventilation System – Basic requirements (25,000 TPD Plan). SME Preprint No. 98-57. Littleton, CO: SME.
- [6] Duckworth I, Casten T, Loomis I, 2010. Understanding fire risk at P.T. Freeport Indonesia. 13th US/N. American Mine Ventilation Symp. Hardcastle & McKinnon (eds).
- [7] Duckworth I, 2008. Fires in vehicular tunnels. 12th US/N. American Mine Vent Symp. Wallace (ed).
- [8] Duckworth I, Loomis I, Prosser B, 2012. Fifteen years of resistance data collected at Freeport Indonesia. 14th US/N. American Mine Ventilation Symp. Calizaya & Nelson (eds).
- [9] Egan M, 1990. Summary of Combustion Products From Mine Materials: Their Relevance to Mine Fire Detection. USBM Information Circular 9272. US Dept of Interior.
- [10] Haack A (ed), 2010. Design Fire Scenarios. Tech report Part 1. European Thematic Network Fire in Tunnels.
- [11] Hansen, R and Ingason, H, 2013. Full-scale fire experiments with mining vehicles in an underground mine. Research Report 2013:2. Mälardalen University.
- [12] Leithead C S, Lind A R. 1964. *Heat Stress and Heat Disorders*. London, Cassell.
- [13] NIOSH, 1995. Immediately Dangerous to Life or Health Concentrations (IDLH) Chemical Listing and Documentation of Revised IDLH Values (as of 3/1/95). <http://www.cdc.gov/niosh/idlh/intridl4.html> accessed on 29 January 2015.
- [14] Paveley, 2010. Reference design. Section 24—Fire and Life Safety. Engineering Brief. Sydney Metro.
- [15] Penney, D.G., ed. (2000) *Carbon Monoxide Toxicity*, CRC Press, 560 pp, Chp 6, McGrath J.J. of Texas Tech University School of Medicine
- [16] Purser D, 1989. Modelling Toxic and Physical Hazard in Fire. *J Fire Safety Science*. Vol 2 pp 391-400.
- [17] Varley F, 2004. A study of heat stress exposures and interventions for mine rescue workers. SME annual meeting (Feb 23-25, 2004). SME.
- [18] Zhou, L., Luo, Y., 2010, “Application of the t-squared fire model in MFIRE,” Proc. of 13th United States/North American Mine Ventilation Symposium Hardcastle & McKinnon (Eds.)

Managing the Risk of Spontaneous Combustion in Underground Coal Mines

John W. Grubb^a, Jürgen F. Brune^a, R. Karl Zipf, Jr.^a, Gregory E. Bogin, Jr.^a, Jonathan A. Marts^a,
Richard C. Gilmore^a, Saqib A. Saki^a, Samuel A. Lolon^a

^aColorado School of Mines

Spontaneous combustion events leading to thermal runaway and a fire or explosion in underground coal mines are low in frequency but can have severe consequences in terms of both fatalities and business losses. The propensity of coal seams to spontaneously combust and reach thermal runaway varies and is not fully understood. Recent fire events at Elk Creek Mine in Colorado and Deer Run Mine in Illinois and possibly the Soma Mine in Turkey are reminders that the spontaneous combustion risk remains insufficiently mitigated in some sectors of the coal mining industry.

Coal mine regulations in the United States are minimal in addressing the spontaneous combustion risk in underground mines. As compared to other coal mining risks, the regulations offer minimal prescriptive solutions for managing this risk. In other countries where spontaneous combustion events have been more prevalent in occurrence including the loss of life and business, the regulations and accepted practices are more aggressive in addressing the risk.

Findings from five years of computational fluid dynamics (CFD) modeling conducted at Colorado School of Mines (CSM) under funding from the National Institute for Occupational Safety and Health (NIOSH) have shown that explosive gas zones can exist in a longwall gob in areas where the spontaneous combustion of coal could develop into an ignition source. This paper will summarize measures that have been collected from a leading practice survey for assessing and managing the spontaneous combustion risk. A deductive modeling approach will be presented that can assist mine management teams in their cost-benefit analysis of the extent of implementation of a management program for the risk.

As a minimum, mine management teams must assess the risk of a spontaneous combustion event at their mine. Once technically informed regarding the propensity of their coal and the potential existence of contributing factors, the decision on how extensive a preventative program is required can be made. A major spontaneous combustion event is infrequent but the consequences can be devastating.

Keywords: coal, spontaneous combustion, prevention, cost-benefit analysis

1. What Is Spontaneous Combustion of Coal?

Spontaneous combustion of coal has been and continues to be a risk to be managed in many underground coal mines throughout the world. The mixture of high methane emission levels and spontaneous combustion is a particularly hazardous situation. Spontaneous combustion has led to numerous mine closings, temporary and permanent, and has resulted in mine disasters with multiple loss of life as presented in Table 1. The phenomenon of the spontaneous combustion of coal is not fully understood, but most literature agrees that it is an exothermic reaction of coal with oxygen that initiates at ambient

temperature and can proceed to thermal run-away and a fire event as long as there is a continued supply of oxygen and the heat is not dissipated [1-3]. The most poorly understood stage of spontaneous combustion occurs at ambient temperature and during the early period of heating. It appears that oxygen combines with the carbon compounds of coal to produce “peroxy-complexes” during this early phase. Chemical activity of absorbing oxygen and emitting heat continues around these complexes as the chain reaction continues [1]. The tendency and speed with which different coals chemically react to oxygen and create heat defines their propensity to spontaneously combust [4].

Table 1. Significant spontaneous combustion events over the last four decades [5, 6]

Year	Mine	Consequences
1972	Box Flats (Australia)	18 fatalities
1975	Kianga (Australia)	13 fatalities
1991	Ulan (Australia)	Loss of US\$60 million
1994	Moura No. 2 (Australia)	11 fatalities
1997	Galatia (U.S.A.)	Loss of US\$38 million
1997 - 1998	North Goonyella (Australia)	Loss of longwall
1999	Sanborn Creek (U.S.A.)	Mine idled 9 months
2000	West Elk (U.S.A.)	Loss of US\$60 million
2003	Southland (Now Austar – Australia)	Loss of Longwall – mine closed / sold
2013	Elk Creek (U.S.A.)	Loss of longwall – mine closed
2014	Deer Run Mine (U.S.A.)	Loss of 3 weeks of production

2. Spontaneous Combustion Risk in Underground Coal Mines

The generally accepted definition of risk is the probability of a loss. Risk can be further explained as the combination of the probability that an undesired event will occur and the consequences that result due to the undesired event. The best solution for managing risk is to eliminate the possibility that the event will occur. For instance, to eliminate the risk of health hazards associated with asbestos, the use of asbestos has been eliminated in most applications. The elimination of a risk is usually not entirely possible. The risk can be managed by reducing the probability or frequency and / or mitigating the consequences of the undesired events. Spontaneous combustion of coal is a risk that is inherent in the nature of coal with some coals having a higher susceptibility or propensity to spontaneously combust than other coals. As long as coal is exposed, the three ingredients of the fire triangle of fuel, oxygen and heat may be present so the risk of spontaneous combustion can only be mitigated and not eliminated. If spontaneous combustion develops and a critical velocity of air with sufficient oxygen to sustain the reaction but insufficient velocity to dissipate the sustaining heat continues, eventually a thermal runaway or fire develops.

Leading up to and since the formation of the Mine Enforcement and Safety Administration (MESA) followed by its successor the Mine Safety and Health Administration (MSHA), there have been no fatalities from spontaneous combustion events in coal mines in the United States. Therefore, federal regulations, which have been primarily based on past accidents and disasters, are brief in addressing measures to be undertaken to secure the safety of mines regarding the risk of spontaneous combustion. The provision addressing the spontaneous combustion hazard states “for mines with a demonstrated history of spontaneous combustion, or that are located in a coal seam determined to be susceptible to spontaneous combustion, the approved ventilation plan shall specify the following: 1) Measures to detect methane, carbon monoxide and oxygen concentrations during and after pillar recovery, and in worked-out areas where no pillars have been recovered, to determine if the areas must be ventilated or sealed. 2) Actions that will be taken to protect miners from the hazards of spontaneous combustion. 3) If a bleeder system will not be used, the methods that will be used to control spontaneous combustion, accumulations of methane-air mixtures, and other gases, dusts, and fumes in the worked-out area.” (*Part 75 of Title 30 of the Code of the Federal Register, Paragraph 334f* [7]) In the following paragraphs (*Paragraphs 335 - 339*) the requirements for seal construction and monitoring are stated. These requirements are necessary for a progressively sealed approach to managing the spontaneous combustion risk, and the strength of the seal is increased if monitoring of the atmosphere behind the seal is not undertaken.

The combination of the accumulation of methane at explosive levels and spontaneous combustion is a particularly hazardous situation. In current research funded by NIOSH since 2009 Colorado School of Mines (CSM) researchers have modeled the air flow and gas distribution in the gobs of longwall panels utilizing CFD and information from partnering mines [8, 9]. This work has shown that explosive gas zones (EGZs) can develop in the gob area in both bleeder-ventilated and progressively sealed gobs. Figure 1 displays the location of the EGZs in the bleeder-ventilated and progressively sealed models respectively. The EGZ for the bleeder-ventilated gob surrounds the caved area as the atmosphere transitions from the bleeder to the high methane gob. For the inertized, progressively sealed gob the EGZ is located just inby the back return paralleling the face. Examination of the EGZ locations reveal that the EGZs overlap porous zones in the gob as indicated on the plan views in Figure 1, particularly the void that surrounds the rubble material in the bleeder-ventilated gob and the porous area just inby the back return in the progressively sealed gob. These porous zones, if coal is present, can have the necessary characteristics for spawning a spontaneous combustion event – sufficient oxygen yet insufficient air flow to dissipate the heat. The overlapping zone for the progressively sealed panel is relatively smaller in volume than the zones for the bleeder-ventilated panel.

3. Spontaneous Combustion Preventative Measures

In 2008 a dissertation entitled “Preventative Measures for Spontaneous Combustion in Underground Coal Mines” was completed by John Grubb at Colorado School of Mines [5]. As a part of the research for this dissertation a leading practice survey was conducted with visits to 28 mines and agencies in the United States, Australia, Germany, New Zealand and Poland. Contacts and literature searches were extended to China, India, South Africa and the United Kingdom. Additions and modifications to the list of leading practices have continued since 2008 to the present. The leading practices are classified into seven categories detailed as follows:

- 1) Understanding the spontaneous combustion behavior of the coal seam mined – Leading practices for understanding the propensity and contributing conditions of spontaneous combustion in a particular mine include a) accurate and detailed record-keeping of spontaneous combustion events at the mine both on the surface and underground, b) propensity testing of splits of the seam mined as well as rider seams above and below the seam in zones of caving and fracturing, c) confirmation of the propensity by at least two methods, d) medium to large scale laboratory gas evolution testing to identify signature gases, e) annual small scale and large scale testing as appropriate for changes encountered, f) use of

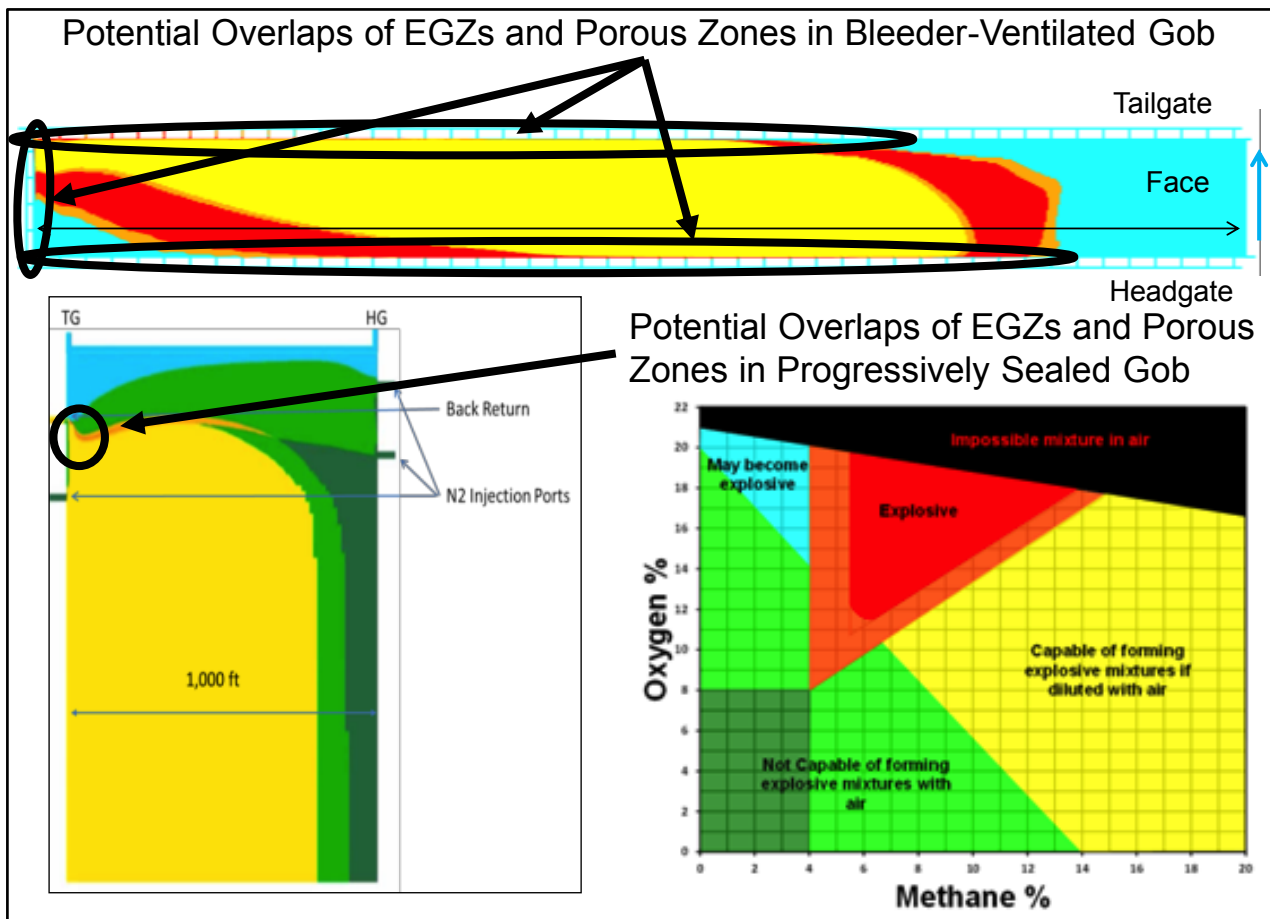


Fig. 1. View at top is longwall panel with bleeder ventilation with potential overlap of EGZs and porous zones on the edges of the gob outlined [8]. View at bottom left is longwall panel with reduced potential overlap of EGZ and porous zones on the edges of the gob when leading practices of sealing, nitrogen inertization and back return are applied [9]. Color code for EGZ for both views is per the Coward Triangle as shown at bottom right. (Elements reprinted with permission)

numerical modeling or an expert system such as NIOSH's SponCom 2.0 to identify contributing factors [10] and g) intensive evaluation of geological and other contributing factors.

2) Detection and monitoring – Leading practices for detecting and monitoring for spontaneous combustion include a) widespread use of hand-held gas meters for detecting carbon monoxide by all workers, b) real-time carbon monoxide, oxygen and methane detection in conveyor, return, intake, bleeder and face areas, c) tube bundle collection and analysis system behind seals and at other critical locations, d) weekly bag samples taken behind seals, e) two or more chromatographs on site for reliable signature gas identification, f) mine control center for data collection, interpretation and communication, g) comprehensive trigger action response plan based on monitored data, h) infrared imaging devices for checking potential hot spots, i) temperature monitoring in pillars subject to high pressure differentials and j) daily patrol in bleeders if utilized.

3) Pressure differential management – Measures for managing pressure differentials are primarily for the purpose of keeping air movement below the critical velocity in areas of potential spontaneous combustion. Leading practices include a) off-setting the fan from

the coal face for drift mines, b) rigorous ventilation modeling and application to minimize the mine operating pressure, c) induced inertized balance chambers at panel seals with a barometric pressure management system, d) seal design, construction and inspections to minimize air leakage across gob and other abandoned areas and e) forward installation and development to main and district air shafts to minimize the mine operating pressure and pressure differentials across sealed areas.

4) Sealing and inertization – The establishment of progressively sealed ventilation for gob areas is a strategy for preventing spontaneous combustion in these areas. Leading practices for sealing and inertizing these areas include a) sealing active panels as mining retreats and inducing inertization with nitrogen, b) use of nitrogen as required to maintain inertization of mined-out and sealed panels, c) use of gob vent boreholes to manage methane levels in the actively ventilated work areas, d) use of a back return where geotechnically feasible to maintain a non-explosive buffer zone between an EGZ in the sealed gob and the working face and e) use of CFD modeling to design and plan the sealing and inertization program.

5) Inhibitors and sealants – Inhibitors of the spontaneous combustion reaction or sealants to stop the

air flow and therefore oxygen supply to the reaction have been used for many years. Leading practices include a) applying (wax-walling) a mixture of water, bentonite, an inhibitor, an emulsifier and a stabilizer or a patented product to the surface of coal pillars that are subject to a high pressure differential and b) applying a sealant to pillars abutting seals of gob areas.

6) Extinguishment planning – Leading practices for extinguishment planning include a) extension of the basic fire-fighting plan to include resources and training of employees for combatting a spontaneous combustion fire, b) timely up-dating of plans for location of seals including remote seals constructed from boreholes so that deployment time is minimized and c) purchase or pre-arrangement of resources, such as nitrogen or water source and other materials for sealing and inertization or flooding of the mine in case of a fire.

7) Other – Other leading practices for spontaneous combustion prevention include a) comprehensive training for all employees and officials in the spontaneous combustion risk and the mine trigger action response plan, b) procedures and training for hot work permits, c) no underground stowage of coal-bearing materials, d) to the extent possible minimizing the amount of coal not mined in longwall panels and if left behind develop a plan for minimizing the risk, e) maximizing the mining rate to minimize the duration of any coal in the critical velocity zone of the gob, f) plugging of methane drainage and other boreholes and g) minimum use of wood including wood supports that may come in contact with spontaneously combusted coal.

Some of the leading practices as applied to a longwall mine lay-out are presented in Figure 2. The leading practices for spontaneous combustion and the net present value of their costs are listed in Table 2.

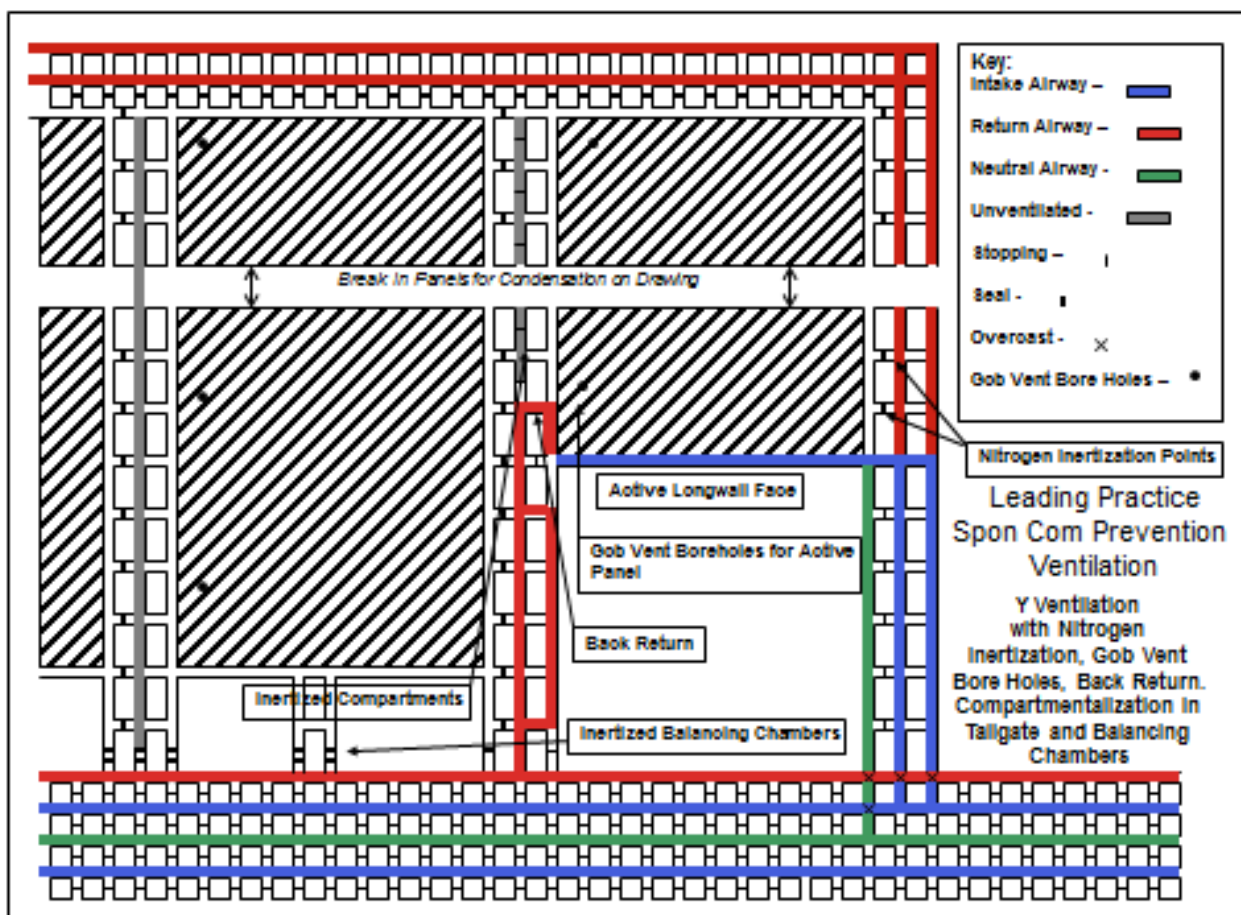


Fig. 2. Longwall mine lay-out with leading practices applied.

Table 2. List of and net present value (NPV) of costs in \$000's for leading and selected practices for spontaneous combustion prevention for the typical coal mine – discount rate of 10% applied on a constant dollar basis.

Leading Preventative Measures by Category	NPV for Costs of All Leading Practices	NPV for Costs of Selected Practices
<u>Understanding the behavior of the coal –</u>		
Initial and annual propensity testing on representative coal samples for the mine including seam splits and upper and lower riders	\$247	\$247
Numerical modeling or expert system utilized	\$161	\$0
Intensive geological evaluation and application of solutions	\$238	\$238
<u>Detection and monitoring –</u>		
Hand-held meters widely distributed	\$104	\$104
Real-time detectors in returns, intakes and face areas	\$731	\$731
Scheduled weekly bag sampling and chromatograph analyses	\$966	\$966
Tube bundle collection and analysis system	\$960	\$960
Data collection, management and interpretation system	\$3,219	\$2,065
Infrared imaging device	\$9	\$9
Temperature monitoring in applicable high pressure pillars	\$15	\$15
Daily patrol in bleeders	\$809	\$0
<u>Pressure differential management -</u>		
Fan off-set from coal face	\$1,126	\$1,126
Maximum operating pressure set and maintained	\$13,365	\$0
Rigorous ventilation system monitoring	\$54	\$54
Inertized balance chambers at panel seals	\$317	\$317
Forward installation and development to air shafts	\$2,153	\$0
<u>Sealing and inertization -</u>		
Progressive sealing of mined-out panels	\$10,387	\$10,387
Nitrogen inertization with membrane plant	\$5,866	\$5,866
Gob vent boreholes in panels for methane control	\$1,848	\$1,848
Inertization planning with CFD or equivalent method	\$135	\$0
<u>Inhibitors and sealants -</u>		
“Wax-walling” of applicable high pressure pillars	\$60	\$2
Sealant application to pillars abutting seals	\$83	\$83
<u>Extinguishment planning -</u>		
Pre-arranged and / or contracted fire-fighting resources	\$28	\$28
Preparatory seals designed and partially constructed	\$68	\$68
<u>Other -</u>		
Comprehensive training in spontaneous combustion prevention	\$315	\$315
No underground stowage of coal-bearing materials	\$208	\$208
Plugging of methane drainage holes	\$93	\$93
Minimum wood in the gob	\$7,166	\$0
Total -	\$50,731	\$25,730

4. Cost-Benefit Analysis

To present the costs versus the benefits of implementing the leading practices for prevention of spontaneous combustion, a net present value model was developed for a typical mine in western Colorado – a single longwall operation with two development units [5]. Table 2 displays the net present costs for the leading practices that were collected for spontaneous combustion prevention in underground coal mines as applied to the model mine. These costs were for additional equipment, materials and labor required to implement the leading practices as compared to the base case with no leading practices applied.

No one mine was found in the survey that applied all of the practices. Most mines that were surveyed did not forward develop and install fans ahead of longwall

panels to minimize operating pressures. Most mines continued to utilize some wood for secondary support but restricted the use in zones of high susceptibility to a spontaneous combustion event. Some mines inertized sealed gobs only when triggered by high signature gas levels taken by bag samples or a tube bundle outlet behind the seals. Some mines progressively inertized behind the seals without any detection system. These and other approaches reduced the cost of prevention without loss of much of the benefits. Even with full implementation of all leading practices, there is no full assurance that there will not be a spontaneous combustion event, but the track record is successful for mines that have diligently implemented at least one or more of the practices in each of the categories as presented. Practices were selected as displayed by the costs in the last column of Table 2 and were applied in

the cost-benefit analysis for the model mine. These practices were some of the most commonly applied practices found in the survey. Figure 3 summarizes the costs for selected leading practices by category of

preventative measure. The total net present cost of a program utilizing the selected leading practices is \$25.7 million or \$0.23 per ton over the life of the mine.

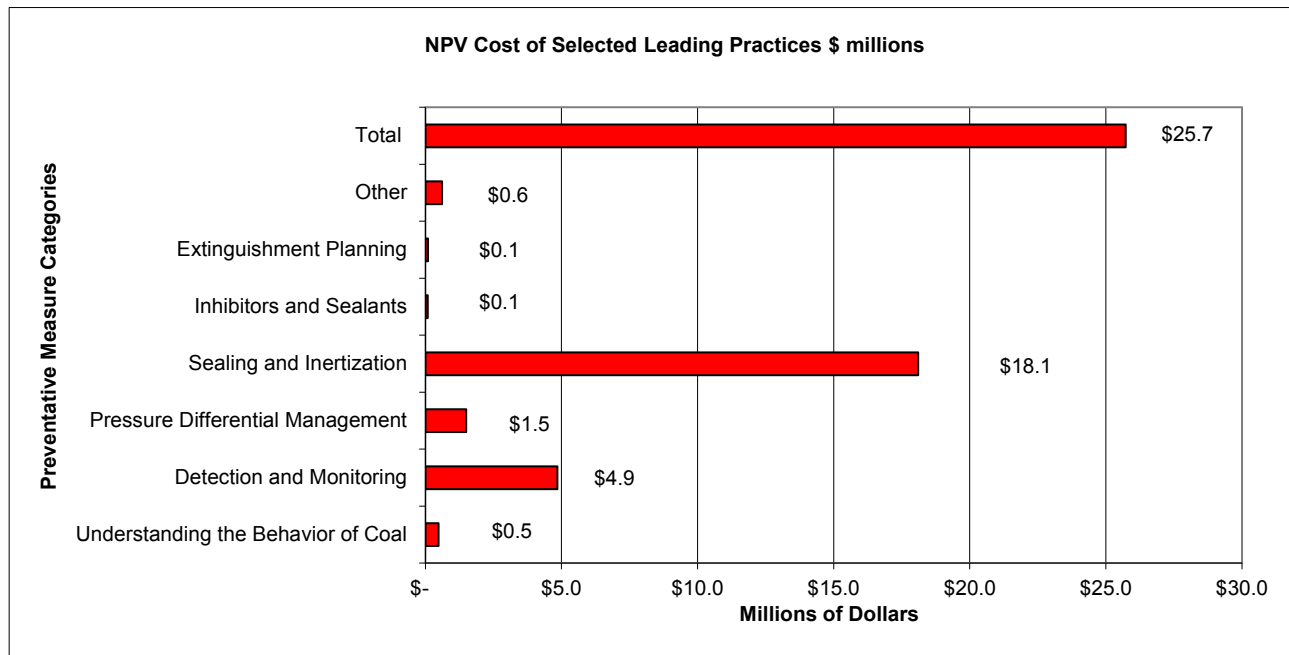


Fig. 3. Summary of spontaneous combustion preventative costs by category

To evaluate the benefits of implementing the leading practices, the cost of spontaneous combustion events of varying degrees of severity were calculated. Although they have and can occur, fatalities were excluded from the cases. Utilizing the same mine model, the net

present cost of the events displayed in Table 3 were computed applying the material costs presented in Table 4. It is assumed labor from the mine would be used to combat the fire.

Table 3. Description of spontaneous combustion events for which net present costs were computed. The assumptions column describes the scope of the costs applied to each event.

Spontaneous Combustion Event	Assumptions for Calculating Costs
All Events	No lay-offs of employees unless noted, no customer penalties, no costs applied for reputational loss
1 Month Lost Production	Sealing, no inertization, delayed development during stoppage
3 Months Lost Production	Sealing, inertization of half panel or equivalent, delayed development during stoppage
6 Months Lost Production	Sealing, inertization of one and half panels or equivalent, delayed development during stoppage
9 months Lost Production	Sealing, inertization of two and half panels or equivalent, delayed development during stoppage
12 Months Lost Production	Sealing, inertization of four panels or equivalent, delayed development during stoppage
6 Months Lost Production and Reserves and Loss of LW Equipment	Sealing, loss of 50% of panel, inertization of up to one and half panels, wait for development and equipment
9 Months Lost Production and Reserves and Loss of LW Equipment	Sealing, loss of 75% of panel, inertization of up to three panels, wait for development and equipment
12 Months Lost Production and Reserves and Loss of LW Equipment	Sealing, loss of 75% of panel, inertization of up to four panels, wait for development and equipment
Loss of Mine and Business	Loss of mine and reserves at no salvage value for surface facilities and equipment, employee severance after 6 months

Table 4. Assumed costs for fire-fighting of spontaneous combustion events - \$ millions for totals.

Item	Unit Cost	Unit	1 Month	3 Months	6 Months	9 Months	12 Months
Cryogenic nitrogen	\$0.0692	Per cubic foot	\$0	\$3.5	\$10.4	\$17.4	\$27.8
Nitrogen transportation	\$0.0512	Per 1000 cubic foot - mile	\$0	\$0.8	\$2.3	\$3.9	\$6.2
Nitrogen tanks - 2	\$3,444	Per day	\$0	\$0.1	\$0.2	\$0.4	\$0.6
Nitrogen pump / vaporizer	\$20,432	Per day	\$0	\$0.4	\$1.3	\$2.1	\$3.4
Underground constructed seals	\$27,000	Each	\$0.2	\$0.2	\$0.2	\$0.2	\$0.2
Remote seals	\$400,000	Each	\$0	\$0	\$3.6	\$3.6	\$3.6
Shaft / borehole / drift caps	\$165,800	For 2 shafts, 5 drifts and 20 boreholes	\$0.2	\$0.2	\$0.2	\$0.2	\$0.2
Fire-fighting mobilization	\$5,000	Per day	\$0.2	\$0.5	\$0.9	\$1.4	\$1.8
Total			\$0.6	\$5.7	\$19.1	\$29.2	\$43.8

Three graphs (Figures 4 through 6) were constructed to demonstrate the net present cost of spontaneous combustion prevention utilizing the selected leading practices with the cost of specific spontaneous combustion events over a 20-year life of the model mine. Figure 4 featured spontaneous combustion events for which the net present costs included the loss of production for periods of one month, three months, six months, nine months and twelve months and the associated fire-fighting costs for the respective events. Figure 5 events were more serious events for which the net present costs were for lost production for six, nine and twelve months respectively plus the net present costs of lost reserves for one panel, lost longwall equipment, additional development and associated fire-fighting costs for the respective events. Figure 6 shows the loss of the mine at net present value due to a spontaneous combustion event in various years during the mine life.

In the first two years represented on the graphs the mine is in development with no longwall production. In the third year investment in the longwall equipment occurs and longwall production begins. In the 11th year

recapitalization of the longwall occurs. These cash flow events as well as factoring for the time value of money accounts for the ups and downs in the net present cost of the various spontaneous combustion scenarios.

Review of the three graphs concludes that production losses alone must be early in the mine life and of six or more months of duration to justify implementation of the selected leading practices. Not only lost production but also delays of development impact the cost of these events. Partial implementation can certainly be justified if losses of three months or more can be avoided. Losses that extend to longer term production, the loss of longwall equipment and the loss of some reserves justify the application of the selected leading practices. Certainly loss of the mine and the business justifies implementation of the selected leading practices. The net present cost of an event is highest in the first longwall panel when the sunk cost for the mine is high but also when the learning curve for the mine management team is also high.

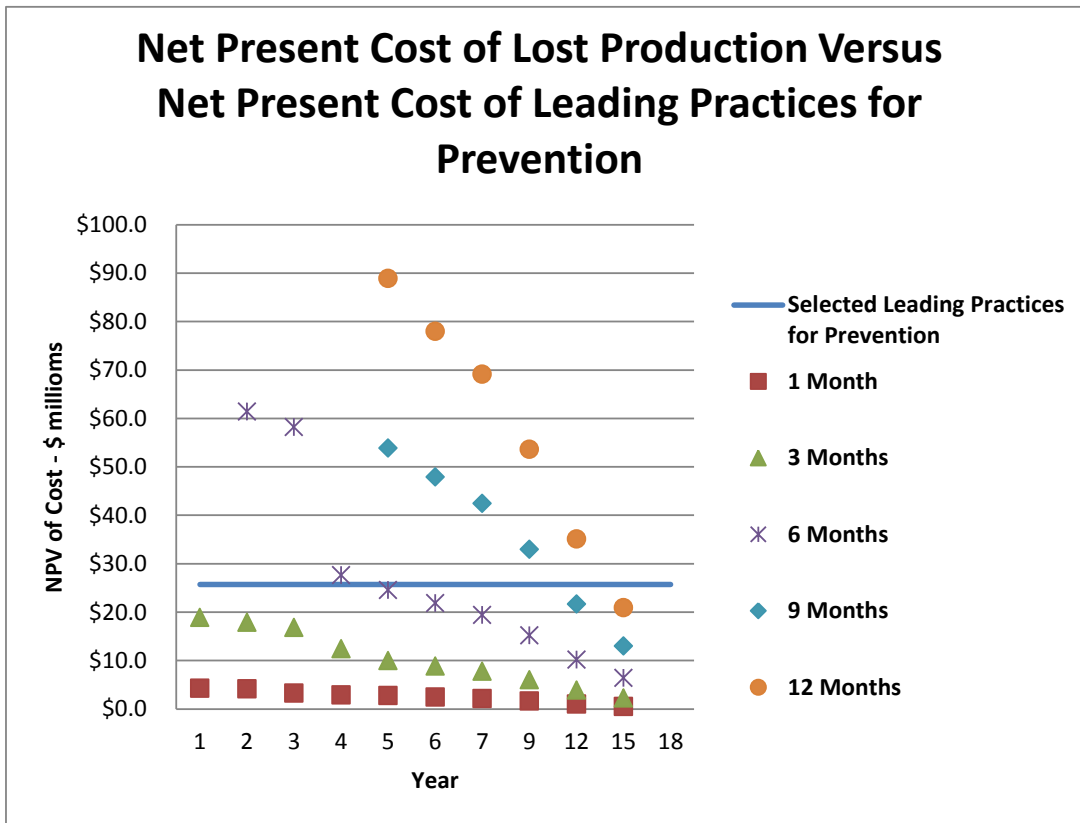


Fig. 4. Comparison of net present cost of spontaneous combustion events with losses of production of varying lengths with net present cost of prevention applying selected leading practices.

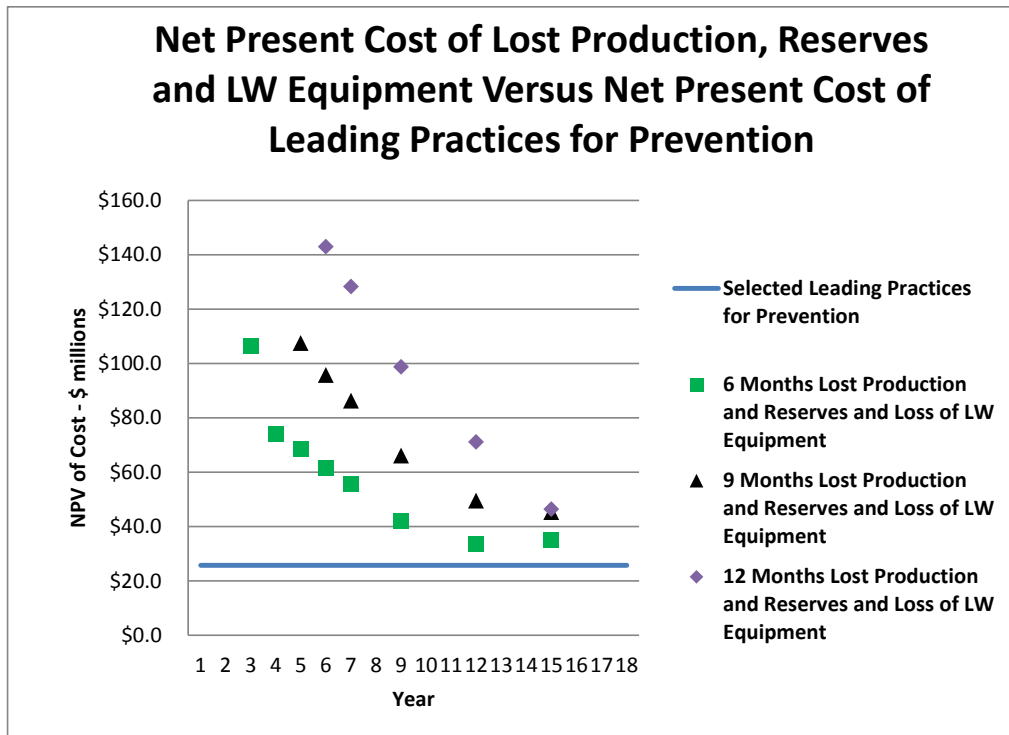


Fig. 5. Comparison of net present cost of spontaneous combustion events with losses of production, reserves in one panel and longwall equipment with net present cost of prevention applying selected leading practices.

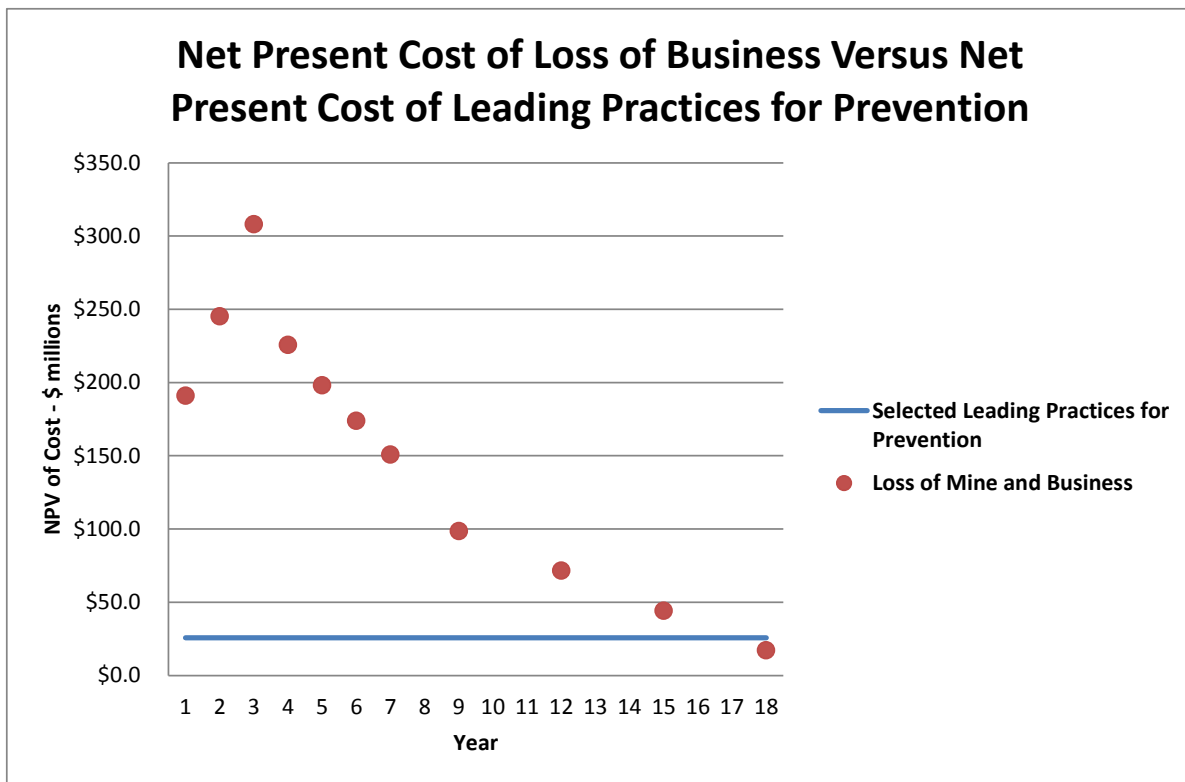


Fig. 6. Comparison of net present cost of spontaneous combustion events resulting in loss of business with net present cost of prevention applying selected leading practices.

The graphs are a visual summary of the scope and size of the investment for preventing a low frequency, serious consequence event and the potential business outcomes over the life of the mine if the event were to occur. Safety concerns that can lead to fatalities must be taken into account in addition to the business considerations. The ultimate decision will depend upon the risk tolerance of the management team. The graphs are a tool for facilitating the decision-making process.

5. Conclusions

Coal mines with a medium or high propensity for spontaneous combustion should consider leading practices identified in the world-wide survey to supplement the mine safety regulations in the United States for the prevention of a spontaneous combustion event. As demonstrated by CFD modeling at CSM, leading practice implementation can reduce the size of the EGZ in a critical velocity zone and minimize the risk of a methane explosion initiated by spontaneous combustion. Leading practice implementation can be justified in a business case for the prevention of losses of production, equipment, reserves and possibly the mine. The low frequency of spontaneous combustion events in underground mines places prevention often outside immediate consideration for mine management, but the serious consequences both from the safety and business aspects should drive a program for implementation of selected leading practices in each of the seven prevention categories. Cost of the program for a typical western U.S. mine is \$0.23 per ton.

Acknowledgement

The authors and researchers at Colorado School of Mines gratefully acknowledge the financial support from NIOSH under contract number 200-2009-31409 and the cooperation of mines in the western United States for providing the data for CFD model construction and validation and the mines and agencies who have openly shared their spontaneous combustion prevention practices.

References

- [1] S.C. Banerjee, Spontaneous combustion of coal and mine fires. A.A. Balkema. Rotterdam. (1985) 168 pages.
- [2] D. Cliff and C. Bofinger, Dissemination of information on spontaneous combustion. Australian Coal Association Research Program. (1998) 180 pages.
- [3] A.C. Smith and C.P. Lazzara, Spontaneous combustion studies of U.S. coals. United States Bureau of Mines (1987) 28 pages.
- [4] B. Beamish, J. Theiler, J. Saurat, and T. Levi, Commissioning adiabatic oven testing – an inter-laboratory comparison. 14th Coal Operators' Conference, University of Wollongong, The Australasian Institute of Mining and Metallurgy & Mine Managers Association of Australia, (2014) 324-329.
- [5] J. Grubb, Preventative measures for spontaneous combustion in underground coal mines. Thesis, Colorado School of Mines, Golden, Colorado, December (2008)

- [6] Coal Age; Aug 2014, Vol. 119 Issue 8, p5
- [7] *Federal Underground Coal Mine Safety Standards* – 30 CFR, Part 75, Paragraphs 334f through 339
- [8] R. Gilmore, J. Marts, J. Brune, G. Bogin, J. Grubb, and S. Saki. CFD modeling explosion hazards - bleeder vs. progressively sealed gobs. 10th International Mine Ventilation Congress (IMVC), Sun City, South Africa (2014).
- [9] J. Marts, R. Gilmore, J. Brune, G. Bogin, J. Grubb, and S. Saki. Accumulations of explosive gases in longwall gobs and mitigation through nitrogen injection and face ventilation method. 6th Aachen International Mining Symposia (AIMS), Aachen, Germany, June (2014).
- [10] NIOSH, Spon Com 2.0, Office of Mine Safety and Health Research, Pittsburgh, Pennsylvania, August 2011.

CFD Analysis of Truck Fire in Large-Opening Limestone Mine

Changwoo Lee^a, Hyogyu Kim^b

^a*Dong-A University, Busan, Korea*

^b*Jusung-GNB Engineering, Seoul, Korea*

In Korea, most of the large open-pit limestone mines have started to go underground due to depletion of the easily-accessible high-grade ore body near the surface and also the strict environmental regulations. The most common underground mining method adopted is room-and-pillar mining with large openings, 10~15m wide and 6~9m high with approximately 10mx10m pillars. Since the domestic limestone deposits are steeply dipped, rampways are developed to connect drifts, 8~20m apart in vertical distance. Almost all equipment deployed for development and mining operations such as drilling, explosive charging, loading, hauling, scaling, rock bolting, etc are diesel-powered. As the mining working sites are getting larger and going deeper, risks of diesel engine fire is becoming one of the major concerns.

This paper aims at analyzing the characteristics of diesel engine fire: propagation of the smoke and heat and impacts of the ventilation in large-opening limestone mines with a CFD tool. Under the scenario with ignition of a 25-ton diesel truck at the working face reaching the maximum heat release rate of 30MW after 600 seconds, factors influencing the fire spread are evaluated. Dependences on the roadway dimension and the ventilation capacity studied, while behavior of smoke layers, choking effects, safety of emergency egress with respect to temperature and visibility are analyzed. The fundamental goal is to provide information about the large mine fire development at the face for designing the mine fire safety plan and ultimately protect the workers as well as the mine facilities.

Keywords: limestone mine, truck fire, CFD analysis, fire propagation, mine egress

1. Introduction

In 2013, over 88 million tons of limestone was produced in Korea from more than 100 mines. Nearly 72 percent of the output was consumed by the cement manufactures and the steel makers consumed 12 percent. Most of the limestone in Korea used to be mined at open pit mines, but depletion of easily accessible reserves along with high standards of environmental regulation have forced most of surface operators to close down their surface operation and go underground. Local limestone seams are steeply folded and faulted. The most common mining method adopted locally is room-and-pillar mining method with rampway of 10~13% grade. Horizontal drifts with vertical elevation difference of 8~20m are developed toward the strike direction, sometimes extending several km's. The number of drifts in each level depends on the width of seam; generally 2~5 drifts. Rooms are developed as large openings, 10~15m wide and 6~9m high mostly with 10mx10m pillars.

Development and mining operations depend heavily on the diesel equipment: drills, loaders, scalers, trucks, utility vehicles, rock bolters, etc. At a face developed in sequence of drilling, blasting, loading and hauling, approximately 1,000 tons of limestone are produced by one blasting operation, a load to fill 40~50 trucks since 25-ton truck is the most common type deployed in local mines. At a working face, a number of diesel equipment are running simultaneously; in general, one loader, one utility vehicle, three trucks and one excavator can be seen. This intense use of diesel equipment raises concerns over the diesel-engine fire. Fires on diesel-powered mining equipment typically are known to arise from leaking high-pressure hydraulic lines which can spray a heated mist of highly combustible liquid onto an ignition source, such as a hot exhaust manifold or turbocharger [1].

This paper studies the outcome of the worst safety

scenario with a heavy 25-ton truck fire equal to 30MW heat release rate; the behavior of fire including spread speed and temporal propagation of temperature, smoke concentration and visibility in the study domain are analyzed. And effects of the drift dimension and the fan capacity on the behavior of smoke and hot airstream are also evaluated. This paper ultimately aims at providing fundamental information for designing fire safety plan for evacuation and equipment protection.

2. Fire Scenario

2.1 Fire characteristics

Incidents such as truck roll-over on the rampway, roof fall or oil spill can result in mine fires where a truck is completely destroyed. Most of the mine fires are oxygen-rich fire where the oxygen content downstream the fire remains relatively high [2]. Once initiated, the fire goes through three different stages: growth stage, peak intensity stages and decay stage. Fire size is of vital importance in the understanding of the behavior of mine fires. Even though there have been extensive fire test in vehicle tunnels to evaluate fire load for ventilation and safety design, there are few studies on full-scale fire test of the mining vehicles in underground mine. The most recent test results can be found in Hansen and Ingason [3]. They conducted a series of full-scale fire experiment with a wheel loader and a drilling rig at a dolomite mine and approximate dimensions of the mine drifts in the test area were 6 x 8m. The maximum heat release rate of the wheel loader was found to be 15.9MW at 11 minutes after ignition while that for the drilling rig was 29.4MW at 21 minutes. The air velocity measured at the time of ignition was 0.02~0.4m/s for the wheel loader test, while the velocity was in the range of 1.2~1.4m/s for the drilling rig fire. Meanwhile, NFPA 502(2008), standards for tunnel[4] recommend 70~200MW for goods tuck. But, 25-ton truck fire load

is not defined in all of the NFPA standards for fire prevention and control in mines[5] [6].

British standard PD 7974-1:2003[7] provides guidelines for the fire growth and size within the enclosure of fire origin as well as enclosures to which the fire has subsequently spread. According to PD 7974-1:2003, the basic fire growth curve follows a time-squared function: $Q = \alpha t^2$ where Q , α and t are heat release rate, constant and time in second. For the 25-ton heavy truck with peak fire size of 30MW, recommended α is 0.0833 and this means the characteristic fire growth time to the peak fire size is 600 seconds. In this paper, maximum heat release rate from a 25-ton truck fire and time to reach the peak are assumed to be 30MW, slightly bigger than the drilling rig fire size in Hansen and Ingason[3] and 600 seconds respectively. Fire size is considered to be linear between consecutive points in time as plotted in Fig. 1. Table 1 shows the truck fire characteristics. This paper takes into consideration radiation loss to the drift wall. Memorial test report[8] states that 30% of the total heat is dissipated to the tunnel wall via radiation and about 70% of this dissipation occurs within 61m of the fire 30%.

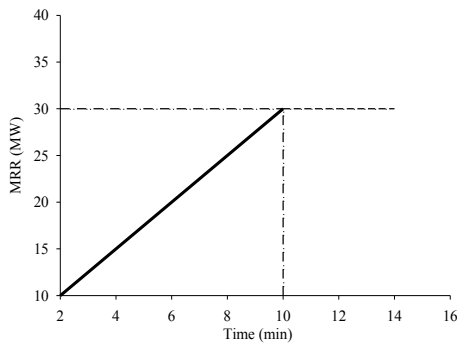


Fig. 1. Fire growth curve for a 25-ton truck

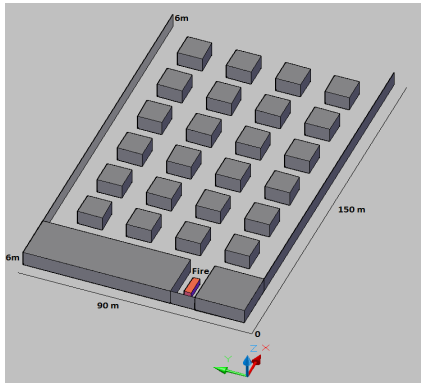


Fig. 2. Entry development face with five entries in Scenario I (150x90x6m)

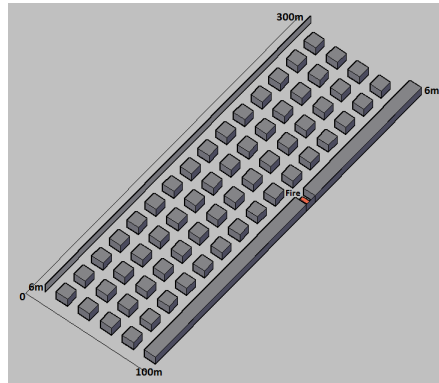


Fig. 3. Cross-cut development face with five entries in Scenario II (300x100x6m)

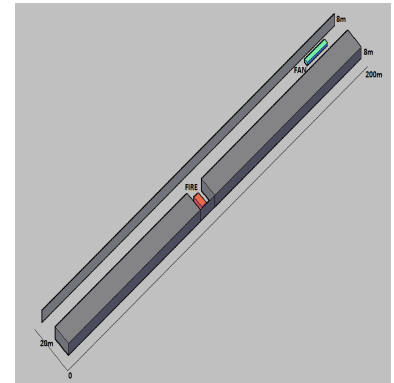


Fig. 4. Cross-cut development face with single entry in Scenario III (200x20x8m)

Table 1. Fire source characteristics

Category	Characteristics
Fire load	30MW
Fire source dimension	2.5m(w)x8.7m(L)x3.5m(H)
Stoichiometric ratio	14.5
Heating value	4.26E+07 J/kg
Fuel consumption rate at 600 seconds	0.704 kg/s
Radiation loss fraction	30%

2.2 Analytical tool and fire scenarios

The computational fluid dynamics tool used in this paper is SOLVENT(version 1.0) developed by Innovative Research, Inc. and Parsons Brinckerhoff as a result of the Memorial Tunnel Ventilation Test Program administered by Commonwealth of Massachusetts from 1993 to 1995[9]. While the model is designed as a computational tool for the simulation of fluid flow, heat transfer and smoke transport in a single-tube tunnel, it can be applied to mine ventilation system with one layer

Depending on the study topic, three different sites are designed for CFD analysis with 10x10m pillars and 10m wide drifts. Scenario I includes the site in Fig. 2 describing a entry development face in five-entry level where a truck catches on fire; two different cases with entry height of 6m and 8m are taken into consideration. In Scenario II and III, fire sources are located in cross-cut development faces in 6m-high five-drift and 8m-high single-drift level as plotted in Fig. 3 and 4, respectively. All the drifts are assumed to have the ventilation resistance (k) of 0.016 kg/m³ which is the typical value measured in local limestone mines.

The characteristics of fan installed are presented in Table 2 and the cases for CFD analysis are summarized in Table 3.

Table 2. Fan characteristics in Scenario I, II and III

Category	Characteristics
Fan type	Axial-flow fan
Fan dimension	L:2m Φ :1m
Fan thrust	250N and 500N in Scenario 1&2, 100N and 200N in Scenario 3
Fan operation	Normal and reverse operation
Fan installation on entry cross-section	Fan center location: 3m high, 2m from pillar sidewall in Senario I & II, 6m high and 4m from pillar sidewall in Scenario 3

Table 3. List of the CFD analysis cases

Scenario	Case	Descriptions
I	1	Without fan operation at 6m-high face
	2	250N fan operated at 6m-high face
	3	250N fan operation reversed at 6m-high face
		500N fan operated at 6m-high face
	4	500N fan operation reversed at 6m-high face
		Without fan operation at 8m-high face
II	1	Intake air velocity of 0.2m/s
	2	Intake air velocity of 0.5m/s
III	1	100N fan operation
	2	200N fan operation

2.3 Analysis of Scenario I

In this scenario, the effects of roadway dimension and local fan operation on the fire development and propagation are analyzed. In addition, reversal of fan operation in the exhaust mode is also simulated for the comparison with the blowing mode. Fig. 5 and 6 show growth of the maximum temperature at the fire source. After the simulation time of 600 seconds, the maximum temperature at the 30MW fire source in the 8m-high drift in the domain shown in Fig. 2 increases to 394.6°C without fan operation, but when a fan is turned on from the ignition in the blowing mode, the increasing rate is higher and the temperature reaches 529.0°C and 553.2°C for the fan thrust of 250N and 500N, respectively. If the fan operation is reversed, the maximum fire source temperatures for the two fans are relatively reduced by 74.7°C and 61.3°C.

In the 6m-high drift, the maximum temperatures at the source are higher than in the 8m-high cases; the differences are 145.7°C for natural spread, 128.0°C for 250N fan and 28.1°C for 500N. This indicates that roadway cross-sectional area influences the fire development and smaller area tends to have higher temperature at the fire source; the same relation was observed in Lonnermark and Ingason [10].

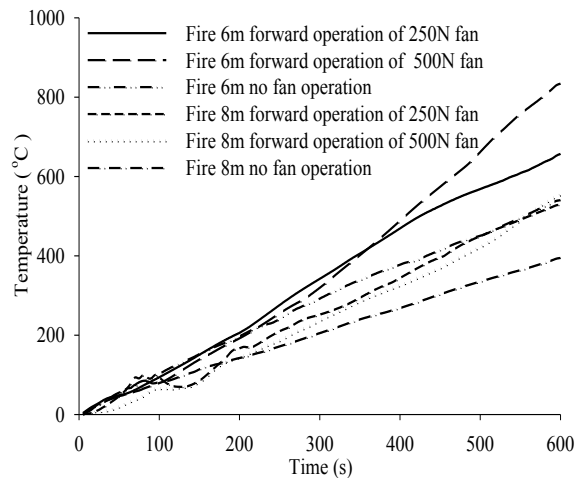


Fig. 5. Fire temperature rise at source

Operating a fan in blowing mode during fire increases the airflow rate toward the fire and subsequently enhances the fire development. When the fan operation is reversed, temperature increases at lower rate after the lapse of 400 seconds as shown in Fig. 6.

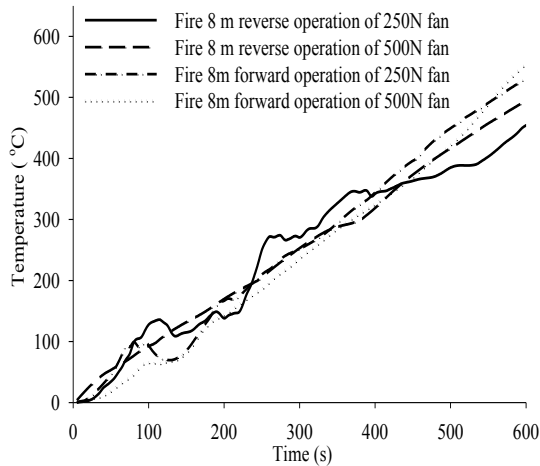


Fig. 6. Fire temperature rise during forward and reverse operation of the fan

Soot, clusters of solid carbon spheres, is the most important constituent of fire smoke that obscures visibility. Based on the fire test in a vehicle tunnel with No.2 distillate fuel oil, an empirical model for visibility was proposed as follows:

$$L_v = \frac{0.67}{(\rho_{air} W_{smoke} W_{soot} 1000)^{0.69}}$$

where L_v is visibility in m, ρ_{air} is air density in kg/m³, W_{smoke} is mass fraction of smoke, and W_{soot} is mass fraction of soot[8]. NFPA 130(Standard for fixed guideway transit and passenger rail systems) recommends a maximum short-term exposure of 60°C for 100% water-vapor saturated air. And the visibility distance to unlighted objects is recommend to be maintained within 10m in NFPA 130[11]. Those NFPA recommendations are used in this paper to define the boundaries of the hot airstream, over 60°C, and the dense smoke of which visibility is less than 10m.

Hot airstream, temperature of over 60°C and dense smoke, visibility of less than 10m expands rapidly in the upper layers above the fire sources, while at the height less than the fire height the propagation is limited only within one cross cut from the sources as shown in Fig. 7 and 8. In Fig. 9, temperature and smoke concentration profiles are plotted on the vertical cross section in the middle of the 8m-high drift with the fire source. The hot

airstream layer near the ceiling is well maintained and expands gradually without fan operation. But after the blowing fan operation, hot air stream is confined near the source and expands at a much lower rate, while in case of fan reversal, the hot airstream layer is moving near the ceiling at higher speed than in the blowing mode, but at lower rate than in case of the natural spread. This result implies that natural spread of the hot layers near the ceiling should not be disturbed and the exhaust fan operation is more efficient to reduce the temperature near the fire source and disperse the fire smoke safely for securing safe escape path.

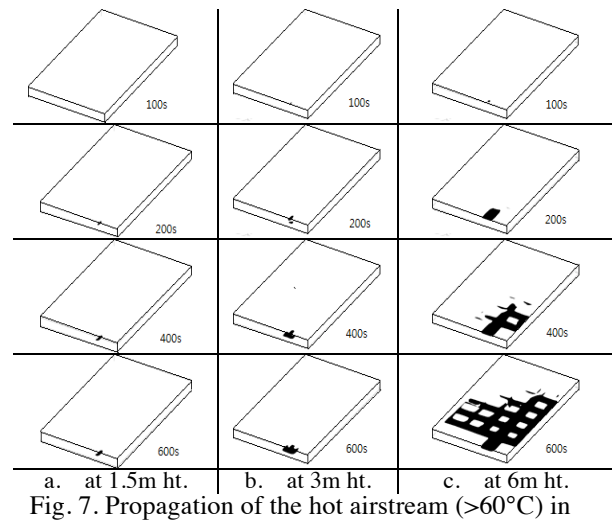


Fig. 7. Propagation of the hot airstream (>60°C) in

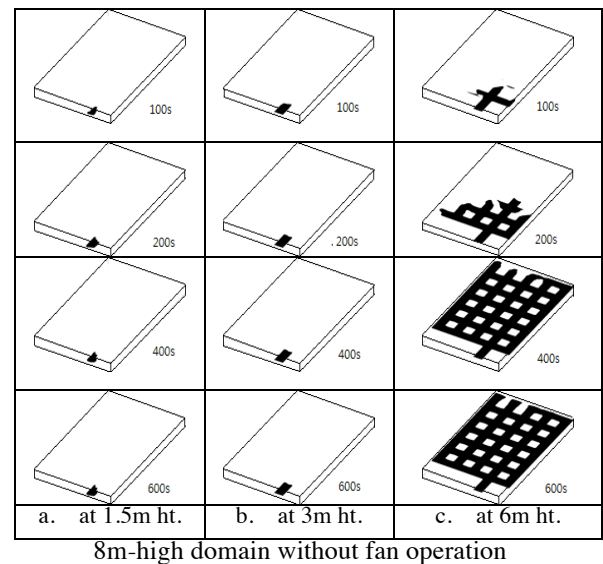
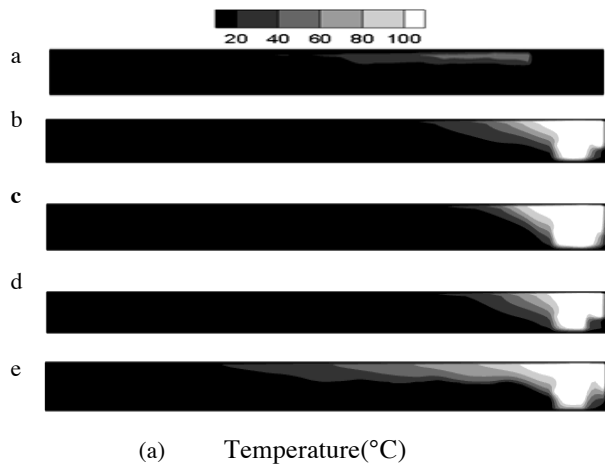
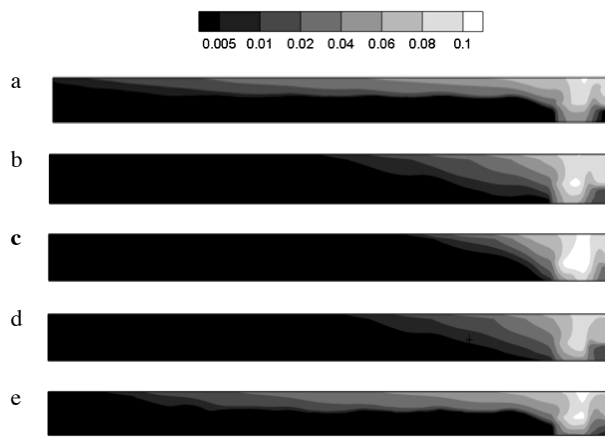


Fig. 8. Expansion of the low visibility region (<10m) in 8m-high domain without fan operation



(a) Temperature(°C)



(b) Smoke concentration((kg smoke/kg mixture))

Fig.9. Temperature(°C) and smoke concentration profiles at 300 seconds on the vertical cross section in the drift with the fire source(a: without fan, b: with 250N blowing fan, c: with 250N exhaust fan, d: with 500N blowing fan, e: with 500N exhaust fan)

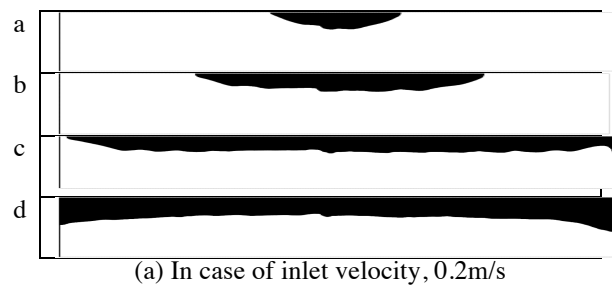
2.4 Analysis of Scenario II

If the ventilation capacity is weak, the upper layers of heated air and smoke may flow in the direction opposite to the ventilation direction due to the buoyancy force, a phenomenon called backlayering. The occurrence of backlayering is affected by many factors such as the fire heat release rate, the entry dimension, the air velocity approaching the fire[12].

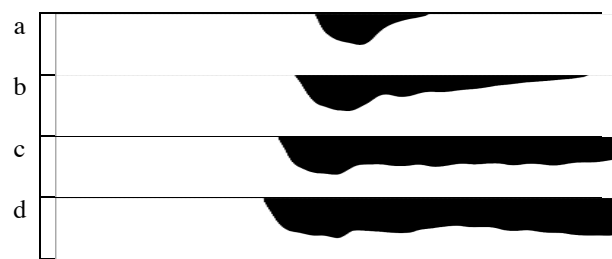
Scenario II evaluates the possibility of backlayering by varying the inlet air velocity: 0.2, 0.5 and 1.0m/s. Fig. 10 shows the distribution of hot air (>60°C) and dense smoke (visibility <10m) layers on the vertical plane in the middle of the nearest drift from the fire source in Fig. 3. At 0.2m/s, the rollback of hot airstream and smoke is considerable and reaches 27.8, 67.5, 138.0 and over 141m at 100, 200, 400 and 600seconds after fire ignition. This backlayering phenomenon is reduced

by increasing the air velocity; at the inlet velocity of 1.0m/s, the rollback extends much shorter distance of 4.7, 15.1, 23.9 and 32.1m/s, respectively. Dense smoke layer propagates along the airflow at the speed of 0.26~0.44, 0.56~0.72 and 0.52~0.69m/s near the ceiling under the inlet air velocity of 0.2, 0.5 and 1.0m/s, while the backlayering extends at the speed of 0.24~0.34, 0.11~0.14 and 0.05~0.08m/s, respectively.

In the 10m(W)x6m(H) drift, securing air velocity of 1.0m/s requires flow rate of 60m³/s which can be hardly achieved in large-opening limestone mines. Therefore, in case of a large fire, the backlayering is inevitable in local limestone mines. Since the thickness increase rate of the rolling-back layer observed at 30m upwind is 0.2~0.4m/min; even after 600seconds, the hot layer is not likely to come down to the workers height in 6m-high drift. This implies that workers can find safe escape routes underneath the hot and dense smoke layers. In order to design economical safety plan, further studies will be performed to identify the so-called critical velocity, the minimum velocity to prevent the smoke rollback at the workers height. In addition, at 30m downwind, the thickness of hot layer increases at the rate of 0.2~0.8m/min.



(a) In case of inlet velocity, 0.2m/s



(b) In case of inlet velocity, 1.0m/s

Fig. 10. Backlayering of the hot smoke at inlet velocity of 0.2 and 1.0m/s on the vertical cross section in the nearest drift from the fire source in Scenario II (a: at 100s, b: at 200s, c: 400s, d: 600s)

Figure 11 shows the backlayering of the hot dense smoke layer over the entire domain in Scenario II at the inlet velocity of 0.2 and 1.0m/s.

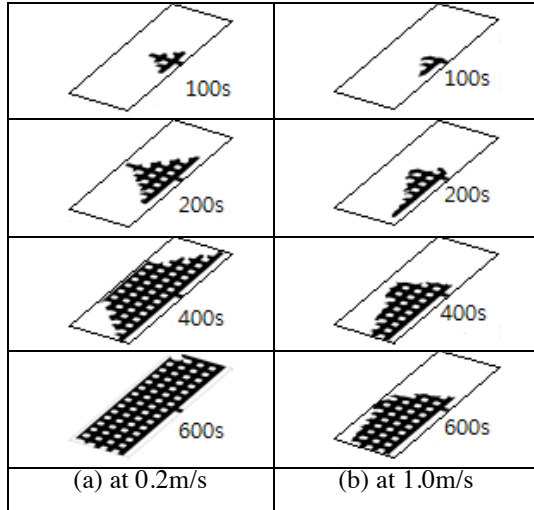
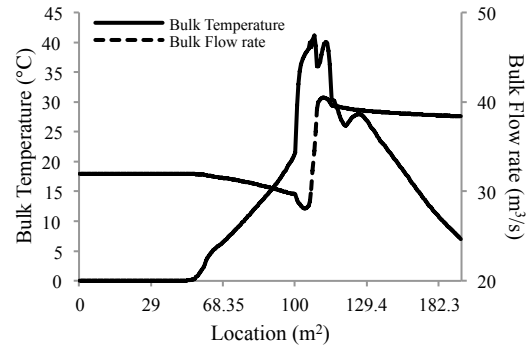


Fig. 11. Backlayering of the dense smoke layer in Scenario II

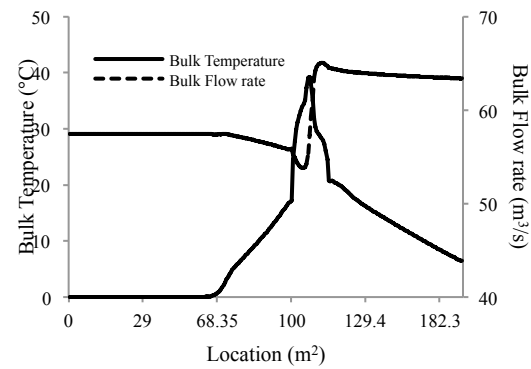
2.5 Analysis of Scenario III

Since the air passing through the vicinity of the fire zone is heated, its volume expands and downstream air velocity increases. This phenomenon is called a throttling or choking effect; and its effects diminish gradually due to the increasing frictional pressure losses[13]. The purpose of deploying Scenario III is to observe this phenomenon. In Scenario III, a 200m-long single drift(10m(W)x8m(H)) is driven and at the middle, a room is being developed in a direction perpendicular. A 30MW fire is simulated in the room and immediately after the ignition, a fan with thrust of 100N and 200N installed at 90m upwind is turn on.

Fig.12 shows bulk temperature and bulk flow rate on the cross section along the drift after 150seconds under the inlet inflow rate of 32.0 and 57.4m/s with the fan capacity of 100N and 200N, respectively. The volume flow rate increase in the downstream of the fire; the flow rate rises are 12.1 and 11.0m³/s corresponding to the velocity increase of 0.30m/s and 0.14m/s. The effects do not completely diminish even at 100m downwind.



(a) With fan thrust of 100N



(b) With fan thrust of 200N

Fig. 12. Choking effect after 150 seconds with fan thrust of 100N and 200N in Scenario III

3. Summary and Conclusion

A 25-ton diesel truck fire in large-opening limestone mine is analyzed to evaluate the fire behavior and effects of the drift dimension and the fan operating capacity and method, and possibility of the backlayering and choking effects. Some of the observations made through CFD analysis are as follows:

- (1) At the fire source without fan operation in Scenario I, the temperature reaches 540.4°C in 6m-high drift and 394.6°C in 8m-high drift after 600 seconds. When fan is turned on either in the blowing or exhaust mode, higher temperature at the fire source is observed. The exhaust fan operation is more effective to maintain lower temperature and layers of the hot airstream near the ceiling along the escape route. Higher fan capacity leads to faster fire growth.
- (2) In Scenario II, the backlayering effects are observed. Under the inlet velocity of 0.2 and 1.0m/s, hot smoke layer expands downwind at the speed of approximately 0.35 and 0.61m/s, while the rollback layers move upwind at

0.29m/s and 0.06m/s, respectively. The thickness of the hot airstream grows at the rate of 0.2~1.0m/min 30m downwind and 0.2~0.4m/min at 30m upwind. Securing the critical velocity by increasing the ventilation rate to prevent the smoke rollback over the entire cross section seems to be economically wasteful; instead, maintaining the safe environment at the workers height is desirable.

- (3) The choking effects, increasing volumetric flow rate near the fire source due to the growing fire are clearly demonstrated. At the inlet velocity of 0.40 and 0.72m/s in 8m-high and 10-m wide drift, the air velocity increases to 0.50 and 0.81m/s near the fires, respectively. The effects exist even at 100m downwind.

Acknowledgments

This research was supported by a grant from the Energy Technology Development Program(grant No. 2013T100100021) of the Korea Institute of Energy Technology Evaluation and Planning, funded by the Ministry of Trade Industrial and Energy of the Korean government.

References

- [1] K.L. Bickel, Analysis of diesel-powered mine equipment. In Proceedings of the Bureau of Mines Technology Transfer Seminar: Diesels in Underground Mines. Information Circular 9141. Washington, DC: Bureau of Mines, 1987
- [2] R. Hansen, Design fires in underground mines, Studies in sustainable technology, Studies in sustainable technology, Research report 2010:2, Malardalen University, Sweden, 2010
- [3] R. Hansen and H. Ingason, Full-scale fire experiments with mining vehicles in an underground mine, Studies in sustainable technology, Research report 2013:2, Malardalen University, Sweden, 2013
- [4] National Fire Protection Association, NFPA 502: Standard for tunnels, bridges, and other limited access highways, 2008
- [5] National Fire Protection Association, NFPA 120: Standard for fire prevention and control in coal mines, 2015
- [6] National Fire Protection Association, NFPA 122: Standard for Fire Prevention and Control in Metal/Nonmetal Mining and Metal Mineral Processing Facilities, 2015
- [7] British Standards Institution, PD 7974-1: Application of fire safety engineering principles to the design of buildings. Initiation and development of fire within the enclosure of origin (Sub-system 1), 2003
- [8] Anon., Memorial tunnel fire ventilation test program, phase IV report, Commonwealth of Massachusetts, prepared by Bechtel/Parsons Brinckerhoff, 1999
- [9] Anon., Users's manual, SOLVENT (ver 1.0), prepared by Innovative Research, Inc., and Parsons Brinckerhoff, 2000
- [10] A. Lonnermark and H. Ingason, The effect of cross-sectional area and air velocity on the conditions in a tunnel during a fire, SP Technical Research Institute of Sweden, SP Report 2007:05, 2007
- [11] National Fire Protection Association, NFPA 130: Standard for fixed guideway transit and passenger rail systems, 2015
- [12] D.J. Brake, Fire modeling in underground mines using Ventsim Visal VentFIRE software, The Australian Mine Ventilation Conference (2013) 265-276
- [13] J. Tubbs and B. Meachan, Egress design solutions: a guide to evacuation and crowd management planning, ARUP, John Wiley & Sons, 200



Photo: Jim Stroup

This book contains the complete proceedings of the 15th North American Mine Ventilation Symposium held on the campus of Virginia Tech in Blacksburg, Virginia, from June 20 to 25, 2015. The symposium series was initiated by the Underground Ventilation Committee of the Society for Mining, Metallurgy, and Exploration (a joint committee of the Coal and Energy Division and Mining and Exploration Division) to facilitate open collaboration between underground mine ventilation professionals from industry, academia, and government in an environment that fosters innovation. The technical papers in these proceedings represent subjects critical to underground mine ventilation, including diesel exhaust and other contaminants in the mine atmosphere, dust in the underground mine environment, mine atmospheric monitoring, mine fans, mine fires, mine gases, mine heating and cooling, case studies, ventilation planning, and ventilation system design.

Proceedings of the 15th North American Mine Ventilation Symposium
Copyright © 2015 Virginia Tech Department of Mining and Minerals Engineering
ISBN 978-0-692-47348-1